Journal of Oncology

Prognosis, Diagnosis and Treatments for Digestive System Cancers

Lead Guest Editor: Alamgeer Yuchi
Guest Editors: Muhammad Wasim Khan and Hafiz Muhammad Irfan

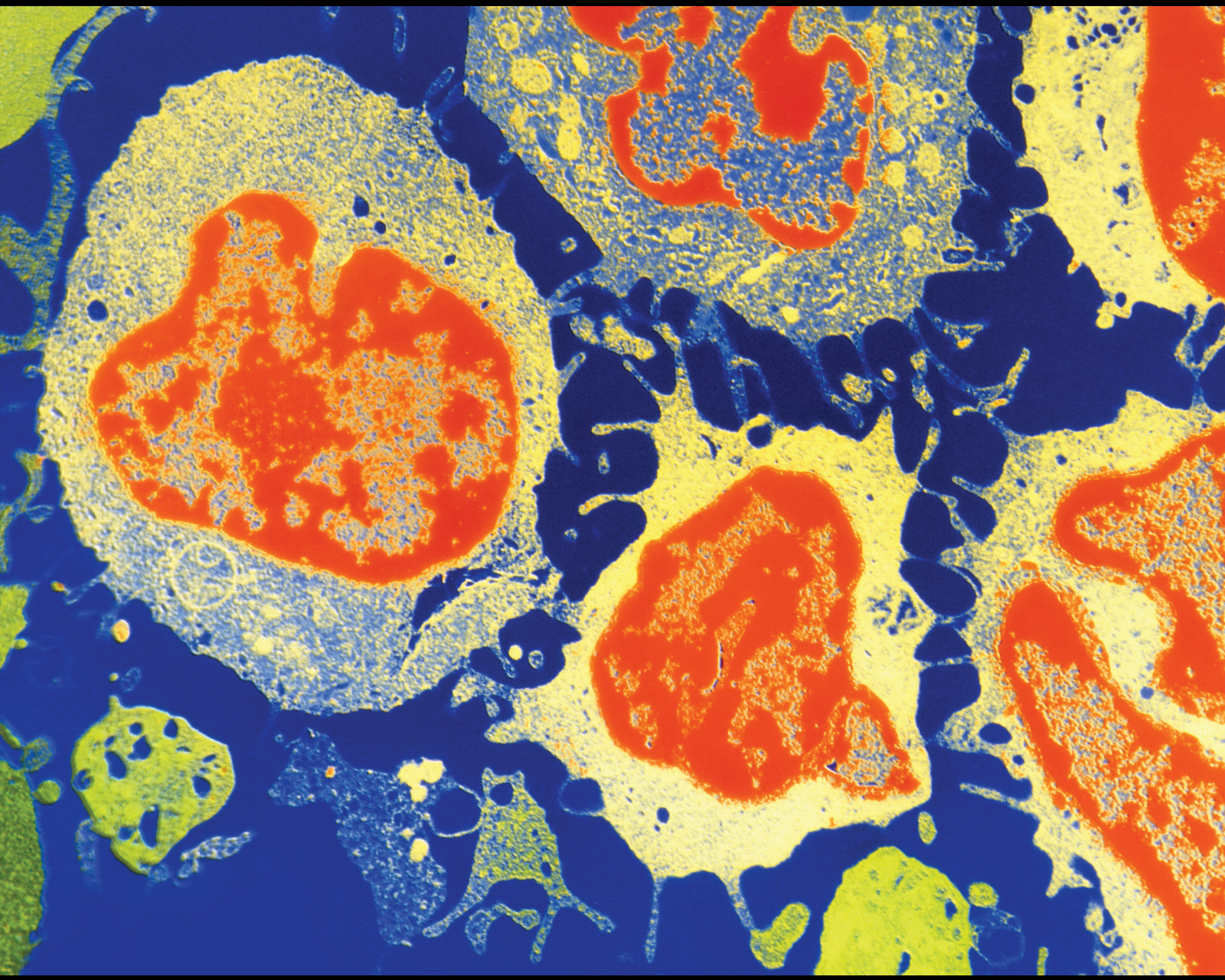

Prognosis, Diagnosis and Treatments for Digestive System Cancers

Journal of Oncology

Prognosis, Diagnosis and Treatments for Digestive System Cancers

Lead Guest Editor: Alamgeer Yuchi
Guest Editors: Muhammad Wasim Khan and Hafiz Muhammad Irfan

Contents

Contents

Contents

Contents

Hindawi
Journal of Oncology
Volume 2022, Article ID 9780315, 5 pages
https://doi.org/10.1155/2022/9780315

Corrigendum

Corrigendum to "LncRNA SNHG3 Promotes Gastric Cancer Cells Proliferation, Migration, and Invasion by Targeting miR-326"

Jun Rao,[1] Jinjin Fu,[1] Chuchen Meng,[2] Jin Huang,[1] Xiangrong Qin,[1] and Shaohua Zhuang[1]

[1]*Department of Gastroenterology, Changzhou No. 2 People's Hospital, The Affiliated Hospital of Nanjing Medical University, No. 29 Xinglong District, Changzhou 213000, China*
[2]*Department of Endocrinology, Changzhou No. 2 People's Hospital, The Affiliated Hospital of Nanjing Medical University, Changzhou, China*

Correspondence should be addressed to Shaohua Zhuang; zhuangshaohua@czehospial.cn

Received 28 June 2022; Accepted 28 June 2022; Published 20 September 2022

In the article titled "LncRNA SNHG3 Promotes Gastric Cancer Cells Proliferation, Migration, and Invasion by Targeting miR-326" [1], concerns with the figures have been identified as initially raised on PubPeer [2].

In the published article, the right side panel of Figure 2(c) is the same as the middle two panels of Figure 6(c), the first left panel of Figure 2(d) is the same as the first left panel of Figure 3(d), and the N-cadherin of Figure 2(b) is the same as TWIST in HGC-27 of Figure 5(e). The authors explained that these errors were introduced during the preparation of the manuscript, and this does not affect the results and conclusions of the article.

While the authors initially responded to provide an explanation to the concerns along with the revised figures, they have not responded to requests to approve this notice. This corrigendum is therefore published with the agreement of the editorial board to ensure the appropriate correction of the issues detailed above. The corrected Figures 2 and 6 are as follows.

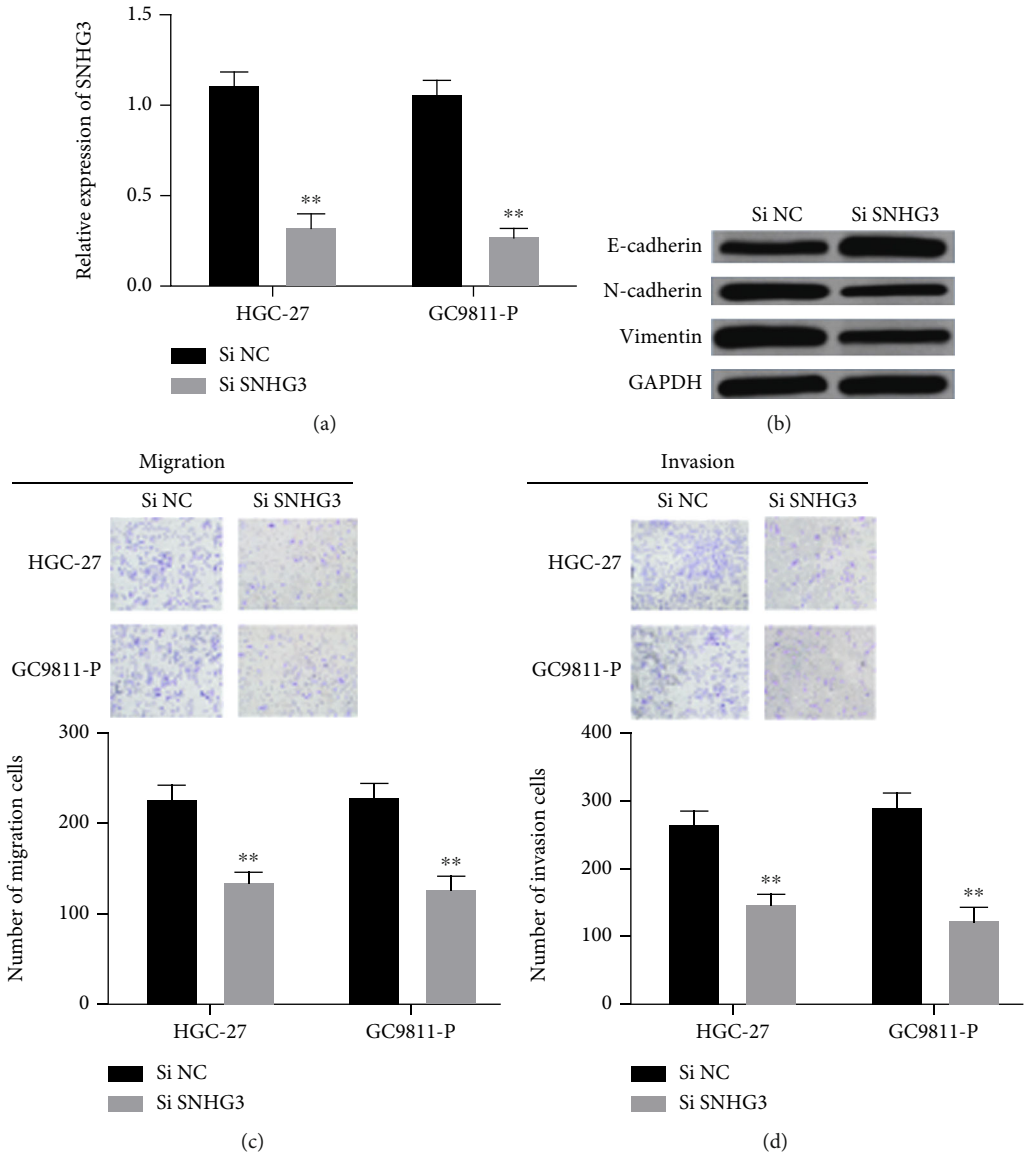

Figure 2: Continued.

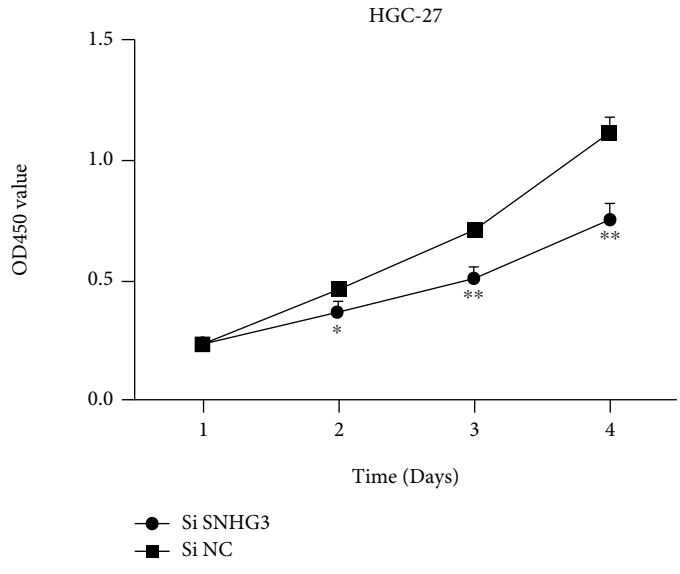

(e)

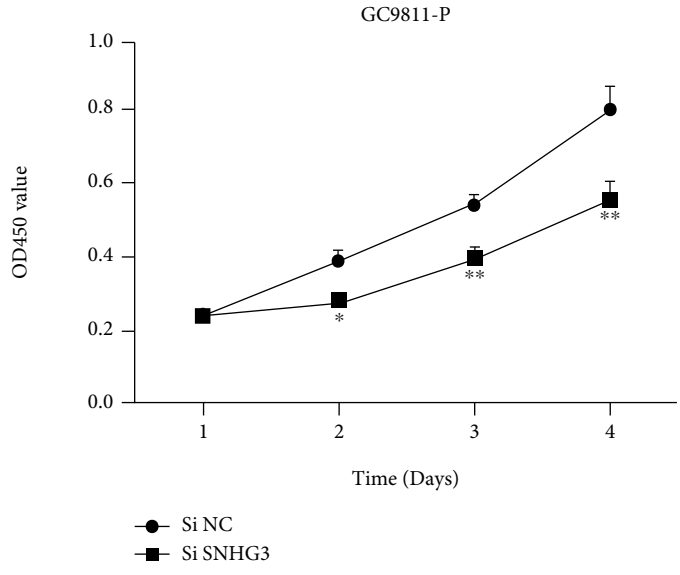

(f)

Figure 2: lncRNA SNHG3 knockdown suppressed HGC-27 and GC9811-P cell proliferation, migration, and invasion in vitro. (a) Expression of lncRNA SNHG3 in GC cells transfected with siSNHG3 or NC. (b) The protein level EMT-related marker in si NC and siSNHG3 groups. (c, d) Effect of lncRNA SNHG3 knockdown on cell migration and invasion. (e, f) Effect of lncRNA SNHG3 knockdown on cell proliferation. $^{*}P < 0.05$ and $^{**}P < 0.01$.

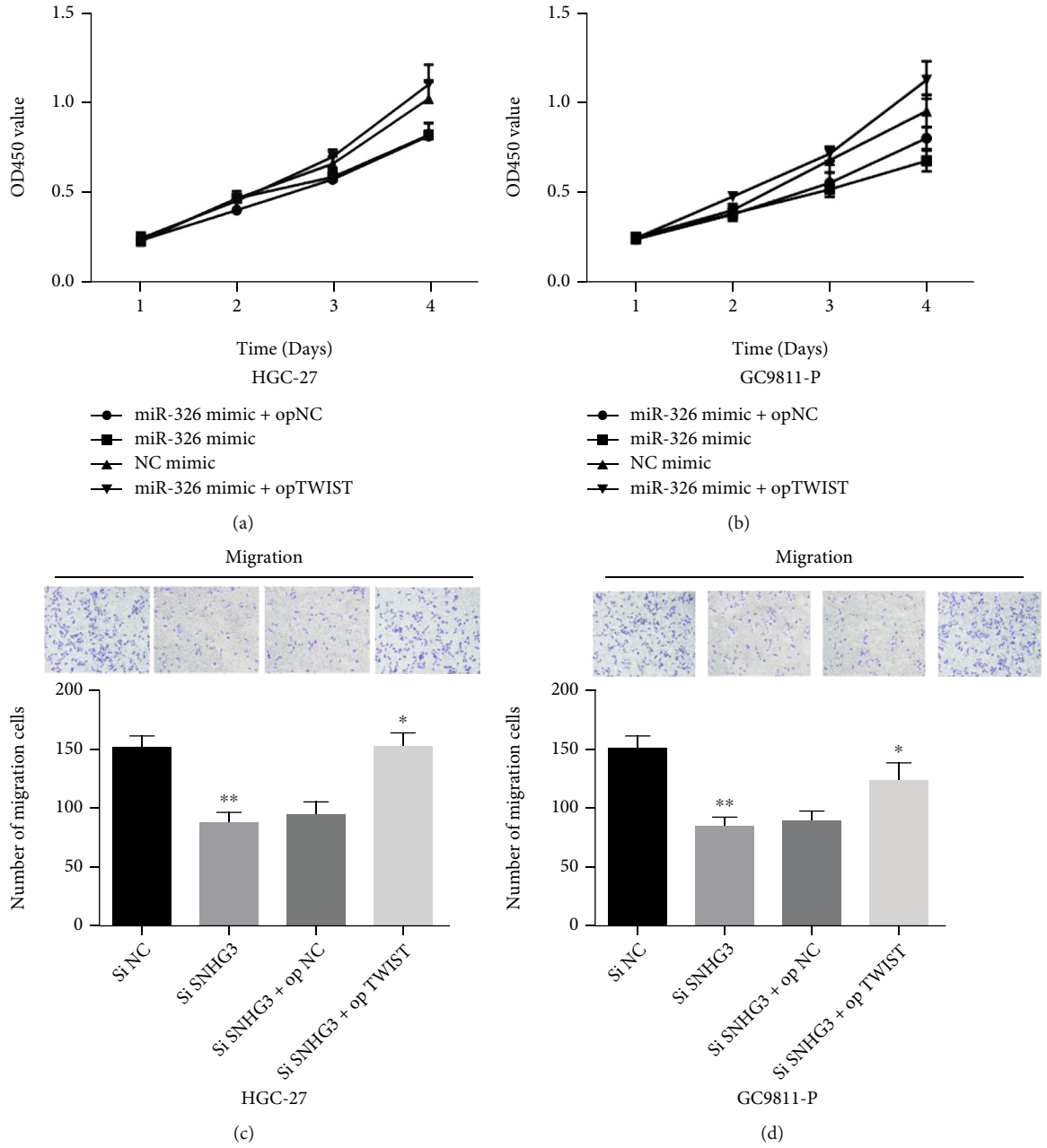

Figure 6: Continued.

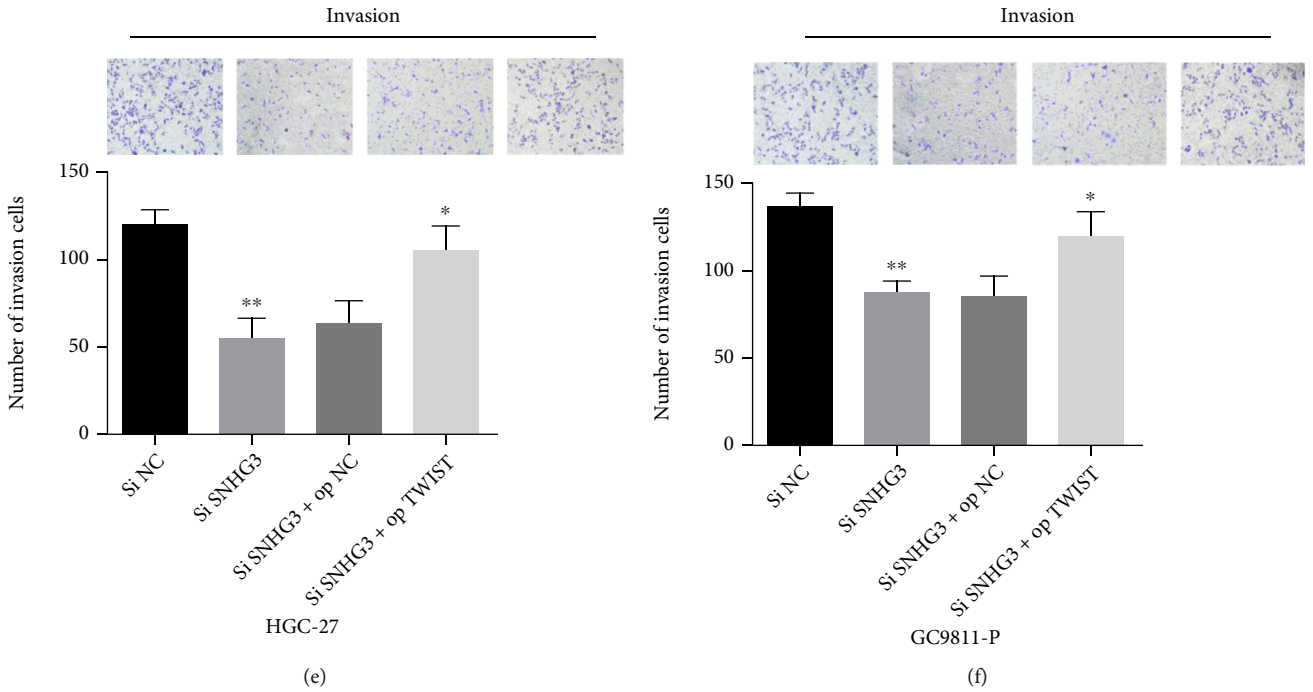

Figure 6: TWIST overexpression overturned lncRNA SNHG3 knockdown or miR-326 overexpression induced suppressive role on cell proliferation, migration, and invasion of GC cells. (a, b) TWIST overexpression overturned the suppressive functions of miR-326 overexpression in GC cell proliferation. (c–f) TWIST overexpression overturned the suppressive functions of SNHG3 knockdown in GC cell migration and invasion. $^{*}P < 0.05$ and $^{**}P < 0.01$.

References

[1] J. Rao, F. Jinjin, C. Meng, J. Huang, X. Qin, and S. Zhuang, "LncRNA SNHG3 Promotes Gastric Cancer Cells Proliferation, Migration, and Invasion by Targeting miR-326," *Journal of Oncology*, vol. 2021, Article ID 9935410, 11 pages, 2021.

[2] R.-D. Gosselin, "LncRNA SNHG3 Promotes Gastric Cancer Cells Proliferation, Migration, and Invasion by Targeting miR-326," July 2021, https://pubpeer.com/publications/135C34EDEF7AED6CF824D84B488745.

Hindawi
Journal of Oncology
Volume 2021, Article ID 5495267, 18 pages
https://doi.org/10.1155/2021/5495267

Research Article

Construction, Validation, and Visualization of Two Web-Based Nomograms to Predict Overall and Cancer-Specific Survival in Patients with Gastric Cancer and Lung Metastases

Honghong Zheng,[1] **Zhehong Li**,[2] **Jianjun Li**,[1] **Shuai Zheng**,[1] **and Enhong Zhao**[1]

[1]*Department of Gastrointestinal Surgery, Affiliated Hospital of Chengde Medical University, Chengde, China*
[2]*Department of Orthopedic, Affiliated Hospital of Chengde Medical University, Chengde, China*

Correspondence should be addressed to Enhong Zhao; zhenghh1215@163.com

Received 28 May 2021; Accepted 21 October 2021; Published 1 November 2021

Academic Editor: Nicola Silvestris

Background. The lung is one of the most common sites of metastasis in gastric cancer. Our study developed two nomograms to achieve individualized prediction of overall survival (OS) and cancer-specific survival (CSS) in patients with gastric cancer and lung metastasis (GCLM) to better guide follow-up and planning of subsequent treatment. *Methods*. We reviewed data of patients diagnosed with GCLM in the Surveillance, Epidemiology, and End Results (SEER) database from 2010 to 2015. The endpoints of the study were the OS and CSS. We used the "caret" package to randomly divide patients into training and validation cohorts in a 7 : 3 ratio. Multivariate Cox regression analysis was performed using univariate Cox regression analysis to confirm the independent prognostic factors. Afterward, we built the OS and CSS nomograms with the "rms" package. Subsequently, we evaluated the two nomograms through calibration curves, receiver operating characteristic (ROC) curves, and decision curve analysis (DCA). Finally, two web-based nomograms were built on the basis of effective nomograms. *Results*. The OS analysis included 640 patients, and the results of the multivariate Cox regression analysis showed that grade, chemotherapy, and liver metastasis were independent prognostic factors for patients with GCLM. The CSS analysis included 524 patients, and the results of the multivariate Cox regression analysis showed that the independent prognostic factors for patients with GCLM were chemotherapy, liver metastasis, marital status, and tumor site. The ROC curves, calibration curves, and DCA revealed favorable predictive power in the OS and CSS nomograms. We created web-based nomograms for OS (https://zhenghh.shinyapps.io/aclmos/) and CSS (https://zhenghh.shinyapps.io/aslmcss/). *Conclusions*. We created two web-based nomograms to predict OS and CSS in patients with GCLM. Both web-based nomograms had satisfactory accuracy and clinical usefulness and may help clinicians make individualized treatment decisions for patients.

1. Introduction

Gastric cancer (GC) is one of the most common malignant tumors of the gastrointestinal tract, accounting for the third and fifth causes of cancer deaths in men and women worldwide, respectively [1]. According to the 2018 Global Cancer Center statistics [1], there were approximately one million new cases of GC and approximately 780,000 GC-related deaths worldwide. Although radical surgery is currently effective in treating localized GC, recurrence or metastasis still occurs in 25% to 40% of patients after surgery [2–4]. According to relevant studies, the lung is a frequent metastatic organ in patients with GC [5], and the incidence of lung metastasis (LM) after GC surgery ranges from 1.3% to 3.8% [6–10]. Moreover, there is a lack of mature therapy standards for gastric cancer and lung metastasis (GCLM), and the 5-year survival rate of patients with GCLM is <5% [11]. At this stage, few studies have reported prognostic factors regarding the survival of patients with GCLM. Therefore, establishing a prediction model for patients with GCLM is clinically significant.

The treatment of GCLM has been recently diversified [12–15]; however, the poor surgical outcome and complications associated with lung-occupying lesions in patients with GCLM lead to worse prognosis. Kong et al. [16] reported that the median survival of patients with GCLM is only four months. Moreover, studies have shown that the prognostic influences of GCLM generally include tumor histological grade, T stage, concurrent pulmonary metastases, primary lesions not subjected to surgery, bilateral pulmonary metastases, combined extrapulmonary metastases, and chemotherapy [17]. Regrettably, no studies have combined the relevant variables to assess the prognosis of GCLM.

A nomogram is a simple, multivariate visualization tool in oncology for predicting and quantifying individual patient survival, to aid clinical decision-making and promote precision medicine [18–21]. In addition, the web-based nomogram, also known as "predictive probability web page calculator," is a web page based on Shiny. This nomogram is a product of the electronic era, and the user just has to select the appropriate variable and click "Predict" to draw the probability of occurrence of the corresponding characteristics of patients, which is convenient and more practical [22]. Consequently, we aimed to devise two web-based nomograms to predict the overall survival (OS) and cancer-specific survival (CSS) in patients with GCLM based on the Surveillance, Epidemiology, and End Results (SEER) database.

2. Materials and Methods

2.1. Data Source and Inclusion Criteria. In this study, our data were obtained by downloading the SEER∗Stat software version 8.3.6. The SEER database is a public database, exempt from medical ethics review, and does not require informed consent. Strict inclusion and exclusion criteria were also developed, and the nadir criteria are listed below. The inclusion criteria were as follows: (I) patients diagnosed with GCLM between 2010 and 2015; (II) demographic variables, including age, race and gender, marital status, and insurance status; and (III) available tumor characteristics, including histological grade, T stage, N stage, brain metastasis, bone metastasis, and liver metastasis. The exclusion criterion was incomplete information. Next, we randomized the patients into training (70%) and validation cohorts (30%). In this study, patients in the training and validation cohorts were used to develop and validate the nomograms, respectively.

2.2. Clinicopathological Factors. Clinicopathological factors for the following variables were extracted: age (<60 and ≥60 years), race (white, black, and other), sex (female and male), histologic type (adenocarcinoma, signet ring cel1, intestinal type, other), T stage (T1, T2, T3, and T4), N stage (NO, N1, and N3), grade (grade I, grade II, grade III, and grade IV), bone metastasis (yes or no), liver metastasis (yes or no), brain metastasis (yes or no), primary site (cardia, fundus, body, gastric antrum, lesser, greater, other), radiotherapy (yes or no), chemotherapy (yes or no), surgery (yes or no), marital status (yes or no), and insurance (yes or no). OS and CSS were considered endpoint times. OS and CSS were, respectively, defined as the time from diagnosis to death from all causes and the time from cancer diagnosis to death.

2.3. Statistical Analysis. All statistical analyses were performed using the R software (version 4.0.2). P value <0.05 (both sides) was considered statistically significant. We obtained relevant prognostic factors through univariate Cox regression analysis and obtained independent prognostic factors through multivariate Cox regression analysis on the basis of univariate Cox regression analysis. The prognostic nomograms for OS and CSS were created separately using the "rms" package, according to the independent prognostic factors. In addition, ROC curves for the prognostic nomograms were established. The area under the curve (AUC) was used to evaluate the discriminative power of the nomograms. In addition, calibration curves and decision curve analysis (DCA) for nomograms were established. Finally, we divided all patients into high- and low-risk groups according to the median risk score and tested the prognostic value of the nomograms using Kaplan-Meier (K-M) analysis.

3. Results

3.1. Flowchart. A detailed workflow is shown in Figure 1.

3.2. Characteristics of the Study Population. For the OS analysis, a total of 640 patients were included, 448 patients in the training cohort and the remaining 192 patients in the validation cohort. Among the 640 patients, the number of male patients (69.69%) was higher than that of the female patients (30.31%). A total of 484 patients (75.63%) were white, 75 patients (11.72%) were black, and 81 patients (12.65%) were classified as "other." Of these patients, 219 were below 60 years of age and 421 were 60 years old or older. The baseline clinicopathological characteristics of patients in the OS group are shown in Table 1.

A total of 524 patients for the CSS analysis were enrolled; 368 patients were included in the training cohort, and the remaining 156 patients were included in the validation cohort. Of the 524 patients, 69.08% were male and 30.92% were female patients. Most of the patients (70.05%) were classified as white. Finally, 197 patients were below 60 years of age, and 327 patients were 60 years old or older. The baseline clinical pathological characteristics of patients in the CSS group are shown in Table 2.

3.3. Prognostic Factors for Patients with GCLM. For grouping status of OS, the detailed information of patients with GCLM in the OS group is shown in Table 3. Univariate Cox regression analysis demonstrated that grade II, liver metastasis, radiotherapy, and chemotherapy were OS-related prognostic factors. Multivariate Cox regression analysis showed that grade I1l (P value = 0.018, hazard ratios (HR) = 1.896, 95% confidence interval (CI) = 1.118–3.214), liver

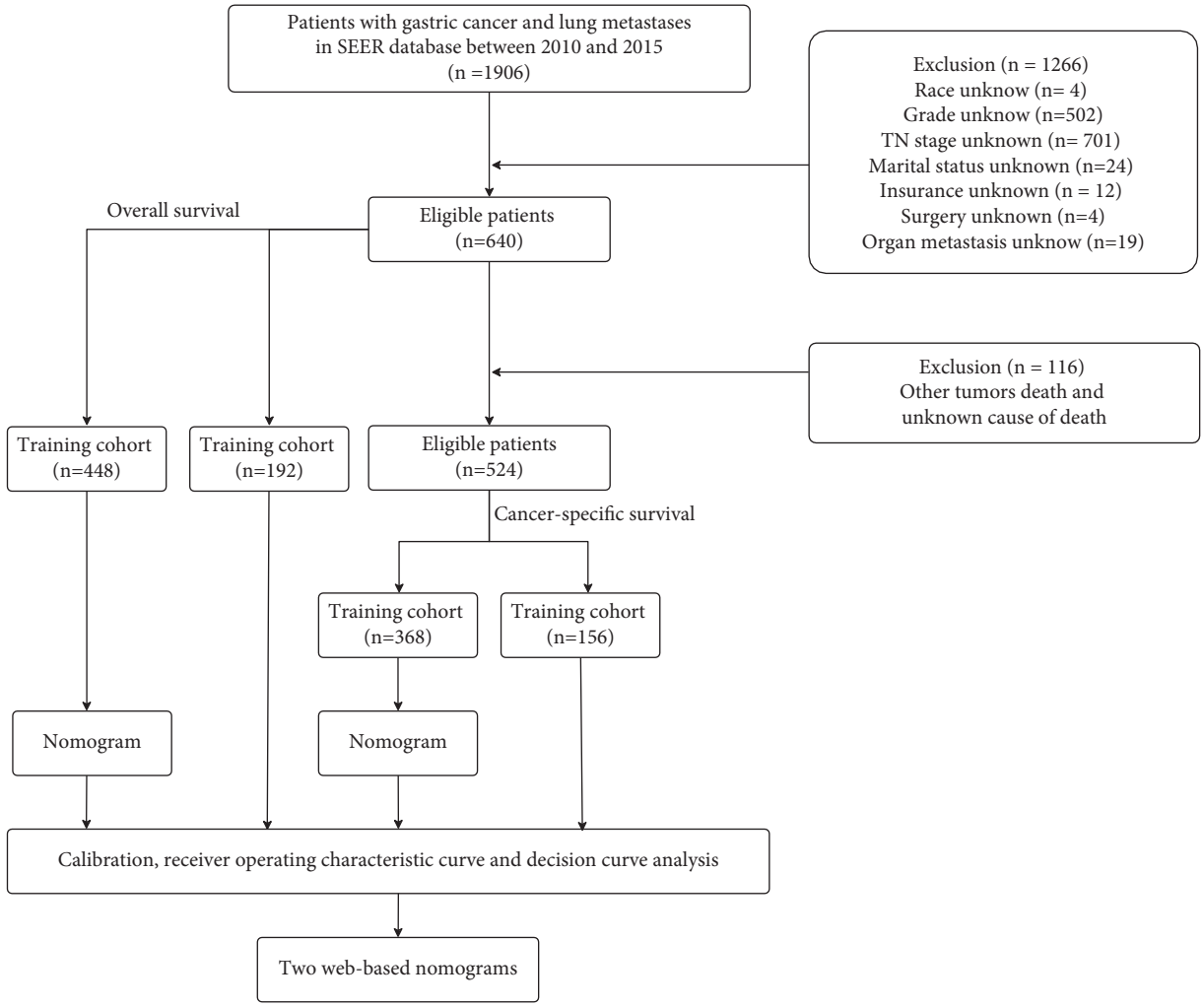

Figure 1: Detailed workflow of study design and analysis.

metastasis (P value <0.001, HR = 1.440, 95% CI = 1.179–1.760), and chemotherapy (P value <0.001, HR = 0.292, 95% CI = 0.235–0.363) were independent prognostic factors in patients with GCLM.

For grouping status of CSS, more details of the patients with GCLM in the CSS group are listed in Table 4. Univariate Cox regression analysis revealed that race, T2, liver metastasis, primary site, chemotherapy, and marital status were CSS-related prognostic factors. Multivariate COX regression analysis revealed that liver metastasis (P value <0.001, HR = 1.524, 95% CI = 1.217–1.909), primary site (greater, P value = 0.001, HR = 2.315, 95% CI = 1.395–3.814), chemotherapy (P value <0.001, HR = 0.398, 95% CI = 0.317–0.501), and marital status (P value = 0.039, HR = 0.778, 95% CI = 0.629–0.988) were independent prognostic factors for GCLM.

3.4. Establishment of Nomogram. Prognostic nomograms of OS were established according to three independent prognostic factors (Figure 2(a)). Prognostic nomograms of CSS were created according to four independent prognostic factors (Figure 2(b)).

3.5. Verification of Nomogram

(i) ROC of OS: The AUCs at 3, 6, and 12 months were 0.753, 0.799, and 0.732, respectively, in the training cohort (Figures 3(a)–3(c)). In the validation cohort, the AUCs at 3, 6, and 12 months were 0.855, 0.755, and 0.686, respectively (Figures 3(d)–3(f)). The time-dependent ROC curves revealed that the AUC value fluctuated at approximately 0.8 from one month to 12 months (Figures 3(g) and 3(h)).

(ii) ROC of CSS: The AUCs at 3, 6, and 12 months were, respectively, 0.820, 0.766, and 0.760, respectively, in the training cohort (Figures 4(a)–4(c)). The AUCs at 3, 6, and 12 months were separately 0.894, 0.764, and 0.720, respectively, in the validation cohort (Figures 4(d)–4(f)). The time-dependent ROC curves also demonstrated that the AUC value fluctuated at approximately 0.8 from one month to 12 months (Figures 4(g) and 4(h)).

(iii) Calibration curves: The calibration curves at 3, 6, and 12 months for the OS probabilities were in good correspondence with the OS predicted with the

Table 1: Baseline data of clinicopathological characteristics of patients with GCLM in OS group.

Variables	Total cohort ($N = 640$)		Training cohort ($N = 448$)		Validation cohort ($N = 192$)	
	n	%	*n*	%	*n*	%
Age						
<60	219	34.2	158	35.3	61	31.8
≥60	421	65.8	290	64.7	131	68.2
Race						
Black	75	11.7	53	11.8	22	11.5
Other	81	12.7	51	11.4	30	15.6
White	484	75.6	344	76.8	140	72.9
Sex						
Female	194	30.3	127	28.3	67	34.9
Male	446	69.7	321	71.7	125	65.1
Histologic type						
Adenocarcinoma	407	63.6	288	64.3	119	62.0
Signet ring cell	94	14.7	66	14.7	28	14.6
Intestinal type	42	6.6	26	5.8	16	8.3
Other	97	15.2	68	15.2	29	15.1
T stage						
T1	252	39.4	168	37.5	84	43.8
T2	40	6.3	28	6.3	12	6.3
T3	147	23	106	23.7	41	21.4
T4	201	31.4	146	32.6	55	28.6
N stage						
N0	262	40.9	185	41.3	77	40.1
N1	292	45.6	198	44.2	94	49.0
N2	43	6.7	35	7.8	8	4.2
N3	43	6.7	30	6.7	13	6.8
Grade						
Grade I	26	4.1	16	3.6	10	5.2
Grade II	178	27.8	124	27.7	54	28.1
Grade III	426	66.6	302	67.4	124	64.6
Grade IV	10	1.6	6	1.3	4	2.1
Bone metastasis						
No	526	82.2	372	83	154	80.2
Yes	114	17.8	76	17	38	19.8
Liver metastasis						
No	325	50.8	222	49.6	103	53.6
Yes	315	49.2	226	50.4	89	46.4
Brain metastasis						
No	622	97.2	436	97.3	186	96.9
Yes	18	2.8	12	2.7	6	3.1
Primary site						
Cardia	291	45.5	201	44.9	90	46.9
Fundus	35	5.5	22	4.9	13	6.8
Body	44	6.9	31	6.9	13	6.8
Gastric antrum	74	11.6	53	11.8	21	10.9
Lesser	28	4.4	21	4.7	7	3.6
Greater	30	4.7	22	4.9	8	4.2
Other	138	21.6	98	21.9	40	20.8
Radiotherapy						
No	492	76.9	348	77.7	144	75.0
Yes	148	23.1	100	22.3	48	25.0
Chemotherapy						
No	256	40	179	40	77	40.1
Yes	384	60	269	60	115	59.9
Surgery						
No	580	90.6	407	90.8	173	90.1
Yes	60	9.4	41	9.2	19	9.9
Marital status						
No	255	39.8	182	40.6	73	38.0

Table 1: Continued.

Variables	Total cohort ($N = 640$)		Training cohort ($N = 448$)		Validation cohort ($N = 192$)	
	n	%	*n*	%	*n*	%
Yes	385	60.2	266	59.4	119	62.0
Insurance						
No	37	5.8	30	6.7	7	3.6
Yes	603	94.2	418	93.3	185	96.4

Table 2: Baseline data of clinicopathological characteristics of patients with GCLM in CSS group.

Variables	Total cohort ($N = 524$)		Training cohort ($N = 368$)		Validation cohort ($N = 156$)	
	n	%	*n*	%	*n*	%
Age						
<60	197	37.6	131	35.6	66	42.3
≥60	327	62.4	237	64.4	90	57.7
Race						
Black	67	12.8	50	13.6	17	10.9
Other	69	13.2	49	13.3	20	12.8
White	388	74	269	73.1	119	76.3
Sex						
Female	162	30.9	109	29.6	53	34.0
Male	362	69.1	259	70.4	103	66.0
Histologic type						
Adenocarcinoma	340	64.9	247	67.1	93	59.6
Signet ring cell	76	14.5	46	12.5	30	19.2
Intestinal type	36	6.9	26	7.1	10	6.4
Other	72	13.7	49	13.3	23	14.7
T stage						
T1	209	39.9	148	40.2	61	39.1
T2	36	6.9	27	7.3	9	5.8
T3	117	22.3	84	22.8	33	21.2
T4	162	30.9	109	29.6	53	34.0
N stage						
N0	207	39.5	144	39.1	63	40.4
N1	254	48.5	187	50.8	67	42.9
N2	26	5	14	3.8	12	7.7
N3	37	7.1	23	6.3	14	9.0
Grade						
Grade I	19	3.6	15	4.1	4	2.6
Grade II	147	28.1	105	28.5	42	26.9
Grade III	349	66.6	242	65.8	107	68.6
Grade IV	9	1.7	6	1.6	3	1.9
Bone metastasis						
No	432	97.1	303	82.3	129	82.7
Yes	92	2.9	65	17.7	27	17.3
Liver metastasis						
No	257	49	179	48.6	78	50.0
Yes	267	51	189	51.4	78	50.0
Brain metastasis						
No	509	97.1	356	96.7	153	98.1
Yes	15	2.9	12	3.3	3	1.9
Primary site						
Cardia	240	45.8	164	44.6	76	48.7
Fundus	33	6.3	22	6	11	7.1
Body	38	7.3	29	7.9	9	5.8
Gastric antrum	63	12	46	12.5	17	10.9
Lesser	20	3.8	11	3	9	5.8
Greater	24	4.6	19	5.2	5	3.2
Other	106	20.2	77	20.9	29	18.6

Table 2: Continued.

Variables	Total cohort ($N = 524$)		Training cohort ($N = 368$)		Validation cohort ($N = 156$)	
	n	%	*n*	%	*n*	%
Radiotherapy						
No	401	76.5	276	75	125	80.1
Yes	123	23.5	92	25	31	19.9
Chemotherapy						
No	205	39.1	158	42.9	47	30.1
Yes	319	60.9	210	57.1	109	69.9
Surgery						
No	481	91.8	340	92.4	141	90.4
Yes	43	8.2	28	7.6	15	9.6
Marital status						
No	209	39.9	152	41.3	57	36.5
Yes	315	60.1	216	58.7	99	63.5
Insurance						
No	31	5.9	22	6	9	5.8
Yes	493	94.1	346	94	147	94.2

Table 3: Univariate and multivariate Cox proportional hazards regression analysis of patients with GCLM in the OS group.

Variables	Univariate Cox regression analysis		Multivariate Cox regression analysis	
	HR (95% CI)	*P*	HR (95% CI)	*P*
Age				
<60	Reference			
≥60	1.044 (0.854–1.277)	0.671		
Race				
Black	Reference			
Other	0.979 (0.658–1.457)	0.918		
White	0.788 (0.586–1.061)	0.117		
Sex				
Female	Reference			
Male	0.99 (0.799–1.225)	0.923		
Histologic type				
Adenocarcinoma	Reference			
Signet ring cell	1.044 (0.786–1.388)	0.765		
Intestinal type	1.358 (0.901–2.047)	0.144		
Other	1.144 (0.873–1.498)	0.33		
T stage				
T1	Reference			
T2	0.705 (0.459–1.083)	0.11		
T3	0.944 (0.735–1.214)	0.656		
T4	1.219 (0.969–1.535)	0.091		
N stage				
N0	Reference			
N1	1.009 (0.820–1.243)	0.929		
N2	0.961 (0.664–1.391)	0.833		
N3	1.166 (0.790–1.721)	0.44		
Grade				
Grade I	Reference		Reference	
Grade II	1.458 (0.850–2.501)	0.171	1.275 (0.738–2.201)	0.383
Grade III	1.864 (1.105–3.144)	0.02	1.896 (1.118–3.214)	0.018
Grade IV	1.238 (0.410–3.743)	0.705	0.942 (0.310–2.864)	0.916
Bone metastasis				
No	Reference			
Yes	1.075 (0.833–1.388)	0.58		
Liver metastasis				
No	Reference			
Yes	1.309 (1.080–1.587)	0.006	1.440 (1.179–1.760)	<0.001

Table 3: Continued.

Variables	Univariate Cox regression analysis		Multivariate Cox regression analysis	
	HR (95% CI)	*P*	HR (95% CI)	*P*
Brain metastasis				
No	Reference			
Yes	1.434 (0.806–2.550)	0.22		
Primary site				
Cardia	Reference			
Fundus	1.487 (0.956–2.315)	0.079		
Body	1.179 (0.792–1.754)	0.418		
Gastric antrum	1.224 (0.893–1.676)	0.208		
Lesser	1.211 (0.764–1.922)	0.416		
Greater	1.182 (0.737–1.895)	0.488		
Other	1.28 (0.995–1.646)	0.054		
Radiotherapy				
No	Reference			
Yes	0.761 (0.606–0.955)	0.019	0.979 (0.770–1.244)	0.859
Chemotherapy				
No	Reference			
Yes	0.312 (0.253–0.384)	<0.001	0.292 (0.235–0.363)	<0.001
Surgery				
No	Reference			
Yes	0.835 (0.598–1.167)	0.291		
Marital status				
No	Reference			
Yes	0.844 (0.694–1.025)	0.087		
Insurance				
No	Reference			
Yes	1.076 (0.723–1.602)	0.718		

Table 4: Univariate and multivariate Cox proportional hazards regression analysis of patients with GCLM in the CSS group.

Variables	Univariate Cox regression analysis		Multivariate Cox regression analysis	
	HR (95% CI)	*P*	HR (95% CI)	*P*
Age				
<60	Reference			
≥60	0.945 (0.759–1.176)	0.612		
Race				
Black	Reference		Reference	
Other	0.823 (0.549–1.232)	0.343	0.916 (0.602–1.393)	0.681
White	0.707 (0.519–0.963)	0.028	0.883 (0.635–1.227)	0.458
Sex				
Female	Reference			
Male	0.976 (0.775–1.230)	0.837		
Histologic type				
Adenocarcinoma	Reference			
Signet ring cell	1.064 (0.763–1.484)	0.715		
Intestinal type	1.207 (0.798–1.825)	0.372		
Other	1.152 (0.846–1.570)	0.368		
T stage				
T1	Reference		Reference	
T2	0.594 (0.378–0.932)	0.024	0.71 (0.446–1.131)	0.149
T3	0.854 (0.648–1.124)	0.26	1.121 (0.840–1.497)	0.436
T4	1.088 (0.844–1.402)	0.513	1.15 (0.882–1.498)	0.302
N stage				
N0	Reference			
N1	0.922 (0.737–1.153)	0.475		
N2	0.864 (0.498–1.500)	0.603		
N3	0.865 (0.551–1.358)	0.528		

Table 4: Continued.

Variables	Univariate Cox regression analysis		Multivariate Cox regression analysis	
	HR (95% CI)	*P*	HR (95% CI)	*P*
Grade				
Grade I	Reference			
Grade II	1.282 (0.732–2.245)	0.385		
Grade III	1.632 (0.950–2.806)	0.076		
Grade IV	2.121 (0.813–5.530)	0.124		
Bone metastasis				
No	Reference			
Yes		0.146		
Liver metastasis				
No	Reference		Reference	
Yes	1.47 (1.186–1.821)	<0.001	1.524 (1.217–1.909)	<0.001
Brain metastasis				
No	Reference			
Yes	1.114 (0.610–2.033)	0.725		
Primary site				
Cardia	Reference		Reference	
Fundus	1.593 (1.006–2.522)	0.047	1.312 (0.824–2.091)	0.253
Body	1.337 (0.880–2.030)	0.173	1.364 (0.882–2.108)	0.163
Gastric antrum	1.498 (1.067–2.105)	0.02	1.206 (0.846–1.718)	0.301
Lesser	1.185 (0.642–2.189)	0.587	1.409 (0.732–2.710)	0.305
Greater	2.024 (1.238–3.308)	0.005	2.315 (1.395–3.841)	0.001
Other	1.367 (1.035–1.805)	0.028	1.26 (0.932–1.704)	0.133
Radiotherapy				
No	Reference			
Yes	0.813 (0.640–1.033)	0.091		
Chemotherapy				
No	Reference		Reference	
Yes	0.388 (0.311–0.484)	<0.001	0.398 (0.317–0.501)	<0.001
Surgery				
No	Reference			
Yes	0.715 (0.474–1.077)	0.109		
Marital status				
No	Reference		Reference	
Yes	0.735 (0.592–0.912)	0.005	0.788 (0.629–0.988)	0.039
Insurance				
No	Reference			
Yes	0.954 (0.600–1.518)	0.843		

nomograms to the actual results (Figures 5(a)–5(f)). The calibration curves for the CSS probabilities at 3, 6, and 12 months also suggested the same better consistency among the CSS forecasted with the nomogram and the actual results (Figures 6(a)–6(f)).

(iv) DCA curves: DCA curves confirmed that nomograms can better predict OS (Figures 7(a)–7(f)) and CSS (Figures 8(a)–8(f)) in patients with GCLM. In addition, K-M survival curves revealed that, for OS (Figures 9(a) and 9(b)) and CSS (Figures 9(c) and 9(d)), patients from the higher risk group had a more unfavorable prognosis than those from the lower risk group.

3.6. Establishment of Two Web-Based Nomograms. Based on the above results, we constructed a probabilistic calculator OS (https://zhenghh.shinyapps.io/aclmos/) and CSS (https://zhenghh.shinyapps.io/aslmcss/) based on a dynamic network, which predicts the OS and CSS of patients with GCLM based on previous nomograms (Figure 10(a)). For example, the CSS of a patient with GCLM, who is a married woman with liver metastases, occurs in the gastric body and without chemotherapy. The survival curve of this patient is shown in Figure 10(b). Survival rates and 95% confidence intervals at three months (Figure 10(c), black line), six months (Figure 10(c), blue line), and 12 months (Figure 10(c), red line) can also be observed at the operation interface. In addition, specific numbers are summarized to improve the prediction accuracy (Figure 10(d)). The OS of patients with GCLM can be predicted in the same way.

4. Discussion

GC is a malignant tumor of the gastrointestinal tract with a low early diagnosis rate, low surgical resection rate, and high mortality rate [23]. The majority of patients with GC are in

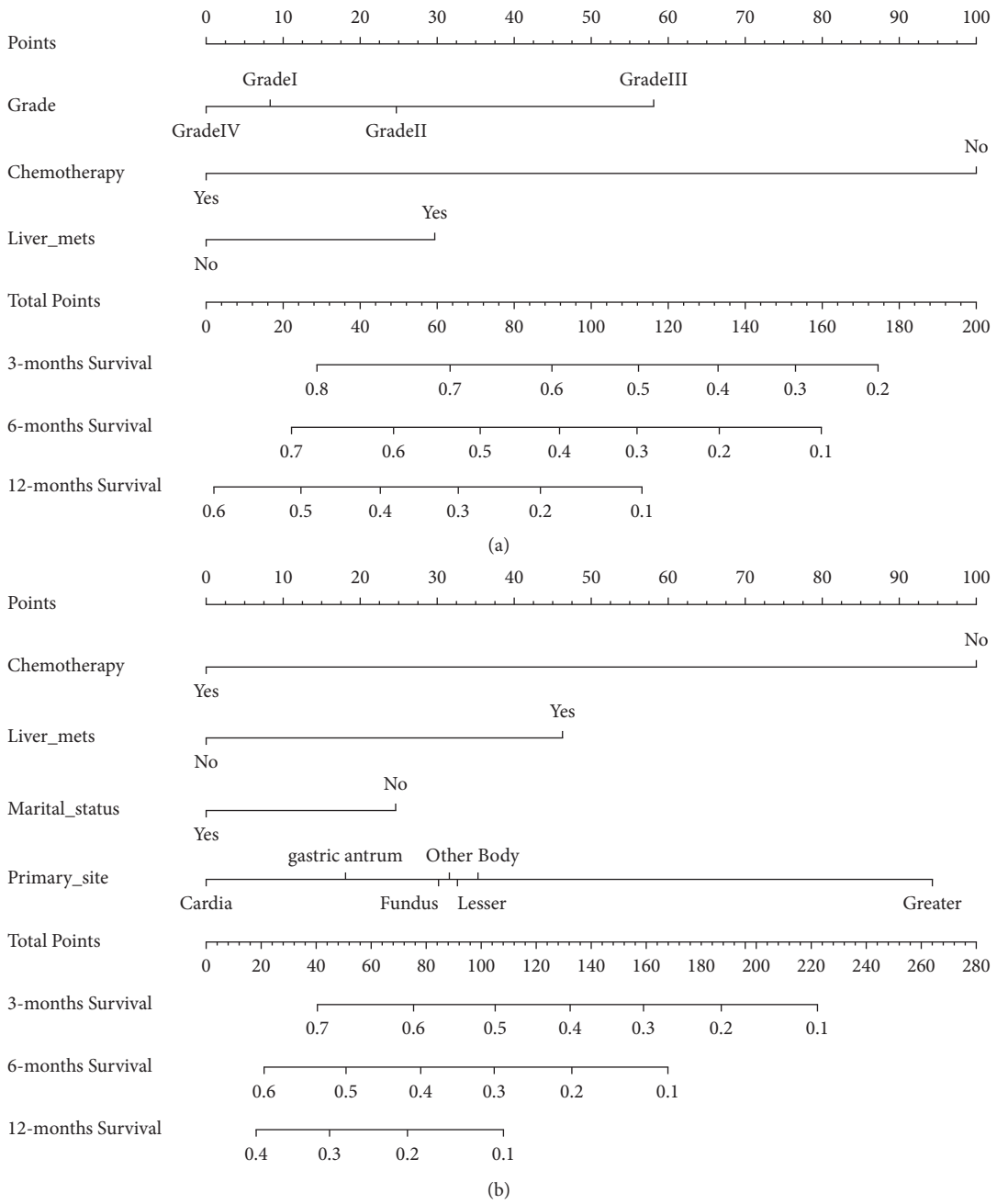

Figure 2: Nomogram. (a) Overall survival (OS) nomogram; (b) cancer-specific survival (CSS) nomogram. OS, overall survival; CSS, cancer-specific survival.

the advanced stage at the time of consultation, and 32.6% have distant metastases [24]. Interestingly, the incidence of LM is 14.9% [24]. LM typically indicates advanced tumors, and when not detected and treated in time, the prognosis is extremely poor. In our study, we created two nomograms to predict the prognosis of patients with GCLM. These two nomograms performed well in predicting OS and CSS in patients with GCLM, allowing more precise individualized clinical decision-making and surveillance. Finally, we built two web-based nomograms based on the nomograms. This prediction model can facilitate the prediction of the survival probability of patients with GCLM at a specific time. Clinicians can also arrange personalized treatment plans based on the prediction results.

As we know, survival statistics of GCLM are not optimistic. Therefore, clinicians can identify the risk and protective factors of GCLM, which can result in a good prognosis for patients with GCLM. A number of potential biomarkers that are involved in cadherin-catenin interaction, integrin signaling, and cancer stem cell identification in gastrointestinal cancers have been observed [25]. However, these biomarkers are difficult to measure, have low sensitivity, are expensive, and have few clinical applications. Therefore, it is necessary to actively identify other clinical

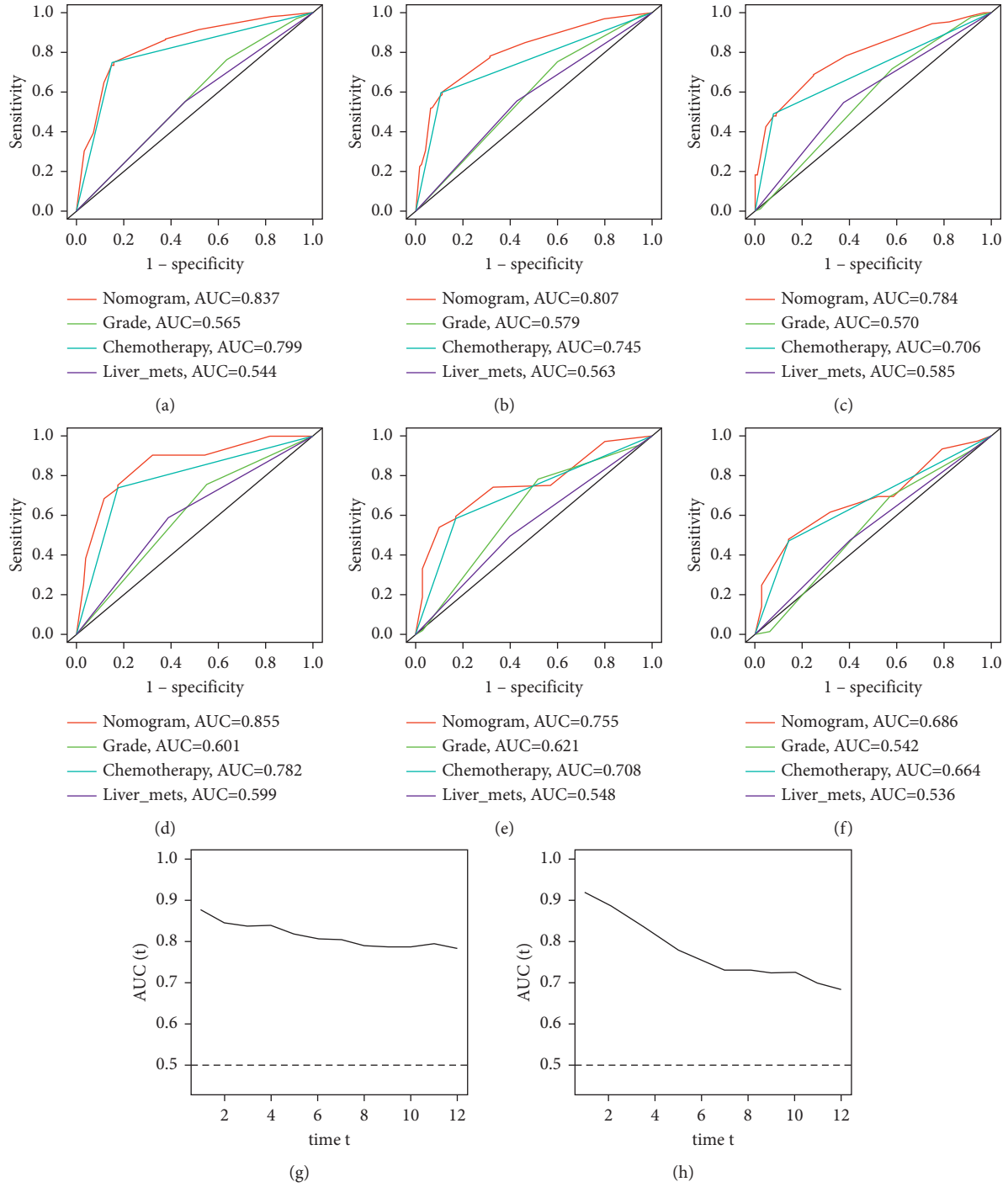

Figure 3: Receiver operating characteristic (ROC) curves of OS. (a–c) ROC curves corresponding to 3, 6, and 12months in the training cohort, respectively; (d–f) ROC curves corresponding to 3, 6, and 12 months in the verification cohort, respectively; (g) the time-dependent ROC curve corresponding to 1 to 12 months in the verification cohort in the training cohort; 3 h, the time-dependent ROC curve corresponding to 1 to 12 months in the verification cohort. ROC, receiver operating characteristic; OS, overall survival.

features related to prognosis in patients with advanced GCLM. In 2019, Wenjie et al. [26] found that age, race, primary site, T stage, and N stage are independently related to CSS in patients with lymph node-positive GC. Studies have shown that the fat content in high muscle tissue is associated with CSS in patients with locally advanced GC [27]. However, so far, few studies have focused on GCLM, and no corresponding nomogram has been established to assess the survival and prognosis of these patients. Previous studies have confirmed that the prognostic factors of liver cancer are quite different from those of liver cancer with bone metastasis [28–31].

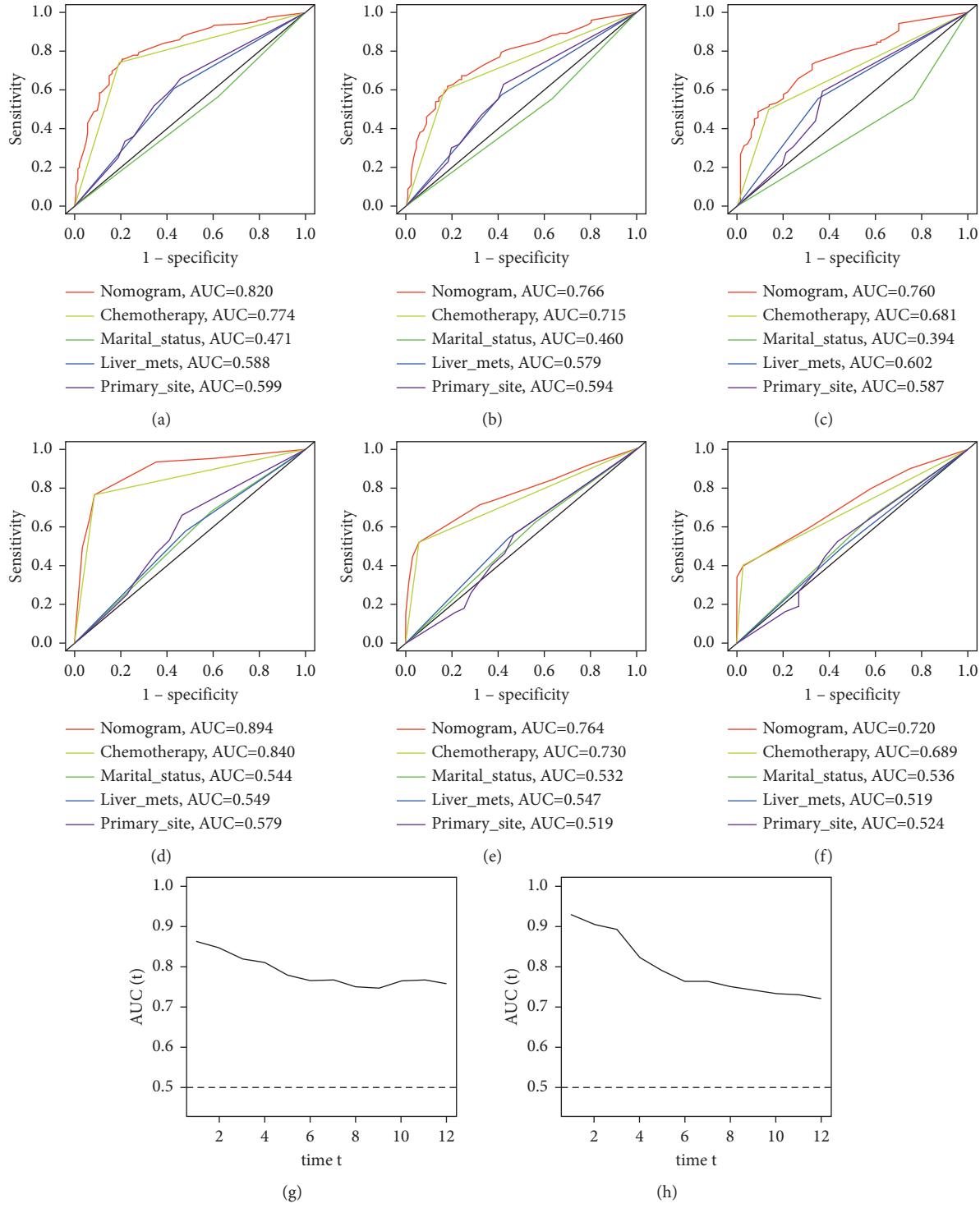

Figure 4: Receiver operating characteristic (ROC) curves of cancer-specific survival (CSS). (a–c) ROC curves corresponding to 3, 6, and 12 months in the training cohort, respectively; (d–f) ROC curves corresponding to 3, 6, and 12 months in the verification cohort, respectively; (g) the time-dependent ROC curve corresponding to 1 to 12 months in the verification cohort in the training cohort; (h) the time-dependent ROC curve corresponding to 1 to 12 months in the verification cohort. ROC, receiver operating characteristic; CSS, cancer-specific survival.

Therefore, it is not possible to evaluate the survival of patients with GCLM solely through the prognostic factors of GC, due to possible biases and errors. In this study, we screened the relevant independent prognostic factors of patients with GCLM. More meaningfully, this study integrates these multiple prognostic factors and visual graphs to predict the survival of patients with GCLM through nomograms, which is a practical tool widely used in oncology [32]. The web-based nomograms were based on further upgraded results.

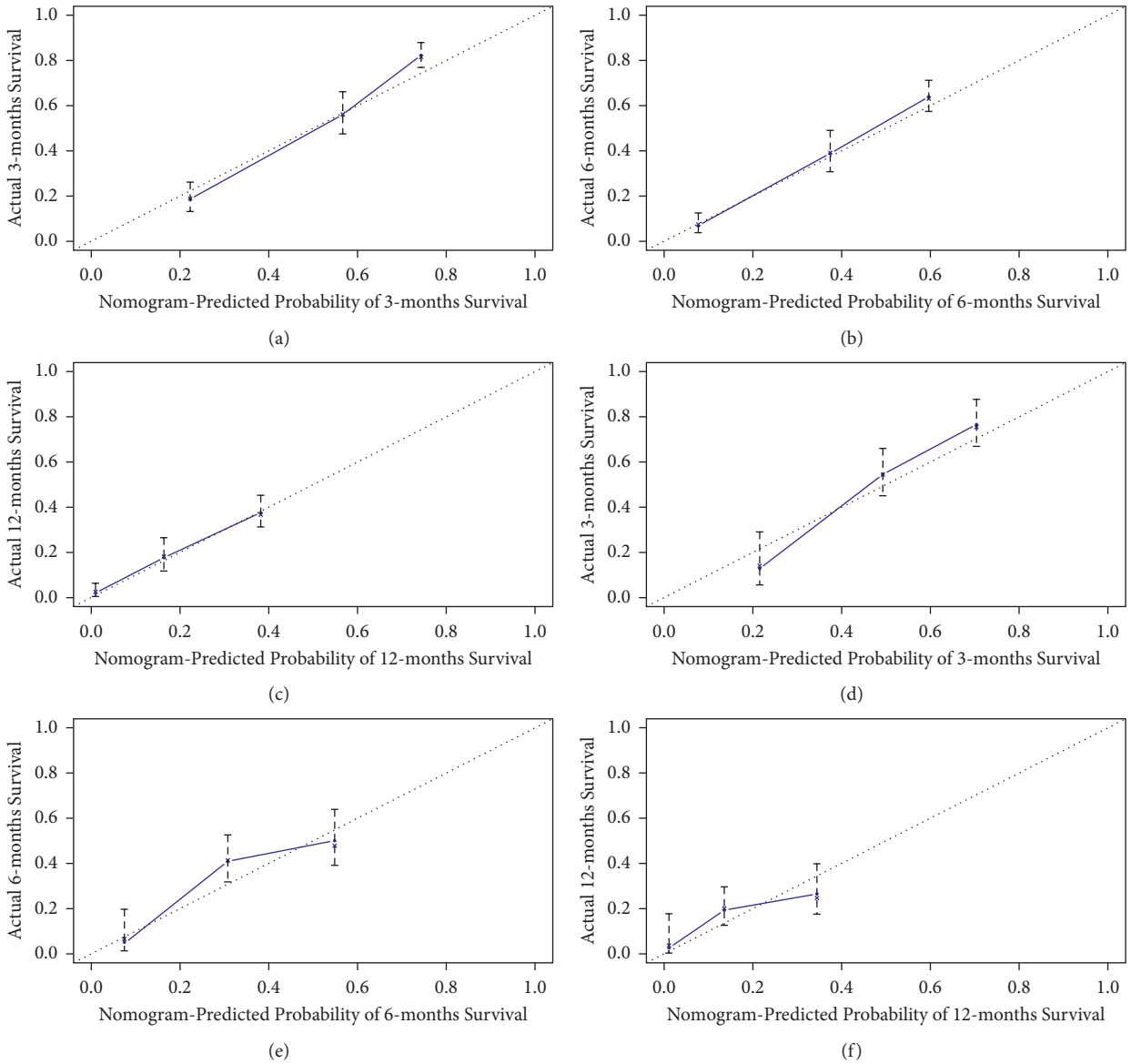

Figure 5: Calibration curves of overall survival (OS). (a–c) Calibration curves corresponding to 3, 6, and 12 months in the training cohort, respectively; (d–f) calibration curves corresponding to 3, 6, and 12 months in the verification cohort, respectively. OS, overall survival.

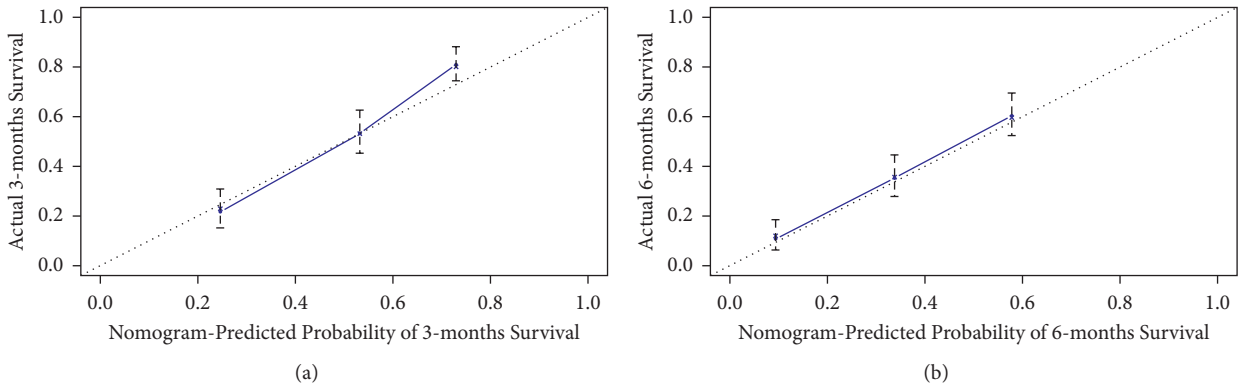

Figure 6: Continued.

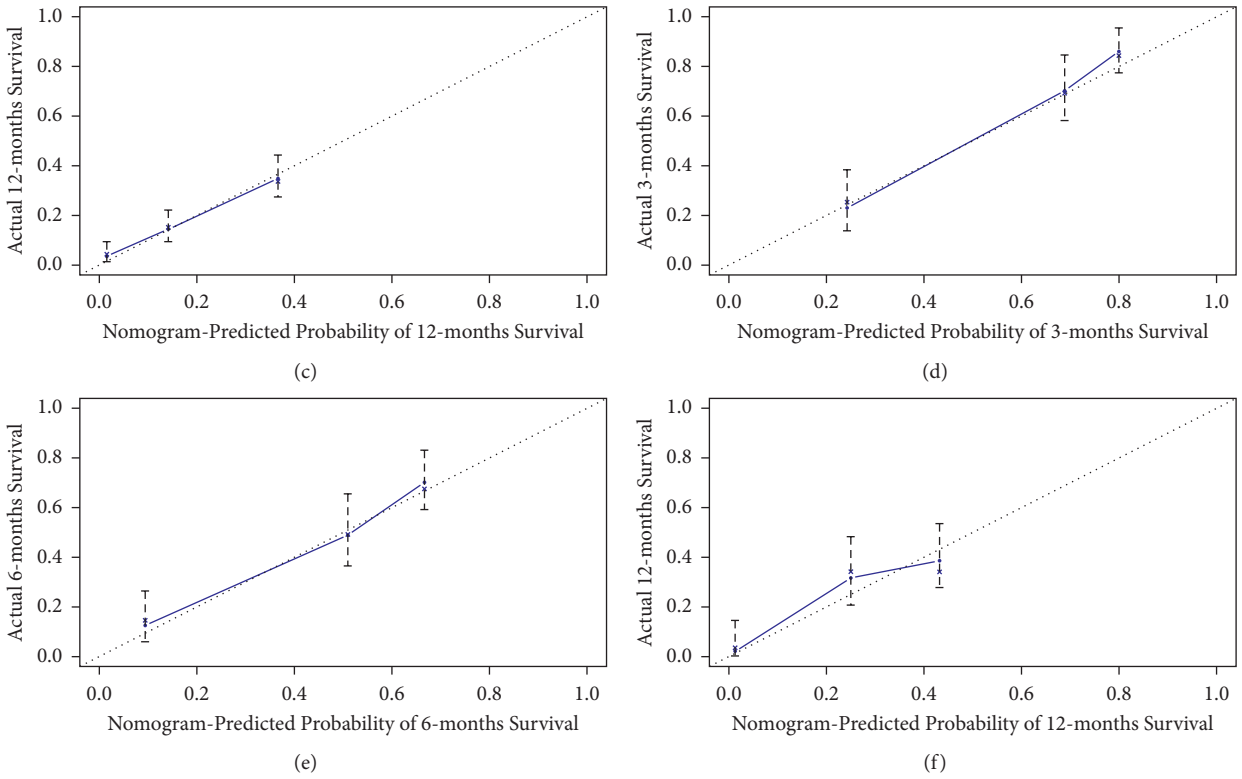

Figure 6: Calibration curves of cancer-specific survival (CSS). (a–c) Calibration curves corresponding to 3, 6, and 12 months in the training cohort, respectively; (d–f) calibration curves corresponding to 3, 6, and 12 months in the verification cohort, respectively. CSS, cancer-specific survival.

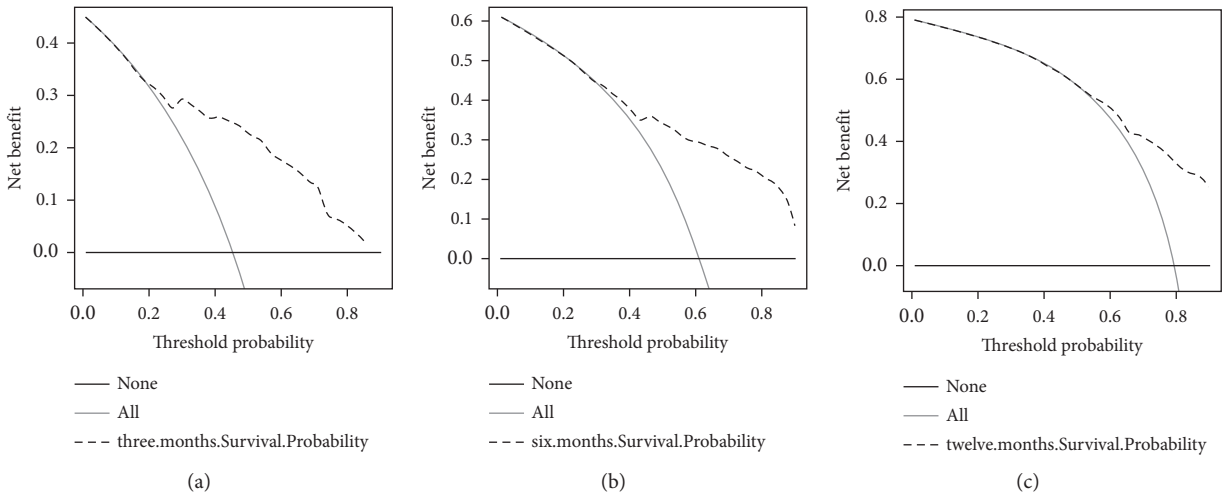

Figure 7: Continued.

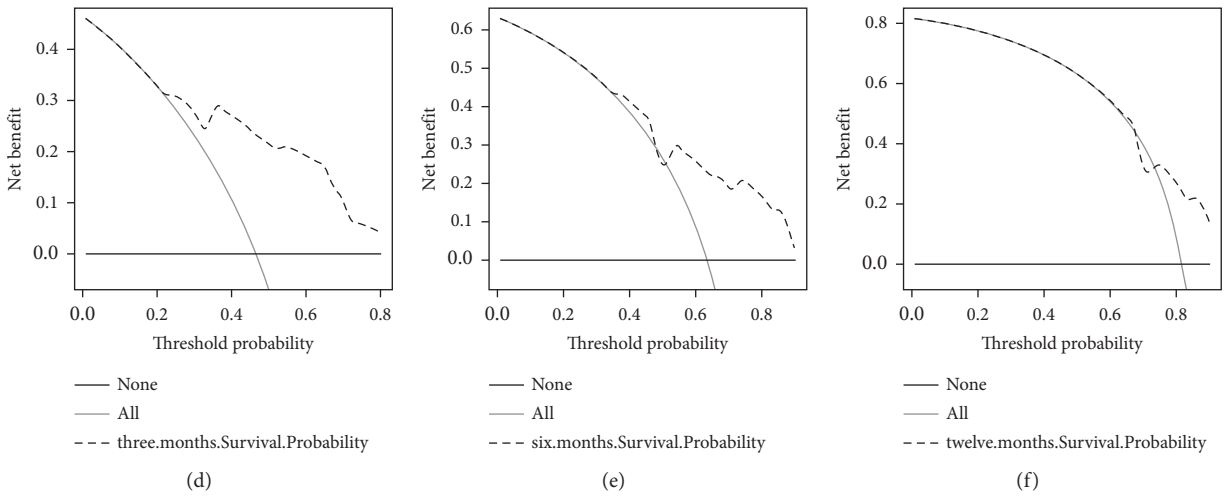

Figure 7: Decision curve analysis (DCA) curves of overall survival (OS). (a–c) DCA corresponding to 3, 6, and 12 months in the training cohort, respectively; (d–f) DCA corresponding to 3, 6, and 12 months in the verification cohort, respectively. DCA, decision curve analysis; OS, overall survival.

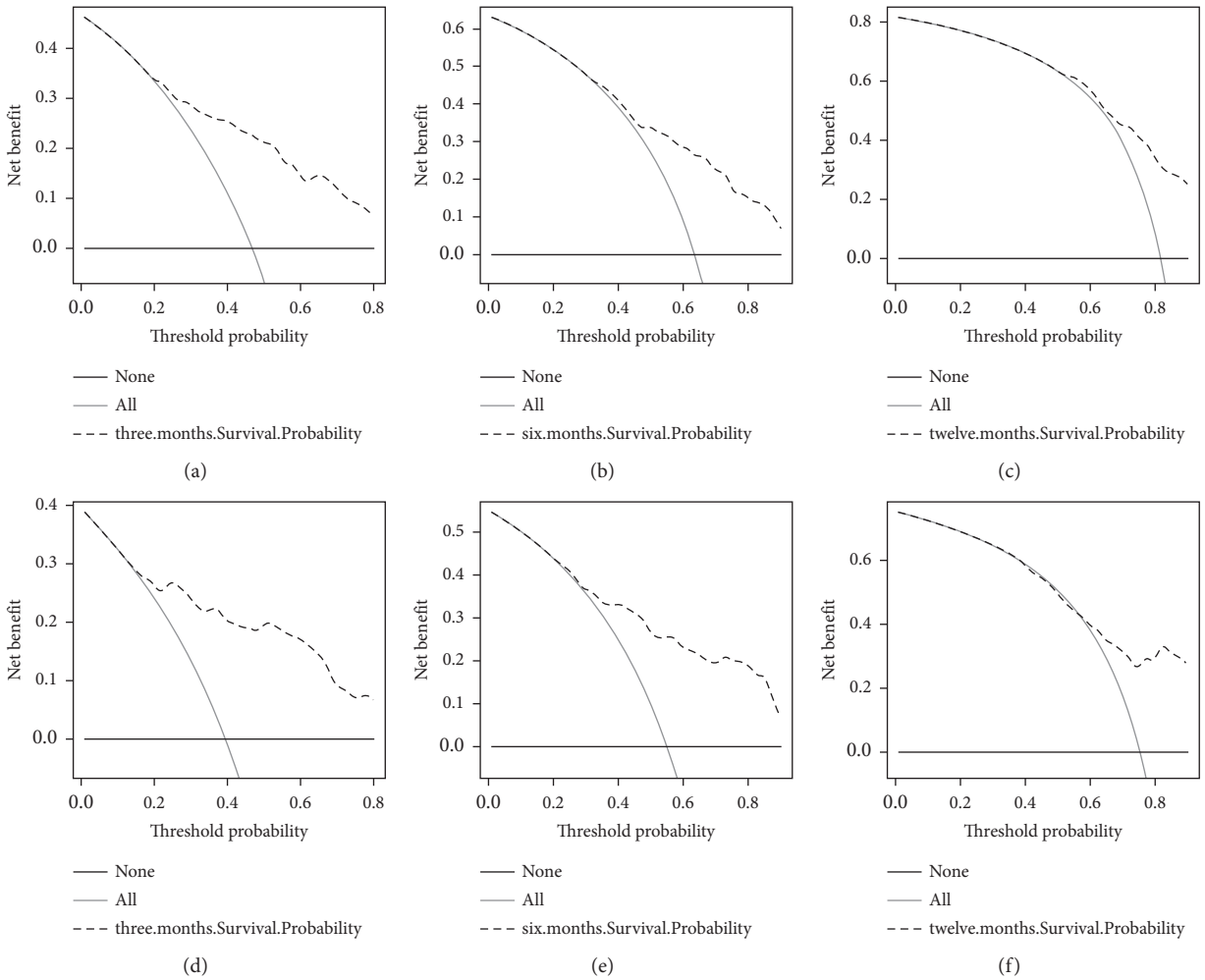

Figure 8: Decision curve analysis (DCA) curves of cancer-specific survival (CSS). (a–c) DCA corresponding to 3, 6, and 12 months in the training cohort, respectively; (d–f) DCA corresponding to 3, 6, and 12 months in the verification cohort, respectively. DCA, decision curve analysis; CSS, cancer-specific survival.

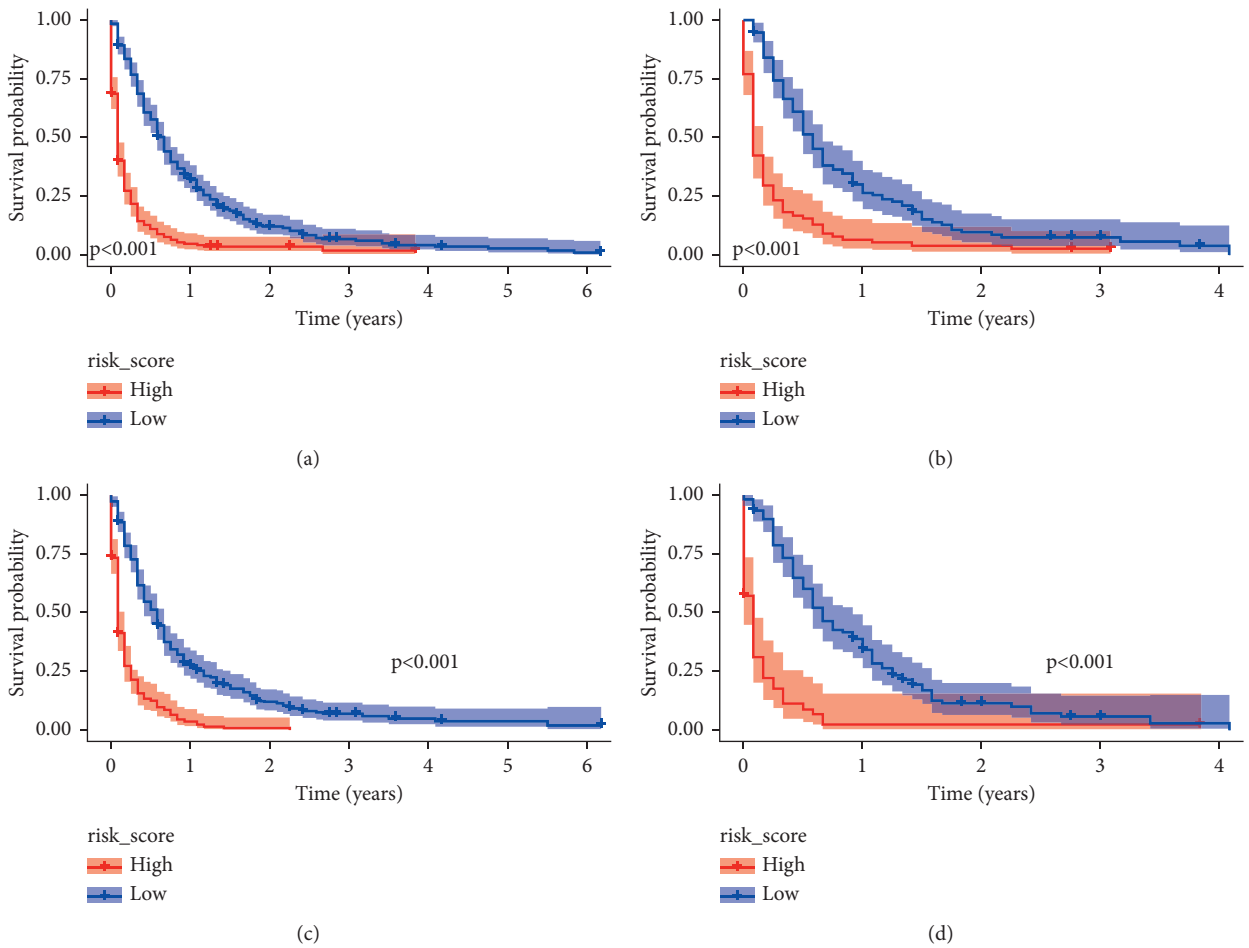

Figure 9: Kaplan-Meier (K-M) survival curves. (a) K-M survival curves in training cohort for OS of GCLM; (b) K-M survival curves in verification queue for OS of GCLM; (c) K-M survival curves in training cohort for CSS of GCLM; (d) K-M survival curves in verification cohort for CSS of GCLM. K-M, Kaplan-Meier; OS, overall survival; CSS, cancer-specific survival.

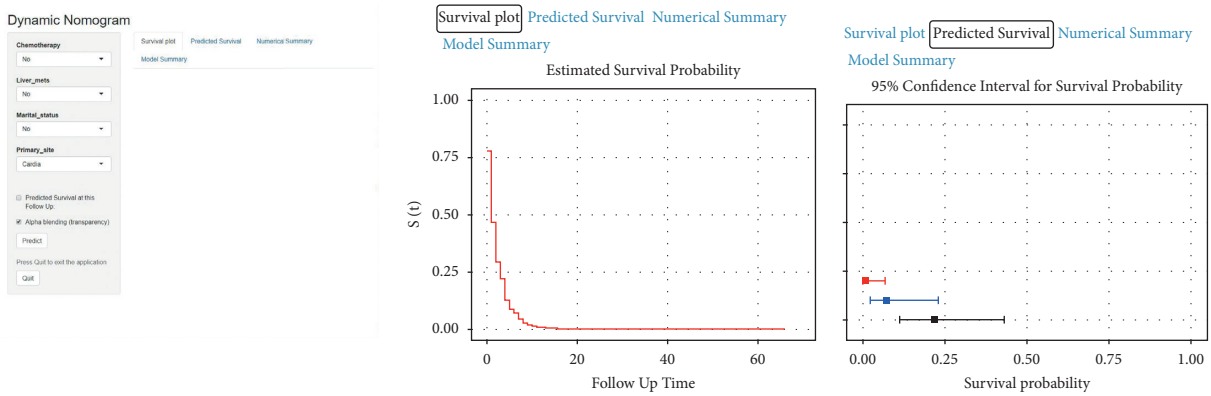

Figure 10: Continued.

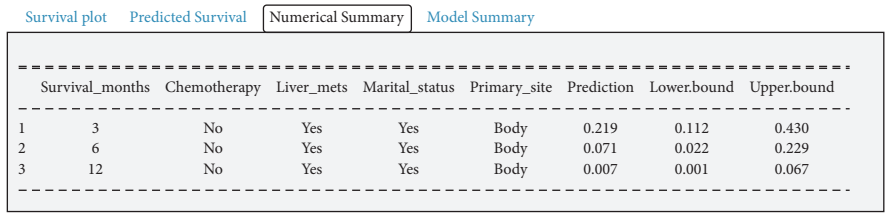

	Survival_months	Chemotherapy	Liver_mets	Marital_status	Primary_site	Prediction	Lower.bound	Upper.bound
1	3	No	Yes	Yes	Body	0.219	0.112	0.430
2	6	No	Yes	Yes	Body	0.071	0.022	0.229
3	12	No	Yes	Yes	Body	0.007	0.001	0.067

(d)

Figure 10: Web-based nomogram. (a) Operation page of web-based nomogram; (b) survival curve of the corresponding patient; (c) survival rates and 95% confidence intervals at 3 months (black line), 6 months (blue line), and 12 months (red line); (d) the prediction accuracy of the corresponding patient.

We found that liver metastasis is an independent risk factor for OS and CSS in patients with GCLM. There are two possible reasons for this. First, the liver contains a rich blood supply, tumor metastasis is rapid, patients are already advanced when symptoms appear, and most of them miss the time of surgery. Second, for patients with GCLM and hepatocellular carcinoma (HCC), the prognosis is worse because the patients are lethargic and weak, and their immunity is reduced, typically when they develop complications associated with advanced HCC (such as jaundice, ascites, peritonitis, and hepatic encephalopathy). Chemotherapy was found to be an independent protective factor for OS and CSS. This result confirmed the importance and necessity of chemotherapy in patients with GCLM. The National Comprehensive Cancer Network guidelines clearly state that chemotherapy is recommended for the treatment of patients with unresectable or metastatic GC [33]. A study reported median OS times of 8.6 and 7.9 months for patients with advanced GC treated with cisplatin combined with S-1 (CS) versus cisplatin combined with 5-FU (CF) regimens, respectively ($P = 0.02$) [34]. Standardized chemotherapy not only relieves the patients' clinical symptoms but also prolongs the survival time. Hence, it is worthwhile to focus on the possibility of liver metastasis in patients with GCLM. To obtain an excellent prognosis, doctors could prefer chemotherapy for the clinical treatment of patients with GCLM. In addition, we incorporated marital status into our study. The results of this study showed that married patients with GCLM had better clinical prognosis than those who were unmarried. It has been shown that marriage plays a humanistic role during the treatment of oncology patients and that care plays a crucial role in influencing tumor progression [35].

However, there are some limitations to our study. First, although we have set strictly incorporated exclusion standards, the deletion of patients is missing and may cause statistical bias. Second, there is no detailed treatment information in the SEER database, such as specific chemotherapy modalities and surgical procedures. Third, the SEER database has limited coverage, and some important factors such as smoking, alcohol consumption, family history of tumor, and other factors that may affect patient prognosis were not assessed.

5. Conclusions

In conclusion, this study revealed that grade, liver metastasis, and chemotherapy were independent prognostic factors for OS, where the risk factors were grade and liver metastasis, and chemotherapy was a protective factor. Liver metastasis, primary site, chemotherapy, and marital status were independent prognostic factors for CSS, where liver metastasis and primary site were risk factors, and chemotherapy and marital status were protective factors. We created two easy-to-use visual web-based nomograms with several clinical and pathological factors to quantitatively predict OS and CSS in patients with GCLM. Moreover, our model may help physicians develop individualized postoperative follow-up strategies.

Abbreviations

AUC: Area under the curve
CSS: Cancer-specific survival
DCA: Decision curve analysis
GC: Gastric cancer
GCLM: Gastric cancer and lung metastasis
LM: Lung metastasis
OS: Overall survival
ROC: Receiver operating characteristic
SEER: Surveillance, Epidemiology, and End Results.

Data Availability

The dataset from the SEER database which was generated and/or analyzed during the current study is available in the SEER dataset repository (https://seer.cancer.gov/).

Ethical Approval

The study's approval was waived by the local ethics committee, as the SEER data were publicly available and deidentified.

Conflicts of Interest

The authors declare that there are no conflicts of interest with respect to the research, authorship, and/or publication of this article.

Authors' Contributions

Honghong Zheng and Zhehong Li contributed equally to this work. HH Z and ZH L conceived and designed the study. Honghong Zheng and Jianjun Li performed the

literature search. Zhehong Li and Shuai Zheng generated the figures and tables. Jianjun Li and Shuai Zheng analyzed the data. Honghong Zheng and Zhehong Li wrote the manuscript, and Enhong Zhao critically reviewed the manuscript. Enhong Zhao supervised the study. All experiments and methods met the standards of relevant guidelines and regulations. All authors have read and approved the manuscript.

Acknowledgments

This study is funded by the 2020 Hebei Provincial Finance Department Grant for Outstanding Talents in Clinical Medicine (no. 2020397).

References

[1] F. Bray, J. Ferlay, I. Soerjomataram, R. L. Siegel, L. A. Torre, and A. Jemal, "Global cancer statistics 2018: GLOBOCAN estimates of incidence and mortality worldwide for 36 cancers in 185 countries," *CA: A Cancer Journal for Clinicians*, vol. 68, no. 6, pp. 394–424, 2018.

[2] Y.-J. Bang, Y.-W. Kim, H.-K. Yang et al., "Adjuvant capecitabine and oxaliplatin for gastric cancer after D2 gastrectomy (CLASSIC): a phase 3 open-label, randomised controlled trial," *The Lancet*, vol. 379, no. 9813, pp. 315–321, 2012.

[3] M. Sasako, S. Sakuramoto, H. Katai et al., "Five-year outcomes of a randomized phase III trial comparing adjuvant chemotherapy with S-1 versus surgery alone in stage II or III gastric cancer," *Journal of Clinical Oncology*, vol. 29, no. 33, pp. 4387–4393, 2011.

[4] K.-Y. Song, S.-M. Park, S.-N. Kim, and C.-H. Park, "The role of surgery in the treatment of recurrent gastric cancer," *The American Journal of Surgery*, vol. 196, no. 1, pp. 19–22, 2008.

[5] T. Cancer and T. Kajitani, "The general rules for the gastric cancer study in surgery and pathology part I," *Japanese Journal of Surgery*, vol. 11, no. 2, pp. 127–139, 1981.

[6] W.-M. Kang, Q.-B. Meng, J.-C. Yu, Z.-Q. Ma, and Z.-T. Li, "Factors associated with early recurrence after curative surgery for gastric cancer," *World Journal of Gastroenterology*, vol. 21, no. 19, pp. 5934–5940, 2015.

[7] G. Spolverato, A. Ejaz, Y. Kim et al., "Rates and patterns of recurrence after curative intent resection for gastric cancer: a United States multi-institutional analysis," *Journal of the American College of Surgeons*, vol. 219, no. 4, pp. 664–675, 2014.

[8] Y. Nakanishi, M. Ohara, H. Domen, T. Shichinohe, S. Hirano, and M. Ishizaka, "Differences in risk factors between patterns of recurrence in patients after curative resection for advanced gastric carcinoma," *World Journal of Surgical Oncology*, vol. 11, no. 1, pp. 98–8, 2013.

[9] J. Deng, H. Liang, D. Wang, D. Sun, Y. Pan, and Y. Liu, "Investigation of the recurrence patterns of gastric cancer following a curative resection," *Surgery Today*, vol. 41, no. 2, pp. 210–215, 2011.

[10] J. Y. Choi, T. K. Ha, and S. J. Kwon, "Clinicopathologic characteristics of gastric cancer patients according to the timing of the recurrence after curative surgery," *Journal of Gastric Cancer*, vol. 11, no. 1, pp. 46–54, 2011.

[11] R. C. Ye, S. H. Dong, S. H. Kong et al., "The value of palliative gastrectomy in gastric cancer with distant metastasis," *Annals of Surgical Oncology*, vol. 19, no. 4, pp. 1231–1239, 2012.

[12] T. Zheng, J. Jin, Y. Zhang, and L. Zhou, "Efficacy and safety of paclitaxel with or without targeted therapy as second-line therapy in advanced gastric cancer: a meta-analysis," *Medicine (Baltimore)*, vol. 99, no. 25, Article ID e20734, 2020.

[13] Y. W. Choi, M. S. Ahn, G. S. Jeong et al., "The role of surgical resection before palliative chemotherapy in advanced gastric cancer," *Scientific Reports*, vol. 9, no. 1, Article ID 4136, 2019.

[14] Y.-K. Kang, N. Boku, T. Satoh et al., "Nivolumab in patients with advanced gastric or gastro-oesophageal junction cancer refractory to, or intolerant of, at least two previous chemotherapy regimens (ONO-4538-12, ATTRACTION-2): a randomised, double-blind, placebo-controlled, phase 3 trial," *The Lancet*, vol. 390, no. 10111, pp. 2461–2471, 2017.

[15] Y. Kobayashi, T. Fukui, S. Ito et al., "Pulmonary metastasectomy for gastric cancer: a 13-year single-institution experience," *Surgery Today*, vol. 43, no. 12, pp. 1382–1389, 2013.

[16] J. H. Kong, J. Lee, C.-A. Yi et al., "Lung metastases in metastatic gastric cancer: pattern of lung metastases and clinical outcome," *Gastric Cancer*, vol. 15, no. 3, pp. 292–298, 2012.

[17] M. A. Tursun and Z. W. Bin, "Analysis of prognostic factors affecting 118 cases of patients with lung metastases from gastric cancer," *Chinese Journal of Cancer Control*, vol. 26, no. 15, pp. 1107–1110, 2019.

[18] M. Chen, S. Li, W. Topatana et al., "Development and validation of a nomogram for predicting survival in gallbladder cancer patients with recurrence after surgery," *Frontiers in Oncology*, vol. 10, Article ID 537789, 2021.

[19] L.-J. Sun, A. Guan, W.-Y. Xu et al., "γ-glutamyl transferase-to-platelet ratio based nomogram predicting overall survival of gallbladder carcinoma," *World Journal of Gastrointestinal Oncology*, vol. 12, no. 9, pp. 1014–1030, 2020.

[20] J. Li, H. Yue, H. Yu, X. Lu, and X. Xue, "Development and validation of SIRT3-related nomogram predictive of overall survival in patients with serous ovarian cancer," *Journal of Ovarian Research*, vol. 12, no. 1, p. 47, 2019.

[21] W. Song, C.-g. Lv, D.-l. Miao et al., "Development and validation of a nomogram for predicting survival in patients with gastrointestinal stromal tumours," *European Journal of Surgical Oncology*, vol. 44, no. 10, pp. 1657–1665, 2018.

[22] T. Yang, Y. Wu, Y. Zuo, S. Fu, Z. Xu, and N. Yu, "Development and validation of prognostic nomograms and a web-based survival rate calculator for sarcomatoid renal cell carcinoma in pre- and post-treatment patients," *Translational Andrology and Urology*, vol. 10, no. 2, pp. 754–764, 2021.

[23] Y. W. Chung, D. S. Han, Y. K. Park et al., "Association of obesity, serum glucose and lipids with the risk of advanced colorectal adenoma and cancer: a case-control study in korea," *Digestive and Liver Disease*, vol. 38, no. 9, pp. 668–672, 2006.

[24] Y. Zhang, Y. Lin, J. Duan, K. Xu, M. Mao, and X. Wang, "A population-based analysis of distant metastasis in stage IV gastric cancer," *Medical Science Monitor: International Medical Journal of Experimental and Clinical Research*, vol. 26, Article ID e923867, 2020.

[25] N. Lui, P. Ronnie Tung Ping, and P. Roberta, "Biomarkers for predicting future metastasis of human gastrointestinal tumors," *Cellular and Molecular Life Sciences: CMLS*, vol. 70, no. 19, 2013.

[26] W. Zhang, G. Zhangyuan, J. Wang et al., "Effect of lymph nodes count in node-positive gastric cancer," *Journal of Cancer*, vol. 10, no. 23, pp. 5646–5653, 2019.

[27] Y. Waki, T. Irino, R. Makuuchi et al., "Impact of preoperative skeletal muscle quality measurement on long-term survival

after curative gastrectomy for locally advanced gastric cancer," *World Journal of Surgery*, vol. 43, no. 12, pp. 3083–3093, 2019.

[28] C.-H. HSIEH, C.-K. WEI, W.-Y. YIN et al., "Vascular invasion affects survival in early hepatocellular carcinoma," *Molecular and clinical oncology*, vol. 3, no. 1, pp. 252–256, 2015.

[29] S.-W. Suh, K.-W. Lee, J.-M. Lee et al., "Prediction of aggressiveness in early-stage hepatocellular carcinoma for selection of surgical resection," *Journal of Hepatology*, vol. 60, no. 6, pp. 1219–1224, 2014.

[30] Y. Tomimaru, H. Eguchi, S. Marubashi et al., "Equivalent outcomes after anatomical and non-anatomical resection of small hepatocellular carcinoma in patients with preserved liver function," *Digestive Diseases and Sciences*, vol. 57, no. 7, pp. 1942–1948, 2012.

[31] C. Hu, J. Yang, Z. Huang et al., "Diagnostic and prognostic nomograms for bone metastasis in hepatocellular carcinoma," *BMC Cancer*, vol. 20, no. 1, p. 494, 2020.

[32] C. Neuzillet, A. Casadei Gardini, B. Brieau et al., "Prediction of survival with second-line therapy in biliary tract cancer: actualisation of the AGEO CT2BIL cohort and European multicentre validations," *European Journal of Cancer*, vol. 111, pp. 94–106, 2019.

[33] J. A. Ajani, T. A. D'Amico, K. Almhanna et al., "Gastric cancer, version 3.2016, NCCN clinical practice guidelines in oncology," *Journal of the National Comprehensive Cancer Network: Journal of the National Comprehensive Cancer Network*, vol. 14, no. 10, pp. 1286–1312, 2016.

[34] J. A. Ajani, W. Rodriguez, G. Bodoky et al., "Multicenter phase III comparison of cisplatin/S-1 with cisplatin/infusional fluorouracil in advanced gastric or gastroesophageal adenocarcinoma study: the FLAGS trial," *Journal of Clinical Oncology*, vol. 28, no. 9, pp. 1547–1553, 2010.

[35] J. J. Jin, W. Wang, F. X. Dai et al., "Marital status and survival in patients with gastric cancer," *Cancer Medicine*, vol. 5, no. 8, pp. 1821–1829, 2016.

Hindawi
Journal of Oncology
Volume 2021, Article ID 9868585, 7 pages
https://doi.org/10.1155/2021/9868585

Research Article

Clinical Research of Combined Application of DCEUS and Dynamic Contrast-Enhanced MSCT in Preoperative cT Staging of Gastric Cancer

Junling Wang,[1] **Xia Li**,[1] **Zhijie Zhang**,[1] **Chao Jing**,[1] **and Jie Li**[2]

[1]*Department of Ultrasound, Dezhou People's Hospital, Dezhou, Shandong 253014, China*
[2]*Department of Ultrasound, Qilu Hospital of Shandong University, Jinan, Shandong 250012, China*

Correspondence should be addressed to Zhijie Zhang; zhangzj198108@126.com

Junling Wang and Xia Li contributed equally to this work.

Received 18 June 2021; Accepted 25 September 2021; Published 19 October 2021

Academic Editor: Alamgeer Yuchi

Purpose. To investigate the clinical value of double contrast-enhanced ultrasound (DCEUS) combined with dynamic contrast-enhanced multislice CT (MSCT) in preoperative T staging of gastric cancer (GC). *Methods*. 206 patients with GC confirmed by preoperative gastroscopy from February 2019 to February 2021 were collected, all patients were examined by DCEUS and dynamic contrast-enhanced MSCT before operation, and the invasion depth (T staging) of GC was evaluated. The diagnosis results of DCEUS, dynamic contrast-enhanced MSCT, and combined diagnosis of DCEUS and MSCT methods (D&M method) were compared with the pathological staging results (gold standard). *Results*. The correct diagnosis rate of MSCT was 27.27% in T1 staging, 55.56% in T2 staging, 42.11% in T3 staging, 59.29% in T4 staging, and 55.34% in summation. The correct diagnosis rate of DCEUS was 90.91% in T1 staging, 88.89% in T2 staging, 78.95% in T3 staging, 82.86% in T4 staging, and 83.98% in summation. The correct diagnosis rate of the D&M method was 100.00% in T1 staging, 94.44% in T2 staging, 89.47% in T3 staging, 93.57% in T4 staging, and 93.69% in summation. The D&M method had higher correct diagnosis rate than MSCT or DCEUS alone, the correct diagnosis rate of the D&M method in T1, T2, T3, and T4 staging was significantly higher than that of MSCT ($P < 0.05$). The correct diagnosis rate of the D&M method in T1, T3, and T4 was significantly higher than that of DCEUS ($P < 0.05$). The Youden index of preoperative T1, T2, T3, and T4 staging of GC by the D&M method was 99.49%, 94.44%, 84.13%, and 90.54%, respectively, and the Kappa values of these were 0.954, 0.966, 0.707, and 0.881, respectively. *Conclusions*. Dynamic contrast-enhanced MSCT combined with DCEUS in the diagnosis of preoperative cT staging of GC has more validity, reliability, and revenue than the using of MSCT or DCEUS alone, which is an image evaluation method worthy of clinical promotion.

1. Introduction

Gastric cancer (GC) is the most common malignant tumor in the world, the incidence rate of malignant tumors is fifth, and the mortality rate is third [1]. At present, although the early diagnosis rate of GC in China is increasing year by year, more than 80% of patients are still in the progressive stage at the first visit. Among all patients with GC who received surgical treatment, the 5-year survival rate of patients with advanced GC was only about 30%, which was significantly lower than that of patients with early GC. Individualized treatment is advocated in patients with early or advanced GC. Accurate evaluation of the clinical staging of GC before formulating the treatment plan is of great significance for the selection of treatment plan and the preliminary evaluation of patients' prognosis. The 8th edition of TNM staging system for GC developed by UICC/AJCC includes pathological staging (pTNM staging), clinical staging (cTNM staging), and pathological staging after neoadjuvant therapy (ypTNM staging) [2]. This system can provide diagnostic basis and theoretical guidance for accurate staging of GC and is of great significance for reasonable selection of treatment

options and prognosis evaluation [3]. The common methods for preoperative diagnosis of GC include fiberoptic gastroscopy and histological examination. These methods can make a preliminary diagnosis of GC before operation, but cannot get the tumor staging [4]. There are a lot of clinical research methods for preoperative clinical T staging (cT) of GC, including endoscopic ultrasonography [5], dynamic contrast-enhanced multislice CT (MSCT) [6], magnetic resonance imaging (MRI) [7], and double contrast-enhanced ultrasound (DCEUS) [8]. In this study, DCEUS and dynamic contrast-enhanced MSCT were used for preoperative examination of GC patients and compared with pathological results to explore the application value of the combined application of the two methods in preoperative cT staging of GC.

2. Patients and Methods

2.1. Clinical Data. The clinical data of 206 patients with GC who were confirmed by gastroscopy before operation, performed abdominal dynamic contrast-enhanced MSCT and DCEUS, underwent radical gastrectomy, and then got the results of pT staging. There were 111 males and 95 females. The age of them ranged from 23 to 81 years old, with an average age of 59.7 ± 11.3 years. This study was approved by the ethics committee of Qilu Hospital of Shandong University. The included patients and their families signed informed consent in advance.

2.2. Inclusion Criteria. (1) Preoperative gastroscopy confirmed GC by pathology, excluding distant metastasis of other organs. (2) No other treatment was given before operation. (3) The patients agreed and tolerated radical gastrectomy. (4) MSCT and DCEUS were performed within one week before operation. (5) There was no massive hemorrhage, gastric perforation, or obstruction within 2 weeks before MSCT and DCEUS. (6) The interval between MSCT/DCEUS and the previous biopsy should be more than 3 days. (7) The clinical and pathological data were complete.

2.3. Exclusion Criteria. (1) Those who are allergic or contraindicated to anisodamine and/or iodine contrast media and those who are allergic to oral or intravenous contrast media. (2) Whose judgment of cT staging was affected by image artifacts. (3) Poor filling of gastric cavity affects the judgment of cT staging. (4) Those who had hemorrhage, perforation, obstruction, gastric retention, and so on. (5) Patients who received endoscopic resection before operation.

2.4. Imaging Equipment and Methods

2.4.1. MSCT. Philips Brilliance 128 row 256 slice spiral CT was used, plain scan and enhanced scan were performed, and the contrast agent was lohexol. Patients should fast for more than 8 hours before examination, drink water 500 ml 30–60 minutes before examination, then intramuscular injection of raceanisodamine hydrochloride injection (produced by Hangzhou Minsheng Pharmaceutical Co., Ltd., 1 ml: 5 mg, H33021707) 10–20 mg, and then drink water 500 ml 15 minutes before examination. The scanning range was from diaphragmatic apex to pubic symphysis. Scanning parameters: 120 kV, 200–250 mAs, pitch 0.938, and collimation 0.625 mm × 128. The contrast agent used in contrast-enhanced scanning was lohexol (iopromide injection, produced by GE Pharmaceutical (Shanghai) Co., Ltd., 100 ml: 30 g (I), H20000595) or ultravist (iopromide injection, produced by Bayer Medical and Health Care Co., Ltd. Guangzhou Branch, 100 ml: 37 g (I), H10970417), with a dose of 1.5 ml/kg body weight and injected through the median cubital vein at a flow rate of 3 ml/s. Low dose test method was used: 16 ml of test dose was injected first, and then the drug was injected in a bolus. The scan was performed in the pulse phase (peak enhancement time was determined by small dose test), portal vein phase (20 s after the arterial phase), and equilibrium phase (60 s after the portal vein phase). The MSCT results and preoperative cT staging evaluation of all patients in this study were performed by two senior doctors in the radiology department of Qilu Hospital of Shandong University.

2.4.2. DCEUS. Acuson Sequoia 512 color ultrasonic diagnostic instrument of Siemens was used. Tianxia brand instant gastrointestinal ultrasound aid (Huzhou East Asia medical supplies Co., Ltd., 50 g/bag, 3230223) was used as an oral contrast agent. Sonovue (sulphur hexafluoride microbubbles for injection, produced by Bracco (Italy) Co., Ltd., 59 mg SF_6, J20080052) was used as an intravenous contrast agent. Light diet 2-3 days, fasting more than 8 hours, and intramuscular injection of 0.5 mg atropine half an hour before examination, in order to reduce the impact of gastric peristalsis on ultrasound examination. After the oral administration of the contrast agent, the gastric fundus and body were scanned dynamically in real time to observe the size, shape, and scope of lesions. During the examination, the patients were asked to change their position to cooperate with the examination. If necessary, the oral contrast agent could be added to obtain clear images. Intravenous contrast agent was mixed with 5 ml normal saline to form suspension, and 2.4 ml was injected through superficial vein of elbow arm quickly. Then, observation and dynamic recording were started to store the enhancement mode, peak value and duration of the lesion and surrounding normal gastric tissue, gastric wall, and perigastric lymph nodes. The low mechanical index of the linear array probe was 0.07–0.10. The offline analysis software was used to analyze the images and generate the time intensity curve. DCEUS examination and preoperative staging of GC in all patients were performed by two senior doctors in the ultrasound department of Qilu Hospital of Shandong University.

2.5. DCEUS Combined with MSCT Image Analysis. The images of the two methods were analyzed by three senior abdominal radiologists (at least 3 years working experience in imaging department) using double-blind method. According to the principle of majority, the cT staging results were obtained.

Table 1: Pathological T staging criteria.

T staging	Infiltration depth
T0	There was no evidence of primary tumor
T1	The tumor invaded the mucosa or submucosa
T2	The tumor infiltrated into the muscularis propria
T3	The tumor penetrated the tissue under serosa, but did not invade the visceral membrane and adjacent structures
T4	The tumor invaded visceral peritoneum or adjacent structures

Table 2: Comparison of pathological T staging and MSCT cT staging.

		cT staging results of MSCT					Summation	Correct diagnosis rate (%)
		T0	T1	T2	T3	T4		
pT staging	T1	5	3	3	0	0	11	27.27
	T2	4	1	20	11	0	36	55.56
	T3	0	0	2	8	9	19	42.11
	T4	0	0	0	57	83	140	59.29
Summation		9	4	25	76	92	206	55.34

Table 3: Comparison of pathological T staging and DCEUS cT staging.

		cT staging results of DCEUS				Summation	Correct diagnosis rate (%)
		T1	T2	T3	T4		
pT staging	T1	10	1	0	0	11	90.91
	T2	3	32	1	0	36	88.89
	T3	0	0	15	4	19	78.95
	T4	0	0	24	116	140	82.86
Summation		13	33	40	120	206	83.98

2.6. Criteria for T Staging GC. According to the theory of Kim et al. [5] and referring to the 8th edition of the TNM staging system of GC [3], the criteria of T staging of GC are summarized in Table 1.

2.7. Statistical Analysis. SPSS 23.0 software (IBM Corp.) was used for the statistical analysis of the data. The differences were compared with each other χ^2 test, $P < 0.05$ was considered to indicate a statistically significant difference. Kappa consistency test was used to analyze the consistency between preoperative cT staging and postoperative PT staging, $0.75 < K \leq 1$ is good consistency, $0.4 < K \leq 0.75$ is general consistency, and $0 < K \leq 0.4$ is poor consistency. The count data is expressed as rate (%), and the comparison between two groups was made by using the four grid table χ^2 inspection. When $n \geq 40$ and $t \geq 5$, Pearson χ^2 test was used for inspection. When $n \geq 40$ and $1 \leq T < 5$, continuous correction was used for inspection.

3. Results

3.1. Results of MSCT Diagnosis in Preoperative T Staging of GC. In all patients, postoperative pathology was regarded as the "gold standard," and pT staging of GC included 11 cases of T1, 36 cases of T2, 19 cases of T3, and 140 cases of T4. According to the gold standard, cT staging results of MSCT diagnosis were: 3 cases of T1, 20 cases of T2, 8 cases of T3, and 83 cases of T4. The correct diagnosis rate was 27.27% in T1, 55.56% in T2, 42.11% in T3, 59.29% in T4, and 55.34% in summation. The specific results are shown in Table 2.

3.2. Results of DCEUS Diagnosis in Preoperative T Staging of GC. According to the gold standard, cT staging results of DCEUS diagnosis were: 10 cases of T1, 32 cases of T2, 15 cases of T3, and 116 cases of T4. The correct diagnosis rate was 90.91% in T1, 88.89% in T2, 78.95% in T3, 82.86% in T4, and 83.98% in summation. The specific results are shown in Table 3, DCEUS and MSCT images of typical cases are shown in Figure 1.

3.3. Results of D&M Method Diagnosis in Preoperative T Staging of GC. According to the gold standard, cT staging results of the D&M method diagnosis were: 11 cases of T1, 34 cases of T2, 17 cases of T3, and 131 cases of T4. The correct diagnosis rate was 100.00% in T1, 94.44% in T2, 89.47% in T3, 93.57% in T4, and 93.69% in summation. The specific results are shown in Table 4.

3.4. Results of Comparison of Correct Diagnosis Rate of cT Staging. The correct diagnosis rate of MSCT, DCEUS, and D&M method diagnosis of cT staging is shown in Figure 2. The DCEUS method had higher correct diagnosis rate than MSCT method in T1 to T4 staging of GC ($P < 0.05$). The D&M method had higher correct diagnosis rate than MSCT or DCEUS alone, the correct diagnosis rate of the D&M method in T1, T2, T3, and T4 staging was significantly

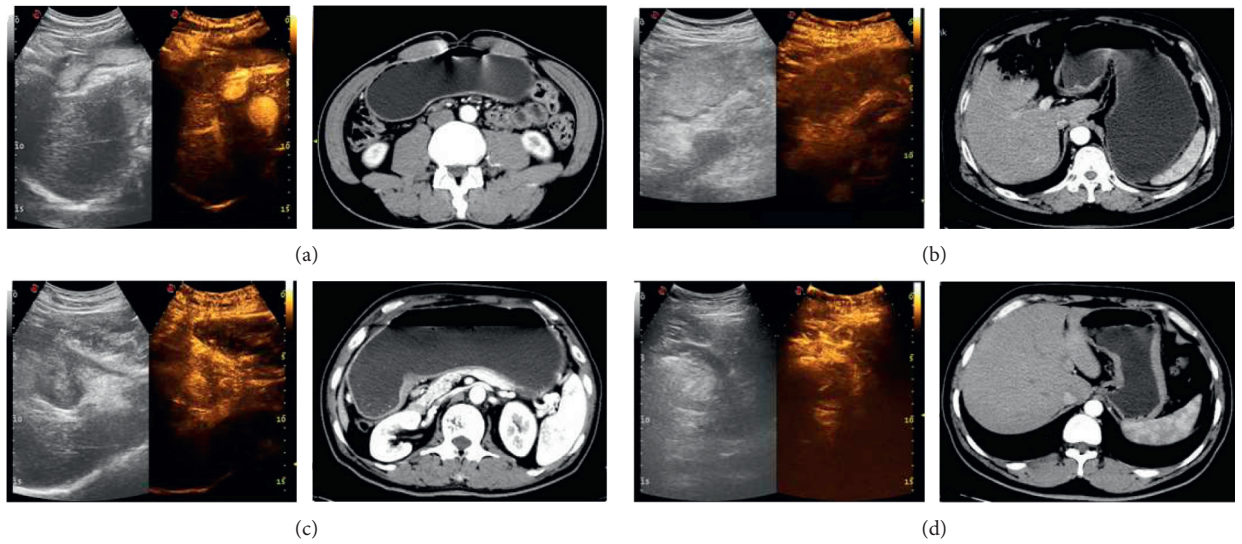

Figure 1: DCEUS image of typical cases. Note: in (a), (b), (c), and (d), the left images were oral gastrointestinal contrast agent ultrasound images, the middle images were double-contrast ultrasound images, and the right images were enhanced MSCT images. (a) An ultrasound image of a 59-year-old male patient; he was finally diagnosed as a moderately differentiated adenocarcinoma of the antrum (pT1 staging). DCEUS showed focal thickening of the gastric wall, with focal positive development of the middle layer in the inner layer of the gastric wall and clear boundary with the outer layer, and it was judged that the tumor infiltrated into the muscularis mucosa. MSCT showed focal gastric wall thickening, and the lesion did not exceed the low-density zone of submucosa (preoperative diagnosis cT1 staging). (b) An ultrasound image of a 60-year-old female patient. She was finally diagnosed as poorly differentiated adenocarcinoma with ulcerative gastric antrum (pT2 staging). DCEUS showed that the whole gastric wall of the lesion was thickened and positively developed, and the outer edge of the lesion was intact and smooth, and it was judged that the tumor infiltrated into the muscle layer; MSCT showed that the gastric wall was thickened, the lesion broke through the slightly strengthened muscle layer of the submucosa, the outer surface of the stomach around the lesion was clear and smooth, and the fat surface around the stomach was clear (preoperative diagnosis of cT2 staging). (c) An ultrasound image of a 64-year-old female patient. She was finally diagnosed as a poorly differentiated adenocarcinoma with an ulcerative type of lesser curvature of stomach (pT3 staging). DCEUS showed that the whole gastric wall of the lesion was obviously thickened and showed positive development, and the outer layer of the tumor was vague and serrated, breaking through the adventitia, but not invading the adjacent structures, and it was judged that the tumor infiltrated into the subserosal layer; MSCT showed gastric wall thickening, irregular fat infiltration around the stomach, and uneven serosal surface (preoperative diagnosis of cT3 staging). (d) An ultrasound image of a 58-year-old male patient. He was finally diagnosed as poorly differentiated adenocarcinoma of the lesser curvature ulcerative type (pT4 staging). DCEUS showed that the whole layer of gastric wall of the lesion was thickened and showed positive development, the tumor invaded the outer serous, and the tumor broke through serosa; MSCT showed that the tumor broke through the perigastric adipose tissue and serosa, accompanied by the expansion and invasion of adjacent organs or structures (preoperative diagnosis of cT4 staging).

Table 4: Comparison of pathological T staging and D&M method cT staging.

		cT staging results of combined diagnosis				Summation	Correct diagnosis rate (%)
		T1	T2	T3	T4		
pT staging	T1	11	0	0	0	11	100.00
	T2	1	34	1	0	36	94.44
	T3	0	0	17	2	19	89.47
	T4	0	0	9	131	140	93.57
Summation		12	34	27	133	206	93.69

higher than that of MSCT ($P < 0.05$). The correct diagnosis rate of the D&M method in T1, T3, and T4 was significantly higher than that of DCEUS ($P < 0.05$).

3.5. Results of Validity, Reliability, and Revenue. The results of validity, reliability, and revenue are shown in Table 5. The Youden index of preoperative T1, T2, T3, and T4 staging was 26.76%, 52.61%, 5.74%, and 45.65%, respectively, by the MSCT method; the same was 89.37%, 88.30%, 65.58%, and 76.80%, respectively, by the DCEUS method; and the same was 99.49%, 94.44%, 84.13%, and 90.54%, respectively, by the D&M method, which shows that the D&M method has better validity in preoperative cT staging of GC. The Kappa value of preoperative T1, T2, T3, and T4 staging was 0.382, 0.598, 0.024, and 0.383, respectively, by the MSCT method; the same was 0.823, 0.913, 0.438, and 0.711, respectively, by the DCEUS method; and the same was 0.954, 0.966, 0.707, and 0.881, respectively, by the D&M method. This means the D&M method has better reliability in preoperative cT staging

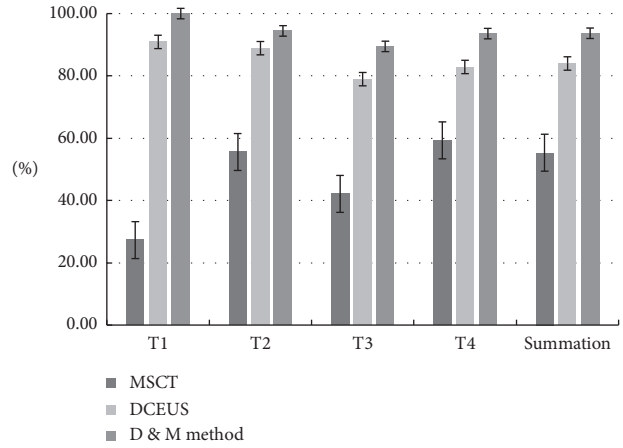

Figure 2: The correct diagnosis rate of T staging results of MSCT, DCEUS, and combined diagnosis. Note: (1) comparison of correct diagnosis rate of MSCT and DCEUS in different T staging: T1 staging, $\chi^2 = 13.015$, $p = 0.000$; T2 staging, $\chi^2 = 6.132$, $p = 0.015$; T3 staging, $\chi^2 = 10.451$, $p = 0.000$; T4 staging, $\chi^2 = 5.177$, $p = 0.019$; summation, $\chi^2 = 7.152$, $p = 0.008$. (2) Comparison of correct diagnosis rate of MSCT and the D&M method in different T staging: T1 staging, $\chi^2 = 16.541$, $p = 0.000$; T2 staging, $\chi^2 = 9.648$, $p = 0.000$; T3 staging, $\chi^2 = 15.224$, $p = 0.000$; T4 staging, $\chi^2 = 8.674$, $p = 0.004$; summation, $\chi^2 = 11.192$, $p = 0.000$; (3) Comparison of correct diagnosis rate of DCEUS and D&M method in different T staging: T1 staging, $\chi^2 = 4.482$, $p = 0.034$; T2 staging, $\chi^2 = 2.697$, $p = 0.187$; T3 staging, $\chi^2 = 4.847$, $p = 0.031$; T4 staging, $\chi^2 = 4.052$, $p = 0.044$; summation, $\chi^2 = 2.387$, $p = 0.163$.

Table 5: Results of validity, reliability, and revenue.

	Validity			Reliability		Revenue	
	Sensitivity (%)	Specificity (%)	Youden index (%)	Coincidence rate (%)	Kappa value	Positive predictive value (%)	Negative predictive value (%)
				MSCT			
T1	27.27	99.49	26.76	95.63	0.382	75.00	96.04
T2	55.56	97.06	52.61	89.81	0.598	80.00	91.16
T3	42.11	63.64	5.74	61.65	0.024	10.53	91.54
T4	59.29	86.36	45.65	67.96	0.383	90.22	50.00
				DCEUS			
T1	90.91	98.46	89.37	98.06	0.823	76.92	99.48
T2	88.89	99.41	88.30	97.57	0.913	96.97	97.69
T3	78.95	86.63	65.58	85.92	0.438	37.50	97.59
T4	82.86	93.94	76.80	86.41	0.711	96.67	72.09
				D&M method			
T1	100.00	99.49	99.49	99.51	0.954	91.67	100.00
T2	94.44	100.00	94.44	99.03	0.966	100.00	98.84
T3	89.47	94.65	84.13	94.17	0.707	62.96	98.88
T4	93.57	96.97	90.54	94.66	0.881	98.50	87.67

of GC. In addition, the positive predictive value and negative predictive value of the D&M method is highest among the three diagnostic methods, that is to say, the revenue of the D&M method is the best.

4. Discussion

The incidence rate of GC is increasing year by year, and surgical treatment is still the first choice. Preoperative accurate staging is very important for the formulation of treatment plan [9]. GC is one of the tumors lacking blood supply; more than 90% of them are adenocarcinoma, and most of them are local thickening and abnormal enhancement of the gastric wall [10]. For tumor tissue, tumor microvessels grow first, and then tumor cells grow and infiltrate [11]. The microvessel perfusion of tumor and peritumoral tissue is consistent, which is different from the surrounding normal tissue structure [12]. Therefore, both MSCT and DCEUS can evaluate the blood supply in tumor. At present, there are some guidelines for preoperative T staging of GC in various staging standards, and the description of imaging features can be used as the basis for the preliminary diagnosis of T staging, but these imaging examination standards are not perfect and need to be further studied.

DCEUS refers to the combination of oral contrast agent and intravenous contrast agent for ultrasound examination [8]. Compared with conventional ultrasound and oral contrast agent ultrasound, it has better contrast and better image quality. In addition, it can dynamically observe and

record the perfusion imaging process of the contrast medium in the lesions and normal tissues, so as to improve the diagnostic ability of lesions, so it has great application value in the preoperative cT staging evaluation of GC [13]. However, the study of DCEUS in preoperative evaluation of GC has some shortcomings [14]. Most scholars evaluate lymph node metastasis according to the presence of lymph node metastasis, rather than the number of lymph node metastasis. Therefore, this method needs further study [15].

MSCT is widely used in preoperative evaluation of GC [16]. Compared with conventional CT, it has the following advantages, such as fast scanning, in the abdominal examination, it can reduce the image of respiration and gastrointestinal movement [17]. The image resolution is high. The image can be reconstructed in many directions with high spatial resolution [18]. Through intravenous injection of contrast agent, we can observe the enhancement mode and degree of different tissues and better distinguish the focus tissue and normal tissue [19]. Studies have shown that dynamic contrast-enhanced MSCT in preoperative cT staging of GC has high accuracy and clinical value, but there are also shortcomings, mainly the accuracy of judging the depth of tumor invasion is low [20].

In this study, the correct diagnosis rate of the cT staging of MSCT and DCEUS were compared, in order to find their respective advantages and disadvantages and further study the accuracy of their combined application in preoperative staging of GC, and then some research results were obtained. We found that the correct diagnosis rate of MSCT and DCEUS were 55.34% and 83.98%, respectively, and the D&M method was 93.69%, which was higher than that of MSCT and DCEUS used alone. In addition, the Kappa values of the D&M method in T1 to T4 were 0.954, 0.966, 0.707, and 0.881, respectively, indicating that the consistency of the D&M method in the diagnosis of preoperative T staging of GC is very reliable.

Therefore, with the development of neoadjuvant therapy for GC, it is urgent to find an examination method with high accuracy, less damage, and easy acceptance by patients to evaluate the effect of neoadjuvant therapy. The results of DCEUS and enhanced MSCT in the preoperative cT staging evaluation of GC will lay a foundation for its research in the evaluation of neoadjuvant therapy.

5. Conclusion

The dynamic contrast-enhanced MSCT can penetrate the vessel wall. DCEUS is pure blood pool imaging, which can accurately reflect the blood supply of the lesions and dynamically observe the tumor invasion. The application of dynamic contrast-enhanced MSCT improves the accuracy of GC staging and the detection rate of lesions. DCEUS can more accurately predict the cT staging of GC, which has the advantages of nonradiation, simple, repeatable, and noninvasive. The correct diagnosis rate of the DCEUS method for preoperative T stage of gastric cancer was significantly higher than that of the MSCT method. Dynamic contrast-enhanced MSCT combined with DCEUS in the diagnosis of preoperative T staging of GC has more validity, reliability, and revenue than using MSCT or DCEUS alone, which is an image evaluation method worthy of clinical promotion.

Data Availability

The datasets used and/or analyzed during the current study are available from the corresponding author on reasonable request.

Ethical Approval

The study was approved by the ethics committee of Qilu Hospital of Shandong University. Patients who participated in the study had complete clinical data.

Consent

Signed written informed consents were obtained from the patients and/or guardians.

Conflicts of Interest

The authors declare that they have no conflicts of interest.

References

[1] S. Wang, M. Zhou, A. Ji, D. Zhang, and J. He, "Milk/dairy products consumption and gastric cancer: an update meta-analysis of epidemiological studies," *Oncotarget*, vol. 9, no. 6, pp. 7126–7135, 2017.

[2] L. A. Torre, F. Bray, R. L. Siegel, J. Ferlay, J. Lortet-Tieulent, and A. Jemal, "Global cancer statistics, 2012," *CA: A Cancer Journal for Clinicians*, vol. 65, no. 2, pp. 87–108, 2015.

[3] J. W. Kim, S. S. Shin, S. H. Heo et al., "Diagnostic performance of 64-section CT using CT gastrography in preoperative T staging of gastric cancer according to 7th edition of AJCC cancer staging manual," *European Radiology*, vol. 22, no. 3, pp. 654–662, 2012.

[4] K. K. F. Tsoi, H. W. Hirai, F. C. H. Chan, S. Griffiths, and J. J. Y. Sung, "Cancer burden with ageing population in urban regions in China: projection on cancer registry data from World Health Organization," *British Medical Bulletin*, vol. 121, no. 1, pp. 83–94, 2017.

[5] Y. N. Kim, D. Choi, S. H. Kim et al., "Gastric cancer staging at isotropic MDCT including coronal and sagittal MPR images: endoscopically diagnosed early vs. advanced gastric cancer," *Abdominal Imaging*, vol. 34, no. 1, pp. 26–34, 2009.

[6] C.-Y. Chen, J.-S. Hsu, D.-C. Wu et al., "Gastric cancer: preoperative local staging with 3D multi-detector row CT-correlation with surgical and histopathologic results," *Radiology*, vol. 242, no. 2, pp. 472–482, 2007.

[7] I. Joo, J. M. Lee, J. H. Kim, C.-I. Shin, J. K. Han, and B. I. Choi, "Prospective comparison of 3T MRI with diffusion-weighted imaging and MDCT for the preoperative TNM staging of gastric cancer," *Journal of Magnetic Resonance Imaging*, vol. 41, no. 3, pp. 814–821, 2015.

[8] L. Wang, X. Wang, H. Kou et al., "Comparing single oral contrast-enhanced ultrasonography and double contrast-enhanced ultrasonography in the preoperative Borrmann classification of advanced gastric cancer," *Oncotarget*, vol. 9, no. 9, pp. 8716–8724, 2018.

[9] H. In, I. Solsky, B. Palis, M. Langdon-Embry, J. Ajani, and T. Sano, "Validation of the 8th edition of the AJCC TNM

staging system for gastric cancer using the National Cancer Database," *Annals of Surgical Oncology*, vol. 24, no. 12, pp. 3683–3691, 2017.

[10] T. Fukagawa, H. Katai, H. Katai et al., "A prospective multi-institutional validity study to evaluate the accuracy of clinical diagnosis of pathological stage III gastric cancer (JCOG1302A)," *Gastric Cancer*, vol. 21, no. 1, pp. 68–73, 2018.

[11] O. Jeong, M. R. Jung, J. H. Kang, and S. Y. Ryu, "Prognostic performance of preoperative staging: assessed by using multidetector computed tomography-between the new clinical classification and the pathological classification in the eighth American Joint Committee on Cancer classification for gastric carcinoma," *Annals of Surgical Oncology*, vol. 27, no. 2, pp. 545–551, 2020.

[12] N. Hasuike, H. Ono, H. Ono et al., "A non-randomized confirmatory trial of an expanded indication for endoscopic submucosal dissection for intestinal-type gastric cancer (cT1a): the Japan clinical oncology group study (JCOG0607)," *Gastric Cancer*, vol. 21, no. 1, pp. 114–123, 2018.

[13] S. Li, P. Huang, Z. Wang et al., "Preoperative T staging of advanced gastric cancer using double contrast-enhanced ultrasound," *Ultraschall in der Medizin*, vol. 33, no. 7, pp. E218–E224, 2012.

[14] L. Rubaltelli, Y. Khadivi, A. Tregnaghi et al., "Evaluation of lymph node perfusion using continuous mode harmonic ultrasonography with a second-generation contrast agent," *Journal of Ultrasound in Medicine*, vol. 23, no. 6, pp. 829–836, 2004.

[15] R. E. Dorfman, M. B. Alpern, B. H. Gross, and M. A. Sandler, "Upper abdominal lymph nodes: criteria for normal size determined with CT," *Radiology*, vol. 180, no. 2, pp. 319–322, 1991.

[16] I. J. Lee, J. M. Lee, S. H. Kim et al., "Diagnostic performance of 64-channel multidetector CT in the evaluation of gastric cancer: differentiation of mucosal cancer (T1a) from submucosal involvement (T1b and T2)," *Radiology*, vol. 255, no. 3, pp. 805–814, 2010.

[17] A. Y. Kim, H. J. Kim, and H. K. Ha, "Gastric cancer by multidetector row CT: preoperative staging," *Abdominal Imaging*, vol. 30, no. 4, pp. 465–472, 2005.

[18] C. Gerardo, E. R. Johel, B. Valmore et al., "Computational assessment of stomach tumor volume from multi-slice computerized tomography images in presence of type 2 cancer," *F1000Research*, vol. 7, pp. 1–15, 2018.

[19] Z. Kristina, K. Irena, and K. Mindaugas, "Comparison of different methods of multislice spiral computed tomography for the preoperative gastric cancer staging," *Surgical Science*, vol. 6, no. 9, pp. 427–435, 2015.

[20] M. Daniele, A. M. Maria, P. Corrado et al., "High accuracy of multislices computed tomography (MSCT) for para-aortic lymph node metastases from gastric cancer: a prospective single-center study," *Annals of Surgical Oncology*, vol. 18, no. 8, pp. 2265–2272, 2011.

Hindawi
Journal of Oncology
Volume 2021, Article ID 7764817, 10 pages
https://doi.org/10.1155/2021/7764817

Review Article

Main Risk Factors of Type 2 Diabetes Mellitus with Nonalcoholic Fatty Liver Disease and Hepatocellular Carcinoma

Yueying Qi,[1] Lirong Fan,[2] Decong Ran,[3] Jieda Xu,[4] Yuansong Wang,[5] Jin Wu,[5] and Zhongyong Zhang[5]

[1]*Department of Gastroenterology and Hepatology, Cangzhou Hospital of Integrated Traditional Chinese Medicine and Western Medicine, 31 West Huanghe Road, Cangzhou, Hebei, China*
[2]*Department of Endocrinology, The Traditional Chinese Medicine Hospital of Botou, West Shengli Road, Botou, Hebei, China*
[3]*Graduate School, Hebei University of Chinese Medicine, Xingyuan Road, Shijiazhuang, Hebei, China*
[4]*Graduate School, Chengde Medical University, Anyuan Road, Chengde, Hebei, China*
[5]*Department of Endocrinology, Hebei Province Cangzhou Hospital of Integrated Traditional Chinese Medicine and Western Medicine, 31 West Huanghe Road, Cangzhou, Hebei, China*

Correspondence should be addressed to Zhongyong Zhang; jiuzai63879572419@163.com

Received 1 July 2021; Accepted 15 September 2021; Published 13 October 2021

Academic Editor: Muhammad Wasim Khan

Type 2 diabetes mellitus (T2DM) with nonalcoholic fatty liver disease (NAFLD) is a pathological metabolic disease characterized by high ketone lipid based on abnormal lipid metabolism. Compared with patients with single T2DM or NAFLD, T2DM complicated with NAFLD has more complicated pathogenic factors and pathological processes. Hepatocellular carcinoma (HCC), the leading malignancy arising from cirrhosis, is the second most lethal cancer globally. The purpose of this study was to clarify the main risk factors of T2DM with NAFLD and HCC. There are many challenges in the diagnosis and treatment of T2DM patients with NAFLD and HCC. The current gold standard is to adjust treatment strategy, optimize metabolic control, and improve liver phenotype. It is necessary to identify further the risk factors driving the progression of T2DM with NAFLD and HCC and evaluate new therapeutic targets, in addition to exploring the syndromic forms of T2DM combined with NAFLD and providing a theoretical basis for early prevention, diagnosis, and treatment of the disease using traditional Chinese medicine (TCM).

1. Introduction

Nonalcoholic fatty liver disease (NAFLD) is prevalent in patients with type 2 diabetes mellitus (T2DM) [1]. Previous studies had shown that 50% of T2DM patients had NAFLD, while the incidence of NAFLD in obese diabetic patients is as high as 100% [2]. There is increasing evidence that patients with T2DM have a particularly high risk of developing nonalcoholic fatty liver disease, nonalcoholic steatohepatitis, and hepatocellular carcinoma (HCC) [3]. HCC is a major life-limiting factor in progressive fibrotic liver disease, mainly caused by a chronic viral infection, alcohol abuse, and nonalcoholic fatty liver disease [4].

In prospective studies, preexisting diabetes mellitus was an independent risk factor for NAFLD progression and liver-related mortality [5, 6]. Studies had shown that the existence of NAFLD predicted the development of T2DM [7]. A cross-sectional study of T2DM patients found that the prevalence of NAFLD identified by ultrasound was 69% [8]. In a Swedish cohort study, most NAFLD patients (78%) were diagnosed with diabetes or impaired glucose tolerance at follow-up [9]. In addition, the interaction of environmental and genetic factors can promote the progress of T2DM with NAFLD. NAFLD increased the incidence of T2DM. At the same time, T2DM can effectively accelerate the development of NAFLD to a more serious form. In most developed

countries, NAFLD is currently the most common liver disease and a major risk factor for HCC [10]. One study showed that diabetes increases the risk of HCC [11]. Whether the interaction between diabetes and the etiology of cirrhosis affects the risk of liver cancer remains controversial.

Although significant progress has been made in discovering new targets and treating chronic liver disease in recent decades, most treatment methods have not achieved satisfactory results [12]. Traditional Chinese medicine (TCM) treatment of the disease has the advantages of stable curative effect, safety, being nontoxic, low price, and multitarget effect [13]. In particular, the TCM syndrome types of different diseases may suggest different TCM treatment schemes.

2. Epidemiology of T2DM

The International Diabetes Federation estimates that 371 million adults worldwide had diabetes [14]. In China, the prevalence of diabetes reached 11.6% in 2010, affecting about 113.9 million adults [15]. It is estimated that, by 2040, about 642 million people will have diabetes, and T2DM is the main type of diabetes [16]. T2DM had become a heavy burden of limited medical resources. Since 1980, the incidence rate and prevalence of T2DM in the world had increased two times, and they are still increasing [17]. It had been reported that the prevalence of T2DM in women was on the rise globally, which was more common in low-income countries where obesity and aging were seen as driving forces [18]. In the United States, about one-third of patients with T2DM are adolescents [19]. It is estimated that the prevalence of T2DM in the population above 20 years of age ranges from 6.6% to 7.0% in Spain and 6.3% in Midi-Pyrénées, while the estimated value in men in these three regions is about more than 2% [20].

3. Epidemiology of NAFLD

NAFLD can be divided into two categories: primary and secondary. Fatty liver associated with metabolic syndrome caused by excess nutrition and cryptogenic fatty liver belongs to the category of primary nonalcoholic fatty liver disease. Fatty liver caused by malnutrition, total parenteral nutrition, drug/environment, and industrial toxicosis belongs to the category of secondary nonalcoholic fatty liver disease. NAFLD refers to all kinds of liver diseases, such as nonalcoholic steatohepatitis (NASH), simple steatosis (NAFL), and fibrosis. The incidence rate of NAFLD is expected to increase worldwide with the increase of obesity and diabetes. Recently, studies concluded that the prevalence of NAFLD worldwide is 25.2%, and the prevalence of NAFLD in the US is expected to increase by 50% by 2030 [21, 22]. The prevalence of NAFLD in China was about 20% [23]. NAFLD patients had not only a risk of progressive liver disease but also a significantly increased risk of cancer death [24]. NAFLD is diagnosed when more than 5% of liver cells show fat accumulation or by histological or imaging evaluation [25]. The pathogenesis of NAFLD is complex and has not been fully elucidated.

4. Epidemiology of HCC

Liver cancer mainly refers to malignant tumors originating from hepatocytes, liver epithelium, or liver mesenchymal tissue. HCC is more specific, mainly hepatocellular carcinoma. The etiology of the two cancers is also slightly different. Hepatocellular carcinoma is mainly caused by hepatitis B and hepatitis C. HCC accounts for >80% of primary liver cancers worldwide [26]. HCC accounted for 72.7% of global deaths in 2015 [27]. In addition, the World Health Organization (WHO) estimates that more than 1 million patients are expected to die from liver cancer within the next 10 years [28]. The incidence of liver cancer varies geographically, with the majority of liver cancer cases occurring in less developed regions, such as East Asia (54.8% of cases) and Southeast Asia (10.8% of cases) [29]. From 2006 to 2017, the incidence of HCC increased by 2-3% per year, mainly due to viral cirrhosis and a high incidence of NAFLD [30].

5. Main Risk Factors of T2DM with NAFLD

5.1. Genetic Factors. TM6SF2rs 58542926 mutation was closely related to NAFLD, age, body mass index (BMI), and T2DM [31]. TM6SF2 is located in ER and Golgi complex and has the function of mobilizing neutral lipids for VLDL assembly. In the absence of lipid droplets, lipids accumulate in the droplets [32]. However, the assessment of insulin resistance (IR) or oral glucose tolerance test did not reduce in the TM6SF2 gene mutation vector [33]. Therefore, the mutation may not be associated with IR.

Not only is PNPLA 3 gene mutation related to NAFLD, but also it has a slightly increased risk of T2DM [34, 35]. In fact, the expression of PNPLA 3 is directly regulated by the insulin regulatory transcription factor sterol regulatory element-binding protein 1c (SREBP-1c). In the case of obesity and IR, the accumulation of pathogenic PNPLA 3 mutation products aggravates liver steatosis, inflammation, and cirrhosis [36].

Adiponectin (HMW) is an adipocytokine and insulin-sensitive substance, which plays an essential role in the pathogenesis of diabetes mellitus and NAFLD [37]. HMWrs 266729 polymorphism is associated with an increased risk of NAFLD patients [38]. Studies on different populations showed that HMW gene polymorphism affected the development of NAFLD [39, 40]. There was a significant correlation between rs1501299 and NAFLD in some female diabetic patients in Japan [41]. HMW is considered a potential biomarker for the detection and prediction of NAFLD complicated with T2DM [42]. Lu et al. found that the mutation frequency of LEPR nucleotide 3057 G > A (rs1805096) was 76.0% in 104 T2DM patients with NAFLD. The results suggested that LEPR gene G3057 A (rs1805096) polymorphism may be involved in NAFLD by regulating lipid metabolism and affecting insulin sensitivity in patients with T2DM [43].

5.2. Insulin Resistance. The close relationship between NAFLD and T2DM is that they have common pathogenesis, namely, IR [44]. IR refers to the decrease of tissue response to insulin [45]. The pathogenesis of NAFLD is described as the "multiple hit hypothesis." IR plays a central role in the first attack, resulting in an imbalance between factors that promote liver fat accumulation and factors that prevent fatty acid accumulation [46, 47]. The steady-state model assessment value of β cell function and the decreased value of β cell function in patients of T2DM with NAFLD were higher than those in patients without NAFLD, including IR of liver and adipocytes [48]. Therefore, NAFLD often coexists with T2DM.

Swollen and inflamed visceral adipose tissue is likely to trigger various factors that may be correlated with the development of IR and NAFLD, such as inflammatory adipocytokines and free fatty acids [49]. The interaction between hepatic steatosis and IR establishes a circle to promote the development of T2DM and NAFLD. In addition, glucose cotransporter 2 can promote renal reabsorption of glucose and reduce urinary glucose excretion by increasing blood glucose and body weight (BW), thus aggravating IR in T2DM and NAFLD patients [50]. This relationship between T2DM, IR, and NAFLD is believed to be due to insulin being delivered directly to the portal vein after secretion in the same way as glucose absorbed. IR plays a crucial role in the pathogenesis of T2DM with NAFLD. Therefore, insulin sensitizer is considered as an effective treatment.

5.3. Lifestyle. A multicenter clinical trial involving 5145 overweight adults with T2DM showed that, after 12 months of intensive lifestyle intervention, steatosis and NAFLD were significantly reduced, and weight loss was at least 7% [51]. Recent randomized controlled trials ($n = 154$) had again shown that lifestyle intervention could effectively alleviate NAFLD in nonobese and obese patients [52]. Numerous studies have shown that developing a reasonable exercise plan is significant for alleviating T2DM and NAFLD. Reasonable exercise plays an important role in controlling the blood sugar and blood lipids of patients and can significantly improve the therapeutic effect of T2DM or NAFLD.

The relationship between diet and T2DM with NAFLD is very complex. Excess of total energy intake can lead to obesity by changing the energy balance. A high carbohydrate diet (50% to 65% of carbohydrate calories) is associated with IR and obesity [53]. All of these are risk factors for damaging NAFLD phenotype and increasing IR [25]. A review study evaluated the effects of probiotics and synbiotics on obesity, T2DM, and NAFLD [54]. The beneficial effects of probiotics and synbiotics improved liver function and metabolic parameters in NAFLD patients.

Lower frequency and level of physical activity and being sedentary for a long time were associated with IR, T2DM, and NAFLD. Sedentary behavior is associated with chronic low-grade inflammation and can lead to obesity [55]. Exercise management can prevent or delay the progress of T2DM [56]. Among large numbers of middle-aged Korean people, being sedentary and reduced physical activity are positively correlated with the prevalence of NAFLD, which supports the importance of increasing physical activity to promoting physical activity [57, 58].

5.4. Obesity. Obesity is a chronic metabolic disease, which is mainly characterized by excessive accumulation of fat and overweight. The current research showed that the causes of obesity are diverse, and the main reasons are divided into congenital factors and exogenous factors. Studies have shown that the congenital factors of obesity are mainly genetic factors, while the exogenous factors are mainly excessive diet, lack of exercise, or pathological obesity.

The incidence rate of obesity and its metabolic complications worldwide had risen sharply in recent years. Obesity is an important risk factor for NAFLD and T2DM and may provide a common link through IR [59]. Recent studies had shown that obesity (whether peripheral or central obesity) usually preceded NAFLD, and NAFLD preceded the development of T2DM [60]. Obesity is closely related to adipose tissue dysfunction in NAFLD patients, which may accelerate IR and pancreatic β cell dysfunction [61]. To a large extent, IR in obese patients is the result of adipose tissue inflammation and adipocyte regulation disorder [62]. Weight loss has a significant effect on T2DM with NAFLD, and the weight loss is mainly due to the reduction of fat mass, especially visceral fat, rather than skeletal muscle mass [63]. Bariatric surgery is an effective method to treat obesity, which has been proved to significantly improve or even cure diabetes and improve the histological characteristics of NAFLD [64].

In addition, a large number of studies have shown that obesity is closely related to the intestinal flora. The change of intestinal microbiota composition has been considered an effective therapy to regulate obesity [65].

5.5. Others. The data showed that NAFLD and diabetes were related to the decrease of CYP3A4 activity in the liver [66]. In human studies, low plasma adiponectin levels are associated with an increased risk of T2DM, and low adiponectin levels are an independent risk factor for NAFLD [67]. In addition, LDL-c, FPG, BMI, FINS, TC, and HOMA-IR were also risk factors of T2DM with NAFLD [44]. In 146 T2DM patients with NAFLD, multivariate analysis showed that dyslipidemia, elevated LDL, HbA1c, and diastolic blood pressure were risk factors [68]. In addition, human and animal intestines are occupied by a variety of microorganisms. These microorganisms play a key role in maintaining intestinal function and regulating host immune response and chronic diseases such as obesity, diabetes, and NAFLD [69–71].

6. Main Risk Factors of HCC

Major risk factors contributing to the rise in HCC include high prevalence of HBV and HCV infection, followed by an increased incidence of alcohol abuse, obesity, NAFLD, and

Table 1: Studies which have evaluated the association between type 2 diabetes and risk of HCC.

Study	Study characteristics	Diabetes diagnosis	Covariate adjustment considered	Main findings
Huo et al., Eur J Gastroenterol Hepatol 2003; 15 : 1203-8	Prospective study: 239 HCC patients (16.3% of whom had DM). Mean follow-up: 2.6 years	Fasting glucose ≥126 mg/dL or 2-hour postload glucose ≥200 mg/dL, or past history	Age, sex, tumor size, anti-HCV-Ab positivity, HBeAg-positivity, cirrhosis, alcohol intake, alpha-fetoprotein, albumin, bilirubin	DM did not affect long-term survival in HCV-related HCC but was a recurrence-independent prognostic factor for HBV-related HCC
Coughlin et al., Am J Epidemiol 2004; 159 : 1160-7	Population cohort study: 467,922 men and 588,321 women without history of cancer at baseline. Mean follow-up: 16 years	Self-reported	BMI	DM was associated with increased risk of incident HCC only in men
El-Serag et al., Gastroenterology 2004; 126 : 460-8	Prospective study: 73,643 patients with DM and 650,620 patients without DM. Mean follow-up: 5 years	Self-reported	Alcoholic liver disease, viral chronic hepatitis, demographic variables	DM was associated with an increased risk of incident HCC. DM carried the highest risk among patients with a follow-up longer than 10 years
Davilla et al., Gut 2005; 54 : 533-9	Population-based case-control study: 2,061 HCC patients (of whom 43% with DM) and 6,183 noncancer controls (of whom 19% with DM)	Electronic register	Age, sex, race, HCV, HBV, alcoholic liver disease, and hemochromatosis	DM was associated with a nearly threefold increased risk of HCC
Inoue et al., Arch Intern Med 2006; 166 : 1871-7	Prospective study: 97,771 Japanese adult individuals followed up for cancer incidence over 5 years. At baseline, 4.7% of them had DM	Self-reported	Age, study area, BMI, prior cardiovascular disease, smoking, alcohol intake, leisure-time physical activity, green vegetable intake, coffee intake	DM was associated with increased risk of total cancer and cancer in specific sites, including HCC
El-Serag et al. Clin Gastroenterol Hepatol 2006; 4 : 369-80	Meta-analysis: a total of 26 studies (of which 13 were case-control studies and 13 were cohort studies), inclusive of approximately 3 million individuals	Self-reported	Alcohol intake, chronic viral hepatitis, diet, BMI	Among 13 cohort studies, DM was associated with an increased risk of HCC
Kawamura et al., J Gastroenterol Hepatol 2008; 23 : 1739-46	Prospective study: 40 consecutive HCC patients (with HCC associated with non-B, non-C hepatitis) and later underwent surgical resection or radiofrequency ablation. Prevalence of DM was 45%. Mean follow-up: 5 years	Fasting glucose ≥126 mg/dL or past history	Age, sex, dyslipidemia, smoking, alcohol intake, history of blood transfusion, state of liver disease (chronic hepatitis or cirrhosis), AST, albumin, bilirubin, alpha-fetoprotein, prothrombin time, tumor size, multiplicity, hypervascularity, and portal vein invasion of HCC	DM was a significant predictor of tumor recurrence after potentially curative therapy for HCC
Donadon et al., World J Gastroenterol 2009; 15 : 2506-11	Case-control study: 465 HCC patients, 618 with cirrhosis, and 490 control subjects. The prevalence of DM was 31.2% in HCC, 23.3% in cirrhotic patients, and 12.7% in control group	Self-reported	Age, sex, BMI, alcohol abuse, HBV, and HCV	DM was an independent risk factor for HCC. Among male patients with DM, there was a positive association of HCC with insulin/sulphonylurea treatment and an inverse association with metformin

Table 1: Continued.

Study	Study characteristics	Diabetes diagnosis	Covariate adjustment considered	Main findings
Hassan et al., Cancer 2010; 116 : 1938-46	Hospital-based case-control study: 420 patients with HCC and 1,104 healthy controls. The prevalence of DM was 33.3% in patients with HCC and 10.4% in controls	Self-reported	Age, sex, race, educational level, smoking, alcohol intake, HCV, HBV, family history of cancer	DM increased the risk of HCC. Treatments with sulfonylureas or insulin were associated with higher HCC risk, whereas treatments with metformin or glitazones were associated with lower HCC risk
Hense et al., Diabetol Metab Syndr 2011; 3 : 15	Community-based study: 26,742 DM patients, who were 40 to 79 years old and resided in the Muenster district. Mean follow-up: 3.3 years	Self-reported	Sex, diabetes duration, BMI, insulin treatment	Risk of any incident cancer in DM was increased, in particular for HCC. Insulin therapy was related to higher cancer risk, while metformin was not
Johnson et al., Diabetologia 2011; 54 : 2263-71	Population-based retrospective cohort study: 185,100 individuals with DM and 185,100 without DM, matched by sex and age. Mean follow-up: 10 years	Electronic register	Age, sex, socioeconomic status, number of physician visits, year of diagnosis	DM was associated with increased risk of selected cancers, including HCC
Li et al., Int J Canc 2012; 131 : 1197-202	Hospital-based case-control study: 1,105 patients with HBV-related HCC and 5,170 patients with chronic HBV. The whole prevalence of DM was 6.7%	Fasting glucose ≥126 mg/dL or past history	Age, family history of HCC, city of residence, HBV-Ag, and cirrhosis	DM was associated with increased risk of HCC, only in women
Wang et al., Int J Cancer 2012; 130 : 1639-48	Meta-analysis: a total of 25 cohort studies, enrolling 1,283,112 persons. Mean follow-up: 8.8 years	Self-report, medical records	Geographic location, alcohol intake, history of cirrhosis, or HBV and HCV infections	DM was associated with increased risk of incident HCC and higher HCC mortality. Longer diabetes duration and use of sulfonylureas or insulin were associated with increased risk of HCC. Metformin treatment was protective
Wang et al., Diabetes Metab Res Rev 2012; 28 : 109-22	Meta-analysis: 17 case-control studies (a total of nearly 6,000 HCC cases and 74,000 controls) and 32 cohort studies (a total of nearly 6,500,000 individuals)	Self-report, medical records	BMI, prior hepatitis, cirrhosis, alcohol intake, smoking, treatment, duration of diabetes	The combined risk estimate of all studies showed a significant increased risk of HCC among DM individuals. In addition, meta-analysis of 7 cohort studies found a significant increased risk of HCC mortality for individuals with DM compared to those without
Lai et al., Am J Gastroenterol 2012; 107 : 46-52	Population-based cohort study: 19,349 newly diagnosed DM patients and 77,396 control subjects without DM. Mean follow-up: 5 years	Electronic register	Age, sex, cirrhosis, alcoholic liver damage, viral hepatitis	DM was associated with increased risk of incident HCC. Use of metformin or glitazones was associated with reduced HCC risk

Table 1: Continued.

Study	Study characteristics	Diabetes diagnosis	Covariate adjustment considered	Main findings
Schlesinger et al., Ann Oncol 2013; 24 : 2449-55	Community-based cohort study: 363,426 participants, after excluding those with cancer at baseline. Mean follow-up: 8.5 years	Self-reported	Age, sex, center, education level, smoking, alcohol intake, BMI, waist-to-height ratio	DM was independently associated with higher risk of incident HCC and biliary tract cancer. HCC risk was higher in those treated with insulin. Results were similar in HCV/HBV-negative individuals
Zheng et al., PLoS One 2013; 8:e84776	Hospital-based retrospective case-control study: 1,568 participants of whom 716 patients were diagnosed with benign liver diseases and 852 patients were diagnosed with HCC. The prevalence of DM was 7.6%	Fasting glucose ≥126 mg/dL or 2-hour postload glucose ≥200 mg/dL, HbA1c ≥ 6.5%	Age, sex, HBV and HCV infections, cirrhosis, gallstone disease, cholinesterase, alkaline phosphatase	DM was associated with increased risk of HCC. However, there was a significant interaction between DM and HBV on HCC occurrence
Koh et al., Br J Cancer 2013; 108 : 1182-8	Community-based cohort study: 63,257 middle-aged and older individuals. The prevalence of DM was 8.6%. Mean follow-up: 14 years	Self-reported	Age, sex, BMI, recruitment year, education level, smoking, alcohol intake, consumption of coffee and tea	DM was associated with an increased risk of incident nonviral HCC
Miele et al., Gastroenterol Res Pract 2015; 2015 : 570356	Hospital-based case-control study: 224 HCC patients and 389 controls. The prevalence of DM was 19.7%	Self-reported	Age, sex, smoking, alcohol intake	DM was associated with increased risk of HCC. Treatment with any glucose-lowering drugs was not associated with increased HCC risk
Adami et al., J Natl Cancer Inst 1996; 88 : 1472-7	Hospital-based cohort: 153,852 patients with DM. Follow-up: from 1 to 24 years	Hospital discharge diagnosis	None	DM was associated with increased risk of incident HCC
La Vecchia et al., Int J Cancer 1997; 73 : 204-7	Case-control study: 428 HCC cases, 59 with gallbladder and bile duct cancers, and 1,502 control subjects from hospital	Self-reported	Age, sex, area of residence, education level, alcohol intake, BMI, smoking, history of chronic hepatitis and cirrhosis, family history of liver cancer	DM was associated with increased risk of incident HCC

uncontrolled type 2 diabetes [10]. In areas with high incidence, 80% of HCC patients test positive for hepatitis B surface antigen (HBsAg) in serum [72]. Moreover, 10–20% of patients with hepatitis B can develop HCC without cirrhosis [73]. Hepatitis C virus (HCV) infection is also a major risk factor for HCC, which leads to a 5- to 20-fold risk of HCC [74]. Indeed, persistent cellular stress, repeated necrosis, and compensatory regeneration of cells, as well as chronic inflammation, lead to cellular senescence and mutagenesis, ultimately leading to hepatocarcinogenesis [75]. The mechanism of NAFLD-induced HCC is not fully understood, and there is no way to prevent NAFLD patients from progressing to HCC [76]. T2DM is a risk factor for NAFLD and increases HCC incidence two- to threefold [77]. NAFLD HCC patients have increased levels of IL-13, which can activate myeloid-derived suppressor cells and promote tumor progression by suppressing tumor immunity [78]. Another mechanism underlying NAFLD HCC is PNPLA3 gene polymorphism, possibly related to by enhancing inflammatory signaling [79]. Table 1 compiles the principal observational investigations and meta-analyses analyzing the association between T2DM and the risk of HCC.

7. TCM Syndrome Types of T2DM with NAFLD

In recent years, TCM and its extracts have been considered a new potential source of therapeutic drugs for preventing and treating fatty liver disease [80]. According to modern TCM theory, type 2 diabetes belongs to the category of diabetes. There are many problems, such as dryness and heat injury, qi and yin deficiency, liver qi and yin deficiency, liver failure, spleen failure, liver blood deficiency, and spleen stomach heat accumulation. Therefore, it can be divided into eight types: stomach heat syndrome, lung dryness syndrome, spleen qi deficiency syndrome, lung qi deficiency syndrome, yin and yang deficiency syndrome, kidney yin deficiency syndrome, blood stasis syndrome, and phlegm retention syndrome.

Statistical analysis showed that spleen deficiency syndrome was the main syndrome type in T2DM with the

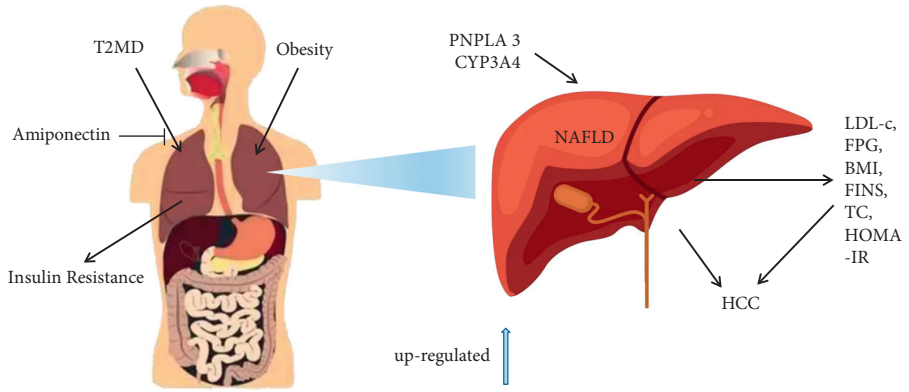

Figure 1: Biological mechanisms linking type 2 diabetes mellitus and NAFLD.

NAFLD group [81]. This has also been confirmed in other studies, and phlegm is one of the main syndrome characteristics [82]. There are also studies suggesting that, in T2DM patients with NAFLD, the proportion of damp-heat accumulation is the highest, followed by yin deficiency heat [83]. Additionally, studies also found that damp-heat trapped spleen syndrome and qi and yin deficiency syndrome are the most important syndrome types [84]. Correct evaluation of TCM syndrome types is helpful to improve the clinical effect of TCM combined with general therapy in the treatment of T2DM with NAFLD.

8. Conclusion and Future Prospect

At present, T2DM with NAFLD is considered as a multifactorial disease with genetic and environmental factors. IR is considered as a key risk factor for the occurrence and development of T2DM with NAFLD. IR in the peripheral tissue and liver is one of the causes of this condition, leading to the increase of circulating glucose and lipid substrates for lipid accumulation in the liver. Changing diet structure is beneficial to delay the progression of T2DM with NAFLD. It supports more extensive application of traditional Chinese medicine, Chinese patent medicine, and acupuncture physiotherapy, which provides theoretical support for the clinical application of traditional Chinese medicine therapy. However, there are still many deficiencies in the treatment of TCM. Therefore, further research and clinical verification are needed (Figure 1).

Prevention and treatment of viral hepatitis and NAFLD were vital factors in reducing the global burden of liver cancer. Implementation of screening for viral hepatitis and surveillance for hepatocellular carcinoma in high-risk patients are essential to improve current poor outcomes for patients with HCC. However, a better understanding of risk factors for liver cancer is required for developing new effective regimens and improving the efficacy of the existing therapies. [85]

Conflicts of Interest

The authors declare that they have no conflicts of interest.

Authors' Contributions

Yueying Qi and Decong Ran have contributed equally to this work.

Acknowledgments

This work was supported by the Research Project of Hebei Administration of Traditional Chinese Medicine (no. 2018479) and Project Support of Yuansong Wang Heritage Studio of Famous Traditional Chinese Medicine in Hebei Province.

References

[1] L. A. Adams, Q. M. Anstee, H. Tilg, and G. Targher, "Non-alcoholic fatty liver disease and its relationship with cardiovascular disease and other extrahepatic diseases," *Gut*, vol. 66, no. 6, pp. 1138–1153, 2017.

[2] S. Chitturi, V. W.-S. Wong, and G. Farrell, "Nonalcoholic fatty liver in Asia: firmly entrenched and rapidly gaining ground," *Journal of Gastroenterology and Hepatology*, vol. 26, no. 1, pp. 163–172, 2011.

[3] N. C. Leite, C. A. Villela-Nogueira, C. R. Cardoso, and G. F. Salles, "Non-alcoholic fatty liver disease and diabetes: from physiopathological interplay to diagnosis and treatment," *World Journal of Gastroenterology*, vol. 20, no. 26, pp. 8377–8392, 2014.

[4] T. Higashi, S. L. Friedman, and Y. Hoshida, "Hepatic stellate cells as key target in liver fibrosis," *Advanced Drug Delivery Reviews*, vol. 121, pp. 27–42, 2017.

[5] Z. M. Younossi, T. Gramlich, C. A. Matteoni, N. Boparai, and A. J. McCullough, "Nonalcoholic fatty liver disease in patients with type 2 diabetes," *Clinical Gastroenterology and Hepatology*, vol. 2, no. 3, pp. 262–265, 2004.

[6] L. Porepa, J. G. Ray, P. Sanchez-Romeu, and G. L. Booth, "Newly diagnosed diabetes mellitus as a risk factor for serious liver disease," *Canadian Medical Association Journal*, vol. 182, no. 11, pp. E526–E531, 2010.

[7] G. Musso, R. Gambino, M. Cassader, and G. Pagano, "Meta-analysis: natural history of non-alcoholic fatty liver disease (NAFLD) and diagnostic accuracy of non-invasive tests for liver disease severity," *Annals of Medicine*, vol. 43, no. 8, pp. 617–649, 2011.

[8] N. C. Leite, G. F. Salles, A. L. E. Araujo, C. A. Villela-Nogueira, and C. R. L. Cardoso, "Prevalence and associated factors of

non-alcoholic fatty liver disease in patients with type-2 diabetes mellitus," *Liver International*, vol. 29, no. 1, pp. 113–119, 2009.

[9] M. Ekstedt, L. E. Franzén, U. L. Mathiesen et al., "Long-term follow-up of patients with NAFLD and elevated liver enzymes," *Hepatology*, vol. 44, no. 4, pp. 865–873, 2006.

[10] J. D. Yang, P. Hainaut, G. J. Gores, A. Amadou, A. Plymoth, and L. R. Roberts, "A global view of hepatocellular carcinoma: trends, risk, prevention and management," *Nature Reviews Gastroenterology & Hepatology*, vol. 16, no. 10, pp. 589–604, 2019.

[11] J. D. Yang, H. A. Mohamed, J. L. Cvinar, G. J. Gores, L. R. Roberts, and R. W. Kim, "Diabetes mellitus heightens the risk of hepatocellular carcinoma except in patients with hepatitis C cirrhosis," *American Journal of Gastroenterology*, vol. 111, no. 11, pp. 1573–1580, 2016.

[12] B. E. Wang, "Treatment of chronic liver diseases with traditional Chinese medicine," *Journal of Gastroenterology and Hepatology*, vol. 15, pp. E67–E70, 2000.

[13] M. Inoue, A. Hayashi, T. Taguchi et al., "Effects of canagliflozin on body composition and hepatic fat content in type 2 diabetes patients with non-alcoholic fatty liver disease," *Journal of Diabetes Investigation*, vol. 10, no. 4, pp. 1004–1011, 2019.

[14] Y. Ren, M. Zhang, J. Zhao et al., "Association of the hypertriglyceridemic waist phenotype and type 2 diabetes mellitus among adults in China," *Journal of Diabetes Investigation*, vol. 7, no. 5, pp. 689–694, 2016.

[15] Y. Xu, L. Wang, J. He et al., "Prevalence and control of diabetes in Chinese adults," *Journal of the American Medical Association*, vol. 310, no. 9, pp. 948–959, 2013.

[16] O. O. Oguntibeju, "Type 2 diabetes mellitus, oxidative stress and inflammation: examining the links," *International journal of physiology, pathophysiology and pharmacology*, vol. 11, no. 3, pp. 45–63, 2019.

[17] A. Bashier, A. Bin Hussain, E. Abdelgadir, F. Alawadi, H. Sabbour, and R. Chilton, "Consensus recommendations for management of patients with type 2 diabetes mellitus and cardiovascular diseases," *Diabetology & Metabolic Syndrome*, vol. 11, no. 1, p. 80, 2019.

[18] G. Roglic, "Diabetes in women: the global perspective," *International Journal of Gynaecology & Obstetrics*, vol. 104, pp. S11–S13, 2009.

[19] M. Silink, "Childhood diabetes: a global perspective," *Hormone Research*, vol. 57, no. Suppl 1, pp. 1–5, 2002.

[20] G. Moulis, B. Ibañez, A. Palmaro et al., "Cross-national health care database utilization between Spain and France: results from the EPICHRONIC study assessing the prevalence of type 2 diabetes mellitus," *Clinical Epidemiology*, vol. 10, pp. 863–874, 2018.

[21] Z. M. Younossi, A. B. Koenig, D. Abdelatif, Y. Fazel, L. Henry, and M. Wymer, "Global epidemiology of nonalcoholic fatty liver disease-Meta-analytic assessment of prevalence, incidence, and outcomes," *Hepatology*, vol. 64, no. 1, pp. 73–84, 2016.

[22] M. W. Fleischman, M. Budoff, I. Zeb, D. Li, and T. Foster, "NAFLD prevalence differs among hispanic subgroups: the Multi-Ethnic Study of Atherosclerosis," *World Journal of Gastroenterology*, vol. 20, no. 17, pp. 4987–4993, 2014.

[23] Z. Li, J. Xue, P. Chen, L. Chen, S. Yan, and L. Liu, "Prevalence of nonalcoholic fatty liver disease in mainland of China: a meta-analysis of published studies," *Journal of Gastroenterology and Hepatology*, vol. 29, no. 1, pp. 42–51, 2014.

[24] L. Calzadilla Bertot and L. A. Adams, "The natural course of non-alcoholic fatty liver disease," *International Journal of Molecular Sciences*, vol. 17, no. 5, 2016.

[25] F. De Chiara, C. Ureta Checcllo, and J. Ramon Azcon, "High protein diet and metabolic plasticity in non-alcoholic fatty liver disease: myths and truths," *Nutrients*, vol. 11, no. 12, 2019.

[26] H. B. El-Serag and K. L. Rudolph, "Hepatocellular carcinoma: epidemiology and molecular carcinogenesis," *Gastroenterology*, vol. 132, no. 7, pp. 2557–2576, 2007.

[27] S. K. Sarin, M. Kumar, M. Eslam et al., "Liver diseases in the asia-pacific region: a lancet gastroenterology and hepatology commission," *The Lancet Gastroenterology and Hepatology*, vol. 5, no. 2, pp. 167–228, 2020.

[28] C. Kole, N. Charalampakis, S. Tsakatikas et al., "Immunotherapy for hepatocellular carcinoma: a 2021 update," *Cancers*, vol. 12, no. 10, 2020.

[29] Z. Chen, H. Xie, M. Hu et al., "Recent progress in treatment of hepatocellular carcinoma," *American journal of cancer research*, vol. 10, no. 9, pp. 2993–3036, 2020.

[30] S. Li, A. Saviano, D. J. Erstad et al., "Risk factors, pathogenesis, and strategies for hepatocellular carcinoma prevention: emphasis on secondary prevention and its translational challenges," *Journal of Clinical Medicine*, vol. 9, no. 12, 2020.

[31] Y.-L. Liu, H. L. Reeves, A. D. Burt et al., "TM6SF2 rs58542926 influences hepatic fibrosis progression in patients with non-alcoholic fatty liver disease," *Nature Communications*, vol. 5, no. 1, p. 4309, 2014.

[32] E. Smagris, S. Gilyard, S. BasuRay, J. C. Cohen, and H. H. Hobbs, "Inactivation of Tm6sf2, a gene defective in fatty liver disease, impairs lipidation but not secretion of very low density lipoproteins," *Journal of Biological Chemistry*, vol. 291, no. 20, pp. 10659–10676, 2016.

[33] Y. Zhou, G. Llauradó, M. Orešič, T. Hyötyläinen, M. Orho-Melander, and H. Yki-Järvinen, "Circulating triacylglycerol signatures and insulin sensitivity in NAFLD associated with the E167K variant in TM6SF2," *Journal of Hepatology*, vol. 62, no. 3, pp. 657–663, 2015.

[34] S. Romeo, J. Kozlitina, C. Xing et al., "Genetic variation in PNPLA3 confers susceptibility to nonalcoholic fatty liver disease," *Nature Genetics*, vol. 40, no. 12, pp. 1461–1465, 2008.

[35] P. Dongiovanni, S. Stender, A. Pietrelli et al., "Causal relationship of hepatic fat with liver damage and insulin resistance in nonalcoholic fatty liver," *Journal of Internal Medicine*, vol. 283, no. 4, pp. 356–370, 2018.

[36] Y. Huang, S. He, J. Z. Li et al., "A feed-forward loop amplifies nutritional regulation of PNPLA3," *Proceedings of the National Academy of Sciences*, vol. 107, no. 17, pp. 7892–7897, 2010.

[37] P.-W. Wang, C.-J. Hsieh, L.-C. Psang et al., "Fatty liver and chronic inflammation in Chinese adults," *Diabetes Research and Clinical Practice*, vol. 81, no. 2, pp. 202–208, 2008.

[38] C.-J. Hsieh, P. W. Wang, and T. H. Hu, "Association of adiponectin gene polymorphism with nonalcoholic fatty liver disease in Taiwanese patients with type 2 diabetes," *PloS One*, vol. 10, no. 6, Article ID e0127521, 2015.

[39] Z. L. Wang, B. Xia, U. Shrestha et al., "Correlation between adiponectin polymorphisms and non-alcoholic fatty liver disease with or without metabolic syndrome in Chinese population," *Journal of Endocrinological Investigation*, vol. 31, no. 12, pp. 1086–1091, 2008.

[40] M. Hashemi, H. Hanafi Bojd, E. Eskandari Nasab et al., "Association of adiponectin rs1501299 and rs266729 gene

polymorphisms with nonalcoholic fatty liver disease," *Hepatitis Monthly*, vol. 13, no. 5, Article ID e9527, 2013.

[41] K. Tokushige, E. Hashimoto, H. Noto et al., "Influence of adiponectin gene polymorphisms in Japanese patients with non-alcoholic fatty liver disease," *Journal of Gastroenterology*, vol. 44, no. 9, pp. 976–982, 2009.

[42] N. C. Leite, G. F. Salles, C. R. L. Cardoso, and C. A. Villela-Nogueira, "Serum biomarkers in type 2 diabetic patients with non-alcoholic steatohepatitis and advanced fibrosis," *Hepatology Research*, vol. 43, no. 5, pp. 508–515, 2013.

[43] H. Lu, J. Sun, L. Sun, X. Shu, Y. Xu, and D. Xie, "Polymorphism of human leptin receptor gene is associated with type 2 diabetic patients complicated with non-alcoholic fatty liver disease in China," *Journal of Gastroenterology and Hepatology*, vol. 24, no. 2, pp. 228–232, 2009.

[44] Z. Zhang, J. Wang, and H. Wang, "Correlation of blood glucose, serum chemerin and insulin resistance with NAFLD in patients with type 2 diabetes mellitus," *Experimental and therapeutic medicine*, vol. 15, no. 3, pp. 2936–2940, 2018.

[45] U. Jung and M.-S. Choi, "Obesity and its metabolic complications: the role of adipokines and the relationship between obesity, inflammation, insulin resistance, dyslipidemia and nonalcoholic fatty liver disease," *International Journal of Molecular Sciences*, vol. 15, no. 4, pp. 6184–6223, 2014.

[46] C. P. Day and O. F. W. James, "Steatohepatitis: a tale of two "hits"?" *Gastroenterology*, vol. 114, no. 4, pp. 842–845, 1998.

[47] G. Targher, C. P. Day, and E. Bonora, "Risk of cardiovascular disease in patients with nonalcoholic fatty liver disease," *New England Journal of Medicine*, vol. 363, no. 14, pp. 1341–1350, 2010.

[48] I. C. M. Simoes, J. Janikiewicz, J. Bauer et al., "Fat and sugar-A dangerous duet. A comparative review on metabolic remodeling in rodent models of nonalcoholic fatty liver disease," *Nutrients*, vol. 11, no. 12, 2019.

[49] S. E. Shoelson, L. Herrero, and A. Naaz, "Obesity, inflammation, and insulin resistance," *Gastroenterology*, vol. 132, no. 6, pp. 2169–2180, 2007.

[50] Y. Arase, K. Shiraishi, K. Anzai et al., "Effect of sodium glucose Co-transporter 2 inhibitors on liver fat mass and body composition in patients with nonalcoholic fatty liver disease and type 2 diabetes mellitus," *Clinical Drug Investigation*, vol. 39, no. 7, pp. 631–641, 2019.

[51] M. Lazo, S. F. Solga, A. Horska et al., "Effect of a 12-month intensive lifestyle intervention on hepatic steatosis in adults with type 2 diabetes," *Diabetes Care*, vol. 33, no. 10, pp. 2156–2163, 2010.

[52] V. W.-S. Wong, G. L.-H. Wong, R. S.-M. Chan et al., "Beneficial effects of lifestyle intervention in non-obese patients with non-alcoholic fatty liver disease," *Journal of Hepatology*, vol. 69, no. 6, pp. 1349–1356, 2018.

[53] S. M. Grundy, N. Abate, and M. Chandalia, "Diet composition and the metabolic syndrome: what is the optimal fat intake?" *Americas Journal of Medicine*, vol. 113, no. Suppl 9B, pp. 25S–9S, 2002.

[54] M. J. Saez-Lara, C. Robles-Sanchez, F. J. Ruiz-Ojeda, J. Plaza-Diaz, and A. Gil, "Effects of probiotics and synbiotics on obesity, insulin resistance syndrome, type 2 diabetes and non-alcoholic fatty liver disease: a review of human clinical trials," *International Journal of Molecular Sciences*, vol. 17, no. 6, 2016.

[55] M. T. Hamilton, D. G. Hamilton, and T. W. Zderic, "Role of low energy expenditure and sitting in obesity, metabolic syndrome, type 2 diabetes, and cardiovascular disease," *Diabetes*, vol. 56, no. 11, pp. 2655–2667, 2007.

[56] B. Wang, X.-L. Mu, J. Zhao et al., "Effects of lifestyle interventions on rural patients with type 2 diabetes mellitus," *World Journal of Diabetes*, vol. 11, no. 6, pp. 261–268, 2020.

[57] N. J. Snowling and W. G. Hopkins, "Effects of different modes of exercise training on glucose control and risk factors for complications in type 2 diabetic patients: a meta-analysis," *Diabetes Care*, vol. 29, no. 11, pp. 2518–2527, 2006.

[58] S. Ryu, Y. Chang, H.-S. Jung et al., "Relationship of sitting time and physical activity with non-alcoholic fatty liver disease," *Journal of Hepatology*, vol. 63, no. 5, pp. 1229–1237, 2015.

[59] E. Hui, A. Xu, H. Bo Yang, and K. S. L. Lam, "Obesity as the common soil of non-alcoholic fatty liver disease and diabetes: role of adipokines," *Journal of Diabetes Investigation*, vol. 4, no. 5, pp. 413–425, 2013.

[60] B. J. Maliakkal, "Pathogenesis of non-alcoholic fatty liver disease and implications on cardiovascular outcomes in liver transplantation," *Translational Gastroenterology and Hepatology*, vol. 5, p. 36, 2020.

[61] G. Firneisz, "Non-alcoholic fatty liver disease and type 2 diabetes mellitus: the liver disease of our age?" *World Journal of Gastroenterology*, vol. 20, no. 27, pp. 9072–9089, 2014.

[62] H. Tilg and A. R. Moschen, "Evolution of inflammation in nonalcoholic fatty liver disease: the multiple parallel hits hypothesis," *Hepatology*, vol. 52, no. 5, pp. 1836–1846, 2010.

[63] C. M. Perdomo, G. Frühbeck, and J. Escalada, "Impact of nutritional changes on nonalcoholic fatty liver disease," *Nutrients*, vol. 11, no. 3, 2019.

[64] J. M. Hazlehurst, C. Woods, T. Marjot, J. F. Cobbold, and J. W. Tomlinson, "Non-alcoholic fatty liver disease and diabetes," *Metabolism*, vol. 65, no. 8, pp. 1096–1108, 2016.

[65] S. Duranti, C. Ferrario, D. van Sinderen, M. Ventura, and F. Turroni, "Obesity and microbiota: an example of an intricate relationship," *Genes & Nutrition*, vol. 12, no. 1, p. 18, 2017.

[66] R. Jamwal, S. M. de la Monte, K. Ogasawara, S. Adusumalli, B. B. Barlock, and F. Akhlaghi, "Nonalcoholic fatty liver disease and diabetes are associated with decreased CYP3A4 protein expression and activity in human liver," *Molecular Pharmaceutics*, vol. 15, no. 7, pp. 2621–2632, 2018.

[67] L. Marino and F. R. Jornayvaz, "Endocrine causes of non-alcoholic fatty liver disease," *World Journal of Gastroenterology*, vol. 21, no. 39, pp. 11053–11076, 2015.

[68] A. S. Butt, S. Hamid, Z. Haider et al., "Nonalcoholic fatty liver diseases among recently diagnosed patients with diabetes mellitus and risk factors," *Euroasian Journal of Hepato-Gastroenterology*, vol. 9, no. 1, pp. 9–13, 2019.

[69] D. Pitocco, M. Di Leo, L. Tartaglione et al., "The role of gut microbiota in mediating obesity and diabetes mellitus," *European Review for Medical and Pharmacological Sciences*, vol. 24, no. 3, pp. 1548–1562, 2020.

[70] K. Mokkala, N. Houttu, T. Cansev, and K. Laitinen, "Interactions of dietary fat with the gut microbiota: evaluation of mechanisms and metabolic consequences," *Clinical Nutrition*, vol. 39, no. 4, pp. 994–1018, 2020.

[71] Y. Ji, Y. Yin, L. Sun, and W. Zhang, "The molecular and mechanistic insights based on gut-liver Axis: nutritional target for non-alcoholic fatty liver disease (NAFLD) improvement," *International Journal of Molecular Sciences*, vol. 21, no. 9, 2020.

[72] Y.-S. Hsu, R.-N. Chien, C.-T. Yeh et al., "Long-term outcome after spontaneous HBeAg seroconversion in patients with chronic hepatitis B," *Hepatology*, vol. 35, no. 6, pp. 1522–1527, 2002.

[73] J. D. Yang, W. R. Kim, R. Coelho et al., "Cirrhosis is present in most patients with hepatitis B and hepatocellular carcinoma," *Clinical Gastroenterology and Hepatology*, vol. 9, no. 1, pp. 64–70, 2011.

[74] S. Dash, Y. Aydin, K. E. Widmer, and L. Nayak, "Hepatocellular carcinoma mechanisms associated with chronic HCV infection and the impact of direct-acting antiviral treatment," *Journal of Hepatocellular Carcinoma*, vol. 7, pp. 45–76, 2020.

[75] J. Giraud, D. Chalopin, J.-F. Blanc, and M. Saleh, "Hepatocellular carcinoma immune landscape and the potential of immunotherapies," *Frontiers in Immunology*, vol. 12, Article ID 655697, 2021.

[76] N. Fujiwara, S. L. Friedman, N. Goossens, and Y. Hoshida, "Risk factors and prevention of hepatocellular carcinoma in the era of precision medicine," *Journal of Hepatology*, vol. 68, no. 3, pp. 526–549, 2018.

[77] N. N. Massarweh and H. B. El-Serag, "Epidemiology of hepatocellular carcinoma and intrahepatic cholangiocarcinoma," *Cancer Control : Journal of the Moffitt Cancer Center*, vol. 24, no. 3, Article ID 1073274817729245, 2017.

[78] F. R. Ponziani, S. Bhoori, C. Castelli et al., "Hepatocellular carcinoma is associated with gut microbiota profile and inflammation in nonalcoholic fatty liver disease," *Hepatology*, vol. 69, no. 1, pp. 107–120, 2019.

[79] K. Friedrich, A. Wannhoff, S. Kattner et al., "PNPLA3 in end-stage liver disease: alcohol consumption, hepatocellular carcinoma development, and transplantation-free survival," *Journal of Gastroenterology and Hepatology*, vol. 29, no. 7, pp. 1477–1484, 2014.

[80] S. Panyod and L.-Y. Sheen, "Beneficial effects of Chinese herbs in the treatment of fatty liver diseases," *Journal of Traditional and Complementary Medicine*, vol. 10, no. 3, pp. 260–267, 2020.

[81] C. Li and J. Pang, "TCM clinical research progress of type 2 diabetes mellitus with nonalcoholic fatty liver disease," *Mass technology*, vol. 21, no. 02, pp. 61–64, 2019.

[82] X. Liu, *Correlation Between TCM Syndrome Types and Islet β Cell Function in Newly Diagnosed Type 2 Diabetes Mellitus Patients with Nonalcoholic Fatty Liver Disease*, Traditional Chinese Medicine University of Gansu, Lanzhou, China, 2017.

[83] Z. Zhang, J. Wu, and Y. Qi, "Clinical study on main risk factors and TCM syndrome types of type 2 diabetes mellitus with nonalcoholic fatty liver disease," *Modern distance education of traditional Chinese medicine in China*, vol. 17, no. 11, pp. 48–50, 2019.

[84] Y. Lu, *Analysis of the Difference and Risk Factors of Insulin Resistance in Different TCM Syndrome Types of Type 2 Diabetes Mellitus with Nonalcoholic Fatty Liver Disease*, Chinese Medical University of Zhejiang, Hangzhou, China, 2013.

[85] T. Gao, L. Yan, and Y. Wang, "Analysis of common TCM syndromes and nonalcoholic fatty liver disease and related risk factors in newly diagnosed type 2 diabetes mellitus," *Journal of Traditional Chinese Medicine in Liaoning*, vol. 38, no. 02, pp. 200–202, 2011.

Hindawi
Journal of Oncology
Volume 2021, Article ID 3392433, 6 pages
https://doi.org/10.1155/2021/3392433

Research Article

Effect of Radiofrequency Ablation with Interventional Therapy of Hepatic Artery on the Recurrence of Primary Liver Cancer and the Analysis of Influencing Factors

Sishuo Zhang,[1] Ge Zhao,[2] and Honglin Dong[3]

[1]*Department of Surgery, Second Hospital of Shanxi Medical University, Taiyuan 030001, Shanxi Province, China*
[2]*Department of General Surgery, Second Hospital of Shanxi Medical University, Taiyuan 030001, Shanxi Province, China*
[3]*Department of Vascular Surgery, Second Hospital of Shanxi Medical University, Taiyuan 030001, Shanxi Province, China*

Correspondence should be addressed to Honglin Dong; donghl645663@163.com

Received 1 June 2021; Accepted 21 September 2021; Published 13 October 2021

Academic Editor: Alamgeer Yuchi

Background. The probability of liver cancer recurring in patients after surgery is a serious threat to liver cancer patients. Radiofrequency ablation is widely employed in liver cancer cases. We explored the therapeutic effects and influencing factors of radiofrequency ablation combined with hepatic artery intervention in patients with recurrence of primary liver cancer surgery. *Methods.* 90 patients with primary liver cancer postoperative recurrence admitted to our hospital from January 2014 to February 2017 were selected as the research objects. The patients were randomly divided into the control group ($n = 45$) and combined treatment group ($n = 45$). The combined treatment group received radiofrequency ablation combined with hepatic artery interventional therapy, and the control group received hepatic artery interventional therapy. The short-term efficacy, AFP levels before and after treatment, and long-term survival results of the two groups were compared. Single-factor and multifactor analyses of the clinical information of the combined treatment group were carried out to find out the factors affecting the therapeutic effect of radiofrequency ablation combined with hepatic artery intervention on patients with recurrence of primary liver cancer. *Results.* The total effective rate of short-term curative effect of the combined treatment group was higher than the control group, and there was a statistically significant difference existing ($P < 0.05$). After treatment, two groups of patients' AFP levels were greatly lower than before treatment, the AFP levels of the combined treatment group were significantly lower than the control group, and there was a statistically significant difference ($P < 0.05$). The survival rates of patients in the combined treatment group at the sixth month, the first year, and the second year after treatment were significantly higher than those of the control group, and there was a statistically significant difference ($P < 0.05$). The univariate results showed that, in the combined treatment group, there were statistically significant differences between the effective group and the ineffective group in tumor diameter, intact capsule, liver cirrhosis, intrahepatic spread, and tumor adjacent to large blood vessels ($P < 0.05$). The outcomes of multivariate analysis indicated that tumor diameter ≥ 3 cm, incomplete capsule, intrahepatic spread, and tumor adjacent to large blood vessels were risk factors for ineffective recurrence of patients with primary liver cancer after radiofrequency ablation combined with hepatic artery intervention ($P < 0.05$). *Discussion.* Tumor diameter ≥ 3 cm, incomplete capsule, intrahepatic spread, and tumor adjacent to large blood vessels are risk factors for the ineffectiveness of radiofrequency ablation combined with hepatic artery interventional therapy for patients with recurrence of primary liver cancer. It is necessary to increase the range of radiofrequency treatment, increase the temperature of the radiofrequency needle, and strengthen postoperative follow-up interventions based on the specific conditions of the patient's tumor.

1. Introduction

Primary liver cancer refers to malignant liver tumors that originate from liver epithelial or mesenchymal tissues. It has the characteristics of high morbidity and high mortality. The clinical manifestations of its patients are pain, fatigue, and jaundice in the liver area [1]. Many patients will have liver cancer recurrence after treatment due to tumor

metastasis, tumor cell residues, and other reasons. Statistics show that the probability of liver cancer recurring in patients within 5 years after surgery is more than 70%, which seriously threatens the long-term postoperative life of liver cancer patients. At present, the clinical treatments commonly used in the therapy of patients with recurrence of liver cancer include radiofrequency ablation and hepatic artery interventional chemotherapy [2, 3]. As thermal ablation therapy, radiofrequency ablation can use its local energy to kill tumor cells and has the advantages of less damage and fewer complications [4]. Radiofrequency ablation is widely applied in the therapy of liver cancer patients. However, there are few clinical reports about the therapeutic effect and influencing factors of radiofrequency ablation combined with hepatic artery intervention in patients with recurrence of primary liver cancer. This study retrospectively analyzed the clinical data and follow-up data of 90 patients with postoperative recurrence of primary liver cancer, observed the therapeutic effect of radiofrequency ablation combined with hepatic artery intervention on patients with postoperative recurrence of primary liver cancer, and analyzed its influencing factors. The research results are reported as follows.

2. Methods

2.1. Normal Information. Ninety patients with postoperative recurrence of primary liver cancer admitted to the Second Hospital of Shanxi Medical University, Taiyuan, Shanxi Province, China, from January 2014 to February 2017 were selected as the research objects. Inclusion criteria were as follows: (1) patients diagnosed with recurrence of primary liver cancer, (2) patients without mental disorders, (3) complete clinical data, and (4) signed informed consent. Exclusion criteria were as follows: (1) patients who have received immunotherapy, (2) patients with extrahepatic metastasis, and (3) patients who do not cooperate with follow-up. This study has been approved by the ethics committee of the Second Hospital of Shanxi Medical University, Taiyuan, Shanxi Province, China.

2.2. Clinical Data Collection. Clinical data of patients, including age, gender, tumor diameter, tumor number, tumor differentiation degree, complete capsule, liver cirrhosis, operation time, intrahepatic spread, pathological type, and tumor adjacent large blood vessels, were collected.

2.3. Radiofrequency Ablation Treatment Methods. Put the patient in the supine position, first locate the tumor, mark the puncture point under CT or B ultrasound, then use lidocaine at a concentration of 0.5% to give the patient local anesthesia, and finally give the patient a radiofrequency ablation treatment [5]. The parameters of the radiofrequency ablation machine are set as follows: the power range is 30–50 W and the temperature range is 90–105°C. When the patient's tumor diameter is less than 3 cm, radiofrequency ablation should be performed after a single-needle single-point puncture, and the ablation time is 8–10 minutes; when the patient's tumor diameter is greater than or equal to 3 cm, multistage multineedle single radiofrequency ablation should be used. The ablation time is 15–20 min [6].

2.4. Hepatic Artery Interventional Therapy. First, the Seldinger technique is used for intubation, and then the patient's celiac trunk arteriography or proper hepatic arteriography is performed to clarify the blood supply arteries of the patient's tumor. Then, under the guidance of DSA, the microcatheter is superselectively pushed into the tumor target vessel to infuse lobaplatin chemotherapeutics, and then a mixture of epirubicin and lipiodol emulsion embolism is injected.

2.5. Observation Index. The clinical efficacy of the two groups of patients was compared, including the following: (1) short-term efficacy: the tumor size was measured one month before and one month after treatment, and the modified solid tumor efficacy evaluation standard (mRECIST) [7, 8] was used to evaluate the efficacy of the patient; efficacy is divided into CR (complete remission: disappearance of all target lesions), PR (partial remission: reduction of the total length of the baseline lesions by at least 30%), SD (stable disease: reduction of the total length of the baseline lesions by less than 30% or the total length diameter increases but the increase is less than 20%), and PD (disease progression: the appearance of new lesions or the total length diameter of the baseline lesions increases by at least 20%); and the total effective rate = (CR + PR) number of cases/total cases × 100%; (2) alpha-fetoprotein (AFP) levels before and after treatment; (3) long-term survival results: the survival rate of patients at the 6th month, 1st year, and 2nd year after treatment. Based on the evaluation results of the solid tumors of the patients, 40 patients in the combined treatment group with complete remission and partial remission were included in the effective group, and 5 patients with disease progression and stable disease in the combined treatment group were included in the ineffective group.

2.6. Statistical Method. Data statistics are carried out using SPSS 23.0 software. Qualitative data are represented by n (%), and the χ^2 test is used for comparison. Quantitative data are represented by $(x \pm s)$, and the t-test is used for comparison. Univariate analysis and logistic regression analysis were conducted to determine the factors affecting the therapeutic effect of radiofrequency ablation combined with hepatic artery intervention on patients with recurrence of primary liver cancer after surgery. $P < 0.05$ indicated statistical differences in the data.

3. Results

3.1. Comparison of the Short-Term Efficacy of the Two Groups of Patients. The total effective rate of combined treatment group was higher than that of control group, and there was a statistically significant difference ($P < 0.05$; Table 1).

Table 1: Comparison of the short-term efficacy of the two groups of patients (n (%)).

Group	n	CR	PR	NC	PD	Total effective rate
Control group	45	20 (44.44)	12 (26.67)	9 (20.0)	4 (8.89)	32 (71.11)
Combined treatment group	45	24 (53.33)	16 (35.56)	4 (8.89)	1 (2.22)	40 (88.89)
χ^2						4.444
P						0.035

Table 2: Comparison of AFP levels and long-term survival results of the two groups of patients (n (%)).

Group	n	AFP (g/L)		Long-term survival outcome		
		Before treatment	After treatment	6 months	1 year	2 years
Control group	45	884.78 ± 78.38	423.64 ± 76.64	39 (86.67)	32 (71.11)	28 (62.22)
Combined treatment group	45	887.36 ± 76.64	218.64 ± 61.47	45 (100.0)	40 (88.89)	37 (82.22)
t/χ^2		0.158	14.003	4.464	4.444	4.486
P		0.875	<0.001	0.026	0.035	0.034

3.2. Comparison of AFP Levels and Long-Term Survival Results between the Two Groups of Patients. No significant difference existed in the AFP levels of the two groups of patients before treatment ($P > 0.05$); the AFP levels of the two groups of patients after treatment were significantly lower than before treatment, and the AFP levels of the combined treatment group were greatly lower than those of the control group. There was a statistically significant difference ($P < 0.05$; Table 2).

3.3. Single-Factor Analysis of the Therapeutic Effect of Radiofrequency Ablation Combined with Hepatic Artery Intervention on Patients with Recurrence of Primary Liver Cancer. Univariate results indicated that no significant difference existed in age, gender, number of tumors, degree of tumor differentiation, intraoperative blood loss, operation time, hepatic port occlusion time, surgical margins, and pathological types between two groups of patients ($P > 0.05$). A statistically significant difference existed between the two groups of patients in tumor diameter, intact capsule, liver cirrhosis, intrahepatic spread, and tumor adjacent to large blood vessels ($P < 0.05$), as shown in Table 3.

3.4. Multifactor Analysis of the Therapeutic Effect of Radiofrequency Ablation Combined with Hepatic Artery Intervention on Patients with Recurrence of Primary Liver Cancer. In univariate analysis, statistically significant influencing factors (tumor diameter, complete capsule, liver cirrhosis, intrahepatic spread, and tumor adjacent to large blood vessels) were used as independent variables, and whether the patient was effective after treatment (effective = 0 and ineffective = 1) is the dependent variable, and the assignment is shown in Table 4. The results of multivariate analysis showed that tumor diameter ≥ 3 cm, incomplete capsule, intrahepatic spread, and tumor adjacent to large blood vessels were risk factors for ineffective recurrence of patients with primary liver cancer after radiofrequency ablation combined with hepatic artery intervention ($P < 0.05$; Table 5).

4. Discussion

The results of this research show that the total effective rate of radiofrequency ablation combined with hepatic artery intervention in patients with recurrence of primary liver cancer after surgery is higher than that of patients with hepatic artery intervention alone. After the treatment, the AFP level of all patients decreased, and the AFP level of the patients who used the radiofrequency ablation combined with hepatic artery intervention method decreased more compared with the patients who used the hepatic artery intervention alone. The survival rates of patients who received radiofrequency ablation combined with hepatic artery interventional therapy at the sixth month, the first year, and the second year were greatly higher than those of patients who received hepatic artery interventional therapy alone. It shows that the therapeutic effect of radiofrequency ablation combined with hepatic artery interventional therapy of patients with recurrence of primary liver cancer after surgery is better.

This study found that tumor diameter ≥ 3 cm, incomplete capsule, intrahepatic spread, and tumor adjacent to large blood vessels were risk factors for ineffective recurrence of patients with primary liver cancer after radiofrequency ablation combined with hepatic artery intervention ($P < 0.05$). The reasons may be as follows: (1) tumor diameter ≥ 3 cm is a risk factor for the ineffectiveness of radiofrequency ablation combined with hepatic artery intervention in patients with recurrence of primary liver cancer after surgery. The larger the diameter of the tumor, the faster the growth of tumor cells and the more likely it is to cause the rupture of the envelope [9], causing the tumor cells to spread to the surrounding tissues beyond the radiofrequency range, causing some tumor cells to fail [10]. Therefore, the efficacy of radiofrequency ablation combined with hepatic artery interventional therapy for patients with recurrent primary liver cancer is not good. Therefore, for patients with larger tumor diameters, the radiofrequency treatment range set by medical staff can be expanded based on the range of the lesion to ensure that all lesions and tumor cells that may be spread in the surrounding tissues are all

Table 3: Single-factor analysis of the therapeutic effect of radiofrequency ablation combined with hepatic artery intervention on patients with recurrence of primary liver cancer after surgery (n (%)).

Factor	Effective group ($n = 40$)	Invalid group ($n = 5$)	t/χ^2	P
Age (years)				
≥60	21 (91.30)	2 (8.70)	0.003	0.958
<60	19 (86.36)	3 (13.64)		
Gender				
Male	22 (91.67)	2 (8.33)	0.025	0.874
Female	18 (85.71)	3 (14.29)		
Tumor diameter (cm)				
≥3	8 (66.67)	4 (33.33)	5.401	0.020
<3	32 (96.97)	1 (3.03)		
Number of tumors (n)				
≥2	17 (85.0)	3 (15.0)	0.070	0.791
<2	23 (92.0)	2 (8.0)		
Tumor differentiation				
I, II grade	28 (93.33)	2 (6.67)	0.703	0.402
III, IV grade	12 (80.0)	3 (20.0)		
Envelope intact				
Yes	33 (97.06)	1 (2.94)	6.321	0.012
No	7 (63.63)	4 (36.36)		
Liver cirrhosis				
Yes	5 (62.50)	3 (37.50)	3.995	0.046
No	35 (94.59)	2 (5.41)		
Intrahepatic spread				
Yes	3 (50.0)	3 (50.0)	6.544	0.011
No	37 (94.87)	2 (5.13)		
Pathological type				
Hepatocellular carcinoma	13 (81.25)	3 (18.75)	0.512	0.474
Cholangiocarcinoma	27 (93.10)	2 (6.90)		
Tumor adjacent to large blood vessels				
Yes	4 (57.14)	3 (42.86)	5.080	0.024
No	36 (94.74)	2 (5.26)		

Table 4: Assignment of factors affecting the therapeutic effect of radiofrequency ablation combined with hepatic artery intervention on patients with recurrence of primary liver cancer after surgery.

Factor	Variable name	Assignment
Tumor diameter	X1	≥3 cm = 1, <3 cm = 0
Envelope intact	X2	No = 1, yes = 0
Liver cirrhosis	X3	No = 1, yes = 0
Intrahepatic spread	X4	No = 1, yes = 0
Tumor adjacent to large blood vessels	X5	No = 1, yes = 0

Table 5: Multifactor analysis of the therapeutic effect of radiofrequency ablation combined with hepatic artery intervention on patients with recurrence of primary liver cancer after surgery.

Factor	B	Wald	P	OR	95% CI
Tumor diameter ≥3 cm	2.399	6.214	0.009	11.021	8.648 (15.636)
Incomplete envelope	2.515	6.587	0.005	12.367	9.347 (16.647)
Liver cirrhosis	1.936	3.987	0.057	6.932	4.624 (8.346)
Intrahepatic spread	2.277	5.947	0.015	9.746	7.348 (13.314)
Tumor adjacent to large blood vessels	2.098	5.647	0.018	8.148	5.364 (11.365)

killed, thereby improving patient efficacy [11, 12]. (2) Incomplete capsule is a risk factor for the failure of radiofrequency ablation combined with hepatic artery intervention in the treatment of patients with recurrence of primary liver cancer. The envelope of liver cancer refers to the extracellular matrix produced by avascular necrosis of the surrounding tissues due to the growth of the tumor [13, 14]. Studies have shown that [15] when the diameter of a

patient's tumor is greater than 5 cm, the capsule is a protective factor for the patient's therapeutic effect. Patients with nonenveloped tumors have a shorter postoperative tumor-free survival period than patients with enveloped tumors. In patients with no tumor envelope, the tumor cells not only easily infiltrate the surrounding blood vessels but also may directly infiltrate the liver. In addition, it will increase the number of microlesions around the tumor [16, 17], resulting in patients without tumor envelope receiving treatment. Sometimes the treatment may be incomplete; there will be residual tumor cells or lesions that have not been cleaned, resulting in poor treatment effects for the patient. Therefore, medical staff should pay more attention to the therapy of patients with noncapsular tumors. After treatment, they should strengthen the follow-up of patients and pay close attention to their prognosis. Once residual lesions are found, they should be treated again in time. (3) Intrahepatic diffusion is a risk factor for the ineffectiveness of radiofrequency ablation combined with hepatic artery intervention in the treatment of patients with recurrence of primary liver cancer. The diffusion and metastasis of intrahepatic tumor in patients may lead to the failure of the lesion to be cleared during the treatment process and the infiltration of intrahepatic blood vessels by HCC cells [13], resulting in poor efficacy of radiofrequency ablation combined with hepatic artery intervention in the treatment of patients with postoperative recurrence of primary liver cancer. Therefore, when locating the tumor location of a patient, medical staff should carefully observe whether the patient has the possibility of intrahepatic metastasis of liver cancer cells [18]. For patients with intrahepatic metastasis of liver cancer cells, medical staff should take effective measures to intervene in time to prevent further diffusion. (4) Tumor adjacent to large blood vessels is a risk factor for the ineffectiveness of radiofrequency ablation combined with hepatic artery intervention in patients with recurrence of primary liver cancer after surgery. When a patient's liver cancer tumor is adjacent to large blood vessels, the temperature around the tumor may decrease due to the flow of blood vessels, thus affecting the effect of radiofrequency ablation and making the ablation incomplete [19]. As a result, the efficacy of radiofrequency ablation combined with hepatic artery intervention in the treatment of patients with recurrent primary liver cancer is not good. On the other hand, the proximity of large blood vessels to the tumor can change the shape of the ablation site, thus affecting the treatment outcome of patients [20, 21]. Therefore, for patients with tumors adjacent to large blood vessels, medical staff should consider increasing the ablation range and increasing the temperature of the radiofrequency needle to improve the treatment effect of the patient [22, 23].

5. Conclusions

In summary, tumor diameter ≥ 3 cm, incomplete capsule, intrahepatic spread, and tumor adjacent to large blood vessels are risk factors for poor therapeutic effect of radiofrequency ablation combined with hepatic artery intervention in patients with recurrent primary liver cancer. It is necessary to increase the range of radiofrequency treatment, increase the temperature of the radiofrequency needle, and strengthen postoperative follow-up interventions based on the specific conditions of the patient's tumor.

Data Availability

All primary data are available from the corresponding author upon reasonable request.

Conflicts of Interest

The authors declare that they have no conflicts of interest.

Authors' Contributions

Sishuo Zhang and Ge Zhao contributed equally to this work.

References

[1] S. T. Orcutt and D. A. Anaya, "Liver resection and surgical strategies for management of primary liver cancer," *Cancer Control : Journal of the Moffitt Cancer Center*, vol. 25, no. 1, Article ID 1073274817744621, 2018.

[2] A. Shiani, S. Narayanan, L. Pena, and M Friedman, "The role of diagnosis and treatment of underlying liver disease for the prognosis of primary liver cancer," *Cancer Control : Journal of the Moffitt Cancer Center*, vol. 24, no. 3, Article ID 1073274817729240, 2017.

[3] S. Jeong, B. Zheng, H. Wang, Q. Xia, and L. Chen, "Nervous system and primary liver cancer," *Biochimica et Biophysica Acta (BBA) - Reviews on Cancer*, vol. 1869, no. 2, pp. 286–292, 2018.

[4] F. Izzo, V. Granata, R. Grassi et al., "Radiofrequency ablation and microwave ablation in liver tumors: an update," *The Oncologist*, vol. 24, no. 10, pp. e990–e1005, 2019.

[5] L. Cui, L. Kong, Y.-H. Bai et al., "Covered stent placement for hepatic artery pseudoaneurysm," *Abdominal Radiology*, vol. 45, no. 10, pp. 3337–3341, 2020.

[6] N. Harada, T. Yoshizumi, H. Uchiyama et al., "Impact of middle hepatic artery reconstruction after living donor liver transplantation using the left lobe," *Clinical Transplantation*, vol. 34, no. 6, Article ID e13850, 2020.

[7] N. Vietti Violi, R. Duran, B. Guiu et al., "Efficacy of microwave ablation versus radiofrequency ablation for the treatment of hepatocellular carcinoma in patients with chronic liver disease: a randomised controlled phase 2 trial," *The Lancet Gastroenterology & Hepatology*, vol. 3, no. 5, pp. 317–325, 2018.

[8] R. Lencioni and J. M. Llovet, "Modified RECIST (mRECIST) assessment for hepatocellular carcinoma," *Seminars in Liver Disease*, vol. 30, no. 1, pp. 52–60, 2010.

[9] X.-D. Zhou, Z.-Y. Tang, Z.-C. Ma et al., "Surgery for large primary liver cancer more than 10 cm in diameter," *Journal of Cancer Research and Clinical Oncology*, vol. 129, no. 9, pp. 543–548, 2003.

[10] S. T. Schindera, R. C. Nelson, D. M. DeLong, and B. Clary, "Intrahepatic tumor recurrence after partial hepatectomy: value of percutaneous radiofrequency ablation," *Journal of Vascular and Interventional Radiology*, vol. 17, no. 10, pp. 1631–1637, 2006.

[11] W.-M. Cong, H. Bu, J. Chen et al., "Practice guidelines for the pathological diagnosis of primary liver cancer: 2015 update,"

World Journal of Gastroenterology, vol. 22, no. 42, pp. 9279–9287, 2016.

[12] F. Yang, Z. Qian, F. Sun et al., "Laparoscopic enucleation of hepatic cysts reduces the recurrence of nonparasitic hepatic cysts," *Journal of Laparoendoscopic & Advanced Surgical Techniques*, vol. 31, no. 3, pp. 314–319, 2021.

[13] L. Song, J. Li, and Y. Luo, "The importance of a nonsmooth tumor margin and incomplete tumor capsule in predicting HCC microvascular invasion on preoperative imaging examination: a systematic review and meta-analysis," *Clinical Imaging*, vol. 76, pp. 77–82, 2020.

[14] G. E. Chung, W. Kim, J.-H. Lee et al., "Negative hepatitis B envelope antigen predicts intrahepatic recurrence in hepatitis B virus-related hepatocellular carcinoma after ablation therapy," *Journal of Gastroenterology and Hepatology*, vol. 26, no. 11, pp. 1638–1645, 2011.

[15] F. Ridouani, S. B. Solomon, Y. Bryce, J. F. Bromberg, C. T. Sofocleous, and A. R. Deipolyi, "Predictors of progression-free survival and local tumor control after percutaneous thermal ablation of oligometastatic breast cancer: retrospective study," *Journal of Vascular and Interventional Radiology*, vol. 31, no. 8, pp. 1201–1209, 2020.

[16] M. Alvarado-Kristensson and C. A. Rosselló, "The biology of the nuclear envelope and its implications in cancer biology," *International Journal of Molecular Sciences*, vol. 20, no. 10, p. 2586, 2019.

[17] M. Gao, C. Liang, X. Song et al., "Erythrocyte-membrane-enveloped perfluorocarbon as nanoscale Artificial red blood cells to relieve tumor hypoxia and enhance cancer radiotherapy," *Advanced Materials*, vol. 29, no. 35, 2017.

[18] P. Karayiannis, "Hepatitis B virus: virology, molecular biology, life cycle and intrahepatic spread," *Hepatology International*, vol. 11, no. 6, pp. 500–508, 2017.

[19] T. Chen, D. Guo, Z. Fang, W. Zhong, J. Zhao, and Y. Jiang, "Preliminary study of whole-brain CT perfusion imaging in patients with intracranial tumours adjacent to large blood vessels," *Clinical Radiology*, vol. 69, no. 1, pp. e25–e32, 2014.

[20] H. Xie, H. Wang, W. An et al., "The efficacy of radiofrequency ablation combined with transcatheter arterial chemoembolization for primary hepatocellular carcinoma in a cohort of 487 patients," *PLoS One*, vol. 9, no. 2, Article ID e89081, 2014.

[21] Y. Zhu, L. Gu, T. Chen, G. Zheng, C. Ye, and W. Jia, "Factors influencing early recurrence of hepatocellular carcinoma after curative resection," *Journal of International Medical Research*, vol. 48, no. 8, Article ID 300060520945552, 2020.

[22] Z.-Y. Lin, J. Chen, and X.-F. Deng, "Treatment of hepatocellular carcinoma adjacent to large blood vessels using 1.5T MRI-guided percutaneous radiofrequency ablation combined with iodine-125 radioactive seed implantation," *European Journal of Radiology*, vol. 81, no. 11, pp. 3079–3083, 2012.

[23] H.-W. Huang, "Influence of blood vessel on the thermal lesion formation during radiofrequency ablation for liver tumors," *Medical Physics*, vol. 40, no. 7, Article ID 073303, 2013 Jul.

Hindawi
Journal of Oncology
Volume 2021, Article ID 2483964, 7 pages
https://doi.org/10.1155/2021/2483964

Research Article

Clinical Value of Serum Thrombospondin-2 Combined with CA19-9 in Early Diagnosis of Gastric Cancer

Lanzhi Li,[1] **Jie Dong**,[2] **Lei Fu**,[3] **Xinhua Xia**,[4] **Feng Pan**,[4] **and Yuan Ning**[5]

[1]*Health Examination Department, Yantaishan Hospital, Yantai 64000, China*
[2]*Department of Clinical Laboratory, Yantai Yuhuangding Hospital Affiliated To Qingdao University, Yantai 264000, China*
[3]*PIVAS, Affiliated Qingdao Central Hospital, Qingdao University, Qingdao 266000, China*
[4]*Ward Department, Zhangqiu District People's Hospital, Jinan 250200, China*
[5]*Supply Support Center, The Central Hospital Affiliated to Shandong First Medical University, 105 Jiefang Road, Jinan 250013, Shandong, China*

Correspondence should be addressed to Yuan Ning; yuanning@jnzxhospital.cn

Received 1 June 2021; Revised 14 July 2021; Accepted 15 September 2021; Published 7 October 2021

Academic Editor: Alamgeer Yuchi

Gastric cancer (GC) is a kind of common cancer worldwide. Too late in diagnosis results in poor prognosis of patients with GC. Thrombospondin-2 (THBS2) is a type of secreted protein that has been found to be a diagnostic biomarker in a variety of cancers. Our study aimed to uncover the clinical value of THBS2 in early detection for patients with gastric cancer. THBS2 was upregulated in gastric cancer tissue compared with normal tissue via analyzing data obtained from The Cancer Genome Atlas (TCGA) database. Additionally, the enzyme-linked immunosorbent assay revealed that the level of serum THBS2 and carcinoembryonic antigen, CA19-9, was higher dramatically in patients with early gastric cancer (EGC) than that in healthy control (HC) in addition to patients with benign gastric tumor (BGT), which suggested that THBS2 indeed associated with GC. Receiver operator characteristic (ROC) curve assay was conducted to demonstrate that serum THBS2 was similar to CA19-9 to distinguish patients with early gastric cancer from healthy control and patients with benign gastric tumor and that THBS2 combined with CA19-9 improved the detective performance of THBS2 for early gastric cancer. Furthermore, we applied the gene set enrichment analysis assay to analyze signaling pathways related to THBS2. We found that THBS2 positively controlled MAPK and WNT signaling pathways, which indicated that THBS2 might exert its functions via the pathway mentioned above. Thus, our study expounded that serum THBS2 could serve as a vital early diagnostic marker for patients with gastric cancer.

1. Introduction

Gastric cancer (GC) as the fourth leading tumor results in third most main death rate that is related to cancers in the world [1]. The disease incidence and mortality of GC maintains high in both East Asian and Central South American countries including China, Korea, Mexico, and Chile [2, 3]. Early gastric cancer can invade either mucosa or submucosa, which is accompanied by metastasis of the lymph node or not [4]. Late detection, in addition to insensitivity to existing treatment options, causes a poor prognosis of GC [5]. For an optimum period of therapy, it is necessary to diagnose GC as early as possible. Recently, advanced technologies such as screening are employed to raise diagnosis proportion of early gastric cancer [6]. Carcinoembryonic antigen, CA19-9, and other detection methods are available to predict GC [7]. Serum markers are easier to detect than other test indexes; therefore, they are used widely to diagnose early gastric cancer [8]. The most sensitive serum index for diagnosing GC, however, is still uncovered [9]. Thus, it is urgent to explore new and highly effective biomarkers to boost the detective accuracy of early GC [10].

Thrombospondins (THBSs), a family belonging to Ca^{2+} binding glycoproteins, are secretions of immune cells and mesenchymal cells in addition to endotheliocytes [11]. They

can bind to plenty of downstream proteins involved in various biological procedures, including cell migration, blood vessel production, apoptosis, and cytoskeletal regulation [12, 13]. In multiple malignancies, THBS2 is tight correlated with progression and prognosis of cancers [14]. Tokunaga et al. discovered that the expression of THBS2 in colon cancer decreased hepatic metastases risk as well as angiogenesis of tumors compared to patients lacking THBS2 [15]. Additionally, THBS2 had been found to exert a vital impact on lung adenocarcinoma, prostate cancer, myeloid tumor, and breast cancer [16, 17]. Nevertheless, the specific effect of THBS2, in addition to its clinical value for gastric cancer, is not disclosed now. Therefore, we are trying to expose its clinical significance in the detection of early gastric cancer.

2. Materials and Methods

2.1. Patients and Samples. This is a prospective study. Blood was obtained from 41 healthy individuals, 33 benign gastric tumor patients, and 46 early gastric cancer patients at Yantaishan Hospital, Yantai, China. The benign or early stage of cancer was confirmed by the principle of the American Joint Committee on Cancer (AJCC) TNM (tumor–node–metastasis) classification. Blood was centrifuged; then, serum was collected and stored at −80°C freezer. Basic information such as age, gender, and amounts of samples are given in Table 1. All participants voluntarily participated in our studies, and all protocols related to human volunteers were abiding by the guidance of the Helsinki Declaration. All patients provided written informed consent, and the study was approved by the Ethics Committee of the Yantaishan Hospital, Yantai, China.

2.2. Gene Set Enrichment Analysis (GSEA). To verify the molecular signaling pathway related to the high expression of THBS2, GSEA was conducted by using GSEA 3.0 software. Specific gene sets were downloaded from the official website (http://software.broadinstitute.org/gsea/index.jsp) and analyzed for pathway enrichment.

2.3. Enzyme-Linked Immunosorbent Assay (ELISA). The protein levels of THBS2 and CA19-9 in serum were examined by the ELISA kit (ThermoFisher, USA). Serum from early gastric cancer (EGC), benign gastric tumor (BGT), or healthy control (HC) was incubated with a microtiter plate which had been treated with capture antibodies for 1 hour at room temperature. Then, the plate was washed and incubated with a specific antibody for 0.5 hour at room temperature, followed by washing the plate. Then, the secondary antibody was added into plate, and reaction was terminated by a stop solution. A microplate reader (BioRad, CA) was employed to record the absorbance at 450 nm. The detailed protocol was in accordance with the reagent specification.

2.4. Statistical Analysis. All data were analyzed by using SPSS 19.0 software (IBM, USA) and GraphPad 8.0 software (CABIT, China) for calculating statistical significance and was presented in a manner of mean ± standard deviation (SD). The correlation between THBS2 and CA19-9 was measured by Pearson's correlation analysis. Receiver operator characteristic (ROC) curves were drawn to estimate the diagnostic performance. All relevant data are given in Table 2. $P < 0.05$ is statistically significant.

Table 1: Basic information.

Diagnosis	Healthy control	Benign gastric tumor	Early gastric cancer
Sex			
Male	22	15	25
Female	19	18	21
Age			
Mean	55	53	58
Range	21–67	20–65	24–71
Amount	41	33	46

Table 2: Data of ROC curve.

	AUC	95% CI
HC vs. EGC		
THBS2	0.816	0.722–0.911
CA19.9	0.901	0.833–0.968
THBS2 + CA19.9	0.951	0.912–0.989
BGT vs. EGC		
THBS2	0.840	0.752–0.927
CA19.9	0.847	0.762–0.931
THBS2 + CA19.9	0.928	0.872–0.984

*$P < 0.05$ in comparison with CA19.9.

3. Results

3.1. The Level of THBS2 Is Increased in Gastric Cancer Tissues. The load of THBS2 in tumor tissues and normal tissues of patients diagnosed with gastric cancers was analyzed by deferential analysis as well as paired differential analysis on the basis of data from The Cancer Genome Atlas (TCGA) database. The mean level of THBS2 in gastric cancer tissues was obviously higher than that in control tissues ($P < 0.001$, Figures 1(a) and 1(b)). The data showed that serum THBS2 was potential to be secreted by gastric cancer tissues.

3.2. Increased Level of THBS2 in Serum of Patients with Early Gastric Cancer. To confirm results mentioned above, an ELISA was conducted to measure the load of serum THBS2 in 46 patients with EGC or 33 patients with BGT in addition to 41 HC. The results illustrated that the protein level of serum THBS2 in people with EGC was upregulated dramatically compared with that in HC and BGT patients. Additionally, the load of serum THBS2 in BGT patients was higher than that in HC ($P < 0.05$, Figure 2(a)). CA19-9, a common biomarker for GC, was also estimated by the ELISA assay. As shown in Figure 2(b), the level of serum CA19-9 was the highest in EGC patients while the lowest in HC, which is consistent with the load of serum THBS2 ($P < 0.05$, Figure 2(b)).

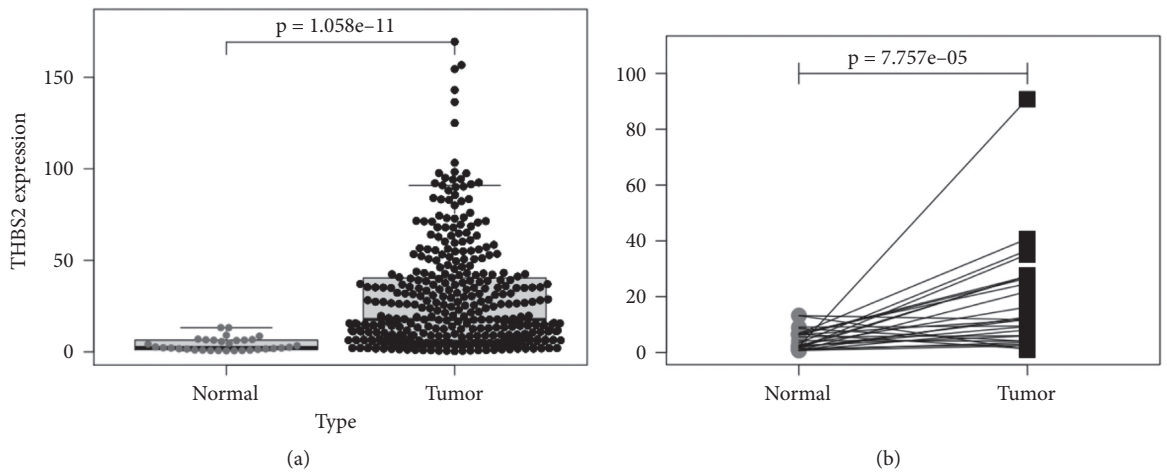

Figure 1: The level of THBS2 increased in gastric cancer tissues. (a) Data from TCGA website are deferential analyzed. (b) Data from TCGA website are paired deferential analyzed.

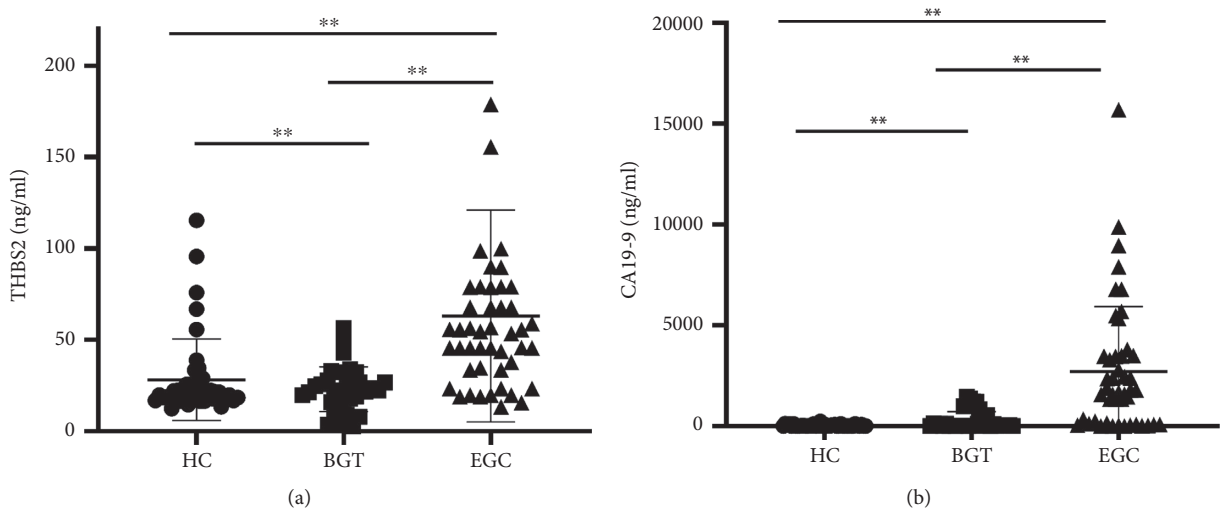

Figure 2: Increased level of THBS2 in serum of patients with early gastric cancer. (a) The level of serum THBS2 in various samples measured by the ELISA assay ($P < 0.05$). (b) The level of serum CA19-9 in various samples measured by the ELISA assay ($P < 0.05$).

3.3. The Correlation between Serum THBS2 and CA19-9. To reveal how serum THBS2 influences the detection of early gastric cancer, we made scatter plots based on the level of serum THBS2 in addition to CA19-9 and analyzed their relationship. Interestingly, there was no obvious correlation between THBS2 and CA19-9 in health controls sample ($P = 0.157$) as well as benign patients sample ($P = 0.292$), while there existed a significant correlation in patients with early gastric cancer ($P = 0.04$) (Figures 3(a)–3(c)).

3.4. The Detected Performance of THBS2 and CA19-9 for Early Gastric Cancer. ROC curve analysis was employed to explore the performance of early diagnosis about serum THBS2 and CA19-9 in patients with GC (Figure 4(a)). Additionally, we listed all data obtained from the above analysis, including area under the curve (AUC) and asymptotic 95% confidence interval in Table 2. Serum THBS2 possessed well capacity to forecast early gastric cancer with the value of AUC: 0.816 (95% CI: 0.722–0.911). Serum CA19-9 distinguished patients with EGC from healthy control with the value of AUC of 0.901 (95% CI: 0.833–0.968). Furthermore, serum THBS2 combined with CA19-9 as a marker could promote the performance of THBS2 or CA19-9 as an individual index (AUC: 0.951, 95% CI: 0.912–0.989). Subsequently, we conducted the ROC curve to uncover whether THBS2 and CA19-9 differentiated patients with EGC from patients with BGT. As shown in Figure 4(b), the data showed that THBS2 or CA19-9 was able to predict early gastric cancer as an individual biomarker and combined THBS2 with CA19-9 could improve the diagnostic performance dramatically. All detailed data are given in Table 2.

3.5. THBS2 Plays a Vital Role in GC via Potentially Regulating MAPK and WNT Signaling Pathway. To further explore the functional mechanism of serum THBS2 on GC, we

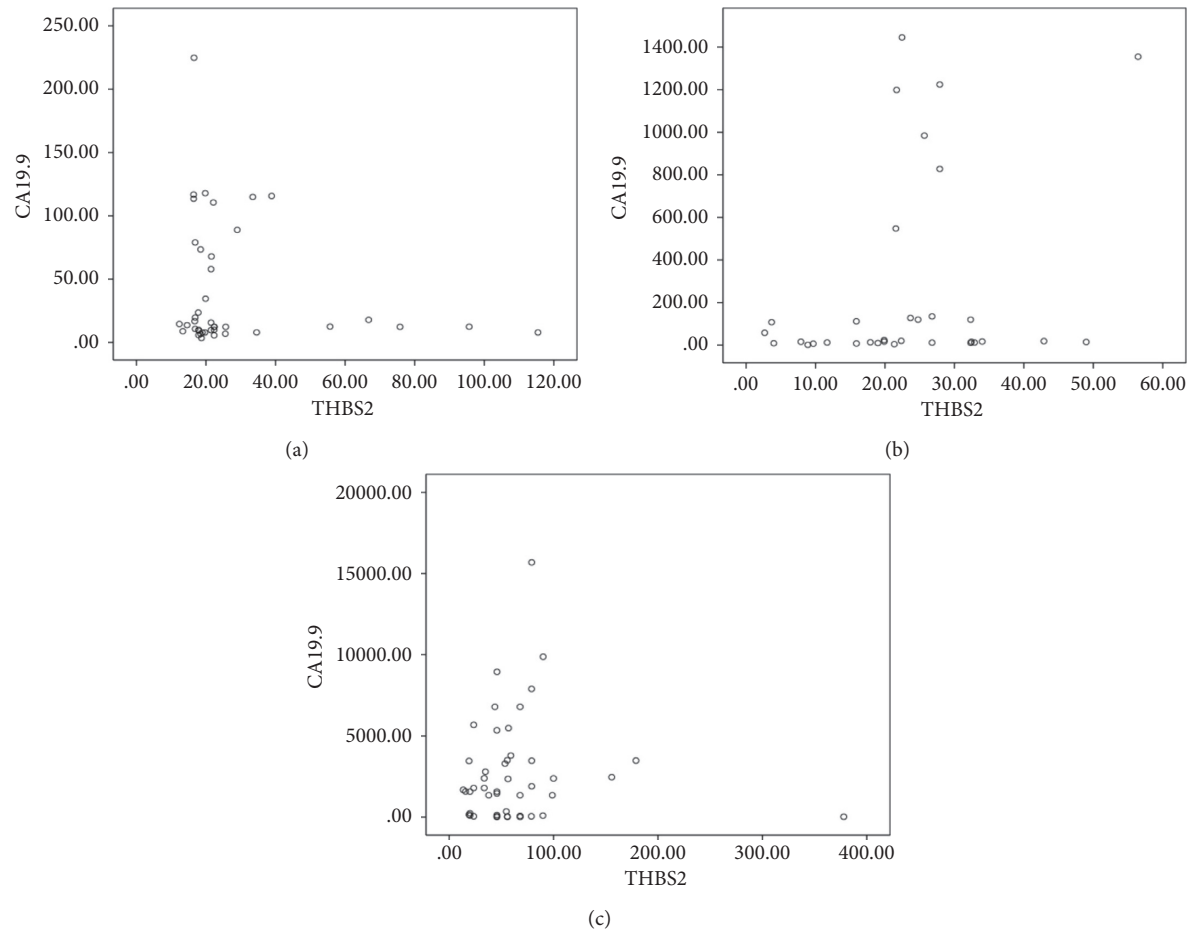

Figure 3: The correlation between serum THBS2 and CA19-9. (a) The correlation between THBS2 and CA19-9 in HC. (b) The correlation between THBS2 and CA19-9 in patients with BGT. (c) The correlation between THBS2 and CA19-9 in patients with EGC.

conducted the GSEA assay with data from the TCGA database and analyzed the THBS2-related pathway. The GSEA enrichment plot showed that high THBS2 expression was positively enriched in mitogen-activated protein kinase (MAPK) as well as Wnt-β/catenin signaling pathway and exhibited a tightly positive relationship with multiple downstream genes involved in the pathway as mentioned earlier (Figures 5(a) and 5(b)).

4. Discussion

Increasing novel technologies, including liquid biopsy, have been employed to diagnose cancers; however, various proteins lack sensitivity in addition to specificity for applying into clinical practice [17]. More blood-based markers such as serum proteins possess the ability to offer information that is associated with the progression of cancers timely [18]. Therefore, serum biomarkers related to the early stage of cancers are required to diagnose and follow up patients with malignancy. Recently, emerging studies have revealed various markers that possess potential to detect gastric cancer in the early stage. For example, serum amyloid A cluster (SAA) and high mobility group box 1 (HMGB1) can be regarded as significant biomarkers for early diagnosis of GC [19]. Thymidine kinase 1 (TK1), CA19-9, and CA72-4 combined with other carcinoembryonic antigen exhibited better detection ability of GC and colorectal cancer (CRC) [20].

THBS2, one of the proteins belonging to thrombospondin family, has been reported to serve as a vital regulator of tumorigenesis [21]. In multiple cancers, decreasing the expression of THBS2 can trigger production of oncogenes or depress production of tumor suppresser genes. Upregulating THBS2 in cancer tissues is correlated to inhibit progression of tumors sometimes [15, 22, 23]. Simpson RE et al. found that THBS2 was a biomarker of pancreatic ductal adenocarcinoma and related to a high rate of dysplasia in sufferers with premalignant symptoms [24]. Liu et al. reported that it accelerates lung cancer progression through producing matrix metalloproteinase-13 [25]. In addition, serum THBS2 has been regarded as a valuable clinical marker for various cancers. For example, THBS2 has the ability to forecast prognosis for patients with colorectal cancer [26]. Downregulating THBS2 exerts utterly opposite functions on the clinical outcome of sufferers with gastric cancer [27, 28]. Nevertheless, no enough research studies devoted into uncovering the clinical value of serum THBS2 for diagnosing early gastric cancer.

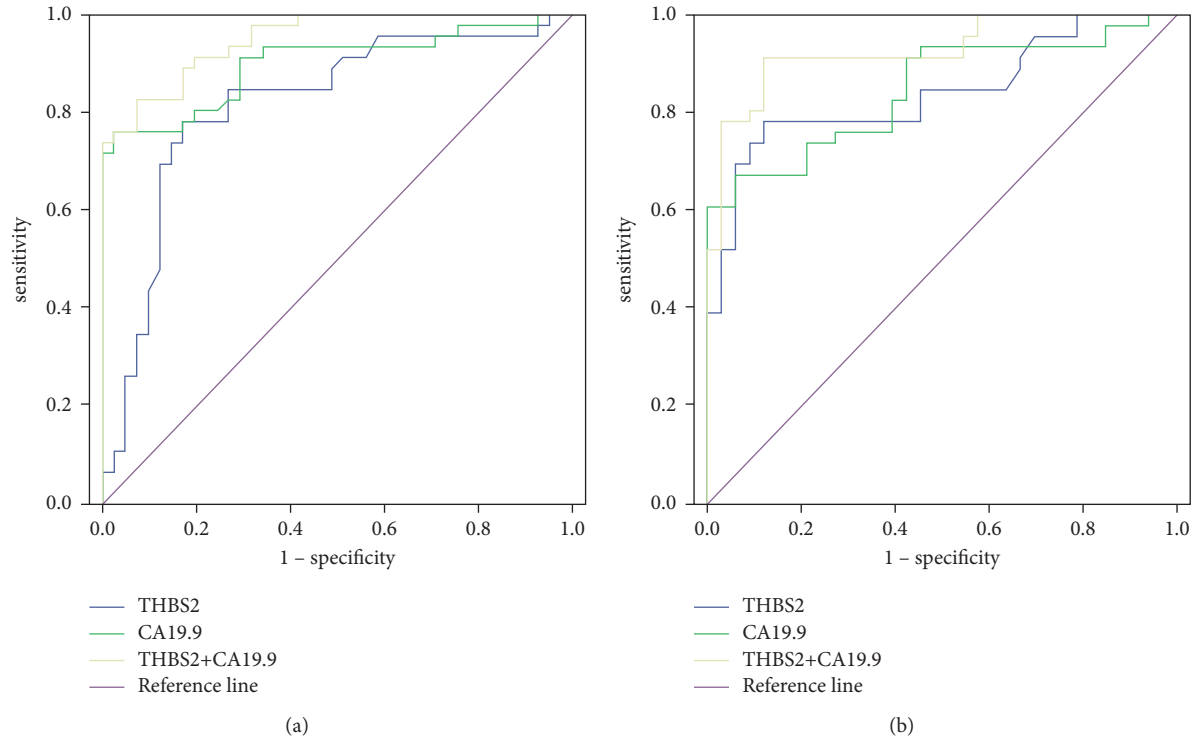

Figure 4: The detected performance of THBS2 and CA19-9 for early gastric cancer. (a) Diagnostic performance of THBST in addition to CA19-9 to differentiate early gastric cancer patients from a healthy control. (b) Diagnostic performance of THBST in addition to CA19-9 to differentiate early gastric cancer patients from benign gastric tumor patients.

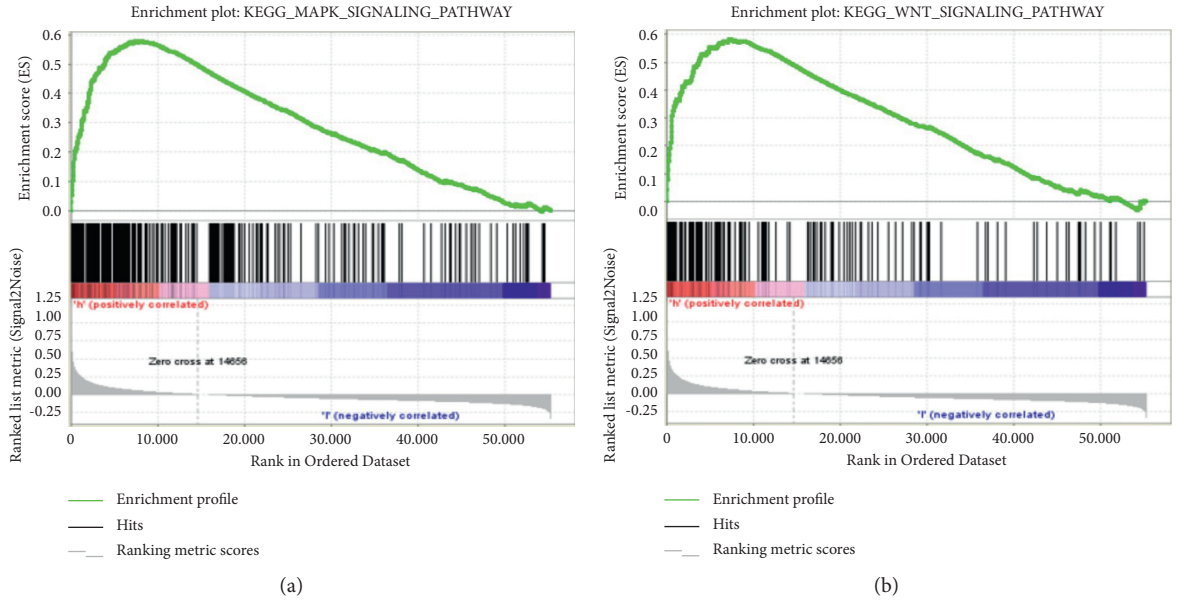

Figure 5: THBS2 playing a vital role in GC via potentially regulating MAPK and WNT signaling pathways. (a) Genes related to MAPK signaling pathway positively enriched by THBS2. (b) Genes related to WNT signaling pathway positively enriched by THBS2.

In our present study, we first analyzed data from the TCGA database and found that THBS2 was upregulated dramatically in gastric cancer tumor, which indicated that THBS2 might exert a crucial role in GC. To confirm the hypothesis, we collected tissue samples from 41 cases of HC and 33 cases of BGT in addition to 46 cases of EGC to measure the serum load of THBS2 by using ELISA assay. The results demonstrated that the level of serum THBST

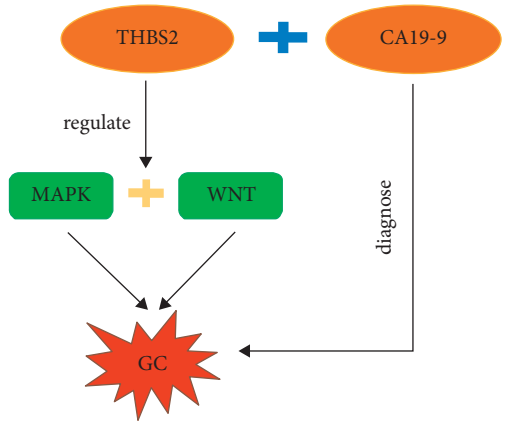

Figure 6: Schematic diagram of THBS2 regulating GC and THBS2 combined CA19-9 existing better performance in diagnosing GC.

was upregulated in patients with EGC compared to patients with BGT as well as HC significantly, implying that the increase of THBS2 was an important marker of GC. According to previous studies, the performance will get better to combine THBS2 and CA19-9 in detecting pancreatic ductal adenocarcinoma and distal cholangiocarcinoma [29]. Bamlet et al. discovered that THBS2 had good detection performance in tumors combined with CA19-9 [30]. Chen et al. revealed that THBS2 as one of biomarkers could be replenished by CA19-9 for diagnosing colorectal cancer [31]. Given these reporters, we assumed THBS2 combined CA19-9 may exert better performance in diagnosing GC. Subsequently, we further conducted the ELISA assay and found the load of CA19-9 in serum of patients diagnosed with EGC was higher than that in EGT as well as in HC, which illustrated that cancer tissues were likely to produce more THBS2 in serum in accordance with former research studies [32, 33]. In addition, there exhibited an obvious correlation between THBS2 and CA19-9 in patients with ECG ($P = 0.04$) but not in HC ($P = 0.157$) and patients with EGT ($P = 0.292$) according to correlation analysis, indicating that both THBS2 and CA19-9 play an essential role in diagnosis of early GC. Next, ROC curve analysis was employed to reveal that THBS2 possessed a comparable ability to differentiate patients with EGC from HC and patients with EGT to CA19-9. Additionally, the detective capacity was notably improved when we combined THBS2 and CA19-9 as the diagnostic marker. Moreover, GSEA was employed to uncover that THBS2 positively related with the MAPK and Wnt-β/catenin signaling pathway, implying the potential regulatory mechanism of serum THBS2 on gastric cancer first, eventhough it was also necessary to conduct more experiments to explore the detailed mechanisms (Figure 6).

There are still some limitations to our study. For example, our investigation did not conduct sufficient experiments to explore the detailed functions of THBS2 combined CA19-9 for GC in vivo. Moreover, we have not identified the direct target gene for THBS2. Additionally, more attention need to be paid to identify that whether THBS2 combined with CA19-9 exert equally dramatic effects on early detection of other cancers.

5. Conclusion

In conclusion, our study uncovered that THBS2 was upregulated in GC tissues and positively regulated MAPK in addition to the WNT signaling pathway. Moreover, both THBS2 and CA19-9 could serve as significant and excellent biomarkers for detecting GC in the early stage. Additionally, THBS2 combined CA19-9 exhibited better performance in the diagnosis of early GC, which may improve diagnostic efficiency for patients with GC.

Data Availability

The data used to support the findings of this study are included within the article.

Conflicts of Interest

The authors declare that they have no conflicts of interest.

Authors' Contributions

Lanzhi Li and Jie Dong contributed equally to this work.

References

[1] L. A. Torre, F. Bray, R. L. Siegel, J. Ferlay, J. Lortet-Tieulent, and A. Jemal, "Global cancer statistics," *CA: A Cancer Journal for Clinicians*, vol. 65, pp. 87–108, 2012.

[2] W. Chen, R. Zheng, P. D. Baade et al., "Cancer statistics in China, 2015," *CA: A Cancer Journal for Clinicians*, vol. 66, no. 2, pp. 115–132, 2016.

[3] M. S. Sierra, P. Cueva, L. E. Bravo, and D. Forman, "Stomach cancer burden in central and South America," *Cancer Epidemiology*, vol. 44, no. Suppl 1, pp. S62–S73, 2016.

[4] F. Feng, L. Sun, G. Xu et al., "Is it reasonable to treat early gastric cancer with mucosal infiltration and well differentiation by endoscopic submucosal resection?" *Journal of Gastrointestinal Surgery*, vol. 19, no. 12, pp. 2111–2119, 2015.

[5] J. Wang, Y. Liu, W. Sun, Q. Zhang, T. Gu, and G. Li, "Plasma exosomes as novel biomarker for the early diagnosis of gastric cancer," *Cancer Biomarkers*, vol. 21, no. 4, pp. 805–812, 2018.

[6] L. Zhu, J. Qin, J. Wang, T. Guo, Z. Wang, and J. Yang, "Early gastric cancer: current advances of endoscopic diagnosis and treatment," *Gastroenterology Research and Practice*, vol. 2016, Article ID 9638041, 7 pages, 2016.

[7] X. Zhu, M. Lv, H. Wang, and W. Guan, "Identification of circulating microRNAs as novel potential biomarkers for gastric cancer detection: a systematic review and meta-analysis," *Digestive Diseases and Sciences*, vol. 59, no. 5, pp. 911–919, 2014.

[8] S.-B. Tian, J.-C. Yu, W.-M. Kang et al., "Combined detection of CEA, CA 19-9, CA 242 and CA 50 in the diagnosis and prognosis of resectable gastric cancer," *Asian Pacific Journal of Cancer Prevention*, vol. 15, no. 15, pp. 6295–6300, 2014.

[9] Z. Jin, W. Jiang, and L. Wang, "Biomarkers for gastric cancer: progression in early diagnosis and prognosis (review)," *Oncology Letters*, vol. 9, no. 4, pp. 1502–1508, 2015.

[10] W. K. Leung, M.-S. Wu, Y. Kakugawa et al., "Screening for gastric cancer in Asia: current evidence and practice," *The Lancet Oncology*, vol. 9, no. 3, pp. 279–287, 2008.

[11] P. Bornstein, "Thrombospondins function as regulators of angiogenesis," *Journal of Cell Communication and Signaling*, vol. 3, no. 3-4, pp. 189–200, 2009.

[12] O. I. Stenina, E. J. Topol, and E. F. Plow, "Thrombospondins, their polymorphisms, and cardiovascular disease," *Arteriosclerosis, Thrombosis, and Vascular Biology*, vol. 27, no. 9, pp. 1886–1894, 2007.

[13] J. C. Adams and J. Lawler, "The thrombospondins," *Cold Spring Harbor Perspectives in Biology*, vol. 3, no. 10, Article ID a009712, 2011.

[14] J. Lawler and M. Detmar, "Tumor progression: the effects of thrombospondin-1 and -2," *The International Journal of Biochemistry & Cell Biology*, vol. 36, no. 6, pp. 1038–1045, 2004.

[15] T. Tokunaga, M. Nakamura, Y. Oshika et al., "Thrombospondin 2 expression is correlated withinhibition of angiogenesis and metastasis of coloncancer," *British Journal of Cancer*, vol. 79, 1999.

[16] T. Chijiwa, Y. Abe, N. Ikoma et al., "Thrombospondin 2 inhibits metastasis of human malignant melanoma through microenvironment-modification in NOD/SCID/γCnull (NOG) mice," *International Journal of Oncology*, vol. 34, 1992.

[17] E. Heitzer, S. Perakis, J. B. Geigl, and M. R. Speicher, "The potential of liquid biopsies for the early detection of cancer," *Npj Precision Oncology*, vol. 1, no. 1, p. 36, 2017.

[18] A. Li, T. Zhang, M. Zheng, Y. Liu, and Z. Chen, "Exosomal proteins as potential markers of tumor diagnosis," *Journal of Hematology & Oncology*, vol. 10, no. 1, p. 175, 2017.

[19] A. A. Ghweil, H. A. Osman, M. H. Hassan et al., "Validity of serum amyloid A and HMGB1 as biomarkers for early diagnosis of gastric cancer," *Cancer Management and Research*, vol. 12, pp. 117–126, 2020.

[20] S. Ning, W. Wei, J. Li et al., "Clinical significance and diagnostic capacity of serum TK1, CEA, CA 19-9 and CA 72-4 levels in gastric and colorectal cancer patients," *Journal of Cancer*, vol. 9, no. 3, pp. 494–501, 2018.

[21] W. Naumnik, M. Ossolińska, I. Płońska, E. Chyczewska, and J. Nikliński, "Circulating thrombospondin-2 and FGF-2 in patients with advanced non-small cell lung cancer: correlation with survival," *Advances in Experimental Medicine and Biology*, vol. 833, pp. 9–14, 2015.

[22] G. Bocci, G. Francia, S. Man, J. Lawler, and R. S. Kerbel, "Thrombospondin 1, amediator of the antiangiogenic effects of low-dose metronomic chemotherapy," *Proceedings of the National Academy of Sciences*, vol. 100, 2003.

[23] M. Streit, L. Riccardi, P. Velasco et al., "Thrombospondin-2: a potent endogenous inhibitor o ftumor growth and angiogenesis," *Proceedings of the National Academy of Sciences*, vol. 96, no. 26, pp. 14888–14893, 1999.

[24] R. E. Simpson, M. T. Yip-Schneider, H. Wu et al., "Circulating Thrombospondin-2 enhances prediction of malignant intraductal papillary mucinous neoplasm," *The American Journal of Surgery*, vol. 217, no. 3, pp. 425–428, 2019.

[25] J.-F. Liu, C.-W. Lee, M.-H. Tsai et al., "Thrombospondin 2 promotes tumor metastasis by inducing matrix metalloproteinase-13 production in lung cancer cells," *Biochemical Pharmacology*, vol. 155, pp. 537–546, 2018.

[26] X. Wang, L. Zhang, H. Li, W. Sun, H. Zhang, and M. Lai, "THBS2 is a potential prognostic biomarker in colorectal cancer," *Scientific Reports*, vol. 6, no. 1, Article ID 33366, 2016.

[27] R. Sun, J. Wu, Y. Chen et al., "Down regulation of Thrombospondin2 predicts poor prognosis in patients with gastric cancer," *Molecular Cancer*, vol. 13, no. 1, p. 225, 2014.

[28] C. Zhuo, X. Li, H. Zhuang et al., "Elevated THBS2, COL1A2, and SPP1 expression levels as predictors of gastric cancer prognosis," *Cellular Physiology and Biochemistry*, vol. 40, no. 6, pp. 1316–1324, 2016.

[29] T. Y. S. Le Large, L. L. Meijer, R. Paleckyte et al., "Combined expression of plasma thrombospondin-2 and CA19-9 for diagnosis of pancreatic cancer and distal cholangiocarcinoma: a proteome approach," *The Oncologist*, vol. 25, pp. e634–e643, 2020.

[30] J. Kim, W. R. Bamlet, A. L. Oberg et al., "Detection of early pancreatic ductal adenocarcinoma with thrombospondin-2 and CA19-9 blood markers," *Science Translational Medicine*, vol. 9, no. 11, pp. 1–13, 2017.

[31] W. Fei, L. Chen, J. Chen et al., "RBP4 and THBS2 are serum biomarkers for diagnosis of colorectal cancer," *Oncotarget*, vol. 8, no. 54, pp. 92254–92264, 2017.

[32] T.-Y. Weng, C.-Y. Wang, Y.-H. Hung, W.-C. Chen, Y.-L. Chen, and M.-D. Lai, "Differential expression pattern of THBS1 and THBS2 in lung cancer: clinical outcome and a systematic-analysis of microarray databases," *PLoS One*, vol. 11, no. 8, Article ID e0161007, 2016.

[33] R. Navab, D. Strumpf, B. Bandarchi et al., "Prognostic gene-expression signature of carcinoma-associated fibroblasts in non-small cell lung cancer," *Proceedings of the National Academy of Sciences*, vol. 108, no. 17, pp. 7160–7165, 2011.

Hindawi
Journal of Oncology
Volume 2021, Article ID 4529915, 5 pages
https://doi.org/10.1155/2021/4529915

Research Article

Effect of Paroxetine Combined with Probiotics in Patients with Type 2 Diabetes Mellitus Complicated with Gastrointestinal Dysfunction and Liver Cancer

Yi Peng,[1] Xingxia Yang,[2] and Yeju Wang[3]

[1]*Department of Emergency, Wuhan Central Hospital Chinese Construction Third Engineering Bureau, Wuhan 430070, Hubei, China*
[2]*Department of Infectious Disease, Shandong Binzhou Optimal Care Hospital, Binzhou 256606, Shandong, China*
[3]*Department of Endocrine, Hanzhong Central Hospital, Hanzhong 723000, Shaanxi, China*

Correspondence should be addressed to Yeju Wang; wangyeju@hzcch.cn

Received 25 June 2021; Accepted 14 July 2021; Published 7 October 2021

Academic Editor: Muhammad Wasim Khan

Background. To explore the effect of paroxetine combined with probiotics in patients with type 2 diabetes mellitus with gastrointestinal dysfunction and liver cancer and its effect on nutritional status. *Materials and Methods*. 96 patients with type 2 diabetes mellitus combined with gastrointestinal dysfunction and liver cancer were selected as subjects from March 2018 to March 2021. They were randomly divided into control group and observation group, with 48 cases in each group. The control group was treated with probiotics, and the observation group was combined with paroxetine on the basis of the control group. After 4 weeks of treatment, the gastrointestinal mucosal function, nutritional status, Hamilton Depression Scale (HAMD) and Hamilton Anxiety Scale (HAMA) score, and the safety were compared between the two groups. *Results*. The levels of D-lactic acid, PCT, and endotoxin in the observation group were (1.75 ± 0.38), (4.39 ± 0.79), and (0.20 ± 0.06), respectively, which were significantly lower than those in the control group (2.69 ± 0.46), (7.84 ± 1.32), and (0.29 ± 0.08) ($P < 0.05$). Moreover, the nutritional status TP, ALB, Hb, PA, and TLC levels of the observation group were higher than those of the control group ($P < 0.05$). The HAMA and HAMD scores in the observation group were (5.76 ± 1.06) and (8.94 ± 1.26), respectively, which were significantly lower than those in the control group (10.69 ± 2.21) and (13.42 ± 2.34) ($P < 0.05$). However, there was no statistical significance in the incidence of nausea and vomiting, blurred vision, chest arthralgia, palpitation, anaesthesia, dizziness, and drowsiness between the two groups ($P > 0.05$). *Conclusions*. Paroxetine combined with probiotics could help to improve the gastrointestinal mucosal function of patients with type 2 diabetes mellitus complicated with gastrointestinal dysfunction and liver cancer, improve the nutritional status of patients, and reduce anxiety and depression, and the drug was safe and worthy of promotion and application.

1. Introduction

Liver cancer can be divided into primary liver cancer and secondary liver cancer. The former originates from the epithelial or mesenchymal tissue of the liver and the latter is caused by the metastasis of other tumors [1]. Epidemiological studies have confirmed that the incidence of primary liver cancer is increasing year by year, with an annual increase of over 700,000 cases, and primary liver cancer has now become the second leading cause of cancer-related deaths worldwide [2]. In China, about 383,000 people die of liver cancer every year, accounting for about 51% of the world's total. Liver cancer has become the fourth most common malignant tumor in China, with a poor prognosis and low survival rate [3, 4].

In recent years, with the change of people's lifestyles, diabetes has become one of the major chronic noncommunicable diseases affecting global health, and its prevalence has been increasing year by year [5]. Gastrointestinal dysfunction is one of the common chronic complications in patients with type 2 diabetes. It is more common in people with a long history of diabetes and older

people and the clinical manifestations are heartburn, early satiety, postprandial discomfort, constipation or diarrhea, etc. [6]. Given the rapidly increasing incidence of liver cancer and type 2 diabetes, the number of people living with both diseases is also growing. Previous studies have shown that the mechanism of type 2 diabetes with gastrointestinal dysfunction and liver cancer has not yet been clarified, which might be related to autonomic nerve dysfunction, intestinal flora imbalance, smooth muscle damage, and gastrointestinal hormonal disorders, etc. [7]. Other studies have shown that dysregulation of the brain-gut axis can cause changes in intestinal movement and visceral perception, and patients are often accompanied by depression and psychological anxiety disorders, aggravating abnormalities and disorders of the digestive system [8, 9].

Probiotics are commonly used clinical gastrointestinal regulators, which can directly supplement the body's normal physiological bacteria and maintain the normal intestinal flora [10, 11]. Paroxetine is a commonly used clinical antidepressant, which can selectively inhibit 5-hydroxytryptamine (5-HT) transporter, block the reuptake of 5-HT by the presynaptic membrane, and exert an antidepressant effect [12]. This present study was aimed to explore the effect of paroxetine combined with probiotics in patients with type 2 diabetes mellitus complicated with gastrointestinal dysfunction and liver cancer. The report was as follows.

2. Materials and Methods

2.1. Clinical Data. Ninety-six patients with type 2 diabetes mellitus combined with gastrointestinal dysfunction and liver cancer were selected from March 2018 to March 2021 at Wuhan Central Hospital Chinese Construction Third Engineering Bureau, Wuhan, Hubei, China, and they were randomly divided into observation group and control group, with 48 cases in each group. Control group: 31 males and 17 females, age (41–73) years old, average (60.39 ± 5.61) years old, body mass index (BMI) (18–29) kg/m^2, average (23.51 ± 3.49) kg/m^2, duration of type 2 diabetes (1–15) years, average (9.15 ± 0.95) years, duration of gastrointestinal disorders (1–6) years, average (3.23 ± 0.51) years, and complications: 3 cases of hypertension, high 6 cases of lipemia. Observation group: 29 males and 19 females, aged (42–74) years old, average (60.46 ± 5.68) years old, BMI (17–30) kg/m^2, average (23.68 ± 3.54) kg/m^2, type 2 diabetes course (1–16) years, average (9.21 ± 0.99) years, gastrointestinal dysfunction course (1–7) years, average (3.32 ± 0.58) years, and complications: 4 cases of hypertension, 5 cases of hyperlipidemia. There was no statistically significant difference in general information between the two groups of patients ($P > 0.05$), and they were comparable. The study was approved by the ethics committee of Wuhan Central Hospital Chinese Construction Third Engineering Bureau, Wuhan, Hubei, China, and informed consent was obtained from the patients.

2.2. Inclusion and Exclusion Criteria. Inclusion criteria: (1) meeting the diagnostic criteria for type 2 diabetes, with different degrees of gastrointestinal dysfunction. (2) Meeting the diagnostic criteria for liver cancer, and diagnosed by pathological examination. (3) Meeting paroxetine, probiotics drug therapy indications; no history of drug allergy. (4) Completing baseline and follow-up data.

Exclusion criteria: (1) severe liver and kidney dysfunction or taking glucocorticoids or immune enhancers in the past 3 months. (2) Mental disorders, organic diseases, or blood system diseases. (3) Cognitive dysfunction; abnormal blood coagulation function.

2.3. Method. After admission, both groups were given symptomatic and supportive treatment intervention. Individuals with type 2 diabetes should eat low-salt and low-fat foods and fresh vegetables and fruits and strengthen the rehabilitation exercise according to the patients' recovery. Control groups were treated with probiotics. Patients took 2 capsules of probiotics (*Bifidobacterium*, *Enterococcus,* and *Lactobacillus acidophilus*) capsules (Shandong Hengjia Biotechnology Co., Ltd., sc11337082906741) each time, orally, 3 times a day. According to the patient's tolerance and response, the drug dose was increased appropriately according to the drug instructions. Observation groups were combined with paroxetine treatment on the basis of the control group. The initial dose of paroxetine (Zhejiang Huahai Pharmaceutical Co., Ltd., National Medicine Standard H20031106, specification: 20 mg) was 5 mg each time, orally, and the drug dose was increased every 5 days (the drug dose is 20 mg), and other psychotropic drugs were avoided during treatment. Effects for each patient were evaluated after 4 weeks of treatment.

2.4. Observation Indicators. (1) Gastrointestinal mucosal function: the modified enzymatic spectrophotometry was used to determine the D-lactic acid level before treatment and 4 weeks after treatment. A quantitative immunoluminescence method was used to determine the patient's procalcitonin (PCT) level [13]. (2) Nutritional status: an automatic biochemical analyzer was used to determine the total protein (TP), hemoglobin (Hb), prealbumin (PA), total lymphocyte count of the patients (TLC), and serum albumin (ALB) levels [14]. (3) Psychological fluctuations: the Hamilton Depression Scale (HAMD) and Hamilton Anxiety Scale (HAMA) were used to evaluate the psychological fluctuations of the patients before and 4 weeks after treatment. The lower the score, the better the effect [15, 16]. (4) Security: the incidence of nausea and vomiting, blurred vision, chest palpitations, palpitation, akathisia, dizziness, and drowsiness during the two groups was recorded.

2.5. Statistical Analysis. SPSS24.0 software was used to measure the statistical data. The count data were analyzed by $\chi 2$ test, expressed by n (%). D-Lactic acid, PCT, endotoxin, and other measurement data were in accordance with the normal distribution and analyzed by t test, expressed by ($\overline{x} \pm s$). $P < 0.05$ was considered as statistically significant.

3. Results

3.1. Comparison of Gastrointestinal Mucosal Function between the Two Groups. The function of gastrointestinal mucosa before treatment in the two groups was not statistically significant ($P > 0.05$). The gastrointestinal mucosal function of the two groups was improved 4 weeks after treatment. The levels of D-lactic acid, PCT, and endotoxin in the observation group were lower than those in the control group ($P < 0.05$), as shown in Table 1.

3.2. Comparison of Nutritional Status between the Two Groups. The nutritional status of the two groups before treatment was not statistically significant ($P > 0.05$). After 4 weeks of treatment, the nutritional status of the two groups was significantly improved, and the nutritional status of the observation group was higher than that of the control group ($P < 0.05$), as shown in Table 2.

3.3. Comparison of Psychological Fluctuations between the Two Groups. Psychological fluctuations before treatment in the two groups were not statistically significant ($P > 0.05$). Four weeks after treatment, the psychological symptoms of the two groups were significantly improved ($P < 0.05$); the HAMA and HAMD scores of the observation group were lower than those of the control group ($P < 0.05$), as shown in Table 3.

3.4. Comparison of the Safety of the Two Groups. The incidence of nausea and vomiting, blurred vision, chest palpitations, akathisia, and dizziness and drowsiness during the treatment of the two groups was not statistically significant ($P > 0.05$), as shown in Table 4.

4. Discussion

With the change of lifestyle, diabetes has become the third most harmful disease to human health after malignant tumors and cardiovascular and cerebrovascular diseases, and its morbidity and mortality have been on the rise year by year. In 2013, 3.82 billion people were diagnosed with diabetes, which is expected to increase to 5.92 billion worldwide [17]. Yancik et al. confirmed that the 30-month mortality of breast cancer patients with diabetes was 76% higher than that of patients without diabetes after adjusting for age and staging [18]. At the same time, another clinical study showed that after adjusting for age, sex, and stage, the mortality rate of colon cancer patients with diabetes increased by 37% [19]. A randomized adjuvant chemotherapy study conducted by Pechlivanis et al. also confirmed that 287 colon cancer patients with diabetes mellitus had a 42% increased risk of death and a 21% increased rate of tumor recurrence [20]. Previous studies have shown that the intestine is the "second brain" of humans. The continuous stress response will cause mental and psychological abnormalities, which will cause hyperesthesia in the intestines and internal organs in patients with type 2 diabetes and gastrointestinal dysfunction. Meanwhile, the increased sensitivity threshold of the intestine will cause intestinal spasms and abnormal motility [21, 22]. Therefore, the search for specific drugs for early prediction of liver cancer with diabetes has important clinical significance.

In recent years, paroxetine combined with probiotics has been used in patients with type 2 diabetes with gastrointestinal dysfunction and liver cancer, and the effect is ideal [23]. In this study, the levels of D-lactic acid, PCT, and endotoxin in the observation group were lower than those in the control group ($P < 0.05$) 4 weeks after treatment, indicating that paroxetine combined with probiotics can improve gastrointestinal dysfunction in patients with type 2 diabetes and liver cancer, which is beneficial to the recovery of patients. Probiotics are commonly used clinical gastrointestinal regulators, which can directly supplement the normal physiological bacteria of the body and maintain the normal intestinal flora [24]. Moreover, probiotics can inhibit and remove potentially harmful bacteria in the intestines and can regulate the disorder of the body's microecological balance [10]. Previous studies have shown that probiotics can help patients rebuild and protect the gastrointestinal flora barrier, thereby organizing the invasion of foreign pathogenic bacteria, inhibiting endotoxins produced by harmful bacteria, reducing the translocation of bacteria and endotoxins in the intestines, maintaining the structural integrity of the gastrointestinal tract and enhancing the local defense ability of the gastrointestinal mucosa [25].

In this study, the nutritional status TP, ALB, Hb, PA, and TLC levels of the observation group were higher than those of the control group 4 weeks after treatment ($P < 0.05$). The HAMA and HAMD scores of the observation group were lower than those of the control group 4 weeks after treatment ($P < 0.05$), indicating that paroxetine can improve the psychological fluctuations of patients with type 2 diabetes and gastrointestinal dysfunction and improve the nutritional status of patients. Clinically, paroxetine combined with probiotics can be used in patients with type 2 diabetes with gastrointestinal dysfunction and liver cancer, which can give play to the advantages of different drugs. Moreover, the combined use of the drugs is safer, which helps to improve patient tolerance and compliance. In addition, the incidence of nausea and vomiting, blurred vision, chest palpitations, akathisia, and dizziness and drowsiness during the treatment of the two groups was not statistically significant ($P > 0.05$), indicating that paroxetine combined with probiotics is safer in the treatment of type 2 diabetes with gastrointestinal dysfunction and liver cancer.

Table 1: Comparison of gastrointestinal mucosal function between the two groups ($\overline{x} \pm s$).

Group		D-Lactic acid (mmol/L)	PCT (ug/L)	Endotoxin (EU/mL)
Observation group ($n = 48$)	Before treatment	3.10 ± 0.53	10.43 ± 2.14	0.33 ± 0.08
	Four weeks after treatment	$1.75 \pm 0.38^{\#*}$	$4.39 \pm 0.79^{\#*}$	$0.20 \pm 0.06^{\#*}$
Control group ($n = 48$)	Before treatment	3.12 ± 0.55	10.45 ± 2.16	0.35 ± 0.10
	Four weeks after treatment	$2.69 \pm 0.46^{*}$	$7.84 \pm 1.32^{*}$	$0.29 \pm 0.08^{*}$

$^{\#}P < 0.05$ vs control group; $^{*}P < 0.05$ vs before treatment.

Table 2: Comparison of nutritional status between the two groups ($\overline{x} \pm s$).

Group		TP (g/L)	ALB (g/L)	Hb (g/L)	PA (mg/L)	TLC ($\times 10^9$/L)
Observation group ($n = 48$)	Before treatment	50.39 ± 2.63	28.51 ± 4.69	97.35 ± 6.73	144.39 ± 12.59	1.16 ± 0.21
	Four weeks after treatment	$64.53 \pm 4.59^{\#*}$	$35.63 \pm 5.71^{\#*}$	$119.69 \pm 10.69^{\#*}$	$191.56 \pm 14.66^{\#*}$	$1.82 \pm 0.53^{\#*}$
Control group ($n = 48$)	Before treatment	50.41 ± 2.64	28.52 ± 4.70	97.37 ± 6.75	145.41 ± 12.62	1.17 ± 0.23
	Four weeks after treatment	$58.59 \pm 4.31^{*}$	$30.59 \pm 5.36^{*}$	$105.63 \pm 8.52^{*}$	$158.96 \pm 13.48^{*}$	$1.35 \pm 0.51^{*}$

$^{\#}P < 0.05$ vs control group; $^{*}P < 0.05$ vs before treatment.

Table 3: Comparison of psychological fluctuations between the two groups (points $\overline{x} \pm s$).

Group	Case	HAMA		HAMD	
		Before treatment	Four weeks after treatment	Before treatment	Four weeks after treatment
Observation group	48	24.69 ± 3.57	$5.76 \pm 1.06^{\#}$	28.63 ± 4.35	$8.94 \pm 1.26^{\#}$
Control group	48	24.72 ± 3.59	$10.69 \pm 2.21^{\#}$	28.66 ± 4.38	$13.42 \pm 2.34^{\#}$
T	—	0.583	12.593	1.448	10.336
P value	—	0.409	<0.001	0.925	<0.001

$^{\#}P < 0.05$ vs before treatment.

Table 4: Comparison of the safety of the two groups (n (%)).

Group	Case	Sick and vomiting	Blurred vision	Chest palpitations	Cannot sit still	Dizziness and drowsiness	Incidence
Observation group	48	0 (0.00)	1 (2.08)	0 (0.00)	1 (2.08)	1 (2.08)	3 (6.25)
Control group	48	1 (2.08)	1 (2.08)	1 (2.08)	0 (0.00)	1 (2.08)	4 (8.3)
x^2	—						0.154
P value	—						0.695

5. Conclusion

Paroxetine combined with probiotics can help improve gastrointestinal mucosal function in patients with type 2 diabetes complicated with gastrointestinal dysfunction and liver cancer, help improve the nutritional status of patients, and reduce anxiety and depression. The drug is safe and worthy of promotion and application.

Data Availability

The datasets used and/or analyzed during the present study are available from the corresponding author on reasonable request.

Disclosure

The funding body had no role in the design of the study, collection, analysis, and interpretation of data, or writing of the manuscript.

Conflicts of Interest

The authors declare that they have no conflicts of interest.

Acknowledgments

The authors sincerely appreciate the contributions to this work made in various ways by all of the participants.

References

[1] C. Young, A. Subramonian, and C. Argaez, *Yttrium-90 Microspheres for Intermediate-or Advanced-Stage Hepatocellular Carcinoma*, Canadian Agency for Drugs and Technologies in Health, Ottawa, Canada, 2021.

[2] J. Ferlay, I. Soerjomataram, R. Dikshit et al., "Cancer incidence and mortality worldwide: sources, methods and major patterns in GLOBOCAN 2012," *International Journal of Cancer*, vol. 136, no. 5, pp. E359–E386, 2015.

[3] F. S. Wang, J. G. Fan, Z. Zhang, B. Gao, and H. Y. Wang, "The global burden of liver disease: the major impact of China," *Hepatology*, vol. 60, no. 6, pp. 2099–2108, 2014.

[4] W. Chen, R. Zheng, P. D. Baade et al., "Cancer statistics in China, 2015," *CA: A Cancer Journal for Clinicians*, vol. 66, no. 2, pp. 115–132, 2016.

[5] D. H. Jiang, B. F. Mundell, N. D. Shah, and R. G. McCoy, "Impact of high deductible health plans on diabetes care

quality and outcomes: systematic review," *Endocrine Practice*, vol. S1530-891X, no. 21, 2021.

[6] M. Y. A. Ghafar, H. Yaakup, R. A. R. Ali, and S. A. Shah, "Evaluation of the efficacy of probiotics (mcp BCMC strains) treating constipation in elderly patients with multiple chronic co-morbidities: a randomized control trial," *The Journal of Nutrition, Health & Aging*, vol. 24, no. 10, pp. 1066–1072, 2020.

[7] V. Annese, G. Bassotti, N. Caruso et al., "Gastrointestinal motor dysfunction, symptoms, and neuropathy in non-insulin-dependent (type 2) diabetes mellitus," *Journal of Clinical Gastroenterology*, vol. 29, no. 2, pp. 171–177, 1999.

[8] C.-M. Chao, C.-C. Hsu, C.-C. Huang et al., "Selective brain cooling achieves peripheral organs protection in hemorrhagic shock resuscitation via preserving the integrity of the brain-gut axis," *International Journal of Medical Sciences*, vol. 18, no. 13, pp. 2920–2929, 2021.

[9] S. H. Jang, Y. S. Woo, S. Y. Lee, and W. M. Bahk, "The brain-gut-microbiome axis in psychiatry," *International Journal of Molecular Sciences*, vol. 21, 2020.

[10] E. Montassier, R. Valdes-Mas, E. Batard et al., "Probiotics impact the antibiotic resistance gene reservoir along the human GI tract in a person-specific and antibiotic-dependent manner," *Nature Microbiology*, vol. 6, pp. 1043–1054, 2021.

[11] S. Salminen, M. C. Collado, A. Endo et al., "Publisher correction: the international scientific association of probiotics and prebiotics (ISAPP) consensus statement on the definition and scope of postbiotics," *Nature Reviews Gastroenterology & Hepatology*, vol. 18, no. 9, p. 671, 2021.

[12] S. C. Waye, O. C. Dinesh, S. N. Hasan et al., "Antidepressant action of transcranial direct current stimulation in olfactory bulbectomised adolescent rats," *Journal of Psychopharmacology*, vol. 35, no. 8, pp. 1003–1016, 2021.

[13] M. Potjo, A. J. Theron, R. Cockeran et al., "Interleukin-10 and interleukin-1 receptor antagonist distinguish between patients with sepsis and the systemic inflammatory response syndrome (SIRS)," *Cytokine*, vol. 120, pp. 227–233, 2019.

[14] X. Zhu, H. Zhang, F. Shang, K. Zang, and X. Zhang, "[Effect of intensive insulin therapy on high mobility group box-1/nuclear factor-kappaB pathway in severe traumatic brain injury patient with stress hyperglycemia]," *Zhonghua Wei Zhong Bing Ji Jiu Yi Xue*, vol. 31, pp. 949–952, 2019.

[15] Q. Chen, G. Yang, S. Lin et al., "The effects of mindfulness-based stress reduction therapy combined with intensive education on the effectiveness of the care and the awareness rate in patients with arthritis and diabetes," *American Journal of Tourism Research*, vol. 13, no. 4, pp. 3190–3197, 2021.

[16] J. Komorousova, J. Beran, Z. Rusavy, and Z. Jankovec, "Glycemic control improvement through treatment of depression using antidepressant drugs in patients with diabetes mellitus type 1," *Neuroendocrinology Letters*, vol. 31, pp. 801–806, 2010.

[17] L. Guariguata, D. R. Whiting, I. Hambleton, J. Beagley, U. Linnenkamp, and J. E. Shaw, "Global estimates of diabetes prevalence for 2013 and projections for 2035," *Diabetes Research and Clinical Practice*, vol. 103, no. 2, pp. 137–149, 2014.

[18] R. Yancik, M. N. Wesley, L. A. G. Ries et al., "Comorbidity and age as predictors of risk for early mortality of male and female colon carcinoma patients: a population-based study," *Cancer*, vol. 82, no. 11, pp. 2123–2134, 1998.

[19] J. A. Meyerhardt, P. J. Catalano, D. G. Haller et al., "Impact of diabetes mellitus on outcomes in patients with colon cancer," *Journal of Clinical Oncology*, vol. 21, no. 3, pp. 433–440, 2003.

[20] S. Pechlivanis, K. Wagner, J. Chang-Claude, M. Hoffmeister, H. Brenner, and A. Försti, "Polymorphisms in the insulin like growth factor 1 and IGF binding protein 3 genes and risk of colorectal cancer," *Cancer Detection and Prevention*, vol. 31, no. 5, pp. 408–416, 2007.

[21] M. Avetisyan, E. M. Schill, and R. O. Heuckeroth, "Building a second brain in the bowel," *Journal of Clinical Investigation*, vol. 125, no. 3, pp. 899–907, 2015.

[22] W.-L. Chou, "Therapeutic potential of targeting intestinal bitter taste receptors in diabetes associated with dyslipidemia," *Pharmacological Research*, vol. 170, Article ID 105693, 2021.

[23] Y. Chen, Y. Wang, H. Jin, D. Zhang, D. Li, and H. Zhang, "The effect of probiotic probio-fit combined with metformin on the efficacy and intestinal flora structure in patients with type 2 diabetes," *Chinese Journal of Food Science*, vol. 19, no. 4, pp. 16–26, 2019.

[24] C. Huang, X. Li, L. Wu et al., "The effect of different dietary structure on gastrointestinal dysfunction in children with cerebral palsy and epilepsy based on gut microbiota," *Brain and Development*, vol. 43, no. 2, pp. 192–199, 2021.

[25] J. He, X. Xia, W. Tian, Y. Li, and Z. Li, "Effects of early enteral nutrition support through nasal jejunum tube combined with probiotics on nutritional status and intestinal mucosal damage in patients with severe acute pancreatitis," *Journal of Clinical and Pathology*, vol. 40, no. 11, pp. 149–155, 2020.

Hindawi
Journal of Oncology
Volume 2021, Article ID 1620891, 6 pages
https://doi.org/10.1155/2021/1620891

Research Article

Intervention Effect of Probiotics in Gastric Cancer Patients with Complications of Coronary Heart Disease and Heart Failure

Hui Yu,[1,2] **Anqin Dong**,[2] **Luosha Zhao**,[1] **Ping Li**,[3] **Qiujun Zhang**,[4] **Juying Lu**,[5] **and Ling Li**[1]

[1]*Department of Cardiology, The First-Affiliated Hospital of Zhengzhou University, Zhengzhou 450052, China*
[2]*Department of Rehabilitation Medicine, The Fifth-Affiliated Hospital of Zhengzhou University, Zhengzhou 450052, China*
[3]*Department of Medicine, Henan Medical College, Zhengzhou 451191, China*
[4]*Department of Nursing, The Fifth-Affiliated Hospital of Zhengzhou, Zhengzhou 450052, China*
[5]*Department of Cardiopulmonary Rehabilitation, The Fifth-Affiliated Hospital of Zhengzhou, Zhengzhou 450052, China*

Correspondence should be addressed to Ling Li; liling875320@163.com

Received 29 June 2021; Accepted 15 September 2021; Published 7 October 2021

Academic Editor: Alamgeer Yuchi

Objective. To investigate the characteristics of intestinal flora in patients with gastric cancer complicated by coronary heart disease and heart failure and the guiding value of probiotics intervention for clinical treatment. *Methods*. (1) One hundred and sixty-eight gastric cancer patients with complications of coronary heart disease and heart failure from August 2017 to December 2020 were selected as the observation group. A total of 125 patients with coronary heart disease treated at the same time were selected as control group 1, and 89 healthy subjects were selected as control group 2. Fecal samples were retained to extract the total RNA, and high-throughput sequencing was applied to complete the analysis of microbial diversity and structure differences, so as to obtain the biological species information of the specimens. (2) Patients in the observation group were randomly divided into two equal groups of 84 patients, namely, group A and group B. Group A was treated with conventional methods, and group B was combined with probiotics intervention on the basis of group A; then, the differences in the intestinal mucosal barrier between the two groups were compared. *Results*. The Chao, ACE, and Simpson index in the observation group were lower than those in control group 1 ($P < 0.05$), and the Shannon index was higher than that in control group 1 ($P < 0.05$). The Chao, ACE, and Shannon index in control group 1 were lower than those in control group 2 ($P < 0.05$), whereas the Simpson index was higher than in control group 2 ($P < 0.05$). The abundance of *Bacteroidetes* in the observation group was lower than that in control group 1 and control group 2 ($P < 0.05$). The abundance of *Firmicutes* was higher than that of control group 1 and control group 2 ($P < 0.05$). Four weeks after treatment, the levels of ET, D-lactic acid, and PCT in the group B were (0.10 ± 0.01), (3.99 ± 0.32), and (0.41 ± 0.10), respectively, which were lower than those in group A (0.19 ± 0.03), (4.51 ± 0.46), and (0.81 0.13). *Conclusion*. Gastric cancer patients with complications of coronary heart disease and heart failure are associated with intestinal flora disorder, which may be involved in the occurrence and development of the disease. Probiotics intervention is helpful to repair the intestinal mucosal barrier in patients, which is worthy of popularization and application.

1. Introduction

Coronary heart disease is a disease caused by coronary artery stenosis or occlusion of myocardial ischemia, hypoxia, or necrosis. As the course of the disease increases, it can increase the incidence of chronic heart failure [1]. At present, the clinical treatment of coronary heart disease mainly focuses on reducing blood lipids, preventing risk factors, and symptomatic treatment. Although good effects can be obtained, how to choose and take measures to reduce disease morbidity and mortality has become a hot research topic [2]. Gastric cancer is a kind of gastric cancer that originates from gastric mucosal cells, which is mainly clinically characterized by abdominal pain. It usually occurs in people aged 40–70. The incidence rate of men is higher than that of women. Its incidence is mostly related to gastrointestinal dysfunction.

Intestinal microbiota refers to the general name of the microorganisms that live in the human gut, which can help the host to complete a variety of physiological and biochemical functions and produce corresponding metabolites [3]. Studies have shown that the host can provide an appropriate environment and necessary nutrition for the intestinal flora, and the intestinal flora can participate in mediating various functions of the human body, provide metabolic nutrients to the host, participate in the promotion of growth and immune regulation, and regulate various functions of the human body [4]. Therefore, strengthening the analysis of the characteristics of the intestinal flora of patients with gastric cancer complicated by coronary heart disease and heart failure can help us understand its role in the pathogenesis of the disease and guide clinical treatment [5, 6]. Probiotics are commonly used as clinical gastrointestinal regulating drugs, regulating intestinal flora, and protecting the intestinal mucosal barrier, but there are few studies on the application of drugs in patients with gastric cancer complicated by coronary heart disease and heart failure [7]. Therefore, this study focused on patients with gastric cancer complicated by coronary heart disease and heart failure to explore the characteristics of the intestinal flora of patients with coronary heart disease combined with heart failure and gastric cancer and the guiding value of probiotic intervention in clinical treatment.

2. Materials and Methods

2.1. Patients. A total of 168 patients with gastric cancer complicated by coronary heart disease and heart failure from August 2017 to December 2020 at the First-Affiliated Hospital of Zhengzhou University, Zhengzhou, China, were prospectively selected as the observation group. There were 89 males and 79 females, aged (42–84) years, with an average of (61.85 ± 6.61) years; body mass index (BMI) was 18–29 kg/m^2, average 23.26 ± 4.61 kg/m^2; coronary heart disease course was 1–9 years, average 4.14 ± 0.61 years; and heart failure course was 1–6 months, with an average of 3.25 ± 0.51 months; patients in the observation group were randomly divided into two groups, A and B, with 84 cases in each group. A total of 125 patients with coronary heart disease who were selected for simultaneous treatment were included in control group 1. There were 67 males and 58 females, aged 43–85 years, with an average of 62.41 ± 6.64 years; BMI was 19–28 kg/m^2, average 23.31 ± 4.64 kg/m^2; and duration of disease was 1–10 years, average 4.19 ± 0.67 years; 89 cases of healthy physical examination during the same period were selected as control group 2, with 48 males and 41 females, aged 43–86 years, with average 61.87 ± 6.69 years; BMI was 17–30 kg/m^2, average 23.86 ± 4.69 kg/m^2. There was no statistically significant difference in the general information of the patients in each group ($P > 0.05$), and the data were comparable. The study was approved by the ethics committee of the First-Affiliated Hospital of Zhengzhou University, Zhengzhou, China, and the patient's informed consent was obtained.

2.2. Inclusion and Exclusion Criteria

2.2.1. Inclusion criteria [8, 9]. (1) Conformed to the diagnostic criteria of coronary heart failure, confirmed by coronary angiography and cardiopulmonary exercise test. (2) Patients in the observation group met the diagnostic criteria for gastric cancer and were diagnosed by pathological examination. (3) All of them could complete the determination of intestinal flora and give probiotics intervention. (4) Complete baseline and follow-up data.

2.2.2. Exclusion criteria. (1) Chronic heart failure caused by valvular disease, hypertension, and cardiomyopathy. (2) Individuals with a mental disorder, abnormal cognitive function, or organic disease. (3) Patients with severely abnormal liver and kidney function accompanied by autoimmune system diseases.

2.3. Methods

2.3.1. Analysis of Characteristics of Intestinal Flora

(1) Specimen collection and extraction of total DNA of samples

After admission, 0.5 g of feces were collected from all three groups and placed in the fecal DNA preservation solution (Shanghai Microcomputer Biotechnology Co., Ltd., Shanghai, China). Total DNA of the samples was extracted according to the instructions (Omega Bio-tek, Norcross, GA, USA), and the concentration and purity of DNA were examined by NanoDrop2000. Subsequently, the DNA was extracted by agarose gel electrophoresis with a concentration of 1% [10].

(2) High-throughput sequencing was carried out to complete the analysis of bacterial diversity and species differences, in order to obtain the species information of the specimens. Relevant primers were designed, and the PCR products were recovered by agarose gel with a concentration of 2%. The purified PCR product fragments were amplified by the Illumina MiSeq platform (Illumina, San Diego, USA) to construct a PE 2 300 library. Sequencing was completed with the MiSeq PE300 platform of Illumina (Shanghai Megei Bio-Pharmaceutical Technology Co., Ltd., Shanghai, China), and the obtained data were transferred to the National Biotechnology Information Generality (NCBI) database for processing. TrimMomatic software was applied for quality control during specimen determination [11]. The analysis was performed with Flash software (diversity analysis was carried out from the Chao, ACE, Simpson, Shannon, and the Coverage indexes to detect intestinal flora), and species classification annotation was completed for different sequences. The comparison threshold of the Silva database was set as 70.0% [12].

Table 1: Comparison of intestinal flora diversity among the three groups ($\overline{x} \pm s$).

Group	Cases	Chao	ACE	Simpson	Shannon	Coverage
Observation group	168	$100.61 \pm 10.83^{\#*}$	$101.21 \pm 14.32^{\#*}$	$0.10 \pm 0.04^{\#*}$	$2.59 \pm 0.56^{\#*}$	1.04 ± 0.21
Control group 1	125	$120.52 \pm 18.53^{\#}$	$112.59 \pm 17.53^{\#}$	$0.28 \pm 0.09^{\#}$	$2.15 \pm 0.41^{\#}$	1.06 ± 0.24
Control group 2	89	170.59 ± 24.62	159.74 ± 21.41	0.14 ± 0.06	3.20 ± 0.63	1.03 ± 0.20

Vs. control group 2, $^{\#}P < 0.05$; vs. control group 1, $^{*}P < 0.05$.

2.4. Intervention in the Observation Group. Both groups were given conventional intervention and conventional symptomatic supportive treatment, such as angiotensin inhibitors Digitalium and diuretics. Group A was utilized conventional methods of treatment. Metoprolol Succinate Sustained-release Tablets (AstraZeneca, Inc., National Drug License: J20150044, specification: 47.5 mg) 95 mg orally every time, once a day, and Trimetazidine Dihydrochloride Tablets (Shanxi C&Y Pharmaceutical Group Co., Ltd., National Drug License: H20123233, specification: 20 mg) 20 mg orally every time, 3 times a day for 4 weeks (1 course of treatment), were given. The treatment of group B is combined with probiotic intervention on the basis of group A. *Bifidobacterium longum*, *Lactobacillus acidophilus*, and *Enterococcus faecalis* Capsules (Shenzhen Xinwanze Pharmaceutical Co., Ltd., National Drug License: S19980004, specification: 0.5 g, containing live bacteria number $\geq 1.0 \times 10^7$ CFU) 2 tablets orally were given in warm water for 30 min after meals, twice a day for 4 weeks (1 course) [13].

2.5. Observation Indicators. (1) The Chao, ACE, Simpson, Shannon, and Coverage indexes of the three groups were recorded to analyze intestinal flora diversity. (2) Routine microflora determination was completed in all three groups, and the characteristics of intestinal microflora were analyzed for the level of phylum, class, and genus. (3) 3 mL of peripheral fasting blood was taken from the two groups before treatment and the day after treatment. ELISA assay was performed to determine the patient's endotoxin (ET) and D-lactic acid levels, and the chemiluminescence method was applied to determine procalcitonin (PCT) level, to assess the intestinal mucosal barrier.

2.6. Statistical Analysis. SPSS24.0 software was used to process these data. A chi-square test was performed, and n (%) was utilized to represent the enumeration data. ET, PCT, and other measurement data were all in line with normal distribution. The $P < 0.05$ was statistically significant.

3. Results

3.1. Comparison of the Diversity of Intestinal Flora among the Three Groups. The Coverage index of the three groups showed no statistical significance ($P > 0.05$). The Chao, ACE, and Simpson index in the observation group were lower than those in control group 1 ($P < 0.05$), whereas the Shannon index was higher than that in control group 1 ($P < 0.05$). The Chao, ACE, and Shannon index in control group 1 were lower than those in control group 2 ($P < 0.5$), whereas the Simpson index was higher than that in control group 2 ($P < 0.05$), as shown in Table 1.

3.2. Analysis of Intestinal Flora Characteristics of the Three Groups. The abundance of *Bacteroidetes* and *Firmicutes* in the three groups was statistically significant ($P < 0.05$), respectively. The abundance of *Bacteroidetes* in the observation group was lower than that in control group 1 and control group 2 ($P < 0.05$), respectively. The abundance of *Firmicutes* was higher than that of control group 1 and control group 2 ($P < 0.05$), respectively. The abundance of *Proteobacteria* and *Actinobacteria* in the three groups was not statistically significant ($P > 0.05$), as shown in Figure 1.

3.3. Comparison of the Intestinal Mucosal Barrier between the Two Groups. Before treatment, there was no statistical significance between the two groups ($P > 0.05$). Intestinal mucosa was improved significantly in both groups 4 weeks after treatment. The levels of ET, D-lactic acid, and PCT in group B at 4 weeks after treatment were lower than those in group A ($P < 0.05$), as shown in Table 2.

4. Discussion

Numerous studies have shown that intestinal flora is involved in the occurrence and development of various diseases, including cardiovascular system disorders [14, 15]. Coronary atherosclerosis is an independent risk factor for coronary heart disease. It is a chronic vascular inflammatory disease and can participate in different stages of plaque, from adhesion molecules to white blood cells to metalloproteinases, causing digestion of fibrous cap and increasing plaque instability [16]. Gastric cancer is a malignant tumor originating from gastric mucosal epithelium, and its incidence has obvious regional differences. In China, it tends to occur on the eastern coast and the northwest. In addition, with the change of dietary structure and the increase of work pressure and other reasons such as *Helicobacter pylori*, gastric cancer tends to be younger. More and more studies have shown that changes in intestinal flora composition and function will cause intestinal flora imbalance, which can accelerate the occurrence of cardiovascular diseases [17]. In this study, the Chao, ACE, and Simpson index of the observation group were lower than those of the control group 1. The Shannon index was higher than that in control group 1. The Chao, ACE, and Shannon index in control group 1 were lower than those in control group. The Simpson index was higher than that in control group 2. The abundance of *Bacteroidetes* in group B was lower than that in group A, while the abundance of *Firmicutes* was higher than that in

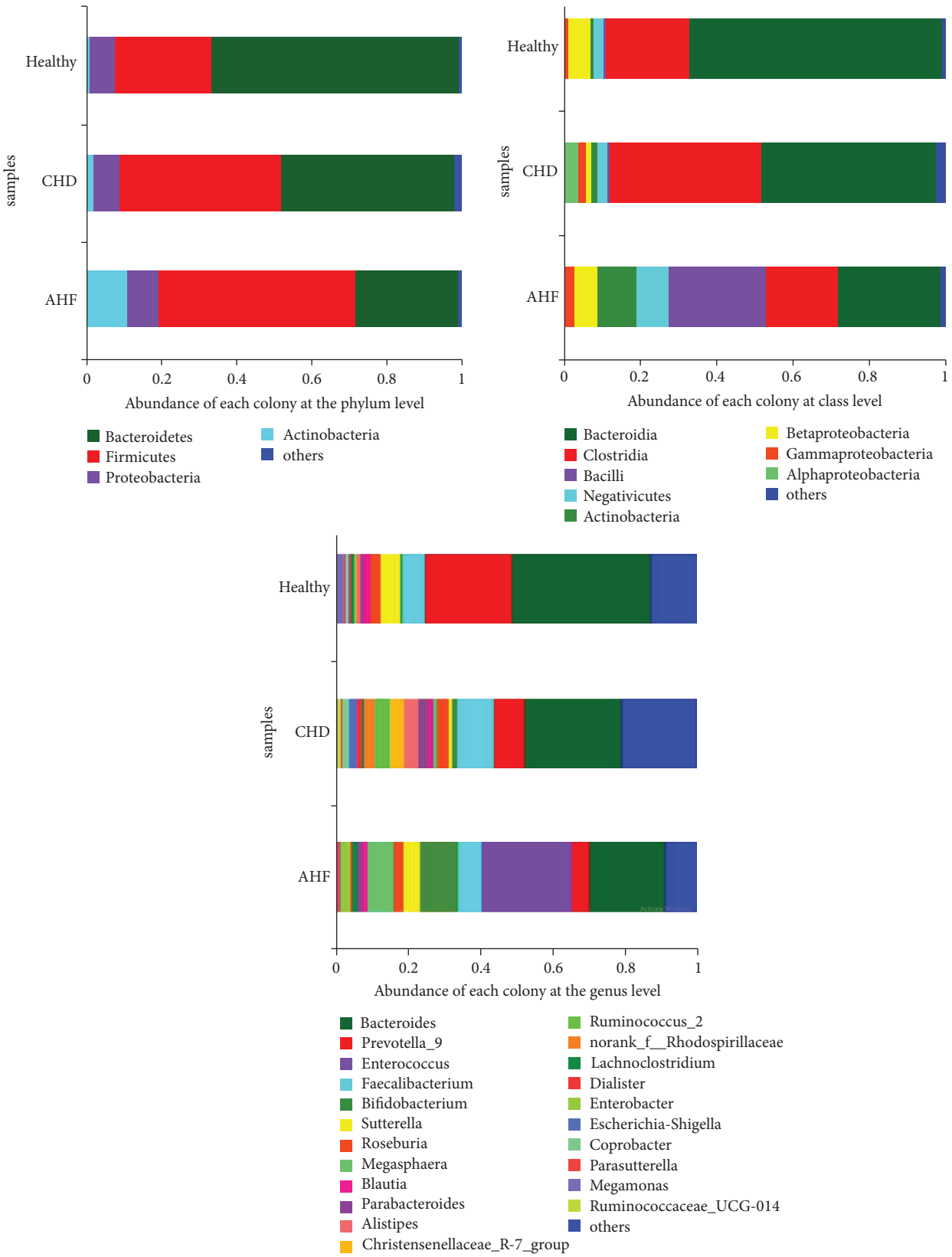

Figure 1: Characteristic analysis of the intestinal flora of the three groups (in phylum, class, and genus level).

group A. According to these pieces of evidence, gastric cancer patients with complications of coronary heart disease and heart failure are accompanied by obvious intestinal flora disorder, which can be directly involved in the pathological process of the disease. It may be due to the intestinal flora disorder of patients, which can cause the increase of the level

Table 2: Comparison of the gastrointestinal mucosal barrier between the two groups ($\overline{x} \pm s$).

Group		ET (EU/mL)	D-lactate (μg/mL)	PCT (μg/L)
Group B($n = 84$)	Before treatment	0.25 ± 0.04	6.42 ± 0.61	0.96 ± 0.13
	4 weeks after treatment	$0.10 \pm 0.01^{\#*}$	$3.99 \pm 0.32^{\#*}$	$0.41 \pm 0.10^{\#*}$
Group A($n = 84$)	Before treatment	0.26 ± 0.05	6.43 ± 0.62	0.98 ± 0.15
	4 weeks after treatment	$0.19 \pm 0.03^{*}$	$4.51 \pm 0.46^{*}$	$0.81 \pm 0.13^{*}$

Vs. group A, $^{\#}P < 0.05$; vs. before treatment, $^{*}P < 0.05$.

of inflammatory factors in the body through its metabolites, thus accelerating the course of atherosclerosis and heart failure and affecting cardiovascular diseases. From the analysis of intestinal flora characteristics of gastric cancer patients with complications of coronary heart disease and heart failure, the intestinal flora of patients contains a higher *Firmicutes* and lower *Bacteroidetes*, mainly because *Bacteroidetes* can participate in the metabolism of a variety of substances, promote the formation of intestinal mucosal blood vessels, and maintain the balanced metabolism of normal intestinal flora [18]. However, in gastric cancer patients with complications of coronary heart disease and heart failure, there are fewer beneficial bacteria that can maintain the intestinal metabolism, which can aggravate the onset in patients [19].

These shreds of evidence have revealed that intestinal flora disturbance can directly participate in the occurrence of coronary heart disease combined with heart failure and gastric cancer patients, being harmful to patients. Probiotics are a commonly used microecological preparation. After oral supplementation of intestinal beneficial bacteria, the beneficial bacteria attach to the intestinal mucosa, then grow, and proliferate in large numbers, which can competitively antagonize the colonization and growth of pathogenic bacteria in the intestinal tract, thus promoting the recovery of normal intestinal flora, helping patients to rebuild and maintain the balance of intestinal flora, and helping patients to construct the intestinal barrier [20]. Previous studies have shown that probiotics can stimulate the local lymphoid tissues of intestinal mucosa, activate the local defense function, and enhance the anti-infection ability of the gastrointestinal tract [21]. In this study, the levels of ET, D-lactic acid, and PCT in group B were lower than those in group A at 4 weeks after treatment, suggesting probiotics for gastric cancer patients with complications of coronary heart disease and heart failure can help to build the intestinal barrier, correct the intestinal flora disorder patients, and reduce the aggravation of the disease caused by intestinal flora. Therefore, the determination of intestinal flora in gastric cancer patients with complications of coronary heart disease and heart failure should be strengthened in clinical practice, and timely probiotics intervention should be given to abnormal patients to promote their recovery.

In conclusion, gastric cancer patients with complications of coronary heart disease and heart failure are often accompanied by intestinal flora disorder, which may be involved in the occurrence and development of various disorders. Probiotics intervention is helpful to repair the intestinal mucosal barrier in patients, which is worthy of popularization and application.

Data Availability

The data used to support the findings of this study are available from the corresponding author upon request.

Conflicts of Interest

The authors declare no conflicts of interest.

Acknowledgments

This study was funded by the Henan Medical Science and Technology Research Program (Hui Yu, No. 2018020250), Henan Provincial Health and Family Planning Science and Technology Talents Overseas Training Project (Hui Yu, No. HWYX2019081), Research on Technology System and Information Management of Full Cycle Rehabilitation for the Elderly (Anqin Dong, No. 2018YFC2002300), and Science and Technology Project of Henan Province (Ping Li, 212102310797).

References

[1] Y. Tian, P. Deng, B. Li et al., "Treatment models of cardiac rehabilitation in patients with coronary heart disease and related factors affecting patient compliance," *Reviews in Cardiovascular Medicine*, vol. 20, no. 1, pp. 27–33, 2019.

[2] L. Qu and H. Jiang, "Clinical efficacy of trimetazidine and holistic management in the treatment of coronary heart disease," *Iranian Journal of Public Health*, vol. 47, no. 6, pp. 824–829, 2018.

[3] S. Zhang, C. Liang, Y. Yang, Z. Zhao, J. Li, and X. Meng, "Effects of Yangxinshi tablet on exercise tolerance in patients with coronary heart disease: a protocol of randomized, double-blind, placebo-controlled, and multi-center trial," *Medicine (Baltimore)*, vol. 99, no. 31, Article ID e21485, 2020.

[4] R. G. Yang, X. K. Xu, Q. L. Zhou, and X. X. Yang, "Analysis of intestinal flora and immune status of patients with hepatitis B virus-associated chronic acute liver failure secondary infection before and after probiotics intervention," *Journal of Third Military Medical University*, vol. 41, no. 08, pp. 794–798, 2019.

[5] F. H. S. Zhu, "Study on etiological characteristics and risk factors of nosocomial pulmonary infection in elderly patients with coronary heart disease complicated with heart failure," *China Preventive Medicine*, vol. 21, no. 07, pp. 749–753, 2020.

[6] G. Yang, H. Q. He, G. Chen, and J. Wang, "Research progress of TCM regulating intestinal flora and intervening coronary heart disease and its risk factors," *China Journal of Chinese Materia Medica*, vol. 45, no. 01, pp. 29–36, 2020.

[7] M. Zhao, Q. Che, Y. Zhang, X. Qian, and T. Huang, "Expression and clinical significance of serum cystatin C in patients with hypertension and coronary heart disease," *Medicine (Baltimore)*, vol. 99, no. 22, Article ID e20029, 2020.

[8] J. Joseph, A. Velasco, F. G. Hage, and E. Reyes, "Guidelines in review: comparison of ESC and ACC/AHA guidelines for the

diagnosis and management of patients with stable coronary artery disease," *Journal of Nuclear Cardiology: Official Publication of the American Society of Nuclear Cardiology*, vol. 25, no. 2, pp. 509–515, 2018.

[9] K. Dickstein, K. Dickstein, P. E. Vardas et al., "Focused Update of ESC Guidelines on device therapy in heart failure: an update of the 2008 ESC Guidelines for the diagnosis and treatment of acute and chronic heart failure and the 2007 ESC guidelines for cardiac and resynchronization therapy. Developed with the special contribution of the Heart Failure Association and the European Heart Rhythm Association," *European Heart Journal*, vol. 31, no. 21, pp. 2677–2687, 2010.

[10] Y. Zhang, Y. L. Wang, C. J. Zhang, and H. F. Zhang, "Effects of probiotics intervention on intestinal flora immune function and related complications in patients with non-small cell lung cancer treated with chemotherapy," *Progress in Modern Biomedicine*, vol. 20, no. 03, pp. 574–577+595, 2020.

[11] P. F. B. J. Liu, "Changes of intestinal flora and serum inflammatory cytokines in patients with subclinical hepatic encephalopathy and the intervention effect of probiotics," *Chinese Journal of Microecology*, vol. 32, no. 02, pp. 180–182+186, 2020.

[12] Y.-D. Chen, X.-C. Yang, V. N. Pham et al., "Resting heart rate control and prognosis in coronary artery disease patients with hypertension previously treated with bisoprolol: a sub-group analysis of the BISO-CAD study," *Chinese Medical Journal*, vol. 133, no. 10, pp. 1155–1165, 2020.

[13] P. Ambalam, M. Raman, R. K. Purama, and M. Doble, "Probiotics, prebiotics and colorectal cancer prevention. Best practice & research," *Best Practice & Research Clinical Gastroenterology*, vol. 30, no. 1, pp. 119–131, 2016.

[14] M. Jin, Z. Qian, J. Yin, W. Xu, and X. Zhou, "The role of intestinal microbiota in cardiovascular disease," *Journal of Cellular and Molecular Medicine*, vol. 23, no. 4, pp. 2343–2350, 2019.

[15] F. X. Li and Y. Zhao, "Characteristics of intestinal flora in elderly patients with coronary heart disease complicated with heart failure," *Chinese Journal of Gerontology*, vol. 38, no. 11, pp. 220–1222, 2019.

[16] M. Trøseid, G. Andersen, K. Broch, and J. R. Hov, "The gut microbiome in coronary artery disease and heart failure: current knowledge and future directions," *EBioMedicine*, vol. 52, Article ID 102649, 2020.

[17] S. M. Grundy, "Management of high serum cholesterol and related disorders in patients at risk for coronary heart disease," *The American Journal of Medicine*, vol. 102, no. 2a, pp. 15–22, 1997.

[18] M. B. Y. Zhang, "The clinical effect of yangxin tongmai prescription combined with aspirin enteric-coated tablet on patients with coronary heart disease with deficiency of qi and blood stasis and its effect on intestinal flora," *Journal of Clinical Medicine in Practice*, vol. 23, no. 13, pp. 92–95, 2019.

[19] Y. Huang, Y. Y. Zhou, Q. Wu, X. Z. Chen, and A. Q. Xiao, "Etiological characteristics and influencing factors of nosocomial infection in patients with coronary heart disease complicated with heart failure," *Chinese Journal Of Nosocomiology*, vol. 29, no. 18, pp. 2783–2786, 2019.

[20] N. Ding, X. Wang, K. L. Tucker et al., "Dietary patterns, bone lead and incident coronary heart disease among middle-aged to elderly men," *Environmental Research*, vol. 168, pp. 222–229, 2019.

[21] Y. K. Lu, Z. Y. Chen, X. M. Zhuang, and B. Huang, "Effect of Sijunzi decoction on regulating intestinal microflora and improving heart failure induced by cardiac hypertrophy in rats," *Research and practice of modern Chinese medicine*, vol. 34, no. 05, pp. 29–33, 2020.

Hindawi
Journal of Oncology
Volume 2021, Article ID 9026610, 5 pages
https://doi.org/10.1155/2021/9026610

Research Article

Analysis of Threshold Changes of Tumor Mutation Burden of Gastric Cancer and Its Relationship with Patients' Prognosis

Nan Zhang, Peiyu Li, Xin Wu, Shaoyou Xia, Xudong Zhao, and Lin Chen

Department of General Surgery, The First Medical Centre, Chinese PLA General Hospital, Beijing 100036, China

Correspondence should be addressed to Lin Chen; chenlin@301yiyuan.cn

Received 24 June 2021; Revised 3 September 2021; Accepted 15 September 2021; Published 27 September 2021

Academic Editor: Alamgeer Yuchi

Objective. Gastric cancer is a malignant tumor originating from gastric mucosal epithelium. Here, we aimed to investigate the analysis of the threshold change of gastric cancer tumor mutation burden (TMB) and its relationship with the prognosis of patients. *Methods*. 256 patients with gastric cancer were selected as subjects. All patients were in the advanced stage and received surgical resection of D2 lymph node dissection. After the operation, a follow-up was performed for 24 months, and the disease-free survival and overall survival of patients were counted. The NGS molecular biological was detected to obtain gastric cancer tumor mutation burden (TMB) data. Pearson correlation analysis software was used to analyze the correlation between TMB threshold and disease-free survival or overall survival of patients with gastric cancer, and the multivariate logistic analysis was performed as well. *Results*. The disease-free survival period and the overall survival period of patients in the low-to-medium TMB group were both longer than those in the high TMB group. Pearson correlation analysis results showed that the TMB threshold was negatively correlated with the disease-free survival and overall survival of gastric cancer patients. Results from multivariate logistic analysis showed that high TMB thresholds have a greater impact on disease-free survival and overall survival of patients, but the impact of medium and low TMB thresholds on disease-free survival and overall survival of patients is weakened. *Conclusions*. The TMB threshold level has a predictive effect on the effect of surgical resection of D2 lymph node dissection, and high levels of TMB can significantly affect disease-free survival and overall survival of patients with advanced gastric cancer.

1. Introduction

Gastric cancer is a malignant tumor that originates from the epithelium of the gastric mucosa, and with the changes in the diet of Chinese residents, increased work pressure, and *Helicobacter pylori* infection, the incidence of the disease is showing a younger trend [1]. Previous studies have shown that gastric cancer is more likely to occur in people over the age of 50, and the incidence of men is slightly higher than that of women, and more than 50.0% of patients occur in the antrum, greater curvature, and lesser curvature of the stomach [2]. Due to the lack of typical clinical symptoms in the early stage of gastric cancer, the diagnosis of most patients is already in the middle and late stages, and the best diagnosis and treatment opportunity are missed [2,3]. Surgical resection of D2 lymph node dissection is a common treatment method for patients with gastric cancer. The lesion tissue can be removed with surgery, but most patients lack effective evaluation methods, resulting in poor long-term prognosis [4,5]. Tumor mutational burden (TMB), an emerging independent biomarker, is the detection of the total number of mutations in the coding region of tumor genes, which is widely used to stratify the patient's response to treatment. Previous studies have shown that TMB refers to the exon coding region of the evaluation gene in the tumor cell genome and the total number of substitution, insertion, or deletion mutations per megabase [6]. Highly mutated tumors are believed to contain increased neoantigen load, making them immunogenic and responsive to immunotherapy [7]. However, there are few studies on the relationship between TMB and the prognosis of patients with gastric cancer.

In this study, gastric cancer patients were selected as subjects to explore the changes of TMB and its relationship with the prognosis of the gastric cancer patients. The report is as follows.

2. Materials and Methods

2.1. Clinical Data. 256 patients with advanced gastric cancer were selected as subjects from May 2017 to January 2019 at the First Medical Centre, Chinese PLA General Hospital, including 185 males and 71 females, aged 45–84 years, with an average of 68.83 ± 5.71 years old. ECOG score: 0 points (149 cases); 1 point (107 cases). Tumor location: 42 cases of upper gastric body, 75 cases of gastric body, and 139 cases of gastric isthmus. Clinical N stage: 34 cases of cN1 stage, 132 cases of cN2 stage, and 90 cases of cN3 stage. The study was approved by the Ethics Committee of the First Medical Centre, Chinese PLA General Hospital, and the informed consent was obtained from the patients.

2.2. Inclusion and Exclusion Criteria. Inclusion criteria: (1) the patients met the diagnostic criteria for gastric cancer, were diagnosed by pathological tissues, and were in the advanced stage. (2) All patients were planned to undergo surgical resection of D2 lymph node dissection, and the patients can tolerate it. (3) The complete baseline and follow-up data were available.

Exclusion criteria: (1) the recurrent gastric cancer, patients undergoing emergency surgery due to tumor perforation, obstruction, or bleeding. (2) Mental disorders, abnormal blood coagulation, or autoimmune system diseases. (3) Tumors in other parts or those undergoing radiotherapy and chemotherapy before surgery.

2.3. Method

2.3.1. Treatment Method. The specific method of surgical removal of D2 lymph node dissection is as follows. The patient takes the supine position and then undergoes general anesthesia, disinfection, and draping. Laparoscopy and other surgical instruments used to separate the omentum, the anterior lobe of the transverse mesocolon to the tail of the pancreas, separate the pancreatic capsule, clip off the left side of the gastric omentum, and the tip splenogastric ligament. The gastrophrenic ligament was opened, and the dissection retrograded to remove lymph nodes around the splenic artery after sweeping the splenic hilar area. The right omentum was peeled to the liver flexure of the colon, the head of the pancreas and the bulb of the duodenum were fully exposed, the right blood vessels of the gastroomentum was clipped off, and the sixth group of lymph node dissection was completed. After the above operations were completed, the omental sac was incised, the lymph nodes of group 12a were cleaned, the tissue separation was completed along the direction of the common hepatic artery, the intrathecal area was routinely cleaned, and the left gastric vein and left gastric artery were dissected, and the lymph nodes of group 8, 9, and 11p were dissected. The posterior wall of the stomach, the cardia, and the lower esophagus were free, and then, a surgical incision in the lower abdomen of the patient was made to complete the cut of the lower esophagus, the specimen was taken out, and the digestive tract reconstruction was completed. After the operation, a follow-up was performed for 24 months, and the disease-free survival and overall survival of patients were counted [8].

2.3.2. Determination of TMB. After the operation, the NGS molecular biological was performed to obtain the TMB data of gastric cancer. The specific methods are as follows. (1) Specimen processing: gastric cancer tissues were fixed with formaldehyde and embedded in paraffin. 6–10 um sections were prepared, and then, hematoxylin-eosin (H&E) staining was performed, and the tumor cell content was judged by pathologists. The tissues with tumor cell content >10.0% were selected. The plasma samples were collected with EDTA anticoagulation tube, centrifuged for 10 min (1800 rpm, centrifugal radius 15 cm), and then placed at −4°C until use. (2) DNA extraction and library preparation: Qiagen company extraction kit was used to extract tissues and the DNA of white blood cells. The KAPA Hyper Prep Kit (Woosen Biotechnology, Shanghai, China) was used as the sequencing library, and the target gene was enriched after PCR amplification and library purification [9]. (3) Enrichment and sequencing of target genes: after the above operations were completed, multiple samples were mixed to obtain 2 ug of DNA mixed library. The colonized biotin-type DNA probe (GeneSeqOne^{TM}) was used to hybridize and capture 415 coding regions of genes related to gastric cancer and 16 introns of genes in the library. Meanwhile, the library DNA was amplified with the help of Illumina p5, p7 primers, and KAPA HiFi HotStart ReadyMix (Sigma-Aldrich, Shanghai, China), and the enriched library was sequenced on the HiSeq 4000 platform using a 2×150 bp sequencing kit [10]. (4) Sequencing data processing: Trimmomatic 25 software was used to filter the sequencing data and remove low-quality bases or N bases. The resulting data and the reference sequence genome were compared through high-throughput sequencing analysis. GATK was used to complete single calculation of mutation and indel gene mutation data. (5) TMB calculation: TMB was defined as the number of tumor-specific mutations contained in the 1 Mb base of the coding region. The data of tumor samples and white blood cells were compared, and the somatic mutations were analyzed and germline mutations were removed [11].

2.3.3. Correlation Analysis. Pearson correlation analysis software was used to analyze the correlation between TMB threshold of gastric cancer patients and disease-free survival and overall survival and multivariate logistic analysis.

2.4. Statistical Analysis. SPSS24.0 software (IBM, NY, USA) was used to measure the statistical data. The count data were analyzed by the χ^2 test, expressed by n (%). The measurement data in the article were all in accordance with the normal distribution and analyzed by the t-test, expressed by $(\overline{x} \pm s)$. Kaplan–Meier survival analysis was carried out for overall survival. $P < 0.05$ was considered as statistical significance.

3. Results

3.1. Comparison of Disease-Free Survival and Overall Survival of Patients with Different TMB Levels in Gastric Cancer. The TMB level in advanced gastric cancer was 5–14, with an average of 8.58 ± 0.61. The patients with gastric cancer were divided into the high TMB group ($n = 131$ cases, TMB≥8) and low-medium TMB group ($n = 125$ cases, TMB<8) by the three-point method. The enrolled patients were followed up for 24 months. Results showed that the disease-free survival time of patients in the low-to-medium TMB group was 14.39 ± 3.23 months, and the overall survival time was 17.41 ± 2.12 months, which were longer than the disease-free survival time (11.51 ± 2.59 months) and the overall survival time of the high TMB group (13.15 ± 2.05 months) ($P < 0.05$; $P < 0.05$) (Figures 1(a) and 1(b)).

3.2. Correlation between TMB Threshold and Disease-Free Survival and Overall Survival of Patients with Gastric Cancer. Results from Pearson correlation analysis showed that the TMB threshold of gastric cancer patients was negatively correlated with disease-free survival and overall survival ($P < 0.05$), as given in Table 1.

3.3. Multivariate Analysis of TMB Threshold and Disease-Free Survival and Overall Survival of Patients with Gastric Cancer. Results from multivariate logistic analysis showed that the high TMB threshold of gastric cancer patients had a greater impact on disease-free survival and overall survival of patients, but the impact of medium and low TMB thresholds on disease-free survival and overall survival of patients was weakened, as given in Table 2 and Table 3.

4. Discussion

In recent years, the number of advanced gastric cancer in China has been increasing, and 60.0%–80.0% of gastric cancer patients are already in the advanced tumor stage [12]. Surgical removal of D2 lymph node dissection is a common surgical treatment method for patients with advanced gastric cancer. However, due to the lack of effective prediction and evaluation indicators during the operation of some patients, disease-free survival and overall survival rate of patients are low, which affects the prognosis of patients. Therefore, effective evaluation indicators are the focus of clinical evaluation and research for gastric cancer.

TMB is currently a hotspot in clinical research. TMB refers to the total number of substitution, insertion, and deletion mutations per megabase in the exon coding region of the evaluated gene in the tumor cell genome [13]. Previous studies have shown that changes in the pathogenicity of cell functions due to changes in the genome are clinically called "driver mutations," which can lead to tumors [14]. In this study, the level of TMB in advanced gastric cancer was 5–14, with an average of 8.58 ± 0.61. The disease-free survival time of patients in the low-to-medium TMB group was 14.39 ± 3.23 months, and the overall survival period was 17.41 ± 2.12 months, both of which were longer than those in the high TMB group, (11.51 ± 2.59) months and (13.15 ± 2.05) months ($P < 0.05$). These results suggest that the survival and overall survival of patients in the high TMB group are lower. Rizzo and Ricci revealed that TMB has a significant effect on the differential expression of hepatocellular cancer genes and the proportion of infiltrating immune cells in tumor tissues [15]. Although this study is not the same disease as this article, it fully illustrates the correlation between TMB and tumors.

NCCN guidelines included TMB testing for the first time in 2019, which further promoted the clinical application of TMB [16]. Increasing research studies have confirmed that high levels of TMB are correlated with the survival rate of patients with different types of tumors, leading to lower patient survival and disease-free survival [17]. TMB reflects the repair and damage of DNA in tumor cells to a certain extent and is related to the ability to produce tumor neoantigens. DNA mismatch repair (MMR) is responsible for repairing DNA replication errors, and mutations associated with MMR often cause picoinstability. Therefore, hypermicrosatellite instability can be used as a surrogate indicator for MMR functional defects. In order to further analyze the relationship between the TMB threshold and the prognosis of patients with gastric cancer, Pearson correlation analysis was performed in this study. Results showed that the TMB threshold of gastric cancer patients was negatively correlated with disease-free survival and overall survival. Multivariate logistic analysis results showed that the high TMB threshold of gastric cancer patients has a greater impact on disease-free survival and overall survival, but the impact of medium and low TMB thresholds on disease-free survival and overall survival of patients was weakened, indicating the close relationship between the TMB of advanced gastric cancer and the patient's prognosis. Therefore, when surgical treatment of patients with diagnosed advanced gastric cancer is performed clinically, the measurement of the patient's TMB level should be strengthened, the long-term prognosis of the patient should be evaluated, and the corresponding measures should be formulated according to the measurement results to intervene to consolidate the surgical effect and promote the recovery of the patient [18].

This study also has its limitations. First, the relatively small sample size may lead to errors in overall survival. Second, the small number of human and environmental factors may also lead to statistical errors. Third, more biological functions in vitro are required to explore in the future studies.

In summary, for patients with advanced gastric cancer, the tumor mutation load threshold level has a predictive effect on the effect of surgical resection of D2 lymph node dissection, and high levels of TMB could significantly affect the disease-free survival and overall survival of patients, which provided a certain reference value for the evaluation of prognosis in gastric cancer patients.

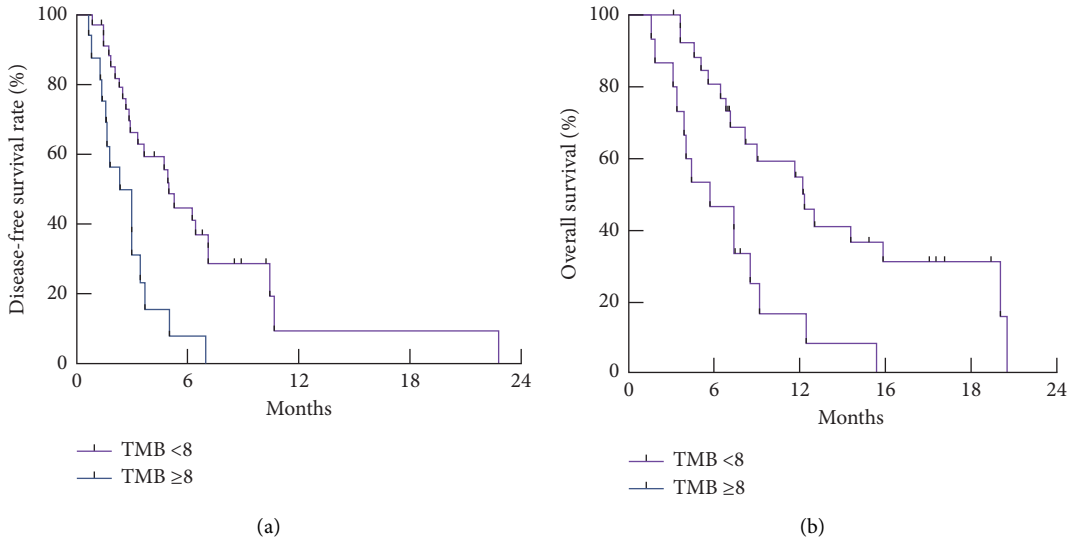

Figure 1: Comparison of disease-free survival and overall survival of patients with different TMB levels in gastric cancer. (a) Kaplan–Meier survival analysis of disease-free survival time of patients with different TMB levels. (b) Kaplan–Meier survival analysis of overall survival time of patients with different TMB levels.

Table 1: Correlation between TMB threshold and disease-free survival and overall survival of patients with gastric cancer (r, P).

Correlation	Disease-free survival	Overall survival
r	−0.715	−0.892
P	<0.001	<0.001

Table 2: Multivariate analysis of TMB threshold and disease-free survival of patients with gastric cancer.

Multivariate	B value	S.E	Wald	P value	OR value	95% CI
High TMB	1.973	0.121	9.434	<0.001	7.982	6.313–8.493
Medium TMB	1.495	0.104	8.498	<0.001	6.791	6.312–7.326
Low TMB	1.213	0.097	7.151	<0.001	5.457	4.698–7132

Table 3: Multivariate analysis of TMB threshold and disease-free survival of patients with gastric cancer.

Multivariate	B value	S.E	Wald	P value	OR value	95% CI
High TMB	1.943	0.133	5.456	<0.001	5.412	4.951–5.838
Medium TMB	1.783	0.214	6.981	<0.001	4.313	3.235–7.491
Low TMB	1.669	0.169	4.341	<0.001	6.323	4.346–7.982

Data Availability

The datasets used and/or analyzed during the present study are available from the corresponding author upon request.

Disclosure

The funding body had no role in the design of the study, collection, analysis, interpretation of data, or writing of the manuscript.

Conflicts of Interest

The authors declare that they have no conflicts of interest.

Acknowledgments

The authors deeply appreciate the contributions to this work made in various ways by all of the participants.

References

[1] Q. Liu, Y. Li, and B. Tan, "The expression of Tat binding protein 30 in gastric cancer tumor tissues and its relationship with patient prognosis," *Chinese General Practice*, vol. 23, no. 6, pp. 55–60, 2020.

[2] J. Sun, X. Ji, and Y. Wang, "Study on the relationship between circulating tumor cells and clinicopathological characteristics and prognosis of patients with gastric cancer," *Chinese Journal of Basic and Clinical Medicine*, vol. 26, no. 1, pp. 25–30, 2019.

[3] J. Li, Y. Luo, and Z. Zhang, "The relationship between HOXC10 expression in gastric cancer tissues and

clinicopathological characteristics and prognosis," *International Journal of Digestive Diseases*, vol. 40, no. 2, pp. 119–124, 2020.

[4] Y. Song and X. Li, "Meta-analysis of the relationship between phosphorylated STAT3 protein and the prognosis and clinicopathological characteristics of patients with gastric cancer," *Journal of Gastroenterology and Hepatology*, vol. 29, no. 2, pp. 148–154, 2020.

[5] H. Xu, Y. Zhang, and F. Liu, "Expression changes of lncRNAMEG3 and GAS5 in gastric cancer tissues and their relationship with the clinicopathological characteristics and prognosis of patients," *Shandong Medicine*, vol. 59, no. 10, pp. 6–9, 2019.

[6] Z. Su, G. Wang, and Y. Yang, "Study on the correlation between the expression of miR-935 and the efficacy and prognosis of platinum-based chemotherapy in patients with advanced gastric cancer," *Chinese Journal of Integrated Traditional Chinese and Western Medicine on Digestion*, vol. 27, no. 5, pp. 15–19+24, 2019.

[7] L. Zhang, X.-y. Liu, G. Zhong, Z. Xin, X.-Y. Sun, and Z.-Y. Wang, "A protocol of systematic review and meta-analysis of narrow band imaging endoscopy in detection of early gastric cancer," *Medicine*, vol. 99, no. 33, Article ID e21420, 2020.

[8] Y. Li, B. Zhong, and W. Zeng, "Expression of GRAP and Treg in gastric cancer and their relationship with clinical features and prognosis," *Guangdong Medicine*, vol. 40, no. 9, pp. 126–129, 2019.

[9] L. Tong, N. Ding, and J. Li, "Study on detection of tumor mutation burden of tumor free DNA in pleural effusion supernatant of patients with advanced lung cancer," *Chinese Journal of Tuberculosis and Respiratory*, vol. 42, no. 8, pp. 596–601, 2019.

[10] A. Avanesyan, A. Sokolenko, and A. Ivantsov, "Gastric cancer in BRCA1 germline mutation carriers: results of endoscopic screening and molecular analysis of tumor tissues," *Pathobiology*, vol. 87, no. 6, pp. 1–8, 2020.

[11] S. Wang, H. Li, and C. Tang, "The relationship between CD44, CD133 and NLR and the pathological characteristics of gastric cancer and their significance in prognostic evaluation," *Practical Journal of Cancer*, vol. 35, no. 11, pp. 34–37, 2020.

[12] X. Wang and B. Liu, "The mechanism of ARID1A gene mutation or loss of expression mediating tumorigenesis and its value in gastric cancer immunotherapy," *Chinese Journal of Oncology*, vol. 47, no. 18, pp. 955–960, 2020.

[13] J. H. Kim, M.-H. Ryu, Y. S. Park et al., "Predictive biomarkers for the efficacy of nivolumab as ≥ third-line therapy in patients with advanced gastric cancer (AGC): from a subset analysis of ATTRACTION-2 phase III trial," *Journal of Clinical Oncology*, vol. 37, no. 4_suppl, p. 152, 2019.

[14] M. Lang, M. Baumgartner, A. Rożalska et al., "Crypt residing bacteria and proximal colonic carcinogenesis in a mouse model of Lynch syndrome," *International Journal of Cancer*, vol. 147, no. 8, pp. 2316–2326, 2020.

[15] A. Rizzo and A. D. Ricci, "PD-L1, TMB, and other potential predictors of response to immunotherapy for hepatocellular carcinoma: how can they assist drug clinical trials?" *Expert Opinion on Investigational Drugs*, vol. 30, pp. 1–9, 2021.

[16] Y. Zhou, S. Xu, and C. Guan, "The regulatory role of GAPLINC in malignant tumors and its relationship with patient prognosis," *Chinese Journal of Pathology*, vol. 48, no. 11, pp. 902–905, 2019.

[17] D. Yang, Y. Xu, L. Huang et al., "A pan-cancer analysis of ARID1A as a potential biomarker for immune checkpoint therapy," *Journal of Clinical Oncology*, vol. 38, no. 15_suppl, p. 3540, 2020.

[18] H. Chu, H. Cao, and H. Lu, "Association analysis between the expression of miRNA182 in gastric cancer tissues and the progression and prognosis of patients," *Air Force Medical Journal*, vol. 35, no. 2, pp. 132–134, 2019.

Hindawi
Journal of Oncology
Volume 2021, Article ID 2929233, 5 pages
https://doi.org/10.1155/2021/2929233

Research Article

Study on the Differential Value of Tumor Marker CA724 on Primary Gastric Cancer

Jieying Ding, Han Zhang, and Zixian Wu

Department of Clinical Laboratory, Shanghai Ninth People's Hospital, Shanghai Jiao Tong University School of Medicine, Shanghai 200011, China

Correspondence should be addressed to Jieying Ding; dingjieying@sh9hospital.com.cn

Received 17 June 2021; Revised 14 September 2021; Accepted 15 September 2021; Published 25 September 2021

Academic Editor: Alamgeer Yuchi

We investigated the diagnostic value of the tumor marker CA724 in patients with primary gastric cancer. One hundred forty-six patients with primary gastric cancer were selected as the observation group; 89 patients with gastritis treated in the same period were included in the control group 1; 91 patients with healthy physical examination during the same period were included in the control group 2. Electrochemiluminescence immunoassay was used to determine the level of carbohydrate antigen CA724 in each group; the pathological data of the observation group were consulted, and the expression level of tumor marker CA724 under different pathological conditions was analyzed; ROC curve was drawn to evaluate the diagnostic value of CA724 in gastric cancer and gastritis. The level of CA724 in primary gastric cancer patients was significantly correlated with tumor diameter, tumor stage, differentiation type, and lymph node metastasis. The ROC curve was drawn with a CA724 cutoff value of 7.94 U/Ml. The AUC value of CA724 in primary gastric cancer patients was 0.815, with a diagnostic sensitivity of 84.68% and a specificity of 71.95%. In conclusion, CA724 was highly expressed in patients with primary gastric cancer, which can achieve the diagnostic differentiation of gastric cancer and gastritis, and obtain a high diagnostic efficiency, providing a reference basis for clinical diagnosis and treatment.

1. Introduction

Gastric cancer is a malignant tumor originating from the epithelium of the gastric mucosa, which is more common in people over 50 years of age and has a slightly higher incidence in men than in women. In recent years, the incidence of gastric cancer has been on the rise due to changes in people's diet, increased work pressure, and *Helicobacter pylori* infection [1]. Previous studies have reported that gastric cancer can occur in any part of the stomach, with most patients occurring in the sinus, greater curvature, and lesser curvature of the stomach [2]. Most patients with gastric cancer are adenocarcinoma, and the symptoms are not obvious in the early stage of development. With the prolongation of the disease, it can be accompanied by nonspecific symptoms such as upper abdominal discomfort and belching, and it is similar to gastritis, which makes clinical diagnosis and treatment more difficult [3]. Although pathological tissue examination is the "gold standard" for diagnosing primary gastric cancer, it can help patients to confirm the diagnosis, but it is difficult to be applied in primary hospitals because of the high diagnostic risk [4, 5].

Tumor marker CA724 is a glycoprotein antigen, with a double antigenic determinant cluster, mainly found in human adenocarcinoma tissues, and is considered a tumor marker in the gastrointestinal tract and ovaries [6]. Previous studies have shown that CA724 is highly expressed in solid tumors such as gastric, breast, and lung cancers, reflecting the severity of the disease [7]. However, the application of CA724 in primary gastric cancer and gastritis has been less investigated. Therefore, this study was conducted to investigate the diagnostic value of CA724 in patients with primary gastric cancer and gastritis.

2. Materials and Methods

2.1. Clinical Data. 146 patients with primary gastric cancer who underwent surgery at Shanghai Ninth People's Hospital, Shanghai Jiao Tong University School of Medicine, Shanghai, China, from January 2018 to December 2020 were selected for the study and also set up as an observation group. The clinical data for the patients were as follows: 84 males and 62 females, aged 37–84 years old, mean: 61.49 ± 6.61 years; disease duration: 1–13 months, mean: 6.93 ± 0.85 months; tumor diameter: 1–6 cm, mean: 3.41±0.89 cm; clinical stage: 81 cases of stages I-II, 65 cases of stages III-IV; differentiation type: 33 cases of low differentiation, 71 cases of medium differentiation, 42 cases of high differentiation, and 51 cases of lymph node metastasis. 89 patients with gastritis treated at the same time were selected as control group 1, 49 men and 40 women, aged 36–85 years old, average, 60.98 ± 6.58; the duration of the disease was 1–12 months, with a mean of 6.91 ± 0.83 months. 91 patients with health check-ups at the same time were selected as control group 2, 53 males and 38 females, aged 35–84 years, with a mean of 60.15 ± 6.51 years. This study was approved by the Ethics Committee of the Shanghai Ninth People's Hospital, Shanghai Jiao Tong University School of Medicine, Shanghai, China. All patients provided written informed consent.

2.2. Inclusion and Exclusion Criteria

Inclusion criteria: (1) patients in the observation group met the diagnostic criteria for primary gastric cancer [8] and were diagnosed by pathological tissue examination; (2) control group 1 met the diagnostic criteria for gastritis and was diagnosed by gastroscopy; (3) everyone had completed the CA724 test and could tolerate it; (4) complete baseline and follow-up data.

Exclusion criteria: (1) patients with mental disorders, cognitive dysfunction, or other malignant tumors; (2) patients with autonomic nervous system diseases and severe liver and kidney dysfunction; (3) patients who had received radiotherapy and chemotherapy before the examination and had autoimmune system diseases.

2.3. Methods

2.3.1. Specimen Collection. 3 mL of peripheral fasting blood was obtained from the patients in the observation group and control group 1 the next day after admission and from the patients in the control group 2 on the day of healthy physical examination. The blood was centrifuged for 10 minutes at a speed of 3000 rpm and stored at a low temperature for further use.

2.3.2. Detection Method. Electrochemiluminescence immunoassay (Roche Cobas e80, Roche, Switzerland) was used to determine the level of CA724 in each group. The pathological data of the observation group (including gender, age, tumor diameter, tumor stage, differentiation type, and lymph node metastasis) were checked, and the expression levels of CA724 under different pathological conditions were evaluated [9, 10].

2.3.3. ROC Curves. ROC curves were drawn to analyze the diagnostic value (diagnostic sensitivity and specificity) of CA724 in gastric cancer and gastritis.

2.4. Statistical Analysis. The statistical analysis was performed by SPSS24.0 software and expressed by n (%). The t-test was used for comparison between groups, and the χ^2 test was used to compare all counting data between groups. The difference was statistically significant when $p < 0.05$.

3. Results

3.1. Comparison of CA724 Levels in the Three Groups. The patients in the three groups all completed the investigation of CA724 levels. As given in Table 1, the results showed that there was no significant difference in the level of the CA724 in control group 1 and control group 2 ($p > 0.05$); in the meantime, the CA724 levels in the observation group were higher than those in the control group 1 and control group 2.

3.2. Comparison of CA724 Levels in the Observation Group under Different Pathological Conditions. The pathological data of all patients were collected, and the results showed that the level of CA724 in patients with primary gastric cancer was not statistically correlated with gender and age ($p > 0.05$). At the same time, it was statistically related to tumor diameter, tumor stage, differentiation type, and lymph node metastasis ($p < 0.05$, Table 2).

3.3. ROC Curve of CA724 in Patients with Primary Gastric Cancer. The ROC curve was drawn with the cutoff value of the CA724 at 7.94 U/mL. The results showed that the AUC value of the CA724 for patients with primary gastric cancer was 0.815, the diagnostic sensitivity was 84.68%, and the specificity was 71.95% (Figure 1).

4. Discussion

Primary gastric cancer is a malignant tumor with high clinical incidence, and with the change of people's lifestyle, it has led to an increasing trend of disease incidence [11]. However, the early diagnosis rate of primary gastric cancer is relatively low, leading to a high clinical mortality rate, and it is clinically important to choose an appropriate diagnostic method to improve the detection rate and patient prognosis [12]. Histopathological examination is a common diagnostic technique to differentiate primary gastric cancer and gastritis, and it is considered the "gold standard" for diagnosis. However, this diagnostic approach is risky, invasive, and requires high instrumentation and equipment, so it is difficult to apply it at the grassroots level [13].

With the improvement and development of medical technology, clinical research in the area of tumor markers has

Table 1: Comparison of CA724 levels in the three groups.

Group	Cases	CA724 (U/mL)
Observation group	146	$52.53 \pm 5.39^{\#*}$
Control group 1	89	4.51 ± 0.64
Control group 2	91	4.42 ± 0.61
F	—	7.195
P	—	

$^{\#}$Compared with the control group 2, $p < 0.05$; *compared with the control group 1, $p < 0.05$.

Table 2: Comparison of CA724 levels in the observation group under different pathological conditions ($\overline{x} \pm s$).

Pathological type		Cases	CA724 (U/mL)	t	P
Gender	Male	84	51.98 ± 5.35	1.593	0.425
	Female	62	53.87 ± 5.51		
Age (years)	≥60	79	51.90 ± 5.31	0.615	0.893
	<60	67	53.89 ± 5.54		
Tumor diameter	≥3 cm	73	79.69 ± 8.51	9.154	≤0.001
	<3 cm	73	43.19 ± 5.12		
Tumor stage	I-II	81	46.96 ± 5.31	8.391	≤0.001
	III-IV	65	80.44 ± 8.78		
Differentiation type	Poorly differentiated	33	91.45 ± 9.51	11.691	≤0.001
	Moderate differentiation	71	54.69 ± 6.13		
	Well differentiated	42	40.31 ± 4.96		
Lymph node metastasis	Yes	51	94.59 ± 9.15	10.529	≤0.001
	No	95	42.33 ± 4.29		

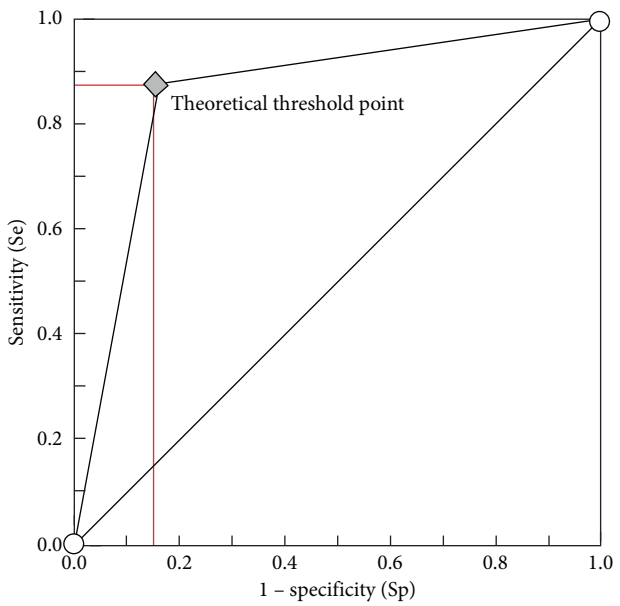

Figure 1: ROC curve of CA724 in patients with primary gastric cancer.

been strengthened. Tumor markers are chemical analogs that reflect the presence of tumors and are expressed at low or no levels in normal tissues and are present only in embryonic tissues. However, their levels are significantly higher in tumor tissues [14, 15]. Previous studies have shown that the existence and quantitative changes of tumor markers can reflect the nature of the tumor to some extent and can reflect the histogenesis, cellular function of the tumor, and thus the severity of the patient's disease [16]. A series of studies have explored the diagnostic and prognostic value of various serum tumor markers in gastric cancer [17, 18]. Tumor biomarker CA724 trended to be considered as an independent prognostic factor [19]. Tong et al. found that CA724 predicted overall survival in locally advanced gastric cancer patients with neoadjuvant chemotherapy [20]. In this study, there was no significant difference between the levels of tumor marker CA724 in control group 1 and control group 2 ($p > 0.05$), while the level of tumor marker CA724 in the observation group was higher than that in both control group 1 and control group 2 ($p < 0.05$). Taken together, we found that tumor marker CA724 was highly expressed in patients with primary gastric cancer. At the same time, it had lower levels in patients with gastritis, suggesting that strengthening CA724 level measurement can achieve the diagnosis and differentiation of primary gastric cancer and gastritis.

CA724 is a gastric cancer antigen, one of the laboratory indicators for detecting gastric cancer and various gastrointestinal cancers, and it is a nonspecific tumor marker. Previous studies have shown that elevated levels of CA724 do not indicate that patients have tumors [21]. They are more common in gastrointestinal tissues and have high sensitivity to gastric cancer and nonsmall cell lung cancer. In this study, the level of the tumor marker CA724 in patients with primary gastric cancer was significantly correlated with tumor diameter, tumor stage, type of differentiation, and lymph node metastasis ($p < 0.05$), indicating that the elevated expression level of CA724 in patients with primary gastric cancer could reflect the severity of the disease. Previously performed studies have reported that CA724 is a second-generation tumor-associated glycoprotein-72 with dual antigenic determinants, and its expression level is

elevated in malignant tumors such as gastric cancer, colon cancer, and lung cancer [22]. However, the increase in the level of CA724 does not mean that the patient must have a tumor disease. The level of this indicator is also elevated in type 2 diabetes, liver cirrhosis, rheumatism, and gastrointestinal disorders. Studies have shown that CA724 is a sugar chain antigen that can act as a cell surface adhesion molecule to participate in the occurrence and development of tumors [23]. In order to further analyze the diagnostic value of CA724 in primary gastric cancer and gastritis, the ROC curve was drawn in this study with a CA724 cutoff value of 7.94 U/mL. The results showed that the AUC value of CA724 in primary gastric cancer patients was 0.815, with a diagnostic sensitivity of 84.68% and a specificity of 71.95%, indicating that CA724 can achieve the diagnostic differentiation between primary gastric cancer and gastritis, and has high diagnostic efficacy. Therefore, clinical attention should be paid to CA724 levels when they are elevated, and other methods of diagnosis should be combined when necessary to help patients with early diagnosis [24].

5. Conclusion

CA724 was highly expressed in patients with primary gastric cancer, which can achieve the diagnostic differentiation of gastric cancer and gastritis, and can obtain a high diagnostic efficacy and provide a reference basis for clinical diagnosis and treatment. In future clinical practice, tumor marker CA724 can be applied to diagnose primary gastric cancer to improve the diagnostic accuracy and provide timely and effective treatment for patients.

Data Availability

The datasets used and/or analyzed during the current study are available from the corresponding author upon request.

Ethical Approval

The study was approved by the Ethics Committee of Shanghai Ninth People's Hospital, Shanghai Jiao Tong University School of Medicine, Shanghai, China.

Conflicts of Interest

The authors declare that they have no conflicts of interest.

Acknowledgments

This research was approved by the Medical and Engineering Cross Research Foundation of Shanghai Jiao Tong University (YG2016QN15).

References

[1] Y. Liu, M. Jiang, L. N. Ni, Z. Xu, and J. Z. Xu, "The value of serum carcinoembryonic antigen, carbohydrate antigen 724 combined with long-chain non-coding RNA MALAT1 in the diagnosis of gastric cancer," *Cancer Research and Clinic*, vol. 31, no. 2, pp. 88–92, 2019.

[2] J. M. Zhang, Z. Luo, Z. M. Fu et al., "Detection of circulating tumor cells and circulating tumor vascular endothelial cells in gastric cancer and its clinical significance," *Chinese Journal of General Surgery*, vol. 36, no. 4, pp. 281–285, 2021.

[3] M. Li, F. Xue, J. Yang, and X. Pan, "Correlation between tumor marker CA72-4 and prognosis of patients with gastric cancer," *Medicine*, vol. 99, no. 52, Article ID e23723, 2020.

[4] N. N. Sun, Y. Liang, and L. Shi, "The clinical value of CA724, CA242 and CEA in predicting the prognosis of colon cancer," *Modern Digestion and Interventional Diagnosis and Treatment*, vol. 24, no. 4, pp. 83–85, 2019.

[5] B. Liu, Y. Zhao, X. S. Pan, B. Fu, and F. W. Wang, "The clinical value of combined detection of pepsinogen and tumor markers in the diagnosis of gastric cancer," *Advances in Modern Chinese General Surgery*, vol. 22, no. 8, pp. 655-656, 2019.

[6] Z. Peng, C. J. Zheng, P. Jiang, L. Chen, and G. Q. Song, "The diagnostic value of serum tumor markers carcinoembryonic antigen and carbohydrate antigen in gastric cancer peritoneal metastasis," *Western Medicine*, vol. 31, no. 5, pp. 782–785, 2019.

[7] Q. Zhu, X. Wu, M. Tang, and L. Wu, "Observation of tumor-associated macrophages expression in gastric cancer and its clinical pathological relationship," *Medicine*, vol. 99, no. 17, Article ID e19839, 2020.

[8] Ministry of Health of the People's Republic of China, *Diagnostic Standards for Gastric Cancer (WS 316-2010)*, China Standards Press, Beijing, China, 2010.

[9] Y. Wang, H. L. Cui, Y. Z. Lin, and Q. Z. Cui, "The differential diagnosis value of multi-slice spiral computed tomography and gastrointestinal tumor markers for advanced gastric cancer and primary gastric lymphoma," *Cancer Progress*, vol. 18, no. 15, pp. 79–82, 2020.

[10] L. H. Yin, "The evaluation value of CEA, AFP, CA199, CA242, CA724 in the diagnosis and prognosis of gastric cancer," *Hebei Medicine*, vol. 42, no. 9, pp. 1348–1350, 2020.

[11] A. B. Sagakyants, O. I. Kit, E. P. Ulianova et al., "Expression of CD44 and CD133 in tumor cells of metastatic and non-metastatic gastric cancer," *Journal of Clinical Oncology*, vol. 37, no. 15s, Article ID e15531, 2019.

[12] H. F. Liu, Z. Wang, L. Wang, and Y. Liang, "The value of tumor markers in the diagnosis and prognosis of gastric cancer and their correlation with immune inflammatory response indexes," *Journal of Hebei Medical University*, vol. 40, no. 7, pp. 855–858, 2019.

[13] R. Guo, X. L. He, and F. Gao, "The value of serum high-sensitivity C-reactive protein, carcinoembryonic antigen, carbohydrate antigen 724 and carbohydrate antigen 199 in the early diagnosis of gastric cancer and related lesions," *Anhui Medicine*, vol. 23, no. 1, pp. 106–109, 2019.

[14] Y. H. Liu, J. F. Song, H. Li, X. Y. Ye, and X. Y. Zeng, "Value analysis of combined detection of serum tumor markers CEA, CA19-9, CA242 and CA724 in the diagnosis of gastric cancer," *Modern Digestive and Interventional Diagnosis and Treatment*, vol. 24, no. 4, pp. 94–98, 2019.

[15] B. Wei, X. Xing, Z. Li et al., "Tumor mutation burden and immunogenicity in gastric cancer with HER2 alterations," *Journal of Clinical Oncology*, vol. 37, no. 15s, p. 4024, 2019.

[16] J. X. Hou and P. Guo, "Value analysis of immunohistochemical markers Her-2 and tumor markers in the diagnosis of gastric cancer," *Shaanxi Medical Journal*, vol. 48, no. 1, pp. 121–124, 2019.

[17] T. Matsuoka and M. Yashiro, "Biomarkers of gastric cancer: current topics and future perspective," *World Journal of Gastroenterology*, vol. 24, no. 26, pp. 2818–2832, 2018.

[18] L. Zou, L. Guo, C. Zhu, Z. Lai, Z. Li, and A. Yang, "Serum phospholipids are potential biomarkers for the early diagnosis of gastric cancer," *Clinica Chimica Acta*, vol. 519, pp. 276–284, 2021.

[19] J. Louhimo, A. Kokkola, H. Alfthan, U.-H. K. Stenman, and C. Haglund, "Preoperative hCGbeta and CA 72-4 are prognostic factors in gastric cancer," *International Journal of Cancer*, vol. 111, no. 6, pp. 929–933, 2004.

[20] Y. Tong, Y. Zhao, Z. Shan, and J. Zhang, "CA724 predicts overall survival in locally advanced gastric cancer patients with neoadjuvant chemotherapy," *BMC Cancer*, vol. 21, no. 1, p. 4, 2021.

[21] C. Q. Wu, Q. L. Wang, P. Li, and X. C. Tu, "Application value of combined detection of P53, PCNA, CA724, gastrin 17 and *Helicobacter pylori* antibody in the identification of atrophic gastritis and early gastric cancer," *Chinese Journal of Microecology*, vol. 32, no. 2, pp. 72–76, 2020.

[22] Y. Chen, G. Chen, J.-N. Xiong et al., "Immunogenomic classification of gastric cancer based on the tumor microenvironments expression of PD-L1 and CD8+ *T*-cell infiltration," *Journal of Clinical Oncology*, vol. 38, no. 15s, Article ID e16578, 2020.

[23] J. H. Chen, H. W. Zhang, and K. M. Ying, "Expression and significance of tumor markers and immunohistochemical indicators in gastric cancer tissues," *Shanxi Medical Journal*, vol. 048, no. 10, pp. 1139–1142, 2019.

[24] J. Y. Liu, J. T. Zhao, L. N. Meng, Y. T. Wang, and J. M. Xiang, "The clinical application of serum amyloid A in the auxiliary diagnosis of gastric cancer," *Marker Immunoassay and Clinic*, vol. 26, no. 9, pp. 77–82, 2019.

Hindawi
Journal of Oncology
Volume 2021, Article ID 8273722, 5 pages
https://doi.org/10.1155/2021/8273722

Research Article

Effects of Combined Epidural Anesthesia and General Anesthesia on Cognitive Function and Stress Responses of Elderly Patients Undergoing Liver Cancer Surgery

Zhixiu Meng, Cao Gao, Xin Li, Jiang Shen, Tao Hong, Xiaofeng He, and Leijun Zhu

Department of Anesthesiology, The Third Affiliated Hospital of Soochow University, Changzhou 213003, Jiangsu, China

Correspondence should be addressed to Leijun Zhu; ziejiuho@163.com

Received 2 June 2021; Revised 13 September 2021; Accepted 14 September 2021; Published 25 September 2021

Academic Editor: Alamgeer Yuchi

This study aimed at exploring the effects of combined epidural anesthesia and general anesthesia on the cognitive function and stress responses of elderly patients undergoing liver cancer surgery. One hundred and fifteen elderly patients were enrolled as research subjects. They were admitted to our hospital and underwent liver cancer surgery from August 2017 to May 2019. Fifty five cases were treated with general anesthesia (GA) (GA group), while the other sixty cases were treated with combined epidural anesthesia and general anesthesia (joint group). Scoring standards of Mini-Mental State Examination (MMSE) were used to evaluate the patients before and after operation. Their operating time, total fluid input (TFI), spontaneous breathing recovery time (SBRT), preoperative and postoperative indices of stress responses (epinephrine (EPI), cortisol (Cor), and norepinephrine (NE)), and postoperative adverse reactions were observed. There were statistically significant differences between the two groups with respect to anesthesia time, TFI, postoperative SBRT, and postoperative directional recovery time (DRT) ($cP < 0.05$). There was no difference in operating time, total fluid loss (TFL), and hospitalization time ($P > 0.05$). After operation, patients in both groups experienced a cognitive decline of different degrees and the MMSE scores decreased. There was no significant difference in the score between the two groups before operation and 3 days and 7 days after operation ($P > 0.05$). The score was significantly better in the joint group than that in the GA group at 6 hours and 1 day after operation ($P < 0.05$). There were no significant differences in levels of EPI, Cor, and NE between the two groups before operation ($P > 0.05$), but there were significant differences after operation. The total incidence of postoperative adverse reactions was 11.67% in the joint group and 25.45% in the GA group. In conclusion, combined epidural anesthesia and general anesthesia can significantly reduce postoperative cognitive dysfunction and inhibit postoperative stress responses in elderly patients undergoing liver cancer surgery. It has good application value in clinical practice.

1. Introduction

As a common malignant tumor in the digestive system, liver cancer has a high mortality rate and a natural survival period of less than 3–6 months [1]. According to statistics of a previous study, the disease is the fifth most common cancer worldwide [2]. It is estimated that there are approximately 780,000 new cases and 740,000 deaths globally every year. Cases in China alone account for 50% of the total number [3]. According to the National Cancer Center, the incidence of liver cancer ranked the second among all cancers in China in 2014 [4], and the incidence in the elderly has been gradually increasing because of the aging population in this country [5]. The global disease burden caused by the disease has resulted in losses of lives, and the disease is still an important public health problem in the world due to its high incidence, mortality rate, and aggressiveness.

The etiology and exact molecular mechanism of primary liver cancer are still unclear. According to epidemiological and experimental research data, hepatitis B virus (HBV) and hepatitis C virus (HCV) infection, aflatoxin, contaminated drinking water, and liver cirrhosis are all related to the pathogenesis of liver cancer [6]. The clinical symptoms of early liver cancer are not apparent, so most patients were already at

the advanced stage once the symptoms appeared. After the early diagnosis of liver cancer, the disease is primarily treated by surgery with a high cure rate [7, 8]. However, the risk of surgical treatment rises with the increasing number of elderly patients. The patients' postoperative cognitive function and stress responses are different due to different anesthesia methods [9, 10]. Although general anesthesia (GA) is commonly used in liver cancer surgery, the incidence of postoperative cognitive dysfunction in elderly patients is high, which is also the focus of this study. Therefore, effects of combined epidural anesthesia and general anesthesia on the cognitive function and stress responses of elderly patients undergoing liver cancer surgery were explored in this study, so as to provide potential basis for future research.

2. Materials and Methods

2.1. Clinical Data. One hundred and fifteen elderly patients were enrolled as the research objects. They were admitted to The Third Affiliated Hospital of Soochow University, Changzhou, Jiangsu, China, and underwent liver cancer surgery from August 2017 to May 2019. Fifty five cases treated with GA were in the GA group, including 36 males and 19 females, with an average age of 67.5 ± 3.2 years. Sixty cases treated with combined epidural anesthesia and general anesthesia were in the joint group, including 33 males and 27 females, with an average age of 67.5 ± 3.1 years.

2.2. Inclusion and Exclusion Criteria

2.2.1. Inclusion Criteria. Patients who met the diagnostic criteria for liver cancer in the guidelines from the National Comprehensive Cancer Network [11]; patients aged 60–77 years old; patients with complete medical records; patients with indications to GA and epidural anesthesia (EA); patients with educational level of primary school and above; patients willing to cooperate in investigation; patients without other serious organ diseases affecting this study. This study has been approved by the ethics committee of The Third Affiliated Hospital of Soochow University, Changzhou, Jiangsu, China, and all study participants provided written informed consent.

2.2.2. Exclusion Criteria. Those with contraindications to anesthesia or liver cancer surgery; those who died during treatment; those with injury in important organs; those complicated with other tumors; those complicated with other cardiovascular and cerebrovascular diseases; those with physical disability; pregnant women; those complicated with other autoimmune diseases; those transferred to other hospitals; those with mental diseases, language dysfunction, or diseases affecting the results of this study.

2.3. Preoperative Preparation. Patients in the two groups fasted for 12 hours and were forbidden to drink water for 4 hours before operation. Venous infusion channels were established to carry out blood gas analysis and monitor vital signs and electrocardiograms of the patients.

2.4. Anesthesia Methods. Patients in the GA group were treated with GA. Anesthesia induction was first conducted with propofol (1.5 mg/kg) + sufentanil (0.2–0.6 μg/kg) + atracurium besylate (0.2 mg/kg). Tracheal intubation was performed for mechanical ventilation, with tidal volume controlled at 8–10 mL/kg, respiratory frequency controlled at 10–12 times/min, and partial pressure end-tidal carbon dioxide maintained at 35–45 mmHg. During operation, the patients after sevoflurane inhalation were continuously administered with remifentanil and propofol by a micropump and intermittently injected intravenously with atracurium to keep the muscle relaxed and ensure the anesthetic effect. Drug dosage was determined by the patients' tolerance degree and stress responses, and their vital signs were closely monitored throughout the operation. Patients in the joint group were treated with combined epidural anesthesia and general anesthesia. Strict disinfection was carried out before puncture. The patients were placed in a lateral position (bend the knees and embrace the knees with both hands) to fully expose the puncture position. Thoracic 8–10 spinous process intervals were selected, which were commonly used puncture sites in the upper abdomen. Local anesthesia was conducted after the puncture position was determined. Lidocaine with a concentration of 1% was selected as the anesthetic drug. After the puncture position was confirmed in the epidural space, ropivacaine (20 mL) with a concentration of 5% was injected, and the needle was pulled out after the puncture. The anesthesia block level was maintained between *T*6 and *T*9. Mask oxygen inhalation was conducted, and GA was performed after the body position was maintained for 10–15 min. The anesthesia method was the same as that in the joint group. After operation, dicaine, flurbiprofen axetil, and granisetron were administrated in both groups for postoperative analgesia. The drug dosage was determined based on the patients' pain tolerance.

2.5. Scoring Standards. Mini-Mental State Examination (MMSE) was used as the scoring standards to evaluate the patients before operation and 6 h, 1 d, 3 d, and 7 d after operation. Its total score was 30 points, and a high score indicated a better cognitive function.

2.6. Outcome Measures. Main outcome measures: the patients' operating time, total fluid input (TFI), spontaneous breathing recovery time (SBRT), cognitive function at each time period, and preoperative and postoperative indices of stress responses were observed.

Secondary outcome measures: the patients' postoperative adverse reactions were observed.

2.7. Statistical Methods. In this study, SPSS20.0 (IBM Corp, Armonk, NY, USA) was used to statistically analyze the collected data. GraphPad 7 was used to plot the required figures. Kolmogorov–Smirnov (K-S) test was used to analyze the distribution of measurement data. The data conforming to normal distribution were expressed by mean ± standard deviation (Mean ± SD). Independent samples *t*-test was used

for comparison between groups, while paired t-test was used for the comparison within groups. Count data were expressed by rate (%), analyzed by chi-square test, and represented by χ^2. When $P < 0.05$, the difference was statistically significant.

3. Results

3.1. Clinical Data. Before operation, there were no significant differences between the GA and joint groups in terms of age, body mass index (BMI), MMSE score, serum alpha-fetoprotein (AFP), gender, place of residence, smoking, drinking, exercise habits, systolic blood pressure (SBP), and diastolic blood pressure (DBP), indicating comparability ($P > 0.05$). See Table 1.

3.2. Operating Time, TFI, and SBRT. There were statistically significant differences between the two groups with respect to anesthesia time, TFI, postoperative SBRT, and postoperative directional recovery time (DRT) ($P < 0.05$). There were no differences in operating time, total fluid loss (TFL), and hospitalization time ($P > 0.05$). See Table 2.

3.3. Cognitive Function at Different Time Periods. After the operation, patients in both groups experienced a cognitive decline of different degrees, and the MMSE scores decreased. There was no significant difference in the score between the two groups before operation and 3 days and 7 days after operation ($P > 0.05$), while the score was significantly better in the joint group than that in the GA group at 6 hours and 1 day after operation ($P < 0.05$). See Table 3.

3.4. Preoperative and Postoperative Indices of Stress Responses. There were no significant differences in levels of epinephrine (EPI), cortisol (Cor), and norepinephrine (NE) between the two groups before operation ($P > 0.05$). There were significant differences after operation ($P < 0.05$). See Figure 1.

3.5. Postoperative Adverse Reactions. The total incidence of postoperative adverse reactions was 11.67% in the joint group and 25.45% in the GA group ($P < 0.05$). See Table 4.

4. Discussion

Liver cancer is mainly induced by alcohol, virus, and fatty liver injury [12]. Its early clinical manifestations are not apparent because of the decline of the sensory function and reaction ability in the elderly, so the disease is basically in the advanced stage when the patients feel the body abnormalities themselves, which definitely delays their treatment and increases the treatment difficulty [13]. Therefore, radiotherapy, chemotherapy, and surgery can be selected to relieve their pain and prolong their life [8, 14–16]. However, the operation is difficult for the elderly patients, because their surgical risk, postoperative cognitive dysfunction, and stress responses are higher than those of young patients with liver cancer. Currently, there are few studies available on the optimal anesthesia methods for the elderly patients. Therefore, in this study, effects of combined epidural anesthesia and general anesthesia on the cognitive function and stress responses of the elderly patients undergoing liver cancer surgery were explored, so as to provide a reference for clinical practice.

In this study, we first observed the intraoperative and postoperative recovery of the patients with liver cancer. There were statistically significant differences between the two groups with respect to anesthesia time, TFI, postoperative SBRT, and postoperative DRT. There were no differences in operating time, THL, and hospitalization time. This indicated that combined epidural anesthesia and general anesthesia could improve the patients' intraoperative and postoperative recovery capability. Liver cancer surgery requires a high level of anesthesia [17, 18], which is more obvious in elderly patients undergoing the surgery. The slight deviation of the level makes the patients prone to pulmonary stretch reflex [19], so it is difficult to achieve accurate anesthesia without affecting respiratory function. Scoring standards of MMSE were used to score the patients before and after operation. After operation, patients in both groups experienced cognitive decline of different degrees and decreasing MMSE scores. There was no significant difference in the score between the two groups before operation and 3 days and 7 days after operation. The score was significantly better in the joint group than that in the GA group at 6 hours and 1 day after operation. This suggested that combined epidural anesthesia and general anesthesia can improve the patients' postoperative cognitive function. We also observed the indices of stress responses before and after operation. There were no significant differences in levels of EPI, Cor, and NE between the two groups before operation, and there were significant differences after operation [20]. This demonstrated that combined epidural anesthesia and general anesthesia could stabilize the patients' indices of stress responses, while GA is slightly inferior. Finally, we observed the postoperative adverse reactions and found that their total incidence in the joint group was lower than that in the GA group. This further reveals the priority of combined epidural anesthesia and general anesthesia. Combined epidural anesthesia and general anesthesia can significantly reduce postoperative cognitive dysfunction and inhibit postoperative stress responses in elderly patients undergoing liver cancer surgery [21], so it has a good application value in clinical practice.

The abovementioned research has preliminarily suggested the effects of combined epidural anesthesia and general anesthesia on the cognitive function and stress responses of the elderly patients undergoing liver cancer surgery, which agree with the results of previous studies [22]. However, this study still has limitations. We did not take a series of neurocognitive tests. We did not follow up the patients for their prognosis. Therefore, we plan to perform more in-depth experimental analyses in future studies, so as to supplement our research results and provide services for clinical practice.

In summary, combined epidural anesthesia and general anesthesia is more effective than GA in reducing the

Table 1: Clinical information of patients (n(%)).

	GA group ($n = 55$)	Joint group ($n = 60$)	χ^2 or t	P value
Age (years)	67.5 ± 3.2	67.5 ± 3.1	0.051	0.956
BMI (kg/cm^2)	28.4 ± 2.61	27.85 ± 3.05	1.072	0.286
Gender			0.277	0.810
Male	36 (65.45)	33 (55.00)		
Female	19 (34.55)	27 (45.00)		
Place of residence			0.479	0.679
City	29 (52.72)	35 (58.83)		
Countryside	26 (47.28)	25 (41.67)		
Smoking			0.206	0.855
Yes	38 (69.09)	36 (60.00)		
No	17 (30.91)	24 (40.00)		
Drinking			0.117	0.917
Yes	39 (70.90)	48 (80.00)		
No	16 (29.10)	12 (20.00)		
Exercise habits			0.148	0.896
Yes	37 (67.27)	44 (73.33)		
No	18 (32.73)	16 (26.64)		
SBP (mmHg)	142.62 ± 12.87	138.86 ± 11.92	1.627	0.106
DBP (mmHg)	86.24 ± 8.67	85.16 ± 8.50	0.674	0.501
MMSE score	27.6 ± 2.83	27.74 ± 2.69	0.272	0.780
Serum AFP (ng/mL)	531 ± 69.20	523 ± 72.50	0.604	0.540

Table 2: Intraoperative and postoperative recovery.

	GA group ($n = 55$)	Joint group ($n = 60$)	t	P value
Operating time (min)	198.72 ± 56.14	187.39 ± 50.11	1.143	0.255
Anesthesia time (min)	214.67 ± 56.89	193.67 ± 55.73	2.073	0.040
TFI (mL)	1906.00 ± 201.00	1739.00 ± 182.00	3.192	0.002
TFL (mL)	375.73 ± 131.06	364.92 ± 120.73	0.460	0.646
Postoperative SBRT (min)	16.08 ± 3.62	13.87 ± 3.55	3.304	0.001
Postoperative DRT (min)	19.63 ± 4.01	17.36 ± 3.80	3.117	0.002
Hospitalization time (d)	18.55 ± 4.85	16.71 ± 5.31	1.934	0.056

Table 3: Cognitive function at different time periods.

	Before operation	6 hours after operation	1 day after operation	3 days after operation	7 days after operation
GA group ($n = 55$)	27.6 ± 2.83	21.77 ± 2.21	22.28 ± 2.51	26.45 ± 2.31	27.28 ± 2.21
Joint group ($n = 60$)	27.74 ± 2.69	23.58 ± 2.46	24.51 ± 2.58	27.09 ± 2.43	27.71 ± 2.11
t	0.272	4.173	4.691	1.000	1.067
P value	0.780	0.001	0.001	0.423	0.288

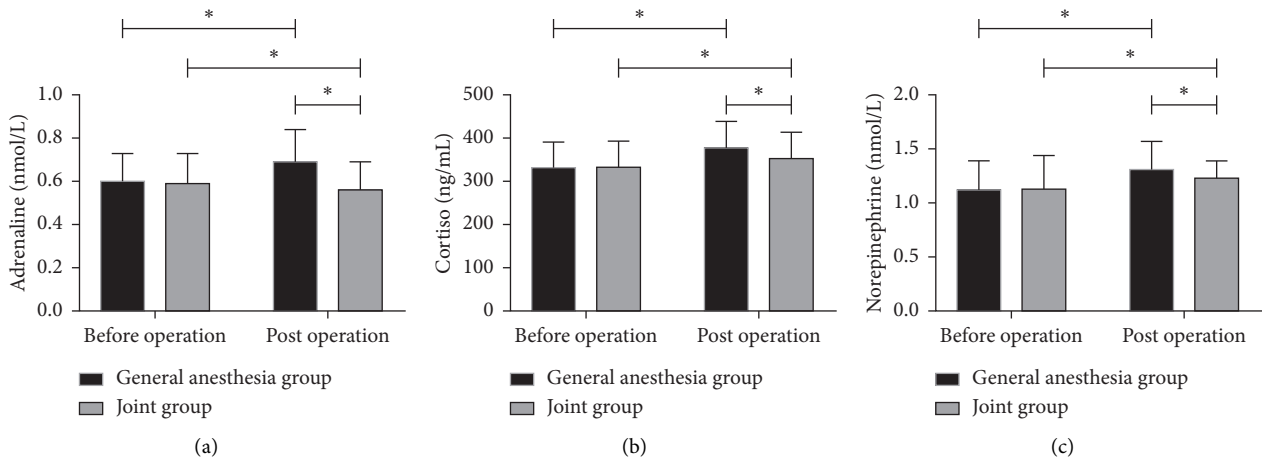

Figure 1: Indices of stress responses. (a) After operation, EPI level in the joint group decreased slightly and was lower than that in the GA group. (b) After operation, Cor level in the joint group increased slightly, but was lower than that in the GA group. (c) After operation, NE level in the joint group increased slightly, but was lower than that in the GA group. *Note.* * indicates a difference between two groups ($P < 0.05$).

Table 4: Postoperative adverse reactions.

	GA group ($n = 55$)	Joint group ($n = 60$)	χ^2/t	P value
Nausea	5(9.09)	1(1.67)		
Vomiting	3(5.45)	1(1.67)		
Dyspnea	2(3.63)	2(3.33)	4.771	0.029
Horner syndrome	4(7.27)	2(3.33)		
Total incidence	14(25.45)	6(11.67)		

postoperative cognitive dysfunction and stress responses of elderly patients undergoing liver cancer surgery, with low incidence of postoperative adverse reactions. Therefore, combined anesthesia, such as combined epidural anesthesia and general anesthesia can significantly reduce the postoperative cognitive dysfunction of the elderly patients undergoing liver cancer surgery.

Data Availability

The datasets used and/or analyzed during the present study are available from the corresponding author on reasonable request.

Conflicts of Interest

The authors declare that they have no conflicts of interest.

References

[1] M. C. S. Wong, J. Y. Jiang, W. B. Goggins et al., "International incidence and mortality trends of liver cancer: a global profile," *Scientific Reports*, vol. 7, no. 1, Article ID 45846, 2017.

[2] X. Zhang, X. Xu, G. Ge et al., "MiR-498 inhibits the growth and metastasis of liver cancer by targeting ZEB2," *Oncology Reports*, vol. 41, pp. 1638–1648, 2019.

[3] W.-M. Cong, H. Bu, J. Chen et al., "Practice guidelines for the pathological diagnosis of primary liver cancer: 2015 update," *World Journal of Gastroenterology*, vol. 22, no. 42, p. 9279, 2016.

[4] W. Chen, K. Sun, R. Zheng et al., "Cancer incidence and mortality in China," *Chinese Journal of Cancer Research*, vol. 30, no. 1, 2014.

[5] J. L. Petrick, M. Braunlin, M. Laversanne, P. C. Valery, F. Bray, and K. A. McGlynn, "International trends in liver cancer incidence, overall and by histologic subtype, 1978-2007," *International Journal of Cancer*, vol. 139, no. 7, pp. 1534–1545, 2016.

[6] M. Minemura and Y. Shimizu, "Gut microbiota and liver diseases," *World Journal of Gastroenterology*, vol. 21, no. 6, p. 1691, 2015.

[7] R. Chatterjee and A. Mitra, "An overview of effective therapies and recent advances in biomarkers for chronic liver diseases and associated liver cancer," *International Immunopharmacology*, vol. 24, no. 2, pp. 335–345, 2015.

[8] A. Vitale, P. Burra, A. C. Frigo et al., "Survival benefit of liver resection for patients with hepatocellular carcinoma across different Barcelona Clinic Liver Cancer stages: a multicentre study," *Journal of Hepatology*, vol. 62, no. 3, pp. 617–624, 2015.

[9] F. Cassinello, I. Prieto, M. del Olmo, S. Rivas, and G. R. Strichartz, "Cancer surgery: how may anesthesia influence outcome?" *Journal of Clinical Anesthesia*, vol. 27, no. 3, pp. 262–272, 2015.

[10] C. Y. Ni, Y. Yang, Y. Q. Chang et al., "Fast-track surgery improves postoperative recovery in patients undergoing partial hepatectomy for primary liver cancer: a prospective randomized controlled trial," *European Journal of Surgical Oncology (EJSO)*, vol. 39, no. 6, pp. 542–547, 2013.

[11] C. Wald, M. W. Russo, J. K. Heimbach, H. K. Hussain, E. A. Pomfret, and J. Bruix, "New OPTN/UNOS policy for liver transplant allocation: standardization of liver imaging, diagnosis, classification, and reporting of hepatocellular carcinoma," *Radiology*, vol. 266, no. 2, pp. 376–382, 2013.

[12] A. Marengo, C. Rosso, and E. Bugianesi, "Liver cancer: connections with obesity, fatty liver, and cirrhosis," *Annual Review of Medicine*, vol. 67, no. 1, pp. 103–117, 2016.

[13] W. Zhang and B. Sun, "Impact of age on the survival of patients with liver cancer: an analysis of 27,255 patients in the SEER database," *Oncotarget*, vol. 6, no. 2, pp. 633–641, 2015.

[14] J.-H. Sun, Q. Luo, L.-L. Liu, and G.-B. Song, "Liver cancer stem cell markers: progression and therapeutic implications," *World Journal of Gastroenterology*, vol. 22, no. 13, p. 3547, 2016.

[15] D. Shao, J. Li, X. Zheng et al., "Janus "nano-bullets" for magnetic targeting liver cancer chemotherapy," *Biomaterials*, vol. 100, pp. 118–133, 2016.

[16] T.-S. Su, P. Liang, J. Liang et al., "Long-term survival analysis of stereotactic ablative radiotherapy versus liver resection for small hepatocellular carcinoma," *International Journal of Radiation Oncology, Biology, Physics*, vol. 98, no. 3, pp. 639–646, 2017.

[17] S. Pathak, A. Hakeem, T. Pike et al., "Anaesthetic and pharmacological techniques to decrease blood loss in liver surgery: a systematic review," *ANZ Journal of Surgery*, vol. 85, no. 12, pp. 923–930, 2015.

[18] S. De La Serna, R. Vilana, S. Sánchez-Cabús et al., "Results of laparoscopic radiofrequency ablation for HCC. Could the location of the tumour influence a complete response to treatment? A single European centre experience," *International Hepato-Pancreato-Biliary Association*, vol. 17, no. 5, pp. 387–393, 2015.

[19] M. Terao, A. Takaki, T. Maruyama et al., "Serum oxidative/anti-oxidative stress balance is dysregulated in potentially pulmonary hypertensive patients with liver cirrhosis: a case control study," *Internal Medicine*, vol. 54, no. 22, pp. 2815–2826, 2015.

[20] Y. Su, Y. Pu, Z. Zhao, and X. Yang, "Influence of combined epidural anesthesia on cognitive function, inflammation and stress response in elderly liver cancer patients undergoing surgery," *Oncology Letters*, vol. 19, no. 4, pp. 2733–2738, 2020.

[21] N. Hadimioglu, H. Ulugol, H. Akbas, N. Coskunfirat, Z. Ertug, and A. Dinckan, "Combination of epidural anesthesia and general anesthesia attenuates stress response to renal transplantation surgery," *Transplantation Proceedings*, vol. 44, no. 10, pp. 2949–2954, 2012.

[22] J. Zhu, X. R. Zhang, and H. Yang, "Effects of combined epidural and general anesthesia on intraoperative hemodynamic responses, postoperative cellular immunity, and prognosis in patients with gallbladder cancer," *Medicine*, vol. 96, no. 10, Article ID e6137, 2017.

Hindawi
Journal of Oncology
Volume 2021, Article ID 6815713, 7 pages
https://doi.org/10.1155/2021/6815713

Research Article

Ginsenoside Rh2 Suppresses Metastasis and Growth of Colon Cancer via miR-491

Wene Wei, Qijing Guo, Cuiping Guo, Xianshu Cui, Xuemei Ma, Xianliang Shen, and Yushuang Luo

Department of Oncology, Qinghai University Affiliated Hospital, Xining 810001, Qinghai, China

Correspondence should be addressed to Yushuang Luo; weiwene@126.com

Received 28 June 2021; Revised 13 September 2021; Accepted 14 September 2021; Published 24 September 2021

Academic Editor: Alamgeer Yuchi

Ginsenoside Rh2 is considered as a new direction for future cancer treatment because of its excellent anticancer effect. However, due to its low bioavailability, it cannot exert its significant anticancer effect when applied directly to the human body. Chitosan (CS), a nanomaterial, has been verified to be able to enhance drug efficacy via its coating for drugs. Thus, we designed this study to investigate the impact of CS-coated ginsenoside Rh2 on the metastasis and growth of colon cancer (CC). First, ginsenoside Rh2 chitosan tripolyphosphate (CS-Rh2-TPP) nanoparticles (NPs) were constructed, and MTT, transwell, scratch adhesion, and flow cytometry assays were carried out for determining the impact of CS-Rh2-TPP at various concentrations on growth, metastasis, and apoptosis of colon cancer cells (CCCs). qRT-PCR was used to detect the expression of mircoRNA-491 (miR-491) in CCCs. According to TEM-based image analysis, CS-Rh2-TPP NPs were spherical or spheroidal in even distribution, with a particle size of about 220 mm and a zeta potential of -44.58 ± 2.84 mV. Additionally, CCCs presented lower miR-491 than normal colon cells, and its relative expression in CCCs showed a stronger increase after intervention of CS-Rh2-TPP than that after intervention of ginsenoside Rh2. Moreover, CS-Rh2-TPP suppressed the activity, invasion, as well as migration of CCCs and accelerated their apoptosis more significantly than ginsenoside Rh2. According to these results, CS-Rh2-TPP is able to upregulate miR-491 in CCCs, thus suppressing the metastasis and growth of CC.

1. Introduction

Due to changes in diet and living structure, gastroenterological diseases present a rising incidence, and colon cancer (CC) is a common one with a comparatively high global incidence [1]. The survey shows that the global incidence of CC is about 6.1% at present. Each year witnesses over 1 million new cases of CC and over 550,000 new deaths from the cancer [2]. Therefore, clinical efforts have been devoted to find solutions. The unfavorable prognosis of patients with CC is mainly caused by the difficulty in early clinical screening of CC and the lack of special clinical symptoms of early CC [3]. In fact, most patients have already entered the middle or late stage at the time diagnosis due to their lack of medical and health knowledge, resulting in the missing of the optimal timing for surgical treatment [4]. At this time, the tumor is usually accompanied by metastasis and invasion, and the commonly used clinical treatment schemes (surgery or combined chemoradiotherapy) generally cannot achieve the best effect of tumor resection [5].

Ginsenoside Rh2 is a primary active substance extracted from Ginseng, with potent pharmacological effects [6]. Its clinical impacts known so far include immunomodulatory activity and increasing cognitive ability [7]. It also plays a crucial part in antioxidant and antitumor activities [8]. According to studies, ginsenoside Rh2 suppresses angiogenesis in patients with prostate cancer through targeting CNNM1 [9] and accelerates the apoptosis of cervical cancer cells during starvation [10]. Additionally, ginsenoside Rh2 has been verified to affect tumors via miRs [11]. MicroRNA (miR) is a research focus in various fields. As a noncoding short-chain RNA in eukaryotes with about 22 nt in length, miR can regulate many intercellular signals via regulation on target genes by binding to downstream target genes 3' UTR,

5' UTR, and coding regions [12]. miR-491, a newly discovered miR, shows low expression in cases with CC according to one early study [13]. Another study [14] revealed that ginsenoside Rh2 can inhibit the growth of lung cancer (LC) via miR-491.

Thanks to the continuous advancement of medical technology, nanomedicine has attracted extensive application in clinical practice [15]. As a polymer colloid particle system (10–500 nm in diameter), NPs have been extensive used in carrying and delivering bioactive substance [16]. Chitosan (CS) is a biomaterial made by deacetylation of chitin from shrimps and crab, with favorable antibacterial and antiviral properties [17]. In one recent study, ginsenoside Rh2-CS NPs have been revealed to suppress the activity of LC cells [18]. However, whether it possesses the same effect in CC is still under investigation.

Accordingly, this study primarily investigated the impact of ginsenoside Rh2-CS NPs on the growth and metastasis of colon cancer cells (CCCs).

2. Materials and Methods

2.1. Preparation of CS NPs. The preparation of ginsenoside Rh2 chitosan tripolyphosphate (CS-RH2-TPP) nanoparticles (NPs) was carried out by referring to the study of Zare-Zardini et al. [19]. CS (4 mg, Shandong AK Biotech Co., Ltd., China) was stirred in 1% acetic acid (4 mL, Sigma-Aldrich, Merck KGaA) until it was completely dissolved, and then, the PH was adjusted to 5 with 2 mol/L NaOH. Ginsenoside Rh2 (1.2 mg, Zhejiang Yake Pharmaceutical Co., Ltd., China) was weighted and dissolved in methanol, which was then dripped into CS solution at 20 drops/min. Afterwards, equal volume of TPP solution was added dropwise and stirred for 30 min crosslinking reaction, followed by filtering via a 0.45 μm filter membrane and freeze drying. Finally, the obtained substance was stored at 4°C.

2.2. Identification of CS NPs. A transmission electron microscope (TEM, Beijing Precise Instrument Co., Ltd., China) was adopted to observe the microscopic morphology of CS NPs. Specifically, 1.0 mL solution was put on a carbon-coated copper grid, restained with phosphotungstic acid (Sigma-Aldrich, Merck KGaA), and then evaluated under a TEM after drying. Subsequently, 1.5 mL solution was made to penetrate a 0.22 μm microporous membrane, followed by analysis via a Malvern particle size analyzer (Zhuhai OMEC Instruments Co., Ltd., China) for understating the particle size and distribution.

2.3. Cell Culture. SW480 and SW620 cells (CCCs) were selected, and FHC cells (normal human colonic epithelial mucosal cells) were adopted as controls, all of which were offered by the American Type Culture Collection. The above cells were incubated (37°C, 5%CO_2) in 10% fetal bovine serum (FBS) + 1% penicillin/streptomycin-contained DMEM (Gibco).

2.4. MTT Assay. Cell viability was detected by MTT assay. Specifically, the transfected cells were transferred to a 96-well plate (2^*10^5 cells/well) after resuspension and cultured at room temperature for 24 h. Then, the plate was treated by 24 h of incubation with CS-Rh2-TPP or ginsenoside Rh2 at various concentrations (5, 10, and 20 μg/mL), followed by 4 h of incubation with 20 μL MTT complete medium per well (Thermo Fisher Scientific, USA), as well as 10 min mixing at 492 nm with complete medium replaced by 200 μL DMSO.

2.5. Transwell Assay. A transwell assay (Corning, USA) was conducted to understand the impact of CS-Rh2-TPP/ginsenoside Rh2 on the invasion of CCCs. Specifically, a Matrigel-coated transfer chamber with an 8 μm porous polycarbonate membrane was adopted. Totally, 100 μL DMEM (serum-free) suspended with 5×10^4 cells were transferred to 500 μL FBS-contained DMEM together with cell culture insert, followed by 24 h of incubation with CS-Rh2-TPP or ginsenoside Rh2 at various concentrations (5, 10, and 20 μg/mL). Afterwards, noninvasive cells on the upper surface of the membrane were scraped off, while the remaining was treated by immobilization via 4% paraformaldehyde and dyeing with 1% crystal violet. Finally, under an optical microscope, cells in a randomly selected area were counted.

2.6. Wound-Healing Assay. To investigate the impact of CS-Rh2-TPP/ginsenoside Rh2 on the migration of CCCs, a wound-healing assay was conducted. Specifically, in a 6-well plate seeded with 4×10^5 cells, two parallel wounds were created in the cell monolayer with a 10 μl pipette tip at the cell confluence of over 90%. Then, PBS was adopted for twice washing of the cell fragments that were then subjected to incubation in serum-free DMEM and then to 24 h of incubation with CS-Rh2-TPP or ginsenoside Rh2 (5, 10, and 20 μg/ml) at different concentrations. Finally, cell images were taken with one optical microscope (×200), followed by calculation of the wound width by a standard caliper.

2.7. Flow Cytometry Assay. The impact of CS-Rh2-TPP/ginsenoside Rh2 on the apoptosis of CCCs was determined with an Annexin V-APC kit (Shanghai Yeasen Biotechnology Co., Ltd., China). CS-Rh2-TPP or ginsenoside Rh2 at various concentrations (5, 10, and 20 μg/mL) were put into CCCs for 24 h of incubation, and the collected cells were determined via a FACS Calibur flow cytometer (BD Biosciences). CCCs collected via EDTA-free trypsin were suspended in binding buffer after two times of washing with cold PBS, followed by 15 min of dyeing with Annexin V-FITC and propidium iodide (PI). Finally, the proportion of apoptotic cells (Annexin V-FITC positive) in the total number of counted cells was calculated.

2.8. qRT-PCR Assay. After extraction of total RNA from collected cells with a TRIzol kit (Thermo Fisher Scientific, USA), its concentration, purity, as well as integrity were confirmed with an ultraviolet spectrophotometer and agarose

gel electrophoresis. Then, the total RNA was reverse transcripted to complementary DNA (cDNA) in strict accordance with the kit (Thermo Fisher Scientific, USA) instructions. The amplification system: 1 μL cDNA, 0.4 μL upstream and downstream primers, respectively, 10 μL 2 × TransTaq® Tip Green qPCR SuperMix, 0.4 μL passive reference dye (50X), and ddH_2O added for volume adjustment (20 μL in total); the amplification conditions: conditions for PCR reaction: 94°C for 30 s, followed by 40 cycles of 94°C for 5 s and 60°C for 30 s. Each sample was determined three times with three duplicate wells, and the obtained data were analyzed via $2^{-\triangle\triangle ct}$ (internal reference of miR: U6).

2.9. Statistical Analyses. In our study, GraphPad 8 was adopted for data analysis and data visualization into corresponding figures. Measurement data were presented by mean ± SD; the intergroup comparison was carried out via the independent-samples *t*-test, and the multigroup comparison was conducted by the one-way ANOVA (expressed in F) and LSD-t post hoc test. Additionally, the comparison of data at various time points was performed by the repeated measures ANOVA (expressed in F), and their post hoc comparison by the Bonferroni post hoc test. $P < 0.05$ denotes a remarkable difference.

3. Results

3.1. Identification of CS NPs. In our study, the constructed CS-Rh2-TPP NPs were identified first. According to TEM-based image analysis, CS-Rh2-TPP NPs were spherical or spheroidal in even distribution, with a particle size of 220 mm (Figure 1), negatively charged surface, and zeta potential of −44.58 ± 2.84 mV.

3.2. MiR-491 in CCCs. We analyzed the expression of miR-491 in CCCs based on the TCGA database through Starbase online and found that it was downregulated in CCCs (Figure 2(a)). We also quantified miR-491 in CCCs via a qRT-PCR assay. It was found that the expression of miR-491 in CCCs was significantly lower than that in normal colon cells, which indicates its low expression in cases with CC (Figure 2(b)).

3.3. Impact of CS-Rh2-TPP on miR-491 in CCCs. We have quantified miR-491 in cases with CC through the above assay. Then, we evaluated the impact of CS-Rh2-TPP/ginsenoside Rh2 on miR-491 in CCCs. According to the qRT-PCR assay, miR-491 in cases with CC increased more notably with the increase of their concentration, and the increase was more significant under the intervention of CS-Rh2-TPP than that under the intervention of ginsenoside Rh2 (Figure 3). The results suggest that CS-Rh2-TPP has a more significant effect on miR-491 in CCCs.

3.4. Impact of CS-Rh2-TPP on Cell Activity. For the purpose of exploring the impact of CS-Rh2-TPP on cell activity, we adopted CS-Rh2-TPP/ginsenoside Rh2 at various concentrations to intervene with CCCs. According to the MTT assay, the cell viability was more notably suppressed as their concentrations increased, and the suppression was stronger under intervention of CS-Rh2-TPP than that of ginsenoside Rh2 (Figure 4).

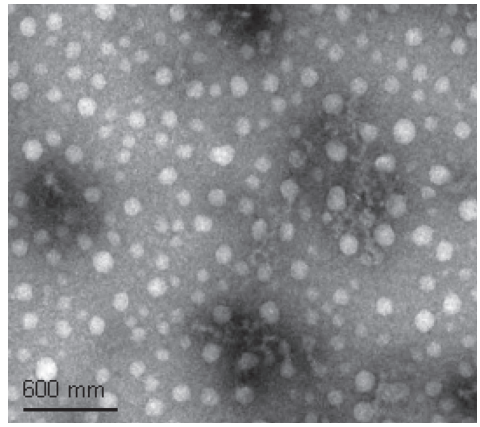

Figure 1: CS-Rh2-TPP nanoparticle morphology.

3.5. Impact of CS-Rh2-TPP on Cell Invasion and Migration. This study also evaluated the impact of CS-Rh2-TPP/ginsenoside Rh2 on the invasion and migration activities of CCCs. According to assay results, under intervention of CS-Rh2-TPP/ginsenoside Rh2, the invasion and migration activities of CCCs were increasingly inhibited as the concentration of CS-Rh2-TPP/ginsenoside Rh2 increased. Moreover, the intergroup comparison showed that the effect of CS-Rh2-TPP on the invasion and migration activities of CCCs was stronger than that of ginsenoside Rh2 (Figures 5(a) and 5(b)).

3.6. Impact of CS-Rh2-TPP on Apoptosis of CCCs. We also evaluated the impact of CS-Rh2-TPP on the apoptosis of CCCs. According to assays, the apoptosis of CCCs increased more notably as the concentration of CS-Rh2-TPP/ginsenoside Rh2 increased, and CS-Rh2-TPP exerted a more notable promotion effect on the apoptosis of CCCs than ginsenoside Rh2 (Figure 6).

4. Discussion

CC is the most common digestive tract malignancy, but its mechanism is still under investigation. In our study, ginsenoside Rh2 suppressed the growth and metastasis of CCCs and the constructed CS-Rh2-TPP exerted a more notable inhibitory action, so CS-Rh2-TPP is expected to be a clinical therapy scheme for CC.

Ginseng is a Chinese herbal medicine widely found in Asian countries, with various beneficial properties, including anti-inflammatory, antioxidation, and anticancer activities [20]. Ginsenoside Rh2, the primary active extract of Ginseng, is considered as a broad anticancer agent [21]. According to one study [22], ginsenoside Rh2 has the advantages of low toxicity, low molecular weight, and good fat

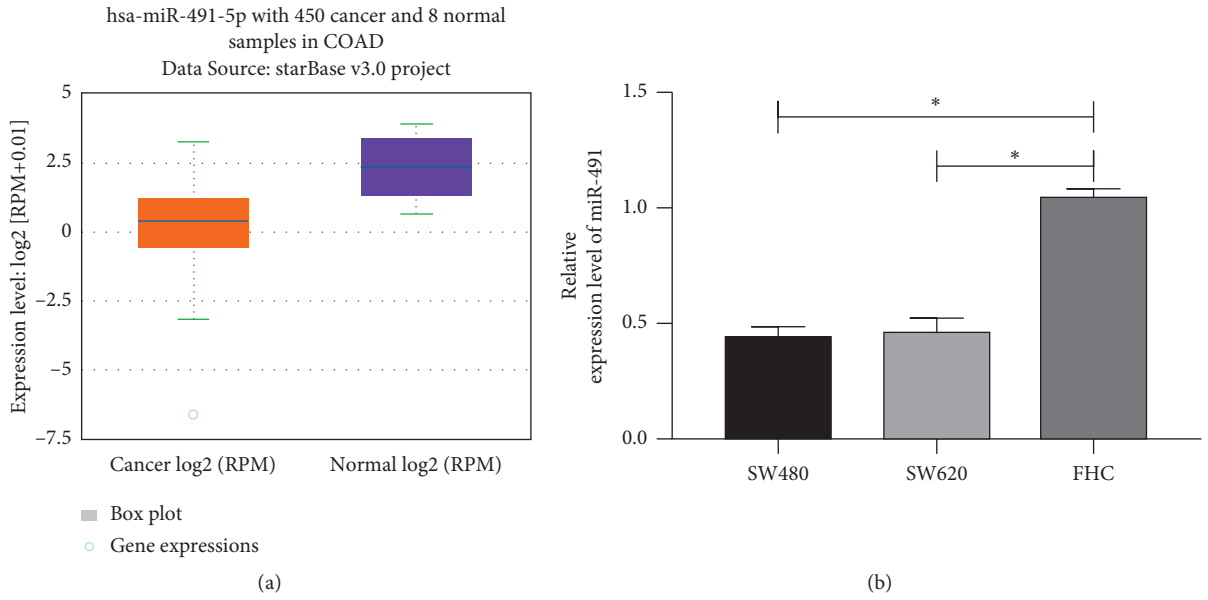

Figure 2: MiR-491 in CC (a). MiR-491 in cases with CC according to online analysis based on TCGA (b). MiR-491 in CCCs according to qRT-PCR assay. * $P < 0.05$. Note: CS-Rh2-TPP, ginsenoside Rh2 chitosan tripolyphosphate; CCCs, colon cancer cells; CC, colon cancer.

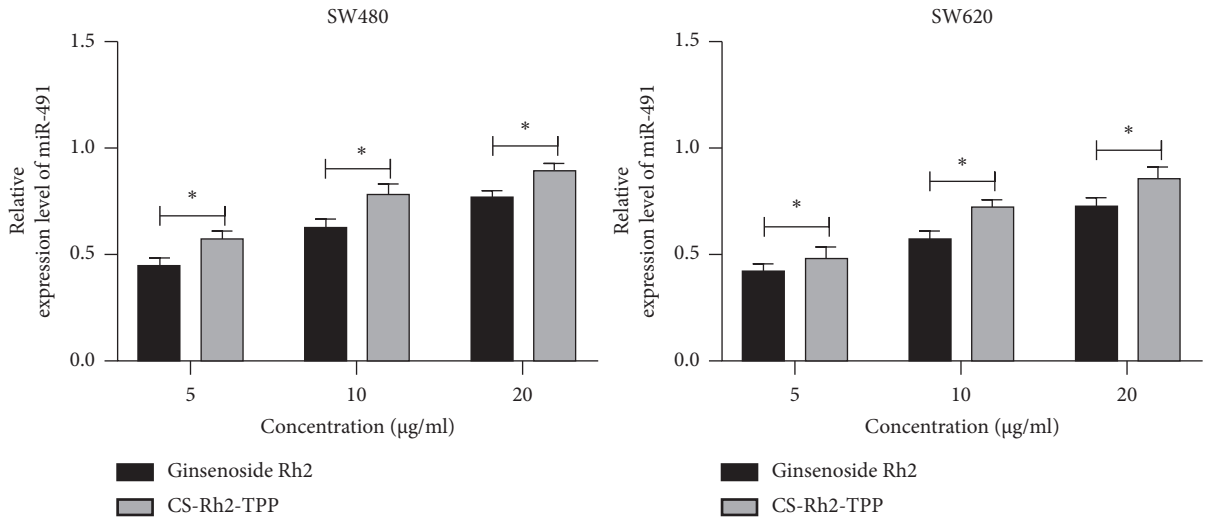

Figure 3: Impact of CS-Rh2-TPP on miR-491 in CCCs. *$P < 0.05$. Note: CS-Rh2-TPP, ginsenoside Rh2 chitosan tripolyphosphate; CCCs, colon cancer cells.

solubility. And its ability to inhibit the proliferation and migration of tumor cells and angiogenesis has been well documented [23]. One study [24] reported that ginsenoside Rh2 affected tumorigenesis through regulating encoded proteins or encoded RNAs [24]. MiR-491, a newly discovered miR, has been shown to inhibit the metastasis and growth of LC [25], bladder cancer [26], and gastric cancer [27]. One study by Lu et al. [28] revealed the anticancer role of miR-491 in colorectal cancer by targeting IGF2 [28]. In our study, ginsenoside Rh2 did lower the activity of CCCs, and under its intervention, the cells presented higher miR-491 and weaker growth and metastasis activities. The results suggest the ability of ginsenoside Rh2 to regulate the metastasis and growth of CCCs via miR-491.

Nanomedicine is one of the research hotspots in recent years and has made outstanding contributions to medical therapy and diagnosis [29]. Drugs coated by nanomaterials have been found to have higher efficacy and less loss during circulation [30]. For instance, solid lipid NPs and those coated by CS are promising tools for silybin delivery [31], and methotrexate-loaded fucoidan/CS NP has anti-inflammatory potential and enhanced skin permeability [32]. CS, as the product of N-deacetylation of chitin, has the advantages of nontoxicity, bacteriostasis, lipid-lowering, and anticancer properties. Reportedly, drugs coated by CS possess stronger efficacy against cancer than such drugs without coating [33]. For instance, doxorubicin/cisplatin combined with hyaluronic acid/CS NPs boosts the efficacy of

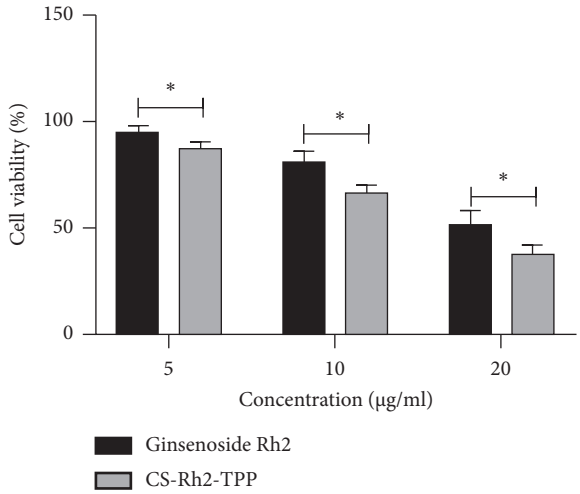

Figure 4: Suppression of CS-Rh2-TPP on viability of CCCs. $^*P < 0.05$. Note: CS-Rh2-TPP, ginsenoside Rh2 chitosan tripolyphosphate; CCCs, colon cancer cells.

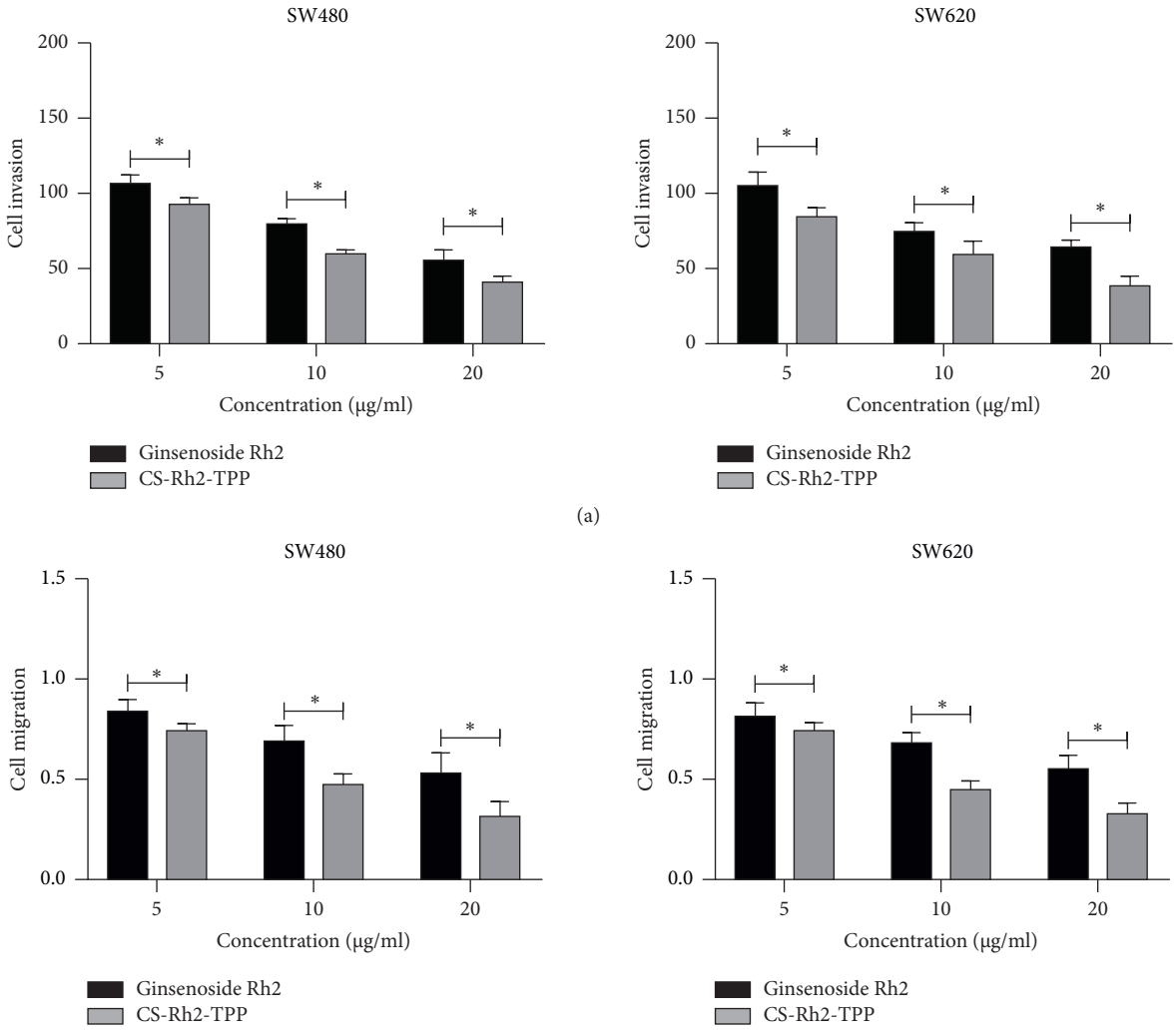

Figure 5: Impact of CS-Rh2-TPP on invasion and migration activities of CCCs (a). Impact of CS-Rh2-TPP/ginsenoside Rh2 on invasion of CCCs according to the transwell assay (b). Impact of CS-Rh2-TPP/ginsenoside Rh2 on migration of CCCs according to the wound-healing assay. $^*P < 0.05$. Note: CS-Rh2-TPP, ginsenoside Rh2 chitosan tripolyphosphate; CCCs, colon cancer cells.

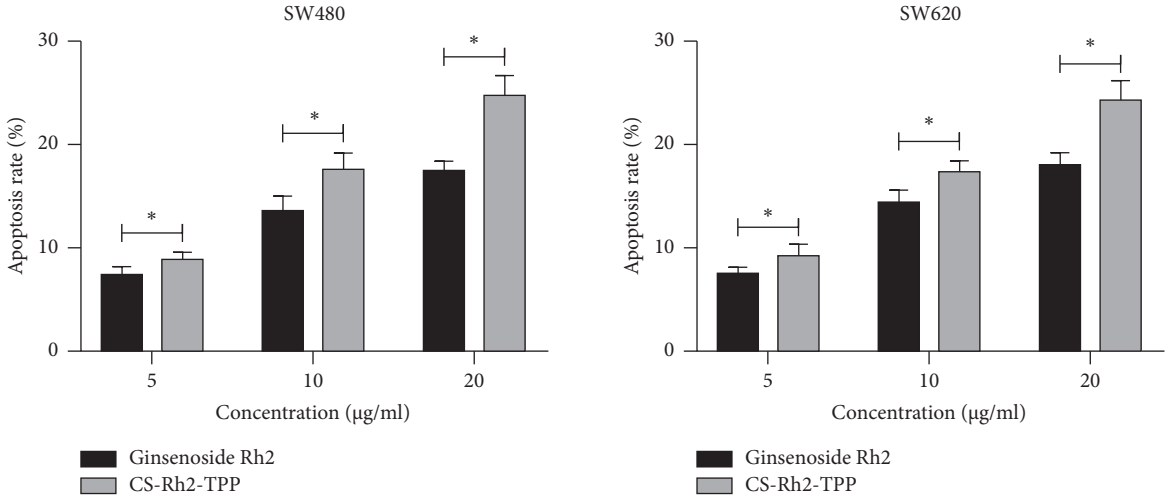

Figure 6: Impact of CS-Rh2-TPP on apoptosis of CCCs. $^*P < 0.05$. Note: CS-Rh2-TPP, ginsenoside Rh2 chitosan tripolyphosphate; CCCs, colon cancer cells.

synergistic combination chemotherapy for breast cancer [34]. CS-capped ZnO NPs have specific apoptosis induction ability via P53 activation and G2/M arrest in breast cancer cells [35]. In our study, we constructed CS-Rh2-TPP materials and found through assays that compared with ginsenoside Rh2, CS-Rh2-TPP exerted a stronger effect in inducing the apoptosis of CCCs, suppressing their activity, migration, and invasion, and upregulating miR-491 in them. The above data show that the anticancer effect of CS-Rh2-TPP is stronger than that of ginsenoside Rh2 alone. As the disease with the highest mortality at present, the main clinical treatment of malignant tumor is still surgery or combined chemoradiotherapy, but the prognosis of patients is not optimistic. With the deepening of research, there is consensus at home and abroad that molecular antitumor will be the key to conquering tumors in the future. On this basis, more and more studies have pointed out that a variety of drugs can inhibit the occurrence and development of tumors through molecular pathways. Among them, ginsenoside Rh2 has this effect. However, ginsenoside Rh2 cannot play its excellent anticancer effect in human body due to its low bioavailability and fast metabolism. Therefore, how to solve this problem has become a hotspot and difficult point in clinical research. In this experiment, CS-RH2-TPP NPs were prepared and achieved a significantly better inhibitory effect on CC than ordinary ginsenoside Rh2. This indicates that CS-RH2-TPP NPs have great clinical application prospects in the future, which can effectively address the application limitations at the present stage and provide new ideas and directions for the treatment of CC, rendering an important guarantee for the prognosis of patients.

However, our study still has its limitations. For instance, it has just determined the impact of CS-Rh2-TPP on biological function of CCCs. In addition, it is an in vitro experiment, so whether CS-Rh2-TPP has such effect on animal models needs further experimental support. Therefore, we hope to further carry out assays to improve our conclusions in the future.

5. Conclusion

To sum up, CS-coated ginsenoside Rh2 can upregulate miR-491 in CCCs, thus suppressing the growth and metastasis of CC.

Data Availability

The data used to support the findings of this study are available from the corresponding author upon request.

Consent

Not applicable.

Conflicts of Interest

The authors declare that they have no conflicts of interest.

Authors' Contributions

Wene Wei and Qijing Guo contributed equally to this work.

References

[1] J. Poblocki, A. Jasińska, A. Syrenicz, E. Andrysiak-Mamos, and M. Szczuko, "The neuroendocrine neoplasms of the digestive tract: diagnosis, treatment and nutrition," *Nutrients*, vol. 12, no. 5, 2020.

[2] F. Bray, J. Ferlay, I. Soerjomataram, R. L. Siegel, L. A. Torre, and A. Jemal, "Global cancer statistics 2018: GLOBOCAN estimates of incidence and mortality worldwide for 36 cancers in 185 countries," *CA: A Cancer Journal for Clinicians*, vol. 68, no. 6, pp. 394–424, 2018.

[3] "Colon cancer," *American Family Physician*, vol. 97, no. 10, 2018.

[4] M. W. Arnold, "Colon cancer: the road traveled," *Surgical Oncology Clinics of North America*, vol. 27, no. 2, 2018.

[5] A. W. Rosen, T. H. Degett, and I. Gogenur, "Individualized treatment of colon cancer," *Ugeskrift for Laeger*, vol. 178, no. 31, pp. 1–15, 2016.

[6] J. Zhuang, J. Yin, C. Xu, Y. Mu, and S. Lv, "20 (S)-Ginsenoside Rh2 induce the apoptosis and autophagy in U937 and K562 cells," *Nutrients*, vol. 10, no. 3, pp. 1–18, 2018.

[7] H. Luo, C. T. Vong, H. Chen et al., "Naturally occurring anti-cancer compounds: shining from Chinese herbal medicine," *Chinese Medicine*, vol. 14, no. 1, p. 48, 2019.

[8] X. Li, S. Chu, M. Lin et al., "Anticancer property of ginsenoside Rh2 from ginseng," *European Journal of Medicinal Chemistry*, vol. 203, Article ID 112627, 2020.

[9] Y. Huang, H. Huang, Z. Han, W. Li, Z. Mai, and R. Yuan, "Ginsenoside Rh2 inhibits angiogenesis in prostate cancer by targeting CNNM1," *Journal of Nanoscience and Nanotechnology*, vol. 19, no. 4, pp. 1942–1950, 2019.

[10] J. Wang, S. Bian, S. Wang et al., "Ginsenoside Rh2 represses autophagy to promote cervical cancer cell apoptosis during starvation," *Chinese Medicine*, vol. 15, no. 1, p. 118, 2020.

[11] X. Wen, H.-D. Zhang, L. Zhao, Y.-F. Yao, J.-H. Zhao, and J.-H. Tang, "Ginsenoside Rh2 differentially mediates microRNA expression to prevent chemoresistance of breast cancer," *Asian Pacific Journal of Cancer Prevention*, vol. 16, no. 3, pp. 1105–1109, 2015.

[12] T. X. Lu and M. E. Rothenberg, "MicroRNA," *The Journal of Allergy and Clinical Immunology*, vol. 141, no. 4, pp. 1202–1207, 2018.

[13] K. Tao, J. Yang, Z. Guo et al., "Prognostic value of miR-221-3p, miR-342-3p and miR-491-5p expression in colon cancer," *American Journal of Tourism Research*, vol. 6, no. 4, pp. 391–401, 2014.

[14] Y. Chen, Y. Zhang, W. Song, Y. Zhang, X. Dong, and M. Tan, "Ginsenoside Rh2 inhibits migration of lung cancer cells under hypoxia via mir-491," *Anti-Cancer Agents in Medicinal Chemistry*, vol. 19, no. 13, pp. 1633–1641, 2019.

[15] R. Zingg and M. Fischer, "The consolidation of nanomedicine," *Wiley interdisciplinary reviews. Nanomedicine and nanobiotechnology*, vol. 11, no. 6, Article ID e1569, 2019.

[16] W. Feng and Y. Chen, "Chemoreactive nanomedicine," *Journal of Materials Chemistry B*, vol. 8, no. 31, pp. 6753–6764, 2020.

[17] A. Muxika, A. Etxabide, J. Uranga, P. Guerrero, and K. de la Caba, "Chitosan as a bioactive polymer: processing, properties and applications," *International Journal of Biological Macromolecules*, vol. 105, pp. 1358–1368, 2017.

[18] G. Qian, Z. Jing, Z. Jianmei et al., "Preparation of ginsenoside Rh2 loaded chitosan nanoparticles and its cytotoxicity to A549 cells," *Food Science*, vol. 14, pp. 1–11, 2020.

[19] H. Zare-Zardini, A. Alemi, A. Taheri-Kafrani et al., "Assessment of a new ginsenoside Rh2 nanoniosomal formulation for enhanced antitumor efficacy on prostate cancer: an in vitro study," *Drug Design, Development and Therapy*, vol. 14, pp. 3315–3324, 2020.

[20] C. Mancuso and R. Santangelo, "Panax ginseng and Panax quinquefolius: from pharmacology to toxicology," *Food and Chemical Toxicology*, vol. 107, pp. 362–372, 2017.

[21] M. Ben-Eltriki, S. Deb, and E. S. T. Guns, "1α,25-Dihydroxyvitamin D3 synergistically enhances anticancer effects of ginsenoside Rh2 in human prostate cancer cells," *The Journal of Steroid Biochemistry and Molecular Biology*, vol. 209, Article ID 105828, 2021.

[22] H. Zhang, S. Park, H. Huang et al., "Anticancer effects and potential mechanisms of ginsenoside Rh2 in various cancer types (Review)," *Oncology Reports*, vol. 45, no. 4, pp. 1–10, 2021.

[23] H. Yan, H. Jin, Y. Fu, Z. Yin, and C. Yin, "Production of rare ginsenosides Rg3 and Rh2 by endophytic bacteria from panax ginseng," *Journal of Agricultural and Food Chemistry*, vol. 67, no. 31, pp. 8493–8499, 2019.

[24] N. Wu, G.-c. Wu, R. Hu, M. Li, and H. Feng, "Ginsenoside Rh2 inhibits glioma cell proliferation by targeting microRNA-128," *Acta Pharmacologica Sinica*, vol. 32, no. 3, pp. 345–353, 2011.

[25] S.-N. Wang, S. Luo, C. Liu et al., "miR-491 inhibits osteosarcoma lung metastasis and chemoresistance by targeting αB-crystallin," *Molecular Therapy*, vol. 25, no. 9, pp. 2140–2149, 2017.

[26] F. Liu, H. Zhang, F. Xie et al., "Hsa_circ_0001361 promotes bladder cancer invasion and metastasis through miR-491-5p/MMP9 axis," *Oncogene*, vol. 39, no. 8, pp. 1696–1709, 2020.

[27] R. Sun, Z. Liu, D. Tong et al., "miR-491-5p, mediated by Foxi1, functions as a tumor suppressor by targeting Wnt3a/β-catenin signaling in the development of gastric cancer," *Cell Death & Disease*, vol. 8, no. 3, Article ID e2714, 2017.

[28] L. Lu, M. Cai, M. Peng, F. Wang, and X. Zhai, "miR-491-5p functions as a tumor suppressor by targeting IGF2 in colorectal cancer," *Cancer Management and Research*, vol. 11, pp. 1805–1816, 2019.

[29] S. Ravindran, A. J. Tambe, J. K. Suthar, D. S. Chahar, J. M. Fernandes, and V. Desai, "Nanomedicine: bioavailability, biotransformation and biokinetics," *Current Drug Metabolism*, vol. 20, no. 7, pp. 542–555, 2019.

[30] H. Xiang and Y. Chen, "Energy-converting nanomedicine," *Small*, vol. 15, no. 13, Article ID e1805339, 2019.

[31] V. Piazzini, L. Cinci, M. D'Ambrosio, C. Luceri, A. R. Bilia, and M. C. Bergonzi, "Solid lipid nanoparticles and chitosan-coated solid lipid nanoparticles as promising tool for silybin delivery: formulation, characterization, and in vitro evaluation," *Current Drug Delivery*, vol. 16, no. 2, pp. 142–152, 2019.

[32] A. I. Barbosa, S. A. Costa Lima, and S. Reis, "Development of methotrexate loaded fucoidan/chitosan nanoparticles with anti-inflammatory potential and enhanced skin permeation," *International Journal of Biological Macromolecules*, vol. 124, pp. 1115–1122, 2019.

[33] P. Sacco, M. Cok, F. Scognamiglio et al., "Glycosylated-chitosan derivatives: a systematic review," *Molecules*, vol. 25, no. 7, pp. 11–28, 2020.

[34] Y. Wang, J. Qian, M. Yang et al., "Doxorubicin/cisplatin co-loaded hyaluronic acid/chitosan-based nanoparticles for in vitro synergistic combination chemotherapy of breast cancer," *Carbohydrate Polymers*, vol. 225, Article ID 115206, 2019.

[35] J. Anitha, R. Selvakumar, and K. Murugan, "Chitosan capped ZnO nanoparticles with cell specific apoptosis induction through P53 activation and G2/M arrest in breast cancer cells - in vitro approaches," *International Journal of Biological Macromolecules*, vol. 136, pp. 686–696, 2019.

Hindawi
Journal of Oncology
Volume 2021, Article ID 6868514, 10 pages
https://doi.org/10.1155/2021/6868514

Research Article

Long Noncoding RNA NR2F1-AS1 Enhances the Migration and Invasion of Hepatocellular Carcinoma via Modulating miR-642a/DEK Pathway

Yingxia Xu,[1] Chunrong Han,[2] Jing Sun,[3] Jingjing Zhao,[4] Qing Liu,[5] and Ping An [6]

[1]*Department of Infectious Diseases, Weifang People's Hospital, Weifang 261041, China*
[2]*Medical Records Room, Jinan Zhangqiu District Hospital of TCM, Jinan 250200, China*
[3]*Department of Medical Administration, Qingdao Central Hospital, Qingdao University, Qingdao 266042, China*
[4]*Department of Surgery, Zhangqiu District People's Hospital, Jinan 250200, China*
[5]*Department of Traditional Chinese Medicine, Zhangqiu District People's Hospital, Jinan 250200, China*
[6]*Department of Disinfection Supply Center, The 5th People's Hospital of Ji'nan, Jinan 250022, China*

Correspondence should be addressed to Ping An; anping@jndwyy.com.cn

Received 8 June 2021; Revised 3 September 2021; Accepted 4 September 2021; Published 21 September 2021

Academic Editor: Muhammad Wasim Khan

Purpose. Hepatocellular carcinoma (HCC), a malignant tumor that exists worldwide, has a high morbidity and mortality rate. Previous studies have reported that lncRNA NR2F1-AS1 plays a critical role in several cancers. Here, we aimed to investigate the biological function of NR2F1-AS1 and its molecular mechanism in the migration and invasion of HCC. *Methods*. Quantitative real-time PCR (qRT-PCR) was performed to analyze NR2F1-AS1 expression in HCC. The biological function was investigated by transwell invasion and migration assays. The protein level was identified by Western blot. In addition, the downstream targets of NR2F1-AS1 and miR-642a were confirmed by luciferase reporter assays. *Results*. NR2F1-AS1 was significantly upregulated in HCC and associated with the poor prognosis of HCC patients. Biological function experiments revealed that the silence of NR2F1-AS1 suppressed cell invasion and migration in HCC. More importantly, NR2F1-AS1 directly interacted with miR-642a and negatively regulated miR-642a. DEK was the target of miR-642a, and NR2F1-AS1 positively regulated DEK expression by suppressing miR-642a. *Conclusion*. Taken together, it is the first time we discovered the interaction of NR2F1-AS1 with miR-642a in modulating HCC cell invasion and migration.

1. Introduction

Hepatocellular carcinoma (HCC) is the most common type of primary liver cancer, which initiates in hepatocytes and has a high mortality rate [1, 2]. Surgical resection has been considered the most effective therapy for HCC; however, it may produce new metastases [3]. Therefore, it is becoming more and more urgent to explore the molecular mechanism for the treatment of HCC.

Long noncoding RNAs (lncRNAs), as a new epigenetic regulatory molecule, have received wide attention in various cellular and biological processes. And dysregulation of lncRNAs is closely related to tumorigenesis, metastasis, and apoptosis by competing for corresponding miRNAs [4]. Recently, lncRNAs have been found to be critical regulators in HCC [5, 6]. For instance, lncRNA OTUD6B-AS1 was highly expressed in HCC and associated with HCC patients' prognosis. Moreover, silencing OTUD6B-AS1 inhibited HCC proliferation and invasion through the Wnt/β-catenin pathway [7]. lncRNA HCG18 was discovered to be increased in HCC and facilitated the progression of HCC via the miR-214-3p/CENPM axis [8]. Recently, a novel lncRNA, NR2F1 antisense RNA 1 (NR2F1-AS1), was functionally identified [9]. Mounting evidence has discovered that NR2F1-AS1 played a critical role in the development of various cancers, including colorectal cancer [10], breast cancer [11], and

esophageal squamous cell carcinoma [12]. However, the biological role of NR2F1-AS1 and the detailed mechanism in HCC cell invasion and migration are yet to be explored.

In this study, NR2F1-AS1 expression was detected in HCC tissues and its correlation with prognosis. Furthermore, the significance and molecular mechanism of NR2F1-AS1 were measured in HCC cell invasion and migration. The findings demonstrated that NR2F1-AS1 was highly expressed in HCC tissues and associated with the prognosis of HCC patients. Moreover, the results elucidated that NR2F1-AS1 enhanced HCC progression via modulating the miR-642a/DEK axis, which strengthened understanding of HCC pathogenesis and the development of effective therapies.

2. Methods

2.1. Clinical Samples. Pairs of HCC tumor tissues ($n = 36$) were taken from patients who received hepatectomy at Weifang People's Hospital, Weifang, Shandong, China. All patients had not received any preoperative chemotherapy or radiotherapy before surgery. This study was approved by the Ethics Committee of the Weifang People's Hospital, Weifang, Shandong, China, and all patients gave informed written consent in advance. The collected samples were stored at −80°C for further use.

2.2. Cell Culture and Cell Transfection. Human HCC cell lines (Huh7 and SK-Hep-1) and normal liver cell line HL-7702 were obtained from Cell Bank of the Chinese Academy of Sciences (Shanghai, China). All cells were cultured in DMEM (Gibco, CA, USA) supplemented with 10% FBS with 5% CO_2 at 37°C. The shRNAs targeting NR2F1-AS1 (sh-NR2F1-AS1) were used to decrease NR2F1-AS1 expression. miR-642a mimic or inhibitor, obtained from Shanghai R&S Biotechnology Co. (Shanghai, China), was used to increase or decrease miR-642 expression. Lipofectamine® 2000 (Invitrogen, CA, USA) was carried out to perform the transfections for 48 h.

2.3. Quantitative Real-Time PCR (qRT-PCR). Isolation of total RNA from HCC tissues or cells was carried out with TRIzol reagent (Invitrogen, NY, USA). cDNA was synthesized using a specific reverse transcription kit (Thermo Fisher). QRT-PCR was performed with SYBR Green (ThermoFisher, MA, USA). U6 or GAPDH was applied as an internal control. The relative quantitation of gene expressions was performed using the $2 - \Delta\Delta Ct$ method. Primers used in this study are listed as follows: NR2F1-AS1-F: 5′-CAGCGGTGCAAACCATGTGC-3′; NR2F1-AS1-R: 5′-GTAAACCAAGTCGGTTGAACG-3′; miR-642a-F: 5′-GCGGTCCCTCT CCAAATGT-3′, miR-642a-R: 5′-AGTGCAGGGTCCGAGGTATT-3′; U6-F: 5′-CTC GCTTCGGCAGCACA-3′, U6-R: 5′-AACGCTTCACGA-ATTTGCGT-3′; DEK-F: 5′-TGTTAAGAAAGCAGATA-GCAGGACC-3′; and DEK-R: 5′-ATTAAAGGTTCAT CATCTGAACTATCCTC-3′.

2.4. Western Blot Assay. 50 μg protein lysates were separated by SDS-PAGE and then transferred to PVDF membranes. Afterwards, the membranes were blocked with 5% skim milk for 2 h at room temperature and incubated with primary antibodies overnight at 4°C. After incubating with a secondary antibody for 2 h at room temperature, the protein bands were visualized by an ECL kit. GAPDH was used as the loading control.

2.5. Transwell Assay. For the migration experiment, HCC cells were seeded into the upper chamber of a transwell insert, and the lower chamber was fixed with a medium with 20% FBS. For the invasion experiment, the upper chamber was coated with Matrigel, and the lower chamber contained a 20% FBS medium. After incubation for 48 h, the cells were fixed, stained, and then counted under a microscope.

2.6. RNA Immunoprecipitation (RIP) Assay. After transfection with miR-642a mimic or inhibitor for 48 h, Huh7 cells were lysed with RIP lysis buffer and incubated with RIP immunoprecipitation buffer mixed with magnetic beads conjugating human anti-Argonaute 2 (Ago2) antibody or negative control mouse IgG (Millipore, MA, USA). Acquired RNAs were analyzed by qRT-PCR. IgG served as control in the RIP assay.

2.7. Luciferase Reporter Assay. The wild and mutant types of NR2F1-AS1 or DEK containing the binding site for miR-642a were cloned into pGL3 reporter vectors, designed as pGL3-NR2F1-AS1-WT and pGL3-NR2F1-AS1-MuT or pGL3-DEK-WT and pGL3-DEK-MuT, and then, they were transfected into Huh7 cells with miR-642a mimic/inhibitor for 48 h using Lipofectamine 2000.

2.8. Statistical Analysis. Independent repetitions of experiments were performed three times. The data were presented as means ± SD. The differences were analyzed using two-tailed Student's *t*-tests or Turkey's post hoc tests in one-way ANOVA. Statistical analysis was performed using SPSS Statistics 20.0 software. $P < 0.05$ was considered statistically significant.

3. Results

3.1. NR2F1-AS1 Was Highly Expressed in HCC Tissues. To investigate the significance of NR2F1-AS1 in HCC, the expressional level of NR2F1-AS1 was first measured in 36 matched pairs of HCC tissues using the qRT-PCR assay. Results displayed that NR2F1-AS1 was highly expressed in HCC tumor tissues when compared to adjacent nontumor tissues (Figure 1(a)). The median value of NR2F1-AS1 expression was used as the cutoff point to divide NR2F1-AS1 expression into high and low expression of NR2F1-AS1. HCC patients with low NR2F1-AS1 expression exhibited high overall survival, while those with high NR2F1-AS1 expression showed low overall survival (Figure 1(b)). Furthermore, NR2F1-AS1 was increased in HCC cells in comparison with normal HL-7702 cells (Figure 1(c)). These

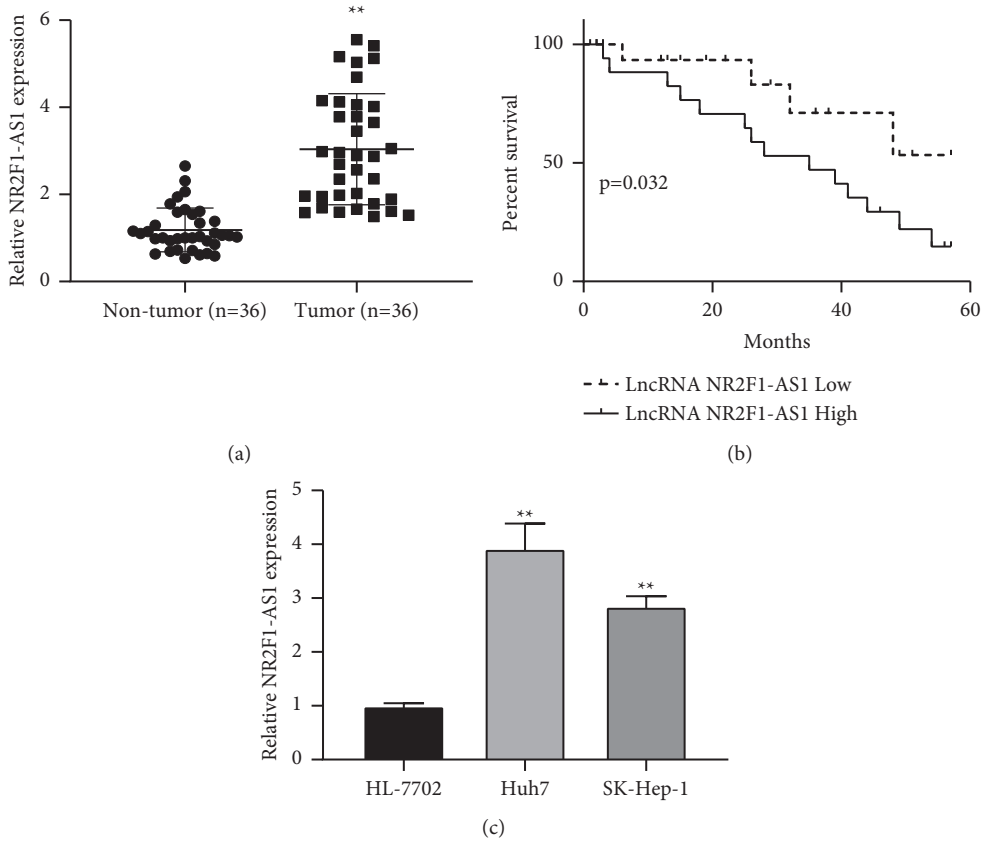

Figure 1: NR2F1-AS1 highly expressed in HCC. (a) High expression of NR2F1-AS1 detected in HCC tumor tissues ($n = 36$). (b) Lower survival of HCC patients with high NR2F1-AS1 expression than ($n = 18$) with low NR2F1-AS1 expression ($n = 18$). (c) High expression of NR2F1-AS1 measured in HCC cell lines. $^{**}P < 0.01$.

results demonstrated that NR2F1-AS1 was closely related to the prognosis of HCC patients and might take part in HCC progression.

3.2. Knockdown of NR2F1-AS1 Inhibited HCC Cell Invasion and Migration. Next, the functional significance of NR2F1-AS1 was explored in Huh7 and SK-Hep-1 cells. NR2F1-AS1 expression was downregulated after transfection with shRNA-NR2F1-AS1 in both two HCC cells (Figure 2(a)). Transwell migration assay manifested that HCC cells migration was decreased in the sh-NR2F1-AS1 group when compared to the control group (Figure 2(b)). Moreover, decreasing NR2F1-AS1 attenuated the invasion of HCC cells compared to the control group (Figure 2(c)). These results indicated that the silence of NR2F1-AS1 suppressed HCC cell invasion and migration.

3.3. NR2F1-AS1 Directly Interacted with miR-642a. Then, the underlying molecular mechanism of NR2F1-AS1 in Huh7 cells was further studied. The starBase database predicted miR-642a as a target of NR2F1-AS1 (Figure 3(a)). MiR-642a expression was increased or decreased after transfection with miR-642a mimic or inhibitor in Huh7 cells by qRT-PCR (Figure 3(b)). Luciferase reporter assay was then performed to validate this prediction, followed by RIP assay. Luciferase reporter assay discovered that miR-642a mimic reduced, while miR-642a inhibitor increased NR2F1-AS1-WT' luciferase activity. However, neither miR-642a mimic nor inhibitor showed any effect on NR2F1-AS1-MuT' luciferase activity (Figure 3(c)). RIP results displayed that NR2F1-AS1 and miR-642a expressions were elevated in the anti-Ago2 group versus the control group (Figure 3(d)). Then, qRT-PCR was applied to investigate the correlation of NR2F1-AS1 with miR-642a, and the findings exhibited that overexpression of NR2F1-AS1 significantly decreased miR-642a expression, while knockdown of NR2F1-AS1 markedly increased miR-642a expression in both two HCC cells (Figure 3(e)), indicating a negative correlation of NR2F1-AS1 with miR-642a. Then, miR-642a expression was detected in HCC tissues, and the findings displayed that miR-642a was underexpressed in HCC tissues versus nontumor tissues (Figure 3(f)). Pearson's correlation analysis discovered that NR2F1-AS1 was inversely associated with miR-642a in HCC tissues (Figure 3(g)). These results suggested that NR2F1-AS1 directly targets miR-642a in HCC.

3.4. NR2F1-AS1 Sponged miR-642a to Modulate Cell Invasion and Migration in HCC. Next, the impact of miR-642a on NR2F1-AS1-regulated cell invasion and migration was investigated in HCC cells. Huh7 and SK-Hep-1 cells were

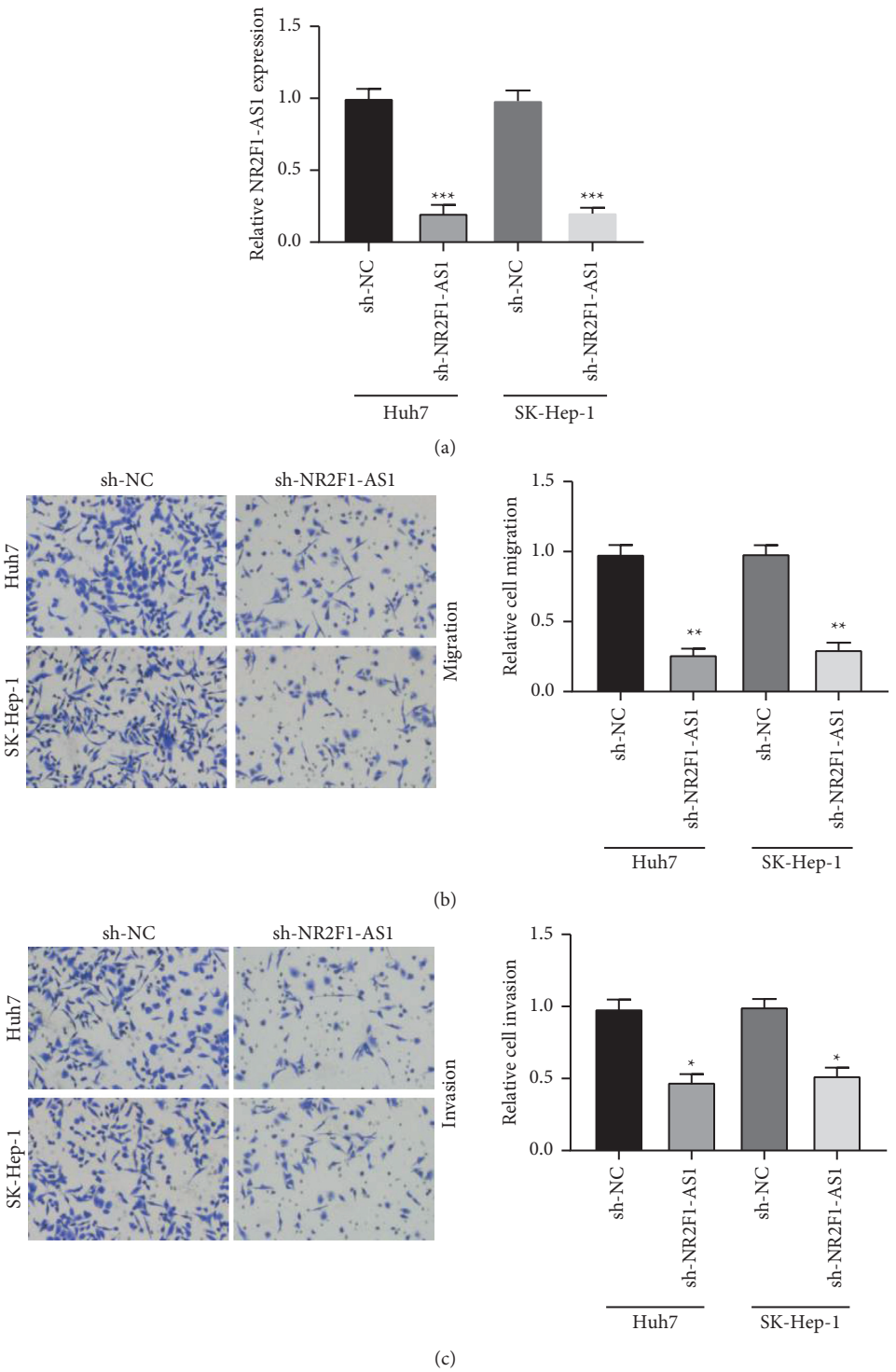

Figure 2: Knockdown of NR2F1-AS1 suppressing cell invasion and migration in HCC. (a) NR2F1-AS1 expression significantly inhibited by sh-NR2F1-AS1 in Huh7 and SK-Hep-1 cells. (b) HCC cells migration suppressed by transfection with sh-NR2F1-AS1. (c) HCC cells invasion repressed by transfection with sh-NR2F1-AS1. $^{*}P < 0.05$, $^{**}P < 0.01$, and $^{***}P < 0.001$.

transfected with sh-NR2F1-AS1 or combined with miR-642a inhibitors. Transwell migration results displayed that the migration of HCC cells reduced by sh-NR2F1-AS1 could be rescued by incorporating miR-642a inhibitor (Figures 4(a) and 4(b)). Moreover, the transwell invasion assay manifested that the sh-NR2F1-AS1 effect on HCC cells invasion was also partly restored by combining with miR-642a inhibitor (Figures 4(c) and 4(d)). These results demonstrated that NR2F1-AS1 modulated HCC cell migration and invasion through miR-642a.

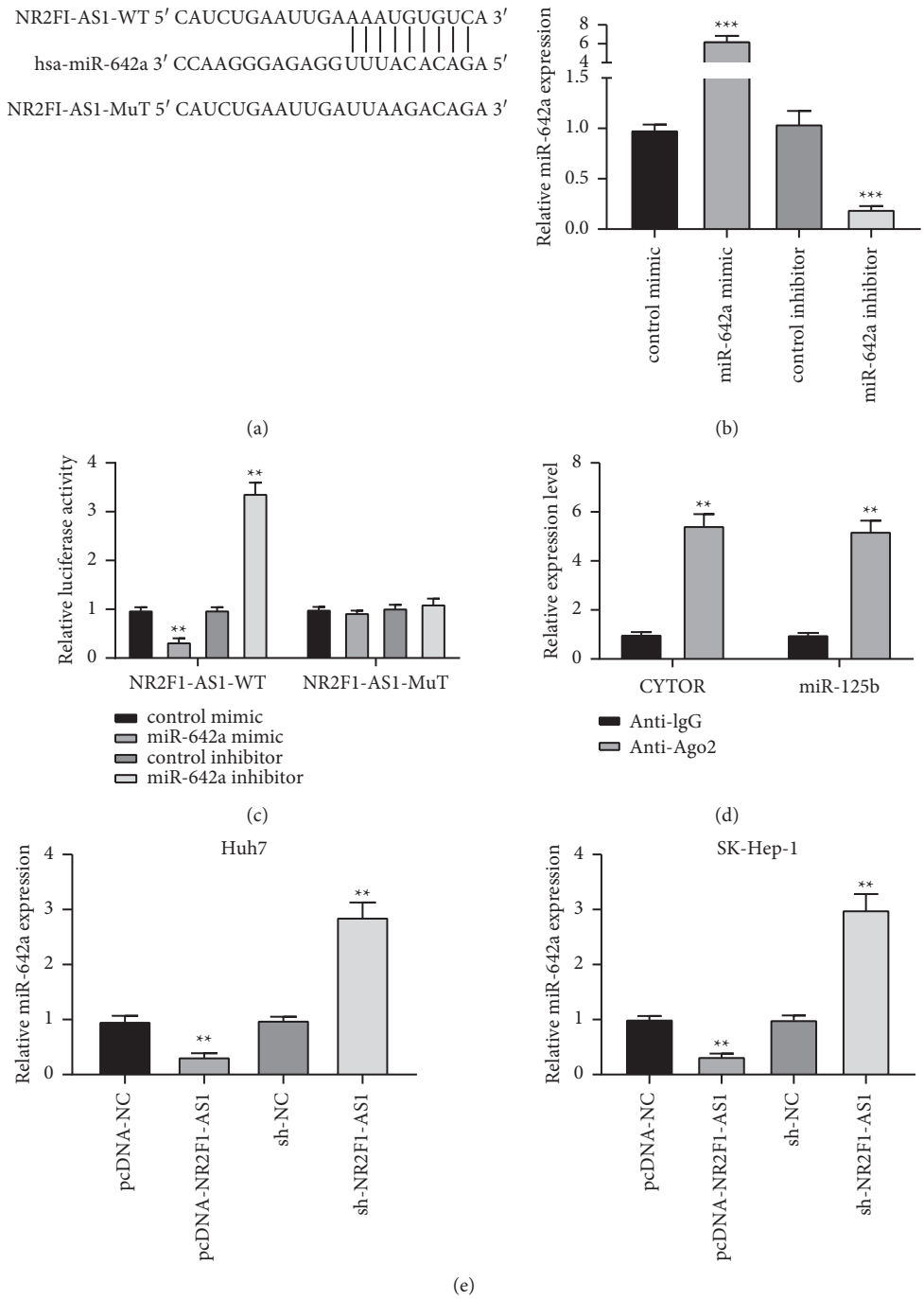

Figure 3: Continued.

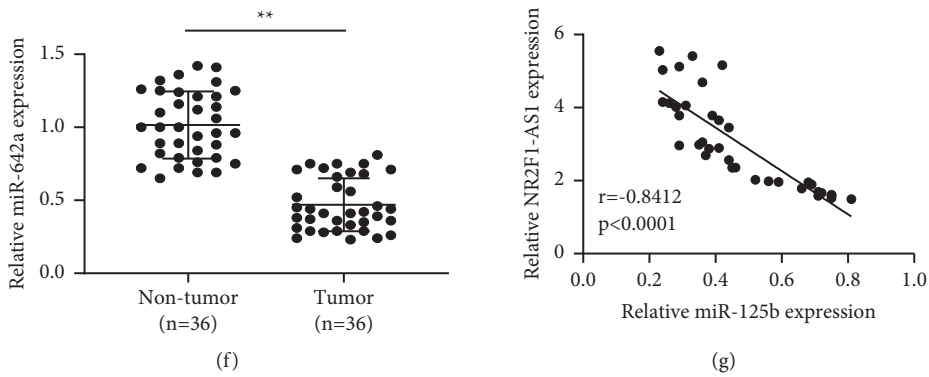

Figure 3: NR2F1-AS1 directly interacted with miR-642a. (a) The predicted binding site between NR2F1-AS1 and miR-642a. (b) qRT-PCR detection of the overexpression and knockdown efficiency for miR-642a. (c) The luciferase activity of the NR2F1-AS1-WT affected by miR-642a overexpression or knockdown. (d) Increased NR2F1-AS1 and miR-642a expression in the anti-Ago2 group compared to the LgG group. (e) NR2F1-AS1 negatively regulating miR-642a expression. (f) Downregulation of miR-642a in HCC tumor tissues versus nontumor tissues ($n = 36$). (g) The inverse correlation between NR2F1-AS1 and miR-642a in HCC tissues ($n = 36$). $^{**}P < 0.01$ and $^{***}P < 0.001$.

3.5. NR2F1-AS1-Regulated DEK through miR-642a in HCC Cells. TargetScan Human 7.2 was applied to predict the potential target genes of miR-642a, and DEK was found to own a binding site for miR-642a (Figure 5(a)). Then, the luciferase assay was carried out to confirm this prediction further, and results discovered that DEK-WT' luciferase activity was remarkably inhibited by miR-642a mimic in Huh7 cells, but not in the DEK-MuT group (Figure 5(b)), indicating that DEK was a downstream target of miR-642a. More importantly, DEK expression was inhibited by miR-642a mimic, while enhanced by miR-642a inhibitor using qRT-PCR and Western blot assays (Figures 5(c) and 5(d)). Afterwards, the relationship between NR2F1-AS1, miR-642a, and DEK was explored, and results showed that DEK expression increased by miR-642a inhibitor could be reduced by sh-NR2F1-AS1 (Figures 5(e) and 5(f)), indicating that NR2F1-AS1 facilitated DEK expression via suppressing miR-642a.

4. Discussion

Hepatocellular carcinoma is one of the most common causes of cancer-related death globally [13]. Recently, lncRNA profile analysis and functional analysis of various types of cancer have provided more and more evidence that lncRNA plays a critical role in tumor growth and development [14]. lncRNA is considered to be a new diagnostic biomarker, effective prognostic predictor, and attractive therapeutic target for HCC through interactions with cellular macromolecules, such as proteins and mRNAs [15, 16]. Thus, it is critically called for to understand the molecular mechanism of lncRNAs in HCC progression.

Prior research confirmed that lncRNA NR2F1-AS1 modulated the pathological progressions of tumors. For instance, NR2F1-AS1 was overexpressed in tumor tissues and involved in endometrial cancer development [17]. NR2F1-AS1 knockdown inhibited thyroid cancer progression in vitro and in vivo [18]. Liet al. discovered that NR2F1-AS1 was highly expressed in osteosarcoma and exhibited an oncogene role in OS development [19]. In this study, we found that NR2F1-AS1 was increased in HCC tissues and associated with the prognosis of HCC patients. Moreover, HCC cell migration and invasion were inhibited distinctly by sh-NR2F1-AS1. These results suggested that NR2F1-AS1 may also play an oncogenic role in HCC.

Accumulating evidence has discovered that lncRNAs exhibited key roles in tumors by sponging miRNAs [20, 21]. In HCC, lncRNA H19 was discovered to promote cell proliferation, invasion, and migration yet suppressed cell apoptosis through miR-520a/LIMK1 axis [22]. Upregulation of CASC15 enhanced the tumorigenicity and epithelial to mesenchymal transition of HCC by increasing TWIST1 gene expression via miR-33a-5p sponging [23]. Xiao et al. found that LINC01123 sponges miR-34a-5p to promote cell proliferation and invasion in HCC through modulating TUFT1 [24]. To identify NR2F1-AS1's underlying mechanism in HCC, the bioinformatics analysis was applied to screen the potential targets of NR2F1-AS1 and found that miR-642a served as the candidate target. Luciferase reporter assay and RIP assay further confirmed miR-642a was a direct target of NR2F1-AS1. Moreover, we observed that NR2F1-AS1 negatively regulated miR-642a expression. Importantly, miR-642a inhibitor could rescue the sh-NR2F1-AS1 effect on HCC cell invasion and migration.

DEK is a potential biomarker and oncogene, which is reported in many cancers [25–27]. DEK was found to involve in the development of pancreatic cancer as a target of miR-200a [28]. Also, miR-1292 inhibited gastric cancer cell growth, migration, and invasion via targeting DEK [29]. However, whether DEK served as the target of miR-642a was not reported until now. In this study, we found that DEK served as the direct target of miR-642a following the luciferase and RIP assays. Prior research has shown that abnormal expression of DEK exists in various tumors. For instance, DEK was significantly elevated in pancreatic cancer and cervical cancer [30, 31]. Soo Yeon Lee et al. discovered that DEK was highly expressed in HCC, and its high expression was associated with poor prognosis of HCC patients [27, 32], which is consistent with our study that DEK was increased significantly in HCC tissues. Our

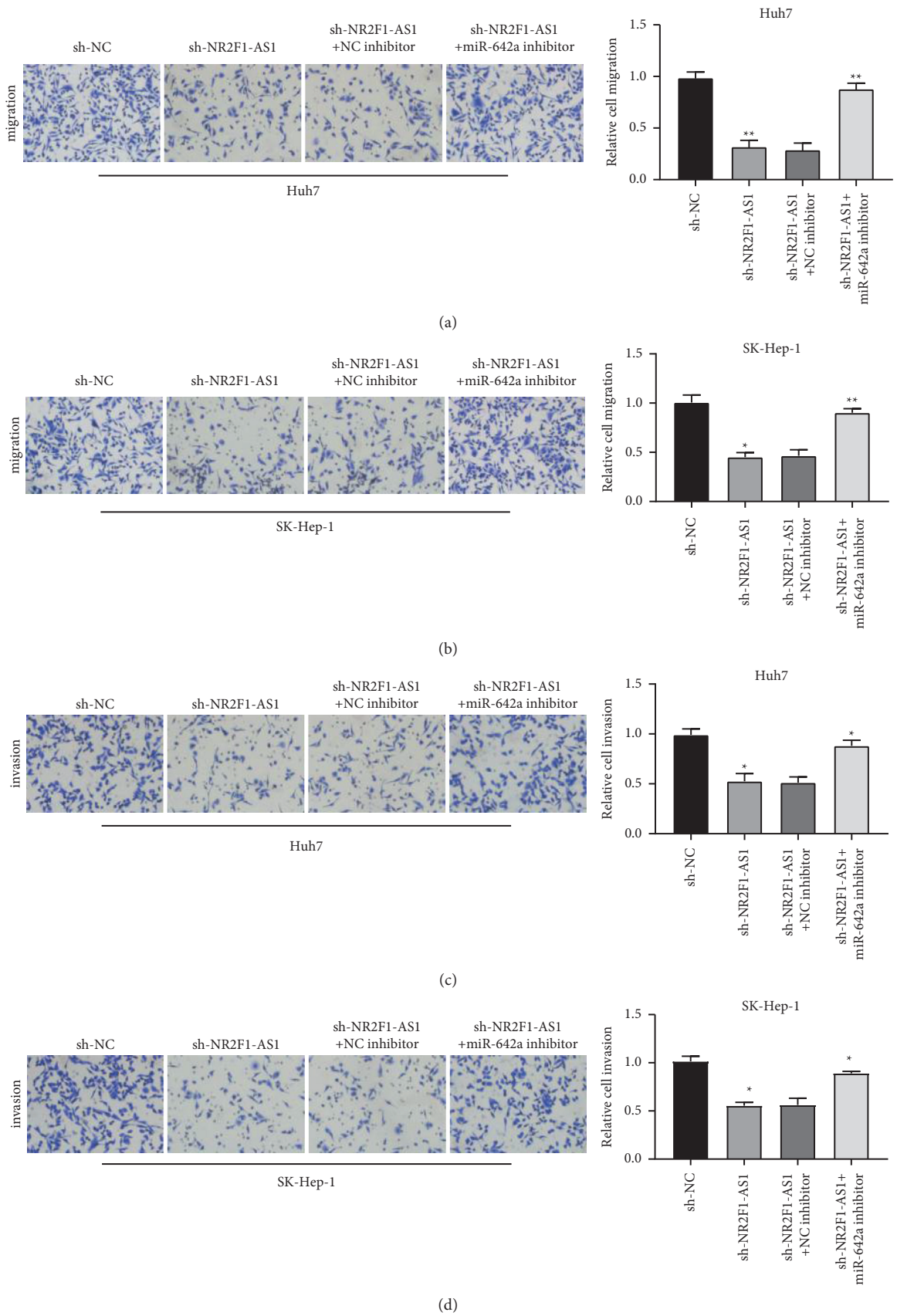

Figure 4: NR2F1-AS1 modulating HCC cell migration and invasion by sponging miR-642a. (a) miR-642a inhibitor increasing the cell migration reduced by sh-NR2F1-AS1 in Huh7 and (b) SK-Hep-1 cells. (c) miR-642a inhibitor increasing the cell invasion reduced by sh-NR2F1-AS1 in Huh7 and (d) SK-Hep-1 cells. $^{*}P < 0.05$ and $^{**}P < 0.01$.

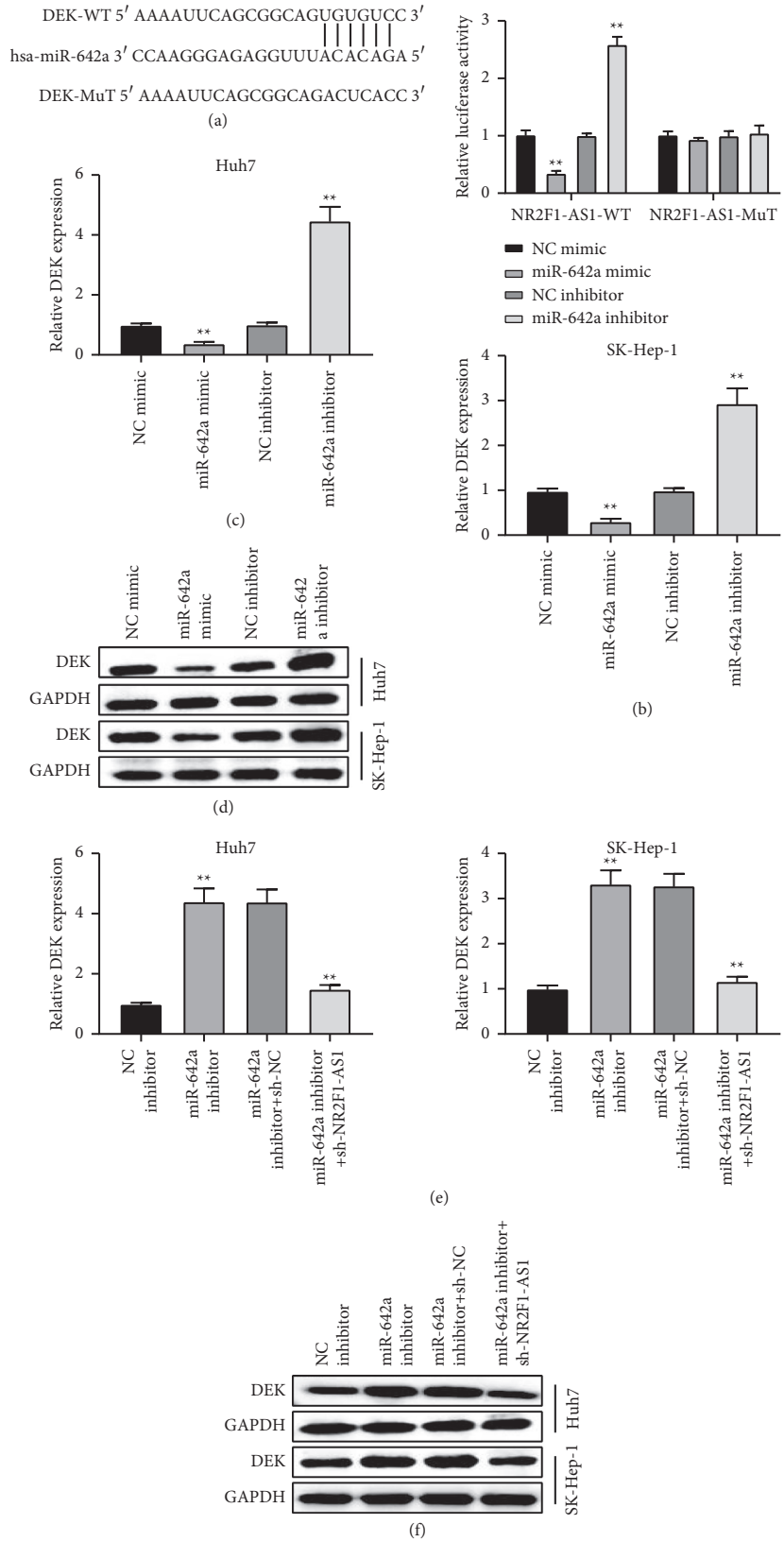

Figure 5: NR2F1-AS1 regulating DEK expression through miR-642a. (a) The putative DEK binding site with miR-642a. (b) Luciferase activities of DEK-WT or -MuT detected after transfection with miR-642a mimic in Huh7 cells. (c) DEK mRNA expression and (d) protein level decreased by miR-642a mimic, while increased by miR-642a inhibitor in HCC cells. (e-f) Upregulation of DEK increased by miR-642a inhibitor reduced by NR2F1-AS1 knockdown. $^{**}P < 0.01$.

study also found that NR2F1-AS1 aggravated the expression of DEK in HCC cells by decreasing the expression of miR-642a.

There are some limitations to this study that we only investigated the biological functions and mechanism of NR2F1-AS1 in cell migration and invasion in vitro. The functional role of NR2F1-AS1 in vivo animal experiments is required to explore in the future studies.

Taken together, our results demonstrated that NR2F1-AS1 was highly expressed in HCC, and silence of NR2F1-AS1 suppressed cell invasion and migration in HCC cells via miR-642a/DEK axis. The NR2F1-AS1/miR-642a/DEK axis might provide new insights for designing promising therapeutic strategies for HCC.

Data Availability

The datasets used and/or analyzed during the present study are available from the corresponding author upon request.

Ethical Approval

The study was approved by the Ethics Committee of the Weifang People's Hospital, Weifang, China.

Consent

Written permission was obtained from all participants.

Conflicts of Interest

The authors declare that they have no conflicts of interest.

Acknowledgments

The authors sincerely appreciate the contributions to this work made in various ways by all of the participants.

References

[1] S. Zhang, Y. Liu, Z. Liu et al., "CircRNA_0000502 promotes hepatocellular carcinoma metastasis and inhibits apoptosis through targeting microRNA-124," *Journal of BUON: Official Journal of the Balkan Union of Oncology*, vol. 24, pp. 2402–2410, 2019.

[2] J. Syrios, M. Logothetis, H. Tountas, A. Grivas, E. Lianos, and A. E. Athanasiou, "Cutaneous metastasis from hepatocellular carcinoma," *Journal of BUON: Official Journal of the Balkan Union of Oncology*, vol. 17, pp. 797-798, 2012.

[3] J. J. Yu, W. Xiao, S. L. Dong et al., "Effect of surgical liver resection on circulating tumor cells in patients with hepatocellular carcinoma," *BMC Cancer*, vol. 18, no. 1, p. 835, 2018.

[4] T. Wang, X. Tang, and Y. Liu, "LncRNA-ATB promotes apoptosis of non-small cell lung cancer cells through MiR-200a/beta-Catenin," *Journal of BUON: Offical Journal of the Balkan Union of Oncology*, vol. 24, pp. 2280–2286, 2019.

[5] X. Yang, B. Yao, Y. Niu et al., "Hypoxia-induced lncRNA EIF3J-AS1 accelerates hepatocellular carcinoma progression via targeting miR-122-5p/CTNND2 axis," *Biochemical and Biophysical Research Communications*, vol. 518, no. 2, pp. 239–245, 2019.

[6] J. Feng, G. Yang, Y. Liu et al., "LncRNA PCNAP1 modulates hepatitis B virus replication and enhances tumor growth of liver cancer," *Theranostics*, vol. 9, no. 18, pp. 5227–5245, 2019.

[7] S. Kong, H. Xue, Y. Li et al., "The long noncoding RNA OTUD6B-AS1 enhances cell proliferation and the invasion of hepatocellular carcinoma cells through modulating GSKIP/Wnt/beta-catenin signalling via the sequestration of miR-664b-3p," *Experimental Cell Research*, vol. 395, no. 1, Article ID 112180, 2020.

[8] Y. Zou, Z. Sun, and S. Sun, "LncRNA HCG18 contributes to the progression of hepatocellular carcinoma via miR-214-3p/CENPM axis," *Journal of Biochemistry*, vol. 168, 2020.

[9] H. Huang, J. Chen, C. M. Ding, X. Jin, Z. M. Jia, and J. Peng, "LncRNA NR2F1-AS1 regulates hepatocellular carcinoma oxaliplatin resistance by targeting ABCC1 via miR-363," *Journal of Cellular and Molecular Medicine*, vol. 22, no. 6, pp. 3238–3245, 2018.

[10] Q. Zhang, T. Li, Z. Wang, X. Kuang, N. Shao, and Y. Lin, "lncRNA NR2F1-AS1 promotes breast cancer angiogenesis through activating IGF-1/IGF-1R/ERK pathway," *Journal of Cellular Molecular Medicine*, vol. 24, 2020.

[11] J. Wang, S. Dong, J. Zhang et al., "LncRNA NR2F1-AS1 Regulates miR-371a-3p/TOB1 axis to suppress the proliferation of colorectal cancer cells," *Cancer Biother Radiopharmaceuticals*, vol. 35, no. 10, pp. 760–764, 2020.

[12] P. Ren, H. Zhang, L. Chang, X. D. Hong, and L. Xing, "LncRNA NR2F1-AS1 promotes proliferation and metastasis of ESCC cells via regulating EMT," *European Review for Medical and Pharmacological Sciences*, vol. 24, pp. 3686–3693, 2020.

[13] H. Jia, H. Qi, Z. Gong et al., "The expression of FOXP3 and its role in human cancers," *Biochimica et Biophysica Acta (BBA)—Reviews on Cancer*, vol. 1871, no. 1, pp. 170–178, 2019.

[14] C. Xu, H. Cui, H. Li, Y. Wu, H. An, and C. Guo, "Long noncoding RNA ZEB2-AS1 expression is associated with disease progression and predicts outcome in gastric cancer patients," *Journal of BUON: Official Journal of the Balkan Union of Oncology*, vol. 24, pp. 663–671, 2019.

[15] N. Xu, L. Qiao, L. Yin, and H. Li, "Long noncoding RNA ROR1-AS1 enhances lung adenocarcinoma metastasis and induces epithelial-mesenchymal transition by sponging miR-375," *Journal of BUON: Official Journal of the Balkan Union of Oncology*, vol. 24, pp. 2273–2279, 2019.

[16] R. Zhang, S. Hao, L. Yang, J. Xie, S. Chen, and G Gu, "LINC00339 promotes cell proliferation and metastasis in pancreatic cancer via miR-497-5p/IGF1R axis," *Journal of BUON: Official Journal of the Balkan Union of Oncology*, vol. 24, pp. 729–738, 2019.

[17] L. Wang, S. Zhao, and Y. U. Mingxin, "LncRNA NR2F1-AS1 is involved in the progression of endometrial cancer by sponging miR-363 to target SOX4," *Die Pharmazie*, vol. 74, pp. 295–300, 2019.

[18] F. Guo, Q. Fu, Y. Wang, and G. Sui, "Long non-coding RNA NR2F1-AS1 promoted proliferation and migration yet suppressed apoptosis of thyroid cancer cells through regulating miRNA-338-3p/CCND1 axis," *Journal of Cellular and Molecular Medicine*, vol. 23, no. 9, pp. 5907–5919, 2019.

[19] S. Li, K. Zheng, Y. Pei, W. Wang, and X. Zhang, "Long noncoding RNA NR2F1-AS1 enhances the malignant properties of osteosarcoma by increasing forkhead box A1 expression via sponging of microRNA-483-3p," *Aging*, vol. 11, no. 23, pp. 11609–11623, 2019.

[20] H. Wang, X. Huo, X. R. Yang et al., "STAT3-mediated upregulation of lncRNA HOXD-AS1 as a ceRNA facilitates

liver cancer metastasis by regulating SOX4," *Molecular Cancer*, vol. 16, no. 1, p. 136, 2017.

[21] S. P. Li, H. X. Xu, Y. Yu et al., "LncRNA HULC enhances epithelial-mesenchymal transition to promote tumorigenesis and metastasis of hepatocellular carcinoma via the miR-200a-3p/ZEB1 signaling pathway," *Oncotarget*, vol. 7, no. 27, pp. 42431–42446, 2016.

[22] D. Wang, N. Xing, T. Yang et al., "Exosomal lncRNA H19 promotes the progression of hepatocellular carcinoma treated with Propofol via miR-520a-3p/LIMK1 axis," *Cancer Medicine*, vol. 9, 2020.

[23] Y. Li, G. Chen, Y. Yan, and Q. Fan, "CASC15 promotes epithelial to mesenchymal transition and facilitates malignancy of hepatocellular carcinoma cells by increasing TWIST1 gene expression via miR-33a-5p sponging," *European Journal of Pharmacology*, vol. 860, Article ID 172589, 2019.

[24] Z. Xiao, Y. Liu, J. Zhao et al., "Long noncoding RNA LINC01123 promotes the proliferation and invasion of hepatocellular carcinoma cells by modulating the miR-34a-5p/TUFT1 axis," *International Journal of Biological Sciences*, vol. 16, no. 13, pp. 2296–2305, 2020.

[25] M. Q. Yang, L. L. Bai, L. Lei et al., "DEK promotes the proliferation and invasion of lung cancers and indicates poor prognosis in lung adenocarcinomas," *Oncology Reports*, vol. 43, pp. 1338–1348, 2020.

[26] K. F. Lee, M. M. Tsai, C. Y. Tsai et al., "DEK is a potential biomarker associated with malignant phenotype in gastric cancer tissues and plasma," *International Journal of Molecular Sciences*, vol. 20, 2019.

[27] S. Y. Lee, W. Jung, J. Lee, A. Kim, H. K. Kim, and B. H. Kim, "High expression of DEK is associated with poor prognosis in hepatocellular carcinoma," *Histology and Histopathology*, vol. 34, pp. 1279–1288, 2019.

[28] C. S. Liu, Q. Zhou, Y. D. Zhang, and Y. Fu, "Long noncoding RNA SOX2OT maintains the stemness of pancreatic cancer cells by regulating DEK via interacting with miR-200a/141," *European Review for Medical and Pharmacological Sciences*, vol. 24, pp. 2368–2379, 2020.

[29] W. Hui, X. Ma, Y. Zan, L. Song, S. Zhang, and L. Dong, "MicroRNA-1292-5p inhibits cell growth, migration and invasion of gastric carcinoma by targeting DEK," *American Journal of Cancer Research*, vol. 8, pp. 1228–1238, 2018.

[30] T. Zhao, B. Qiu, S. Zhou, G. Ding, L. Cao, and Z. Wu, "Expression of DEK in pancreatic cancer and its correlation with clinicopathological features and prognosis," *Journal of Cancer*, vol. 10, no. 4, pp. 911–917, 2019.

[31] X. Xu, L. Zou, Q. Yao, Y. Zhang, L. Gan, and L. Tang, "Silencing DEK downregulates cervical cancer tumorigenesis and metastasis via the DEK/p-Ser9-GSK-3beta/p-Tyr216-GSK-3beta/beta-catenin axis," *Oncology Reports*, vol. 38, no. 2, pp. 1035–1042, 2017.

[32] L. J. Lin and L. T. Chen, "The role of DEK protein in hepatocellular carcinoma for progression and prognosis," *Pakistan Journal of Medical Sciences*, vol. 29, pp. 778–782, 2013.

Hindawi
Journal of Oncology
Volume 2021, Article ID 4312296, 7 pages
https://doi.org/10.1155/2021/4312296

Research Article

The Correlation between ^{18}F-FDG PET/CT Imaging SUVmax of Preoperative Colon Cancer Primary Lesions and Clinicopathological Factors

Dacheng Li,[1,2] **Ying Wang**,[1] **Weili Liu**,[3] **Qiusong Chen**,[1] **Li Cai**,[1] **Xiling Xing**,[1] **and Shuo Gao**[1]

[1]*Department of PET-CT Diagnostic, Tianjin Medical University General Hospital, Tianjin 300052, China*
[2]*Department of Nuclear Medicine, The Affiliated Hospital of Qingdao University, Qingdao 266000, Shandong Province, China*
[3]*Interventional Operation Room, The Affiliated Hospital of Qingdao University, Qingdao 266000, Shandong Province, China*

Correspondence should be addressed to Shuo Gao; yitaosu76@163.com

Received 1 July 2021; Accepted 25 August 2021; Published 17 September 2021

Academic Editor: Alamgeer Yuchi

Background. The purpose of this study is to explore the correlation between the ^{18}F-FDG PET/CT imaging maximum standardized uptake value (SUVmax) of preoperative colon cancer primary lesions and clinicopathological factors. *Methods*. 88 colon cancer patients diagnosed by histopathology were collected from January 2014 to December 2015. ^{18}F-FDG PET/CT imaging was performed before surgery. Kaplan–Meier survival analysis was used to assess the prognosis of colon cancer patients. *Results*. The ^{18}F-FDG PET/CT imaging SUVmax value of preoperative colon cancer primary lesion was significantly correlated with the length of the lesion, clinical stage, histopathological type, and the degree of tumor differentiation. The SUVmax value of tumors with long-diameter, ≥ 3 cm, clinically high-stage, adenocarcinoma, and poorly differentiated lesions was significantly high. In addition, the consistency between PET/CT and surgical pathological results at stage I and IV was higher. Stage II and III PET/CT are basically consistent with the pathological results of surgery. Kaplan–Meier survival analysis showed that the 5-year event-free survival rate of the SUVmax > 18.26 group was significantly lower than that of the SUVmax ≤ 18.26 group. *Conclusion*. ^{18}F-FDG PET/CT imaging SUVmax of preoperative colon cancer primary lesions can not only reflect the proliferation and invasion ability but also monitor the recurrence and metastasis of colon cancer.

1. Introduction

The incidence of colon cancer ranks third among malignant tumors, and its mortality rate is second only to lung cancer, liver cancer, and gastric cancer. Colon cancer is a serious threat to human life and health [1]. With the changes in people's dietary habits and the intensification of population aging, the incidence and mortality of colon cancer in China have shown a continuous upward trend in recent years. In addition, the incidence of colon cancer has risen to the second place among gastrointestinal malignancies [2]. The main method of treating early colon cancer is surgical resection. Postoperative patients with advanced colon cancer have a certain rate of recurrence and metastasis. Therefore, early diagnosis and accurate preoperative evaluation of clinicopathological factors are key factors that guide the treatment and prognosis of colon cancer patients.

Currently, traditional imaging examination methods include CT and MRI. They judge the lesion based on the anatomical shape of the lesion. Sometimes, it is difficult to distinguish between benign and malignant lesions. There are limitations in judging lymph node or distant metastasis [3]. PET/CT combines the advantages of PET and CT. PET can display the pathophysiological function of malignant tumor lesions. CT can accurately display the anatomical structure. PET/CT can realize the same machine fusion of morphological and functional imaging. In addition, PET/CT not only makes up for the deficiencies of CT qualitative

Table 1: Clinicopathological information of 88 patients with colon cancer (n).

Group	n
Gender	
Male	52
Female	36
Age (year)	
<60	43
≥ 60	45
Tumor site	
Left colon	38
Right colon	50
Lesion length (cm)	I
<3	23
≥3	65
Pathological tissue type	
Mucinous adenocarcinoma	22
Adenocarcinoma	66
Tumor differentiation	
Well differentiated	21
Moderate differentiation	33
Poorly differentiated	34
AJCC stage	
0	2
I	4
II	16
III	22
IV	44

difficulties and inaccurate PET positioning but also greatly improves the diagnostic efficiency of malignant tumors [4]. PET/CT has unique advantages over traditional imaging in monitoring the recurrence, metastasis, and prognosis of colon cancer [5]. The maximum standardized uptake value (SUVmax) is a semiquantitative index of PET/CT. Understanding the correlation between SUVmax and clinicopathological factors can further guide clinical treatment and evaluate prognosis.

In this study, preoperative ^{18}F-FDG PET/CT imaging data of 88 colon cancer patients were retrospectively analyzed to evaluate the correlation between SUVmax and clinicopathological factors. This study can provide the basis for guiding the treatment and prognostic follow-up of colon cancer.

2. Materials and Methods

2.1. Patients. 88 patients with colon cancer diagnosed by histopathology participated in our research. ^{18}F-FDG PET/CT imaging was performed before surgery. Surgery or colonoscopy histopathological examination was performed within 2 weeks after PET/CT examination. Clinical stage refers to the TNM staging standard for colon cancer proposed by the American Joint Committee on Cancer (AJCC) and the Union for International Cancer Control (UICC) [6]. The clinicopathological factors of 88 patients with colon cancer are shown in Table 1.

2.2. Inclusion and Exclusion Criteria. Inclusion criteria: ① All patients were diagnosed for the first time and were cancers of the colon primary site. ② All patients had not received antitumor treatment within half a year before the examination. ③ All patients underwent ^{18}F-FDG PET/CT examination before operation. ④ All patients and their families in this study signed informed consent.

Exclusion criteria: ① patients with other malignant tumors; ② pregnant, breastfeeding, or diabetic patients; and ③ patients with incomplete data.

2.3. PET/CT Examination. Before the examination, the patient fasted for 4–6 hours. Fasting blood glucose should be maintained below 7.1 mmol/L. After injecting 18 F-FDG into the elbow vein at a dose of 4.0 MBq/kg, the patient rested quietly for 50–60 minutes. After the patient has passed the urine, a regular PET/CT scan (from the top of the skull to the middle of the femur) was performed. If necessary, the lower limbs or soles of the feet were also scanned. Then, 6~8 beds were collected (3 min/bed). The tube voltage and tube current are 120 kV and 150 mA, respectively. The layer thickness is 3.75 mm. Three-dimensional acquisition is performed during the PET scan, and the layer thickness is 3.25 mm. The CT data are used for attenuation correction, and the maximum expected value iteration method of ordered subsets is used for image reconstruction. The reconstruction data are uploaded to the AW4.5 workstation for image display and data processing.

2.4. Image Analysis. Two experienced nuclear medicine physicians observe and analyze each PET/CT image. When the diagnosis is inconsistent, the result after discussion by 2 or more nuclear medicine doctors shall prevail. Semiquantitative analysis is used to select the layer with the highest radioactive concentration of the lesion to delineate the region of interest (ROI). Also, the system automatically measures the SUVmax of the lesion.

2.5. PET/CT Preoperative Stage Standard. PET/CT preoperative staging is based on the TNM staging system for colon cancer proposed by the American Joint Committee on Cancer (AJCC), the Union for International Cancer Control (UICC) [6], and other PET studies [7].

T0: no primary tumor was found.

T1~T2: the lumen is locally thickened, but the outer wall is still smooth. The fat spaces around is still clear. Also, the radioactivity of the lesion was concentrated on the PET image (SUVmax ≥ 2.5).

T3: the tube wall is locally thickened, and the lumen is obviously narrowed. The shape of the tube wall is irregular and uneven. The fat gap is not clear and fuzzy. The primary focus and the main lesions and affected organs or tissues show radioactivity concentration on the PET image.

T4: the tumor breaks through the serosal layer, and the tube wall thickens more obviously. Also, the lumen becomes narrower. The density of peripheral fat interstices is increased, which invades the structure of adjacent organs. The mass and the invaded organs showed radioactivity concentration on the PET image.

N0: no regional lymph node metastasis was found.

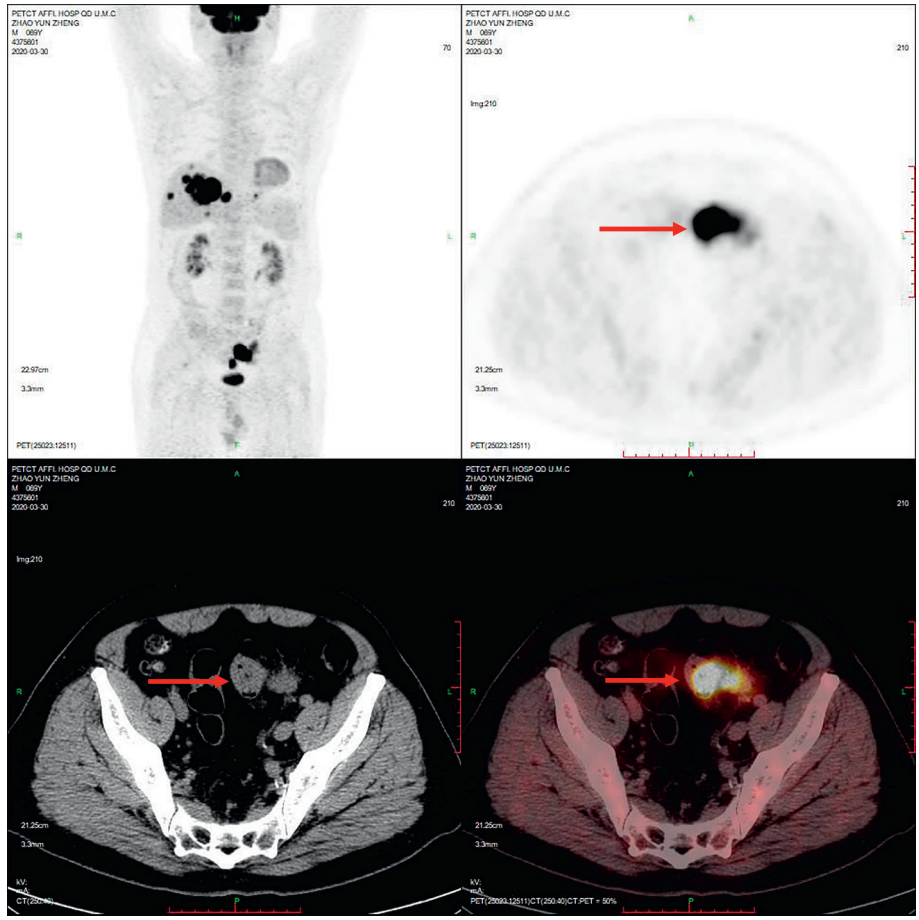

Figure 1: Male, 69 years old. Sigmoid colon cancer lesions significantly uptake FDG (SUVmax, 37.6). The SUVmax of peri-intestinal metastases was about 8.4.

N1: there are 1 to 3 regional lymph node metastases. CT shows that the long diameter of the lymph node is >1.0 cm. The long diameter is less than 1.0 cm, but SUVmax ≥ 2.0.

N2: there are more than 4 regional lymph node metastases.

M0: no distant metastasis was found.

M1: distant metastasis was exhibited. The PET image of the metastasis shows the radioactivity concentration. Also, the shadow of the lesion can be seen on CT.

2.6. Follow-Up and Prognostic Evaluation. After initial treatment (surgery, radiotherapy, and chemotherapy), 88 patients with colon cancer were followed up by a combination of outpatient review, telephone, and electronic medical record system. The follow-up end point was December 2020. The follow-up time was 3–60 months (1 time/3–6 months).

The patients received CT, ^{18}F-FDG PET/CT and colonoscopy regularly. The occurrence of recurrence, new metastasis, or death is defined as an "event." Event-free survival refers to the absence of recurrence, new metastasis, or death from the end of initial treatment to the end of follow-up.

2.7. Statistical Analysis. The data were analyzed using SPSS 22.0. Data are expressed as mean ± SD. The independent sample *t*-test was used to compare the average SUVmax between the two groups. PET/CT was calculated to determine the sensitivity, specificity, accuracy, positive predictive value (PPV), and negative predictive value (NPV) of colon cancer clinical stage. The kappa test was used to evaluate the consistency of PET/CT in the preoperative clinical stage and pathological diagnosis. Kappa value < 0.4 indicates that the consistency of the test results is poor. The kappa value is generally consistent between 0.4 and 0.75. Kappa value > 0.75 means higher consistency. The Kaplan–Meier method and log-rank test were used for survival analysis. $P < 0.05$ indicates that the difference is statistically significant.

3. Results

3.1. Uptake of 18 F-FDG in Primary Lesions and Metastases. Eighty-eight colon cancer lesions uptake 18 F-FDG significantly. As shown in Figure 1, the sigmoid colon cancer lesions significantly uptake FDG, and the SUVmax was about 37.6. The SUVmax of peri-intestinal metastases was about approximately 8.4. Figure 2 shows that the SUVmax of

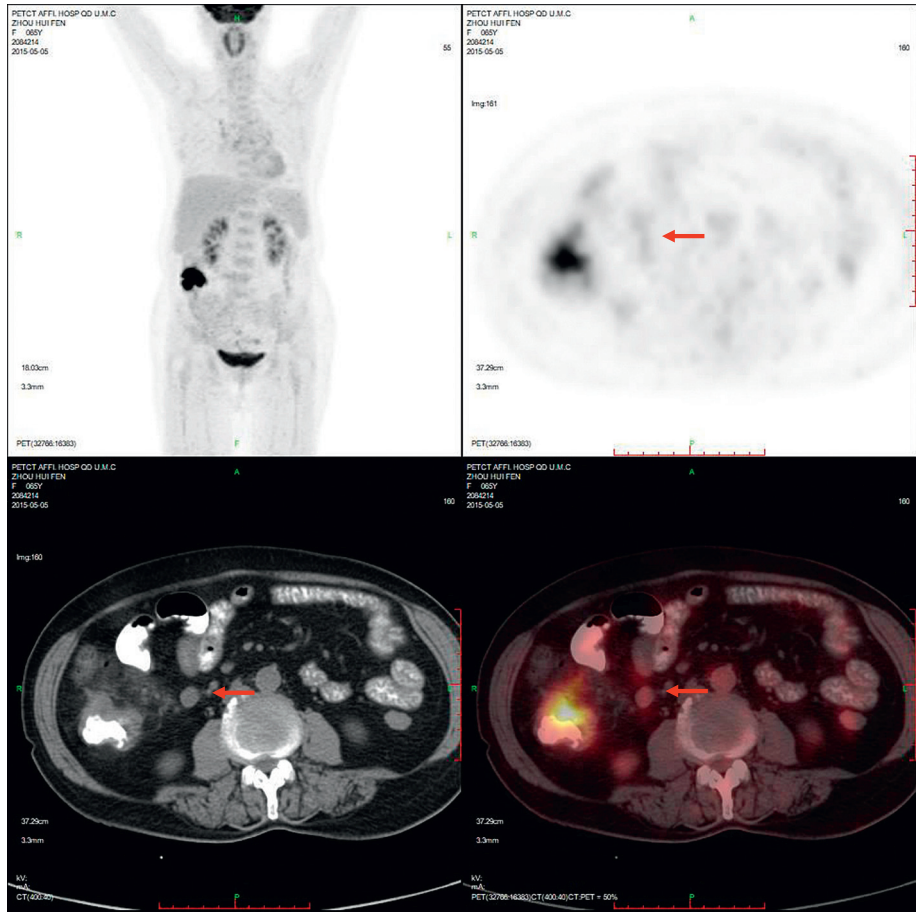

Figure 2: Female, 65 years old, colon cancer (SUVmax, 17.0). The SUVmax of enlarged lymph nodes beside the right colon (10 ∗ 11 mm) is about 4.6.

colon cancer was about 17.0. The size of the enlarged lymph node next to the right colon was about 10 ∗ 11 mm, and the SUVmax was about 4.6. Figure 3 showed sigmoid colon cancer (SUVmax, 20.5) with multiple lung metastases (SUVmax, 15.3).

3.2. The Correlation between ^{18}F-FDG PET/CT Imaging SUVmax Value before Colon Cancer Surgery and Clinicopathological Factors. The ^{18}F-FDG PET/CT imaging lesion SUVmax of colon cancer before surgery was not significantly correlated with the patient's gender, age, and tumor location ($P > 0.05$, Table 2). But, it was closely related to the length of the lesion, clinical stage, histopathological type, and the degree of tumor differentiation ($P < 0.01$, Table 2). The SUVmax value of tumor with long-diameter, ≥ 3 cm, clinically high-stage, adenocarcinoma, and poorly differentiated lesions was significantly higher than that of short-diameter, <3 cm, clinically low-stage, mucinous adenocarcinoma, and well-differentiated tumor lesions ($P < 0.01$, Table 2).

3.3. Comparison of Clinical Stage Judged by ^{18}F-FDG PET/CT Imaging and the Pathological Stage. Taking pathological diagnosis as the gold standard, the pathological stage results of 88 colon cancer patients and the sensitivity, specificity, accuracy, PPV, NPV, and kappa value of PET/CT stage are shown in Table 3. The consistency between PET/CT and surgical pathological results at stage I and IV was high (kappa = 0.789, 1.000; $P < 0.05$). The consistency between PET/CT and surgical pathological results at stage II and III was moderate (kappa = 0.553, 0.722; $P < 0.05$).

3.4. The Effect of the ^{18}F-FDG PET/CT Imaging SUVmax Value of Primary Colon Cancer before Surgery on the Prognosis of Patients. Kaplan–Meier survival analysis showed that the 5-year event-free survival rate of the ^{18}F-FDG PET/CT imaging SUVmax > 18.26 group (preoperative primary colon cancer) was significantly lower than that of the SUVmax ≤ 18.26 group ($x^2 = 14.363$, $P < 0.01$, Figure 4).

4. Discussion

Colon cancer is one of the common malignant tumors of the digestive system, which can easily cause metastasis. When colon cancer has lymph node metastasis, the 5-year survival rate of the patients drops from 75% to about 30% [8]. Therefore, it is very important to conduct accurate clinicopathological factors analysis before colon cancer surgery. In addition to clarifying the location, size, and nature of the tumor lesions before surgery, it is also necessary to clarify the

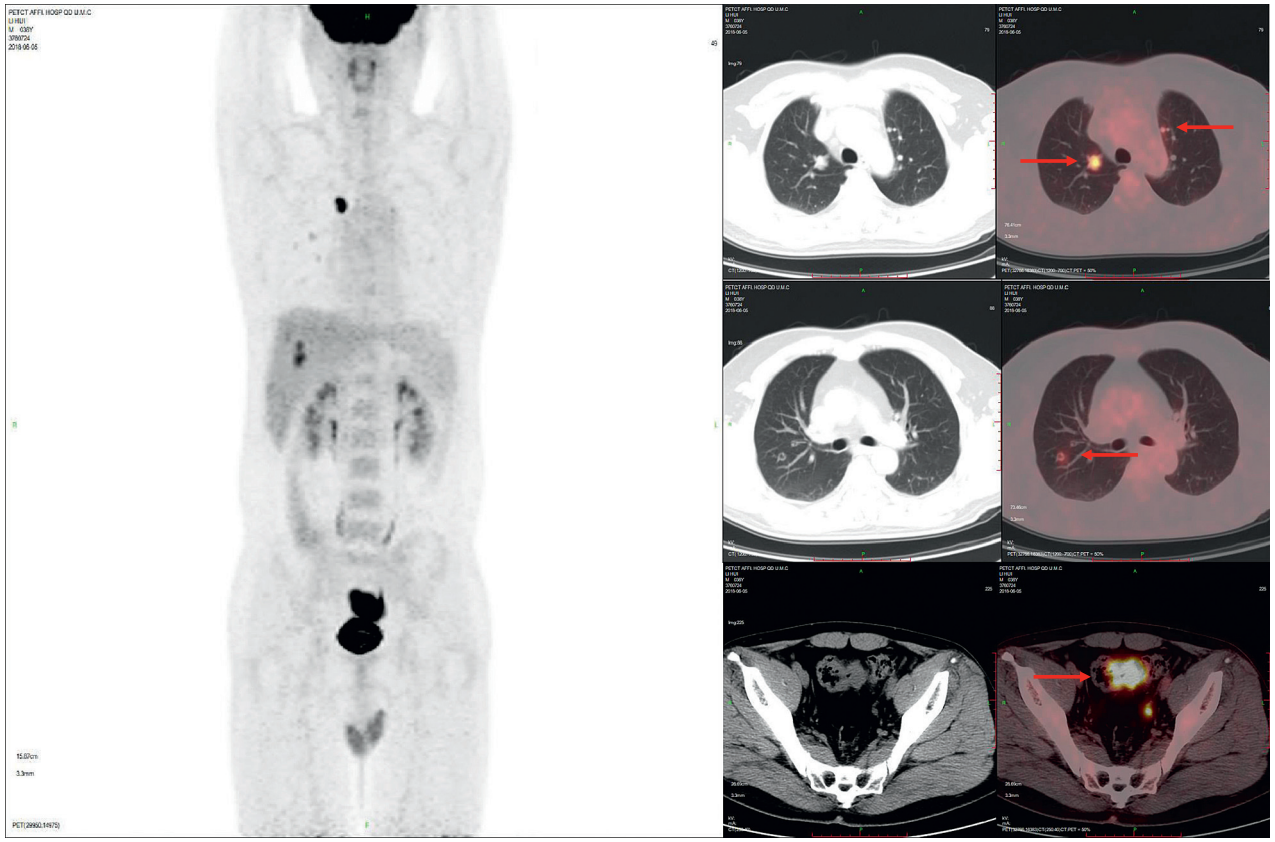

Figure 3: Male, 38 years old, having sigmoid colon cancer (SUVmax, 20.5) and multiple lung metastases (SUVmax, 15.3).

Table 2: Correlation analysis between the SUVmax value of ^{18}F-FDG PET/CT imaging and clinicopathological factors before colon cancer surgery.

Group	n	SUVmax	T	*P* value
Gender				
Male	52	16.38 ± 8.12^{a}	0.290	0.773
Female	36	15.32 ± 7.01		
Age (year)				
<60	43	15.67 ± 6.89^{a}	0.283	0.775
≥60	45	15.79 ± 7.25		
Tumor site				
Left colon	38	16.53 ± 8.01^{a}	0.501	0.623
Right colon	50	15.12 ± 7.32		
Lesion length (cm)				
<3	23	9.12 ± 4.31^{b}	8.796	$P \leq 0.001^{**}$
≥3	65	20.39 ± 9.63		
Clinical stage				
0 + I + II	16	5.35 ± 2.67^{b}	7.863	$P \leq 0.001^{**}$
III + IV	72	23.78 ± 9.02		
Pathological tissue type				
Mucinous adenocarcinoma	22	8.75 ± 3.54^{b}	10.356	$P \leq 0.001^{**}$
Adenocarcinoma	66	21.32 ± 9.76		
Tumor differentiation				
Poorly differentiated	34	25.67 ± 12.31^{b}	9.265	$P \leq 0.001^{**}$
Well and moderately differentiated	54	11.36 ± 5.06		

$^{**}P \leq 0.01$.

biological behaviors such as the extent of local infiltration, clinical stage, and the degree of lesion differentiation. Accurate analysis of clinicopathological factors can guide individualized treatment and optimize the treatment plan for colon cancer patients. It also reduces the risk and complications of blind surgery and improves the prognosis of patients [9].

Table 3: Comparison of results of clinical staging and pathological staging of 88 cases of colon cancer by 18 F-FDG PET/CT imaging.

PET/CT clinical stage	Postoperative pathological clinical stage					Sensitivity (%)	Specificity (%)	Accuracy (%)	PPV (%)	NPV (%)	Kappa	*P*
	0	I	II	III	IV							
I	2	4	0	0	0	100.0	97.6	97.7	66.7	100.0	0.788	<0.01
II	0	0	8	2	0	50.0	97.2	88.6	80.0	89.7	0.553	<0.01
III	0	0	8	20	0	90.1	87.9	88.6	71.4	97.1	0.722	<0.01
IV	0	0	0	0	44	100.0	100.0	100.0	100.0	100.0	100.0	<0.01

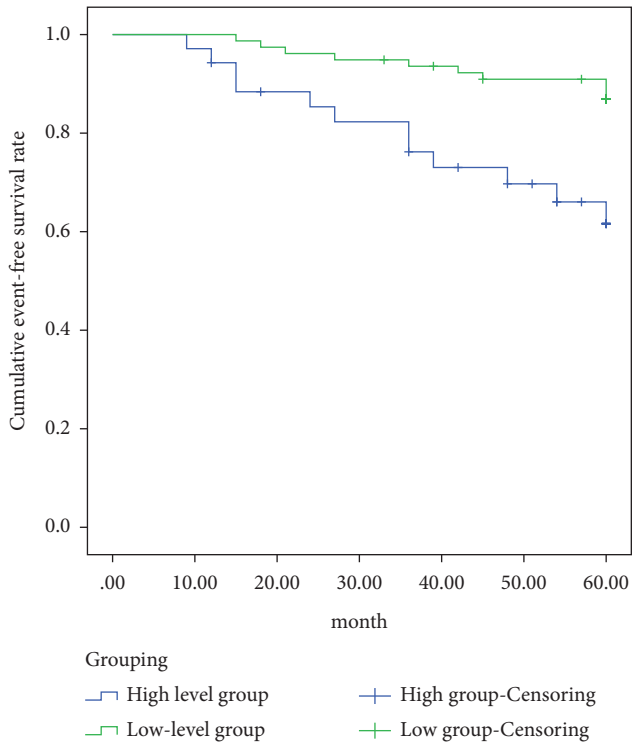

Figure 4: 5-year event-free survival rate.

At present, imaging examination has become one of the main methods for preoperative diagnosis of cancer lymph node metastasis. Compared with other imaging methods, CT has the characteristics of high sensitivity and specificity in judging lymph node metastasis, low false positive rate, less trauma to patients, and economical benefits [10]. Malignant tumor cells have active metabolism and high level of glycolysis. 18 F-FDG uptake increases and accumulates in cells. For small lesions, PET/CT may detect slight metabolic changes at an early stage [11]. PET/CT imaging can detect lesions early and immediately observe tumor cell proliferation and metabolic changes [9]. ^{18}F-FDG PET/CT uses a semiquantitative index SUV to reflect the metabolism of the lesion. Also, the morphological changes of the lesions are observed by CT. ^{18}F-FDG PET/CT can distinguish the nature of lesions together [12]. ^{18}F-FDG PET/CT is suitable for patients of all ages, especially those who cannot undergo colonoscopy. In addition, ^{18}F-FDG PET/CT plays an important role in tumor localization, staging, efficacy monitoring, and detection of distant metastases. In recent years, ^{18}F-FDG PET/CT has gradually been used to assess the preoperative clinicopathological factors of colon cancer [13]. ^{18}F-FDG PET/CT realizes the simultaneous fusion of functional metabolic imaging and anatomical morphology imaging. One imaging can simultaneously display the distribution, morphology, and metabolic status of multiple organs throughout the body. Its advantages in tumor diagnosis, stage, efficacy evaluation, and prognosis prediction are also increasingly prominent.

PET/CT uses SUV to measure the uptake of 18 F-FDG by colon cancer lesions, and SUVmax is usually used as an evaluation index. Analyzing the correlation between SUVmax and patients' clinicopathological factors is crucial to formulating preoperative treatment plans. This study showed that SUVmax was significantly related to lesion length, clinical stage, pathological type, and histological differentiation. Mucinous adenocarcinoma lesions require less ^{18}F-FDG due to more mucus. Adenocarcinoma, especially poorly differentiated adenocarcinoma, has many malignant cells and high levels of metabolism. Therefore, adenocarcinoma requires more 18 F-FDG [14], which has a higher SUVmax value. In this study, the SUVmax of poorly differentiated and adenocarcinoma lesions was significantly higher than that of well-differentiated and mucinous adenocarcinoma. Accurately judging the clinical stage before surgery is particularly critical for guiding the choice of surgical plan. The National Comprehensive Cancer Network (NCCN) diagnosis and treatment guidelines proposed that neoadjuvant radiotherapy and chemotherapy should be performed for patients at stage III and IV to reduce the recurrence rate after surgery. Patients at stage I and II can be directly operated on [15]. The size of the lesion reflects the proliferation ability of the tumor. The invasion of surrounding tissues, lymph nodes, or distant metastasis reflects the tumor's invasion ability. In this study, the SUVmax value of tumor lesions with a long diameter, ≥ 3 cm, was significantly higher than that of tumor lesions with a short diameter, less than 3 cm. Lymph node metastasis is the most common way of colon cancer metastasis [16]. Approximately 20% of newly diagnosed colon cancer patients have distant metastases [17]. The most common site of metastasis is the liver. The number and location of liver metastases will affect the choice of surgical methods [18]. Previous studies have shown that the distant metastases accuracy of CT detection varies greatly, ranging from 55% [19] to 100% [15]. The sensitivity of PET/CT to distant metastases is higher than that of CT and MRI [20]. In this study, the consistency

of between PET/CT and surgical pathological results at stage I and IV was high, and the consistency of between PET/CT and surgical pathological results at stage II and III was moderate. Therefore, the use of ^{18}F-FDG PET/CT imaging SUVmax to assess the biological behavior of colon cancer is of great significance for guiding the choice of clinical treatment options.

This study also analyzed the relationship between the SUVmax of preoperative colon cancer primary lesions and the prognosis. The results showed that the 5-year event-free survival rate of the SUVmax > 18.26 group was significantly lower than that of the SUVmax ≤ 18.26 group. Therefore, the prognosis of colon cancer patients can be evaluated based on the SUVmax value of the primary tumor before surgery.

5. Conclusions

Exploring the correlation between preoperative ^{18}F-FDG PET/CT imaging SUVmax of primary colon cancer and clinicopathological factors can guide the treatment and prognosis evaluation of colon cancer patients.

Data Availability

The datasets used during the present study are available from the corresponding author upon reasonable request.

Conflicts of Interest

The authors declare no conflicts of interest.

References

[1] J. Ferlay, I. Soerjomataram, R. Dikshit et al., "Cancer incidence and mortality worldwide: sources, methods and major patterns in GLOBOCAN 2012," *International Journal of Cancer*, vol. 136, no. 5, pp. E359–E386, 2015.

[2] H. G. Welch and W. C. Black, "Overdiagnosis in cancer," *JNCI Journal of the National Cancer Institute*, vol. 102, no. 9, pp. 605–613, 2010.

[3] S. Kijima, T. Sasaki, K. Nagata, K. Utano, A. T. Lefor, and H. Sugimoto, "Preoperative evaluation of colorectal cancer using CT colonography, MRI, and PET/CT," *World Journal of Gastroenterology*, vol. 20, no. 45, pp. 16964–16975, 2014.

[4] J. W. Huh, J. J. Min, J. H. Lee, H. R. Kim, and Y. J. Kim, "The predictive role of sequential FDG-PET/CT in response of locally advanced rectal cancer to neoadjuvant chemoradiation," *American Journal of Clinical Oncology*, vol. 35, no. 4, pp. 340–344, 2012.

[5] I. J. Park, H. C. Kim, C. S. Yu et al., "Efficacy of PET/CT in the accurate evaluation of primary colorectal carcinoma," *European Journal of Surgical Oncology*, vol. 32, no. 9, pp. 941–947, 2006.

[6] M. B. Amin, F. L. Greene, S. B. Edge et al., "The Eighth Edition AJCC Cancer Staging Manual: continuing to build a bridge from a population-based to a more "personalized" approach to cancer staging," *CA: A Cancer Journal for Clinicians*, vol. 67, no. 2, pp. 93–99, 2017.

[7] B. E. Engelmann, A. Loft, A. Kjær et al., "Positron emission tomography/computed tomography for optimized colon cancer staging and follow up," *Scandinavian Journal of Gastroenterology*, vol. 49, no. 2, pp. 191–201, 2014.

[8] J. Lykke, O. Roikjaer, P. Jess, and Danish Colorectal Cancer Group, "The relation between lymph node status and survival in stage I-III colon cancer: results from a prospective nationwide cohort study," *Colorectal Disease*, vol. 15, no. 5, pp. 559–565, 2013.

[9] Y. Tsunoda, M. Ito, H. Fujii, H. Kuwano, and N. Saito, "Preoperative diagnosis of lymph node metastases of colorectal cancer by FDG-PET/CT," *Japanese Journal of Clinical Oncology*, vol. 38, no. 5, pp. 347–353, 2008.

[10] S. Bipat, A. S. Glas, F. J. M. Slors, A. H. Zwinderman, P. M. M. Bossuyt, and J. Stoker, "Rectal cancer: local staging and assessment of lymph node involvement with endoluminal US, CT, and MR imaging-a meta-analysis," *Radiology*, vol. 232, no. 3, pp. 773–783, 2004.

[11] V. X. Nguyen, B. D. Nguyen, and P. C. Ram, "Occult colon cancer with initial cutaneous metastatic manifestation," *Clinical Nuclear Medicine*, vol. 37, no. 5, pp. 506–508, 2012.

[12] V. Malik, C. Johnston, C. Donohoe et al., "18F-FDG PET-detected synchronous primary neoplasms in the staging of esophageal cancer," *Clinical Nuclear Medicine*, vol. 37, no. 12, pp. 1152–1158, 2012.

[13] A. M. Maffione, E. Lopci, C. Bluemel, F. Giammarile, K. Herrmann, and D. Rubello, "Diagnostic accuracy and impact on management of 18F-FDG PET and PET/CT in colorectal liver metastasis: a meta-analysis and systematic review," *European Journal of Nuclear Medicine and Molecular Imaging*, vol. 42, no. 1, pp. 152–163, 2015.

[14] M. Yun, J. S. Lim, S. H. Noh et al., "Lymph node staging of gastric cancer using (18)F-FDG PET: a comparison study with CT," *Journal of Nuclear Medicine: Official Publication, Society of Nuclear Medicine*, vol. 46, pp. 1582–1588, 2005.

[15] F. Cademartiri, G. Luccichenti, A. Rossi, and P. Pavone, "Spiral hydro-CT in the evaluation of colo-sigmoideal cancer," *La Radiologia Medica*, vol. 104, pp. 295–306, 2002.

[16] E. Nerad, M. J. Lahaye, M. Maas et al., "Diagnostic accuracy of CT for local staging of colon cancer: a systematic review and meta-analysis," *American Journal of Roentgenology*, vol. 207, no. 5, pp. 984–995, 2016.

[17] A. M. Leufkens, M. A. A. J. van den Bosch, M. S. van Leeuwen, and P. D. Siersema, "Diagnostic accuracy of computed tomography for colon cancer staging: a systematic review," *Scandinavian Journal of Gastroenterology*, vol. 46, no. 7-8, pp. 887–894, 2011.

[18] T. Ruers and R. P. Bleichrodt, "Treatment of liver metastases, an update on the possibilities and results," *European Journal of Cancer*, vol. 38, no. 7, pp. 1023–1033, 2002.

[19] M. R. McAndrew and A. K. Saba, "Efficacy of routine preoperative computed tomography scans in colon cancer," *The American Surgeon*, vol. 65, pp. 205–208, 1999.

[20] S. Bipat, M. S. van Leeuwen, E. F. I. Comans et al., "Colorectal liver metastases: CT, MR imaging, and PET for diagnosis-meta-analysis," *Radiology*, vol. 237, no. 1, pp. 123–131, 2005.

Hindawi
Journal of Oncology
Volume 2021, Article ID 4470778, 10 pages
https://doi.org/10.1155/2021/4470778

Research Article

MiR-200b Suppresses Gastric Cancer Cell Migration and Invasion by Inhibiting NRG1 through ERBB2/ERBB3 Signaling

Tonglei Xu,[1] Fangliang Xie,[1] Dazhou Xu,[2] Weidong Xu,[1] Xuming Ge,[1] Shengxiang Lv,[2] and Shouying Li[2]

[1]*Department of Hepatobiliary Surgery, First People's Hospital of Lianyungang, Lianyungang 222061, Jiangsu Province, China*
[2]*Department of Gastroenterology, First People's Hospital of Lianyungang, Lianyungang 222061, Jiangsu Province, China*

Correspondence should be addressed to Shouying Li; lishouying@lyghospital.cn

Received 8 June 2021; Accepted 20 August 2021; Published 7 September 2021

Academic Editor: Alamgeer Yuchi

Purpose. Accumulating evidence indicates that miRNAs (miRs) play crucial roles in the modulation of tumors development. However, the accurately mechanisms have not been entirely clarified. In this study, we aimed to explore the role of miR-200b in the development of gastric cancer (GC). *Methods*. Western blot and RT-PCR were applied to detect epithelial-mesenchymal transition (EMT) marker expression and mRNA expression. Transwell assay was used for measuring the metastasis and invasiveness of GC cells. TargetScan system, luciferase reporter assay, and rescue experiments were applied for validating the direct target of miR-200b. *Results*. MiR-200b was prominently decreased in GC tissues and cells, and its downregulation was an indicator of poor prognosis of GC patients. Reexpression of miR-200b suppressed EMT along with GC cell migration and invasion. Neuregulin 1 (NRG1) was validated as the target of miR-200b, and it rescued miR-200b inhibitory effect on GC progression. In GC tissues, the correlation of miR-200b with NRG1 was inverse. *Conclusion*. MiR-200b suppressed EMT-related migration and invasion of GC through the ERBB2/ERBB3 signaling pathway via targeting NRG1.

1. Introduction

As a malignant tumor originating from the gastric mucosa epithelium, gastric cancer (GC) occupies the first place among various malignant tumors in China [1, 2]. The vast majority of GC belongs to adenocarcinoma, and there are no obvious symptoms at the early stage. It is often similar to gastritis, gastric ulcer, and other chronic gastric disease symptoms, which are easy to be ignored. Therefore, the early diagnosis rate of GC is still low in China [3, 4]. Although significant improvements including surgery, radiotherapy, and targeted therapy have been made in treating GC, most patients will experience postoperative recurrence and metastasis, leading to poor survival [5]. Thus, it is imperative to investigate the metastatic mechanism in GC.

MiRNAs (miRs) have been proved to serve as oncogenes or tumor suppressors via modulating the expression of target genes at the posttranscriptional level in various tumors [6, 7]. Accumulating evidence has shown that miRs take part in many tumors development, including migration and invasion. For example, Ye et al. displayed that downregulation of miR-7 facilitated GC metastasis via promoting p65-mediated NF-κB activation [8]. Also, miR-214 was decreased in GC, and its downregulation contributed to GC cell migration and invasion via inducing EMT [9]. Moreover, miR-1292 suppressed GC cell invasion and migration via DEK [10]. Furthermore, miR-200b was reported to take part in GC development [11]. However, the molecular mechanism of miR-200b in the modulation of GC invasion and migration has not been fully clarified. Epithelial-mesenchymal transition (EMT) plays important roles in the metastasis of various cancers, and it is an important biological process in which epidermal malignant cells acquire the ability to migrate and invade [12–14]. Thus, understanding the mechanism of miR-200b in regulating EMT is very important.

Neuregulin 1(NRG1), a member of the NRG family, is an emerging potential oncogene in tumors [15]. NRG1 has been

proved to participate in the progression of multiple cancers [16, 17]. For instance, Jones et al. displayed that NRG1 played important roles in the treatment for metastatic cancer [16]. Moreover, Yun et al. showed that NRG1 served as a potential biomarker for prognosis and treatment of GC patients [18]. However, the role of NRG1 in GC progression has not been reported. NRG1 was verified as the target of miR-125 in the regulation of the apoptosis and invasion of glioma [19]. Besides, miR-296 targeted NRG1 to suppress hepatocellular carcinoma progression [20]. Here, we investigated the role of NRG1 and its underlying mechanism in the modulation of GC cell migration and invasion.

Previous studies have been reported that NRG1 played important roles in cancers by directly binding to ERBB3 or ERBB4 and ERBB3 or ERBB4 interacts with ERBB2 or ligand-receptor, leading to receptor phosphorylation and signal cascade activation [21]. In the present study, we explored miR-200b's role in GC progression and explored whether the ERBB2/ERBB3 signaling pathway was involved in GC progression modulated by the miR-200b/NRG1 axis.

2. Methods

2.1. Study Design. From January 2014 to December 2014, 60 patients with GC resection were recruited in the First People's Hospital of Lianyungang. No patients had received preoperative chemotherapy or targeted therapy. Before collection of tissue specimens, written informed consent should be signed by all patients, and the ethics committee of the First People's Hospital of Lianyungang approved this study. The GC specimens were determined by pathologists, and they were stored at −80°C for further analysis.

2.2. Cell Culture and Cell Transfection. Two GC cell lines (MGC-803 and BGC-823) and normal gastric epithelial cell (GES-1) were provided by the Cell Bank of the Chinese Academy of Science (Shanghai, China). All cells were maintained in the RPMI-1640 medium supplemented with 10% FBS (Fatal bovine serum) at 37°C and 5% CO_2.

MiR-200b mimic/inhibitor or NRG1 siRNA/vector synthesized by RiboBio (Guangzhou, China) was transfected into MGC-803 and BGC-823 cells, respectively. The transfection was conducted for 48 h with the aid of Lipofectamine 2000 (Invitrogen, Carlsbad, USA) following the manufacturer's instructions.

2.3. Real-Time PCR (RT-PCR) Assay. Total RNA was isolated by Trizol reagent (Invitrogen, Grand Island, USA). The synthesis of cDNA was performed using a M-MLV Reverse Transcriptase Kit (Invitrogen). RT-PCR was performed using an SYBR Green Real-Time PCR Assay Kit (ThermoFisher, Waltham, USA). The sequences of primers were as follows: miR-200b-F: 5′-CACACTGAAATCCTGTCAGCTTC-3′, miR-200b-R: 5′- ACGUGACACGUU CGGAGAATT-3′; NRG1-F: 5'-CGGTGTCCATGCCTTC CAT-3', NRG1-R: 5'-GTGTCA CGAGAAGTAGAGGTCT-3'; U6-F: 5′-GCTT CGGCAGCACATATACTAAAAT-3′, U6-R: 5′-CGCTTCACGAATTTGCGTG TCAT-3′; and GAPDH-F: 5'-GGGGCTCTCCA GAACATCATCC-3', GAPDH-R: 5'-ACGCCTGCTTCACCACCTCTT-3'. U6 and GAPDH were served as the internal control. Relative expression was calculated using the $2^{-\Delta\Delta Ct}$ method.

2.4. Western Blotting Assay. Total protein was extracted from cells or tissue specimens. After the proteins were separated by SDS-PAGE, followed by transfer to NC membranes, they were blocked with 5% skimmed milk for 1 h. Subsequently, the membranes were incubated with primary antibodies at 4°C overnight, followed by second antibodies for 1 h. Lastly, BeyoECL (Thermo Fisher Scientific) was applied for detecting the immune complexes. GAPDH assay served as internal control.

2.5. Transwell Assay. Transwell migration assay and Transwell invasion assay were almost the same except for the membranes with or without 25 μg Matrigel coating. A total of 5×10^4 cells were placed onto the upper chamber, and the complete medium containing with 5% FBS was seeded in the lower chamber as a chemoattractant. After incubation for 24 h, the cells in the upper chamber migrated or invaded to the lower chamber. The cells in the lower chamber were stained with crystal violet, photographed, and calculated under a light microscope.

2.6. Dual-Luciferase Reporter Assay. Firstly, we amplified the 3'-UTR of NRG1 and then cloned it into a pGL3-reporter vector (Promega, WI, USA), named NRG1-WT. The 3'-UTR mutant type of NRG1 (NRG1-MUT) was generated by using the site-directed mutagenesis kit (TaKaRa, Shiga, Japan). The HEK-293T cells were cotransfected with miR-200b mimic or inhibitor and NRG1-WT or -MUT by Lipofectamine 2000 (Invitrogen). After transfection for 48 h, the luciferase activity was tested by using the dual-luciferase reporter assay system (Promega, Madison, WI, USA). Renilla luciferase activity served as a reference control.

2.7. Statistics. Data were presented as mean ± SD. The values were analyzed by SPSS 22.0 software (IBM, NY, USA). MiR-200b high expression and low expression were cut by using the mean value. The chi square test or two-tailed Pearson's correlation analysis were applied to detect the correlation of miR-200b with the clinicopathological features of GC patients or miR-200b with NRG1, E-cadherin, or vimentin. Overall survival rate was analyzed by the Kaplan–Meier method, and the difference analysis between the survival curves was measured by the log-rank test. The statistical significance of differences between two groups was determined by Student's *t*-test, and when more than two groups, one-way analysis of variance (ANOVA) with Tukey's *post hoc* test was applied to determine the differences. $p < 0.05$ was considered as statistically significant.

3. Results

3.1. MiR-200b Was Negatively Correlated with GC Aggressiveness. To investigate whether miR-200b was abnormally expressed during GC metastasis, we first detected miR-200b expression in GC tissue specimens. As Figure 1(a) shows, miR-200b was dramatically decreased in GC tissues relative to the normal control group. The median value of miR-200b expression was used as the cutoff point to divide miR-200b expression into high and low expression of miR-200b. Then, we measured the clinical significance of miR-200b in GC. As Table 1 shows, miR-200b was significantly associated with clinical features of GC patients. Moreover, we revealed that high expression of miR-200b predicted high overall survival time, while low expression of miR-200b served as an indicator of poor prognosis of GC patients (Figure 1(b)). More strikingly, the relationship between miR-200b and E-cadherin was positive (Figure 1(c)), while miR-200b negatively correlated with vimentin expression (Figure 1(d)). These findings indicated that miR-200b might be a favorable diagnostic maker.

3.2. MiR-200b Inhibited GC Metastasis through EMT. To verify the specific role of miR-200b in GC metastasis *in vitro*, miR-200b expressional level in GC cells (MGC-803 and BGC-823) was tested firstly. As Figure 2(a) shows, miR-200b was significantly downregulated in both two GC cell lines compared with normal cells (GES-1). Then, the two GC cells were transfected with miR-200b mimic or inhibitor to overexpress or knockdown of miR-200b expression. Results showed that the transfection was very successful (Figure 2(b)). EMT-related markers were then detected by western blot, and the results displayed that N-cadherin and vimentin level were reduced and E-cadherin level was elevated in miR-200b mimic GC cells, while N-cadherin and vimentin level were elevated and E-cadherin was reduced in miR-200b inhibitor GC cells (Figure 2(c)). Transwell assay was then applied for measuring the migration and invasion of GC cells. The findings displayed that miR-200b mimic decreased and miR-200b inhibitor increased the migratory ability of GC cells (Figure 2(d)). Similar results were observed in the invasion of GC cells after transfection with miR-200b mimic or inhibitor (Figure 2(e)). Correlatively, the observations implied that miR-200b showed a suppressive effect on the invasion and migration of GC through EMT.

3.3. NRG1 Was the Target of miR-200b. To explore the underlying mechanism of miR-200b in GC metastasis, bioinformatics approaches (miRanda and TargetScan) were applied for seeking for the target of miR-200b. As Figure 3(a) shows, NRG1 was the selected candidate target of miR-200b. Then, dual-luciferase reporter assay was selected to further verify whether NRG1 was the direct target of miR-200b. Results displayed that miR-200b mimic showed a decreased luciferase activity, while miR-200b inhibitor showed an increased luciferase activity in wild-type reporter, but not with mutant (Figure 3(b)), indicating that miR-200b modulated NRG1 by binding its 3'UTR. Furthermore, NRG1 protein (Figure 3(c)) and mRNA level (Figure 3(d)) were reduced by miR-200b mimic, while elevated by miR-200b inhibitor in both two GC cell lines. Moreover, the findings displayed that miR-200b and NRG1 were negatively correlated in GC tissues (Figure 3(e)). These observations suggested that NRG1 was the direct target of miR-200b.

3.4. NRG1 Rescued the MiR-200b Effect on GC EMT and Metastasis. To uncover the role of NRG1 in the EMT and metastasis modulated by miR-200b *in vitro*, NRG1 expressional level in GC cells was measured firstly. As shown in Figure 4(a), NRG1 was upregulated obviously in both two GC cell lines compared with normal cells. Then, GC cells were transfected with NRG1 siRNA to silence NRG1 expression. As Figure 4(b) shows, the transfection was very successful. EMT-related markers were then detected by western blot, and the results displayed that N-cadherin and vimentin level was elevated and E-cadherin level was reduced in miR-200b inhibitor GC cells, while their expression was reversed by NRG1 siRNA (Figure 4(c)). Transwell assay was then applied to measure the migration and invasion of GC. The findings displayed that miR-200b inhibitor increased, while combined with NRG1 siRNA decreased the migratory ability of GC cells (Figure 4(d)). Similar results were found in cell invasion in GC cells after transfection with miR-200b inhibitor or combining with NRG1 siRNA (Figure 4(e)). Correlatively, these observations implied that NRG1 overturned the miR-200b effect on GC cell invasion and migration through EMT.

3.5. ERBB2/ERBB3 Pathway Was Critical for MiR-200b Biological Behavior in GC. As described above, NRG1 and ERBB2 or ERBB3 interaction could activate a series of signaling, resulting in cell migration and invasion [22]. Here, we investigated whether the NRG1/ERBB2/ERBB3 pathway was modulated by miR-200b in GC. Western blotting was carried out for exploring the downstream genes of ERBB2/ERBB3 in GC cells after treated with miR-200b mimic, miR-200b inhibitor, or combined with NRG1 siRNA. The results showed that the phosphorylation of ERBB2 or ERBB3 was downregulated in miR-200b mimic GC cells and upregulated in miR-200b inhibitor GC cells. Furthermore, p-ERBB2 or p-ERBB3 expression was decreased by NRG1 siRNA induced by miR-200b inhibitor in GC cells (Figures 5(a) and 5(b)). These findings suggested that miR-200b regulated GC cell invasion and migration via modulating NRG1 through the ERBB2/ERBB3 signaling pathway.

4. Discussion

Increasing evidence has displayed that miRs played critical roles in GC metastasis. Therefore, it is very essential to identify the metastasis-related miRs for understanding the potential mechanism in GC development. It has been revealed that miR-200b was involved in the progression of several cancers. For instance, miR-200b took part in bladder cancer migration and invasion as a tumor suppressor [23].

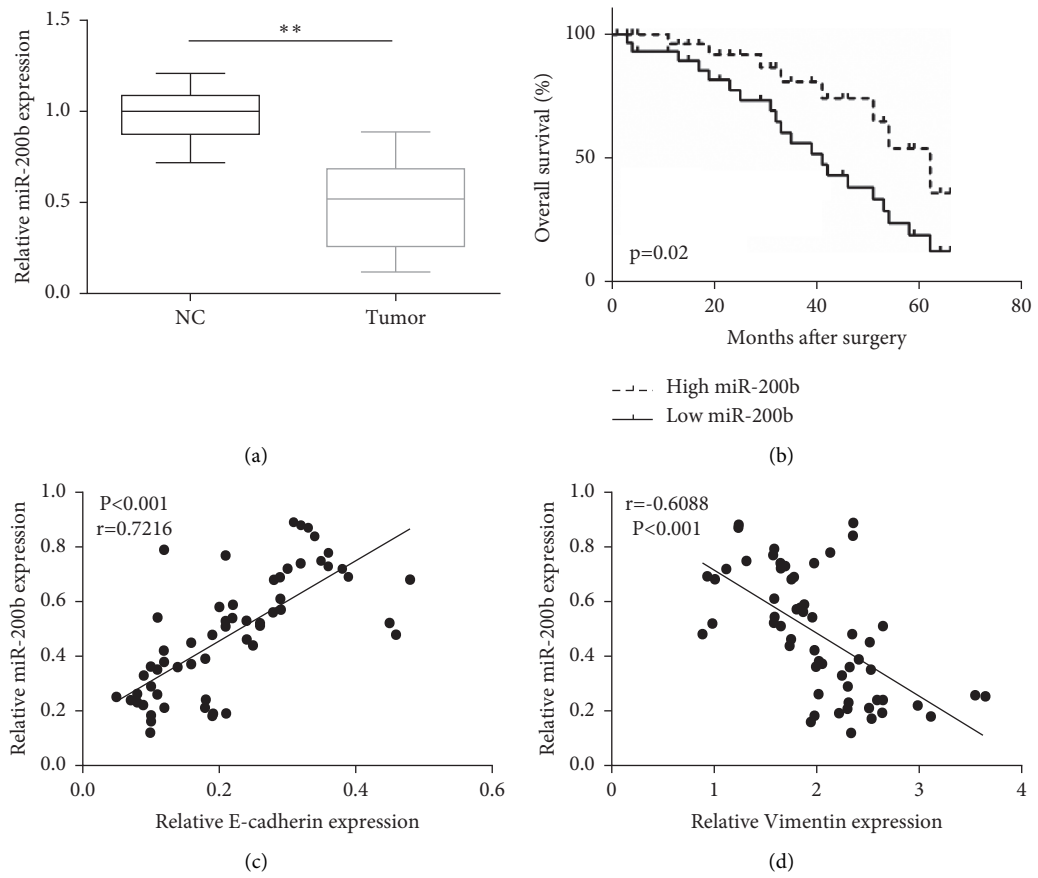

Figure 1: MiR-200b was negatively associated with GC aggressiveness. (a) MiR-200b expression was measured in GC tissue specimens and normal control (NC) tissue specimens ($n = 60$). (b) Overall survival was detected in GC patients with high or low miR-200b expression. (c) Positive association of miR-200b expression with EMT-related marker (E-cadherin) expression. (d) Negative association of miR-200b expression with EMT-related marker (vimentin) expression ($^{**}p < 0.01$).

Table 1: Correlation with miR-200b expression and clinicopathological features in gastric cancer patients.

Item	MiR-200b		p value
	High ($n = 29$)	Low ($n = 31$)	
Age (years)			0.205
< 60	14	20	
≥60	15	11	
Gender			0.809
Female	15	17	
Male	14	14	
AJCC stage			0.017*
I-II	21	13	
III-IV	8	18	
Tumor size, cm			0.009*
<3	21	12	
≥3	8	19	
Lymph node metastasis			0.190
Negative	18	14	
Positive	11	17	
Invasion into the serous layer			0.305
Yes	16	13	
No	13	18	

Statistical analyses were performed by the $\chi 2$ test. $^{*}p < 0.05$ was considered significant.

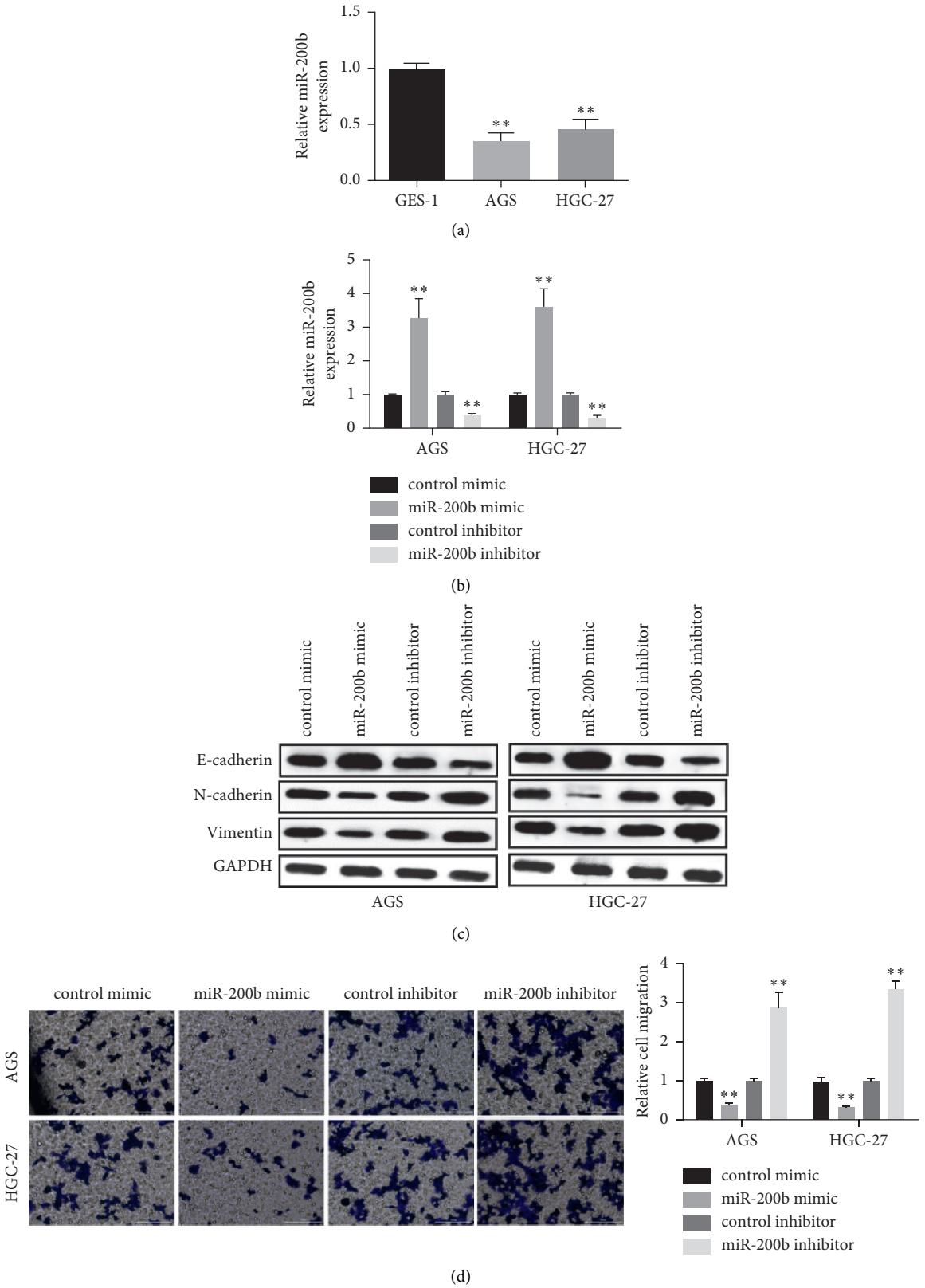

Figure 2: Continued.

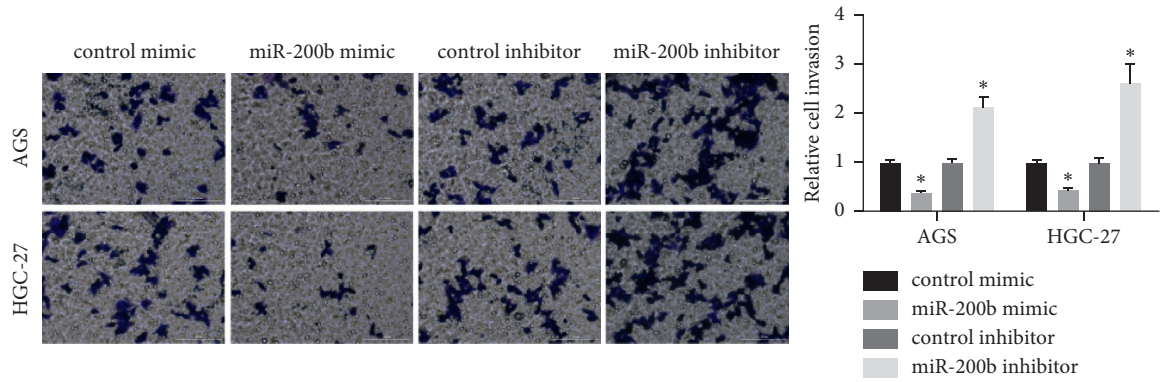

(e)

Figure 2: MiR-200b inhibited the invasion and migration of GC through EMT. (a) Relative expression of miR-200b tested in GC cells. (b) MiR-200b expression measured in GC cells treated with miR-200b mimic or inhibitor. (c) The protein levels of EMT markers tested in GC cells after treatment with miR-200b mimic or inhibitor. (d) GC cell migration and (e) invasion detected after transfected with miR-200b mimic or inhibitor ($^{*}p < 0.05$, $^{**}p < 0.01$).

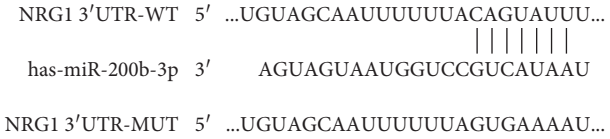

(a)

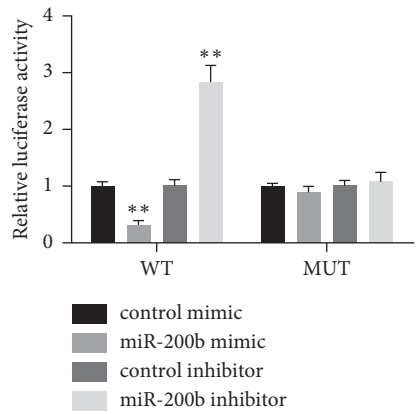

(b)

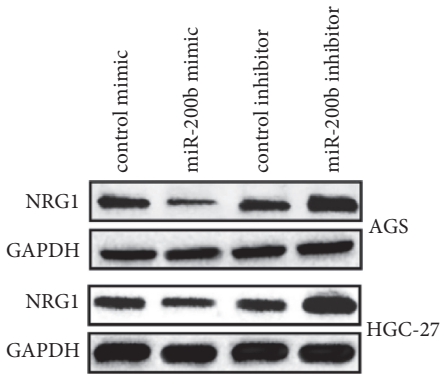

(c)

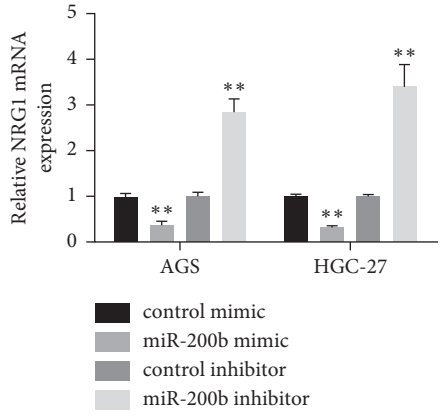

(d)

Figure 3: Continued.

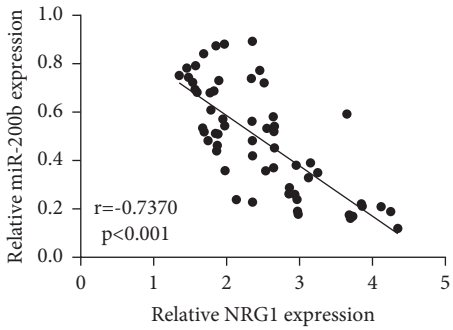

(e)

Figure 3: MiR-200b targeted NRG1. (a) Display of the NRG1 3'UTR-WT or -MUT sequences with miR-200b sequences. (b) Luciferase activity of NRG1 3'UTR-WT or -MUT in HEK-293T cells after increasing or decreasing miR-200b. (c) Protein level of NRG1 and (d) mRNA expression of NRG1 detected in GC cells after increasing or decreasing miR-200b. (e) Relationship between miR-200b expression and NRG1 expression ($^{*}p < 0.05$, $^{**}p < 0.01$).

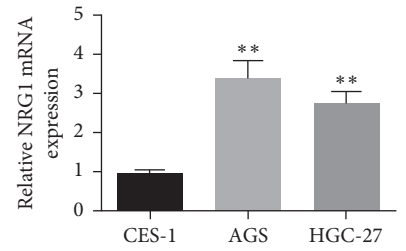

(a)

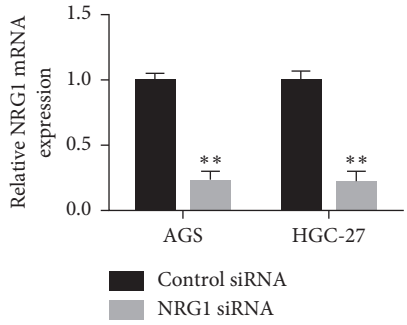

(b)

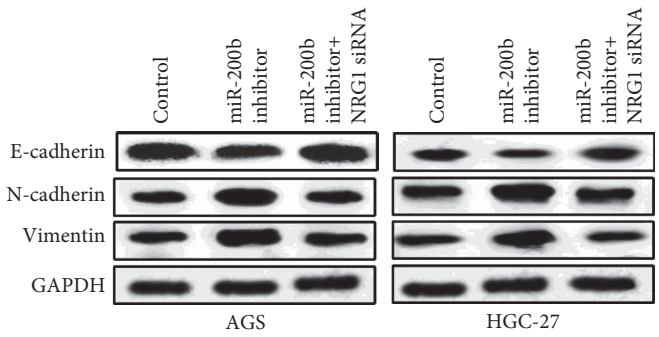

(c)

Figure 4: Continued.

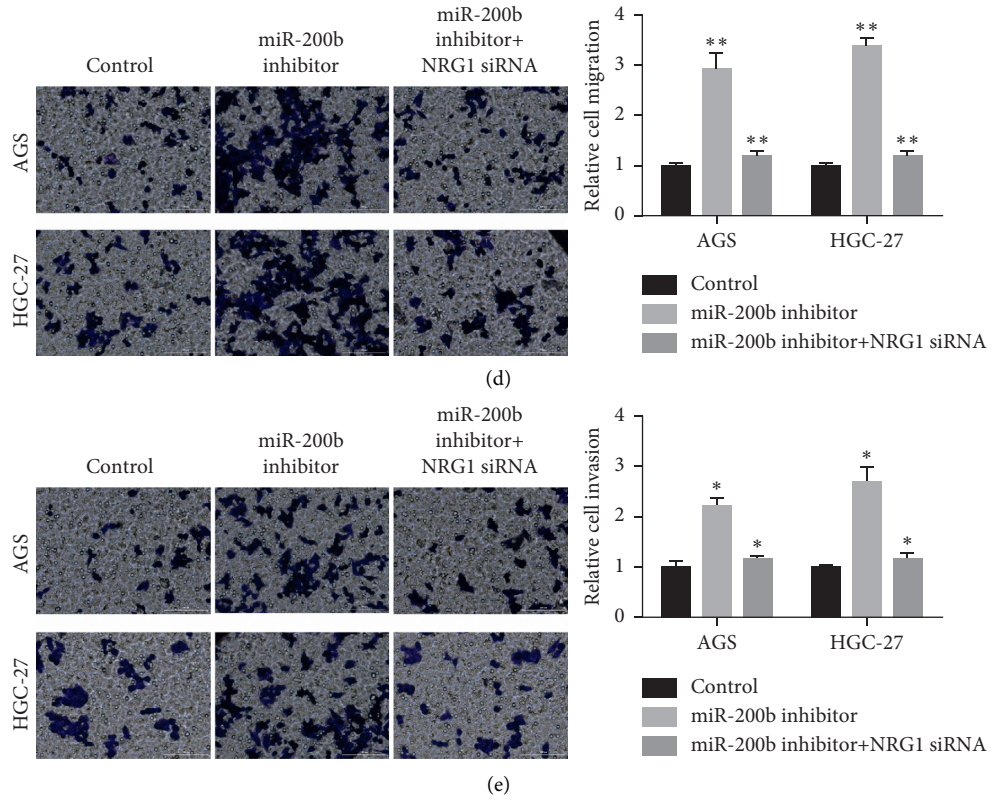

Figure 4: NRG1 overturned the miR-200b effect on GC cell invasion and migration. (a) Relative expression of NRG1 tested in two GC cells. (b) Detection of NRG1 expression in GC cells after silence NRG1. (c) The protein levels of EMT markers detected in GC cells after transfected with miR-200b inhibitor or combined with NRG1 siRNA. (d) Cell migration and (e) cell invasion detected in GC cells after transfected with miR-200b inhibitor or combined with NRG1 siRNA ($^{*}p < 0.05$, $^{**}p < 0.01$).

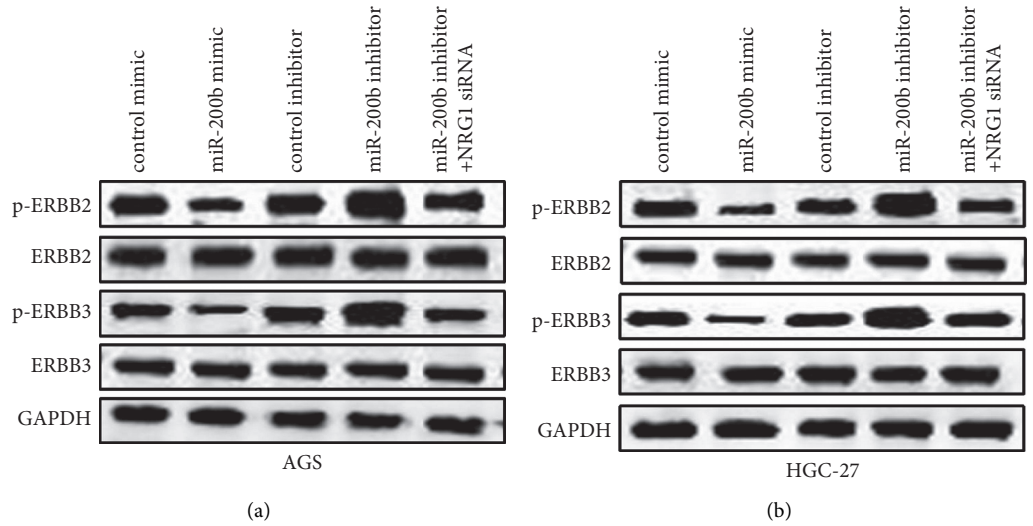

Figure 5: MiR-200b modulated GC cell migration and invasion through the ERBB2/ERBB3 signaling pathway. (a), (b) The protein level of p-ERBB2, ERBB2, p-ERBB3, and ERBB2 measured in GC cells after increasing miR-200b, decreasing miR-200b, or combined with decreasing NRG1.

MiR-200b showed an oncogene behavior in colorectal and cervical cancer [24, 25]. Moreover, Tang et al. showed that miR-200b served as a prognostic factor and mediator of GC progression [26]. In this study, the results displayed that miR-200b was dramatically decreased in GC and its downregulation predicted poor prognosis of GC patients. Moreover, we also displayed that miR-200b repressed GC cell invasion and migration.

Tumor metastasis is a complex process involving a series of events [27]. EMT displays an important role in the metastasis of tumors and acts an important biological process in which epidermal malignant cells acquire the ability to migrate and invade. Previous studies have proved the role of miRs in EMT progression [28, 29]. In our study, we displayed that miR-200b was significantly associated with EMT-related markers and reexpression of miR-200b was repressed, whereas silence of miR-200b promoted EMT-associated markers.

NRG1 was reported to act as an oncogene in various tumor development [20, 30]. In this study, we showed that NRG1 was upregulated in GC and it was inversely associated with miR-200b expression. More importantly, NRG1 could reverse the miR-200b effect on GC cell migration and invasion. A previous study displayed that NRG1 exerted its roles in tumors by binding to ERBB2 or ERBB3, resulting in tumor cell proliferation, invasion, and migration [21]. Our study revealed that the phosphorylation of ERBB2 or ERBB3 was markedly inhibited in GC cells after overexpression of miR-200b, while it was elevated after inhibiting miR-200b and decreasing NRG1 overturned the miR-200b inhibitor effect on the ERBB2/ERBB3 signaling pathway.

This study has its limitations that it only investigated the biological functions of the miR-200b/NRG1 axis on cell migration and invasion in vitro. The functional role of miR-200b in in vivo animal experiments is required to explore in the future studies.

In conclusion, miR-200b inhibited GC cell migration and invasion through EMT via the NRG1/ERBB2/ERBB3 signaling pathway, and miR-200b might be a potential biomarker for GC progression, which provides a clue for treating GC.

Data Availability

The datasets used and/or analyzed during the present study are available from the corresponding author on reasonable request.

Ethical Approval

The study was approved by the First People's Hospital of Lianyungang.

Consent

Written consent was obtained from all participants.

Conflicts of Interest

The authors declare no conflicts of interest.

Acknowledgments

This study was supported by the Lianyungang High-Tech Zone Science and Technology Project (Grant no. ZD201929).

References

[1] F. Bray, J. Ferlay, I. Soerjomataram, R. L. Siegel, L. A. Torre, and A. Jemal, "Global cancer statistics 2018: GLOBOCAN estimates of incidence and mortality worldwide for 36 cancers in 185 countries," *CA: A Cancer Journal for Clinicians*, vol. 68, no. 6, pp. 394–424, 2018.

[2] J. Ferlay, I. Soerjomataram, R. Dikshit et al., "Cancer incidence and mortality worldwide: sources, methods and major patterns in GLOBOCAN 2012," *International Journal of Cancer*, vol. 136, no. 5, pp. E359–E386, 2015.

[3] H. Suzuki, I. Oda, S. Abe et al., "High rate of 5-year survival among patients with early gastric cancer undergoing curative endoscopic submucosal dissection," *Gastric Cancer*, vol. 19, no. 1, pp. 198–205, 2016.

[4] H. Yu, A. M. Yang, X. H. Lu et al., "Magnifying narrow-band imaging endoscopy is superior in diagnosis of early gastric cancer," *World Journal of Gastroenterology*, vol. 21, no. 30, pp. 9156–9162, 2015.

[5] Y. Gao and J. Chen, "Low expression of lncRNA NBAT-1 promotes gastric cancer development and is associated with poor prognosis," *Journal of B. U. ON.: Official Journal of the Balkan Union of Oncology*, vol. 24, pp. 656–662, 2019.

[6] S. Chen, S. Ke, S. Cheng, T. Wu, Y. Yang, and B. Liao, "MicroRNA-151 regulates the growth, chemosensitivity and metastasis of human prostate cancer cells by targeting PI3K/AKT," *Journal of B. U. ON.: Official Journal of the Balkan Union of Oncology*, vol. 25, pp. 2045–2050, 2020.

[7] Z. Cheng, H. Geng, Y. Cheng et al., "Effects of MiR-210 on proliferation, apoptosis and invasion abilities of esophageal cancer cells," *Journal of B. U. ON.: Official Journal of the Balkan Union of Oncology*, vol. 23, pp. 814–819, 2018.

[8] T. Ye, M. Yang, D. Huang et al., "MicroRNA-7 as a potential therapeutic target for aberrant NF-κB-driven distant metastasis of gastric cancer," *Journal of Experimental & Clinical Cancer Research*, vol. 38, no. 1, p. 55, 2019.

[9] R. Wang, Y. Sun, W. Yu et al., "Downregulation of miRNA-214 in cancer-associated fibroblasts contributes to migration and invasion of gastric cancer cells through targeting FGF9 and inducing EMT," *Journal of Experimental & Clinical Cancer Research*, vol. 38, no. 1, p. 20, 2019.

[10] W. Hui, X. Ma, Y. Zan, L. Song, S. Zhang, and L. Dong, "MicroRNA-1292-5p inhibits cell growth, migration and invasion of gastric carcinoma by targeting DEK," *American Journal of Cancer Research*, vol. 8, pp. 1228–1238, 2018.

[11] Y.-K. Minn, D. H. Lee, W. J. Hyung et al., "MicroRNA-200 family members and ZEB2 are associated with brain metastasis in gastric adenocarcinoma," *International Journal of Oncology*, vol. 45, no. 6, pp. 2403–2410, 2014.

[12] X. Liang, "EMT: new signals from the invasive front," *Oral Oncology*, vol. 47, no. 8, pp. 686-687, 2011.

[13] K. Okubo, Y. Uenosono, T. Arigami et al., "Clinical significance of altering epithelial-mesenchymal transition in metastatic lymph nodes of gastric cancer," *Gastric Cancer*, vol. 20, no. 5, pp. 802–810, 2017.

[14] P. Xia and X. Y. Xu, "Epithelial-mesenchymal transition and gastric cancer stem cell," *Tumour Biology: The Journal of the International Society for Oncodevelopmental Biology and Medicine*, vol. 39, 2017.

[15] A. Drilon, R. Somwar, B. P. Mangatt et al., "Response to ERBB3-directed targeted therapy in NRG1-rearranged cancers," *Cancer Discovery*, vol. 8, no. 6, pp. 686–695, 2018.

[16] M. R. Jones, H. Lim, Y. Shen et al., "Successful targeting of the NRG1 pathway indicates novel treatment strategy for

metastatic cancer," *Annals of Oncology*, vol. 28, no. 12, pp. 3092–3097, 2017.

[17] S. Jonna, R. A. Feldman, J. Swensen et al., "Detection of NRG1 gene fusions in solid tumors," *Clinical Cancer Research: An Official Journal of the American Association for Cancer Research*, vol. 25, no. 16, pp. 4966–4972, 2019.

[18] S. Yun, J. Koh, S. K. Nam et al., "Clinical significance of overexpression of NRG1 and its receptors, HER3 and HER4, in gastric cancer patients," *Gastric Cancer*, vol. 21, no. 2, pp. 225–236, 2018.

[19] F. Yin, J. N. Zhang, S. W. Wang et al., "MiR-125a-3p regulates glioma apoptosis and invasion by regulating Nrg1," *PLoS One*, vol. 10, no. 1, Article ID e0116759, 2015.

[20] D.-M. Shi, L.-X. Li, X.-Y. Bian et al., "miR-296-5p suppresses EMT of hepatocellular carcinoma via attenuating NRG1/ERBB2/ERBB3 signaling," *Journal of Experimental & Clinical Cancer Research*, vol. 37, no. 1, p. 294, 2018.

[21] H. Jeong, J. Kim, Y. Lee, J. H. Seo, S. R. Hong, and A. Kim, "Neuregulin-1 induces cancer stem cell characteristics in breast cancer cell lines," *Oncology Reports*, vol. 32, no. 3, pp. 1218–1224, 2014.

[22] U. Vijapurkar, M. S. Kim, and J. G. Koland, "Roles of mitogen-activated protein kinase and phosphoinositide 3'-kinase in ErbB2/ErbB3 coreceptor-mediated heregulin signaling," *Experimental Cell Research*, vol. 284, pp. 291–302, 2003.

[23] R. Gao, N. Zhang, J. Yang et al., "Long non-coding RNA ZEB1-AS1 regulates miR-200b/FSCN1 signaling and enhances migration and invasion induced by TGF-β1 in bladder cancer cells," *Journal of Experimental & Clinical Cancer Research*, vol. 38, no. 1, p. 111, 2019.

[24] Z. Zhang, T. Xing, Y. Chen, and J. Xiao, "Exosome-mediated miR-200b promotes colorectal cancer proliferation upon TGF-β1 exposure," *Biomedicine & Pharmacotherapy*, vol. 106, pp. 1135–1143, 2018.

[25] F. Zeng, M. Xue, T. Xiao et al., "MiR-200b promotes the cell proliferation and metastasis of cervical cancer by inhibiting FOXG1," *Biomedicine & Pharmacotherapy*, vol. 79, pp. 294–301, 2016.

[26] H. Tang, M. Deng, Y. Tang et al., "miR-200b and miR-200c as prognostic factors and mediators of gastric cancer cell progression," *Clinical Cancer Research*, vol. 19, no. 20, pp. 5602–5612, 2013.

[27] N. Machairas and Z. Garoufalia, "Correlation of tumor biology and optimal colorectal liver metastasis resection margin: existing evidence and future directions," *Journal of B. U. ON.: Official Journal of the Balkan Union of Oncology*, vol. 23, pp. 1561-1562, 2018.

[28] Y. Qi, W. Zha, and W. Zhang, "Exosomal miR-660-5p promotes tumor growth and metastasis in non-small cell lung cancer," *Journal of B. U. ON.: Official Journal of the Balkan Union of Oncology*, vol. 24, pp. 599–607, 2019.

[29] S. Liu, J. Chen, T. Zhang, and H. Chen, "MicroRNA-133 inhibits the growth and metastasis of the human lung cancer cells by targeting epidermal growth factor receptor," *Journal of B. U. ON.: Official Journal of the Balkan Union of Oncology*, vol. 24, pp. 929–935, 2019.

[30] T. T. Zhang, N. Qu, G. H. Sun et al., "NRG1 regulates redox homeostasis via NRF2 in papillary thyroid cancer," *International Journal of Oncology*, vol. 53, pp. 685–693, 2018.

Hindawi
Journal of Oncology
Volume 2021, Article ID 5646589, 8 pages
https://doi.org/10.1155/2021/5646589

Research Article

Combining Fluorescent Cell Sorting and Single B Cell Amplification to Screen the Monoclonal Antibody Gene against Human Glypican-1 in Pancreatic Cancer

Mi Huang,[1,2] Yingying Ma,[1,2] Xiaoyan Gao,[1,2] Xinyang Li,[1,3] Quan Ding,[2] Chuxin Liu,[1] Xiaopan Liu,[1] Hang Zhang,[2] and Naibo Yang [1,2,3,4]

[1]*BGI-Shenzhen, Shenzhen, Guangdong 518083, China*
[2]*BGI-Wuhan, Wuhan 430074, China*
[3]*BGI Education Center, University of Chinese Academy of Sciences, Shenzhen, Guangdong 518083, China*
[4]*Complete Genomics Inc., San Jose, CA, USA*

Correspondence should be addressed to Naibo Yang; yangnaibo@genomics.cn

Received 1 July 2021; Accepted 6 August 2021; Published 6 September 2021

Academic Editor: Muhammad Wasim Khan

In this report, one novel method has been developed to screen the monoclonal antibody against human pancreatic cancer biomarker glypican-1 (GPC1) through the combination of fluorescent cell sorting and single B cell amplification. GPC1-positive B cells were sorted out from the peripheral blood mononuclear cells (PBMCs) by fluorescent cell sorting after the GPC1 immunization to the New Zealand white rabbit. Then, total RNA was extracted and reversely transcribed into cDNA, which was used as the template, and the variable region sequences of both heavy and light chains were amplified from the same B cell. Next, their recombinant antibody was expressed and purified from the human 293T cell after the antibody gene amplification and expression vector construction. The enzyme-linked immunosorbent assay (ELISA) and flow cytometry assays were used to determine the antibody affinity. The antibody named GPC-12 that we screened and obtained was proven to have natural heavy-light chain pairing information, and it was highly specific to the GPC1 antigen, and the affinity could reach 1×10^{-7} M. Overall, an effective and novel method has been successfully developed to screen the antibody by combining the fluorescent cell sorting and single-cell amplifying technologies, which was proved to be workable in our setting.

1. Introduction

Pancreatic cancer is a malignant gastrointestinal malignancy, with the prognosis being rather grim [1]. In recent years, the incidence of pancreatic cancer has been shown to have an upward trend, and it is predicted that pancreatic cancer causes more than 331,000 deaths every year [2, 3]. Overall survival rate of pancreatic cancer ranked the lowest among all kinds of malignant tumors. The five-year survival rate was only 2%–9%, with an average being no more than 6% [2], and the morbidity/mortality rate was close to 100% [4]. Therefore, it is essential to develop the new diagnostic method for pancreatic cancer, known as the king of cancer, which makes the early diagnosis of pancreatic cancer become possible.

The diagnosis of pancreatic cancer is mainly based on a comprehensive diagnostic method, that is, imaging, tumor markers, and tissue biopsy [5]. However, the diameter of early pancreatic cancer is usually less than two centimeters; and it is confined to the pancreatic parenchyma and does not invade the pancreatic capsule. Traditional imaging methods are not sensitive and specific enough to detect pancreatic cancer lesions. All these make it extremely difficult to measure and detect the pancreatic cancer. Therefore, it is required to develop the novel method to earlier detect the multiple tumor markers, which plays an important role in improving the positive detection rate of cancer patients, cancer screening in high-risk groups without clinical symptoms, and early detection of pancreatic cancer [6, 7].

At present, CA19-9 and CEA are commonly used tumor markers for detection of pancreatic cancer, but the two biomarkers were less specific in that they are also related antigens in other cancers, such as colorectal cancer or ovarian cancer [8, 9]. The positive rate of CA19-9 was over 80%, but the positive rate of CA19-9 in small pancreatic cancer patients was not high (60.7% in adenocarcinoma patients less than 2 cm), while the positive rate of CEA was only 78.9%. Therefore, there is an urgent need to find a more specific antibody for pancreatic cancer, that is to say, a detection reagent with higher diagnostic positive rate, which can be used as a common detection marker for pancreatic cancer [10, 11]. As early as 1998, it has been reported that Glypican-1 (GPC1) was overexpressed in pancreatic cancer cells; and that Glypican-1 could regulate the metastasis and angiogenesis of pancreatic cancer cells, playing a pivotal role in the oncogenesis of pancreatic ductal adenocarcinoma [12]. These previous findings suggest that GPC1 can be a potential diagnostic biomarker. In addition, in 2015, one study reported that GPC1 had nearly 100% sensitivity and specificity in both animal models and clinical patients with pancreatic cancer, being able to accurately detect early pancreatic cancer, indicating that GPC1 has great potential as a tumor marker for early detection of pancreatic cancer [13–15].

Consequently, to screen the monoclonal antibody against human pancreatic cancer biomarker GPC1, in this study, a single B cell clone against human pancreatic cancer GPC1 was sorted out by flow cytometry; and then a natural pair of antibody heavy and light chain sequences were amplified from a single B cell by PCR. In performing PCR, the codons preferred by adult mammalian cells were optimized. After gene synthesis, the expression vector was constructed and transfected into HEK293T cells for expression. The binding activity of antibody to antigen was evaluated by ELISA, and the affinity kinetics between antibody protein and antigen GPC1 were verified by surface plasmon resonance (SPR).

2. Materials and Methods

2.1. Materials. New Zealand white rabbits were purchased and reared in the Food and Drug Safety Evaluation Center of Hubei Province. Sample homogenate device (instrumental model: T10) was purchased from IKA-Werke GmbH & Co. KG (Staufen, Germany). Analytical flow cytometry (CytoFLEX S) was purchased from Beckman Coulter Inc. (Beckman Coulter, Brea, CA, USA). Sorting flow cytometry (MoFlo XDP) was purchased from Beckman Coulter Inc. (Beckman Coulter, Brea, CA, USA). Horizontal hanging basket centrifuge (H1850R) was from Hunan Xiangyi, and 1 × RPMI1640 basic medium was purchased from Gibco Company. Fetal bovine serum (FBS) was from HyClone Company. Horseradish peroxidase labeled sheep anti-rabbit IgG was purchased from GeneTex Company. SuperScript II Reverse Transcriptase was purchased from Invitrogen Inc. (Life Technologies, Carlsbad, CA, USA). Fluorescein Isothiocyanate (FITC) was purchased from Sigma Chemical Co. (St. Louis, MO, USA). Ficoll-Paque PREMIUM for PBMC separation was purchased from GE Healthcare (San Diego, CA, USA). D2000 DNA ladder was purchased from Tiangen Biochemical Technology Co., Ltd. (Beijing, China). rTaq enzyme and TA clone are from TaKaRa (TaKaRa, Japan) with pMD18-T vector, *E. coli* competent cell DH5-alpha, and template switch oligos (TSO). Master Mix was purchased from Kapa Biosystems (Boston, MA, USA). Bovine serum albumin, Triton X-100, Freund's complete adjuvant, Freund's incomplete adjuvant, and GPC1 polypeptide were purchased from Sigma Chemical Co. (St. Louis, MO, USA). PCR product purification kit and agarose gel recovery kit were purchased from QIAGEN Company (Germany). pFUSE-Fc mammalian cell expression plasmid was purchased from Invitrogen Inc. (Life, Carlsbad, CA, USA). Commercial anti-GPC1 monoclonal antibodies were purchased from GeneTex (CA, USA).

2.2. Animal Immunization. The experimental animal immunization and blood collection program were approved by the Animal Ethics Committee of Shenzhen Huada Academy of Life Sciences (ethics approval number FT15149). Two New Zealand white rabbits aged 5-6 weeks were immunized by subcutaneous injection on the back. They were immunized once every two weeks, four times in total. 500 μl antigen (200 micrograms of antigen protein dissolved in 500 μl of sterile water to form a solution of 0.4 mg/mL) and 500 μl Freund's complete adjuvant were used uniformly. The pulp machine emulsified evenly and was used for the first time before immunization. The other three immunizations used a mixture of Freund's incomplete adjuvant and antigen emulsifies evenly and equally.

2.3. Blood Collection and Cell Separation. Before or two weeks after the final immunization, blood samples were collected from the ear vein of two white rabbits. The serum of 100 μl before and after immunization was used to test the titer of anti-positive antibody. The peripheral blood of a white rabbit with strong immune response was collected and separated by Ficoll lymphocyte gradient centrifugation.

2.4. Detection of Serum and Antibody Titers by ELISA. The antigen was dissolved in coating solution (50 mM Na_2CO_3, pH 9.6) at an appropriate concentration, and 100 μl antigen was added to the corresponding pore overnight at 4°C. The liquid was discarded and the residual liquid was dried, followed by rinsing with the detergent PBST (1 × PBS pH 7.4 plus 0.05% Tween 20, the same as below) three times. Each pore was incubated at 37°C for 1 h with 200 μl blocking solution (3% BSA). The liquid was emptied and the remaining liquid was dried. The washing liquid was used for rinsing three times. Each pore was incubated with 100 μl diluted serum or antibody, at 37°C for 1 hour. The liquid was emptied and the remaining liquid was dried. The washing liquid was used for rinsing three times. Each pore was incubated with 100 μl secondary antibody (1 : 5000 diluted horseradish peroxidase labeled sheep anti-rabbit IgG) for 1 hour at 37°C. The liquid was emptied and the remaining

liquid was dried. The washing liquid was used for rinsing five times. The residual liquids in the dry holes were patted, and 100 μl color developing solution was added to each hole, and the color was visualized for 10 minutes without light. Each hole was terminated by adding 50 μl 2M H_2SO_4, and the 450 nm OD value was read immediately.

2.5. Cell Staining and Selection. The 1 mg GPC1 antigen was dissolved in 0.1 M carbonate buffer of 0.5 mL pH9.0. FITC (sigma F4274) was dissolved with DMSO, and the final concentration of FITC was 1 mg/mL. FITC-DMSO solution was slowly added to antigen solution, and 50 μl FITC-DMSO solution was added to antigen solution. The reaction time was 8 h at 4°C. The reaction was terminated by adding NH_4CL with the final concentration of 50 mM and reacted at 4°C for 2 h. Ultrafiltration removes unreacted FITC.

The isolated rabbit PBMC was suspended to the final volume of 20 μl PBS and 2 μl GPC1-FITC was added. The PBMC was gently vortexed and blended. The light-avoiding reaction lasted 1 hour at room temperature (a small number of cells without GPC1-FITC were reserved as negative control). After the reaction, 1 mL PBS was added; the supernatant was discarded by centrifugation for 5 minutes and precipitated by 1 mL PBS. The supernatant was discarded by centrifugation for 5 minutes and precipitated by 1 mL PBS. The samples were prepared by centrifugation for 5 min at 400 ×g, discarding the supernatant, and resuspension precipitation with 500 μl PBS. The density of the samples was about 10^7/mL.

2.6. Preparation of Cell Lysate. A 4 μl lysate [1.86 μl nonnuclease water, 1 μl Oligo(dT)18 (10 mu-ol/L), 0.1 μl RNase inhibitor (4 U), and 0.04 μl Triton X-100 (100 mL/L)] was prepared. The lysate was placed in a 0.2 mL PCR tube (8 rows of 96-well plate). The selected cells were directly added to the cell lysate. One tube of negative pore (0 cells, i.e., no cell sorting) was reserved for each row; one tube of positive pore (i.e., 10 cells sorted) was used as control, and 10 tubes of single-cell pore were reserved for each row. Twelve PCR tubes can be selected as one group for each experiment, and the rest can be frozen to −80°C group. After two weeks of use, the success rate of amplification will be greatly reduced.

2.7. Separation of GPC1-FITC-Positive Cells by Flow Cytometry. Conventional flow cytometry was subjected to calibration, and then calibration was undertaken for sorting parameters; the latency value of side fluid flow and droplets were adjusted to make the left bright spot farthest and most concentrated in the side fluid flow window; then the coordinate value of cell sorting around the coordinate window was adjusted to ensure that the sheath fluid can hit the bottom of the PCR tube (cells cannot hit the wall of the side tube; otherwise, it would affect the success rate of amplification). At last, the rate of cell sorting was checked, such as setting 10 cells to be sorted; looking at the actual number of cells under the microscope, more than 90% of the cells were qualified and could be sorted in the next step. After all the above steps were completed, the sorting commenced.

2.8. Cell Lysis and Reverse Transcription. The PCR tube containing lysate was placed in the PCR instrument at 72°C for 3 minutes; the hot cover was set at 75°C for 1 min on ice immediately after lysis and centrifuged at 10,000 r/min for 30 seconds. 6 μl reverse transcription system [2 μl SuperScript II First-Strand Buffer (5×), 2 μl betaine (5 mol/L), 0.9 mu-L $MgCl_2$ (100 mmol/L), 0.25 μl DTT (100 mmol/L), 0.1 μl TSO (100 μmol/L), 0.25 μl RNA inhibitor (4 U), and 0.5 μl SuperScript II Reverse Transcriptase (20 U)] was prepared. Reverse transcription was performed under the following conditions: 42°C for 90 min, 50°C for 2 min, 42°C for 2 min, 10 cycles, 70°C for 15 min, and 12°C. The DNA was obtained.

2.9. Amplification of the Antibody Sequence. Primer Premier 5 software was used to design primers. The products of single-tube cDNA system obtained by the above methods were used as templates for two rounds of nested PCR. In the first round, Ld primers (rIgH-Ld1, rIgK-Ld1, rIgL-Ld1-1, and rIgL-Ld1-2) and downstream primers of heavy and light chain C region (rIgHG-C1, rIgK-C1, and rIgL-C1) were used to prepare 25 μl PCR system [12.5 μl KAPA ReadyMix (2×∗), 0.5 μl Ld primers (10 μmol/L), 10 μl reverse transcription products, and 1.5 μl nuclease-free water]. The second round of PCR used FR primers (rIgH-FR1 and rIgK-FR1) and J primers (rIgH-J, rIgK-J-1, rIgK-J-2, and rIgL-J). A 25 μl PCR system [12.5 μl KAPA ReadyMix (2×), 0.5 μl FR primer (10 μmol/L), 0.5 μl J primer (10 μmol/L), 1 μl first-round PCR product, and 10.5 μl ribonuclease-free water] was prepared. The amplification conditions for both rounds of PCR were as follows: 95°C for 3 min, 98°C for 15 s, 60°C for 20 s, 72°C for 2 min, 25 cycles, 72°C for 5 min, and 12°C. The amplification system could be amplified as needed. Here, a nested amplification primer was designed (Table 1), TSO and oligo(dT) primers were used in the reverse transcription stage; Ld and C primers were annealed to the upstream sequence of TSO and the downstream CH1 region of antibody subtypes in the first round of PCR, respectively, and the primers of 10 mm/L were mixed equally; the other primers were the second round of PCR primers.

2.10. TA Cloning, Gene Synthesis, and Expression Vector Construction. 10 g/L agarose gel was used to detect the amplified products of PCR, and the target bands (380 BP) were cut and recovered by gel recovery kit. Then, rTaq enzyme was used to add A to the end of the gel-cut recovery product, and the product was purified by the PCR product purification kit and then linked to the pMD18 T vector overnight at 16°C. The conjugates were transferred into competent cells DH5α and cultured in antibiotic-free Luria-Bertani (LB) medium at 37°C for 1 hour. The conjugates were coated on ampicillin-containing LB solid medium overnight. The next day, the monoclonal colony in good condition was selected for shaking culture for 3 to 5 hours, and then the liquid was sent to Shanghai Shanggong

Table 1: Primer name and sequence.

Name	Sequence (5′ to 3′)
TSO[12]	AAGCAGTGGTATCAACGCAGAGTACrGrG + G[a]
Oligo(dT)18	TTTTTTTTTTTTTTTTTT
rIgH-Ld1	CTTCTCCTGGTCGCTGTGCT
rIgH-FR1	CACTCACCTGCACAGYCTCTGGA
rIgK-Ld1	CTGCTGGGGCTCCTGCT
rIgK-FR1	GCTGTGGGAGGCACAGTCAC
rIgL-Ld1-1	CCTCACAGTCCTGGCTCACTGCACA
rIgL-Ld1-2	CCYCCTCCTCKCTCACTGCACA
rIgH-J	TGARGAGAYRGTGACSAGGGT
rIgK-J-1	CGACGACCACCTYGGTCC
rIgK-J-2	TGATTTCCACCTTGGTGCC
rIgL-J	CTGTGACGGTCAGCTKGGTC
rIgHG-C1	GAAGACTGAYGGAGCCTTAGGT
rIgK-C1	GGTGGGAAGATGAGGACAGTAG
rIgL-C1	CCTCTGAGGAGGGCGGRAACA

Company for DNA sequencing to verify whether the antibody sequence is correct and also to verify whether the expression contains both heavy chain and light chain in the correct pairing. According to the preference of human cell expression system, the codon of the amplified heavy and light chain genes was optimized, and then the whole gene of variable region was synthesized and cloned directly into the commercial mammalian cell expression vector pFUSE-rabbit Fc, which contained the Fc constant region of rabbit antibody.

2.11. Expression of Mammalian Cells and Purification of the Antibody. Trypsinase digestive cells were counted and paved and cultured overnight at 37°C and 5% CO_2, and the confluence of cells was 70%–80% at transfection. The plasmid was diluted with a certain volume of Opti-MEM (Invitrogen 11058-021), carefully mixed, and labeled as liquid A. The transfection reagent PEI (Polyscience 23966-2) was diluted with the same volume of Opti-MEM, named liquid B. The mass ratio of plasmid to PEI was 1 : 2. It was kept at room temperature for 15 minutes. Liquid B was slowly added to liquid A and it was mixed. It was kept at room temperature for 20 minutes. The DNA-PEI mixture was slowly added to the cell culture medium and it was gently mixed. 48 hours after transfection, the supernatant was collected and centrifuged for 5 minutes to remove the cells. The supernatant was centrifuged for 10 minutes to remove the cell debris. The antibody was purified by affinity purification column coupled with GPC1 antigen.

2.12. Antigen-Antibody Binding Kinetics (Affinity Test). The GPC1 antigen was dissolved in the coating solution (50 mM Na_2CO_3, pH 9.6) at an appropriate concentration, and 100 μl antigen was added to the corresponding pore for overnight stay at 4°C. The liquid was emptied and the residual liquid was pat-dried; the PBST was washed (PBST and pat dry the residual liquid, add 1 mL/L Tween 20, the same as below) and rinsing was performed three times. Each pore was incubated with 200 μl blocking solution (3 g/L bovine serum albumin) for 2 hours at 37°C. The liquid was emptied and the remaining liquid was dried. Wash the PBST detergent was washed three times. Each pore was incubated at 37°C for 1 hour with 100 μl diluted antibody. The liquid was emptied and the remaining liquid was dried. The washing liquid was used for rinsing three times. Each pore was incubated with 100 μl secondary antibody (1 : 5000 diluted horseradish peroxidase labeled sheep anti-rabbit IgG) for 1 hour at 37°C. The liquid was emptied and the remaining liquid was dried. The washing liquid was used for rinsing five times. The residual liquid in the dry hole was patted, adding 100 μl color developing solution to each hole, and coloring at 37°C for 5 minutes. Each hole was added with 50 μl 2M HCL to stop the color rendering and 450 nm OD value was read immediately.

2.13. Detection of Antibody Binding to Natural GPC1 on the Cell Surface. MDA-MB-231 (China Typical Culture Preservation Center) in logarithmic growth phase was digested into single-cell suspension, counted, and centrifuged to remove the medium. Cell suspension was separated into three centrifugal tubes according to 50 μl/tube with proper volume of PBS suspension cells. No. 1 was without antibody, No. 2 was added with 0.5 μl positive GPC1 antibody (GeneTex GTX42664), and No. 3 was added with 1 μl purified GPC1 antibody and incubated at room temperature for 30 minutes. Each tube was centrifuged with 1 mL PBS for 5 min at 300 × g for supernatant. 1 mL PBS suspended cells were precipitated and centrifuged for 5 min at 300 × g, and then the supernatant was discarded twice. The 50 μl PBS suspended cells were precipitated and incubated at room temperature for 30 minutes with the corresponding fluorescent labeled antibody. Each tube was centrifuged with 1 mL PBS for 5 min at 300 × g for supernatant for three times. Flow detection was done on computer.

2.14. Statistical Analysis. All data were analyzed using SPSS 21.0 statistical software. The data were expressed as mean ± standard deviation. One-way ANOVA (Bonferroni) was used for comparisons among multiple groups. Tukey's post hoc test was used for pairwise comparisons of the mean values between multiple groups. Independent-sample t-test was used to analyze the difference between two groups where the data had normal distribution. $P < 0.05$ was considered to be statistically significant.

3. Results

3.1. Detection of the Serum-Positive Conversion Titer. To make the titer of the antibodies we produced clear, ELSIA was performed. As shown in Table 2, the blank group refers to the blank control without serum and with 100 μl PBS. The negative group was the negative control with 100 μl serum before immunization. The immune group refers to the serum diluted by 100 μl ratio after the fourth immunization. The positive detection group still had a high absorbance value from 1 : 1000 dilution to 1 : 32000, and the positive/negative ratio was >8 (generally, the value was greater than 4; that is to say, the immune serum was positive), which

Table 2: Detection of the serum-positive conversion titer.

Rabbit number	Detection of the antigen	Blank group	Negative group (1 : 1000)	Immune group (1 : 1000)	Immune group (1 : 4000)	Immune group (1 : 16000)	Immune group (1 : 32000)
Rabbit 1	GPC1	0.070	0.111	2.922	2.132	1.424	0.987
Rabbit 2	GPC1	0.062	0.082	2.536	2.071	1.054	0.663

indicated that specific antibodies against human GPC1 had been produced in rabbits, and Rabbit 1 was selected for the next experiment.

3.2. Cell Staining and Flow Cytometry. To stain fluorescently the cells of interest, GPC1-FITC was used. As shown in Figure 1(a), NC- was not stained with GPC1-FITC for immunized rabbit lymphocytes, NC+ was stained with GPC1-FITC for immunized rabbit lymphocytes, GPC1 was not stained with GPC1-FITC for immunized rabbit lymphocytes, and GPC1+ was stained with GPC1-FITC for immunized rabbit lymphocytes. It can be seen that the lymphocyte without GPC1-FITC staining was in the same fluorescence intensity range regardless of immunization, and the lymphocyte without GPC1-FITC staining also showed positive deviation and nonspecific binding, but the fluorescence intensity was lower than that of immunized rabbit lymphocyte. Therefore, this part was the cells that need to be further sorted, as shown in Figure 1(b).

3.3. Amplification and Sequencing of the Monocyte Antibody Gene. To purify the cells that were fluorescently stained with GPC1-FITC, cell sorting was employed based on flow cytometry. As shown in Figure 2, one cell was selected from lane 2 to lane 15 as a PCR template, from 18 to 19 as a positive control, 10 cells were selected as templates, and 20 to 21 as a negative control, which was no cells. The size of target protein was about 380 bp. It can be seen that, in lanes 11, 12, and 14, as well as in positive control, there was the size of target band. The corresponding PCR products of lanes 11, 12, and 14 were gelatinized, cloned, and sequenced by TA. By comparing the results of sequencing, it was found that lane 12 was a rabbit antibody sequence and paired with light chain. This sequence was named GPC1-12. The next step was to construct GPC1-12 on the vector for expression.

3.4. ELISA Detection of Antibody Transfection Supernatant. To understand the titer of antibody we produced, ELSIA was undertaken. As shown in Figure 3(a), bovine serum albumin (BSA) and cell culture medium (Medium) were negative controls, and positive control (abbreviated as PC) was polyclonal antibodies purified from rabbit serum by affinity purification column. The expression of GPC1-12 was detected in the supernatant of transfection. The next step was affinity purification of the supernatant.

3.5. Affinity Determination of the Purified Antibody. In order to further verify the binding activity of the purified antibody and GPC1 antigen, we carried out ELISA binding test. The initial concentration of the purified antibody was 100 μg/mL, and then it was diluted twice. The results showed that, as shown in Figure 3(b), compared with the uncoated antigen group and blank control, GPC1-12 purified antibody was shown to have specific binding performance with GPC1 antigen.

3.6. Detection of Antibody Binding Abilities to Natural Surface Protein. To verify the affinity of antibody we generated, evaluation was performed with flow cytometry. As shown in Figure 4, GPC1-12 monoclonal antibody (blue solid line) could bind well to cells but had a significant positive deviation from the negative control (red line).

4. Discussion

Pancreatic cancer is a highly malignant tumor, ranking near the eighth place among all kinds of lethal tumors. In addition, its cure rate and five-year survival rate are very low. Therefore, early diagnosis of pancreatic cancer is of particularly import, and there is a huge potential demand in patients with pancreatic cancer. Biomarker-based early diagnosis of cancer has always been prevailing, such as CA19-9-based diagnostic kit, but its specificity and sensitivity for the diagnosis of pancreatic cancer still need to be improved. It has been reported that GPC1 has a higher specificity for pancreatic cancer than CA19-9 [7]. The aim of this study was to develop and establish one effective method to screen out the more specific diagnostic antibodies for pancreatic cancer GPC1 by means of flow cytometry and single-cell amplification.

Similar to our previous report regarding single-cell study [16], three batches of rabbit single B cells were selected, 17 antibody sequences against human GPC1 were screened, and using these sequences, expression vectors were constructed, and antibodies were expressed. GPC1-12 was turned out to be the best antibody sequence in this screening process in our setting, which guaranteed the affinity of antibody antigen and the relative expression quantity. It was proved to be higher than those of other clones. There might be several reasons for the low expression of other antibodies. Firstly, after many rounds of PCR reaction, mutation could occur to some key bases of the antibody gene, which would greatly affect its expression level; secondly, the commercial expression vector pFUSE-rabbit Fc might have low expression efficiency, and other expression vectors could be replaced, such as pc-DNA serial vectors.

Traditional methods of antibody preparation mainly include hybridoma cell method and phage display method [17]. Outside of animal immunity, both of them have a lot of library building and screening work, which lasts for several months or even half a year. In this study, the period

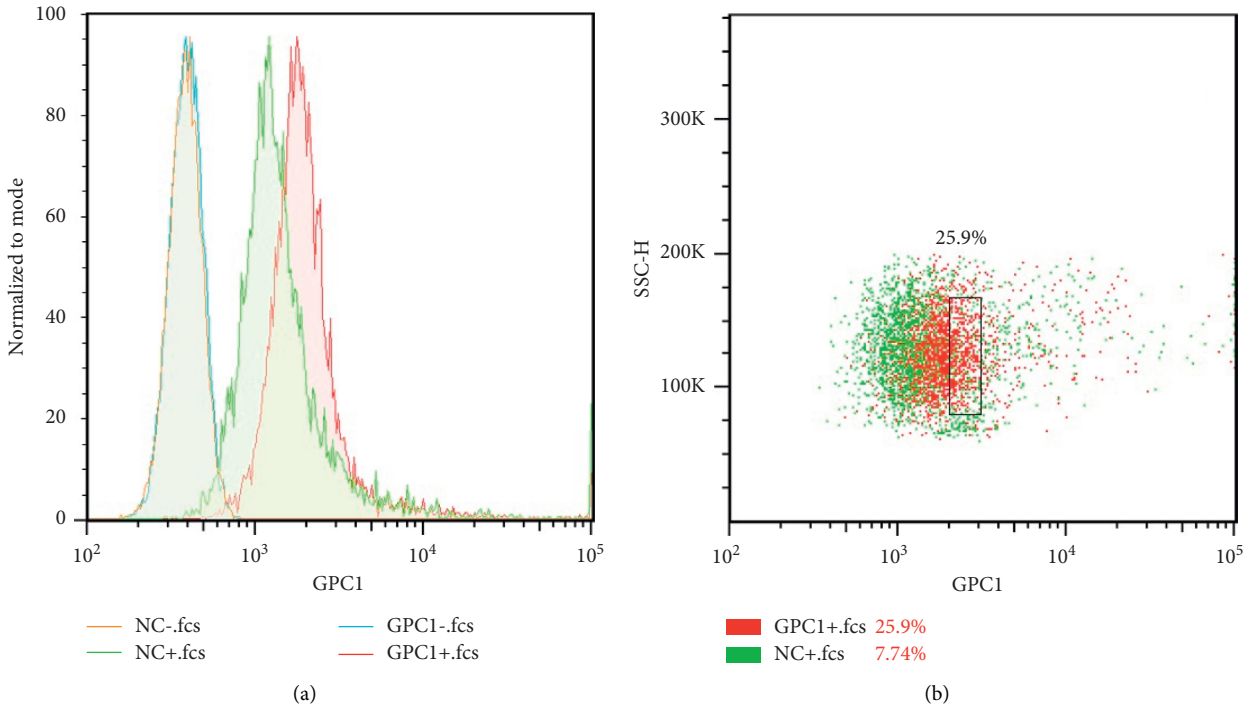

Figure 1: Cell fluorescent staining and sorting of single cell by flow cytometry. (a) Cell fluorescent staining; NC− means lymphocytes without GPC1-FITC staining. The lymphocytes were sampled from rabbits without immunization. NC+ means lymphocytes stained with GPC1-FITC. The lymphocytes were sampled from rabbits without immunization. GPC1− represents lymphocytes that were not stained with GPC1-FITC from immunized rabbits; GPC1+ denotes lymphocytes that were stained with GPC1-FITC from immunized rabbits. (b) B cell sorting by flow cytometry. GPC1+ cells were all that we want which were sorted by flow cytometry.

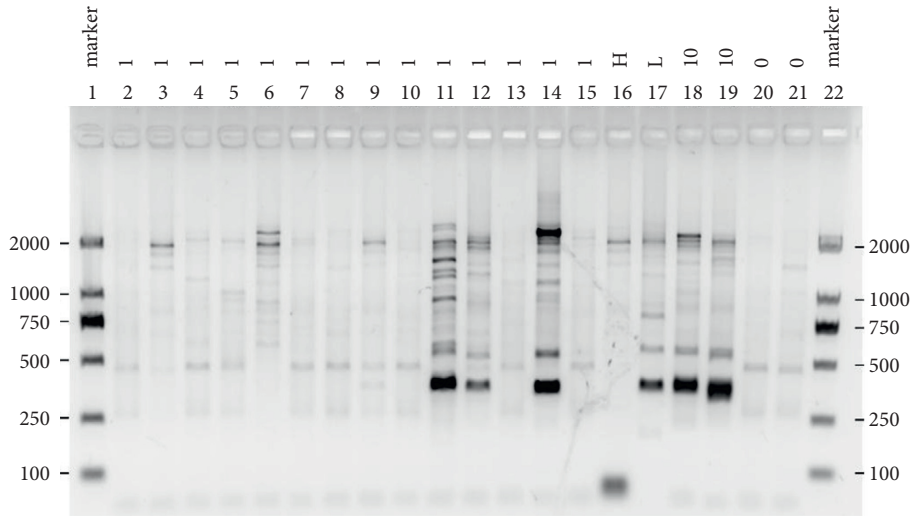

Figure 2: Electrophoresis of single-cell amplification. As shown in the electrophoretic gel, lanes 2–15 denote that only one cell sorted was used as the PCR template; lanes 18 and 19 were set as the positive control, where 10 cells sorted were utilized as the PCR template; lanes 20 and 21 were set as the negative control in which no cell was used in PCR. The gene of interest was around 380 bp. Lanes 11, 12, and 14, as well as positive controls, in which the bands of interest can be visibly achieved can be seen.

of antibody screening using immune antigens can be directly and remarkably shortened with the aid of flow cytometric cell sorting; moreover, the B cell clones isolated need not be cultured and expanded any more. The advantage of the methods we established here is that the amplification of antibody heavy chain and light chain genes can be directly obtained. It can directly obtain the matching information of antibody heavy chain and light chain, thus eliminating the cumbersome steps of cDNA library establishment and cell culture, therefore substantially greatly improving the efficiency of screening antibodies.

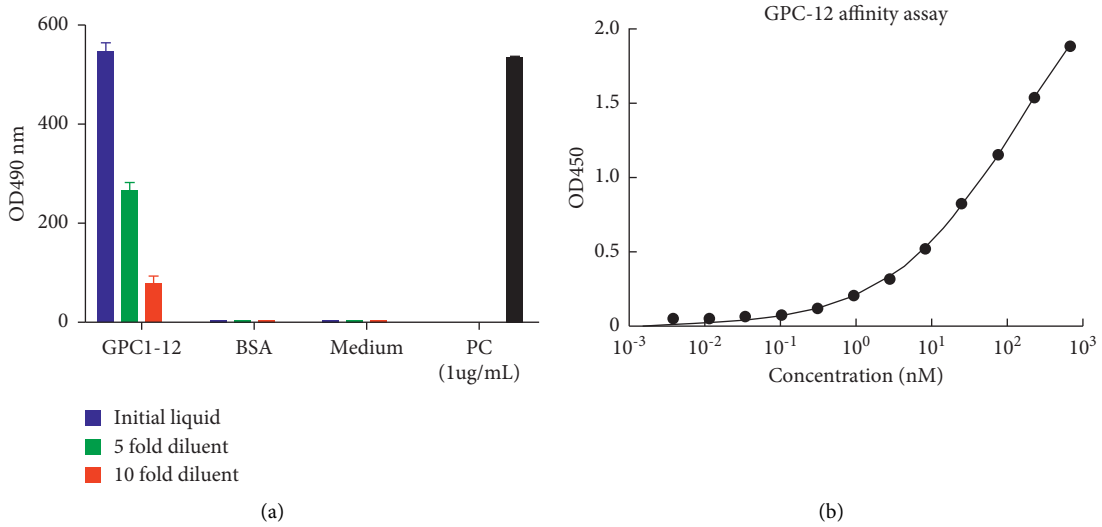

Figure 3: Detection of GPC1-12 in transfection supernatant was determined using ELISA and GPC1-12 affinity approaches. (a) Both BSA and medium were set as the negative control; PC (positive control): poly-IgG purified by affinity chromatography from positive rabbit serum. (b) GPC1-12 affinity determination. Enzyme-linked immunosorbent assay (ELISA) was performed to test the binding ability. The initial concentration of the coated antigen was 100 μg/mL, and then it was double diluted. It was shown that compared with antigen and blank control groups, GPC1-12 antibodies purified can specifically bind to GPC1 antigens.

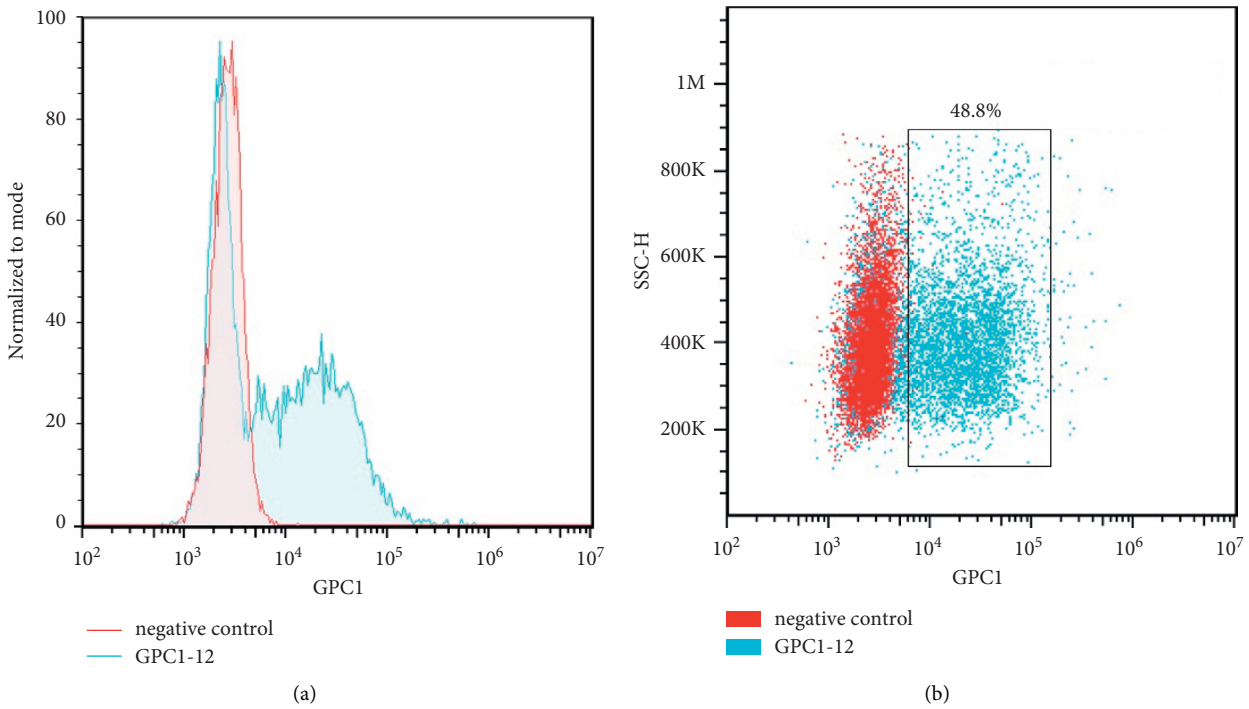

Figure 4: Feasibility of monoantibody GPC1-12 we obtained was validated using surface natural protein from the MDA-MB-231 cell line. The blue line represents monoantibody GPC1-12; the red line represents the negative control.

Based on the sequence of the antibody obtained in this experiment, the experiment that follows need to be considered, including the following: Firstly, the screened antibodies could be used to prepare early diagnostic kits for pancreatic cancer based on ELISA or flow cytometry. Secondly, with going deep in the research work, it has been reported that exosomes played an increasingly important role in the diagnosis and treatment of diseases, especially in cancer [18]. Considering this, the antibodies we screened can be used to isolate the antigen-specific exosomes by flow cytometry for subsequent clinical diagnosis and treatment. In conclusion, the method we established and developed here obtained highly specific antibody sequences and was able to substantially shorten the experimental cycle, which

would be also suitable for screening other targets one is interested in.

Abbreviations

GPC1: Glypican-1
PBMCs: Peripheral blood mononuclear cells
ELISA: Enzyme-linked immunosorbent assay
FITC: Fluorescein-5-isothiocyanate
DMSO: Dimethyl sulfoxide
PBS: Phosphate-buffered saline
PCR: Polymerase chain reaction.

Data Availability

All data generated or analyzed during this study are truthfully presented. Relevant data are available upon request.

Ethical Approval

The animal procedures were approved by the Institutional Animal Care and Use Committee at BGI, Shenzhen. All procedures were in compliance with the guidance released by the Care and Use of Laboratory Animals Regulations of BGI, Shenzhen.

Disclosure

Mi Huang and Yingying Ma are the co-first authors.

Conflicts of Interest

The authors declare that they have no conflicts of interest.

Authors' Contributions

Mi Huang and Yingying Ma contributed equally to this work. Both performed the experiments involved and collected the data. XYL and QD provided help in statistical analysis. CXL and XPL did some favor in cell culture and reagents purchase. YL and HZ contributed to the writing and revising of the manuscript. NY conceived the idea and was in charge of the whole project.

Acknowledgments

This work was supported by the Shenzhen Science and Technology Innovation Committee (no. JCYJ20160531194232631).

References

[1] S. A. El-Zahaby, Y. S. R. Elnaggar, and O. Y. Abdallah, "Reviewing two decades of nanomedicine implementations in targeted treatment and diagnosis of pancreatic cancer: an emphasis on state of art," *Journal of Controlled Release*, vol. 293, pp. 21–35, 2019.

[2] P. Maisonneuve, "Epidemiology and burden of pancreatic cancer," *La Presse Médicale*, vol. 48, no. 3, pp. e113–e123, 2019.

[3] W. Chen, R. Zheng, P. D. Baade et al., "Cancer statistics in China, 2015," *CA: A Cancer Journal for Clinicians*, vol. 66, no. 2, pp. 115–132, 2016.

[4] T. Kamisawa, L. D. Wood, T. Itoi, and K. Takaori, "Pancreatic cancer," *The Lancet*, vol. 388, no. 10039, pp. 73–85, 2016.

[5] B. Zhou, J.-W. Xu, Y.-G. Cheng et al., "Early detection of pancreatic cancer: where are we now and where are we going?" *International Journal of Cancer*, vol. 141, no. 2, pp. 231–241, 2017.

[6] M. R. Young, P. D. Wagner, S. Ghosh et al., "Validation of biomarkers for early detection of pancreatic cancer," *Pancreas*, vol. 47, no. 2, pp. 135–141, 2018.

[7] M. Herreros-Villanueva and L. Bujanda, "Glypican-1 in exosomes as biomarker for early detection of pancreatic cancer," *Annals of Translational Medicine*, vol. 4, no. 4, p. 64, 2016.

[8] R. Peltonen, P. Österlund, M. Lempinen, A. Nordin, U.-H. Stenman, and H. Isoniemi, "Postoperative CEA is a better prognostic marker than CA19-9, hCGβ or TATI after resection of colorectal liver metastases," *Tumor Biology*, vol. 40, no. 1, 2018.

[9] J. Guo, J. Yu, X. Song, and H. Mi, "Serum CA125, CA199 and CEA combined detection for epithelial ovarian cancer diagnosis: a meta-analysis," *Open Medicine*, vol. 12, no. 1, pp. 131–137, 2017.

[10] J. Song, L. J. Sokoll, J. J. Pasay et al., "Identification of serum biomarker panels for the early detection of pancreatic cancer," *Cancer Epidemiology Biomarkers & Prevention*, vol. 28, no. 1, pp. 174–182, 2019.

[11] X. Zou, J. Wei, Z. Huang et al., "Identification of a six-miRNA panel in serum benefiting pancreatic cancer diagnosis," *Cancer Medicine*, vol. 8, no. 6, pp. 2810–2822, 2019.

[12] J. Kleeff, T. Ishiwata, A. Kumbasar et al., "The cell-surface heparan sulfate proteoglycan glypican-1 regulates growth factor action in pancreatic carcinoma cells and is overexpressed in human pancreatic cancer," *Journal of Clinical Investigation*, vol. 102, no. 9, pp. 1662–1673, 1998.

[13] C.-y. Zhou, Y.-p. Dong, X. Sun et al., "High levels of serum glypican-1 indicate poor prognosis in pancreatic ductal adenocarcinoma," *Cancer Medicine*, vol. 7, no. 11, pp. 5525–5533, 2018.

[14] W. Qiu, H. Zhang, X. Chen et al., "A GPC1-targeted and gemcitabine-loaded biocompatible nanoplatform for pancreatic cancer multimodal imaging and therapy," *Nanomedicine*, vol. 14, no. 17, pp. 2339–2353, 2019.

[15] S. A. Melo, L. B. Luecke, C. Kahlert et al., "Glypican-1 identifies cancer exosomes and detects early pancreatic cancer," *Nature*, vol. 523, no. 7559, pp. 177–182, 2015.

[16] X. Li, P. Yang, and N. Yang, "A set of methods of amplification of human monoclonal antibody heavy and light chain genes from one single B cell," *Xi Bao Yu Fen Zi Mian Yi Xue Za Zhi*, vol. 34, no. 4, pp. 367–372, 2018.

[17] A. F. U. H. Saeed, R. Wang, S. Ling, and S. Wang, "Antibody engineering for pursuing a healthier future," *Frontiers in Microbiology*, vol. 8, p. 495, 2017.

[18] S. Kamerkar, V. S. LeBleu, H. Sugimoto et al., "Exosomes facilitate therapeutic targeting of oncogenic KRAS in pancreatic cancer," *Nature*, vol. 546, no. 7659, pp. 498–503, 2017.

Hindawi
Journal of Oncology
Volume 2021, Article ID 1281031, 9 pages
https://doi.org/10.1155/2021/1281031

Research Article

LncRNA NKILA Promotes Epithelial-Mesenchymal Transition of Liver Cancer Cells by Targeting miR-485-5p

Yuxu Wang, Chao Li, Yuyi Shi, and Jing Kuai

Department of Hepatobiliary Surgery, Weifang People's Hospital, Weifang 261000, Shandong Province, China

Correspondence should be addressed to Jing Kuai; laohetip@163.com

Received 21 June 2021; Accepted 23 July 2021; Published 3 September 2021

Academic Editor: Alamgeer Yuchi

Objective. Liver cancer (LC), one of the familiar malignancies, has a very high morbidity all over the world. The onset of the disease is hidden, and the patients usually do not express any special symptoms. Most of them will have been developed to the middle and later stage when they are diagnosed. This is one of the main reasons why the prognosis of LC is extremely pessimistic all the year round. Recently, researchers have focused mainly on molecular studies, among which LncRNA is a hot spot. This research aims to explore the biological behaviors of LncRNA NKILA and miR-485-5p in LC cells and verify the relationship between them, thereby providing a new theoretical basis for future prevention and treatment. *Methods*. Ninety-four early LC patients admitted to our hospital from January 2015 to January 2017 were regarded as the research objects. In addition, human LC cells SMMC-7721, HepG2, and normal liver cells HL-7702 were purchased. The LncRNA NKILA and miR-485-5p level in cancer and adjacent tissues, LC, and normal liver cells of patients was tested by PCR. Patients were followed up for 3 years. Then, LncRNA NKILA and miR-485-5p's effects on prognosis and cell biological behavior were analyzed. At last, the relationship between LncRNA NKILA and miR-485-5p was assessed by a dual-luciferase reporter assay. *Results*. The LncRNA NKILA expression was high in LC tissues and cells ($P < 0.050$), while miR-485-5p was low compared with the normal adjacent tissues ($P < 0.050$). Prognostic follow-up manifested that high LncRNA NKILA or low miR-485-5p could predict the poor prognosis and high mortality risk of the patients ($P < 0.050$). LC cells with downregulated LncRNA NKILA documented inhibited proliferation, invasion, and EMT, while the apoptosis level of the cells increased ($P < 0.050$). The proliferation, invasion, and EMT were inhibited by miR-485-5p increase, while the apoptosis of the cells decreased after upregulating miR-485-5p ($P < 0.050$). Online websites predicted that LncRNA NKILA had a binding site with miR-485-5p, and dual-luciferase reporter assay confirmed that LncRNA NKILA could directly target with miR-485-5p ($P < 0.050$). The miR-485-5p in LC cells increased after LncRNA NKILA was silenced ($P < 0.050$). The rescue experiment documented that LncRNA NKILA inhibition on LC cells was reversed by inhibiting miR-485-5p ($P < 0.050$). *Conclusion*. The LncRNA NKILA with high expression advances LC cell proliferation, invasion, and EMT by targeting miR-485-5p.

1. Introduction

As "the world's three major malignancies," liver cancer (LC), esophageal cancer (EC), and gastric cancer (GC), have very high morbidity worldwide [1]. On the basis of statistics, the morbidity of LC is about 274/100,000 [2]. It is a malignancy with hidden onset and no special symptoms. Once the clinical disease appears, the tumor has developed to the middle and late stages [3]. It is also one of the main reasons why the prognosis of LC is extremely pessimistic year by year. It is estimated that the number of people who die from LC every year in the world is as high as 745,000 [4]. Because of this, LC has always been a hot spot in clinical research. Researchers are trying to probe into the pathogenesis of LC to effectively counter this disease [5]. Research has shown that the occurrence of LC may be related to hepatitis, liver fluke, and infection [6]. Researchers have focused mainly on molecular studies, among which LncRNA is a major research hotspot [7, 8].

LncRNA, as a kind of RNA which can regulate many cytokines in human and animal bodies, has been proved to be relevant to many tumor diseases such as EC and GC

[9, 10]. According to the different localization and function of LncRNA in the body, it may promote or inhibit the progression of tumors [11]. Looking up related studies, we found that LncRNA NKILA, a member of LncRNA family, was first determined to have an abnormal expression in retinoblastoma [12]. Furthermore, it has been found that LncRNA NKILA has a certain influence on epithelial-mesenchymal transition (EMT) of breast cancer [13]. EMT promotes cell metastasis and invasion, thereby accelerating tumor development [14]. Tu et al. [15] found that LncRNA NKILA might be related to LC. Besides, we suspect that LncRNA NKILA may also affect the EMT of LC cells, but there is still no research to prove our point. When reviewing related studies, we discovered that miR-485-5p was also abnormally expressed in LC [16], and LncRNA NKILA had the same binding site with miR-485-5p through ENCORI online website. Thus, this research focuses on investigating the biological behavior and EMT of LncRNA NKILA and miR-485-5p in LC cells and verifying the relationship between them, thus supplying a new theoretical basis for future prevention and treatment.

2. Experimental Preparation and Methods

2.1. Experimental Subjects

2.1.1. Source of Patients. Ninety-four early LC patients admitted to our hospital from January 2015 to January 2017 were considered as the research objects. Inclusion criteria are as follows: people diagnosed as primary LC by biopsy in pathology department; those with early pathological stage; the patients with complete case data; 20–70-year-old patients; and those agreeing to take part in the research work. Exclusion criteria are as follows: the patients with multiple tumors; the patients with other cardiovascular and cerebrovascular diseases, autoimmune defects, infectious diseases, and organ dysfunction; pregnant and lactating patients; those who have transferred from one hospital to another; and those who have received antibiotics, surgery, radiotherapy, and chemotherapy six months before. All the investigators signed an informed consent form. This experiment was ratified by the Ethics Committee of our hospital.

2.2. Cell Sources. Human LC cells SMMC-7721 and HepG2 and normal liver cells HL-7702 were all bought from ATCC and preserved in CM1-1 medium. The three all grew adhering to the wall and were cultured in 5% CO_2 at 37°C. SMMC-7721 was epithelial-like, polygonal, and short spindle-shaped. HepG2 was epithelial-like and clustered. HL-7702 was epithelial-like, polygonal, and round.

3. Experimental Methods

3.1. Sample Collection. Upon approval, the samples of cancer tissues and normal tissues adjacent to cancer (≥5 cm away from cancer tissues) were obtained when patients underwent pathological biopsy. Two minutes later, the samples were stored in liquid nitrogen.

3.2. qRT-PCR Detection. About 40 mg of cancer tissue and adjacent tissue samples were collected and put into a mortar. Then, a proper amount of liquid nitrogen and 1 mL TRIzol were added to mix them well. Thus, total RNA was extracted. The purity of total RNA was verified by ultraviolet spectrophotometer, and then it was reverse-transcribed into cDNA by reverse transcription kit. The reverse transcription system is as follows: 10 μL RNA sample without gDNA, 1 μL PrimerScript RT Enzyme Mix I, 4 μL RT Primer Mix, 24 μL Sx PrimerScript Buffer, and 1 μL RNase-free water, 20 μL in total. Afterwards, it was tested by the PCR method. The primer sequence was designed by Invitrogen. The reaction system is as follows: FastStart Universal SYBR Green Master (ROX) 25 μL, forward primer and reverse primer sequences 0.5 μL each, and RNase-free water 19 μL, totally 45 μL. Reaction conditions are as follows: 95°C for 10 min, 95°C for 15 s, and 60°C for 60 s, totally 40 cycles. The LncRNA NKILA and miR-485-5p levels were calculated via $2^{-\Delta\Delta Ct}$.

3.3. Prognostic Follow-Up. All patients were followed up for 3 years by reexamination in the hospital. Their 3-year survival was recorded and the survival curves were drawn.

3.4. Cell Passage. SMMC-7721, HepG2, and HL-7702 proliferated to about 80% in a culture dish and then were subcultured. The old culture solution was absorbed and washed twice with PBS. Next, 6 mL (/100 mm dish) pancreatin was added and observed under a microscope. During the period, the culture dish was not allowed to be shaken. Most of the pancreatin was absorbed when the cells just fell off, leaving about 0.5 mL. After that, it was moved to the incubator, digested, and taken out in about 2 min. After passage, the digestion was terminated with a 12 mL CM1-1 culture medium, and the cells were gently blown. After that, those could be cultured in 3–6 dishes.

3.5. Cell Transfection. The logarithmic phase SMMC-7721 and HepG2 were inoculated into the 6-hole plate. When the cells covered 70%–80% of the bottom, a certain titer of lentivirus and 5 μg/mL polybrene were added into each well with a multiplicity of infection 10. The LncRNA NKILA group and the empty vector NC group were constructed. After 24 h, it was changed to complete medium and expanded. After 72 h, fluorescence intensity was observed under an inverted fluorescence microscope to judge transfection efficiency. The mimics, inhibitor, and negative control of miR-485-5p were transfected with Lipofectamine®2000, respectively, and were set as miR-485-5p overexpression group (miR-mimics), miR-485-5p inhibition group (miR-inhibitor), and blank group (miR-NC). The efficiency of cell transfection was examined by qRT-PCR, the same as 2.2. The cells were added to lysate to prepare tissue homogenate before PCR detection.

3.6. CCK-8 Test. The transfected cells were seeded into 96-hole plates at a density of 1×10^4 cells/hole. Those were transfected when the fusion reached 80%, the same as 2.4.

CCK-8 solution was supplemented after 0, 24, 48, and 72 h and cultured for another 4 h. The absorbance values were detected by microplate reader at 450 nm and the cell growth curves were drawn.

3.7. Transwell Experiment. Matrigel diluent 50–100 μL was evenly applied to the basement membrane at the bottom of the Transwell chamber and air-dried at 4°C. Then, 100 μL culture medium was added to each Transwell chamber to hydrate the basement membrane and stood at 37°C for 1 h. The cells were resuspended to 1×10^5 cells/mL with a culture solution containing 1% fetal bovine serum (FBS). The liquid in the upper chamber was discarded, and 900 μL solution with 10% FBS was supplemented outside the chamber and cultured for another 24 h. Subsequently, the chamber was taken out, immobilized with 4% paraformaldehyde, dyed with crystal violet for 30 min, and observed in five fields randomly under a microscope (400x). The average cell number in each field was counted.

3.8. Flow Cytometry. After cells were cleaned by PBS, trypsin without EDTA was added and digested for 2 min. Then, the digestion was terminated by adding a proper complete medium. Cells were adjusted to 1×10^6 cells/mL with pre-cooled PBS and centrifuged for 10 min (500xg). After that, the liquid of the tubes was discarded, and 500 μL binding buffer was supplemented. Annexin V-FITC and PI 5 μL each were added under dark conditions, shaken and mixed well, standing at indoor temperature for 30 min. The apoptosis rate was monitored using a flow cytometer.

3.9. Western Blot Detection. A total of 200 μL protein lysate was added. Then, the cells were lysed and the total protein was extracted. The sample was mixed with the loading buffer, and the protein was denatured by boiling water bath for 10 min. Soon afterwards, 30 μg of each well was sampled and transferred to PVDF membrane after SDS-PAGE electrophoresis. After 5% FBS albumin was blocked, the primary antibody was added. The cells were incubated at 4°C overnight, and the second antibody was added the next day. They were developed by ECL and photographed under dark conditions. The expression of protein is the optical density ratio of the target band to internal reference GAPDH.

3.10. Verification of Targeted Relationship. The binding site between LncRNA NKILA and miR-485-5p was predicted by the Starbase online website (http://starbase.sysu.edu.cn/). Wild-type LncRNA NKILA (LncRNA NKILAA-WT) and mutant LncRNA NKILA (LncRNA NKILAA-MUT) lacking miR-218-5p binding region were obtained. The LncRNA NKILAA-WT and LncRNA NKILAA-MUT fluorescein reporter vectors were transfected into SMMC-7721 and HepG2 cells, respectively. After 48 h, the luciferase activity was tested using a dual-luciferase reporter kit.

3.11. Statistical Methods. The results were plotted and statistically calculated by GraphPad7 software, marked by mean ± standard deviation. The data were analyzed via the independent-samples *t*-test, while the difference among multiple groups was assessed through one-way analysis of variance (ANOVA) and LSD backtesting. Multiple time points were compared via repeated measures ANOVA and Bonferroni backtesting. The survival rate was counted via the Kaplan–Meier method and assessed via the log-rank test. $P < 0.05$ denotes that the difference is statistically marked, while $P < 0.001$ means that is remarkable.

4. Experimental Results

4.1. LncRNA NKILA in Cancer Tissues Is Higher than That in Adjacent Normal Tissues While miR-485-5p Is Lower. The LncRNA NKILA expression in LC tissues was higher than that in adjacent tissues ($P < 0.05$), while the miR-485-5p level was lower ($P < 0.05$) (Figure 1).

4.2. High-Expressed LncRNA NKILA and Low-Expressed miR-485-5p Indicate Poor Prognosis. Eighty-nine patients were successfully followed up within 3 years, and the success rate was 93.68%. Among them, 15 patients died, with a total mortality of 16.85% after 3 years of prognosis. It was found that LncRNA NKILA in dead patients was higher than that in survivors, while miR-485-5p was lower. ROC curve analysis manifested that when LncRNA NKILA >5.325, the sensitivity and specificity of death prediction within 3 years were 80.00% and 89.19% (AUC: 0.854, 95% CI: 0.728–0.980, $P < 0.001$). When miR-485-5p <1.905, the sensitivity and specificity were 73.33% and 85.14% (AUC: 0.805, 95% CI: 0.661–0.950, $P < 0.001$). On the basis of the cut-off value, they were divided into group A (LncRNA NKILA >5.325, $n = 20$), group B (LncRNA NKILA ≤5.325, $n = 69$), group C (miR-485-5p ≥1.905, $n = 67$), and group D (miR-485-5p <1.905, $n = 22$). According to the prognosis and survival curve, the survival of group B was better than group A, while group C was better than group D ($P < 0.05$) (Figure 2).

4.3. Silencing LncRNA NKILA Can Inhibit the Activity and EMT of LC Cells. The expression of LncRNA NKILA in SMMC-7721, HepG2, and HL-7702 was higher than that in HL-7702 ($P < 0.05$). The proliferation, invasion, and EMT in SMMC-7721 and HepG2 si-LncRNA NKILA group were lower than those in NC group, but the apoptosis was higher ($P < 0.05$) (Figure 3).

4.4. Inhibiting miR-485-5p Promotes LC Cell Activity and EMT and Vice Versa. It was found that the miR-485-5p levels in SMMC-7721 and HepG2 were lower than that in HL-7702 ($P < 0.05$). MiR-485-5p mimics, inhibitor, and negative control groups were transfected into the cells in the miR-mimics, inhibitor, and negative control groups, respectively. The cell proliferation, invasion, and EMT of the miR-mimics group were low but the apoptosis was high compared with the other two groups ($P < 0.05$). The three in

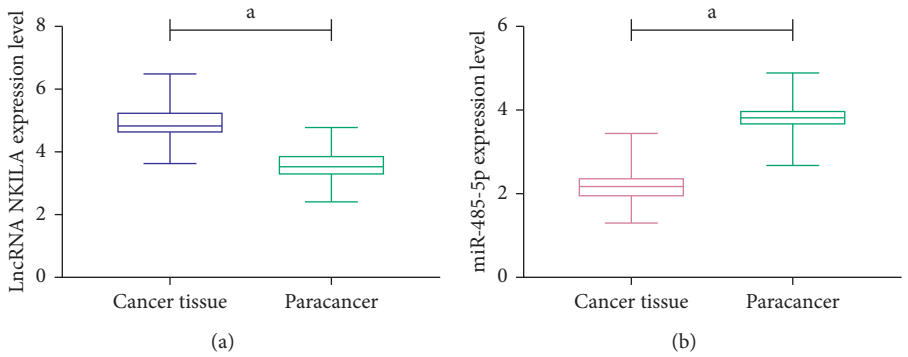

Figure 1: LncRNA NKILA and miR-485-5p expression. (a) The LncRNA NKILA expression in cancer tissues was higher than that in adjacent tissues ($^aP < 0.05$). (b) The miR-485-5p level in cancer tissues was lower than that in adjacent tissues ($^aP < 0.05$).

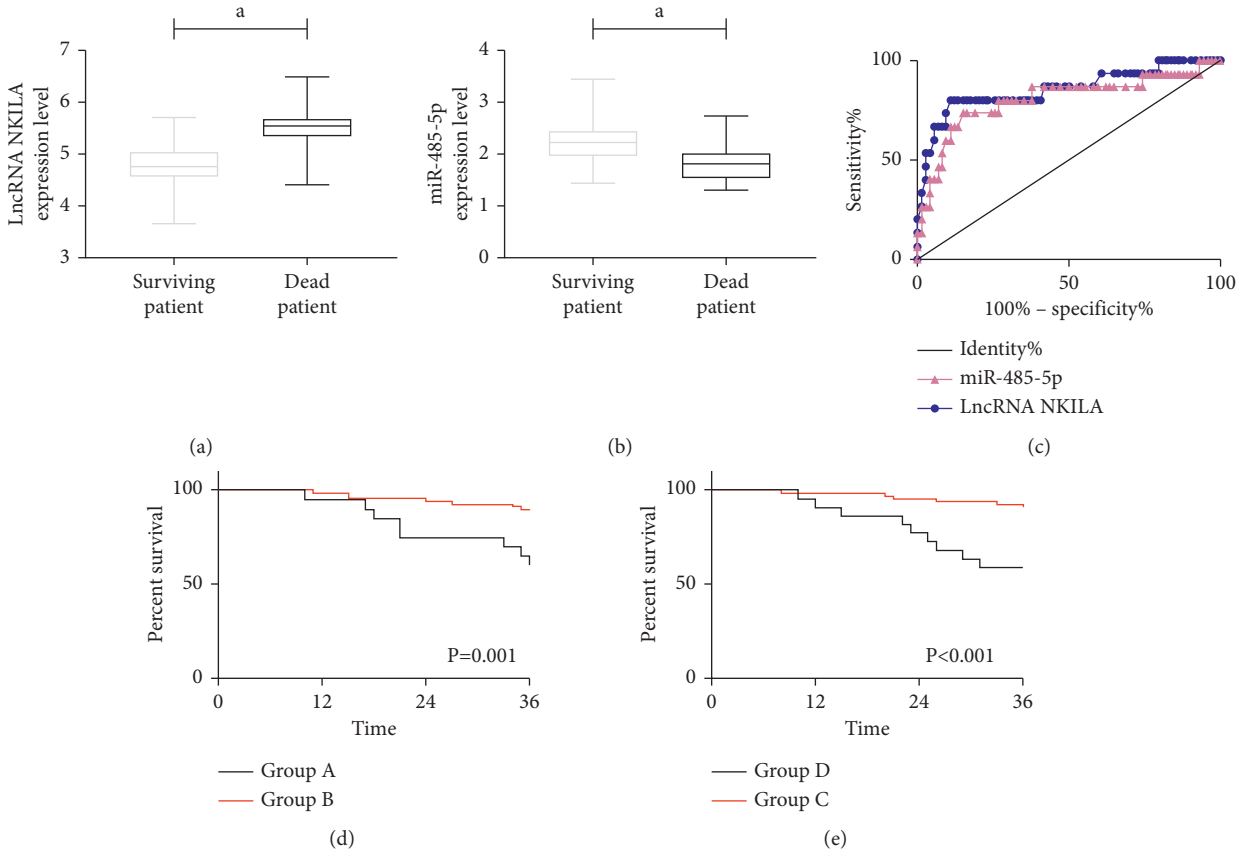

Figure 2: Influence of LncRNA NKILA and miR-485-5p on prognosis of LC patients. (a) The LncRNA NKILA expression in dead patients was higher than that in those who survived ($^aP < 0.05$). (b) The miR-485-5p expression in dead patients was lower than that in those who survived ($^aP < 0.05$). (c) ROC curve of LncRNA NKILA and miR-485-5p in death prediction within 3 years. (d) Three-year survival curves of prognosis between groups A and B (e) Three-year survival curves of prognosis between groups C and D.

the miR-inhibitor group were higher than those in the miR-NC group, but the apoptosis was lower ($P < 0.05$) (Figure 4).

4.5. Relationship between LncRNA NKILA and miR-485-5p. The Starbase online website manifested that there were binding sites between LncRNA NKILA and miR-485-5p. Dual-luciferase reporter assay documented that the fluorescence activity of LncRNA NKILAA-WT was inhibited by overexpressed miR-485-5p ($P < 0.05$), while the miR-485-5p expression in SMMC-7721 and HepG2 after transfection of LncRNA NKILA lentivirus inhibition and empty vector was higher than that in NC group ($P < 0.05$) (Figure 5).

4.6. Rescue Experiment. The LncRNA NKILA lentivirus inhibition and miR-485-5p inhibitor were cotransfected into SMMC-7721 and HepG2 cells as cotransfection

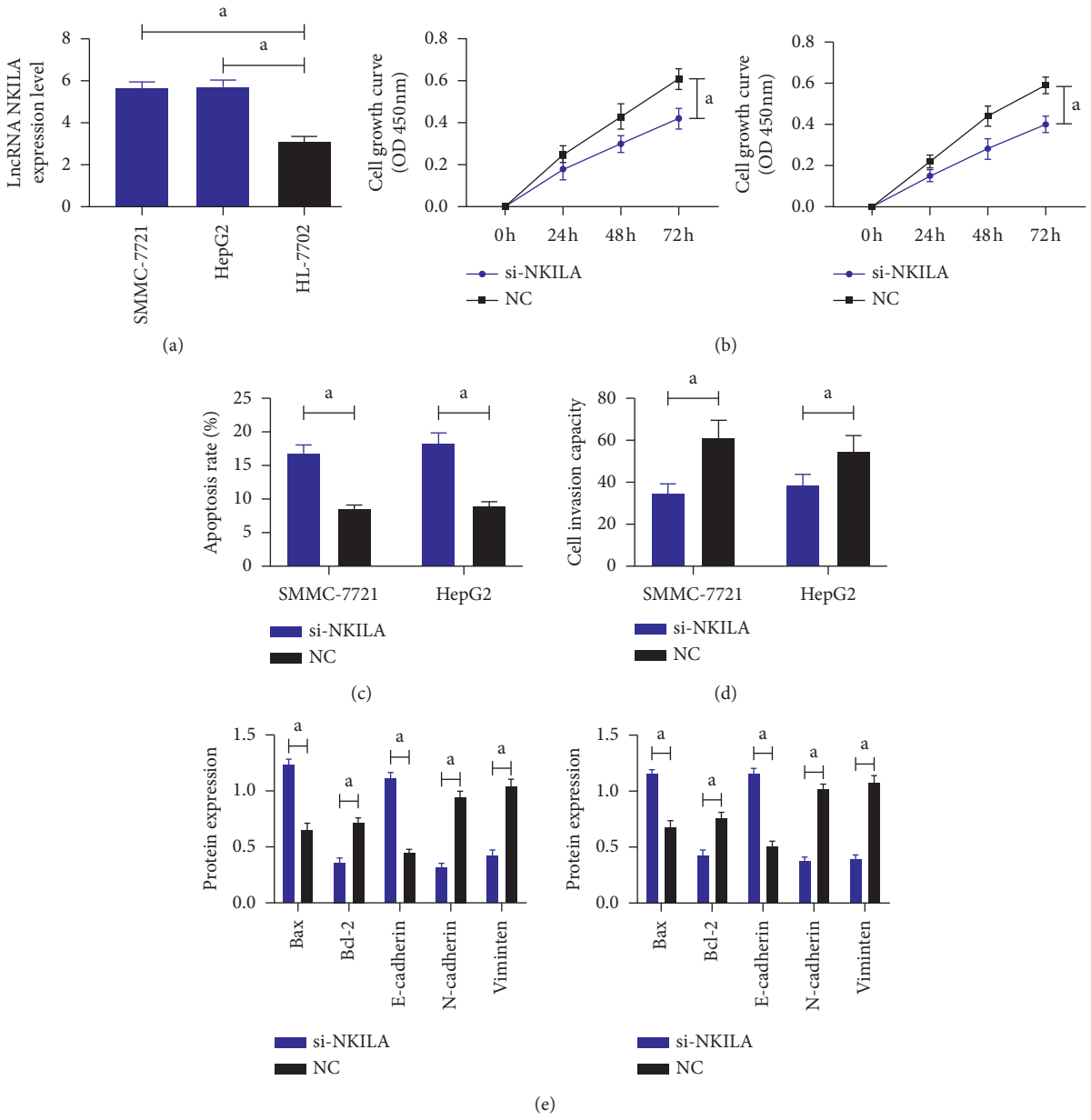

Figure 3: Effect of LncRNA NKILA on LC cells. (a) The expression of LncRNA NKILA in SMMC-7721, HepG2, and HL-7702 was higher than that in HL-7702 ($^aP < 0.05$). (b) Comparison of growth curves of SMMC-7721 and HepG2 ($^aP < 0.05$). (c) Comparison of apoptosis rates of SMMC-7721 and HepG2 ($^aP < 0.05$). (d) Comparison of invasion of SMMC-7721 and HepG2 ($^aP < 0.05$). (e) Comparison of expression of SMMC-7721, HepG2 apoptosis-related protein, and EMT-related protein ($^aP < 0.05$).

group. LncRNA NKILA lentivirus inhibition, miR-485-5p inhibitor, and LncRNA NKILA empty vector were transfected alone. The biological behavior of cells showed that there was no difference in proliferation, invasion, and apoptosis between cotransfected and NC groups ($P > 0.05$). The proliferation and invasion of the cells transfected with si-LncRNA NKILAA were lower than those of the cells in cotransfection and NC groups, while the apoptosis level of the cells transfected with si-LncRNA NKILAA was higher than that of the cell in other groups ($P < 0.05$) (Figure 6).

5. Discussion

Along with the increasing morbidity of LC, it is more and more urgent to investigate its pathogenesis clinically [17]. It is quite valuable to explore at the molecular level [18]. In the first place, molecular detection can be used as a tumor diagnostic marker, which improves tumors' early detection rate and improves patients' prognosis. In the second place, through molecular detection, it can help clinical judgment of disease progress and assist clinicians to take effective intervention measures as soon as possible. In the third place,

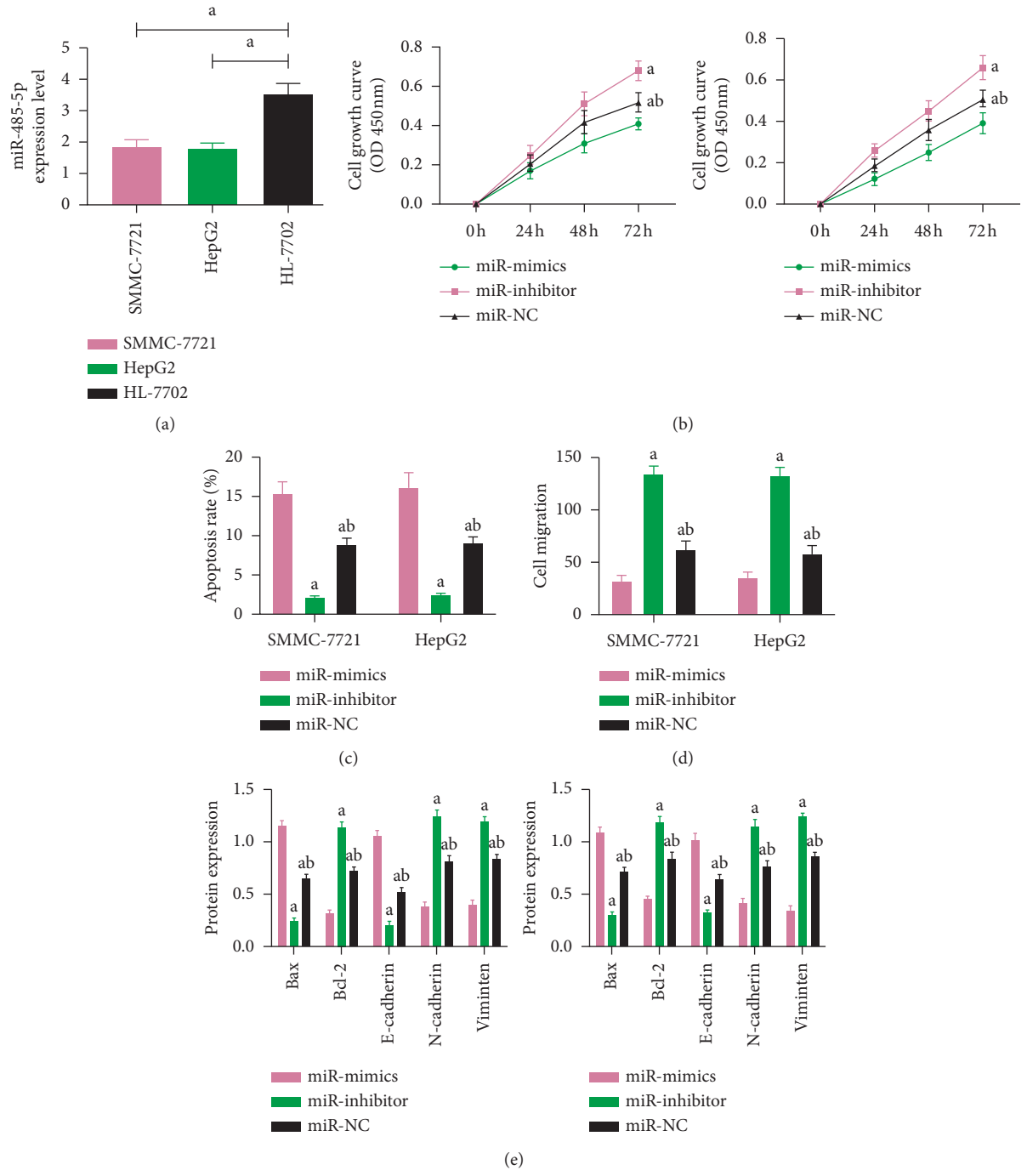

Figure 4: miR-485-5p effect on LC cells. (a) The miR-485-5p expression in SMMC-7721, HepG2, and HL-7702 was lower than that in HL-7702 ($^{a}P < 0.05$). (b) Comparison of growth curves between SMMC-7721 and HepG2. (c) Comparison of apoptosis rates between SMMC-7721 and HepG2. (d) Comparison of SMMC-7721 and HepG2 invasion. (e) Comparison of apoptosis- and EMT-related protein expression between SMMC-7721 and HepG2. ^{a}Comparison with the miR-mimics group, $P < 0.05$; ^{b}comparison with the miR-inhibitor group, $P < 0.05$.

through molecular targeted therapy, it is possible to achieve better results and higher safety than surgery, radiotherapy, and chemotherapy. Hence, after exploring the effect of miR-485-5p targeted by LncRNA NKILA on LC cells, this experiment is quite marked for future diagnosis and treatment.

We detected the LncRNA NKILA and miR-485-5p levels in cancer and adjacent tissues of patients and found that LncRNA NKILA was highly expressed in the former, while miR-485-5p was low. The abnormal expressions of LncRNA NKILA and miR-485-5p suggested that they might be relevant to LC occurrence and development. The studies have also discovered that the LncRNA NKILA and miR-485-5p levels were also consistent in laryngeal cancer, rectal cancer, and tongue cancer [19–21]. It manifested that LncRNA

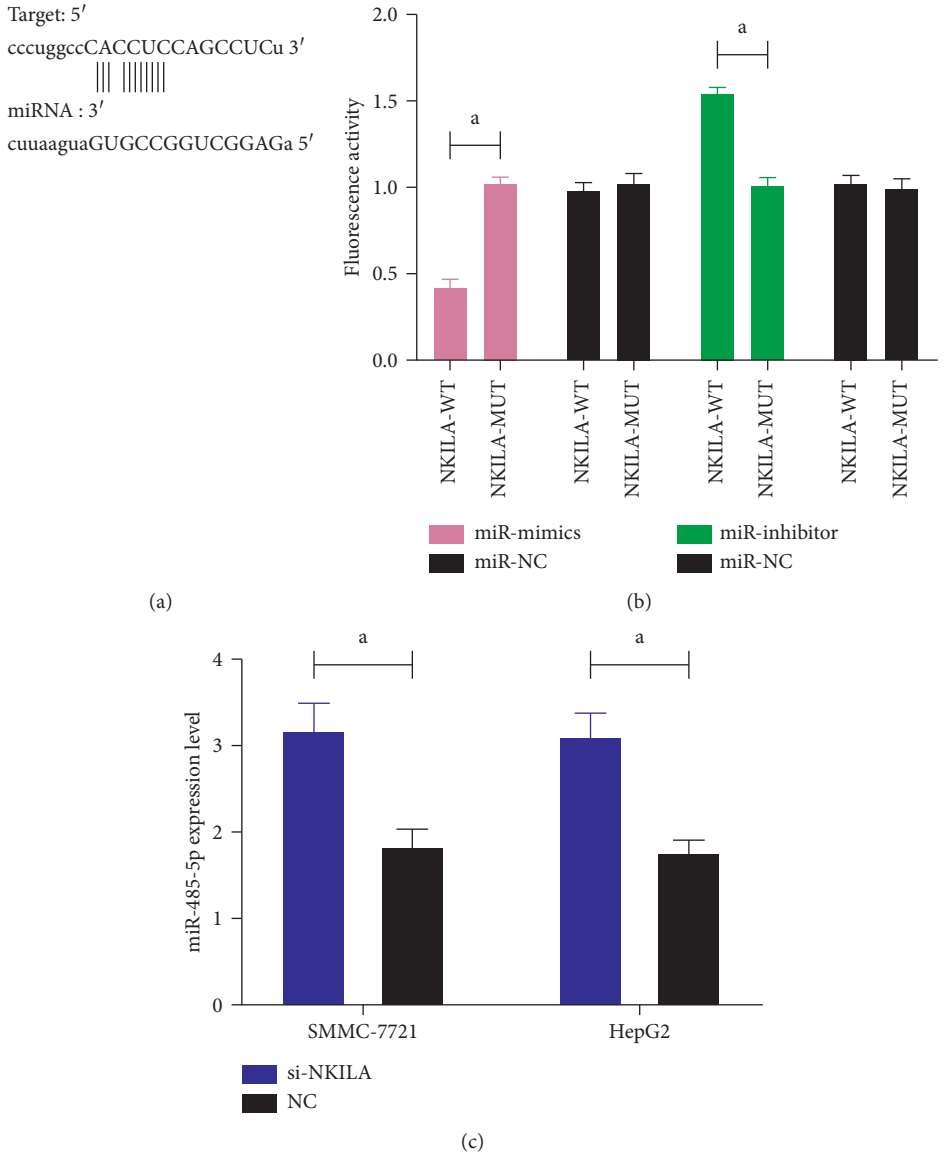

Figure 5: Relationship between LncRNA NKILA and miR-485-5p. (a) Binding sites of LncRNA NKILA and miR-485-5p. (b) Fluorescence activity of dual-luciferase reporter enzyme ($^aP < 0.05$). (c) The miR-485-5p expression in SMMC-7721 and HepG2 of the si-LncRNA NKILAA group was higher than that of the NC group after transfection of LncRNA NKILA lentivirus inhibition and empty vector ($^aP < 0.05$).

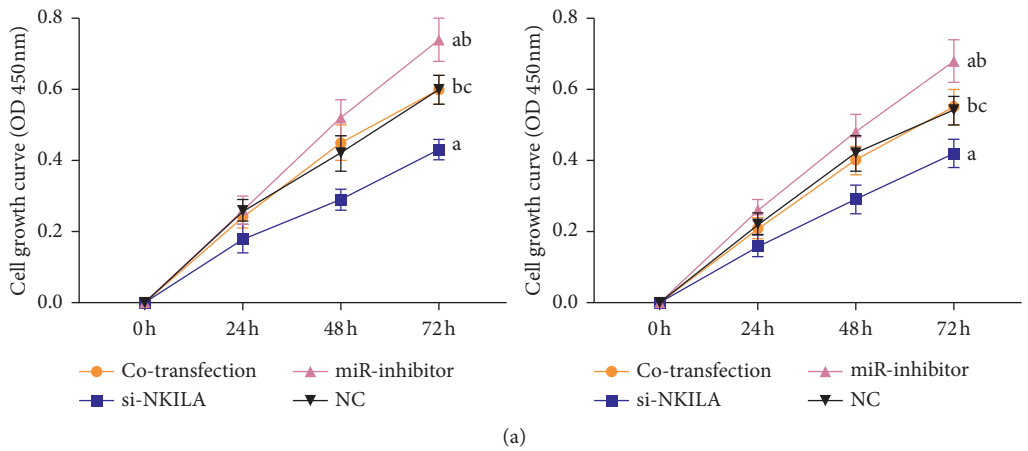

Figure 6: Continued.

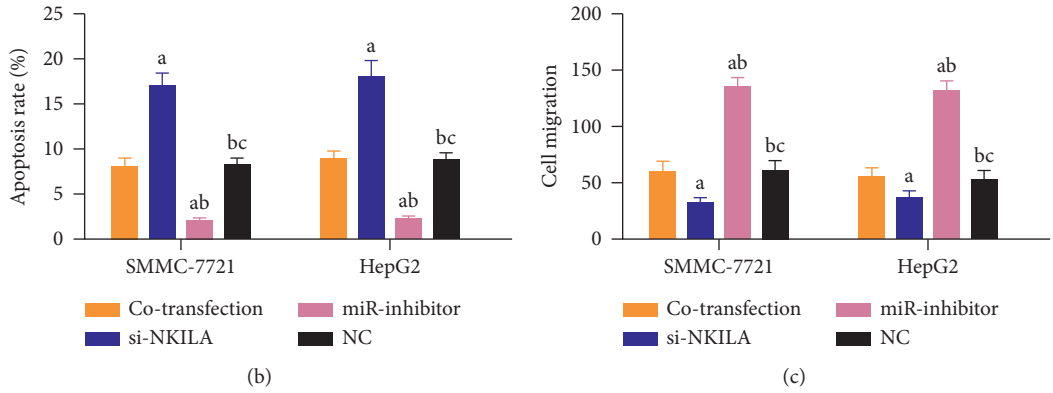

Figure 6: Rescue experiment. (a) Comparison of growth curves between SMMC-7721 and HepG2. (b) Comparison of apoptosis rates between SMMC-7721 and HepG2. (c) Comparison of SMMC-7721 and HepG2 invasion. [a]Comparison with the cotransfection group, $P < 0.05$; [b]comparison with si-LncRNA NKILAA, $P < 0.05$; [c]comparison with the miR-inhibitor group, $P < 0.05$.

NKILA and miR-485-5p might play the same role in many diseases. Through prognostic follow-up, we found that the LncRNA NKILA levels of prognostic dead patients were higher than those of survival patients, while the miR-485-5p level expressed a contrary situation. It revealed that high expression of LncRNA NKILA and low expression of miR-485-5p could predict poor prognosis of the patients with LC. To verify their influence on prognosis, we first analyzed the predictive value of LncRNA NKILA and miR-485-5p on patients' death within 3 years by ROC curve. The result also accords with our above inference. The cut-off value shows that high LncRNA NKILA and low miR-485-5p were related to the high mortality risk of the patients. With the cut-off value as the boundary, we divided patients into high- and low-expression groups. By observing their prognosis and survival curves, we also found that those with high expression of LncRNA NKILA and low expression of miR-485-5p had higher mortality. So, we can judge the prognosis of patients by monitoring the LncRNA NKILA and miR-485-5p levels in the future.

Above, we have a preliminary understanding of the clinical role of LncRNA NKILA and miR-485-5p in LC, but the mechanism on cancer cells is ambiguous. So, we purchased LC and normal liver cells, to detect LncRNA NKILA and miR-485-5p expression. It was found that the results were consistent with ours mentioned above, which confirmed our experimental results. Then, we transfected a lentiviral vector that inhibits LncRNA NKILA with miR-485-5p mimics and inhibitor into LC cells and detected their biological behavior. It was found that silencing LncRNA NKILA could inhibit the activities of LC cells, suggesting that highly expressed LncRNA NKILA acted as an oncogene in LC. Inhibiting miR-485-5p can promote LC cell activity and vice versa. Looking at previous studies, we found that LncRNA NKILA and miR-485-5p also regulated colorectal cancer and mandatory spondylitis progression [22, 23], which can also support our experimental results. Besides, because we speculated that LncRNA NKILA and miR-485-5p had a certain influence on EMT, we also detected the expression of E-cadherin, N-cadherin, and vimentin hepatoma cells. E-Cadherin, N-cadherin, and vimentin, as effective indicators of EMT, have been unanimously recognized in clinical practice [24, 25], so they will not be described in detail here. We found that inhibiting LncRNA NKILA and overexpressing miR-485-5p suppressed LC cell EMT. It suggests that LncRNA NKILA and miR-485-5p may be potential therapeutic targets. Hence, targeted silencing of LncRNA NKILA or enhancement of miR-485-5p can reduce the EMT and inhibit the spread of cancer cells. Of course, the clinical application still needs to be confirmed by a large number of experiments. At last, in order to assess the relationship between LncRNA NKILA and miR-485-5p, we first confirmed the binding sites between them through the online website. The dual-luciferase reporter enzyme experiment documented that there was a targeted regulation relationship between them. The miR-485-5p expression in LC cells increased after transfection of lentiviral vector inhibiting LncRNA NKILA. Thus, we can know that LncRNA NKILA has an impact on the targeted regulation of miR-485-5p in LC. The rescue experiment documented that the biological behavior of LC cells cotransfected with lentiviral vector inhibiting LncRNA NKILA and miR-485-5p inhibitor was not different from the cells transfected with LncRNA NKILA empty vector, indicating that the effect of silencing LncRNA NKILA was completely changed by inhibiting miR-485-5p.

Hence, we can finally conclude that highly expressed LncRNA NKILA boosts cell proliferation, invasion, and EMT by targeting miR-485-5p.

There are still many shortcomings in this research. The LncRNA NKILA and miR-485-5p expression in normal samples and blood of LC patients are not detected, and their diagnostic value is not assessed. Furthermore, we have not yet known the signal pathway that LncRNA NKILA targets miR-485-5p to affect LC cells, which needs to be verified by much research and experimental analysis. In addition, we need to carry out tumor-forming experiments in nude mice to verify the effects of LncRNA NKILA and miR-485-5p to make a better experimental analysis and get more effective results.

Data Availability

All data used to support this study are available from the corresponding author upon request.

Conflicts of Interest

The authors declare that they have no conflicts of interest.

References

[1] M. C. S. Wong, J. Y. Jiang, W. B. Goggins et al., "International incidence and mortality trends of liver cancer: a global profile," *Scientific Reports*, vol. 7, no. 1, Article ID 45846, 2017.

[2] C.-C. Chien, M.-M. Han, Y.-H. Chiu et al., "Epidemiology of cancer in end-stage renal disease dialysis patients: a national cohort study in Taiwan," *Journal of Cancer*, vol. 8, no. 1, pp. 9–18, 2017.

[3] M. Ringehan, J. A. McKeating, and U. Protzer, "Viral hepatitis and liver cancer," *Philosophical Transactions of the Royal Society B: Biological Sciences*, vol. 372, no. 1732, Article ID 20160274, 2017.

[4] E. W. Beal, D. Tumin, A. Kabir et al., "Trends in the mortality of hepatocellular carcinoma in the United States," *Journal of Gastrointestinal Surgery*, vol. 21, no. 12, pp. 2033–2038, 2017.

[5] M. Seehawer, F. Heinzmann, L. D'Artista et al., "Necroptosis microenvironment directs lineage commitment in liver cancer," *Nature*, vol. 562, no. 7725, pp. 69–75, 2018.

[6] D. Maucort-Boulch, C. de Martel, S. Franceschi, and M. Plummer, "Fraction and incidence of liver cancer attributable to hepatitis B and C viruses worldwide," *International Journal of Cancer*, vol. 142, no. 12, pp. 2471–2477, 2018.

[7] X. Huo, S. Han, G. Wu et al., "Dysregulated long noncoding RNAs (lncRNAs) in hepatocellular carcinoma: implications for tumorigenesis, disease progression, and liver cancer stem cells," *Molecular Cancer*, vol. 16, no. 1, p. 165, 2017.

[8] J. Zhao, Y. Fu, J. Wu, J. Li, G. Huang, and L. Qin, "The diverse mechanisms of miRNAs and lncRNAs in the maintenance of liver cancer stem cells," *BioMed Research International*, vol. 2018, Article ID 8686027, , 2018.

[9] N.-B. Hao, Y.-F. He, X.-Q. Li, K. Wang, and R.-L. Wang, "The role of miRNA and lncRNA in gastric cancer," *Oncotarget*, vol. 8, no. 46, pp. 81572–81582, 2017.

[10] Z. Dong, A. Zhang, S. Liu et al., "Aberrant methylation-mediated silencing of lncRNA MEG3 functions as a ceRNA in esophageal cancer," *Molecular Cancer Research*, vol. 15, no. 7, pp. 800–810, 2017.

[11] W.-X. Peng, P. Koirala, and Y.-Y. Mo, "LncRNA-mediated regulation of cell signaling in cancer," *Oncogene*, vol. 36, no. 41, pp. 5661–5667, 2017.

[12] X. Lyu, Y. Ma, F. Wu, L. Wang, and L. Wang, "LncRNA NKILA inhibits retinoblastoma by downregulating lncRNA XIST," *Current Eye Research*, vol. 44, no. 9, pp. 975–979, 2019.

[13] W. Wu, F. Chen, X. Cui et al., "LncRNA NKILA suppresses TGF-β-induced epithelial-mesenchymal transition by blocking NF-κB signaling in breast cancer," *International Journal of Cancer*, vol. 143, no. 9, pp. 2213–2224, 2018.

[14] A. Dongre and R. A. Weinberg, "New insights into the mechanisms of epithelial-mesenchymal transition and implications for cancer," *Nature Reviews Molecular Cell Biology*, vol. 20, no. 2, pp. 69–84, 2019.

[15] J. Tu, Z. Zhao, M. Xu, M. Chen, Q. Weng, and J. Ji, "LINC00460 promotes hepatocellular carcinoma development through sponging miR-485-5p to up-regulate PAK1," *Biomedicine & Pharmacotherapy*, vol. 118, Article ID 109213, 2019.

[16] X. Sun, Y. Liu, M. Li, M. Wang, and Y. Wang, "Involvement of miR-485-5p in hepatocellular carcinoma progression targeting EMMPRIN," *Biomedicine & Pharmacotherapy*, vol. 72, pp. 58–65, 2015.

[17] C. Klec, T. Gutschner, K. Panzitt, and M. Pichler, "Involvement of long non-coding RNA HULC (highly up-regulated in liver cancer) in pathogenesis and implications for therapeutic intervention," *Expert Opinion on Therapeutic Targets*, vol. 23, no. 3, pp. 177–186, 2019.

[18] M. Kudo, "Molecular targeted agents for hepatocellular carcinoma: current status and future perspectives," *Liver Cancer*, vol. 6, no. 2, pp. 101–112, 2017.

[19] T. Yang, S. Li, J. Liu, D. Yin, X. Yang, and Q. Tang, "LncRNA-NKILA/NF-κB feedback loop modulates laryngeal cancer cell proliferation, invasion, and radioresistance," *Cancer medicine*, vol. 7, no. 5, pp. 2048–2063, 2018.

[20] F. Tao, Y. Xu, D. Yang et al., "LncRNA NKILA correlates with the malignant status and serves as a tumor-suppressive role in rectal cancer," *Journal of Cellular Biochemistry*, vol. 119, no. 12, pp. 9809–9816, 2018.

[21] X.-J. Lin, C.-L. He, T. Sun, X.-J. Duan, Y. Sun, and S.-J. Xiong, "hsa-miR-485-5p reverses epithelial to mesenchymal transition and promotes cisplatin-induced cell death by targeting PAK1 in oral tongue squamous cell carcinoma," *International Journal of Molecular Medicine*, vol. 40, no. 1, pp. 83–89, 2017.

[22] X. Gai and L. Li, "Overexpression of long noncoding RNAs (lncRNA) NF-$\kappa\beta$-Interacting long noncoding RNA (NKILA) in ankylosing spondylitis is correlated with transforming growth factor β1 (TGF-β1), active disease and predicts length of treatment," *Medical Science Monitor*, vol. 25, pp. 4244–4249, 2019.

[23] Y. Pan, J. Qin, H. Sun, T. Xu, S. Wang, and B. He, "MiR-485-5p as a potential biomarker and tumor suppressor in human colorectal cancer," *Biomarkers in Medicine*, vol. 14, no. 3, pp. 239–248, 2020.

[24] S. Liao, C. Yu, H. Liu, C. Zhang, Y. Li, and X. Zhong, "Long non-coding RNA H19 promotes the proliferation and invasion of lung cancer cells and regulates the expression of E-cadherin, N-cadherin, and vimentin," *OncoTargets and Therapy*, vol. 12, pp. 4099–4107, 2019.

[25] Y. Li, T. Zhang, S. Qin et al., "Effects of UPF1 expression on EMT process by targeting E-cadherin, N-cadherin, vimentin and twist in a hepatocellular carcinoma cell line," *Molecular Medicine Reports*, vol. 19, no. 3, pp. 2137–2143, 2019.

Hindawi
Journal of Oncology
Volume 2021, Article ID 2341719, 8 pages
https://doi.org/10.1155/2021/2341719

Research Article

High Expression of ROMO1 Aggravates the Malignancy of Hepatoblastoma

Jiangfeng Lv,[1] **Yan Wu**,[2] **Wei Li**,[3] **and Huaping Fan**[4]

[1]*Department of Clinical Laboratory, Jinan City People's Hospital, Jinan People's Hospital Affiliated to Shandong First Medical University, Jinan, Shandong 271199, China*
[2]*Department of Clinical Laboratory, Yantai Yuhuagding Hospital Affiliated to Qingdao University, Yantai, Shandong 264000, China*
[3]*Department of Oncology (II), Qingdao Central Hospital Affiliated to Qingdao University, Qingdao, Shandong 266042, China*
[4]*Department of Pediatrics, Yantai Maternal and Child Health Care Hospital, Yantaishan Hospital, Yantai, Shandong 264000, China*

Correspondence should be addressed to Huaping Fan; yibi41758@163.com

Received 14 June 2021; Accepted 20 August 2021; Published 1 September 2021

Academic Editor: Alamgeer Yuchi

Hepatoblastoma (HB) is a kind of tumor that occurs frequently in children and is highly malignant. Here, the function of ROS modulator 1 (ROMO1) was identified in the development of HB. In this study, the mRNA expression of ROMO1 was measured by RT-qPCR. Colony formation assay, MTT assay, and flow cytometric analysis were applied to detect cell viability. The cell migrative and invasive ability was measured by wound healing and transwell assays. Tumor xenografts were performed to examine tumor growth. The results showed that upregulation of ROMO1 was identified in liver hepatocellular carcinoma (LIHC) tissues and predicted poor prognosis in LIHC patients. And ROMO1 expression was also increased in HB tissues and cells. Functionally, ROMO1 knockdown restrained cell viability, migration, and invasion in HB. In addition, knockdown of ROMO1 was found to suppress tumor formation *in vivo*. In conclusion, upregulation of ROMO1 promotes tumor growth and cell aggressiveness in HB.

1. Introduction

Hepatoblastoma (HB) develops from hepatocyte precursor cells and is a malignant embryonic tumor with multiple differentiation modes [1]. The cause of HB is not clear. Some genetic diseases and congenital factors may be related to the occurrence of HB [2]. HB is the most common liver malignant tumor in children, accounting for 90% of the primary malignant tumors of the liver in children. The incidence of HB is about 0.7 to 1/100 million, and the male-to-female ratio is approximately (1.5 to 2) : 1 [3]. Infants and young children, especially those who have been infected with hepatitis B virus, have an increased risk of HB [4]. Additionally, the early symptoms of HB are not obvious, and the child usually looks good. After that, the tumor grows rapidly, and an abdominal mass may appear, which is the most common symptom of HB [5]. The treatment of HB is mainly surgery combined with chemotherapy. If the patient is actively treated, the overall survival rate of HB is about 80%, and the prognosis is good [6]. Therefore, early detection, early diagnosis, and early treatment are extremely important for improving the survival rate of patients with HB.

In the past few years, many RNAs and genes have been found to be involved in the development of HB. For example, microRNA-26-5p functioned as a new inhibitor of HB by repressing the LIN28B-RAN-AURKA pathway [7]. LncRNA CRNDE promoted the angiogenesis of HB by regulating the miR-203/VEGFA axis [8]. Circ-STAT3 promoted HB progression through acting as a sponge for miR-29a/b/c-3p [9]. In addition, DPEP1 has been reported to promote HB progression by the PI3K/Akt/mTOR pathway [10]. In this study, the role of ROMO1 in HB was investigated.

ROS modulator 1 (ROMO1) is well known to regulate intracellular ROS production. And in many human cancers,

the important role of ROMO1 has been found. For example, ROMO1 predicted unfavorable prognosis in colorectal cancer patients [11]. And ROMO1 was also found to regulate ROS production and cellular growth in gliomas [12]. In addition, it has been reported that ROMO1 overexpression predicted worse survival in patients with NSCLC [13]. More importantly, overexpression of ROMO1 was found to promote the production of ROS and hepatic tumor cell invasion [14]. However, the function of ROMO1 in HB has not been reported in previous studies.

To investigate whether ROMO1 is involved in the pathogenesis of HB, the expression of ROMO1 in HB tissues and cells was examined. At the same time, the effect of ROMO1 on tumor growth and cell aggressiveness was also identified in HB. ROMO1 may be a potential biological target for HB.

2. Materials and Methods

2.1. Clinical Samples. HB tissues and adjacent normal tissues were collected from 18 patients in Yantai Maternal and Child Health Care Hospital, Yantaishan Hospital, between January 2014 and December 2020. The average age of these patients was 4.8 years between 2 and 9 (from 2 to 9 years old). Among them, there were 11 male and 7 female patients. Written informed consent was obtained from every patient or their direct relatives. Our research was approved by the Ethics Committee of Yantai Maternal and Child Health Care Hospital, Yantaishan Hospital.

2.2. Bioinformatics Analysis of ROMO1. The expression of ROMO1 in human cancers was analyzed in the GEPIA (http://gepia.cancer-pku.cn/) database. The expression level and prognosis of ROMO1 in liver hepatocellular carcinoma (LIHC) were analyzed by box plots and survival plots.

2.3. Cell Cultures. Normal hepatocyte cell lines LO2 and HepG2 and HuH-6 HB cells were purchased from the Chinese Academy of Sciences Cell Bank. LO2 and HuH-6 cells were incubated in the DMEM medium with 10% FBS at 37°C under an atmosphere with 5% CO_2.

2.4. Cell Transfection. ROMO1 siRNAs (si-ROMO1) and negative control (si-NC) were purchased from RiboBio (Guangzhou, China). For *in vitro* experiments, si-ROMO1 and si-NC were transfected into HuH-6 cells using Lipofectamine 3000 (Invitrogen, CA, USA). For *in vivo* experiments, ROMO1 knockdown lentivirus (sh-ROMO1) and empty lentivirus control (Mock) were constructed into HuH-6 cells.

2.5. RT-qPCR. Total RNA of ROMO1 was isolated from HB tissues and cells by TRIzol reagent (Invitrogen, CA, USA). cDNA was synthesized using the High-Capacity cDNA Reverse Transcription Kit (Applied Biosystems, CA, USA). RT-qPCR assay was performed on the StepOnePlus Real-Time PCR System by using the Power SYBR Green PCR Master Mix (Applied Biosystems). GAPDH was an internal control. ROMO1 expression was analyzed using the $2^{-\triangle\triangle Cq}$ method.

2.6. MTT Assay. The transfected HuH-6 cells were reseeded in a 96-well plate (4×10^3 cells/well). MTT solution (0.5 mg/ml) was used to incubate these cells based on the MTT assay. The absorbance was detected at 490 nm with a spectrophotometer.

2.7. Colony Formation Assay. The transfected HuH-6 cells were seeded into 6-well plates (4×10^3 cells/well). Next, the cells were cultured in a cell incubator for 10 days. Then, the colonies were fixed with 4% paraformaldehyde and stained with 0.1% crystal violet. Finally, cell colonies were counted and photographed.

2.8. Flow Cytometric Analysis. Annexin V-FITC/propidium iodide Apoptosis Detection Kit I (BD Biosciences, Franklin Lakes, NJ, USA) was used to detect apoptotic cells. In brief, 0.25% EDTA-free trypsin was added to digest HuH-6 cells. Then, the cells were resuspended in 100 mL binding buffer. Next, 5 ml Annexin V-FITC and PI were added to incubate these cells for 30 min at 37°C in the dark. Finally, flow cytometry (Becton, Dickinson and Company, CA, USA) was applied to measure the apoptotic cells.

2.9. Wound Healing Assay. HuH-6 cells (4×10^5 cells/well) were seeded into six-well plates. After reaching 90% confluence, a 1 mm-wide wound was made by a 200 mL sterile needle tip. The wound area was measured and photographed under a microscope every 24 h.

2.10. Transwell Assay. Transwell chamber (10 μm pore membrane, BD Biosciences) was used to assess the cell migrative and invasive ability. The transfected HuH-6 cells (5×10^3 cells/well) were added to the upper chamber. DMEM medium with 20% FBS was added in the bottom well. After 24 h, HuH-6 cells in the chamber were fixed with methanol for 30 min and stained with crystal violet for 15 min. Migrated cells were observed and counted under a light microscope. For cell invasion, Matrigel (BD Biosciences) was added in the top side of the upper chamber. Besides this, the whole experiment was similar to the cell migration method.

2.11. Tumor Xenografts. The male BALB/c nude mice (4–6 weeks) were obtained from Beijing Vital River Laboratory (Beijing, China). HuH-6 cells with sh-ROMO1 and Mock were subcutaneously injected into the lower flank of nude mice. Tumor growth was detected every 4 days. Mice were euthanized after 28 days. Finally, tumors were dissected and weighed. Before this study, the Animal Health Committee of Yantai Maternal and Child Health Care Hospital, Yantaishan Hospital, approved this experiment.

2.12. Statistical Analysis. GraphPad Prism 6 software was used for statistical analysis. Data were expressed as mean ± SD. Difference was analyzed by Student's *t*-test or one-way ANOVA, with the significant level specified as $P < 0.05$.

3. Results

3.1. Upregulation of ROMO1 Is Identified in LIHC Tissues and Predicts Poor Prognosis in Liver Hepatocellular Carcinoma (LIHC) Patients. First, the expression of ROMO1 in different human cancers was analyzed by using the GEPIA database (TCGA and GTEX). We found that ROMO1 expression was increased in most cancers ($P < 0.05$, Figure 1(a)). At the same time, upregulation of ROMO1 was also found in LIHC tissues in comparison with normal tissues ($P < 0.05$, Figure 1(b)). In addition, LIHC patients with higher ROMO1 expression were found to have lower overall survival (OS) and disease-free survival (DFS) than patients with low ROMO1 expression ($P < 0.05$, Figures 1(c) and 1(d)). These results demonstrate that ROMO1 is upregulated in LIHC tissues. And upregulation of ROMO1 predicts poor prognosis in LIHC patients.

3.2. ROMO1 Expression Is Also Increased in HB Tissues and Cells. Although the expression of ROMO1 in LIHC is known, the alternation of ROMO1 expression in HB remains unclear. Thus, ROMO1 mRNA expression was detected in 18 HB tissues in our study. Compared with normal tissues, upregulation of ROMO1 was detected in HB tissues ($P < 0.05$, Figure 2(a)). In addition, ROMO1 expression in HB cells was also detected. Compared with normal hepatocyte cell line LO2, ROMO1 was upregulated in HuH-6 and HepG2 HB cells ($P < 0.05$, Figure 2(b)). Based on these results, we infer that ROMO1 may be involved in the pathogenesis of HB. We also found that the difference of ROMO1 expression in HuH-6 cells was more significant than HepG2 cells (Figure 2(b)). Therefore, HuH-6 was selected to explore the function of ROMO1 in HB.

3.3. Knockdown of ROMO1 Restrains Cell Viability in HB. Next, si-ROMO1 or si-NC was transfected into HuH-6 cells. RT-qPCR showed that ROMO1 expression in the si-ROMO1 group was reduced in comparison with the si-NC group ($P < 0.01$, Figure 3(a)). Functionally, ROMO1 downregulation suppressed cell proliferation in HuH-6 cells compared to the si-NC group ($P < 0.01$, Figure 3(b)). Meanwhile, we found that the colony-forming ability of HuH-6 cells was reduced after ROMO1 knockdown ($P < 0.05$, Figure 3(c)). To further explore the effect of ROMO1 on cell viability, flow cytometric analysis was performed to detect cell apoptosis. Compared with the si-NC group, knockdown of ROMO1 significantly promoted apoptosis of HuH-6 cells ($P < 0.05$, Figure 3(d)). In brief, knockdown of ROMO1 restrains cell proliferation and induces apoptosis in HB.

3.4. Downregulation of ROMO1 Decreases the Cell Migrative and Invasive Ability in HB. To investigate how ROMO1 regulates cell migration and invasion, transwell and wound healing assays were performed in HuH-6 cells. We found that the scratch healing ability of HuH-6 cells in the si-ROMO1 group was reduced in comparison with the si-NC group ($P < 0.05$, Figure 4(a)). It indicates that downregulation of ROMO1 can decrease the cell migrative ability of HB cells. In the meantime, transwell assay also showed the same results ($P < 0.01$, Figure 4(b)). In addition, transwell assay also suggested that ROMO1 knockdown significantly restrained cell invasion in HuH-6 cells ($P < 0.01$, Figure 4(c)). All these results revealed that ROMO1 silencing can decrease the cell migrative and invasive ability in HB.

3.5. Downregulation of ROMO1 Suppresses Tumor Growth of HB In Vivo. Finally, HuH-6 cells with sh-ROMO1 were injected into nude mice to explore the effect of ROMO1 on tumor growth in HB. We found that tumor growth, as shown by tumor volumes at different time points, was suppressed in the sh-ROMO1 group compared to the Mock group ($P < 0.05$, Figure 5(a)). At the same time, tumor weight in the sh-ROMO1 group was lower than that in the Mock group ($P < 0.01$, Figures 5(b) and 5(c)). The *in vivo* experiment indicates that knockdown of ROMO1 can restrain the tumor formation of HB.

4. Discussion

HB accounts for approximately 62% of primary liver malignancies in children. And HB is highly malignant and can be widely metastasized through blood and lymphatic pathways [15]. The first choice of HB treatment is surgical resection, and comprehensive treatment such as corresponding chemotherapy can also be used after the operation [16]. Moreover, the development of HB is slow. When HB is discovered, the tumor is already large. It is difficult to perform operation, and the prognosis of HB is poor [17]. Therefore, the development of new molecular markers for early detection of HB is very important.

Here, we found that ROMO1 was upregulated in LIHC tissues. Upregulation of ROMO1 predicted poor prognosis in LIHC patients. Based on the above results, we speculate that ROMO1 may be involved in the tumorigenesis of HB. As we predicted, upregulation of ROMO1 was also found in HB tissues and cells. Similar to our results, increased expression of ROMO1 was also identified in other cancers, such as bladder cancer [18] and glioblastoma [19]. In addition, it has been reported that high ROMO1 expression predicted unfavorable prognosis and lymphatic metastasis in NSCLC patients [20]. More importantly, ROMO1 has been reported to be a novel potential target for cancer diagnosis and treatment [21]. To investigate whether ROMO1 regulates the tumorigenesis of HB, both *in vitro* and *in vivo* experiments were performed.

Our study demonstrated that ROMO1 knockdown restrained cell proliferation and induced apoptosis in HB. Similar to our results, upregulation of ROMO1 was also

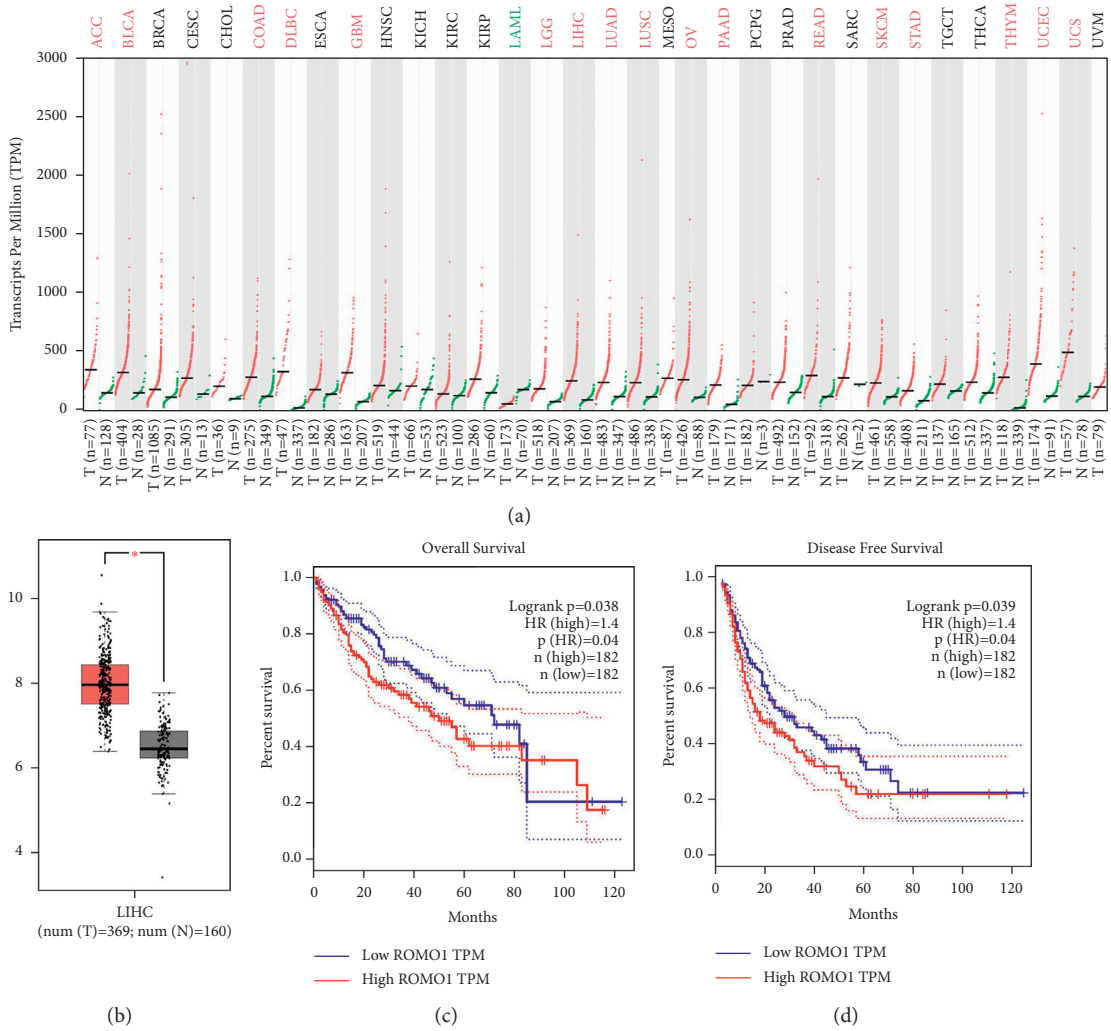

Figure 1: Upregulation of ROMO1 is identified in LIHC tissues and predicts poor prognosis in LIHC patients. (a) ROMO1 expression in human cancers was analyzed in the GEPIA database. (b) ROMO1 expression in LIHC tissues. (c, d) Analysis of OS and DFS rates in LIHC patients with high or low ROMO1 expression. $^{*}P < 0.05$.

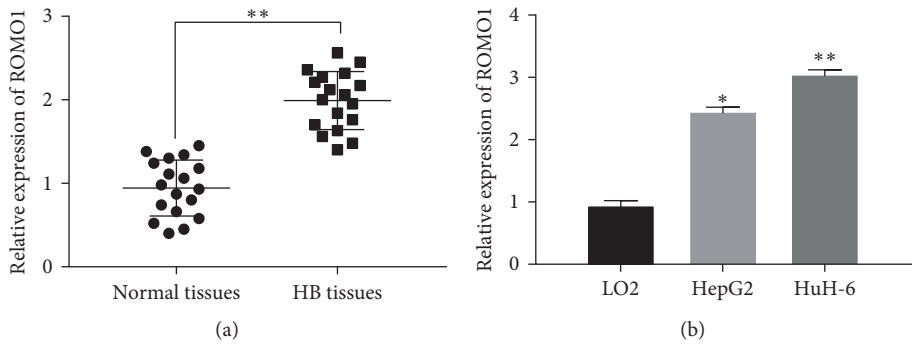

Figure 2: ROMO1 expression is also increased in HB tissues and cells. (a) ROMO1 expression was detected in HB tissues and normal tissues by RT-qPCR. (b) ROMO1 expression was detected in normal hepatocyte cell lines LO2 and HepG2 and HuH-6 HB cells. $^{*}P < 0.05$ and $^{**}P < 0.01$.

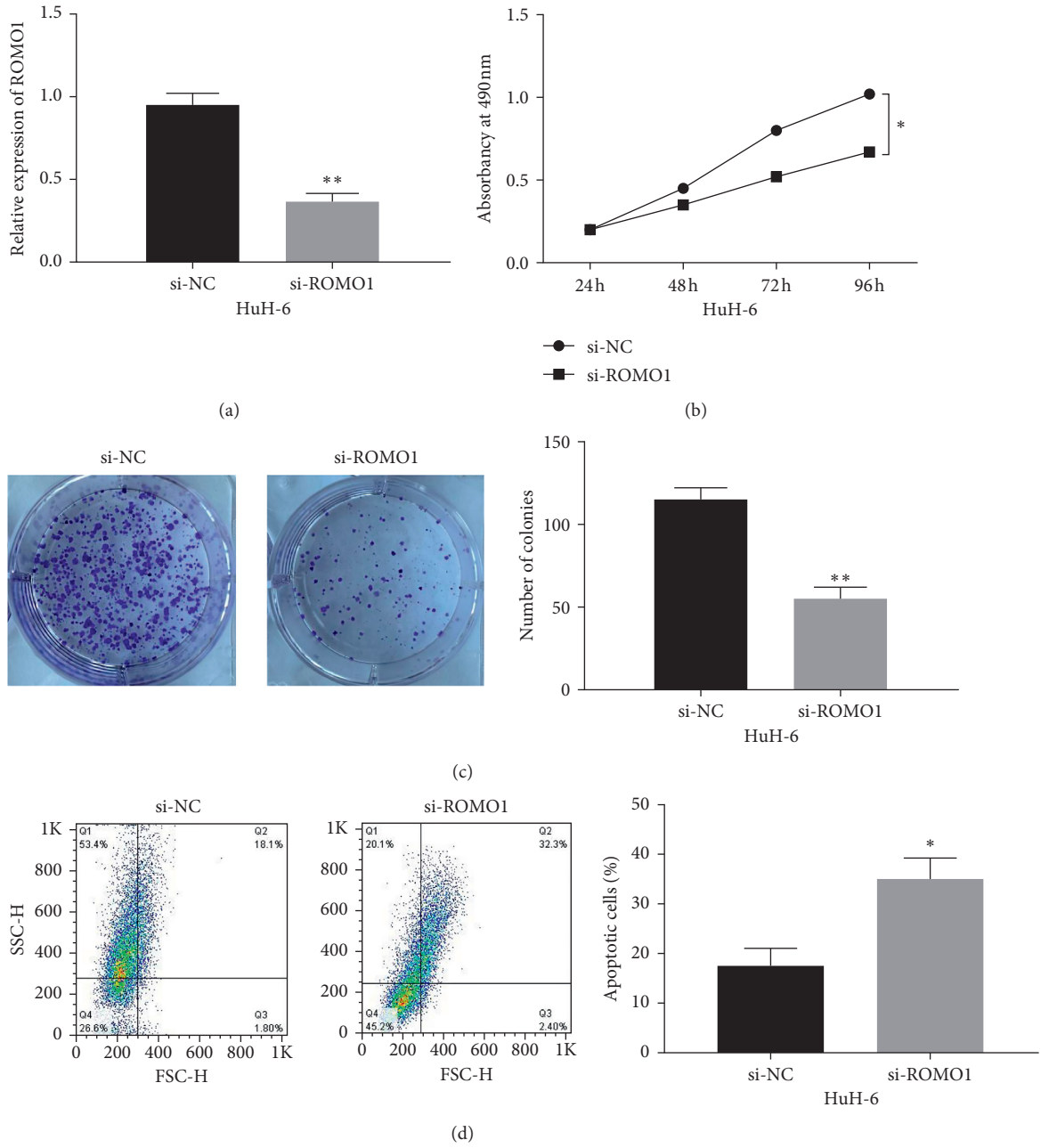

Figure 3: Knockdown of ROMO1 restrains cell viability in HB. (a) ROMO1 expression was detected in HuH-6 cells with si-ROMO1 or si-NC. (b) Cell proliferation was detected by the MTT assay in HuH-6 cells with si-ROMO1 or si-NC. (c) Colony-forming ability was assessed in HuH-6 cells with si-ROMO1 or si-NC. (d) Annexin V-FITC/PI flow cytometry was used to evaluate apoptosis in HuH-6 cells with si-ROMO1 or si-NC. $^{*}P < 0.05$ and $^{**}P < 0.01$.

found to promote cellular growth in human gliomas [12]. And ROMO1 inhibition induced TRAIL-mediated apoptosis in colorectal cancer [22]. In addition, downregulation of ROMO1 decreased the cell migrative and invasive ability in HB. Lee et al. also reported that ROMO1 and the NF-κB pathway can regulate tumor cell invasion induced by oxidative stress [23]. However, the relationship between ROMO1 and the NF-κB pathway in HB has not been investigated in this study, which needs to be explained in the future. Besides the above results, our study revealed that knockdown of ROMO1 suppressed HB tumor formation *in vivo*. The result has not been found in previous studies.

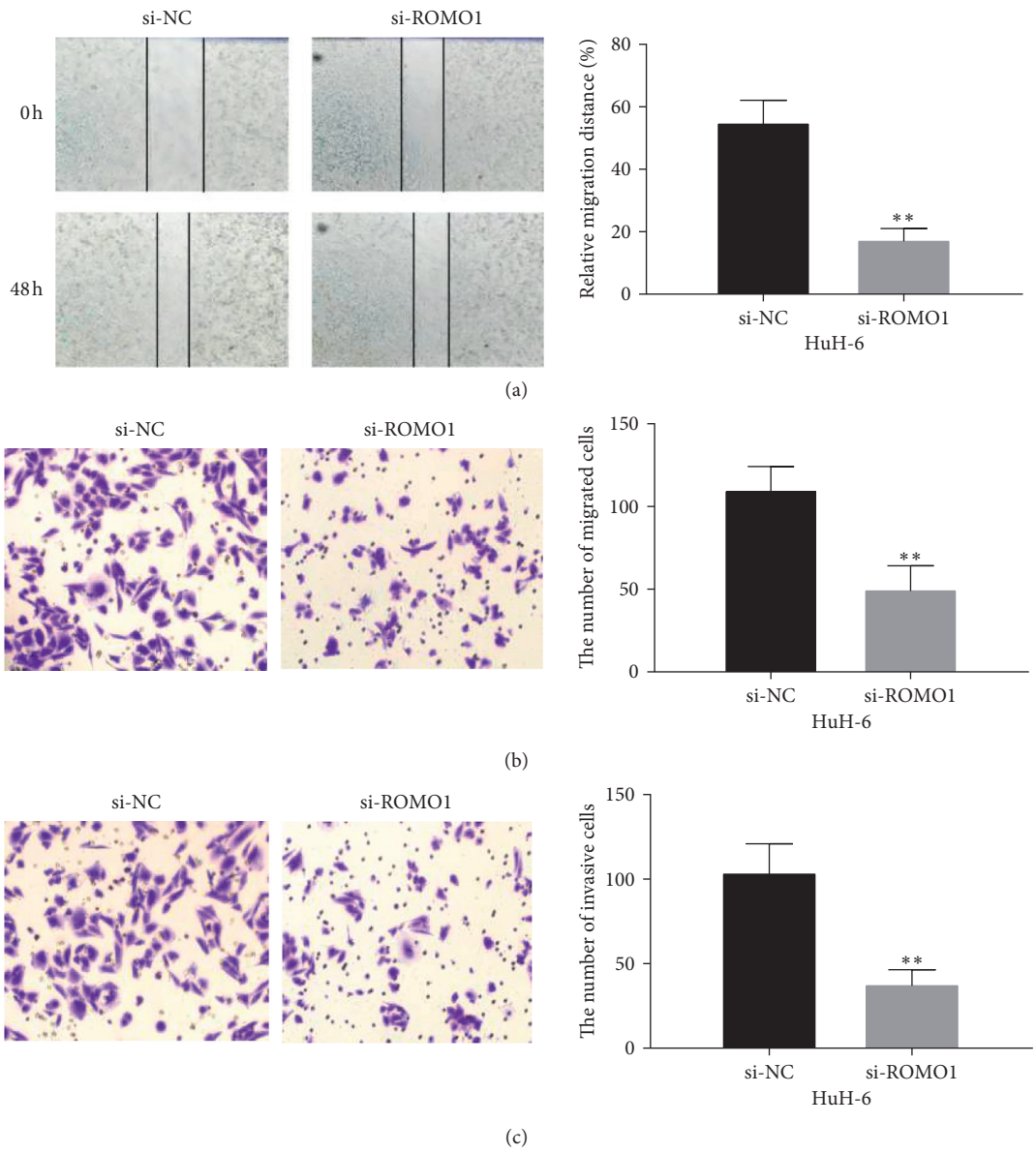

Figure 4: Downregulation of ROMO1 decreases the cell migrative and invasive ability in HB. (a) Wound healing assay showed HuH-6 cell migration capability in the si-ROMO1 or si-NC group. (b, c) Cell migration and invasion were detected in HuH-6 cells with si-ROMO1 or si-NC by the transwell assay. $^{**}P < 0.01$.

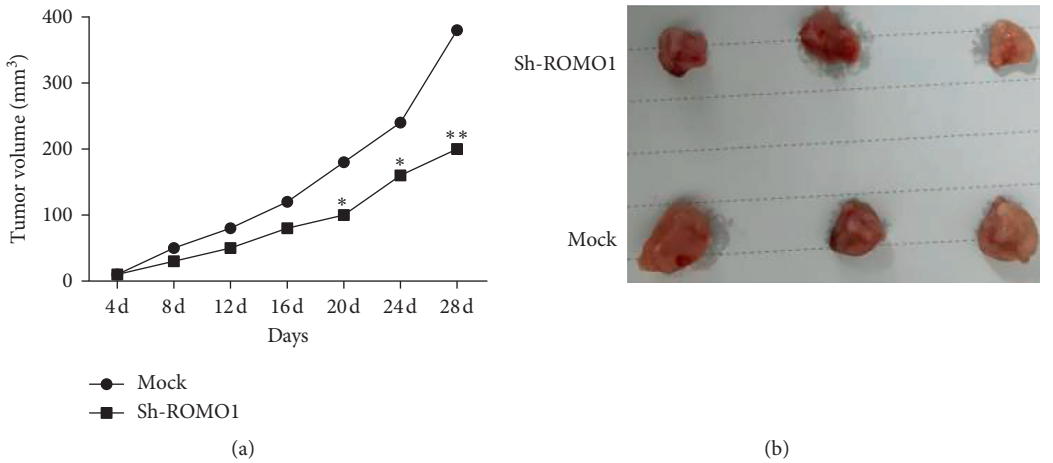

Figure 5: Continued.

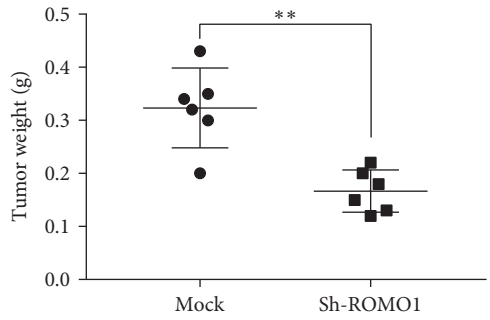

Figure 5: Knockdown of ROMO1 suppresses tumor formation *in vivo*. (a) Tumor size was detected every 4 d. (b) Representative HB tumors at 28 d. (c) Tumor weights were measured in the sh-ROMO1 and Mock group at 28 d. $^{*}P < 0.05$ and $^{**}P < 0.01$.

5. Conclusion

Similarly, upregulation of ROMO1 is found in LIHC and predicts poor prognosis in LIHC patients. High expression of ROMO1 is also identified in HB, and it acts as a tumor promoter in the development of HB. Our study provides a potential target for the diagnosis and treatment of HB. However, future investigation is still needed to explain the underlying mechanisms of ROMO1 in HB.

Data Availability

The datasets used and/or analyzed during the present study are available from the corresponding author upon reasonable request.

Disclosure

Jiangfeng Lv and Yan Wu are the co-first authors.

Conflicts of Interest

The authors declare that they have no conflicts of interest.

Authors' Contributions

Jiangfeng Lv and Yan Wu contributed equally to this work.

References

[1] G. E. Tomlinson and R. Kappler, "Genetics and epigenetics of hepatoblastoma," *Pediatric Blood and Cancer*, vol. 59, no. 5, pp. 785–792, 2012.

[2] Y.-T. Zhang, L.-H. Feng, X.-D. Zhong, L.-Z. Wang, and J. Chang, "Vincristine and irinotecan in children with relapsed hepatoblastoma: a single-institution experience," *Pediatric Hematology & Oncology*, vol. 32, no. 1, pp. 18–25, 2015.

[3] B. Haeberle, A. Rangaswami, M. Krailo et al., "The importance of age as prognostic factor for the outcome of patients with hepatoblastoma: analysis from the Children's Hepatic tumors International Collaboration (CHIC) database," *Pediatric Blood & Cancer*, vol. 67, Article ID e28350, 2020.

[4] F. X. Bosch, J. Ribes, M. Díaz, and R. Cléries, "Primary liver cancer: worldwide incidence and trends," *Gastroenterology*, vol. 127, no. 5, pp. S5–S16, 2004.

[5] A. D. Trobaugh-Lotrario, R. L. Meyers, A. F. O'Neill, and J. H. Feusner, "Unresectable hepatoblastoma: current perspectives," *Hepatic Medicine: Evidence and Research*, vol. 9, pp. 1–6, 2017.

[6] D. Aronson, P. Czauderna, R. Maibach, G. Perilongo, and B. Morland, "The treatment of hepatoblastoma: its evolution and the current status as per the SIOPEL trials," *Journal of Indian Association of Pediatric Surgeons*, vol. 19, no. 4, pp. 201–207, 2014.

[7] Y. Zhang, Y. Zhao, J. Wu, S. Liangpunsakul, J. Niu, and L. Wang, "MicroRNA-26-5p functions as a new inhibitor of hepatoblastoma by repressing lin-28 homolog B and aurora kinase a expression," *Hepatology Communications*, vol. 2, no. 7, pp. 861–871, 2018.

[8] L.-J. Chen, M.-X. Yuan, C.-Y. Ji et al., "Long non-coding RNA CRNDE regulates angiogenesis in hepatoblastoma by targeting the MiR-203/VEGFA Axis," *Pathobiology*, vol. 87, no. 3, pp. 161–170, 2020.

[9] Y. Liu, J. Song, Y. Liu, Z. Zhou, and X. Wang, "Transcription activation of circ-STAT3 induced by Gli2 promotes the progression of hepatoblastoma via acting as a sponge for miR-29a/b/c-3p to upregulate STAT3/Gli2," *Journal of Experimental & Clinical Cancer Research*, vol. 39, no. 1, p. 101, 2020.

[10] X. Cui, X. Liu, Q. Han et al., "DPEP1 is a direct target of miR-193a-5p and promotes hepatoblastoma progression by PI3K/Akt/mTOR pathway," *Cell Death & Disease*, vol. 10, no. 10, p. 701, 2019.

[11] H. J. Kim, M. J. Jo, B. R. Kim et al., "Reactive oxygen species modulator-1 (Romo1) predicts unfavorable prognosis in colorectal cancer patients," *PloS One*, vol. 12, no. 5, Article ID e0176834, 2017.

[12] M. O. Yu, N.-H. Song, K.-J. Park et al., "Romo1 is associated with ROS production and cellular growth in human gliomas," *Journal of Neuro-Oncology*, vol. 121, no. 1, pp. 73–81, 2015.

[13] S. H. Lee, J. W. Min, J. S. Lee et al., K. H. In, Reactive oxygen species modulator 1 (Romo1) overexpression is an independent predictor of poor survival in NSCLC patients who undergo surgical resection," *Lung Cancer*, vol. 87, pp. 45–52, 2015.

[14] J. S. Chung, S. Park, S. H. Park et al., "Overexpression of Romo1 promotes production of reactive oxygen species and invasiveness of hepatic tumor cells," *Gastroenterology*, vol. 143, pp. 1084–1094, 2012.

[15] W. Chen, R. Zheng, P. D. Baade et al., "Cancer statistics in China, 2015," *A Cancer Journal for Clinicians*, vol. 66, pp. 115–132, 2016.

[16] P. Czauderna, J. B. Otte, D. J. Roebuck, D. von Schweinitz, and J. Plaschkes, "Surgical treatment of hepatoblastoma in children," *Pediatric Radiology*, vol. 36, pp. 187–191, 2006.

[17] F. Bray and I. Soerjomataram, "The changing global burden of cancer: transitions in human development and implications for cancer prevention and control," in *Cancer: Disease Control Priorities*, H. Gelband, P. Jha, R. Sankaranarayanan, and S. Horton, Eds., vol. 3, 3rd Edition, 2015.

[18] Y. Yang, F. Zhang, H. Huang et al., "Long noncoding RNA LINC00319 regulates ROMO1 expression and promotes bladder cancer progression via miR-4492/ROMO1 axis," *Journal of Cellular Physiology*, vol. 235, pp. 3768–3775, 2020.

[19] G. Sun, Y. Cao, C. Qian et al., "Romo1 is involved in the immune response of glioblastoma by regulating the function of macrophages," *Aging*, vol. 12, pp. 1114–1127, 2020.

[20] H. J. Kim, M. J. Jo, B. R. Kim et al., "Overexpression of Romo1 is an unfavorable prognostic biomarker and a predictor of lymphatic metastasis in non-small cell lung cancer patients," *OncoTargets and Therapy*, vol. 11, pp. 4233–4246, 2018.

[21] M. A. Amini, S. S. Talebi, and J. Karimi, "Reactive oxygen species modulator 1 (ROMO1), a new potential target for cancer diagnosis and treatment," *Chonnam Medical Journal*, vol. 55, pp. 136–143, 2019.

[22] M. J. Jo, B. G. Kim, S. H. Park et al., "Romo1 inhibition induces TRAIL-mediated apoptosis in colorectal cancer," *Cancers*, vol. 12, 2020.

[23] S. Lee, Y. H. Park, J. S. Chung, and Y. D. Yoo, "Romo1 and the NF-kappaB pathway are involved in oxidative stress-induced tumor cell invasion," *International Journal of Oncology*, vol. 46, pp. 2021–2028, 2015.

Hindawi
Journal of Oncology
Volume 2021, Article ID 8114327, 5 pages
https://doi.org/10.1155/2021/8114327

Research Article

Involvement of *TRPC7-AS1* Expression in Hepatitis B Virus-Related Hepatocellular Carcinoma

Shaoliang Zhu,[1] Hang Ye,[1] Xiaojie Xu,[1] Weiru Huang,[1] Ziyu Peng,[1] Yingyang Liao,[2] and Ningfu Peng[1]

[1]*Department of Hepatobiliary Surgery, Guangxi Medical University Cancer Hospital, Nanning 530021, China*
[2]*Department of Clinical Nutrition, Guangxi Medical University Cancer Hospital, Nanning 530021, China*

Correspondence should be addressed to Ningfu Peng; pengnfu2020@163.com

Received 28 June 2021; Accepted 30 July 2021; Published 1 September 2021

Academic Editor: Muhammad Wasim Khan

Objective. To investigate the expression of transient receptor potential (TRP) superfamily genes, especially *TRPC7-AS1* in hepatitis B virus- (HBV-) related hepatocellular carcinoma (HCC). *Methods*. Three cancer samples of HBV-related HCC at phase IV and matched paracancerous liver tissues were included in the study. Total RNA was extracted, and differential expression of RNA was screened by high-throughput transcriptome sequencing. The expression of *TRPC7-AS1* was detected by quantitative real-time PCR. The N6-adenosyl methylation RNA in MHCC97H, HepG2, and HL-7702 was enriched by coimmunoprecipitation with m6A antibody, and the relative level of N6-adenosyl methylation RNA in *TRPC7-AS1* was detected. *Results*. The expression of TRP family genes in cancer tissues was higher than that in paracancerous liver tissues, including *TRPC7-AS1*, *TRPC4AP*, *PKD1P6*, and *PKD1P1*. Moreover, the expression level of *TRPC7-AS1* in MHCC97H and HepG2 was also significantly higher than that in L02, a normal liver cell. The methylation level of N6-adenosine of *TRPC7-AS1* was lower in HepG2 cells than that in L02 cells. *Conclusion*. TRP superfamily genes, especially *TRPC7-AS1*, were highly expressed in HBV-related HCC. *TRPC7-AS1* could be a potential therapeutic target or diagnostic marker for HCC.

1. Introduction

Transient receptor potential (TRP) ion channel is a transmembrane protein, which plays key roles in mechanical injury, pain, temperature perception, and osmotic pressure perception by changing cell membrane potential or intracellular calcium concentration [1–4]. According to homology, the TRP ion channel family genes in mammals can be divided into six subgroups: TRP canonical (TRPC), TRP vanilloid (TRPV), TRP melastatin (TRPV), TRP ankyrin (TRPA), TRP mucolipin (TRPML), and TRP polycrystalline (TRPP). Among them, the first four subgroups belong to one class, and the latter two subgroups are classified as one group [5]. It has been reported that the dysfunction of the TRP ion channel (TRPV4, TRPV1, TRPM4, and TRPM) is considered to be related to obesity or diabetes, and these disorders are related to appetite, insulin secretion, and autoimmune response [6–10].

The downstream of the TRP ion channel family has a function in cell proliferation and is also considered to be related to cancer development (ref). TRPC6 was reported to be upregulated in glioblastoma, while TRPV2 was highly expressed in ovarian cancer [11, 12]. However, the involvement of TRP family genes in hepatocellular carcinoma (HCC) is still rarely reported.

In this study, the paracancerous tissues and the corresponding cancer tissues of three patients with stage IV hepatitis B virus- (HBV-) related HCC were taken as samples for high-throughput transcriptome sequencing. The expression levels of TRP family genes were analyzed, especially *TRPC7-AS1*. Additionally, the level of N6 adenosine methylation in HCC was also detected. This study would

provide a potential therapeutic target or diagnostic marker for HBV-related HCC.

2. Materials and Methods

2.1. Patients. The paracancerous tissues and corresponding cancer tissues of three patients with phase IV HBV-related HCC were provided by Hepatobiliary Surgery, Cancer Hospital Affiliated to Guangxi Medical University. HepG2 cells (SCSP-510), HL-7702 cells (GNHu 6), and MHCC97H cells (SCSP-528) were provided by Cell Bank of Chinese Academy of Sciences (Shanghai, China). The study was approved by the Ethics Committee of Guangxi Medical University Cancer Hospital.

2.2. High-Throughput Sequencing. The paracancerous tissues and corresponding cancer tissues of three patients with stage IV HBV-related HCC were frozen, and the high-throughput sequencing was conducted by Shanghai Sangon Biotechnology Co., Ltd. (Shanghai, China) as previously described (ref).

2.3. Fluorescence Quantitative PCR. HepG2 cells, HL-7702 cells, and MHCC97H cells were cultured in DMEM supplied with 10% FBS (ThermoFisher, Massachusetts, USA). All cells were purchased from Wuhan Shangen Biotechnology Co., Ltd. (Wuhan, China). RNA was extracted from the cells in logarithmic growth using the ultrapure RNA extraction kit (CW0581M and CWBIO). After RNA was extracted, cDNA was synthesized according to the reverse transcription kit (CW2569M, CWBIO), and PCR reaction was carried out on the fluorescent quantitative PCR instrument with cDNA as template. The primers were synthesized by Shanghai Sangon Biotechnology Co., Ltd. (Shanghai, China). The primers included ENST00000514459F: 5′-GCCTCCTCCTTCCATAACG-3′, ENST00000514459R: 5′-CCCACAGCCTAGACCCATT-3'; GAPDH F: 5′-TGACTTCAACAGCGACACCCA-3′, and GAPDH R: 5′-TGACTTCAACAGCGACACCCA-3'.

2.4. RNA Coimmunoprecipitation (Co-IP). With RNase inhibitors (cat.no), 5×10^6 cells were lysed in 500 μL lysate, and the lysate was used as the sample for Co-IP. 100 μL of cell lysate was used as the input sample and another 100 μL of cell lysate also used mouse lgG (provided by kit) for Co-IP experiment to get the IgG sample. Another 100 μL cell lysate was incubated with m6A antibody (ab15123, Abcam, Cambridge, UK). The total RNA was extracted from the samples and reversely transcribed in the 50 μL system to obtain cDNA. The cDNA was used as template, and *TRPC7-AS1* was used as the index for fluorescence quantitative PCR detection.

2.5. Statistical Analysis. All the data were presented as mean and standard deviation and analyzed by one-way ANOVA followed by the post hoc test by SPSS 19.0, with $P < 0.05$ as the significant difference.

3. Results

3.1. Expression Abundance of TRP Family Genes in HBV-Related HCC. The paracancerous tissues (A1, A2, and A3) and the corresponding cancer tissues (B1, B2, and B3) of three patients with HBV-related HCC at stage IV were used as samples for high-throughput sequencing. The expression abundance of TRP family genes in the sample is shown in Figure 1. If TRP ion channel family genes were not detected in 4 or more samples, those genes are not shown in Figure 1, i.e., TRPC7 was not detected in 6 samples. The expression of TRP ion channel family genes in cancer tissue was higher than those in paracancerous tissue, and the expressions of TRPV6 (in B1 sample), TRPM4 (in B3 sample), TRPC1 (in B3 sample), and *PKD1P1* (in B2 sample) were significantly upregulated compared with those in paracancerous tissues.

The expression of TRP channel genes in cancer tissues was higher than those in paracancerous tissues.

The results of high-throughput sequencing showed that TRP ion channel-related genes, such as *TRPC7-AS1*, *TRPC4AP*, *PKD1P6*, and *PKD1P1*, were highly expressed in cancer tissues than those in paracancerous tissues (Table 1).

3.2. Expression Level of TRPC7-AS1 in MHCC97H, HepG2, and L02 Cell Lines. The PCR results of *TRPC7-AS1* (transcript ID: enst0000514459) in MHCC97H, HepG2, and L02 cells are shown in Figure 2. MHCC97H and HepG2 were hepatoma cell lines, while L02 was normal cell line. Compared with L02 cells, the expression level of *TRPC7-AS1* in MHCC97H and HepG2 was significantly upregulated.

3.3. The level of N6-Adenosyl Methylation (m6A) of TRPC7-AS1 in MHCC97H, HepG2, and L02 Cells. Through Co-IP with m6A antibody to enrich N6-adenosine methylation RNA in cells, the expression level of *TRPC7-AS1* was detected. Compared with the expression level of *TRPC7-AS1* in total RNA of the same amount of input samples, the relative level of N6 adenosine methylated in *TRPC7-AS1* was obtained (Figure 3, $P < 0.05$). The methylation level of N6 adenosine in *TRPC7-AS1* was lower in HepG2 cells than that in L02, but there was no significant difference between MHCC97H cells and L02 cells.

4. Discussion

In this study, we analyzed the expression abundance of TRP family genes in three cases of HBV-related HCC at stage IV. We found that the expression of TRP family genes in cancer tissues was higher than those in paracancerous tissues. In addition, we also found that TRP ion channel family genes (TRPV4, TRPV1, TRPM4, and TRPM5) related to obesity or diabetes were highly expressed in HBV-related HCC.

Compared with the paracancerous tissues, the high expression of TRPV4, low expression of TRPV1, and high expression of TRPM4 were found in HCC tissues, but TRPM 5 was not detected in 5 samples. The expression trends of TRPV1 and TRPM4 in the patients with diabetes are similar to the patients with obesity [6, 8]. TRPV4 has a regulatory

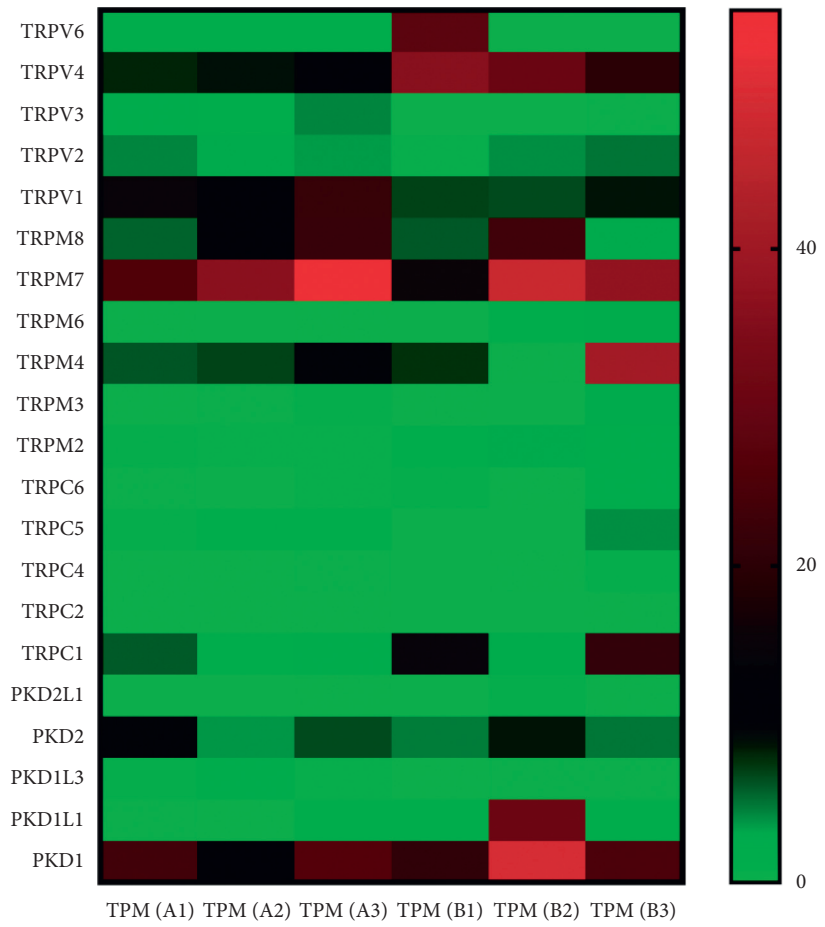

Figure 1: Expression abundance of TRP family genes in HBV-related HCC. Right side is the scale corresponding to the color and value. TPM, transcripts per million.

Table 1: The expression of TRP channel-related genes.

Gene name	Position	TPM (A1)	TPM (A2)	TPM (A3)	TPM (B1)	TPM (B2)	TPM (B3)	Gene description
TRPC7-AS1	5[+]136214048-136222159	0.00	0.00	0.00	24.65	1.98	6.89	TRPC7 antisense RNA 1
TRPC4AP	20[-]35002404-35092871	29.08	23.56	18.38	41.96	39.70	59.08	Transient receptor potential cation channel subfamily C member 4 associated protein
PKD1P6	16[-]15125242-15154564	14.68	12.48	15.99	17.64	43.34	22.32	Polycystin 1, transient receptor potential channel interacting pseudogene 6
PKD1P1	16[+]16310341-16334190	6.01	4.23	5.66	15.63	11.46	5.30	Polycystin 1, transient receptor potential channel interacting pseudogene 1 (source: HGNC Symbol; Acc: HGNC:30065)

effect on bodyweight and autoimmune inflammation, but whether it is positive or negative regulation is controversial [9, 10]. Diabetes is a risk factor of liver cancer, obesity, energy metabolism imbalance, and other states, which are indeed related to liver cancer [13]. Therefore, it can be inferred that the imbalance of TRP ion channel family gene expression is related to HCC.

We also found that the expression of TRP ion channel-related genes such as *TRPC7-AS1*, *TRPC4AP*, *PKD1P6*, and *PKD1P1* in cancer tissues was higher than those in adjacent tissues. Among them, the protein encoded by *TRPC4AP* gene is believed to be able to interact with TRPC ion channel and promote calcium release into cells, which is found to be related to Alzheimer's disease [14].

TRPC7-AS1, *PKD1P6*, and *PKD1P1* belong to lncRNA. More than 98% of the regions in human genome are noncoding regions. lncRNA is a kind of RNA which is widely transcribed but not translated to produce functional proteins. In recent years, lncRNA has been gradually found to play an important role in gene expression regulation [15]. *PKD1P6* and *PKD1P1* are pseudogenes of PKD1. Pseudogene is presumed to be a gene produced in the process of

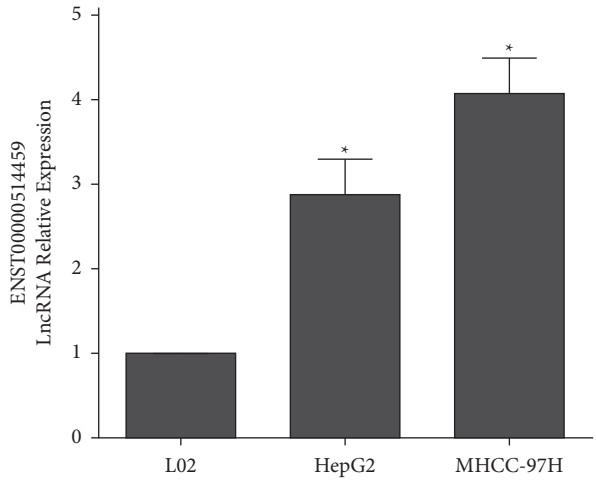

Figure 2: PCR results of *TRPC7-AS1* expression in L02, HepG2, and MHCC97H cells. Data are presented as mean and standard deviation. $^{*}P < 0.05$ vs. L02.

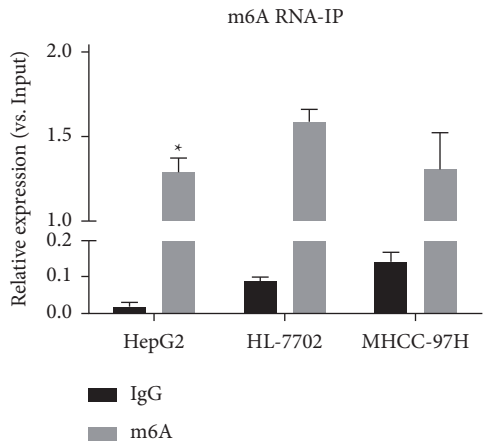

Figure 3: RNA Co-IP test results of the N6-adenosyl methylation (m6A) level of *TRPC7-AS1*. m6A: $^{*}p < 0.05$ vs. L02 cells.

tandem doubling, gene mutation, or gene recombination of the parent gene without effective coding. In recent years, studies have found that pseudogene often has a regulatory effect on the parent gene, and the expression of pseudogene varies significantly in different cells, which may be supposed as the diagnostic and prognostic markers of cancer [16, 17]. The expression of *TRPC7-AS1* in the antisense chain of the intron region of TRPC7 gene was selected for further study. TRPC7 gene itself has not been detected in high-throughput sequencing of liver cancer samples, which may indicate that *TRPC7-AS1* cannot regulate the expression of TRPC7 gene in liver cancer. In this study, we found that the expression level of *TRPC7-AS1* in hepatoma cell lines was significantly higher than that in normal hepatoma cell lines, which was consistent with the high-throughput sequencing results of hepatitis B-related hepatoma samples. It was also found that the methylation level of N6-adenosine in *TRPC7-AS1* was higher in normal hepatocytes than that in hepatoma cells.

N6-adenosyl methylation (m6A) is the most common type of RNA modification, which is involved in the regulation of RNA cutting, transport, and degradation. For lncRNA, the increased m6A level often means poor stability of the structure [18, 19]. Moreover, the genes such as mettl3 and FTO which can regulate m6A have been also reported to be involved in the occurrence and development of cancer such as liver cancer [20, 21]. *TRPC7-AS1* has a low level of m6A in hepatoma cells, which is consistent with the high expression of *TRPC7-AS1* in hepatoma tissues and cells. It can be inferred that regulating the expression of m6A-related genes can play a role in regulating *TRPC7-AS1*.

In conclusion, the expression of TRP family genes in HCC and the correlation between *TRPC7-AS1* and HCC can be concluded by analyzing the experimental results of this study. In the future, we will select more target genes and carry out relevant functional experiments to explore the regulatory mechanism of *TRPC7-AS1* in the target genes.

Data Availability

The data used to support the findings of this study are available from the corresponding author upon request.

Conflicts of Interest

The authors declare that they have no conflicts of interest.

Acknowledgments

This research was supported by the National Natural Science Foundation of China (81560460/H1602) and the Youth Foundation of Guangxi Medical University (GXMUSF201726).

References

[1] M. M. Moran, "TRP channels as potential drug targets," *Annual Review of Pharmacology and Toxicology*, vol. 58, no. 1, 2018.

[2] B. Nilius and G. Appendino, "Spices: the savory and beneficial science of pungency," *Reviews of Physiology, Biochemistry & Pharmacology*, vol. 164, pp. 1–76, 2013.

[3] A. Patapoutian, S. Tate, and C. J. Woolf, "Transient receptor potential channels: targeting pain at the source," *Nature Reviews Drug Discovery*, vol. 8, no. 1, pp. 55–68, 2009.

[4] F. Guilak, H. A. Leddy, and W. Liedtke, "Transient receptor potential vanilloid 4," *Annals of the new york Academy of Sciences*, vol. 1192, no. 1, pp. 404–409, 2010.

[5] A. Samanta, T. E. T. Hughes, and V. Y. Moiseenkova-Bell, "Transient receptor potential (TRP) channels," *Subcellular Biochemistry*, vol. 87, pp. 141–165, 2018.

[6] R. Vennekens, B. Nilius, and B. Colsoul, "Transient receptor potential (TRP) cation channels in diabetes," *Current Topics in Medicinal Chemistry*, vol. 13, no. 3, 2013.

[7] G. A. Kyriazis, M. M. Soundarapandian, and B. Tyrberg, "Sweet taste receptor signaling in beta cells mediates fructose-induced potentiation of glucose-stimulated insulin secretion," *Proceedings of the National Academy of Sciences of the united states of america*, vol. 109, no. 8, pp. E524–E532, 2012.

[8] N. J. Marshall, L. Liang, J. Bodkin et al., "A role for TRPV1 in influencing the onset of cardiovascular disease in obesity," *Hypertension*, vol. 61, no. 1, pp. 246–252, 2013.

[9] C. J. O'Conor, T. M. Griffin, W. Liedtke et al., "Increased susceptibility of trpv4-deficient mice to obesity and obesity-induced osteoarthritis with very high-fat diet," *Annals of the Rheumatic Diseases*, vol. 72, no. 2, 2012.
[10] Y. Li, K. Sandra, W. Jun et al., "TRPV4 is a regulator of adipose oxidative metabolism, inflammation, and energy homeostasis," *Cell*, vol. 151, no. 1, pp. 96–110, 2012.
[11] G. Santoni and V. Farfariello, "TRP channels and cancer: new targets for diagnosis and chemotherapy," *Endocrine, Metabolic & Immune Disorders - Drug Targets*, vol. 11, no. 1, 2011.
[12] S. George, V. 'y. Lehen'kyi, S. Roman et al., "TRP channels in cell survival and cell death in normal and transformed cells," *Cell Calcium*, vol. 50, no. 3, pp. 295–302, 2011.
[13] P. Wang, D. Kang, W. Cao et al., "Diabetes mellitus and risk of hepatocellular carcinoma: a systematic review and meta-analysis," *Diabetes/metabolism Research & Reviews*, vol. 28, no. 2, 2012.
[14] S. E. Poduslo, R. Huang, J. Huang, and S. Smith, "Genome screen of late-onset Alzheimer's extended pedigrees identifies TRPC4AP by haplotype analysis," *American Journal of Medical Genetics Part B: Neuropsychiatric Genetics*, vol. 150B, no. 1, pp. 50–55, 2009.
[15] W. Run and Y. Yao, "Cellular functions of long noncoding RNAs," *Nature Cell Biology*, 2019.
[16] L. Xiao-Jie, G. Ai-Mei, J. Li-Juan, and X. Jiang, "Pseudogene in cancer: real functions and promising signature," *Journal of Medical Genetics*, vol. 52, no. 1, pp. 17–24, 2015.
[17] P. Laura, M. Andrea, and P. Pier Paolo, "Pseudogenes in human cancer," *Frontiers of Medicine*, vol. 2, 2015.
[18] X. Wang, Z. Lu, A. Gomez et al., "N6-methyladenosine -dependent regulation of messenger RNA stability," *Nature*, 2014.
[19] B. Slobodin, R. Han, V. Calderone et al., "Transcription impacts the efficiency of mRNA translation via Co-transcriptional N6-adenosine methylation," *Cell*, vol. 169, no. 2, pp. 326–337, 2017.
[20] M. Chen, L. Wei, C.-T. Law et al., "RNA N6-methyladenosine methyltransferase-like 3 promotes liver cancer progression through YTHDF2-dependent posttranscriptional silencing of SOCS2," *Hepatology*, vol. 67, no. 6, pp. 2254–2270, 2018.
[21] G. Jia, Y. Fu, X. Zhao et al., "N6-Methyladenosine in nuclear RNA is a major substrate of the obesity-associated FTO," *Nature Chemical Biology*, vol. 7, no. 12, pp. 885–887, 2011.

Hindawi
Journal of Oncology
Volume 2021, Article ID 6147962, 9 pages
https://doi.org/10.1155/2021/6147962

Research Article

LncRNA SNHG7 Regulates Gastric Cancer Progression by miR-485-5p

Zhongsong Zhao and Xueping Liu

Department of Gastroenterology, Shandong Provincial Third Hospital, Cheeloo College of Medicine, Shandong University, Jinan 250031, China

Correspondence should be addressed to Xueping Liu; shuiccywlsd372@163.com

Received 2 June 2021; Accepted 20 August 2021; Published 31 August 2021

Academic Editor: Alamgeer Yuchi

Background. Long noncoding ribonucleic acids (lncRNAs) were closely related to the development of gastric cancer. This study investigated the effect of SNHG7 on gastric cancer progression and its potential molecular mechanism. *Methods*. SNHG7 and microRNA-485-5p (miR-485-5p) expressions in gastric cancer tissues and cells were detected by quantitative real-time polymerase chain reaction (qRT-PCR). Cell counting kit-8 (CCK-8), wound healing, and transwell experiments were used to detect cell proliferation, migration, and invasion. The dual luciferase reporter assay, RNA immunoprecipitation (RIP) experiment, and Pearson's correlation analysis were used to confirm the relationship between SNHG7 and miR-485-5p. *Results*. SNHG7 expression was increased in human gastric cancer tissues and cells. Knockdown of SNHG7 could notably inhibit the gastric cancer cells proliferation, migration, and invasion. The dual-luciferase reporter assay and RIP experiments proved that miR-485-5p was a direct target of SNHG7. At the same time, further experiments demonstrated that miR-485-5p inhibition reversed the suppression of SNHG7 knockdown on gastric cancer cells proliferation, migration, and invasion. *Conclusions*. SNHG7 knockdown could hamper gastric cancer progression via inhibiting miR-485-5p expression, providing a novel understanding for gastric cancer development.

1. Introduction

Gastric cancer is one of the most common malignant tumors of the digestive tract [1]. The incidence and death rate of gastric cancer have been decreasing in the past half century, but it is still the second deadliest cancer in the world [2]. Gastric cancer mainly originates from epithelial cells of the gastric mucosa and occurs in the gastric antrum and gastric pylorus [3]. The etiology of gastric cancer is complex, such as genetics, adverse environment, diet, *Helicobacter pylori* (HP) infection, and others [4]. The occurrence and development of gastric cancer are related to multiple factors and genes. Despite the continuous development of surgical techniques, new chemotherapeutic drugs, and a variety of new treatment options [5–8], the current treatment effect for gastric cancer is still limited. Therefore, a deeper understanding of the pathogenesis has great significance for the diagnosis and treatment of gastric cancer patients. At present, lncRNA has become a research focus of antitumor therapy, and its reports in gastric cancer are also increasing.

LncRNA is a class of RNA molecules in which transcripts are more than 200 nucleotides in length and cannot encode proteins [9]. LncRNA can participate in various intracellular signal regulation processes through chromatin modification, transcription activation or interference, and others [10]. Some studies have shown that dysregulation of lncRNA is closely related to gastric cancer invasion, migration, metastasis, prognosis, and et cetera [11, 12]. For example, Xu et al. suggested that ZFAS1 knockdown hampered malignant behavior of gastric cancer cells through the Wnt/β-catenin pathway [13]. XIST inhibition suppressed gastric cancer progression and metastasis through regulating miR-101/EZH2 [14]. CCAT2 overexpression accompanied poor prognosis and overall survival for gastric cancer patients [15].

SNHG7 located at 9q34.3 is a potential molecular marker for malignant tumors, such as pancreatic cancer, osteosarcoma, esophageal cancer, bladder cancer, colorectal cancer, and breast cancer, cervical cancer, as well as gastric cancer [16, 17]. Boone et al. reported that SNHG7 involved in the proliferation and apoptosis of breast cancer cells regulated by IGF1 [18]. Zhong et al. found SNHG7 was upregulated, and inhibition of SNHG7 expression could promote cell apoptosis and suppress cell proliferation and invasion in bladder cancer [19]. SNHG7 facilitated cell proliferation and invasion and closely related to poor prognosis in cervical cancer [20]. In esophageal cancer, SNHG7 repressed cell apoptosis and accelerated cell proliferation [21]. These studies indicate that SNHG7 might have certain biological functions in the occurrence, development, and progression of tumor cells. Similarly, SNHG7 also contributed to the progression and development of gastric cancer [22–24]. However, there are few studies on the molecular mechanism of SNHG7 in gastric cancer.

Currently, this study intends to explore the expression and role of SNHG7 and the possible molecule mechanisms in gastric cancer. First, we measured the expression of SNHG7 in gastric cancer. Besides, whether SNHG7 affects gastric cancer cell biological behavior through miR-485-5p was also explored.

2. Materials and Methods

2.1. Tissues Samples. 36 cases of primary gastric cancer specimens were surgically resected and pathologically diagnosed in our hospital from January 2016 to December 2019 were collected, and adjacent tissues were selected as controls. There were 16 males and 20 females with an average age of (51.86 ± 9.38) years, ranging from 32 to 71 years old. The postoperative tissue was quickly stored in liquid nitrogen for subsequent RNA extraction. Inclusion criteria are as follows. (1) All patients were diagnosed with gastric cancer by pathological examination. (2) All patients received surgical treatment and did not undergo related chemotherapy and other related treatment. and (3) Patients with complete clinical data. Exclusion criteria are as follows: (1) Patients with other malignant tumors. (2) Patients with severe liver, kidney, and heart dysfunction and metabolic abnormalities. (3) Patients with previous history of mental illness. and (4) Patients with incomplete clinical data. This study was approved by our hospital Ethics Committee (Approval No. 2015–04). The collection of all specimens was informed by the patients and their families, and informed consent was signed.

2.2. Cell Culture. Gastric cancer cells including HS746 T, HGC-27, SNU-1, AGS, and human gastric mucosa epithelial line GES-1 were cultured in the RPMI-1640 medium (Gibco, USA) containing 10% FBS (Gibco, USA) and placed in an incubator with saturated humidity at 37°C and 5% CO_2. For every 1-2 days, fresh medium was changed. Subculture was performed when the cell fusion reached 80–90%. Logarithmic growth phase cells were taken for subsequent experiments. Each experiment was repeated at least 3 times.

2.3. Cell Transfections. Small interfering RNA against SNHG7 (si-SNHG7), si-NC, miR-485-5p mimic (mimic), and inhibitor and their corresponding controls were obtained from Shanghai GenePharma. Cells transfection was performed by Lipofectamine 2000 (Invitrogen, USA). In brief, 5 μl Lipofectamine 2000 was also added into 250 μl serum-free medium. 5 μl si-SNHG7 mimic or controls was added into 250 μl serum-free medium, respectively. Above liquids were mixed and added 1 ml serum-free medium. After 24 h of incubation at 37°C, the cells were harvested for further analysis.

2.4. CCK-8 Assay. Cell with 5×10^3 cells/ml was placed in a 96-well plate and incubated for 1, 2, 3, and 4 days, respectively. 10 μl CCK-8 solution (Dojindo, Japan) was added. Each well was measured for absorbance at 450 nm on an enzyme immunosorbent detector.

2.5. Wound-Healing Assay. Gastric cancer cells were placed in a 6-well plate. One 200 μl disinfection tip was used to draw a vertical line when the cell fusion degree grew at 90%. The initial distance of scratches (0 h) was measured under a microscope. After 48 h incubation in a constant temperature incubator, the scratch distance was measured and the cell mobility was calculated as described previously [25]. The cell migration rate = (migration distance (0 h) − migration distance (48 h))/migration distance (0 h) × 100%.

2.6. Transwell Assay. Cell invasion was assessed by the transwell chamber of 8 mm (Corning, USA) as described previously [26]. Basement membrane matrix (Matrigel, BD, USA) was added to the upper chamber. Cell suspension (1×10^5 cells) was added to the upper chamber. Next, the lower chamber was inserted with 500 μl of RPMI 1640 containing 10% FBS. Cells were incubated for 24 hours in a humidified incubator with 5% CO_2. Then, the removed cells were fixed and stained. Five fields were randomly selected to count the number of cell invasions.

2.7. Dual-Luciferase Reporter Assay. The starBase database (http://starbase.sysu.edu.cn/index.php) was used to predict the binding sites of miR-485-5p and SNHG7. SNHG7-3′UTR fragment containing the binding site and the mutation binding site were inserted into PGL3 vector to construct the wild-type (wt) and mutant-type (mut) vectors of SNHG7. Vectors were cotransfected with miR-485-5p mimic or miR-NC into gastric cancer cells, and cells were cultured for 48 h to detect the luciferase activity of each group.

2.8. RIP Assay. RIP experiments were performed using the Magna RIP™ kit (Millipore, USA) as described previously [27]. Cells were lysed by lysis buffer, and the lysate was incubated with magnetic bead-conjugated IgG or Ago2 antibody (Millipore, USA). Coimmunoprecipitated products were collected, and RNA was extracted and purified.

QRT-PCR was used to detect the expression of SNHG7 and miR-485-5p.

2.9. qRT-PCR. Total RNA was extracted according to the TRIzol method, and cDNA was synthesized by the PrimeScript^{TM} RT Master Mix kit (Takara, Japan). U6 and GAPDH were used as the internal reference. The qRT-PCR amplification reaction was performed in an ABI 7500 instrument (Applied Biosystems, USA) according to the instructions of the SYBR Green PCR detection kit (Takara, Japan). The $2^{-\Delta\Delta Ct}$ method was used to calculate RNAs expression [28]. The primers are given in Table 1.

2.10. Statistical analysis. Data were processed using GraphPad Prism5 software and expressed as mean ± SD, and the *t*-test was used for pairwise comparison. Correlation analysis uses Pearson correlation coefficient. $P < 0.05$ was considered statistically significant.

3. Results

3.1. SNHG7 Expression Is Increased in Gastric Cancer. SNHG7 expression was detected in 36 pairs of gastric cancer and adjacent tissues by qRT-PCR. The results revealed that SNHG7 expression in gastric cancer tissues was significantly higher than that of adjacent tissues (Figure 1(a)). To investigate whether there were differences in the expression of SNHG7 between gastric cancer cells and human normal gastric epithelial cells, we tested SNHG7 expression in, HS746 T, HGC-27, SNU-1, and AGS, four gastric cancer cells. Findings suggested that SNHG7 expression was obviously enhanced in all gastric cancer cells versus GES1 (Figure 1(b)). These results suggested that SNHG7 may play an oncogenic role in gastric cancer. It was also found that the expression of SNHG7 in HS746 T cells was higher than that in other gastric cancer cells (Figure 1(b)). Therefore, the HS746 T cell was selected to perform the follow-up experiments.

3.2. SNHG7 Knockdown Suppresses Gastric Cancer Cell Proliferation, Migration, and Invasion. The biological effects of SNHG7 in gastric cancer cells were further explored. The results showed that SNHG7 expression was notably decreased by si-SNHG7 (Figure 2(a)), suggesting that si-SNHG7 could successfully inhibit the expression of SNHG7 in HS746 T cells. The CCK-8 assay proved that si-SNHG7 could markedly reduce the absorbance value of HS746 T cells versus the si-NC group (Figure 2(b)). The migration rate of the si-SNHG7 group was also decreased versus si-NC (Figure 2(c)). Similarly, transwell experiments showed that the invasive capacity of si-SNHG7-transfected gastric cancer cells was reduced than that of si-NC cells (Figure 2(d). These results indicated that SNHG7 knockdown could significantly inhibit the proliferation, migration, and invasion ability of gastric cancer cells.

3.3. miR-485-5p Directly Binds to SNHG7. In order to explore the molecular mechanism of SNHG7 regulating the biological behavior of gastric cancer cells, we predicted miRNAs targeted by SNHG7. We found the complementary binding site of miR-485-5p and SNHG7 (Figure 3(a)). The results of the dual luciferase experiment suggested that in HS746 T cells, miR-485-5p mimic obviously inhibited the luciferase activity in the SNHG7-wt group, while remaining unchanged in cells cotransfected with others (Figure 3(b)). Moreover, expressions of SNHG7 and miR-485-5p were enriched in the Ago2 group (Figure 3(c)). Besides, we detected miR-485-5p expression by the qRT-PCR assay in si-SNHG7-transfected cells. Findings revealed that downregulation of SNHG7 could increase miR-485-5p expression (Figure 3(d)). This suggested that SNHG7 may negatively regulate miR-485-5p expression in HS746 T cells. Since the transfection of SNHG7-mut + mimic had no effect on luciferase activity in HS746 T cells, it was further suggested that their negative regulatory effect was achieved through specific binding in the seed region.

3.4. Expression of miR-485-5p in Gastric Cancer. In order to confirm miR-485-5p expression in gastric cancer, we used qRT-PCR to detect its expression in gastric cancer tissues and cells. The results showed that compared with adjacent tissues, the expression of miR-485-5p was significantly downregulated in gastric cancer tissues (Figure 4(a)). In addition, miR-485-5p expression levels were obviously decreased in gastric cancer cells versus GES1 cells (Figure 4(b)). After pairing the SNHG7 and miR-485-5p expression data in each sample of gastric cancer tissues, we analyzed whether there is a correlation between their expressions. Interestingly, miR-485-5p expression negatively correlated with SNHG7 expression in gastric cancer tissues (Figure 4(c)).

3.5. SNHG7 Facilitates Gastric Cancer Progression via Targeting miR-485-5p. To further verify whether SNHG7 regulated the malignant behavior of HS746 T cells through miR-485-5p, the inhibitor was transfected into HS746 T cells. Then, qRT-PCR experiments verified that miR-485-5p expression was reduced by the inhibitor (Figure 5(a)). CCK-8 experimental results showed that the inhibitor reversed the effect of SNHG7 knockdown on HS746 T cell proliferation (Figure 5(b)). Moreover, inhibition of miR-485-5p prominently abated SNHG7 silencing-induced cell migration in HS746 T cells (Figure 5(c)). At the same time, the inhibitor attenuated the suppression of si-SNHG7 on cell invasion ability (Figure 5(d)). The above results indicated that SNHG7 regulated the gastric cancer cells malignant behavior by targeting miR-485-5p.

4. Discussion

Gastric cancer is a heterogeneous, multifactorial malignant tumor with poor prognosis and difficult to cure [29]. There are no special clinical symptoms in early gastric cancer, most gastric cancer patients are diagnosed as progressive with metastases, and the 5-year survival rate is still low [30]. At present, there is no effective screening method for gastric

Table 1: Primer sequences for real-time fluorescence quantification PCR.

Gene name	Primer sequences (5′-3′)
GAPDH	F TCCTCTGACTTCAACAGCGACAC R CACCCTGTTGCTGTAGCCAAATTC
U6	F CTCGCTTCGGCAGCACA R AACGCTTCACGAATTTGCGT
SNHG7	F TTGCTGGCGTCTCGGTTAAT R GGAAGTCCATCACAGGCGAA
miR-485-5p	F GGAGAGGCTGGCCGTGAT R CAGTGCGTGTCGTGGAGT

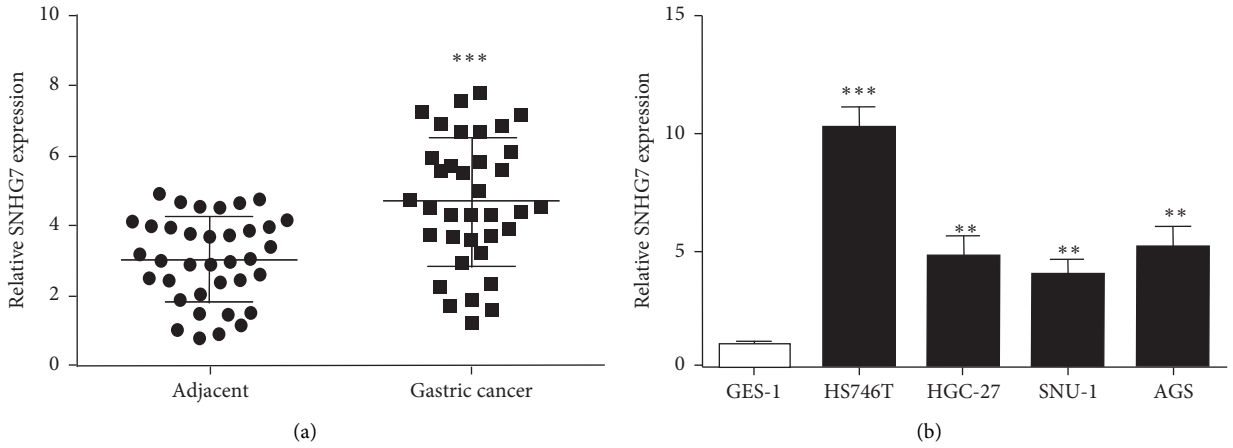

Figure 1: SNHG7's expression detected in gastric cancer tissues and cells. (a) Expression of SNHG7 in gastric cancer tissues. (b) SNHG7 expression elevated in gastric cancer cells. $^{**}P < 0.01$. $^{***}P < 0.001$.

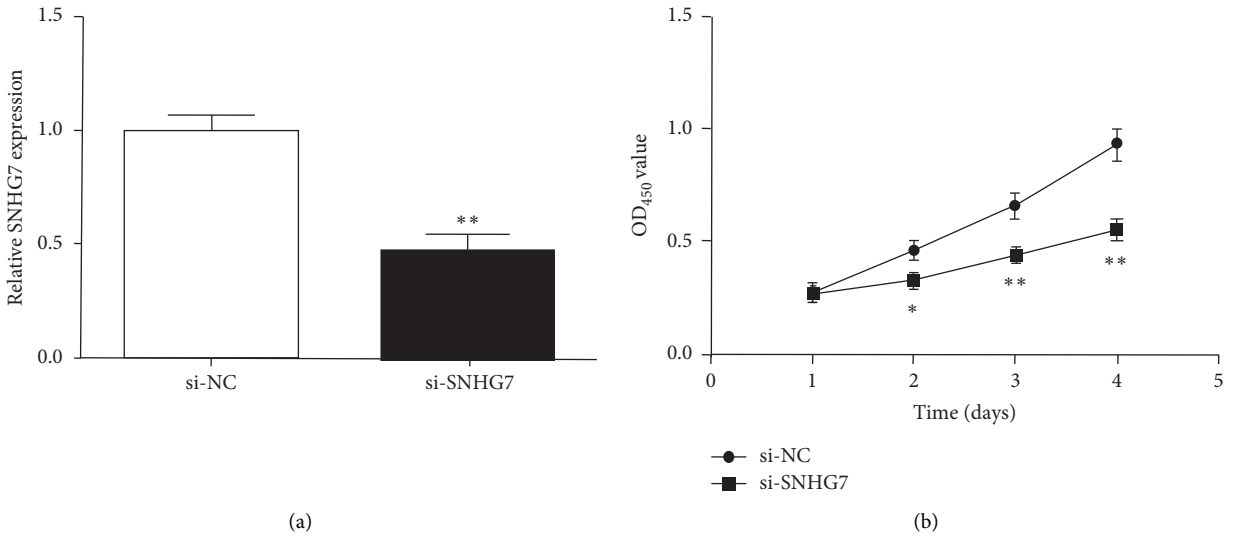

Figure 2: Continued.

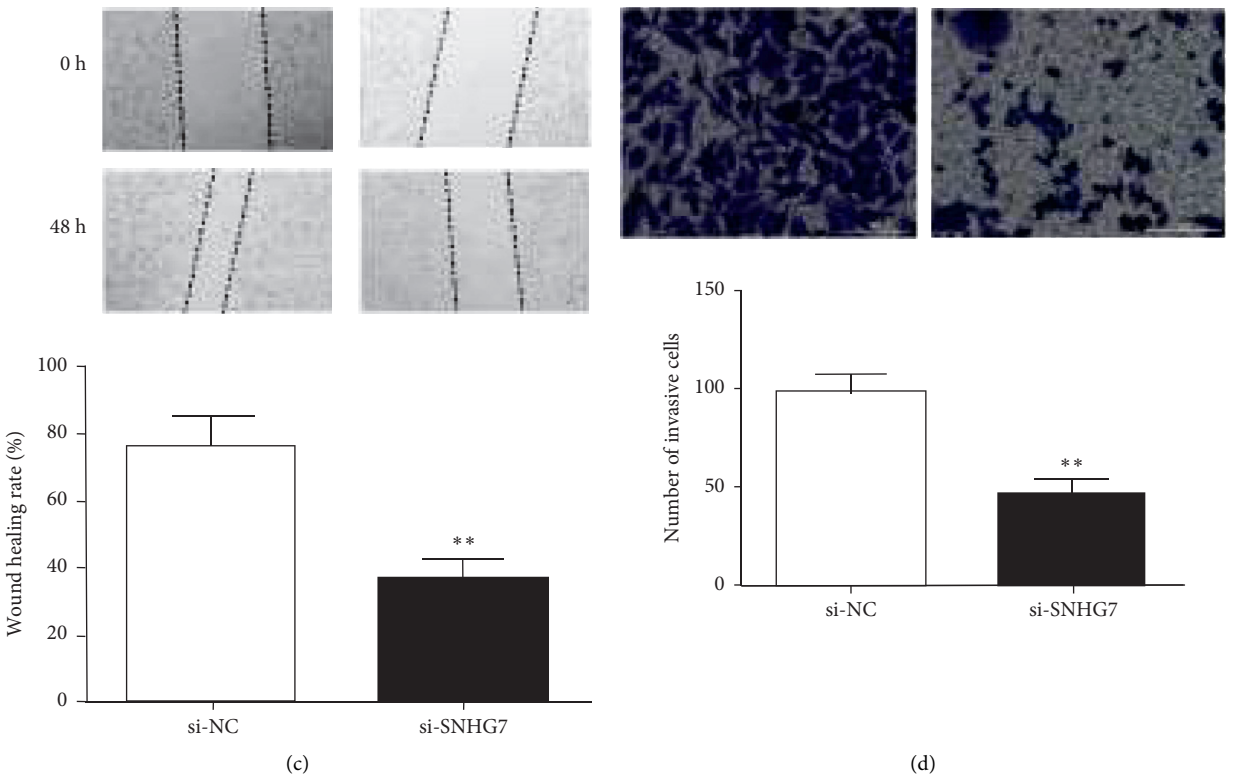

Figure 2: SNHG7 knockdown repressed malignant behavior of HS746 T cells. (a) SNHG7 expression in HS746 T cells after si-SNHG7 transfected. (b) Cell proliferation of HS746 T cells after SNHG7 inhibition. (c) Cell migration rate of HS746 T cells after SNHG7 knockdown. (d) Number of invading HS746 T cells after SNHG7 knockdown. $^{*}P < 0.05$. $^{**}P < 0.01$.

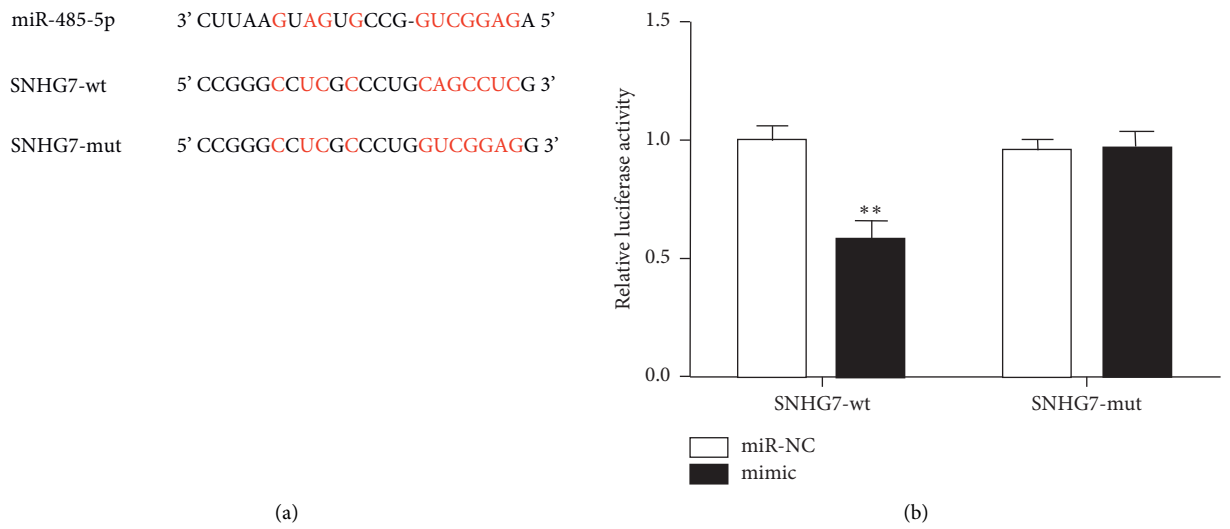

Figure 3: Continued.

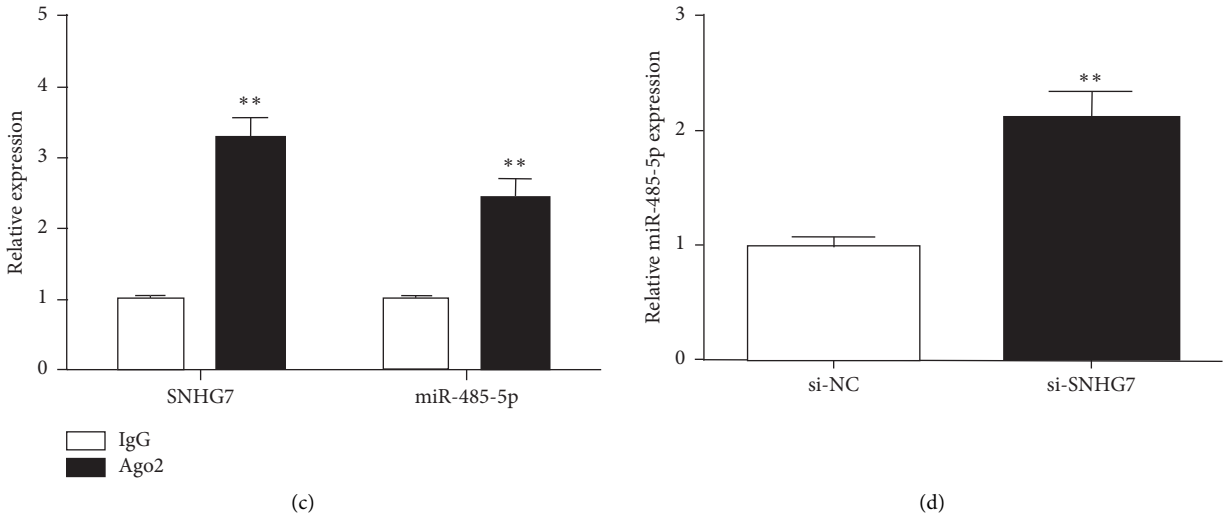

Figure 3: SNHG7 directly targets miR-485-5p. (a) Predicted binding site between miR-485-5p and SNHG7. (b) The luciferase activity in HS746 T cells. (c) SNHG7 and miR-485-5p expressions detected in the RIP assay. (d) miR-485-5p expression in HS746 T cells treated with si-SNHG7. $^{**}P < 0.01$.

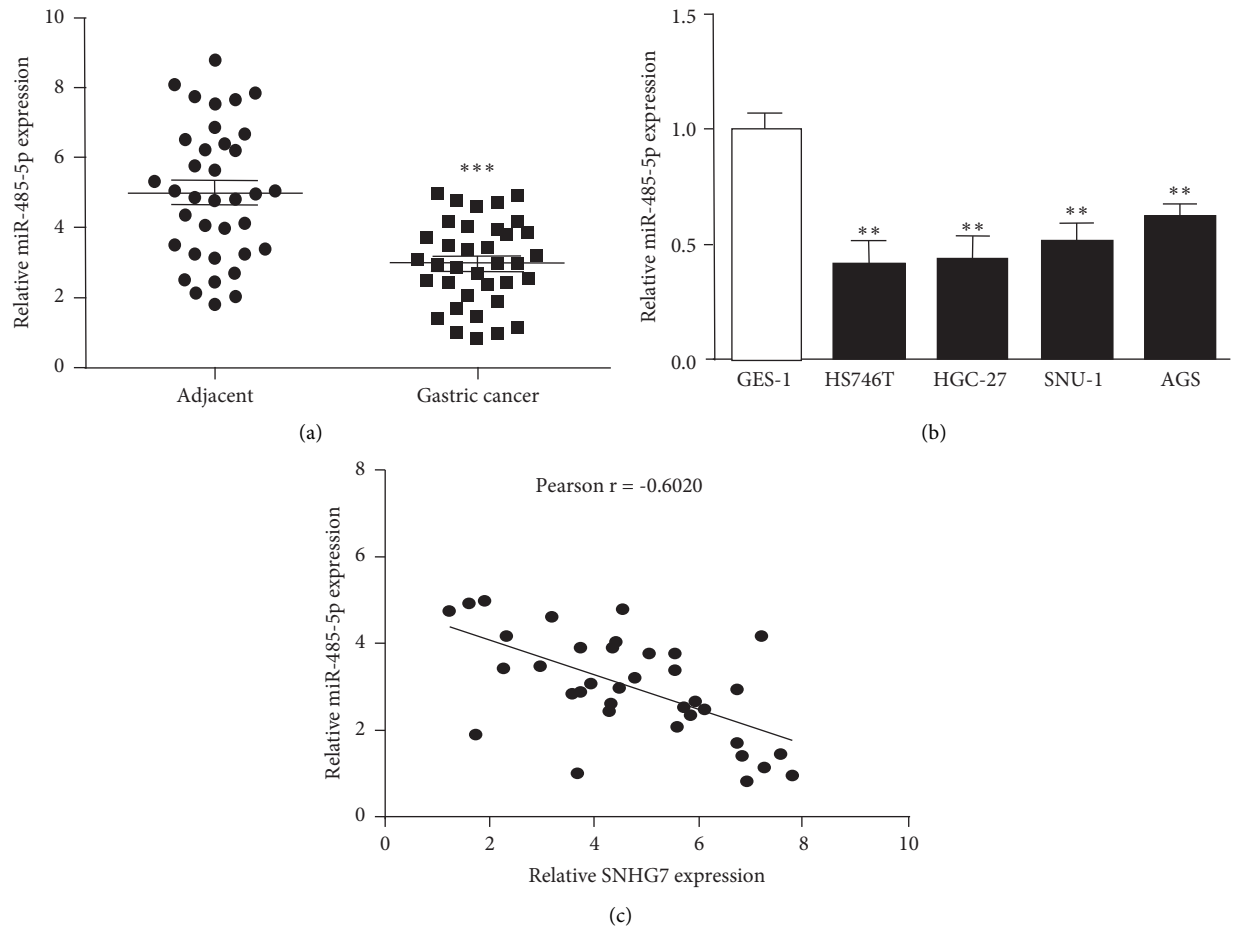

Figure 4: miR-485-5p's expression reduced in gastric cancer. (a) Expression of miR-485-5p decreased in gastric cancer tissue. (b) Expression of miR-485-5p reduced in gastric cancer cells. (c) Correlation analysis between SNHG7 expression and miR-485-5p expression in gastric cancer tissues. $^{**}P < 0.01$. $^{***}P < 0.001$.

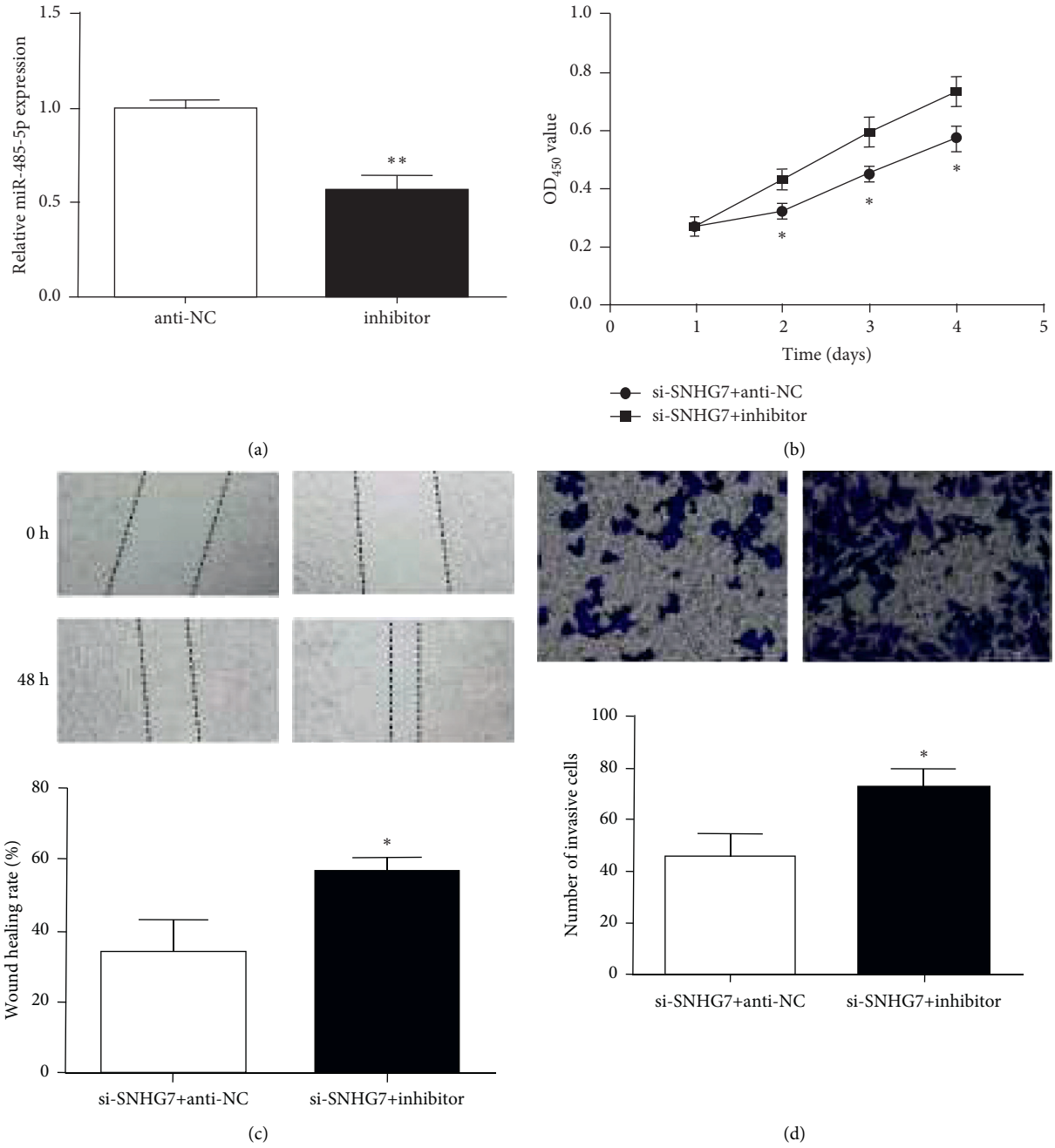

Figure 5: SNHG7 regulated gastric cancer malignant behavior through miR-485-5p. (a) miR-485-5p expression inhibited in HS746 T cells treated with the miR-485-5p inhibitor. (b) Cell proliferation in HS746 T cells transfected with the miR-485-5p inhibitor and si-SNHG7. (c) Cell migration rate in HS746 T cells transfected with the miR-485-5p inhibitor and si-SNHG7. (d) Number of invading HS746 T cells transfected with the miR-485-5p inhibitor and si-SNHG7. $^{*}P < 0.05$. $^{**}P < 0.01$.

cancer. In order to prolong the survival time of tumor patients and improve the quality of their life, researchers are encouraged to develop new technologies and methods of cancer treatment. It is necessary to understand the gastric cancer regulatory mechanism at the molecular level. Combined with the currently popular targeted therapy, it will provide important evidence for gastric cancer diagnosis, treatment, and prognosis. This study aimed to provide new biomarkers for the early diagnosis and treatment of gastric cancer by exploring SNHG7 expression and its effect and mechanism in gastric cancer.

SNHG7 was commonly overexpressed in a variety of cancers as an oncogene [17]. Wang et al. found SNHG7 could inhibit P15 and P16 to suppress apoptosis and facilitate the proliferation of gastric cancer cells [22]. Zhang et al. reported that gastric cancer cell migration and invasion were promoted through the miR-34a-Snail-EMT axis by SNHG7 [23]. Here, we conducted a preliminary study on

SNHG7 expression in gastric cancer, as well as its functions and regulatory mechanisms. The results found that SNHG7 expression was increased in gastric cancer. After SNHG7 was inhibited in gastric cancer cells, the cell proliferation, migration, and invasion ability were signally repressed. Results suggested that SNHG7 inhibition may hamper the progression of gastric cancer.

A large number of studies have found that miRNAs are related to gastric cancer as tumor suppressor or oncogenic genes [31]. For example, Cao et al. proposed that miR-381 could inhibit TMEM16 A expression to hamper gastric cancer metastasis [32]. Guan et al. reported miR-93 could target TIMP2 to facilitate proliferation and metastasis of gastric cancer [33]. And miR-485-5p was significantly decreased in colorectal cancer (CC), breast cancer (BC), and nonsmall cell lung cancer (NSCLC) and could inhibit the progression of cancers by targeting downstream genes [34–36]. In gastric cancer, miR-485-5p was related to prognosis and overall survival of gastric cancer patients and exerted a suppressor in gastric cancer cell growth and motility by inhibiting NUDT1 [37, 38]. It shows that the antitumor effect of miR-485-5p has biodiversity, which is worthy of further study. Based on previous research, we hypothesized that miR-485-5p plays an important role in gastric cancer progression. Interestingly, miR-485-5p expression was decreased and was inversely related to SNHG7 expression in gastric cancer tissues.

LncRNAs act as a sponge of ceRNA or miRNA molecules by interacting with and inhibiting miRNAs [39]. The bioinformatics analysis revealed that SNHG7 has a complementary nucleotide binding site to miR-485-5p. SNHG7 could specifically target miR-485-5p by the dual-luciferase assay and RIP assay. At the same time, knockdown of SNHG7 in gastric cancer cells was found to increase miR-485-5p expression, indicating that SNHG7 could negatively regulate miR-485-5p. miR-485-5p silencing in cells could partially reverse the inhibition of biological behavior caused by SNHG7 knockdown. Since inhibition of miR-485-5p only partially reversed SNHG7 function, there might be other binding sites or pathways for SNHG7 to participate in tumor promotion.

Since this study was conducted in vitro in cell lines, there are still some deficiencies, including the relatively small number of patients, and the preliminary results may not accurately reflect its expression in gastric cancer, which needs to be repeated in large samples. In addition, how the effect of upregulating SNHG7 or downregulating miR-485-5p on gastric cancer and the results in animals need to be further studied. Although the incidence of gastric cancer has improved in recent years, it still faces tremendous pressure for prevention and treatment due to atypical clinical symptoms in the early stages of gastric cancer. There is an urgent need to discover new molecular markers that provide opportunities for the prevention and control of gastric cancer.

5. Conclusion

In summary, expression of SNHG7 was significantly reduced, and SNHG7 inhibition could repress the biological behavior of gastric cancer cells. Rescue experiments confirmed that SNHG7 regulated the gastric cancer cells malignant behavior via the regulation of miR-485-5p. Subsequent research will further explore related mechanisms and signaling pathways on this basis, in order to provide experimental evidence for treatment of gastric cancer.

Data Availability

The datasets used and/or analyzed during the present study are available from the corresponding author on reasonable request.

Conflicts of Interest

The authors declare that they have no conflicts of interest.

References

[1] H.-R. Qian and Y. Yang, "Functional role of autophagy in gastric cancer," *Oncotarget*, vol. 7, no. 14, pp. 17641–17651, 2016.

[2] M.-L. Pärn, K. Innos, A. Baburin, R.-A. Kiivet, and J. Jaal, "Gastric cancer trends in Estonia 1995-2014 by age, subsite, morphology and stage," *Acta Oncologica*, vol. 58, no. 3, pp. 283–289, 2019.

[3] S. Lai, "A human mode of intestinal type gastric carcinoma," *Medical Hypotheses*, vol. 123, pp. 27–29, 2019.

[4] P. Rawla and A. Barsouk, "Epidemiology of gastric cancer: global trends, risk factors and prevention," *Gastroenterology Review*, vol. 14, no. 1, pp. 26–38, 2019.

[5] F. Raza, Y. Zhu, L. Chen et al., "Paclitaxel-loaded pH responsive hydrogel based on self-assembled peptides for tumor targeting," *Biomaterials Science*, vol. 7, no. 5, pp. 2023–2036, 2019.

[6] F. Raza, H. Zafar, X. You, A. Khan, J. Wu, and L. Ge, "Cancer nanomedicine: focus on recent developments and self-assembled peptide nanocarriers," *Journal of Materials Chemistry B*, vol. 7, no. 48, pp. 7639–7655, 2019.

[7] F. Raza, H. Zafar, S. Zhang et al., "Recent advances in cell membrane-derived biomimetic nanotechnology for cancer immunotherapy," *Advanced Healthcare Materials*, vol. 10, no. 6, Article ID e2002081, 2021.

[8] R. E. Sexton, M. N. Al Hallak, M. Diab, and A. S. Azmi, "Gastric cancer: a comprehensive review of current and future treatment strategies," *Cancer and Metastasis Reviews*, vol. 39, no. 4, pp. 1179–1203, 2020.

[9] J. J. Quinn and H. Y. Chang, "Unique features of long noncoding RNA biogenesis and function," *Nature Reviews Genetics*, vol. 17, no. 1, pp. 47–62, 2016.

[10] M. B. Clark and J. S. Mattick, "Long noncoding RNAs in cell biology," *Seminars in Cell & Developmental Biology*, vol. 22, no. 4, pp. 366–376, 2011.

[11] T. Li, X. Mo, L. Fu, B. Xiao, and J. Guo, "Molecular mechanisms of long noncoding RNAs on gastric cancer," *Oncotarget*, vol. 7, no. 8, pp. 8601–8612, 2016.

[12] M. Sun, F. Q. Nie, Z. X. Wang, and W. De, "Involvement of lncRNA dysregulation in gastric cancer," *Histology & Histopathology*, vol. 31, no. 1, pp. 33–39, 2016.

[13] W. Xu, L. He, Y. Li, Y. Tan, F. Zhang, and H. Xu, "Silencing of lncRNA ZFAS1 inhibits malignancies by blocking Wnt/β-catenin signaling in gastric cancer cells," *Bioscience Biotechnology and Biochemistry*, vol. 82, no. 138, pp. 456–465, 2018.

[14] D.-L. Chen, H.-Q. Ju, Y.-X. Lu et al., "Long non-coding RNA XIST regulates gastric cancer progression by acting as a molecular sponge of miR-101 to modulate EZH2 expression," *Journal of Experimental & Clinical Cancer Research*, vol. 35, no. 1, p. 142, 2016.

[15] C. Y. Wang, L. Hua, K. H. Yao, J. T. Chen, J. J. Zhang, and J. H. Hu, "Long non-coding RNA CCAT2 is up-regulated in gastric cancer and associated with poor prognosis," *International Journal of Clinical and Experimental Pathology*, vol. 8, no. 1, pp. 779–785, 2015.

[16] D. Cheng, J. Fan, Y. Ma et al., "LncRNA SNHG7 promotes pancreatic cancer proliferation through ID4 by sponging miR-342-3p," *Cell & Bioscience*, vol. 9, no. 1, p. 28, 2019.

[17] Y. Zhou, B. Tian, J. Tang et al., "SNHG7: a novel vital oncogenic lncRNA in human cancers," *Biomedicine & Pharmacotherapy*, vol. 124, Article ID 109921, 2020.

[18] D. N. Boone, A. Warburton, S. Som, and A. V. Lee, "SNHG7 is a lncRNA oncogene controlled by Insulin-like Growth Factor signaling through a negative feedback loop to tightly regulate proliferation," *Scientific Reports*, vol. 10, no. 1, p. 8583, 2020.

[19] X. Zhong, Z. Long, S. Wu, M. Xiao, and W. Hu, "LncRNA-SNHG7 regulates proliferation, apoptosis and invasion of bladder cancer cells assurance guidelines," *Journal of B. U. ON.: Official Journal of the Balkan Union of Oncology*, vol. 23, no. 3, pp. 776–781, 2018.

[20] J. Zeng, Y. X. Ma, Z. H. Liu, and Y. L. Zeng, "LncRNA SNHG7 contributes to cell proliferation, invasion and prognosis of cervical cancer," *European Review for Medical and Pharmacological Sciences*, vol. 23, no. 21, pp. 9277–9285, 2019.

[21] L. J. Xu, X. J. Yu, B. Wei et al., "LncRNA SNHG7 promotes the proliferation of esophageal cancer cells and inhibits its apoptosis," *European Review for Medical and Pharmacological Sciences*, vol. 22, no. 9, pp. 2653–2661, 2018.

[22] M. W. Wang, J. Liu, Q. Liu et al., "LncRNA SNHG7 promotes the proliferation and inhibits apoptosis of gastric cancer cells by repressing the P15 and P16 expression," *European Review for Medical and Pharmacological Sciences*, vol. 21, no. 20, pp. 4613–4622, 2017.

[23] Y. Zhang, Y. Yuan, Y. Zhang, L. Cheng, X. Zhou, and K. Chen, "SNHG7 accelerates cell migration and invasion through regulating miR-34a-Snail-EMT axis in gastric cancer," *Cell Cycle*, vol. 19, no. 1, pp. 142–152, 2020.

[24] L.-J. Pei, P.-J. Sun, K. Ma, Y.-Y. Guo, L.-Y. Wang, and F.-D. Liu, "LncRNA-SNHG7 interferes with miR-34a to desensitize gastric cancer cells to cisplatin," *Cancer Biomarkers*, vol. 30, no. 1, pp. 127–137, 2021.

[25] S. Chen, L. Zhang, S. Kim et al., "Arsenic sulfide inhibits cell migration and invasion of gastric cancer in vitro and in vivo," *Drug Design, Development and Therapy*, vol. 9, pp. 5579–5590, 2015.

[26] J. Bai, B. Yao, L. Wang et al., "lncRNA A1BG-AS1 suppresses proliferation and invasion of hepatocellular carcinoma cells by targeting miR-216a-5p," *Journal of Cellular Biochemistry*, vol. 120, no. 6, pp. 10310–10322, 2018.

[27] X. Cai, X. Wang, C. Cao et al., "HBXIP-elevated methyltransferase METTL3 promotes the progression of breast cancer via inhibiting tumor suppressor let-7 g," *Cancer Letters*, vol. 415, pp. 11–19, 2017.

[28] K. J. Livak and T. D. Schmittgen, "Analysis of relative gene expression data using real-time quantitative PCR," *Methods*, vol. 25, no. 4, pp. 402–408, 2002.

[29] M. A. Shah and J. A. Ajani, "Gastric cancer-an enigmatic and heterogeneous disease," *Jama*, vol. 303, no. 17, pp. 1753-1754, 2010.

[30] M. L. M. Kwong, C. Ihemelandu, and P. H. Sugarbaker, "Prevention and treatment of peritoneal metastases from gastric cancer," *Surgery for Gastric Cancer*, Springer, pp. 277–291, New York, NY, USA, 2019.

[31] M. Zhang and X. Du, "Noncoding RNAs in gastric cancer: research progress and prospects," *World Journal of Gastroenterology*, vol. 22, no. 29, p. 6610, 2016.

[32] Q. Cao, F. Liu, K. Ji et al., "MicroRNA-381 inhibits the metastasis of gastric cancer by targeting TMEM16A expression," *Journal of Experimental & Clinical Cancer Research*, vol. 36, no. 1, p. 29, 2017.

[33] G. Hao, L. Weiming, L. Yuanyuan et al., "MicroRNA-93 promotes proliferation and metastasis of gastric cancer via targeting TIMP2," *PloS One*, vol. 12, no. 12, Article ID e0189490, 2017.

[34] M. Wang, W.-R. Cai, R. Meng et al., "miR-485-5p suppresses breast cancer progression and chemosensitivity by targeting survivin," *Biochemical and Biophysical Research Communications*, vol. 501, no. 1, pp. 48–54, 2018.

[35] R.-S. Huang, Y.-L. Zheng, C. Li, C. Ding, C. Xu, and J. Zhao, "MicroRNA-485-5p suppresses growth and metastasis in non-small cell lung cancer cells by targeting IGF2BP2," *Life Sciences*, vol. 199, pp. 104–111, 2018.

[36] X.-X. Hu, X.-N. Xu, B.-S. He et al., "microRNA-485-5p functions as a tumor suppressor in colorectal cancer cells by targeting CD147," *Journal of Cancer*, vol. 9, no. 15, pp. 2603–2611, 2018.

[37] L. L. Jing and X. M. Mo, "Reduced miR-485-5p expression predicts poor prognosis in patients with gastric cancer," *European Review for Medical and Pharmacological Sciences*, vol. 20, no. 8, pp. 1516–1520, 2016.

[38] J. Duan, H. Zhang, S. Li et al., "The role of miR-485-5p/NUDT1 axis in gastric cancer," *Cancer Cell International*, vol. 17, no. 1, p. 92, 2017.

[39] M. D. Paraskevopoulou and A. G. Hatzigeorgiou, "Analyzing MiRNA-LncRNA interactions," *Long Non-Coding RNAs*, vol. 1402, no. 1, pp. 271–286, 2016.

Hindawi
Journal of Oncology
Volume 2021, Article ID 8943353, 6 pages
https://doi.org/10.1155/2021/8943353

Research Article

Application of NRS2002 in Preoperative Nutritional Screening for Patients with Liver Cancer

Suling Huang,[1] Shijie Wang,[1] Yuankang Xie,[1] Xiao He,[1] Xiuying Yi,[1] Jianhong Zhang,[2] Zuomei Deng,[3] and Ling Yin [1]

[1]*Department of Hepatological Surgery, First Affiliated Hospital of Gannan Medical University, Ganzhou 341000, Jiangxi Province, China*
[2]*Department of Pharmacy, First Affiliated Hospital of Gannan Medical University, Ganzhou 341000, Jiangxi Province, China*
[3]*Department of Thyroid Hernia Surgery, First Affiliated Hospital of Gannan Medical University, Ganzhou 341000, Jiangxi Province, China*

Correspondence should be addressed to Ling Yin; yinling20210701@163.com

Received 1 July 2021; Accepted 17 August 2021; Published 27 August 2021

Academic Editor: Muhammad Wasim Khan

Objective. To explore the application of NRS2002 in preoperative nutritional screening of patients with liver cancer (LC). *Methods*. 60 LC patients treated in the First Affiliated Hospital of Gannan Medical University (January 2018–May 2021) were chosen as the research objects, and split into group J without nutritional risk and group Q with nutritional risk according to the results of NRS2002 to compare the preoperative situation, surgery-related indexes, hematological indexes, postoperative recovery, and incidence of complications between the two groups. *Results*. Group J ($n = 28$) and group Q ($n = 32$) showed no obvious difference in preoperative situation, and patients' liver function indexes were within the normal range. The duration of surgery in group J was notably shorter compared with group Q ($P < 0.05$). Alanine aminotransferase (ALT), aspartate aminotransferase (AST), direct bilirubin (DBIL), and albumin in group J were notably different from those of group Q ($P < 0.001$) at 1 day after surgery. ALT and AST in group J were notably different from those of group Q at 3 days after surgery ($P < 0.001$). No obvious differences were observed in the hematological indexes between the two groups at 5 days after surgery ($P > 0.05$). The total amount of albumin infusion, postoperative hospitalization time, and hospitalization cost in group J were notably lower compared with group Q ($P < 0.001$). The incidence of complications in group J was notably lower compared with group Q ($P < 0.05$). *Conclusion*. Postoperative recovery of LC patients is closely related to their preoperative nutritional status, and those with poor nutritional status have a high incidence of postoperative complications and long recovery time. NRS2002 can effectively screen the nutritional status of patients and provide reference for prognosis evaluation.

1. Introduction

Liver cancer (LC) is a common clinical disease. According to the data of International Agency for Research on Cancer (IARC), the number of LC cases in China accounts for 55% of the total cases worldwide, and about 70% of the patients are in the middle and late stages when diagnosed, with an increasing annual mortality rate, endangering the life and health of Chinese residents. At present, surgical treatment is generally performed in practice to radically treat it. However, LC patients are often complicated with other diseases such as liver cirrhosis, their liver cells are seriously damaged, their metabolic function is reduced, and the inactivated function of steroid hormones is weakened, which jointly lead to the nutritional and metabolic imbalances in patients. Therefore, the possibility of malnutrition in patients with liver cancer during perioperative period reaches 80%, and severe malnutrition will increase the probability of surgical complications, enhance the adverse reactions of radiotherapy and chemotherapy, and affect the prognosis of patients [1–3]. In recent years, precise requirements have been put forward for surgical procedures. Preoperative assessment

has become an integral part of surgical procedures, including liver function classification and imaging examination in LC patients. However, there were few preoperative examinations related to nutritional assessment. Since clinical practice shows that there is a close relationship between the nutritional status of patients and their postoperative recovery, it is extremely important to add preoperative nutritional assessment to the scope of preoperative examination [4–6]. NRS2002 is a common nutritional risk-screening scale in clinical practice, which can be applied in various types of hospitalized patients. Based on this, this paper aims to explore the application of NRS2002 in preoperative nutritional screening of LC patients, summarized as follows.

2. Materials and Methods

2.1. Preoperative Assessment. Sixty LC patients treated in the First Affiliated Hospital of Gannan Medical University (January 2018–May 2021) were chosen as the research objects and underwent preoperative evaluation, with steps as follows. (1) All the patients received routine examination. (2) The patients received indocyanine green excretive test with 15-minute retention and other methods to evaluate their liver function [7, 8]. (3) The patients underwent imaging examinations, including MRI examination and ultrasound examination to observe the tumor size, location, and other information and to determine whether extrahepatic metastasis occurred.

This study was in line with the principles of Declaration of Helsinki and was approved by the Ethics Committee of the First Affiliated Hospital of Gannan Medical University.

2.2. Inclusion Criteria. (1) The patients or their families fully recognized the study process and signed the informed consent. (2) The patients were diagnosed with LC after examination, and the lesions could be removed by hepatectomy. (3) The liver function of patients was graded as A [9, 10]. (4) The 15-minute retention rate of indocyanine green excretion test was 20% and below.

2.3. Exclusion Criteria. (1) The patients had mental problems or could not communicate with others. (2) The patients had other organic diseases. (3) The patients had liver function grade below A. (4) The patients had extrahepatic metastasis of cancer or tumor thrombus in the portal vein and primary branches. (5) The patients received radiotherapy and chemotherapy before surgery. (6) The patients quit the study halfway.

2.4. Methods

2.4.1. Surgical Methods. (1) All surgeries of the patients were operated by the same surgical group. The surgical plans were selected according to the actual situation of the patients, and the ultrasound-assisted technology was adopted to clarify the sites for resection. (2) Portal triad clamping (Pringle) was selected for hepatic inflow occlusion. The liver tissue was separated by the fine clamp method, and the pipeline structure of the section was sutured, except for the liver section.

2.4.2. Perioperative Nutrition Support Schemes. (1) The patient did not take nutritional support before surgery and continued to follow the routine dietary. (2) After surgery, enteral nutrition support was given to the patients. The patients could drink water at 12 h after surgery. With low amount and high frequency, the patients drank enteral nutrient solution (Nutricia Pharmaceutical Co., Ltd., Wuxi Branch; NMPA approval no. H20030012) at 24 h after surgery with 500 ml each day and was increased to 1000 mL within 3 days, accompanied by semiliquid diet.

2.5. Observation Criteria

(1) Grouping of patients: the patients were split into group J without nutritional risk (NRS2002 score <3 points) and group Q with nutritional risk (NRS2002 score ≥3 points) according to the results of NRS2002, and the number of each group was counted [11–14].

(2) Preoperative situation: the comparison items included gender, age, underlying diseases, alanine aminotransferase (ALT) level, aspartate aminotransferase (AST) level, total bilirubin (TBIL) level, direct bilirubin (DBIL) level, and albumin level.

(3) Surgery-related indexes: the range of liver resection, duration of surgery, hepatic portal occlusion, intraoperative blood loss, and intraoperative blood transfusion were compared.

(4) Hematological indexes: the ALT, AST, TBIL, DBIL, and albumin levels [15–18] at 1 day, 3 days, and 5 days after surgery were compared.

(5) Postoperative recovery: the total amount of albumin infusion, postoperative ventilation time, postoperative hospitalization time, and hospitalization cost were compared.

(6) Incidence of complications: complications included ascites, bile leakage, abdominal infection, and postoperative hemorrhage. The number of patients with complications was counted.

2.6. Statistical Treatment. In this study, the data were processed by SPSS 20.0 and graphed by GraphPad Prism 7 (GraphPad Software, San Diego, USA). This study included enumeration data and measurement data, tested by X^2 and t-test. The difference was statistically significant when $P < 0.05$.

3. Results

3.1. Analysis of Patient Grouping. The grouping of patients is shown in Figure 1.

3.2. Comparison of Preoperative Situation. No obvious difference in preoperative situation was found between the two

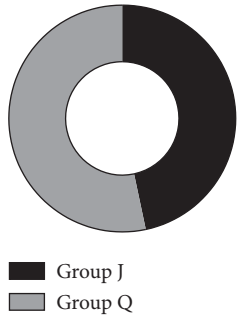

Figure 1: Analysis of patient grouping (n(%)). The black area represents group J ($n = 28$, 46.7%), and the gray area represents group Q ($n = 32$, 53.3%).

groups ($P > 0.05$), and the liver function indexes of all patients were within the normal range (Table 1).

3.3. Comparison of Surgery-Related Indexes. The duration of surgery in group J was notably shorter compared with group Q ($P < 0.05$; Figure 2 and Table 2).

Group J included 14 patients (50%) with a resection of 3 segments or less and 14 patients (50%) with a resection of more than 3 segments. Group Q included 12 patients (37.5%) with a resection of 3 segments or less and 20 patients (62.5%) with a resection of more than 3 segments. The comparison between the two groups showed $X^2 = 0.950$ and $P = 0.330$.

3.4. Comparison of Hematological Indexes. ALT, AST, DBIL, and albumin in group J were notably different from those of group Q ($P < 0.001$) at 1 day after surgery. ALT and AST in group J were notably different from those of group Q at 3 days after surgery ($P < 0.001$). No obvious differences were observed in the hematological indexes between the two groups at 5 days after surgery ($P > 0.005$) (see Table 3).

3.5. Comparison of Postoperative Recovery. The total amount of albumin infusion, postoperative hospitalization time, and hospitalization cost in group J were notably lower compared with group Q ($P < 0.001$; Table 4).

3.6. Comparison of the Incidence of Complications. The incidence of complications in group J was notably lower compared with group Q ($P < 0.05$; Figure 3).

4. Discussion

With the continuous progress of relevant medical technology in recent years and significantly improved level of liver cancer surgery in China, how to optimize the prognosis of LC patients undergoing surgery by preoperative assessment has become the focus of clinical research. Complication with underlying liver diseases such as liver cirrhosis in LC patients in China can increase the damage to liver cells and affect liver nutritional and metabolic functions. At the same time, due to the decline of appetite in LC patients and

Table 1: Comparison of preoperative situation.

Group	Group J ($n = 28$)	Group Q ($n = 32$)	X^2/t	P
Gender			0.234	0.628
Male	14 (50.0%)	14 (43.8%)		
Female	14 (50.0%)	18 (56.3%)		
Age (years old)				
Range	32–74	33–74		
Average age	51.21 ± 6.20	51.23 ± 6.21	0.012	0.990
Underlying diseases				
Diabetes	6 (21.4%)	10 (31.3%)	0.737	0.391
Hypertension	3 (10.7%)	6 (18.8%)	0.756	0.384
ALT (U/L)	38.98 ± 9.12	42.11 ± 9.65	1.286	0.204
AST (U/L)	30.15 ± 4.65	32.15 ± 5.36	1.533	0.131
TBIL (μmol/L)	14.99 ± 0.54	15.10 ± 0.65	0.707	0.482
DBIL (μmol/L)	4.10 ± 0.35	4.24 ± 0.65	1.017	0.313
Albumin (g/L)	40.10 ± 0.68	39.98 ± 1.54	0.381	0.705

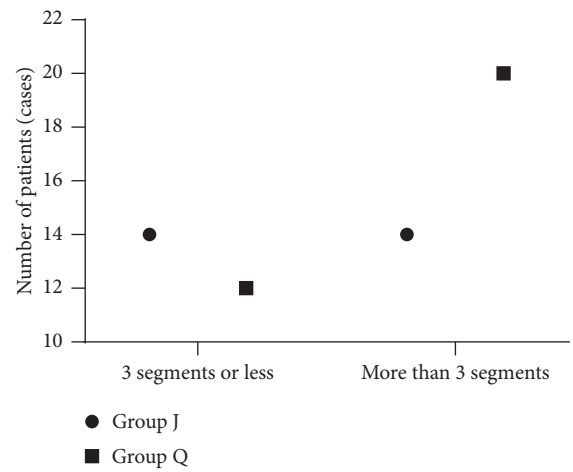

Figure 2: Scope of liver resection. The abscissa from left to right represent 3 segments or less and more than 3 segments, respectively, and the ordinate represents the number of patients (cases). The dots represent group J, and the squares represent group Q.

reduced nutrition intake with different degrees of Warburg effect, the incidence of malnutrition in patients can reach 80%, adversely affecting the postoperative recovery of patients [19–21]. At present, the preoperative assessment of liver cancer patients includes liver function classification and hepatic functional reserve test, while nutritional assessment is not included. However, clinical practice has confirmed the key role of nutritional assessment, so close attention should be paid to the selection of appropriate preoperative nutritional assessment tools in doctors.

As a common preoperative nutritional assessment tool in clinical practice, NRS2002 is superior to other assessment scales in sensitivity, which can be adopted to screen nutritional risk indicators of hospitalized patients and is associated with the prognosis of patients [22, 23]. NRS2002 can be used in the preoperative assessment of various diseases. In this study, it was applied to the preoperative nutritional assessment of LC patients, and 60 patients were split into group J ($n = 28$) without nutritional risk and

Table 2: Comparison of surgery-related indexes.

Items	Group J ($n = 28$)	Group Q ($n = 32$)	X^2/t	P
Duration of surgery (min)	215.68 ± 26.87	365.98 ± 35.15	18.399	<0.001
Hepatic portal occlusion			0.950	0.330
Yes	14 (50.0%)	20 (62.5%)		
No	14 (50.0%)	12 (37.5%)		
Intraoperative blood loss (ml)	295.12 ± 60.98	565.98 ± 48.45	19.156	<0.001
Intraoperative blood transfusion			2.402	0.121
Yes	4 (14.3%)	10 (31.3%)		
No	24 (85.7%)	22 (68.8%)		

Table 3: Comparison of hematological indexes ($\overline{x} \pm s$).

Items	Group J ($n = 28$)	Group Q ($n = 32$)	t	P
1 day after surgery				
ALT (U/L)	205.65 ± 28.54	489.35 ± 65.12	21.314	<0.001
AST (U/L)	180.54 ± 25.48	470.65 ± 98.54	15.128	<0.001
TBIL (μmol/L)	20.99 ± 2.54	22.65 ± 5.21	1.533	0.131
DBIL (μmol/L)	6.10 ± 0.54	13.54 ± 3.68	10.588	<0.001
Albumin (g/L)	32.11 ± 0.65	30.98 ± 1.20	4.442	<0.001
3 days after surgery				
ALT (U/L)	178.65 ± 24.65	356.98 ± 98.52	9.317	<0.001
AST (U/L)	75.45 ± 10.58	210.65 ± 92.12	7.714	<0.001
TBIL (μmol/L)	22.65 ± 2.54	23.65 ± 2.14	1.655	0.103
DBIL (μmol/L)	8.21 ± 1.68	9.11 ± 2.15	1.788	0.079
Albumin (g/L)	34.12 ± 1.65	33.68 ± 0.65	1.391	0.169
5 days after surgery				
ALT (U/L)	120.65 ± 25.65	125.98 ± 26.98	0.781	0.438
AST (U/L)	46.98 ± 4.25	49.11 ± 5.87	1.589	0.117
TBIL (μmol/L)	20.12 ± 2.35	20.98 ± 2.68	1.313	0.195
DBIL (μmol/L)	7.10 ± 1.24	7.65 ± 1.64	1.448	0.153
Albumin (g/L)	35.98 ± 0.64	35.87 ± 0.98	0.507	0.614

Table 4: Comparison of postoperative recovery ($\overline{x} \pm s$).

Items	Group J ($n = 28$)	Group Q ($n = 32$)	t	P
Total amount of albumin infusion (g)	13.10 ± 3.48	41.65 ± 13.57	10.815	<0.001
Postoperative ventilation time (d)	2.56 ± 0.35	2.68 ± 0.35	1.325	0.190
Postoperative	9.25 ± 0.30	13.11 ± 0.58	31.680	<0.001

group Q ($n = 32$) with nutritional risk according to the classification of NRS2002. The two groups showed no obvious difference in preoperative situation, and patients' liver function indexes were within the normal range, which could be used for study.

Anesthesia, trauma, and other factors during liver cancer surgery can cause high catabolism. If patients have poor preoperative nutritional status and low surgical tolerance, their perioperative body consumption will be higher than that of ordinary patients, further increasing the possibility of metabolic disorders after surgery and seriously affecting the recovery during anesthesia. Moreover, liver cancer surgery will lead to serious damage to liver function. Malnutrition will further aggravate liver damage, significantly reduce the frequency of albumin synthesis, and increase the incidence of complications such as hypoproteinemia, infection, and poor healing, thus slowing the recovery of patients after surgery. This study showed that the duration of surgery and postoperative hospitalization time in group J were notably shorter compared with group Q ($P < 0.05$), indicating that malnutrition will worsen the body condition of patients and increase the surgical risk. ALT, AST, DBIL, and albumin in group J were notably different compared with group Q ($P < 0.001$) at 1 day after surgery. ALT and AST in group J were notably different compared with group Q at 3 days after surgery ($P < 0.001$). The above results indicated that patients with malnutrition had more serious liver damage, with unsatisfactory postoperative recovery.

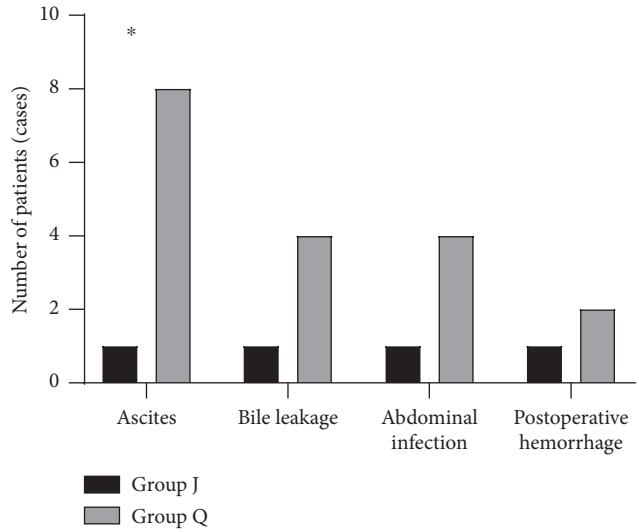

Figure 3: Comparison of the incidence of complications. The abscissa from left to right represent ascites, bile leakage, abdominal infection, and postoperative hemorrhage, and the ordinate represents the number of patients (cases). The black area represents group J, and the gray area represents group. Q $^{*}P < 0.05$. Ascites occurred in 1 case of group J and 8 cases of group Q. Bile leakage occurred in 1 case of group J and 4 cases of group Q. Abdominal infection occurred in 1 case of group J and 4 cases of group Q. Postoperative hemorrhage occurred in 1 case of group J and 2 cases of group Q.

The study also found that the hospitalization cost in group J was notably lower compared with group Q ($P < 0.001$), which may be related to the higher incidence of complications in group Q. Group Q received more albumin infusion, resulting in an obvious increase of the hospitalization cost. This study also showed that patients with malnutrition were more likely to have complications such as ascites and bile leakage compared with group J, but no serious complications or death occurred. This is because the patients in this study received comprehensive evaluation and perioperative management before surgery, as well as enteral nutrition support after surgery. Therefore, both groups of patients had certain recovery.

According to the study of Debanjan et al., the albumin infusion volume of patients with malnutrition undergoing liver cancer surgery was (41.65 ± 13.57) g, which was significantly higher than that of patients with normal nutrition ($P < 0.001$) [24], revealing that malnutrition can affect the body state and aggravate the perioperative consumption of patients. Therefore, it is of great importance to deepen the study on chronic nutritional consumption of such patients.

In conclusion, liver cancer is a common malignant disease affecting life and health of Chinese residents. This study has confirmed that postoperative recovery of LC patients is closely related to their preoperative nutritional status, and those with poor nutritional status have a high incidence of postoperative complications and long recovery time. NRS2002 can effectively screen the nutritional status of patients and provide reference for prognosis evaluation and the application of nutritional support programs.

Data Availability

All data can be provided by the corresponding author upon request.

Conflicts of Interest

The authors declare that they have no conflicts of interest.

Authors' Contributions

Suling Huang and Shijie Wang contributed equally to this work.

Acknowledgments

This article was funded by "Ganzhou Guiding Science and Technology Plan Task (GZ2018ZSF088)."

References

[1] R. Boulhosa, R. P. Loureno, D. M. Crtes et al., "Comparison between criteria for diagnosing malnutrition in patients with advanced chronic liver disease: GLIM group proposal versus different nutritional screening tools," *Journal of Human Nutrition and Dietetics*, vol. 33, no. 6, 2020.

[2] G. Giorgetti, F. Fabiocchi, G. Brandimarte, and A. Tursi, "Acute diverticulitis is at significant risk of malnutrition: an analysis of hospitalized patients in a medicine department," *Journal of gastrointestinal and liver diseases: JGLD*, vol. 28, no. 4, pp. 53–56, 2019.

[3] A. Adiamah, P. Skorepa, A. Weimann et al., "The impact of preoperative immune modulating nutrition on outcomes in patients undergoing surgery for gastrointestinal cancer: a systematic review and meta-analysis," *Annals of Surgery*, vol. 270, no. 2, pp. 247–256, 2019.

[4] K. Russell, H. G. Zhang, L. K. Gillanders et al., "Preoperative immunonutrition in patients undergoing liver resection: a prospective randomized trial," *World Journal of Hepatology*, vol. 11, no. 3, pp. 305–317, 2019.

[5] I. Bachini, V. Ariu, F. Canaletti et al., "IMMUNO-ERAS: preoperative immunonutrition IN patients undergoing

elective liver surgery within eras pathway," *Nutrition*, vol. 75-76, Article ID 110926, 2020.

[6] A. Demagistris, V. Ariu, I. Bachini et al., "Preoperative immunonutrition in liver surgery within eras pathway: a post-hoc analysis in the subgroup of patients at nutritional risk," *Nutrition*, vol. 75-76, Article ID 110918, 2020.

[7] P. Probst, J. Fuchs, M. R. Schön et al., "Prospective study to evaluate the prognostic value of different nutritional assessment scores in liver surgery: NURIMAS Liver (DRKS00006340)," *Hepatobiliary Surgery and Nutrition*, vol. 9, no. 4, pp. 400–413, 2020.

[8] P. Achilli, M. Mazzola, C. L. Bertoglio et al., "Preoperative immunonutrition in frail patients with colorectal cancer: an intervention to improve postoperative outcomes," *International Journal of Colorectal Disease*, vol. 35, no. 9868, 2020.

[9] R. Tokunaga, S. Nakagawa, Y. Miyamoto et al., "The clinical impact of preoperative body composition differs between male and female colorectal cancer patients," *Colorectal Disease*, vol. 22, no. 1, pp. 62–70, 2020.

[10] L. A. Robinson, T. Tanvetyanon, D. Grubbs et al., "Preoperative nutrition-enhanced recovery after surgery (N-ERAS) protocol for thoracic neoplasms," *The Journal of Thoracic and Cardiovascular Surgery*, vol. 162, no. 3, pp. 710.e1–720.e1, 2020.

[11] Y. Okugawa, "P2-080 clinical burden of prognostic nutrition index in patients with rectal cancer who receive preoperative chemoradiotherapy," *Annals of Oncology*, vol. 29, no. 7, 2018.

[12] N. Kamo, T. Kaido, Y. Miyachi et al., "Preoperative abnormal body composition is closely related to bacteremia after living donor liver transplantation," *Nutrition*, vol. 77, Article ID 110798, 2020.

[13] D. Atieh, M. Darbandi, A. Shariati et al., "The effects of probiotics on reducing the colorectal cancer surgery complications: a periodic review during 2007–2017," *Clinical Nutrition*, vol. 39, no. 8, pp. 2358–2367, 2019.

[14] Korean Liver Cancer Association and National Cancer Center, "2018 Korean liver cancer association-national cancer center korea practice guidelines for the management of hepatocellular carcinoma," *Gut & Liver*, vol. 13, no. 3, pp. 227–299, 2019.

[15] E. B. Tapper and N. D. Parikh, "Mortality due to cirrhosis and liver cancer in the United States, 1999–2016: observational study," *BMJ*, vol. 362, p. k2817, 2018.

[16] J. L. Petrick, T. Jake, Z. J. Anne et al., "Body mass index, diabetes and intrahepatic cholangiocarcinoma risk: the liver cancer pooling project and meta-analysis," *The American Journal of Gastroenterology*, vol. 113, no. 10, pp. 1494–1505, 2018.

[17] P. C. Valery, M. Laversanne, P. J. Clark, J. L. Petrick, K. A. McGlynn, and F. Bray, "Projections of primary liver cancer to 2030 in 30 countries worldwide," *Hepatology*, vol. 67, pp. 600–611, 2018.

[18] A. Chatterjee, J. Biswas, A. Chatterjee, S. Bhattacharya, B. Mukhopadhyay, and S. Mandal, "Psorinum therapy in treating stomach, gall bladder, pancreatic, and liver cancers: a prospective clinical study," *Evidence-Based Complementary and Alternative Medicine*, vol. 2018, Article ID 724743, 7 pages, 2018.

[19] A. Cast, L. Valanejad, M. Wright et al., "C/EBPα-dependent preneoplastic tumor foci are the origin of hepatocellular carcinoma and aggressive pediatric liver cancer," *Hepatology*, vol. 67, no. 5, 2018.

[20] Y. Pang, C. Kartsonaki, I. Turnbull et al., "Diabetes, plasma glucose and incidence of fatty liver, cirrhosis and liver cancer: a prospective study of 0.5 million people," *Hepatology*, vol. 68, 2018.

[21] A. W. Singer, K. R. Reddy, L. E. Telep et al., "Direct-acting antiviral treatment for hepatitis C virus infection and risk of incident liver cancer: a retrospective cohort study," *Alimentary Pharmacology & Therapeutics*, vol. 47, no. 9, pp. 1278–1287, 2018.

[22] E. I. Cohen, D. Field, G. E. Lynskey, and A. Y. Kim, "Technology of irreversible electroporation and review of its clinical data on liver cancers," *Expert Review of Medical Devices*, vol. 15, no. 2, pp. 99–106, 2018.

[23] S. T. Orcutt and D. A. Anaya, "Liver resection and surgical strategies for management of primary liver cancer," *Cancer Control: Journal of the Moffitt Cancer Center*, vol. 25, no. 1, 2018.

[24] D. Debanjan, A. Laura, N. Hayato et al., "The application value of NRS2002 in patients with liver cancer, the relationship between nutritional status and patient prognosis," *Cancer Cell*, vol. 33, no. 6, pp. 1061.e6–1077.e6, 2018.

Hindawi
Journal of Oncology
Volume 2021, Article ID 5140621, 8 pages
https://doi.org/10.1155/2021/5140621

Research Article

Effect of Gambogic Acid on miR-199a-3p Expression and Cell Biological Behavior in Colorectal Cancer Cells

Xiaodong Wang, Yingchun Li, Haihua Zhou, Ning Han, Linlin Pan, and Chen Yu

Department of Anus & Intestine Surgery, Taizhou People's Hospital,
Taizhou Clinical Medical College of Nanjing Medical University, Taizhou 225300, Jiangsu, China

Correspondence should be addressed to Yingchun Li; wxd5018@163.com

Received 28 June 2021; Accepted 7 August 2021; Published 27 August 2021

Academic Editor: Muhammad Wasim Khan

Colorectal cancer (CC), as a malignancy threatening life and health, has a rising incidence in recent years. It has been reported that gambogic acid (GA) has antitumor activity in various tumors, but its effect on CC remains to be elucidated. In this investigation, the influence of GA nanoparticles on microRNA-199a-3p (miR-199a-3p) in CC was analyzed to provide a reliable reference for future clinical practice. Through PCR detection, we first determined that miR-199a-3p presented low expression in CC and had a significant effect in predicting the onset and prognosis of CC. Through in vitro experiments, the enhanced CC cell viability after inhibition was determined; however, decreased cell viability and increased miR-199a-3p level were also observed after GA nanoparticles addition. Hence, GA nanoparticles may influence CC cell biological behaviors by modulating miR-199a-3p, providing a novel treatment scheme for CC in the future.

1. Introduction

As a malignant disease threatening life and health, colorectal cancer (CC) has a very high prevalence on the global scale [1, 2]. According to research reports, the incidence of CC is as high as 4-5%, and the susceptibility is linked to personal characteristics and habits, such as age, history of chronic diseases, and lifestyle [3, 4]. In such a case, the gut microbiome plays a related role, while malnutrition can trigger CC through a chronic inflammatory mechanism [5]. The prevalence of CC rises along with the development of society and the change of people's living habits [6], and it is more pervasive in middle-aged people over 40 years old, with more males than females [7]. At the beginning of CC, the cure rate is extremely high. Whereas, the disease can be ignored easily due to the absence of obvious symptoms in the early stage, and as a result, most patients are in the middle stage when diagnosed [8, 9]. Referring to previous relevant data, it is found that the prognosis of patients in the advanced stage is unfavorable after surgical treatment, which seriously affects the therapeutic effect [10]. In recent years, as the traditional Chinese medicine (TCM) has risen to prominence in clinical treatment, its treatment of major diseases such as malignancies has attracted increasing attention [11].

Gambogic acid (GA) is a potential anticancer compound [12], which is extracted from *Garcia hanburyi*'s resin and has potent anticancer activity [13]. Studies have found that GA has an obvious inhibitory effect on liver cancer [14]. Besides, many related studies confirmed that GA has certain curative effects on breast cancer, lymphoma, skin cancer, and gastric cancer [15]. Moreover, miR-199a-3p interferes with the onset and progression of various malignant tumors. Author Callegari E [16] observed that in hepatocellular carcinoma transgenic mouse models, MTOR and PAK4 pathways were modulated and tumor growth was suppressed by miR-199a-3p. Author Cui Y [17] revealed enhanced cisplatin sensitivity of ovarian cancer cells by miR-199a-3p. Whereas, the lack of research data hinders the elucidation of the clinical value of miR-199a-3p in CC. Considering its clinical manifestations in other malignant tumors, we presumed that it might benefit the treatment of CC.

In recent years, the research of nanomedicine is a research hotspot in the medical field. Nanomedicine can not only improve the effect and half-life of the drug but also reduce its toxic and side effects [18]. GA nanobodies have also been confirmed to have a higher clinical application value than traditional GA [19]. Therefore, this study will analyze the effects of GA nanobodies on the expression of miR-199a-3p in colorectal cancer cells as well as cell proliferation and apoptosis and provide new ideas and theoretical foundations for the treatment of colorectal cancer in the future.

2. Materials and Methods

2.1. Patient Data. From April 2013 to May 2015, fifty-six CC patients treated at Taizhou People's Hospital, Taizhou, Jiangsu, PR China, were selected as the research group (RG), while 61 healthy individuals as the control group (CG). The study was approved by the Ethics Committee of the Taizhou People's Hospital, Jiangsu, PR China, and all patients provided written informed consent.

2.2. Inclusion and Exclusion Criteria. All the included patients were confirmed by endoscopy, laboratory examination, and imaging and met the diagnostic criteria for CC. All the primary lesions were CC, and all the patients were aged 35 or older.

Patients with pregnancy or lactation were excluded, as well as those with other tumors or immunodeficiency.

2.3. Cell Data. Human CC cell line SW480 and normal human colon epithelial cell line NCM-460 were purchased from BeNa Culture Collection, a subsidiary of ATCC, USA, while gambogic acid was from Shanghai PureOne Biotechnology. After resuscitation, the cells were inoculated into the corresponding culture medium and cultivated in a 5% CO_2 incubator at 37°C. The passage was carried out when the confluence reached 80%, and cells used in experiments were in a growth period.

2.4. Cell Intervention. After transfection with the corresponding vector according to the Lipofectamine 2000 kit instructions, the miR-199a-3p-NC group (intervened by miR-199a-3p negative control), miR-199a-3p-mim group (intervened by miR-199a-3p mimic sequence), and miR-199a-3p-inh group (intervened by miR-199a-3p inhibitor sequence) were set up.

2.5. Preparation of GA Nanoparticles. Dephosphatidylcholine (PC) 60 mg, cholesterol (Chol) 30 mg, and GA 4 mg was mixed and add 15 mL of chloroform to dissolve in a rotary evaporator (0.01 MPa, 30°C) to form a film, remove the solvent, and then increase the vacuum to remove traces of chloroform. Add phosphate-buffered saline solution and glass beads (2 mm), spin, and hydrate for 5 min. After 10 minutes of sonication, GA nanoparticles were prepared.

2.6. GA Nanobody Intervention Cell. SW480 was added to the culture medium containing GA nanoparticles to incubate for 48 hours and then subcultured. When the growth length reached 80%, the follow-up test was performed.

2.7. PCR. The total RNA, after extraction, was reverse transcribed into cDNA according to PrimeScript™ RT reagent Kit and used SYBR Green PCR Master Mix for PCR detection. The internal reference was U6, and the expression level was calculated by $2^{-\triangle\triangle CT}$.

2.8. CCK-8. Cells seeded in the 96-well plates following 24, 48, 72, and 96 h of culture were immersed in 20 μL CCK-8, and the absorbance (450 nm) of each well was measured following another 4 h of culture. After the removal of culture solution, 200 μL GA was added to each well, followed by the replenishing of culture solution, with a final concentration of 4.0 μg/mL. After the addition of 20 μL CCK-8, the absorbance (450 nm) of each well was determined following another 4 h of culture, in order to draw the cell growth curve.

2.9. Flow Cytometry Test. The apoptosis level of the cells was observed by flow cytometry assay. The cells were diluted at 2×10^3 cells/mL by ice Annexin V-FITC binding buffer. Cells were cultured in fresh Gibco 1640 solution with 0 μg/mL as a blank group. They were treated with 10 μL of propidium iodide (PI 20 μg/ml) and 5 μL of Annexin V-FITC/PI (10 μg/ml) cell apoptosis assay 24 later and cultivated at ambient temperature for 10 min for apoptosis determination. Finally, the apoptosis level of the cells was instantly observed by a flow cytometry equipment (BD Biosciences, State of New Jersey, USA).

2.10. Transwell Experiment. Transwell upper chamber and lower chamber were added with cells adjusted to 1×10^6/mL and fetal bovine serum culture medium, respectively. After 24 h, the cells in the upper chamber were wiped off, immobilized, stained, and counted under the microscope.

2.11. Western Blot. Fishing extraction from RIPA lysate, the total protein was processed for SDS-PAGE electrophoresis isolation and membrane transfer. Then, it was processed for 2 h of sealing with 50 g/L skimmed milk powder and 24 h of cultivation mixed with Bax, Bcl-2 (1 : 1000, AB_2533042), and β-actin (1 : 1000, AB_11004139) at 4°C, followed by TBST rinsing and 2 h of cultivation with II antibody (1 : 2000). Image *J* analyzed the band gray value. All antibodies were purchased from ThermoFisher (Massachusetts, USA).

2.12. Statistical Analysis. Data were processed by SPSS22.0 and visualized using Graphpad7. The average value of the experimental results was calculated and recorded as mean ± standard deviation; the comparison between groups was realized by the independent sample *t*-test, the comparison among groups by one-way ANOVA and LSD post-hoc test. Receiver operating characteristic (ROC) curves

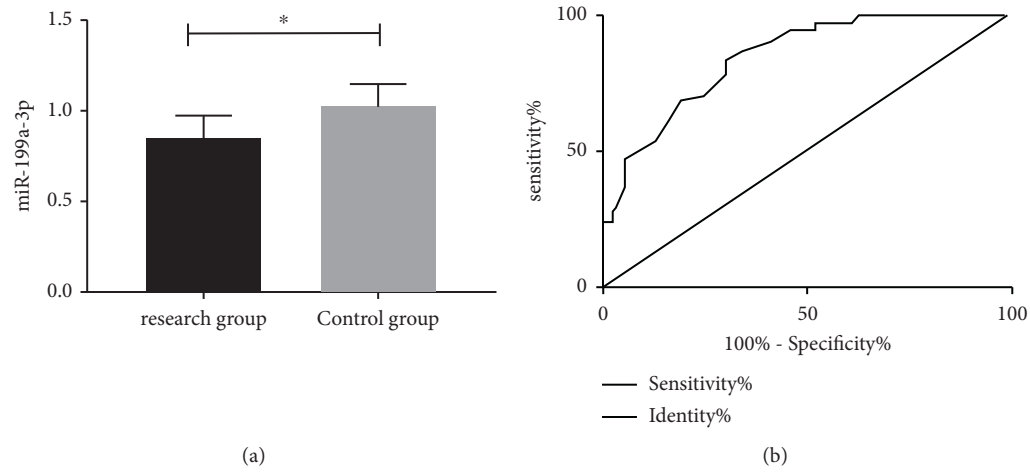

Figure 1: miR-199a-3p expression. (a) miR-199a-3p expression in the research group and control group. (b) Predictive significance of miR-199a-3p in the onset of CC. Note: $^{*}P < 0.05$.

analyzed the predicted value. Statistical difference was considered when $P < 0.05$.

3. Results

3.1. miR-199a-3p Expression Profiles in CC. miR-199a-3p showed lower levels in RG (0.83 ± 0.13) than in CG (1.02 ± 0.12) ($P < 0.05$, Figure 1(a)). ROC revealed that miR-199a-3p < 0.925, and the sensitivity, specificity, area under the curve (AUC), and standard error were 83.61%, 69.64%, 0.846, and 0.035, respectively ($P < 0.001$, Figure 1(b), Table 1).

3.2. Influence of miR-199a-3p on Patient Prognosis. The 5-year follow-up rate was 100%. The follow-up results indicated that miR-199a-3p was (0.34 ± 0.09) among the 20 dead, while miR-199a-3p was (0.50 ± 0.11) among the 36 survivors (Figure 2(a) and Table 2). ROC exhibited that when miR-199a-3p < 0.35, it had a sensitivity of 80.56%, a specificity of 65.00%, an AUC of 0.804, and standard error of 0.064 ($P < 0.001$, Figure 2(b) and Table 2). The patients were subdivided into high and low expression groups based on the cutoff value, and prognosis and survival curves determined a remarkably higher mortality rate in the low expression group compared with the high expression group ($P < 0.05$, Figure 2(c) and Table 2).

3.3. Influence of miR-199a-3p on SW480 of Human CC Cell Strain. miR-199a-3p expression in human CC cell strain SW480 and normal human colon epithelial cell NCM-460 was detected. The results identified statistically lower miR-199a-3p in SW480 than in NCM-460 ($P < 0.05$, Figure 3(a)). Besides, the miR-199a-3p-mim group showed declined proliferation and invasion capacity and elevated apoptosis rate, while the miR-199a-3p-inh group presented enhanced proliferation and invasion ability and reduced apoptosis ($P < 0.05$, Figures 3(b)–3(d)).

3.4. Influence of GA on Human CC Cell Strain SW480. Under TEM, the particle size of GA nanobodies is about 200 nm (Figure 4(a)). Changes in proliferation, invasion, and apoptosis rate of human CC cell strain SW480 after GA intervention were analyzed. It showed that the tumorigenic phenotype of CC cells SW480 was reduced following GA intervention, and the apoptosis rate was increased compared with those without GA intervention ($P < 0.05$, Figures 4(b)–4(d)).

3.5. miR-199a-3p Expression Changes in Cells following GA Addition. miR-199a-3p expression in the CC cells after GA intervention (0.96 ± 0.13) was significantly higher than the CC cells without GA intervention (0.73 ± 0.14) ($P < 0.05$, Figure 5).

3.6. Influence of miR-199a-3p on Human CC Cell Strain SW480 following GA Addition. Transfection of GA-interfered SW480 resulted in the lowered proliferation and invasion ability and increased apoptosis in miR-199a-3p-mim group, while the reverse results were obtained in the miR-199a-3p-inh group ($P < 0.05$, Figure 6).

4. Discussion

Due to people's unhealthy living habits, the incidence of CC is on the rise [20, 21]. Molecular exploration and analysis is now a trending topic in the research of malignant tumor diseases, which carries huge implications for future prevention and treatment of tumors [22]. This study, through preliminary investigation of the influence of miR-199a-3p and GA nanoparticles on CC, may provide potential basis for future clinical practice.

First, low miR-199a-3p in serum was observed in CC patients, implying that miR-199a-3p may interfere with CC progression. Similar results were obtained in the previous research [23], which can testify to our experimental results. Then, for the sake of determining its clinical significance, we

Table 1: Primer sequence.

	Forward primer	Reverse primer
miR-199a-3p	5′-GCCACAGTAGTCTGCACAT-3′	5′-CAGTGCGTGTCGTGGAGT-3′
U6	5′-CTCGCTTCGGCAGCACA-3′	5′-AACGCTTCACGAATTTGCGT-3′

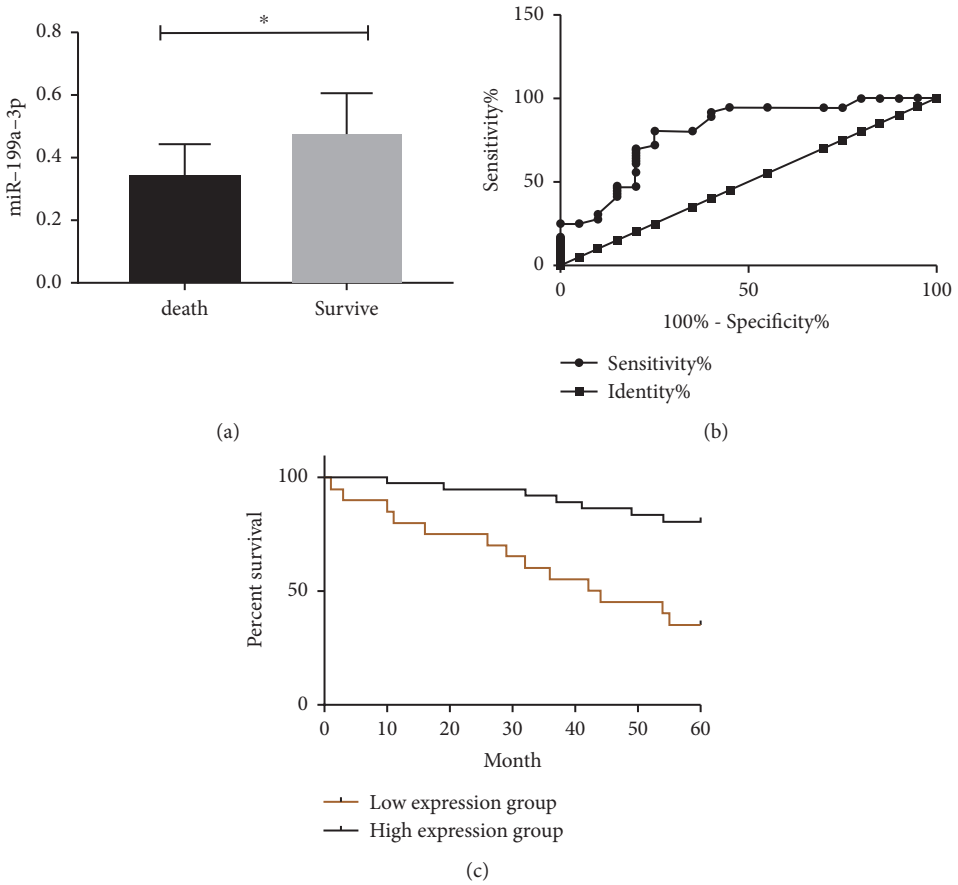

Figure 2: Influence of miR-199a-3p on patient prognosis. (a) miR-199a-3p expression in patients with survival and death. (b) ROC curves of miR-199a-3p for predicting patient death. (c) Prognostic survival curves. Note: $^{*}P < 0.05$.

Table 2: Diagnostic effect of miR-199a-3p on CC.

	miR-199a-3p
AUC	0.846
Standard error	0.035
95% CI	0.777–0.914
Cutoff	>0.925
Sensitivity (%)	83.61
Specificity (%)	69.64
Youden index	53.25
P	<0.001

determined miR-199a-3p's predictive value in CC by ROC curve analysis. The results showed that the predictive sensitivity and specificity of miR-199a-3p for CC were 83.61% and 69.64%, respectively, demonstrating its plausible predictive effect on the onset of CC, for it not only has a better response ability to CC but also has a superior recognition specificity. The current tumor markers commonly used in the clinic, such as CEA, CA125, and CA199, can basically show a strong response to all tumor diseases [24]. There are also pieces of evidence pointing out that the traditional cancer markers increase in conditions such as chronic inflammatory diseases or tissue injuries [25], so the ability of early screening for tumor diseases is getting lower and lower. The diagnostic value of miR-199a-3p for CC can effectively make up for the deficiencies of traditional cancer targets, bolster the early diagnosis rate of CC, and improve the prognosis of patients. Furthermore, according to a previous study, miR-199a-3p is a candidate diagnostic marker for renal cell carcinoma [26], which further confirms its significant clinical application potential in the future. Of course, ROC curve analysis usually requires a large number of research bases for analysis, so that the cutoff value obtained and the diagnostic performance can be more accurate [27]. However, the included case number is relatively small, and consequently, there may be errors in reverifying the results. Therefore, large sample size and multicenter evaluation will provide more potential basis regarding this

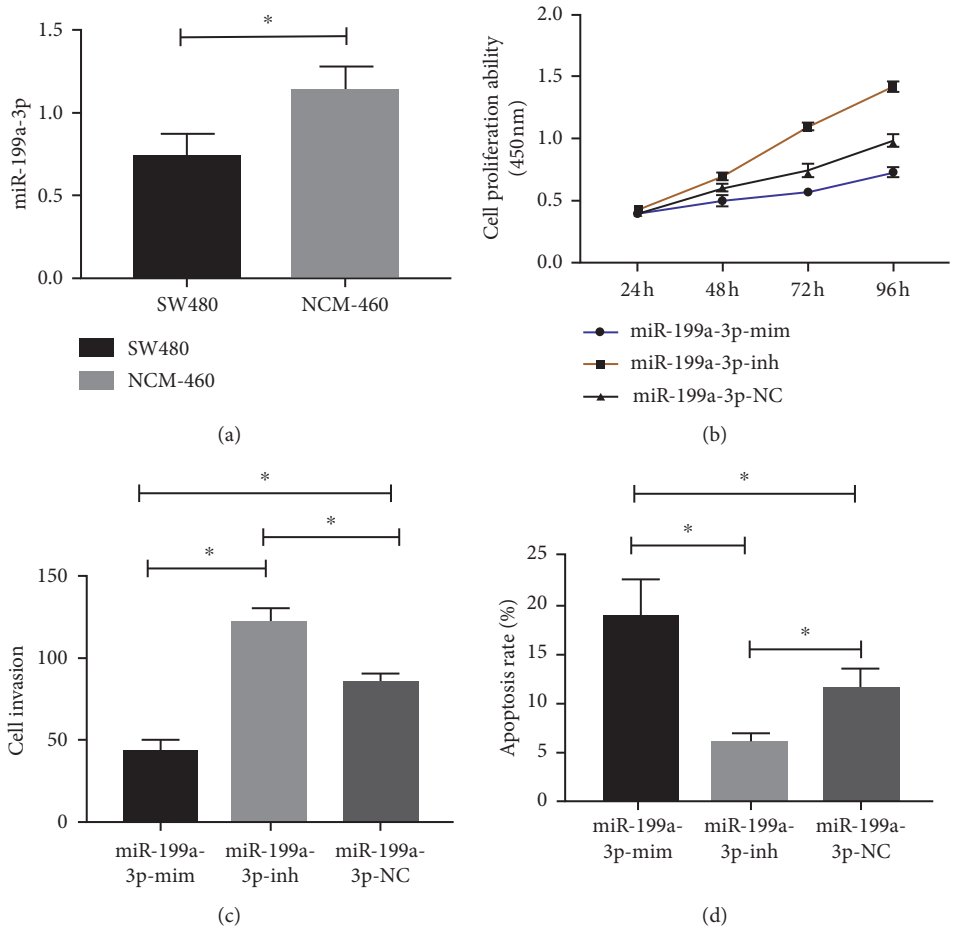

Figure 3: Influence of miR-199a-3p on SW480. (a) miR-199a-3p expression. (b) Cell proliferation. (c) Cell invasion. (d) Apoptosis rate. Note: $^{*}P < 0.05$.

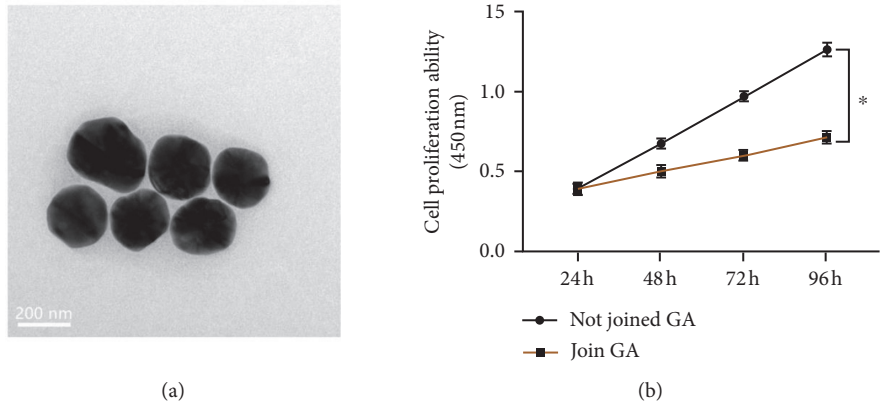

Figure 4: Continued.

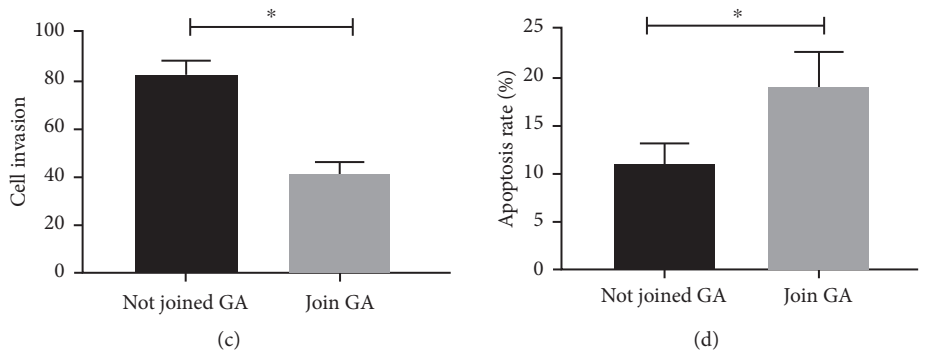

Figure 4: Influence of GA on SW480. (a) Observe GA nanoparticles under TEM. (b) Cell proliferation. (c) Cell invasion. (d) Apoptosis rate. Note: $^{*}P < 0.05$.

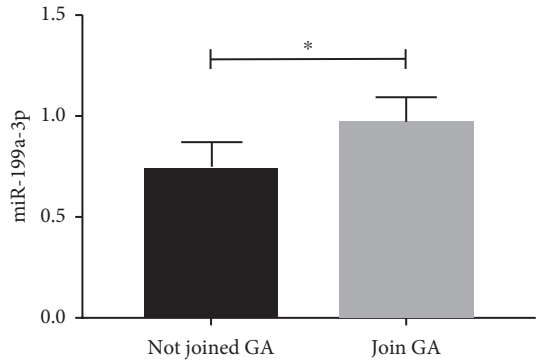

Figure 5: miR-199a-3p expression changes in cells following GA addition.

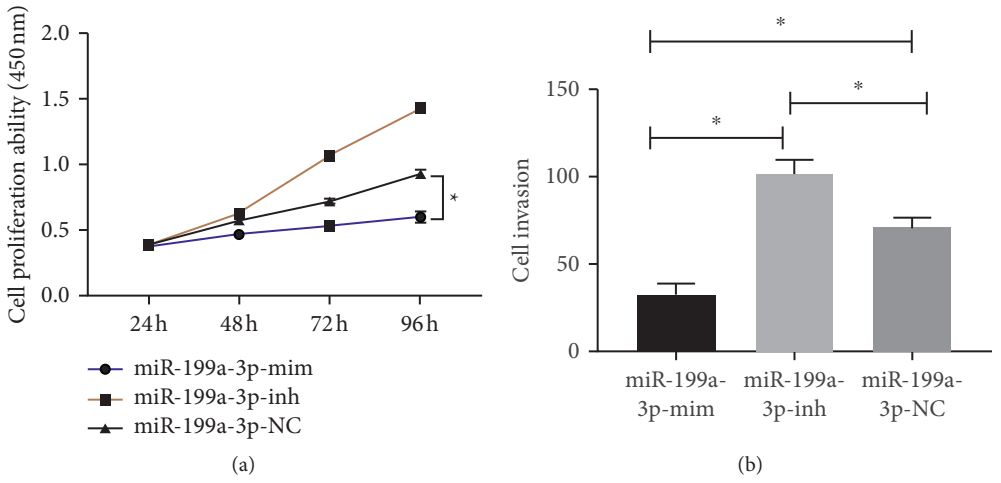

Figure 6: Continued.

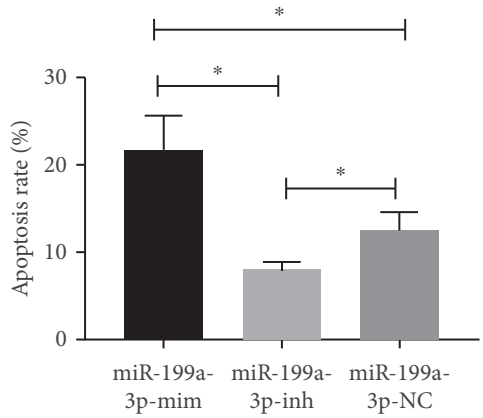

Figure 6: Influence of miR-199a-3p on SW480 following GA addition. (a) Cell proliferation. (b) Cell invasion. (c) Apoptosis. Note: $^{*}P < 0.05$.

concept. Subsequently, we analyzed the influence of miR-199a-3p on patient prognosis through the prognostic follow-up. The results identified notably lowermiR-199a-3p levels among the dead, which was basically consistent with the results of our above analysis. And through ROC curve analysis, we found that miR-199a-3p has an excellent predictive value for the prognostic death of CC patients. Moreover, the prognostic survival curves identified an increased risk of death confronted by patients with low miR-199a-3p expression. Based on the above results, we can see that the lower the miR-199a-3p expression is, the more severe the development of CC may be, which also provides a reliable reference for future clinical understanding of the patient's condition.

Although some studies have analyzed the action mechanism of miR-199a-3p [28], the mechanism of its action on CC is not clear. Hence, the biological effects of miR-199a-3p on CC cells were investigated through in vitro experiments. The results revealed enhanced CC cell viability following miR-199a-3p suppression, but increased miR-199a-3p lead to the opposite. Thus, it is clear that low-expressed miR-199a-3p promotes the activity of tumor cells and accelerates CC progression, which is consistent with the previous research [29] and our above experimental. Then, we tested the biological behavior of CC cells under GA intervention and found obviously inhibited cell viability and enhanced apoptosis rate. Hence, GA nanoparticles can play a role in the treatment of CC, which verifies the effect of GA nanoparticles. Furthermore, an increased miR-199a-3p increased was observed under GA nanoparticles intervention, so we speculated that the influence of GA nanoparticles on CC cells might be associated with miR-199a-3p. Finally, miR-199a-3p mimics and inhibitors were introduced into CC cells under GA nanoparticles intervention. The results were found to be roughly the same as those after miR-199a-3p transfection as mentioned above, except that cell viability and apoptosis showed more distinct differences under GA nanoparticles intervention. The study has indicated that GA could effectively inhibit the progression of the nonsmall cell lung cancer via inducing the autophagy progression of the tumor cells [30]. Therefore, we can preliminarily infer that through modulating miR-199a-3p, GA nanoparticles exert their effect on CC cells. However, due to the short experimental period, how miR-199a-3p interferes with the long-term prognosis of CC patients remains unresolved. Besides, the influence of GA nanoparticles on CC cells may not only be carried out by affecting miR-199a-3p, so further exploration of other mechanisms is warranted. Moreover, we did not compare the effect of cisplatin and other commonly used CC treatment drugs in clinical practice with that of GA nanoparticles, so it is still unclear which drug has a more significant effect on tumor cells. Last but not least, the deeper and more intricate relationship and relevant pathways of GA nanoparticles and miR-199a-3p on CC cells are worthy of further experimental analysis.

5. Conclusion

GA may affect CC cell biological behaviors by modulating miR-199a-3p, which usually shows low expression in CC, providing a novel treatment approach for CC in the future.

Data Availability

The data used to support the findings of this study are available from the corresponding author upon request.

Conflicts of Interest

The authors declare that they have no conflicts of interest.

References

[1] E. Dekker, P. J. Tanis, J. L. A. Vleugels, P. M. Kasi, and M. B. Wallace, "Colorectal cancer," *The Lancet*, vol. 394, no. 10207, pp. 1467–1480, 2019.

[2] K. Thanikachalam and G. Khan, "Colorectal cancer and nutrition," *Nutrients*, vol. 11, no. 1, 2019.

[3] C. Lucas, N. Barnich, and H. T. T. Nguyen, "Microbiota, inflammation and colorectal cancer," *International Journal of Molecular Sciences*, vol. 18, no. 6, 2017.

[4] I. Mármol, C. Sánchez-De-Diego, A. Pradilla Dieste, E. Cerrada, and M. J. Rodriguez Yoldi, "Colorectal carcinoma: a general overview and future perspectives in colorectal cancer," *International Journal of Molecular Sciences*, vol. 18, no. 1, 2017.

[5] J. S. Moore and T. H. Aulet, "Colorectal cancer screening," *Surgical Clinics of North America*, vol. 97, no. 3, pp. 487–502, 2017.

[6] R. Gao, Z. Gao, L. Huang, and H. Qin, "Gut microbiota and colorectal cancer," *European Journal of Clinical Microbiology & Infectious Diseases*, vol. 36, no. 5, pp. 757–769, 2017.

[7] I. A. Issa and M. Noureddine, "Colorectal cancer screening: an updated review of the available options," *World Journal of Gastroenterology*, vol. 23, no. 28, pp. 5086–5096, 2017.

[8] M. J. Munro, S. K. Wickremesekera, L. Peng, S. T. Tan, and T. Itinteang, "Cancer stem cells in colorectal cancer: a review," *Journal of Clinical Pathology*, vol. 71, no. 2, pp. 110–116, 2018.

[9] G. Mauri, A. Sartore-Bianchi, A. G. Russo, S. Marsoni, A. Bardelli, and S. Siena, "Early-onset colorectal cancer in young individuals," *Molecular Oncology*, vol. 13, no. 2, pp. 109–131, 2019.

[10] S. H. Wong and J. Yu, "Gut microbiota in colorectal cancer: mechanisms of action and clinical applications," *Nature Reviews Gastroenterology & Hepatology*, vol. 16, no. 11, pp. 690–704, 2019.

[11] K. Y. Tan, C. B. Liu, A. H. Chen et al., "The role of traditional Chinese medicine in colorectal cancer treatment," *Techniques in Coloproctology*, vol. 12, no. 1, pp. 1–6, 2008.

[12] X. Sun, T. T. H. Ng, K. W. Y. Sham, L. Zhang, M. T. V. Chan, and W. K. K. Wu, "Bufalin, a traditional Chinese medicine compound, prevents tumor formation in two murine models of colorectal cancer," *Cancer prevention research (Philadelphia*, vol. 12, no. 10, pp. 653–666, 2019.

[13] H. Wang, Z. Zhao, S. Lei et al., "Gambogic acid induces autophagy and combines synergistically with chloroquine to suppress pancreatic cancer by increasing the accumulation of reactive oxygen species," *Cancer Cell International*, vol. 19, no. 1, p. 7, 2019.

[14] K. Zhao, S. Zhang, X. Song et al., "Gambogic acid suppresses cancer invasion and migration by inhibiting TGFβ1-induced epithelial-to-mesenchymal transition," *Oncotarget*, vol. 8, no. 16, pp. 27120–27136, 2017.

[15] G. Xia, H. Wang, Z. Song, Q. Meng, X. Huang, and X. Huang, "Gambogic acid sensitizes gemcitabine efficacy in pancreatic cancer by reducing the expression of ribonucleotide reductase subunit-M2 (RRM2)," *Journal of Experimental & Clinical Cancer Research*, vol. 36, no. 1, p. 107, 2017.

[16] E. Callegari, L. D'Abundo, P. Guerriero et al., "miR-199a-3p modulates MTOR and PAK4 pathways and inhibits tumor growth in a hepatocellular carcinoma transgenic mouse model," *Molecular Therapy-Nucleic Acids*, vol. 11, pp. 485–493, 2018.

[17] Y. Cui, F. Wu, D Tian et al., "miR-199a-3p enhances cisplatin sensitivity of ovarian cancer cells by targeting ITGB8," *Oncology Reports*, vol. 39, no. 4, pp. 1649–1657, 2018.

[18] J. K. Patra, G. Das, L. F. Fraceto et al., "Nano based drug delivery systems: recent developments and future prospects," *Journal of Nanobiotechnology*, vol. 16, no. 1, p. 71, 2018.

[19] L. Han, Y. Wang, X. Huang et al., "Specific-oxygen-supply functionalized core-shell nanoparticles for smart mutual-promotion between photodynamic therapy and gambogic acid-induced chemotherapy," *Biomaterials*, vol. 257, Article ID 120228, 2020.

[20] A. Grancher, P. Michel, F. Di Fiore, and D. Sefrioui, "Aspirine et cancer colorectal," *Bulletin du Cancer*, vol. 105, no. 2, pp. 171–180, 2018.

[21] K. M. Smith and J. Desai, "Nivolumab for the treatment of colorectal cancer," *Expert Review of Anticancer Therapy*, vol. 18, no. 7, pp. 611–618, 2018.

[22] E. Saus, S. Iraola-Guzmán, J. R. Willis, A. Brunet-Vega, and T. Gabaldón, "Microbiome and colorectal cancer: roles in carcinogenesis and clinical potential," *Molecular Aspects of Medicine*, vol. 69, pp. 93–106, 2019.

[23] E. Pashaei, E. Pashaei, M. Ahmady, M. Ozen, and N. Aydin, "Meta-analysis of miRNA expression profiles for prostate cancer recurrence following radical prostatectomy," *PLoS One*, vol. 12, no. 6, Article ID e0179543, 2017.

[24] M. Campos-da-Paz, J. G. Dórea, A. S. Galdino, Z. G. M. Lacava, and M. A. S. De Fatima, "Carcinoembryonic antigen (CEA) and hepatic metastasis in colorectal cancer: update on biomarker for clinical and biotechnological approaches," *Recent Patents on Biotechnology*, vol. 12, no. 4, pp. 269–279, 2018.

[25] W. Lei, C. Yan, J. Ya, D. Yong, B. Yujun, and L. Kai, "MiR-199a-3p affects the multi-chemoresistance of osteosarcoma through targeting AK4," *BMC Cancer*, vol. 18, no. 1, p. 631, 2018.

[26] J. Liu, B. Liu, Y. Guo et al., "MiR-199a-3p acts as a tumor suppressor in clear cell renal cell carcinoma," *Pathology, Research & Practice*, vol. 214, no. 6, pp. 806–813, 2018.

[27] N. A. Obuchowski and J. A. Bullen, "Receiver operating characteristic (ROC) curves: review of methods with applications in diagnostic medicine," *Physics in Medicine and Biology*, vol. 63, no. 7, Article ID 07TR01, 2018.

[28] P. Phatak, W. M. Burrows, I. E. Chesnick et al., "MiR-199a-3p decreases esophageal cancer cell proliferation by targeting p21 activated kinase 4," *Oncotarget*, vol. 9, no. 47, pp. 28391–28407, 2018.

[29] Q. D. Zhu, Q. Q. Zhou, L. Dong, Z. Huang, F. Wu, and X. Deng, "MiR-199a-5p inhibits the growth and metastasis of colorectal cancer cells by targeting ROCK1," *Technology in Cancer Research & Treatment*, vol. 17, Article ID 1533034618775509, 2018.

[30] L. Ye, J. Zhou, W. Zhao, P. Jiao, G. Ren, and S. Wang, "Gambogic acid-induced autophagy in nonsmall cell lung cancer NCI-H441 cells through a reactive oxygen species pathway," *Journal of Cancer Research and Therapeutics*, vol. 14, no. Supplement, pp. S942–S947, 2018.

Hindawi
Journal of Oncology
Volume 2021, Article ID 9162346, 5 pages
https://doi.org/10.1155/2021/9162346

Research Article

Effect of Entecavir Combined with Adefovir Dipivoxil on Clinical Efficacy and TNF-α and IL-6 Levels in Patients with Hepatitis B Cirrhosis

Yonghuan Yu,[1] **Xinfeng Cui**,[2] **Jingjing Zhao**,[3] **Ting Jia**,[4] **Baofeng Ren**,[5] **and Xiaoyan Zhang**[6]

[1]*Department of Blood Transfusion, Yantaishan Hospital, Yantai 264000, China*
[2]*Department of Stomatology, Chengyang People's Hospital, Chengyang 266109, China*
[3]*Department of Surgery, Zhangqiu District People's Hospital, Jinan 250200, China*
[4]*Department of Gynaecology, Zhangqiu District People's Hospital, Jinan 250200, China*
[5]*Medical Insurance Department, Zhangqiu District People's Hospital, Jinan 250200, China*
[6]*PIVAS, Weifang People's Hospital, Weifang 261041, China*

Correspondence should be addressed to Xiaoyan Zhang; zhangxiaoyan@sdwfph.cn

Received 3 June 2021; Accepted 17 August 2021; Published 25 August 2021

Academic Editor: Muhammad Wasim Khan

Objective. The purpose of the study was to investigate the effect of entecavir combined with adefovir dipivoxil on clinical efficacy and TNF-α and IL-6 levels in patients with hepatitis B cirrhosis. *Methods*. A total of 100 patients with hepatitis B cirrhosis admitted to our hospital between January 2018 and June 2019 were randomly selected and divided into the control group ($n = 50$) and experimental group ($n = 50$) according to the order of admission. Among them, the control group patients were treated with entecavir, while the patients in the experimental group received entecavir combined with adefovir dipivoxil. After that, the effective rate of treatment, the incidence of adverse reactions, liver function indexes, liver fibrosis condition, and TNF-α and IL-6 expression levels were all compared between the two groups. *Results*. The effective rate of treatment in the experimental group was significantly higher than that in the control group, with statistical significance ($p < 0.001$); the incidence of adverse reactions of the patients in the experimental group was significantly lower than that in the control group, with statistical significance ($p < 0.001$); the liver function indexes in the experimental group were significantly better than those in the control group, with statistical significance ($p < 0.001$); the number of patients with liver fibrosis in the experimental group was significantly less than that in the control group, with statistical significance ($p < 0.001$); the TNF-α and IL-6 expression levels in the experimental group were significantly lower than those in the control group, with statistical significance ($p < 0.001$). *Conclusion*. Entecavir combined with adefovir dipivoxil in the treatment of hepatitis B cirrhosis can effectively improve the therapeutic effect and reduce the serum inflammatory factor levels, with high safety, which is worthy of application and popularization.

1. Introduction

Hepatitis B cirrhosis refers to clinically common chronic liver cirrhosis caused by hepatitis B, which poses a great threat to people's daily life [1]. Due to the infection of hepatitis B virus (HBV), the liver function of patients is affected to some extent, resulting in a higher risk of liver cirrhosis [2–4]. Liver fibrosis refers to the pathological process of abnormal hyperplasia of connective tissue in the liver, which is an important factor affecting the prognosis of chronic liver disease. Clinical trials have found that patients with hepatitis B cirrhosis may show liver fibrosis and increased expression levels of serum inflammatory factors during treatment, leaving them in a microinflammatory state for a long time and thus affecting the therapeutic effect [5]. Entecavir, adefovir dipivoxil, and lamivudine, with antibacterial and antivirus effects, are common and effective clinical drugs to treat liver cirrhosis [6]. Although entecavir

has a good antiviral effect for newly diagnosed patients with hepatitis, they are easily affected by high variability of the virus. In addition, long-term administration will increase drug resistance and reduce the therapeutic effect. Therefore, the combination of entecavir with other drugs in the treatment of hepatitis B cirrhosis has become a hot spot in clinical research [7]. Adefovir dipivoxil is a pentacyclic purine nucleotide analogue that inhibits HBV replication [8]. In order to explore the better treatment method for patients with hepatitis B cirrhosis, patients with hepatitis B cirrhosis were selected as the research objects of this study, and different treatment methods were adopted to compare the effective rate of treatment, the incidence of adverse reactions, liver fibrosis condition, and the expression levels of inflammatory factors, specifically reported as follows.

2. Materials and Methods

2.1. General Information. A total of 100 patients with hepatitis B cirrhosis admitted to our hospital between January 2018 and June 2019 were randomly selected and divided into the control group ($n = 50$) and experimental group ($n = 50$) according to the order of admission, with aging from 26 to 66 years old in the experimental group and from 25 to 67 years old in the control group. There was no statistical significance in the comparison of general information such as gender and age, between the two groups ($p > 0.05$), as given in Table 1.

Table 1: Comparison of general information between the two groups (n (%), $\overline{x} \pm s$).

Group	Experimental group	Control group	X^2/t	P
Gender (male/female)	23/27	26/24	0.36	0.55
Age (years old)	43.39 ± 6.21	43.77 ± 6.39	0.30	0.76
Height (cm)	165.32 ± 10.01	165.64 ± 10.37	0.16	0.88
Weight (kg)	71.45 ± 5.90	71.39 ± 5.64	0.05	0.96
Disease course (months)	5.68 ± 1.69	5.72 ± 1.73	0.12	0.91
Smoking history (years)	4.31 ± 1.33	4.27 ± 1.38	0.15	0.88
Drinking history (years)	10.96 ± 1.38	10.52 ± 1.22	1.69	0.09
Hypertension (cases)	13	15	0.20	0.66
Diabetes (cases)	8	7	0.08	0.78
Hyperlipidemia (cases)	4	6	0.44	0.51

2.2. Inclusion/Exclusion Criteria

2.2.1. Inclusion Criteria

(i) Patients met the diagnostic criteria of hepatitis B cirrhosis in basic and clinical features of hepatitis B cirrhosis [9] and were confirmed by pathological or imaging diagnosis

(ii) Patients were 18 years of age or older

(iii) Patients had no history of drug allergy, drug abuse, and bad addiction

(iv) Patients had no other organic diseases

(v) This study was approved by the hospital ethics committee, and the patients all voluntarily participated in this study and signed the informed consent.

2.2.2. Exclusion Criteria

(i) Patients had disturbance of consciousness and could not cooperate with the study

(ii) Patients suffered from liver cancer

(iii) Patients with severe hepatic and renal dysfunction

2.3. Methods. All patients underwent routine physical examinations. 3 ml of fasting venous blood examples was collected from the patients to evaluate their liver and kidney functions and routine blood indexes.

All patients orally took entecavir tablets (Manufacturer: Sino-American Shanghai Squibb Pharmaceutical Co., Ltd.; NMPA approval no. H20052237; specification: 0.5 mg), 1 tablet each time, once a day, for 24 weeks.

The patients in the experimental group were additionally treated with adefovir dipivoxil (Manufacturer: Fujian Cosunter Pharmaceutical Co., Ltd.; NMPA approval no. H20070198; specification: 10 mg) orally, 1 tablet each time, once a day, for 24 weeks.

2.4. Observation Indexes. The effective rate of treatment, the incidence of adverse reactions, liver function indexes, liver fibrosis condition and TNF-α and IL-6 expression levels were all compared between the two groups.

2.4.1. Serum Detection. 5 ml of fasting venous blood was collected from patients in both groups after treatment, and the upper serum was taken after centrifugation. The serum TNF-α and IL-6 expression levels were determined by the enzyme-linked immunosorbent assay (ELISA). The kits were purchased from Kamai Shu (Shanghai) Biotechnology Co., Ltd., and the operation was strictly conducted according to the kit instructions. The normal range was 740–1540 pg/ml for TNF-α and 56.37–150.33 pg/ml for IL-6.

The markedly effective referred to that patients' clinical manifestations and the detection of hepatitis B virus basically disappeared and liver function obviously improved; the effective referred to that patients' clinical manifestations obviously relieved, the detection of hepatitis B virus obviously decreased, and liver function improved; the ineffective referred to that patients' clinical manifestations had no obvious remission but aggravation, the detection of hepatitis B virus had no obvious decrease, and liver function had no improvement. Total effective rate = (the number of markedly effective + the number of effective)/total number × 100%.

Liver function test indexes included serum total protein (TP), glutamic-pyruvic transaminase (ALT), glutamic-

oxaloacetic transaminase (AST), total bilirubin (TBIL), and total bile acid (TBA) [10–12].

2.4.2. Diagnosis of Liver Fibrosis. After treatment, all patients received ultrasound-guided liver biopsy, and the number of cases with liver fibrosis was compared between the two both groups.

2.5. Statistical Treatment. The selected data processing software for this study was SPSS20.0 (IBM, Armonk, NY, USA), and GraphPad Prism 7 (GraphPad Software, San Diego, USA) was used to draw the pictures of the data. Measurement data were expressed by ($\overline{x} \pm s$) and tested by the t-test. Enumeration data were expressed as (n (%)) and tested by the X^2 test. The differences had statistical significance when $p < 0.05$.

3. Results

3.1. Comparison of the Effective Rate of Treatment between the Two Groups. The comparison of the effective rate of treatment between the two groups showed that the effective rate of treatment of 94% in the experimental group was significantly higher than that of 76% in the control group, with statistical significance ($p < 0.05$), as given in Table 2.

3.2. Comparison of the Incidence of Adverse Reactions between the Two Groups. The patients suffered from ascites, gastrointestinal bleeding, and portal hypertension during treatment, and the incidence of adverse reactions in the experimental group was significantly lower than that in the control group, with statistical significance ($p < 0.05$), as given in Table 3.

3.3. Comparison of Liver Function between the Two Groups. The comparison of liver function between the two groups showed that liver function test indexes in the experimental group were all significantly better than those in the control group, with statistical significance ($p < 0.05$), as given in Table 4.

3.4. Comparison of Liver Fibrosis Condition between the Two Groups. The number of patients suffering from liver fibrosis in the two groups was recorded and compared, and the results showed that the number of patients suffering from liver fibrosis in the experimental group was significantly lower than that in the control group, with statistical significance ($p < 0.05$), as shown in Figure 1.

3.5. Comparison of TNF-α and IL-6 Expression Levels between the Two Groups. The comparison of TNF-α and IL-6 expression levels between the two groups revealed that the TNF-α and IL-6 expression levels in the experimental group were significantly lower than those in the control group, with statistical significance ($p < 0.05$), as shown in Figure 2.

4. Discussion

Further spread of hepatitis B virus (HBV) in human body can cause liver dysfunction and cirrhosis, and the majority of the patients with hepatitis B will be affected by cirrhosis and liver dysfunction, posing a great threat to their physical health [13–15]; therefore, timely treatment should be carried out to prevent the development of related complications. With antibacterial, anti-infection, and anti-HBV functions, drugs such as entecavir and adefovir dipivoxil are commonly used for hepatitis B cirrhosis, and their main components were guanine nucleoside analogues, which can inhibit hepatitis B polymerase and have been confirmed in the treatment of chronic hepatitis B [16]. Liver fibrosis is a pathological repairing reaction of the liver to chronic injury. The further development of liver fibrosis can cause the disorder of liver structure, nodular regeneration of liver cells, and formation of cirrhosis. Therefore, it is of great significance to effectively control the process of liver fibrosis in patients and improve the prognosis of patients [17, 18]. Although both drugs have good therapeutic efficacy in clinical treatment, their effect on controlling liver fibrosis and inflammatory factors in patients is not obvious [15, 19]. In order to deeply investigate the effective treatment method and analyze the clinical efficacy of the combination of entecavir and adefovir dipivoxil, in this study, the patients with hepatitis B cirrhosis were selected as the study subjects to explore the effects of entecavir combined with adefovir dipivoxil as well as entecavir dipivoxil alone on liver function, inflammatory factor levels, and so on.

Our study results showed that the effective rate of treatment in the experimental group was significantly higher than that in the control group, with statistical significance ($p < 0.05$), indicating that entecavir combined with adefovir dipivoxil can greatly improve the therapeutic effect. In this study, the evaluation indexes of the effective rate of treatment included the liver function test, clinical manifestations, and hepatitis B virus testing, and the results revealed that entecavir combined with adefovir dipivoxil could significantly relieve patients' clinical manifestations, eliminate hepatitis B virus, and improve their liver function and that the liver function indexes in the experimental group were significantly better than those in the control group, with statistical significance ($p < 0.05$). TNF-α and IL-6 are proinflammatory factors with the synergistic effect, which can promote the progress of liver fibrosis and inflammation in patients, while the incidence of adverse reactions in patients is the key index to evaluate the effect of drug therapy [20]. In addition, the cases of liver fibrosis, the incidence of adverse reactions, and serum TNF-α and IL-6 expression levels in the experimental group were significantly lower than those in the control group ($p < 0.05$), which was similar to the results of Ren et al. [21] who have pointed in their study that entecavir combined with adefovir dipivoxil has significantly better efficacy in reducing HBeAg-negative chronic hepatitis B than entecavir alone. All these demonstrate that entecavir combined with adefovir dipivoxil can significantly reduce the incidence of adverse

Table 2: Comparison of the effective rate of treatment between the two groups (n (%)).

Group	Markedly effective	Effective	Ineffective	Total effective rate (%)
Experimental group	33	14	3	94%
Control group	10	28	12	76%
X^2	—	—	—	6.35
P	—	—	—	0.01

Table 3: Comparison of the incidence of adverse reactions between the two groups (n (%)).

Group	Ascites	Gastrointestinal bleeding	Portal hypertension	Total incidence (%)
Experimental group	1	1	0	4%
Control group	3	5	8	32%
X^2	—	—	—	13.28
P	—	—	—	<0.001

Table 4: Comparison of liver function between the two groups ($\overline{x} \pm s$).

Group	TP (g/L)	ALT (U/L)	AST (U/L)	TBIL (μmol/L)	TBA (μmol/L)
Experimental group	73.59 ± 3.66	24.39 ± 2.74	30.66 ± 3.48	15.52 ± 2.51	5.21 ± 0.52
Control group	66.75 ± 2.51	97.71 ± 5.68	77.61 ± 4.45	23.69 ± 3.30	11.48 ± 2.23
t	10.90	82.21	58.77	13.93	19.36
P	<0.001	<0.001	<0.001	<0.001	<0.001

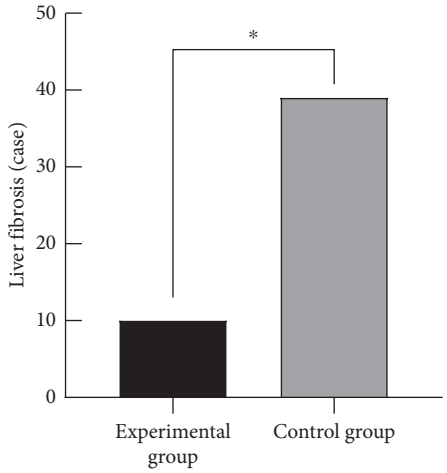

Figure 1: Comparison of liver fibrosis condition between the two groups (n (%)). Note: the abscissa represented the experimental group and control group, while the ordinate represented the cases of liver fibrosis. *The comparison between 10 patients with liver fibrosis in the experimental group and 39 patients with liver fibrosis in the control group, $X^2 = 33.65$, $p < 0.001$, with statistical significance.

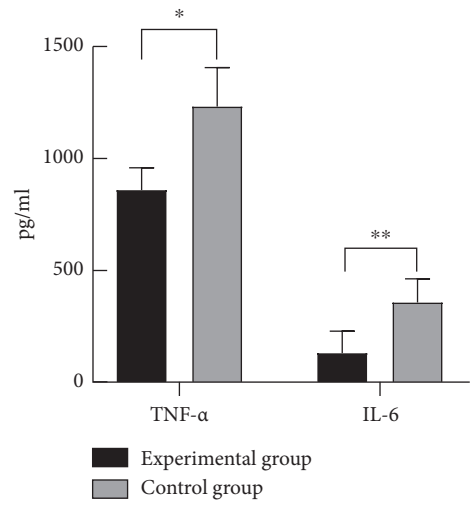

Figure 2: Comparison of TNF-α and IL-6 expression levels between the two groups ($\overline{x} \pm s$). Note: the abscissa represented TNF-α and IL-6, while the ordinate represented the expression level (pg/ml). *The comparison of TNF-α expression levels between the experimental group of (862.38 ± 100.01) pg/ml and the control group of (1237.25 ± 174.16) pg/ml, $t = 13.20$, $p < 0.001$, with statistical significance. **The comparison of IL-6 expression levels between the experimental group of (129.66 ± 98.24) pg/ml and the control group of (357.19 ± 105.39) pg/ml, $t = 11.17$, $p < 0.001$, with statistical significance.

reactions, inflammatory factors expression levels, and the incidence of liver fibrosis during the treatment of hepatitis B cirrhosis. Regina et al. [22] in their studies have pointed out that entecavir combined with adefovir dipivoxil can obviously increase the effective rate in the treatment of hepatitis B cirrhosis combined with liver fibrosis and can effectively improve liver fibrosis and liver function; therefore, entecavir combined with adefovir dipivoxil in patients with hepatitis B cirrhosis combined with liver fibrosis has a high application value, which is consistent with the conclusion of this study, fully demonstrating the scientific reliability of the findings of this study. This study also has some limitations. For example, the sample size is small, the influence of disease staging on the results is not considered, and long-term efficacy is not included in this study.

In conclusion, entecavir combined with adefovir dipivoxil in the treatment of hepatitis B cirrhosis can effectively improve the therapeutic effect and reduce the serum inflammatory factor levels, with high safety, which is worthy of popularization.

Data Availability

The data used to support the findings of this study are available from the corresponding author upon request.

Conflicts of Interest

The authors declare that they have no conflicts of interest.

Authors' Contributions

Yonghuan Yu and Xinfeng Cui contributed equally.

References

[1] S. Pol, N. C. Lusivika, and F. Carrat, "Letter: tenofovir may be superior to entecavir for treatment-naïve chronic hepatitis B patients—authors' reply," *Alimentary Pharmacology & Therapeutics*, vol. 53, no. 9, 2021.

[2] Y. Liu, R. Chen, W. Liu et al., "Investigation of multidrug-resistance mutations of hepatitis B virus (HBV) in a large cohort of chronic HBV-infected patients with treatment of nucleoside/nucleotide analogs," *Antiviral Research*, vol. 189, no. S1, 2021.

[3] L.-Y. Mak, Q. Huang, D. K.-H. Wong et al., "Residual HBV DNA and pgRNA viraemia is associated with hepatocellular carcinoma in chronic hepatitis B patients on antiviral therapy," *Journal of Gastroenterology*, vol. 56, no. 5, pp. 479–488, 2021.

[4] A. Naz, I. Tabish, A. Naseer, A. Z. Siddiqi, F. A. Siddiqui, and A. Z. Mirza, "Green chemistry approach: method development and validation for identification and quantification of entecavir using FT-IR in bulk and pharmaceutical dosage form," *Future Journal of Pharmaceutical Sciences*, vol. 7, no. 1, 2021.

[5] V. W.-K. Hui, T. C.-F. Yip, and V. W.-S. Wong, "Aspirin reduces the incidence of hepatocellular carcinoma in patients with chronic hepatitis B receiving oral nucleos(t)ide analog," *Clinical and Translational Gastroenterology*, vol. 12, no. 3, 2021.

[6] T. Kakiuchi, H. Takahashi, S. Iwane, A. Koji, and M. Matsuo, "Entecavir administration to pregnant Japanese woman with chronic hepatitis B and hepatocellular carcinoma: a case report," *Clinical case reports*, vol. 9, no. 3, pp. 1752–1758, 2021.

[7] S. Yang, X. Ma, C. Cai, H. Wang, F. Xiao, and C. Yu, "Tenofovir disoproxil fumarate is superior to entecavir in reducing hepatitis B surface antigen for chronic hepatitis B in China: 2-year comprehensive comparative result of a matched comparative study," *Frontiers in Medicine*, vol. 8, 2021.

[8] G. V. Papatheodoridis, G. N. Dalekos, and R. Idilman, "Similar risk of hepatocellular carcinoma during long-term entecavir or tenofovir therapy in Caucasian patients with chronic hepatitis B," *Journal of Hepatology*, vol. 73, no. 5, pp. 1037–1045, 2020.

[9] C.-L. Lin, K.-C. Tseng, K.-Y. Chen, L.-Y. Liao, and J.-H. Kao, "Factors predicting outcomes of hepatitis B-related cirrhosis patients with long-term antiviral therapy," *Journal of the Formosan Medical Association*, vol. 119, no. 10, pp. 1483–1489, 2020.

[10] J.-L. Ma, L.-L. He, P. Li, and L. Jiang, H.-S. Wei, "Prognosis of endotherapy versus splenectomy and devascularization for variceal bleeding in patients with hepatitis B-related cirrhosis," *Surgical Endoscopy*, vol. 35, no. 6, pp. 2620–2628, 2020.

[11] L. Ni, C. Li, and Y. Li, "Correlation of APOBEC3G expression with liver function indexes of patients with chronic hepatitis B and comparison in chronic hepatitis B, liver cirrhosis and liver cancer," *Oncology letters*, vol. 19, no. 3, pp. 2562–2567, 2020.

[12] T.-H. Su, C.-Y. Peng, T.-C. Tseng et al., "Serum mac-2-binding protein glycosylation isomer at virological remission predicts hepatocellular carcinoma and death in chronic hepatitis B-related cirrhosis," *The Journal of Infectious Diseases*, vol. 221, no. 4, pp. 589–597, 2020.

[13] X. Jin and X. Li, "Factors predicting outcomes of hepatitis B-related cirrhosis patients with long-term antiviral therapy," *Journal of the Formosan Medical Association*, vol. 119, no. 10, pp. 1483–1489, 2020.

[14] J. Q. Yang, R. Zeng, J. M. Cao et al., "Predicting gastro-oesophageal variceal bleeding in hepatitis B-related cirrhosis by CT radiomics signature," *Clinical Radiology*, vol. 74, no. 12, pp. 976.e1–976.e9, 2019.

[15] L. He, X. Ye, J. Ma et al., "Antiviral therapy reduces rebleeding rate in patients with hepatitis B-related cirrhosis with acute variceal bleeding after endotherapy," *BMC Gastroenterology*, vol. 19, no. 1, p. 101, 2019.

[16] T.-H. Hung, C.-C. Tsai, and H.-F. Lee, "Population-based study of entecavir and long-term mortality in chronic hepatitis B–related decompensated liver cirrhosis," *Clinics and Research in Hepatology and Gastroenterology*, vol. 43, no. 6, pp. 694–699, 2019.

[17] L. L. Zhang, Y. F. Li, C. Zhang, X. F. Wu, Y. Ma, and L. Li, "Study on the risk of hepatitis B-related cirrhosis combined with type 2 diabetes mellitus for the occurrence of primary hepatocellular carcinoma," *Zhonghua Gan Zang Bing Za Zhi = Zhonghua Ganzangbing Zazhi = Chinese Journal of Hepatology*, vol. 27, no. 10, pp. 788–792, 2019.

[18] J. Wang, Z. Zhang, X. Yan et al., "Albumin-Bilirubin (ALBI) as an accurate and simple prognostic score for chronic hepatitis B-related liver cirrhosis," *Digestive and Liver Disease*, vol. 51, no. 8, pp. 1172–1178, 2019.

[19] M. Ren, J. Li, R. Xue, Z. Wang, S. Li Coll, and Q. Meng, "Liver function and energy metabolism in hepatocellular carcinoma developed in patients with hepatitis B-related cirrhosis," *Medicine*, vol. 98, no. 19, Article ID e15528, 2019.

[20] M. J. Lian, J. Q. Zhang, S. D. Chen, D. D. Zhang, Y. Y. Yang, and G. L. Hong, "Diagnostic accuracy of γ-glutamyl transpeptidase-to-platelet ratio for predicting hepatitis B-related fibrosis: a meta-analysis," *European Journal of Gastroenterology & Hepatology*, vol. 31, no. 5, pp. 599–606, 2019.

[21] M. Ren, J. Li, R. Xue, Z. Wang, S. L. Coll, and Q. Meng, "Liver function and energy metabolism in hepatocellular carcinoma developed in patients with hepatitis B-related cirrhosis," *Medicine*, vol. 98, no. 19, Article ID e15528, 2019.

[22] Regina, C. Zhao and H. Niu, "Effects of entecavir combined with adefovir dipivoxil on liver fibrosis and serum ALT and FFA levels in patients with chronic hepatitis B," *Systemic Medicine*, vol. 5, no. 5, pp. 120–122, 202.

Hindawi
Journal of Oncology
Volume 2021, Article ID 7462012, 7 pages
https://doi.org/10.1155/2021/7462012

Research Article

Effect of Prophylactic Radiotherapy on Patients with Stage II-III Esophageal Cancer after Esophageal Cancer Radical Operation and Influencing Factors in Its Recurrence

Dan Guo[1] **and Kang Zheng**[2]

[1]*Radiotherapy in One Ward of the Chest, Shanxi Provincial Cancer Hospital, Taiyuan 030013, Shanxi, China*
[2]*Special Ward, Shanxi Provincial Cancer Hospital, Taiyuan 030013, Shanxi, China*

Correspondence should be addressed to Kang Zheng; poduilu8@163.com

Received 22 June 2021; Revised 29 July 2021; Accepted 10 August 2021; Published 21 August 2021

Academic Editor: Muhammad Wasim Khan

Objective. To explore the effect of prophylactic radiotherapy on patients with stage II-III esophageal cancer (EC) after esophageal cancer radical operation (ECRO) and influencing factors on EC recurrence. *Methods*. Totally, 65 patients with EC in our hospital were enrolled. Among them, 30 patients were treated by routine ECRO as a control group (Con group) and 35 patients by prophylactic radiotherapy as a research group (Res group). Then, the following measures were taken: record the efficacy on both groups, quantify their C-reactive protein (CRP) and white blood cell count (WBC) before and after therapy, evaluate their mental state through the revised piper fatigue scale (PFS-R) before and after therapy, determine their changes in Self-Rating Depression Scale (SDS) and Self-Rating Anxiety Scale (SAS) before and after therapy, compare them in terms of lymph-node metastatic rate (LNMR), hematogenous metastasis rate (HMR), anastomotic recurrence rate (ARR), and 3-year survival rate, compare them in terms of life quality after therapy via the Quality of Life-Core Questionnaire (QLQ-C30), and analyze influencing factors on their recurrence. *Results*. The Res group showed a notably higher total effective rate (TER) than the Con group ($P = 0.037$). After therapy, CRP and WBC in both groups increased, but their levels were not considerably different in both ($P > 0.05$). Additionally, after therapy, in contrast to the Con group, the Res group got notably lower PFS-R, SDS, and SAS scores, showed notably lower LNMR and ARR and notably higher 3-year survival rate, and experienced notably higher life quality (all $P < 0.05$), and the HMR results were not considerably different in both groups ($P > 0.05$). Moreover, carcinoembryonic antigen (CEA), carbohydrate antigen 125 (CA125), esophageal inflammation history, family medical history, postoperative complications, and lymphatic and vascular infiltration were risk factors for the disease recurrence, and treatment method was the protective factor for it. *Conclusion*. For patients with stage II-III EC after ECRO, prophylactic radiotherapy is highly effective and safe and can lower the recurrence rate, so it is worth popularizing in clinical practice.

1. Introduction

Esophageal cancer (EC) is a malignancy frequently found in males [1] and also a primary fatal malignancy worldwide [2]. Its primary histological subtypes are squamous cell carcinoma and adenocarcinoma. Obesity, smoking, excessive drinking, and unhealthy eating habits are crucial factors inducing EC [3]. Its symptoms are bound up with its progress. Early EC has no evident symptoms, but middle or late EC is manifested by dysphagia, persistent retrosternal pain, and emaciation [4]. Roughly, EC ranks sixth among all cancers in mortality, gravely threatening patients' lives and safety [5]. Currently, EC is primarily treated based on the principle of individualized comprehensive therapy, including surgery and radiotherapy [6]. Esophageal cancer radical operation (ECRO) is usually selected for patients with early EC, and tumor resection, peripheral lymph-node dissection, and digestive tract reconstruction are adopted [7]. After such therapy, their prognosis is relatively favorable. However, most patients are at the middle/late stage at

the time of diagnosis, so they are prone to lymph-node metastasis and thus suffer deterioration [8]. Therefore, in addition to timely surgical therapy, auxiliary radiotherapy is also necessary to improve the efficacy in patients with EC.

According to earlier clinical data, prophylactic radiotherapy can strongly alleviate the deterioration of cancers like small-cell lung cancer and cervical cancer and boost the therapeutic effect against it [9]. For instance, in a study by Nishii et al. [10], prophylactic radiotherapy can lower the complication rate of oral cancer. Roge et al. also pointed out that [11] prophylactic lymph-node radiotherapy is a crucial therapy for early breast cancer. However, its clinical efficacy in EC is rarely studied, and experimental data are insufficient to verify the influence of prophylactic radiotherapy on patients after ECRO and their prognosis. Thus, this study probed into the impact of prophylactic radiotherapy on patients with stage II-III EC after ECRO and influencing factors on EC recurrence, with the aim of offering reliable guidance and potential basis for future clinical therapy of EC.

2. Study Design and Treatment

Totally, 65 patients with EC at Shanxi Provincial Cancer Hospital, Taiyuan, Shanxi, PR China, between January 2016 and November 2017 were enrolled. Among them, 30 patients were randomly included in the control group (Con group) treated with routine ECRO, and the remaining 35 patients were included in the research group (Res group) treated with prophylactic radiotherapy. All study participants provided written informed consent. The study was approved by the Ethics Committee of Shanxi Provincial Cancer Hospital, Taiyuan, Shanxi, PR China (20151121), and all experiments conformed to the provisions of the Declaration of Helsinki.

2.1. Inclusion and Exclusion Criteria.

(1) The inclusion criteria: patients confirmed with stage II-III EC via examinations in pathology, laboratory examination, and imaging in our hospital, patients with detailed case data, and those consenting to cooperate with the study

(2) The exclusion criteria: patients with other comorbid malignancies, patients with liver or kidney dysfunction, patients with a surgical contraindication, coagulant function abnormality, or immune deficiency, lactating women, pregnant women, referred patients, and those with poor compliance

2.2. Methods. All patients were given ECRO. Firstly, in a cutting direction selected according to the pathological tissue of the patient, the cancerous tissue tumors were resected and the surrounding lymph nodes that can be cleaned were cleaned under a maximized operation field or visual field. The proper digestive tract function of the patient after surgery should be ensured, so the patient was given enteral and parenteral nutrition support while he was required to take liquid food as staple food so that he can get faster recovery. Patients in the Res group were given prophylactic radiotherapy four weeks after surgery. Each patient was irradiated after a target radiotherapy area was selected according to his situation. Specifically, single anterior-field radiotherapy was adopted at a dosage of 40 Gy 20 times during the first four weeks, and then the horizontal fields on both sides were irradiated at 20 Gy 10 times during the next 2 weeks and 60 Gy 30 times during the next 6 weeks.

2.3. Outcome Measures. The efficacy in the two groups after therapy was recorded. The efficacy was classified into complete remission, partial remission, no change, and progression. Total effective rate (TER) = complete remission rate + partial remission rate [12]. Then, before and after therapy, the C-reactive protein (CRP) and white blood cell count (WBC) in the two groups were quantified and their mental state was evaluated through the revised piper fatigue scale (PFS-R) [13]. Additionally, the psychological changes of the two groups were evaluated using the Self-Rating Depression Scale (SDS) and Self-Rating Anxiety Scale (SAS), and the lymph-node metastatic rate (LNMR), hematogenous metastasis rate (HMR), anastomotic recurrence rate (ARR), and 3-year recurrence rate were compared between them. Moreover, the life quality of both groups was evaluated via the EORTC Quality of Life Questionnaire (QLQ-C30), and influencing factors on the disease recurrence were analyzed.

2.4. Statistical Analyses. In this study, SPSS22.0 was used for data processing and GraphPad7 for visualization of data into corresponding figures. Intergroup comparison of enumeration data, presented by (%), was carried out via the chi-square test, while intergroup and multigroup comparisons of measurement data, presented as the mean ± SD, were conducted via the t-test and one-way ANOVA, respectively, and the LSD post hoc test was conducted. Additionally, data at multiple times were analyzed via the repeated measures analysis of variance and Bonferroni post hoc test. $P < 0.05$ denotes a notable difference.

3. Results

3.1. Baseline Data of Patients. The two groups were not considerably different in age, body mass index (BMI), sex, course of disease, living environment, smoking history, drinking history, and nationality (all $P > 0.05$) (Table 1).

3.2. Efficacy in the Two Groups. From the comparison of efficacy between the two groups, the Res group showed a TER of 85.71% (30 patients), with complete remission in 19 patients (54.29%), partial remission in 11 patients (31.43%), no change in 4 patients (11.43%), and progression in 1 patient (2.86%), while the Con group showed a TER of 63.33% (19 patients), with complete remission in 7 patients (23.33%), partial remission in 12 patients (40.00%), no change in 6 patients (20.00%), and progression in 5 patients (16.67%), so the TER in the Res group was notably higher ($p = 0.037$) (Table 2).

Table 1: Comparison of clinical baseline data.

	The Res group ($n = 35$)	The Con group ($n = 30$)	$\chi 2$ or t/P
Age (Y)	58.6 ± 5.4	59.3 ± 5.2	0.530/0.598
BMI (kg/cm^2)	24.2 ± 1.4	24.5 ± 1.7	0.780/0.438
Sex			
Male	22 (62.86%)	19 (63.33%)	0.002/0.968
Female	13 (37.14%)	11 (36.67%)	
Course of disease (month)	15.2 ± 2.3	15.6 ± 2.5	0.672/0.504
Residential environment			
Urban area	20 (57.14%)	16 (53.33%)	0.094/0.758
Rural area	15 (42.86%)	14 (46.67%)	
Smoking history			
Yes	28 (80.00)	26 (86.67)	0.511/0.475
No	7 (20.00)	4 (13.33)	
Drinking history			
Yes	30 (85.71)	27 (90.00)	0.275/0.600
No	5 (14.29)	3 (10.00)	
Nationality			
Han nationality	35 (100.00%)	28 (93.33%)	2.407/0.121
Minority nationality	0 (0.00%)	2 (6.67%)	

Table 2: Efficacy in the two groups.

	The Res group ($n = 35$)	The Con group ($n = 30$)	$\chi 2$	P value
Complete remission	19 (54.29)	7 (23.33)		
Partial remission	11 (31.43)	12 (40.00)		
No change	4 (11.43)	6 (20.00)		
Progress	1 (2.86)	5 (16.67)		
Total effective rate (%)	30 (85.71)	19 (63.33)	4.361	0.037

3.3. Changes of CRP and WBC in the Two Groups. According to quantification of CRP and WBC in the two groups before and after therapy, after therapy, both groups showed notably increased levels of CRP and WBC (both $P < 0.05$), but in both groups, the levels were not significantly different ($P > 0.05$) (Figure 1).

3.4. PFS-R Scores of the Two Groups. The comparison of mental state between the two groups via PFS-R before and after therapy showed that, before therapy, the two groups were not considerably different in PFS-R score ($P > 0.05$), while after therapy, the score of both groups declined and the decline in the Res group was more notable ($P < 0.05$) (Figure 2).

3.5. Psychological Changes of the Two Groups. According to the comparison of the two groups in alleviation of mental depression and anxiety before and after therapy, before therapy, the two groups were not significantly different in SDS and SAS scores (both $P > 0.05$), while after therapy, SDS and SAS scores of both groups declined and the scores of the Res group were low (all $P < 0.05$) (Figure 3).

3.6. Incidence of Posttherapy Complications. According to a comparison of LNMR, HMR, ARR, and 3-year survival rate between the two groups after therapy, the Res group presented notably lower LNMR and ARR and considerably higher 3-year survival rate and the HMR results were not considerably different in both groups (all $P < 0.05$) (Table 3).

3.7. Posttherapy Life Quality of the Two Groups. The posttherapy life quality of the two groups was evaluated via the functional, symptom, and general health subscales. As a result, after therapy, the functional and general health scores of the two increased and the scores of the Res group were notably higher than those of the Con group (both $P > 0.05$). Additionally, after therapy, the symptom scores of both groups decreased, and the score of the Res group was notably lower (both $P < 0.05$) (Figure 4).

3.8. Influencing Factors of Disease Recurrence. Logistic regression analysis on influencing factors of disease recurrence showed that carcinoembryonic antigen (CEA), carbohydrate antigen 125 (CA125), esophageal inflammation history, family medical history, postoperative complications, and lymphatic and vascular infiltration were risk factors for the disease recurrence, and the treatment method was the protective factor (Tables 4 and 5).

4. Discussion

EC is the most prevalent gastrointestinal cancer [14]. Its morbidity and mortality have been brought under control, but it is still a serious threat to the life and health of the

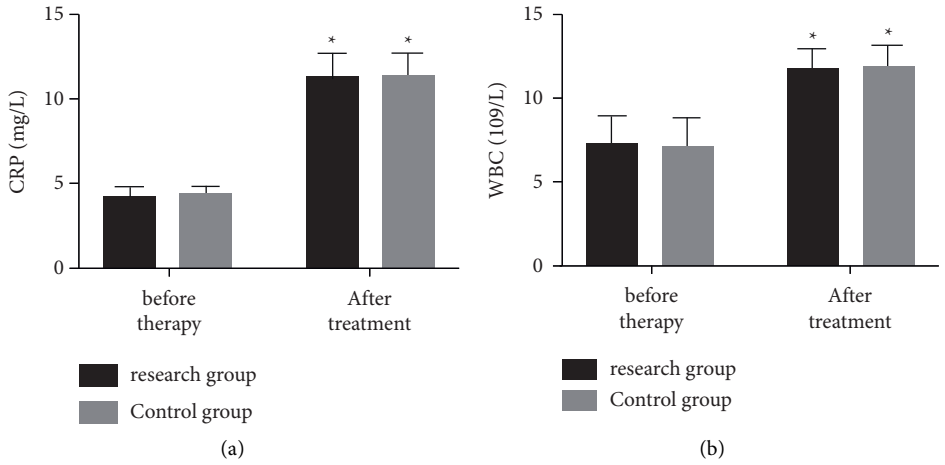

Figure 1: Changes of CRP and WBC. Pretherapy and posttherapy (a) CRP and (b) WBC of the two groups. The symbol ∗ signifies vs. the situation before treatment.

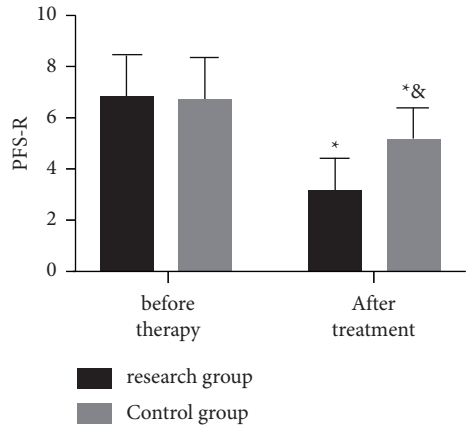

Figure 2: Pretherapy and posttherapy PFS-R scores of the two groups. The symbol ∗ signifies vs. the situation before treatment; &, vs. the Res group.

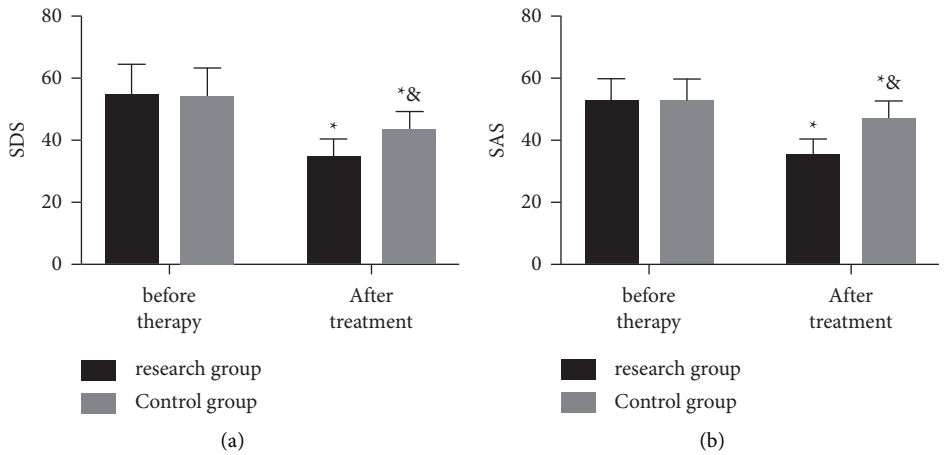

Figure 3: Psychological changes of the two groups before and after treatment. Pretherapy and posttherapy (a) SDS and (b) SAS of the two groups. The symbol ∗ signifies vs. the situation before treatment; &, vs. the Res group.

Table 3: Prognosis of the patients after therapy.

	The Res group ($n = 35$)	The Con group ($n = 30$)	$\chi 2$	P value
Lymph-node metastatic rate %	3 (8.57)	9 (30.00)	4.928	0.026*
Hematogenous metastasis rate %	3 (8.57)	4 (13.33)	0.381	0.537
Anastomotic recurrence rate %	2 (5.71)	7 (23.33)	4.204	0.040*
3-year survival rate %	25 (71.43)	14 (46.67)	4.127	0.042*

*meant that the differences of the two groups were significant.

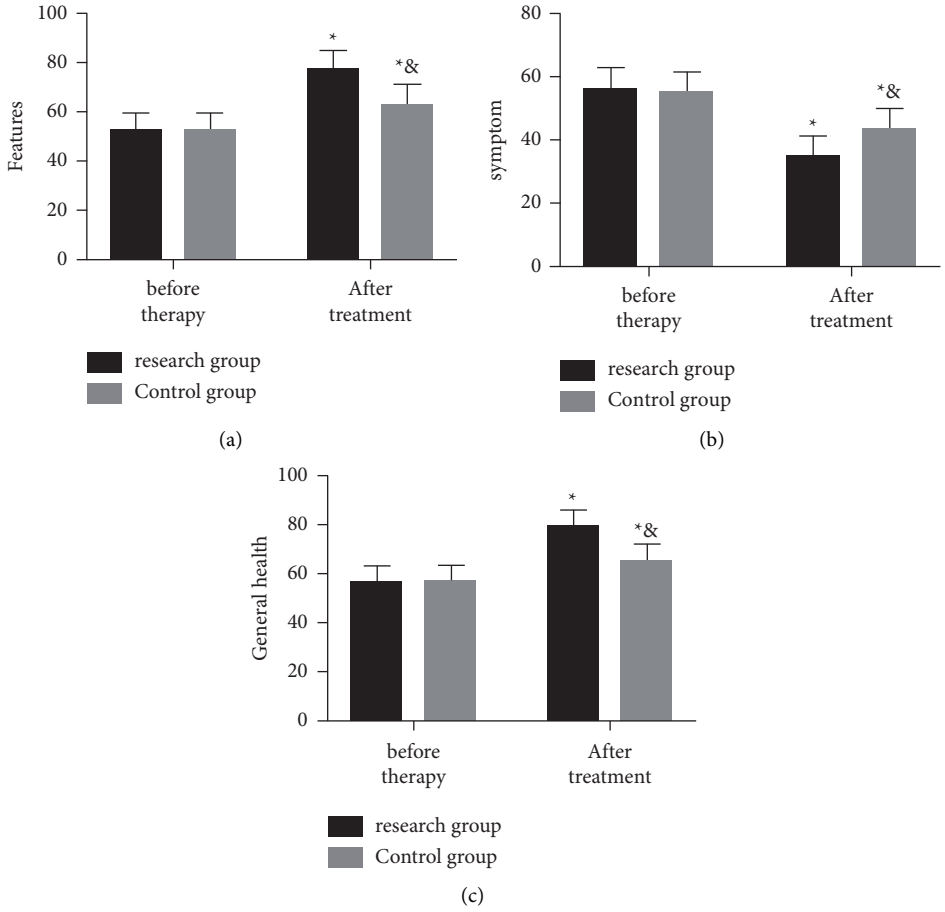

Figure 4: Posttherapy life quality of the two groups. Posttherapy (a) functional scores, (b) symptom scores, and (c) general health scores of the two groups. The symbol ∗ signifies vs. ∗ the situation before treatment; &, the Res group.

Table 4: The information of assignment.

Assignment	
CEA	Raw data were used for analysis
CA125	Raw data were used for analysis
Esophageal inflammation history	0 was assigned to No and 1 to Yes
Family medical history	0 was assigned to No and 1 to Yes
Postoperative complications	0 was assigned to No and 1 to Yes
Lymphatic vessel invasion	0 was assigned to No and 1 to Yes
Treatment methods	0 was assigned to postoperative prophylactic radiotherapy and 1 to no postoperative prophylactic radiotherapy

Chinese due to its various pathogenic factors [15]. Radical surgery is the primary therapy for EC [16], but the selection of adjuvant treatments such as radiotherapy after ECRO is still controversial in clinical practice. For improving the survival rate of Chinese people with EC, this study probed into the effect of prophylactic radiotherapy on patients with stage II-III EC after ECRO and influencing factors on EC recurrence.

Table 5: Univariate and multivariate analysis on influencing factors of disease recurrence.

	Univariate			Multivariate		
	OR	95% CI	*P* value	OR	95% CI	*P* value
CEA	15.63	4.63–26.63	0.019	4.63	2.54–9.63	0.021
CA125	12.6063	7.63–13.41	0.029	6.63	2.63–12.63	0.018
Esophageal inflammation history	2.63	1.16–3.84	0.019	1.63	0.54–2.63	0.187
Family medical history	1.33	0.42–3.63	0.184	—	—	—
Postoperative complications	1.63	0.23–4.63	0.002	1.14	0.18–1.63	0.006
Lymphatic vessel invasion	1.85	0.15–3.63	0.009	1.56	0.06–1.92	0.001
Treatment methods	0.42	0.06–1.06	0.004	0.75	0.12–1.15	0.002

Before the study, we collected baseline data of the two groups and found no notable difference between them in age, BMI, sex, course of disease, living environment, smoking history, drinking history, and nationality, which suggests their comparability. Firstly, we evaluated the efficacy in the two groups. The efficacy was classified into complete remission, partial remission, no change, and progression. As our results showed, the Res group presented a notably higher TER than the Con group (85.71% (30 patients) vs. 63.33% (19 patients)). The data imply that prophylactic radiotherapy can contribute to stronger clinical efficacy in patients with EC, with a beneficial influence on their clinical symptoms and survival rate. According to associated references, Sun et al. [17] pointed out the remarkable efficacy of prophylactic radiotherapy in patients with nasopharyngeal carcinoma. There are also studies which support the idea that prophylactic radiotherapy can strongly prevent recurrence and metastasis of tumor diseases [18]. These conclusions can verify the results of our study. The tumor of patients with middle or late EC is large, so the postoperative effect is inconsistent due to the difference of their tumor location or tumor size, and prophylactic radiotherapy can further kill the residual tumor, which may be one major reason for the efficacy improvement by prophylactic radiotherapy. We quantified CRP and WBC in the two groups and found after therapy that both groups showed notably increased CRP and WBC, but the levels were not considerably different in both groups, which were in line with results discovered previously [19]. We reason that for patients with EC, after surgery or postoperative radiotherapy, their body will produce stress response and their CRP and WBC will increase. At the same time, the two groups showed no notable difference in CRP and WBC after therapy, which further reflected the effectiveness and safety of prophylactic radiotherapy. One study by Kugele et al. [20] has pointed out that prophylactic radiotherapy can strongly enhance local control and survival among patients undergoing radical mastectomy. It is similar to our study result, which supports the conclusion that prophylactic radiotherapy can deliver a strong inhibitory influence on postoperative tumor recurrence. We also adopted PFS-R for analyzing and comparing the mental state of the two groups. As the results showed, before therapy, the two groups were not greatly different in PFS-R score, while after therapy, the scores of both groups declined and the decline in the Res group was more notable. The results imply the crucial role of prophylactic radiotherapy in alleviating the fatigue state of patients and improving their life quality. Cancer-associated fatigue is a prevalent clinical symptom of EC. Diseases take a serious toll on patients' mental and physical strength, which is prone to aggravating their negative emotions and increasing the difficulty of treating muscle diseases [21]. Prophylactic radiotherapy may greatly alleviate patients' clinical symptoms, which is the primary task to improve their life quality [22]. We compared the two groups for alleviation of mental depression and anxiety before and after therapy and found that before therapy, the two groups were not significantly different in SDS and SAS scores, while after therapy, SDS and SAS scores of both groups declined and the scores of the Res group were low. The results further demonstrate the favorable clinical efficacy of prophylactic radiotherapy because of its function in strongly alleviating patients' symptoms and unhealthy emotions. Moreover, we compared the LNMR, HMR, ARR, and 3-year survival rates of the two groups after therapy, finding that the Res group presented notably lower LNMR and ARR and notably higher 3-year survival rate, but they were not considerably different in HMR. The acquired data reflect the safety and effectiveness of prophylactic radiotherapy in the Res group from one angle and further reflect the reason for the higher survival rate in the Res group. The data also confirm the crucial clinical value of prophylactic radiotherapy after ECRO. We evaluated the posttherapy life quality of the two groups via the functional, symptom, and general health subscales. As a result, after therapy, the functional and general health scores of the two increased and the scores of the Res group were notably higher than those of the Con group. Additionally, after therapy, the symptom scores of both groups decreased and the score of the Res group was notably lower. The results were in step with our above analysis. Finally, we carried out logistic regression analysis on influencing factors of disease recurrence, finding that CEA, CA125, esophageal inflammation history, family medical history, postoperative complications, and lymphatic and vascular infiltration were risk factors for the disease recurrence and postoperative prophylactic radiotherapy was the protective factor for it. Thus, postoperative prophylactic radiotherapy is pivotal for patients. The study has indicated that low-dose, prophylactic, extended-field, intensity-modulated radiotherapy combined with cisplatin could effectively improve the prognosis of patients with cervical cancer [23].

However, due to the short experimental period, we were unable to evaluate the long-run prognosis of patients, and

some experimental results may not be highly representative because of the small sample size of included subjects. It provides potential basis for further experimental analysis. In addition, it is required to understand the exact mechanism of prophylactic radiotherapy through basic experiments to provide more perfect clinical references.

To sum up, for patients with stage I-II EC after ECRO, prophylactic radiotherapy is highly effective and safe and can lower the recurrence rate, so it is worth popularizing in clinical practice.

Data Availability

All data are available from the corresponding author upon request.

Conflicts of Interest

The authors declare no conflicts of interest associated with this work.

References

[1] F.-L. Huang and S.-J. Yu, "Esophageal cancer: risk factors, genetic association, and treatment," *Asian Journal of Surgery*, vol. 41, no. 3, pp. 210–215, 2018.

[2] M. W. Short, K. G. Burgers, and V. T. Fry, "Esophageal cancer," *American Family Physician*, vol. 95, no. 1, pp. 22–28, 2017.

[3] M. Watanabe, R. Otake, R. Kozuki et al., "Recent progress in multidisciplinary treatment for patients with esophageal cancer," *Surgery Today*, vol. 50, no. 1, pp. 12–20, 2020.

[4] T.-X. Huang and L. Fu, "The immune landscape of esophageal cancer," *Cancer Communications*, vol. 39, no. 1, p. 79, 2019.

[5] D. Vrána, M. Matzenauer, Č. Neoral et al., "From tumor immunology to immunotherapy in gastric and esophageal cancer," *International Journal of Molecular Sciences*, vol. 20, no. 1, p. 13, 2018.

[6] B.-R. Sah, K. Owczarczyk, M. Siddique, G. J. R. Cook, and V. Goh, "Radiomics in esophageal and gastric cancer," *Abdominal Radiology*, vol. 44, no. 6, pp. 2048–2058, 2019.

[7] R. J. Gillies and M. B. Schabath, "Radiomics improves cancer screening and early detection, Cancer Epidemiology," *Biomarkers & Prevention*, vol. 29, no. 12, pp. 2556–2567, 2020.

[8] Q. Zhao, J. Yu, and X. Meng, "A good start of immunotherapy in esophageal cancer," *Cancer Medicine*, vol. 8, no. 10, pp. 4519–4526, 2019 Aug.

[9] M. Jarosz-Biej, R. Smolarczyk, N. Cichoń, and N. Kułach, "Tumor microenvironment as A "game changer" in cancer radiotherapy," *International Journal of Molecular Sciences*, vol. 20, no. 13, p. 3212, 2019.

[10] M. Nishii, S. Soutome, A. Kawakita et al., "Factors associated with severe oral mucositis and candidiasis in patients undergoing radiotherapy for oral and oropharyngeal carcinomas: a retrospective multicenter study of 326 patients," *Supportive Care in Cancer*, vol. 28, no. 3, pp. 1069–1075, 2020.

[11] M. Rogé, S. Thureau, J. Dampierre, B. Dubray, and S. Rivera, "Irradiation des aires ganglionnaires prophylactiques pour le cancer du sein," *Cancer Radiotherapie*, vol. 23, no. 8, pp. 904–912, 2019.

[12] F. Coccolini, M. Nardi, G. Montori et al., "Neoadjuvant chemotherapy in advanced gastric and esophago-gastric cancer. Meta-analysis of randomized trials," *International Journal of Surgery*, vol. 51, pp. 120–127, 2018.

[13] K. M. Mustian, C. M. Alfano, C. Heckler et al., "Comparison of pharmaceutical, psychological, and exercise treatments for cancer-related fatigue," *JAMA Oncology*, vol. 3, no. 7, pp. 961–968, 2017.

[14] Y. Kitagawa, T. Uno, T. Oyama et al., "Esophageal cancer practice guidelines 2017 edited by the Japan Esophageal Society: part 1," *Esophagus*, vol. 16, no. 1, pp. 1–24, 2019.

[15] H. Kikuchi and H. Takeuchi, "Future perspectives of surgery for esophageal cancer," *Annals of Thoracic and Cardiovascular Surgery*, vol. 24, no. 5, pp. 219–222, 2018.

[16] M. Sohda and H. Kuwano, "Current status and future prospects for esophageal cancer treatment," *Annals of Thoracic and Cardiovascular Surgery*, vol. 23, no. 1, pp. 1–11, 2017.

[17] X.-S. Sun, X.-Y. Li, Q.-Y. Chen, L.-Q. Tang, and H.-Q. Mai, "Future of radiotherapy in nasopharyngeal carcinoma," *British Journal of Radiology*, vol. 92, no. 1102, Article ID 20190209, 2019.

[18] C. E. Coles, C. L. Griffin, A. M. Kirby et al., "Partial-breast radiotherapy after breast conservation surgery for patients with early breast cancer (UK IMPORT LOW trial): 5-year results from a multicentre, randomised, controlled, phase 3, non-inferiority trial," *The Lancet*, vol. 390, no. 10099, pp. 1048–1060, 2017.

[19] L. Bai, B.-S. Zhou, and Y.-X. Zhao, "Dynamic changes in T-cell subsets and C-reactive protein after radiation therapy in lung cancer patients and correlation with symptomatic radiation pneumonitis treated with steroid therapy," *Cancer Management and Research*, vol. 11, pp. 7925–7931, 2019.

[20] M. Kügele, A. Mannerberg, S. Nørring Bekke et al., "Surface guided radiotherapy (SGRT) improves breast cancer patient setup accuracy," *Journal of Applied Clinical Medical Physics*, vol. 20, no. 9, pp. 61–68, 2019.

[21] O. Shen, J. Wang, W. Li, W. Yi, and W. Wang, "Assessment of health-related quality of life of patients with esophageal squamous cell carcinoma following esophagectomy using EORTC quality of life questionnaires," *Molecular and Clinical Oncology*, vol. 3, no. 1, pp. 133–138, 2015.

[22] J.-K. Peng, N. Hepgul, I. J. Higginson, and W. Gao, "Symptom prevalence and quality of life of patients with end-stage liver disease: a systematic review and meta-analysis," *Palliative Medicine*, vol. 33, no. 1, pp. 24–36, 2019.

[23] J.-A. Liang, S.-W. Chen, Y.-C. Hung et al., "Low-dose, prophylactic, extended-field, intensity-modulated radiotherapy plus concurrent weekly cisplatin for patients with stage IB2-IIIB cervical cancer, positive pelvic lymph nodes, and negative para-aortic lymph nodes," *International Journal of Gynecological Cancer*, vol. 24, no. 5, pp. 901–907, 2014.

Hindawi
Journal of Oncology
Volume 2021, Article ID 5391977, 7 pages
https://doi.org/10.1155/2021/5391977

Research Article

miR-651-3p Enhances the Sensitivity of Hepatocellular Carcinoma to Cisplatin via Targeting ATG3-Mediated Cell Autophagy

Lei Zou, Peng Sun, and Lei Zhang

Department of Gastroenterology, Zibo Central Hospital, Zibo 255036, Shandong Province, China

Correspondence should be addressed to Lei Zhang; shibayej@163.com

Received 30 June 2021; Accepted 10 August 2021; Published 19 August 2021

Academic Editor: Muhammad Wasim Khan

Drug resistance is a major challenge for hepatocellular carcinoma (HCC) treatment in a clinic, which limits the therapeutic effect of the chemotherapeutic drugs, including cisplatin (CDDP), in this disease. Mounting evidence has identified that miRNAs dysfunction is related to the resistance of tumor cells to CDDP, and miR-651-3p has been identified as a tumor inhibitor to suppress the progression of multiple tumors. However, the role of miR-651-3p in HCC remains unclear. In this study, the relative expression of miR-651-3p in HCC tissues and cell lines were measured, and the functions of miR-651-3p were also observed by CCK-8 assay, flow cytometry assay, and Western blot. Moreover, the downstream target of miR-651-3p was predicted and verified via TargetScan and dual-luciferase reporter assay, and its functions were also investigated. The results showed that miR-651-3p was significantly downregulated in HCC tissues and cell lines, and the decreased miR-651-3p was also observed in CDDP-induced cells. miR-651-3p upregulation could effectively inhibit the proliferation and induce the apoptosis of R-HepG2. It was also found that ATG3 was a downstream target of miR-651-3p, and ATG3 was highly upregulated in HCC tissues. Moreover, the upregulated ATG3 could partly reverse the effects of miR-651-3p on R-HepG2. Besides, miR-651-3p involved the autophagy pathway of the HCC cells via targeting ATG3. In conclusion, miR-651-3p could regulate the autophagy to enhance the sensitivity of HepG2 cells to CDDP via targeting ATG3.

1. Introduction

Hepatocellular carcinoma (HCC) is the fifth most common malignant disease in the world, which is also the major leading cause of cancer-related death [1]. Statistically, more than 60% of patients have advanced HCC at the time of diagnosis [2]. Several chemotherapy drugs approved by the Food and Drug Administration (FDA) have shown high efficacy in controlling the symptoms of the patients in the early stage, while their therapeutic effects are reducing significantly with the decrease of the sensitivity of tumor cells to the drugs [3, 4]. Chemotherapy drugs involved some special targets in tumor cells, and tumor cells can develop a serious mechanism to weaken the injury and escape the apoptosis induced by drugs, which is a major cause leading to the failure of chemotherapy in the long-term intervention [5, 6]. Autophagy, a natural survival mechanism formed in cell involution, protects cells from apoptosis induced by injury of toxicants, oxidative stress, and physical damages [7, 8]. The activated autophagy has been observed in multiple tumor cells, and some studies have indicated that activated autophagy effectively suppresses the malignant progressions of tumor cells in the early stage [9]. However, accumulating evidence has indicated that autophagy may decrease the drug's toxicity in cells and minimize their therapeutic effect on tumor cells.

MiRNAs consisted of 18–22 nucleotides and play essential roles in cells activities [10]. MiRNAs dysfunction involves proliferation and invasion, and increasing studies have confirmed that some miRNAs are involved in the regulation of HCC cells to chemotherapeutical drugs [11]. For instance, miR-124 downregulation is related to the stem

formation and sorafenib resistance of HCC cells [12]. A previous study has identified miR-651-3p as a tumor inhibitor that can effectively suppress the progression of glioma cancer [13]. However, the role of miR-651-3p in HCC remains unclear. This study focused on investigating the connection of miR-651-3p and HCC and intended to illustrate the regulation mechanism of miR-651-3p on HCC.

This study attempted to investigate the role of miR-651-3p in HCC and provide a potential basis for HCC treatment.

2. Materials and Methods

2.1. Pathological Tissue. The tumor tissues and normal tissues of the 15 patients at ZiBo Central Hospital, Zibo, Shandong, China, were collected for this investigation. All tissues were frozen at −80°C after sample collection. The study was approved by the Ethics Committee of the ZiBo Central Hospital, Zibo, Shandong, China, and all patients provided informed written consent.

2.2. Cell Culture. The HCC cells lines, including HepG2 and Huh7, purchased from (BioWit Technologies Co., Ltd., Shenzhen, China) were used for this study. All cells were cultured with Dulbecco's modified Eagle's medium containing 10% fetal calf serum (DMEM+10% FBS, BioWit Technologies Co., Ltd., Shenzhen, China). The cells were cultured in an incubator with 5% CO_2 and 37°C.

The expression vectors of ATG3, miR-651-3p mimics, and their related negative controls were purchased from Generay Biotech (Shanghai, China). The cells were seeded in 6-well plates and cultured at the incubator with 37°C and 5% CO_2, and the cell transfection was performed when cells confluence at 70%. In brief, 100 pmol of RNA or 4 μg of DNA was incubated with 250 μL serum-free medium for 5 min, and 10 μL of Lipofectamine 2000 (Generay Biotech, Shanghai, China) was also diluted with the 250 μL serum-free medium. After that, the medium containing the expression vectors of ATG3 or miR-651-3p mimics was incubated with isometric-diluted Lipofectamine 2000 at 25°C for 20 min. Finally, 500 μL of the mixtures was added to each well, and then, the cells were cultured for 24 hours.

2.3. qRT-PCR. The total RNAs were extracted from the tissues and cells with TRIzol reagent, and the concentrations of the extracts were measured by ultraviolet spectrophotometry. 1 μg of RNAs was reversed as cDNA with TaqMan MicroRNA Reverse Transcription Kit (Applied Biosystems, Foster City, CA). The primers were synthesized and purified by RiboBio (Guangzhou, China). 10 μL of reaction system was prepared according to the instructions of the KAPA qRT-PCR kit (Sigma-Aldrich, Missouri, USA). The reaction conditions included the denaturation at 95°C for 3 min, followed by amplification for 40 cycles at 95°C for 12 s, 56°C for 40 s, and 70°C for 30 s. The relative expression levels of miR-651-3p were calculated with the $2^{-(\Delta\Delta Ct)}$ method. The primers of miR-651-3p, ATG3, and U6 are listed in Table 1.

Table 1: Primer sequence of miR-493-5p, E2F3, and U6.

Name of primer	Sequences
miR-493-5p-F	5′-GCGCAAAGGAAAGTGTATCC-3′
miR-493-5p-R	5′-CAGTGCGTGTCGTGGAGT-3′
ATG3-F	5′-GCAAACAAGAACCTATGACCTG-3
ATG3-R	5′-GTCTTCATACATGTGCTCAACTG-3′
U6-F	5′-CTCGCTTCGGCAGCACA-3′
U6-R	5′-AACGCTTCACGAATTTGCGT-3′

2.4. Cell Viability Assay. The viability of the cells was observed by CCK-8 assay. 5×10^4 cells were seeded into the 96-well plates. After cell transfection, the viability of the cells at 0, 24, 48, and 72 hours were measured by CCK-8 assay. Briefly, 10 μL of CCK-8 solution (Solarbio Biotechnology Co., Ltd., Shanghai, China) was added into each well, and then, the cells were further cultured in the dark for 4 hours. The viability of the cells was observed by a microplate reader (Molecular devices, Shanghai, China) at 450 nm.

2.5. Flow Cytometry Assay. Flow cytometry assay was performed to observe the effects of miR-651-3p on the apoptosis of HCC cells. 2×10^3 cells were suspended by 1 mL of ice Annexin V-FITC binding buffer, and then, 10 μL of propidium iodide (PI 20 μg/ml, Shanghai Yuanye Biotechnology Co., Ltd, Shanghai, China) and 5 μl of Annexin V-FITC (10 μg/ml, Shanghai Yuanye Biotechnology Co., Ltd, Shanghai, China) were added into the cells. After incubation for 15 min, the apoptosis level of the cells was observed by flow cytometry equipment (BD Biosciences, State of New Jersey, USA).

2.6. Western Blot. Total proteins were extracted from the tissues and cell lines with RIPA buffer, and BCA kit (ThermoFisher, Massachusetts, USA) and UV spectrophotometry were used to measure the concentration of the proteins. The proteins were boiled for 5 mins, and then, they were separated with sodium dodecyl sulfate polyacrylamide gels. Subsequently, the proteins in gels were translated on the polyvinylidene fluoride membranes (BioRad, CA, USA) with a wet translation method. After that, the membranes were blocked with 5% fat-free milk, and the related primary antibodies including anti-ATG3(1 : 1000, ab2577009 ThermoFisher, Massachusetts, USA), anti-LC3B (1 : 1000, ab2234770, ThermoFisher, Massachusetts, USA), and anti-β-actin (1 : 1000, sc-47,778, Santa Cruz) were used for membrane incubation at 4°C overnight. The membranes were washed with TBST for three times (15 min/time), and then, they were incubated with second antibodies for 2 hours. After membranes washing (3×10 min), the chemiluminescence detection system was used to observe and calculate the relative expressions of the related proteins.

2.7. Statistical Analysis. All experiments in this study were performed three times, independently. The data were analyzed with SPSS 20.0 and expressed by GraphPad Prism 8. The difference between the two groups was analyzed and

calculated with the chi-squared test or ANOVA (Tukey's post hoc test). $P < 0.05$ means that the difference was statistically significant.

3. Results

3.1. miR-651-3p Was Downregulated in HCC Tissues and Cells. To investigate the involvement of miR-651-3p in HCC, the qRT-PCR was used to measure the expression levels of miR-651-3p in HCC tissues and cell lines. The results showed that miR-651-3p was highly downregulated in the HCC tissues compared with the paracancerous tissues of the patients. Subsequently, the expression level of miR-651-3p was also measured in CDDP-sensitive and CDDP-resistant tissues. The results showed that miR-651-3p was significantly downregulated in CDDP-resistance tissues (Figure 1(a), $p < 0.01$). Moreover, the miR-651-3p levels were also investigated in CDDP-resistant HepG2 cells (R-HepG2) and CDDP-resistant Huh7 (R-Huh7). It was found that miR-651-3p was significantly downregulated in R-HepG2 cells (Figure 1(b), $p < 0.01$). Those observations suggested that decreased miR-651-3p was involved in the resistance of HepG2 cells.

3.2. miR-651-3p Enhanced the Sensitivity of R-HepG2 on CDDP. To evaluate the function of miR-651-3p in resistance of HepG2, the miR-651-3p mimics and related miR-NC were, respectively, transfected into R-HepG2 cells, and the cells were cultured with the medium containing a different dose of CDDP range from 0 μM to 50 μg/mL. The CCK-8 and cytometry assay were used to observe the viability and apoptosis of the cells with 5 μM of CDDP. The results showed that the viability levels of R-HepG2 transfected with miR-NC in different doses were significantly high compared with the cells transfected with miR-651-3p (Figure 2(a), $p < 0.01$). Moreover, the flow cytometry assay showed that HepG2 cells with the high miR-651-3p level expressed a high apoptosis rate compared with the cells with the low miR-651-3p level (Figure 2(b), $p < 0.01$). Those observations suggested that miR-651-3p could effectively enhance the resistance of R-HepG2 on CDDP.

3.3. miR-651-3p Directly Targets ATG3, and ATG3 Involved Resistance of HepG2. To explore the downstream target of miR-651-3p, MiRDB was used to search the downstream target of miR-651-3p. The results showed that the 3′-UTR of ATG3 could match with the sequence of miR-651-3p (Figure 3(a), $p < 0.01$). Subsequently, the miR-651-3p mimics, miR-NC, ATG3-wt, and ATG3-mut were, respectively, transfected into the HEK-293T cells to verify the binding effects of miR-651-3p and ATG3. It was found that miR-651-3p remarkably suppressed the activity of ATG3-wt, while it did not express any significant effect on ATG3-mut (Figure 3(b), $p < 0.01$). Besides, the expression levels of ATG3 were also measured in HepG2 and R-HepG2 cells. The results showed that ATG3 was significantly upregulated in R-HepG2 cells compared with HepG2 cells (Figure 3(c), $p < 0.01$). Those observations suggested that ATG3 could be targeted by miR-651-3p and involved the chemotherapeutic resistance of HepG2 cells.

3.4. ATG3 Reversed the Effects of miR-651-3p on R-HepG2. Although it was confirmed that ATG3 was significantly upregulated in R-HepG2 cells, whether ATG3 plays a key role in the regulation of miR-651-3p on R-HepG2 remains unknown. The cells were cultured with the medium containing 5 μM of CDDP, and the miR-651-3p mimics and ATG3 expressed vectors were cotransfected into the R-HepG2 to observe the changes in viability and apoptosis levels. CCK-8 assay showed that the enhanced sensitivity of R-HepG2 induced by miR-651-3p upregulation could be reversed by ATG3 (Figure 4(a), $p < 0.01$). The flow cytometry assay showed that ATG3 could effectively inhibit the apoptosis of R-HepG2 with a high miR-651-3p level (Figure 4(b), $p < 0.01$). Those observations suggested that miR-651-3p could elevate the sensitivity of R-HepG2 on CDDP.

3.5. miR-651-3p Regulated Autophagy Level of R-HepG2 via Targeting ATG3. To illustrate the regulation mechanism of miR-651-3p in resistance of HCC, the related proteins of the autophagy pathway in R-HepG2 cells were measured by Western blot after transfecting with miR-651-3p mimics and ATG3 vectors. The result showed that the miR-651-3p significantly increased LC3-I and reduced LC3-II in R-HepG2 cells. However, the effects of miR-651-3p on the cells could be reversed by ATG3. Besides, it was also found that increased miR-339-5p significantly inhibited the expression of p-AMPK in R-HepG2 cells (Figure 5, $p < 0.01$). Those observations suggested that miR-651-3p inhibited the AMPK-induced cell autophagy via targeting ATG3.

4. Discussion

Remarkable progression has been made in HCC treatment in recent ten years [14]. However, completely healing HCC remains quite difficult. At present, chemotherapy failure induced by drug resistance has become a major challenge in the clinical field of HCC treatment [15]. This study investigated the role of miR-651-3p in HCC and revealed the regulation mechanism of miR-651-3p involved resistance in HCC to CDDP.

MiRNAs dysfunction has been confirmed as a major reason for cancer development. Increasing studies have also indicated that the malignant progression of HCC is related to the miRNAs dysfunctions [16]. In this study, it was found that miR-651-3p was obviously downregulated in HCC tissues and cell lines. miR-651-5p locates on the chromosome 3, p13 of humans, and the miR-651-5p involves the artery remodeling. The reduced miR-651-3p in gastric cancer cells has been observed by a recent study, while the role of miR-651-3p in other tumors remains unclear [17]. This study proved that miR-651-3p downregulation was related to the resistance of HCC cells to CDDP. Decreased miR-651-3p has been found in gastric cancer, and the

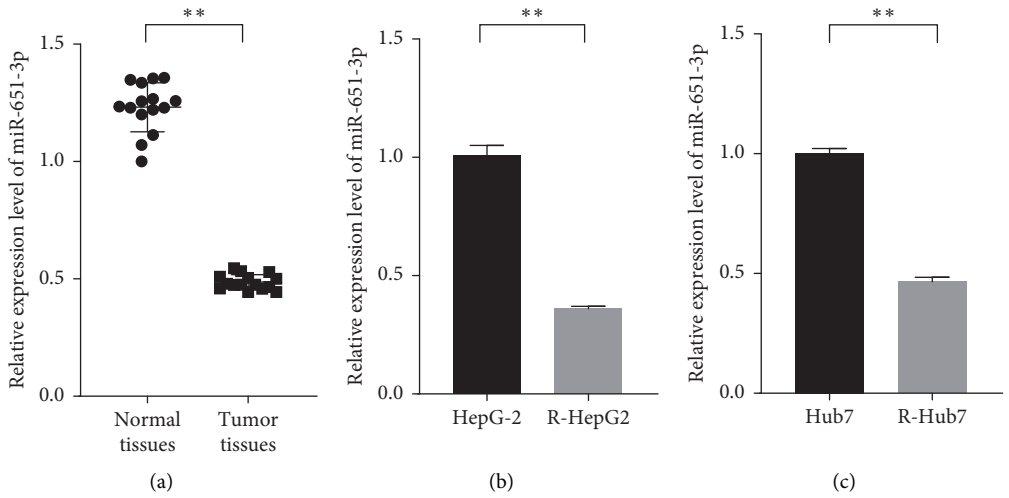

Figure 1: miR-651-3p was downregulated in HCC tissues and drug-resistant HCC cells. (a) The relative expression levels of miR-651-3p in normal and tumor tissues measured by qRT-PCR. (b) The expression levels of miR-651-3p in HepG2 cells and resistant HepG2 (R-HepG2) were measured by qRT-PCR; (c) The expression levels of miR-651-3p in Hub7 cells and resistant Hub7 (R-Hub7) measured by qRT-PCR.

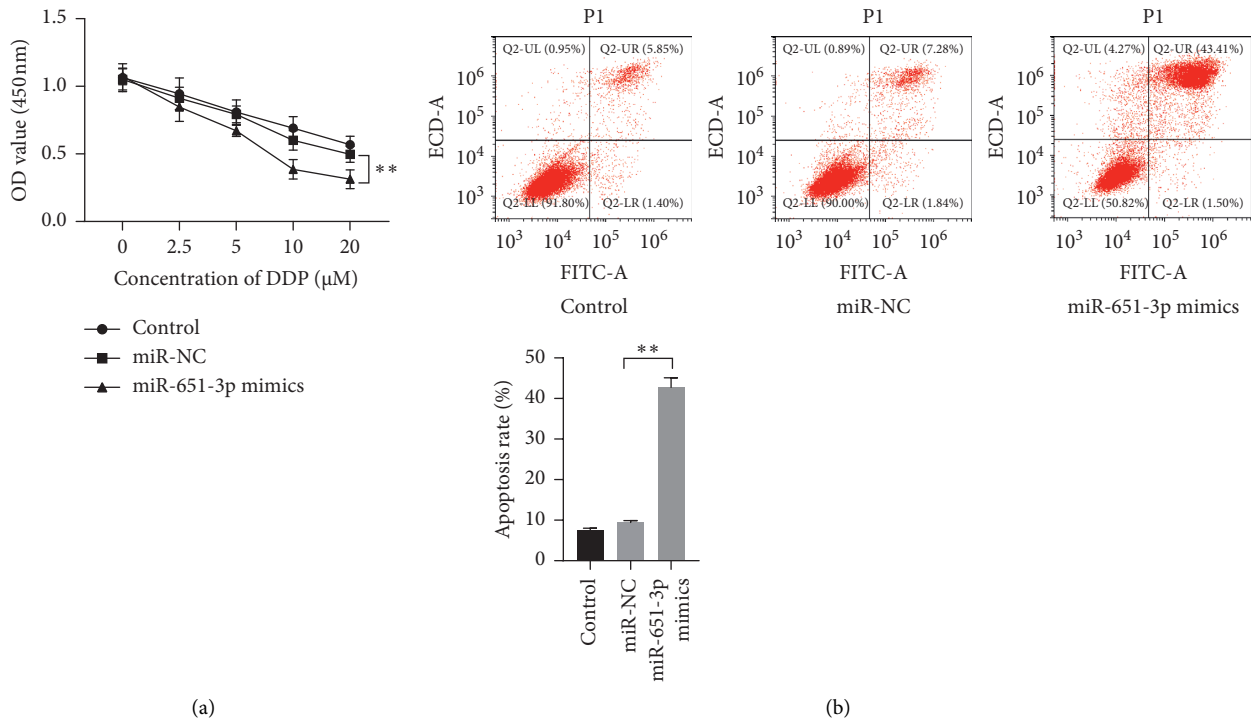

Figure 2: miR-651-3p increased the sensitivity of R-HepG2 cells on CDDP. (a) The viability of the R-HepG2 after serial dosage DDP treatment observed by CCK-8. (b) The apoptosis level of R-HepG2 with 5 μM of CDDP measured by flow cytometry assay.

proliferation and migration of the tumor cells can be effectively inhibited when miR-651-3p is overexpressed [13]. Therefore, it was hypothesized in this study that miR-651-3p involved the progression of HCC. In this study, it was also observed that miR-651-3p was highly downregulated in CDDP-resistant HepG2 cells. CDDP is one of the effective drugs for cancer intervention, which has been widely used in cancer treatment [18, 19]. Moreover, the study also found that miR-651-3p upregulation could effectively reduce the viability and promote the apoptosis of R-HepG2 cells. Thus, this study supports that miR-651-3p deficiency is a major reason for the resistance of HepG2 on CDDP.

MiRNAs are characterized by regulating the expression of proteins to involve the progressions of cells via targeting the 3′-UTR of the related mRNAs [20]. Given the characters of miRNAs in regulating the expression of proteins, the downstream target of miR-651-3p was searched by TargetScan. It was found that ATG3 was a target of miR-651-3p.

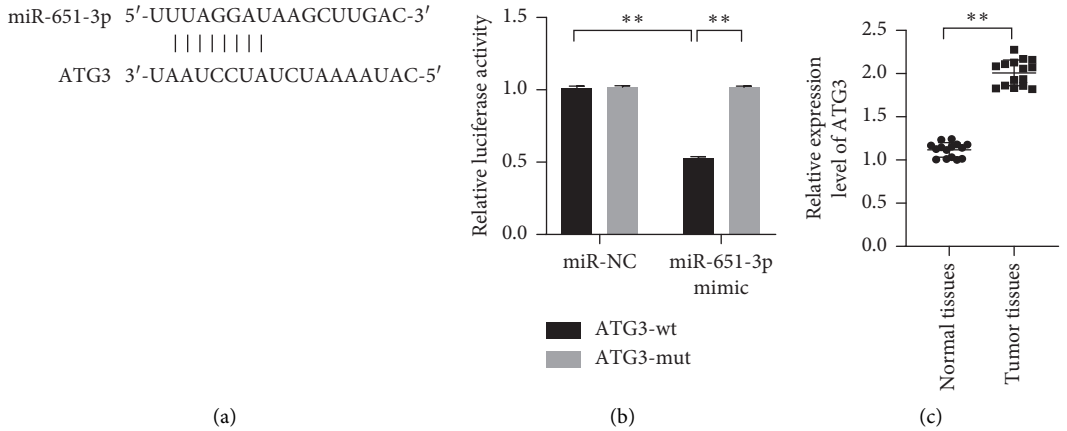

FIGURE 3: ATG3 was a downstream target of miR-651-3p and was significantly upregulated in tumor tissues. (a) The binding sites of miR-651-3p and ATG3. (b) The binding effect of miR-651-3p and ATG3 observed by dual-luciferase reporter assay. (c) The mRNAs level of miR-651-3p significantly upregulated in tumor tissues.

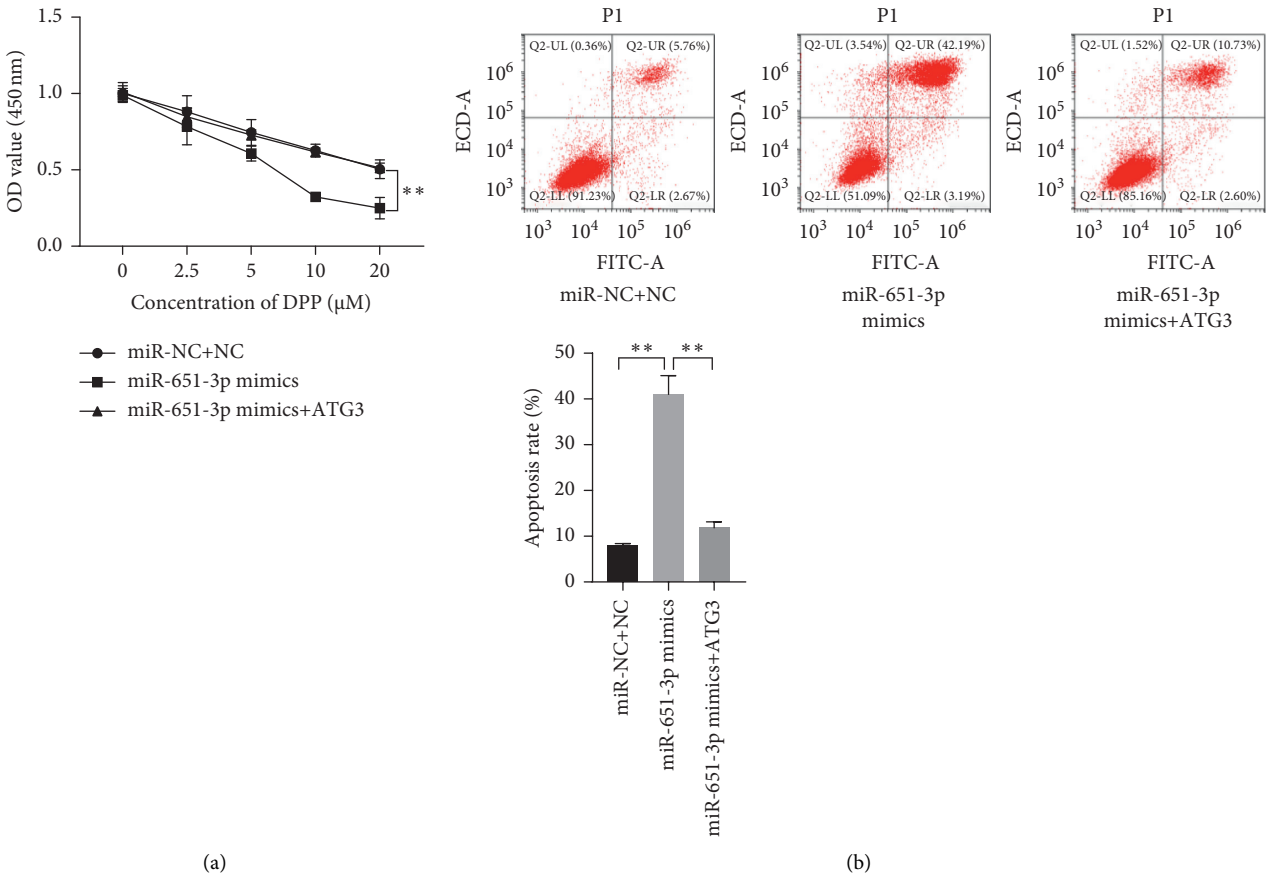

FIGURE 4: ATG3 reversed the effect of miR-651-3p on the CDDP-resistance of R-HepG2 cells. (a) The viability of the resistant HepG2 after serial dosage DDP treatment observed by CCK-8. (b) The apoptosis level of resistant HepG2 with 5 μM of CDDP measured by flow cytometry assay.

ATG3 has been found as a tumor promoter that involves the malignant behaviors of multiple tumors [21]. The promotion of ATG3 on tumor cells has been confirmed by several studies, and ATG3 was regulated by multiple miRNAs to involve the malignant progression of some tumor cells [22, 23]. Moreover, ATG3 is also related to the sensibility of the cell on DNA injury [24].

Several studies have proved that ATG3 was significantly upregulated in multiple cancers, and ATG3 downregulation could effectively inhibit the proliferation invasive abilities of

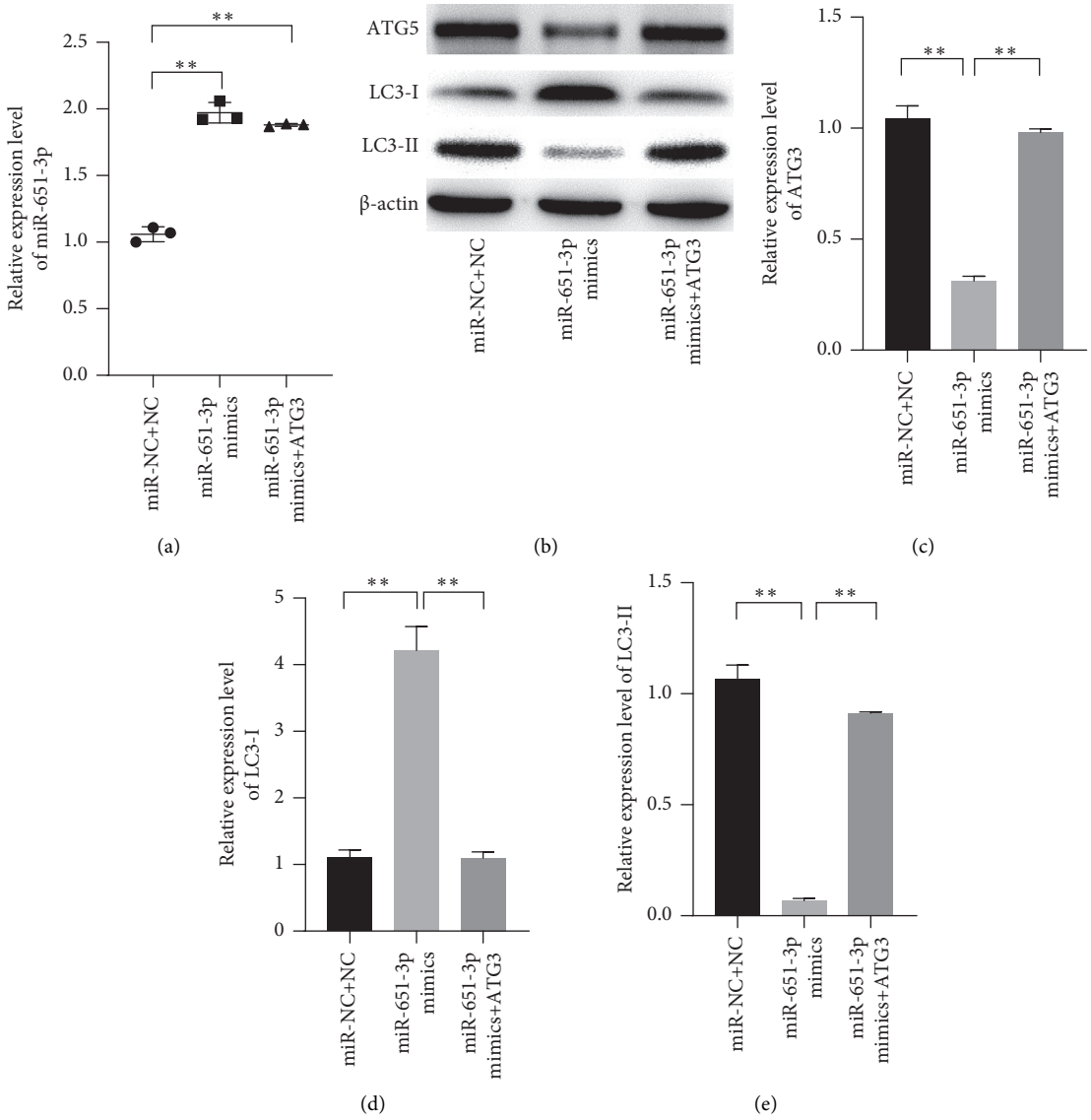

Figure 5: miR-651-3p regulating the cell autophagy of R-HepG2 via targeting ATG3. (a) The relative expression level of miR-651-3p measured by qRT-PCR. (b–e) The relative expression levels of ATG3, LC3-I, and LC3-II measured by Western blot, respectively.

tumor cells [25]. Huang et al. have found that ATG3 downregulation significantly inhibited the proliferation, migration, and invasion of nonsmall cell lung cancer [26]. In this study, it was proved that ATG3 restoration could partly rescue the enhanced sensitivity of R-HCC cells to CDDP induced by miR-651-3p and reduce the apoptosis rate of the cells when suffered CDDP treatment. Thus, this study suggested that ATG3 involved the regulation of miR-651-3p on the resistance of HCC. Drug-resistance is related to the autophagy progression of the cells, and tumor cells can reduce the effect drug toxicity of chemotherapy drugs via promoting cell autophagy [27]. ATG3 is related to cell autophagy, and several studies have found that aberrant expression of ATG3 can increase cell autophagy, which is related to enhanced drug-resistance of tumor cells [28]. In this study, the expression of the related proteins in the autophagy pathway was observed, and the obvious changes in the expression levels of LC3-I and LC3-II were observed. Thus, this study supported that miR-651-3p could inhibit the ATG3-mediated cell autophagy to enhance the sensitivity of HCC cells to CDDP.

This study revealed miR-651-3p as a tumor inhibitor in HCC cells and illustrated that miR-651-3p could enhance the sensitivity of HCC cells on CDDP via regulating the aberrant autophagy levels of HCC cells induced by increased ATG3. However, the presumption in this study was only confirmed with cell experiments, and more evidence from animal experiments is still necessary to validate the resistance-inhibited effects of miR-651-3p on HCC.

Data Availability

The data used to support the findings of this study are available from the corresponding author upon request.

Conflicts of Interest

The authors declare that they have no conflicts of interest.

References

[1] A. Caines, R. Selim, and R. Salgia, "The changing global epidemiology of hepatocellular carcinoma," *Clinics in Liver Disease*, vol. 24, no. 4, pp. 535–547, 2020.

[2] Z. Liu, M. Ma, L. Yan et al., "miR-370 regulates ISG15 expression and influences IFN-α sensitivity in hepatocellular carcinoma cells," *Cancer Biomarkers*, vol. 22, no. 3, pp. 453–466, 2018.

[3] Y.-J. Liao, S.-M. Hsu, C.-Y. Chien, Y.-H. Wang, M.-H. Hsu, and F.-M. Suk, "Treatment with a new barbituric acid derivative exerts antiproliferative and antimigratory effects against sorafenib resistance in hepatocellular carcinoma," *Molecules*, vol. 25, no. 12, Article ID 2856, 2020.

[4] K. Regan-Fendt, D. Li, R. Reyes et al., "Transcriptomics-based drug repurposing approach identifies novel drugs against sorafenib-resistant hepatocellular carcinoma," *Cancers*, vol. 12, no. 10, Article ID 2730, 2020.

[5] Y. Ren, Y. K. Gu, Z. Li et al., "CXCR3 confers sorafenib resistance of HCC cells through regulating metabolic alteration and AMPK pathway," *American Journal of Tourism Research*, vol. 12, no. 3, pp. 825–836, 2020.

[6] Y. Zhou, R.-G. Fan, C.-L. Qin, J. Jia, X.-D. Wu, and W.-Z. Zha, "LncRNA-H19 activates CDC42/PAK1 pathway to promote cell proliferation, migration and invasion by targeting miR-15b in hepatocellular carcinoma," *Genomics*, vol. 111, no. 6, pp. 1862–1872, 2019.

[7] E. Lee, Y. Koo, A. Ng et al., "Autophagy is essential for cardiac morphogenesis during vertebrate development," *Autophagy*, vol. 10, no. 4, pp. 572–587, 2014.

[8] N. Wojciechowska, I. Smugarzewska, K. Marzec-Schmidt, A. Zarzyńska-Nowak, and A. Bagniewska-Zadworna, "Occurrence of autophagy during pioneer root and stem development in Populus trichocarpa," *Planta*, vol. 250, no. 6, pp. 1789–1801, 2019.

[9] Y.-F. Peng, Y.-H. Shi, Z.-B. Ding et al., "Autophagy inhibition suppresses pulmonary metastasis of HCC in mice via impairing anoikis resistance and colonization of HCC cells," *Autophagy*, vol. 9, no. 12, pp. 2056–2068, 2013.

[10] S. Zhang, L. Chen, Y. Wang, W. Tang, Y. Chen, and L. Liu, "Investigation of the association of *miRNA-499, miRNA-146a, miRNA-196a2* loci with hepatocellular carcinoma risk: a case-control study involving 1507 subjects," *DNA and Cell Biology*, vol. 39, no. 3, pp. 379–388, 2020.

[11] Y. Zhou, H. Ren, B. Dai et al., "Hepatocellular carcinoma-derived exosomal miRNA-21 contributes to tumor progression by converting hepatocyte stellate cells to cancer-associated fibroblasts," *Journal of Experimental & Clinical Cancer Research*, vol. 37, no. 1, p. 324, 2018.

[12] Y. Feng, W. Jiang, W. Zhao, Z. Lu, Y. Gu, and Y. Dong, "miR-124 regulates liver cancer stem cells expansion and sorafenib resistance," *Experimental Cell Research*, vol. 394, no. 2, Article ID 112162, 2020.

[13] S. Yu, X. Ruan, X. Liu et al., "HNRNPD interacts with ZHX2 regulating the vasculogenic mimicry formation of glioma cells via linc00707/miR-651-3p/SP2 axis," *Cell Death & Disease*, vol. 12, no. 2, p. 153, 2021.

[14] Q. Ruan, H. Wang, L. J. Burke et al., "Therapeutic modulators of hepatic stellate cells for hepatocellular carcinoma," *International Journal of Cancer*, vol. 147, no. 6, pp. 1519–1527, 2020.

[15] L. Wei, D. Lee, C.-T. Law et al., "Genome-wide CRISPR/Cas9 library screening identified PHGDH as a critical driver for Sorafenib resistance in HCC," *Nature Communications*, vol. 10, no. 1, p. 4681, 2019.

[16] J. Wang, Y. Zhang, L. Lu, Y. Lu, Q. Tang, and J. Pu, "Insight into the molecular mechanism of LINC00152/miR-215/CDK13 axis in hepatocellular carcinoma progression," *Journal of Cellular Biochemistry*, vol. 120, no. 11, pp. 18816–18825, 2019.

[17] G. Hu, Y. Shi, X Zhao et al., "CBFβ/RUNX3-miR10b-TIAM1 molecular axis inhibits proliferation, migration, and invasion of gastric cancer cells," *International Journal of Clinical and Experimental Pathology*, vol. 12, no. 9, pp. 3185–3196, 2019.

[18] Y. Xiao, F. T. Lin, and W. C. Lin, "ACTL6A promotes repair of cisplatin-induced DNA damage, a new mechanism of platinum resistance in cancer," *Proceedings of the National Academy of Sciences of the United States of America*, vol. 118, no. 3, Article ID e2015808118, 2021.

[19] M. D. Tharmalingam, G. Matilionyte, W. H. B. Wallace et al., "Cisplatin and carboplatin result in similar gonadotoxicity in immature human testis with implications for fertility preservation in childhood cancer," *BMC Medicine*, vol. 18, no. 1, p. 374, 2020.

[20] Z. Hongfeng, J. Andong, S. Liwen et al., "lncRNA RMRP knockdown suppress hepatocellular carcinoma biological activities via regulation miRNA-206/TACR1," *Journal of Cellular Biochemistry*, vol. 121, no. 2, pp. 1690–1702, 2020.

[21] Y. Kang, Y. Jia, Q. Wang et al., "Long noncoding RNA KCNQ1OT1 promotes the progression of non-small cell lung cancer via regulating miR-204-5p/ATG3 Axis," *OncoTargets and Therapy*, vol. 12, pp. 10787–10797, 2019.

[22] X. Li, Y. Zhou, L. Yang et al., "LncRNA NEAT1 promotes autophagy via regulating miR-204/ATG3 and enhanced cell resistance to sorafenib in hepatocellular carcinoma," *Journal of Cellular Physiology*, vol. 235, no. 4, pp. 3402–3413, 2020.

[23] H. Wang, Y. Zhang, Q. Wu, Y. B. Wang, and W. Wang, "miR-16 mimics inhibit TGF-β1-induced epithelial-to-mesenchymal transition via activation of autophagy in non-small cell lung carcinoma cells," *Oncology Reports*, vol. 39, no. 1, pp. 247–254, 2018.

[24] K. Ma, W. Fu, M. Tang et al., "PTK2-mediated degradation of ATG3 impedes cancer cells susceptible to DNA damage treatment," *Autophagy*, vol. 13, no. 3, pp. 579–591, 2017.

[25] S. Lin, H. Wang, W. Yang, A. Wang, and C. Geng, "Silencing of long non-coding RNA colon cancer-associated transcript 2 inhibits the growth and metastasis of gastric cancer through blocking mTOR signaling," *OncoTargets and Therapy*, vol. 13, pp. 337–349, 2020.

[26] W. Huang, C. Zeng, S. Hu, L. Wang, and J. Liu, "ATG3, a target of miR-431-5p, promotes proliferation and invasion of colon cancer via promoting autophagy," *Cancer Management and Research*, vol. 11, pp. 10275–10285, 2019.

[27] Y. Zhang, F. Li, L. Liu et al., "Salinomycin-induced autophagy blocks apoptosis via the ATG3/AKT/mTOR signaling axis in PC-3 cells," *Life Sciences*, vol. 207, pp. 451–460, 2018.

[28] F. Nazio, M. Bordi, V. Cianfanelli, F. Locatelli, and F. Cecconi, "Autophagy and cancer stem cells: molecular mechanisms and therapeutic applications," *Cell Death & Differentiation*, vol. 26, no. 4, pp. 690–702, 2019.

Hindawi
Journal of Oncology
Volume 2021, Article ID 7517379, 5 pages
https://doi.org/10.1155/2021/7517379

Research Article

Analysis of Changes of Intestinal Flora in Elderly Patients with Alzheimer's Disease and Liver Cancer and Its Correlation with Abnormal Gastrointestinal Motility

Weiwei Zhang,[1,2] **Xuelian Zhang**,[1] **Yanyan Zhang**,[1] **Huanyu Wu**,[1] **Qiaoling Liu**,[1] **Xinyu Zhou**,[1] **and Yunxia Meng**[1]

[1]*Department of Geriatrics, The First People's Hospital of Lianyungang, Lianyungang 222000, China*
[2]*Department of Geriatrics, The First Affiliated Hospital of Kangda College of Nanjing Medical University, Lianyungang 222000, China*

Correspondence should be addressed to Yunxia Meng; mengyunxia@lyghospital.cn

Received 24 June 2021; Accepted 3 August 2021; Published 13 August 2021

Academic Editor: Muhammad Wasim Khan

Objective. To investigate the changes of intestinal flora in elderly patients with Alzheimer's disease and liver cancer and its correlation with abnormal gastrointestinal motility. *Methods*. From January 2018 to December 2020, 102 elderly patients with Alzheimer's disease and liver cancer were selected as the observation group. Eighty-nine healthy patients during the same period were selected as the control group. The two groups of intestinal flora (intestinal microbial diversity) were detected by real-time fluorescent quantitative PCR (RT-qPCR) and high-throughput sequencing. The two groups of serum motilin (MTL) and gastrin (GAS) levels were measured by the Hitachi automatic biochemical analyzer 7600. Pearson correlation analysis software was used to analyze the relationship between changes in the intestinal flora and gastrointestinal motility in elderly patients with Alzheimer's disease and liver cancer. *Results*. The contents of *Bifidobacteria* and *Lactobacilli* in the observation group were lower than those in the control group, and the contents of *Escherichia coli*, *Helicobacter pylori,* and *Streptococcus* were higher than those in the control group. The Chaol index and Shannon index in the observation group were higher than those in the control group. The gastrointestinal motility levels MTL and GAS of the observation group were higher than those of the control group. The results of Pearson correlation analysis showed that the Chaol index and Shannon index of elderly patients with Alzheimer's disease and liver cancer were positively correlated with MTL and GAS. *Conclusion*. Elderly patients with Alzheimer's disease and liver cancer often have changes in the intestinal flora, which are correlated with abnormal gastrointestinal motility. Strengthening the analysis of changes in patients' intestinal flora can enhance clinical medication knowledge and improve gastrointestinal motility in patients.

1. Introduction

Alzheimer's disease is a degenerative disease of the nervous system with relatively insidious onset and progressive development in the elderly. The clinical manifestations are memory impairment, aphasia, ignorance, impairment of visual and spatial skills, and executive dysfunction [1]. Current studies show that the onset of Alzheimer's disease in the elderly may be related to family history, head trauma, viral infection, etc., but its specific pathogenesis is still not clear. With the increasing aging of the population in China, elderly Alzheimer's disease incidence is on the rise [2, 3]. Liver cancer is a malignant tumor that occurs in the liver, and its incidence is mainly related to viral hepatitis, drinking, eating moldy food, and heredity. The clinical symptoms in the early stage of the disease lack typicality, and as the course of the disease prolongs, they usually manifest as pain, fever, and fatigue in the liver area. Previous studies have shown that intestinal flora belongs to the "second genome" of the human body and is also an important defense line of the body's immune system [4]. Its dynamic balance is the basis for maintaining the body's normal function, and it has essential physiological and pathological significance for the human body. In addition, the intestinal

flora can also affect the body's protein, neurotoxicity, and neuronal absorption [5]. For patients with intestinal flora disorder or imbalance, it will not only aggravate the damage and loss of neurons in the brain but also cause gastrointestinal dysfunction, thereby aggravating the occurrence and development of the disease. However, there are few clinical studies on the relationship of intestinal microflora changes in elderly Alzheimer's disease patients with liver cancer and its correlation with gastrointestinal motility abnormalities [6, 7]. Therefore, this study selected elderly patients with Alzheimer's disease and liver cancer and healthy subjects to explore the changes of intestinal flora in elderly patients with Alzheimer's disease complicated with liver cancer and their correlation with gastrointestinal motility abnormalities.

2. Materials and Methods

2.1. Clinical Information. From January 2018 to December 2020 at the First People's Hospital of Lianyungang, Lianyungang, China, 102 elderly patients with Alzheimer's disease and liver cancer were selected as the observation group and 89 cases of healthy physical examination during the same period were included in the control group. There was no statistically significant difference in the general information of the two groups of patients, and they were comparable (Table 1). The study was approved by the ethics committee of the First People's Hospital of Lianyungang, Lianyungang, China, and the patient's informed consent was obtained.

2.2. Inclusion and Exclusion Criteria. Inclusion criteria: (1) patients who meet the diagnostic criteria for Alzheimer's disease according to the American Psychiatric Association "Diagnosis and Statistical Work Manual of Mental Disorders Fourth Edition Revised Edition" [8]; patients with liver cancer diagnosed by pathological tissue examination; (2) patients with age ≥60 years, with complete baseline and follow-up data; and (3) patients with complete intestinal flora and gastrointestinal motility examinations and who can tolerate them. Exclusion criteria: (1) patients with autoimmune diseases, language communication disorders, or other mental illnesses; (2) patients who have taken neurotrophic drugs, microecological agents, and cardiovascular diseases within the past month; and (3) patients with severe liver and kidney dysfunction, accompanied by autoimmune system diseases.

3. Method

3.1. Intestinal Flora Determination

3.1.1. Determination of Intestinal Flora. The RT-qPCR method was used to detect the total load of the intestinal flora in the two groups, including two types of intestinal probiotics (such as *Bifidobacterium* and *Lactobacillus*) and six types of intestinal pathogenic bacteria (*Escherichia coli*, *Staphylococcus*, *Veillonella*, *Helicobacter pylori*, *Streptococcus*, and *Pseudomonas aeruginosa*) levels. 300 mg of feces (middle feces) after admission of both groups were collected, and we completed the extraction of fecal bacterial DNA according to the instructions of the fecal bacterial genomic DNA extraction kit (Tiangen Biochemical Technology Co., Ltd., Beijing) and the PCR reaction. The primer is designed by Shanghai Yingjun Biotechnology Co., Ltd. According to the test content, the measurement of relevant parameters was completed: 10 min at 30°C; 30 min at 42°C; 5 min at 99°C; and 5 min at 5°C. A total of 35 cycles are completed, the final 10 min is extended, and the temperature is 72°C.

A standard calibration and negative control are set up for each experiment. After the reaction is completed, the specificity of the PCR product is analyzed according to the melting curve, and the final product is placed for agarose gel electrophoresis with a concentration of 1.5%. The result is the bacterial copy coefficient using logarithm/g feces mentioned above [9, 10].

Table 1: Comparison of general data between the two groups.

Clinical data	Observation	Control	χ^2/t	P
Gender				
Male	61	51	1.214	0.793
Female	41	38		
Age (years)	71.49 ± 6.38	71.64 ± 6.42	0.591	0.325
BMI (kg/m^2)	23.52 ± 3.26	24.97 ± 3.31	1.025	0.782
Disease duration (years)	12.52 ± 3.21	—	—	—
Education				
Junior high school and below	41	36	1.491	0.678
High school	54	47		
High school or above	7	6		
Electroencephalogram (EEG) examination				
Mild diffuse abnormalities	43	—	—	—
Moderate abnormalities	40	—	—	—
Severe abnormalities	19	—	—	—

3.1.2. Diversity Detection of Intestinal Flora. High-throughput sequencing was used to detect the intestinal flora (intestinal microbial diversity) of the two groups. Stool samples were obtained from the abovementioned samples, and the intestinal flora diversity test was completed by Shanghai Shenggong Biological Engineering Co., Ltd. The Chaol index and Shannon index were calculated to complete the relative abundance analysis of the flora [11].

3.2. Measurement and Correlation of Gastrointestinal Motility Level

3.2.1. Collection of Blood Samples. 3 mL of peripheral fasting blood was taken from the observation group in the morning of the next day after admission, and 3 mL of peripheral blood was taken from the control group took on the day of physical examination and centrifuged for 30 min at a speed of 2500 rpm. Samples were placed at low temperature for use after the serum separation.

3.2.2. Detection Method. The Hitachi 7600 automatic biochemical analyzer was used to determine the levels of serum MTL and GAS in the two groups. The detection method was

enzyme-linked immunosorbent assay (ELISA). All kits were purchased from the Beijing East Asia Institute of Immunology. All operations were completed in strict accordance with the instrument instructions [12, 13].

3.2.3. Correlation Analysis. Pearson correlation analysis software was used to analyze the relationship between changes in the intestinal flora and gastrointestinal motility in elderly patients with Alzheimer's disease and liver cancer.

3.3. Statistical Analysis. SPSS24.0 software was used to process and analyze the data. The counting data were tested by χ^2 and expressed by n (%). Measurement data such as intestinal flora content were in line with normal distribution and were performed by the t test and expressed by ($\overline{x} \pm s$). $P < 0.05$ was considered statistically significant.

4. Results

4.1. Comparison of Intestinal Flora between the Two Groups. The contents of *Staphylococcus*, *Pseudomonas aeruginosa,* and *Veillonella* in the two groups were not statistically significant (Table 2). The contents of *Bifidobacteria* and *Lactobacilli* in the observation group were lower than those in the control group, and the contents of *Escherichia coli*, *Helicobacter pylori*, and *Streptococcus* were higher than those in the control group (Table 2).

4.2. Comparison of the Diversity of Intestinal Flora between the Two Groups. The Chaol index and Shannon index of elderly patients in the observation group were higher than those in the control group (Table 3).

4.3. Comparison and Correlation Analysis of Gastrointestinal Motility between the Two Groups. The gastrointestinal motility levels MTL and GAS of the observation group were higher than those of the control group (Table 4). The results of Pearson correlation analysis showed that the Chaol index and Shannon index of elderly patients with Alzheimer's disease and liver cancer were positively correlated with MTL and GAS (Table 5).

5. Discussion

Alzheimer's disease occurs more frequently in older adults, and common pathogenic factors include gene mutation and unhealthy lifestyle, but the specific pathogenesis of the disease has not been clarified clinically [14]. Liver cancer is also a malignant tumor with a high incidence rate. It occurs in people over the age of 40, and it is also an important cause of death among Chinese residents. Studies have shown that the brain tissues of elderly patients with Alzheimer's disease and liver cancer have obvious pathological changes [15]. Patients are often accompanied by amyloid deposition and neurofibrillary tangles after the onset of disease, which can cause nerve cell atrophy and death, and a serious condition of patients can cause cognitive dysfunction [15]. At the same time, Alzheimer's disease and liver cancer can interact and exacerbate, affecting the prognosis of patients.

In recent years, more and more research results have confirmed that intestinal microecological disorders are more common in elderly patients with Alzheimer's disease. The imbalance of the intestinal flora after the onset of the patient can affect the neuro-immune-endocrine system through the flora-brain-gut axis, which can damage the structure and function of the central nervous system [16, 17]. For normal people, intestinal flora is in a state of dynamic balance, but the imbalance of intestinal flora caused by various reasons will lead to the occurrence of a variety of diseases, increasing the incidence of chronic enteritis, gastrointestinal ulcer, stroke, and other diseases [18]. In this study, the contents of *Bifidobacterium* and *Lactobacillus* in the observation group were lower than those in the control group. In comparison, the contents of *Escherichia coli*, *Helicobacter pylori,* and *Streptococcus* in the observation group were higher than those in the control group, indicating that the elderly Alzheimer's disease and liver cancer patients were often accompanied by intestinal flora disorders, resulting in a decrease in the number of beneficial bacteria and an increase in the number of harmful bacteria.

Previous studies have shown that when the intestinal microecology is unbalanced and beneficial bacteria are reduced, a large amount of endotoxin will be produced, which will damage multiple tissues and organs throughout the body and increase the risk of damage to the central nervous system [19]. In addition, the reduction of beneficial bacteria and the increase of harmful bacteria in the intestines can affect the neuroendocrine system of patients, leading to neurotransmitter disorders [20]. In this study, the Chaol index and Shannon index of observation group were higher than those in the control group. The gastrointestinal motility levels MTL and GAS of the observation group were higher than those of the control group. It shows that the intestinal tract of elderly patients with Alzheimer's disease and liver cancer has the characteristics of diversity and complexity, which can cause the reduction of beneficial bacteria, can lead to abnormal gastrointestinal function, and aggravate the occurrence and development of the disease.

It has been reported that the decrease of beneficial bacteria in the intestine and the increase of harmful bacteria can cause a microinflammatory state and cause systemic oxidative stress, which are independent risk factors for Alzheimer's disease [21]. It can be seen that there is a close connection between intestinal microecological disorder and the occurrence of Alzheimer's disease. Thus, the correlation analysis between the changes of the intestinal flora of patients and the level of gastrointestinal motility was conducted in this study. The results show that the Chaol index and Shannon index of elderly patients with Alzheimer's disease and liver cancer are positively correlated with MTL and GAS, indicating that there is a strong correlation between the changes of intestinal flora and gastrointestinal motility in elderly patients with Alzheimer's disease and liver cancer. Therefore, at a clinic for elderly patients with Alzheimer's disease and liver cancer, there is a need to

Table 2: Comparison of intestinal flora between the two groups (logarithm/g feces, $\overline{x} \pm s$).

Group	Observation ($n = 102$)	Control ($n = 89$)	t	P
Staphylococcus	4.39 ± 0.56	4.41 ± 0.58	1.394	0.785
Escherichia coli	8.63 ± 0.83	4.12 ± 0.43	7.451	≤0.01
Helicobacter pylori	8.81 ± 0.88	5.29 ± 0.52	9.229	≤0.01
Streptococcus	7.40 ± 0.79	3.25 ± 0.45	6.672	≤0.01
Veillonella	4.21 ± 0.56	4.23 ± 0.58	2.142	0.561
Pseudomonas aeruginosa	4.06 ± 0.51	4.08 ± 0.53	0.638	0.829
Bifidobacteria	2.59 ± 0.41	6.63 ± 0.64	5.982	≤0.01
Lactobacilli	1.02 ± 0.25	5.49 ± 0.42	9.142	≤0.01

Table 3: Comparison of intestinal flora diversity between the two groups ($\overline{x} \pm s$).

Group	Cases	Chaol index	Shannon index
Observation	102	543.59 ± 35.61	5.70 ± 0.53
Control	89	287.43 ± 26.98	3.71 ± 0.41
t	—	7.813	6.092
P	—	≤0.01	≤0.01

Table 4: Comparison of gastrointestinal motility levels between the two groups ($\overline{x} \pm s$).

Group	Cases	MTL (ng/L)	GAS (pg/mL)
Observation	102	83.23 ± 4.51	96.49 ± 6.63
Control	89	51.16 ± 3.20	70.32 ± 4.74
t	—	8.142	5.091
P	—	≤0.01	≤0.01

Table 5: Correlation analysis of intestinal flora and gastrointestinal motility in elderly patients with Alzheimer's disease and liver cancer (r, P).

Correlation	MTL	GAS
Chaol index	0.774 (≤0.01)	0.815 (≤0.01)
Shannon index	0.698 (≤0.01)	0.791 (≤0.01)

strengthen the measurement of the changes in the intestinal flora of the patients, evaluate and predict the gastrointestinal motility level of the patients, and adjust the treatment plan according to the measurement results, so that specific treatment is provided. However, there are some limitations to this study. The ELISA kit has some defects (such as operation errors), which may lead to data deviation. The patients enrolled in this study all took drugs for a long time, which may cause some interference to the study results.

In summary, elderly patients with Alzheimer's disease and liver cancer are often accompanied by changes in intestinal flora, which are correlated with abnormal gastrointestinal motility. Strengthening the analysis of changes in patients' intestinal flora can provide potential basis for clinical medication use and improve patients' health.

Data Availability

All data generated or analyzed during this study are included in the published article. The datasets used and/or analyzed during the present study are available from the corresponding author on reasonable request.

Conflicts of Interest

The authors declare no conflicts of interest.

Acknowledgments

This work was supported by the Medical Technology Support Project (Advanced Sign Technology) of the First People's Hospital of Lianyungang (No. XJ1905).

References

[1] Z. Sun, H. Chen, and S. Chen, "Expression of serum Lp-PLA2 and NLRP3 in elderly patients with Alzheimer's disease and its relationship with cognitive impairment," *Journal of Modern Laboratory Medicine*, vol. 35, no. 1, pp. 55–58, 2020.

[2] S. Zhang and W. Xu, "Recent advance in relations of intracerebral chronic inflammation and gut-brain axis with Alzheimer's disease," *Chinese Journal of Neuromedicine*, vol. 19, no. 11, pp. 1176–1180, 2020.

[3] Q. Cai, W. Chen, Q. Huang, M. Ma, and Y. Huo, "Discussion on the theoretical basis of treating Alzheimer's disease from the spleen and stomach based on "intestinal flora"" *Journal of Sichuan of Traditional Chinese Medicine*, vol. 37, no. 2, pp. 28–30, 2019.

[4] S. Shao, Y. Tang, Y. Guo, Z. Tian, D. Xiang, and J. Wu, "Effects of acupuncture on patients with Alzheimer's disease," *Medicine*, vol. 98, no. 4, Article ID e14242, 2019.

[5] Y. Zhang, S. Wang, J. Li, M. Song, S. Wang, and P. Yan, "Association of serum thioredoxin and melatonin levels with MMSE score in patients with Alzheimer's disease," *Zhejiang Medical Journal*, vol. 42, no. 1, pp. 55–57, 2020.

[6] H. Wang, C. Niu, H. Wang, and C. Zhao, "Understanding the underlying pathogenesis of Alzheimer's disease from the perspective of gut microbiota," *Journal of Microbes and Infections*, vol. 14, no. 5, pp. 310–316, 2019.

[7] D. Zhou, M. Wang, and H. Jiang, "Correlation between intestinal microecological changes and cognitive function in elderly patients with Alzheimer's disease," *Chinese Journal of Microecology*, vol. 32, no. 6, pp. 86–90, 2020.

[8] N. Franzmeier, J. Neitzel, J. Neitzel et al., "Functional brain architecture is associated with the rate of tau accumulation in Alzheimer's disease," *Nature Communications*, vol. 11, no. 1, p. 347, 2020.

[9] M. Guo, D. Jin, P. Wang, and J. Li, "Analysis of correlation between cognitive function and levels of IL-6, hs-CRP, Hcy and CysC in patients with senile dementia," *Journal of Clinical Research*, vol. 36, no. 2, pp. 280-281, 2019.

[10] J. Xiang, K. Cao, Y. Dong et al., "SOD2 and SIRT3 expression levels in the different brain regions of patients with

Alzheimer's disease and their correlation," *Journal of Guangxi Medical University*, vol. 44, no. 5, pp. 497–502, 2019.

[11] Y. Zhang, Y. Liu, P. Xu, and L. Wen, "Exploring the mechanism of Jiedu Huayu decoction to improve the cognitive function of Alzheimer's disease mice based on the regulation of the brain-gut axis," *Chinese Journal of Pharmacology and Toxicology*, vol. 33, no. 9, p. 42, 2019.

[12] L. Liu, H. Sun, F. Nie, and X. Hu, "Prognostic value of abnormal ankle–brachial index in patients with coronary artery disease: a meta-analysis," *Angiology*, vol. 71, no. 6, Article ID 000331972091158, 2020.

[13] Y. Zhou and X. Pan, "Effect of deep sea fish oil on Alzheimer's disease and intestinal microecology in rats," *Chinese Journal of Microecology*, vol. 32, no. 12, pp. 21–27, 2020.

[14] D. Xu, Z. Cai, C. Gu, J. Luo, and L. Wu, "Funding of national natural science foundation of China to pharmacological research on alzheimer disease drugs from 2009 to 2018," *Chinese Journal of Pharmacology and Toxicology*, vol. 33, no. 5, pp. 327–333, 2019.

[15] H. Yan, Q. Qi, L. Yang, and J. Xu, "Correlation between serum homocysteine, folate levels and the incidence of Alzheimer's disease in the elderly," *Chinese Journal of Health Laboratory Technology*, vol. 30, no. 6, pp. 68–74, 2020.

[16] M. Koszewiczz, J. Jaroch, A. Brzecka, M. Ejma, and G. Aliev, "Dysbiosis is one of the risk factor for stroke and cognitive impairment and potential target for treatment," *Pharmacological Research*, vol. 164, no. 4, Article ID 105277, 2020.

[17] H. Li, W. Zhou, T. Zeng, and D. Yang, "Correlation between sleep structure abnormalities and cognitive function scores (MMSE and MoCA) in patients with Alzheimer's disease," *Journal of Clinical Research*, vol. 36, no. 10, pp. 1890–1892, 2019.

[18] J. Wu, Z. Lin, K. Yang, Y. Li, and X. Liu, "Analysis on correlations between serum 8-OHdG, MnSOD and cognitive function in patients with Alzheimer's disease," *Chongqing Medicine*, vol. 49, no. 10, pp. 97–100, 2020.

[19] T. Zhang, C. Liu, and A. Yin, "Correlation analysis of care burden and sadness of 161 cases of Alzheimer's disease patients," *Journal of Nursing*, vol. 26, no. 11, pp. 65–67, 2019.

[20] X. Wu, L. Zhu, T. Zhu, H. Li, Y. Chen, and Q. Tang, "Advance in intestinal flora affecting central nervous system diseases (review)," *Chinese Journal of Rehabilitation Theory and Practice*, vol. 24, no. 5, pp. 539–543, 2018.

[21] Y. Li, Z. Lv, J. Zhang et al., "Profiling of differentially expressed circular RNAs in peripheral blood mononuclear cells from Alzheimer's disease patients," *Metabolic Brain Disease*, vol. 35, no. 3, pp. 201–213, 2020.

Hindawi
Journal of Oncology
Volume 2021, Article ID 9120265, 6 pages
https://doi.org/10.1155/2021/9120265

Research Article

Efficacy of Sorafenib Combined with Interventional Therapy on Primary Liver Cancer Patients and Its Effect on Serum AFP, VEGF, and GGT

Ying Jia,[1] Yufei Xing,[2] and Meitian Yang[2]

[1]*Department of Laboratory, Tianjin Jianhua Hospital, Tianjin 300122, China*
[2]*Department of Laboratory, The Second People' Hospital of Dongying, Dongying 257335, China*

Correspondence should be addressed to Meitian Yang; weiqian9729176690@163.com

Received 1 July 2021; Accepted 30 July 2021; Published 11 August 2021

Academic Editor: Muhammad Wasim Khan

Objective. To explore the efficacy of sorafenib combined with interventional therapy on primary liver cancer (PLC) patients and its effect on serum AFP, VEGF, and GGT. *Methods*. 120 PLC patients admitted to our hospital from January 2016 to January 2020 were selected as the research object and divided into group A and group B according to the admission order, with 60 cases each. Interventional therapy was performed to both groups, and sorafenib was given to group A additionally to compare their treatment effect, survival, adverse reaction rate (ARR), and serum AFP, VEGF, and GGT levels. *Results*. After treatment, group A obtained significantly higher objective remission rate (ORR) and disease control rate (DCR) ($p < 0.05$), higher one-year survival rate and two-year survival rate ($p < 0.05$), lower ARR of skin reactions, gastrointestinal reactions, hepatorenal reactions, and hyperbilirubinemia ($p < 0.05$), and lower serum AFP, VEGF, and GGT levels ($p < 0.001$). *Conclusion*. The combination of sorafenib and interventional therapy can inhibit the growth and migration of PLC, improve the immune function, prolong the survival period of patients, and lower ARR, so it should be promoted in practice.

1. Introduction

Primary liver cancer (PLC) is one of the most common malignant tumors in the clinic, and its lethality rate ranks the third place in all malignant tumors after lung cancer and gastric cancer with more than a million patients dying each year due to the disease. PLC is characterized by insidious onset and slow tumor growth, so most patients have missed the optimal surgical time when being diagnosed and can no longer receive radical treatment [1–3]. For PLC patients in advanced or middle advanced stages, local nonsurgical treatment options are the preferred measures to control the further spread of cancer cells, and interventional treatment is the most commonly used in the clinic, which is able to block the blood supply to the hepatic artery, make the cancer cells ischemic and necrotic, and then extend the survival of patients [4–7]. But recent studies have revealed that blocking the blood supply would cause residual cancer cells to release the hypoxia inducible factor and elevate the VEGF expression level, and the state of hypoxia and ischemia would accelerate the frequency of neovascularization, greatly improving the chance of PLC recurrence and affecting the long-term prognosis of patients [3, 8, 9]. In order to improve the application effect of interventional treatment, other target therapeutic measures should be adopted at the same time. Sorafenib, a novel multimolecular targeted therapeutic drug, is currently available in China, which can reduce VEGF expression, regulate the Mcl-1 protein level, and then inhibit tumor growth. In addition, some studies have shown that sorafenib can reverse the immunosuppression of hepatocellular carcinoma and improve the immunosenescence condition of patients [10], with a more comprehensive effect.

At present, there have been studies combining interventional treatment with sorafenib in academia, but mostly focusing on the survival rate of patients with few explorations on other aspects. This study aimed to explore the

enhancement of sorafenib on the efficacy of interventional treatment comprehensively, with the results reported as follows.

2. Materials and Methods

2.1. General Information. 120 PLC patients admitted to The Second People's Hospital of Dongying from January 2016 to January 2020 were selected as the research object and divided into group A and group B according to the admission order, with 60 cases each and no statistical difference in their general information ($p > 0.05$), as given in Table 1. The study was approved by the Ethics Committee of The Second People's Hospital of Dongying.

2.2. Inclusion Criteria. The inclusion criteria of the study were as follows. (1) The patients or their family members fully understood the study process and signed the informed consent; (2) the patients were diagnosed with PLC by clinical and pathological examinations and met the diagnose criteria in the Primary Liver Cancer Diagnose and Treatment Standard (2011 Ver.) [11]; (3) the expected survival time of the patients was over 3 months, and their clinical materials were complete; (4) the patients were at least 18 years old; (5) the liver function class of the patients was A or B [12]; (6) the Karnofsky (KPS) scores of the patients were over 60 points [13]; (7) the follow-up visit was acceptable to the patients; and (8) the patients did not meet the surgical indication and were required to undergo interventional treatment [14].

2.3. Exclusion Criteria. The exclusion criteria for the patients of the study were as follows. (1) Presence of mental problems or inability to communicate with others; (2) suffering from other organic diseases, coagulation disorders, or second primary tumor; (3) allergy to the drugs involved in the study; (4) in pregnancy or lactation; (5) presence of alimentary tract hemorrhage; and (6) suffering from inferior vena cava thrombus.

2.4. Methods. Both groups of patients received interventional therapy, and sorafenib was given to group A additionally, with the following specific steps. (1) Intervention therapy: after routine skin preparation and disinfection, the patients received local anesthesia. The 5-FRH catheter was inserted to the superior mesenteric artery, common hepatic artery, and proper hepatic artery for visualization, and then, the blood supply artery puncture targeted at primary lesions was conducted according to the lesion condition of the patients, and the ultrasmooth guide wire was used to fix the catheter; then, the mixture of 55 mg/m^2 of oxaliplatin (manufactured: Harbin Pharmaceutical Group Bioengineering Co., Ltd.; NMPA Approval No. H20133094), 40 mg/m^2 of hydroxyacetophenone (manufactured: Zhejiang Kancheer Pharmaceutical Co., Ltd.; NMPA Approval No. H42021857), 40 mg/m2 of epirubicin (manufactured: Jiangsu Hengrui Medicine Co., Ltd.; NMPA Approval No. H20020542), and ultraliquid iodized oil was administered once every month for 12 weeks. (2) Sorafenib treatment: the patients orally took 0.5 g of sorafenib (manufactured: Jiangxi Shanxiang Pharmaceutical Co., Ltd.; NMPA Approval No. H20203397) twice every day with warm water. A course lasted for two weeks, and after 1 course, administration was stopped for 2 weeks before entering into a new one. The entire treatment lasted for 12 weeks.

Patients in both groups were followed up for 24 months.

2.5. Observation Criteria

(1) Treatment effect: according to the RECIST (Response Evaluation Criteria in Solid Tumors) of the WHO, patients' conditions were classified as complete response (CR, disappearance of all lesions, no new lesions, and tumor markers returned to normal for a month), partial response (PR, ≥30% decrease of SLD (the sum of the longest diameters) for a month), stable disease (SD, <30% decrease of SLD or <20% increase of SLD), and progressive disease (PD, ≥20% increase of SLD, or new lesions). The objective remission rate (ORR) = CR + PR and the disease control rate (DCR) = CR + PR + SD were used to compare the treatment effect [15].

(2) Survival: the one-year survival rate and two-year condition rate of patients were compared between the two groups.

(3) Adverse reaction rate (ARR): the adverse reactions included skin reactions, gastrointestinal reactions, hepatorenal reactions, rash, fatigue and drowsiness, and hyperbilirubinemia, and the numbers of patients with adverse reactions were counted.

(4) Serum AFP, VEGF, and GGT levels: 5 ml of fasting elbow vein blood was extracted from the patients before treatment and at the 4th week and 12th week of treatment to detect their AFP, VEGF, and GGT levels with the ELISA assay (Beijing Kewei Clinical Diagnostic Reagent Inc.; NMPA Approval No. S20060028).

2.6. Statistical Processing. In this study, the data processing software was SPSS20.0, the picture drawing software was GraphPad Prism 7 (GraphPad Software, San Diego, USA), items included were enumeration data and measurement data, methods used were the X^2 test and t-test, and differences were considered statistically significant at $p < 0.05$.

3. Results

3.1. Comparison of the Patients' Treatment Effect. Group A obtained significantly higher ORR and DCR than group B ($p < 0.05$), as given in Table 2.

3.2. Comparison of Patients' Survival. Compared with group B, group A obtained significantly higher one-year survival rate (95.0% (57/60) vs. 68.3% (41/60), $p < 0.05$) and two-year survival rate (80.0% (48/60) vs. 60.0% (36/60), $p < 0.05$), as shown in Figure 1.

Table 1: Comparison of patients' general information.

Group	Group A ($n = 60$)	Group B ($n = 60$)	X^2/t	P
Gender				
Male	52	50	0.261	0.609
Female	8	10		
Age (years)				
Range	34–76	35–76		
Mean age	46.32 ± 5.21	46.98 ± 5.25	0.691	0.491
Liver function class				
A	48	47	0.051	0.822
B	12	13		
Hepatitis type				
Hepatitis C	10	12	0.223	0.637
Hepatitis B	50	48		
Complication				
Ascites	30	32	0.134	0.715
Portal vein tumor thrombus	10	9	0.063	0.803
Cirrhosis	42	40	0.154	0.695
TNM staging				
II	24	25	0.035	0.853
III	26	25	0.034	0.853
IV	10	10	0.000	1.000
Clinical type				
Diffused	10	12	0.223	0.637
Nodal	20	21	0.037	0.847
Massive	30	27	0.301	0.583
Maximum diameter of tumor (mm)				
Range	50–140	48–142		
Mean diameter	85.65 ± 20.65	86.98 ± 20.66	0.353	0.725
ECOG score*				
0 point	35	36	0.035	0.853
1 point	25	24		
Educational degree				
Senior high school and below	22	21	0.036	0.849
College and above	38	39		

*The physical health and therapy resistance of patients.

Table 2: Comparison of patients' overall efficacy (n (%)).

Group	CR	PR	SD	PD	ORR	DCR
Group A	24 (40.0)	30 (50.0)	2 (3.3)	4 (6.7)	54 (90.0)	56 (93.3)
Group B	18 (30.0)	20 (33.3)	10 (16.7)	12 (20.0)	38 (63.3)	48 (80.0)
X^2	1.319	3.429	5.926	4.615	11.926	4.615
P	0.251	0.064	0.015	0.032	0.001	0.032

3.3. Comparison of Patients' ARR. The ARRs of skin reactions, gastrointestinal reactions, hepatorenal reactions, and hyperbilirubinemia of group A were significantly lower than those of group B ($p < 0.05$), as shown in Figure 2.

No statistical differences were shown in the ARRs of rash and fatigue and drowsiness (9 vs. 10, 14 vs. 15, $p > 0.05$), and the ARRs of skin reactions, gastrointestinal reactions, hepatorenal reactions, and hyperbilirubinemia of group A were significantly lower than those of group B (5 vs. 15, 6 vs. 18, 6 vs. 15, 2 vs. 10, $p < 0.05$).

3.4. Comparison of Patients' Serum AFP, VEGF, and GGT Levels. The treated serum AFP, VEGF, and GGT levels of group A were significantly lower than those of group B ($p < 0.001$), as shown in Figure 3.

Figure 3(a) shows the serum AFP level. No statistical differences are shown in the serum AFP levels between the two groups before treatment (321.65 ± 75.26 vs. 322.69 ± 74.98, $p > 0.05$); at 4th week and 12th week of treatment, group A obtained significantly lower serum AFP levels than group B (180.65 ± 45.98 vs. 225.99 ± 55.98 and 88.95 ± 22.62 vs. 140.95 ± 26.98, $p < 0.001$).

Figure 3(b) shows the serum VEGF level. No statistical differences are shown in the serum VEGF levels between the two groups before treatment (442.56 ± 60.89 vs. 445.66 ± 61.55, $p > 0.05$); at 4th week and 12th week of treatment, group A obtained significantly lower serum VEGF levels than group B (299.65 ± 46.98 vs. 350.98 ± 47.99 and 199.98 ± 35.87 vs. 264.48 ± 36.98, $p < 0.001$).

Figure 3(c) shows the serum GGT level. No statistical differences are shown in the serum GGT levels between the

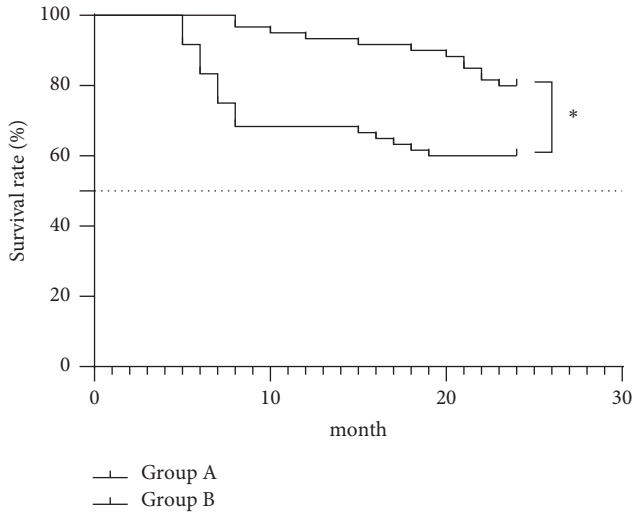

Figure 1: Comparison of patients' survival. The horizontal axis indicates the month, and the vertical axis indicates the survival rate (%). $^{*}P < 0.05$.

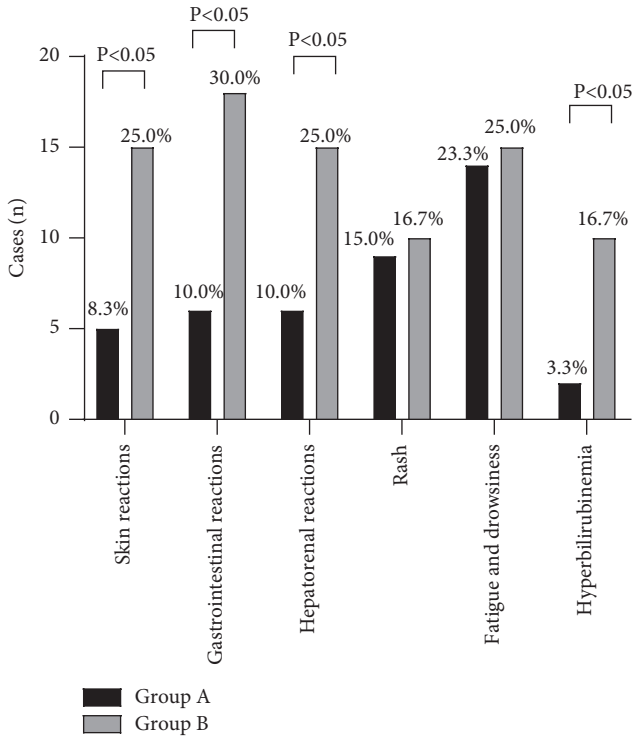

Figure 2: Comparison of patients' ARR (n (%)). The horizontal axis from left to right indicates the skin reactions, gastrointestinal reactions, hepatorenal reactions, rash, fatigue and drowsiness, and hyperbilirubinemia, and the vertical axis indicates the cases (n); the black areas indicate group A and the gray areas indicate group B.

two groups before treatment (178.98 ± 31.25 vs. 180.56 ± 32.65, $p > 0.05$); at 4^{th} week and 12^{th} week of treatment, group A obtained significantly lower serum GGT levels than group B (95.41 ± 24.56 vs. 126.98 ± 30.11 and 80.54 ± 12.10 vs. 110.98 ± 14.65, $p < 0.001$).

4. Discussion

PLC has an insidious onset, and the patients who are diagnosed with PLC are mostly in the middle and late stages of the disease, so they can only be treated with local nonsurgical modalities to prolong survival rather than radical surgery. 90% of PLCs are hepatocellular carcinomas (HCC), and the blood supply of HCC is mainly from the hepatic artery, and only a small amount is from the portal vein; in contrast to the blood supply ratio of normal liver tissue, the interventional therapy can target the blocking of the hepatic artery supply, so that the tumor tissue loses its blood supply source without affecting normal liver tissue, which is the preferred nonsurgical treatment option for patients [16–18]. Notably, interventional therapy, although it can substantially prolong the survival time of patients, cannot eliminate all cancer cells, and residual cells in hypoxic and ischemic conditions elevate the expression of the hypoxia inducible factor, which can increase VEGF transcription and then accelerate the frequency of neoangiogenesis, so that patients are prone to recurrence and metastasis of liver cancer. Therefore, combining other target therapeutic measures with the interventional therapy to optimize the long-term outcome is the key to lower the mortality in PLC patients [19].

Molecular targeted therapy is an important way to inhibit the growth of cancer cells, which can act in the links of cancer cell survival, growth, or neoangiogenesis with the toxicity significantly lower than chemotherapy, thus playing a specific antitumor role and being able to combine with different interventional therapies. Sorafenib, a novel molecular targeted therapeutic agent, can block the signal pathway of receptor tyrosine kinase, reduce VEGF activity in the hepatic artery, slow down the neoangiogenesis for oxygen and blood supply, and thus inhibit cancer cell metastasis [20, 21], so the treated VEGF level of patients in group A who received both treatment modalities was significantly lower than that in group B ($p < 0.001$), indicating a reduced migration rate of the cancer tissue.

In addition to receptor tyrosine kinase, there are several other receptors for sorafenib, which can suppress multiple protein expression levels of cell proliferation through other pathways, alleviate cytotoxicity, and accelerate the repair process of liver function. In this study, GGT was selected as an indicator of liver function, which mostly presented in the human liver and was able to monitor hepatobiliary disease. The GGT level in PLC patients can be over dozens of times higher than the normal person, and the decrease of GGT directly indicates the improvement of liver function in patients and indirectly suggests the reduction of liver cancer cells [22]. The result showed that group A achieved significantly lower GGT level than group B ($p < 0.001$), reflecting that recovery was seen in the patients' liver function and the likelihood of experiencing liver toxic side effects decreased concomitantly. Moreover, Pereira et al.' study confirmed that sorafenib could also induce the movement of lymphocytes to HCC tissues and reverse the immunosuppression of HCC [23], while Meizhen et al.' study showed that this drug could downregulate AFP expression and relieve immunosuppression in hepatitis B

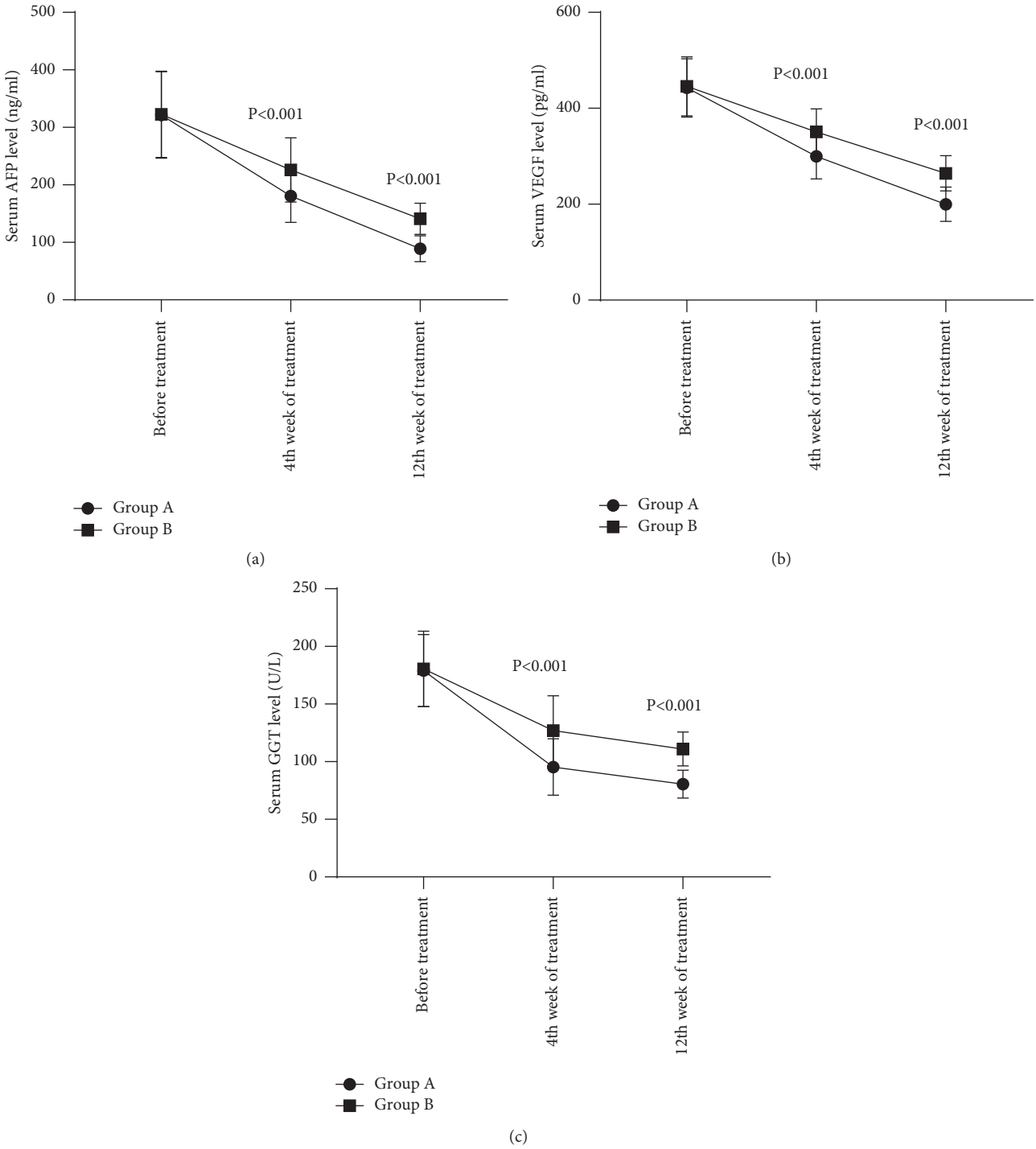

Figure 3: Comparison of patients' AFP, VEGF, and GGT levels ($\overline{x} \pm s$). The horizontal axis from left to right indicates before treatment, 4th week of treatment, and 12th week of treatment; the lines with dots indicate group A and the lines with blocks indicate group B.

patients [24]. AFP is a class of protein with immunosuppression that can reduce the proliferation rate of T lymphocytes and inhibit the activity of tumor cytokines. This study showed that AFP levels after treatment in both groups were reduced because the intervention could accelerate the frequency of cancer cell necrosis and scavenge immunosuppressive factors, thus improving the immune function of patients, and group A obtained obviously lower AFP levels than group B ($p < 0.001$), confirming that the combined therapy could achieve a better immune recovery effect and enhance the patient body resistance, which further lowered the ARR and comprehensively promoted the overall efficacy of PLC patients. Therefore, the ORR, DCR, and survival rate of group A were significantly higher than those

of group B ($p < 0.05$), indicating that the combined therapy obtained a remarkably better effect than intervention alone in terms of long-term outcomes.

To sum up, sorafenib combined with interventional therapy can inhibit PLC, enhance the body immunity, and prolong the survival time of patients, which should be promoted in practice.

Data Availability

The data used to support the findings of this study are available from the corresponding author upon reasonable request.

Conflicts of Interest

The authors declare that they have no conflicts of interest.

References

[1] R. González, M. D. L. Hernández, M. N. González et al., "Downregulation of thioredoxin-1-dependent CD95 S-nitrosation by Sorafenib reduces liver cancer," *Redox Biology*, vol. 34, 2020.

[2] F. Piscaglia and S. Ogasawara, "Patient selection for transarterial chemoembolization in hepatocellular carcinoma: importance of benefit/risk assessment," *Liver Cancer*, vol. 7, no. 1, pp. 104–119, 2018.

[3] D. E. Kaplan, R. Mehta, K. D'Addeo et al., "Sorafenib prescribed by gastroenterologists and hepatologists for hepatocellular carcinoma," *Medicine*, vol. 97, no. 4, 2018.

[4] P. Hsiao, K. C. Hsieh, Y. S. Chen et al., "Sorafenib with concurrent multiple-line therapies improves overall survival in advanced stage hepatocellular carcinoma," *Medicine*, vol. 98, no. 25, Article ID e16074, 2019.

[5] B. Foglia and M. Parola, "Of FACT complex and oxidative stress response: a KEAP1/NRF2-dependent novel mechanism sustaining hepatocellular carcinoma progression," *Gut*, vol. 69, no. 2, 2019.

[6] T. Duval, D. S. Troquier, O. de Souza Silva, N. Demartines, and O. Dormond, "Diclofenac potentiates sorafenib-based treatments of hepatocellular carcinoma by enhancing oxidative stress," *Cancers*, vol. 11, no. 10, p. 1453, 2019.

[7] S. H. Tella, A. Mahipal, A. Kommalapati, and Z. Jin, "Evaluating the safety and efficacy of nivolumab in patients with advanced hepatocellular carcinoma: evidence to date," *OncoTargets and Therapy*, vol. 12, pp. 10335–10342, 2019.

[8] J. P. Plastaras, K. T. Nead, and J. E. Meyer, *Primary Liver Tumors: Hepatocellular Carcinoma and Intrahepatic Cholangiocarcinoma*, 2018.

[9] D. Schizas, A. Mastoraki, E. Routsi et al., "Combined hepatocellular-cholangiocarcinoma: an update on epidemiology, classification, diagnosis and management," *Hepatobiliary and Pancreatic Diseases International: HBPD INT*, vol. 19, no. 6, 2020.

[10] E. D. Mattia, E. Cecchin, M. Guardascione et al., "Pharmacogenetics of the systemic treatment in advanced hepatocellular carcinoma," *World Journal of Gastroenterology*, vol. 25, no. 29, pp. 3870–3896, 2019.

[11] V. Longo, O. Brunetti, A. Gnoni et al., "Emerging role of immune checkpoint inhibitors in hepatocellular carcinoma," *Medicina*, vol. 55, no. 10, 2019.

[12] L. Gailhouste, L. C. Liew, K. Yasukawa et al., "Differentiation therapy by epigenetic reconditioning exerts antitumor effects on liver cancer cells," *Molecular Therapy*, vol. 26, 2018.

[13] K. Ueshima, S. Ogasawara, M. Ikeda et al., "Hepatic arterial infusion chemotherapy versus sorafenib in patients with advanced hepatocellular carcinoma," *Liver Cancer*, vol. 9, no. 5, pp. 1–13, 2020.

[14] S. Yozo, N. Hideyuki, Y. Taku et al., "Multicenter phase II clinical trial of sorafenib combined with transarterial chemoembolization for advanced stage hepatocellular carcinomas (barcelona clinic liver cancer stage C): STAB study," *Journal of Vascular and Interventional Radiology*, vol. 29, 2018.

[15] B. Ren, W. Wang, J. Shen et al., "Transarterial chemoembolization (TACE) combined with sorafenib versus TACE alone for unresectable hepatocellular carcinoma: a propensity score matching study," *Journal of Cancer*, vol. 10, 2019.

[16] O. Abdel-Rahman, "Impact of baseline characteristics on outcomes of advanced HCC patients treated with sorafenib: a secondary analysis of a phase III study," *Journal of Cancer Research and Clinical Oncology*, vol. 38, no. 2, pp. 1–8, 2018.

[17] S. Llerena, N. García-Díaz, S. Curiel-Olmo et al., "Applied diagnostics in liver cancer. Efficient combinations of sorafenib with targeted inhibitors blocking AKT/mTOR," *Oncotarget*, vol. 9, 2018.

[18] S. Caruso, A. L. Calatayud, J. Pilet et al., "Analysis of liver cancer cell lines identifies agents with likely efficacy against hepatocellular carcinoma and markers of response," *Gastroenterology*, vol. 157, no. 3, 2019.

[19] F. Piñero, S. Marciano, N. Fernández et al., "Intermediate-advanced hepatocellular carcinoma in Argentina: treatment and survival analysis," *World Journal of Gastroenterology*, vol. 25, no. 27, pp. 3607–3618, 2019.

[20] S. Lee, M. Loecher, and R. Iyer, "Immunomodulation in hepatocellular cancer," *Journal of Gastrointestinal Oncology*, vol. 9, no. 1, pp. 208–219, 2018.

[21] L. Goyal, Z. Hui, T. A. Abrams et al., "A phase II and biomarker study of sorafenib combined with FOLFOX in patients with advanced hepatocellular carcinoma (HCC)," *Clinical Cancer Research*, vol. 25, no. 1, 2018.

[22] A. Mori, A. Arimoto, Y. Hamaguchi, M. Kajiwara, A. Nakajima, and S. Kanaya, "Risk factors and outcome of portal vein thrombosis after laparoscopic and open hepatectomy for primary liver cancer: a single-center experience," *World Journal of Surgery*, vol. 44, no. 9, pp. 3093–3099, 2020.

[23] S. Pereira, L. Rodrigues, D. Castven et al., "Dual role of transforming growth factor Beta1&2 during tumor promotion and metastasis in primary liver cancer," *Zeitschrift für Gastroenterologie*, vol. 58, no. 1, 2020.

[24] L. Meizhen, Z. Rui and S. Min, Antineoplastic effects of sorafenib on primary liver cancer: a systematic review and meta-analysis," *International Journal of Clinical and Experimental Pathology*, vol. 12, no. 7, pp. 2389–2397, 2019.

Hindawi
Journal of Oncology
Volume 2021, Article ID 5046981, 8 pages
https://doi.org/10.1155/2021/5046981

Research Article

Downregulated KIF3B Induced by miR-605-3p Inhibits the Progression of Colon Cancer via Inactivating Wnt/β-Catenin

Qilong Wang,[1] Xiaomin Hao,[2] Gang Xu,[3] and Tiesheng Lv[1]

[1]*Department of General Surgery, The Third Affiliated Hospital of Xi'an Medical University, Xi'an 710068, Shaanxi Province, China*
[2]*Department of Internal Medicine, Shaanxi Province Tuberculosis Hospital, Xi'an 710068, Shaanxi Province, China*
[3]*Department of Oncology Surgery, The First Affiliated Hospital of Xi'an Jiaotong University, Xi'an 710068, Shaanxi Province, China*

Correspondence should be addressed to Tiesheng Lv; zipazhif@163.com

Received 10 June 2021; Accepted 4 August 2021; Published 11 August 2021

Academic Editor: Muhammad Wasim Khan

Colon cancer is a common malignant disease with high morbidity and mortality, and miRNA dysfunction has been confirmed as an important reason for cancer development. Several studies have verified miR-605-3p as a tumor inhibitor while its roles in colon cancer remain uncertain. In this study, the specimen of the patients and the cell lines of colon cancer were used to observe the expression of miR-605-3p, and the CCK-8, Transwell assay, and flow cytometry assay were used to observe the functions of miR-605-3p in colon cancer cells. The downstream factors of miR-605-3p were predicted by TargetScan and then were verified by dual-luciferase reporter assay. Moreover, western blot was used to investigate the effect of miR-605-3p on Wnt/β-catenin signal pathway. The result showed that miR-605-3p was extremely downregulated in the pathological tissues and tumor cells, and miR-605-3p could effectively induce the apoptosis and impede the proliferation and invasion of the tumor cells. It was found that KIF3B was a target of KIF3B; decreased KIF3B could reverse the effects of miR-605-3p on colon cancer. Besides, the inactivated Wnt/β-catenin pathway was also observed in colon cells when miR-605-3p was upregulated, and the phenomenon could be rescued by KIF3B upregulation. In conclusion, miR-605-3p could inactivate the Wnt/β-catenin pathway induced via promoting KIF3B expression.

1. Introduction

Colon cancer still remains one the most intractable diseases in the world which seriously threaten the health of human beings. Statistically, more than 1 million patients were diagnosed with colon cancer in 2018 [1, 2]. At present, drug, radiotherapy, and surgery interventions have been used to restrain the symptoms of the patients [1, 3]. However, the early symptoms of colon cancer usually do not express special natures, thus it may be mistaken as inflammation [4]. Patients' conditions have been become serious when they are first diagnosed as colon cancer [5]. Hence, even with current medical level, the prognosis and over-survival rate of the patients remain unsatisfactory. More studies are still necessary to delve the pathogenic mechanism of colon cancer. In the recent ten years, the pathological mechanism of colon cancer has received wide attention, which continually boosts the development of drug in colon cancer treatment [6, 7].

In the last decade, the functions of microRNAs in cellular activities have been confirmed by growing evidences, and the dysfunctions of miRNAs have also been observed in multiple cancers [8, 9]. miRNA dysfunction is major driving force behind the progression and recurrence [10]. Several studies have indicated that miRNA profiles in colon cancer tissues are different from normal tissues, and miRNA dysfunction has been proved as a major lead for tumor formation and development [11, 12]. Consequently, the drug therapies involved in miRNAs have been thought as prospective strategies for colon cancer treatment. miR-605-3p

serves as a tumor mimic in multiple tumors while its role in colon cancer remains unclear [13].

This study aimed to provide some new target and research points for cancer development by investigating the connection of miR-605-3p and colon cancer and revealing the regulation mechanism of miR-605-3p in the progression of colon cancer.

2. Material and Methods

2.1. Specimen Preparation. This study has been approved by the hospital Ethics Committee. The tumor tissues and matched adjacent health tissues donated by the patients were used in this study. All tissues were stored at −80°C. Prior consents of the patients and authorizations from hospitals were obtained.

2.2. Cell Culture and Transfection. Normal human colon cell lines including FHC and HEK-293T and human hepatocellular carcinoma cell lines including HCT116, CaCO-2, SW620, and RKO were used in this study. All cells were purchased from Hunan Fenghui Biotechnology Co., Ltd. (Changsha, China). All cells were cultured with Dulbecco's modified eagle medium (DMEM, Procell Life Science and Technology Co., Ltd., China) containing 10% fetal bovine serum (FBS, Thermo Fisher, USA) at 37°C and 5% CO_2. Subculture of the cells was performed when the cellular confluence was at 90%.

The cells were seeded into the 6-well plates, and the cell transfections were performed when the confluences of the cells were at 70%. The miR-605-3p mimics, miRNA negative control (miR-NC), pcDNA-KIF3B, and pcDNA-NC were synthesized by Generay Biotech Co., Ltd. (Shanghai, China). In short, 4 g of DNA, 100 pmol of RNA, or 10 μl Lipofectamine 2000 were respectively diluted and incubated with 250 μl serum-free medium for 5 min. The diluted DNA and RNA were respectively mixed with isometric diluted Lipofectamine 2000 (Thermo Fisher, Massachusetts, USA) and then were incubated at 25°C for 20 min. After that, 500 μl of mixtures were added in each well, and then the cells were cultured for 24 hours.

2.3. Real-Time Quantitative Reverse Transcription PCR (qRT-PCR). The miR-605-3p levels in the tissues and cell lines have been measured by qRT-PCR. The TRIzol reagent was used to perform the extractions of the total RNA in the tissues or HCC cell lines. The concentration of the total RNAs was measured by a spectrophotometer. 1 μg of RNA was used to transcribe as cDNA, and a PrimeScript® RT Reagent Kit performed the cDNA transcribe with random hexamers. The reaction systems (10 μL) of qRT-PCR were prepared according to the operational instruction of a KAPA qRT-PCR Kit (Sigma-Aldrich, Missouri, USA). U6 was used as the endogenous controls. The following conditions were used: denaturation at 95°C for 3 min, followed by amplification for 40 cycles at 95°C for 12 s and at 53°C for 40 s and 70°C for 30 s. The relative levels of miRNAs were calculated with the $2^{-(\Delta\Delta Ct)}$ method. The primers of miR-605-3p and U6 were synthesized and purified by RiboBio (Guangzhou, China). The primer sequences of miR-605-3p, KIF3B, and U6 are listed in Table 1.

2.4. Western Blot. The total proteins in the tissues and cell lines were extracted by RIPA buffer in an ice box, and the concentration of the extractions was measured by a BCA protein assay kit (Thermo Fisher, Massachusetts, USA). The extractions were mixed with quadruple SDS-PAGE sample loading buffer, and then the extractions were boiled at 100°C for 5 min. The proteins were transferred onto polyvinylidene fluoride (PVDF) membranes by wet transfer method. After that, the membranes were blocked with 5% fat-free milk at 4°C for 1 hour, and then the membranes were added with the related primary antibodies and incubated at 4°C overnight. The membranes were washed three times (15 min per time) by Tris buffered saline Tween (TBST), and then the membranes were incubated with second antibodies at 25°C for 1 hour. Finally, the membranes were washed three times (10 min per time) by TBST and added with ECL reagent (Thermo Fisher, USA) for observation under a chemiluminescence detection system. The antibodies purchased from Thermo Fisher (Massachusetts, USA) were used as follows: anti-KIF3B (1 : 1000), anti-β-catenin (1 : 1000), anti-Wnt (1 : 1000), anticleaved caspase-3 (1 : 1000), and anti-β-actin (1 : 1000).

2.5. Transwell Assay. For the invasion assay, Matrigel was diluted with eight-times DMEM, and the diluted Matrigel was added into the upper chambers of Transwells. 5×10^4 cells with 200 μL serum-free DMEM were seed into the upper chambers, and 600 μL and DMEM containing 10% FBS were added into the cell in lower chambers. The cells were cultured for 24 hours. After that, the cell on the upper surfaces of the chambers were removed by cotton buds, and the migrated cells on the lower surface of the upper chamber were fixed by methanol for 10 min and then dried at 25°C. The cells were stained with 0.1% w/v crystal violet (Cat#G1062, Solarbio, Beijing, China) for 30 min and washed with tap water. The number of invaded cells was calculated and photographed under a Leica DMi8 microscope.

2.6. CCK-8 Assay. The cells (3×10^3) were seeded into 96-well plates and incubated for 24 hours. The transfections were added into the related wells for further incubation. After that, the viability of the cells at 0, 24, 48, and 72 hours was measured by CCK-8 Kit (Amyjet, Wuhan, China). In short, 10 μL of CCK-8 solution (Solarbio Biotechnology Co., Ltd., Shanghai, China) was added into each well, and then the cells were incubated at 25°C in dark for 4 hours. Finally, the absorbance value of each well was measured at 450 nm by a microplate reader (Molecular Devices, Shanghai, China).

2.7. Dual-Luciferase Reporter Gene Assay. The mutant or wild 3'-UTR sequences of FMNL2 were inserted into the pmirGLO luciferase reporter vectors (Yangjiang Bio Co.,

Table 1: Primer sequences of miR-605-3p, KIF3B, and U6.

Name of primers	Sequences
miR-605-3p-F	5'-AACGAGACGACGACAGAC-3'
miR-605-3p-R	5'-AGAAGGCACTATGAGATTTAGA-3'
KIF3B-F	5'- GATGTTAAGCTGGGGCAGGT-3'
KIF3B-R	5'-TTTGCCGTCCACTAGAGCAG-3'
U6-F	5'-CTCGCTTCGGCAGCACA-3'
U6-R	5'-AACGCTTCACGAATTTGCGT-3'

Ltd., China) to establish the FMNL2-mutant type (FMNL2-mut) and FMNL2-wild type (FMNL2-wt), respectively. FMNL2-mut and FMNL21-wt were respectively cotransfected with miR-466 mimics or miR-NC into HEK-293T cells. After that, the cells were incubated for 48 hours. Finally, the binding effect of miR-466 and FMNL2 was observed by a dual-luciferase reporter assay system.

2.8. Flow Cytometry Assay. HCT116 cells were harvested by trypsinase (0.25%, EDTA-free). The harvested cells were washed by 3 mL of ice phosphate-buffered saline (PBS) for once and then were fixed by alcohol. After that, 1×10^6 of the cells were suspended by 100 μl incubation buffer. 5 μl of ice Annexin V-FITC and 5 μL of propidium iodide (PI 20 μg/ml) were added into the cells, and then the cells were incubated in dark for 15 min. Finally, the apoptosis level of the cells was instantly observed by a flow cytometry equipment (BD Biosciences, State of New Jersey, USA).

2.9. Statistical Analysis. All experiments were performed at least 3 times, independently. The data were analyzed by SPSS 20.0, and the figures were charted by GraphPad Prism 8.0. The difference of the data was tested with chi-squared test or ANOVA with Tukey's post hoc test. $P < 0.05$ means the difference of two groups is significant.

3. Results

3.1. miR-605-3p Was Extremely Downregulated in the Pathological Tissues and Tumor Cell Lines. The specimens of paracancerous and tumor tissues were used to confirm the difference in miR-605-3p levels. In the experiments, miR-605-3p was observably downregulated in the pathological samples compared with the normal parts (Figure 1(a); $P < 0.01$). Moreover, the decreased miR-605-3p was also observed in the colon cancer cells including HCT116, CaCO-2, SW620, and RKO compared with FHC cells (Figure 1(b); $P < 0.01$). Those observations suggested that miR-605-3p dysfunctions were related with the progression of colon cancer.

3.2. miR-605-3p Blocked the Progression of CaCO-2 Cells. For exploring the functions of the miR-605-3p on colon cancer development, the miR-605-3p level in HCT116 cells was downregulated by the specific mimics, and the phenotypic changes in the cell growth, invasion, and apoptosis were detected by CCK-8 assay, Transwell assay, and flow cytometry assay, respectively. The results uncovered that the HCT116 cells with reduced miR-605-3p expressed low viability and invasive ability and serious apoptosis level compared to the cells without the intervention of miR-605-3p mimics (Figure 2; $P < 0.01$). Those observations suggested that declined miR-605-3p could impede the growth and invasion of HCT116 cells.

3.3. KIF3B Was a Target of miR-605-3p and Was Significantly Downregulated in Pathological Tissues. Given the translation barriers of miRNAs on special mRNAs, the database, TargetScan, was used to search the downstream target of miR-605-3p. It was found that miR-605-3p could directly target the 3'-UTR of KIF3B. To further verify the prediction results, the luciferase vectors containing the wild type and mutant type in the 3'-UTR sequences of KIF3B were respectively cotransfected with miR-605-3p into HEK-293T cells to observe the effect of miR-605-3p on KIF3B (Figure 3(a); $P < 0.01$). In the results, miR-605-3p expressed visible effect on wt-KIF3B rather than that on mut-KIF3B. Moreover, the increased mRNA levels of KIF3B were also found in tumor tissues (Figure 3(b); $P < 0.01$).

3.4. KIF3B Upregulation Reversed the Effects of miR-605-3p on Phenotype of the Cells. To verify whether KIF3B involves in the regulation of miR-605-3p in colon cells, the miR-605-3p mimics and KIF3B were cotransfected into the cells to observe the phenotypic changes of the cells. In the results, the reduced viability of the cells induced by miR-605-3p downregulation was reversed by KIF3B, and the cells cotransfected with miR-605-3p mimics and KIF3B expressed high invasion ability compared with the cells only transfected with miR-605-3p mimics (Figures 4(a) and 4(c); $P < 0.01$). Besides, the high apoptosis level of the cells induced by miR-605-3p was rescued by KIF3B downregulation (Figure 4(b); $P < 0.01$). Those observations suggested that the regulation of miR-605-3p in colon cancer was related with KIF3B, respectively.

3.5. miR-605-3p Impeded the Progression of Colon Cancer via Activating Wnt/β-Catenin Pathway. To further delve the mechanism of miR-605-3p in colon cancer, the activity of Wnt/β-catenin pathway was observed by western blot. The results indicated that the expressions of Wnt and β-catenin were significantly inhibited when miR-605-3p level decreased, suggesting that the level of miR-605-3p was related with the activity of Wnt/β-catenin pathway (Figure 5; $P < 0.01$). However, compared with the cells singly transfected with miR-605-3p mimics, the inactivated Wnt/β-catenin pathway of the cells was reversed after cotransfected with KIF3B, suggesting that the tumor promotion effects of miR-605-3p were related with inactivation of Wnt/

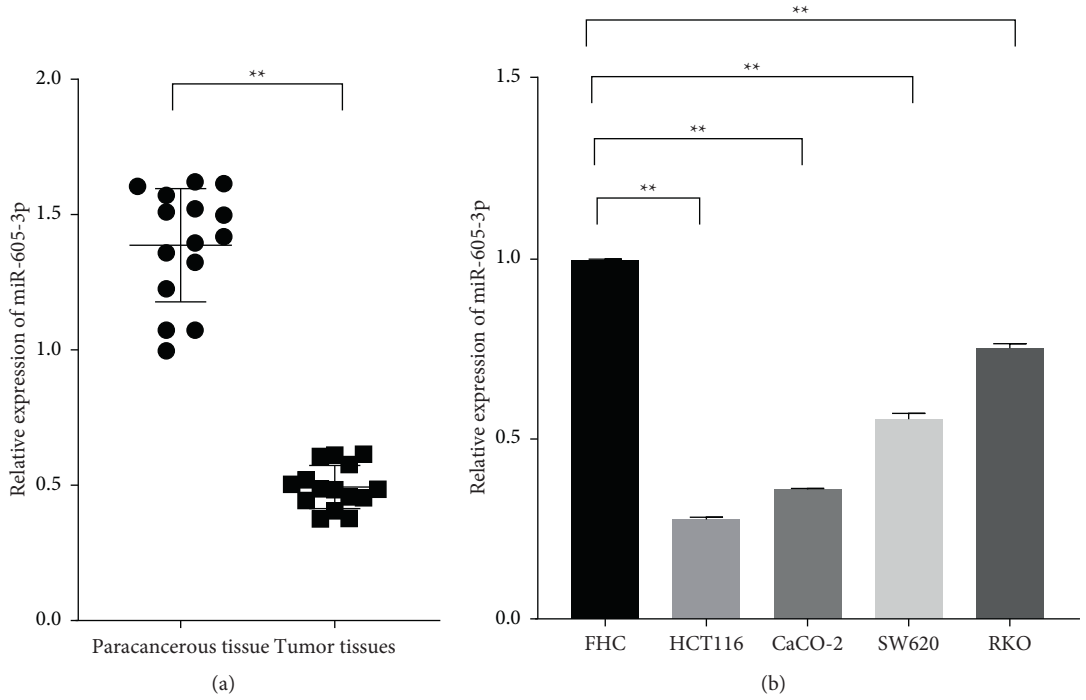

FIGURE 1: miR-605-3p was significantly downregulated in the colon cancer tissues and cell lines. (a) The relative expression levels of miR-605-3p in the paracancerous and tumor tissues of the patients with colon cancer were measured by qRT-PCR. (b) The relative expression levels of miR-605-3p in the nonneoplastic colon cells (FHC) and colon cancer cells (HCT116, CaCO-2, SW620, and RKO) were measured by qRT-PCR. $^{*}P < 0.05$ and $^{**}P < 0.01$.

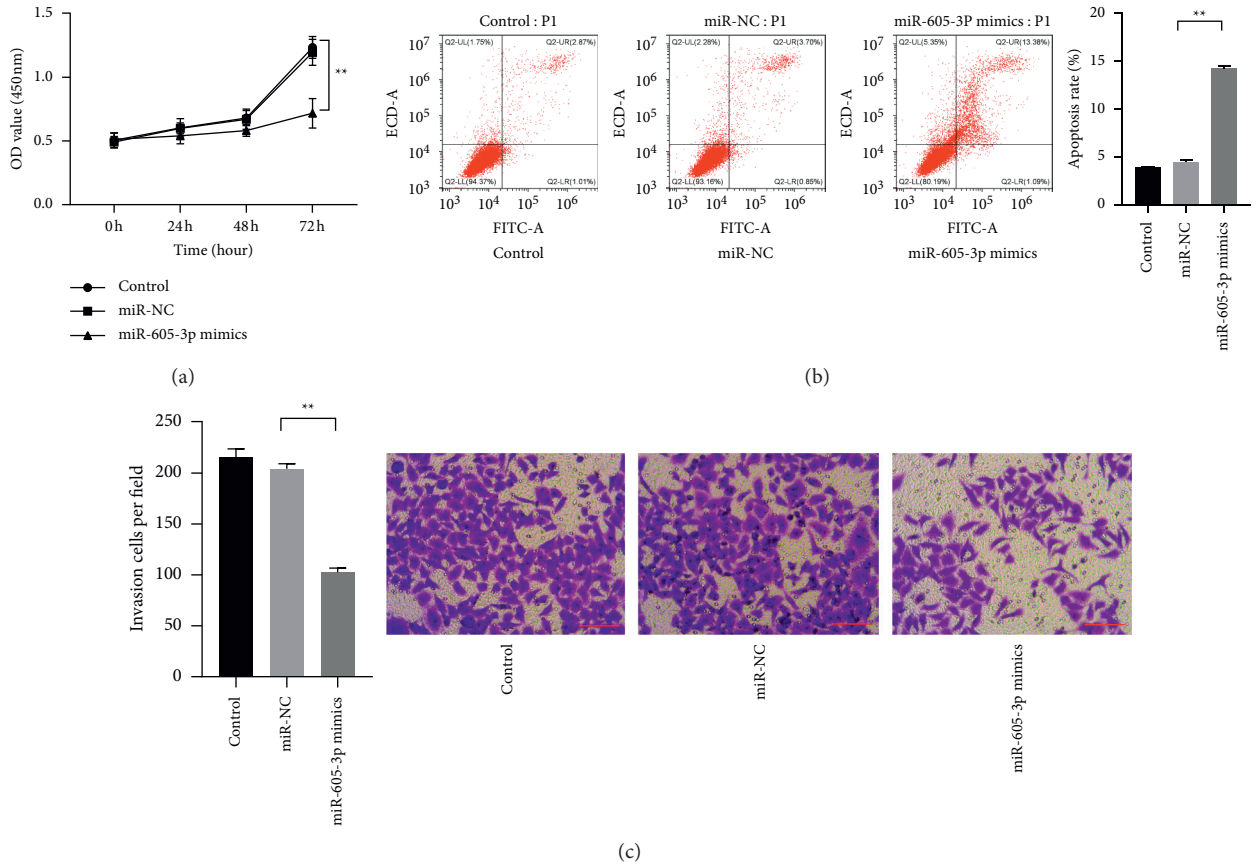

FIGURE 2: miR-605-3p inhibited the progression of colon cancer. (a) The effect of miR-605-3p on the viability of HCT116 cells was observed by CCK-8 assay. (b) The effect of miR-605-3p on the apoptosis of HCT116 cells was observed by flow cytometry assay. (c) The effect of miR-605-3p on the invasive ability of HCT116 cells was observed by Transwell assay (scale bar = 50 μm). $^{*}P < 0.05$ and $^{**}P < 0.01$.

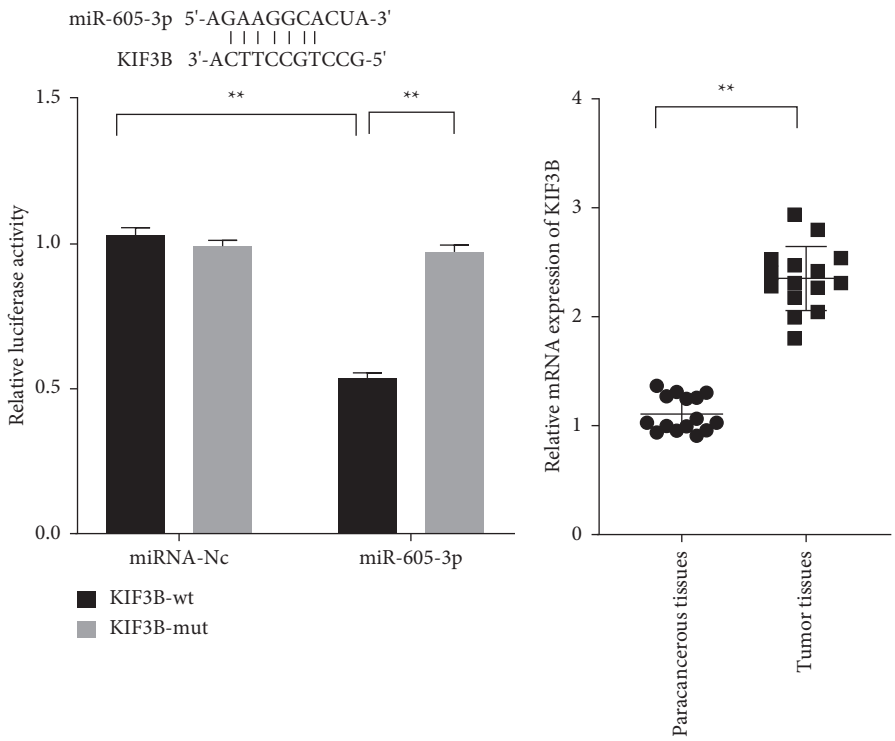

(a) (b)

FIGURE 3: KIF3B was a target of miR-605-3p, and KIF3B was significantly upregulated in the paracancerous and tumor tissues of colon cancer. (a) The binding effect of miR-605-3p and KIF3B was measured by dual-luciferase reporter assay. (b) The relative mRNA levels of KIF3B in the specimens were measured by qRT-PCR. $^{*}P < 0.05$ and $^{**}P < 0.01$.

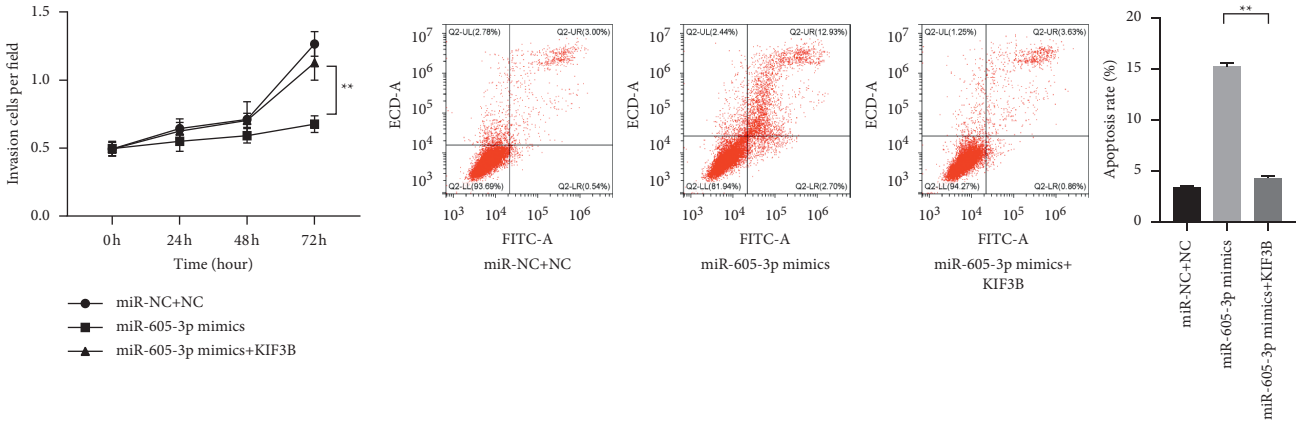

(a) (b)

FIGURE 4: Continued.

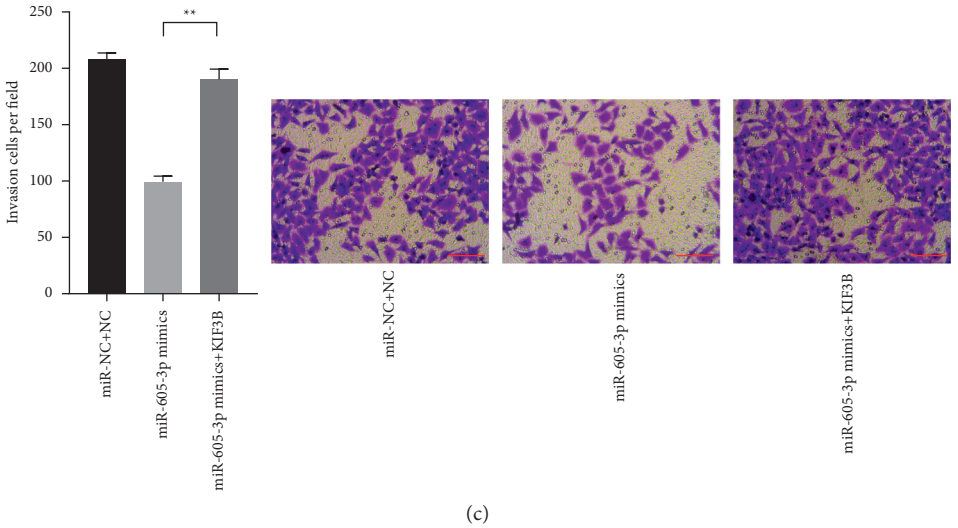

(c)

Figure 4: KIF3B could reverse the effects of miR-605-3p on the phenotype of colon cancer cells. (a) The effect of KIF3B on the viability of HCT116 cells with high miR-605-3p level was observed by CCK-8 assay. (b) The effect of KIF3B on the apoptosis of HCT116 cells with high miR-605-3p level was observed by flow cytometry assay. (c) The effect of KIF3B on the invasion of HCT116 cells with high miR-605-3p level was observed by Transwell assay (scale bar = 50 μm). $^{*}P < 0.05$ and $^{**}P < 0.01$.

β-catenin pathway induced by KIF3B downregulation (Figure 5; $P < 0.01$).

4. Discussion

Despite recent advances in diagnosis and treatments, many patients with colon cancer still experience relapse and metastasis, primarily involving the liver, abdomen, and lung [14]. Colon cancer therefore remains an incurable disease. Previous researches have indicated that increased malignancy of CSCs serves as important reason for cancer development and resistance [15]. This study investigated the connection of miR-605-3p and colon cancer, revealed the downstream target of miR-605-3p on the progression of CSCs, and delved the regulation mechanism of miR-605-3p on colon cancer.

The profiles of miRNAs express visible difference in tumor and normal tissues of the patients, and regulation on the expression of special miRNAs has been thought as a feasible therapeutic strategy for cancer [16, 17]. For instance, one study has found that miR-34a was significantly overexpressed in colon cancer cell, and downregulated miR-34a could promote the metastasis for the cells and poor prognosis for the patients, which is analogical with the observation from the previous study [18]. This study determined that miR-605-3p was significantly downregulated in the colon cancer tissues and cell lines. The recent studies have confirmed that miR-605-3p may play a tumor support role in the diverse human tumors and involves in the malignant growth, resistance, and invasive ability [19]. In this study, it was observed that miR-605-3p inhibition could extremely inhibit the proliferation, viability, and invasive ability of CSCs.

Several studies have showed that miRNAs exert the regulation functions in cells involved in the expression of some key proteins [20]. Xi et al. have indicated that miR-204-3p upregulation counts against the growth and invasion of the colon cancer, and those effects are related with the downregulation of HMGA2 which is the downstream target of miR-204-3p [21]. Considering the natures of miRNAs on transcription restraining of proteins via targeting the 3'-UTR of the related mRNAs, the downstream targets were searched by databases including TargetScan and miRDB, and it was found that KIF3B was a downstream target of miR-605-3p. KIF3B has been confirmed to be involved in the formation and development of multiple diseases including inflammations and acute injury [22, 23]. Recently, increasing studies have indicated that aberrant KIF3B involves in the progression of some tumors [24]. Song et al. have found that KIF3B was extremely upregulated in the tissues of pancreatic cancer and related with the pTNM stage of the patients [25]. Moreover, it has been also observed that the reduced KIF3B inhibited the viability and induced the apoptosis of colon cancer [26]. In this study, KIF3B was also determined as a key factor which could visibly reverse the effects of miR-605-3p on the phenotype of the colon cancer cells. Therefore, the present proofs suggest that miR-605-3p blocked the progression of colon cancer via targeting KIF3B.

The formation and development of cancers generally involve in the activity changes of multiple signal pathways. The changes in activities of pathways in cells such as PI3K/AKT, NF-κB, Hippo, and Wnt/β-catenin are inner force to impetus the formation and development of colon cancer [27]. The study has determined activated PI3K/AKT pathway induced by LINC00657 as a major cause leading the progression of colon cancer [28]. The related consideration has been given in the changes of the signal pathways in this study, and it was observed that the tumor cells expressed low activity of Wnt/β-catenin when miR-605-3p was upregulated. Moreover, KIF3B downregulation could reverse the phenomenon induced by miR-605-3p downregulation. The

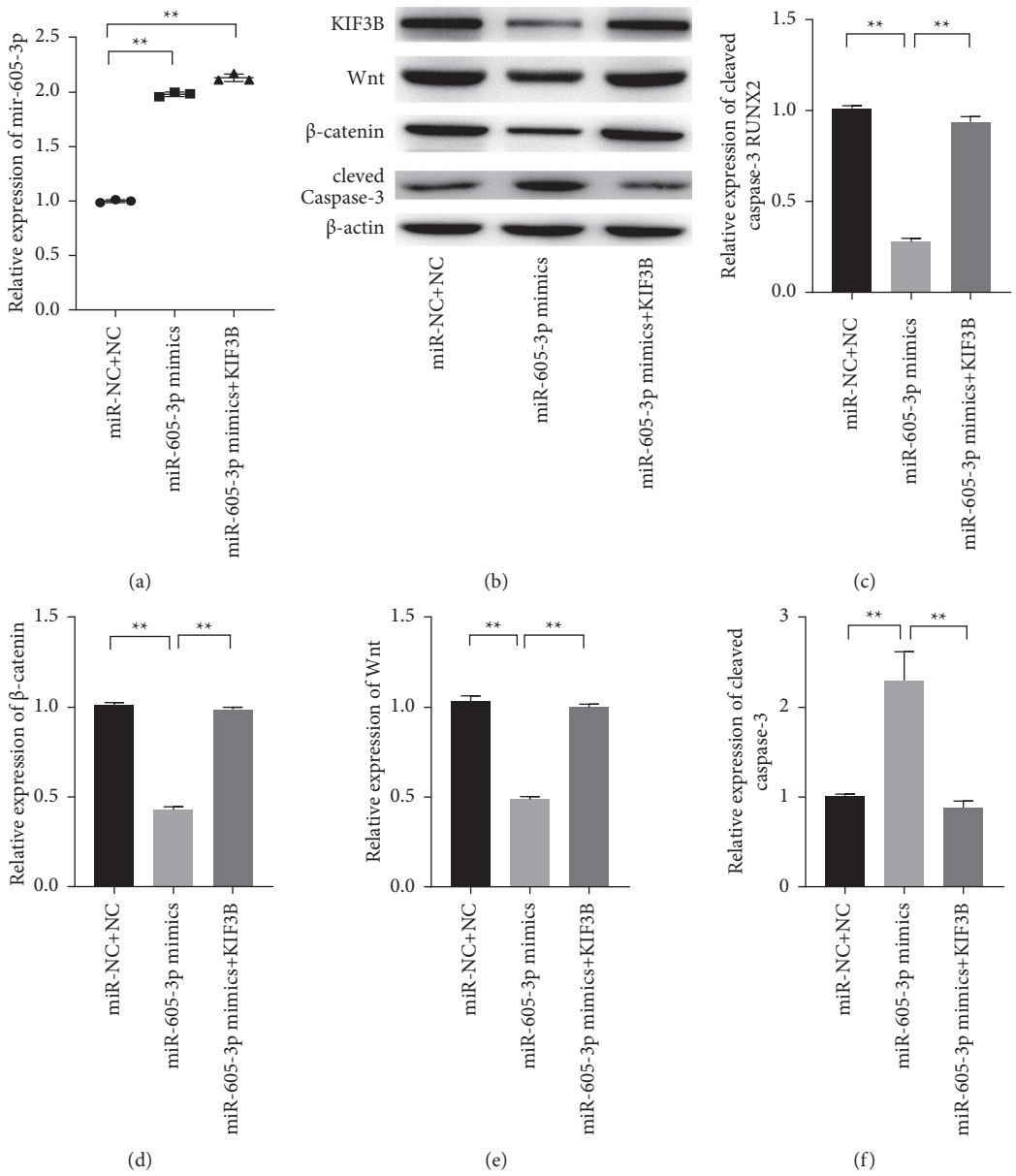

Figure 5: miR-605-3p inactivated the Wnt/β-catenin pathway via targeting KIF3B. (a) The relative expression level of miR-605-3p was measured by qRT-PCR. (b–f) The expression levels of KIF3B, Wnt, β-catenin, and cleaved caspase-3 were observed by western blot. $^{*}P < 0.05$ and $^{**}P < 0.01$.

study has indicated that the activation of Wnt/β-catenin mediated by KIF3B directly promote the growth, invasion, and epithelial-mesenchymal transition of breast cancer cells [29]. Hence, this study suggests that miR-605-3p serves as a tumor inhibitor in colon cancer via suppressing the activation of Wnt/β-catenin induced by KIF3B.

In this study, the evidence of miR-605-3p involving in the progression of colon cancer was provided, the downstream target of miR-605-3p was determined, and the regulation mechanism of miR-605-3p in colon cancer was revealed and elaborated. However, for further verifying the practical therapeutic effects of miR-605-3p on colon cancer, the oncogenicity of miR-605-3p should be validated by animal experiments.

Data Availability

The datasets used and/or analyzed during the present study are available from the corresponding author on reasonable request.

Conflicts of Interest

The authors declare that they have no conflicts of interest.

References

[1] Y. Zhao, X. Hu, X. Zuo, and M. Wang, "Chemopreventive effects of some popular phytochemicals on human colon cancer: a review," *Food & Function*, vol. 9, no. 9, pp. 4548–4568, 2018.

[2] X. Ji, Q. Peng, and M. Wang, "Anti-colon-cancer effects of polysaccharides: a mini-review of the mechanisms," *International Journal of Biological Macromolecules*, vol. 114, pp. 1127–1133, 2018.

[3] J. S. Souris, H. J. Zhang, U. Dougherty et al., "A novel mouse model of sporadic colon cancer induced by combination of conditional Apc genes and chemical carcinogen in the absence of Cre recombinase," *Carcinogenesis*, vol. 40, no. 11, pp. 1376–1386, 2019.

[4] V. R. M. Lombardi, I. Carrera, L. Corzo, and R. Cacabelos, "Role of bioactive lipofishins in prevention of inflammation and colon cancer," *Seminars in Cancer Biology*, vol. 56, pp. 175–184, 2019.

[5] Z. Baster, L. Li, S. Kukkurainen et al., "Cyanidin-3-glucoside binds to talin and modulates colon cancer cell adhesions and 3D growth," *The FASEB Journal*, vol. 34, no. 2, pp. 2227–2237, 2020.

[6] D. Hu, B. Zhang, M. Yu, W. Shi, and L. Zhang, "Identification of prognostic biomarkers and drug target prediction for colon cancer according to a competitive endogenous RNA network," *Molecular Medicine Reports*, vol. 22, no. 2, pp. 620–632, 2020.

[7] Y. Li, J. Wang, S. Zhong, J. Li, and W. Du, "Scutellarein inhibits the development of colon cancer via CDC4-mediated RAGE ubiquitination," *International Journal of Molecular Medicine*, vol. 45, no. 4, pp. 1059–1072, 2020.

[8] X. Lai, M. Eberhardt, U. Schmitz, and J. Vera, "Systems biology-based investigation of cooperating microRNAs as monotherapy or adjuvant therapy in cancer," *Nucleic Acids Research*, vol. 47, no. 15, pp. 7753–7766, 2019.

[9] W. H. Chen, G. F. Luo, Y. S. Sohn, R. Nechushtai, and I. Willner, "miRNA-specific unlocking of drug-loaded metal-organic framework nanoparticles: targeted cytotoxicity toward cancer cells," *Small*, vol. 15, no. 17, Article ID e1900935, 2019.

[10] M. Eckstein, V. Sailer, B. S. Nielsen et al., "Co-staining of microRNAs and their target proteins by miRNA in situ hybridization and immunohistofluorescence on prostate cancer tissue microarrays," *Laboratory Investigation*, vol. 99, no. 10, pp. 1527–1534, 2019.

[11] Q. Zhang, C. Zhang, J.-X. Ma, H. Ren, Y. Sun, and J.-Z. Xu, "Circular RNA PIP5K1A promotes colon cancer development through inhibiting miR-1273a," *World Journal of Gastroenterology*, vol. 25, no. 35, pp. 5300–5309, 2019.

[12] Z. He, J. Dang, A. Song, X. Cui, Z. Ma, and Z. Zhang, "NEAT1 promotes colon cancer progression through sponging miR-495-3p and activating CDK6 in vitro and in vivo," *Journal of Cellular Physiology*, vol. 234, no. 11, pp. 19582–19591, 2019.

[13] M. Z. Pan, Y. L. Song, and F. Gao, "miR-605-3p inhibits malignant progression of prostate cancer by up-regulating EZH2," *European Review for Medical and Pharmacological Sciences*, vol. 23, no. 20, pp. 8795–8805, 2019.

[14] W. Dai, Y. Li, S. Mo et al., "A robust gene signature for the prediction of early relapse in stage I-III colon cancer," *Molecular Oncology*, vol. 12, no. 4, pp. 463–475, 2018.

[15] S. Mo, W. Dai, W. Xiang et al., "Prognostic and predictive value of an autophagy-related signature for early relapse in stages I-III colon cancer," *Carcinogenesis*, vol. 40, no. 7, pp. 861–870, 2019.

[16] J. Xu, K. Liao, Z. Fu, and Z. Xiong, "A new method for early detection of pancreatic cancer biomarkers: detection of microRNAs by nanochannels," *Artificial Cells, Nanomedicine, and Biotechnology*, vol. 47, no. 1, pp. 2634–2640, 2019.

[17] G. Wilk and R. Braun, "Integrative analysis reveals disrupted pathways regulated by microRNAs in cancer," *Nucleic Acids Research*, vol. 46, no. 3, pp. 1089–1101, 2018.

[18] H. Luo, C. Xu, W. Le, B. Ge, and T. Wang, "lncRNA CASC11 promotes cancer cell proliferation in bladder cancer through miRNA-150," *Journal of Cellular Biochemistry*, vol. 120, no. 8, pp. 13487–13493, 2019.

[19] Y. Z. Su, M. F. Cui, J. Du, and B. Song, "LncRNA DCST1-AS1 regulated cell proliferation, migration, invasion and apoptosis in gastric cancer by targeting miR-605-3p," *European Review for Medical and Pharmacological Sciences*, vol. 24, no. 3, pp. 1158–1167, 2020.

[20] J. Y. Chen, L. F. Xu, H. L. Hu, Y. Q. Wen, D. Chen, and W. H. Liu, "MiRNA-215-5p alleviates the metastasis of prostate cancer by targeting PGK1," *European Review for Medical and Pharmacological Sciences*, vol. 24, no. 2, pp. 639–646, 2020.

[21] X. Xi, M. Teng, L. Zhang, L. Xia, J. Chen, and Z. Cui, "Retracted: MicroRNA-204-3p represses colon cancer cells proliferation, migration, and invasion by targeting HMGA2," *Journal of Cellular Physiology*, vol. 235, no. 2, pp. 1330–1338, 2020.

[22] W. Zhou, T. Yuan, Y. Gao et al., "IL-1β-induces NF-κB and upregulates microRNA-372 to inhibit spinal cord injury recovery," *Journal of Neurophysiology*, vol. 117, no. 6, pp. 2282–2291, 2017.

[23] M. Kaur, D. Panikkath, X. Yan et al., "Perianal Crohn's disease is associated with distal colonic disease, stricturing disease behavior, IBD-associated serologies and genetic variation in the JAK-STAT pathway," *Inflammatory Bowel Diseases*, vol. 22, no. 4, pp. 862–869, 2016.

[24] F. Z. Yao and D. G. Kong, "Identification of kinesin family member 3B (KIF3B) as a molecular target for gastric cancer," *The Kaohsiung Journal of Medical Sciences*, vol. 36, no. 7, pp. 515–522, 2020.

[25] J. Song, Y. Liu, T. Wang, B. Li, and S. Zhang, "miR-17-5p promotes cellular proliferation and invasiveness by targeting RUNX3 in gastric cancer," *Biomedicine & Pharmacotherapy*, vol. 128, Article ID 110246, 2020.

[26] C. Pan, J. Luo, and J. Zhang, "Computational identification of RNA-seq based miRNA-mediated prognostic modules in cancer," *IEEE Journal of Biomedical and Health Informatics*, vol. 24, no. 2, pp. 626–633, 2020.

[27] X. Y. Gong and A. L. Huang, "LEF-AS1 participates in occurrence of colorectal cancer through adsorbing miR-505 and promoting KIF3B expression," *European Review for Medical and Pharmacological Sciences*, vol. 23, no. 21, pp. 9362–9370, 2019.

[28] Y. Lei, Y. H. Wang, X. F. Wang, and J. Bai, "LINC00657 promotes the development of colon cancer by activating PI3K/AKT pathway," *European Review for Medical and Pharmacological Sciences*, vol. 22, no. 19, pp. 6315–6323, 2018.

[29] C. Wang, R. Zhang, X. Wang et al., "Silencing of KIF3B suppresses breast cancer progression by regulating EMT and wnt/β-catenin signaling," *Frontiers in Oncology*, vol. 10, Article ID 597464, 2021.

Hindawi
Journal of Oncology
Volume 2021, Article ID 5177140, 6 pages
https://doi.org/10.1155/2021/5177140

Research Article

Safety Analysis of Apatinib Combined with Chemotherapy in the Treatment of Advanced Gastric Carcinoma: A Randomised Controlled Trial

Min Yuan,[1] Zhaohui Wang,[2] Yibo Zhang,[3] Liying Chen,[1] Yuting Liu,[4] Cui Cui,[5] and Bo Sun[6]

[1]*Department of Nursing, Weifang People's Hospital, Weifang 261041, China*
[2]*Department of Liver Disease, Qingdao No. 6 People's Hospital, Qingdao 266033, China*
[3]*Department of Wound and Ostomy Outpatient, Weifang People's Hospital, Weifang 261041, China*
[4]*Department of Dentistry, Weifang People's Hospital, Weifang 261041, China*
[5]*Ward 2, Department of Neurology, Yidu Central Hospital of Weifang, Qingzhou 262500, China*
[6]*Department of Vascular Surgery, Weifang People's Hospital, Weifang 261041, China*

Correspondence should be addressed to Yibo Zhang; yituiciz@163.com

Received 1 July 2021; Accepted 31 July 2021; Published 10 August 2021

Academic Editor: Muhammad Wasim Khan

Objective. To study the safety of apatinib combined with chemotherapy in the treatment of advanced gastric carcinoma (GCA). *Methods*. 74 patients with advanced GCA treated in the oncology department of Weifang People's Hospital (January 2019–January 2020) were enrolled in this study and equally split into study group (SG) and reference group (RG) according to the odd and even admission numbers. RG underwent chemotherapy alone, while SG received apatinib combined with chemotherapy. The clinical indicators of serum matrix metalloproteinase 9 (MMP-9), serum interleukin-2 receptor (SIL-2R), and immune cell level were detected in the two groups before and after treatment to analyze the therapeutic effect of different treatment methods on patients with advanced gastric carcinoma. *Results*. No obvious differences in gender ratio, average age, average BMI, pathological staging, pathological types, organ metastasis types, and residence were observed between the two groups ($P > 0.05$). The short-term follow-up results showed that the disease control rate (DCR) in SG was markedly higher compared with RG ($P < 0.05$). The MMP-9 and SIL-2R levels in both groups after treatment decreased ($P < 0.05$), and the levels in SG after treatment were notably lower compared with RG ($P < 0.001$). Compared with RG, $CD3^+$, $CD4^+$, and $CD4^+/CD8^+$ levels in SG after treatment were notably higher ($P < 0.001$), while the $CD8^+$ level was notably lower ($P < 0.001$). The median progression-free survival (MPFS) and overall survival (OS) in SG were markedly higher compared with RG ($P < 0.001$). The GQOLI-74 scores in both groups after treatment increased ($P < 0.001$), and the GQOLI-74 score in SG after treatment was markedly higher compared with RG ($P < 0.001$). The total incidence of adverse reactions was lower in SG than in RG ($P < 0.05$). *Conclusion*. Apatinib combined with chemotherapy is superior to chemotherapy alone in effectively improving treatment outcomes in patients with advanced GCA.

1. Introduction

Gastric carcinoma (GCA) is a common tumor disease in gastroenterology. China is a country with a high incidence of GCA, and about 350,000 people die from GCA every year. Therefore, GCA has become the main cancer that endangers human life and health [1–3]. In recent years, due to unreasonable diet structure, high working pressure, chronic atrophic gastritis, and other reasons, GCA patients tend to be younger. Since the early clinical symptoms of GCA are not obvious, most patients have missed the best treatment opportunity. Chemotherapy is the main treatment for prolonging the survival period of patients at present, and there is no standard scheme for chemotherapy. Oxaliplatin is widely applied to slow down the disease progression and relieve the clinical symptoms, with good short-term curative

effect and prognosis [4–7]. However, chemotherapy can not only cause strong side effects and increase the pain of treatment but also increase the drug resistance of tumor cells, resulting in poor efficacy. Studies have found that apatinib is a highly selective tyrosinase inhibitor acting on vascular endothelial growth factor 2 (VEGFR-2), and its efficacy and safety in advanced pancreatic cancer have been confirmed [8–10]. Based on this, the paper aims to investigate the safety of apatinib combined with chemotherapy for treating patients with advanced GCA.

2. Materials and Methods

2.1. General Information. 74 patients with advanced GCA treated in the oncology department of Weifang People's Hospital (January 2019–January 2020) were enrolled in this study, and equally split into the study group (SG) and reference group (RG) according to the odd and even admission numbers.

2.2. Inclusion Criteria

(1) All enrolled patients met the diagnostic criteria of advanced GCA in Guidelines for Diagnosis and Treatment of Primary Gastric Cancer [10] of Chinese Society of Clinical Oncology (CSCO) and confirmed by clinical diagnosis and imaging.

(2) The expected survival period was more than 3 months.

(3) The patients had normal blood routine, electrolyte, and liver function with no contraindication to chemotherapy.

(4) Eastern Cooperative Oncology Group (ECOG) score was 0–2.

(5) This study got the approval of the ethics committee of Weifang people's Hospital, and the patients had signed the informed consent.

2.3. Exclusion Criteria

(1) The patients had other malignant tumors

(2) The blood pressure of the patients could not be controlled

(3) The patients were receiving anticoagulant therapy or thrombolytic therapy

(4) The patients had a contraindication to apatinib

(5) The patients did not recover from the adverse reactions of early chemotherapy

2.4. Methods. RG was treated with chemotherapy alone, with the regimen of 5-fluorouracil (5-Fu), oxaliplatin, and calcium folinate (FOLFOX6 regimen or its improved regimen). The patients received 400 mg/m^2 of 5-Fu (manufacturer: Shanghai Acmec Biochemical Co., Ltd; art. no: F93580-100 g) by intravenous drip on the 1st day, with 2400–3000 mg/m^2 of continuous intravenous drip for 46 hours. The patients received 80–95 mg/m^2 of oxaliplatin (SFDA approval no.: H20143023; manufacturer: Hainan Jinrui Pharmaceutical Co., Ltd; specification: 50 mg) by intravenous drip for 3 hours on the 1st day. The patients received 200 mg/m^2 of calcium folinate (SFDA approval no.: H20040612; manufacturer: Guangdong Lingnan Pharmaceutical Co., Ltd.; specification: 0.1 g) by intravenous drip on the 1st day, with 14 days as a cycle. On this basis, SG was given oral apatinib (SFDA approval no.: H20140103; manufacturer: Jiangsu Hengrui Pharmaceutical Co., Ltd.; specification: 0.25 g × 10 tablets/box) at a dose of 250–850 mg/d. 14 days was a course of treatment, and 6 courses were performed.

2.5. Observation Indexes

2.5.1. Disease Control Rate. The response evaluation criteria in solid tumor (RECIST1.1) [11] was applied to evaluate the efficacy in the two groups. (1) Complete response (CR): the tumor disappeared completely. (2) Partial response (PR): the maximum tumor diameter decreased by 30%. (3) Stable disease (SD): the change of diameter was between PR and PD. (4) Progressive disease (PD): the diameter increased by 20% or new lesions were found. Disease control rate (DCR) = CR + PR + SD.

3 ml of fasting venous blood was collected from patients before and after treatment. The upper serum was taken after centrifugation, and the MMP-9 and SIL-2R levels were determined by ELISA. The kits were purchased from Jiangsu Jingmei Biotechnology Co., Ltd.

2.5.2. Immune Function. The FACSVia flow cytometer (manufacturer: Shanghai Huanxi Medical Equipment Co., Ltd.) was used to measure the $CD4^+$, $CD8^+$, $CD3^+$, and $CD4^+/CD8^+$ levels before and after treatment.

The patients were followed up until July 2020, and returned to the hospital for magnetic resonance imaging and computed tomography after one month. The median progression-free survival (MPFS) and overall survival (OS) of patients were recorded.

Generic Quality of Life Inventory-74 (GQOLI-74) [12] was used to score the quality of life (QOL) before and after intervention, including psychological function, somatic function, social function, and material life. Higher scores represented better QOL.

The incidence of adverse reactions during treatment was recorded, including alimentary tract hemorrhage, myelosuppression, liver function damage, skin and mucosal reaction, and thrombocytopenia.

2.6. Statistical Methods. All the experimental data were processed by SPSS21.0 software and graphed by GraphPad Prism 7 (GraphPad Software, San Diego, USA). The count data were tested by X^2, expressed by (n (%)), and the measurement data were measured by t-test, expressed by ($\bar{x} \pm s$). The differences were statistically significant at $P < 0.05$.

3. Results

3.1. Comparison of Clinical Data. No obvious differences in gender ratio, average age, average BMI, pathological staging, pathological types, organ metastasis types, and residence were observed between the two groups ($P > 0.05$), as shown in Table 1.

3.2. Comparison of Short-Term Efficacy. The short-term follow-up results showed that the DCR in SG was markedly higher compared with RG ($P < 0.05$), as shown in Table 2.

3.3. Comparison of Serum Indexes before and after Treatment. The MMP-9 and SIL-2R levels in both groups after treatment decreased ($P < 0.05$), and the levels in SG after treatment were markedly lower compared with RG ($P < 0.05$), as shown in Figure 1.

3.4. Comparison of Immune Function after Treatment. Compared with RG, $CD3^+$, $CD4^+$, and $CD4^+/CD8^+$ levels in SG after treatment were notably higher ($P < 0.001$), while the $CD8^+$ level was notably lower ($P < 0.001$), as shown in Table 3.

3.5. Comparison of Survival Period. The MPFS and OS in SG were markedly higher compared with RG ($P < 0.001$), as shown in Table 4.

3.6. Comparison of GQOLI-74 Scores before and after Treatment. The GQOLI-74 scores in both groups after treatment increased ($P < 0.001$), and the GQOLI-74 score in SG after treatment was notably higher compared with RG ($P < 0.001$), as shown in Figure 2.

3.7. Comparison of the Incidence of Adverse Reactions. The total incidence of adverse reactions in SG was markedly lower compared with RG ($P < 0.05$), as shown in Table 5.

4. Discussion

The pathological mechanism of GCA may be related to the following factors. (1) *Helicobacter pylori* infection: *Helicobacter pylori* infection leads to injury and apoptosis of gastrointestinal mucosal epithelial cells, increases oxygen free radicals, and cell proliferation and deterioration, eventually resulting in gastric cancer. (2) Life style and dietary habits: long-term eating of charcoal roasted or salted food increases the incidence of GCA. In addition, smoking is also the main factor leading to GCA. Chemotherapy is the main way to prolong the survival time of patients with advanced GCA, but there is no standard scheme for chemotherapy at present. The common chemotherapy drugs include antimicrotubule, fluorouracil, and platinum drugs, which can reduce the gastrointestinal reaction of patients to a certain extent and delay the disease progression [13, 14]. Clinical studies have found that abnormal angiogenesis is one of the basic features of malignant tumors and also one of the main ways of tumor progression [15]. Vascular endothelial growth factor (VEGF) plays an important role in the process of abnormal angiogenesis, which is mainly secreted by tumor cells or tumor stromal cells. During tumor enlargement, abnormal tumor vascular system causes the increased VEGF expression level, thus promoting the formation of abnormal angiogenesis. Therefore, the targeted therapy of VEGF has become a new method for the treatment of advanced GCA [16–18]. VEGFR-2 facilitates the proliferation of vascular endothelial cells by activating the MAPK signaling pathway. Apatinib, as an oral small molecule TKI against angiogenesis, can block VEGFR-2 in advanced GCA patients and reduce the activation of mitogen-activated protein kinase, thus inhibiting the proliferation of vascular endothelial cells [19–21].

As an interleukin receptor, SIL-2R can combine with IL-2 to reduce the activity of IL-2. If SIL-2R is highly expressed in serum, the cellular immunity induced by IL-2 will be inhibited, resulting in the decline of immune function and thereby accelerating the infiltration and proliferation of tumor cells [22–24]. This study confirmed that the serum SIL-2R level after apatinib combined with chemotherapy was markedly lower than that after chemotherapy alone, indicating that apatinib combined with chemotherapy reduces the serum SIL-2R level in advanced GCA patients, slows down the proliferation of tumor cells, and improves the prognosis. This study also found that the DCR in SG was markedly higher compared with RG, demonstrating that efficacy of the combined therapy in treating advanced GCA is markedly better than that of chemotherapy alone. Kano et al. [25] pointed out in their study that the disease control rate was 43.52% in the patients with lung cancer treated with chemotherapy alone, while that was 68.25% in the patients treated with apatinib combined with chemotherapy, suggesting that the effect of the combined therapy is better in treating lung cancer. In this study, both groups of patients had different types of adverse reactions during treatment, mainly including thrombocytopenia and alimentary tract hemorrhage. Most adverse reactions of patients could be relieved after symptomatic treatment, and some patients stopped medication due to intolerance. However, the incidence of adverse reactions of apatinib combined with chemotherapy was notably lower than that of chemotherapy alone, suggesting that apatinib combined with chemotherapy was safer than chemotherapy alone. This study also has some deficiencies such as the small size of selected samples. Therefore, the sample size should be further expanded for in-depth studies.

In conclusion, for advanced GCA patients, apatinib combined with chemotherapy has a high DCR with convenient and simple administration and can alleviate the clinical symptoms of patients with obvious clinical efficacy. Therefore, it is worth applying and promoting in clinic.

Table 1: Comparison of clinical data.

Items	SG ($n = 37$)	RG ($n = 37$)	χ^2/t	P
Gender			0.492	0.483
Male	22 (59.46%)	19 (51.35%)		
Female	15 (40.54%)	18 (48.65%)		
Average age (years old)	53.21 ± 6.51	53.25 ± 6.38	0.027	0.979
Average BMI (kg/m^2)	22.84 ± 1.73	22.86 ± 1.78	0.049	0.961
Pathological staging			0.237	0.626
III	23 (62.16%)	25 (67.57%)		
IV	14 (37.84%)	12 (32.43%)		
Pathological types				
Poorly differentiated adenocarcinoma	16 (43.24%)	14 (37.84%)	1.458	0.227
Medium differentiated adenocarcinoma	17 (45.95%)	18 (48.65%)	0.046	0.831
Carcinoma mucocellulare	4 (10.81%)	5 (13.51%)	0.127	0.722
Organ metastasis types			0.237	0.626
Single organ metastasis	14 (37.84%)	12 (32.43%)		
Multiple organ metastasis	23 (62.16%)	25 (67.57%)		
Residence			0.218	0.641
Urban area	19 (51.35%)	21 (56.76%)		
Rural area	18 (48.65%)	16 (43.24%)		

Table 2: Comparison of short-term efficacy (n (%)).

Group	n	CR	PR	SD	PD	DCR (%)
SG	37	5 (13.51%)	16 (43.24%)	5 (13.51%)	11 (29.73%)	70.27% (26/37)
RG	37	2 (5.41%)	7 (18.92%)	8 (21.62%)	20 (54.05%)	45.95% (17/37)
X^2						4.497
P						0.034

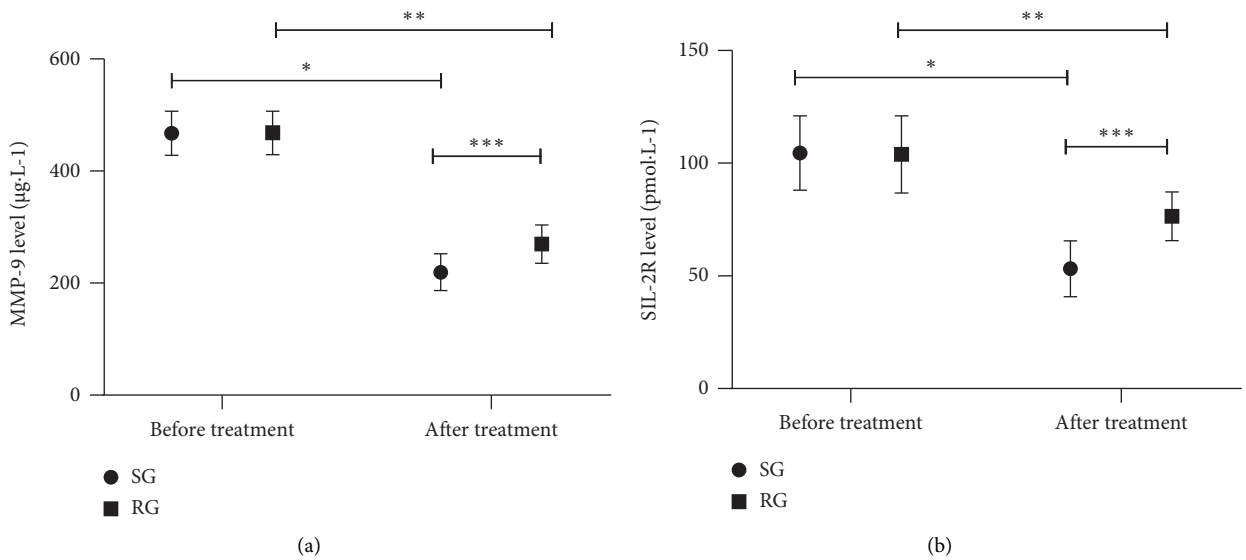

Figure 1: Comparison of serum indexes between the two groups before and after treatment ($\bar{x} \pm s$). (a) Comparison of MMP-9 levels before and after treatment. The abscissa represents before treatment and after treatment, and the ordinate represents the MMP-9 level ($\mu g \cdot L^{-1}$). The MMP-9 levels in SG before and after treatment were (467.34 ± 39.56) $\mu g \cdot L^{-1}$ and (219.46 ± 32.54) $\mu g \cdot L^{-1}$, respectively. The MMP-9 levels in RG before and after treatment were (468.12 ± 38.74) $\mu g \cdot L^{-1}$ and (269.56 ± 34.17) $\mu g \cdot L^{-1}$, respectively. * indicated an obvious difference in the MMP-9 levels of SG before and after treatment ($t = 29.436$, $P < 0.05$). ** indicated an obvious difference in the MMP-9 levels of RG before and after treatment ($t = 23.381$, $P < 0.05$). *** indicated an obvious difference in the MMP-9 levels between the two groups after treatment ($t = 6.459$, $P < 0.05$). (b) Comparison of SIL-2R levels before and after treatment. The abscissa represented before treatment and after treatment, and the ordinate represented the SIL-2R level ($pmol \cdot L^{-1}$). The SIL-2R levels in SG before and after treatment were (104.57 ± 16.54) $pmol \cdot L^{-1}$ and (53.17 ± 12.34) $pmol \cdot L^{-1}$, respectively. The SIL-2R levels in RG before and after treatment were (103.92 ± 17.12) $pmol \cdot L^{-1}$ and (76.46 ± 10.83) $pmol \cdot L^{-1}$, respectively. * indicated an obvious difference in the SIL-2R levels of SG before and after treatment ($t = 15.151$, $P < 0.05$); ** indicated an obvious difference in the SIL-2R levels of RG before and after treatment ($t = 8.245$, $P < 0.05$); *** indicated an obvious difference in the SIL-2R levels between the two groups after treatment ($t = 8.629$, $P < 0.05$).

Table 3: Comparison of immune function after treatment ($\bar{x} \pm s$).

Group	n	$CD3^+$ (%)	$CD4^+$ (%)	$CD8^+$ (%)	$CD4^+/CD8^+$
SG	37	62.31 ± 5.29	42.56 ± 4.19	25.71 ± 3.62	1.57 ± 0.18
RG	37	53.62 ± 5.17	33.18 ± 3.84	31.21 ± 3.41	1.14 ± 0.14
t		7.146	10.039	6.727	11.470
P		<0.001	<0.001	<0.001	<0.001

Table 4: Comparison of survival period ($\bar{x} \pm s$, months).

Group	n	MPFS	OS
SG	37	4.31 ± 0.58	7.62 ± 1.34
RG	37	2.72 ± 0.41	5.48 ± 1.21
t		13.617	7.210
P		<0.001	<0.001

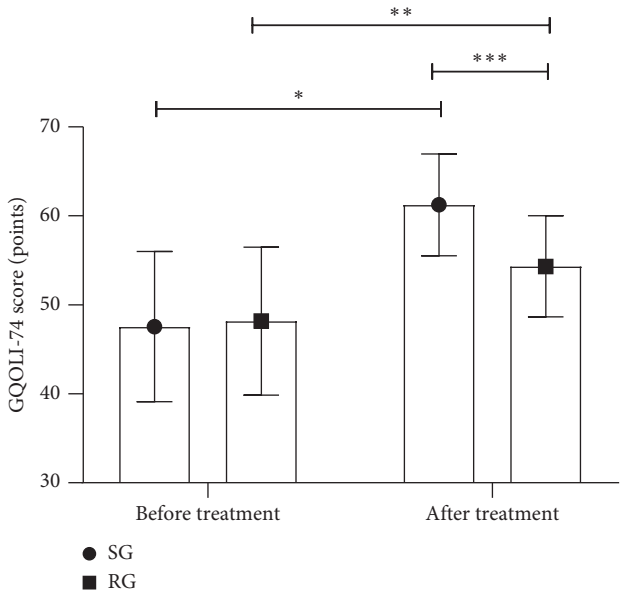

Figure 2: Comparison of GQOLI-74 scores before and after treatment ($\bar{x} \pm s$). *Note*. The abscissa represented before treatment and after treatment, and the ordinate represented the GQOLI-74 score (points). The GQOLI-74 scores in SG before and after treatment were (47.56 ± 8.45) and (61.24 ± 5.72), respectively. The GQOLI-74 scores in RG before and after treatment were (48.17 ± 8.32) and (54.33 ± 5.68), respectively. *indicated an obvious difference in the GQOLI-74 scores of SG before and after treatment ($t = 8.155$, $P < 0.001$); **indicated an obvious difference in the GQOLI-74 scores of RG before and after treatment ($t = 3.719$, $P < 0.001$); ***indicated an obvious difference in the GQOLI-74 scores between the two groups after treatment ($t = 5.214$, $P < 0.001$).

Table 5: Comparison of the incidence of adverse reactions (n (%)).

Group	n	Alimentary tract hemorrhage	Myelosuppression	Liver function damage	Skin and mucosal reaction	Thrombocytopenia	Total incidence
SG	37	2 (5.41%)	1 (2.70%)	1 (2.70%)	0 (0.00%)	2 (5.41%)	16.22% (6/37)
RG	37	3 (8.11%)	4 (10.81%)	2 (5.41%)	3 (8.11%)	4 (10.81%)	43.24% (16/37)
t							6.469
P							0.011

Data Availability

The datasets used and/or analyzed during the present study are available from the corresponding author on reasonable request.

Conflicts of Interest

The authors declare that they have no conflicts of interest.

References

[1] S. Mishima, A. Kawazoe, and K. Shitara, "Safety of pembrolizumab in recurrent or advanced gastric cancer expressing PD-L1 refractory to platinum and fluoropyrimidine," *Expert Opinion on Drug Safety*, vol. 19, no. 9, pp. 1063–1068, 2020.

[2] J. Sato, S. Iwasa, Y. Honma et al., "Impact of oxaliplatin-induced neuropathy on subsequent paclitaxel for advanced gastric cancer," *International Journal of Clinical Medicine*, vol. 11, no. 9, pp. 526–537, 2020.

[3] C. Ran and G. Gong, "Clinical application and research progress of accelerated rehabilitation surgery in perioperative period of advanced gastric cancer in the elderly," *International Journal of Clinical Medicine*, vol. 11, no. 3, pp. 101–110, 2020.

[4] K. Harada, M. Zhao, N. Shanbhag, H. Baba, and J. a. Ajani, "Palliative care for advanced gastric cancer," *Expert Review of Anticancer Therapy*, vol. 20, no. 7, pp. 575–580, 2020.

[5] J.-W. Wang and C.-Y. Chen, "Prognostic value of total retrieved lymph nodes on the survival of patients with advanced gastric cancer," *Journal of the Chinese Medical Association*, vol. 83, no. 8, pp. 691-692, 2020.

[6] V. T. Chivere, P. P. D. Kondiah, Y. E. Choonara, and V. Pillay, "Nanotechnology-Based biopolymeric oral delivery platforms for advanced cancer treatment," *Cancers*, vol. 12, no. 2, p. 522, 2020.

[7] A. Kawazoe and K. Shitara, "Trifluridine/tipiracil for the treatment of metastatic gastric cancer," *Expert Review of Gastroenterology and Hepatology*, vol. 14, no. 2, pp. 65–70, 2020.

[8] J. J. Han, J. W. Kim, K. J. Suh et al., "Clinical characteristics and outcomes of patients enrolled in clinical trials compared with those of patients outside clinical trials in advanced gastric cancer," *Asia-Pacific Journal of Clinical Oncology*, vol. 15, no. 3, pp. 158–165, 2019.

[9] Z. Li, Y. Zhao, B. Lian, Y. Liu, and Q. Zhao, "Long-term oncological outcomes in laparoscopic versus open gastrectomy for advanced gastric cancer: a meta-analysis of high-quality nonrandomized studies," *The American Journal of Surgery*, vol. 218, no. 3, pp. 631–638, 2019.

[10] H. Liang, Z. Liu, X. Cai et al., "PD-(L)1 inhibitors vs . chemotherapy vs . their combination in front-line treatment for NSCLC: an indirect comparison," *International Journal of Cancer*, vol. 145, no. 11, pp. 3011–3021, 2019.

[11] T. Omori, Y. Fujiwara, K. Yamamoto et al., "The safety and feasibility of single-port laparoscopic gastrectomy for advanced gastric cancer," *Journal of Gastrointestinal Surgery*, vol. 23, no. 7, pp. 1329–1339, 2019.

[12] K. Shibuya, H. Kawamura, S. Takahashi et al., "Short-term and long-term outcomes following laparoscopic gastrectomy for advanced gastric cancer compared with open gastrectomy," *Surgical Laparoscopy Endoscopy and Percutaneous Techniques*, vol. 29, no. 4, pp. 297–303, 2019.

[13] J. Ding, X.-Y. Cheng, S. Liu et al., "Apatinib exerts anti-tumour effects on ovarian cancer cells," *Gynecologic Oncology*, vol. 153, no. 1, pp. 165–174, 2019.

[14] Y. Hu, P. Zhou, Y. Lin, D. Yang, and B. Wang, "Anti-colorectal cancer effect via application of polyethylene glycol modified liposomal apatinib," *Journal of Biomedical Nanotechnology*, vol. 15, no. 6, pp. 1256–1266, 2019.

[15] Z. Gao, M. Shi, Y. Wang, J. Chen, and Y. Ou, "Apatinib enhanced anti-tumor activity of cisplatin on triple-negative breast cancer through inhibition of VEGFR-2," *Pathology, Research and Practice*, vol. 215, no. 7, Article ID 152422, 2019.

[16] Y. Wang, M. Deng, Q. Chen et al., "Apatinib exerts anti-tumor activity to non-hodgkin lymphoma by inhibition of the Ras pathway," *European Journal of Pharmacology*, vol. 843, pp. 145–153, 2019.

[17] M. J. Choi, J. Y. Noh, A.-Y. Jang et al., "Age-stratified analysis of serotype-specific baseline immunity against group B streptococcus," *Human Vaccines and Immunotherapeutics*, vol. 16, no. 6, pp. 1338–1344, 2020.

[18] C. Ranasinghe, C. Ozemek, and R. Arena, "Exercise and well-being during COVID 19 - time to boost your immunity," *Expert Review of Anti-infective Therapy*, vol. 18, no. 12, pp. 1195–1200, 2020.

[19] Y. Shao, J. Saredy, W. Y. Yang et al., "Vascular endothelial cells and innate immunity," *Arteriosclerosis, Thrombosis, and Vascular Biology*, vol. 40, no. 6, pp. e138–e152, 2020.

[20] A. Marchant, N. Amenyogbe, T. R. Kollmann, and T. Goetghebuer, "Maternal HIV infection alters antimicrobial immunity in exposed and uninfected infants," *The Pediatric Infectious Disease Journal*, vol. 39, no. 5, pp. e47–e48, 2020.

[21] M. L. Compton and J. M. M. Cates, "Evidence-based tumor staging of skeletal chondrosarcoma," *The American Journal of Surgical Pathology*, vol. 44, no. 1, pp. 111–119, 2020.

[22] W. Chen, X. Tan, J. Ye, Y. Zhang, J. Liang, and M. Huang, "Impact of primary tumor site on the prognosis in T4 colorectal cancer patients," *International Journal of Clinical Medicine*, vol. 11, no. 9, pp. 504–515, 2020.

[23] S. Syed, S. P. Basourakos, F. S. Ali, J. L. Garcia, A. Zurita-Saavedra, and Z. Gong, "A limited-versus-extensive staging strategy for small cell prostate cancer," *American Journal of Clinical Oncology*, vol. 43, no. 2, pp. 87–93, 2020.

[24] A. P. Punke and J. Waddell, "Creation and evaluation of a cancer chemotherapy order review guide for use at a community hospital," *Journal of Oncology Pharmacy Practice*, vol. 25, no. 1, pp. 25–43, 2019.

[25] M. Kano, K. Hayano, H. Hayashi et al., "Survival benefit of neoadjuvant chemotherapy with S-1 plus docetaxel for locally advanced gastric cancer: a propensity score-matched analysis," *Annals of Surgical Oncology*, vol. 26, no. 6, pp. 1805–1813, 2019.

Hindawi
Journal of Oncology
Volume 2021, Article ID 3711699, 6 pages
https://doi.org/10.1155/2021/3711699

Research Article

Rehabilitation Nursing Intervention Can Improve Dysphagia and Quality of Life of Patients Undergoing Radiotherapy for Esophageal Cancer

Xiange Zeng,[1] Ling Li,[2] Wenjing Wang,[1] and Lihui Zhu[1]

[1]*Department of Gastroenterology, The Second Affiliated Hospital, Hengyang Medical School, University of South China, Hengyang, China*
[2]*Digestive Endoscopy Center, The Second Affiliated Hospital, Hengyang Medical School, University of South China, Hengyang, China*

Correspondence should be addressed to Lihui Zhu; anzagou5@163.com

Received 3 June 2021; Accepted 29 July 2021; Published 5 August 2021

Academic Editor: Alamgeer Yuchi

Objective. To seek the improvement of rehabilitation nursing intervention on dysphagia and quality of life of patients with esophageal cancer undergoing radiotherapy. *Methods*. A total of 109 patients with esophageal cancer undergoing radiotherapy were selected as research objects. According to the random number table, they were separated into the control group (CG) and intervention group (IG), with 45 cases in CG and 64 cases in IG. In CG, patients were given routine nursing intervention, while those in IG were given rehabilitation nursing intervention. After intervention, the degree of acute radiation injury and the improvement of swallowing function were observed to compare the self-nursing ability, quality of life, and incidence of complications between the two groups. *Results*. The degree of injury in CG was heavier than that in IG. The improvement of swallowing function in IG was better than that in CG. The scores of self-nursing ability and life quality in IG were higher than those in CG, with statistically significant differences ($p < 0.05$). The incidence of complications in IG was obviously lower than that in CG ($p < 0.05$). *Conclusion*. Rehabilitation nursing intervention can ameliorate dysphagia, improve the quality of life, and reduce the incidence of complications for patients with esophageal cancer undergoing radiotherapy. It is worthy of clinical application.

1. Introduction

Esophageal cancer, also known as esophagus cancer, is a malignant tumor disease that develops in esophageal epithelial tissue, mostly occurring in people over 40 years old [1]. Its early symptoms are not obvious, but patients will show progressive dysphagia and other symptoms in the middle and late stages, which seriously threatens their life health [2]. The occurrence and distribution of esophageal cancer are related to many factors, including age, gender, race, living environment, and geographical distribution [3–5]. China is a country with a high incidence of esophageal cancer. Due to the improvement of diet and living habits, the incidence of esophageal cancer in China has declined in recent years, but its mortality rate remains high [6, 7]. Because there are no obvious clinical symptoms in the early stage of esophageal cancer, 80% of sufferers have entered the middle and late stages when they are diagnosed, often missing the best opportunity to radically cure it [8].

Surgery [9], radiopharmaceutical therapy (radiotherapy) [10], and chemotherapy [11] are the basic methods to treat esophageal cancer. If timely and effective treatment measures are given at the early stage of the patient's disease development, it is highly curative, so it is very necessary to give effective surgical treatment in the early and middle stage of patients' disease development [12]. However, most patients lose the chance of operation because of the location of tumor or the rapid progress of disease, so radiotherapy needs to be given to patients with advanced disease. However, the spread of cancer cells cannot be controlled when the radiotherapy measures are implemented, so the incidence of adverse reactions is higher after treatment [13, 14], which

leads to greater psychological pressure of patients, directly affects their psychological state and quality of life, and has a certain negative impact on the therapeutic effect [15, 16]. Moreover, radiation injury to esophageal mucosa is one of the most common side effects of radiotherapy, which can lead to mucosal edema, congestion, ulcer, and erosion causing patients to feel esophageal burning, esophageal swelling and pain, and then suffering from dysphagia, swallowing pain, pain behind the sternum, and other symptoms when eating [17–19]. Therefore, the implementation of scientific and effective rehabilitation training and health guidance is conducive to improve the swallowing function for esophageal cancer patients with difficulty in opening mouth after radiotherapy, so as to supplement enough nutrition and water to improve the body's resistance, which is of great significance for the rehabilitation of disease and psychology. In this study, rehabilitation nursing was mainly used to intervene patients with esophageal cancer undergoing radiotherapy and observe its application effect.

2. Materials and Methods

2.1. Research Objects. A total of 109 patients with esophageal cancer were selected as the research objects, and the patients were admitted to hospital from June 2019 to June 2020. They were randomly divided into CG and IG in accordance with the random number table. There were 45 cases in CG, including 29 men and 16 women, with an mean age of 47.68 ± 3.51 years old. There were 64 cases in IG, including 37 men and 27 women, with a mean age of 48.05 ± 3.57 years old.

Inclusion criteria are as follows: all of them met the diagnostic criteria of esophageal cancer, and all patients received radiotherapy.

Exclusion criteria are as follows: comorbid with other tumors, cognitive impairment, and severe hepatic insufficiency.

There was no statistically significant difference in baseline data in both groups ($p > 0.05$), which was comparable. In both groups, patients and their families have affixed informed consent, and this research has been ratified by the ethics committee of our hospital.

2.2. Methods. In both groups, patients received radiotherapy. During radiotherapy, patients in CG were provided with corresponding nursing measures according to the routine nursing process of esophageal cancer. The vital signs, blood routine, and systemic reactions of patients were closely observed, and symptomatic treatment was given in time. The ward was ventilated regularly to keep the air fresh, and the ward was kept quiet. The ward was regularly disinfected, and patients with low leucocyte or infection should be placed in protective isolation. The patient was placed in a comfortable position and kept the respiratory tract smooth.

In IG, patients were treated with rehabilitation nursing intervention. Specific measures: (1) preparatory work. Medical staff explained the importance and positive role of rehabilitation exercise to patients and their families and introduced the content of rehabilitation exercise, so that patients and their families could get a basic understanding, so as to establish a good attitude towards treatment and preparation. (2) Rehabilitation exercises: rehabilitators and nursing staff assisted patients in rehabilitation exercises, including mouth opening exercises, neck massage, oral organ coordination training, and direct feeding training. (3) Oral and pharyngeal nursing. The swallowing therapeutic apparatus with frequency of 30–80 Hz, wave width of 700 ms, and current intensity of 0–25 mA was used for treatment, and it could be adjusted according to the specific condition and tolerance of patients. The patient was treated for 30 min/time, once/d, and continued for 2 weeks. (4) Psychological nursing. When patients received radiotherapy, they needed to be enlightened by nursing staff to relieve their anxiety and fear and give appropriate psychological comfort to enhance their self-confidence to overcome the disease.

2.3. Outcome Measures. Mucosal injury degree: it was judged according to the grading standard of acute radiation injury of tumor cooperative organization in radiotherapy, which was divided into four grades, and the severity was decreased in turn according to the grades. Grade 4: the patient had a large area of ulcer, fistula, and perforation, and the pain was intense. Grade 3: the patient suffered from severe dysphagia with complications such as weight loss and severe dehydration. The patient needed to be fed by intravenous fluids infusion or nasal feeding. Grade 2: the patient suffered from moderate dysphagia with labor pains. The patient might take a liquid diet or rely on some anesthetic to relieve the pain. Grade 1: the patients suffered from mild dysphagia and could take semiliquid food, and the epidermal anesthetics could be used to relieve discomfort. Grade 0: there was no symptom.

Swallowing X-ray video (VFSS) was used to evaluate the improvement of swallowing function. Cure: the swallowing time was normal, without error aspiration, residual barium meal, and epiglottic vallecula. Effective: the swallowing time was shortened by more than 1/2 compared with before treatment, and there was no error aspiration, residual barium meal, and epiglottic vallecula. Ineffective: the swallowing time was shortened by less than 1/2 compared with before treatment, and there was error aspiration, residual barium meal, and epiglottic vallecula, or even the patient was unable to swallow.

Self-nursing ability: the self-nursing ability scale ESCA was applied to assess the self-nursing ability of the patients in both groups. The scale included four parts: self-concept, self-care responsibility, self-care skills, and health knowledge cognition, with a total of 43 items. Each item was scored by 1–4 grades. The higher the score, the higher the self-nursing ability.

The quality of life core scale (EORTC QLQ-C30) was applied to evaluate patients' life quality, which was divided into somatic function, role function, cognitive impairment, emotional function, and society function, with 30 items in total. The higher the score, the better the life quality of patients.

Incidence of complications: the complications mainly included esophagitis, tracheitis, esophageal fistula, and hemorrhage.

2.4. Statistical Methods. SPSS22.0 statistical software was applied to analyze the research data. The quantitative data were represented by mean number ± standard deviation ($x \pm s$), and the t-test was applied. The enumeration data were represented by rate (%), and the χ^2 test was applied. The difference was statistically significant with $p < 0.05$.

3. Results

3.1. Degree of Mucosal Injury in the Two Groups. The number of patients with grade 0 and grade 1 mucosal injury in IG was higher than that in CG, and the number of grade 2, grade 3, and grade 4 was lower than that in CG. The difference was statistically significant ($p < 0.05$), indicating that the degree of injury in CG was heavier than that in IG (Table 1).

3.2. Improvement of Swallowing Function in the Two Groups. Observing the improvement of swallowing function in both groups, the findings showed that the total response rate in IG (82.8%) was higher than 57.8% in CG, and the difference was statistically significant ($p < 0.05$) (Table 2).

3.3. Self-Care Ability of Patients in Both Groups. The self-nursing ability of patients was observed in the two groups. Before intervention, there was no obvious difference in scores of self-concept, self-care responsibility, self-care skills, and health knowledge cognition in both groups ($p < 0.05$). After intervention, the scores of patients in both groups increased, and the scores of patients in IG were obviously higher than those in CG ($p < 0.05$) (Table 3).

3.4. Life Quality of Patients in the Two Groups. There was no significant difference in EORTC QLQ-C30 scores in both groups before intervention. After intervention, the EORTC QLQ-C30 scores of the two groups were higher than those before intervention, and the scores in IG were obviously higher than those in CG ($p < 0.05$) (Figure 1).

3.5. Incidence of Complications in Both Groups. In IG, there were 1 case with esophagitis, 2 cases with tracheitis, 1 case with esophageal fistula, and 0 cases with bleeding, with a total of 4 cases (6.3%). In CG, there were 3 cases with esophagitis, 3 cases with tracheitis, 2 cases with esophageal fistula, and 2 cases with bleeding, with a total of 10 cases (22.2%). There was a statistical difference in the incidence of complications in both groups ($p < 0.05$) (Table 4).

4. Discussion

With the change of people's diet structure, the prevalence of esophageal cancer is increasing year by year. Radiotherapy has become the main treatment for esophageal cancer due to less trauma than surgery and less restrictions by surrounding tissues and trachea [20–22]. However, this treatment can lead to serious side effects and increase the psychological burden of patients [23, 24]. Therefore, it is of positive significance to carry out necessary nursing intervention for patients with esophageal cancer during chemotherapy to improve the clinical prognosis.

In this study, rehabilitation nursing was used to intervene patients undergoing radiotherapy for esophageal cancer. The results showed that the total effective rate of improving swallowing function in IG was 82.8% (53/64), significantly higher than 57.8% in the control group, which was consistent with the findings in stroke patients with hemiplegia [25]. Radiotherapy can cause different degrees of radiotherapy reaction during the treatment of esophageal cancer. The main toxic side effect is acute radiation esophagitis. The clinical manifestation of acute radiation injury is pain aggravated by eating or burning sensation behind sternum, and its incidence increases with the increase of dose, which has adverse effects on the treatment effect, life quality, and survival rate of patients. The results showed that rehabilitation nursing intervention could effectively reduce the degree of acute radiation injury. The scores of self-nursing ability and life quality in IG were higher than those in CG, and the incidence of complications in IG was 6.3% (4/64), obviously lower than 22.2% (10/45) in CG. Rehabilitation nursing is designed to make every link in the nursing process continuous and systematic and provide high-efficiency and high-quality nursing services for patients, so as to effectively relieve the psychological and physiological pressure of patients and improve the quality of nursing work. Through rehabilitation exercise, oropharyngeal care, psychological intervention, and other measures, the correct and effective rehabilitation nursing in the radiotherapy process can improve the clinical symptoms and reduce the psychological burden of patients, so that patients take the initiative to cooperate with radiotherapy to improve compliance. The results suggested that rehabilitation nursing intervention could obviously ameliorate patients' self-nursing ability and their life quality. Patients with esophageal cancer should be evaluated and take functional exercise as early as possible. Rehabilitation nursing intervention measures (the main content is to understand their condition and psychological characteristics, formulate nursing plans, give health education, rehabilitation training, specialized nursing, and psychological counseling) can significantly ameliorate the degree of swallowing difficulties of patients and prevent the development and progression of complications. This study also has some limitations. For example, the effect of patient disease types on the results of the study

Table 1: Degree of mucosal injury in the two groups.

	Grade 0	Grade 1	Grade 2	Grade 3	Grade 4
CG ($n = 45$)	1 (2.2)	10 (22.2)	22 (48.9)	8 (17.8)	4 (8.9)
IG ($n = 64$)	9 (14.1)*	37 (57.8)*	15 (23.4)*	3 (4.7)	0 (0)*
χ^2/t	4.4451	13.6510	7.6331	1.6881	5.9061
P	0.0350	0.0002	0.0057	0.1939	0.0151

*Comparison with the CG group ($p < 0.05$).

Table 2: Improvement of swallowing function in the two groups.

	Cure	Effective	Ineffective	Total effective rate
CG ($n = 45$)	5 (11.1)	21 (45.7)	19 (42.2)	26 (57.8)
IG ($n = 64$)	16 (25.0)	37 (57.8)	10 (17.2)	53 (82.8)*
χ^2/t				8.3011
P				0.0040

*Comparison with the CG group ($p < 0.05$).

Table 3: Self-care ability of patients in the two groups.

	Before intervention		χ^2/t	P	After intervention		χ^2/t	P
	CG ($n = 45$)	IG ($n = 64$)			CG ($n = 45$)	IG ($n = 64$)		
Self-concept	24.75 ± 4.26	24.94 ± 4.03	0.2367	0.8133	29.03 ± 5.12	32.68 ± 5.39*	3.5530	0.0005
Self-care responsibility	25.37 ± 3.97	25.56 ± 4.11	0.2410	0.8100	29.77 ± 5.69	34.82 ± 5.61*	4.6000	<0.0001
Self-care skills	25.77 ± 4.51	25.93 ± 4.22	0.1894	0.8501	29.06 ± 5.97	36.81 ± 6.23*	6.5046	<0.0001
Health knowledge cognition	26.08 ± 4.87	26.21 ± 4.93	0.1362	0.8919	30.19 ± 6.06	36.49 ± 6.17*	5.2871	<0.0001

*Comparison with the CG group after intervention ($p < 0.05$).

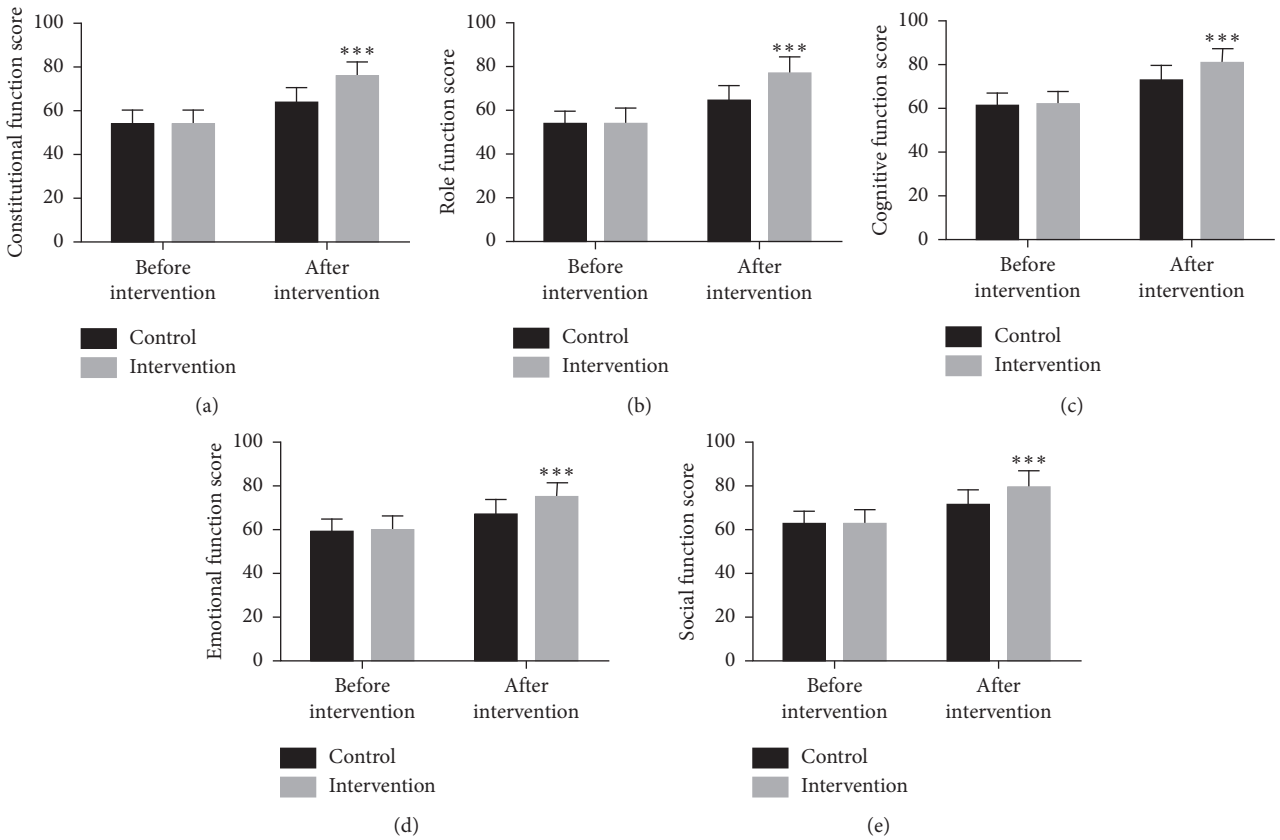

Figure 1: Quality of life of patients in the two groups. (a) Physical function scores of patients in the two groups. (b) Role function scores of patients in the two groups. (c) Cognitive function scores of patients in the two groups. (d) Emotional function scores of patients in the two groups. (e) Social function scores of patients in the two groups. Compared with the CG, *** $p < 0.0001$).

Table 4: Incidence of complications in the two groups.

	Esophagitis	Tracheitis	Esophageal fistula	Hemorrhage	Overall incidence
CG ($n = 45$)	3 (6.7)	3 (6.7)	2 (4.4)	2 (4.4)	10 (22.2)
IG ($n = 64$)	1 (1.6)	2 (3.1)	1 (1.6)	0 (0)	4 (6.3)*
χ^2/t					6.0211
P					0.0141

*Comparison with the CG group ($p < 0.05$).

was not considered, and the small number of included cases may lead to bias in the results.

5. Conclusion

In conclusion, rehabilitation nursing intervention has a remarkable effect on dysphagia in patients undergoing radiotherapy for esophageal cancer, which can ameliorate their pain symptoms, improve the quality of life, and reduce the incidence of complications. It is worthy of popularization and application in radiotherapy.

Data Availability

The data used to support the findings of this study are included within the article.

Conflicts of Interest

The authors declare that there are no conflicts of interest.

Acknowledgments

This study was financially supported by Hunan Health Commission Major Project (A2017014).

References

[1] W. Short Matthew, G. Burgers Kristina, and T. Fry Vincent, "Esophageal cancer," *American Family Physician*, vol. 95, pp. 22–28, 2017.

[2] S. Joseph, M. Zfass Alvin, S. Mitchell et al., "Early esophageal cancer: a gastroenterologist's disease," *Digestive Diseases and Sciences*, vol. 64, pp. 3048–3058, 2019.

[3] H. Fang-Liang and S.-J. Yu, "Esophageal cancer: risk factors, genetic association, and treatment," *Asian Journal of Surgery*, vol. 41, pp. 210–215, 2018.

[4] G. K. Malhotra, U. Yanala, A. Follet, M. Vijayakumar, and C. Are, "Global trends in esophageal cancer," *Journal of Surgical Oncology*, vol. 115, no. 5, pp. 564–579, 2017.

[5] D. R. S. Middleton, L. Bouaoun, R. Bray et al., "Esophageal cancer male to female incidence ratios in Africa: a systematic review and meta-analysis of geographic, time and age trends," *Cancer Epidemiology*, vol. 53, pp. 119–128, 2018.

[6] R. Chen, R. S. Zheng, S. W. Zhang et al., "Analysis of incidence and mortality of esophageal cancer in China, 2015," *Zhonghua Yu Fang Yi Xue Za Zhi*, vol. 53, pp. 1094–1097, 2019.

[7] Y. Y. Li, L. B. Du, X. Q. Hu et al., "A suggested framework for conducting esophageal cancer screening in China," *Journal of Digestive Diseases*, vol. 19, pp. 722–729, 2018.

[8] Y. Horie, T. Yoshio, K. Yoshimizu et al., "Diagnostic outcomes of esophageal cancer by artificial intelligence using convolutional neural networks," *Gastrointestinal Endoscopy*, vol. 89, pp. 25–32, 2019.

[9] H. Kikuchi and H. Takeuchi, "Future perspectives of surgery for esophageal cancer," *Annals of Thoracic and Cardiovascular Surgery*, vol. 24, no. 5, pp. 219–222, 2018.

[10] J. Lyu, T. Li, C. Xie et al., "Enteral nutrition in esophageal cancer patients treated with radiotherapy: a Chinese expert consensus 2018," *Future Oncology*, vol. 15, no. 5, pp. 517–531, 2019.

[11] G. Y. Ku, "Systemic therapy for esophageal cancer: chemotherapy," *Chinese Clinical Oncology*, vol. 6, no. 5, p. 49, 2017.

[12] S. Makoto and K. Hiroyuki, "Current status and future prospects for esophageal cancer treatment," *Annals of Thoracic and Cardiovascular Surgery*, vol. 23, pp. 1–11, 2017.

[13] C. Zhu, S. Wang, Y. You, K. Nie, and Y. Ji, "Risk factors for esophageal fistula in esophageal cancer patients treated with radiotherapy: a systematic review and meta-analysis," *Oncology Research and Treatment*, vol. 43, no. 1-2, pp. 34–41, 2020.

[14] H. Song, F. Fang, U. Lu et al., "Waiting time for cancer treatment and mental health among patients with newly diagnosed esophageal or gastric cancer: a nationwide cohort study," *BMC Cancer*, vol. 17, no. 1, p. 2, 2017.

[15] V. Lancellotta, F. Cellini, B. De Sanctis et al., "The role of palliative interventional radiotherapy (brachytherapy) in esophageal cancer: an AIRO (Italian Association of Radiotherapy and Clinical Oncology) systematic review focused on dysphagia-free survival," *Brachytherapy*, vol. 19, pp. 104–110, 2020.

[16] K. Terufumi, N. Keiji, S. Keisuke et al., "Palliative radiotherapy and chemoradiotherapy in stage IVA/B esophageal cancer patients with dysphagia," *International Journal of Clinical Oncology*, vol. 23, pp. 1076–1083, 2018.

[17] W. Li, B. Zheng, S. Zhang, H. Chen, W. Zheng, and C. Chen, "Feasibility and outcomes of modified enhanced recovery after surgery for nursing management of aged patients undergoing esophagectomy," *Journal of Thoracic Disease*, vol. 9, no. 12, pp. 5212–5219, 2017.

[18] Y. Lian, X. Niu, H. Cai et al., "Clinicopathological significance of c-MYC in esophageal squamous cell carcinoma," *Tumour Biology: The Journal of the International Society for Oncodevelopmental Biology and Medicine*, vol. 39, Article ID 1010428317715804, 2017.

[19] J. Y. Cho, D. Y. Cheung, T. J. Kim, and J. K. Kim, "A case of esophageal squamous cell carcinoma in situ arising from esophageal squamous papilloma," *Clinical Endoscopy*, vol. 52, no. 1, pp. 72–75, 2019.

[20] M. . Stefan, C. Mickael, N. Nadja et al., "Early esophageal cancer: the significance of surgery, endoscopy, and chemoradiation," *Annals of the New York Academy of Sciences*, vol. 1434, pp. 115–123, 2018.

[21] C. C. Abnet, M. Arnold, and W.-Q. Wei, "Epidemiology of esophageal squamous cell carcinoma," *Gastroenterology*, vol. 154, no. 2, pp. 360–373, 2018.

[22] X. C. Li, M. Y. Wang, M. Yang et al., "A mutational signature associated with alcohol consumption and prognostically significantly mutated driver genes in esophageal squamous cell carcinoma," *Annals of Oncology*, vol. 29, no. 4, pp. 938–944, 2018.

[23] L. Zheng, S. Liu, H. Chen et al., "[Relationship between lifestyle and dietary habits and the occurrence of squamous cell carcinoma in different subsites of the esophagus]," *Wei Sheng Yan Jiu*, vol. 48, pp. 757–764, 2019.

[24] N.-B. Chen, B. Qiu, J. Zhang et al., "Intensity-modulated radiotherapy versus three-dimensional conformal radiotherapy in definitive chemoradiotherapy for cervical esophageal squamous cell carcinoma: comparison of survival outcomes and toxicities," *Cancer Research and Treatment*, vol. 52, no. 1, pp. 31–40, 2020.

[25] P. Jelvehgaran, D. M. de Bruin, G. Borst et al., "Optical coherence tomography to detect acute esophageal radiation-induced damage in mice: a validation study," *Journal of Biophotonics*, vol. 12, Article ID e201800440, 2019.

Hindawi
Journal of Oncology
Volume 2021, Article ID 6199732, 6 pages
https://doi.org/10.1155/2021/6199732

Research Article

Clinical Effect of Iodine-125 Seed Implantation in Patients with Primary Liver Cancer and Its Effect on Th1/Th2 Cells in Peripheral Blood

Xiaoyan Chen,[1] **Fan Zhu**,[2] **Bin Wang**,[1] **Yu Zhou**,[1] **Hao Xiong**,[1] **Tao Fan**,[3] **and Wenjie Ke**[4]

[1]*Department of Hepatobiliary Surgery, Renmin Hospital of Wuhan University, Wuhan 430060, China*
[2]*Department of Hepatobiliary Surgery, Ezhou Central Hospital, Ezhou 436099, China*
[3]*Department of Outpatient, Chengdu Wuhou District Enxi Medical Cosmetology Hospital, Chengdu 610047, China*
[4]*Department of Henia and Abdominal Wall Surgery, The Central Hospital of Wuhan, Tongji Medical College, Huazhong Univerity of Science and Technology, Wuhan 430030, China*

Correspondence should be addressed to Xiaoyan Chen; tululupai@163.com and Wenjie Ke; buyi58693@163.com

Received 1 July 2021; Revised 12 July 2021; Accepted 20 July 2021; Published 29 July 2021

Academic Editor: Muhammad Wasim Khan

Objective. To investigate the clinical effect of iodine-125 seed implantation combined with chemotherapy in patients with primary liver cancer and the effect on peripheral blood Th1/Th2 cells. *Methods*. A total of 136 patients with primary liver cancer from April 2017 to June 2018 were selected as subjects and randomly divided into the control group and observation group with 68 cases in each group. The control group was treated with chemotherapy, and the observation group was treated with iodine-125 seed implantation on the basis of the control group. After 3 months of treatment, the curative effect was investigated. Serum tumor markers, peripheral blood Th1/Th2 cells, and side effects and recurrence rate were compared between the two groups. *Results*. The levels of serum tumor markers in both groups at 3 months after treatment were lower than before treatment ($P < 0.05$). Three months after treatment, the levels of tumor markers AFP, AFP-L3, and GP73 in the observation group were $14.61 \pm 3.49\,\mu g/L$, 3.29 ± 0.41 ng/mL, and $51.24 \pm 4.51\,\mu g/L$, respectively, which were lower than those in the control group, $32.53 \pm 4.59\,\mu g/L$, 5.63 ± 0.63 ng/mL, and $71.52 \pm 6.05\,\mu g/L$ ($P < 0.05$). At 3 months after treatment, the level of including interleukin-2 (IL-2) and tumor necrosis factor-α (TNF-α) in Th1 cells of the observation group was higher than that of the control group ($P < 0.05$), whereas the levels of IL-4, IL-6, and IL-10 in Th2 cells were lower than those in the control group ($P < 0.05$). There was no statistical significance in the incidence of leukopenia, thrombocytopenia, and gastrointestinal reactions between the two groups ($P > 0.05$). The recurrence rate of the observation group at 12, 24, and 36 months after treatment was lower than that of the control group ($P < 0.05$). *Conclusion*. Iodine-125 seed implantation combined with chemotherapy in patients with primary liver cancer can reduce the level of serum tumor markers, improve the level of peripheral blood Th1/Th2 cells, and reduce the recurrence rate of patients without increasing the incidence of side effects, which is worthy of promoting the application of iodine-125 seed implantation.

1. Introduction

Primary liver cancer is a common malignant tumor in clinical practice, which tends to occur in people aged 40–50 years, and the incidence of in primary liver cancer in men is slightly higher than that in women. The incidence of primary liver cancer was slightly higher in men than in women. The pathogenesis of primary liver cancer has not been clarified, but is generally believed to be related to cirrhosis viral hepatitis and chemical carcinogens such as aflatoxin [1]. Due to the lack of typical clinical symptoms in the early stage of primary liver cancer, with the prolongation of the course of the disease, the clinical manifestations are mostly liver pain, systemic and digestive tract symptoms, and liver enlargement, leading to great difficulty in clinical diagnosis and treatment; therefore, most patients are diagnosed in the middle and late stages [2, 3]. Chemotherapy is a common method for the clinical treatment of primary liver cancer.

Chemotherapy drugs can kill tumor cells and prolong the life of patients [4]. However, the incidence of side effects of chemotherapy is high, and drugs can affect normal cells, leading to poor treatment tolerance and compliance of patients [5, 6]. Iodine-125 (^{125}I) seed implantation can continuously emit gamma rays through implanting ^{125}I seeds from a tiny radioactive source, which can damage tumor cells, cause DNA double-strand emission break, and cause the loss of the proliferation ability of tumor cells [7, 8].

However, there are few clinical studies on the effect of iodine-125 seed implantation combined with chemotherapy on the level of Th1/Th2 cells in peripheral blood of patients with primary liver cancer. Therefore, this study took patients with primary liver cancer as the object to explore the clinical effect of iodine-125 seed implantation combined with chemotherapy in patients with primary liver cancer.

2. Materials and Methods

2.1. Clinical Data. A total of 136 patients with primary liver cancer from April 2017 to June 2018 at Renmin Hospital of Wuhan University, Wuhan, China, were prospectively selected as the subjects and randomly divided into two groups, control group and observation group. In the control group, there were 68 patients, 41 males and 27 females, age 44–68 years, average 56.71 ± 5.69 years old. Body mass index (BMI) was 18–29 kg/m^2, with an average of 23.51 ± 3.48 kg/m^2. Liver function grade: grade A (13 cases), grade B (32 cases), and grade C (23 cases). Complications: 4 cases of hypertension, 6 cases of diabetes, and 5 cases of hyperlipidemia. In the observation group, there were 68 patients, 39 males and 29 females, aged 43–69 years, with an average of 56.79 ± 5.83 years old. BMI was 17–28 kg/m^2, with an average of 23.58 ± 3.52 kg/m^2. The liver function grade: grade A (11 cases), grade B (33 cases), and grade C (24 cases). Complications: 5 cases of hypertension, 4 cases of diabetes, and 6 cases of hyperlipidemia. The demographic characteristics of patients are shown in Table 1. This study was approved by the ethics committee of the Renmin Hospital of Wuhan University, and all patients signed informed consent.

2.2. Inclusion and Exclusion Criteria. The inclusion criteria were as follows: (1) all patients met the diagnostic criteria for primary liver cancer [9, 10] and were diagnosed by CT-guided percutaneous liver biopsy. (2) It meets the indications for iodine-125 seed implantation combined with chemotherapy and is tolerated by all patients. (3) Complete baseline and follow-up data were available. The exclusion criteria were as follows: (1) patients with mental abnormalities and other malignant tumors or associated with autoimmune system diseases; (2) patients with severe cardiac and renal dysfunction or abnormal coagulation function; (3) metastatic hepatic carcinoma or liver cyst.

2.3. Methods. After admission, both groups were routinely given liver-protective treatment to strengthen nutritional support intervention for patients. Liver-protective drugs were routinely given to patients with cirrhosis to improve liver function and inhibit the progression of cirrhosis. At the same time, routine antiviral treatment intervention was strengthened for patients [11]. The right femoral artery was intubated through the skin. After a successful puncture, the catheter was selectively intubated and reached the common hepatic artery. Digital subtraction angiography (DSA) was completed, intrahepatic tumor staining was visible, and chemotherapy drugs were injected. Chemotherapy drugs used were epirubicin (Shenzhen Main Luck Pharmaceuticals Inc., National Drug Approval no. H10930106, specification: 20 mg) 40–60 mg, 5-fluorouracil (Heilongjiang Fuhe Huaxing Pharmaceutical Group Co., Ltd., National Drug Approval no. H23021711, specifications:10 mL, 0.25 g) 0.75–1 g, mitomycin (Jiangsu Hengrui Medicine Co., Ltd., National Drug Approval no. H20023070) 6–12 mg, and 30 mL superliquefied iodide oil (Guerbet, Hong Kong, China). The patients were treated once every 4 weeks for 3 months (3 courses) [12].

Observation group: on the basis of the control group, iodine-125 seed implantation was combined. The radioactive seed implantation planning system was used to delineate the treatment target area (i.e., primary tumor and intrahepatic metastases) and set the puncture path for ^{125}I seed, and the treatment was carried out according to the principle of 100.0% prescription dose covering 95.0% planned target area to determine the quantity and dose of iodine-125 seed implantation. After the above procedures, ^{125}I seeds were routinely implanted into the lesions with the aid of a particle gun according to the implantation plan, followed by CT scan for reexamination and verification. After 3 months of treatment, the curative effect was investigated. All patients were followed up for 36 months.

2.4. Observation Indicators.

(1) Serum tumor markers: peripheral fasting blood (3 mL) was collected on the day before treatment and the day after 3 months of treatment, respectively. Peripheral fasting blood was stored at −80°C. After centrifugation, the electrochemiluminescence was carried out to determine the level of alpha-fetoprotein (AFP) [13]. Enzyme-linked immunosorbent assay was utilized to determine the levels of alpha-fetoprotein variants (AFP-L3) and Golgi body protein 73 (GP73) [14]. (2) Th1/Th2 cells in peripheral blood: serum specimens were collected from the isolated peripheral blood samples and then stored at −80°C. The levels of Th1 (including interleukin-2 (IL-2) and tumor necrosis factor-α (TNF-α)) and Th2 cells (interleukin-4, 6, and 10) in peripheral blood of patients were determined by the enzyme-linked immunosorbent assay [15, 16]. (3) Side effect and recurrence rates: the incidence of leukopenia, thrombocytopenia, and gastrointestinal reactions in the two groups was recorded. After the treatment, both groups were followed up for 36 months, and the recurrence rates were recorded at 12, 24, and 36 months after the treatment.

Table 1: The demographic characteristics of patients.

Demographic characteristics (n)	Control group ($n = 68$)	Observation group ($n = 68$)
Male	41	39
Female	27	29
Age ($\overline{\chi} \pm$ SD)	44–68 (56.71 ± 5.69)	43–69 (56.79 ± 5.83)
BMI ($\overline{\chi} \pm$ SD)	18–29 (23.51 ± 3.48)	17–28 (23.58 ± 3.52)
Liver function grade		
Grade A	13	11
Grade B	32	33
Grade C	23	24
Complications		
Hypertension	4	5
Diabetes	6	4
Hyperlipidemia	5	6

2.5. Statistical Analysis. SPSS 24.0 software was applied to analyze the data. The enumeration data were tested by χ^2 test and represented by N (%), while the measurement data were tested by t-test and represented by ($\overline{x} \pm s$). $P < 0.05$ was considered statistically significant.

3. Results

3.1. Comparison of Tumor Markers before and after Treatment. Before treatment, the levels of tumor markers in the two groups were not statistically significant ($P > 0.05$). Three months after treatment, the levels of serum tumor markers in both groups were lower than those before treatment ($P < 0.05$). Three months after treatment, the levels of tumor markers (AFP, AFP-L3, and GP73) in the observation group were lower than those in the control group ($P < 0.05$), as shown in Table 2.

3.2. Comparison of Th1/Th2 Cells between the Two Groups. Before treatment, the levels of Th1/Th2 cells were not statistically significant between the observation group and control group ($P > 0.05$). Three months after treatment, the level of Th1 cells in both groups was higher than that before treatment ($P < 0.05$). The level of Th2 cells was lower than before treatment ($P < 0.05$). The level of IL-2 and TNF-α in Th1 cells of the observation group was higher than that of the control group at 3 months after treatment ($P < 0.05$), whereas the levels of IL-4, IL-6, and IL-10 in Th2 cells of the observation group were lower than those in the control group ($P < 0.05$), as shown in Table 3.

3.3. Comparison of Side Effects and Recurrence Rate between the Two Groups. There was no statistical significance in the incidence of leucopenia, thrombocytopenia, and gastrointestinal reactions between the observation group and control group ($P > 0.05$). The recurrence rate of the observation group at 12, 24, and 36 months after treatment was lower than that of the control group ($P < 0.05$), as shown in Table 4.

4. Discussion

Chemotherapy is the preferred treatment for patients with primary liver cancer; transarterial chemoembolization (TACE) is the main treatment [17, 18]. High concentration of chemotherapeutic drugs can be injected into the tumor lesions, and then the tumor supplying blood vessels can be embolized through an embolization agent, which can make the tumor inactivated under the dual effects of ischemia and hypoxia. At the same time, through the injection of chemotherapy drugs, the effect of toxic inactivating of tumor cells can be achieved, playing a good antitumor effect. Previous studies showed that the application of TACE in patients with primary liver cancer is helpful to improve the quality of life, but with the extension of the chemotherapy cycle, the incidence of clinical drug resistance is higher, leading to poor patient prognosis [19]. In recent years, iodine-125 seed implantation combined with chemotherapy has been applied in patients with primary liver cancer with satisfactory results [20, 21]. In this study, 3 months after treatment, the levels of tumor markers (AFP, AFP-L3, and GP73) in the observation group were lower than those in the control group ($P < 0.05$), indicating that iodine-125 seed implantation combined with chemotherapy is beneficial to reduce the level of tumor markers in patients with primary liver cancer and is conducive to the recovery of patients. Iodine-125 seed implantation continuously emits gamma rays, which is conducive to the destruction of tumor tissue, causes the DNA double-strand emission break, and causes the loss of tumor cell activity [22–24]. At the same time, γ-rays have a direct damage effect on the tumor DNA molecular chain, can also ionize water molecules in the body, produce free radicals and biological molecular interaction, and further aggravate the tumor tissue cell damage. Some Chinese scholars [25] took 76 patients with advanced primary liver cancer as the subjects and gave them chemotherapy combined with iodine-125 seed implantation. The results showed that the tumor control rate of patients was 85.8%. In this study, the incidence of leucopenia, thrombocytopenia, and gastrointestinal reactions between the

Table 2: Comparison of tumor markers before and after treatment.

Group	n	AFP (ug/L)		AFP-L3 (ng/mL)		GP73 (ng/mL)	
		Before treatment	Three months after treatment	Before treatment	Three months after treatment	Before treatment	Three months after treatment
Observation group	68	57.93 ± 5.61	$14.61 \pm 3.49^{\#}$	8.12 ± 0.69	$3.29 \pm 0.41^{\#}$	92.41 ± 7.46	$51.24 \pm 4.51^{\#}$
Control group	68	57.97 ± 5.64	$32.53 \pm 4.59^{\#}$	8.14 ± 0.72	$5.63 \pm 0.63^{\#}$	92.45 ± 7.49	$71.52 \pm 6.05^{\#}$
T	—	1.593	7.846	0.951	6.315	1.229	8.893
P	—	0.315	0.000	0.692	0.000	0.646	0.000

$^{\#}P < 0.05$ vs. before treatment.

Table 3: Comparison of Th1/Th2 cell levels between the two groups.

Group		IL-2 (pg/mL)	TNF-α (pg/mL)	IL-4 (pg/mL)	IL-6 (pg/mL)	IL-10 (pg/mL)
Observation group ($n = 68$)	Before treatment	16.92 ± 2.51	1.28 ± 0.51	174.34 ± 11.69	19.43 ± 3.21	9.83 ± 0.52
	Three months after treatment	$23.59 \pm 3.69^{\#*}$	$1.74 \pm 0.64^{\#*}$	$98.87 \pm 15.41^{\#*}$	$13.23 \pm 2.14^{\#*}$	$4.26 \pm 0.43^{\#*}$
Control group ($n = 68$)	Before treatment	16.94 ± 2.54	1.29 ± 0.53	176.41 ± 24.81	19.45 ± 3.24	9.84 ± 0.54
	Three months after treatment	$20.12 \pm 3.24^{*}$	$1.45 \pm 0.59^{*}$	$123.59 \pm 18.42^{*}$	$16.69 \pm 3.02^{*}$	$7.19 \pm 0.49^{*}$

$^{\#}P < 0.05$ vs. the control group. $^{*}P < 0.05$ vs. before treatment.

Table 4: Comparison of side effects and recurrence rate between the two groups.

Group	n	Side effect			Recurrence rate		
		Leucopenia	Thrombocytopenia	Gastrointestinal reactions	12 months	24 months	36 months
Observation group	68	3 (4.41)	4 (5.88)	2 (2.94)	1 (1.47)	4 (5.88)	8 (11.76)
Control group	68	4 (5.88)	5 (7.35)	1 (1.47)	7 (10.29)	17 (25.00)	24 (35.29)
x^2	—		0.061		4.781	9.517	10.462
P	—		0.805		0.029	0.002	0.001

observation group and control group had no statistical significance, whereas the recurrence rate of the observation group at 12, 24, and 36 months after treatment was lower than that of the control group ($P < 0.05$), indicating that iodine-125 seed implantation combined with chemotherapy in the treatment of primary liver cancer is safe and can improve the survival of patients.

Helper T lymphocytes play a crucial role in the occurrence and development of primary liver cancer. Clinically, helper T lymphocytes can be divided into two subsets, Th1 and Th2, according to the cytokines secreted by helper T lymphocytes. Th1 can secrete IL-2 and TNF-α, whereas Th2 cells can secrete IL-4, IL-6, and IL-10. In the normal human body, Th1 and Th2 maintain a dynamic balance [26]. Previous studies [27] have shown that Th1 can enhance the cytotoxic effect of killing cells and mediate cellular immunity. On the contrary, Th2 can promote the production of antibodies, inhibit Th1 cells, and mediate humoral immunity. For patients with primary liver cancer, Th1 cells will be in a dominant state, and the body has active immunity to the tumor. However, with the continuous development of the disease course, Th1 cells will drift to Th2 cells, and the antitumor response of the body will be inhibited. Therefore, the current study investigated the effect of iodine-125 seed implantation combined with chemotherapy on the level of Th1/Th2 in peripheral blood of patients with primary liver cancer. The results showed that the level of IL-2 and TNF-α in Th1 cells in the observation group was higher than that in the control group at 3 months after treatment ($P < 0.05$), whereas the levels of IL-4, IL-6, and IL-10 in Th2 cells were lower than those in the control group ($P < 0.05$) indicating that iodine-125 seed implantation combined with chemotherapy in patients with primary liver cancer can maintain the balance of Th1/Th2 cells in peripheral blood, enhance the body's immunity, and facilitate the recovery of patients. Clinically, iodine-125 seed implantation combined with chemotherapy in patients with primary liver cancer can exert the advantages of different treatment methods, help to maintain the body's immune level, and achieve good results. In this study, the recurrence rate of the observation group at 12, 24, and 36 months after treatment was lower than that of the control group ($P < 0.05$).

We are the first to study the changes of Th1/Th2 cell levels in peripheral blood of patients with iodine-125 seed implantation combined with chemotherapy in the treatment of primary liver cancer and, for the first time, to elucidate the effect of this combination therapy on the immune system. However, the mechanism of its influence still needs further study.

In conclusion, iodine-125 seed implantation combined with chemotherapy in patients with primary liver cancer can reduce the level of serum tumor markers, improve the level

of Th1/Th2 cells in peripheral blood, and reduce the recurrence rate of patients without increasing the incidence of side effects, which is worthy of promotion and application.

Data Availability

The data used to support the findings of this study are available from the corresponding author upon request.

Disclosure

Xiaoyan Chen and Fan Zhu are the co-first authors.

Conflicts of Interest

The authors declare that they have no conflicts of interest.

References

[1] Y. D. Z. Xihui and C. Li, "Preliminary study on radiofrequency ablation of primary hepatocellular carcinoma with radiofrequency implantation," *Chinese Medical Journal*, vol. 100, no. 17, pp. 1310–1314, 2020.

[2] Y. X. Gao, T. W. Yang, J. M. Yin et al., "Progress and prospects of biomarkers in primary liver cancer (review)," *International Journal of Oncology*, vol. 57, no. 1, pp. 54–66, 2020.

[3] W. T. W. Yonghua, "Clinical application and progress of transcatheter arterial chemoembolization combined with $\sim^{(125)}$I radioactive particles in the treatment of liver cancer," *Chinese Journal of Nuclear Medicine and Molecular Imaging*, vol. 39, no. 2, pp. 112–115, 2019.

[4] W. Z. L. Jiahuan, "Efficacy of ^{125}I radiation seed implantation combined with hepatic artery embolization in the treatment of primary liver cancer and its effect on the expression of TRF1 and TRF2 in liver," *Liver*, vol. 25, no. 4, pp. 402–406, 2020.

[5] H. Y. L. Hong and W. Xin, "Clinical study of iodine-125 seed implantation brachytherapy combined with chemotherapy in the treatment of advanced non-small cell lung cancer in the elderly," *Journal of Practical Hepatology*, vol. 23, no. 2, pp. 268–271, 2020.

[6] J. C. Mejia and J. Pasko, "Primary liver cancers," *Surgical Clinics of North America*, vol. 100, no. 3, pp. 535–549, 2020.

[7] W. B. L. Chunrong and X. Debing, "Clinical study of iodine-125 seed implantation brachytherapy combined with chemotherapy in the treatment of advanced non-small cell lung cancer in the elderly," *Guangxi Medical Journal*, vol. 42, no. 19, pp. 2487–2491, 2020.

[8] Z. H. M. Yan and W. Shufen, "Expression of BUB1B in primary hepatocellular carcinoma and its effect on proliferation and invasion of hepatocellular carcinoma cells," *Journal of New Medicine*, vol. 50, no. 4, pp. 272–277, 2019.

[9] A. Mori, A. Arimoto, Y. Hamaguchi, M. Kajiwara, A. Nakajima, and S. Kanaya, "Risk factors and outcome of portal vein thrombosis after laparoscopic and open hepatectomy for primary liver cancer: a single-center experience," *World Journal of Surgery*, vol. 44, no. 9, pp. 3093–3099, 2020.

[10] National Health and Family Planning Commission, "Guidelines for diagnosis and treatment of primary liver cancer (2017 edition)," *Journal of Clinical Hepatology*, vol. 33, no. 8, pp. 1419–1431, 2017.

[11] L. G. Z. Dong and S. Zhongpei, "Effects of addy injection combined with hepatic arterial chemoembolization on vascular growth factors and cellular immune function in patients with primary liver cancer," *Journal of Hainan Medical University*, vol. 25, no. 23, pp. 1770–1775, 2019.

[12] T. Li, X. Zhang, S. Xu, H. Cheng, and H. Zhang, "Effectiveness and safety of adjunctive traditional Chinese medicine therapy for primary liver cancer patients," *Medicine*, vol. 99, no. 31, Article ID e21281, 2020.

[13] L. Y. L. Xiao and S. Chunhui, "Clinical observation of iodine-125 seed implantation combined with chemotherapy in 18 cases of small cell lung cancer," *Journal of Oncology*, vol. 25, no. 3, pp. 268–270, 2019.

[14] W. L. T. Wenjuan and G. Min, "Clinical study on the effect of tonifying kidney and promoting blood circulation combined with active immunotherapy on serum Th1 and Th2 cytokines and related hormones in recurrent homoimmune abortion," *World Journal of Traditional Chinese Medicine*, vol. 14, no. 5, pp. 1258–1261, 2019.

[15] Z. T. W. Yue and Y. Zhendong, "Effect of TIPS combined with ^{125}I seed implantation in the treatment of main portal emboli and complications of liver cancer," *Journal of Interventional Radiology*, vol. 29, no. 1, pp. 89–95, 2020.

[16] Y. T. Z. Lixin and W. Qiang, "Efficacy of ultrasound-guided microwave ablation combined with TACE in the treatment of advanced primary liver cancer and its effect on immune function," *Chinese Journal of Ultrasound in Medicine*, vol. 36, no. 5, pp. 428–432, 2020.

[17] L.-C. Chen, W.-Y. Chiou, H.-Y. Lin et al., "Comparing stereotactic ablative radiotherapy (SABR) versus re-trans-catheter arterial chemoembolization (re-TACE) for hepatocellular carcinoma patients who had incomplete response after initial TACE (TASABR): a randomized controlled trial," *BMC Cancer*, vol. 19, no. 1, p. 275, 2019.

[18] T. Zhang, W. Huang, H. Dong, and Y. Chen, "Trans-catheter arterial chemoembolization plus sorafenib, an unsuccessful therapy in the treatment of hepatocellular carcinoma?" *Medicine*, vol. 99, no. 29, Article ID e20962, 2020.

[19] J.-C. Nault, A.-L. Cheng, B. Sangro, and J. M. Llovet, "Milestones in the pathogenesis and management of primary liver cancer," *Journal of Hepatology*, vol. 72, no. 2, pp. 209–214, 2020.

[20] J. Luo, J. P. Zheng, G. L. Shao et al., "[Comparison of therapeutics effects of transcatheter arterial chemoembolization combined with iodine-125 seed implantation and sorafenib for the treatment of hepatocellular carcinoma with portal vein tumor thrombosis]," *Zhonghua Gan Zang Bing Za Zhi = Zhonghua Ganzangbing Zazhi = Chinese Journal of Hepatology*, vol. 26, no. 4, pp. 298–304, 2018.

[21] Z.-X. Zhu, X.-X. Wang, K.-F. Yuan, J.-W. Huang, and Y. Zeng, "Transarterial chemoembolization plus iodine-125 implantation for hepatocellular carcinoma: a systematic review and meta-analysis," *HPB*, vol. 20, no. 9, pp. 795–802, 2018.

[22] Y. Yang, Z.-H. Ma, X.-G. Li et al., "Iodine-125 irradiation inhibits invasion of gastric cancer cells by reactivating microRNA-181c expression," *Oncology Letters*, vol. 12, no. 4, pp. 2789–2795, 2016.

[23] N. Idota, M. Nakamura, K. Masui, Y. Kakiuchi, K. Yamada, and H. Ikegaya, "Lessons learned from autopsying an unidentified body with iodine-125 seeds implanted for prostate brachytherapy," *Journal of Forensic Sciences*, vol. 62, no. 2, pp. 536–540, 2017.

[24] Z.-H. Ma, Y. Yang, L. Zou, and K.-Y. Luo, "^{125}I seed irradiation induces up-regulation of the genes associated with apoptosis and cell cycle arrest and inhibits growth of gastric

cancer xenografts," *Journal of Experimental & Clinical Cancer Research*, vol. 31, no. 1, p. 61, 2012.

[25] Z. Y. W. Xiao and Y. Miao, "Effect of radioactive iodine seed implantation on immune function and therapeutic effect in patients with primary liver cancer," *Oncology Progress*, vol. 17, no. 4, pp. 435–438, 2019.

[26] L. M. L. Ping and W. Wei, "Effect of heatongxiao granules combined with hepatic arterial chemoembolization in the treatment of primary hepatocellular carcinoma and its effect on interleukin-12 interleukin-10 interferon," *Chinese General Practice*, vol. 22, no. 18, pp. 2230–2236, 2019.

[27] C. L. L. Wang and B. Li, "Feasibility evaluation of electromagneticpositioning and navigation ^{125}I seed implantation in the treatment of advanced primary liver cancer," *Journal of Clinical and Experimental Medicine*, vol. 18, no. 14, pp. 1525–1528, 2019.

Hindawi
Journal of Oncology
Volume 2021, Article ID 2102890, 9 pages
https://doi.org/10.1155/2021/2102890

Research Article

Upregulation of ECT2 Predicts Adverse Clinical Outcomes and Increases 5-Fluorouracil Resistance in Gastric Cancer Patients

Hua Zhang,[1] **Yuan Geng**,[2] **Chunhui Sun**,[3] **and Jin Yu**[4]

[1]*Department of Pharmacy, Yantaishan Hospital, Yantai 264000, Shandong, China*
[2]*Department of Obstetrics, Medical Insurance Office, Qingdao Municipal Hospital, Qingdao 266000, Shandong, China*
[3]*Department of Hepatobiliary Surgery, The Third People's Hospital of Qingdao, Qingdao 266041, Shandong, China*
[4]*Department of Oncology, Jinan Central Hospital, Cheeloo College of Medicine, Shandong University, Jinan 250013, Shandong, China*

Correspondence should be addressed to Jin Yu; guaojingq@163.com

Received 1 July 2021; Revised 15 July 2021; Accepted 16 July 2021; Published 28 July 2021

Academic Editor: Muhammad Wasim Khan

Background. The abnormal expression and prognosis prediction of epithelial cell transforming sequence 2 (ECT2) in gastric cancer (GC) has been reported. However, the effect of ECT2 on 5-fluorouracil (5-Fu) resistance in GC is unclear. This research aims to solve the abovementioned problems. *Methods*. Gene expression was detected by RT-qPCR and Western blot analysis. Cell viability was evaluated by the colony formation assay, MTT assay, and flow cytometric analysis. Transwell and wound healing assays were used to detect cell metastasis. *Results*. Upregulation of ECT2 was found in stomach adenocarcinoma (STAD) and GC tissues. In addition, high ECT2 expression can predict adverse clinical outcomes in GC patients. More importantly, ECT2 knockdown weakened the resistance of 5-FU in GC cells. ECT2 silencing reduced the cell migratory and invasive abilities of GC cells treated with 5-FU. We also found that downregulation of ECT2 increased 5-FU sensitivity in GC cells by downregulating P-gp, MRP1, and Bcl-2. *Conclusion*. Upregulation of ECT2 can predict adverse clinical outcomes and increase 5-FU resistance in GC patients.

1. Introduction

Gastric cancer (GC) is one of the cancers with the highest incidence in the world [1]. Various gastric diseases, *Helicobacter pylori* (Hp) infection, poor diet, environment, and genetics can cause GC [2]. The incidence of GC increases significantly with age, and the peak age of onset is 50–80 years [3]. China is a high incidence area of GC. GC accounts for nearly a quarter of cancer deaths in China [4]. Moreover, the early diagnosis rate of GC is low, about 10%. Most patients with GC are in the middle and advanced stages at the time of diagnosis. The 5-year survival rate is about 7–34% [5]. Recently, more and more methods are being used to treat GC, such as radiotherapy, chemotherapy, cell membrane-derived biomimetic nanotechnology, and cancer nanomedicine [6, 7]. Preoperative chemotherapy can shrink the tumor and increase the chance of radical surgery and cure. However, the resistance of cancer cells to chemotherapy drugs can lead to chemotherapy failure [8]. Therefore, exploring new methods to weaken the drug resistance of cancer cells is of great significance to improve the success rate of chemotherapy.

Commonly used chemotherapy drugs are 5-fluorouracil (5-Fu), tegafur, mitomycin, doxorubicin, paclitaxel, cisplatin, or carboplatin [9, 10]. Many studies have shown that no-coding RNAs or genes can affect the resistance of cancer cells. For example, TRIM37 increased the resistance to CDDP in GC [11]. MiR-95-3p acted as a contributing factor for cisplatin resistance in human GC cells by targeting EMP1/PI3K/AKT signaling [12]. The exosomal miR-223 enhanced the resistance of doxorubicin in GC [13]. In addition, it was found that upregulation of KLF17 increased 5-Fu sensitivity in GC cells [14]. Here, the effect of ECT2 on 5-Fu resistance was investigated in GC.

ECT2 has been found to be involved in the development of various human cancers. Increased expression of ECT2 has been found in many malignant tumors, such as breast cancer [15], cholangiocarcinoma [16], and hepatocellular carcinoma [17]. Functionally, the ECT2/PSMD14/PTTG1 axis promoted the proliferation of gliomas by stabilizing E2F1 [18]. The inhibition of ECT2 induced by small interfering RNA suppressed the progression of osteosarcoma [19]. ECT2 overexpression also promoted the polarization of tumor-associated macrophages in hepatocellular carcinoma [20]. More importantly, upregulation of ECT2 has been found in stomach adenocarcinoma (STAD) and GC tissues [21]. However, the effect of ECT2 on 5-Fu resistance in GC cells has not been reported yet.

Here, the expression level of ECT2 was first detected in GC. The correlation between the expression of ECT2 and the clinical outcome of GC patients was also confirmed. In addition, we have also explored how ECT2 affects 5-Fu resistant in GC cells. Our research may provide a new way of thinking about weakening 5-Fu resistance.

2. Materials and Methods

2.1. Patients. Tissue samples of 66GC patients were collected from Jinan Central Hospital between July 2018 and July 2020. The content of the study is informed to everyone, and we have obtained their informed consents. All participants received only surgical treatment. Our study was approved by the Institutional Ethics Committee of Jinan Central Hospital.

2.2. Bioinformatics Analysis. The expression and prognosis of ECT2 in GC patients were analyzed by box plots and survival plots in the GEPIA database (http://gepia.cancer-pku.cn/).

2.3. Cell Culture and Transfection. Normal gastric mucosal cell lines GES-1 and AGS and NCI-N87GC cells were purchased from ATCC (Manassas, VA, USA). The above cells were cultured in RPMI-1640 medium (Gibco, USA) containing 10% FBS (37°C, 5% CO_2). ECT2 siRNA (si-ECT2) and si-control (si-NC) were purchased from GenePharma (Shanghai, China). Lipofectamine 2000 (Invitrogen, Carlsbad, USA) was used for cell transfection according to the manufacturer's instructions.

2.4. RT-qPCR. The total RNA was extracted with TRIzol reagent (Thermo Fisher Scientific). PrimeScript-RT Kit (Madison, WI, USA) was used to synthesize complementary DNA (cDNA). RT-qPCR was performed using SYBR® Premix-Ex-Taq™ (Takara, TX, USA). The internal reference is GAPDH. The specific primer pairs were as follows: ECT2, sense: 5′-ACT ACT GGG AGG ACT AGC TTG-3′ and antisense: 5′-CAC TCT TGT TTC AAT CTG AGG CA-3′; GAPDH, sense: 5′-GGA GCG AGA TCC CTC CAA AAT-3′ and antisense: 5′-GGC TGT TGT CAT ACT TCT CAT GG-3′. The $2^{-\triangle\triangle ct}$ method was used to measure the relative expression of ECT2.

2.5. Western Blot Analysis. Protein samples were isolated by using RIPA lysis buffer (Beyotime Biotechnology). Then, the protein samples were separated by 10% SDS-PAGE. After transferring to the PVDF membrane, the protein was blocked with 5% skimmed milk. Next, the protein samples were incubated with Bax, Bcl-2, MRP1, P-gp, GST-π, and GAPDH primary antibodies (Abcam, Cambridge, MA, USA) at 4°C overnight. After washing 3 times, the protein samples were incubated with the corresponding secondary antibody (Abcam, USA) for 2 h. Finally, the ECL detection system (Thermo Fisher Scientific, Inc.) was used to visualize the blots. The relative level of protein expression was analyzed using ImagePro plus software (version 6.0; Media Cybernetics Inc., Rockville, MD, USA) and is represented as the density ratio versus GAPDH.

2.6. Cell Viability Assay. The half maximal inhibitory concentration (IC50) of AGS on 5-FU was detected by the MTT assay. AGS cells were cultured in 96-well plates for 24 h. Next, different concentrations of 5-FU were added to treat the AGS cells for 48 h. After that, MTT solution was added to incubate the cells at 37°C for 4 h. Finally, the absorbance value (OD = 490 nm) was measured.

2.7. Colony Formation Assay. The transfected AGS cells were cultured in 6-well plates (1000 cells/well) for three days. Then, 5-FU was added to treat the cells for 10 days. Next, the cells were stained with 0.1% crystal violet. Finally, colonies were observed by a light microscope.

2.8. Flow Cytometric Analysis. The transfected AGS cells were suspended in Annexin-binding buffer and harvested. Then, the cells were stained with Annexin V/FITC and PI solution (KeyGEN Biotech, Nanjing, China) and incubated in the dark for 15 min at room temperature. Finally, flow cytometry analysis was used to assess cell apoptosis.

2.9. Wound Healing Assay. AGS cells (1×10^3 cells/well) were cultured in a 6-well plate for 24 h. After reaching 90% confluence, scratches were generated by a 200 μl pipette tip. A light microscope was used to evaluate the wound width at 0 and 24 h. Images were captured by THUNDER Imagers (Leica Microsystems). Wound distance was quantified by ImageJ Software version 1.6 (National Institutes of Health, Bethesda, MD, USA).

2.10. Transwell Assay. Cell migration and invasion were analyzed by performing transwell assays. Transwell chambers (8 μm pore size; Millipore) were applied to evaluate cell migration and invasion. For the invasion assay, AGS cells

(4×10^3 cells/well) were added into the upper chamber, which was precoated with Matrigel (3.9 ug/ul). For the migration assay, AGS cells (4×10^3 cells/well) were added into the upper chamber, which was not precoated with Matrigel. Lower chamber was added with RPMI-1640 medium (10% FBS). Following incubation for 24 h at 37°C with 5% CO_2, the migrated and invasive cells were stained with 0.1% crystal violet. The number of moved cells was observed under a light microscope.

2.11. Statistical Analysis. GraphPad Prism 6 or SPSS 21.0 is used to analyze experimental data. The results are shown as mean ± SD. The difference among groups was analyzed by using the chi-squared test or one-way ANOVA with the Bonferroni post hoc test. Significant difference means $p < 0.05$.

3. Results

3.1. Upregulation of ECT2 Predicts Adverse Clinical Outcomes in GC Patients. First, the expression level of ECT2 was analyzed in the GEPIA database (http://gepia.cancer-pku.cn/). Compared with the control, the expression of ECT2 was increased in stomach adenocarcinoma (STAD) tissues ($p < 0.05$, Figure 1(a)). Consistently, upregulation of ECT2 in GC tissues was also found in GC samples ($p < 0.05$, Figure 1(b)). In addition, the GEPIA database showed that GC patients with high ECT2 expression had a reduced overall survival (OS) rate ($p < 0.05$, Figure 1(c)). We also found that the high expression of ECT2 was related to lymph node metastasis and TNM stage in GC patients ($p < 0.05$, Table 1). These findings imply that ECT2 may affect the development of GC.

3.2. Knockdown of ECT2 Enhances 5-FU Sensitivity in GC Cells. Next, the expression of ECT2 in GC cells was measured. Compared with GES-1, ECT2 expression was increased in AGS and NCI-N87GC cells ($p < 0.05$, Figure 2(a)). In order to verify the effect of ECT2 on the sensitivity of 5-FU in GC cells, si-ECT2 or si-NC was transfected into AGS cells. Compared with the si-NC group, si-ECT2 reduced the expression of ECT2 in AGS cells ($p < 0.01$, Figure 2(b)). In addition, the downregulation of ECT2 enhanced the sensitivity of 5-FU in AGS cells ($p < 0.01$, Figure 2(c)). The IC50 value of the si-ECT2 group was higher than that of the si-NC group ($p < 0.05$, Figure 2(d)). At the same time, the colony formation assay also showed that knockdown of ECT2 weakened the cloning ability of AGS cells treated with 5-FU ($p < 0.05$, Figure 2(e)). The apoptosis of AGS cells treated with 5-FU was promoted by downregulation of ECT2 ($p < 0.05$, Figure 2(f)). In short, ECT2 knockdown weakens 5-FU resistance in GC cells.

3.3. ECT2 Silencing Inhibits the Metastasis of GC Cells Treated by 5-FU. In order to further explore the role of ECT2 in the development of GC, the effect of ECT2 on the metastasis of 5-FU-treated AGS cell was also investigated. Both the wound healing assay and the transwell assay showed that ECT2 downregulation significantly inhibited cell migration in AGS cells treated with 5-FU ($p < 0.05$, Figures 3(a) and 3(b)). Compared with the si-NC group, cell invasion was also suppressed by ECT2 silencing in AGS cells treated with 5-FU ($p < 0.01$, Figure 3(c)). Briefly, ECT2 silencing reduced the migratory and invasive ability of 5-FU-treated GC cells.

3.4. ECT2 Downregulation Increases the 5-FU Sensitivity of GC Cells by Inhibiting P-gp, MRP1, and Bcl-2. Finally, the effect of ECT2 on P-gp, MRP1, and GST-π related to drug resistance was investigated to explore the regulatory mechanism of ECT2 on 5-FU sensitivity of GC cells. We found that the expression of P-gp and MRP1 in the si-ECT2 group was significantly reduced ($p < 0.05$, Figure 4(a)). However, ECT2 has little effect on GST-π expression. In addition, we also explored how ECT2 regulates the apoptosis-related proteins Bcl-2 and Bax. Downregulation of ECT2 reduced Bcl-2 expression and enhanced Bax expression in AGS cells treated with 5-FU ($p < 0.05$, Figure 4(b)). Taken together, ECT2 affects the 5-FU sensitivity of GC cells by regulating cell viability, metastasis, and apoptosis-related proteins (Figure 5).

4. Discussion

Recently, important functions of ECT2 have been discovered in many human diseases. In addition, the effect of ECT2 on chemoresistance has also been investigated in previous studies. For example, ECT2 can regulate the growth of triple-negative breast cancer cells through the intervention of paclitaxel [22]. In this study, the effect of ECT2 on 5-FU resistance was explored in GC cells. ECT2 expression was increased in STAD and GC tissues. Previous study also proposed the upregulation of ECT2 in STAD and GC tissues [21]. In addition, high ECT2 expression can predict adverse clinical outcomes in GC patients. More importantly, ECT2 knockdown weakened the resistance of 5-FU in GC cells. ECT2 silencing reduced the migratory and invasive ability of GC cells treated with 5-FU. The above findings reveal that ECT2 may act as a tumor promoter in the progression of GC and increase 5-Fu resistance in GC patients.

Consistent with our results, Yan Chen et al. also found the upregulation and carcinogenic effects of ECT2 in GC [23]. In addition, upregulation of ECT2 also related to the poor prognosis of GC patients [24]. The same result is also found in our research. Besides that, it has been found that upregulation of ECT2 can predict adverse clinical outcomes in GC [25]. The histologic differentiation, TNM stages, and lymph node metastasis were related to ECT2 expression in GC patients [26]. This study also demonstrated the same conclusion. Functionally, upregulation of ECT2 promoted the tumor progression of renal cell carcinoma [27]. Overexpression of ECT2 also promoted the growth and metastasis of pancreatic cancer cells [28]. In this study, ECT2 silencing

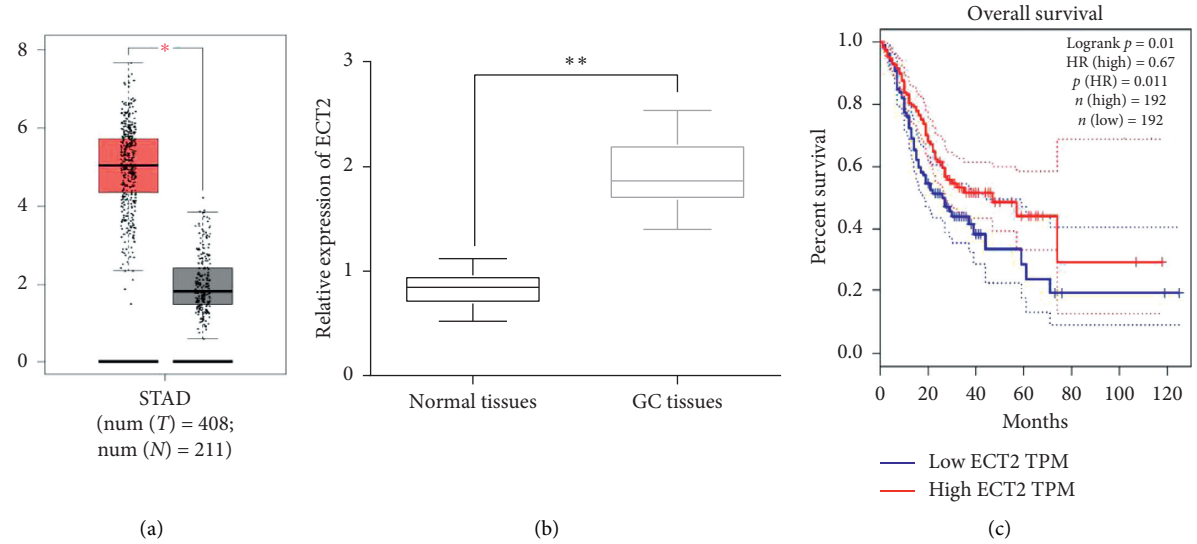

Figure 1: Upregulation of ECT2 predicting adverse clinical outcomes in GC patients. (a) ECT2 mRNA expression in STAD tissues ($n = 408$) and normal tissues ($n = 211$) analyzed in the GEPIA database. (b) ECT2 expression in 66GC tissues and adjacent normal tissues ($n = 66$). (c) OS rate was compared in GC patients with low or high ECT2 expression ($n = 192$). $^{*}P < 0.05$. $^{**}P < 0.01$.

Table 1: Relationship between ECT2 expression and clinic-pathological characteristics of GC patients.

Characteristics	Cases	ECT2		P value
		High	Low	
Age (years)				
≥55	30	18	12	0.083
<55	36	30	6	
Gender				
Male	38	28	10	0.124
Female	28	20	8	
Tumor size (mm)				
≤5.0	26	18	8	0.095
>5.0	40	30	10	
Differentiation				
Well/moderate	22	16	6	0.064
Poor	44	32	12	
Lymph node metastasis				
Yes	42	30	12	0.042*
No	24	18	6	
TNM stage				
I-II	22	15	7	0.024*
III-IV	44	33	22	

restrained the proliferation and metastasis of 5-FU-treated GC cells. These findings have not been found in previous studies.

In addition, we also found that downregulation of ECT2 increased the 5-FU sensitivity of GC cells by inhibiting Bcl-2, MRP1, and P-gp. P-gp can induce drug resistance by transporting drugs outside the cell [29]. MRP1 is an important gene that triggers cell resistance [30]. Apoptosis is not only related to tumor progression but also correlated with chemotherapy resistance. Among them, Bcl-2 is an antiapoptotic protein, and Bax is a proapoptotic protein [31]. Here, downregulation of ECT2 reduced the expression of Bcl-2, MRP1, and P-gp in GC cells. On the other hand, these results prove that ECT2 can increase 5-FU sensitivity in GC cells. However, our conclusion has not been verified in in vivo experiment. The function of ECT2 will be explored in vivo in the future.

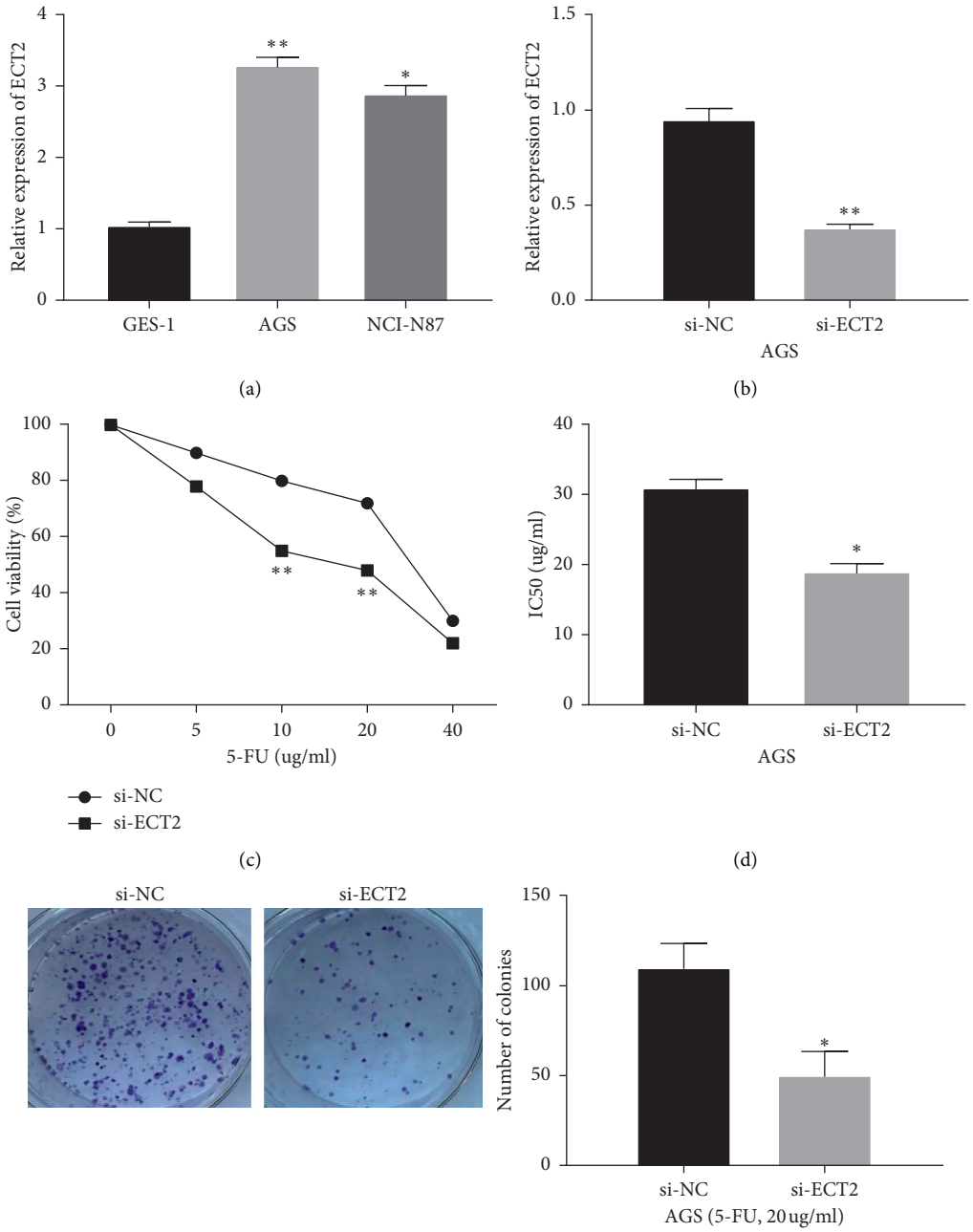

Figure 2: Continued.

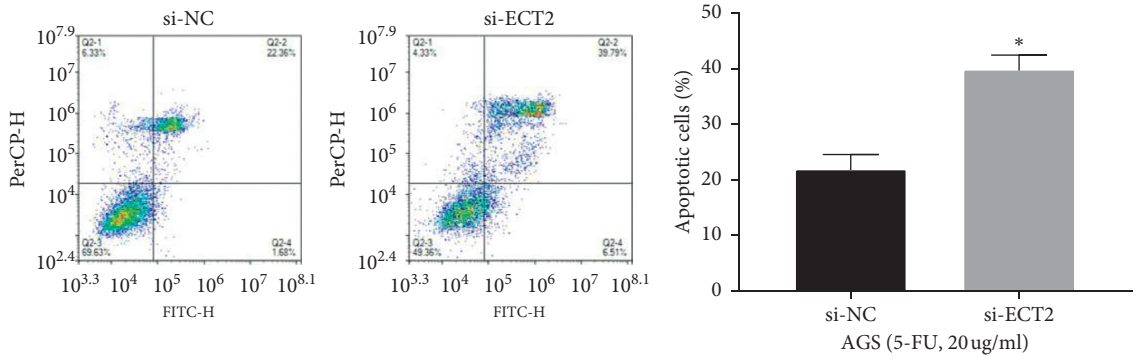

(f)

Figure 2: Knockdown of ECT2 enhancing 5-FU sensitivity in GC cells. (a) ECT2 expression in normal gastric mucosal cell line GES-1 and human GC cell lines AGS and NCI-N87. (b) ECT2 expression in AGS cells with si-ECT2 or si-NC. (c) Cell viability of si-NC and si-ECT2 with 5-FU treatment. (d) The IC50 value of AGS cells with si-NC and si-ECT2. (e) 5-FU sensitivity detection reconfirmed by the colony formation assay. (f) Apoptosis of AGS cells treated with 5-FU in si-NC and si-ECT2 groups. $^{*}P < 0.05$. $^{**}P < 0.01$.

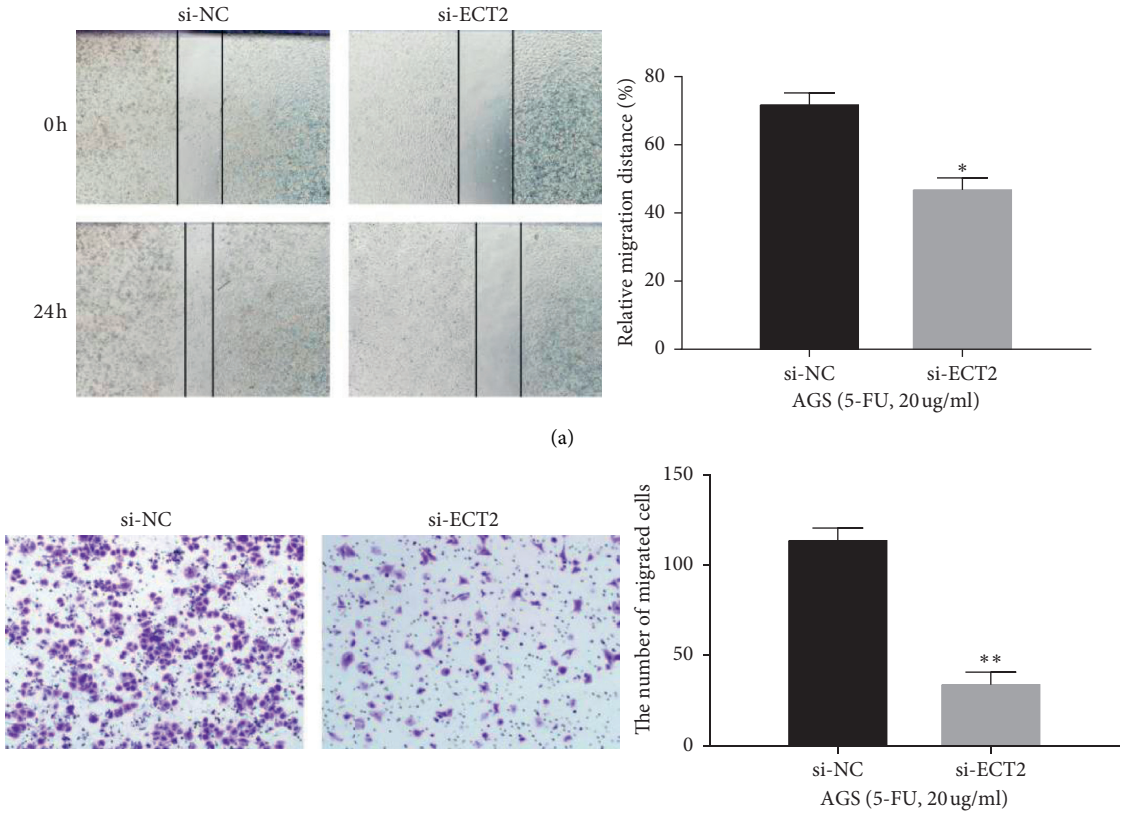

(a)

(b)

Figure 3: Continued.

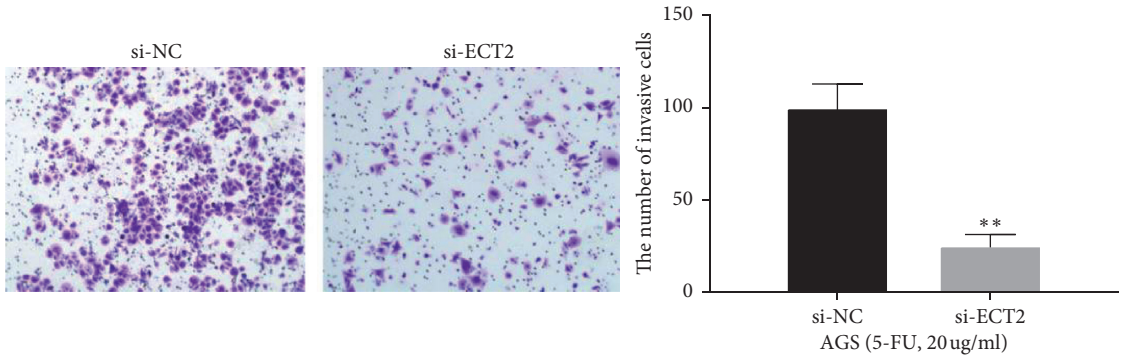

(c)

Figure 3: ECT2 silencing inhibiting the metastasis of GC cell lines treated by 5-FU. (a) The migration of AGS cells treated with 5-FU in si-NC and si-ECT2 groups detected by the wound healing assay. (b, c) The migration and invasion of AGS cells treated with 5-FU in si-NC and si-ECT2 groups detected by the transwell assay. $^{*}P < 0.05$. $^{**}P < 0.01$.

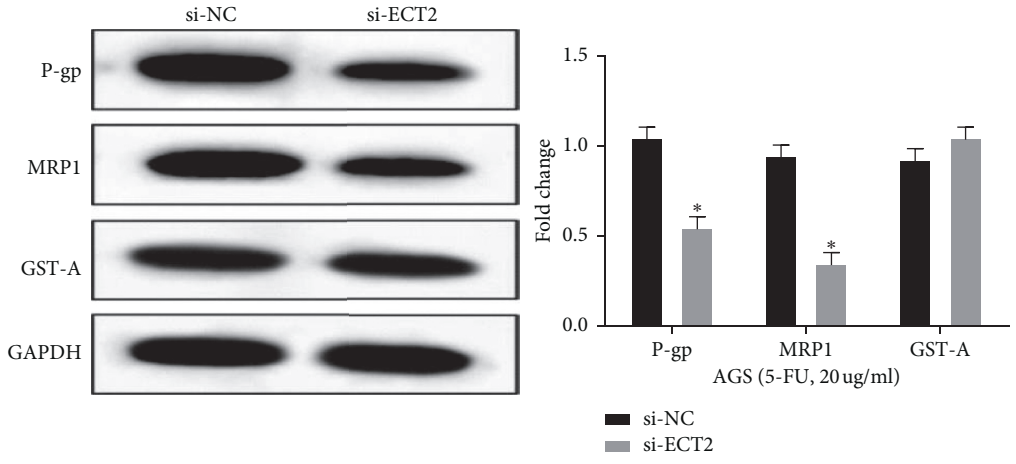

(a)

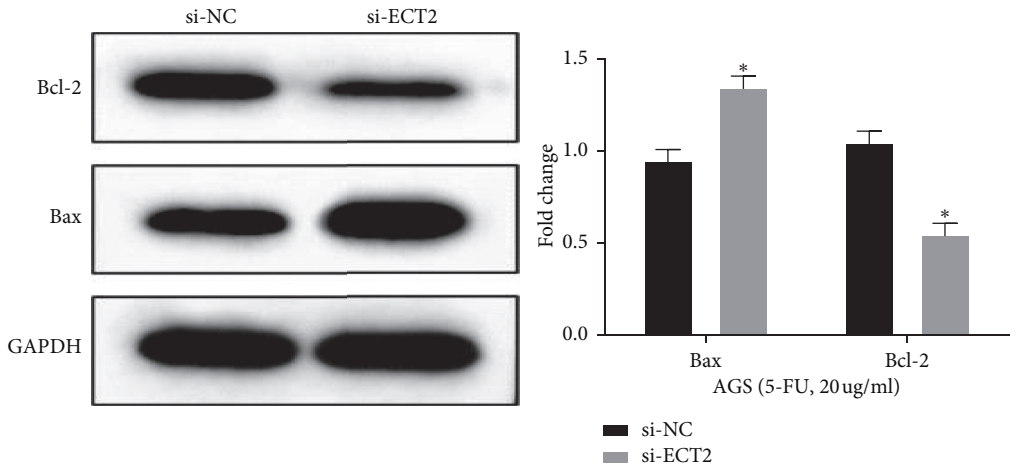

(b)

Figure 4: ECT2 downregulation increasing the sensitivity of GC cell lines to 5-FU by reducing the expressions of P-gp, MRP1, and Bcl-2. (a) Drug resistance-related proteins P-gp, MRP1, GST-π detected in AGS cells treated with 5-FU in si-NC and si-ECT2 groups. (b) Apoptosis-related proteins Bcl-2 and Bax detected in AGS cells treated with 5-FU in si-NC and si-ECT2 groups. $^{*}P < 0.05$.

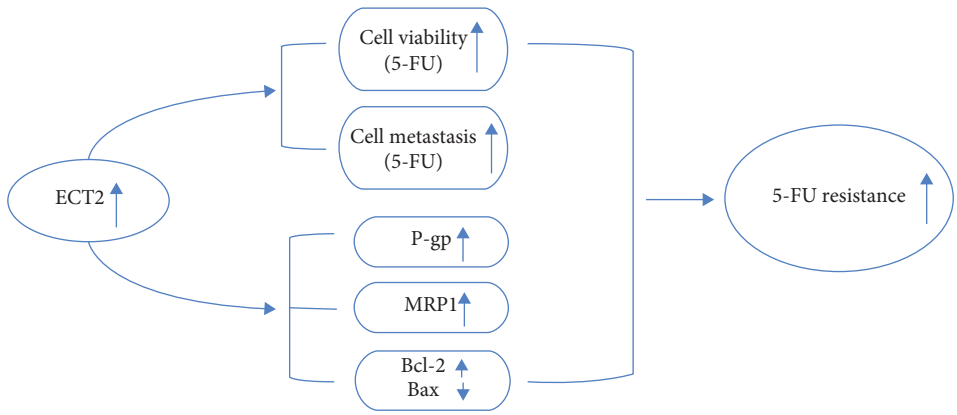

Figure 5: ECT2 affecting 5-FU sensitivity in GC cells by regulating cell viability, metastasis, and apoptosis-related proteins.

5. Conclusion

In conclusion, upregulation of ECT2 is observed in GC, which predicts adverse clinical outcomes in GC patients. Importantly, ECT2 knockdown attenuates 5-FU resistance in GC cells. Innovatively, we found that ECT2 may affect 5-FU sensitivity in GC cells by regulating cell viability, metastasis, and apoptosis-related proteins. This study can provide a promising treatment option for GC patients.

Data Availability

The datasets used to support the findings of this study are available from the corresponding author upon request.

Conflicts of Interest

The authors declare that they have no conflicts of interest.

References

[1] M. Riihimäki, A. Hemminki, K. Sundquist, J. Sundquist, and K. Hemminki, "Metastatic spread in patients with gastric cancer," *Oncotarget*, vol. 7, no. 32, pp. 52307–52316, 2016.

[2] S. Ishaq and L. Nunn, "Helicobacter pylori and gastric cancer: a state of the art review," *Gastroenterology and Hepatology from Bed to Bench*, vol. 8, pp. S6–S14, 2015.

[3] R. L. Siegel, K. D. Miller, and A. Jemal, "Cancer statistics, 2019," *CA: A Cancer Journal for Clinicians*, vol. 69, no. 1, pp. 7–34, 2019.

[4] W. Chen, "Cancer statistics: updated cancer burden in China," *Chinese Journal of Cancer Research*, vol. 27, p. 1, 2015.

[5] A. Biagioni, I. Skalamera, S. Peri et al., "Update on gastric cancer treatments and gene therapies," *Cancer and Metastasis Reviews*, vol. 38, no. 3, pp. 537–548, 2019.

[6] F. Raza, H. Zafar, S. Zhang et al., "Recent advances in cell membrane-derived biomimetic nanotechnology for cancer immunotherapy," *Advanced Healthcare Materials*, vol. 10, no. 6, Article ID e2002081, 2021.

[7] F. Raza, H. Zafar, X. You, A. Khan, J. Wu, and L. Ge, "Cancer nanomedicine: focus on recent developments and self-assembled peptide nanocarriers," *Journal of Materials Chemistry B*, vol. 7, no. 48, pp. 7639–7655, 2019.

[8] H. Arai and T. E. Nakajima, "Recent developments of systemic chemotherapy for gastric cancer," *Cancers*, vol. 12, 2020.

[9] W.-J. Shi and J.-B. Gao, "Molecular mechanisms of chemoresistance in gastric cancer," *World Journal of Gastrointestinal Oncology*, vol. 8, no. 9, pp. 673–681, 2016.

[10] F. Raza, Y. Zhu, L. Chen et al., "Paclitaxel-loaded pH responsive hydrogel based on self-assembled peptides for tumor targeting," *Biomaterials Science*, vol. 7, no. 5, pp. 2023–2036, 2019.

[11] K. Nishibeppu, S. Komatsu, J. Kiuchi et al., "TRIM37 contributes to malignant outcomes and CDDP resistance in gastric cancer," *Journal of Cancer*, vol. 12, no. 2, pp. 316–325, 2021.

[12] Q. Ni, Y. Zhang, R. Tao, X. Li, and J. Zhu, "MicroRNA-95-3p serves as a contributor to cisplatin resistance in human gastric cancer cells by targeting EMP1/PI3K/AKT signaling," *Aging*, vol. 13, no. 6, pp. 8665–8687, 2021.

[13] H. Gao, J. Ma, Y. Cheng, and P. Zheng, "Exosomal transfer of macrophage-derived miR-223 confers doxorubicin resistance in gastric cancer," *OncoTargets and Therapy*, vol. 13, pp. 12169–12179, 2020.

[14] Z. J. An, Y. Li, B. B. Tan et al., "Up-regulation of KLF17 expression increases the sensitivity of gastric cancer to 5-fluorouracil," *International Journal of Immunopathology and Pharmacology*, vol. 35, Article ID 20587384211010925, 2021.

[15] X. Wang, Z. Tong, and H. Liu, "MiR-223-3p targeting epithelial cell transforming sequence 2 oncogene inhibits the activity, apoptosis, invasion and migration of MDA-MB-468 breast cancer cells," *OncoTargets and Therapy*, vol. 12, pp. 7675–7684, 2019.

[16] J. Gao, C. Dai, X. Yu, X. B. Yin, and F. Zhou, "Upregulated microRNA-194 impairs stemness of cholangiocarcinoma cells through the Rho pathway via inhibition of ECT2," *Journal of Cellular Biochemistry*, vol. 121, no. 10, pp. 4239–4250, 2020.

[17] Y. Yu, O. Cai, P. Wu, and S. Tan, "MiR-490-5p inhibits the stemness of hepatocellular carcinoma cells by targeting ECT2," *Journal of Cellular Biochemistry*, vol. 120, no. 1, pp. 967–976, 2019.

[18] T. Zhi, K. Jiang, X. Xu et al., "ECT2/PSMD14/PTTG1 axis promotes the proliferation of glioma through stabilizing E2F1," *Neuro-Oncology*, vol. 21, no. 4, pp. 462–473, 2019.

[19] J. Xie, P. Lei, and Y. Hu, "Small interfering RNA-induced inhibition of epithelial cell transforming sequence 2 suppresses the proliferation, migration and invasion of osteosarcoma cells," *Experimental and Therapeutic Medicine*, vol. 9, no. 5, pp. 1881–1886, 2015.

[20] D. Xu, Y. Wang, J. Wu et al., "ECT2 overexpression promotes the polarization of tumor-associated macrophages in

hepatocellular carcinoma via the ECT2/PLK1/PTEN pathway," *Cell Death & Disease*, vol. 12, no. 2, p. 162, 2021.

[21] J. Liu, M. Zhou, Y. Ouyang, L. Du, L. Xu, and H. Li, "Identification of potential biomarkers and their clinical significance in gastric cancer using bioinformatics analysis methods," *PeerJ*, vol. 8, Article ID e9174, 2020.

[22] H. Wang, H. Liu, J. Li et al., "Effect of Ect2 expression on the growth of triple-negative breast cancer cells with paclitaxel intervention," *OncoTargets and Therapy*, vol. 13, pp. 12905–12918, 2020.

[23] Y. Chen, P. Tian, and Y. Liu, "P53 and protein phosphorylation regulate the oncogenic role of epithelial cell transforming 2 (ECT2)," *Medical Science Monitor*, vol. 23, pp. 3154–3160, 2017.

[24] Y. Jin, Y. Yu, Q. Shao et al., "Up-regulation of ECT2 is associated with poor prognosis in gastric cancer patients," *International Journal of Clinical and Experimental Pathology*, vol. 7, pp. 8724–8731, 2014.

[25] D. Y. Gong, X. Chen, T. L. Yang et al., "Upregulation of ECT2 is associated with transcriptional program of cancer stem cells and predicts poor clinical outcome in gastric cancer," *Oncology Letters*, vol. 20, p. 54, 2020.

[26] H.-B. Wang, H.-C. Yan, and Y. Liu, "Clinical significance of ECT2 expression in tissue and serum of gastric cancer patients," *Clinical and Translational Oncology*, vol. 18, no. 7, pp. 735–742, 2016.

[27] K. Zhou, H. Mai, S. Zheng et al., "OTUB1-mediated deubiquitination of FOXM1 up-regulates ECT-2 to promote tumor progression in renal cell carcinoma," *Cell & Bioscience*, vol. 10, no. 1, p. 50, 2020.

[28] C. Li, Z. Peng, Y. Wang et al., "Epithelial cell transforming 2 is regulated by yes-associated protein 1 and mediates pancreatic cancer progression and metastasis," *American Journal of Physiology-Gastrointestinal and Liver Physiology*, vol. 320, no. 3, pp. G380–G395, 2021.

[29] H. Zhang, H. Jiang, H. Zhang, J. Liu, X. Hu, and L. Chen, "Ribophorin II potentiates P-glycoprotein- and ABCG2-mediated multidrug resistance via activating ERK pathway in gastric cancer," *International Journal of Biological Macromolecules*, vol. 128, pp. 574–582, 2019.

[30] B. Tan, Y. Li, Q. Zhao, L. Fan, and D. Wang, "ZNF139 increases multidrug resistance in gastric cancer cells by inhibiting miR-185," *Bioscience Reports*, vol. 38, 2018.

[31] L. Singh, N. Pushker, N. Saini et al., "Expression of pro-apoptotic Bax and anti-apoptotic Bcl-2 proteins in human retinoblastoma," *Clinical & Experimental Ophthalmology*, vol. 43, no. 3, pp. 259–267, 2015.

Hindawi
Journal of Oncology
Volume 2021, Article ID 1642852, 10 pages
https://doi.org/10.1155/2021/1642852

Research Article

SPP1 Regulates Radiotherapy Sensitivity of Gastric Adenocarcinoma via the Wnt/Beta-Catenin Pathway

Gangyi Sun,[1] **Ziyi Shang**,[2] **and Wenjia Liu**[3]

[1]*Department of Massage, The Affiliated Hospital of Shandong University of Traditional Chinese Medicine, Jinan 250000, China*
[2]*Treating Potential Diseases Branch, The Affiliated Hospital of Shandong University of Traditional Chinese Medicine, Jinan 250000, China*
[3]*Department of Oncology, The Affiliated Hospital of Shandong University of Traditional Chinese Medicine, Jinan 250000, China*

Correspondence should be addressed to Wenjia Liu; wujiapiii@163.com

Received 29 June 2021; Accepted 15 July 2021; Published 28 July 2021

Academic Editor: Muhammad Wasim Khan

Purpose. Radiotherapy has been widely applied for the treatment of locally advanced and metastatic gastric adenocarcinoma (GAC). The aberrant expression of secreted phosphoprotein 1 (SPP1) is involved in radiosensitivity in a variety of cancers. The present study aims to characterize the clinical significance of SPP1 expression in GAC and its role and underlying mechanism of radiosensitivity. *Methods*. The SPP1 expression in GAC tissues and pericarcinomatous tissues was determined by QRT-PCR and immunohistochemistry, and the SPP1 expression in GAC cell lines (BGC823, AGS, and SGC7901) and normal human gastric epithelial cell line (GES-1) was determined by western blot. *T*-test, one-way ANOVA, Cox regression model, and Kaplan–Meier plotter were applied to further assess the association between SPP1 expression and the prognosis of the patients with GAC. After irradiation and transfection with si-SPP1 combined with or without Wnt/*β*-catenin pathway inhibitor (XAV939), western blot, transwell, flow cytometry, and TOP-flash reporter assay were applied to detect DNA damage, invasion, apoptosis, cell cycle, and activation of Wnt/*β*-catenin pathway, respectively. *Results*. SPP1 mRNA and protein levels in GAC tissues were both dramatically higher than those in pericarcinomatous tissues. SPP1 overexpression was positively associated with tumor size, nodal status, and histological grade of GAC patients. SPP1 overexpression, depth of invasion, and nodal status were independent prognostic factors for the patients. High SPP1 expression was negatively related to the overall survival in patients with GAC. We found that SPP1 knockdown enhanced the radiosensitivity of GAC cell lines (AGS and SGC7901). Increasing H2AX phosphorylation, apoptosis and G2/M phase arrest, and decreasing invasion were observed after the administration of si-SPP1 and irradiation. Radiosensitivity of SPP1 was mainly dependent on the Wnt/*β*-catenin signal pathway. XAV939 could enhance these phenomena induced by irradiation combined with SPP1 knockdown. *Conclusion*. This study demonstrates that SPP1 suppresses Wnt/*β*-catenin signaling to enhance the radiosensitivity of GAC via inhibiting invasion and accelerating DNA damage, G2/M phase arrest, and apoptosis.

1. Introduction

Gastric cancer (GC) is an aggressive malignancy with an extremely poor prognosis and a high incidence [1]. The incidence of gastric adenocarcinoma (GAC) accounts for 95 percent of gastric malignant tumors [2]. Accumulated evidence has demonstrated that radiotherapy has a role in the management of neoadjuvant, adjuvant, and palliative treatment of GC [3, 4]. However, because of the low radiosensitivity of GC, no difference in survival was observed in GAC patients receiving radiotherapy [5, 6]. Therefore, it is urgent and imperative to find an effective radiosensitizer to enhance the curative effect of radiotherapy and alleviate its toxicity to the tissues and organs around the radiation field.

Secreted phosphoprotein 1 (SPP1), which is also known as bone sialoprotein 1, osteopontin (OPN), early T-lymphocyte activation 1, and Eta-1 protein, controls the cell growth, proliferation, apoptosis, and migration [7]. High plasma concentrations of SPP1 are correlated with a poor prospect for patients with head and neck cancer after

radiotherapy, which can prognosticate clinically relevant hypoxia, and might determine patients who will benefit from modifying hypoxia during radiotherapy [8]. Studies have indicated that SPP1 is elevated in many malignancies, such as ovarian cancer [9], cervical cancer [10], and breast cancer [11]. And, high SPP1 expression level at the end of radiotherapy is correlated with poor survival, such as glioma [12] and non-small-cell lung cancer [13]. However, the role of SPP1 in radiosensitivity in GAC remains unclear. Consequently, the association between SPP1 and radiosensitivity in GAC needs to be investigated further.

In this study, we found that high SPP1 was associated with poor prognosis in GAC patients. We observed that SPP1 knockdown pretreatment increased H2AX phosphorylation, apoptosis and G2/M phase arrest, and decreased invasion in response to irradiation in AGS and SGC7901 cells. Additionally, we noticed that SPP1 could activate the Wnt/β-catenin signal pathway in GAC cells through TOP-flash reporter assay and western blot validation, and pretreatment with Wnt/β-catenin signal pathway inhibitor (XAV939) sensitized GAC cells to IR.

2. Methods

2.1. Patients. A total of 198 tissue specimens, including 72 cases of adjacent tissues (3-4 cm from the tumor tissue) and 126 cases of gastric adenocarcinomas, were collected from patients with GAC who underwent surgery from September 2010 to September 2015 at the Affiliated Hospital of Shandong University of Traditional Chinese Medicine, Jinan, China. The specimens were confirmed by immunohistochemistry (IHC) and included in the clinical/prognostic analysis. Participants who met the following criteria were included: histologically confirmed diagnosis of GAC, no history of prior anticancer therapies, underwent radical surgery, and complete follow-up data available. Written informed consents were signed by all participants. Ethical approval to conduct this study was obtained from the ethics committee of the Affiliated Hospital of Shandong University of Traditional Chinese Medicine.

2.2. Immunohistochemistry. All specimens were routinely fixed in 10% buffered formalin and embedded in paraffin. And, the 4-μm-thick tissue sections that were cut from wax blocks were prepared on APES-coated glass slides. Slides were deparaffinized in xylene, rehydrated in graded ethanol, and immersed in 3% hydrogen peroxidase-methanol for 15 minutes to eliminate endogenous peroxidase activity. A microwave antigen retrieval procedure was performed for 5 min in 10 mM citrate buffer (pH 6.0). The sections were incubated with a primary anti-SPP1 antibody (1 : 200, ab8448, Abcam, Shanghai, China) at 4°C for overnight. After incubation with HRP-conjugated secondary antibody (1 : 50, ab6721, Abcam) at room temperature for 30 minutes, they are visualized by using 3,3′-diaminobenzidine and then counterstained with hematoxylin for 3 min.

Two experienced pathologists blinded to the clinical data were responsible for reviewing the immunoreactivity of SPP1. The score of staining intensity as well as the proportion of immunostaining positive cells was between 0–3 and 0–4, respectively. The proportions were as follows: 0, negative; 1, ≤10% positive cells; 2, >10% but ≤50% positive cells; 3, >50% but ≤75% positive cells; and 4, >75% positive cells. The staining intensity was as follows: 0, absent; 1, weak; 2, moderate; and 3, strong. The two scores were multiplied to obtain an overall protein expression score. For statistical analysis, the final evaluation criteria of SPP1 expression were as follows: 0–4 as low expression and 5–12 as high expression.

2.3. RNA Extraction and RT-qPCR. Total RNA from GAC tissues and pericarcinomatous tissue was extracted by TRIzol solution (Invitrogen, CA, USA). To synthesized cDNA, PrimeScript™ IV 1st strand cDNA Synthesis Mix (Takara, Dalian, China) was applied. The QPCR was carried out by the SYBR Premix ExTaq TM II (Takara, Dalian, China) by ABI 7900 qRT-PCR system (Applied Biosystems, Foster City, CA, United States). The cDNA was then subjected to qRT-qPCR by SYBR Premix ExTaq TM II (Takara, Dalian, China) to evaluate the relative mRNA levels of SPP1 on an Applied Biosystems real-time PCR machine (ABI 7900HT, CA, USA), and β-actin was applied as the internal control. And, the relative mRNA level was calculated by utilizing the $2^{-\Delta\Delta Ct}$ method.

Primer sequence:

SPP1 F: 5′-TTTGTTGTAAAGCTGCTTTTCCTC-3′

R: 5′-GAATTGCAGTGATTTGCTTTTGC-3′

β-Actin F: 5′-CTCTCTCTACCTACATCTCTACTAAAA-3′

R: 5′-AACTCTAACTCTCTCTCTAACTACTTCTC-3′

2.4. Cell Culture. Normal human gastric epithelial cell line (GES-1) and human stomach gastric adenocarcinoma cell line (AGS, SGC7901, and BGC823) were obtained from the Center for Chinese Typical Cultures Preservation, Wuhan University. All cell lines were cultured in 1640 media supplemented with 10% fetal bovine serum (FBS) at 37°C in 5% CO_2 incubator. In the subsequent experiments, cells were pretreated with or without a β-catenin inhibitor XAV939 (10 μM, Sigma-Aldrich, Darmstadt, Germany) for 48 h and then were exposed to 4 Gy for 24 h with X-ray irradiator RS2000 (RAD SOURCE, USA).

2.5. Transfection. The AGS and SGC7901 cells (5×10^6/ml) were cultivated at 37°C under 5% CO_2 water-saturated atmosphere in 1640 medium supplemented with 10% FBS. Two si-RNAs were synthesized by GenePharma (Shanghai, China) and transfected into GAC cell lines using lipofectamine 3000 reagent (siRNA: lipofectamine = 10 nM:1 μL) (Invitrogen, Shanghai, China) for 24 h. Then, serum-free transfection solution was discarded and replaced with 1640 medium supplemented with 10% FBS for further culture. After 48 h, cellular proteins can be extracted to verify the knockdown efficiency.

The siRNA sequences were as follows:

Si-SPP1-1, 5′-CGAUCGAUAGUGCCGAGAAGC-3′
Si-SPP1-2, 5′-AGCUAGUCCUAGACCCUAAGA-3′

2.6. Western Blot. Total protein was isolated by RIPA lysis buffer (Abcam, Shanghai, China), and then the protein concentration was measured using a Pierce BCA assay (Abcam, Shanghai, China). Protein (40 μg) was separated on SDS-PAGE and transferred to polyvinylidene (PVDE) membrane. After being blocked with 5% nonfat milk at room temperature for 1 h, the membranes were incubated with the primary antibodies anti-SPP1 (1 : 1000, ab8448), γ-H2AX (1 : 1000, ab81299), Bax (1 : 1000, ab32503), Bcl-2 (1 : 1000, ab32124), c-JUN (1 : 1000, ab40766), c-myc (1 : 1000, ab32072), cyclin-D1 (1 : 1000, ab16663), β-catenin (1 : 1000, ab223075), and β-actin (ab8227, 1 : 2000) overnight and then probed with HRP-conjugated anti-IgG antibody (1 : 1000, ab133470, all obtained from Abcam, Shanghai, China) for 1 h. Immunoreactive bands were visualized with an enhanced chemiluminescence system (Thermo Scientific, Shanghai, China).

2.7. Transwell Assay. Total 1×10^4 cells (AGS and SGC7901) were seeded into Matrigel upper chambers (BD Bioscience, USA). The lower chamber contained a complete medium. After 24 hours of culture, the cells passing through the Matrigel membrane were fixed in methanol, stained, and counted in five fields under a microscope (Olympus, Japan).

2.8. Cell Cycle Detection. A total of 2×10^5 cells/well were plated into a six-well plate. Before any treatment, the cell culture medium was changed to a serum-free medium to culture the cells for 12 h, ensuring it enters a similar phase. IR with or without siRNA transfection and XAV939 treatment was carried out as described in the previous methods. After 48 h, the cells were centrifuged, collected, then were fixed in 700 μl of 75% ethanol (−20°C precooled). Subsequently, the cells were suspended in 400 μl of propidium iodide (PI) solutions (50 μg/ml) containing 100 μl of 1 mg/ml RNAse (Solarbio, Shanghai, China) for 10 min. Cellular DNA content was analyzed using flow cytometer (Accuri C6, BD Biosciences).

2.9. Cell Apoptosis Assay. A total of 2×10^5 cells/well were plated in 6-well plates and incubated for 24 h. GAC cells were transfected with siRNA combined with XAV939, followed by IR (4 Gy). Subsequently, all cells were collected and stained with 100 ul of 1× binding buffer, 5 μl of Annexin V-FITC, and 5 ul of Annexin PI in the dark for 15 min at 4°C. Apoptotic cells were analyzed using a flow cytometer (BD Biosciences).

2.10. Luciferase Reporter Assay. A total of 1×10^5 cells/well were plated in a 24-well plate and incubated with RPMI-1640 medium at 37°C for 24 h. Cells were transfected with a 0.8 μg TOP-flash or FOP-flash vector and 0.02 μg Renilla luciferase vector as an internal control (EMD Millipore, Billerica, MA, USA). After transfection for 24 h, cells were harvested in passive lysis buffer (Promega), and the reporter activities were assayed by Dual-Luciferase Assay System kit (Promega Corporation). Renilla reniformis luciferase expression was used for normalization.

2.11. Statistical Analysis. The significance among two or more comparisons was analyzed by a two-tailed Student's *t*-test or one-way ANOVA. All data were expressed as mean ± standard deviation (SD) and a p value <0.05 was indicated statistically significant.

3. Results

3.1. SPP1 Is Upregulated in Gastric Adenocarcinoma. RT-qPCR was carried out to measure SPP1 mRNA levels in GAC tissues and adjacent normal tissues. SPP1 was overexpressed in GAC tissues compared with normal gastric tissues ($p < 0.01$, Figure 1(a)). This result was confirmed by detecting the level of SPP1 protein. As shown in Figure 1(b), negative staining could be discovered in adjacent normal tissues. It was found that SPP1 protein was mainly located at the cytoplasm of the GAC cell. 169 GAC tissues (85.4%) expressed SPP1. Among the 198 GAC tissues, 110 samples (55.6%) expressed high levels, and 88 samples (44.4%) expressed low levels of SPP1.

3.2. Correlations between SPP1 Expression and Clinicopathological Characteristics. To implore the clinical value of SPP1 in GAC, we further examined the correlation between SPP1 expression and the clinicopathological parameters, including age, gender, tumor location, lymphatic/venous invasion, depth of invasion, tumor size, histological grade, and nodal status of patients with GAC, as shown in Table 1. No significant correlations were observed between SPP1 expression and age, gender, tumor location, lymphatic/venous invasion, and depth of invasion ($p > 0.05$) of GAC patients. Interestingly, SPP1 overexpression was positively associated with tumor size ($p = 0.035$), histological grade ($p = 0.003$), and nodal status ($p = 0.002$) of GAC patients.

Univariate analysis revealed the following: SPP1 overexpression (hazard ratio (HR), 2.399; $p < 0.001$), histological grade (HR, 1.782; $p = 0.005$), lymphatic/venous invasion (HR, 1.605; $p = 0.022$), depth of invasion (HR, 1.471; $p = 0.002$), and nodal status (HR, 1.672; $p < 0.001$) (Table 2). Further multivariate analysis presented that SPP1 overexpression (HR, 3.303; $p = 0.001$), depth of invasion (HR, 0.511; $p = 0.025$), and nodal status (HR, 1.432; $p = 0.001$) were independent prognostic factors for the patients (Table 2). Survival analysis showed that the overall survival (OS) of all GAC patients with SPP1 overexpression was dramatically less than for patients with SPP1 low expression (Figure 1(c)).

3.3. Suppression of SPP1 Expression Affected DNA Damage, Invasion, and Apoptosis of GAC Cells. The western blot results verified that SPP1 was overexpressed in AGS and

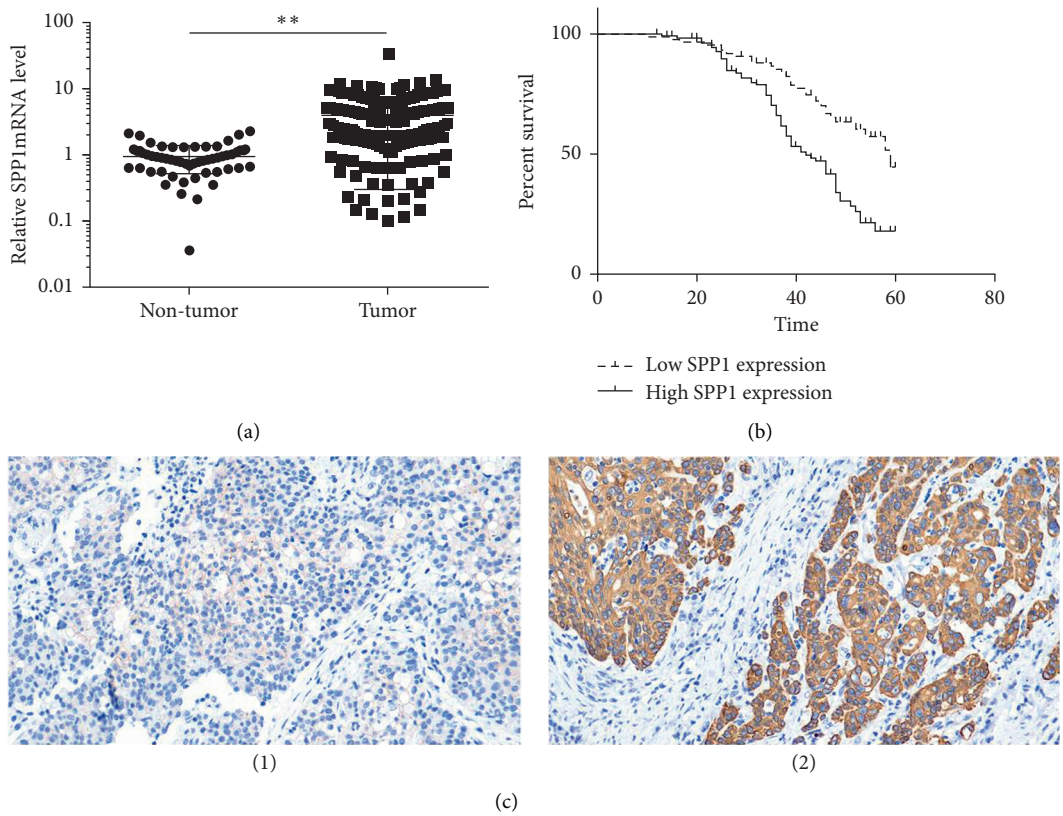

Figure 1: SPP1 was elevated in GAC tissues. (a) The SPP1 mRNA levels in GAC tissues and adjacent normal tissues were measured by RT-qPCR vs. normal tissues, $^{**}p < 0.01$. (b) The SPP1 protein levels in GAC tissues and adjacent normal tissues were measured by immumohistochemical staining. (c) (1) low expression; (2) high expression.

Table 1: Association between SPP1 expression and clinicopathologic characteristics in patients with GAC.

Characteristics	SPP1 expression		p value
	Low expression ($n = 88$)	High expression ($n = 110$)	
Gender			
Male	42	52	0.901
Female	46	58	
Age (years)			
<60	43	52	0.693
≥60	45	58	
Tumor location			
Proximal	49	51	0.192
Distant	29	37	
Total	10	22	
Tumor size (cm)			
<5	49	44	0.035
≥5	39	66	
Histological grade			
Well/moderately differentiated	51	45	0.003
Poorly differentiated	37	65	
Lymphatic/venous invasion			
No	58	48	0.845
Yes	30	62	
Depth of invasion			
T2	49	17	0.894
T3	29	39	
T4a	10	54	
Nodal status			
N1	42	10	0.002
N2	24	41	
N3	22	59	

Table 2: Univariate and multivariable analysis of prognostic factors for 5-year survival in GAC.

Variables	Univariate analysis		Multivariate analysis	
	HR (95% CI)	p value	HR (95% CI)	p value
Gender	1.345 (0.899–2.012)	0.150		
Age	1.335 (0.894–1.995)	0.158		
Tumor location	1.258 (0.972–1.628)	0.081		
Tumor size (cm)	1.216 (0.889–1.662)	0.221		
Histological grade	1.782 (1.195–2.657)	0.005	1.051 (0.288–3.842)	0.940
Lymphatic/venous invasion	1.605 (1.072–2.404)	0.022	0.616 (0.183–2.076)	0.434
Depth of invasion	1.471 (1.151–1.878)	0.002	0.511 (0.283–0.921)	0.025
Nodal status	1.672 (1.288–2.171)	<0.001	1.432 (0.820–2.502)	0.001
SPP1 expression	2.399 (1.560–3.687)	<0.001	3.303 (1.673–6.523)	0.001

SGC7901 cells compared with control GES-1 cells (Figure 2(a)). To evaluate the effect of SSP1 on radiosensitivity in GAC, we transfected the GAC cell lines AGS and SGC-7901 with SPP1-specific siRNAs or a control siRNA (si-NC). Two siRNAs targeting SPP1 were tested (si-SPP1#1 and si-SPP1#2). Si-SPP1#1 was the most effective in suppressing SPP1 expression and was adopted for subsequent study (Figure 2(b)). To investigate the effect of SPP1 on radiotherapy-mediated invasion and apoptosis, we performed experiments in vitro. The phosphorylation of H2AX was elevated in AGS and SGC-7901 cells after irradiation compared with that in the control cells, whereas in the si-SPP1 group, it was enhanced upon irradiation, indicating that SPP1 may exert an important function in DNA damage repair via inducing the phosphorylation of SPP1 (Figure 2(c)). Additionally, the invasive capacity of AGS and SGC-7901 cells was prominently restricted compared with that in the control cells. Concurrently, SPP1 depletion enormously reinforced the effect of irradiation-induced reduction in invasiveness (Figure 2(d)). Compared with the control cells ($5.68\% \pm 0.36$, $6.47\% \pm 0.44$), AGS and SGC-7901 cells exposed irradiation and led to markedly increased apoptosis ratio ($15.59 \pm 0.50\%$, $16.08 \pm 0.87\%$). Concurrently, transfection of AGS and SGC-7901 cells with si-SPP1 enhanced the augment in apoptosis ratio induced by irradiation ($55.12 \pm 0.87\%$, $54.46 \pm 0.59\%$) (Figure 2(e)). There is a perceptible enrichment of GAC cells observed in the G2/M phase when AGS and SGC-7901 cells exposed irradiation, and the suppression of SPP1 remarkably enhanced the irradiation-induced G2/M phase arrest (Figure 2(f)). The irradiation notably increased Bax expression and decreased Bcl-2 expression, while knockdown of SPP1 significantly accelerated the irradiation-induced increase in Bax expression and decrease in Bcl-2 expression (Figure 2(g)). The observations indicated that suppression of SPP1 tremendously enhanced the radiosensitivity of GAC cell lines via inhibiting invasion and accelerating DNA damage, G2/M phase arrest, and apoptosis.

3.4. SPP1 Enhanced the Radiosensitivity of GAC Cell Lines via Wnt/β-Catenin Pathway. Next, we examined the effect of SPP1 knockdown on the activity of the Wnt pathway enabling the TOP-flash/FOP-flash reporter system. SPP1 knockdown induced a 40% to 50% decrease in Wnt-activity in AGS and SGC-7901 cells (Figure 3(a)). The irradiation downregulated the expression of endogenous β-catenin, c-JUN, c-myc, and cyclin-D1 both in AGS and SGC-7901 cells, and SPP1 knockdown enormously enhanced the irradiation-induced suppression effect on the Wnt/β-catenin pathway (Figure 3(b)). To further verify the role of the Wnt/β-catenin pathway in radiosensitivity of GAC, we pretreated cells with the recombinant Wnt inhibitors XAV939. In western blot analysis, inhibitors XAV939 resulted in the reinforcement in the phosphorylation of H2AX-induced by irradiation combined with SPP1 depletion (Figure 3(c)). Additionally, XAV939 enormously reinforced the effect of irradiation combined with SPP1 depletion-induced reduction in invasiveness (Figure 3(d)). Treatment with XAV939 ($84.56\% \pm 1.85$, $83.65\% \pm 0.98$) in AGS and SGC7901 cell lines enhanced the augment in apoptosis ratio induced by irradiation combined with SPP1 depletion ($54.30\% \pm 0.66$, $51.91\% \pm 1.52$) (Figure 3(e)). XAV939 remarkably enhanced the irradiation combined with SPP1 depletion-induced G2/M phase arrest (Figure 3(f)). XAV939 significantly accelerated the irradiation combined with SPP1 depletion-induced increase in Bax expression and decrease in Bcl-2 expression (Figure 3(g)). This evidence indicated that SPP1 enhanced the radiosensitivity of GAC cell lines via the Wnt/β-catenin pathway.

4. Discussion

Radiotherapy has been widely applied for the treatment of locally advanced and metastatic GAC [14, 15]. The search for an effective gene target to enhance the sensitivity of radiotherapy is a vital and urgent issue for the therapy of GAC. Previous studies revealed that SPP1 is involved in the radiosensitivity of a variety of cancers [16, 17]. In the current study, we found that SPPI overexpression was associated with poor prognosis in GAC patients, and si-SPP1 pretreatment decreased invasion and increased irradiation-induced DNA damage, cell cycle arrest, and cell death in GAC cells; the underlying mechanism involves suppression of the Wnt/β-catenin pathway.

It is reported that SPP1 overexpression is associated with high invasive and metastatic potential, poor prognosis, and recurrent disease for cancer patients, such as breast cancer [18] and gastric cancer [19]. In this study, we confirmed that SPP1 was elevated in GAC tissues and cell lines, and SPP1

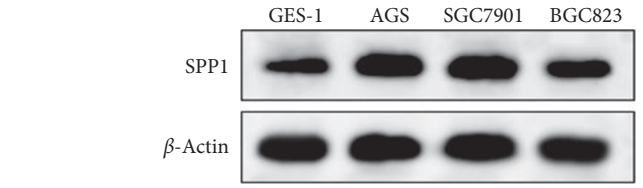

(a)

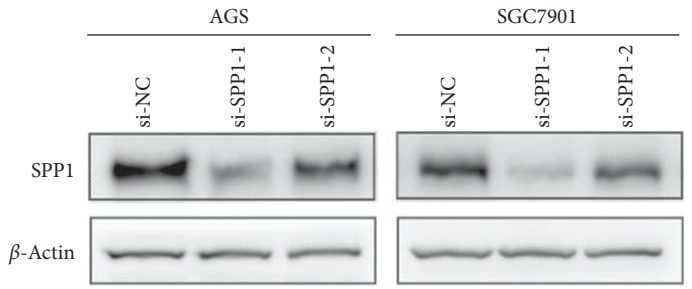

(b)

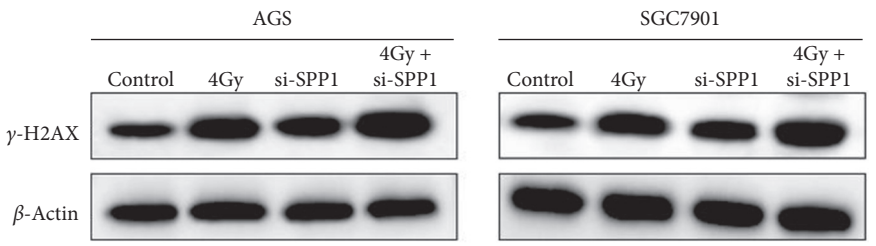

(c)

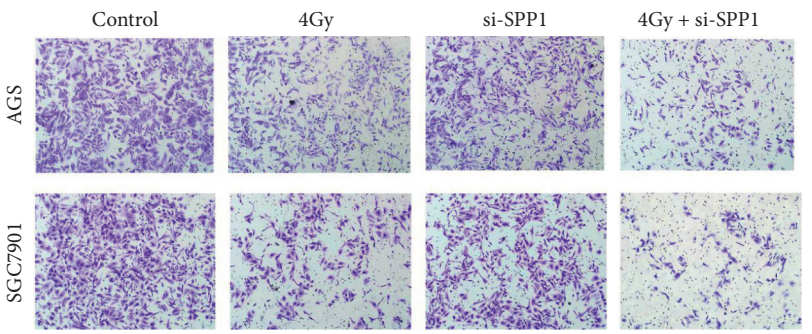

(d)

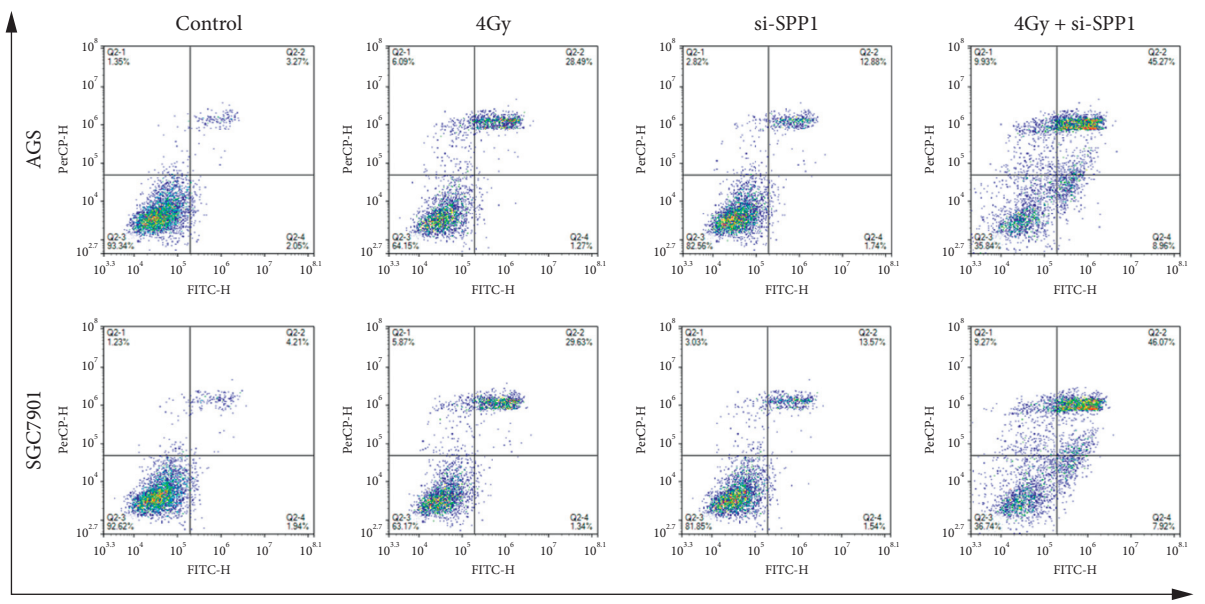

(e)

Figure 2: Continued.

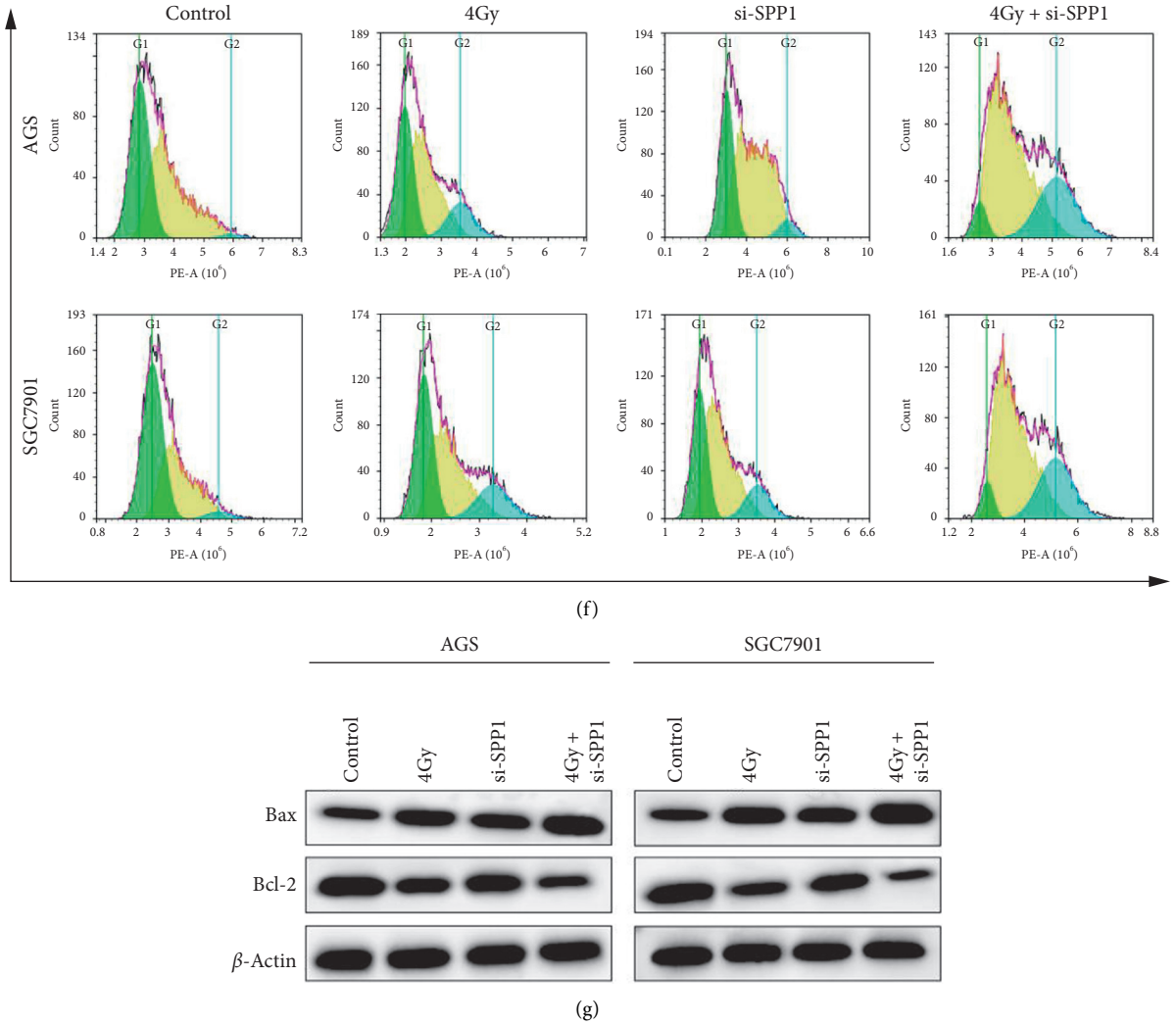

Figure 2: Suppression of SPP1 expression affected DNA damage, invasion, and apoptosis of GAC cells. (a) The western blot results verified that SPP1 was overexpressed in AGS and SGC7901 cells compared with control GES-1 cells. (b) The transfected efficiency of si-SPP1 in GAC cells. (c) The phosphorylation of H2AX in AGS and SGC-7901 cells was measured by western blot. (d) The invasiveness in AGS and SGC-7901 cells was measured by transwell assay. (e) The apoptosis ratio in AGS and SGC-7901 cells was measured by flow cytometry. (f) The cell cycle in AGS and SGC-7901 cells was measured by flow cytometry. (g) The apoptosis-related protein in AGS and SGC-7901 cells was measured by western blot.

overexpression was positively associated with tumor size, nodal status, and histological grade of GAC patients. SPP1 overexpression, nodal status, and depth of invasion were independent prognostic factors for the patients. High SPP1 expression was negatively correlated with survival time in patients with GAC. These pieces of evidence were consistent with the previous study.

In the human response to nascent DNA damage, one of the earliest events is the phosphorylation of histone H2A variant H2AX to form γ-H2AX [20]. Within 10–30 minutes after DNA damage induction [21], the reaction is highly amplified, and many H2AX molecules flanking the DNA double-strand break site are phosphorylated. In the past decade, γ-H2AX has developed into a vital biomarker for quantifying DNA double-strand break levels in cells and tissues [22, 23]. To further investigate the role of SPP1 in radiosensitivity in GAC, we transfected GAC cell lines with SPP1 knockdown plasmid and found that knockdown of SPP1 enhanced the radiation-induced increase in DNA damage, apoptosis, and G2/M phase arrest and decrease in the invasion, which indicates that SPP1 knockdown can enhance the radiosensitivity in GAC.

Signaling transduction after irradiation plays a vital role in mediating damage repair, thereby controlling the fate of cancer cells receiving irradiation [24, 25]. Studies have found that activation of the β-catenin pathway can effectively accelerate the repair of DNA double-strand breaks in osteoblasts after irradiation [26], and β-catenin overexpression aggrandized the capability of DNA double-strand break repair in cancer cells [27]. Therefore, it is adjudged that the function of β-catenin in DNA damage repair may be a factor that affects cell radiosensitivity. Finding gene targets that interfere with radiation-related signaling pathways is an absorbing aim. In the current study, we found that SPP1

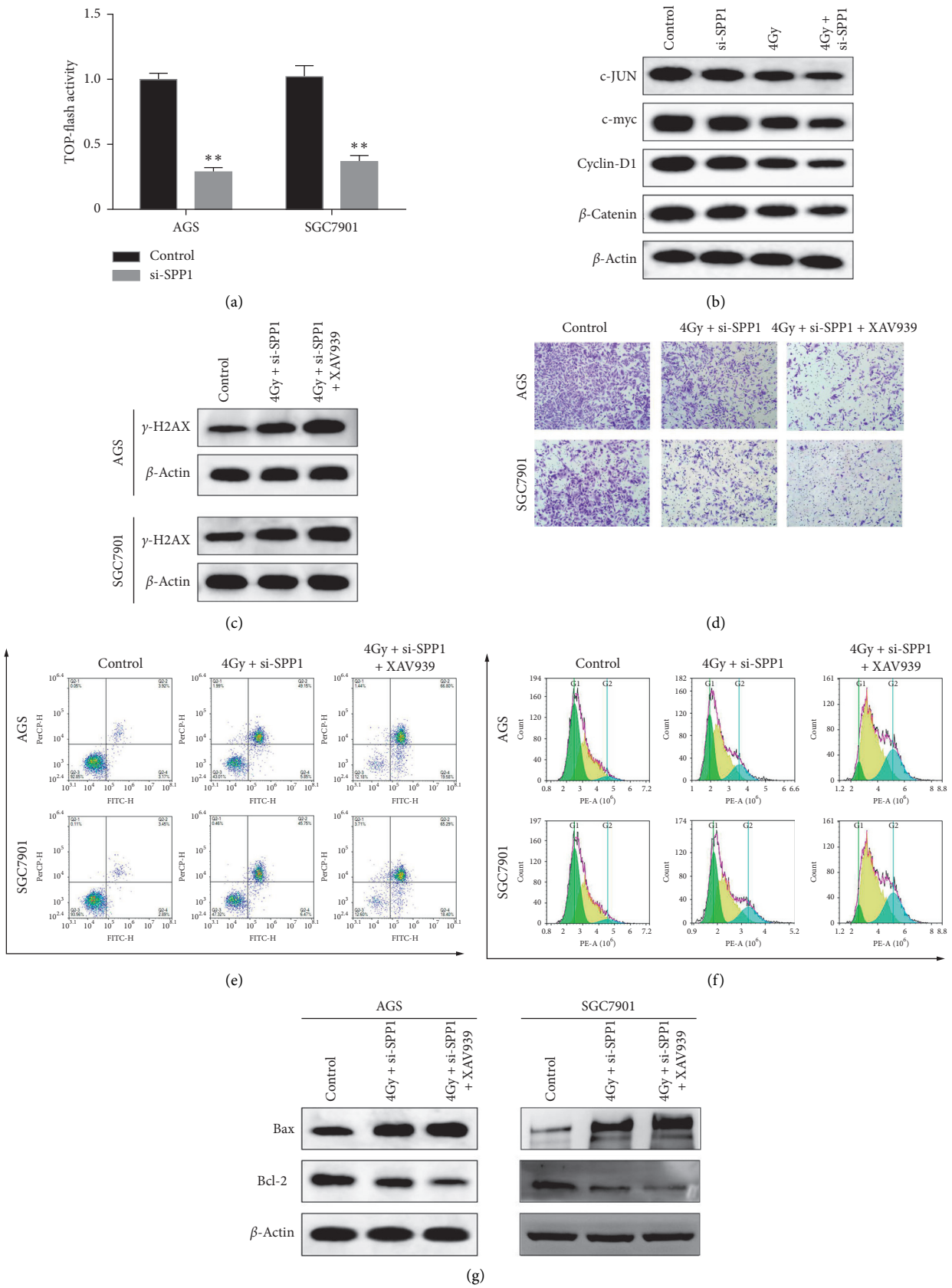

FIGURE 3: SPP1 enhanced the radiosensitivity of GAC cell lines via the Wnt/β-catenin pathway. (a) The Wnt pathway in AGS and SGC-7901 cells was measured by TOP-flash/FOP-flash reporter system vs. control group, ** $p < 0.01$. (b) The Wnt/β-catenin pathway-related protein in AGS and SGC-7901 cells was measured by western blot. (c) The phosphorylation of H2AX in AGS and SGC-7901 cells was measured by western blot. (d) The invasiveness in AGS and SGC-7901 cells was measured by transwell assay. (e) The apoptosis ratio in AGS and SGC-7901 cells was measured by flow cytometry. (f) The cell cycle in AGS and SGC-7901 cells was measured by flow cytometry. (g) The apoptosis-related protein in AGS and SGC-7901 cells was measured by western blot.

knockdown induced a decrease in the Wnt/β-catenin-activity in AGS and SGC-7901 cells through the TOP-flash/FOP-flash reporter system and western blot, indicating that the radiosensitivity of SPP1 was mainly dependent on the Wnt/β-catenin signal pathway. To further verify this hypothesis, we introduced Wnt/β-catenin signal pathway inhibitors (XAV939), which could enhance these phenomena induced by irradiation combined with SPP1 knockdown. This evidence revealed that SPP1 suppresses Wnt/β-catenin signaling to enhance the radiosensitivity of GAC via inhibiting invasion and accelerating DNA damage, G2/M phase arrest, and apoptosis.

This study is the first to indicate that SPP1 can be utilized as a gene target for enhancing radiotherapy sensitivity of gastric adenocarcinoma, triggering the Wnt/β-catenin pathway. However, these inclusions were only conducted at the cellular level, and animal experiments are still needed for further verification.

In conclusion, in the current study, we illustrated for the first time that the knockdown of SPP1 combined with irradiation exerted additive effects on inducing DNA damage, apoptosis and G2/M phase arrest, and suppressing invasion via the Wnt/β-catenin signal pathway. This indicates that SPP1 is a potential target for enhancing the efficacy of radiotherapy.

Data Availability

The data used to support the findings of this study are available from the corresponding author upon request.

Conflicts of Interest

The authors declare that they have no conflicts of interest.

Authors' Contributions

Gangyi Sun and Ziyi Shang contributed equally to this work.

References

[1] O. Özcan, A. K. Belli, A. Korkut Belli et al., "Upregulation of SIRT1 gene in gastric adenocarcinoma," *The Turkish Journal of Gastroenterology*, vol. 30, no. 4, pp. 326–330, 2019.

[2] K. Ghaffarzadehgan, M. Jafarzadeh, H. R. Raziee et al., "Expression of cell adhesion molecule CD44 in gastric adenocarcinoma and its prognostic importance," *World Journal of Gastroenterology*, vol. 14, no. 41, pp. 6376–6381, 2008.

[3] J. S. Macdonald, "Clinical overview: adjuvant therapy of gastrointestinal cancer," *Cancer Chemotherapy and Pharmacology*, vol. 54, no. 1, pp. S4–S11, 2004.

[4] N. G. Coburn, A. Govindarajan, C. H. L. Law et al., "Stage-specific effect of adjuvant therapy following gastric cancer resection: a population-based analysis of 4,041 patients," *Annals of Surgical Oncology*, vol. 15, no. 2, pp. 500–507, 2008.

[5] M. M. Kim, M. M. Kim, V. Rana et al., "Clinical benefit of palliative radiation therapy in advanced gastric cancer," *Acta Oncologica*, vol. 47, no. 3, pp. 421–427, 2008.

[6] J.-G. Park, B. S. Kramer, S.-L. Lai, L. J. Goldstein, and A. F. Gazdar, "Chemosensitivity patterns and expression of human multidrug resistance-associated MDR1 gene by human gastric and colorectal carcinoma cell lines," *JNCI Journal of the National Cancer Institute*, vol. 82, no. 3, pp. 193–198, 1990.

[7] H. Qin, R. Wang, G. Wei et al., "Overexpression of osteopontin promotes cell proliferation and migration in human nasopharyngeal carcinoma and is associated with poor prognosis," *European Archives of Oto-Rhino-Laryngology*, vol. 275, no. 2, pp. 525–534, 2018.

[8] J. Overgaard, J. G. Eriksen, M. Nordsmark, J. Alsner, and M. R. Horsman, "Plasma osteopontin, hypoxia, and response to the hypoxia sensitiser nimorazole in radiotherapy of head and neck cancer: results from the DAHANCA 5 randomised double-blind placebo-controlled trial," *The Lancet Oncology*, vol. 6, no. 10, pp. 757–764, 2005.

[9] H. Hu, Z. Liu, and C. Liu, "Correlation of OPN gene expression with proliferation and apoptosis of ovarian cancer cells and prognosis of patients," *Oncology Letters*, vol. 17, no. 3, pp. 2788–2794, 2019.

[10] H. Cho, S. W. Hong, Y. J. Oh et al., "Clinical significance of osteopontin expression in cervical cancer," *Journal of Cancer Research and Clinical Oncology*, vol. 134, no. 8, pp. 909–917, 2008.

[11] M. Kovacheva, M. Zepp, M. Schraad, S. Berger, and M. R. Berger, "Conditional knockdown of osteopontin inhibits breast cancer skeletal metastasis," *International Journal of Molecular Sciences*, vol. 20, no. 19, 2019.

[12] A. Güttler, M. Giebler, P. Cuno et al., "Osteopontin and splice variant expression level in human malignant glioma: radiobiologic effects and prognosis after radiotherapy," *Radiotherapy and Oncology*, vol. 108, no. 3, pp. 535–540, 2013.

[13] C. Ostheimer, M. Bache, A. Güttler, T. Reese, and D. Vordermark, "Prognostic information of serial plasma osteopontin measurement in radiotherapy of non-small-cell lung cancer," *BMC Cancer*, vol. 14, no. 1, p. 858, 2014.

[14] M. Caudry, J. L. Ratoanina, P. Escarmant, and J. P. Maire, "Les volumes-cibles de la radiothérapie des adénocarcinomes gastriques," *Cancer/Radiothérapie*, vol. 5, no. 5, pp. 523–533, 2001.

[15] P. K. Stumpf, A. Amini, B. L. Jones et al., "Adjuvant radiotherapy improves overall survival in patients with resected gastric adenocarcinoma: a national cancer data base analysis," *Cancer*, vol. 123, no. 17, pp. 3402–3409, 2017.

[16] A. Henry, M.-J. Nokin, N. Leroi et al., "New role of osteopontin in DNA repair and impact on human glioblastoma radiosensitivity," *Oncotarget*, vol. 7, no. 39, pp. 63708–63721, 2016.

[17] A. Hahnel, H. Wichmann, M. Kappler et al., "Effects of osteopontin inhibition on radiosensitivityof MDA-MB-231 breast cancer cells," *Radiation Oncology*, vol. 5, no. 1, p. 82, 2010.

[18] V. H. C. Bramwell, G. S. Doig, A. B. Tuck et al., "Serial plasma osteopontin levels have prognostic value in metastatic breast cancer," *Clinical Cancer Research*, vol. 12, no. 11, pp. 3337–3343, 2006.

[19] C.-Y. Wu, M.-S. Wu, E.-P. Chiang et al., "Elevated plasma osteopontin associated with gastric cancer development, invasion and survival," *Gut*, vol. 56, no. 6, pp. 782–789, 2007.

[20] E. P. Rogakou, D. R. Pilch, A. H. Orr, V. S. Ivanova, and W. M. Bonner, "DNA double-stranded breaks induce histone H2AX phosphorylation on serine 139," *Journal of Biological Chemistry*, vol. 273, no. 10, pp. 5858–5868, 1998.

[21] C. Redon, D. Pilch, E. Rogakou, O. Sedelnikova, K. Newrock, and W. Bonner, "Histone H2A variants H2AX and H2AZ,"

Current Opinion in Genetics & Development, vol. 12, no. 2, pp. 162–169, 2002.

[22] C. E. Redon, A. J. Nakamura, O. A. Martin, P. R. Parekh, U. S. Weyemi, and W. M. Bonner, "Recent developments in the use of γ -H2AX as a quantitative DNA double-strand break biomarker," *Aging*, vol. 3, no. 2, pp. 168–174, 2011.

[23] O. A. Sedelnikova and W. M. Bonner, "GammaH2AX in cancer cells: a potential biomarker for cancer diagnostics, prediction and recurrence," *Cell Cycle (Georgetown, Tex.)*, vol. 5, no. 24, pp. 2909–2913, 2006.

[24] T. D. Lama-Sherpa, V. T. G. Lin, B. J. Metge et al., "Hedgehog signaling enables repair of ribosomal DNA double-strand breaks," *Nucleic Acids Research*, vol. 48, no. 18, pp. 10342–10352, 2020.

[25] Y. Yang, H. Zhou, G. Zhang, and X. Xue, "Targeting the canonical Wnt/β-catenin pathway in cancer radioresistance: updates on the molecular mechanisms," *Journal of Cancer Research and Therapeutics*, vol. 15, no. 2, pp. 272–277, 2019.

[26] A. Chandra, T. Lin, J. Zhu et al., "PTH1-34 blocks radiation-induced osteoblast apoptosis by enhancing DNA repair through canonical Wnt pathway," *Journal of Biological Chemistry*, vol. 290, no. 1, pp. 157–167, 2015.

[27] R. Deng, J. Tang, J.-G. Ma et al., "PKB/Akt promotes DSB repair in cancer cells through upregulating Mre11 expression following ionizing radiation," *Oncogene*, vol. 30, no. 8, pp. 944–955, 2011.

Hindawi
Journal of Oncology
Volume 2021, Article ID 2380958, 8 pages
https://doi.org/10.1155/2021/2380958

Research Article

Clinical Significance of Color Ultrasound, MRI, miR-21, and CA199 in the Diagnosis of Pancreatic Cancer

Jing Yu, Xue Yang, Hongmei Wu, and Jiansheng Li

Department of Abdominal Ultrasound, The Affiliated Hospital of Qingdao University, Qingdao 266000, China

Correspondence should be addressed to Jiansheng Li; lijiansheng@qduah.cn

Received 29 June 2021; Accepted 15 July 2021; Published 28 July 2021

Academic Editor: Muhammad Wasim Khan

Background. To investigate the clinical significance of color ultrasound, magnetic resonance imaging (MRI), miR-21, and CA199 in the diagnosis of pancreatic cancer (PC). *Methods*. A total of 160 patients with PC admitted to our hospital from April 2018 to February 2021 were included in the PC group, and another 100 patients with benign pancreatic disease during the same period were included in the pancreatic benign disease group. Color ultrasound and MRI were used for imaging examination of the two groups of PC patients, and the sensitivity, accuracy, and specificity of the two methods for preoperative diagnosis of PC were calculated, respectively. A total of 100 healthy people who underwent physical examination during the same period were included in the control group. Serum CA199 levels of the three groups were detected by ELISA assay. The level of serum miR-21 in the three groups was detected by qRT-PCR. A receiver operating curve (ROC) was drawn to analyze and calculate the sensitivity, specificity, and accuracy of the two serum markers and the combination of color ultrasound and MRI in the detection of PC. *Results*. Serum CA199 and miR-21 levels in the PC group were significantly higher than those in the benign lesion group and control group. CA199 and miR-21 levels in the benign lesion group were higher than those in the control group. Both color ultrasound and MRI showed a higher detection rate for PC, and the sensitivity and accuracy were significantly higher than those of CA199 and miR-21. The sensitivity, specificity, and accuracy of combined detection were 91.88%, 96.00%, and 93.46%, respectively, which were significantly higher than those of single detection. *Conclusion*. The combined detection of color ultrasound, MRI, miR-21, and CA199 have a high application value in the early diagnosis of PC, which can effectively improve the sensitivity and accuracy of clinical diagnosis, reduce the probability of missed diagnosis and misdiagnosis, and provide a reference for the rational clinical treatment plan and prognosis.

1. Introduction

Pancreatic cancer (PC) is a malignant digestive tumor with high clinical morbidity and mortality and challenging to treat [1]. In recent years, due to changes in dietary habits, PC is more common in middle-aged and older adults, and the incidence has been increasing year by year [2]. The early clinical symptoms of PC have no apparent specificity, the clinical detection rate is low, and there are many cases of missed diagnosis and misdiagnosis. Most patients have been diagnosed in the middle and late stages. The particularity of the location of cancer makes patients lose the opportunity of radical surgery. Patients can only receive surgery and postoperative chemotherapy, with poor quality of life and poor prognosis [3]. Clinically, pathological tissue biopsy is used as the "gold standard" for the diagnosis of PC, but this examination method may cause a certain degree of trauma in patients and has limitations [4]. Therefore, early diagnosis and accurate assessment of preoperative staging of PC are crucial to the treatment effect and survival time of patients [5].

MiR-21 is abnormally expressed in a variety of malignant tumor tissues. MiR-21 plays an important role in the development and progression of PC, which can be used as a new target for diagnosing and treating PC [6]. At present, one of the methods commonly used in the clinical detection of various malignant tumors is the detection of serum tumor markers [7]. CEA [8] and CA199 [9] are widely used clinical serum markers for PC. However, CEA has a low sensitivity in the diagnosis of PC. Although CA199 has a high

sensitivity in the diagnosis of PC, it has certain limitations [10]. Magnetic resonance imaging (MRI) is a common means for the clinical diagnosis of malignant tumors. With fast scanning speed and clear images, it can clearly show the situation of vascular invasion without ionizing radiation and can also be used for further observation of the surrounding tissues of the pancreas [11, 12]. Color ultrasound not only has the advantages of two-dimensional ultrasound structure image but also provides rich hemodynamic information, simple operation, and high accuracy of examination [13]. However, each method alone has advantages and limitations in the diagnosis of PC, and the combination of multiple methods can combine these advantages and significantly improve the diagnostic accuracy.

In this study, we studied the clinical diagnostic value of color ultrasound, MRI, miR-21, and CA199 combined examination in patients with PC, aiming to provide a reference for the early diagnosis, treatment, and prognosis of PC.

2. Materials and Methods

2.1. General Data. A total of 160 patients with PC admitted to the Affiliated Hospital of Qingdao University (Qingdao, China) from April 2018 to February 2021 were included in the study group, aged from 26 to 71 years, with an average of 46.77 ± 10.65 years. The pathological biopsy results showed that 46 cases were TNM I stage, 68 cases were TNM II stage, 31 cases were TNM III stage, and 15 cases were TNM IV stage (Figure 1). Tumor diameter: 94 patients were <5 cm, and 66 patients were ≥5 cm. Types of disease: 131 cases were pancreatic head carcinoma, and 29 cases were pancreatic body carcinoma. Pathological types: 136 cases were ductal adenocarcinoma, 17 cases were mucinous adenocarcinoma, and 7 cases were adenosquamous carcinoma. Tumor differentiation: 45 cases were highly differentiated, 62 cases were moderately differentiated, and 53 cases were poorly differentiated. There were 83 patients with lymph node metastasis and 77 patients without lymph node metastasis. Vascular infiltration was found in 36 cases and not in 124 cases. Inclusion criteria: patients who did not receive surgical treatment before the examination; all patients confirmed by clinical examination and pathological examination; and complete clinical medical records. Exclusion criteria: patients with cirrhosis; patients with coagulation dysfunction or liver cancer metastatic; patients with cardiovascular and visceral diseases; complicated with other malignant tumors; confused consciousness or accompanied by mental illness; and patients with MRI contraindication.

A total of 100 patients with benign pancreatic lesions, aged from 25 to 74 years, with an average age of 47.52 ± 11.43 years, were included in the benign lesions group. Another 100 healthy subjects, aged from 26 to 73 years, with an average age of 48.13 ± 10.71 years, were enrolled into the control group during the same period. There was no statistical significance in the comparison of general information among the three groups (Table 1). All participants in this study signed the informed consent and were approved by the ethics committee of the Affiliated Hospital of Qingdao University (approval number: LIHAO:20180317).

2.2. CA199 and miR-21 Detection Methods. 5 mL fasting venous blood in the morning was collected from the three groups and centrifuged at 3 000 r/min for 10 min. The upper serum was divided into two parts and stored in a refrigerator at −80°C for measurement. CA199 was detected by Enzyme Linked Immunosorbent Assay (ELISA). The ELISA kit was purchased from Sigma Company (United States), and the specific operation was strictly in accordance with the kit instructions.

MiR-21 level was detected by the qRT-PCR method. Total RNA was extracted by the Trizol method and dissolved in DEPC water, and its concentration and purity were detected by using an ultraviolet spectrophotometer. 1 μg total RNA was used as a template to synthesize cDNA. Then, qRT-PCR was performed. The reaction conditions were as follows: 90°C for 2 min, 90°C for 20 s, 65°C for 30 s, 70°C for 10 s, and a total of 39 cycles. The primer sequences were miR-21 forward 5′-CGGCGGTTAGCTTATCAGACTGA-3′ and reverse 5′-CCAGTGCAGGGTCCGAGGGAGTAT-3′; U6 forward 5′-GCGCGTCGTG AAGCG TTC-3′ and reverse 5′- GTGCAGGGTCCGAGGT-3′. The results were analyzed by $2^{-\Delta\Delta CT}$.

2.3. Color Ultrasound Examination. The instrument for color ultrasound was Toshiba Aplio 500, and the probe frequency was set at 3.5 MHz. The patient was supine with the upper abdomen fully exposed and the entire epigastric area scanned. The internal diameters of intrahepatic and extrahepatic bile ducts and pancreatic ducts were measured, and space-occupying lesions in the ampulla and head of the pancreas were examined. The tumor location was determined, and the tumor size, shape, boundary, internal echo, lymph node metastasis, and its relationship with adjacent organs were observed. The size, contour, and shape of the pancreatic duct were examined. The subjects kept breathing deeply during the entire examination to obtain a clear image.

2.4. MRI Examination. The MRI instrument was a Ge3.0T Signa HDX MRI scanner. First, conventional *T*1 WI and *T*2 WI sequences were scanned. The scanning parameters of *T*1 WI were TR 295 ms, TE 3.5 ms, layer thickness 6 mm, layer spacing 3 mm, and matrix 256×256. The scanning parameters of *T*2 WI were TR 6000 ms, TE 90 ms, layer thickness 6 mm, layer spacing 3 mm, and matrix 325×226. The scanning range of both sequences was from the diaphragmatic apex to duodenal level. After the location of the lesion was determined, SE *T*1 WI and fat suppression sequence scanning were performed on the pancreatic layer. The thickness of the adjusted layer was 5 mm, and the spacing was 1 mm. Then dynamic enhanced scanning was performed, and the patient was injected with Magenweir contrast agent (1.5 mL/kg, 3 mL/s) through the cubital vein. The obtained imaging data will be uploaded to the workstation for image postprocessing. The final imaging data of

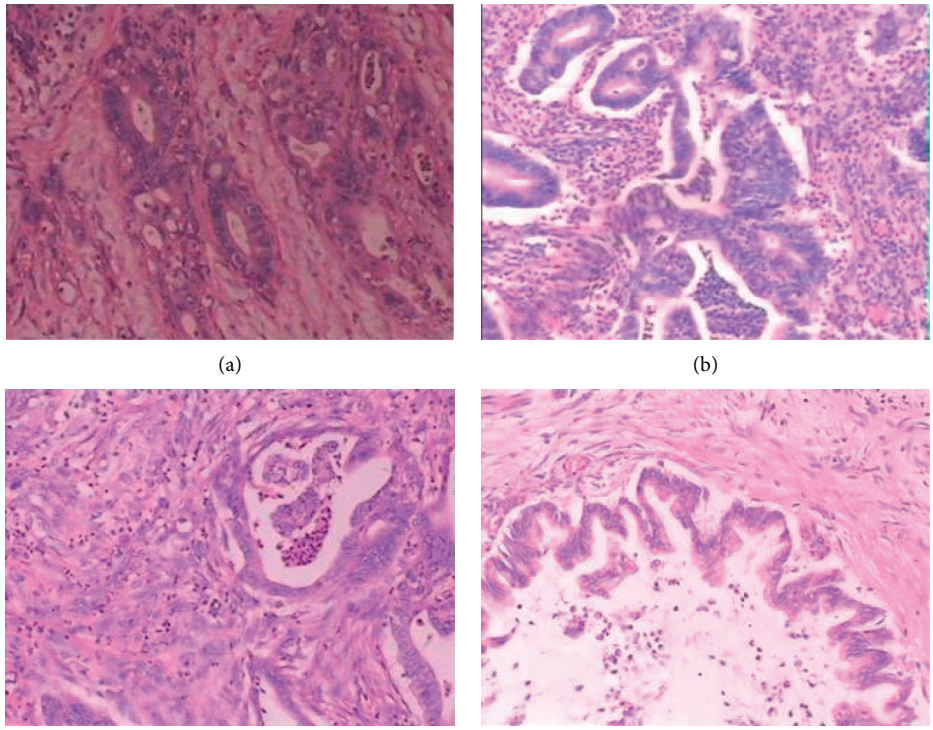

Figure 1: Pathologic biopsy of PC. (a) PC stage I in a 34-year-old woman with moderate to poorly differentiated adenocarcinoma (size 1.9 cm), not invading the pancreatic capsule. (b) PC stage II in a 57-year-old man with moderately differentiated adenocarcinoma (2.5 cm in diameter), invading the pancreatic capsule. (c) PC stage III in a 45-year-old male with moderately differentiated adenocarcinoma (31.5 cm) and high-grade ductal intraepithelial neoplasia extending into the pancreatic capsule to surrounding adipose tissue and the muscular layer. (d) PC stage IV in a 66-year-old male with stage IV pancreatic carcinoma presented with pathologic, moderately differentiated adenocarcinoma that invaded and punctured the pancreas.

Table 1: Comparison of general data of the three groups.

Group		PC group	Benign lesion group	Control group	X^2	P value
Cases		160	100	100		
Gender	Male	97	62	66	0.773	0.679
	Female	63	38	34		
Age (years)	≤45	76	57	55	2.654	0.265
	>45	84	43	45		
Education degree	Junior high school and below	62	31	34	1.718	0.424
	High school or above	98	69	66		
Occupation	Worker	107	68	71	1.917	0.751
	Self-employed	39	27	23		
	No job	14	5	6		

all the subjects were reviewed by two experienced radiologists. For cases with inconsistent judgment results, the two doctors discussed or consulted experts and finally reached the same diagnosis results, and the final report was given.

2.5. Observation Indexes. The sensitivity, specificity, and accuracy of color ultrasound and MRI in the diagnosis of PC were compared, respectively. MiR-21 and CA199 levels in the PC group, benign lesion group, and control group were compared. The sensitivity, specificity, and accuracy of miR-21, CA199, combined with color ultrasound and MRI, in the detection of PC were compared. Sensitivity calculation method: true positive number/(true positive number + false negative number) × 100%. Specificity calculation method: true negative number/(true negative number + false positive number) × 100%. Accuracy calculation method: (true positive number + true negative number)/total number of cases × 100%.

2.6. Statistical Analysis. SPSS23.0 software was used for data analysis. Enumeration data were expressed as rate (%), and the $\chi 2$ test was used for comparison between groups.

Measurement data were expressed as ($x \pm s$), and the $\chi 2$ test was performed between groups. Receiver operating curve (ROC) was used to analyze the diagnostic value of miR-21 and CA199 in PC. $P < 0.05$ was considered statistically significant.

3. Results

3.1. Comparison of CA199 and miR-21 Levels in the Three Groups. Compared with the PC group, CA199 and miR-21 levels in the benign lesion group and control group were significantly downregulated ($P < 0.01$). CA199 and miR-21 levels were the lowest in the control group (Figures 2 and 3).

3.2. Color Ultrasound Images of PC Patients. Color ultrasound images of patients with PC are as shown in Figure 4.

3.3. MRI Images of PC Patients. MRI images of patients with PC are as shown in Figure 5.

3.4. Comparison of the Diagnostic Value of Color Ultrasound and MRI in PC. Both color ultrasound and MRI had high detection rates for PC, and the difference between them was not statistically significant ($P > 0.05$, Tables 2 and 3).

3.5. Comparison of the Diagnostic Value of miR-21 and CA199 and Their Combined Detection in PC. The sensitivity, specificity, and accuracy of miR-21 were 58.13%, 79.00%, and 66.15%, respectively (Figure 6). The sensitivity, specificity, and accuracy of CA199 were 69.38%, 74.00%, and 71.15%, respectively (Figure 7). The sensitivity, specificity, and accuracy of color ultrasonography were 83.13%, 89.00%, and 85.38%, respectively. The sensitivity, specificity, and accuracy of MRI were 81.25%, 90.00%, and 84.62%, respectively. The sensitivity, specificity, and accuracy of the combined detection were 91.88%, 96.00%, and 93.46%, respectively (Table 4). The sensitivity, specificity, and accuracy of the combined detection were all higher than those of the single detection.

4. Discussion

PC is one of the most common clinical malignant tumors of the digestive system. It has no typical features in the early stage and is highly occultive, which is easily ignored by patients [14]. With the extension of time, the disease began to deteriorate, and the patient had missed the best opportunity for radical treatment when diagnosed [15]. At present, the treatment of PC includes surgery, radiotherapy and chemotherapy, and targeted therapy. However, the treatment effect is poor, and the patients are prone to local recurrence and distant metastasis after surgery, and the 5-year survival rate is low, which seriously threatens the quality of human life [16]. The pancreas has a unique anatomical structure and biological characteristics, which are easily confused with other digestive system diseases. Currently, there is no effective and reliable method for diagnosing PC in clinical practice [17]. In recent years, with the continuous development of laboratory medicine and science and technology, some tumor markers can be applied in immunological detection, which increases the efficiency of early tumor diagnosis to a certain extent [18].

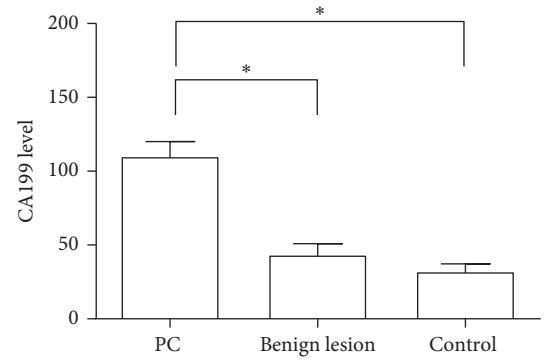

Figure 2: The level of CA199 in three groups.

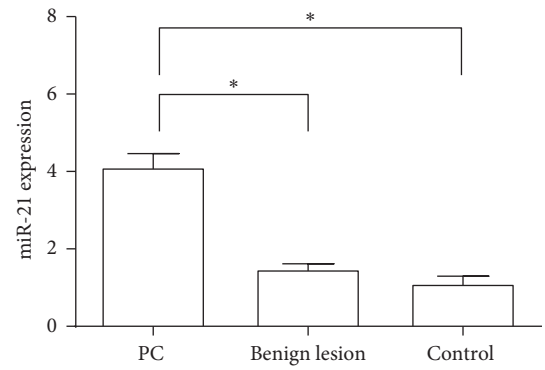

Figure 3: The expression of miR-21 in three groups.

CA199 is currently the most commonly used marker for the diagnosis of pancreatic cancer. The expression level of CA199 is low in normal pancreatic tissues, but it is gradually upregulated when malignant lesions occur in pancreatic ductal epithelial cells [19]. With the continuous deterioration of the disease, the pancreatic duct and small pancreatic ducts are blocked by the tumor, and CA199 invades the stroma around the lesion, leading to a significant increase in the serum level of CA199 [20]. Ge et al. [21] showed that the serum CA199 level in the PC group was significantly higher than that in the pancreatic benign lesion group. Shi et al. [22] reported that serum CA199 levels in the PC group were significantly higher than those in the benign pancreatic disease group and normal control group. MiRNA is a class of short noncoding RNA molecules that can specifically recognize and bind to target genes and play a role in regulating the expression level of target genes [23]. Studies have reported that miR-21 is abnormally expressed in various malignant tumors, such as breast cancer and lung cancer, and can promote the proliferation, invasion, and metastasis of tumor cells [24, 25]. In this study, CA199 and miR-21 in the PC group were significantly upregulated compared with the benign disease group and control group, which was

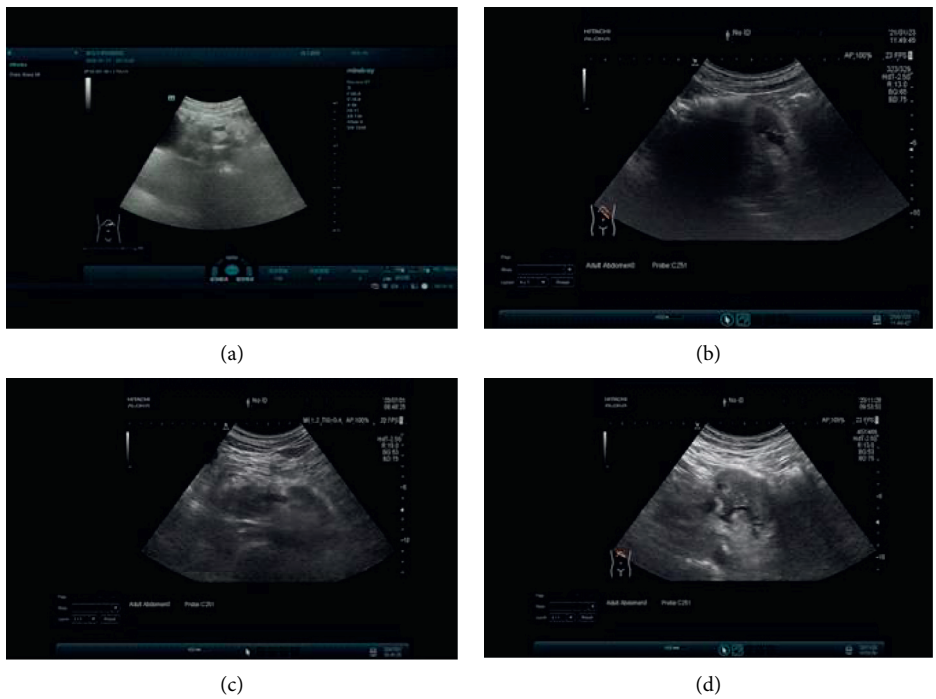

(a) (b) (c) (d)

Figure 4: Color ultrasound image of a pancreatic cancer patient. (a) PC stage I: ultrasound showed hypoechoic nodules in the head of the pancreas with irregular shape and ill-defined boundaries, 1.9×1.7 cm. (b) PC stage II: ultrasound showed a hypoechoic nodule in the head of the pancreas with irregular shape and ill-defined boundaries, 2.6×1.7 cm. (c) PC stage III: ultrasound showed a low-echoing mass in the head and body of the pancreas, with irregular shape, poorly defined boundary, and poorly defined with surrounding tissues, 5.5×3.5 cm. (d) PC stage IV: ultrasound showed a hypoechoic mass in the tail of the pancreatic body, with irregular shape, ill-defined boundary, and unclear boundary with surrounding tissue, 6.9×4.2 cm, surrounded by adjacent arteries.

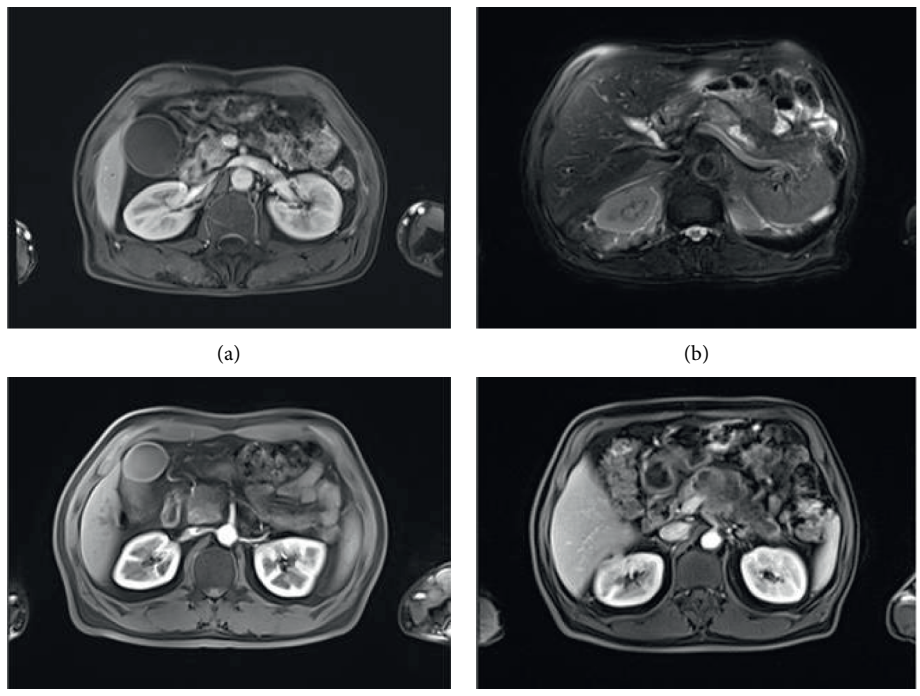

(a) (b) (c) (d)

Figure 5: MRI images of patients with PC. (a) PC stage I: there is a nodular, slightly longer *T*1 shadow in the head of the pancreas, about 10 mm in diameter, with delayed enhancement and dilation of the main pancreatic duct. (b) PC stage II: there was a long *T*1 and *T*2 signal shadow in the body of the pancreas, with obvious hyperintensity on DWI and unclear boundary, 29 mm × 18 mm, and enhanced scanning showed mild enhancement and distal pancreatic duct dilation. (c) PC stage III: the pancreatic head is enlarged, and the pancreatic body and tail are atrophic. In the pancreatic head area, there are lump-like long *T*1 signal shadows, 43 mm × 40 mm, and mild enhancement. (d) PC stage IV: there were lump-like long *T*1 shadows in the body of the pancreas, with an unclear boundary, 40 mm × 85 mm, the enhancement degree was lower than that of the pancreatic parenchyma on an enhanced scan, and the adjacent peritoneal trunk was surrounded in it.

Table 2: Diagnosis of PC by color ultrasonography.

	Clinical stage				Total
	I stage	II stage	III stage	IV stage	
I stage	40	9	0	0	49
II stage	6	54	3	0	63
III stage	0	5	26	2	33
IV stage	0	0	2	13	15
Total	46	68	31	15	160

Table 3: Diagnosis of PC by MRI.

	Clinical stage				Total
	I stage	II stage	III stage	IV stage	
I stage	38	7	0	0	45
II stage	5	55	4	0	64
III stage	3	6	24	2	35
IV stage	0	0	3	13	15
Total	46	68	31	15	160

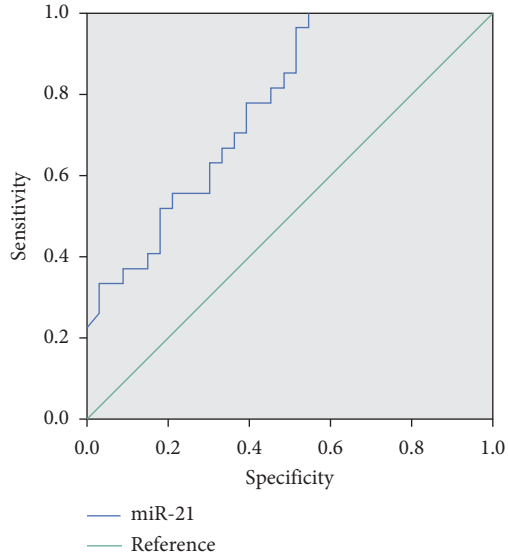

Figure 6: ROC curve of miR-21 in the diagnosis of PC.

consistent with the abovementioned expression results. Our findings suggested that CA199 and miR-21 could be used as serological indicators for the clinical diagnosis of PC.

Ultrasound, MSCT, MRI, and other imaging techniques are widely used in the early diagnosis of PC. Imaging techniques can be used to directly observe the location, size, shape, invasion, and surrounding organ tissue of the lesion, so as to make an effective differential diagnosis and more accurate clinical staging evaluation of PC [26–28]. MRI is a chemical imaging technology, which has the advantages of high soft-tissue resolution, multiple imaging sequences and no ionizing radiation, etc. It has a better effect in detail display and can detect small lesions of PC, which has certain advantages in the diagnosis of PC [29]. Color ultrasound is a diagnostic technology based on two-dimensional ultrasound and has the characteristics of rapidness and noninvasiveness [30]. On color ultrasound, PC is characterized by smooth dilation and interruption of the pancreatic duct. PC is caused mainly by cancerous changes in the epithelial cells of the pancreatic duct. With the continuous deterioration of the cancer cells, the pancreatic duct in patients will be obstructed and narrowed, eventually resulting in smooth dilation and interruption of the pancreatic duct [31].

This study showed that the sensitivity, specificity, and accuracy of miR-21 were 58.13%, 79.00%, and 66.15%, respectively. The sensitivity, specificity, and accuracy of CA199 were 69.38%, 74.00%, and 71.15%, respectively. The sensitivity, specificity, and accuracy of color ultrasonography were 83.13%, 89.00%, and 85.38%, respectively. The sensitivity, specificity, and accuracy of MRI were 81.25%, 90.00%, and 84.62%, respectively. The sensitivity, specificity, and accuracy of the combined assay were 91.88%, 96.00%, and 93.46%, respectively. The detection rate of the combined assay was significantly higher than that of the single assay. The results showed that a single test in the diagnosis of PC has a higher rate of missed diagnosis and

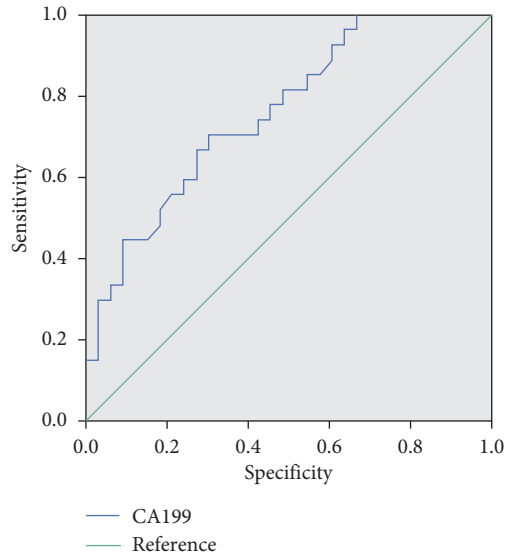

Figure 7: ROC curve of CA199 in the diagnosis of PC.

Table 4: Comparison of diagnostic value (%).

Diagnosis method	Sensitivity	Specificity	Accuracy	Positive prediction rate	Negative prediction rate
miR-21	58.13 (93/160)	79.00 (79/100)	66.15 (172/260)	81.58 (93/114)	54.11 (79/146)
CA199	69.38 (111/160)	74.00 (74/100)	71.15 (185/260)	81.02 (111/137)	60.16 (74/123)
Color ultrasonography	83.13 (133/160)	89.00 (89/100)	85.38 (222/260)	92.36 (133/144)	76.72 (89/116)
MRI	81.25 (130/160)	90.00 (90/100)	84.62 (220/260)	92.85 (130/140)	75.00 (90/120)
Combined diagnosis	91.88 (147/160)	96.00 (96/100)	93.46 (243/260)	97.35 (147/151)	88.07 (96/109)

misdiagnosis, and the combination of multiple detection methods can make up for the limitations of each and significantly increase the sensitivity and accuracy of PC diagnosis. However, the sample size of this study is small, and it is a retrospective analysis, so there may be some deviation in the study results, and it is necessary to further improve the study in the future.

5. Conclusions

In conclusion, color ultrasound and MRI examination of PC have a high detection rate, providing imaging information for patients' treatment plans. Serum CA199 and miR-21 levels were significantly overexpressed in the serum of PC patients. Combined color ultrasound and MRI examination can significantly improve the sensitivity, specificity, and accuracy of the diagnosis of early PC, which is conducive to the clinical judgment of the severity of the disease of PC patients.

Data Availability

The data used to support the findings of this study are available from the corresponding author upon request.

Conflicts of Interest

The authors declare no conflicts of interest.

References

[1] M. Ilic and I. Ilic, "Epidemiology of pancreatic cancer," *World Journal of Gastroenterology*, vol. 22, no. 44, pp. 9694–9705, 2016.

[2] V. Goral, "Pancreatic cancer: pathogenesis and diagnosis," *Asian Pacific Journal of Cancer Prevention*, vol. 16, no. 14, pp. 5619–5624, 2015.

[3] D. Ansari, B. Tingstedt, B. Andersson et al., "Pancreatic cancer: yesterday, today and tomorrow," *Future Oncology*, vol. 12, no. 16, pp. 1929–1946, 2016.

[4] L. C. Chu, M. G. Goggins, and E. K. Fishman, "Diagnosis and detection of pancreatic cancer," *The Cancer Journal*, vol. 23, no. 6, pp. 333–342, 2017.

[5] J. Benzel and V. Fendrich, "Familial pancreatic cancer," *Oncology Research and Treatment*, vol. 41, no. 10, pp. 611–618, 2018.

[6] F. J. Sheedy, "Turning 21: induction of miR-21 as a key switch in the inflammatory response," *Frontiers in Immunology*, vol. 6, p. 19, 2015.

[7] P. Zeng, H. Li, Y. Chen, H. Pei, and L. Zhang, "Serum CA199 levels are significantly increased in patients suffering from liver, lung, and other diseases," *Progress in Molecular Biology and Translational Science*, vol. 162, pp. 253–264, 2019.

[8] M. Campos-da-Paz, J. G. Dórea, A. S. Galdino, Z. G. M. Lacava, and M. d. F. M. A. Santos, "Carcinoembryonic antigen (CEA) and hepatic metastasis in colorectal cancer: update on biomarker for clinical and biotechnological approaches," *Recent Patents on Biotechnology*, vol. 12, no. 4, pp. 269–279, 2018.

[9] D. Teng, K. Wu, Y. Sun et al., "Significant increased CA199 levels in acute pancreatitis patients predicts the presence of pancreatic cancer," *Oncotarget*, vol. 9, no. 16, pp. 12745–12753, 2018.

[10] W.-Y. Xu, H.-H. Zhang, X.-B. Yang et al., "Prognostic significance of combined preoperative fibrinogen and CA199 in gallbladder cancer patients," *World Journal of Gastroenterology*, vol. 24, no. 13, pp. 1451–1463, 2018.

[11] T. Yousaf, G. Dervenoulas, and M. Politis, "Advances in MRI methodology," *International Review of Neurobiology*, vol. 141, pp. 31–76, 2018.

[12] M. Manfredi, F. Mele, D. Garrou et al., "Multiparametric prostate MRI: technical conduct, standardized report and clinical use," *Minerva Urology and Nephrology*, vol. 70, no. 1, pp. 9–21, 2018.

[13] X. Li, L. Zhang, Z. Peng et al., "The impact of ultrasonic treatment on blueberry wine anthocyanin color and its in-vitro anti-oxidant capacity," *Food Chemistry*, vol. 333, Article ID 127455, 2020.

[14] S. Heinrich and H. Lang, "Neoadjuvant therapy of pancreatic cancer: definitions and benefits," *International Journal of Molecular Sciences*, vol. 18, no. 8, p. 1622, 2017.

[15] M. A. Tempero, "NCCN guidelines updates: pancreatic cancer," *Journal of the National Comprehensive Cancer Network: JNCCN*, vol. 17, no. 5.5, pp. 603–605, 2019.

[16] R. Gupta, I. Amanam, and V. Chung, "Current and future therapies for advanced pancreatic cancer," *Journal of Surgical Oncology*, vol. 116, no. 1, pp. 25–34, 2017.

[17] B. M. Wolpin, "Pancreatic cancer," *Hematology/Oncology Clinics of North America*, vol. 29, no. 4, pp. xiii–xiv, 2015.

[18] A. Wang, B. Sun, M. Wang et al., "Predictive value of CONUT score combined with serum CA199 levels in postoperative survival of patients with pancreatic ductal adenocarcinoma: a retrospective study," *PeerJ*, vol. 8, p. e8811, 2020.

[19] D. Huang, Q. Lin, J. Song, and B. Xu, "Prognostic value of pretreatment serum CA199 in patients with locally advanced rectal cancer treated with CRT followed by TME with normal pretreatment carcinoembryonic antigen levels," *Digestive Surgery*, vol. 38, no. 1, pp. 24–29, 2021.

[20] Y. Lu, H. Yu, S. Qin et al., "Single and combined use of preoperative inflammatory biomarkers and CA199 in diagnosing pancreatic cancer," *Clinical Laboratory*, vol. 66, no. 11, 2020.

[21] L. Ge, B. Pan, F. Song et al., "Comparing the diagnostic accuracy of five common tumour biomarkers and CA19-9 for pancreatic cancer: a protocol for a network meta-analysis of diagnostic test accuracy," *BMJ Open*, vol. 7, no. 12, Article ID e018175, 2017.

[22] Q. Shi, K. Feng, L. Xia, C. Wang, and J. Zhu, "Combined use of serum miR-499a-5p and CA199 increases the diagnostic sensitivity of pancreatic cancer," *Clinical Laboratory*, vol. 65, no. 11, 2019.

[23] V. L. Nasci, S. Chuppa, L. Griswold, K. A. Goodreau, R. K. Dash, and A. J. Kriegel, "miR-21-5p regulates mitochondrial respiration and lipid content in H9C2 cells," *American Journal of Physiology-Heart and Circulatory Physiology*, vol. 316, no. 3, pp. H710–H721, 2019.

[24] J. Yuan, H. Chen, D. Ge et al., "Mir-21 promotes cardiac fibrosis after myocardial infarction via targeting Smad7," *Cellular Physiology and Biochemistry*, vol. 42, no. 6, pp. 2207–2219, 2017.

[25] H. Y. Liu, Y. Y. Zhang, B. L. Zhu et al., "miR-21 regulates the proliferation and apoptosis of ovarian cancer cells through PTEN/PI3K/AKT," *European Review for Medical and Pharmacological Sciences*, vol. 23, no. 10, pp. 4149–4155, 2019.

[26] L. Sahlani, L. Thompson, A. Vira, and A. R. Panchal, "Bedside ultrasound procedures: musculoskeletal and non-musculoskeletal," *European Journal of Trauma and Emergency Surgery*, vol. 42, no. 2, pp. 127–138, 2016.

[27] G. Widmann and A. A. Al-Ekrish, "Ultralow dose MSCT imaging in dental implantology," *The Open Dentistry Journal*, vol. 12, no. 1, pp. 87–93, 2018.

[28] J. P. Marques, F. F. J. Simonis, and A. G. Webb, "Low-field MRI: an MR physics perspective," *Journal of Magnetic Resonance Imaging*, vol. 49, no. 6, pp. 1528–1542, 2019.

[29] A.-M. Hespel and R. C. Cole, "Advances in high-field MRI," *Veterinary Clinics of North America: Small Animal Practice*, vol. 48, no. 1, pp. 11–29, 2018.

[30] E. d. O. Barcaui, A. C. P. Carvalho, F. P. P. L. Lopes, J. Piñeiro-Maceira, and C. B. Barcaui, "High frequency ultrasound with color doppler in dermatology," *Anais Brasileiros de Dermatologia*, vol. 91, no. 3, pp. 262–273, 2016.

[31] E. Ozan, G. K. Atac, and S. Gundogdu, "Twinkling artifact on color doppler ultrasound: an advantage or a pitfall?" *Journal of Medical Ultrasonics (2016)*, vol. 43, no. 3, pp. 361–371, 2016.

Hindawi
Journal of Oncology
Volume 2021, Article ID 6880473, 8 pages
https://doi.org/10.1155/2021/6880473

Research Article

Propofol Suppresses Cell Progression by Inhibiting CCL18 Expression in Hepatoblastoma

Hua Zhang,[1] **Pingling Lin**,[2] **Lei Fu**,[3] **Zhijun Li**,[4] **and Yan Ding**[5]

[1]*Department of Pharmacy, Yantaishan Hospital, Yantai 264000, China*
[2]*Department of Pediatrics (I), Jiyang People's Hospital, Jinan 251400, China*
[3]*PIVAS, Qingdao Central Hospital Affiliated to Qingdao University, Qingdao 266042, China*
[4]*Department of Pediatrics, Zhangqiu District People's Hospital, Jinan 250200, China*
[5]*Department of Pediatric Ward (II), Rizhao People's Hospital, Rizhao 276800, China*

Correspondence should be addressed to Yan Ding; dingyan@sdrzph.cn

Received 25 June 2021; Accepted 8 July 2021; Published 27 July 2021

Academic Editor: Muhammad Wasim Khan

Background. Propofol is an anesthetic commonly used clinically and has been found to have antitumor activity in various cancers. The purpose of this study was to investigate the role of propofol in hepatoblastoma (HB). *Methods*. CCK-8 and transwell were used to measure cell proliferation, migration, and invasion in HB cells. Cell apoptosis rate was measured by FCM. The expression of CCL18 in HB tissues and cells was detected by RT-qPCR. Western blotting was used to explore the protein expression of CCK18- and PI3K/AKT-related proteins. *Results*. The expression of CCL18 in HB tissues and cells was overexpressed compared with control groups. CCL18 knockdown was found to notably block cell proliferation and progression, while enhancing cell apoptosis in HuH-6 and HepT1 cells. Furthermore, propofol suppressed the proliferation of HB cells in a dose-dependent manner. According to the results, we chose 5 μg/mL of propofol-treated cells for 48 hours as the subsequent experimental conditions. We found that propofol (5 μg/mL, 48 h) significantly blocked cell migration and invasion, but induced cell apoptosis in HuH-6 and HepT1 cells. In addition, CCK18 overexpression facilitated cell progression in HB cells, while propofol dramatically suppressed the effect of CCK18. Besides that, propofol suppressed the PI3K/AKT pathway. *Conclusion*. Propofol suppressed the development of HB cells by inhibiting CCK18 expression and the PI3K/AKT pathway. Therefore, we infer that propofol plays a role in the treatment of HB.

1. Introduction

Hepatoblastoma (HB) is mainly derived from human immature liver precursor cells [1]. HB is the most common primary liver malignant tumor in children, and 90% of patients are affected before the age of 5 years [2]. HB is an increasingly common tumor worldwide, especially in North America and Europe. HB is treated by adjuvant chemotherapy, radiotherapy, and transplantation, and the survival rate for patients with HB has increased dramatically. However, for patients with advanced HB, the prognosis is still poor [3]. Therefore, it is essential to explore the early biomarkers of HB and find effective treatment methods for patients with HB.

Propofol is a short-acting intravenous anesthetic of alkyl phenols, which is widely used in clinical practice [4]. It plays a sedative and hypnotic role by activating the GABA receptor-chloride ion complex [5]. Propofol has the advantages of rapid onset of anesthesia induction, rapid recovery and complete functional recovery, and low incidence of postoperative malignant vomiting [6]. In addition to the anesthetic effect, propofol can also affect the biological process of tumors and have different effects on different tumor cells [7]. Propofol has been reported to affect the epigenetic pathways such as lncRNAs, miRNAs, and cancer-related proteins and regulate the genetic signaling pathways such as MAPK, PI3K/AKT, NF-κB, SLUG, and Nrf2 [8]. A growing number of studies have shown that propofol may

exert an antitumor effect in human tumors, such as colon cancer [9], ovarian cancer [10], and lung cancer [11]. At present, propofol is widely used in HB surgery and postoperative sedation. Therefore, the effect of propofol on the biological behavior of HB cells has gradually attracted researchers' attention.

CCL18 is a member of the chemokines family. CCL18 has been found to play a special role in the development of human tumors. It is reported that the role of CCL18 in tumors appears after TAM involvement into the tumor niche [12]. Lane et al. reported that CCL18 in ascites accelerated cell migration by regulating Pyk2 in ovarian cancer [13]. In oral cancer, CCL18 was found to facilitate cell progression by activating the JAK2/STAT3 pathway [14]. However, the role of CCL18 in HB is not well understood.

In this study, we aimed to investigate the effect of propofol on the progression of HB. Furthermore, propofol was confirmed to suppress HB tumor progression by regulating CCL18.

2. Materials and Methods

2.1. Patient Samples. HB tissues were obtained from 20 children in Yantaishan Hospital (Yantai, China). All patients were diagnosed as HB preoperatively. Twenty paracancer tissues were at least 2 cm from the tumor margin. All specimens were placed in liquid nitrogen within 30 minutes after isolation and then stored in a −80°C refrigerator. This study was approved by the ethics committee of Yantaishan Hospital, and informed consent of the patients was obtained before surgery.

2.2. Cell Lines and Propofol. Human HB cell lines HepG2, HuH-6, and HepT1 and normal liver cells MIHA were collected from Yantaishan Hospital. After resuscitation at 37°C, the cells were resuspended on Dulbecco's Modified Eagle Medium (DMEM) containing 100 ml/L fetal bovine serum (FBS) and 10 ml/L penicillin and streptomycin. The cells were cultured in a constant-temperature incubator at 37°C and 5% CO_2 for 3-4 days. After cell fusion, the cells were subcultured into a cell culture flask (5 ml/L). Cells were cultured for 4-5 generations for subsequent experiments. Propofol was obtained from Qingyuan JiaBo Pharmaceutical Co. Ltd. (China). The final concentrations of propofol were 0, 2, 5, and 10 μg/mL with complete medium.

2.3. Transfection of si-CCL18. Cells (1×10^6/mL) were inoculated into a 6-well plate. HuH-6 and HepT1 cells were transfected with CCL18 si-RNA (5′-ACAAGTTGGTACCAACAAATT-3′), pcDNA3.1-CCL18, and the corresponding negative control oligonucleotides mixed with LipofectamineTM 2000, respectively. After transfection for 48 h, the cells were collected for subsequent experiments.

2.4. Cell Proliferation. Proliferative ability of HuH-6 and HepT1 cells was evaluated by using the cell counting kit-8 (CCK-8) method. Cell suspension was evenly planted in a 96-well plate with a density of 3ч 10^3 cells/well. Cells were cultured in an incubator for 24, 48, and 72 h and then added with 100 μl DMEM medium and 10 μl CCK-8 solution. The cells were replaced in the incubator for further incubation for 1 to 4 hours. A microplate analyzer was used to detect the OD value of cells at 450 nm.

2.5. Cell Migration and Invasion. Transwell assay was performed to measure cell migration and invasion in HuH-6 and HepT1 cells. Cells are routinely digested to prepare cell suspensions. 100 μl cell suspension was inoculated in the upper transwell chamber, and 500 μl DMEM was added to the lower chamber. The cells were cultured in a constant-temperature cell incubator a 37°C and 5% CO_2. After 24 hours, 200 μl paraformaldehyde was added to fix cells for 15 min. Then, cells were stained with crystal violet for 20 min. Photographs were taken under a microscope, and the number of migrated and invaded cells was counted.

2.6. Cell Apoptosis. Flow cytometry (FCM) was used to measure cell apoptosis in HuH-6 and HepT1 cells. Cells were seeded into a 24-well plate and incubated in an incubator at 37°C and 5% CO_2 for 24 h. After centrifugation at 1500 r/min for 5 min, the supernatant was discarded. Cells were labeled with 1 mL Annexin V and 1 mL Sytox Green. After incubation at 37°C for 15 min, FCM (Beckman Coulter, Germany) was performed to detect cell apoptosis rate within 4 h.

2.7. Real-Time PCR. Total RNA was extracted by Trizol reagent. Reverse transcription system: 5xPrimer Script Buffer 2 μl, RT Enzyme Mix 0.5 μl, primer 0.5 μl, RNA1 μl, and RNAase-free ddH_2O 6 μl. The cDNA was obtained by reverse transcription and then diluted to 50 ng/μl. Real-time PCR transcription system: SYBR premix ExTaqTM II (2x) 10 μl, forward primer 1 μl, reverse primer 1 μl, cDNA 1 μl, and ddH2O 7 μl. The primers were CCL18 forward: 5′-TGGCAGATTCCACAAAAGTTCA-3′, reverse 5′-GGATGACACCTGGCTTGGG-3′; GAPDH forward 5′-GCACCGTCAAGGCTGAGAAC-3′, and reverse 5′-TGGTGAAGACGCCAGTGGA-3′.

2.8. Western Blotting. After transfection for 24–48 hours, cell proteins were extracted by RIPA lysate. The BCA kit was used to detect protein concentration and purity. The protein samples were subjected to SDS-PAGE gel electrophoresis at 80 V and for 2 hours. After the protein was transferred to the PVDF membrane, it was sealed with milk powder at room temperature for 1–2 hours. Subsequently, the PVDF membrane was added with primary antibody and incubated overnight at 4°C. Then, the PVDF membrane was incubated with secondary antibody at room temperature for 2 hours. Finally, ECL chemiluminescence solution was added into the gel imaging system to collect images, and the protein bands were quantitatively analyzed with Image J.

2.9. Statistical Analysis. SPSS23.0 statistical software and GraphPadPrism software were used for statistical analysis. The *t*-test was used to compare the differences between the two experimental groups. Univariate ANOVA analysis was used for comparison between groups. $p < 0.05$ indicated that the comparison results between the experimental groups were statistically significant. All data are mean ± SD from three or more independent trials.

3. Results

3.1. Overexpression of CCL18 Was Observed in HB. According to the RT-qPCR assay, tumor tissues assumed the overexpression of CCL18 compared with normal tissues (Figure 1(a)). Next, western blot results showed that CCL18 was higher expressed in HepG2, HuH-6, and HepT1 cells than in MIHA cells (Figure 1(b)). Therefore, we speculated that CCL18 might play a specific role in HB progression.

3.2. CCL18 Depletion Played an Antitumor Role in HuH-6 and HepT1 Cells. To investigate the specific role of CCL18 in HB, we knock down its expression in HuH-6 and HepT1 cells. As shown in Figure 2(a), the expression of CCL18 was notably reduced by CCL18 si-RNA. CCK-8, transwell, and FCM were used to assess the effect of CCL18 knockdown in HB cells. As we expected, cell proliferation was significantly declined in HuH-6 and HepT1 cells when transfected with CCL18 knockdown (Figure 2(b)). Furthermore, after CCL18 knockdown transfection, the invasiveness of HuH-6 and HepT1 cells was significantly decreased (Figure 2(c)). Similarly, the migration ability of HuH-6 and HepT1 cells transfected with CCL18 knockdown was notably reduced (Figure 2(d)), whereas FCM results verified that CCL18 depletion significantly accelerated cell apoptosis in HB cells (Figure 2(e)). Taken together, we assumed that CCL18 knockdown played a role as a tumor suppressor in HB cells.

3.3. Propofol Suppressed Cell Growth, Migration, and Invasion in HB Cells. To investigate the effect of propofol in HB cells, the concentration and treatment time of propofol were first determined by CCK-8 results. We found that cell viability of HuH-6 and HepT1 cells was notably reduced in a concentration-dependent effect of propofol (0, 2, 5, and 10 μg/mL) (Figure 3(a)). Next, cell viability was suppressed in HuH-6 and HepT1 cells treated with 5 μg/mL propofol for 24, 48, or 96 h (Figure 3(b)). According to the experimental results, 5 μg/mL propofol treatment for 48 hours ($p < 0.01$) was selected for the subsequent experimental condition. CCK-8 assay indicated that propofol (5 μg/mL, 48 h) suppressed cell viability in HB cells (Figure 3(c)). Transwell assay displayed that propofol (5 μg/mL, 48 h) significantly reduced cell invasion (Figure 3(d)). Not surprisingly, cell migration ability was notably reduced by propofol (Figure 3(e)). In addition, propofol dramatically accelerated cell apoptosis in HuH-6 and HepT1 cells (Figure 3(f)).

3.4. Propofol Suppressed Cell Progression by Inhibiting CCL18 Expression and Downregulating the PI3K/AKT Pathway in HB. In order to study the effect of propofol on CCL18 in the progression of HB cells, HuH-6 and HepT1 cells transfected with CCL18 vector were treated with propofol. As shown in Figure 4(a), propofol decreased the expression of CCL18 vector in HuH-6 and HepT1 cells. Next, functional experiments were performed to verify the interaction between propofol and CCL18 in HB cells. We noticed that CCL18 vector accelerated the proliferation of HB cells, while propofol weakened the effect of CCL18 (Figure 4(b)). Likewise, propofol neutralized the stimulative effect of CCL18 on cell migration and invasion (Figures 4(c) and 4(d)).

The PI3K-Akt pathway is a classic antiapoptotic and prosurvival signal transduction pathway, which plays an important role in the occurrence, proliferation, invasion, and metastasis of tumors [15]. Western blot assay was used to study the effect of propofol/CCL18 on the PI3K/AKT pathway. The results displayed that CCL18 vector increased the phosphorylation of PI3K and AKT, while propofol suppressed the phosphorylation of PI3K and AKT (Figure 4(e)).

4. Discussion

The expression and function of CCL18 in HB were evaluated in this study. We found that CCL18 was obviously overexpressed in HB tissues. Additionally, CCL18 was also overexpressed in HB cell lines (HepG2, HuH-6, and HepT1 cells) compared with MIHA cells. CCK-8, transwell, and FCM assay were used to study the effect of CCL18 on tumor progression in vitro. In HuH-6 and HepT1 cells, knockdown of CCL18 significantly reduced cell proliferation, invasion, and migration, but significantly promoted cell apoptosis. Combined with the experimental results, we speculated that CCL18 plays a role as a procancer factor in HB. Many previous studies have confirmed that CCL18 plays an oncogenic role in a variety of cancers. Lin et al. found that CCL18 facilitated cell progression and EMT by regulating the NF-κB pathway in hepatocellular carcinoma [16], which is consistent with our findings. Furthermore, CCL18 promoted cell growth and cell motility in squamous cell carcinoma of the head and neck [17]. In osteosarcoma, Su et al. confirmed that CCL18 promoted tumor progression by increasing UCA1 expression [18].

Propofol is the most widely used intravenous anesthetic in clinical anesthesia. Propofol is characterized by quick action, strong effect, and quick recovery. At present, the role of propofol in human tumors has become a research hotspot. Previous studies have shown that propofol obviously suppresses tumor development. Zhou et al. reported that propofol inhibited tumor growth in mice with liver cancer [19]. Propofol was verified to reduce proinflammatory factors and increase anti-inflammatory factors, so as to effectively improve the immune function of patients with pancreatic cancer [20]. In pancreatic cancer, propofol suppressed cell proliferation and migration by inhibiting the ERK/MMPs pathway [21]. In hepatocellular carcinoma,

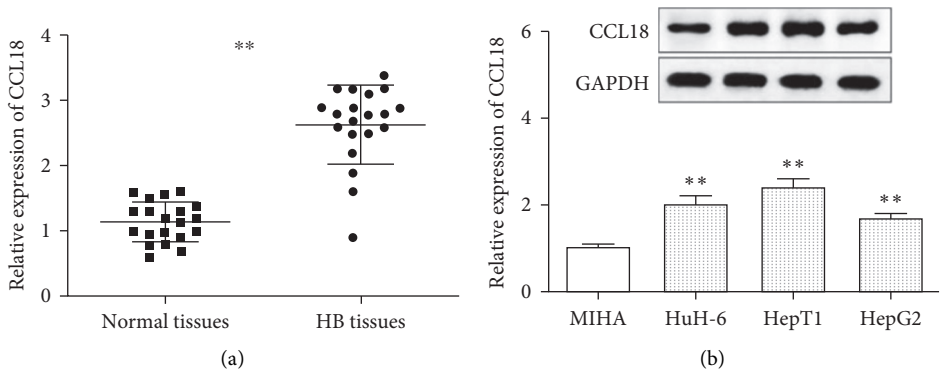

Figure 1: Overexpression of CCL18 was observed in HB. (a) CCL18 was significantly upregulated in 20 HB tissues compared with normal tissues. (b) CCL18 was overexpressed in HuH-6, HepT1, and HepG2 cells compared with MIHA cells. $^{**}p < 0.01$.

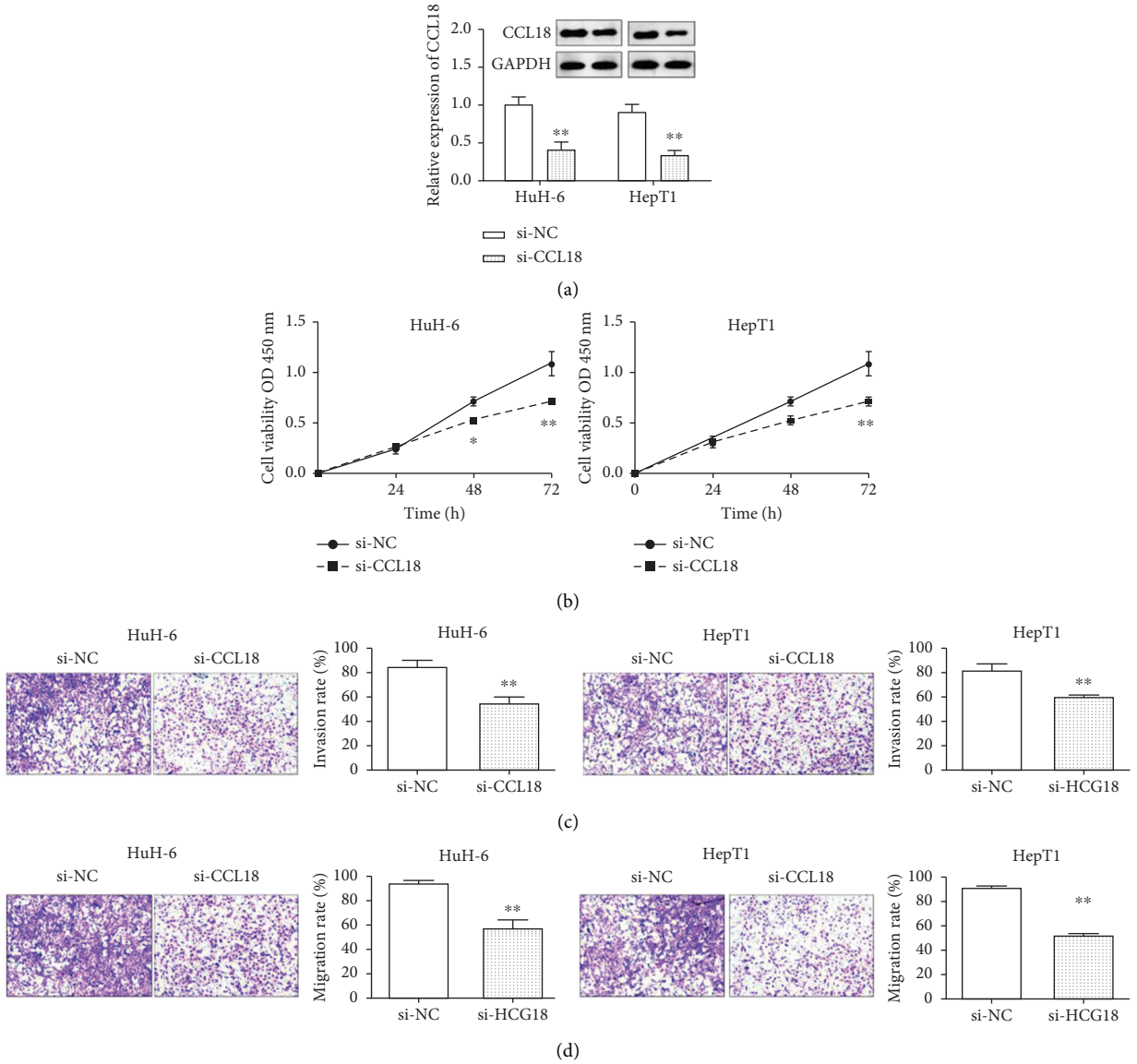

Figure 2: Continued.

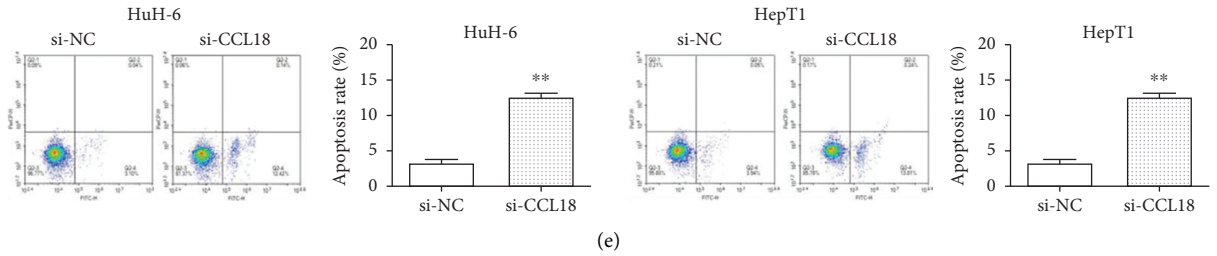

Figure 2: CCL18 depletion played an antitumor role in HuH-6 and HepT1 cells. (a) The expression of CCL18 in HuH-6 and HepT1 cells transfected with CCL18 si-RNA. (b), Cell proliferation was notably suppressed by CCL18 knockdown in HuH-6 and HepT1 cells. (c) Cell invasion was notably inhibited by CCL18 knockdown in HuH-6 and HepT1 cells (scale bar = 100 μm). (d) Cell migration was notably suppressed by CCL18 knockdown in HuH-6 and HepT1 cells (scale bar = 100 μm). (e) Cell apoptosis was notably promoted by CCL18 knockdown in HuH-6 and HepT1 cells. $^{**}p < 0.01$.

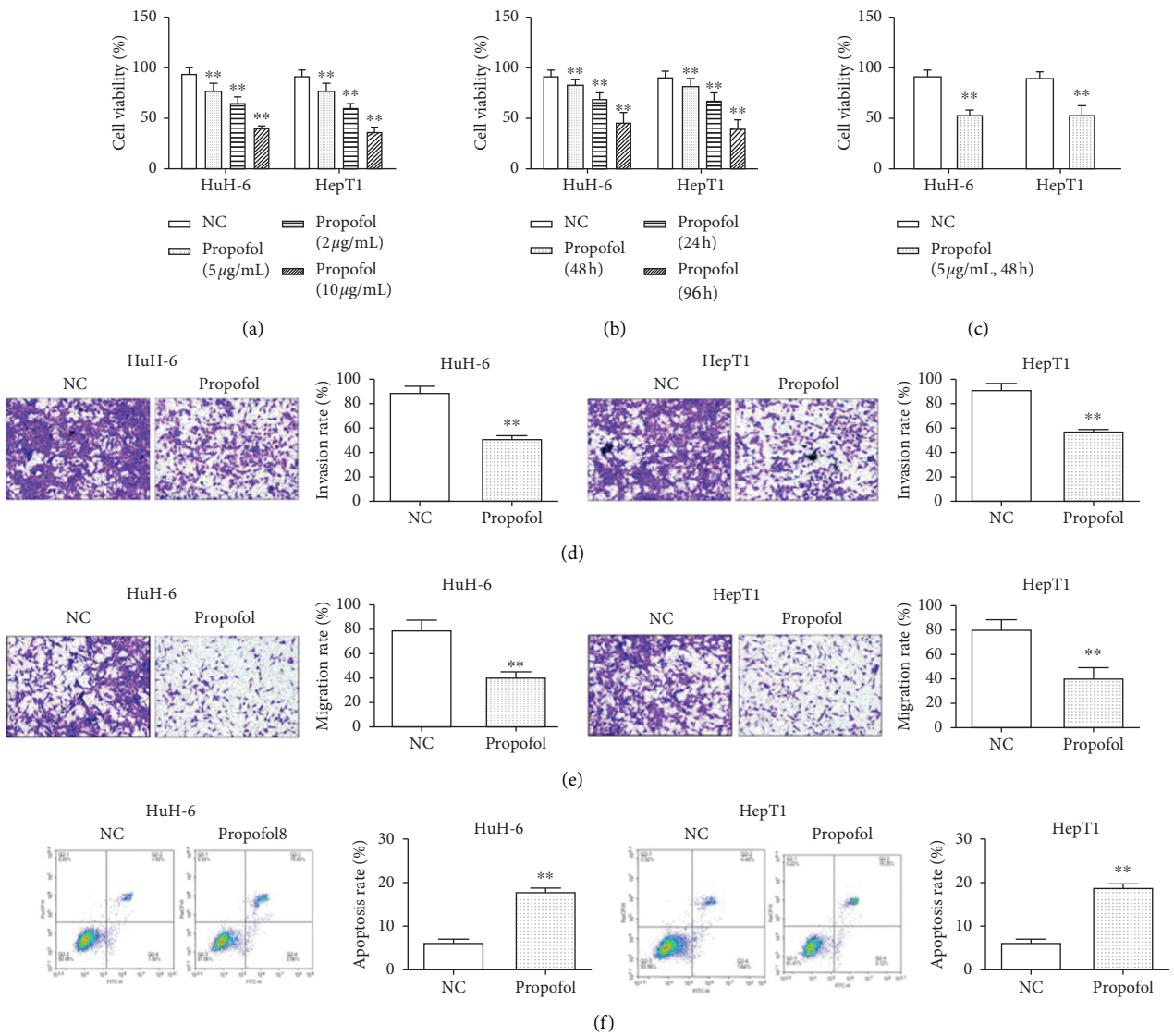

Figure 3: Propofol suppressed cell growth, migration, and invasion in HB cells. (a) The effect of different concentrations of propofol (0, 2, 5, and 10 μg/mL) on HB cell viability. (b) The effect of different treatment time of propofol (0, 24, 48, and 96 h) on HB cell viability. (c) Propofol (5 μg/mL, 48 h) suppressed cell viability in HuH-6 and HepT1 cells. (d) Propofol (5 μg/mL, 48 h) suppressed cell invasion in HuH-6 and HepT1 cells (scale bar = 100 μm). (e) Propofol (5 μg/mL, 48 h) inhibited cell migration in HuH-6 and HepT1 cells (scale bar = 100 μm). (f) Propofol (5 μg/mL, 48 h) enhances cell apoptosis in HuH-6 and HepT1 cells. $^{**}p < 0.01$.

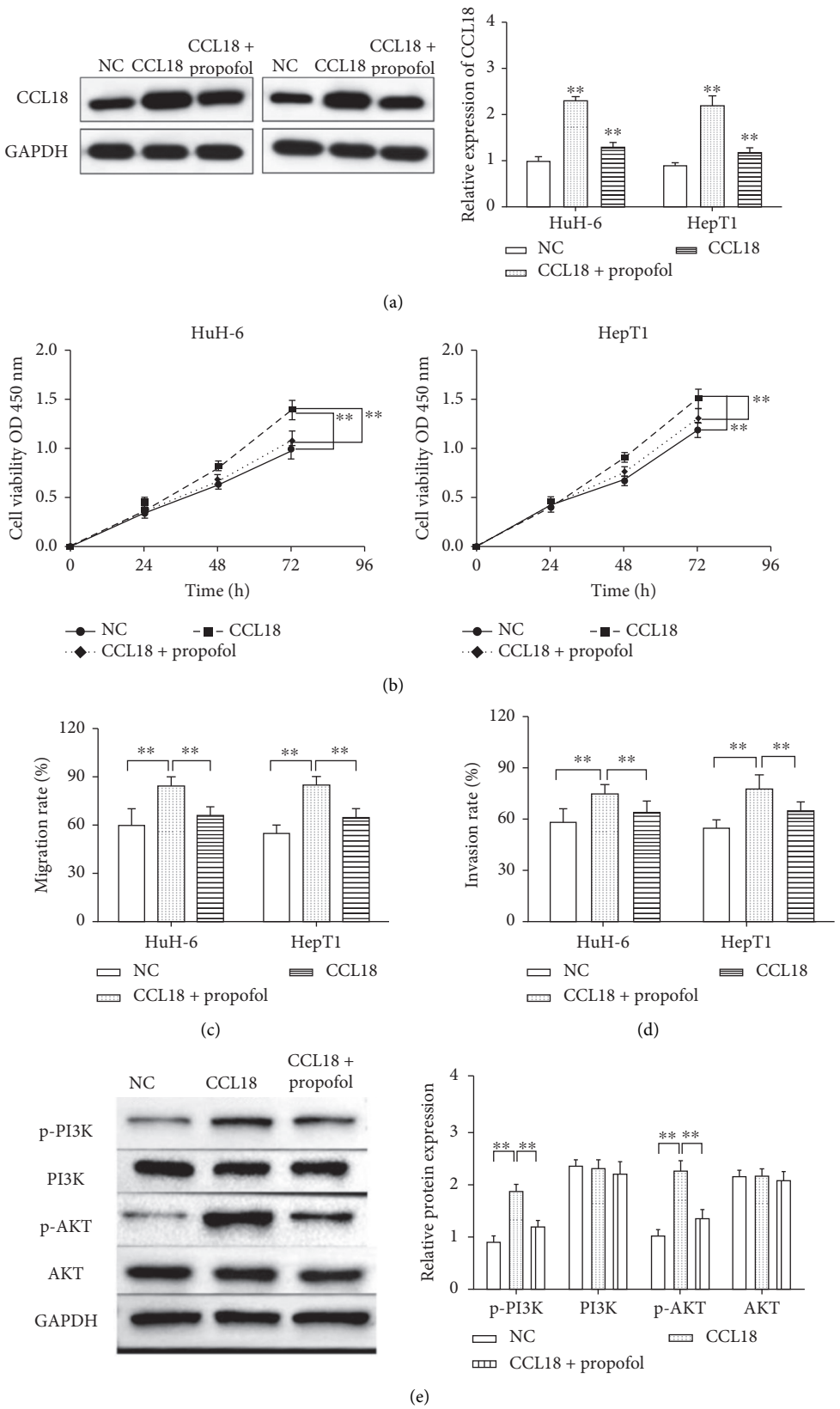

Figure 4: Propofol suppressed cell progression by inhibiting CCL18 expression and downregulating the PI3K/AKT pathway in HB. (a) The expression of CCL18 after treated with propofol. (b) After treated with propofol, cell proliferation induced by CCL18 was suppressed. (c)-(d) After propofol, cell invasion and migration promoted by CCL18 was decreased. (e) CCL18 vector promoted the phosphorylation of PI3K and AKT, while propofol suppressed the phosphorylation of PI3K and AKT. $^{**}p < 0.01$.

propofol has been shown to block the progression [22–24]. Similarly, we found that propofol inhibited extracellular activity in HB. Unlike the previous results, we studied the effect of propofol on CCL18 expression in HB cells. We noticed that propofol reduced the expression level of CCL18. Above all, the promotional effect of CCL18 in HB was suppressed by propofol.

The PI3K/AKT pathway is a classical signaling pathway involved in the regulation of various cellular functions such as proliferation, differentiation, apoptosis, and glucose transport [25]. In recent years, the PI3K/AKT signaling pathway has been found to be closely related to the occurrence and development of human tumors [26, 27]. This pathway regulates the proliferation and survival of tumor cells and is related to tumor cell migration, adhesion, angiogenesis, and degradation of the extracellular matrix [28, 29]. Furthermore, propofol was found to suppress the phosphorylation of PI3K and AKT. Therefore, the results showed that propofol/CCK18 suppressed the development by inhibiting the PI3K/AKT pathway.

To sum up, we found that propofol notably suppressed the progression in HB cells. In addition, propofol played an inhibitory role by blocking the CCL18 expression and PI3K/AKT pathway in HB. However, the dual effect of propofol in relieving the pain of tumor patients and inhibiting tumor progression needs to be confirmed by animal models and clinical trials.

Data Availability

The data used to support the findings of this study are available from the corresponding author upon request.

Conflicts of Interest

The authors declare no conflicts of interest.

References

[1] D. Sharma, G. Subbarao, and R. Saxena, "Hepatoblastoma," *Seminars in Diagnostic Pathology*, vol. 34, no. 2, pp. 192–200, 2017.

[2] S. Ranganathan, D. Lopez-Terrada, and R. Alaggio, "Hepatoblastoma and pediatric hepatocellular carcinoma: an update," *Pediatric and Developmental Pathology*, vol. 23, no. 2, pp. 79–95, 2020.

[3] K. B. Hooks, J. Audoux, H. Fazli et al., "New insights into diagnosis and therapeutic options for proliferative hepatoblastoma," *Hepatology*, vol. 68, no. 1, pp. 89–102, 2018.

[4] R. Vellinga, L. N. Hannivoort, M. Introna et al., "Prospective clinical validation of the Eleveld propofol pharmacokinetic-pharmacodynamic model in general anaesthesia," *British Journal of Anaesthesia*, vol. 126, no. 2, pp. 386–394, 2021.

[5] M. M. Sahinovic, M. M. R. F. Struys, and A. R. Absalom, "Clinical pharmacokinetics and pharmacodynamics of propofol," *Clinical Pharmacokinetics*, vol. 57, no. 12, pp. 1539–1558, 2018.

[6] S. Kim, S. Hahn, M.-J. Jang et al., "Evaluation of the safety of using propofol for paediatric procedural sedation: a systematic review and meta-analysis," *Scientific Reports*, vol. 9, no. 1, Article ID 12245, 2019.

[7] Y. Xu, S. Pan, W. Jiang, F. Xue, and X. Zhu, "Effects of propofol on the development of cancer in humans," *Cell Proliferation*, vol. 53, no. 8, Article ID e12867, 2020.

[8] Y. Ogawa, M. Irifune, A. Mukai et al., "The indirect γ-aminobutyric acid (GABA) receptor agonist gabaculine-induced loss of the righting reflex may inhibit the descending analgesic pathway," *Pharmacology Biochemistry and Behavior*, vol. 198, Article ID 173034, 2020.

[9] Y. F. Zhang, C. S. Li, Y. Zhou, and X. H. Lu, "Effects of propofol on colon cancer metastasis through STAT3/HOTAIR axis by activating WIF-1 and suppressing Wnt pathway," *Cancer Medicine*, vol. 9, no. 5, pp. 1842–1854, 2020.

[10] Y. Sun, Y. Peng, L. Ye, L. Ma, M. Zou, and Z. Cheng, "Propofol inhibits proliferation and cisplatin resistance in ovarian cancer cells through regulating the microRNA-374a/forkhead box O1 signaling axis," *Molecular Medicine Reports*, vol. 21, no. 3, pp. 1471–1480, 2020.

[11] Y. Huang, L. Lei, and Y. Liu, "Propofol improves sensitivity of lung cancer cells to cisplatin and its mechanism," *Medical Science Monitor: International Medical Journal of Experimental and Clinical Research*, vol. 26, Article ID e919786, 2020.

[12] J. Korbecki, M. Olbromski, and P. Dzięgiel, "CCL18 in the progression of cancer," *International Journal of Molecular Sciences*, vol. 21, no. 21, 2020.

[13] D. Lane, I. Matte, C. Laplante et al., "CCL18 from ascites promotes ovarian cancer cell migration through proline-rich tyrosine kinase 2 signaling," *Molecular Cancer*, vol. 15, no. 1, p. 58, 2016.

[14] X. Jiang, Z. Huang, X. Sun et al., "CCL18-NIR1 promotes oral cancer cell growth and metastasis by activating the JAK2/STAT3 signaling pathway," *BMC Cancer*, vol. 20, no. 1, p. 632, 2020.

[15] N. Jiang, Q. Dai, X. Su, J. Fu, X. Feng, and J. Peng, "Role of PI3K/AKT pathway in cancer: the framework of malignant behavior," *Molecular Biology Reports*, vol. 47, no. 6, pp. 4587–4629, 2020.

[16] Z. Lin, W. Li, H. Zhang et al., "CCL18/PITPNM3 enhances migration, invasion, and EMT through the NF-κB signaling pathway in hepatocellular carcinoma," *Tumor Biology*, vol. 37, no. 3, pp. 3461–3468, 2016.

[17] Y. Qin, J. Wang, G. Zhu et al., "CCL18 promotes the metastasis of squamous cell carcinoma of the head and neck through MTDH-NF-κB signalling pathway," *Journal of Cellular and Molecular Medicine*, vol. 23, no. 4, pp. 2689–2701, 2019.

[18] Y. Su, Y. Zhou, Y.-J. Sun et al., "Macrophage-derived CCL18 promotes osteosarcoma proliferation and migration by upregulating the expression of UCA1," *Journal of Molecular Medicine*, vol. 97, no. 1, pp. 49–61, 2019.

[19] Q. Zhou, H. Wu, Y. Liu et al., "Effects of different doses of propofol on the growth and expression of PCNA, CD34 and pAKT proteins in xenografted tumor of BALB/C mice with liver cancer," *Clinical and Translational Oncology*, vol. 22, no. 10, pp. 1741–1749, 2020.

[20] Z. Wang and S. Zhou, "Effect of compound propofol nanoemulsion on immune function in patients with pancreatic cancer," *Journal of Nanoscience and Nanotechnology*, vol. 21, no. 2, pp. 1390–1396, 2021.

[21] X. Yu, J. Shi, X. Wang, and F. Zhang, "Propofol affects the growth and metastasis of pancreatic cancer via ADAM8," *Pharmacological Reports*, vol. 72, no. 2, pp. 418–426, 2020.

[22] Y. Sun and H. Sun, "Retracted: Propofol exerts anticancer activity on hepatocellular carcinoma cells by raising lncRNA

DGCR5," *Journal of Cellular Physiology*, vol. 235, no. 3, pp. 2963–2972, 2020.

[23] H. Zheng, Y. Fu, and T. Yang, "Propofol inhibits proliferation, migration, and invasion of hepatocellular carcinoma cells by downregulating twist," *Journal of Cellular Biochemistry*, vol. 120, no. 8, pp. 12803–12809, 2019.

[24] S.-Q. Liu, J.-L. Zhang, Z.-W. Li, Z.-H. Hu, Z. Liu, and Y. Li, "Propofol inhibits proliferation, migration, invasion and promotes apoptosis through down-regulating miR-374a in hepatocarcinoma cell lines," *Cellular Physiology and Biochemistry*, vol. 49, no. 6, pp. 2099–2110, 2018.

[25] H. Sakai, I. Shiina, T. Shinomiya, and Y. Nagahara, "BRAP2 inhibits the Ras/Raf/MEK and PI3K/Akt pathways in leukemia cells, thereby inducing apoptosis and inhibiting cell growth," *Experimental and Therapeutic Medicine*, vol. 21, no. 5, p. 463, 2021.

[26] H. Lin, G. Zhang, X.-C. Zhang et al., "Germline variation networks in the PI3K/AKT pathway corresponding to familial high-incidence lung cancer pedigrees," *BMC Cancer*, vol. 20, no. 1, p. 1209, 2020.

[27] L. Zhang, J. Wu, M. T. Ling, L. Zhao, and K.-N. Zhao, "The role of the PI3K/Akt/mTOR signalling pathway in human cancers induced by infection with human papillomaviruses," *Molecular Cancer*, vol. 14, no. 1, p. 87, 2015.

[28] R. Liu, Y. Chen, G. Liu et al., "PI3K/AKT pathway as a key link modulates the multidrug resistance of cancers," *Cell Death & Disease*, vol. 11, no. 9, p. 797, 2020.

[29] X. Li, D. Dai, B. Chen, H. Tang, X. Xie, and W. Wei, "Efficacy of PI3K/AKT/mTOR pathway inhibitors for the treatment of advanced solid cancers: a literature-based meta-analysis of 46 randomised control trials," *PLoS One*, vol. 13, no. 2, Article ID e0192464, 2018.

Hindawi
Journal of Oncology
Volume 2021, Article ID 3374939, 6 pages
https://doi.org/10.1155/2021/3374939

Research Article

Analysis of Threshold Change of Tumor Mutation Burden in Gastric Cancer

Xinwei He,[1] **Ming Yu**,[1] **Xuezhong Wang**,[2] **Jixian Chen**,[1] **and Xianglin Li**[3]

[1]*Department of General Surgery, Ruian People's Hospital, Wenzhou 325200, China*
[2]*Department of General Surgery, Ruian Hospital of Traditional Chinese Medicine, Wenzhou 325200, China*
[3]*Department of General Surgery, Yongjia People's Hospital, Wenzhou 325107, China*

Correspondence should be addressed to Xianglin Li; lixianglin@yjxrmyy.com.cn

Received 23 June 2021; Accepted 14 July 2021; Published 22 July 2021

Academic Editor: Muhammad Wasim Khan

Background. The purpose of this study was to investigate the change of tumor mutation burden (TMB) in gastric cancer (GC) and its relationship with prognosis. *Methods*. A total of 262 patients with GC from January 2018 to December 2019 were included in this study. All patients were in the advanced stage and were treated with surgical removal of D2 lymph nodes and dissection. Clinical data and gene expression profile data of the GC dataset in The Cancer Genome Atlas were collected. Patients were randomly divided into a high-level group and a low-level group according to the TMB of 8 mutations/Mb. TMB of GC was calculated based on cell mutation data. Cox regression model was used to evaluate the relationship between TMB and prognosis of GC patients. *Results*. The total mutation rate of 262GC patients was 92.85%. The top 5 mutant genes were TP53, RB1, ARID1A, KMT2B, and RET. The expression level of TMB in GC patients was statistically significant with age, drinking history, and differentiation type. 94 of the 262 patients died, and 168 survived during the follow-up period. Patients with a high level of TMB had a worse prognosis than those with low level of TMB. The results of univariate and multivariate logistic analysis showed that the overall survival rate of GC patients was statistically significant with age, drinking history, clinical stage, differentiation type, and TMB. *Conclusion*. GC patients are often accompanied by changes in TMB, and its expression level is closely related to the degree of pathological differentiation, which is an independent factor affecting the prognosis of GC patients. High TMB value can evaluate the prognosis and provide a reference for the formulation of clinical treatment plans for GC patients.

1. Introduction

Gastric cancer (GC) is a malignant tumor originating from gastric mucosal epithelium, which is more common in people over 50 years old, and has a slightly higher incidence rate in males than in females [1], in recent years, with the change of dietary structure, the increase of work pressure, and the infection of *Helicobacter pylori*. And, GC is also increasingly being diagnosed in younger patients [2, 3]. The early clinical symptoms of GC patients are lack of typical symptoms, such as epigastric discomfort, belching, and other nonspecific symptoms. It is often similar to the symptoms of chronic gastric diseases such as gastritis and gastric ulcer, which increases the difficulty of clinical diagnosis and treatment of GC [4]. Surgical resection of D2 lymph node dissection is the preferred method for patients with GC. Surgery can remove the lesion tissue, prolong the life of patients, and quickly improve their symptoms [5]. However, due to the lack of effective evaluation methods in perioperative period of some GC patients, the long-term prognosis of patients is relatively long [6]. Tumor mutation burden (TMB) is defined as the total number of somatic coding errors, base substitutions, gene insertion, or deletion errors detected per million bases, which can be obtained by the NGS method. Previous studies have shown that TMB is a new biomarker, and its expression level is closely related to the clinical course of treatment, and patients with high TMB benefit more clinically [7]. However, there are a few studies on the change of TMB in GC and its relationship with the prognosis of patients. Therefore, this study aimed to explore

the relationship between TMB changes and prognosis of GC patients.

2. Methods

2.1. Clinical Data. A total of 262 patients with GC from January 2018 to December 2019 were prospectively selected as subjects at Ruian People's Hospital (Wenzhou, China), including 165 males and 97 females, aged 33–64 years old, with an average of 45.98 ± 5.69 years old. The tumor diameter was 1–8 cm, with an average of 4.12 ± 0.61 cm. Tumor sites: lower part of the stomach, 102 cases; middle part of the stomach, 75 cases; and upper part of the stomach, 85 cases. Preoperative staging of GC: 121 cases of stage II, 141 cases of stage III complications, 14 cases of hypertension, 19 cases of diabetes, and 17 cases of hyperlipidemia. This study was approved by the ethics committee of the Ruian People's Hospital, and all patients provided informed consent.

2.2. Inclusion and Exclusion Criteria. Inclusion criteria: (1) patients who met the diagnostic criteria for GC and were confirmed by pathological examination [8]; (2) patients who were in accordance with the indications for surgical removal of D2 lymph node dissection, and all patients had complete baseline and follow-up data; (3) TMB detection of gastric cancer was completed in all patients, and local lesions or metastatic lesions were measurable in all patients.

Exclusion criteria: (1) patients with abnormal cognitive function, routine preoperative chemoradiotherapy, or biological immunotherapy; (2) pathological classification is not clear or routine proton pump inhibitors, antibiotics before examination; (3) patients with autoimmune system diseases or malignant tumors in other parts.

2.3. Surgical Method. All patients were in the advanced stage and were treated with D2 lymph node dissection by surgical resection. Routinely, a 5-well method was used to operate the hole 1 cm below the umbilicus of the patient. Artificial pneumoperitoneum was established, the pneumoperitoneum pressure was controlled at 10–12 mmHg, and Trocar 10 mm was inserted. With the amplification effect of laparoscopy, the location and size of the lesion were determined, as well as the presence of distant metastasis, and a detailed surgical plan was formulated. At the umbilical plane of the bilateral midline of the clavicle, Trocar 5 mm was inserted as the auxiliary operation hole and assistant operation hole. At the same time, Trocar 12 mm was placed 2 cm at the costal margin of the left front axillary as the main operating hole. After the above operations, the gastric body and pylorus were routinely separated by an ultrasonic scalpel, and the area from the duodenum to 3 cm below the pylorus was fully dissected. Routine dissection of the greater omentum was performed to dissect the pancreatic capsule and anterior lobe of the transverse mesocolon. Routine dissection of right omental artery and vein was performed to complete subpyloric lymph node dissection. Routine dissection of the right gastric artery to the root was performed, and the surrounding lymph nodes were dissected and the duodenum was cut off. The gastric tissue was lifted up, and the liver, spleen, abdominal cavity and the root of the left gastric artery were fully exposed. After the dissection, the root of the left gastric vessel was routinely clipped to complete the perivascular lymph node dissection. At the same time, the lesser omentum was excised with an ultrasound knife, and the gastric cardia and the lesser curvature lymph nodes were dissected. A 4 cm long surgical incision was made in the middle of the upper abdomen. The incision protection coil was routinely placed, and the stomach was lifted up and removed after reaching the outside of the abdominal cavity. The lesion specimens were collected for examination, and the digestive tract reconstruction was completed [9, 10].

2.4. TMB Determination and Its Relationship with Prognosis. Total exon sequencing was used to detect the TMB level of the samples. The clinical follow-up data of the patients were collected, summarized, and analyzed. Combined with the pathological diagnosis of the patients, the tumor stage of the patients was further determined, and the TMB level and related factors in the tumors and tumor tissues were analyzed. Clinical data and gene expression profile data of 262 cases of GC in The Cancer Genome Atlas were collected. The QIAGEN genome extraction kit was used to determine the DNA, and the gel electrophoresis method and NanoDrop2000 were used to complete the quality inspection of the whole DNA samples. After the completion of the quality inspection, the results will be processed to determine whether there are problems with the samples. The qualified samples were hybridized and captured and sequenced on a computer. Then, we further processed the data and counted the indexes of the sequencing library, including ratio, repetition rate, data volume, capture efficiency, coverage rate, and average depth. After enrichment, conventional analysis and spectrum analysis were performed, and TMB of GC was calculated based on cell mutation data using the bioinformatics method (in this study, somatic cell mutation data was calculated after processing by downloading VANScan software) [11, 12]. Patients were randomly divided into the high level group and low level group according to TMB of 8 mutations/Mb. After surgery, all patients were followed up for 24 months to evaluate the relationship between TMB and prognosis of GC and overall survival (OS)).

2.5. Statistical Analysis. SPSS24.0 software was used to analyze the data. The enumeration data were expressed as N (%), and analyzed by χ^2 test. The measurement data were expressed by $(\overline{x} \pm s)$ and analyzed by t-test. Cox regression model was used to evaluate the relationship between TMB and prognosis of GC patients. Kaplan–Meier method was used to draw the survival curve, and the differences were analyzed by log-rank test. $P < 0.05$ was statistically significant.

3. Results

3.1. Relationship between TMB and Clinicopathological Parameters in GC Patients. A total of 262 patients with GC were included, and the total mutation rate was 92.85%. The top 5 mutations are TP53, RB1, ARID1A, KMT2B, and RET (Figure 1). TMB determination ranges from 0.1 to 95.3

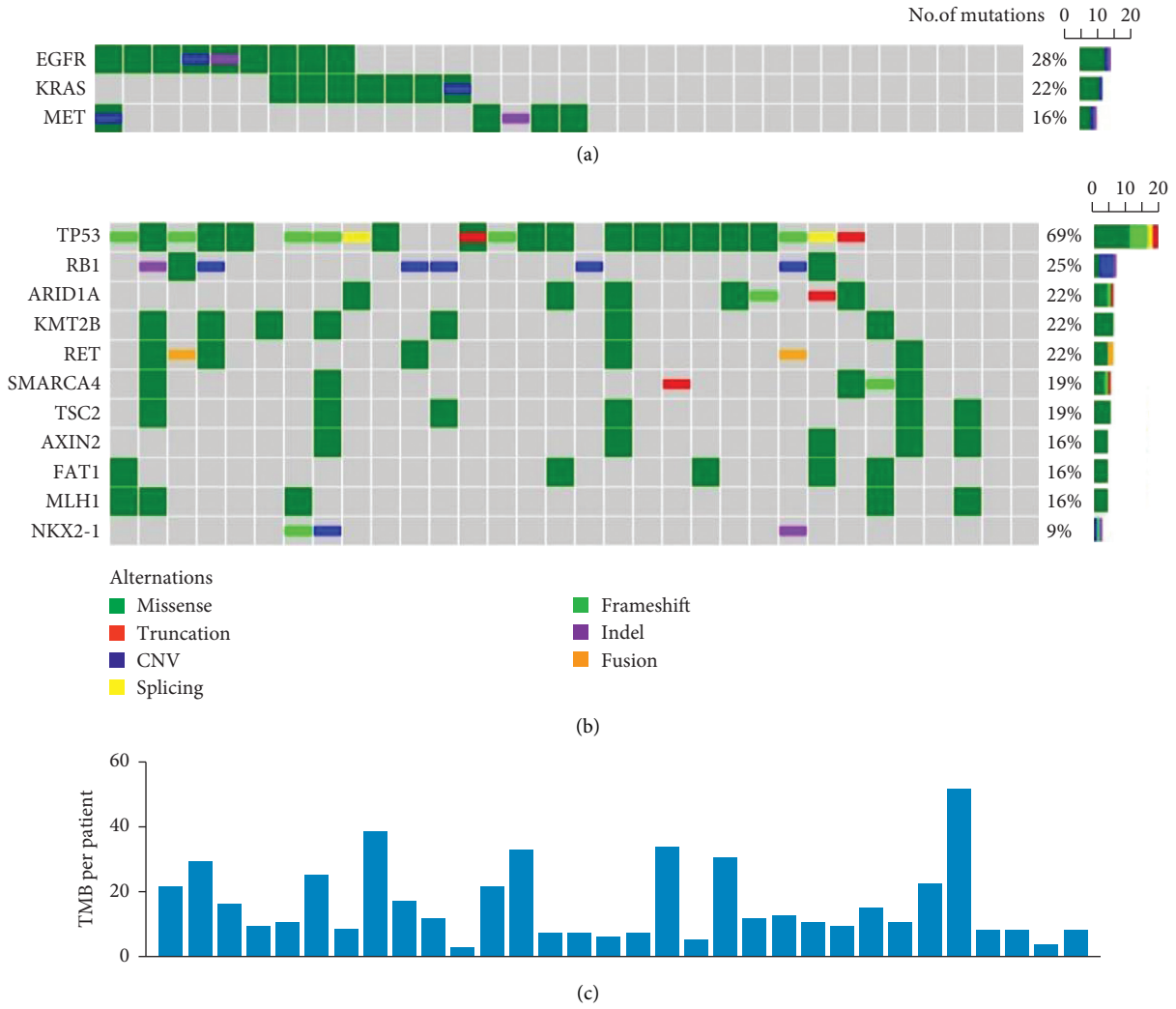

Figure 1: TMB gene mutation in patients with GC. (a, b) Genes with higher mutation frequency in GC patients. (c) The number of TMB in typical GC patients.

mutations/Mb (median position: 3.1). Patients were randomly divided into a high-level group and a low-level group according to TMB 8 mutations/Mb. The results showed that the expression level of TMB in GC patients has no statistical significance with gender, race, smoking history, and clinical stage ($P > 0.05$), while it was statistically significant with age, drinking history, and differentiation type ($P < 0.05$, Figure 1 and Table 1).

3.2. Multivariate Logistic Analysis of TMB in GC. Multivariate logistic analysis showed that the TMB value was statistically significant with age, drinking history, and differentiation type ($P < 0.05$, Table 2).

3.3. Relationship between TMB and Prognosis in GC Patients. In this study, the relationship between TMB and OS in patients with GC was analyzed, and the patients were followed up for 24 months. The results showed that 94 of the 262 patients died and 168 survived during the follow-up period. Patients with a high level of TMB had a poorer prognosis compared with patients with a low level of TMB (Figure 2).

Univariate analysis showed that the overall survival rate of GC patients was not statistically significant with gender, race, and smoking history ($P > 0.05$), while it was statistically significant with age, drinking history, clinical-stage, differentiation type, and TMB level ($P < 0.05$, Table 3).

3.4. Multivariate Logistic Analysis of Prognosis in GC Patients. Multivariate logistic analysis showed that the overall survival rate of GC patients was statistically significant with age, drinking history, clinical stage, differentiation type, and TMB level ($P < 0.05$, Table 4).

4. Discussion

Surgical resection of D2 lymph node dissection is a commonly used treatment method for GC patients, and the life span of patients can be prolonged by resection of lesion

Table 1: Relationship between TMB and clinicopathological parameters in GC patients.

Clinicopathological parameters		n	High ($n = 85$)	Low ($n = 177$)	χ^2	P
Gender	Male	165	51	114	1.593	0.771
	Female	97	34	63		
Age	≥60 years	141	61	80	7.312	0.025*
	<60 years	121	24	97		
Race	Han	214	68	146	0.781	0.602
	Others	48	17	31		
Smoking history	Yes	151	48	103	0.449	0.294
	No	111	37	74		
Drinking history	Yes	205	71	134	6.791	0.029*
	No	57	14	43		
Clinical stages	I-II	127	21	106	0.782	0.391
	III-IV	135	64	71		
Differentiation type	Low	63	34	29	6.342	0.034*
	Moderate	102	30	72		
	High	97	21	76		

*$P < 0.05$.

Table 2: Multivariate logistic analysis of the effect of TMB on GC.

Variable	β	S.E.	Wald	P	OR	95% CI
Age	1.535	0.059	8.681	<0.001	8.514	7.104–8.991
Drinking history	1.024	0.042	6.456	<0.001	5.451	5.102–7.513
Differentiation type	1.382	0.038	5.319	<0.001	4.096	3.241–5.692

S.E.: standard error.

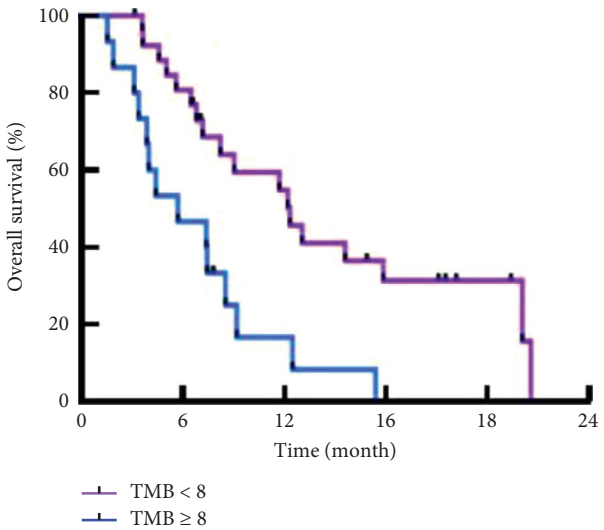

Figure 2: The overall survival time in high TMB expression group was shorter than in low TMB expression group.

tissues [13]. However, due to the lack of effective evaluation and prediction methods for most patients after surgery, the local recurrence rate and metastasis rate are high, leading to poor prognosis of patients. Somatic mutations in GC are caused by relatively many factors, including DNA repair defects, inherent errors in DNA replication mechanism, DNA enzyme modification, and exogenous exposure [14]. Previous studies [15] have shown that there are relatively many forms of mutations during the onset of GC, including nonsynonymous mutations, synonymous mutations, insertion and deletion, and copy number changes. In this study, the total mutation rate of 262GC patients was 92.85%. The top 5 mutated genes were TP53, RB1, ARID1A, KMT2B, and RET, indicating that the gene mutation rate of GC patients was high and there were many types, all of which were directly involved in the occurrence and development of GC.

TMB is the total number of somatic mutations per Mb base in the exon coding region, and its level can reflect the stability level of tumor genome and the heterogeneity of microenvironment [16]. In recent years, with the continuous development of medical technology, TMB has become a new marker in GC patients. At the same time, with the wide application of next-generation sequencing, the role of TMB in tumor screening, monitoring, and treatment has become a focus of current research [17]. Previous studies have shown that TMB, as a biomarker that can identify immunotherapeutic responses, is differentially expressed in different tissues of GC [18]. In this study, the GC patients were routinely divided into a high-level group and a low-level group according to TMB 8 mutations/Mb. The results showed that the expression level of TMB in GC patients was statistically significant with age, drinking history, and differentiation type ($P < 0.05$), indicating that the expression level of TMB in GC is affected by many factors, which can reflect and evaluate the prognosis of patients.

Studies have shown that [19] the level of TMB is related to the response of patients to immunosuppressants; the higher the level of TMB, the more neoantigens that T lymphocytes can recognize and the better the effect of surgery and immunotherapy. In order to further analyze the relationship between TMB and prognosis in patients with GC, patients were followed up for 24

Table 3: Univariate analysis of prognosis in GC patients.

Clinicopathological parameters		n	Death group ($n = 94$)	Survival group ($n = 168$)	χ^2	P
Gender	Male	165	53	112	0.682	0.194
	Female	97	41	56		
Age	≥60 years	141	67	74	8.415	0.021*
	<60 years	121	27	94		
Race	Han	214	78	136	1.325	0.993
	Others	48	16	32		
Smoking history	Yes	151	59	92	0.591	0.781
	No	111	35	76		
Drinking history	Yes	205	81	124	6.791	0.029*
	No	57	13	44		
Clinical stages	I-II	127	25	102	5.678	0.035*
	III-IV	135	69	66		
Differentiation type	Low	63	43	20	8.331	0.024*
	Moderate	102	40	62		
	High	97	11	86		
TMB expression	≥8	104	87	17	12.194	<0.001**
	<8	158	7	151		

*$P < 0.05$; **$P < 0.01$.

Table 4: Multivariate logistic analysis on the influence of prognosis in GC patients.

Variable	B	S.E.	Wald	P	OR	95% CI
Age	1.783	0.194	9.515	<0.001	10.591	9.671–12.562
Drinking history	1.569	0.151	6.391	<0.001	8.515	7.813–8.948
Differentiation type	1.447	0.132	6.874	<0.001	6.679	6.013–7.331
Clinical stages	1.361	0.084	7.891	<0.001	5.093	4.375–5.993
TMB	1.201	0.073	5.923	<0.001	3.591	3.025–4.682

S.E.: standard error.

months in this study. During the follow-up period, 94 of 262 patients died and 168 of them survived. Patients with low levels of TMB had a worse prognosis than those with high levels of TMB. The results of univariate and multivariate logistic analysis showed that the overall survival rate of GC patients was statistically significant with age, drinking history, clinical-stage, differentiation type, and TMB. This indicated that the higher the level of TMB in GC patients, the lower the overall survival rate. This is mainly due to the high TMB level of patients given surgical treatment, local recurrence rate, and metastasis rate are higher. Moreover, patients with high TMB level are less sensitive to chemotherapy and radiotherapy, which will affect the prognosis of patients. Therefore, the determination of TMB level in GC patients should be strengthened, and treatment regimens should be adjusted according to the determination results, so as to improve the prognosis of patients and prolong the life of patients [20]. However, TMB is a relatively new biomarker, and there are still some limitations in the current detection of TMB, which requires intensive research in the future.

5. Conclusion

In conclusion, patients with GC are often accompanied by TMB changes. The expression level of TMB is closely related to the degree of pathological differentiation and is an independent factor affecting the prognosis of GC patients. High TMB value can evaluate the prognosis of GC patients and provide a reference for the formulation of the clinical treatment plan.

Data Availability

The data used to support the findings of this study are available from the corresponding author upon request.

Conflicts of Interest

The authors declare no conflicts of interest.

References

[1] Q. W. Liu, Y. Li, B. B. Tan et al., "Expression of TIP30 in gastric cancer and its relationship with prognosis," *Chinese General Practice*, vol. 23, no. 6, pp. 55–60, 2020.

[2] Y. Jin, Y. M. Chen, X. Hu et al., "Analysis of the feasibility and prognostic value of circulating tumor DNA in detecting gene mutations in small cell lung cancer," *National Medical Journal of China*, vol. 100, no. 45, pp. 3614–3621, 2020.

[3] L. Zhang, X.-y. Liu, G. Zhong, Z. Xin, X.-Y. Sun, and Z.-Y. Wang, "A protocol of systematic review and meta-analysis of narrow band imaging endoscopy in detection of

early gastric cancer," *Medicine*, vol. 99, no. 33, Article ID e21420, 2020.

[4] P. Yu, W. Y. Zhu, W. B. Peng, and Y. E. Fan, "Analysis of the relationship between Hp infection and TNM stage and tumor malignancy in patients with gastric cancer," *Chinese Journal of Integrated Traditional and Western Medicine on Digestion*, vol. 28, no. 9, pp. 19–23, 2020.

[5] W. Zhang, W. Q. Liang, A. Z. Cai et al., "Clinicopathological characteristics of gastric cancer in adolescents aged 10-24 years: 17-year experience of 17 years in a single institute," *Chinese Journal of Gastrointestinal Surgery*, vol. 23, no. 10, pp. 963–968, 2020.

[6] C. Chen, J. Tian, J. Zhou, X. Ni, J. Lei, and X. Wang, "Bacterial growth, morphology, and cell component changes in Herbaspirillum sp. WT00C exposed to high concentration of selenate," *Journal of Basic Microbiology*, vol. 60, no. 4, pp. 304–321, 2020.

[7] Y. Liu, Y. Zhang, J. Zhang et al., *Diagnostic Criteria for Gastric Cancer (WS 316-2010)*, Standards Press of China, Beijing, China, 2010.

[8] M. Zhang, Y. P. Liu, X. X. Chen, D. Y. Wu, K. L. Wu, and C. Y. Xie, "Changes in stroke volume variation to predict fluid responsiveness in elderly patients undergoing laparoscopic-assisted radical gastrectomy," *International Journal of Anesthesiology and Resuscitation*, vol. 41, no. 5, pp. 437–441, 2020.

[9] M. Wang and Y. Zhang, "Clinical analysis of coagulation factors, gastrointestinal motility related hormones and tumor markers in patients with gastric cancer undergoing laparoscopic gastrectomy," *Chinese Journal of Thrombosis and Hemostasis*, vol. 26, no. 5, pp. 99-100, 2020.

[10] L. S. Lino-Silva, P. Anchondo-Núñez, A. Chit-Huerta et al., "Stage I-III colon cancer patients with tumor deposits behave similarly to stage IV patients. Cross-section analysis of 392 patients," *Surgical Oncology*, vol. 120, no. 2, pp. 300–307, 2019.

[11] Y. Tian, P. G. Yang, Y. Li et al., "Clinicopathologic parameters and prognostic analysis of progressive disease after neoadjuvant therapy for locally advanced gastric cancer," *Chinese Journal of General Surgery*, vol. 36, no. 4, pp. 249–253, 2021.

[12] W. Gao, K. Xu, Y. X. Lai, P. Xu, L. Zhang, and W. W. Sun, "Clinical, endoscopic and pathological characteristics of synchronous multiple early gastric cancer," *Chinese Journal of Digestive Endoscopy*, vol. 38, no. 5, pp. 373–378, 2021.

[13] G. M. Gao, Q. G. Jiang, B. Tang et al., "Influencing factors for the number of lymph node harvested after Da Vinci robotic and laparoscopic radical gastrectomy for gastric cancer: a report of 1 396 cases," *Chinese Journal of Digestive Surgery*, vol. 20, no. 5, pp. 512–518, 2021.

[14] T. Adar, M. Friedman, L. H. Rodgers, K. M. Shannon, L. R. Zukerberg, and D. C. Chung, "Gastric cancer in Lynch syndrome is associated with underlying immune gastritis," *Journal of Medical Genetics*, vol. 56, no. 12, pp. 844-845, 2019.

[15] G. Y. Chen and S. F. Huang, "Interpretation of the fifth edition of World Health Organization classification of tumors of the digestive system: selected topic on early gastric cancer," *Chinese Journal of Pathology*, vol. 49, no. 9, pp. 882–885, 2020.

[16] Y. J. Zhu, Y. Li, J. Jiang et al., "Predictive value of quantitative dynamic contrast? enhanced magnetic resonance imaging for the efficacy of neoadjuvant chemotherapy in locally advanced gastric cancer," *Chinese Journal of Oncology*, vol. 41, no. 10, pp. 765–770, 2019.

[17] G. Deng, Y. Chen, C. Guo et al., "BMP4 promotes the metastasis of gastric cancer by inducing epithelial-mesenchymal transition via Id1," *Journal of Cell Science*, vol. 133, no. 11, Article ID jcs237222, 2020.

[18] W. Wei, H. K. Huang, J. M. Lu, and L. Zhou, "Changes of tumor markers, vascular endothelial growth factor and gastrointestinal hormones in patients with gastric cancer at different pathological stages," *Journal of Preventive Medicine of Chinese People's Liberation Army*, vol. 37, no. 9, pp. 109–111, 2019.

[19] X. Y. Liu, Y. H. Wang, R. M. Zhang et al., "Changes of Sonic Hedgehog and Wnt3A/β-catenin expression in different pathological stages of Correa cascade in intestinal gastric cancer," *Chinese Journal of Cancer Prevention and Treatment*, vol. 26, no. 20, pp. 39–44, 2019.

[20] R. L. Miao, Z. Y. Li, and J. F. Ji, "Current treatment status and trends of early gastric cancer in China: analyzed based on the data of China Gastrointestinal Cancer Surgery Union," *Chinese Journal of Practical Surgery*, vol. 39, no. 5, pp. 419–423, 2019.

Hindawi
Journal of Oncology
Volume 2021, Article ID 5338934, 10 pages
https://doi.org/10.1155/2021/5338934

Research Article

All-Trans Retinoic Acid Enhances Chemosensitivity to 5-FU by Targeting miR-378c/E2F7 Axis in Colorectal Cancer

Ji Li,[1] Qing Xiang,[2] Mei Wang,[3] Hongchang Zhang,[4] and Rong Liang[5]

[1]*Department of Pharmacy, Qilu Hospital (Qingdao), Cheeloo College of Medicine, Shandong University, Qingdao, Shandong 266035, China*
[2]*Department of Emergency, Rizhao Hospital of TCM, Rizhao 276800, China*
[3]*PIVAS, Qingdao Central Hospital Affiliated to Qingdao University, Qingdao 266000, China*
[4]*Infectious Diseases Department, Zhangqiu District People's Hospital, Jinan 250200, China*
[5]*Department of Proctology(II), Qilu Hospital (Qingdao), Cheeloo College of Medicine, Shandong University, Qingdao 266035, Shandong, China*

Correspondence should be addressed to Rong Liang; linxiaofei@sdqiluhospital.cn

Received 17 June 2021; Accepted 6 July 2021; Published 21 July 2021

Academic Editor: Muhammad Wasim Khan

Colorectal carcinoma (CRC), a life-threatening malignancy, has been found to present resistance to 5-fluorouracil (5-FU) and cause a poor prognosis for patients. Previous studies have proved that all-trans retinoic acid (ATRA) could inhibit the development of CRC cells. In addition, miR-378c was discovered to exert a vital role in various cancers. In this study, we utilized MTT (3-(4,5-dimethylthiazol-2-yl)-2,5-diphenyltetrazolium bromide), transwell assay, and flow cytometry to confirm that ATRA was able to enhance the inhibitory effects of 5-FU on HCT116 cells effectively by promoting cell apoptosis. Then, ENCORI database (http://starbase.sysu.edu.cn/) was employed to predict that miR-378c was downregulated dramatically in CRC and E2F7 was the direct target of miR-378c. QRT-PCR (quantitative real-time polymerase chain reaction) was conducted to verify that the expression level of miR-378c was decreased while E2F7 expression was upregulated in CRC tissues compared with para-carcinoma tissues. Additionally, treatment of 5-FU combined with ATRA could increase miR-378c expression, whereas it decreased the expression of E2F7. Dual-Luciferase Reporter assay results revealed that miR-378c could regulate the load of E2F7 by binding to its 3′UTR directly. Furthermore, miR-378c inhibitor or vector with E2F7 partially counteracted the effects of 5-FU combined with ATRA on viability, migration, invasion, and apoptosis of HCT116 cells. In conclusion, our study aims to confirm that ATRA enhances chemosensitivity to 5-FU of patients with CRC and expound the potential molecular mechanisms.

1. Introduction

Increasing developments had been made in treating CRC recently. However, CRC remains the second main reason for death associated with tumors and is graded as the fourth diagnosed malignancy worldwide [1–3]. Chemotherapies were the foundation of treatment for patients with CRC in recent decades even though they exhibited obvious toxicity in addition to being ineffective [4]. Due to the limitations of early symptoms as well as screening technologies, many patients with CRC are diagnosed at the advanced stage [5]. The reason that contributes to poor results for patients is mainly recurrence in addition to metastasis of CRC [6]. Over the past few decades, the useful therapy for patients with CRC is the chemotherapy based on fluorouracil. Nevertheless, patients are becoming more and more resistant to 5-FU, which is the major barrier for treating effectively [7, 8]. Therefore, multiple anticancer agents are employed to combine with 5-FU to enhance therapeutic effectiveness for CRC at present [9]. ATRA, one of the important metabolites of vitamin A, has great potential to prevent and treat cancer [10]. ATRA plays promising roles in various cancers including breast cancer, glioblastoma, and head-and-neck cancer [11, 12]. Additionally, Yang et al. found that ATRA is able to inhibit colon cancer cells from proliferating via mediating sponge miR3666 [11]. María Ángeles Castro et al.

primarily revealed that retinoids and 5-FU have synergistic effects on Caco-2 cells [13]. However, the detailed functions and mechanisms underlying 5-FU in addition to ATRA are uncovered now.

MicroRNAs, as the endogenous, non-coding RNAs, have the ability to regulate target genes, and a variety of witnesses have testified that microRNAs are correlated to the progression of various cancers [14–16]. MicroRNAs can serve as either cancer suppressor genes or oncogenes to affect the proliferation, migration, and therapy of cancers [17]. A load of certain genes related to metabolism, stress responses, and cell apoptosis will be regulated by the aberrant transcription of specific miRNAs [18, 19]. Take miR-433, for example; it decreases resistance of cervical cancer cells to 5-FU through regulating the expression of TYMS [20]. Mir-20313, in addition to miR-197, could regulate the reactivity of colorectal cells to 5-FU by changing TYMS expression [21, 22]. MiR-378c belonging to the miR-378 family has been found to have a close relationship with cancers. For example, miR-378c is decreased in gastric cancer tissues, according to previous reports [23]. Furthermore, we consulted the database and found that miR-378c was downregulated significantly in COAD (colon adenocarcinoma), but its effects on CRC are unclear.

Therefore, our study reveals the functions and detailed molecular mechanisms of ATRA combined with 5-FU for CRC via the miR-378c/E2F7 axis.

2. Materials and Methods

2.1. Patients and Tissue Samples. CRC and para-carcinoma tissues were extracted from 15 patients diagnosed with early CRC and treated with radical surgery at Qilu Hospital, Jinan, Shandong, China. In addition, no patients were treated systematically before surgery. All patients provided written informed consent. The isolated tissues were put in liquid nitrogen immediately. All experiments involved in this study were in accordance with the ethics committee of the Qilu Hospital, Jinan, Shandong, China.

2.2. Cell Culture. The HCT116 cell line was purchased from COBIOER in Nanjing and was cultured with McCoy's 5A (Gibco, USA), including 10% FBS (fetal bovine serum) at 37°C.

2.3. Cell Treatment. Different concentrations of 5-FU and ATRA were dissolved in dimethylsulfoxide (DMSO, Thermofisher) solution. HCT116 cells were cultured overnight and treated with the indicated concentration of 5-FU in addition to ATRA for 24 hours. Additionally, the control group referred to DMSO solution with the same volume.

2.4. Cell Transfection. HCT116 cells (1×10^5 cells/well) were planted in specific well plates. Indicated mimic, inhibitor, or vector was transfected into HCT116 cells when cells reached 70% confluence with Lipofectamine 3000 (Thermofisher, USA). After culturing for 24 hours, HCT116 cells were collected for the following assay.

2.5. MTT Assay. HCT116 cells (1×10^3 cells/well) were planted in a 96-well plate and cultured for a night. Then, different doses of 5-FU and ATRA were used to treat HCT116 cells which have been transfected with indicated vectors. After 24 hours, 0.5 mg/ml MTT was added into every well for 4 hours. Finally, the OD value at 550 nm was recorded with a Flash reader (Thermofisher, USA) to represent cell viability.

2.6. Cell Apoptosis. HCT116 cells were planted in 6-well plate overnight. Then, different doses of 5-FU and ATRA were used to treat HCT116 cells which were transfected with indicated vectors. After 24 hours, all cells were obtained in HEPES buffer (119.15 g HEPES (4-hydroxyethyl piperazine ethanesulfonic acid), 0.5–1 M NaOH, PH 6.8–8.2, capacity to 500 ml), and the mixture was centrifuged to abandon supernatant. Next, cells were stained by Annexin V/PI for half hour. Subsequently, flow cytometry was conducted to analyse cell apoptosis rate by using CellQuest software (Becton, USA). The four quadrants represent normal (third quartile), early apoptosis (second quartile), late apoptosis (fourth quartile), and necrotic (first quartile) cells.

2.7. Transwell Assay. For migration assay, HCT116 cells (5×10^4 cells) in serum-free medium were planted in the upper transwell chamber containing an insert (8-mm pore; Corning, USA). Nevertheless, cells were seeded in the upper transwell chamber containing an insert prepared with Matrigel. Medium with 10% FBS as the chemoattractant was placed in the lower transwell chamber. After 24 hours, cells still staying on the upper part were cleared away by using cotton wool; however, cells migrating or invading to the lower chamber were fixed, stained, and recorded with an inverted microscope (Olympus, Japan).

2.8. Dual-Luciferase Reporter Assay. The sequence of E2F7-WT or E2F7-MUT was amplified and constructed into pGL3 plasmid (Thermofisher, USA). Specific mimic or vector was transfected into HCT116 cells by Lipofectamine 3000. After 36–72 hours, a microplate reader was used to measure and record the luciferase activity. Among this assay, a negative control was the luciferase activity of Renilla.

2.9. Quantitative Real-Time PCR. Total RNA of tissues or HCT116 cells was obtained by TRIzol reagent (Invitrogen, USA). The mRNA level of indicated gene was detected by utilizing a qRT-PCR system (Bio-rad, USA). U6, in addition to GAPDH, was used to be the reference of miR-378c and E2F7, respectively. Relative load of a gene was measured in the $2^{-\Delta\Delta Ct}$ method. The primer sequence information is provided in Table 1.

Table 1: The sequence of primer.

Gene	RT-PCT primer
MiR-378c	Forward: 5′ GAGGCCATCACTGGACTTGG-3′ Reverse: 5′-GAGGCACTCACCACCTTCAAA-3′
U6	Forward: 5′ CTCGCTTCGGCAGCACA-3′ Reverse: 5′-AACGCTTCACGAATTTGCGT-3′
E2F7	Forward: 5′-AATGCAGTGGTTGTTTCTGT-3′ Reverse: 5′-TGCCATTGCTTCTTCACTAC-3′
GAPDH	Forward: 5′-GGGAAACTGTGGCGTGAT-3′ Reverse: 5′-GAGTGGGTGTCGCTGTTGA -3′

2.10. Western Blot. Total proteins were extracted from HCT116 cells with lysis buffer (Monad, China) and were isolated by10% SDS PAGE, which were next transferred to PVDF membrane (Thermofisher, USA). Then, the membrane was incubated with primary antibodies GAPDH (glyceraldehyde-3-phosphate dehydrogenase) (#2118, Cell Signaling Technology), Bcl-2 (#15071, Cell Signaling Technology), Bax (#5023, Cell Signaling Technology), or cleaved-Caspase-3 (#9661, Cell Signaling Technology) overnight. Subsequently, the membrane was incubated with secondary antibodies and then photographed by the Odyssey Infrared Imaging System (LI-COR, USA).

2.11. Statistical Analysis. All data in this study were presented in the manner of mean ± SD. Statistical difference was measured by using SPSS 19.0 system (IBM, USA) with Student's *t*-test and ANOVA. Comparisons were calculated and $P < 0.05$ was regarded to be significant statistically.

3. Results

3.1. ATRA Enhanced the Inhibitory Effect of 5-FU on Progression of HCT116 Cells and Induced Cell Apoptosis in a Concentration-Dependent Manner. To reveal the impacts of 5-FU as well as ARTA combined with 5-FU on colorectal cancer cells, HCT116 cells were employed and treated with 5-FU or 5-FU plus ATRA in indicated doses. The data illustrated that 5-FU decreased the proliferation ability of HCT116 cells and adding ATRA further downregulated cell viability compared with the control group ($P < 0.05$, Figure 1(a)). Additionally, we conducted flow cytometry and found that compared with control group, 5 μM 5-FU increased the apoptosis rate of HCT116 cells and 5 μM 5-FU combined with 5 μM ATRA induced more cell apoptosis significantly ($P < 0.05$, Figure 1(b)). Proteins related to apoptosis were measured and the results showed that the level of Bax in addition to cleaved-Caspase-3 was upregulated while the level of Bcl2 was downregulated by 5-FU. Meanwhile, the changes were enhanced dramatically by 5-FU combined with ATRA as shown in Figure 1(c). Furthermore, treating cells with 5-FU plus ATRA exhibited the worst migration and invasion ability compared to the control group as well as the 5-FU group ($P < 0.05$, Figures 1(d) and 1(e)). Thus, ATRA enhanced the series of effects of 5-FU on HCT116 cells.

3.2. MiR-378c Is Downregulated in CRC and Is Positively Regulated by Treatment of 5-FU Combined with ATRA Significantly. According to ENCORI database, we discovered that the level of miR-378c was notably lower in CRC samples compared with normal samples (Figure 2(a)). In addition, we collected CRC and para-carcinoma tissues from 15 patients and conducted qRT-PCR; the results confirmed that the expression level of miR-378c was decreased dramatically in CRC tissues ($P < 0.05$, Figure 2(b)). To uncover the relationship between miR-378c and 5-FU combined with ATRA, qRT-PCR assay was applied to detect the load of miR-378c after treating with 5-FU combined with ATRA. Interestingly, we found that 5-FU increased the expression level of miR-378c and 5-FU combined with ATRA further increased the load of miR-378c in HCT116 cells ($P < 0.05$, Figure 2(c)).

3.3. Effects of 5-FU Combined with ATRA Are Mediated by miR-378c. To verify whether 5-FU combined with ATRA affected developments of HCT116 cells by miR-378c, we conducted MTT, transwell assay, and flow cytometry. The combined impacts of 5 μM FU + 5 μM ATRA (this combination possessed capacity to decrease cell viability no less than 50%) and miR-378c on progression of HCT116 were detected. The data illustrated that the effects of 5 μM FU + 5 μM ATRA on downregulated cell proliferation, migration in addition to invasion ($P < 0.05$, Figures 3(a)–3(c)), upregulated cell apoptosis (Figure 3(d)), and changed apoptosis-related proteins (Figure 3(e)) were partially counteracted by miR-378c inhibitor in HCT116 cells.

3.4. E2F7 Is the Direct Target of miR-378c. To reveal how miR-378c affected CRC, we predicated the targets of miR-378c by using ENCORI website. As presented in Figures 4(a) and 4(b), E2F7 was the direct target of miR-378c and luciferase reporter assay was used to show that the 3′UTR of E2F7 could be bound by miR-378c ($P < 0.05$). Subsequently, the expression level of E2F7 was measured after transfecting miR-378c mimic or miR-378c inhibitor. Consistently, the E2F7 expression was decreased significantly by miR-378c mimic while increased dramatically by miR-378c inhibitor in HCT116 cells ($P < 0.05$, Figure 3(c)). Thus, miR-378c was able to negatively control the expression of E2F7.

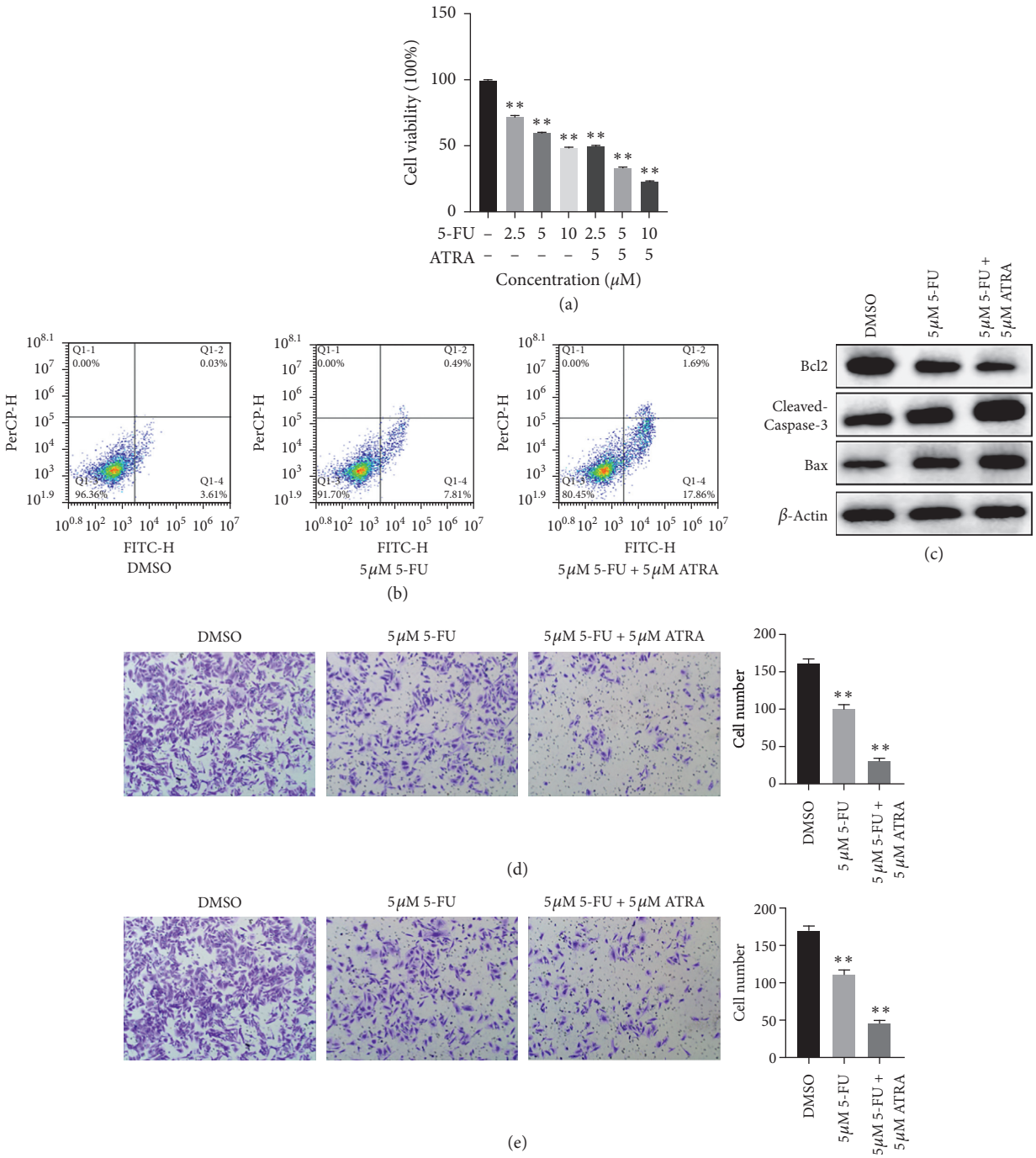

Figure 1: ATRA enhanced the inhibitory effects of 5-Fu on progression of HCT116 cells and induced cell apoptosis in a concentration-dependent manner. (a) Cell viability measured by MTT assay ($P < 0.05$). (b) Cell apoptosis after treating with indicated reagents. (c) The level of proteins related to cell apoptosis. (d) Migration of HCT116 cells after indicated treatment ($P < 0.05$). (e) Invasion of HCT116 cells after indicated treatment ($P < 0.05$).

3.5. E2F7 Is Upregulated in CRC and Is Negatively Regulated by Treatment of 5-FU Combined with ATRA Significantly. The expression of E2F7 was suppressed significantly in CRC samples than that in normal samples according to the GEPIA database (Figure 5(a)). Consistently, the mRNA level of E2F7 in CRC tissues from 15 cases of patients was higher obviously than that in para-carcinoma tissues via using qRT-PCR experiment ($P < 0.05$, Figure 5(b)). HCT116 cells were treated with 5-FU plus ATRA, and we measured the load of E2F7 to explore the correlation between 5-FU combined with ATRA and E2F7. We discovered that 5-FU inhibited the expression level of E2F7 and its expression was further decreased by treatment of 5-FU combined with ATRA ($P < 0.05$, Figure 5(c)).

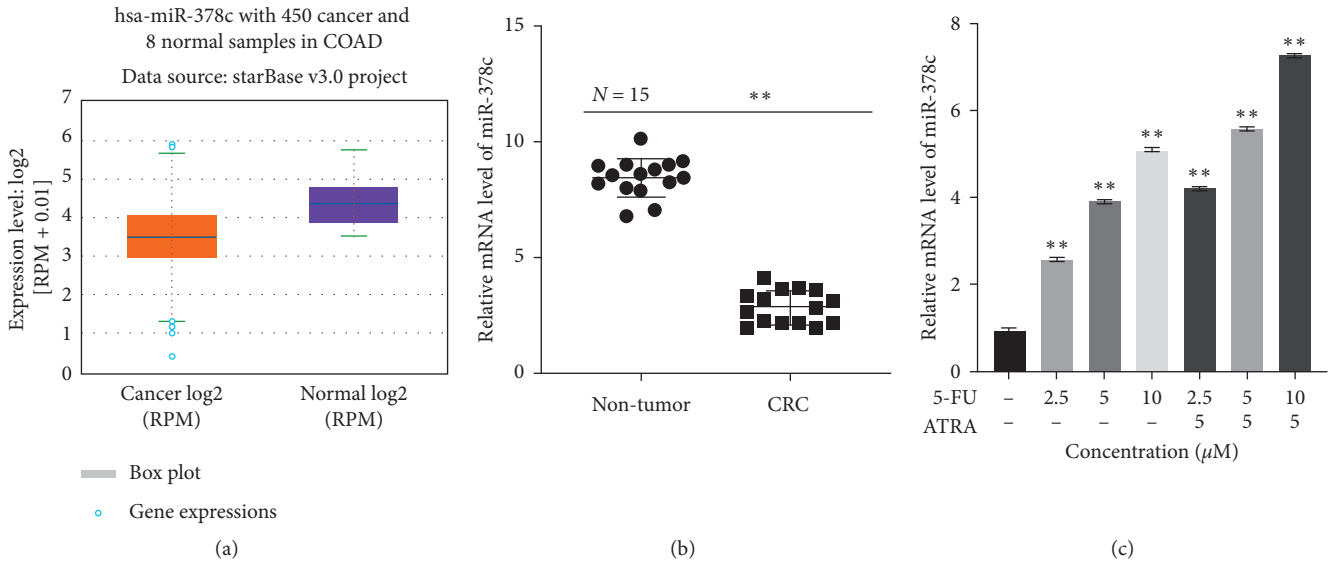

Figure 2: MiR-378c is downregulated in CRC and is positively regulated by treatment of 5-FU combined with ATRA significantly. (a) The expression level of miR-378c in CRC according to ENCORI database. (b) The mRNA level of miR-378c in CRC tissues and para-carcinoma tissues ($N = 15$) was detected by qRT-PCR ($P < 0.05$). (c) The relationship between miR-378c and 5-FU in addition to ATRA ($P < 0.05$).

3.6. Effects of 5-FU Combined with ATRA Are Mediated by E2F7. To confirm that 5-FU plus ATRA inhibited the progress of CRC cells via miR-378c/E2F7 axis, we further investigated the combined effects of 5 μM FU + 5 μM ATRA and E2F7 on viability, migration, invasion, and apoptosis of HCT116 cells. 5 μM FU + 5 μM ATRA still decreased the ability of cell proliferation (Figure 6(a)), migration (Figure 6(b)), and invasion (Figure 6(c)), increased cell apoptosis rate (Figure 6(d)), and changed apoptosis-related protein expression (Figure 6(e)), which however partly were reversed by overexpressing E2F7 significantly ($P < 0.05$). Thus, E2F7 could partially counteract the inhibitory effects of 5-FU combined with E2F7 on CRC cells.

4. Discussion

CRC results in the second highest mortality related to cancers across the world. The reason why life expectancy of patients with CRC usually no more than 1 year is that most of them are definite diagnoses in terminal stages [24]. Chemotherapy based on 5-FU has achieved good performance in treating patients with cancer; however, resistance to 5-FU is the leading limitation for good prognosis [25]. The detailed mechanisms of resistance to 5-FU remain unclear now because of fickle biological processes [26]. Clinical trials revealed that ATRA could inhibit proliferation and promote cell apoptosis in CRC and it was then discovered to alter gene expression for exerting its functions [27]. In our study, we found that using 5-FU alone was able to decrease the viability of HCT116 cells in a dose-dependent manner, while 5-FU combined with ATRA further blocked cells to proliferate significantly. Meanwhile, combined inhibitory effects of 5-FU and ATRA also appeared in migration as well as invasion of HCT116 cells. In addition, 5-FU could promote cell apoptosis and apoptosis rate will be further increased after treatment of 5-FU plus ATRA. All above data illustrated that ATRA had the potential to enhance the anticancer effects of 5-FU and chemosensitivity of patients to 5-FU.

Previous research has reported that multiple microRNAs are associated with chemotherapy. For example, miR-100-5p is connected with cisplatin resistance of patients with lung cancer [28]. MiR-32-5p, produced in resistant cells, could trigger the PI3K/Akt signaling pathway in cancer cells [29]. MiR-145, in addition to miR-34a, serves as tumor-inhibiting factors to be associated with 5-FU resistance in CRC [30]. Notably, miRNA-378 family has been found to exert roles in cell viability, migration, invasion, and apoptosis in various cancers, including ovarian cancer [31], colon cancer [32], and so on [33, 34]. MiR-378c, one of the members of miRNA-378 family, has been reported to play a vital role in cancers such as gastric cancer and lung cancer [35, 36]. We discovered that miR-378c was downregulated in CRC according to the ENCORI database. Next, qRT-PCR was employed to confirm that the level of miR-378c was decreased in CRC tissues compared with para-carcinoma tissues. Interestingly, miR-378c could be upregulated by 5-FU alone in a concentration-dependent manner and the increase will be enhanced by adding ATRA, indicating the tight relationship between miR-378c and 5-FU combined with ATRA. Given this correlation, MTT assay, transwell assay, flow cytometry, and western blotting were conducted, and the results showed that miR-378c partially eliminated the series of effects of 5-FU combined with ATRA on CRC cells. Furthermore, E2F7 was predicted to be

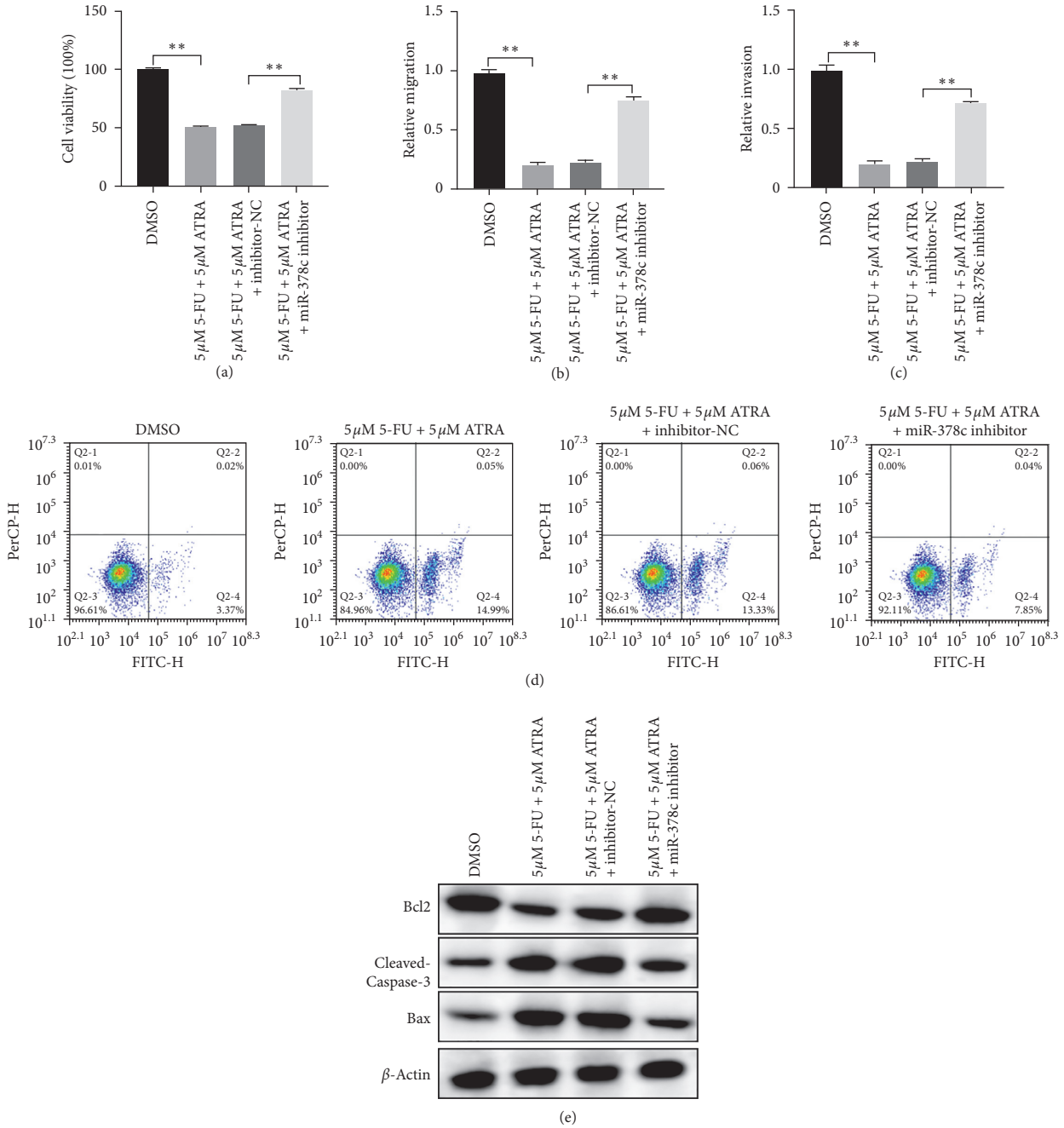

Figure 3: Effects of 5-FU combined with ATRA are mediated by miR-378c. (a) Cell viability after specific treatment ($P < 0.05$). (b) Migration of HC116 cells after specific treatment ($P < 0.05$). (c) Invasion of HC116 cells after specific treatment ($P < 0.05$). (d) Cell apoptosis after specific treatment. (e) The changes of proteins related to cell apoptosis.

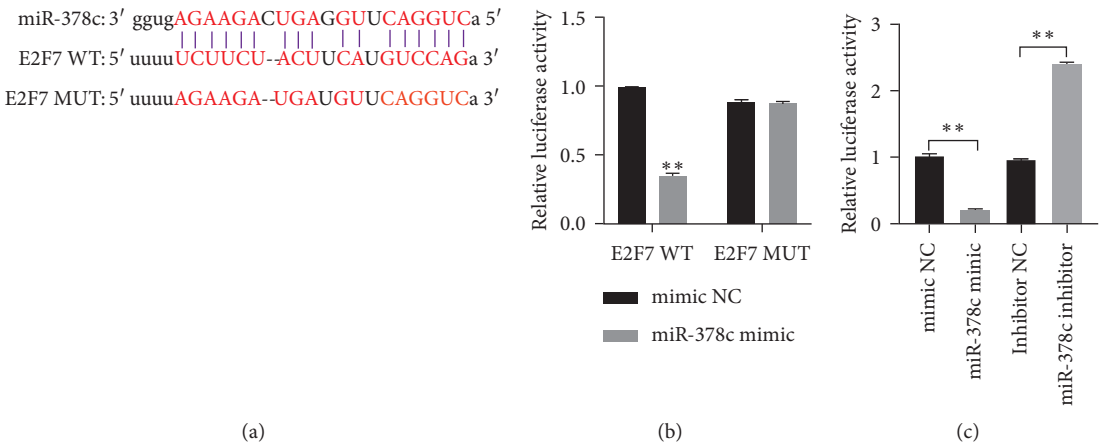

Figure 4: (a) E2F7 was the direct target of miR-378c. (b) The luciferase activity of wild-type E2F7 but not mutant E2F7 was regulated by miR-378c mimic ($P < 0.05$). (c) E2F7 was downregulated by miR-378c mimic but upregulated by miR-378c inhibitor ($P < 0.05$).

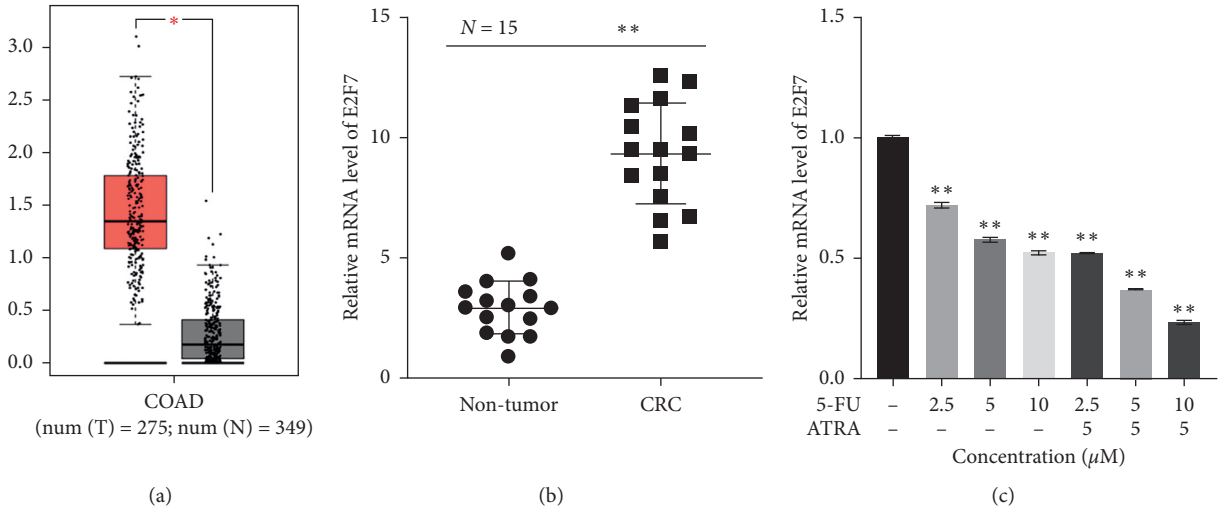

Figure 5: E2F7 is upregulated in CRC and is negatively regulated by treatment of 5-FU combined with ATRA significantly. (a) The level of E2F7 was lower dramatically in CRC, according to GEPIA database. (b) The mRNA level of E2F7 in CRC tissues and para-carcinoma tissues was detected by qRT-PCR ($N = 15$, $P < 0.05$). (c) The relationship between E2F7 and 5-FU in addition to ATRA ($P < 0.05$).

the direct target of miR-378c and it serves as a transcriptional suppressor to inhibit cell viability. E2F7 could play a significant role in various cancers, such as cutaneous squamous cell carcinomas [37], endometrial carcinoma [38], gallbladder cancer [39], and breast cancer cells [40]. In this study, we verified that E2F7 was regulated by miR-378c and downregulated in CRC tissues. In addition, the expression level of E2F7 was decreased by 5-FU alone and further suppressed dramatically by 5-FU combined with ATRA. Expected data illustrated that overexpression of E2F7 could partly reverse the

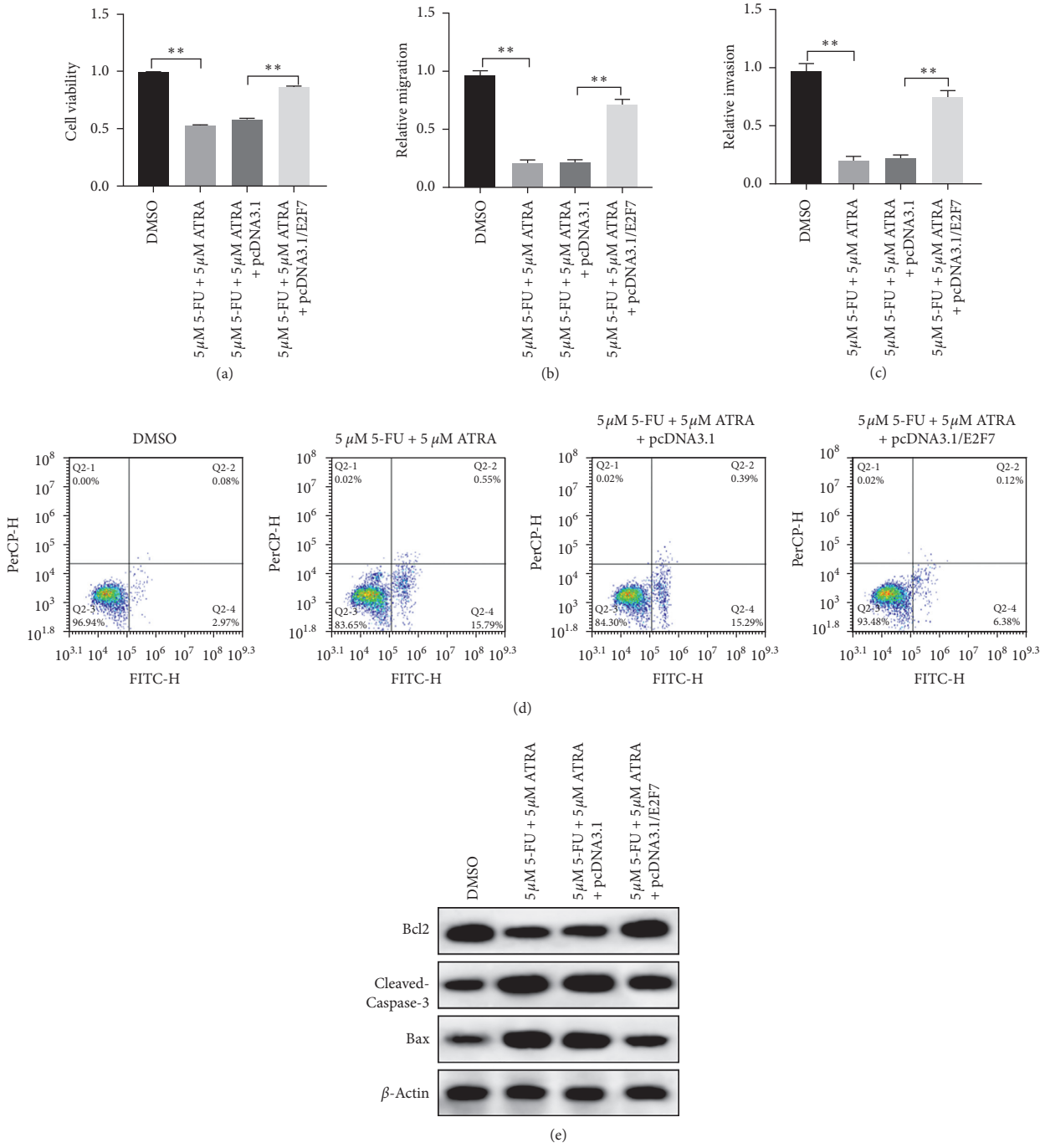

Figure 6: Effects of 5-FU combined with ATRA are mediated by E2F7. (a) Cell viability after specific treatment ($P < 0.05$). (b) Migration of HC116 cells after specific treatment ($P < 0.05$). (c) Invasion of HC116 cells after specific treatment ($P < 0.05$). (d) Cell apoptosis after specific treatment. (e) The changes of proteins related to cell apoptosis.

effects of 5-FU plus ATRA on HCT116 cells, indicating that 5-FU combined with ATRA exerts its functions via miR-378c/E2F7 axis.

5. Conclusion

In conclusion, our study primarily revealed that ATRA enhanced the inhibitory effects of 5-FU on CRC cells through the miR-378c/E2F7 axis, which provides a type of potential therapy regimen for patients diagnosed with CRC.

Data Availability

The data used to support the findings of this study are included within the article.

Conflicts of Interest

The authors declare that they have no conflicts of interest.

References

[1] L. Wang, L. Qian, X. Li, and J. Yan, "MicroRNA-195 inhibits colorectal cancer cell proliferation, colony-formation and invasion through targeting CARMA3," *Molecular Medicine Reports*, vol. 10, no. 1, pp. 473–478, 2014.

[2] M. A. Mansour, T. Hyodo, S. Ito et al., "SATB2 suppresses the progression of colorectal cancer cells via inactivation of MEK5/ERK5 signaling," *FEBS Journal*, vol. 282, no. 8, pp. 1394–1405, 2015.

[3] Q. Zhang, R.-X. Liu, K.-W. Chan et al., "Exosomal transfer of p-STAT3 promotes acquired 5-FU resistance in colorectal cancer cells," *Journal of Experimental & Clinical Cancer Research*, vol. 38, no. 1, p. 320, 2019.

[4] L. E. Dow, K. P. O'Rourke, J. Simon et al., "Apc restoration promotes cellular differentiation and reestablishes crypt homeostasis in colorectal cancer," *Cell*, vol. 161, no. 7, pp. 1539–1552, 2015.

[5] A. Sadanandam, C. A. Lyssiotis, K. Homicsko et al., "A colorectal cancer classification system that associates cellular phenotype and responses to therapy," *Nature Medicine*, vol. 19, no. 5, pp. 619–625, 2013.

[6] M. Xu, X. Chen, K. Lin et al., "lncRNA SNHG6 regulates EZH2 expression by sponging miR-26a/b and miR-214 in colorectal cancer," *Journal of Hematology & Oncology*, vol. 12, no. 1, p. 3, 2019.

[7] H. K. Kim, I. J. Choi, C. G. Kim et al., "A gene expression signature of acquired chemoresistance to cisplatin and fluorouracil combination chemotherapy in gastric cancer patients," *PLoS One*, vol. 6, no. 2, Article ID e16694, 2011.

[8] C. Tournigand, T. André, E. Achille et al., "FOLFIRI followed by FOLFOX6 or the reverse sequence in advanced colorectal cancer: a randomized GERCOR study," *Journal of Clinical Oncology*, vol. 22, no. 2, pp. 229–237, 2004.

[9] Y. Wang, C. Zhang, S. Zhang et al., "Kanglaite sensitizes colorectal cancer cells to Taxol via NF-κB inhibition and connexin 43 upregulation," *Scientific Reports*, vol. 7, no. 1, p. 1280, 2017.

[10] C. Siddikuzzaman, V. M. Guruvayoorappan, C. Guruvayoorappan, and V. M. Berlin Grace, "All trans retinoic acid and cancer," *Immunopharmacology and Immunotoxicology*, vol. 33, no. 2, pp. 241–249, 2011.

[11] W. Liu, Y. Song, C. Zhang, P. Gao, B. Huang, and J. Yang, "The protective role of all-transretinoic acid (ATRA) against colorectal cancer development is achieved via increasing miR-3666 expression and decreasing E2F7 expression," *Biomedicine & Pharmacotherapy*, vol. 104, pp. 94–101, 2018.

[12] S. Huang, Y. Chen, Z.-M. Liang et al., "Targeting pin1 by all-trans retinoic acid (ATRA) overcomes tamoxifen resistance in breast cancer via multifactorial mechanisms," *Frontiers in Cell and Developmental Biology*, vol. 7, p. 322, 2019.

[13] M. R. Abdelaal, S. H. Soror, M. R. Elnagar, and H. Haffez, "Revealing the potential application of EC-synthetic retinoid analogues in anticancer therapy," *Molecules*, vol. 26, no. 2, 2021.

[14] E. Anastasiadou, L. S. Jacob, and F. J. Slack, "Non-coding RNA networks in cancer," *Nature Reviews Cancer*, vol. 18, no. 1, pp. 5–18, 2018.

[15] A. Wojciechowska, A. Braniewska, and K. Kozar-Kamińska, "MicroRNA in cardiovascular biology and disease," *Advances in Clinical and Experimental Medicine: Official Organ Wroclaw Medical University*, vol. 26, no. 5, pp. 865–874, 2017.

[16] O. Volný, L. Kašičková, D. Coufalová, P. Cimflová, and J. Novák, "microRNAs in cerebrovascular disease," *Advances in Experimental Medicine and Biology*, vol. 888, pp. 155–195, 2015.

[17] A. A. Svoronos, D. M. Engelman, and F. J. Slack, "OncomiR or tumor suppressor? The duplicity of MicroRNAs in cancer," *Cancer Research*, vol. 76, no. 13, pp. 3666–3670, 2016.

[18] X. An, C. Sarmiento, T. Tan, and H. Zhu, "Regulation of multidrug resistance by microRNAs in anti-cancer therapy," *Acta Pharmaceutica Sinica B*, vol. 7, no. 1, pp. 38–51, 2017.

[19] T. Fojo, "Multiple paths to a drug resistance phenotype: mutations, translocations, deletions and amplification of coding genes or promoter regions, epigenetic changes and microRNAs," *Drug Resistance Updates : Reviews and Commentaries in Antimicrobial and Anticancer Chemotherapy*, vol. 10, no. 1-2, pp. 59–67, 2007.

[20] K. Gotanda, T. Hirota, N. Matsumoto, and I. Ieiri, "MicroRNA-433 negatively regulates the expression of thymidylate synthase (TYMS) responsible for 5-fluorouracil sensitivity in HeLa cells," *BMC Cancer*, vol. 13, no. 1, p. 369, 2013.

[21] T. Li, F. Gao, and X.-P. Zhang, "miR-203 enhances chemosensitivity to 5-fluorouracil by targeting thymidylate synthase in colorectal cancer," *Oncology Reports*, vol. 33, no. 2, pp. 607–614, 2015.

[22] Z. Sun, N. Zhou, Q. Han et al., "MicroRNA-197 influences 5-fluorouracil resistance via thymidylate synthase in colorectal cancer," *Clinical and Translational Oncology*, vol. 17, no. 11, pp. 876–883, 2015.

[23] K. Tian, W. Liu, J. Zhang et al., "MicroRNA-125b exerts antitumor functions in cutaneous squamous cell carcinoma by targeting the STAT3 pathway," *Cellular & Molecular Biology Letters*, vol. 25, no. 1, p. 12, 2020.

[24] L. N. Kwong and W. F. Dove, "APC and its modifiers in colon cancer," *Advances in Experimental Medicine and Biology*, vol. 656, pp. 85–106, 2009.

[25] D. J. Jonker, J. A. Maroun, and W. Kocha, "Survival benefit of chemotherapy in metastatic colorectal cancer: a meta-analysis of randomized controlled trials," *British Journal of Cancer*, vol. 82, no. 11, pp. 1789–1794, 2000.

[26] H.-J. R. T. H. Lippert and M. Volm, "Intrinsic and acquired drug resistance in malignant tumors," *Arzneimittel-Forschung (Drug Research)*, vol. 58, no. 6, pp. 261–264, 2008.

[27] H. Gronemeyer, J.-A. Gustafsson, and V. Laudet, "Principles for modulation of the nuclear receptor superfamily," *Nature Reviews Drug Discovery*, vol. 3, no. 11, pp. 950–964, 2004.

[28] X. Qin, S. Yu, L. Zhou et al., "Cisplatin-resistant lung cancer cell–derived exosomes increase cisplatin resistance of recipient cells in exosomal miR-100–5p-dependent manner," *International Journal of Nanomedicine*, vol. 12, pp. 3721–3733, 2017.

[29] X. Fu, M. Liu, S. Qu et al., "Exosomal microRNA-32-5p induces multidrug resistance in hepatocellular carcinoma via the PI3K/Akt pathway," *Journal of Experimental & Clinical Cancer Research*, vol. 37, no. 1, p. 52, 2018.

[30] Y. Akao, F. Khoo, M. Kumazaki, H. Shinohara, K. Miki, and N. Yamada, "Extracellular disposal of tumor-suppressor miRs-145 and -34a via microvesicles and 5-FU resistance of human colon cancer cells," *International Journal of Molecular Sciences*, vol. 15, no. 1, pp. 1392–1401, 2014.

[31] M. Zeng, L. Zhu, L. Li, and C. Kang, "miR-378 suppresses the proliferation, migration and invasion of colon cancer cells by inhibiting SDAD1," *Cellular & Molecular Biology Letters*, vol. 22, no. 1, p. 12, 2017.

[32] Z.-H. Xu, T.-Z. Yao, and W. Liu, "miR-378a-3p sensitizes ovarian cancer cells to cisplatin through targeting MAPK1/GRB2," *Biomedicine & Pharmacotherapy*, vol. 107, pp. 1410–1417, 2018.

[33] S. Li, F. Yang, M. Wang, W. Cao, and Z. Yang, "miR-378 functions as an onco-miRNA by targeting the ST7L/Wnt/β-catenin pathway in cervical cancer," *International Journal of Molecular Medicine*, vol. 40, no. 4, pp. 1047–1056, 2017.

[34] Q.-G. Chen, W. Zhou, T. Han et al., "MiR-378 suppresses prostate cancer cell growth through downregulation of MAPK1 in vitro and in vivo," *Tumor Biology*, vol. 37, no. 2, pp. 2095–2103, 2016.

[35] L. Zhang, L. Zou, and P. Sun, "Relationship between miR-378c and YY1 expression in patients with gastric cancer and the clinicopathological features," *Cellular & Molecular Biology Letters*, vol. 26, no. 1, p. 12, 2021.

[36] H. Xia, Z. Zhang, J. Yuan, and Q. Niu, "The lncRNA PVT1 promotes invasive growth of lung adenocarcinoma cells by targeting miR-378c to regulate SLC2A1 expression," *Human Cell*, vol. 34, no. 1, pp. 201–210, 2021.

[37] L. Endo-Munoz, A. Dahler, N. Teakle et al., "E2F7 can regulate proliferation, differentiation, and apoptotic responses in human keratinocytes: implications for cutaneous squamous cell carcinoma formation," *Cancer Research*, vol. 69, no. 5, pp. 1800–1808, 2009.

[38] Q. Li, X.-M. Qiu, Q.-H. Li et al., "MicroRNA-424 may function as a tumor suppressor in endometrial carcinoma cells by targeting E2F7," *Oncology Reports*, vol. 33, no. 5, pp. 2354–2360, 2015.

[39] J. Chu, Y. Zhu, Y. Liu et al., "E2F7 overexpression leads to tamoxifen resistance in breast cancer cells by competing with E2F1 at miR-15a/16 promoter," *Oncotarget*, vol. 6, no. 31, pp. 31944–31957, 2015.

[40] S. Karmakar, N. L. Banik, and S. K. Ray, "Combination of all-trans retinoic acid and paclitaxel-induced differentiation and apoptosis in human glioblastoma U87MG xenografts in nude mice," *Cancer*, vol. 112, no. 3, pp. 596–607, 2008.

Hindawi
Journal of Oncology
Volume 2021, Article ID 9949492, 18 pages
https://doi.org/10.1155/2021/9949492

Research Article

Identification of New Biomarker for Prediction of Hepatocellular Carcinoma Development in Early-Stage Cirrhosis Patients

Gang Ning, Yongqiang Li, Wenji Chen, Wenjuan Tang, Diwen Shou, Qingling Luo, Huiting Chen, and Yongjian Zhou

Department of Gastroenterology and Hepatology, Guangzhou Digestive Diseases Center, Guangzhou First People's Hospital, South China University of Technology, Guangzhou, Guangdong Province, China

Correspondence should be addressed to Huiting Chen; eychenhuiting@scut.edu.cn and Yongjian Zhou; eyzhouyongjian@scut.edu.cn

Received 9 March 2021; Accepted 30 June 2021; Published 21 July 2021

Academic Editor: Muhammad Wasim Khan

Background. Liver cirrhosis is one of the major drivers of hepatocellular carcinoma (HCC). In the present study, we aimed to identify and validate new biomarker for early prediction of HCC development in early-stage cirrhosis patients. *Methods*. mRNA expression and clinical parameters of GSE63898, GSE89377, GSE15654, GSE14520, and TCGA-HCC cohort and ICGC-HCC cohort were downloaded for analysis. Wilcoxon test was performed to identify DEGs. Univariate and multivariate Cox regression analysis were used to develop the risk signature, and ROC analysis was performed to analyze the predictive accuracy and sensitivity of the risk signature. *Results*. There were 42 DEGs (including 28 upregulated genes and 14 downregulated genes) found in early-stage liver cirrhosis patients before developing HCC from GSE1565442. Then, a risk signature consisting of 8 DEGs could effectively classify early-stage cirrhosis patients into high-risk group with shorter HCC development time and low-risk group with longer HCC development time from GSE15654. Multivariate Cox analysis indicated that the risk signature was an independent prognostic factor for the prediction of HCC development and ROC analysis showed that the signature exhibited good predictive efficiency in predicting 2-, 5-, and 10-year HCC development. Mechanistically, significantly higher proportions of CD8 T cells were found to be enriched in cirrhosis patients with low risk score, and higher CD8 T cells were associated with longer HCC development time. Besides, the signature was an independent prognostic factor for poorer prognosis of early-stage liver cirrhosis patients of GSE15654. Moreover, the signature could also separate HCC patients from healthy controls and was also associated with the poorer prognosis of HCC patients from three HCC cohorts. Finally, we also identified HDAC inhibitors, such as trichostatin A, to be a potential chemopreventive treatment for the prevention of HCC development by targeting risk signature based on CMap analysis. *Conclusion*. A risk signature was developed and validated for early prediction of HCC development, which may be a useful tool to set up individualized follow-up interval schedules.

1. Introduction

Hepatocellular carcinoma (HCC) continues to be a serious threat and burden to public health as it represents the sixth most common cancers and the fourth leading cause of cancer-related death worldwide [1]. Moreover, the incidence of HCC has increased rapidly in regions, previously identified as lower rates, such as Oceania, Western Europe, and Northern America [2]. Much achievement has been made in treating HCC. However, the disease is still tackled with low remission rate, high recurrence, and low survival rate. To date, no effective adjuvant therapy is available for prevention of recurrence [3, 4]. Furthermore, at times of the diagnosis of HCC is made, 40% to 50% of the patients are at their advanced stages and the treatment options are very limited [5]. This comes to great clinical urgency in identification of a potential new efficient method for the diagnosis of HCC.

HCC is known to be related to inflammation and liver damage [6]. Liver cirrhosis is a notable risk factor for HCC and is often found prior to the development of HCC [7, 8]. The incidence of HCC in non-cirrhosis patients is 0.5% to 1.0%, but the incidence of HCC in cirrhosis patients reaches

as much as 3%–6%. Current practice guideline suggests the necessity of regular HCC surveillance [9–12]. However, there were up to 12% of HCC patients could be diagnosed through current surveillance recommendation [13]. Other effective prognostic signature is needed to identify cirrhosis patients who are at high risk for HCC development and should be further justified.

Recent applications of microarray and high-throughput technologies have provided a better method to better understand the molecular mechanism of the transformation from liver cirrhosis to HCC [14, 15], through which new biomarkers in screening HCC in cirrhosis patients could be explored. In the present study, we first screened out differentially expressed genes (DEGs) between cirrhosis patients and early HCC patients and then further identified those DEGs whose expression had been altered in early-stage liver cirrhosis patients before development of HCC. Next, we developed and validated a risk signature for prediction of HCC development for early-stage liver cirrhosis patients and analyzed the association of the risk signature with infiltrating immune cells. Besides, we assessed the prognostic value of this signature in HCC patients. Moreover, we sought to identify potential bioactive compounds which could be potential chemopreventive treatment for the prevention of HCC development by targeting the risk signature.

2. Materials and Methods

2.1. Ethics Statement. All the data used for analysis in the present study were downloaded from The Cancer Genome Atlas (TCGA), Gene Expression Omnibus (GEO), and International Cancer Genome Consortium (ICGC) database, so written consents had already been obtained before our study.

2.2. Data Acquisition. mRNA expression profiles of GSE63898, GSE89377, GSE15654, and GSE14520 were downloaded from GEO database (https://www.ncbi.nlm.nih.gov/geo/). mRNA expression profile of TCGA-HCC cohort was got from GDC Data portal (https://cancergenome.nih.gov/). mRNA expression profile of ICGC Japan HCC cohort was attained from the ICGC portal (https://dcc.icgc.org/projects/LIRI-JP). All the data were log2-trasformed for data normalization.

In GSE63898, there were 196 early HCC patients (defined as BCLC 0/A stage) and 168 liver cirrhosis patients. In GSE89377, there were 12 liver cirrhosis patients, 22 patients with dysplastic nodules, 5 early HCC patients, and 23 advanced HCC patients. GSE63898 and GSE89377 were used to identify DEGs and KEGG pathways between liver cirrhosis patients and early HCC patients. DEGs were identified with a cut-off value of $p < 0.05$. KEGG pathways enriched by these DEGs were identified in DAVID (https://david.ncifcrf.gov/summary.jsp), and a cut-off value of $p < 0.05$ was considered as statistically significant.

In GSE15654, gene expression profile of formalin-fixed needle biopsy specimens from the livers of 216 patients with hepatitis C-related early-stage (Child–Pugh class A) cirrhosis were available. These patients were prospectively followed up for a median of 10 years at an Italian center, and there were 65 liver cirrhosis who finally developed HCC. GSE15654 was used to identify the DEGs and KEGG pathways between liver cirrhosis patients who would or would not develop HCC with similar method as described above. Besides, GSE15654 was also used to develop a risk signature for prediction of HCC development for early-stage liver cirrhosis patients. Basic characteristics of 216 patients with early-stage cirrhosis were summarized in Table 1.

Three HCC cohorts, including TCGA-HCC cohort (377 HCC patients and 50 normal controls), GSE14520 HCC cohort (220 HCC patients), and ICGC HCC cohort (232 HCC patients), were used to examine the prognostic value of the risk signature in HCC patients. Basic characteristics of HCC patients from these three cohorts were summarized in Table 2.

2.3. Development and Validation of Risk Signature for Early Prediction of HCC Development for Liver Cirrhosis Patients. First, these 216 early-stage liver cirrhosis patients were randomly divided into training cohort ($N = 108$) and validation cohort ($N = 108$) with an allocation of 1 : 1. Next, univariate and multivariate Cox regression analysis were performed to screen out the HCC development-associated genes in the training cohort. Then, a risk signature was constructed based on the coefficients weighted by multivariate Cox regression analysis. With the help of this signature, risk score for each patient was calculated and they were divided into high-risk group and low-risk group with the best cut-off value calculated by X-Tile software (http://tissuearray.org/, version 3.6.1). After that, the prognostic and predictive values of this signature were analyzed by univariate and multivariate Cox regression analysis and time-dependent ROC analysis. Finally, the applicability of the signature was also validated in the validation cohort and the whole cohort.

2.4. CIBORSORT. CIBERSORT (https://cibersort.stanford.edu), an online tool designed for estimating the abundances of infiltrating immune cells, was used for estimating infiltrating immune cells of 216 liver cirrhosis patients on the basis of mRNA expression profiles [16].

2.5. CMap Analysis. HCC development-associated genes identified by multivariate Cox regression analysis were classified into upregulated genes with the $HR > 1$ and downregulated genes with the $HR < 1$. Next, these genes were uploaded to the CMap web tool (https://portals.broadinstitute.org) to screen out compounds that may be potential chemopreventive treatment for the prevention of HCC development. Scores that ranged from −1 to 1 represented the correlation between compounds and risk signature genes. A negative score indicated that the corresponding compounds could reverse the expression of related genes and thus may be more likely to be used for

Table 1: Basic characteristics of 216 patients with early-stage liver cirrhosis from GSE15654.

Variables	Liver cirrhosis patients ($N = 216$)
Varices (yes/no/NA)	52/159/5
Bilirubin (<1.0 mg/dl/ ≥1.0 mg/dl)	108/108
Platelet (<100,000/mm^3/≥100,000/mm^3)	99/117
Development of HCC (yes/no)	65/151
Times to develop HCC (days, median)	3230 (175–8256)
Development of death (yes/no)	66/150
Times to death (days, median)	3580.5 (194–8256)

Table 2: Basic characteristics of HCC patients from TCGA, GSE14520, and ICGC HCC cohorts.

Variables	TCGA cohort ($N = 377$)	GSE14520 cohort ($N = 220$)	ICGC cohort ($N = 232$)
Gender (male/female)	255/122	190/30	171/61
Age (years, ≤60/>60/NA)	180/196/1	181/39	50/182
Cirrhosis (yes/no/NA)	81/137/159	202/18	NA
Histologic grade (*G*1/*G*2/*G*3/*G*4/NA)	55/180/124/13/5	NA	NA
T stage (I/II/III/IV/TX/NA)	185/95/81/13/1/2	NA	NA
N stage (*N*0/*N*1 + NX/NA)	257/119/1	NA	NA
M stage (*M*0/*M*1 + MX)	272/105	NA	189/43
TNM stage (I/II/III/IV/NA)	175/87/86/5/24	93/77/48/-/2	36/106/71/76

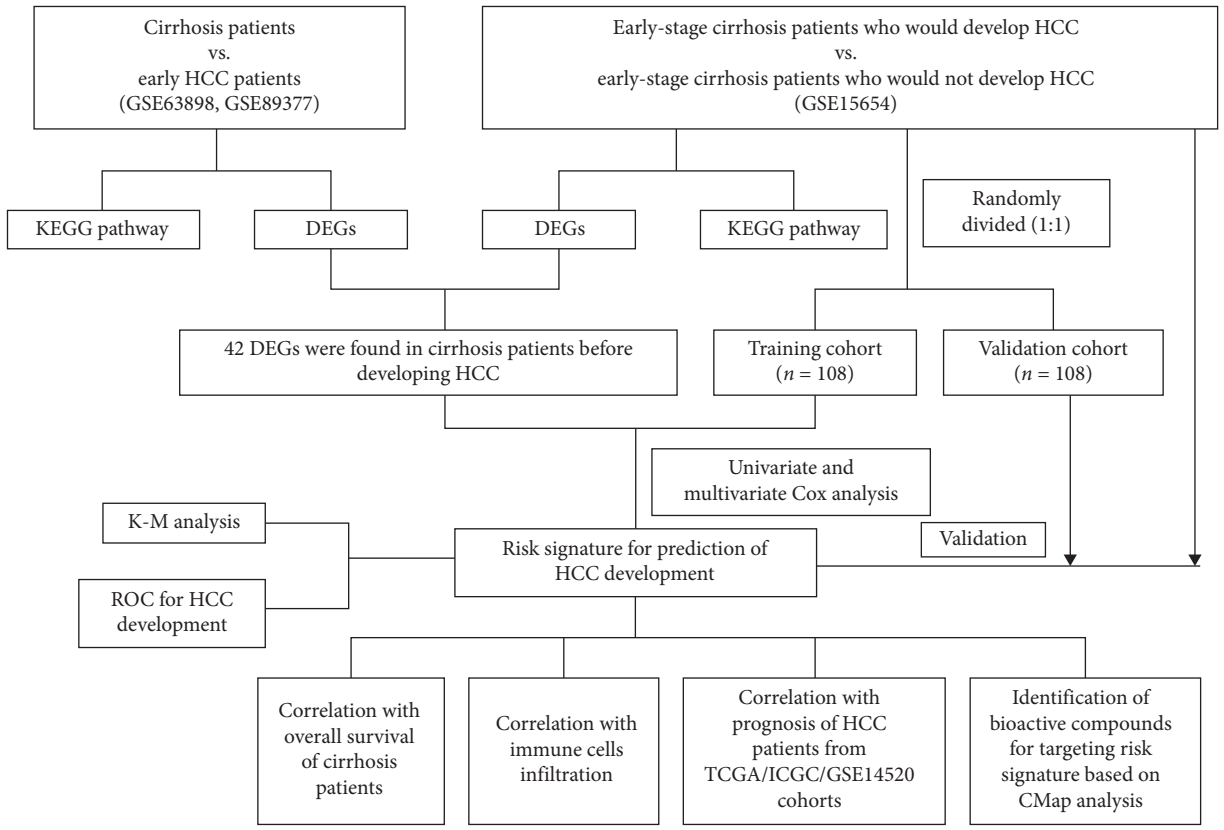

Figure 1: The workflow chart of the present study.

chemopreventive treatment for prevention of HCC development, and vice versa [17].

2.6. Data Analysis Flowchart. A workflow of the study was depicted and is shown in Figure 1.

2.7. Statistical Analysis. R software (version 3.5.1) and GraphPad Prism 6 (GraphPad Software, La Jolla, CA, USA) were used for statistical analysis. Wilcoxon test was performed to identify DEGs between patients with liver cirrhosis and early HCC patients, or early-stage liver cirrhosis patients who would or would not develop HCC. Unpaired

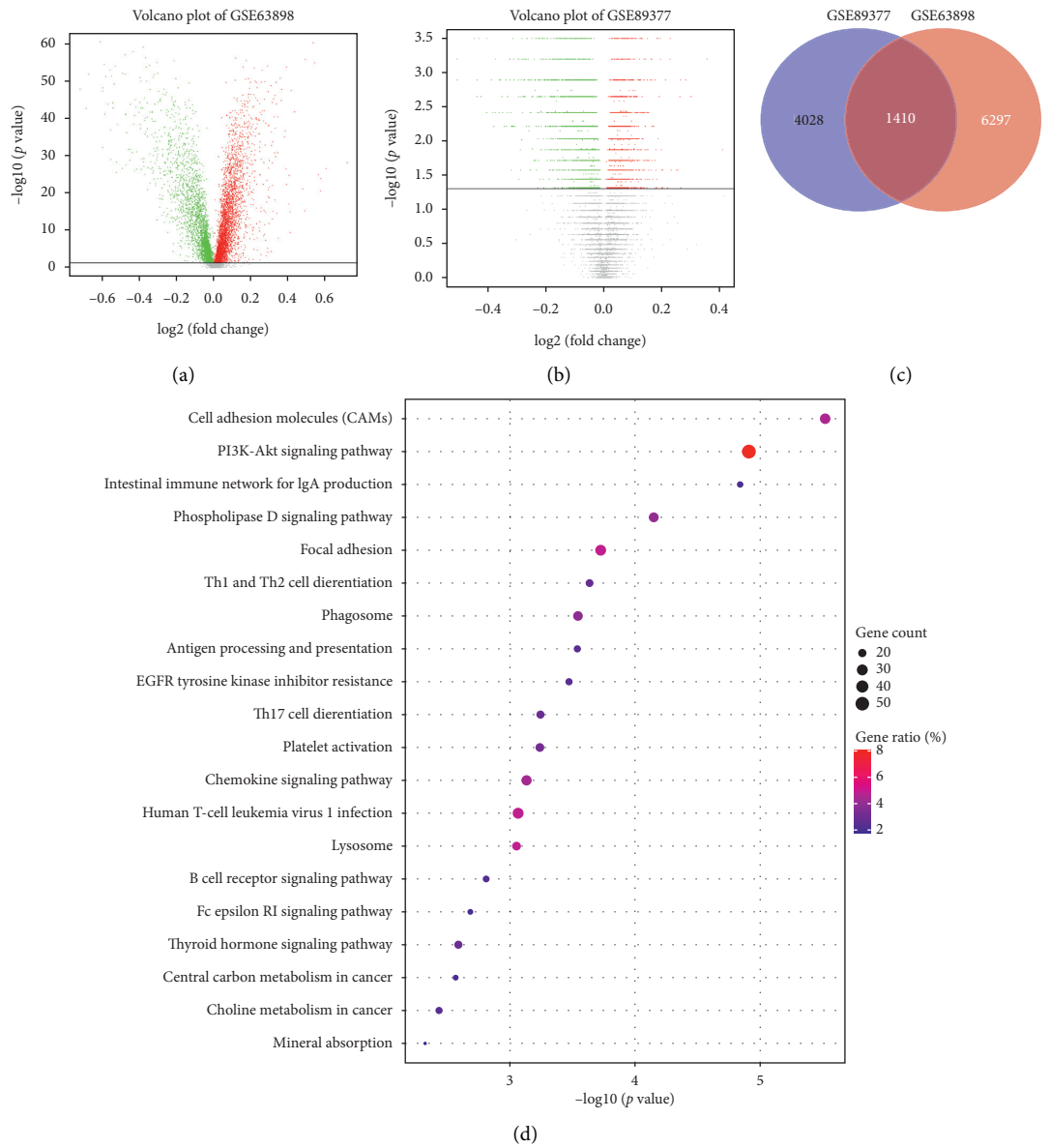

Figure 2: Differentially expressed genes (DEGs) and KEGG pathways between liver cirrhosis patients and early HCC patients. (a) Volcano figure of DEGs identified between liver cirrhosis patients and early HCC patients of GSE63898. (b) Volcano figure of DEGs identified between liver cirrhosis patients and early HCC patients of GSE89377. (c) Venn diagram of overlapped DEGs from GSE63898 and GSE89377. (d) KEGG pathways enriched in early HCC patients.

Student's *t*-tests or ANOVA tests were performed to compare the difference of risk score between two groups or more than three groups. Kaplan–Meier analysis with two-side log-rank test was performed to analyze the difference of HCC development time, overall survival (OS), or disease-free survival (DFS) between patients of different risk scores. Univariate and multivariate Cox regression analysis were performed to analyze the prognostic value of the risk signature. Time-dependent ROC was performed to analyze the predictive accuracy and sensitivity of the risk signature. Additional statistical analyses were performed with STAMP [18]. $p < 0.05$ was considered as statistically significant.

3. Results

3.1. DEGs and KEGG Pathways between Liver Cirrhosis Patients and Early HCC Patients. First, 7707 DEGs, including 4288 upregulated genes and 3419 downregulated genes, were found at early HCC patients (BCLC 0/A stage) compared to liver cirrhosis patients from GSE63898 (Figure 2(a)). Next, in order to reduce the selection bias, DEGs between 12 liver cirrhosis patients and 5 early HCC patients from GSE89377 were also identified, and 5438 DEGs, including 2782 upregulated genes and 2656 downregulated genes, were identified in early HCC patients compared to liver cirrhosis

patients (Figure 2(b)). In total, 1410 DEGs, including 662 upregulated genes and 748 downregulated genes, were identified in early HCC patients by overlapping DEGs from GSE63898 and GSE89377 (Figure 2(c), Supplementary Material 1). These 1410 DEGs were mainly enriched in KEGG pathways, such as cell adhesion molecules (CAMs), PI3K-Akt signaling pathway, focal adhesion, antigen processing and presentation, chemokine signaling pathway, central carbon metabolism in cancer, and choline metabolism in cancer (Figure 2(d)), which had been found to be related with the development and progression of HCC. These results indicated that the above DEGs and KEGG pathways may play an important role in the transformation of liver cirrhosis to early HCC.

3.2. DEGs and KEGG Pathways between Early-Stage Liver Cirrhosis Patients Who Would or Would Not Develop HCC. After identifying the DEGs and KEGG pathways between liver cirrhosis patients and early HCC patients, we next aimed to identify the DEGs and KEGG pathways between early-stage liver cirrhosis patients who would or would not develop HCC. In total, 1511 DEGs, including 972 upregulated genes and 539 downregulated genes, were found at liver cirrhosis patients who developed HCC compared to liver cirrhosis patients who would not develop HCC (Figure 3(a)). These DEGs were mainly enriched in KEGG pathways, such as complement and coagulation cascades, chemical carcinogenesis, retinol metabolism, valine, leucine and isoleucine degradation, tyrosine metabolism, and metabolism of xenobiotics by cytochrome P450 (Figure 3(b)). Compared to the KEGG pathways enriched in early HCC patients, abnormal metabolism of nutrient substance, such as carbon, choline, and amino acid, had been found at early-stage liver cirrhosis patients who would develop HCC. Moreover, compared to the DEGs identified in early HCC patients, 42 DEGs, including 28 upregulated genes and 14 downregulated genes, were found to be already abnormal in early-stage liver cirrhosis patients before developing HCC (Figure 3(c), Supplementary Material 2), suggesting that these abnormally expressed genes may be served as biomarkers for the identification of early-stage liver cirrhosis patients who were at high risk for HCC development.

3.3. Construction of a Risk Signature for Early Prediction of HCC Development for Early-Stage Liver Cirrhosis Patients of the Training Cohort. Having found 42 abnormally expressed genes, which may be served as biomarkers for the identification of early-stage liver cirrhosis patients who were at high risk for HCC, we then tried to comprehensively explore the association of these abnormally expressed genes with the development of HCC. First, 216 early-stage liver cirrhosis patients were randomly divided into training cohort ($N = 108$) and validation cohort ($N = 108$). Next, 14 genes were found to be associated with HCC development in patients of the training cohort by univariate Cox regression analysis (Supplementary Material 3). Then, multivariate Cox regression analysis was performed to further screen out the most HCC development-associated genes (including SEMA4D, RBM28, RPS3A, AGPAT1, COPS4, DPP3, NPLOC4, and YEATS2). Finally, a risk signature was constructed based on the coefficients weighted by multivariate Cox regression analysis. The risk score was calculated as follows: risk score = (−2.07 ∗ SEMA4D expression) + (1.71 ∗ RBM28 expression) + (0.83 ∗ RPS3A expression) + (0.73 ∗ AGPAT1 expression) − (1.23 ∗ COPS4 expression) + (1.44 ∗ DPP3 expression) + (0.32 ∗ NPLOC4 expression) + (0.67 ∗ YEATS2 expression). We calculated the risk score for each patient. Patients with a risk score > 4 were classified into high-risk group ($N = 24$), and others with a risk score < 4 were assigned to low-risk group ($N = 84$) by the X-Tile software (http://tissuearray.org/, version 3.6.1). Higher risk scores were found in liver cirrhosis patients who would develop HCC compared to those patients who would not develop HCC ($p < 0.001$, Figure 4(a)). Patients in the high-risk group had shorter HCC development time than that of the low-risk group (HR = 12.24, 95% CI: 5.8–25.86, $p < 0.001$, Figure 4(b)). Besides, univariate Cox regression analysis and multivariate Cox regression analysis also indicated that the risk signature was an independent prognostic factor for HCC development (HR = 11.02, 95% CI: 5.12–23.70, $p < 0.001$, Figures 4(c) and 4(d)). Moreover, the areas under ROC curve (AUC) of the risk signature for predicting 2-, 5-, and 10-year HCC development were 0.767, 0.909, and 0.859, respectively (Figure 4(e)), which showed good predictive value of the risk signature in predicting HCC development.

3.4. Validation of the Risk Signature in Patients of the Validation Cohort and the Whole Cohort. To further test the applicability of the risk signature, we further examined its prognostic value in the validation cohort and the whole cohort. Similarly, risk score for each patient was also calculated, and then they were assigned into high-risk group ($N = 22$) and low-risk group ($N = 86$) in the validation cohort and high-risk group ($N = 46$) and low-risk group ($N = 170$) in the whole cohort with the same cut-off value. Likewise, higher risk scores were found in liver cirrhosis patients who would develop HCC compared to those patients who would not develop HCC in the validation cohort and the whole cohort (all $p < 0.05$, Figures 5(a) and 6(a)). Patients in the high-risk group had shorter HCC development time than that of the low-risk group in the validation cohort (HR = 3.84, 95% CI: 1.66–8.88, $p = 0.002$, Figure 5(b)) and in the whole cohort (HR = 5.92, 95% CI: 3.61–9.70, $p < 0.001$, Figure 6(b)). Besides, univariate Cox regression analysis and multivariate Cox regression analysis also suggested that the risk signature was an independent prognostic factor for HCC development in the validation cohort (HR = 3.89, 95% CI: 1.68–9.04, $p = 0.002$, Figures 5(c) and 5(d)) and in the whole cohort (HR = 5.32, 95% CI: 3.23–8.78, $p = 0.002$, Figures 6(c) and 6(d)). Moreover, the AUC of the risk signature for predicting 2-, 5-, and 10-year HCC development were 0.828, 0.748, and 0.658 in the validation cohort (Figure 5(e)) and 0.791, 0.846, and 0.766 in the whole cohort (Figure 6(e)), which validated

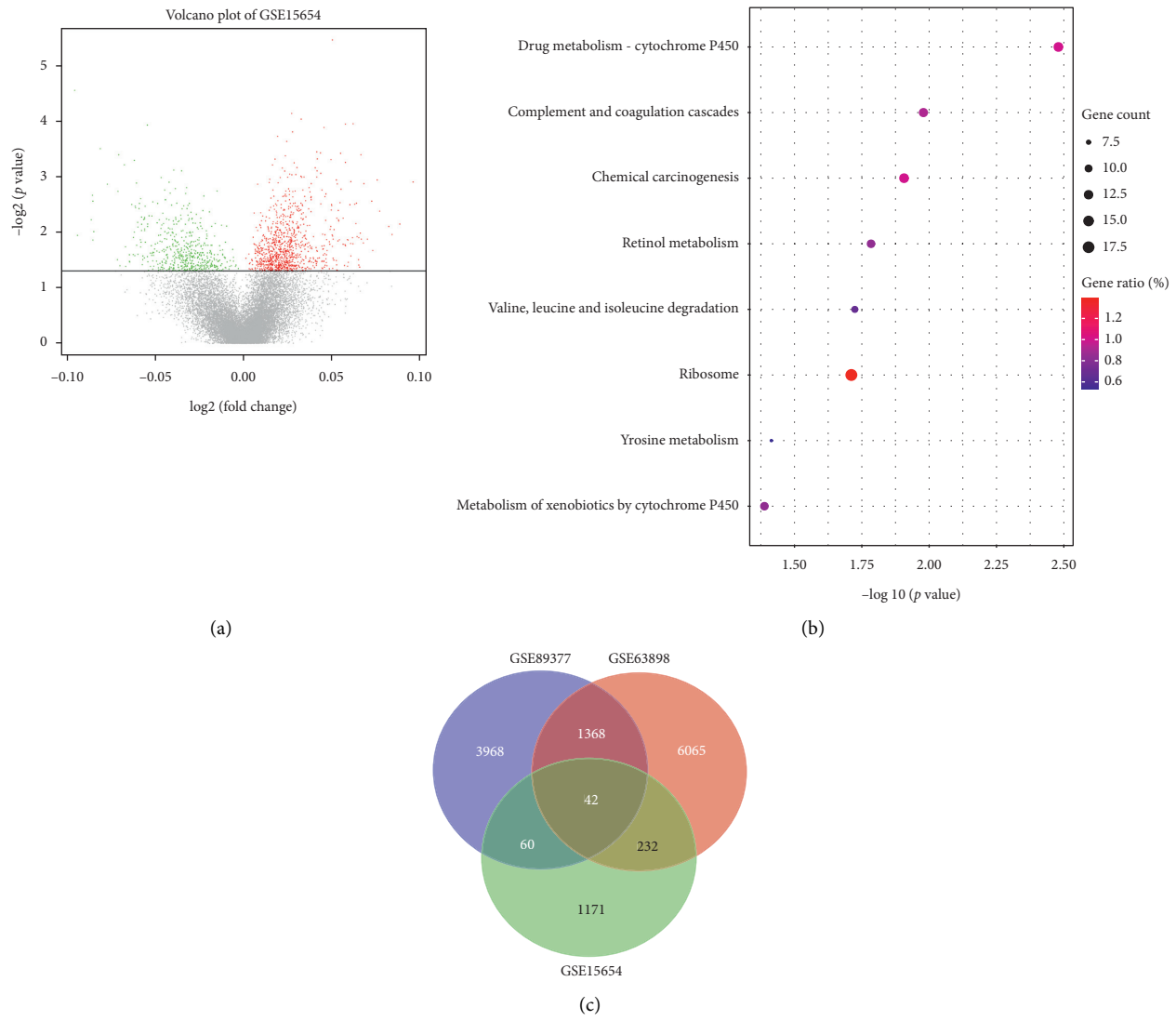

Figure 3: DEGs and KEGG pathways between early-stage liver cirrhosis patients who would or would not develop HCC of GSE15654. (a) Volcano figure of DEGs between early-stage liver cirrhosis patients who would or would not develop HCC of GSE15654. (b) KEGG pathways enriched in early-stage liver cirrhosis patients who would develop HCC. (c) Venn diagram of overlapped DEGs from GSE63898 and GSE89377 and GSE15654.

the good predictive value of the risk signature in predicting HCC development.

3.5. Association of the Risk Signature with the OS of Early-Stage Liver Cirrhosis Patients. After validation of the risk signature in the prediction of HCC development, we next further analyzed the association of the risk signature with the OS of early-stage liver cirrhosis patients in the whole cohort. Similarly, higher risk scores were found in liver cirrhosis patients who would develop death compared to liver cirrhosis patients who would not ($p < 0.01$, Figure 7(a)). Patients in the high-risk group had shorter OS time than that of the low-risk group (HR = 2.15, 95% CI: 1.28–3.62, $p = 0.003$, Figure 7(b)). Besides, univariate Cox regression analysis and multivariate Cox regression analysis also indicated that the risk signature was an independent prognostic factor for OS (HR = 1.71, 95% CI: 1.003–2.91, $p = 0.048$, Figures 7(c) and 7(d)). Moreover, the AUC of the risk signature for predicting 2-, 5-, and 10-year OS were 0.832, 0.703, and 0.676, respectively (Figure 7(e)), which also suggested good predictive value of the risk signature in predicting OS of early-stage liver cirrhosis patients.

3.6. Association of the Risk Signature with the Infiltrating Immune Cells of Early-Stage Liver Cirrhosis Patients. Previous researches had showed that immune system played an important role in protecting against cancer development [19], so we next tried to analyze the relationship of the risk signature with the infiltrating immune cells of early-stage liver cirrhosis patients. We used CIBERSOR to calculate infiltrating immune cells in early-stage liver cirrhosis patients. As is shown in Figure 8(a), significant proportions of resting mast cells, neutrophils, CD8 T cells, and total T cells were found to be enriched

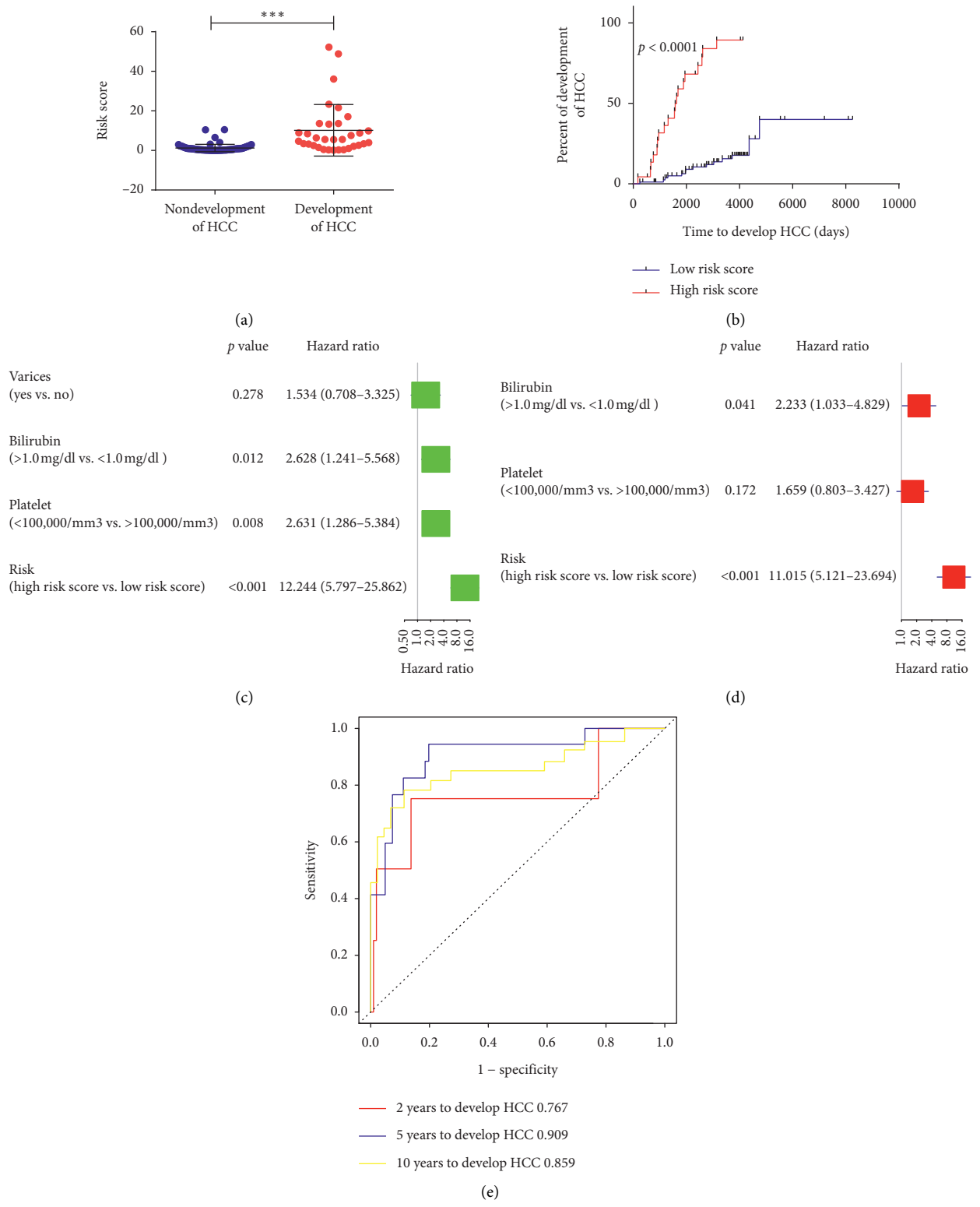

Figure 4: Construction of a risk signature for prediction of HCC development for early-stage liver cirrhosis patients of the training cohort. (a) Risk score between early-stage liver cirrhosis patients who would or would not develop HCC. (b) Kaplan–Meier analysis of HCC development time of patients different risk score. (c)-(d) Univariate and multivariate analysis of the risk signature for HCC development time for early-stage liver cirrhosis patients. (e) AUC of the risk signature in predicting 2-year, 5-year, and 10-year HCC development for early-stage liver cirrhosis patients.

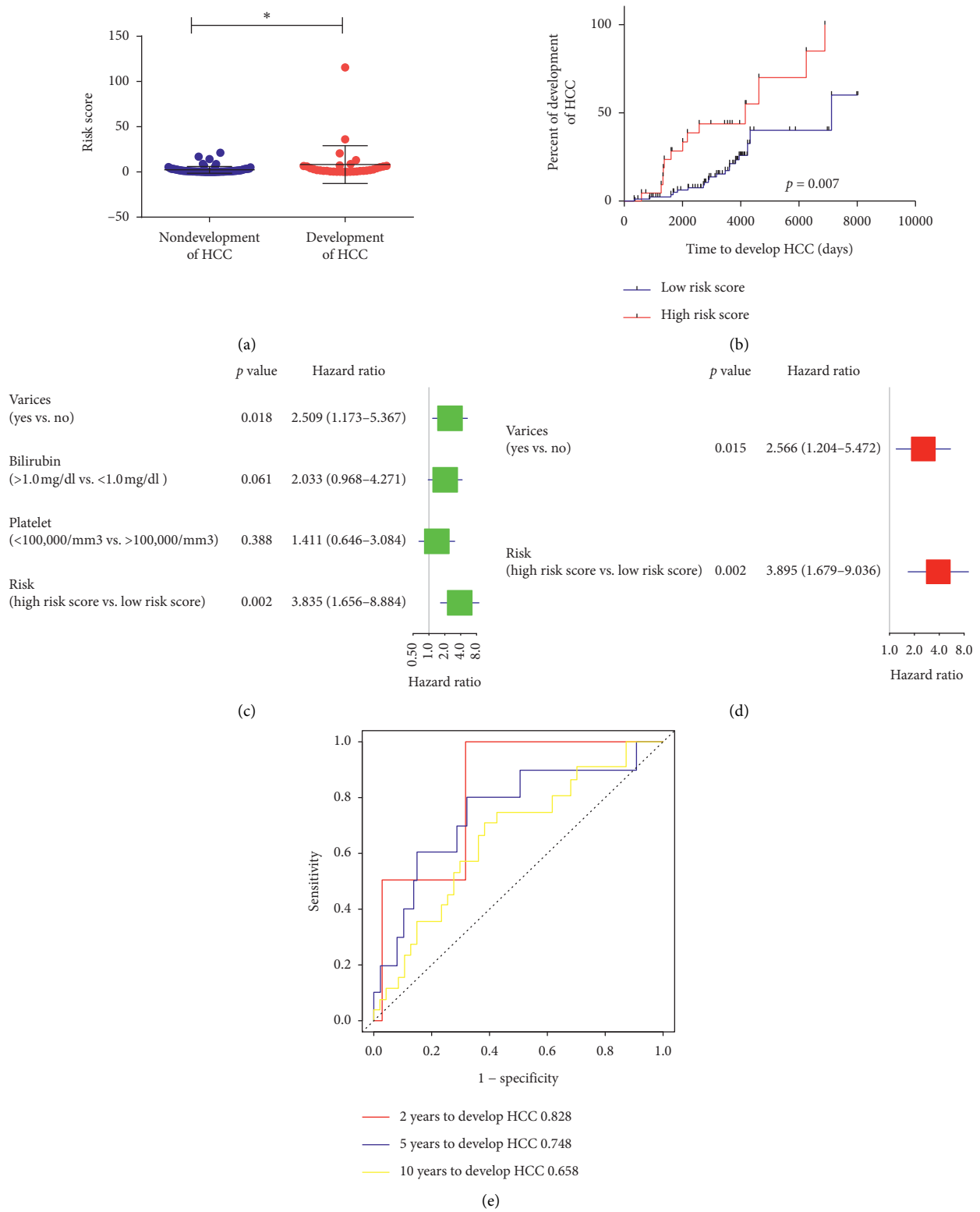

Figure 5: Validation of the risk signature in patients of the validation cohort. (a) Risk score between early-stage liver cirrhosis patients who would or would not develop HCC. (b) Kaplan–Meier analysis of HCC development time of patients different risk score. (c)-(d) Univariate and multivariate analysis of the risk signature for HCC development time for early-stage liver cirrhosis patients. (e) AUC of the risk signature in predicting 2-year, 5-year, and 10-year HCC development for early-stage liver cirrhosis patients.

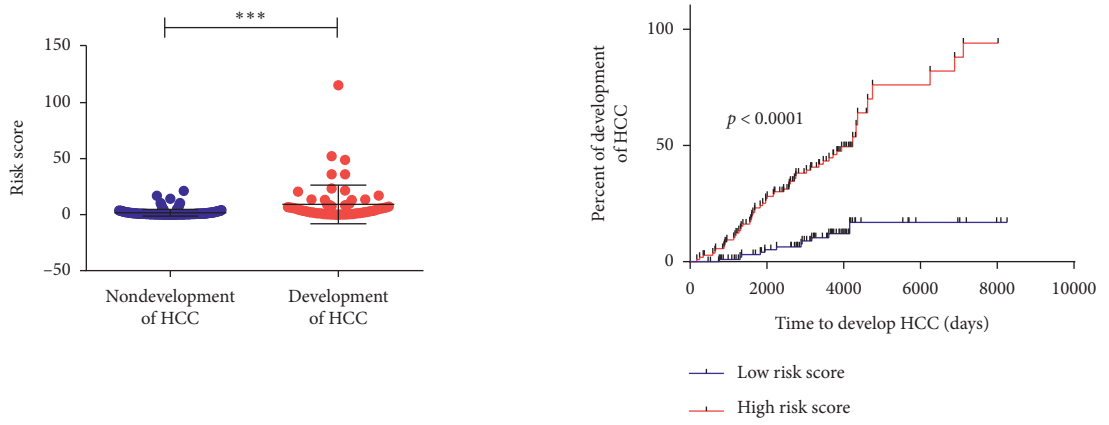

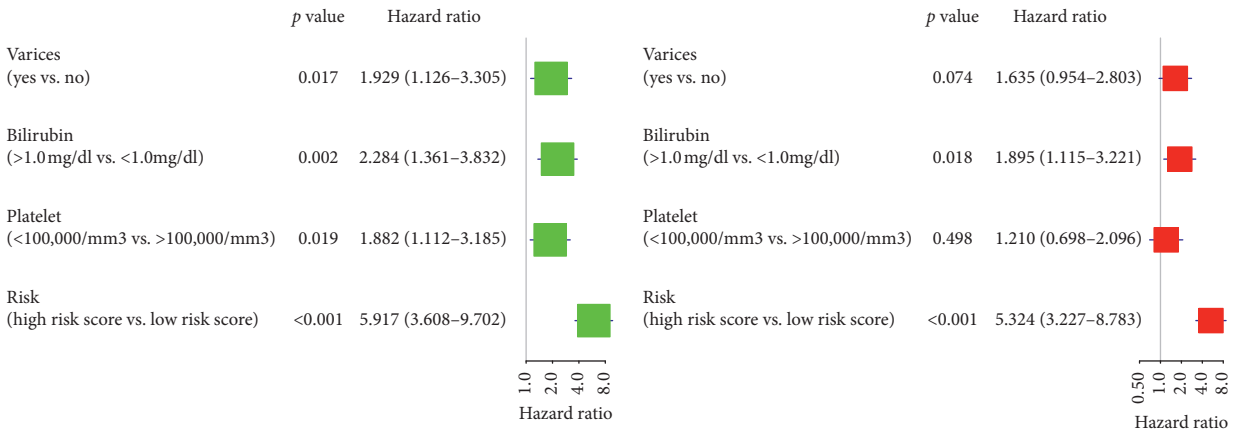

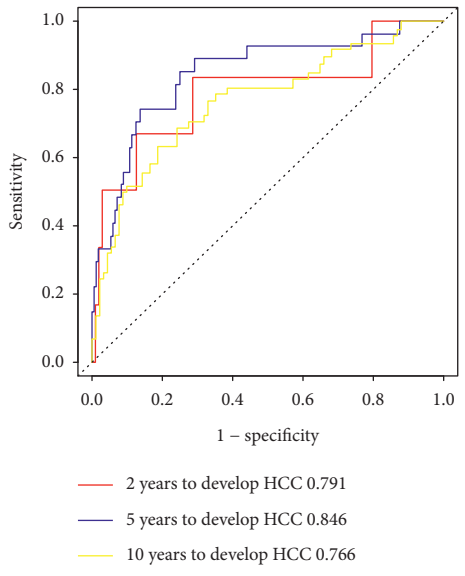

Figure 6: Validation of the risk signature in patients of the whole cohort. (a) Risk score between early-stage liver cirrhosis patients who would or would not develop HCC. (b) Kaplan–Meier analysis of HCC development time of patients different risk score. (c)-(d) Univariate and multivariate analysis of the risk signature for HCC development time for early-stage liver cirrhosis patients. (e) AUC of the risk signature in predicting 2-year, 5-year, and 10-year HCC development for early-stage liver cirrhosis patients.

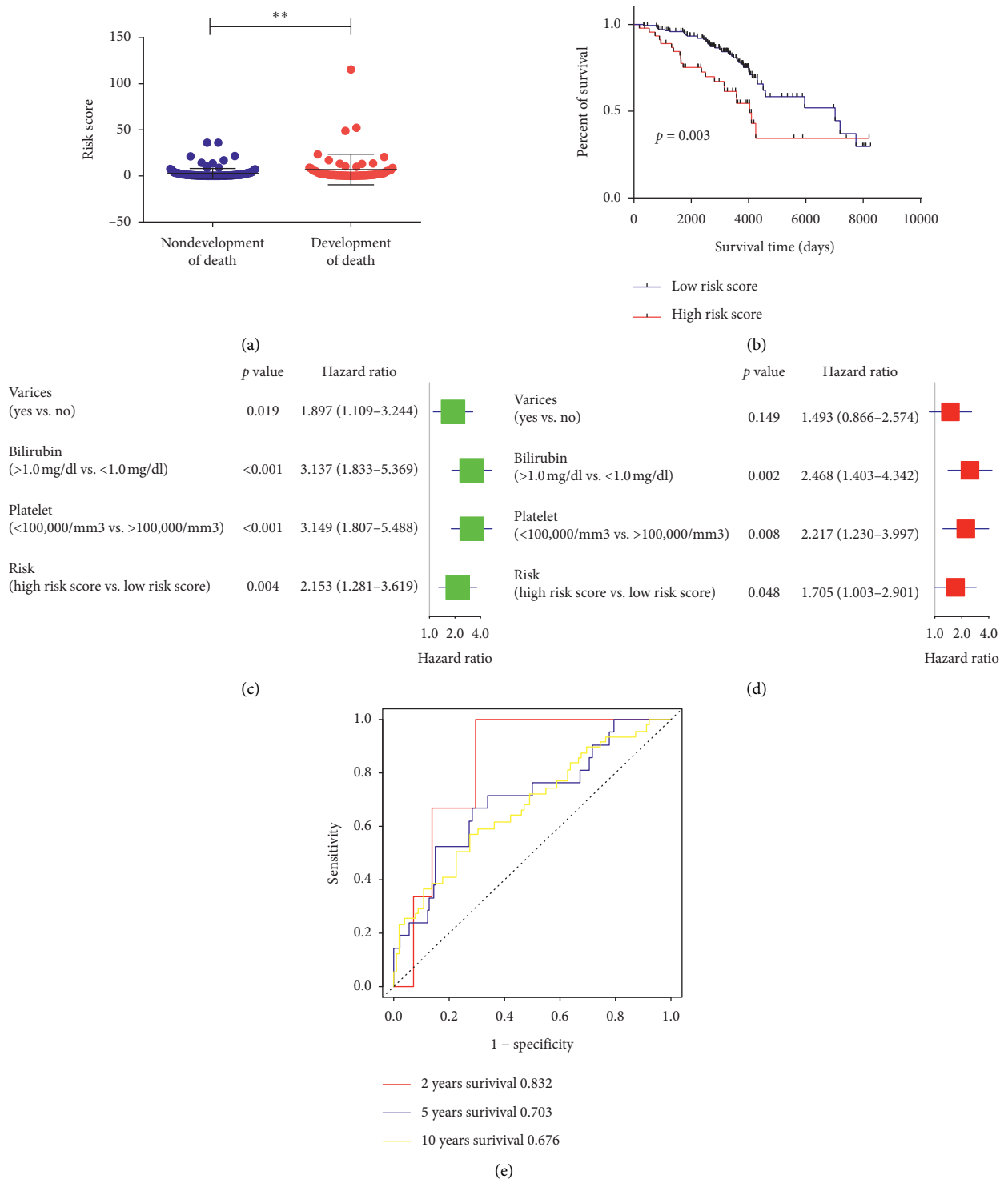

Figure 7: Association of the risk signature with the overall survival (OS) of early-stage liver cirrhosis patients. (a) Risk score between early-stage liver cirrhosis patients who would or would not develop death. (b) Kaplan–Meier analysis of OS time of patients different risk score. (c)-(d) Univariate and multivariate analysis of the risk signature for OS time for early-stage liver cirrhosis patients. (e) AUC of the risk signature in predicting 2-year, 5-year, and 10-year OS for early-stage liver cirrhosis patients.

in HCC patients with low risk score, while only activated mast cells were found to be enriched at patients with high risk score (all $p < 0.05$, Figure 8(a)). Further analysis showed that higher CD8 T cells were associated with longer HCC development time (HR = 1.96, 95% CI: 1.11–3.40, $p = 0.02$, Figure 8(b)), which may indicate that the signature may affect HCC development of early-stage liver cirrhosis patients by the regulation of the infiltration of CD8 T cells.

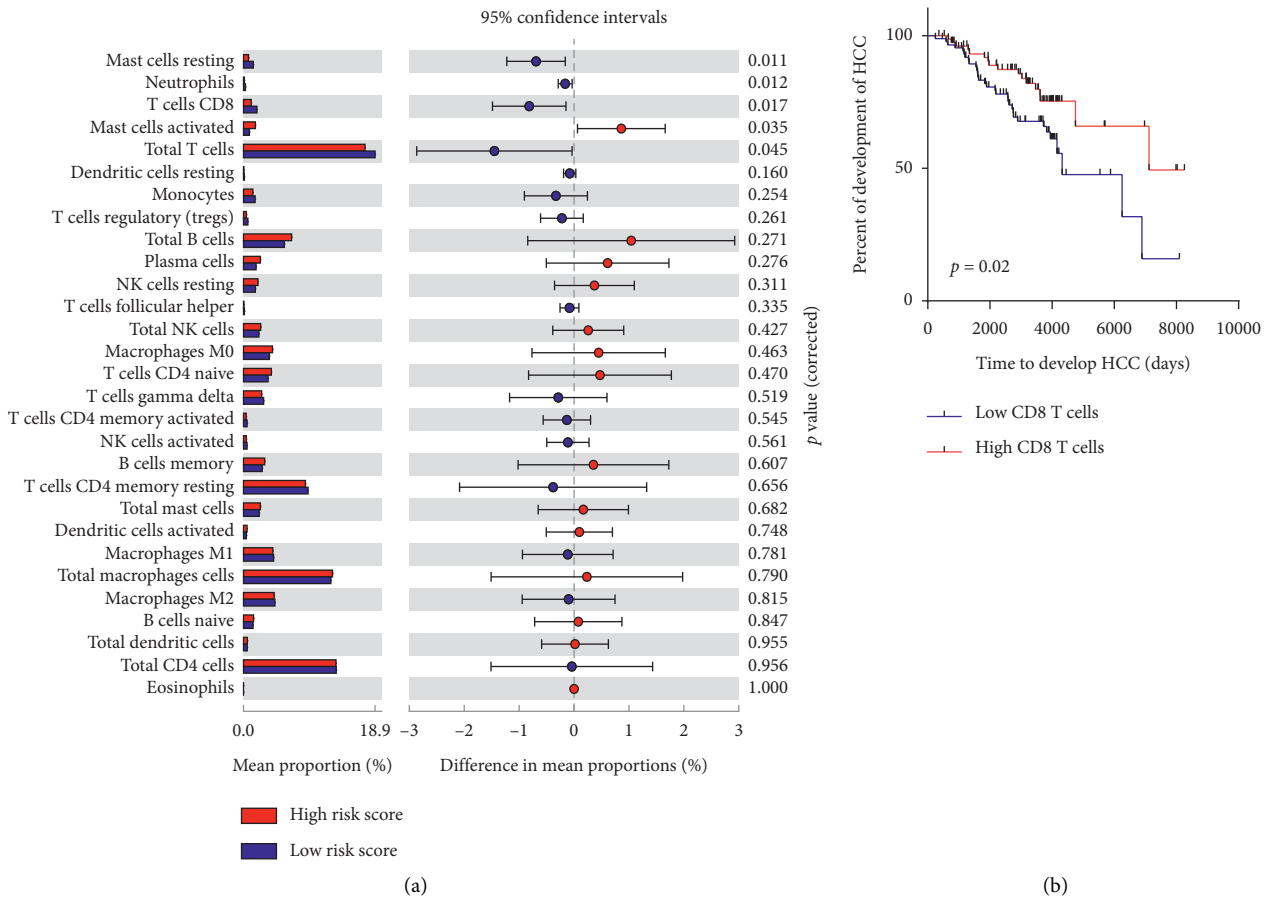

Figure 8: Association of the risk signature with the infiltrating immune cells of early-stage liver cirrhosis patients. (a) Landscape of tumor-infiltrating immune cells in early-stage liver cirrhosis patients of different risk score. (b) Kaplan–Meier analysis of HCC development time of patients with different levels of CD8 T cells.

3.7. Prognostic Value of the Risk Signature in HCC Patients from TCGA Cohort, GSE14520 Cohort, and ICGC Cohort. Having found that the risk signature was significantly associated with HCC development and OS of early-stage liver cirrhosis patients, we then aimed to examine whether the risk signature was associated with the prognosis of HCC patients. Likewise, risk score for each HCC patients was calculated and then assigned into high-risk group and low-risk group by the X-Tile software. In TCGA cohort, higher risk scores were found in HCC patients compared to normal controls ($p < 0.001$, Figure 9(a)), indicating that the signature may also be used to serve as biomarker to distinguish HCC patients from healthy controls. Moreover, patients in the high risk group had shorter OS and DFS time than that of the low-risk group (OS : HR = 2.46, 95% CI: 1.60–3.79, $p < 0.001$; DFS : HR = 1.84, 95% CI: 1.32–2.56, $p < 0.001$, Figures 9(b), and 9(c)); univariate and multivariate Cox regression analysis also suggested that the risk signature was an independent prognostic factor for OS and DFS time for HCC patients (OS : HR = 2.23, 95% CI: 1.40–3.53, $p < 0.001$; DFS : HR = 1.64, 95% CI: 1.16–2.31, $p = 0.005$, Figures 9(d)–9(g)). Similar results were found in GSE14520 cohort and ICGC cohort. In GSE14520 cohort, patients in the high-risk group had shorter OS and DFS time than that of the low-risk group (OS : HR = 2.20, 95% CI: 1.25–3.28, $P = 0.004$; DFS : HR = 1.89, 95% CI: 1.25–2.87, $P = 0.002$, Figures 9(h) and 9(i)); univariate and multivariate Cox regression analysis also suggested that the risk signature was an independent prognostic factor for OS and DFS time of HCC patients (OS : HR = 1.76, 95% CI: 1.08–2.88, $P = 0.05$; DFS : HR = 1.83, 95% CI: 1.20–2.79, $P = 0.005$, Figures 9(j)–9(m)). In ICGC cohort, patients in the high risk group had shorter OS than that of the low risk group (HR = 5.24, 95% CI: 2.87–9.57, $P < 0.001$ Figure 9(n)); univariate and multivariate Cox regression analysis also suggested that the risk signature was an independent prognostic factor for OS and DFS time for HCC patients (HR = 5.33, 95% CI: 2.84–10.0, $P < 0.001$; Figures 9(o) and 9(p)). Taken together, the signature was also associated with the prognosis of HCC patients.

3.8. Identification of Bioactive Compounds as Chemopreventive Treatment for Prevention of HCC Development Based on CMap Analysis. We performed KEGG analysis to explore the underlying pathological pathways by which the signature used to influence the development of HCC for early-stage liver cirrhosis patients. As was shown in Supplementary Figure A, pathological pathways, such as "negative regulation of apoptotic process," "positive regulation of NF-kappaB transcription factor activity,"

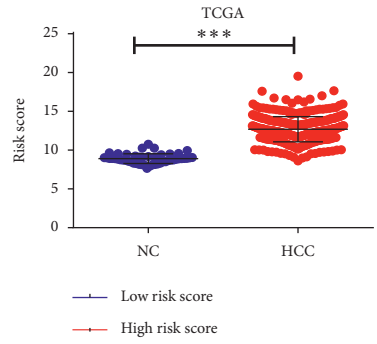

(a)

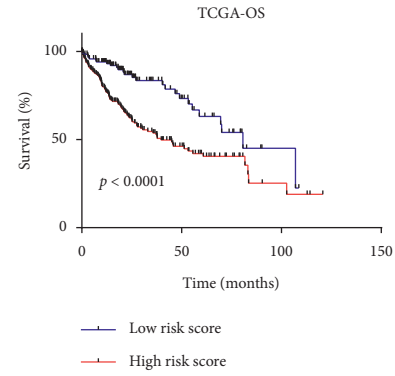

(b)

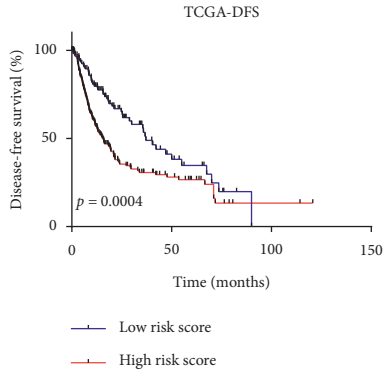

(c)

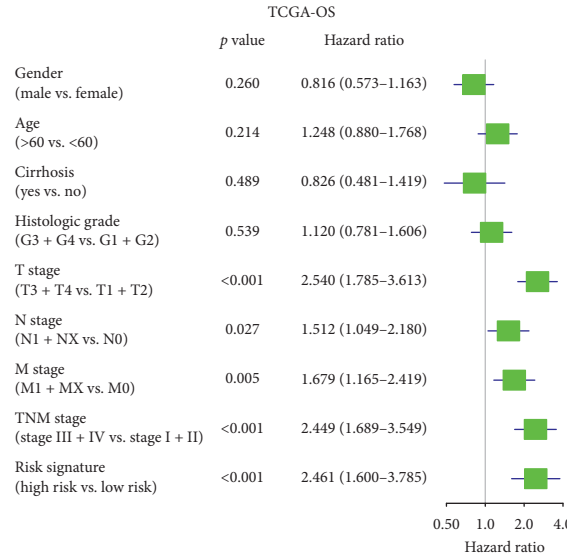

(d)

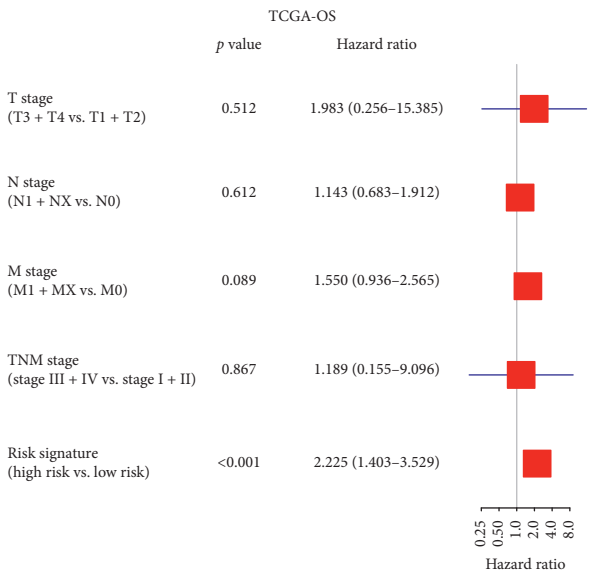

(e)

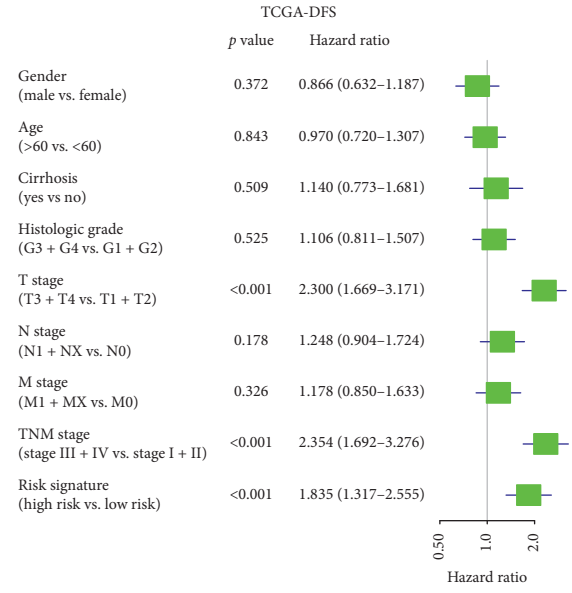

(f)

Figure 9: Continued.

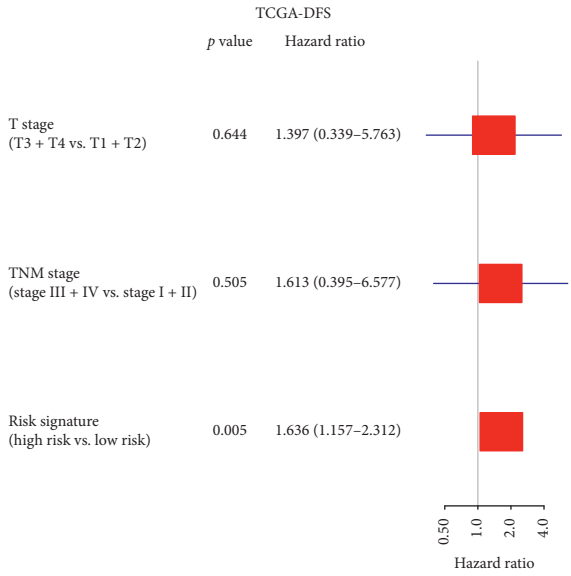

(g)

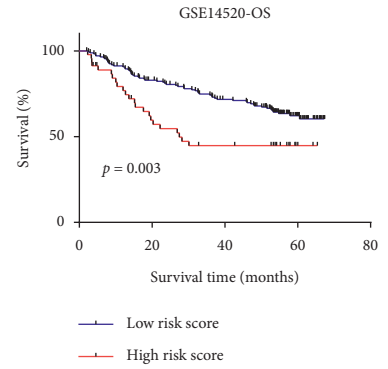

(h)

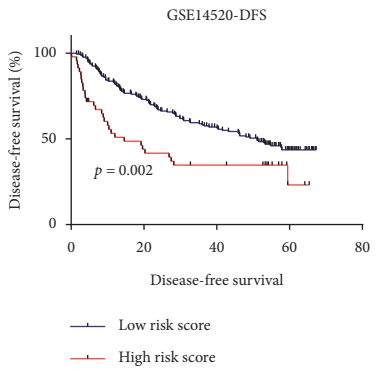

(i)

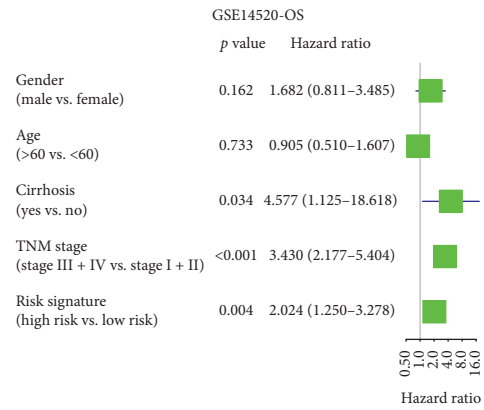

(j)

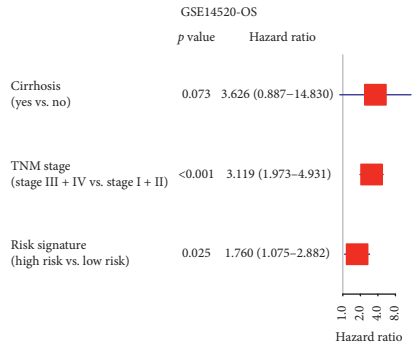

(k)

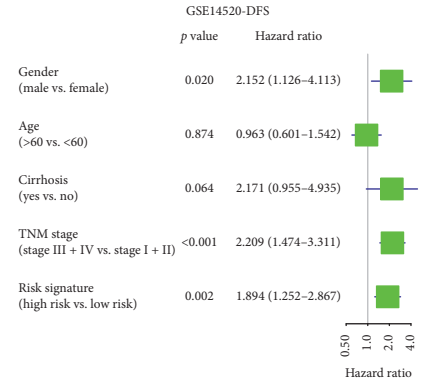

(l)

Figure 9: Continued.

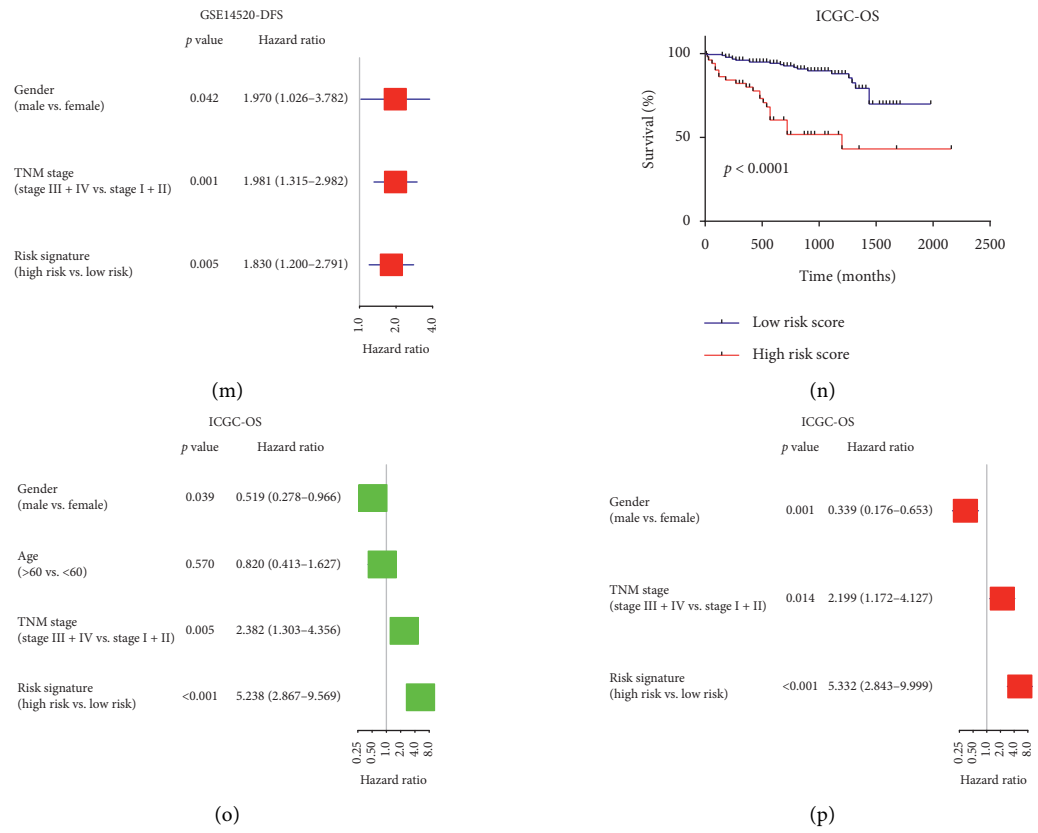

Figure 9: Prognostic value of the risk signature in HCC patients from TCGA cohort, GSE14520 cohort, and ICGC cohort. (a) Risk score between normal controls and HCC patients. (b)-(c) Kaplan–Meier analysis of OS and DFS time of patients with different risk score of TCGA cohort. (d)–(g) Univariate and multivariate analysis of risk signature for OS and DFS time of HCC patients of TCGA cohort. (h)-(i) Kaplan–Meier analysis of OS and DFS time of patients with different risk score of GSE14520 cohort. (j)–(m) Univariate and multivariate analysis of risk signature for OS and DFS time of HCC patients of GSE14520 cohort. (n) Kaplan–Meier analysis of OS time of patients with different risk score of ICGC cohort. (o)-(p) Univariate and multivariate analysis of risk signature for OS time of HCC patients of ICGC cohort.

"nucleotide-excision repair, preincision complex assembly," "glycogen biosynthetic process," "positive regulation of vascular endothelial growth factor receptor signaling pathway," "regulation of angiogenesis," "regulation of cyclin-dependent protein serine/threonine kinase activity," and KEGG pathways, such as "chemical carcinogenesis," "base excision repair," "glucagon signaling pathway," and "glycolysis/gluconeogenesis," were significantly enriched in patients with high risk scores compared to patients with low risk scores, suggesting that the aforementioned pathological pathways played an important roles of the risk signature in influencing the development of HCC. With the help of the CMap dataset, four bioactive compounds including trichostatin A, vorinostat, valproic acid, and tinidazole were identified as potential chemopreventive compounds. Among all these four bioactive compounds, trichostatin A, vorinostat, and valproic acid were histone deacetylases (HDAC) inhibitors, which had been demonstrated to exhibit antitumor efficacy via activation of classic and alternative cell death molecular cascades [20, 21]. So, these bioactive compounds may prevent cirrhosis from development of HCC by targeting the pathological pathways that are mediated by the genes used for construction of the risk signature (Supplementary Figure B). Information of these bioactive compounds is shown in Table 3.

4. Discussion

Liver cirrhosis is highly related to hepatitis B virus infection, hepatitis C virus infection, nonalcoholic fatty liver disease (NAFLD), and alcoholic fatty liver disease and is the major driver of HCC [6]. The initial manifestation of HCC patients was often a cirrhotic liver. [7, 8] Further understanding of the molecular mechanism in the transformation of liver cirrhosis to HCC, especially early HCC, would be of great help for the identification of potential new biomarkers for HCC screening in cirrhosis patients. Previously, He et al. and Jiang et al. analyzed pivotal genes and pathways involved in the transformation of liver cirrhosis to HCC. They found that Hub genes, such as CDK1, RRM2, CDKN3, and KEGG pathways, such as cell cycle and p53 signaling pathways, were the key genes and KEGG pathways for the transformation of liver cirrhosis to early HCC [14, 15]. Different from their studies, in the present study, we mainly focused on the key genes and KEGG pathways for the transformation of liver cirrhosis to early HCC, which may provide other

Table 3: Bioactive compounds identified as a potential chemopreventive treatment for the prevention of HCC development based on CMap analysis.

Drug name	Dose	Cell line	Score	Instance ID
Trichostatin A	100 nM	PC3	−0.877	4184
Vorinostat	10 μM	MCF7	−0.862	1645
Trichostatin A	100 nM	PC3	−0.856	1212
Trichostatin A	100 nM	HL60	−0.847	1561
Trichostatin A	100 nM	MCF7	−0.835	4237
Trichostatin A	100 nM	PC3	−0.826	4237
Valproic acid	1 mM	HL60	−0.821	1150
Tinidazole	16 μM	MCF7	−0.820	3430
Trichostatin A	100 nM	HL60	−0.809	1612
Trichostatin A	100 nM	PC3	−0.800	6316

valuable information in understanding the molecular mechanism for the occurrence of HCC. We found that KEGG pathways, such as cell adhesion molecules (CAMs), PI3K-Akt signaling pathway, focal adhesion, antigen processing and presentation, chemokine signaling pathway, central carbon metabolism in cancer, and choline metabolism in cancer, play a pivotal role in the development of HCC [22–26]. For example, chemokine signaling pathway plays a central role in mediating inflammation and regeneration in chronic liver diseases. Inflammatory chemokines recruited innate and adaptive immune cells and thus promoted the composition of the local disease-specific microenvironment, which was the basis for the development of HCC. Besides, regulatory T cells and myeloid-derived suppressor cells could be recruited to liver by chemokine signaling pathway to exert their immunosuppressive effects by inhibiting NK and CD8+ T cells, and thus promoting the initiation and progression of liver cancer [25]. We also found that KEGG pathways, such as T cells differentiation (including Th1, Th2, and Th17 cells), B cells receptor signaling pathway, antigen processing and presentation, central carbon metabolism in cancer, and choline metabolism in cancer were the key pathways for the transformation of early HCC from cirrhosis, indicating that changes in cell immune and nutrient metabolism may be early events on the occurrence of HCC [27–29]. Moreover, we identified 42 genes, such as SEMA4D, RBM28, and RPS3A, whose expression had become abnormal in early-stage liver cirrhosis patients before HCC development, indicating that these 42 abnormally expressed genes may play an important role in the transformation of cirrhosis to early HCC and they may be served as biomarkers for the identification of early-stage liver cirrhosis patients who were at high risk for HCC development.

Although antiviral therapies could reduce the risk of HCC development in viral hepatitis patients, once liver cirrhosis is established, no available preventive strategies could eliminate the risk of HCC development [30–33]. Considering only 12% of new HCC patients could be diagnosed through current surveillance strategy [13], we hope to explore new effective prognostic signature to identify cirrhosis patients who are at high risk for HCC development. In order to address this problem, Hoshida et al. and King et al. developed a 186-gene signature for prognosis of cirrhosis patients of GSE15654, and they found the signature was an independent predictor of HCC development, but the risk for HCC development in high-risk patients was no more than 3.5 times than that in low-risk patients [34, 35]. Recently, Moeini et al. developed a risk signature for the prediction of HCC development in cirrhosis patients of GSE15654 on the basis of identifying genes that regulate immune response which could contribute to hepatocarcinogenesis. They found that the signature was an independent predictor of HCC occurrence. There was a 2.4-times risk of HCC development for high-risk patients compared to that in low-risk patients [36]. However, the signature developed for discrimination was with fair hazard ratios smaller than 3.5, and none of the them further calculated the ROC for the prediction of HCC development. Differently, in the present study, we developed and validated an 8-gene risk signature for the prediction of HCC development for early-stage cirrhosis patients on the basis of 42 abnormally expressed genes whose expression had been altered in early cirrhosis patient before HCC development. Among all these 8 genes, only the mechanism of RPS3A in the HCC had been explored. Lim et al. found that overexpressed RPS3A could promote the stability and functional activity of HBx protein by its chaperoning activity and thus promote HBx to exert effective viral oncogenic activity and contribute to HCC development [37]. Although there were no reports about the role of the other 7 genes in HCC, future characterization of them may provide new insights into the development and progression of HCC and discovery of potential novel therapeutic targets. With the help of this signature, liver cirrhosis patients could be divided into two distinct subgroups, and the risk for HCC development in high-risk patients was 5.42 times than that in low-risk patients. Besides, the risk signature was an independent prognostic factor for HCC development in cirrhosis patients. Moreover, the AUC of risk signature for predicting 2-, 5-, and 10-year HCC development were 0.791, 0.846, and 0.766, indicating good predictive value of the risk signature in predicting HCC development. Therefore, the risk signature may exhibit great underlying clinical implications for management of cirrhosis patients. In this regard, high-risk cirrhosis patients may need more intensive surveillance and even active chemopreventive treatment to reduce the occurrence of HCC and improve prognosis, while low-risk cirrhosis patients may receive less active follow-up and even can avoid the unnecessary adjuvant therapies.

Previous researches have showed that immune system played an important role in protecting against cancer development. In short, innate immune cells, such as macrophages, dendritic cells, and NK cells, could monitor and destroy external and internal pathogens and nascent tumor cells by directly and indirectly in conjunction with adaptive immune T cells and B cells [19]. In the present study, we also found that the risk signature was associated with infiltrating immune cells of cirrhosis patients. Higher proportions of resting mast cells, neutrophils, CD8 T cells, and total T cells were found to be enriched in HCC patients with low risk score, while only activated mast cells was found to be higher

at patients with high risk score, which indicates the immune-enriched phenotype in low-risk patients and immune-depleted phenotype in high-risk patients. Moreover, further analysis found that higher CD8 T cells was associated with longer HCC development time, suggesting an important antitumorigenic role played by CD8 T cells in HCC development. It is well known that CD8 T cells could eradicate established tumors [19]. Broz et al. have found that CD103 + DC-mediated cross-presentation of tumor antigens could activate CD8 T cells to be cytotoxic CD8 T cells (CTLs), which could effectively control tumor outgrowth and mediate efficient tumor [38]. Similar to the results by Broz et al. and Garnelo et al., the degree of infiltrated T cells and B cells of tumor tissues is significantly associated with improved prognosis in HCC patients [28]. Moreover, Shalapour et al. also found that CTLs could actively prevent HCC occurrence in a mouse models of NASH-promoted HCC as unleashing CTL activity causes regression of established HCC while interference with activation of CTLs by IgA + cells promotes HCC development [39]. Therefore, the above studies may indicate that the risk signature may affect the HCC development of early-stage liver cirrhosis patients by regulation of the infiltration of CD8 T cells.

Up to date, there is still no established preventive treatment for cirrhosis patients who are at risk for HCC development [30]. Reducing the incidence and mortality of HCC patients requires not only the advances in development of curative treatment for early lesions, but also identifying cirrhosis patients who are at high risk for HCC development and development of chemopreventive. In this scenario, we developed and validated a risk signature for prediction of HCC development of cirrhosis patients. Besides, we also found that "negative regulation of apoptotic process," "glycogen biosynthetic process," "regulation of angiogenesis," "regulation of cyclin-dependent protein serine/threonine kinase activity," "glucagon signaling pathway," and "glycolysis/gluconeogenesis" were found to be significantly enriched in patients with high risk scores, indicating that the aforementioned pathological pathways played an important role of the risk signature in influencing the development of HCC. On the basis of the risk signature, we also identified that trichostatin A, vorinostat, and valproic acid may be the promising potential bioactive compounds as novel chemopreventive treatment for the prevention of HCC development by targeting the genes used for construction of the risk signature. These bioactive compounds are all HDAC inhibitors and exhibit preclinical antitumor efficacy. HDAC inhibitors can affect various pathways and lead to transformed cell death. They can induce DNA damage and repair, modify gene expression, cause cell growth arrest, induce apoptosis, and act as antiangiogenic and antimetastatic factors [20, 21], and cell cycle (regulation of cyclin-dependent protein serine/threonine kinase activity), reduced apoptosis (negative regulation of apoptotic process), and angiogenesis (regulation of angiogenesis) were found to be significantly enriched in patients with high risk scores (Supplementary Figure A). For example, Zhou et al. have found that vorinostat can lead to HCC cell morphology changes, growth inhibition, cell cycle blockage, and apoptosis in vitro and suppressed the growth of subcutaneous HCC xenograft tumours in vivo via upregulation of $p21^{Waf1/Cip1}$ and $p19^{INK4d}$ [40]. Freeze et al. have shown that trichostatin A and valproic acid could not only inhibit the proliferation, clonogenicity, and migration of HCC cells, but also enhance the efficacy of sorafenib in killing sorafenib-susceptible cells and reestablished sorafenib sensitivity in resistant HCC cells [41]. It is proved that alterations in homeostasis of glucose play an important role in the development of tumors, loss of fructose-1, 6-bisphosphatase (FBP1), a rate-limiting enzyme in gluconeogenesis, was found to be oncogenic in various cancer cells including HCC and colon cancer cells [42], suggesting that modulation of gluconeogenesis also plays an equal role in tumorigenesis. Consistent with this, we also found "glycolysis/gluconeogenesis" to be significantly enriched in patients with high risk scores. Yang et al. have found that inhibition of histone deacetylases by HDAC inhibitors suppresses glucose metabolism and hepatocellular carcinoma growth by restoring FBP1 expression [43]. Taken together, HDAC inhibitors, such as trichostatin A, vorinostat, and valproic acid, may be exploited to be potential chemopreventive treatment for prevention of HCC development for cirrhosis patients. However, future clinical studies are still needed for further confirmation.

Compared with previous studies, our study has several strengths. First, the risk signature was developed on the basis of 42 DEGs identified between liver cirrhosis patients and early HCC patients. The expression of those genes had been altered in early-stage liver cirrhosis patients before HCC development, so the signature could effectively discriminate cirrhosis patients who were at high risk for HCC development from cirrhosis patients who were at low risk for HCC development with hazard ratios more than 5.0. It also showed good predictive value in predicting HCC development. Second, the prognostic and predictive value of the risk signature were validated in an internal cohort. Finally, the risk signature could also effectively stratify HCC patients into high-risk patients with shorter OS and DFS time and low-risk patients with longer OS and DFS time and it was an independent prognostic factor for OS and DFS time in HCC patients from three different HCC cohorts.

Although the risk signature exhibited good performance for the prediction of HCC development in cirrhosis patients, some limitations should be addressed. First, some basic parameters of the cirrhosis patients from GSE15654, such as age, gender, especially AFP level were missing, so we could not further perform a comparative analysis of predictive value between the risk signature and AFP. Second, limited information was provided to explore the relation between the risk signature and regulation of CD8 T cells. Third, we did not validate the prognostic value of the risk signature in an external cohort, especially in prospective cohorts with larger sample sizes. Finally, we also did not validate chemopreventive efficacy of trichostatin A, vorinostat, and valproic acid for prevention of HCC development in vivo and in vitro experiment.

In conclusion, we developed and validated an 8-gene risk signature for prediction of HCC development, which showed good performance in the discrimination ability and

predictive ability for cirrhosis patients. The risk signature may be a useful tool to set up more individualized follow-up interval schedules and HDAC inhibitors, such as trichostatin A, vorinostat, and valproic acid, may be exploited to be a potential chemopreventive treatment for the prevention of HCC development for cirrhosis patients.

Abbreviations

HCC: Hepatocellular carcinoma
DEGs: Differentially expressed genes
TCGA: The Cancer Genome Atlas
GEO: Gene expression omnibus
ICGC: International Cancer Genome Consortium
OS: Overall survival
DFS: Disease-free status
AUC: Areas under ROC curve
HDAC: Histone deacetylases
NAFLD: Nonalcoholic fatty liver disease
CTLs: Cytotoxic CD8 T cells
FBP1: Fructose-1,6-bisphosphatase.

Data Availability

The data of this study are available from the corresponding web page link, including GDC data portal (https://cancergenome.nih.gov/), ICGC portal (https://dcc.icgc.org/projects/LIRI-JP), and GEO database (https://www.ncbi.nlm.nih.gov/geo/).

Conflicts of Interest

The authors declare that they have no conflicts of interest.

Authors' Contributions

GN and L-YQ performed most of the data analysis and wrote the manuscript. C-WJ assisted in the data collection and analysis of the study. T-WJ assisted in data collection and analysis. S-DW was involved in writing the manuscript. L-QL assisted in the revision of the manuscript. Z-YJ and C-HT designed the study and obtained funding to support this research. GN and YL contributed equally to this work.

Acknowledgments

The study was supported by National Natural Science Foundation of China (81970507), Natural Science Foundation of Guangdong Province (2020A1515010100), Technology Planning Project of Guangzhou City (201904010132 and 202102010023), Guangzhou High Technology Project (2019GX05), and Guangdong Medical Science and Research Foundation (A2020411).

Supplementary Materials

Supplementary Figure A. The underlying pathological pathways by which the signature used to influence the development of HCC for early-stage liver cirrhosis patients. *Supplementary Figure B*. Schematic depicting the pathological pathways mediated by signature and inhibited by suggested bioactive compounds (HDAC inhibitors). *Supplementary Material 1*. DEGs between early HCC patients and cirrhosis patients identified by overlapping GSE63898 and GSE89377 datasets. *Supplementary Material 2*. DEGs identified by overlapping GSE63898, GSE89377, and GSE15654 datasets. *Supplementary Material 3*. HCC development related genes identified by univariate analysis in the patients of the training cohort. (*Supplementary Materials*)

References

[1] F. Bray, J. Ferlay, I. Soerjomataram, R. L. Siegel, L. A. Torre, and A. Jemal, "Global cancer statistics 2018: GLOBOCAN estimates of incidence and mortality worldwide for 36 cancers in 185 countries," *CA: A Cancer Journal for Clinicians*, vol. 68, no. 6, pp. 394–424, 2018.

[2] L. A. Torre, F. Bray, R. L. Siegel, J. Ferlay, J. Lortet-Tieulent, and A. Jemal, "Global cancer statistics," *CA: A Cancer Journal for Clinicians*, vol. 65, no. 2, pp. 87–108, 2012.

[3] T. Uehara, G. R. Ainslie, K. Kutanzi et al., "Molecular mechanisms of fibrosis-associated promotion of liver carcinogenesis," *Toxicological Sciences*, vol. 132, no. 1, pp. 53–63, 2013.

[4] P. Tabrizian, G. Jibara, B. Shrager, M. Schwartz, and S. Roayaie, "Recurrence of hepatocellular cancer after resection," *Annals of Surgery*, vol. 261, no. 5, pp. 947–955, 2015.

[5] S. F. Altekruse, J. S. Henley, J. E. Cucinelli, and K. A. McGlynn, "Changing hepatocellular carcinoma incidence and liver cancer mortality rates in the United States," *American Journal of Gastroenterology*, vol. 109, no. 4, pp. 542–553, 2014.

[6] R. Bataller and D. A. Brenner, "Liver fibrosis," *Journal of Clinical Investigation*, vol. 115, no. 2, pp. 209–218, 2005.

[7] L. A. Beste, S. L. Leipertz, P. K. Green, J. A. Dominitz, D. Ross, and G. N. Ioannou, "Trends in burden of cirrhosis and hepatocellular carcinoma by underlying liver disease in US veterans, 2001-2013," *Gastroenterology*, vol. 149, no. 6, pp. 1471–1482, 2015.

[8] M. Walker, H. B. El-Serag, Y. Sada et al., "Cirrhosis is underrecognised in patients subsequently diagnosed with hepatocellular cancer," *Alimentary Pharmacology and Therapeutics*, vol. 43, no. 5, pp. 621–630, 2016.

[9] G. Fattovich, F. Bortolotti, and F. Donato, "Natural history of chronic hepatitis B: special emphasis on disease progression and prognostic factors," *Journal of Hepatology*, vol. 48, no. 2, pp. 335–352, 2008.

[10] C.-M. Chu and Y.-F. Liaw, "Hepatitis B virus-related cirrhosis: natural history and treatment," *Seminars in Liver Disease*, vol. 26, no. 2, pp. 142–152, 2006.

[11] J. Bruix and M. Sherman, "Management of hepatocellular carcinoma: an update," *Hepatology*, vol. 53, no. 3, pp. 1020–1022, 2011.

[12] European Association for the Study of the Liver; European Organisation for Research and Treatment of Cancer, "EASL-EORTC clinical practice guidelines: management of hepatocellular carcinoma," *Journal of Hepatology*, vol. 56, no. 4, pp. 908–943, 2012.

[13] J. A. Davila, L. Henderson, J. R. Kramer et al., "Utilization of surveillance for hepatocellular carcinoma among hepatitis C virus-infected veterans in the United States," *Annals of Internal Medicine*, vol. 154, no. 2, pp. 85–93, 2011.

[14] B. He, J. Yin, S. Gong et al., "Bioinformatics analysis of key genes and pathways for hepatocellular carcinoma transformed from cirrhosis," *Medicine*, vol. 96, no. 25, Article ID e6938, 2017.

[15] C. H. Jiang, X. Yuan, J. F. Li et al., "Bioinformatics-based screening of key genes for transformation of liver cirrhosis to hepatocellular carcinoma," *Journal of Translational Medicine*, vol. 18, no. 1, p. 40, 2020.

[16] A. M. Newman, C. L. Liu, M. R. Green et al., "Robust enumeration of cell subsets from tissue expression profiles," *Nature Methods*, vol. 12, no. 5, pp. 453–457, 2015.

[17] A. Musa, L. S. Ghoraie, S.-D. Zhang et al., "A review of connectivity map and computational approaches in pharmacogenomics," *Briefings in Bioinformatics*, vol. 18, no. 5, p. 903, 2017.

[18] D. H. Parks, G. W. Tyson, P. Hugenholtz, and R. G. Beiko, "STAMP: statistical analysis of taxonomic and functional profiles," *Bioinformatics*, vol. 30, no. 21, pp. 3123-3124, 2014.

[19] A. Corthay, "Does the immune system naturally protect against cancer?" *Frontiers in Immunology*, vol. 5, p. 197, 2014.

[20] D. I. Tsilimigras, I. Ntanasis-Stathopoulos, D. Moris, E. Spartalis, and T. M. Pawlik, "Histone deacetylase inhibitors in hepatocellular carcinoma: a therapeutic perspective," *Surgical Oncology*, vol. 27, no. 4, pp. 611–618, 2018.

[21] A. Garmpi, N. Garmpis, C. Damaskos et al., "Histone deacetylase inhibitors as a new anticancer option: how far can we go with expectations? delivery systems," *Journal of BUON: Official Journal of the Balkan Union of Oncology*, vol. 23, no. 4, pp. 846–861, 2018.

[22] Y. Wu, X. Qiao, S. Qiao, and L. Yu, "Targeting integrins in hepatocellular carcinoma," *Expert Opinion on Therapeutic Targets*, vol. 15, no. 4, pp. 421–437, 2011.

[23] J. Torresi, B. M. Tran, D. Christiansen, L. Earnest-Silveira, R. H. M. Schwab, and E. Vincan, "HBV-related hepatocarcinogenesis: the role of signalling pathways and innovative ex vivo research models," *BMC Cancer*, vol. 19, no. 1, p. 707, 2019.

[24] N. Panera, A. Crudele, I. Romito, D. Gnani, and A. Alisi, "Focal adhesion kinase: insight into molecular roles and functions in hepatocellular carcinoma," *International Journal of Molecular Sciences*, vol. 18, no. 1, 2017.

[25] J. Ehling and F. Tacke, "Role of chemokine pathways in hepatobiliary cancer," *Cancer Letters*, vol. 379, no. 2, pp. 173–183, 2016.

[26] Z. Chen, J. Chen, X. Huang et al., "Identification of potential key genes for hepatitis B virus-associated hepatocellular carcinoma by bioinformatics analysis," *Journal of Computational Biology*, vol. 26, no. 5, pp. 485–494, 2019.

[27] A. L. Gomes, A. Teijeiro, S. Burén et al., "Metabolic inflammation-associated IL-17a causes non-alcoholic steatohepatitis and hepatocellular carcinoma," *Cancer Cell*, vol. 30, no. 1, pp. 161–175, 2016.

[28] M. Garnelo, A. Tan, Z. Her et al., "Interaction between tumour-infiltrating B cells and T cells controls the progression of hepatocellular carcinoma," *Gut*, vol. 66, no. 2, pp. 342–351, 2017.

[29] K. Wang, X. Nie, Z. Rong et al., "B lymphocytes repress hepatic tumorigenesis but not development in Hras12V transgenic mice," *International Journal of Cancer*, vol. 141, no. 6, pp. 1201–1214, 2017.

[30] N. Fujiwara, S. L. Friedman, N. Goossens, and Y. Hoshida, "Risk factors and prevention of hepatocellular carcinoma in the era of precision medicine," *Journal of Hepatology*, vol. 68, no. 3, pp. 526–549, 2018.

[31] EASL Clinical Practice Guidelines, "Management of hepatocellular carcinoma," *Journal of Hepatology*, vol. 69, no. 1, pp. 182–236, 2018.

[32] V. Calvaruso, G. Cabibbo, I. Cacciola et al., "Incidence of hepatocellular carcinoma in patients with HCV-associated cirrhosis treated with direct-acting antiviral agents," *Gastroenterology*, vol. 155, no. 2, pp. 411–421, 2018.

[33] F. Kanwal, J. Kramer, S. M. Asch, M. Chayanupatkul, Y. Cao, and H. B. El-Serag, "Risk of hepatocellular cancer in HCV patients treated with direct-acting antiviral agents," *Gastroenterology*, vol. 153, no. 4, pp. 996–1005, 2017.

[34] Y. Hoshida, A. Villanueva, A. Sangiovanni et al., "Prognostic gene expression signature for patients with hepatitis C-related early-stage cirrhosis," *Gastroenterology*, vol. 144, no. 5, pp. 1024–1030, 2013.

[35] L. Y. King, C. Canasto-Chibuque, K. B. Johnson et al., "A genomic and clinical prognostic index for hepatitis C-related early-stage cirrhosis that predicts clinical deterioration," *Gut*, vol. 64, no. 8, pp. 1296–1302, 2015.

[36] A. Moeini, S. Torrecilla, V. Tovar et al., "An immune gene expression signature associated with development of human hepatocellular carcinoma identifies mice that respond to chemopreventive agents," *Gastroenterology*, vol. 157, no. 5, pp. 1383–1397, 2019.

[37] K.-H. Lim, K.-H. Kim, S. I. Choi et al., "RPS3a over-expressed in HBV-associated hepatocellular carcinoma enhances the HBx-induced NF-κB signaling via its novel chaperoning function," *PLoS One*, vol. 6, no. 8, Article ID e22258, 2011.

[38] M. L. Broz, M. Binnewies, B. Boldajipour et al., "Dissecting the tumor myeloid compartment reveals rare activating antigen-presenting cells critical for T cell immunity," *Cancer Cell*, vol. 26, no. 5, pp. 638–652, 2014.

[39] S. Shalapour, X.-J. Lin, I. N. Bastian et al., "Inflammation-induced IgA+ cells dismantle anti-liver cancer immunity," *Nature*, vol. 551, no. 7680, pp. 340–345, 2017.

[40] H. Zhou, Y. Cai, D. Liu et al., "Pharmacological or transcriptional inhibition of both HDAC1 and 2 leads to cell cycle blockage and apoptosis via p21Waf1/Cip1 and p19INK4d upregulation in hepatocellular carcinoma," *Cell Proliferation*, vol. 51, no. 3, Article ID e12447, 2018.

[41] K. Freese, T. Seitz, P. Dietrich et al., "Histone deacetylase expressions in hepatocellular carcinoma and functional effects of histone deacetylase inhibitors on liver cancer cells in vitro," *Cancers*, vol. 11, no. 10, Article ID 11101587, 2019.

[42] M. Chen, J. Zhang, N. Li et al., "Promoter hypermethylation mediated downregulation of FBP1 in human hepatocellular carcinoma and colon cancer," *PLoS One*, vol. 6, no. 10, Article ID e25564, 2011.

[43] J. Yang, X. Jin, Y. Yan et al., "Inhibiting histone deacetylases suppresses glucose metabolism and hepatocellular carcinoma growth by restoring FBP1 expression," *Scientific Reports*, vol. 7, no. 1, Article ID 43864, 2017.

Hindawi
Journal of Oncology
Volume 2021, Article ID 2790958, 5 pages
https://doi.org/10.1155/2021/2790958

Research Article

The Auxiliary Diagnosis and Imaging Characteristics of MRI Combined with CT in Patients with Cholangiocarcinoma

Jing Li,[1] **Yuanlin Yu**,[1] **and Qing He**[2]

[1]*Department of Radiology, The First Affiliated Hospital of Fujian Medical University, Fuzhou, Fujian Province, China*
[2]*Department of Radiotherapy, The First Affiliated Hospital of Fujian Medical University, Fuzhou, Fujian Province, China*

Correspondence should be addressed to Qing He; xr212229@163.com

Received 18 June 2021; Revised 5 July 2021; Accepted 11 July 2021; Published 20 July 2021

Academic Editor: Muhammad Wasim Khan

Background. Patients with cholangiocarcinoma (CCA) have poor prognosis and high mortality. Therefore, early detection and early diagnosis are extremely important to control the development of CCA. This study aims to explore the diagnostic effect in patients with CCA and imaging characteristics of MRI combined with CT. *Methods*. 109 patients with suspected CCA underwent CT and MRI before diagnosis. The examination results were compared with the "gold standard." ROC curve was drawn to analyze the diagnostic efficacy of MRI combined with CT for CCA patients. *Results*. The diagnosis rate of suspected CCA patients was 95.41%. The diagnostic coincidence rate of CT and MRI examination was 89.42% and 92.31%, respectively. The diagnostic coincidence rate of MRI combined with CT examination was 100.00%. The number of CT delayed enhancement, peripheral bile duct dilatation, and hepatic capsular depression were more than those of MRI. The number of circular enhancement cases in the CT group was less than that in the MRI group. ROC curve results showed that the sensitivity and specificity of MRI combined with CT for the diagnosis of CCA patients were higher than those of MRI or CT alone. *Conclusion*. MRI combined with CT has high diagnostic sensitivity and specificity and can provide imaging evidence for the clinical diagnosis and treatment of CCA.

1. Introduction

Cholangiocarcinoma (CCA) is a primary liver cancer that occurs in the bile ducts of the liver. The prognosis of CCA patients is poor and the mortality rate is high. Most patients cannot be cured, and a small number of patients with early CCA can be clinically cured. CCA lacks typical clinical symptoms in the early stage of onset. In the advanced stage of CCA, symptoms such as upper abdominal discomfort and hepatomegaly may appear [1]. Therefore, the clinical diagnosis and treatment of CAA is more difficult.

Previous studies have shown that CCA is a tumor that occurs from the confluence of the left and right hepatic ducts (hilar) to peripheral bile duct epithelial cells [2]. Histopathological examination is a commonly used diagnostic method for CCA patients and is regarded as the "gold standard." However, this method has poor reproducibility and requires the professional skills of doctors. It is easy to result in poor diagnosis compliance and tolerability in CCA patients [3, 4]. Therefore, simple and effective diagnostic methods are of great significance to patients with CCA.

CT is a commonly used imaging method, which has a good effect on the display of microcalcification in the lesion. MRI is more sensitive to intratumoral hemorrhage [5]. It has been shown that MRI combined with CT can give full play to the advantages of different imaging methods in the diagnosis and identification of malignant tumors [6]. At the same time, MRI combined with CT detection can evaluate the severity of the patient's disease according to different imaging features [7]. Therefore, this study aims to explore the auxiliary diagnosis in CCA patients and imaging characteristics of MRI combined with CT.

2. Materials and Methods

2.1. Patients. This is a retrospective study. 109 suspected CCA patients in the First Affiliated Hospital of Fujian Medical University were selected from February 2017 and

December 2020. They are between 31 and 79 years old, with an average age of 59.39 ± 5.65 years old. The diameter of the tumor is between 23 and 135 mm, with an average diameter of 64.29 ± 6.61 mm. The clinicopathological factors of these patients are shown in Table 1. The study was approved by the Ethics Committee of the First Affiliated Hospital of Fujian Medical University. And the informed consent forms of these patients were obtained.

2.2. Inclusion and Exclusion Criteria. Inclusion criteria include the following: (1) patients are diagnosed by pathological examination and in line with CCA diagnostic criteria [8]. (2) Patients can tolerate and meet CT, MRI plain scan, or enhanced indications. (3) Patients have complete baseline and follow-up data.

Exclusion criteria include the following: (1) patients with mental disorders, cognitive dysfunction, or other malignant tumors; (2) patients receiving radiotherapy, chemotherapy, and biological immunotherapy before the examination; (3) patients with autoimmune system diseases and abnormal blood coagulation function.

2.3. Treatment Method. All patients were diagnosed by histopathological examination (gold standard). Before the diagnosis, all patients underwent CT and MRI examinations.

2.4. CT Examination. The Lightspeed VCT scanner is used to examine patients. Before the examination, the pathogenesis, clinical manifestations, and examination methods of CCA were explained to patients and their families to improve the cooperation of the patients. Patients were instructed to perform routine fasting examinations and routinely take 800–1000 mL of negative contrast agent before the examination. During the examination, the patient was placed in a supine position. And the relevant parameter settings were completed according to the patient's condition. Finally, the unscanned and enhanced 5 mm layer thickness image was reconstructed as a 0.625 mm image. And the coronal and sagittal image reconstruction was completed [9, 10].

2.5. MRI Examination. After completing the CT examination, MRI examination is performed according to the patient's wishes. The instrument is a 3.0 T Inegenia superconducting magnetic resonance scanner (Philips, Netherlands) using a 32-channel volume phased array coil. It takes about 18–23 s to complete the liver scan and imaging. Relevant parameters were set according to the patient's condition. The obtained images are transferred to the processing software. The examination results are compared with the "gold standard." Finally, the diagnostic coincidence rate of different imaging examinations is analyzed. And the imaging characteristics of CT and MRI are recorded [11, 12].

2.6. Statistical Analysis. SPSS24.0 software was used to analyze the data. The difference between the two groups was analyzed by the χ^2 text. The ROC curve was used to analyze the diagnostic efficacy (sensitivity and specificity) of MRI combined with CT in CCA patients. $P < 0.05$ indicates that the difference is statistically significant.

3. Results

3.1. Comparison of the Diagnostic Coincidence Rate of MRI and CT in Patients with CCA. Among the 109 suspected CCA patients, 104 patients were confirmed by histopathological examination. And the diagnosis rate was 95.41%. CT examination confirmed 93 cases, and the diagnosis coincidence rate was 89.42% ($P < 0.05$, Figure 1). 96 cases were confirmed by MRI examination. The coincidence rate of MRI diagnosis was 92.31% ($P < 0.05$, Figure 1). 104 cases were diagnosed by MRI combined with CT examination, and the diagnosis coincidence rate was 100.00% ($P > 0.05$, Figure 1).

3.2. Comparison of Imaging Characteristics between MRI and CT in Patients with CCA. The CT group and the MRI group had no significant difference in enhancement, "fast-in and fast-out" enhancement, smooth enhancement ring, flatness, hepatic lobe atrophy, DWI high signal, and abnormal perfusion ($P > 0.05$, Table 2). The number of delayed enhancement, peripheral bile duct dilation, and hepatic capsule depression in the CT group were more than those of MRI ($P < 0.05$, Table 2). The number of uneven enhancement cases in the circular-enhanced CT group was less than that of the MRI group ($P < 0.05$, Table 2).

3.3. Diagnostic Efficacy of MRI Combined with CT in Patients with CCA. ROC curve results showed that the sensitivity and specificity of MRI combined with CT for CCA patients were higher than those of MRI and CT alone ($P < 0.05$, Table 3, Figure 2).

4. Discussion

CCA is a malignant tumor with high clinical incidence. At present, it is generally believed that the incidence of CCA is related to intrahepatic bile duct stones, long-term chronic inflammation, or related physical and chemical stimulation [13, 14]. Even worse, the clinical diagnosis and treatment of CCA is difficult because of the lack of typical clinical symptoms in the early stage of CCA. Therefore, most patients are already in the middle and advanced stages at the time of diagnosis. Now, histopathological examination is still the "gold standard" for the diagnosis of patients with CCA. Although pathological examination is helpful for diagnosis, diagnostic compliance and tolerance are poor [15, 16]. Therefore, it is very important to explore new diagnostic methods of CCA in clinical practice.

In recent years, MRI combined with CT has been used in patients with CCA. Moreover, the diagnostic accuracy of MRI combined with CT is satisfactory [17]. In this study, 104 of 109 suspected CCA patients were confirmed by histopathological examination. The diagnosis rate of histopathological examination was 95.41%. In addition, the diagnosis

Table 1: Clinicopathological information of 109 patients with cholangiocarcinoma.

Features	Gender		Symptom				Examination		
	Male	Female	Abdominal pain	Jaundice	Fever	Fatigue	CT	MRI	CT + MRI
Cases	65	44	32	16	19	29	57	29	23

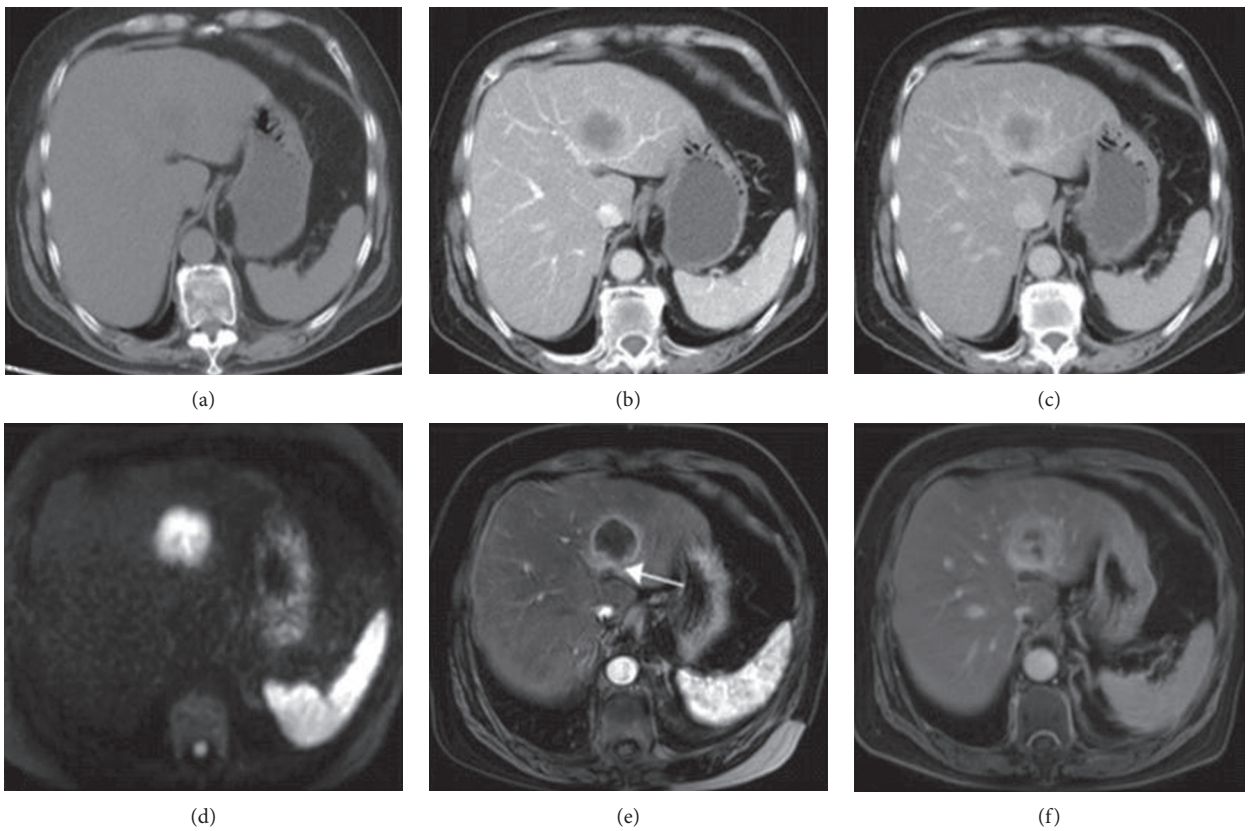

Figure 1: Typical pathological MRI and CT images. In 63 patients with CCA, the lesion was located in the left lobe of the liver. And all patients underwent MRI and CT examinations. (a) CT picture of a typical case, (b) a circular enhancement at the edge of the lesion in the arterial phase, (c) an enhanced inward filling in the equilibrium phase, and (d) DWI picture of the MRI shows high signal intensity. (e) A circular enhancement shows at the edge of the tumor, but the strengthening ring is incomplete. (f) The inward filling of the mass in the equilibrium phase.

Table 2: Comparison of imaging characteristics between MRI and CT in patients with CCA (n (%)).

	Characteristics	CT ($n = 57$)	MRI ($n = 29$)	χ^2	P
Enhanced features	Annular strengthening uneven strengthening	41 (71.93)	28 (96.55)	6.351	0.035*
	Delayed reinforcement	14 (24.56)	3 (10.34)	9.672	0.021*
	No obvious enhancement	2 (3.51)	0 (0.00)	1.491	0.958
	"Fast-in and fast-out" enhancement	2 (3.51)	0 (0.00)	1.491	0.958
	Smooth and flat strengthening ring	0 (0.00)	0 (0.00)	0.000	1.000
	DWI high signal	57 (100.00)	29 (100.00)	0.000	1.000
Arterial passage lesions	Peripheral bile duct dilation	29 (50.88)	16 (55.17)	6.094	0.020*
	Depressed liver capsule sign	42 (73.68)	11 (37.93)	7.103	0.013*
	Hepatic lobe atrophy	9 (15.79)	5 (17.24)	1.593	0.615
	Abnormal perfusion	18 (31.58)	10 (34.48)	0.834	0.058

* $P < 0.05$.

coincidence rate of CT and MRI examination was 89.42% and 92.31%, respectively. More importantly, the diagnosis coincidence rate of CT combined with MRI reached 100.00% in this study. These results indicate that the diagnostic accuracy of MRI combined with CT is very high. Qi et al. [18] also reported that MRI combined with CT can achieve a

Table 3: Diagnostic efficacy of MRI combined with CT in patients with CCA.

Variable	AUC	SD	P	95% confidence interval		Sensitivity	Specificity
				Lower limit	Upper limit		
CT	0.746	0.061	$P \leq 0.001$	0.713	0.858	0.794	0.671
MRI	0.812	0.074	$P \leq 0.001$	0.794	0.871	0.841	0.657
CT + MRI	0.894	0.083	$P \leq 0.001$	0.845	0.932	0.931	0.612

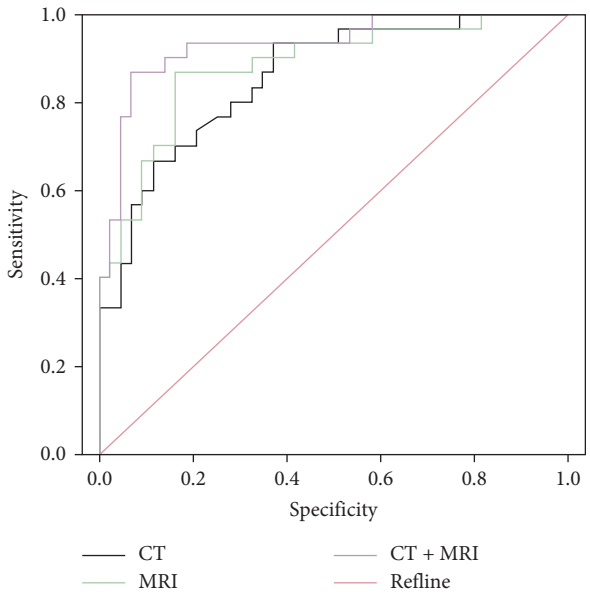

Figure 2: The diagnostic ROC curve of MRI combined with CT in patients with CCA.

higher detection rate in patients with CCA. Briefly, MRI combined with CT examination is helpful to the early diagnosis of CCA patients and can guide the clinical diagnosis and treatment.

It is well-known that fibrous tissue, mucin, coagulative necrosis, and malignant tumor tissue cells are the main components of the mass. And according to the area, tissue type, and distribution characteristics of the tumor, there are obvious differences between different components [19]. It has been found that the imaging manifestations of CCA mainly depend on the pathological type, the distribution of fibrous tissue, and tumor cells [20]. The tumor cells are distributed around the tumor, and the proliferating fibrous tissue is located in the center of the tumor. The contrast agent diffuses slowly in the fibrous tissue and can obtain clear images [21].

In this study, the CT group had more cases of delayed enhancement, peripheral bile duct dilation, and hepatic capsule depression than MRI. The number of uneven enhancement cases in the CT group was less than that of MRI. The above results indicate that MRI and CT have typical imaging characteristics in patients with CCA. The diagnosis of different lesions can be confirmed through imaging features. In order to further analyze the diagnostic value of MRI and CT in patients with CCA, ROC curves were drawn in this study. The results showed that the diagnostic sensitivity and specificity of MRI combined with CT in patients with CCA were higher than those of single MRI and CT. Therefore, MRI combined with CT examinations should be strengthened for patients with suspected CCA. However, the number of samples in our study is a little small. We will continue to collect data in the follow-up to better confirm our conclusions.

5. Conclusion

In conclusion, MRI combined with CT can achieve a high diagnostic coincidence rate in patients with CCA and has typical imaging features. Moreover, the sensitivity and specificity of the combined examination are high. Therefore, MRI combined with CT can provide imaging basis for the clinical diagnosis and treatment of CCA.

Data Availability

The datasets used and/or analyzed during the present study are available from the corresponding author on reasonable request.

Conflicts of Interest

The authors declare that they have no conflicts of interest.

References

[1] P. X. Huang, Q. L. Song, S. J. Di et al., "The diagnostic value of endoscopic balloon dilatation combined with biliary cytology in cholangiocarcinoma," *Chinese Journal of Hepatobiliary Surgery*, vol. 27, no. 3, pp. 202–205, 2021.

[2] Z. F. Wang, F. E. Hao, L. Zhu et al., "CT and MRI imaging features of pancreatic acinar cell carcinoma," *Chinese Journal of Digestive Surgery*, vol. 19, no. 5, pp. 552–558, 2020.

[3] Y.-H. Yang, Q. Deng, T.-B. Yang et al., "A case report of cholangiocarcinoma combined with moderately differentiated gastric adenocarcinoma," *Medicine*, vol. 98, no. 30, Article ID e16332, 2019.

[4] Y. Zhou, D. Li, L. Long et al., "Analysis of enhanced mode of mixed liver cancer and the diagnostic value of contrast-enhanced ultrasound combined with enhanced CT/MRI and tumor markers," *Chinese Journal of Ultrasound Imaging*, vol. 29, no. 9, pp. 754–760, 2020.

[5] Z. P. Qi, J. L. Li, X. L. Zhang et al., "The diagnostic value of serum tumor markers combined with multi-slice spiral CT and MRI in the diagnosis of cholangiocarcinoma and its relationship with tissue invasion molecules," *Advances in Modern Biomedicine*, vol. 19, no. 20, pp. 161–164, 2019.

[6] D. T. Jing and D. Li, "The diagnostic efficacy and imaging characteristics of CT combined with MRI in primary central nervous system lymphoma," *Guizhou Medicine*, vol. 43, no. 9, pp. 1469–1471, 2019.

[7] H. Y. Heng, X. Ding, G. Q. Chen et al., "Analysis of CT and MRI imaging features of massive intrahepatic cholangiocarcinoma," *Chongqing Medicine*, vol. 49, no. 8, pp. 118–121, 2020.

[8] Biliary Surgery Group of the Chinese Medical Association Surgery Branch, PLA Committee of Hepatobiliary Surgery of the PLA, "Guidelines for the diagnosis and treatment of hilar cholangiocarcinoma (2013 edition)," *Chinese Journal of Surgery*, no. 10, pp. 865–871, 2013.

[9] Y. C. Fang, Q. Wang, Q. Tang et al., "Analysis of the diagnostic value of MSCT and MRI dynamic enhancement scan for high blood supply intrahepatic cholangiocarcinoma and hepatocellular carcinoma," *Journal of Practical Hepatology*, vol. 23, no. 6, pp. 131–134, 2020.

[10] S. H. Yang, Z. J. Liao, S. Hu et al., "Expression and significance of eukaryotic translation initiation factor-5A2 in intrahepatic cholangiocarcinoma," *Journal of Kunming Medical University*, vol. 42, no. 5, pp. 24–28, 2021.

[11] D. Xiao, T. Han, C. Zhai et al., "The value of MRI combined with MSCT in the diagnosis of preoperative T and N staging of colorectal cancer," *Chinese Journal of CT and MRI*, vol. 18, no. 10, pp. 139–141, 2020.

[12] A. J. Donato, D. R. Machin, and L. A. Lesniewski, "Mechanisms of dysfunction in the aging vasculature and role in age-related disease," *Circulation Research*, vol. 123, no. 7, pp. 825–848, 2018.

[13] H. Li, S. He, K. Fan et al., "Relationship between the onset date of the Meiyu and the South Asian anticyclone in April and the related mechanisms," *Climate Dynamics*, vol. 52, no. 1-2, pp. 209–226, 2019.

[14] T. Song, J. Y. Liu, and J. P. Lu, "Computed tomography and magnetic resonance imaging features analysis of pancreatic acinar cell carcinoma," *Journal of Second Military Medical University*, vol. 40, no. 3, pp. 110–114, 2019.

[15] I. Roy and R. H. Kripalani, "The role of natural factors (part 1): addressing on mechanism of different types of ENSO, related teleconnections and solar influence," *Theoret Applied Climatol*, vol. 137, no. 1-2, pp. 469–480, 2019.

[16] Y. P. Zeng, J. D. Luo, X. M. Leng et al., "CT and MRI differential diagnosis of hepatocellular carcinoma with cholangiocarcinoma thrombus and intrahepatic cholangiocarcinoma," *Modern Oncology*, vol. 28, no. 1, pp. 108–113, 2020.

[17] C. Q. Long, Z. Q. Zhou, W. J. He et al., "Application of multislice spiral CT multiplanar reconstruction technology in the diagnosis of cholangiocarcinoma," *Chinese Journal of CT and MRI*, vol. 18, no. 5, pp. 32–34, 2020.

[18] Y. Qi, J. Guo, X. H. Zhou, and X. B. Fan, "CT and MRI differential diagnosis of intrahepatic cholangiocarcinoma and atypical liver abscess," *Journal of Medical Imaging*, vol. 30, no. 8, pp. 103–106, 2020.

[19] J. Vlachogiannakos, T. Voulgaris, D. Karagiannakis et al., "Tu1586-do ppis affect the incidence of liver-related complications and overall survival in patients with cirrhosis? The experience of a Greek tertiary hospital," *Gastroenterology*, vol. 156, no. 6, 1369 pages, 2019.

[20] Q. J. Wu, M. L. Xiong, X. Y. Wang et al., "Clinical case analysis of dual primary carcinomas of simultaneous hepatocellular carcinoma and intrahepatic cholangiocarcinoma," *West China Medicine*, vol. 34, no. 3, pp. 94–99, 2019.

[21] B. S. Yang, M. Yuan, T. Y. Chen et al., "Predictive value of enhanced MRI texture analysis for the efficacy and prognosis of intrahepatic cholangiocarcinoma patients undergoing hepatic artery infusion chemotherapy," *Journal of Interventional Radiology*, vol. 29, no. 12, pp. 29–35, 2020.

Hindawi
Journal of Oncology
Volume 2021, Article ID 1071490, 6 pages
https://doi.org/10.1155/2021/1071490

Research Article

Influence of Psychological Nursing Intervention on Psychological State, Treatment Compliance, and Immune Function of Postoperative Patients with Rectal Cancer

Xicai Sun,[1] **Weifeng Zhong**,[2] **Jingjing Lu**,[3] **and Wenzhen Zhuang**[4]

[1]*Department of Health Management, Weifang People's Hospital, Weifang 261041, China*
[2]*Hospital Infection-Control Department, Zhangqiu District People's Hospital, Jinan 250200, China*
[3]*Department of Geriatrics (II), Qingdao Mental Health Center, Qingdao Seventh People's Hospital, Qingdao 266034, China*
[4]*Medical Record Management Section, Weifang People's Hospital, Weifang 261041, China*

Correspondence should be addressed to Wenzhen Zhuang; judi66815@163.com

Received 23 June 2021; Accepted 8 July 2021; Published 20 July 2021

Academic Editor: Muhammad Wasim Khan

In order to explore the clinical effect of psychological nursing intervention on postoperative chemotherapy for rectal cancer, 120 cases of rectal cancer patients were selected as the research subjects. The control group received conventional nursing treatment after operation, and the research group received comprehensive psychological nursing intervention on this basis. The self-rating anxiety scale (SAS) scores, self-rating depression scale (SDS) scores, hope level scores, nursing satisfaction, mental state changes, treatment compliance, and immune function of two groups were analyzed and compared. There was no significant difference between the two groups of patients in the preoperative SAS, SDS, and hope level scale scores. After the intervention, postoperative SAS and SDS scores and $CD8^+$ value of the research group were significantly lower than those of the control group. In contrast, the postoperative hope level score, treatment compliance, and postoperative $CD4^+/CD8^+$ of the research group were significantly higher, and the nursing satisfaction was better than that of the control group. The application of psychological nursing intervention in postoperative chemotherapy for patients with rectal cancer can effectively relieve anxiety and depression of patients, promote patients to establish a healthy and coordinated mental state, improve treatment compliance, improve immune function, and promote disease recovery.

1. Introduction

Rectal cancer is a relatively common type of gastrointestinal malignant tumor, which has clinical treatment difficulties such as high incidence, difficult operation, and many postoperative complications [1]. According to the latest global cancer burden data released by the International Agency for Research on Cancer (IARC) of the World Health Organization in 2020, more than 1.93 million people worldwide were diagnosed with colorectal cancer in 2020, and the cumulative number of deaths reached 930,000 cases, which confirmed that the mortality rate of colorectal cancer ranks third in the mortality rate of malignant tumors [2]. The induction of rectal cancer is caused by many life factors and genetic factors [3]. Factors such as high protein, high fat, low fiber, low vitamins, and excessive intake of sulfite compounds, obesity, and related family genetic diseases are all important factors that promote the induction of rectal cancer [4, 5].

At present, surgical treatment is still the first choice for the treatment of rectal cancer [6]; the stoma (Mile surgery) combined with abdominal perineal resection is often used for patients with low rectal cancer. However, a colon-abdominal stoma changes the patients' normal defecation method, and patients are prone to negative emotions such as depression and anxiety after surgery [7]. Studies have shown that negative emotions such as depression and anxiety affect the immune system, manifested as immunosuppression, and its state is related to tumor growth, metastasis, and other

factors [8]. Drastic emotional changes can lead to the disorder of the body's neuroimmune endocrine network, cause the body's immune function disorders, and lose its normal inhibitory effect on the occurrence and development of tumors [9, 10]. Therefore, psychological problems have an adverse effect on the safety, compliance, and immune function of cancer patients [4, 11], and the evaluation of patients' anxiety, depression, and other psychological emotions has received more and more clinical attention [12, 13].

Psychological intervention nursing mainly refers to the use of psychological theory and technology by nursing staff to solve the psychological problems of patients [14, 15]. According to the objects of intervention, it can be divided into psychological treatment, psychological prevention, psychological support, and mental health. Psychotherapy mainly aimed at the diagnosis and early standard treatment of psychological disorders. The goal of treatment is to alleviate the suffering of patients with mental disorders. Psychological prevention is the use of mental health education to guide people with psychological problems. The goal of treatment is to reduce the risk of psychological disorders.

By comparing the treatment status of the patients in the control group and the research group in terms of psychological status, treatment compliance, and immune function, the efficacy of psychological intervention in the comprehensive treatment of rectal cancer patients with neoadjuvant chemotherapy was evaluated in this study. This further lays a solid theoretical foundation for strengthening and standardizing the status and role of supportive psychological intervention treatment in the comprehensive treatment plan for patients with rectal cancer.

2. Materials and Methods

2.1. Clinical Data. The 120 patients undergoing rectal cancer surgery at Weifang People's Hospital, Weifang, China, from March 2020 to March 2021 were included in this study. The clinical data of 120 patients with rectal cancer undergoing surgical treatment in the hospital were selected and randomly divided into the control group ($n = 56$) and the research group ($n = 64$). The 56 cases in the control group had a male-to-female ratio of 4 : 3, aged from 38 to 78 years, with an average age of 53.29 ± 18.61 years; the education level was 15 cases of junior high school and above, 32 cases of high school and junior college, and 9 cases of bachelor degree and above. The 64 cases in the research group had a male-to-female ratio of 37 : 27, and they were 38–78 years old, with an average age of 52.56 ± 8.25 years; the educational level was 18 cases were junior high school and above, 35 cases were high school and junior college, and 11 cases were bachelor degree or above. There was no statistically significant difference between the two groups of patients in gender, age, and educational level, and they were comparable. This study was approved by the Ethics Committee of the Weifang People's Hospital, Weifang, China.

2.2. Inclusion and Exclusion Criteria. Inclusion criteria were as follows. (1) Patients understand the intention of this study and participate voluntarily and signed the "Informed Consent." (2) The patient is between 38 and 70 years old, and the diagnosis of rectal cancer TNM staging T1~T2, NO~N2, and MO. Under rectal cancer Miles surgery, the patient has a basic understanding of the condition. (3) The patient has no heart, kidney, liver, and other dysfunction, no other malignant tumors, no history of thyroid disease, no history of mental illness or family history of mental illness, and no history of special medication. (4) The patient with a junior high school education level or above can correctly understand the content of the questionnaire, answer the question autonomously, and normally listen, speak, read, and write in Chinese language.

Exclusion criteria were as follows. (1) Patients with chemotherapy, radiotherapy, or immunotherapy before Miles surgery; patients with a history of tumor metastasis in the brain; patients with severe dysfunction of the heart, liver, and kidney, hyperthyroidism, or hypothyroidism. (2) Patients with severe medical diseases and those who have a history of severe mental illness or neurosis. (3) Patients who were more than 70 years old or younger than 18 years old and TNM staging >T2 and >N2, patients with adjuvant radiotherapy or chemotherapy, or patients with distant metastases. (4) Those who cannot correctly understand the content of the questionnaire and answer the questions on their own initiative, and the patient has severe communication barriers and cannot normally listen, speak, read, and write in Chinese language. (5) The family members ask for concealment, the patient does not understand the condition, or the patient refuses to receive psychological care.

2.3. Nursing Methods. The control group received routine care, including hospital admissions, environmental care, patient introduction to the surgeon, and medication guidance to the patient, and close monitoring of the patient's condition and the occurrence of complications. Once abnormalities occur, they will immediately inform the doctor and deal with it effectively. On this basis, the research group implemented comprehensive, personalized, and comprehensive psychological nursing intervention. The intervention time for both groups of patients was 3 months. The specific measures were as follows.

2.4. Psychological Nursing Intervention. Psychological counseling was provided to the treated patients to understand their true inner thoughts and negative emotions in detail and evaluate them. Relevant theoretical knowledge is retrieved in a targeted manner, and questions were answered in a timely manner to eliminate patients' doubts. Psychological intervention methods such as enlightenment, careful conversation, encouragement, and comfort was applied to alleviate further or eliminate the patients' inner worries, instruct patients to master effective methods to adjust bad

emotions, prompt patients to adjust their own bad emotions correctly, establish correct cognition, and face the operation with a good attitude.

2.5. Cognitive and Behavioral Intervention. According to the patients' awareness of the disease, we used multimedia, text, and pictures to promote the disease and comprehensively and systematically explain to the patient and his family the cause of rectal cancer, the procedure, the abnormal conditions that may occur after the operation, and the corresponding treatment methods. The method of combining procedural muscle relaxation training and physical function training was adopted, 30 min/time, 2 times/week, all under soothing and soft music. We instruct patients to learn psychological coping strategies and behavioral training strategies, such as postoperative exercises, methods of turning over, and precautions related to diet.

2.6. Quality of Life Intervention. Patients with rectal cancer are often accompanied by changes in various living habits after surgery, so nursing staff should promptly correct the patients' unhealthy living conditions. For those with sleep disorders, the causes of sleep disorders should be understood and effective solutions should be provided. In view of the changes in bowel habits brought about by colostomy, which seriously affects the patients' physical and psychological state, the patients' diet and self-care methods were instructed to reduce the patients' dependence on nursing staff and family members, improve the patients' quality of life, and help them establish confidence to overcome disease.

2.7. Supervisory Feedback. The patients' emotional changes were recorded. Presentation of patient status, effect of preventive interventions, and discussion of improvement measures were performed during daily shift.

3. Observation Index

3.1. Evaluation Standards. The improvement of the mental status of the two groups was assessed by the SAS and SDS. SAS is based on the results of the Chinese norm. Those with a standard score of less than 50 are considered normal, 50–60 are considered mild anxiety, 61–70 are considered moderate anxiety, and more than 70 are considered severe anxiety. According to the Chinese norm of SDS, the standard cutoff value is 53 points, 53~62 points for mild depression, 63~72 points for moderate depression, and 72 points or more for severe depression. During the treatment, the patient strictly abides by the doctor's advice and adheres to standard treatment as complete compliance. During the treatment period, the patient basically follows the doctor's advice for treatment and occasionally does not receive standard treatment as the basic compliance. During the period, the patient does not strictly follow the doctor's advice for treatment, and the treatment is interrupted as noncompliance. Compliance = (complete compliance + basic compliance)/total number of cases × 100%. The two groups of immune function indicators were recorded and compared, mainly including $CD4^+$, $CD8^+$, and $CD4^+/CD8^+$.

3.2. Nursing Satisfaction Evaluation. According to the detailed rules of nursing satisfaction evaluation, the basis of satisfaction scoring was formulated in combination with the stoma of patients with colorectal cancer. The content includes whether the patients' bowel movement is smooth, whether the bedding is changed in time, whether the nurse's attitude is enthusiastic and positive, and whether the nurse often communicates with the patient. A score of >84 indicates very satisfied, a score of 60–84 indicates basic satisfaction, and a score below 60 indicates dissatisfaction. The treatment satisfaction of the two groups of patients was evaluated after the operation. Total nursing satisfaction = (very satisfied + basic satisfaction)/total number of cases × 100%.

3.3. Hope Level Evaluation. The Herth Hope Index (HHI) was used to evaluate the patients' hope in life. The scale includes three dimensions: a positive attitude toward reality and the future, an attitude to take positive actions, and an attitude to maintain an intimate relationship with others. It is scored by four levels, namely, strongly disagree, disagree, agree, and strongly agree, and the total score is 12–48; the higher the score, the higher the level of hope. 12–23 are divided into the low level; 24–35 are divided into the medium level; and 36–48 are divided into the high level. The hope levels of the two groups of patients were evaluated before and after the operation.

3.4. Statistical Analysis. The data were all analyzed by SPSS 20.0 statistical software, and the normal measurement data were described in the form of mean ± standard deviation ($\overline{x} \pm s$). The comparison of the two groups of normal measurement data between groups and within groups adopts the t test; the count data are described in the form of frequency and percentage $n(\%)$, and the comparison of count data $n(\%)$ adopts the χ^2 test. $P < 0.05$ means that the difference is statistically significant.

4. Results

4.1. Comparison of General Information of the Two Groups of Patients. There are 64 patients in the research group, and the male-to-female ratio is 37 : 27. There were 56 cases in the control group, and the ratio of male-to-female was 4 : 3. The age of the included patients fluctuated between 35 and 78 years old. There was no significant difference in gender between the two groups ($P > 0.05$). In addition, there was no statistically significant difference between the two groups of patients in terms of general information such as gender, age, education, and marital status ($P > 0.05$). As given in Table 1, it describes that the general baseline data of the two groups of patients are basically the same.

Table 1: Comparison of general information of subjects in the intervention group and the control group, n(%).

Variables	Control ($n = 56$)	Research ($n = 64$)	t/χ^2	P
Gender			0.368	0.926
Male	32 (57.14)	37 (57.81)		
Female	24 (42.86)	27 (42.19)		
Age (years)	53.29 ± 8.61	52.56 ± 8.25	0.429	0.713
<40	4 (7.14)	6 (9.37)		
40~50	12 (21.42)	18 (28.13)		
51~60	20 (35.72)	22 (34.37)		
>60	20 (35.72)	18 (28.13)		
Education			0.942	0.246
Junior high school and above	15 (26.79)	18 (28.12)		
High school and junior college	32 (57.14)	35 (54.69)		
Bachelor degree or above	9 (16.07)	11 (17.19)		
Marriage status			1.946	0.425
Unmarried	4 (7.14)	4 (6.25)		
Married	46 (82.14)	50 (78.13)		
Divorced	6 (10.72)	10 (15.62)		

4.2. Changes in the Mental State of the Two Groups. There was no statistically significant difference in the SAS and SDS scores of the two groups of patients upon admission ($P > 0.05$). After the intervention, the SAS and SDS scores of the research group were significantly lower than those of the control group, and the difference was statistically significant ($P < 0.05$), as given in Table 2 and Figure 1.

4.3. Comparison of Nursing Satisfaction between the Two Groups. Through psychological nursing intervention, the satisfaction degree of the research group reached 96.88%, which was significantly better than that of the control group (80.36%), and the difference was statistically significant (Table 3) ($P < 0.05$).

4.4. Two Groups of Hope Level Evaluation. There was no significant difference in the preoperative HHI score between the two groups ($P > 0.05$). The postoperative research group's attitude towards reality and the future, the attitude of taking positive actions, and the attitude of other people's intimacy and the total score were significantly higher than those of the control group, and the difference was statistically significant (Table 4) ($P < 0.05$).

4.5. Two Sets of Compliance. The compliance of the research group and the control group is given in Table 5. The treatment compliance of the research group (89.06%) is higher than that of the control group (71.43%).

4.6. Two Groups of Immune Function. The immune function indexes of the research group and the control group are given in Table 6. After the intervention, $CD4^+$ and $CD4^+/CD8^+$ of the research group were higher than those of the control group.

Table 2: Comparison of SAS and SDS scores between the two groups.

Grading index	Scoring stage	Control	Research	t	P
SAS	Preoperation	58.2 ± 8.6	58.1 ± 8.8	0.35	0.625
	Postoperative	47.5 ± 7.3	39.8 ± 7.5	6.24	0.035
SDS	Preoperation	56.5 ± 7.9	55.6 ± 7.9	0.29	0.158
	Postoperative	45.9 ± 7.5	38.4 ± 7.3	7.01	0.022

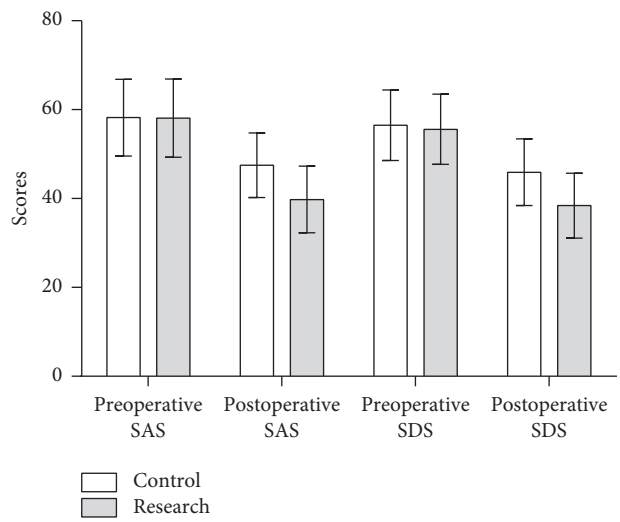

Figure 1: Comparison of SAS and SDS scores between the two groups.

5. Discussion

Rectal cancer is a serious life-threatening disease, and patients are prone to severe psychological stress. In addition, patients' lifestyles and habits often undergo major changes after surgery, and patients are prone to negative emotions such as depression and anxiety. If this emotion is not properly adjusted, it will have

Table 3: Comparison of SAS and SDS scores between the two groups before and after nursing n (%).

Group	Case	Very satisfied	Basic satisfaction	Dissatisfaction	Total satisfaction
Research	64	33 (51.56)	29 (45.31)	2 (3.13)	62 (96.88)
Control	56	24 (42.86)	21 (37.50)	11 (19.64)	45 (80.36)
χ^2					6.124
P					0.014

Table 4: Comparison of HHI scores between the two groups ($\overline{x} \pm s$).

Group	Attitude towards reality and the future		Attitude of taking positive actions		Attitude of other people's intimacy		Total score	
	Preoperation	Postoperative	Preoperation	Postoperative	Preoperation	Postoperative	Preoperation	Postoperative
Research	7.38 ± 1.36	12.11 ± 1.72	8.69 ± 1.78	13.81 ± 1.49	8.04 ± 1.92	13.82 ± 1.86	24.55 ± 2.18	39.85 ± 2.24
Control	7.04 ± 1.31	10.99 ± 1.38	8.82 ± 1.66	11.34 ± 1.56	7.96 ± 1.98	12.56 ± 1.88	24.13 ± 2.11	34.62 ± 2.16
t	−0.871	−2.972	0.245	−5.956	0.069	−2.561	−0.278	−7.922
P	0.554	0.038	0.721	0.011	1.116	0.024	0.714	0.008

Table 5: Compliance comparison between the two groups, n(%).

Group	Case	Complete compliance	Basic compliance	Noncompliance	Total compliance
Research	64	31 (48.44)	26 (40.63)	7 (10.93)	57 (89.06)
Control	56	16 (28.57)	24 (42.86)	16 (28.57)	40 (71.43)
χ^2					5.05
P					0.032

Table 6: Comparison of immune function between the two groups ($\overline{x} \pm s$).

Scoring index	Scoring stage	Control	Research	t	P
$CD4^+$	Before intervention	38.3 ± 7.26	38.1 ± 7.32	0.24	0.152
	After intervention	39.5 ± 8.01	46.9 ± 7.95	5.91	0.031
$CD8^+$	Before intervention	37.2 ± 7.44	36.8 ± 7.06	0.21	0.445
	After intervention	37.8 ± 7.52	31.2 ± 7.13	3.98	0.021
$CD4^+/CD8^+$	Before intervention	1.03 ± 0.28	1.03 ± 0.24	0	0.351
	After intervention	1.09 ± 0.29	1.5 ± 0.34	7.51	0.015

adverse effects on the patients' physiology, immunity, and social activities. It is easy for the patients to lose confidence and be unable to actively cooperate with the doctor's treatment, which affects the compliance of treatment and the quality of life and reduces the survival rate of the patients.

According to the results of the study, the changes in the psychological state of the patients in the research group, the evaluation of satisfaction with care, the evaluation of hope level, and the compliance with treatment were all significantly higher than before, and the immunity of the patients was also enhanced compared with before. In comparison between the groups, the evaluation of treatment compliance, satisfaction with care, and hope level of patients in the research group was significantly higher than that of the control group, and the difference was statistically significant. Through the detection of relevant indicators of the patients' immune function, the results showed that there was no significant difference in the indicators of peripheral blood T cell subsets between the two groups of patients before surgery. After the psychological nursing intervention, the research group's $CD4^+$, $CD8^+$, and $CD4^+/CD8^+$ all changed significantly compared with before the intervention, and the ratio of $CD4^+$ to $CD4^+/CD8^+$ was significantly higher than that of the control group.

To sum up, in the treatment of patients with rectal cancer and colostomy, psychological nursing interventions for different treatment stages of the disease can effectively reduce the patients' anxiety and depression, improve patients' compliance with treatment, and enhance the patients' immune function. It also can promote patients to establish a healthy and coordinated mental state, build confidence in life, improve the level of hope, improve nursing satisfaction, and promote recovery. However, due to the limitations of the environment, sample, time, and other factors, the survival prognosis of the two groups of patients has not been analyzed, and further studies are needed to supplement it.

Data Availability

All data generated or analyzed during this study are included in the published article. The datasets used and/or analyzed during the present study are available from the corresponding author on reasonable request.

Conflicts of Interest

The authors declare that they have no conflicts of interest.

References

[1] W. Q. Chen, R. S. Zheng, and H. M. Zeng, "Report of cancer incidence and mortality in China," *China Cancer*, vol. 24, no. 1, pp. 1–10, 2011.

[2] N. M. Verweij, M. E. Hamaker, D. Zimmerman, Y. Loon, and A. Schiphorst, "The impact of an ostomy on older colorectal cancer patients: a cross-sectional survey," *International Journal of Colorectal Disease*, vol. 32, no. 1, pp. 1–6, 2016.

[3] D. Dorcaratto, L. Grande, J. M. Ramón, and M. Pera, "Quality of life of patients with cancer of the oesophagus and stomach," *Cirugía Española (English Edition)*, vol. 89, no. 10, pp. 635–644, 2011.

[4] H.-P. Kapfhammer, "Comorbid depressive and anxiety disorders in patients with cancer," *Der Nervenarzt*, vol. 86, no. 3, pp. 291–301, 2015.

[5] L. Petty and J. Lester, "Distress screening in chronic disease: essential for cancer survivors," *Journal of the Advanced Practitioner in Oncology*, vol. 5, no. 2, pp. 107–14, 2014.

[6] M. P. Schellekens, D. G. van den Hurk, J. B. Prins et al., "Study protocol of a randomized controlled trial comparing mindfulness-based stress reduction with treatment as usual in reducing psychological distress in patients with lung cancer and their partners: the MILON study," *BMC Cancer*, vol. 14, no. 1, p. 3, 2014.

[7] V. Lohne, C. Miaskowski, and T. Rustøen, "The relationship between hope and caregiver strain in family caregivers of patients with advanced cancer," *Cancer Nursing*, vol. 35, no. 2, pp. 99–105, 2012.

[8] L. Fillion, R. Dupuis, I. Tremblay, G.-R. De Grâce, and W. Breitbart, "Enhancing meaning in palliative care practice: a meaning-centered intervention to promote job satisfaction," *Palliative and Supportive Care*, vol. 4, no. 4, pp. 333–344, 2006.

[9] I. Bdvarsdóttir and A. Elklit, "Psychological reactions in Icelandic earthquake survivors," *Scandinavian Journal of Psychology*, vol. 45, no. 1, pp. 3–13, 2004.

[10] M. Kangas, J. L. Henry, and R. A. Bryant, "The relationship between acute stress disorder and posttraumatic stress disorder following cancer," *Journal of Consulting and Clinical Psychology*, vol. 73, no. 2, pp. 360–364, 2005.

[11] D. Spiegel, L. D. Butler, J. Giese-Davis et al., "Effects of supportive-expressive group therapy on survival of patients with metastatic breast cancer," *Cancer*, vol. 110, no. 5, pp. 1130–1138, 2007.

[12] M. Baur, M. Horvath, S. Stättner et al., "Chemoradiotherapy with 5-fluorouracil/leucovorin, surgery and adjuvant chemotherapy for locally advanced rectal cancer," *Oncology Letters*, vol. 1, no. 1, pp. 189–194, 2010.

[13] R. Sauer, H. Becker, W. Hohenberger et al., "Preoperative versus postoperative chemoradiotherapy for rectal cancer," *Journal of Clinical Oncology*, vol. 351, no. 16, pp. 1926–1933, 2004.

[14] G. L. Cohen and D. K. Sherman, "The psychology of change: self-affirmation and social psychological intervention," *Annual Review of Psychology*, vol. 65, no. 1, pp. 333–371, 2014.

[15] L. J. Hodges, J. Walker, A. M. Kleiboer et al., "What is a psychological intervention? A metareview and practical proposal," *Psycho-Oncology*, vol. 20, no. 5, pp. 470–478, 2011.

Hindawi
Journal of Oncology
Volume 2021, Article ID 2804478, 10 pages
https://doi.org/10.1155/2021/2804478

Research Article

miR-193a Directly Targets PSEN1 and Inhibits Gastric Cancer Cell Growth, the Activation of PI3K/Akt Signaling Pathway, and the Epithelial-to-Mesenchymal Transition

Xuemei Pan,[1] Ting Zhao,[1] Saisai Mu,[2] and Shouchuan Li[2]

[1]*General Surgery Ward I, Qingdao Hospital of Traditional Chinese Medicine, Qingdao Hiser Hospital, Qingdao 266000, China*
[2]*General Surgery Ward III, Qingdao Hospital of Traditional Chinese Medicine, Qingdao Hiser Hospital, Qingdao 266000, China*

Correspondence should be addressed to Shouchuan Li; lishouchuan@qdzyhospital.cn

Received 31 May 2021; Accepted 5 July 2021; Published 15 July 2021

Academic Editor: Muhammad Wasim Khan

Background. Gastric cancer, a kind of gastrointestinal malignancy, is the second type of leading death cancer. miR-193a is a key tumor suppressor in several diseases. PSEN1 is mainly related to Alzheimer's disease and may be involved in the cleavage of the Notch receptor. *Material and Methods*. RT-PCR and western blot were applied to evaluate miR-193a and the expression level of PSEN1. Luciferase reporter assay was applied to verify whether PSEN1 was a target of miR-193a. The Kaplan–Meier method was employed to calculate the 5-year overall survival of gastric cancer patients. *Results*. miR-193a was downregulated in gastric cancer tissues and cell lines, and downregulation of miR-193a predicted poor 5-year overall survival of gastric cancer. miR-193a inhibited the proliferation and the activation of the PI3K/AKT signaling pathway in gastric cancer cells. miR-193a inhibited gastric cancer tumor growth in vivo. miR-193a impaired cell invasion and epithelial-to-mesenchymal transition (EMT) in HGC-27 cells. In addition, PSEN1 was a direct target of miR-193a and PSEN1 reversed partial functions of miR-193a in cell proliferation and invasion. *Conclusion*. miR-193a prominently decreased the proliferation, invasion, and activation of the PI3K/Akt signaling pathway and the abilities of epithelial-to-mesenchymal transition in gastric cancer cells. The newly identified miR-193a/PSEN1 axis provides novel insight into the pathogenesis of gastric cancer.

1. Introduction

Gastric cancer (GC), the second leading death cancer, is a kind of gastrointestinal malignancy [1]. Lamentably, gastric cancers patients at an early stage are difficult to diagnose due to no specific symptoms [2]. Thus, exploring new biomarkers for the early diagnosis and treatment of gastric cancer is urgent.

Micro-RNAs (miRNAs), short noncoding RNAs, could cause mRNA degradation or translational inhibition through binding to target mRNAs 3′-UTR at the post-transcriptional level [3, 4]. Recently, accumulating evidence indicated that miRNAs play a vital role in tumor progression in gastric cancer, including proliferation, metastasis, and apoptosis [5–7]. miR-193a acted as a critical tumor suppressor in various cancers, including colon cancer, acute myeloid leukemia, bladder cancer, and malignant pleural mesothelioma [8–11]. In non-small cell lung cancer, Yu et al. illuminated that miR-193a suppressed cell migration, invasion, and EMT [12]. Similarly, Fang et al. demonstrated that miR-193a inhibited cell proliferation and metastasis in pancreatic cancer [13]. Therefore, we strongly believe miR-193a inhibited cell proliferation and invasion in gastric cancer.

Presenilin-1 (PSEN1), a primary component of the γ-secretase complex, is mainly related to Alzheimer's disease and may be involved in the cleavage of the Notch receptor [14, 15]. The mutation of PSEN1 was associated with spasticity and parkinsonism in the dominant Alzheimer's family [16]. Zhao et al. indicated that PSEN1 overexpression results in attenuated phagocytic uptake of Aβ by microglia and regulated intracellular trafficking and

pathophysiological function in myeloid cells [17]. In addition, Meng et al. illuminated that PSEN1 was a target gene of miR-193a and miR-193a regulated chemoradiation resistance through PSEN1 in oesophageal cancer [18].

In this present study, we aimed to investigate the biological effect of miR-193a on gastric cancer. To translate these findings to clinical practice, it is essential to explore the molecular mechanism of miR-193a in the development of gastric cancer.

2. Materials and Methods

2.1. Patients and Tissue Samples. We selected 50 patients that underwent an operation at Qingdao Hospital of Traditional Chinese Medicine, Qingdao, China, and obtained 50 pairs of gastric cancer tissues and corresponding peritumoral normal tissues. The specimens were immediately frozen in liquid nitrogen and followed storage at −80°C. Informed consent was obtained from each patient and this investigation was approved by the ethics committee of the Qingdao Hospital of Traditional Chinese Medicine, Qingdao, China.

2.2. Cell Lines and Culture Conditions. We obtained two human gastric cancer cells HGC-27 and MGC-803 and a normal gastric epithelial cell GES-1 from American Type Culture Collection (ATCC, Rockville, MD, USA). RPMI-1640 (Gibco-BRL; Rockville, MD, USA) medium contained with 10% FBS (Haoyang Biological, Tianjin, China) were conducted to culture the cells at 37°C with 5% CO_2.

2.3. Plasmid Construction and Transfection. We purchased the miR-193a mimic and miR-193a inhibitor oligo fragments from Gene-Pharma (Shanghai, China), which was conducted to upregulate or downregulate miR-193a. HGC-27 cells were seeded in a 6-well plate, and the transfection was performed using Lipofectamine 2000 (Invitrogen, Carlsbad, USA) reagent as described previously [19]. In brief, the Opti-MEM/reduced serum medium (Thermo Fisher Scientific, Shanghai, China) was employed to dilute the Lipofectamine 2000 reagent and the oligo fragments, respectively. After mixing the two solutions, the mixture was added to the cells. For the transiently transfected cells, the cells were harvest after 48 h. On the contrary, for the cells with stable transfection, we applied Geneticin (G418, Thermo Scientific, Shanghai, China) to select.

2.4. RNA Extraction and Quantitative Real-Time PCR. TRIzol reagent (Invitrogen) and mirVana miRNA Isolation Kit (Thermo, Shanghai, China) were employed to extract the total RNAs and total miRNAs, respectively. The first cDNA chains of mRNA and miRNA were synthesized by the Prime Script RT Reagent Kit (Takara Biotechnology Co., Ltd., Dalian, China) and the miRNA Reverse Transcription Kit (Life Technologies, Foster, CA, USA), respectively. The qPCR was performed by using the SYBR Premix Ex Taq (Takara) and MystiCq microRNA qPCR Assay Primer (Sigma, Missouri, USA) on Applied Biosystems StepOnePlus™ Real-Time PCR System. The normalization for miR-193a and PIK3CG was used as U6 and GAPDH, respectively. The primers were miR-193a F: 5′-ACTGGCCTACAAAGTCCCAGT-3′, R: 5′-GTGC AGGGTCCGAGGT-3'; U6 F: 5′-CTTCGGCAGCACA-TATAC-3′, R: 5′-GAACGCTTCACGAATTTGC-3'; PSEN1 F: 5′-TATGGCAGAAGGAGACCCG-3′, R: 5′-CCATTCCTCACTGAACCCG-3'; GAPDH F: 5′-AAGGTGAAGGTCGGAGTCAA-3′, R: 5′-AAT-GAAGGGGTCATTGATGG-3'.

2.5. Western Blot Analysis. RIPA Lysis Buffer (Sigma, USA) containing 10% PMSF (Sigma, USA) was conducted to lyse the HGC-27 cells on ice for 30 min. We centrifuged the protein solving liquid at 4°C for 20 min with 12,000 × g speeds and then collected the supernatants. We separated the proteins by electrophoresis utilized 10% SDS-PAGE and then transferred the blots on a PVDF membrane (Millipore, USA). After blocking by 5% fat-free milk in TBST buffer at room temperature for 1 h, the blots were incubated with the primary antibodies at 4°C overnight. The membrane was incubated by primary antibodies, including PSEN1 (1 : 1000; Abcam, Cambridge, USA), EMT proteins (E-cadherin (1 : 1000; Abcam), and N-cadherin (1 : 1000; Abcam) and the proteins on the PI3K pathway (p-PI3K (1 : 1000, Cell Signaling, San Jose, CA, USA), PI3K (1 : 1000, Cell Signaling), p-AKT (1 : 1000, Cell Signaling), AKT (1 : 1000, Cell Signaling)), and GAPDH (1 : 1000, Santa Cruz, Shanghai, China). Subsequently, we incubated the membranes by anti-rabbit or mouse HRP-conjugated secondary antibody for 2 h at room temperature. In the end, Enhanced Chemiluminescence (ECL, Pharmacia Biotech, Arlington, USA) was employed to evaluate the signals.

2.6. CCK-8 Assay. The cell proliferative ability was conducted by Cell Counting Kit-8 (CCK8, Dojindo, Japan) [19]. HGC-27 cells were seeded in a 96-well plate and cultured for 24 h, 48 h, 72 h, or 96 h at 37°C incubator. After being cultured, 10 μl of CCK8 solutions was added to each well and cultured at 37°C for 1 h; then, the absorbance was assessed at 450 nm using a microplate reader (BioTek, Winooski, USA).

2.7. Transwell Assays. The cell invasive ability was measured by transwell insert (8 μm membrane, Corning, Cambridge, MA) with matrigel (BD Biosciences) covered [19]. The inserts were put in a 24-well plate to form the upper and lower chambers. The 200 μl HGC-27 cells' suspension was added in the upper chamber, which was suspended by RPMI-1640 medium without PBS. Meanwhile, the lower chamber was filled with a 500 μl RPMI-1640 medium containing 15% FBS. After incubating the cells at 37°C for 24 h, the noninvasive cells on the upper surface were removed using a cotton swab. For the invaded cells, they were fixed and then stained using 4% paraformaldehyde and 10% crystal violet in sequence; and then, the cells were counted under the microscope (Olympus Corporation, Tokyo, Japan).

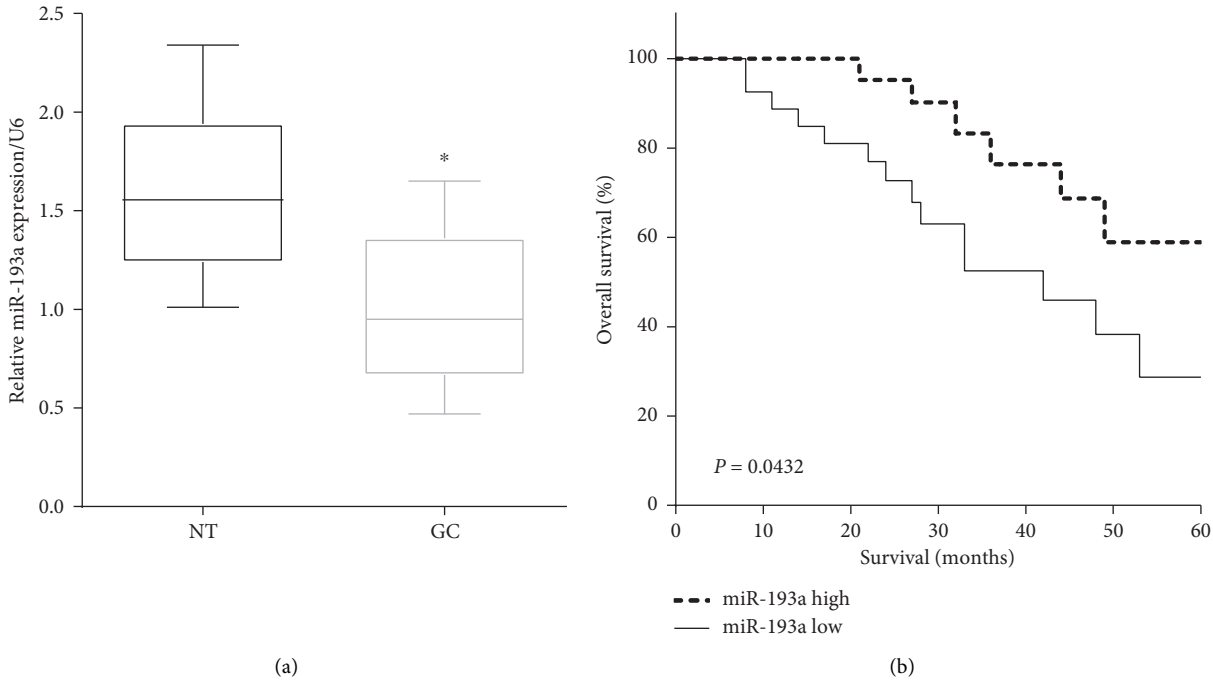

Figure 1: Downregulation of miR-193a predicts poor prognosis of gastric cancer. (a) miR-193a expression was low in GC tissues versus corresponding peritumoral normal tissues. (b) Low expression of miR-193a predicted poor prognosis of gastric cancer patients. $^{*}P < 0.05$.

2.8. Dual-Luciferase Reporter Assay. TargetScan predicted PSEN1 was a target gene of miR-193a, and the binding site was located at 697–703 on PSEN1 mRNA 3′-UTR. To verify whether miR-193a directly binds to PIK3CG mRNA 3′-UTR, the binding sequences were mutated from GGCCAGU to CCGGUCA and inserted in pmirGLO luciferase reporter vector. The HGC-27 cells were cotransfected with miR-193a mimic and the wild-type 3′-UTR or the mutant 3′-UTR of PSEN1. We utilized the dual-luciferase reporter assay system (Promega) to evaluate the firefly luciferase activity with Renilla luciferase activity as the normalization.

2.9. Tumor Xenograft Model in Nude Mice. The 4-week-old nude mice were purchased from Charles River Laboratories (Beijing, China). The nude mice were randomly classified into two groups, miR-193a mimic miR-193a control groups, with two mice in each group. HGC-27 cells were inoculated into the nude mice through subcutaneous injection. The mice were raised in the same environment and were observed every week. We measured and recorded the tumor lengths and widths and then calculated the tumor volume every three days. All animal experiments were performed in the animal laboratory center of Qingdao Hospital of Traditional Chinese Medicine and approved by the Care and Use Committee of Qingdao Hospital of Traditional Chinese Medicine.

2.10. Statistical Analysis. All the data were analyzed by SPSS statistical software version 16.0 (SPSS, Chicago, IL, USA), which were presented as the mean ± standard deviation. The significance between two groups and multiple groups was compared by a two-tailed Student's *t*-test and one-way analysis of variance followed by an LSD test. P value < 0.05 was found to be statistically significant.

3. Results

3.1. Downregulation of miR-193a Predicts Poor Prognosis of Gastric Cancer. We evaluated the mRNA levels of miR-193a in 50 pairs of gastric cancer and peritumoral normal tissues. As expected, the expression of miR-193a was lower in GC tissues than that in the corresponding peritumoral normal tissues ($P < 0.05$) (Figure 1(a)). According to the median level of miR-193a, patients were divided into a low expression group and a high expression group [20]. Results showed that high expression of miR-193a was associated with poor prognosis in gastric cancer ($P < 0.05$) (Figure 1(b)).

3.2. miR-193a Suppresses Cell Proliferation and Inhibits the Activation of PI3K/Akt Signaling Pathway in Gastric Cancer Cells. We calculated miR-193a expression in two gastric cancer cells (HGC-27 and MGC-803) and a normal epithelial cell GES-1. The same as the tissues, miR-193a was low expressed in GES-1 cells versus HGC-27 ($P < 0.01$) and MGC-803 ($P < 0.05$) cells (Figure 2(a)). To detect the significant roles of miR-193a, miR-193a mimic and miR-193a inhibitor were conducted to upregulate ($P < 0.01$) or downregulate ($P < 0.05$) miR-193a in HGC-27 cells measured by RT-qPCR (Figure 2(b)).

CCK8 assay indicated that miR-193a mimic suppressed ($P < 0.05$) cell proliferation, while miR-193a inhibitor

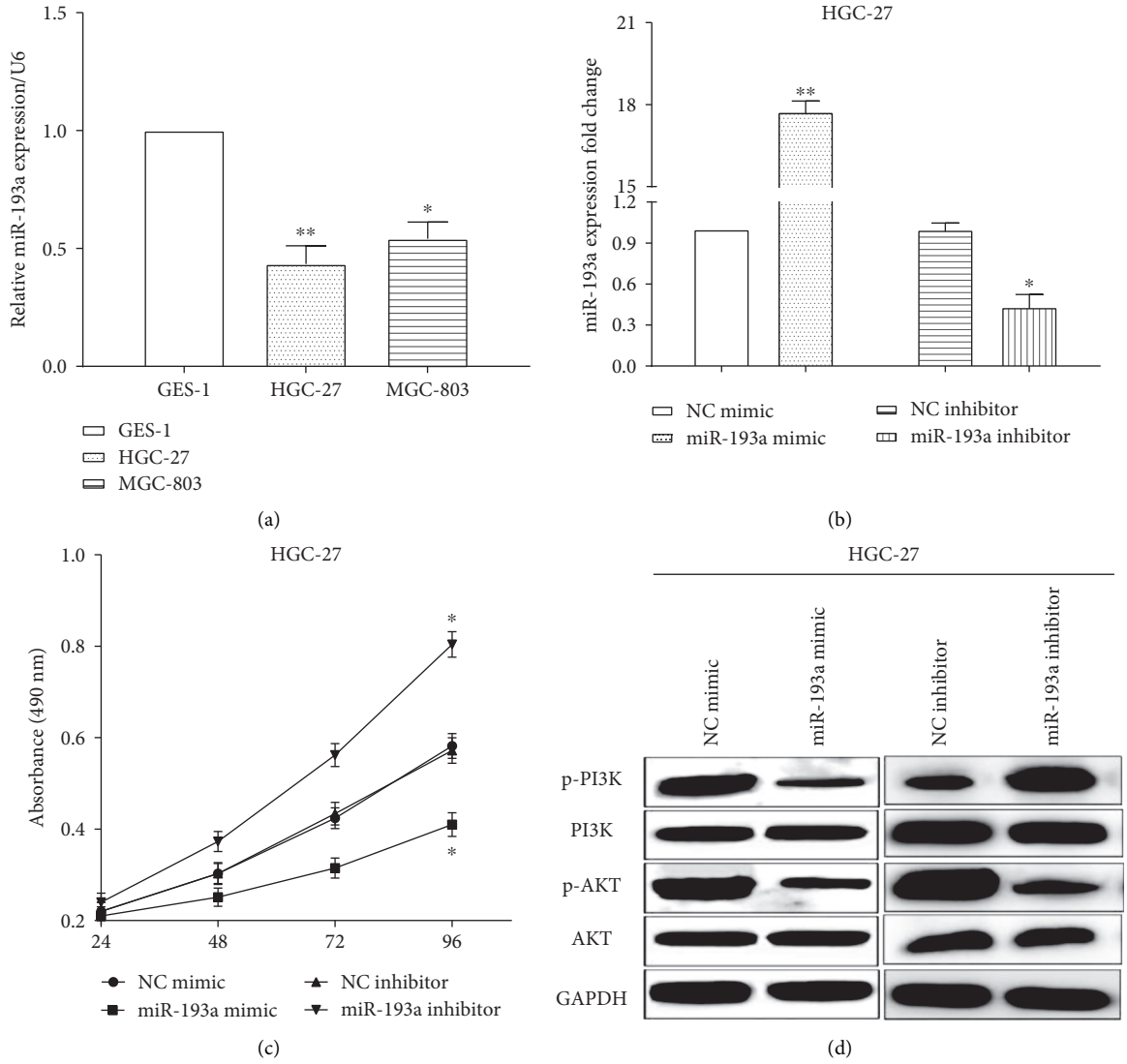

Figure 2: miR-193a suppresses the activation of PI3K/AKT pathway in gastric cancer cells. (a) miR-193a expression was low in GES-1 cells versus HGC-27 and MGC-803 cells. (b) The miR-193a mimic and miR-193a inhibitor were conducted to upregulate or downregulate miR-193a in HGC-27 cells measured by RT-qPCR. (c) CCK8 assay indicated miR-193a mimic suppressed cell proliferation, while miR-193a inhibitor promoted cell proliferative ability in HGC-27 cells. (d) miR-193a inhibited the activation of PI3K/AKT pathway. $^{*}P < 0.05$; $^{**}P < 0.01$.

promoted ($P < 0.05$) cell proliferative ability in HGC-27 cells (Figure 2(c)). Western blot assay was conducted to assess the expression of PI3K pathway-associated proteins in HGC-27 cells. We discovered that miR-193a overexpression suppressed p-PI3K and p-AKT expression in HGC-27 cells, whereas miR-193a inhibitor enhanced the expression of p-PI3K and p-AKT, which elucidated that miR-193a inhibited the activation of PI3K/Akt signaling pathway (Figure 2(d)).

3.3. miR-193a Suppresses the Gastric Cancer Growth In Vivo. HGC-27 cells stably transfected with miR-193a mimic or control plasmid were applied to inject into the nude mice at subcutaneous. The xenograft tumors volumes were calculated every 3 days and the group of transfecting miR-193a mimic had a slower growth rate than the control group (Figure 3(a)). After 26 days of culture, the nude mice were dissected and the tumor volume was calculated and recorded. Furthermore, we discovered that the tumor volumes in miR-193a overexpression group were smaller than those in control group, which indicated that overexpressed miR-193a inhibited gastric cancer growth *in vivo* ($P < 0.05$) (Figure 3(b)).

3.4. miR-193a Inhibits Cell Invasion and the EMT in HGC-27 Cells. Transwell assay elucidated that miR-193a mimic suppressed ($P < 0.05$) cell invasive ability whereas miR-193a inhibitor enhanced cell invasive ability ($P < 0.05$) (Figure 4(a)). All the findings revealed miR-193a inhibited the abilities of proliferation and invasion in gastric cancer

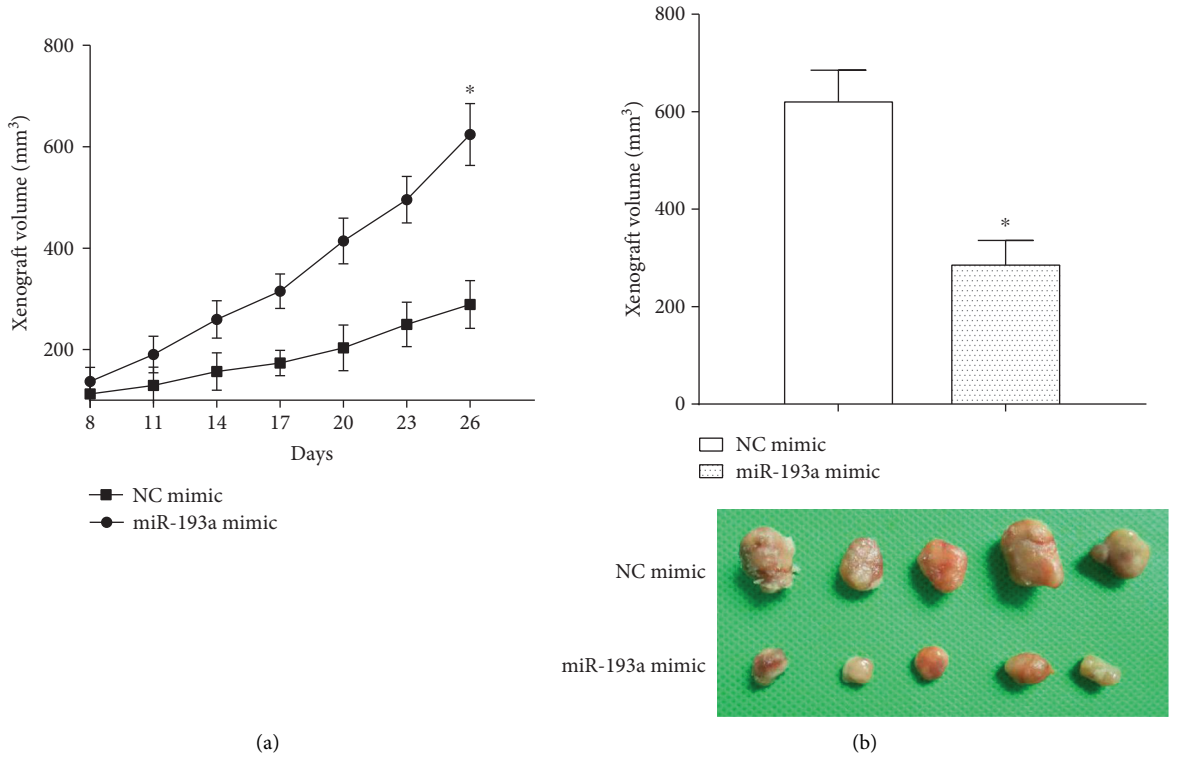

Figure 3: miR-193a suppresses the xenograft growth in vivo. (a) miR-193a overexpression inhibited gastric cancer xenograft growth. (b) The tumor volume of cells overexpressed miR-193a was smaller than the control group. $^{*}P < 0.05$.

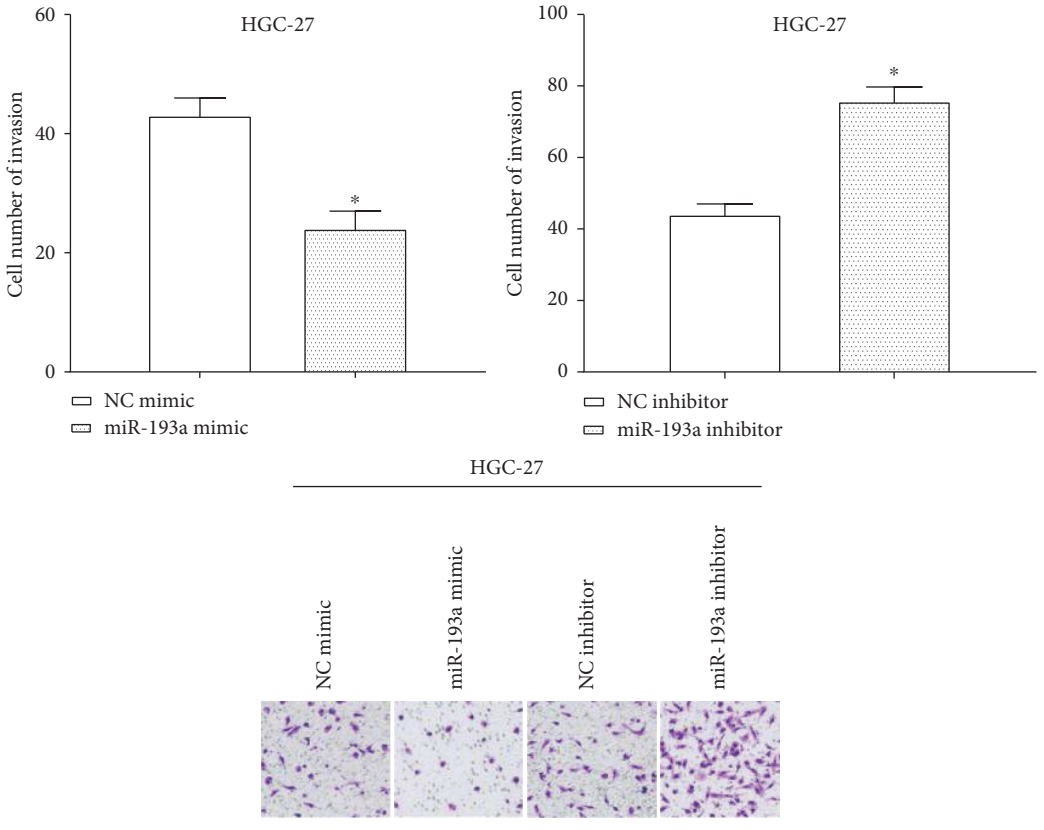

Figure 4: Continued.

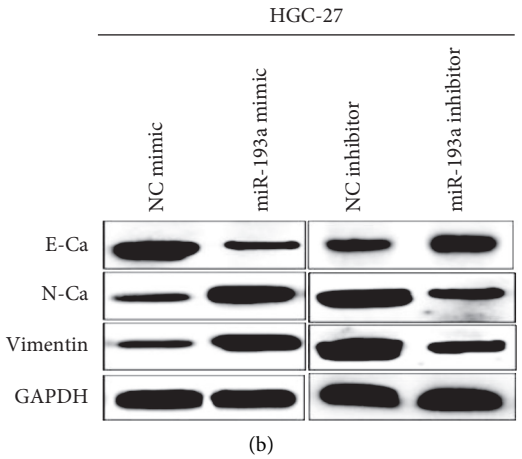

Figure 4: miR-193a suppresses cell invasion and EMT in gastric cancer cells. (a) Transwell assay elucidated that miR-193a inhibited the abilities of invasion in gastric cancer cell HGC-27. (b) miR-193a inhibited the EMT in HGC-27 cells. $^{*}P < 0.05$.

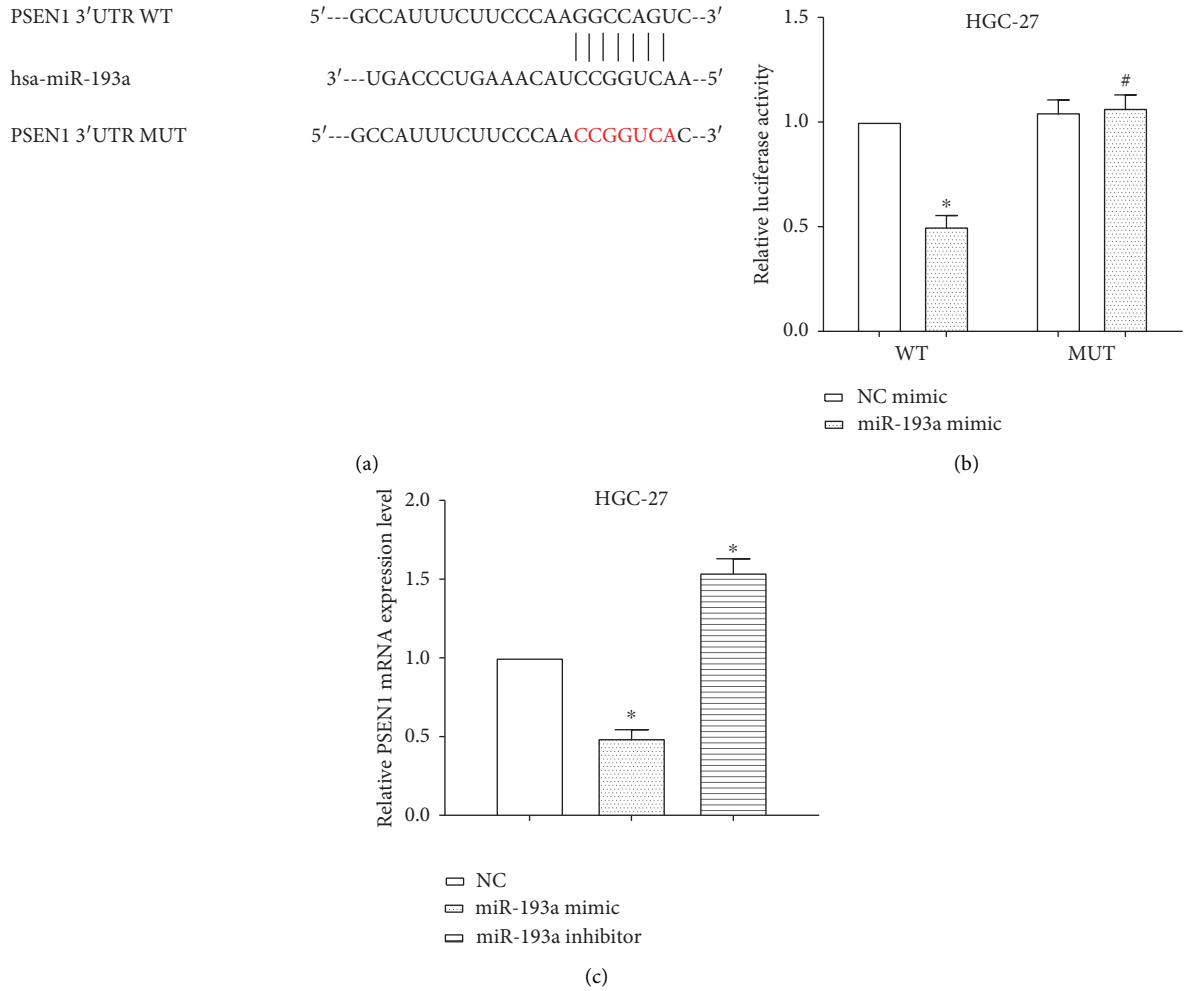

Figure 5: miR-193a regulates PSEN1 expression through binding to PSEN1 mRNA 3′-UTR. (a) PSEN1 was a target gene of miR-193a, and the binding site was located at the 3′-UTR of PSEN1 mRNA. (b) Luciferase reporter assay elucidated miR-193a and decreased the luciferase activity of HGC-27 cells transfected with wild-type PSEN1 3′-UTR, while it did not alter the luciferase activity of cells transfected with mutant PSEN1 3′-UTR. (c) Overexpression of miR-193a inhibited the mRNA level of PSEN1, while knockdown of miR-193a enhanced the expression of PSEN1 in HGC-27 cells. $^{*}P < 0.05$; $^{\#}P < 0.05$.

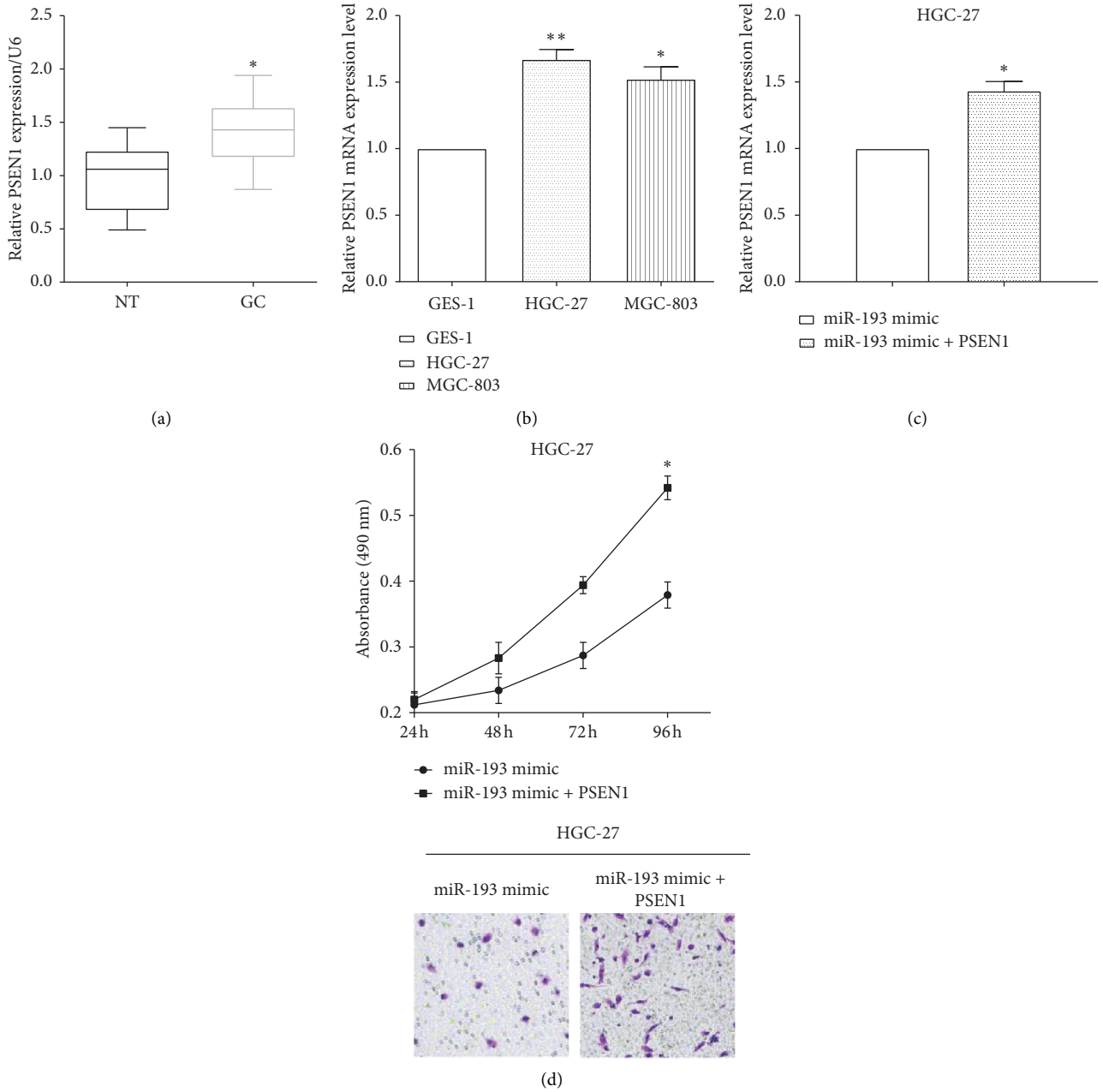

Figure 6: Continued.

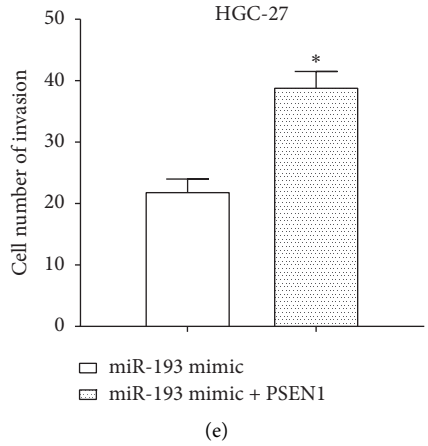

Figure 6: PSEN1 reverses the roles of miR-193a on cell proliferation and invasion. (a) PSEN1 was upregulated in gastric cancer tissues compared to peritumoral normal tissues. (b) PSEN1 expression was higher in HGC-27 and MGC-803 cells than that in GES-1 cells. (c) PSEN1 overexpression plasmid was transfected in miR-193a overexpressed HGC-27 cells. (d) Upregulation of PSEN1 enhanced cell proliferation in miR-193a mimic-transfected HGC-27 cells. (e) PSEN1 reversed partial roles of miR-193a on cell invasion. $^{*}P < 0.05$; $^{**}P < 0.01$.

cell HGC-27. The EMT ability was evaluated by detecting the expression of EMT-associated proteins by western blot. As we expected, miR-193a mimic suppressed the expression of N-cadherin, while improving the expression of E-cadherin in HGC-27 cells. On the contrary, miR-193a inhibitor enhanced the expression of N-cadherin and decreased E-cadherin expression, which suggested that miR-193a inhibited cell EMT through PSEN1 (Figure 4(b)).

3.5. miR-193a Regulates the Expression of PSEN1 through Directly Binding to 3′-UTR of PSEN1 mRNA. TargetScan predicted one of the target genes of miR-193a was PSEN1, and the binding site was located at 697–703 on PSEN1 mRNA 3′-UTR. To verify miR-193a binding to the potential binding site of PSEN1, the binding sequences were mutated from GGCCAGU to CCGGUCA, and then the luciferase activity was calculated (Figure 5(a)). The luciferase reporter assay elucidated that miR-193a decreased ($P < 0.05$) the luciferase activity of HGC-27 cells transfected with wild-type PSEN1 3′-UTR, while it did not alter ($P > 0.05$) the luciferase activity of cells transfected with mutant PSEN1 3′-UTR (Figure 5(b)). PSEN1 mRNA levels were evaluated after transfection of miR-193a mimic or miR-193a inhibitor in HGC-27 cells. As expected, overexpression of miR-193a inhibited ($P < 0.05$) the mRNA level of PSEN1, while knockdown of miR-193a enhanced ($P < 0.05$) PSEN1 expression in HGC-27 cells (Figure 5(c)). All the results indicated that miR-193a regulated the expression of PSEN1 in gastric cancer cells HGC-27.

3.6. PSEN1 Reverses the Roles of miR-193a in Gastric Cancer Development. The expression of PSEN1 was evaluated by RT-qPCR and we found that it was downregulated in peritumoral normal tissues compared to that in gastric cancer tissues ($P < 0.05$) (Figure 6(a)). Similarly, the expression of PSEN1 was higher in HGC-27 ($P < 0.01$) and MGC-803 ($P < 0.05$) cells than that in GES-1 cells (Figure 6(b)).

To investigate the effect of PSEN1 on the suppressive role of miR-193a, PSEN1 overexpression plasmid was transfected in miR-193a overexpressed HGC-27 cells (Figure 6(c)). Upregulation of PSEN1 enhanced cell proliferation and invasion in miR-193a mimic-transfected HGC-27 cells (Figures 6(d) and 6(e)). All the results revealed that PSEN1 partially reversed the roles of miR-193a on cell proliferation and invasion.

4. Discussion

Gastric cancer, a kind of gastrointestinal malignancy, is the second leading death cancer, and the early diagnosis is very difficult [1, 2]. Thus, exploring new biomarkers for the early diagnosis and treatment of gastric cancer is urgent.

Micro-RNAs caused mRNA degradation or translational inhibition through binding to target mRNAs 3′-UTR at the posttranscriptional level [21, 22]. Accumulating evidence indicated that multiple miRNAs were involved in tumor prognosis in gastric cancer, including miR-127, miR-575, miR-31, and miR-520c [23–26]. miR-193a acted as a key tumor suppressor in various cancers and played significant roles in tumor growth and metastasis [8, 11]. miR-193a inhibited cell viability, proliferation, and colony formation and induced *G*1 phase arrest in prostate cancer cells [27]. Consistent with all the findings above, we discovered that miR-193a was downregulated in gastric cancer tissues and cells, and downregulation of miR-193a predicted poor 5-year overall survival of gastric cancer patients. miR-193a inhibited tumor growth in vitro and in vivo and suppressed tumor metastasis in gastric cancer cells HGC-27. Pan et al. indicated that miR-193a inhibited cell proliferation and invasion through PI3K/AKT pathway in renal cell carcinoma [28]. Our results are consistent with Pan

et al.; miR-193a suppressed the activation of PI3K/AKT pathway in gastric cancer. What is more, we first propose that miR-193a inhibited the epithelial-to-mesenchymal transition (EMT) of gastric cancer cells. However, miR-193a promoted cell proliferation and migration in esophageal squamous cell carcinoma [29]; therefore, we conjectured that miR-193a might have tissue specificity.

PSEN1 is a primary component of the γ-secretase complex, which is mainly related to Alzheimer's disease [14, 15]. PSEN1 downregulation caused decreased neuronal survival and protected neurons from glucose deprivation-induced death [30]. Even in gastric cancer, Li et al. indicated that PSEN1 enhanced carcinogenesis and metastasis [31]. PSEN1 is a direct target gene of miR-193a, and PSEN1 promoted cell apoptosis and enhanced the sensitization to a drug in bladder cancer [32]. Consistent with Meng et al. [18, 32], we found that PSEN1 was a target of miR-193a and its expression was mediated by miR-193a in gastric cancer cells HGC-27. PSEN1 partially reversed the functions of miR-193a in cell proliferation and invasion in HGC-27 cells. The shortcoming of our study is that it has not further explored the mechanism of the miRNA/PSEN1/PI3K/Akt axis in gastric cancer.

5. Conclusions

miR-193a inhibits gastric cancer cell proliferation, invasion, and the epithelial-to-mesenchymal transition and suppresses the activation of the PI3K/Akt signaling pathway. This study evaluates the therapeutic potential of miR-193a in gastric cancer and provides a new target for the prevention and treatment of gastric cancer.

Data Availability

The datasets used and/or analyzed during the present study are available from the corresponding author on reasonable request.

Ethical Approval

The study was approved by the Qingdao Hospital of Traditional Chinese Medicine.

Consent

Written permission was obtained from all participants.

Disclosure

The funding body had no role in the design of the study, collection, analysis, interpretation of data, or writing of the manuscript.

Conflicts of Interest

The authors declare that they have no conflicts of interest.

Authors' Contributions

XP contributed to the conception, design, experiments, and drafting of the article. TZ and SM contributed to the collection of human samples, data analysis, and statistical analysis. SL contributed to the conception, interpretation of data, and critical revision of the manuscript.

Acknowledgments

The authors deeply appreciate the contributions to this work made in various ways by all of the participants.

References

[1] A. Jemal, F. Bray, M. M. Center, J. Ferlay, E. Ward, and D. Forman, "Global cancer statistics," *CA: A Cancer Journal for Clinicians*, vol. 61, no. 2, pp. 69–90, 2011.

[2] W.-M. Chen, M.-D. Huang, D.-P. Sun et al., "Long intergenic non-coding RNA 00152 promotes tumor cell cycle progression by binding to EZH2 and repressing p15 and p21 in gastric cancer," *Oncotarget*, vol. 7, no. 9, pp. 9773–9787, 2016.

[3] Y. Yang, Y. Liu, W. Liu et al., "miR-122 inhibits the cervical cancer development by targeting the oncogene RAD21," *Biochemical Genetics*, 2021, Internet.

[4] X. Lin, Z. Yang, P. Zhang, Y. Liu, and G. Shao, "[Retracted] miR-154 inhibits migration and invasion of human non-small cell lung cancer by targeting ZEB2," *Oncology Letters*, vol. 22, no. 2, p. 612, 2021.

[5] Y. Saito, H. Suzuki, and T. Hibi, "The role of microRNAs in gastrointestinal cancers," *Journal of Gastroenterology*, vol. 44, no. Suppl 19, pp. 18–22, 2009.

[6] T. Ueda, S. Volinia, H. Okumura et al., "Relation between microRNA expression and progression and prognosis of gastric cancer: a microRNA expression analysis," *The Lancet Oncology*, vol. 11, no. 2, pp. 136–146, 2010.

[7] F. Xiao, Z Zuo, G Cai, S Kang, X Gao, and T Li, "miRecords: an integrated resource for microRNA-target interactions," *Nucleic Acids Research*, vol. 37, no. Database issue, pp. D105–D110, 2009.

[8] J. Pekow, K. Meckel, U. Dougherty et al., "miR-193a-3p is a key tumor suppressor in ulcerative colitis-associated colon cancer and promotes carcinogenesis through upregulation of IL17RD," *Clinical Cancer Research*, vol. 23, no. 17, pp. 5281–5291, 2017.

[9] X.-N. Gao, J. Lin, Y.-H. Li et al., "MicroRNA-193a represses c-kit expression and functions as a methylation-silenced tumor suppressor in acute myeloid leukemia," *Oncogene*, vol. 30, no. 31, pp. 3416–3428, 2011.

[10] Y. Li, H. Deng, L. Lv et al., "The miR-193a-3p-regulated ING5 gene activates the DNA damage response pathway and inhibits multi-chemoresistance in bladder cancer," *Oncotarget*, vol. 6, no. 12, pp. 10195–10206, 2015.

[11] M. Williams, M. B. Kirschner, Y. Y. Cheng et al., "miR-193a-3p is a potential tumor suppressor in malignant pleural mesothelioma," *Oncotarget*, vol. 6, no. 27, pp. 23480–23495, 2015.

[12] T. Yu, J. Li, M. Yan et al., "MicroRNA-193a-3p and -5p suppress the metastasis of human non-small-cell lung cancer by downregulating the ERBB4/PIK3R3/mTOR/S6K2 signaling pathway," *Oncogene*, vol. 34, no. 4, pp. 413–423, 2015.

[13] C. Fang, C.-Y. Dai, Z. Mei et al., "microRNA-193a stimulates pancreatic cancer cell repopulation and metastasis through

modulating TGF-β2/TGF-βRIII signalings," *Journal of Experimental and Clinical Cancer Research*, vol. 37, no. 1, p. 25, 2018.

[14] H. Jin, N. Sanjo, T. Uchihara et al., "Presenilin-1 holoprotein is an interacting partner of sarco endoplasmic reticulum calcium-ATPase and confers resistance to endoplasmic reticulum stress," *Journal of Alzheimer's Disease*, vol. 20, no. 1, pp. 261–273, 2010.

[15] J. Wang, R. Lu, J. Yang et al., "TRPC6 specifically interacts with APP to inhibit its cleavage by γ-secretase and reduce Aβ production," *Nature Communications*, vol. 6, no. 1, p. 8876, 2015.

[16] Y. Takahashi, Y. Ohta, R. Sasaki et al., "A novel presenilin 1 mutation (Leu418Trp) associated with spasticity, parkinsonism, and white matter lesion in a dominant alzheimer's family," *Journal of the Neurological Sciences*, vol. 387, pp. 166–169, 2018.

[17] Y. Zhao, X. Li, T. Huang et al., "Intracellular trafficking of TREM2 is regulated by presenilin 1," *Experimental and Molecular Medicine*, vol. 49, no. 12, p. e405, 2017.

[18] F. Meng, L. Qian, L. Lv et al., "miR-193a-3p regulation of chemoradiation resistance in oesophageal cancer cells via the PSEN1 gene," *Gene*, vol. 579, no. 2, pp. 139–145, 2016.

[19] S. Wang, Y. Wu, S. Yang et al., "miR -874 directly targets AQP3 to inhibit cell proliferation, mobility and EMT in non-small cell lung cancer," *Thoracic Cancer*, vol. 11, no. 6, pp. 1550–1558, 2020.

[20] D. D. Zhou, H. L Li, W. Liu et al., "miR-193a-3p promotes the invasion, migration, and mesenchymal transition in glioma through regulating BTRC," *BioMed Research International*, vol. 2021, Article ID 8928509, 22 pages, 2021.

[21] E. C. Lai, "Micro RNAs are complementary to 3′ UTR sequence motifs that mediate negative post-transcriptional regulation," *Nature Genetics*, vol. 30, no. 4, pp. 363-364, 2002.

[22] A. Gargalionis and E. Basdra, "Insights in microRNAs biology," *Current Topics in Medicinal Chemistry*, vol. 13, no. 13, pp. 1493–1502, 2013.

[23] L. Wang, X. Wang, and X. Jiang, "miR-127 suppresses gastric cancer cell migration and invasion via targeting Wnt7a," *Oncology Letters*, vol. 17, no. 3, pp. 3219–3226, 2019.

[24] Y.-N. Wang, F. Xu, P. Zhang et al., "MicroRNA-575 regulates development of gastric cancer by targeting PTEN," *Biomedicine and Pharmacotherapy*, vol. 113, Article ID 108716, 2019.

[25] A. Korourian, Z. Madjd, R. Roudi, A. Shariftabrizi, and M. Soleimani, "Induction of miR-31 causes increased sensitivity to 5-FU and decreased migration and cell invasion in gastric adenocarcinoma," *Bratislavské lekárske listy*, vol. 120, no. 1, pp. 35–39, 2019.

[26] A. Azimzadeh-Isfanjani, R. Safaralizadeh, M. Hosseinpour-Feizi, B. Shokouhi, M. Nemati, and S.-Y. Moaddab, "Expression of miR-520c in intestinal type gastric adenocarcinoma," *Journal of Gastrointestinal Oncology*, vol. 9, no. 6, pp. 1184–1189, 2018.

[27] Y. Liu, X Xu, X. Xu et al., "MicroRNA-193a-3p inhibits cell proliferation in prostate cancer by targeting cyclin D1," *Oncology Letters*, vol. 14, no. 5, pp. 5121–5128, 2017.

[28] Y. Pan, J. Hu, J. Ma et al., "MiR-193a-3p and miR-224 mediate renal cell carcinoma progression by targeting alpha-2,3-sialyltransferase IV and the phosphatidylinositol 3 kinase/Akt pathway," *Molecular Carcinogenesis*, vol. 57, no. 8, pp. 1067–1077, 2018.

[29] Y. Yi, J. Chen, C. Jiao et al., "Upregulated miR-193a-3p as an oncogene in esophageal squamous cell carcinoma regulating cellular proliferation, migration and apoptosis," *Oncology Letters*, vol. 12, no. 6, pp. 4779–4784, 2016.

[30] Q. Huang, G. Voloudakis, Y. Ren et al., "Presenilin1/γ-secretase protects neurons from glucose deprivation-induced death by regulating miR-212 and PEA15," *The FASEB Journal*, vol. 32, no. 1, pp. 243–253, 2018.

[31] P. Li, X. Lin, J.-R. Zhang et al., "The expression of presenilin 1 enhances carcinogenesis and metastasis in gastric cancer," *Oncotarget*, vol. 7, no. 9, pp. 10650–10662, 2016.

[32] H. Deng, L. Lv, Y. Li et al., "The miR-193a-3p regulated PSEN1 gene suppresses the multi-chemoresistance of bladder cancer," *Biochimica et Biophysica Acta (BBA) - Molecular Basis of Disease*, vol. 1852, no. 3, pp. 520–528, 2015.

Hindawi
Journal of Oncology
Volume 2021, Article ID 3881932, 10 pages
https://doi.org/10.1155/2021/3881932

Research Article

The Effect and Mechanism of lncRNA NR2F1-As1/miR-493-5p/MAP3K2 Axis in the Progression of Gastric Cancer

Xiaobin Liao,[1] **Linbao Wen**,[2] **and Liqiong Luo**[3]

[1]*Department of General Surgery, South Hospital of Tongchuan People's Hospital, Tongchuan 727100, China*
[2]*Department of Neurosurgery, The Second Affiliated Hospital of Guizhou University of Traditional Chinese Medicine, Guiyang 550003, China*
[3]*Department of Oncology, Lanzhou New District First People's Hospital, Lanzhou 730300, China*

Correspondence should be addressed to Liqiong Luo; luoliqiong@lzdyyy.cn

Received 8 June 2021; Accepted 2 July 2021; Published 14 July 2021

Academic Editor: Muhammad Wasim Khan

Background. LncRNA NR2F1-AS1 has been identified as an oncogene in some human tumors, such as breast cancer, nonsmall cell lung cancer, and esophageal squamous cell carcinoma. Nonetheless, whether NR2F1-AS1 is involved in the progression of gastric cancer (GC) remains unknown. *Methods*. The expression patterns of NR2F1-AS1, MAP3K2, and miR-493-5p in GC tissues and cells were detected by RT-qPCR. The protein expression of MAP3K2 was assessed by the Western blotting assay. The MTT assay and flow cytometry were performed to measure cell proliferation and cell apoptosis in GC cells. The transwell assay was adopted to assess cell migration in GC cells. The relationship between NR2F1-AS1, MAP3K2, and miR-493-5p was verified by a dual-luciferase reporter assay. *Results*. The increased NR2F1-AS1 and MAP3K2 expressions were discovered in GC tissues and cells compared with control groups. Knockdown of NR2F1-AS1 and MAP3K2 dramatically suppressed cell proliferation and migration, while it enhanced cell apoptosis in GC cells. In addition, NR2F1-AS1 was found to be a sponge of miR-493-5p, and MAP3K2 was a downstream gene of miR-493-5p. Moreover, the expression of MAP3K2 was notably reduced by miR-493-5p, and NR2F1-AS1 counteracted the inhibition of miR-493-5p. *Conclusion*. Thus, NR2F1-AS1 was verified to regulate GC cell progression by sponging miR-493-5p to upregulate MAP3K2 expression.

1. Introduction

Gastric cancer (GC) is a malignant tumor derived from the epithelium of the gastric mucosal epithelium. GC accounts for the third in all malignant tumors, the first among gastrointestinal cancer, and 95% of gastric malignancies. The morbidity and mortality of GC are the third and fifth among human malignant tumors, respectively [1]. In view of the high morbidity and mortality of GC, the study on the etiology of GC has attracted many scholars. Studies have shown that obesity, gastroesophageal reflux, unreasonable diet, *Helicobacter pylori* infection, and atrophic gastritis are all high-risk factors for GC [2–4]. At present, surgical resection of the tumor is still the main method for the treatment of GC in clinical practice [5]. But the recurrence rate of GC patients after surgery is high, leading to a poor prognosis [6]. The key of targeted therapy is to find the genes and proteins that play a key role in the development of GC and to intervene against them, so as to achieve the purpose of treatment. At present, the targeted therapy of GC has made a substantial progress [7, 8].

LncRNAs regulate gene expression at multiple levels, including changing chromatin status, binding to miRNAs and mRNAs to regulate genes' expression, and binding to RNA-binding proteins to mediate intracellular signaling [9, 10]. In recent years, great progress has been made in the research on the relationship between lncRNAs and tumor development and metastasis [11, 12]. H19 was negatively correlated with the prognosis of GC and played the carcinogenic role by regulating miRNAs and genes in GC [13–15]. PINT was found to suppress tumor progression by the crosstalk with miR-21 in GC [16]. LncRNA NR2F1-AS1

was found to play a special role in some cancers. NR2F1-AS1 was found to accelerate cell angiogenesis in breast cancer and was associated with breast cancer recurrence [17, 18]. In addition, previous research studies have verified that NR2F1-AS1 functions as an oncogene in nonsmall cell lung cancer, endometrial cancer, and esophageal squamous cell carcinoma [19–21]. On the contrary, NR2F1-AS1 suppressed cell growth by modulating miR-371-3p/TOB1 axis in colorectal cancer [22]. However, the information on the effect of NR2F1-AS1 in GC is limited.

In the current article, we first examined the expression levels of NR2F1-AS1 and MAP3K2 in GC and explored their effect on cell proliferation, cell apoptosis, and cell migration in GC. Furthermore, the regulatory network of NR2F1-AS1/miR-493-5p/MAP3K2 in GC was also explored.

2. Materials and Methods

2.1. Patients and Clinical Tissues Samples. The tissue samples of 44 GC patients at South Hospital of Tongchuan People's Hospital were collected for our experiments. Specimens from each patient included GC tissues and matched distal nontumor tissues. Before surgery, none of the patients had received any preoperative radiotherapy, chemotherapy, or immunotherapy. This study was approved by the Ethics Committee of South Hospital of Tongchuan People's Hospital. The patients or their families have signed the informed consent.

2.2. Cell Lines. Human normal gastric mucosa epithelial cell line (GES-1) and GC cell lines (HGC-27, AGS, MKN-74, and SNU-5) were obtained from the Typical Cell Bank of Chines Academy of Sciences (Shanghai, China). The cells were cultured in the Roswell Park Memorial Institute 1640 (RPMI-1640) medium containing 10% foetal bovine serum (FBS), penicillin, and streptomycin. The culture atmosphere of the cell incubator was 37°C, 5% CO_2, and 95% humidity. Cell passage was carried out when the cell confluence reached 80%.

2.3. RT-qPCR. Total RNA was obtained from GC tissues or cells by using TRIzol. Then, the cDNA was synthesized by using a reverse transcription kit. 2 μl reverse transcription product was taken for PCR reaction. The PCR reaction system was SYBR Green Master Mix 10 μL, forward and reverse primers 0.8 μL each, cDNA 3 μL, and ddH_2O 7.4 μL. Reaction conditions were 95°C for 2 min; 95°C for 15 s, 60°C for 30 s, 72°C for 30 s, and a total of 40 cycles. GAPDH was used as an internal reference for NR2F1-AS1 and MAP3K2, while U6 was used as an internal reference for miR-493-5p. The relative expressions of NR2F1-AS1, MAP3K2, and miR-493-5p were calculated by the $2^{-\triangle\triangle CT}$ method. Primer sequences are given in Table 1.

2.4. Cell Transfection. AGS and MKN-74 cells were selected for the functional experiments. NR2F1-AS1 si-RNA (5′-UAAUAGAAAUAUUGAGAACAU-3′), MAP3K2 si-RNA, and their corresponding negative control si-NC (5′-AAGACAUUGUGUGUCCGCCTT-3′), pcDNA-NR2F1-AS1, and its negative control pcDNA, miR-493-5p mimic, and its negative control miR-NC were obtained from GenePharma (Shanghai, China). The transfections were carried out by Lipofectamine 3000. AGS and MKN-74 cells were cultured in an incubator at 37°C and 5% CO_2. After transfection for 48 h, AGS and MKN-74 cells were collected for the functional experiments.

Table 1: Primers sequences.

Gene		Primer sequences
NR2F1-AS1	Forward	5′- CAGCGGTGCAAACCATGTGC-3′
	Reverse	5′- GCAAGTTGGCTGAACCAAATG-3′
miR-493-5p	Forward	5′- TCCTACGGAGAGGCTCAG-3′
	Reverse	5′- TCCTCGTAGTCCAACACG-3′
MAP3K2	Forward	5′-GCTTACGGTCTCCTGTGAGTT-3′
	Reverse	5′-AGGATTGTCTATGTCACTTCCCC-3′
U6	Forward	5′-CTCGCTTCGGCAGCACA-3′
	Reverse	5′-AACGCTTCACGAATTTGCGT-3′
GAPDH	Forward	5′-GAGTCAACGGATTTGGTCGT-3′
	Reverse	5′-TTGATTTTGGAGGGATCTCG-3′

2.5. Western Blot Assay. The protein expression of MAP3K2 was detected by the Western blot assay. Cells in each group were collected to extract the total protein, and the protein concentration was detected by the BCA method. 30 μg protein was electrophoresized by SDS-PAGE and then transferred to the PVDF membrane. Next, it was sealed with 5% skim milk for 2 h and added primary antibody (anti-MAP3K2, 1 : 1000) at 4°C overnight. After washing with TBST, secondary antibody (goat-anti-mouse, 1 : 1000) was added to incubate for 1 h. The gray values of each strip were measured by the gel imaging analysis system and Image J software.

2.6. Cell Proliferation. Cells were seeded in a 96-well plate with a cell density of 5×10^3 cells/well. After cultured at 37°C for 1–3 days, 10 μl MTT (5 g/L) was added. After incubation for 4 h, cells were added with 150 μl dimethyl sulfoxide and incubated for 10 min. Cell proliferation was indirectly reflected by measuring the OD at 490 nm.

2.7. Cell Migration. AGS and MKN-74 cells were seeded in the upper chamber of the transwell chamber. We added 600 μl Dulbecco's Modified Eagle Medium (DMEM) medium with 10% FBS to the lower chamber. The chamber was incubated in a 5% CO_2 incubator at 37°C for 24 h. After washing with phosphate buffer saline (PBS), cells were fixed and stained by paraformaldehyde and 0.1% crystal violet. Finally, the number of migrated cells was measured by the microscope.

2.8. Cell Apoptosis. AGS and MKN-74 cells were centrifuged at 1000 r/min for 5 min, and the supernatant was discarded.

Then, cells were added with 5 μL Annexin V-FITC and PI. Finally, cell apoptosis was detected by flow cytometry after incubation at room temperature in dark.

2.9. Dual-Luciferase Reporter Assay. NR2F1-AS1-WT, NR2F1-AS1-MUT, MAP3K2-WT, and MAP3K2-MUT were obtained from GenePharma (Shanghai, China). Cells were transfected with miR-493-5p mimic and miR-NC, respectively. After transfection for 48 h, the luciferase activity was detected according to the requirements of the dual-luciferase reporter kit.

2.10. Statistical Analysis. The measurement data were presented as mean ± SD. Data were analyzed by using SPSS 21.0 statistical software. The comparison between the two groups was analyzed by the t-test. The chi-square test was performed to compare the two groups. $P < 0.05$ was the result of the statistical difference.

3. Results

3.1. NR2F1-AS1 and MAP3K2 Were Overexpressed in GC Tissues and Cells. To investigate the role of NR2F1-AS1 and MAP3K2 in the progression of GC, the expression levels of NR2F1-AS1 and MAP3K2 were assessed by RT-qPCR. Results reflected an upward trend of NEAT1 expression in GC tissues compared with control tissues (Figure 1(a)). Next, NR2F1-AS1 was obviously upregulated in GC cells (AGS, HGC-27, MKN-74, and SNU-5) compared with GES-1 cells (Figure 1(b)). Next, we investigated the relationship between NEAT1 expression and overall survival rate. GC patients with high NR2F1-AS1 expression had a shorter survival time than those with low NR2F1-AS1 expression (Figure 1(c)). Moreover, MAP3K2 was identified as an ascending expression in GC tissues compared with control tissues (Figure 1(d)). Subsequently, MAP3K2 was highly expressed in GC cells compared to the normal cells (Figure 1(e)). Furthermore, there was a positive correlation between NR2F1-AS1 and MAP3K2 in GC tissues (Figure 1(f)). Therefore, NR2F1-AS1 and MAP3K2 may play a special role in the development of GC.

3.2. Knockdown of NR2F1-AS1 Repressed Cell Proliferation and Migration, While It Induced Cell Apoptosis of Cells. The expression of NR2F1-AS1 was significantly decreased when AGS and MKN-74 cells were transfected with NR2F1-AS1 si-RNA (Figure 2(a)). Then, the effect of NR2F1-AS1 on GC cell progression was detected by MTT, transwell assay, and FCM. As shown in Figures 2(b) and 2(c), after transfection with NR2F1-AS1 si-RNA, the OD value in GC cells decreased significantly. Compared with the control group, the migration ability of GC cells was obviously suppressed by NR2F1-AS1 knockdown (Figure 2(e)). In contrast, NR2F1-AS1 knockdown obviously accelerated the cell apoptosis rate of GC cells (Figure 2(d)).

3.3. Inhibition of MAP3K2 Suppressed Cell Proliferation and Migration and Enhanced Cell Apoptosis of GC Cells. In the same way, AGS and MKN-74 cells were transfected with MAP3K2 si-RNA. As shown in Figure 3(a), the protein expression of MAP3K2 was obviously reduced after cells were transfected with MAP3K2 si-RNA. Compared with the control group, MAP3K2 knockdown notably blocked cell proliferation in GC cells (Figures 3(b) and 3(c)). Similarly, MAP3K2 knockdown suppressed GC cell migration in cells compared with the control group (Figure 3(d)). As we expected, the cell apoptosis rate was ascended when GC cells were transfected with MAP3K2 knockdown (Figure 3(e)).

3.4. NR2F1-AS1 Targeted miR-493-5p, and MAP3K2 Was a Target Gene of miR-493-5p in GC Cells. LncRNAs have been reported to play their roles in human cancers by targeting miRNAs to regulate the downstream genes. In the current study, StarBase and TargetScan were used to predict the binding sequences between NR2F1-AS1, miR-493-5p, and MAP3K2 (Figures 4(a) and 4(b)). Then, we found that the luciferase activity of the NR2F1-AS1-WT group was notably declined after treatment with miR-493-5p mimic, while transfection of miR-493-5p mimic had no significant effect on the luciferase activity of the NR2F1-AS1-MUT group (Figures 4(c) and 4(d)). Next, RT-qPCR results displayed that the expression of miR-493-5p was increased in GC cells treated with NR2F1-AS1 knockdown, but declined when cells were treated with NR2F1-AS1 (Figures 4(e) and 4(f)). Similar experiments displayed that miR-493-5p mimic decreased the luciferase activity of MAP3K2-WT, but not MAP3K2-MUT (Figures 4(g) and 4(h)). In addition, the expression of MAP3K2 was notably descended by miR-493-5p mimic, while it was increased by the miR-493-5p inhibitor (Figures 4(i) and 4(j)).

3.5. Downregulation of MAP3K2 Induced by miR-493-5p Could Be Recovered by Transfection with NR2F1-AS1 in GC Cells. We noticed that the protein expression of MAP3K2 was notably reduced by miR-493-5p mimic, while NR2F1-AS1 retarded the inhibiting effect of miR-493-5p on MAP3K2 expression (Figures 5(a) and 5(b)). Therefore, NR2F1-AS1 regulated GC cell progression by inhibiting miR-493-5p to upregulate MAP3K2 expression.

4. Discussion

NR2F1-AS1 is verified to be aberrantly expressed in several human tumors and plays an important role in the development of tumors. NR2F1-AS1 was upregulated in hepatocellular carcinoma (HCC), and downregulated NR2F1-AS1 was found to suppress cell growth and EMT progression and promote cell apoptosis of HCC cells [23]. Moreover, high NR2F1-AS1 expression was associated with poor OS, and silencing of NR2F1-AS1 blocked HCC cell hypoxia-induced glycolysis [24]. Furthermore, NR2F1-AS1 knockdown was reported to suppress cell invasion, migration, and cell growth, while it induced cell apoptosis in osteosarcoma cells by miR-483-3p and FOXA1 [25]. Whereas, the role of

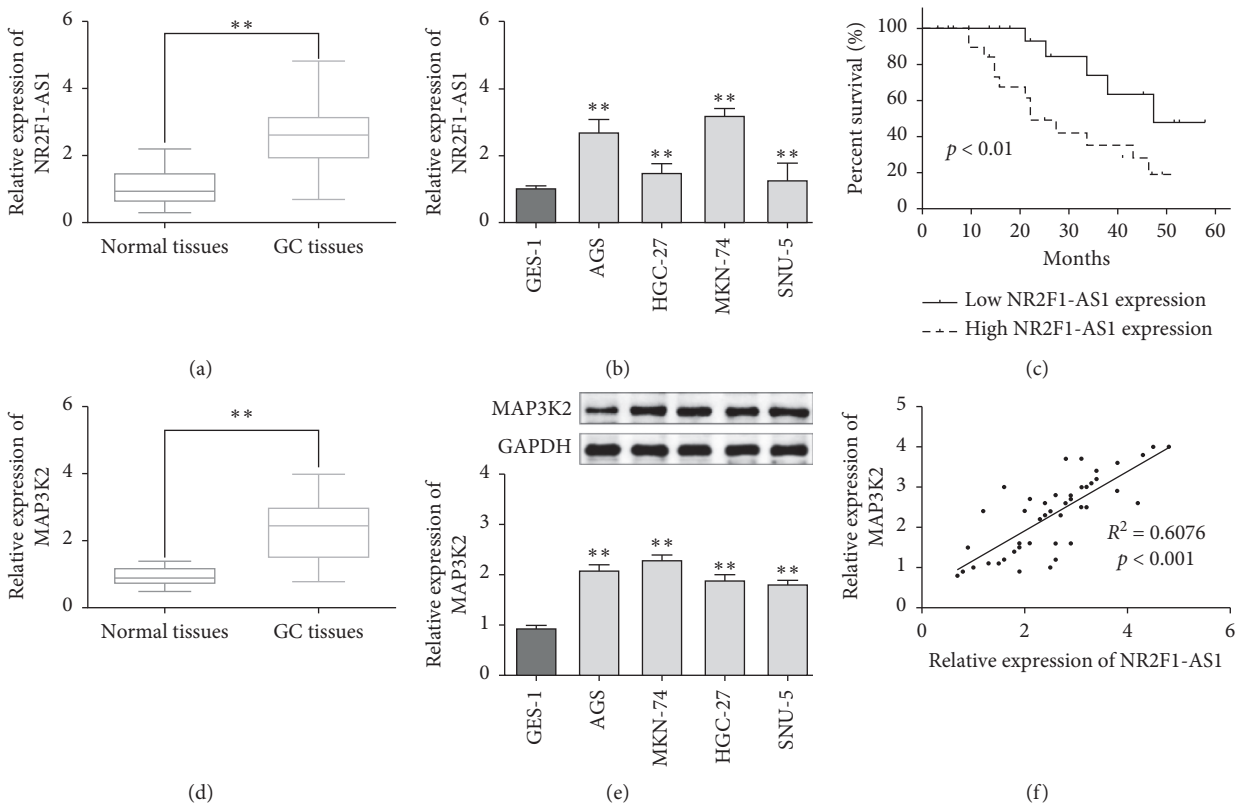

Figure 1: NR2F1-AS1 and MAP3K2 highly expressed in GC tissues and cells. (a, b) The expression of NR2F1-AS1 in 44 GC tissues and cell lines. (c) The relationship between NR2F1-AS1 and overall survival of GC patients. (d, e) The expression of NR2F1-AS1 in 44 GC tissues and cell lines. (f) The relationship between NR2F1-AS1 and MAP3K2 in GC tissues. $^{**}P < 0.01$.

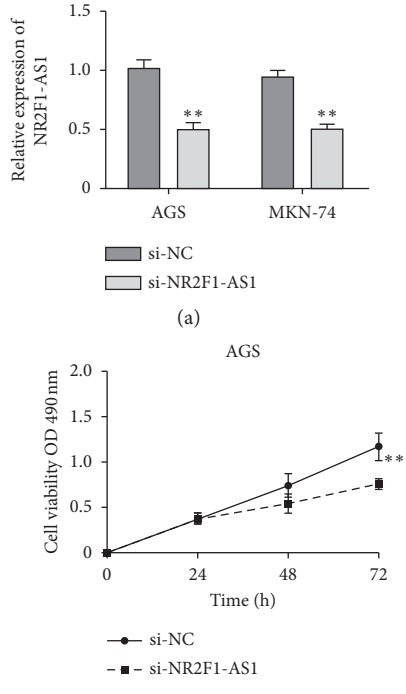

Figure 2: Continued.

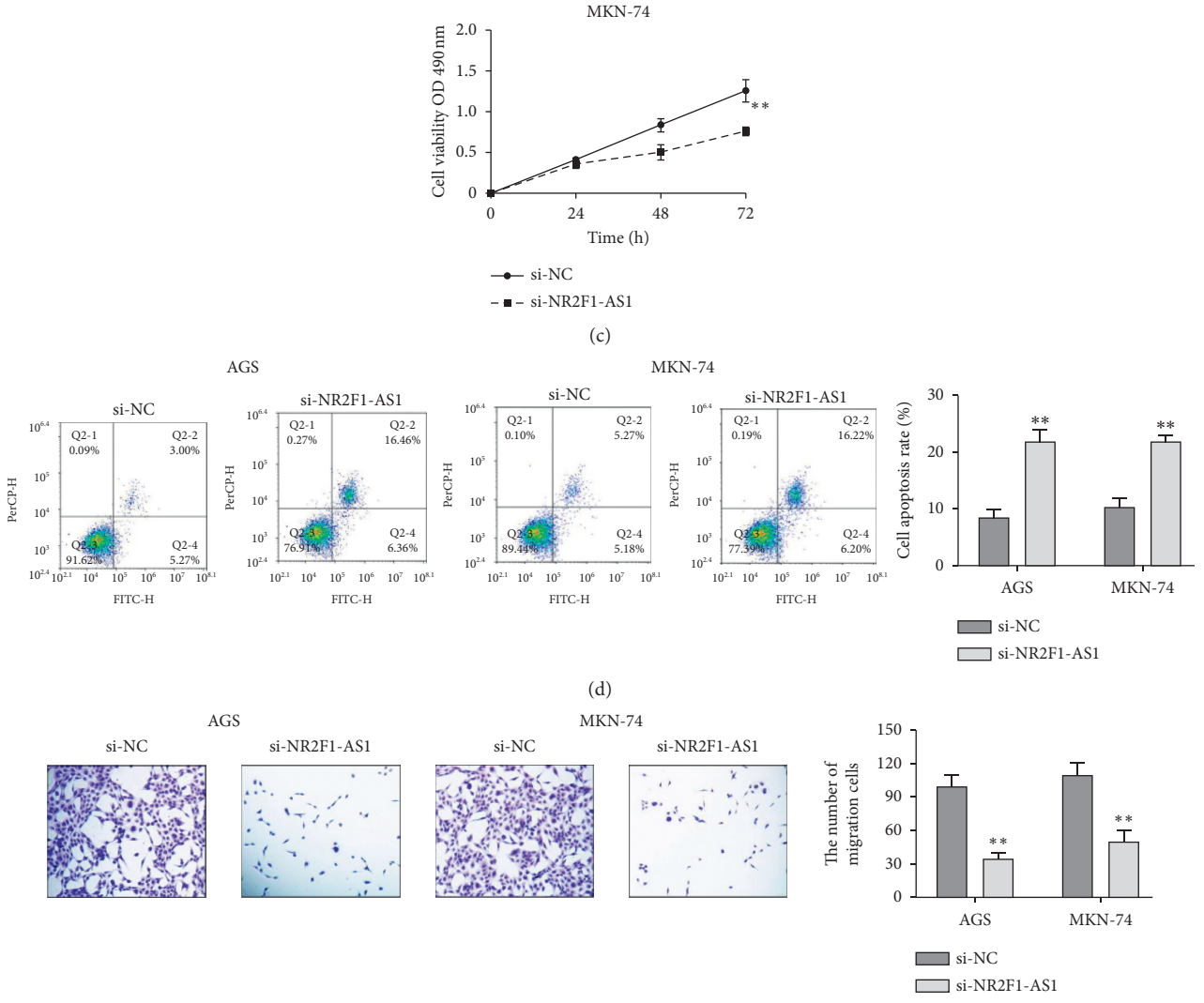

Figure 2: Knockdown of NR2F1-AS1 repressed cell proliferation and migration, while induced cell apoptosis of cells. (a) The expression of NR2F1-AS1 in AGS cells and MKN-74 cells transfected with NR2F1-AS1 si-RNA. (b, c) Cell proliferation in AGS cells and MKN-74 cells with si-NR2F1-AS1. (d) Cell apoptosis in AGS cells and MKN-74 cells with si-NR2F1-AS1. (e) Cell migration in AGS cells and MKN-74 cells with si-NR2F1-AS1 (scale bar = 100 μm). $^{**}P < 0.01$.

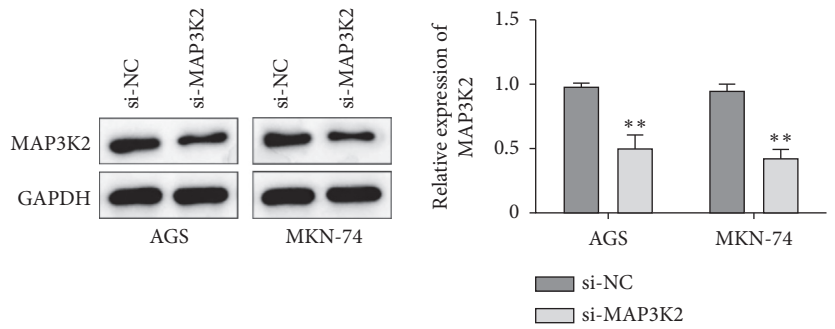

Figure 3: Continued.

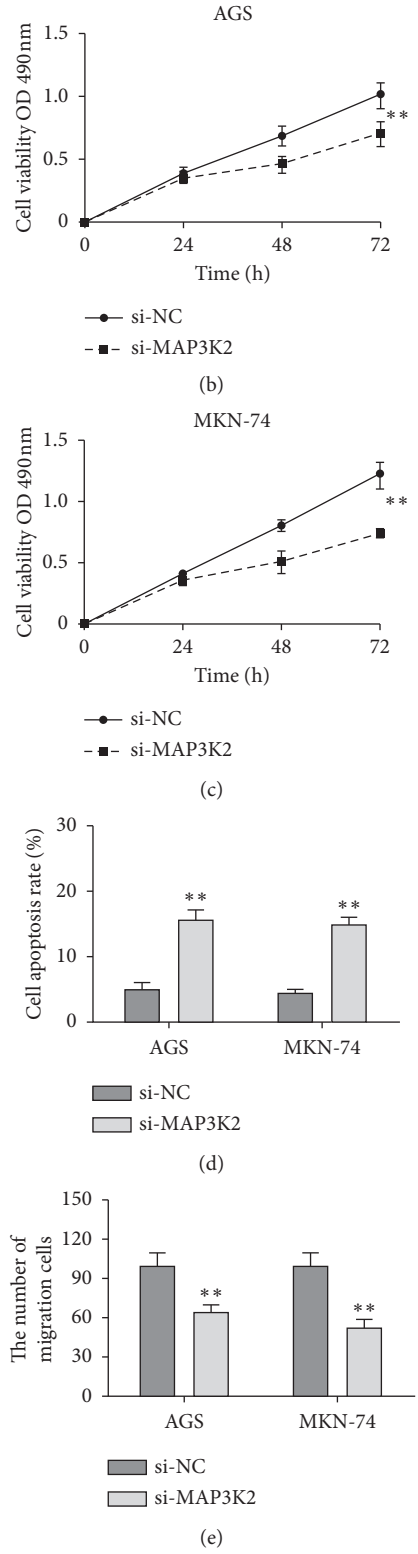

Figure 3: Inhibition of MAP3K2 suppressed cell proliferation and migration and enhanced cell apoptosis of GC cells. (a) The expression of MAP3K2 in AGS cells and MKN-74 cells with si-MAP3K2. (b, c) Cell proliferation in AGS cells and MKN-74 cells with si-MAP3K2. (d) Cell apoptosis in AGS cells and MKN-74 cells with si-MAP3K2. (e) Cell migration in AGS cells and MKN-74 cells with si-MAP3K2. $^{**}P < 0.01$.

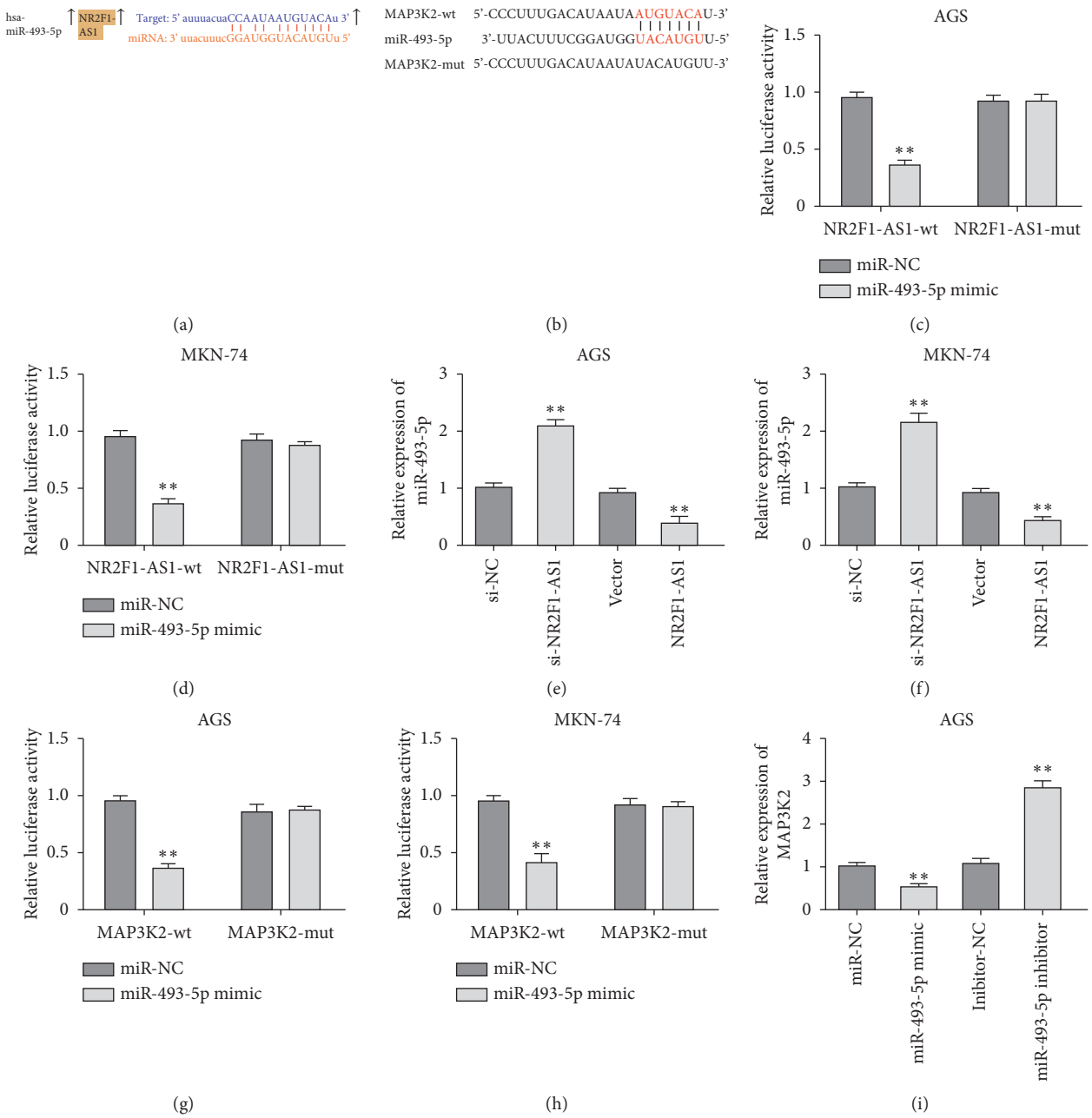

Figure 4: Continued.

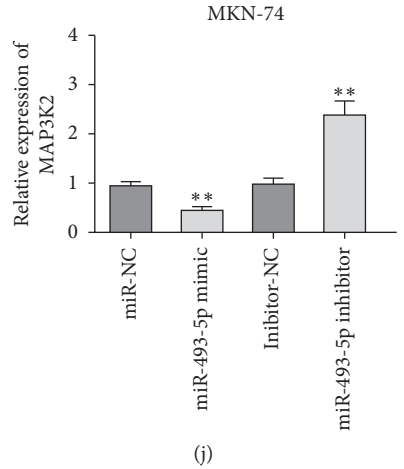

Figure 4: NR2F1-AS1 targeted miR-493-5p, while MAP3K2 was a target gene of miR-493-5p in GC cells. (a) The binding sites between NR2F1-AS1 and miR-493-5p. (b) The binding sites between MAP3K2 and miR-493-5p. (c, d) The effect of miR-493-5p on the luciferase activity of NR2F1-AS1-WT and NR2F1-AS1-MUT. (e, f) The expression of miR-493-5p in AGS cells and MKN-74 cells with si-NR2F1-AS1 or NR2F1-AS1. (g, h) The effect of miR-493-5p on the luciferase activity of MAP3K2-WT and MAP3K2-MUT. (i, j) The expression of MAP3K2 in AGS cells and MKN-74 cells with miR-493-5p mimic or miR-493-5p inhibitor. $^{**}P < 0.01$.

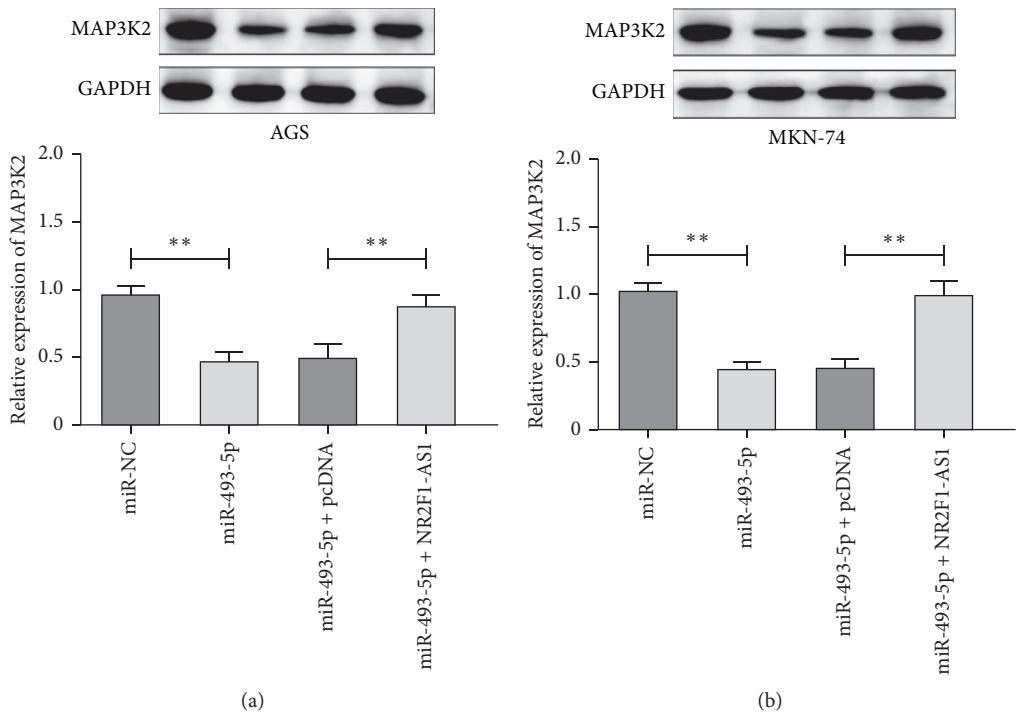

Figure 5: Downregulation of MAP3K2 induced by miR-493-5p could be recovered by transfection with NR2F1-AS1 in GC cells. (a) The expression of MAP3K2 in AGS cells with miR-493-5p or NR2F1-AS1. (b) The expression of MAP3K2 in MKN-74 cells with miR-493-5p or NR2F1-AS1. $^{**}P < 0.01$.

NR2F1-AS1 in GC is not well-understood. In our experiment, we detected the expression level of NR2F1-AS1 in GC. Moreover, functional experiments were performed to measure the effect of NR2F1-AS1 on GC progression. Additionally, the possible carcinogenic mechanism of NR2F1-AS1 in GC was discussed through molecular biology experiments.

We noticed that NR2F1-AS1 was notably overexpressed in GC tissues and cell lines. Our results were similar to previous reports. NR2F1-AS1 was highly expressed in melanoma, endometrial cancer, and cancer esophageal squamous cell carcinoma [19, 26, 27]. Furthermore, to detect the role of NR2F1-AS1 on GC progression, we knocked down the expression of NR2F1-AS1 in AGS and MKN-74

cells. Our results displayed that NR2F1-AS1 knockdown dramatically blocked cell proliferation and migration, while it enhanced cell apoptosis of GC cells. Similarly, NR2F1-AS1 downregulation was found to inhibit cell growth, migration, invasion, and the EMT process in esophageal squamous cell carcinoma cells [26]. Contrary to our findings, NR2F1-AS1 was displayed to play as an antigene in colorectal cancer and cervical squamous cell carcinoma [22, 28].

LncRNAs were reported to play vital roles in tumor progression by sponging miRNAs to regulate downstream genes. In papillary thyroid carcinoma, NR2F1-AS1 acted as an oncogene by sponging miR-423-5p to upregulate SOX12 expression [29]. In the current study, miR-493-5p was a target of NR2F1-AS1, and MAP3K was a downstream gene of miR-493-5p. Mitogen-activated protein kinase 2 (MAP3K2) is a member of the MAP3K family with known roles in activating JNK and other kinases in the MAP pathway [30, 31]. MAP3K2 is reported to be necessary for the activation of ERK1/2 and MEK1/2 [32]. We found that MAP3K2 was significantly overexpressed in GC, and silence of MAP3K2 inhibited cell proliferation and migration, but facilitated cell apoptosis in GC cells. In line with our data, MAP3K2 was reported to be an oncogene in nonsmall cell lung cancer and triple-negative breast cancer [33, 34]. Furthermore, MAP3K2 was significantly reduced by miR-493-5p mimic, while NR2F1-AS1 retarded the inhibitory effect of miR-493-5p. Finally, the network of NR2F1-AS1/miR-493-5p/MAP3K2 in GC progression was constructed.

5. Conclusion

In sum, NR2F1-AS1 was verified to be an oncogene in GC. Furthermore, we confirmed that NR2F1-AS1 regulated GC progression by sponging miR-493-5p to accelerate MAP3K2 expression. Therefore, our results suggested that NR2F1-AS1 might be a therapeutic target for patients with GC. However, the effect of NR2F1-AS1/miR-493-5p/MAP3K2 on the relevant pathways and the possible regulatory mechanism in the process of GC progression still need to be further studied.

Data Availability

The data used to support the findings of this study are available from the corresponding author upon request.

Conflicts of Interest

The authors declare that they have no conflicts of interest.

Authors' Contributions

Xiaobin Liao and Linbao Wen contributed equally to the article.

References

[1] F. Bray, J. Ferlay, I. Soerjomataram, R. L. Siegel, L. A. Torre, and A. Jemal, "Global cancer statistics 2018: GLOBOCAN estimates of incidence and mortality worldwide for 36 cancers in 185 countries," *CA: A Cancer Journal for Clinicians*, vol. 68, no. 6, pp. 394–424, 2018.

[2] M. Plummer, S. Franceschi, J. Vignat, D. Forman, and C. de Martel, "Global burden of gastric cancer attributable toHelicobacterpylori," *International Journal of Cancer*, vol. 136, no. 2, pp. 487–490, 2015.

[3] A. Ferro, V. Rosato, M. Rota et al., "Meat intake and risk of gastric cancer in the stomach cancer pooling (StoP) project," *International Journal of Cancer*, vol. 147, no. 1, pp. 45–55, 2020.

[4] H. Zafar, M. H. Kiani, F. Raza et al., "Design of enzyme decorated mucopermeating nanocarriers for eradication of *H. pylori* infection," *Journal of Nanoparticle Research*, vol. 22, no. 1, p. 4, 2020.

[5] F. Raza, H. Zafar, S Zhang et al., "Recent advances in cell membrane-derived biomimetic nanotechnology for cancer immunotherapy," *Advanced Healthcare Materials*, vol. 10, no. 6, Article ID e2002081, 2021.

[6] T. Hanyu, A. Wakai, T. Ishikawa, H. Ichikawa, H. Kameyama, and T. Wakai, "Carcinoma in the remnant stomach during long-term follow-up after distal gastrectomy for gastric cancer: analysis of cumulative incidence and associated risk factors," *World Journal of Surgery*, vol. 42, no. 3, pp. 782–787, 2018.

[7] L. Jiang, X. Gong, W. Liao, N. Lv, and R. Yan, "Molecular targeted treatment and drug delivery system for gastric cancer," *Journal of Cancer Research and Clinical Oncology*, vol. 147, no. 4, pp. 973–986, 2021.

[8] T. Seidlitz, Y.-T. Chen, H. Uhlemann et al., "Mouse models of human gastric cancer subtypes with stomach-specific CreERT2-mediated pathway alterations," *Gastroenterology*, vol. 157, no. 6, pp. 1599–1614, 2019.

[9] J. Zhou, J. Liu, H. Xing et al., "Implications of protein ubiquitination modulated by lncRNAs in gastrointestinal cancers," *Biochemical Pharmacology*, vol. 188, Article ID 114558, 2021.

[10] G. Militello, T. Weirick, D. John, C. Döring, S. Dimmeler, and S. Uchida, "Screening and validation of lncRNAs and circRNAs as miRNA sponges," *Briefings in Bioinformatics*, vol. 18, no. 5, pp. 780–788, 2017.

[11] K. Taniue and N. Akimitsu, "The functions and unique features of LncRNAs in cancer development and tumorigenesis," *International Journal of Molecular Sciences*, vol. 22, no. 2, p. 632, 2021.

[12] K.-T. Jin, J.-Y. Yao, X.-L. Fang, H. Di, and Y.-Y. Ma, "Roles of lncRNAs in cancer: focusing on angiogenesis," *Life Sciences*, vol. 252, Article ID 117647, 2020.

[13] H. Zhou, W. Shen, H. Zou, Q. Lv, and P. Shao, "Circulating exosomal long non-coding RNA H19 as a potential novel diagnostic and prognostic biomarker for gastric cancer," *Journal of International Medical Research*, vol. 48, no. 7, Article ID 300060520934297, 2020.

[14] J. Yan, Y. Zhang, Q. She et al., "Long noncoding RNA H19/miR-675 Axis promotes gastric cancer via FADD/caspase 8/caspase 3 signaling pathway," *Cellular Physiology and Biochemistry*, vol. 42, no. 6, pp. 2364–2376, 2017.

[15] G. Liu, T. Xiang, Q.-F. Wu, and W.-X. Wang, "Long noncoding RNA H19-derived miR-675 enhances proliferation and invasion via RUNX1 in gastric cancer cells," *Oncology Research Featuring Preclinical and Clinical Cancer Therapeutics*, vol. 23, no. 3, pp. 99–107, 2016.

[16] H. Feng, J. Zhang, Y. Shi, L. Wang, C. Zhang, and L. Wu, "Long noncoding RNA LINC-PINT is inhibited in gastric

cancer and predicts poor survival," *Journal of Cellular Biochemistry*, vol. 120, no. 6, pp. 9594–9600, 2019.

[17] A. Sanchez Calle, T. Yamamoto, Y. Kawamura et al., "Long non-coding NR2F1-AS1 is associated with tumor recurrence in estrogen receptor-positive breast cancers," *Molecular Oncology*, vol. 14, no. 9, pp. 2271–2287, 2020.

[18] Q. Zhang, T. Li, Z. Wang, X. Kuang, N. Shao, and Y. Lin, "lncRNA NR2F1-AS1 promotes breast cancer angiogenesis through activating IGF-1/IGF-1R/ERK pathway," *Journal of Cellular and Molecular Medicine*, vol. 24, no. 14, pp. 8236–8247, 2020.

[19] L. Wang, S. Zhao, and Y. U. Mingxin, "LncRNA NR2F1-AS1 is involved in the progression of endometrial cancer by sponging miR-363 to target SOX4," *Die Pharmazie*, vol. 74, no. 5, pp. 295–300, 2019.

[20] P. Ren, H. Zhang, L. Chang, X. D. Hong, and L. Xing, "LncRNA NR2F1-AS1 promotes proliferation and metastasis of ESCC cells via regulating EMT," *European Review for Medical and Pharmacological Sciences*, vol. 24, no. 7, pp. 3686–3693, 2020.

[21] C. Zhang, S. Wu, R. Song, and C. Liu, "Long noncoding RNA NR2F1-AS1 promotes the malignancy of non-small cell lung cancer via sponging microRNA-493-5p and thereby increasing ITGB1 expression," *Aging*, vol. 13, no. 5, pp. 7660–7675, 2020.

[22] J. Wang, S. Dong, J. Zhang et al., "LncRNA NR2F1-AS1 regulates miR-371a-3p/TOB1 Axis to suppress proliferation of colorectal cancer cells," *Cancer Biotherapy and Radiopharmaceuticals*, vol. 35, no. 10, pp. 760–764, 2020.

[23] W.-C. Ji, G.-J. Bao, F.-W. Yang, L. Sun, and R. Han, "Role of lncRNA NR2F1-AS1 and lncRNA H19 genes in hepatocellular carcinoma and their effects on biological function of huh-7," *Cancer Management and Research*, vol. 13, pp. 941–951, 2021.

[24] X. Li, Y. Li, S. Bai, J. Zhang, Z. Liu, and J. Yang, "NR2F1-AS1/miR-140/HK2 Axis regulates hypoxia-induced glycolysis and migration in hepatocellular carcinoma," *Cancer Management and Research*, vol. 13, pp. 427–437, 2021.

[25] S. Li, K. Zheng, Y. Pei, W. Wang, and X. Zhang, "Long noncoding RNA NR2F1-AS1 enhances the malignant properties of osteosarcoma by increasing forkhead box A1 expression via sponging of microRNA-483-3p," *Aging*, vol. 11, no. 23, pp. 11609–11623, 2019.

[26] Y. Zhang, A. Zheng, R. Xu et al., "NR2F1-induced NR2F1-AS1 promotes esophageal squamous cell carcinoma progression via activating Hedgehog signaling pathway," *Biochemical and Biophysical Research Communications*, vol. 519, no. 3, pp. 497–504, 2019.

[27] M. Bai, Z. Z. Wu, Y. L. Huang, J. Ke, Q. Xu, and X. Wang, "STAT3 activates the transcription of lncRNA NR2F1-AS1 to promote the progression of melanoma via regulating the miR-493-5p/GOLM1 axis," *The Journal of Gene Medicine*, vol. 23, no. 7, Article ID e3338, 2021.

[28] J. Peng, F. Hou, W. Zhu, J. Li, and Z. Teng, "lncRNA NR2F1-AS1 regulates miR-17/SIK1 Axis to suppress the invasion and migration of cervical squamous cell carcinoma cells," *Reproductive Sciences*, vol. 27, no. 7, pp. 1534–1539, 2020.

[29] C. Yang, Z. Liu, X. Chang et al., "NR2F1-AS1 regulated miR-423-5p/SOX12 to promote proliferation and invasion of papillary thyroid carcinoma," *Journal of Cellular Biochemistry*, vol. 121, no. 2, pp. 2009–2018, 2020.

[30] B. Su, J. Cheng, J. Yang, and Z. Guo, "MEKK2 is required for T-cell receptor signals in JNK activation and interleukin-2 gene expression," *Journal of Biological Chemistry*, vol. 276, no. 18, pp. 14784–14790, 2001.

[31] C.-D. Ji, Y.-X. Wang, D.-F. Xiang et al., "Kir2.1 interaction with Stk38 promotes invasion and metastasis of human gastric cancer by enhancing MEKK2-MEK1/2-ERK1/2 signaling," *Cancer Research*, vol. 78, no. 11, pp. 3041–3053, 2018.

[32] P. Colón-Bolea and P. Crespo, "Lysine methylation in cancer: SMYD3-MAP3K2 teaches us new lessons in the Ras-ERK pathway," *BioEssays*, vol. 36, no. 12, pp. 1162–1169, 2014.

[33] T. Huang, K. She, G. Peng et al., "MicroRNA-186 suppresses cell proliferation and metastasis through targeting MAP3K2 in non-small cell lung cancer," *International Journal of Oncology*, vol. 49, no. 4, pp. 1437–1444, 2016.

[34] J. Wu, W.-Z. Li, M.-L. Huang et al., "Regulation of cancerous progression and epithelial-mesenchymal transition by miR-34c-3p via modulation of MAP3K2 signaling in triple-negative breast cancer cells," *Biochemical and Biophysical Research Communications*, vol. 483, no. 1, pp. 10–16, 2017.

Hindawi
Journal of Oncology
Volume 2021, Article ID 9994535, 9 pages
https://doi.org/10.1155/2021/9994535

Research Article

Advanced Xenograft Model with Cotransplantation of Patient-Derived Organoids and Endothelial Colony-Forming Cells for Precision Medicine

Junhye Kwon,[1] Sungryong Oh,[2,3] Misun Park,[1] Joon Seog Kong,[4] Sunyi Lee,[2,3] Hyunsook Lee,[2,3] Younjoo Kim,[5] Kyu-Tae Kang,[2,3] Ui Sup Shin,[6] and Joohee Jung[2,3]

[1]*Department of Radiological & Clinical Research, Korea Cancer Center Hospital, Korea Institute of Radiological and Medical Sciences (KIRAMS), Seoul 01812, Republic of Korea*
[2]*College of Pharmacy, Duksung Women's University, Seoul 01369, Republic of Korea*
[3]*Duksung Innovative Drug Center, Duksung Women's University, Seoul 01369, Republic of Korea*
[4]*Department of Pathology, Korea Cancer Center Hospital, KIRAMS, Seoul 01812, Republic of Korea*
[5]*Department of Internal Medicine, Korea Cancer Center Hospital, KIRAMS, Seoul 01812, Republic of Korea*
[6]*Department of Surgery, Korea Cancer Center Hospital, KIRAMS, Seoul 01812, Republic of Korea*

Correspondence should be addressed to Kyu-Tae Kang; ktkang@duksung.ac.kr, Ui Sup Shin; uisupshin@kirams.re.kr, and Joohee Jung; joohee@duksung.ac.kr

Received 22 March 2021; Accepted 2 July 2021; Published 14 July 2021

Academic Editor: Muhammad Wasim Khan

Preclinical evaluation models have been developed for precision medicine, with patient-derived xenograft models (PDXs) and patient-derived organoids (PDOs) attracting increasing attention. However, each of these models has application limitations. In this study, an advanced xenograft model was established and used for drug screening. PDO and endothelial colony-forming cells (ECFCs) were cotransplanted in NRGA mice (PDOXwE) to prepare the model, which could also be subcultured in Balb/c nude mice. Our DNA sequencing analysis and immunohistochemistry results indicated that PDOXwE maintained patient genetic information and tumor heterogeneity. Moreover, the model enhanced tumor growth more than the PDO-bearing xenograft model (PDOX). The PDO, PDOXwE, and clinical data were also compared in the liver metastasis of a colorectal cancer patient, demonstrating that the chemosensitivity of PDO and PDOXwE coincided with the clinical data. These results suggest that PDOXwE is an improvement of PDOX and is suitable as an evaluation model for precision medicine.

1. Introduction

Precision medicine, which encompasses personalized medicine, is important for the implementation of optimized anticancer therapy. Moreover, preclinical evaluation models are indispensable in screening for the sensitivity of anticancer drugs. Patient-derived organoids (PDOs) have been established as an *in vitro* model for various cancers [1]. This model embodies the function and genetic information of a patient's tissue and could be maintained for an expanded period [2]. PDOs have emerged as a high-throughput screening system in anticancer drug prognosis and development [3]. Although PDOs recapitulate the features of tissues, they cannot emulate the tumor microenvironment. Therefore, several anticancer drugs that interrupt the crosstalk between cancer cells and surrounding cells could not be evaluated using this model. Consequently, *in vivo* animal models are required for an accurate prognosis before clinical application. Recently, patient-derived xenograft models (PDXs) directly transplanted with patient tissue and PDO-bearing xenograft models (PDOXs) have been established [4]. By contrast, PDXs and PDOX can preserve cancer

heterogeneity and the genetic information of the patient's tissue, as well as mimic the tumor microenvironment. However, the establishment rate of PDXs remain low [5, 6] because patient tissue is composed of cancer cells and stroma and this ratio is not constant. The PDOX could improve on the disadvantages of PDX. Nevertheless, the PDX and PDOX protocols have not yet been optimized because they differ depending on the cancer type. Furthermore, the time required for the establishment of PDX and PDOX remains a limiting factor in their application on anticancer drug screening.

In this study, an advanced xenograft model was developed using colorectal cancer (CRC) patient-derived tissues to overcome the limitations of PDOX. CRC is known to cause liver metastasis, and its progression can lead to death [7]. Thus, a strategy for the inhibition of CRC progression is important in increasing survival rate. In particular, there is an urgent need for anticancer drugs optimized for accuracy in anticancer therapy applications. Hence, we investigated the sensitivity of anticancer drugs in advanced xenograft models of CRC and liver metastatic CRC.

2. Materials and Methods

2.1. Human Tissue Acquisition and Patient Treatment. The protocol for this section of the study was approved by the Ethics Committee of the Korea Cancer Center Hospital (approval no. KIRAMS-2017-07-001 and KIRAMS-2017-09-009) and was performed in accordance with the approved guidelines and regulations of the institution. All samples were obtained from patients who provided written informed consent for the use of their tissues. Surgically resected liver metastatic intestinal cancer tissue (LMT) and endoscopic biopsy intestinal cancer tissues were obtained from patients diagnosed with CRC and treated at the Korea Cancer Center Hospital. The collected samples were also histologically verified as adenocarcinoma by a pathologist using hematoxylin and eosin (H&E) staining. The isolation of the tumor epithelium was performed as previously described with minor modifications [8, 9].

For chemotherapy, the LMT patient was treated with an irinotecan-based regimen (FOLFIRI). The FOLFIRI regimen consisted of 180 mg/m^2 irinotecan, 400 mg/m^2 bolus 5-fluorouracil (5-FU), and 2400 mg/m^2 infusional 5-FU every two weeks. The patient's response to chemotherapy was evaluated after every three cycles with computed tomography (CT, Ingenuity, Philips Healthcare, Amsterdam, the Netherlands) as scored using Response Evaluation Criteria In Solid Tumors 1.1.

2.2. Organoid Culture. The tumor organoids were isolated as previously described [10]. Briefly, cancer tissues were incubated with collagenase type II (Sigma-Aldrich, Louis, MO, USA), dispase type II (Roche Applied Science, Mannheim, Germany), and Y-27632 (BioVision, Mountain View, CA, USA) for 1 h at 37°C. Isolated cells were washed with PBS and centrifuged at 300 ×g for 3 min. The cells were then embedded in Matrigel (growth factor reduced, phenol red free; Corning, NY, USA) and seeded in 4-well plates, followed by the addition of the culture medium. The composition of the CRC organoid culture medium was 1 × B27 (Gibco, Grand Island, NY, USA), 1.25 mM N-acetyl cysteine (United States Pharmacopeia, Rockville, MD, USA), 50 ng/mL human epidermal growth factor (BioVision), 50 ng/mL human Noggin (Peprotech, Rocky Hill, NJ, USA), 10 nM gastrin (Sigma-Aldrich), 500 nM A83-01 (BioVision), and 100 mg/mL primocin (InvivoGen, San Diego, CA, USA). To prevent anoikis, 10 μM Y-27632 was added to the culture medium during the first 2-3 days. When organoids were >200 μm, they were passaged by pipetting using the Gentle Cell Dissociation Reagent (STEMCELL Technologies, Vancouver, Canada) according to the manufacturer's instructions.

2.3. Organoid Viability. LMT organoids in good condition were harvested, passaged, and seeded in 96-well cell culture plates. The organoid density was adjusted to 50–60/10 μL Matrigel with 200 μL culture medium. For drug testing, the organoid culture medium was removed and replaced with a 200 μL drug-containing culture medium: 2.5 mg/mL cetuximab (Erbitux, Merck), irinotecan (I1406, Merck), or oxaliplatin (O9512, Sigma). Organoids were photographed seven days after drug treatment (EVOS FL Cell Imaging System, Thermo Fisher Scientific), and cell viability was also evaluated at seven days by the CellTiter 96 Aqueous One Solution cell assay (Promega, G3580) according to the manufacturer's instructions.

2.4. Culture of Human Endothelial Colony-Forming Cells. Endothelial colony-forming cells (ECFCs) were isolated from the adherent mononuclear cell fraction of human peripheral blood using CD31-coated magnetic beads (Invitrogen, MA, USA) as previously described [11]. Isolated ECFCs were expanded on 1% gelatin-coated plates (BD Biosciences, NJ, USA) using an endothelial cell growth medium MV 2 (EGM-MV 2 without hydrocortisone; PromoCell, Heidelberg, Germany) supplemented with 10% fetal bovine serum (Atlas Biologicals, CO, USA) and 1% glutamine-penicillin-streptomycin (Gibco, MA, USA). ECFCs between passages seven and ten were used in all of the experiments. The protocol for this section of the study was approved by the institutional review board of Duksung Women's University (IRB Nos. 2017-002-001 and 2018-007-006).

2.5. Animal Handling. All animal experiments were carried out following the protocol approved by the Institutional Animal Care and Use Committee of Duksung Women's University (No. 2019-012-001). Five-week-old female and male NOD/ShiLtJ-Rag2em1AMC (NRGA) mice and Balb/c nude mice were purchased from JUNGA Bio (Gyeonggi, Korea). All animals were acclimated to the animal laboratory of Duksung Women's University for one week prior

to any procedural work. The room conditions were maintained at 20°C, 50% humidity, and a 12/12 h light/dark cycle. The diet was provided with drinking water ad libitum.

2.6. Organoid-Derived Xenograft Models. Cultured organoids were collected and implanted into the subcutaneous pockets of NRGA mice. For the coimplantation of organoids and ECFCs, ECFCs were prepared at 1×106 cells/100 μL in 10% Matrigel (YoungIn Frontier, Korea) and injected subcutaneously around the implanted organoid. To subculture the organoid-derived xenograft model, organoid-derived tumors were isolated and sliced into 1-2 mm^3 sections. One piece of tumor tissue was subcutaneously implanted into the second generation of Balb/c nude mice (G2). Subsequently, the G2 xenograft mouse models were used to investigate the efficacy of anticancer drugs. Tumor size was measured using a caliper (Mitutoyo Corporation, Japan) three times per week. The tumor volume was calculated as follows:

$$\text{Tumor volume}\left(mm^3\right) = \frac{(\text{longest length}) \times (\text{shortest length})^2}{2}. \quad (1)$$

When the tumor volume reached approximately 100 mm^3, the mice were randomly divided into groups ($n = 5$/group).

2.7. Immunohistochemistry. To characterize organoids and their tissues of origin, immunohistochemistry was performed using the colorectal marker CDX2 (1 : 200; cat. no. 235R-16; Cellmarque), CK7 (1 : 10000; cat. no. ab181598; Abcam), and CK20 (1 : 500; cat. no. 320M-16; Cellmarque) in 5 μm formalin-fixed paraffin-embedded tissues and organoid sections (28114961). All images were acquired using an OLYMPUS IX73 (Olympus, Germany).

2.8. Tumor Organoid DNA Sequencing and Analysis. To analyze the mutational status of patient tissues, organoids, and PDOX tissues, DNA extraction and library construction were performed using the Qiagen Gentra Puregene kit (Valencia, CA, USA) and Agilent SureSelect XT library prep kit (Santa Clara, CA, USA). Deep targeted sequencing using Axen Cancer Panel 2 (170 cancer-related genes, Macrogen) and the NextSeq 500 midoutput system platform (Illumina) was conducted on tumor tissues, organoids, and PDOX samples. Libraries consisting of 150 bp paired-end reads were sequenced by high-throughput sequencing using synthesis technology to a depth coverage of approximately 2000x. An oncoplot was used for the visualization of the mutations of the tissue, organoid, and PDOX.

2.9. Drug Treatment. Intraperitoneal injections of the test drugs were administered following this treatment schedule: oxaliplatin (5 mg/kg, three times/week), irinotecan (20 mg/kg, five times/week), and/or cetuximab (10 mg/kg, twice a week).

2.10. Statistics. Data are presented as the mean ± standard deviation. Statistical significance was set at $p < 0.05$ and was calculated using Student's t test and one-way ANOVA followed by Tukey's post hoc test.

3. Results

3.1. PDOX Maintains Patient-Derived Properties. The sensitivity of anticancer drugs was predicted by screening using the PDO and PDOX models (Figure 1(a)). In our study, we cotransplanted PDO with ECFCs in NRGA mice (G1) and subcultured PDOX (G1) with ECFCs in Balb/c nude mice (G2). First, we investigated whether PDOX maintained the characteristics of PDO. As shown in Figure 1(b), the gene expression of PDO, PDOX (G1), and PDOX (G2) coincided with each other. Moreover, the establishment period of PDO correlated with that of PDOX ($R = 0.6007$) (Figure 1(c)). The establishment period of an *in vivo* model is their limitation in precision medicine applications. Hence, we investigated whether advanced xenograft models can improve the original PDOX.

3.2. PDOX with ECFCs Overcomes the Obstacles of PDOX. The tumor growth of PDOX with ECFCs (PDOXwE) was compared with that of PDOX, because the establishment period of PDOX is an obstacle for its utilization. In 19T-PDO, the establishment of PDOX (G1) failed, but cotransplantation POD with ECFCs showed tumorigenicity (Figure 2(a), left). Furthermore, PDOXwE stimulated tumor growth more than PDOXs in the case of 5T-PDO and 8T-PDO (Figure 2(a), middle and right, respectively). Among them, 5T-PDO was also confirmed to maintain the 5T patient's properties (Figure 2(b)). Additionally, gene expression in PDOXwE coincided with that in PDO (Figure 2(c)). These results indicate that PDOXwE overcomes the obstacle of PDOX by enhancing tumorigenicity and tumor growth while maintaining the advantages of PDOX.

3.3. Drug Sensitivity Is Consistent in PDO and PDOXwE. Our results indicate that PDOX drug sensitivity was consistent with that of the patient. The chemotherapeutic efficacy of anticancer drugs was evaluated in PDOXwE and PDO, and the application validity of PDOXwE as an advanced xenograft model is shown in Figure 2. To compare preclinical data with clinical data, we used liver metastatic CRC patient-derived organoids.

As shown in Figures 3(a) and 3(b), the histopathology and DNA sequence analyses demonstrate that PDO and PDOXwE also coincided with the LMT patient's tissue. The expression of several genes was different among the tissue, PDO, and PDOXwE; nevertheless, the gene profile of PDOXwE (G2) for preclinical evaluation was almost similar to that of the tissue. After seven days of observation of the PDO model, the cytotoxicity of cetuximab was not

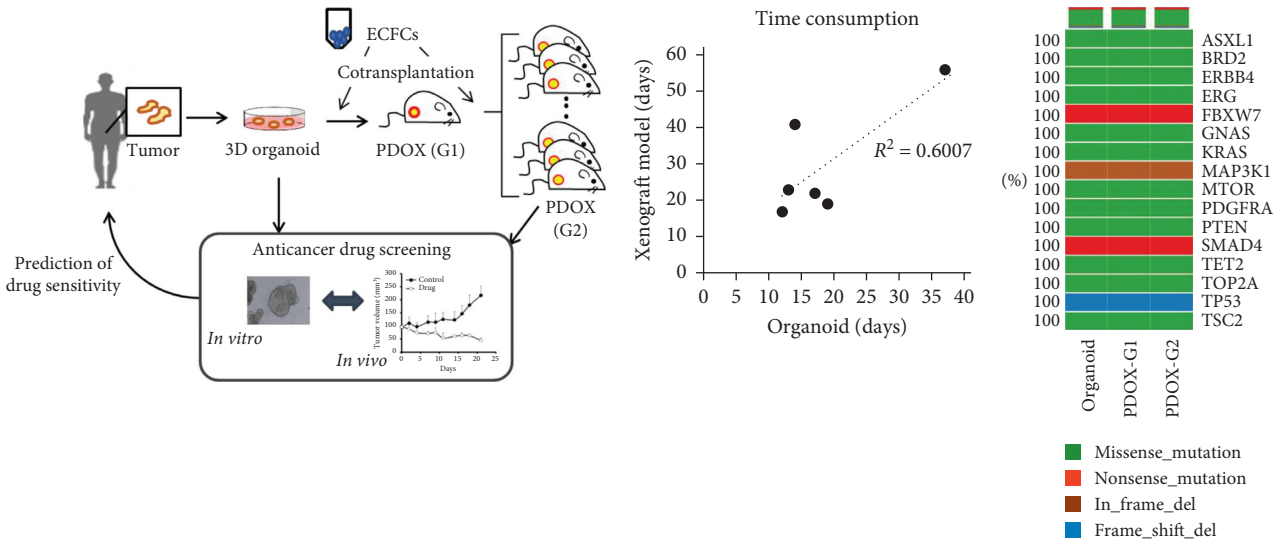

(a) (b) (c)

Figure 1: Cancer-patient-derived organoid and organoid-derived xenograft model. (a) Scheme of the *in vitro* and *in vivo* model for precision medicine. The patient-derived organoid (PDO, *in vitro* model) and patient-derived organoid-bearing xenograft models (PDOX, *in vivo* model) are utilized for anticancer drug screening. The advanced xenograft model is a PDOX cotransplanted with endothelial colony-forming cells (ECFCs). For screening, tumor tissues obtained from PDOX (1st generation, G1) were transplanted into Balb/c nude mice (2nd generation, G2). (b) Correlation of the production period between PDO and PDOX. Six cases of colorectal cancer patients were used for production of organoid and xenograft models. (c) Retention of representative gene expression in organoids and PDOX. Sixteen major genes were compared between the organoid and PDOX (G1 and G2).

significantly enhanced; by contrast, the combination of cetuximab and irinotecan significantly enhanced cytotoxicity compared to cetuximab alone (Figure 3(c)). On the other hand, the combination of cetuximab and oxaliplatin showed no difference with the use of cetuximab alone. The tumor growth of PDOXwE was significantly suppressed only when the combination of cetuximab and irinotecan was used (Figure 3(d)). Moreover, the chemotherapeutic efficacy of PDOXwE was the same as that in the PDO model. However, tumor size and weight significantly decreased in all drug-treated groups on the final day after the 3-week treatment period (Figure 3(e)). The combination of cetuximab and irinotecan inhibited the suppression of tumor growth, tumor size, and tumor weight.

3.4. Monitoring of the LMT Patient Receiving the Irinotecan-Based Regimen. As shown in Figure 3, our results suggest that irinotecan is more effective than oxaliplatin in the LMT organoid and the LMT organoid-bearing xenograft models. In the LMT organoid-supplied patient, a liver metastasis of approximately 2 cm was detected at the edge of liver segment IIb. Thus, we decided to use the FOLFIRI regimen for palliative chemotherapy based on the results of preclinical tests. We monitored the chemotherapeutic efficacy every 3 cycles using CT (Figure 4(a)). Four lesions were analyzed in every detection, and the total lesion size was calculated (Figure 4(b)). The best response to chemotherapy was achieved after the 6th cycle, and the patient remained at the stable disease status until the 9th cycle. After the 12th cycle, the size of the target lesions increased by more than 20% of the size of the best response, and we determined that the disease has progressed.

4. Discussion

In this study, chemotherapeutic efficacy was evaluated in an *in vitro* and an *in vivo* model. Drug sensitivity of the LMT patient was extrapolated based on these results and monitored using CT.

In the preclinical test, these models were expected to predict chemosensitivity in cancer patients. PDO and PDOX models must represent some of the cancer patients' attributes (growth and gene expression); thus, PDOX exhibits different sensitivities to anticancer drugs depending on a patient's organoid (Supplementary Figure 1). Practically, time constraints are addressed to applicate the results of these preclinical assessments for cancer patients. Thus, advanced xenograft models were developed through the cotransplantation of PDO and ECFCs (Figure 1(a)). The PDOXwE model improved the period of establishment, which is a limitation in the utilization of such models for preclinical evaluation (Figure 2). Moreover, our results suggest that PDOXwE could have an edge as an *in vivo* model and, particularly, as an anticancer drug screening system for precision medicine.

PDO is emerging as a model of pathophysiology because it exhibits intratumor heterogeneity [12]. Furthermore, PDO has maintainability with long-term expansion culture [2]. Thus, PDO could be used for high-throughput screening in an *in vitro* model. PDO must be an attractive *in vitro* model for development of anticancer drugs. Nevertheless, PDO

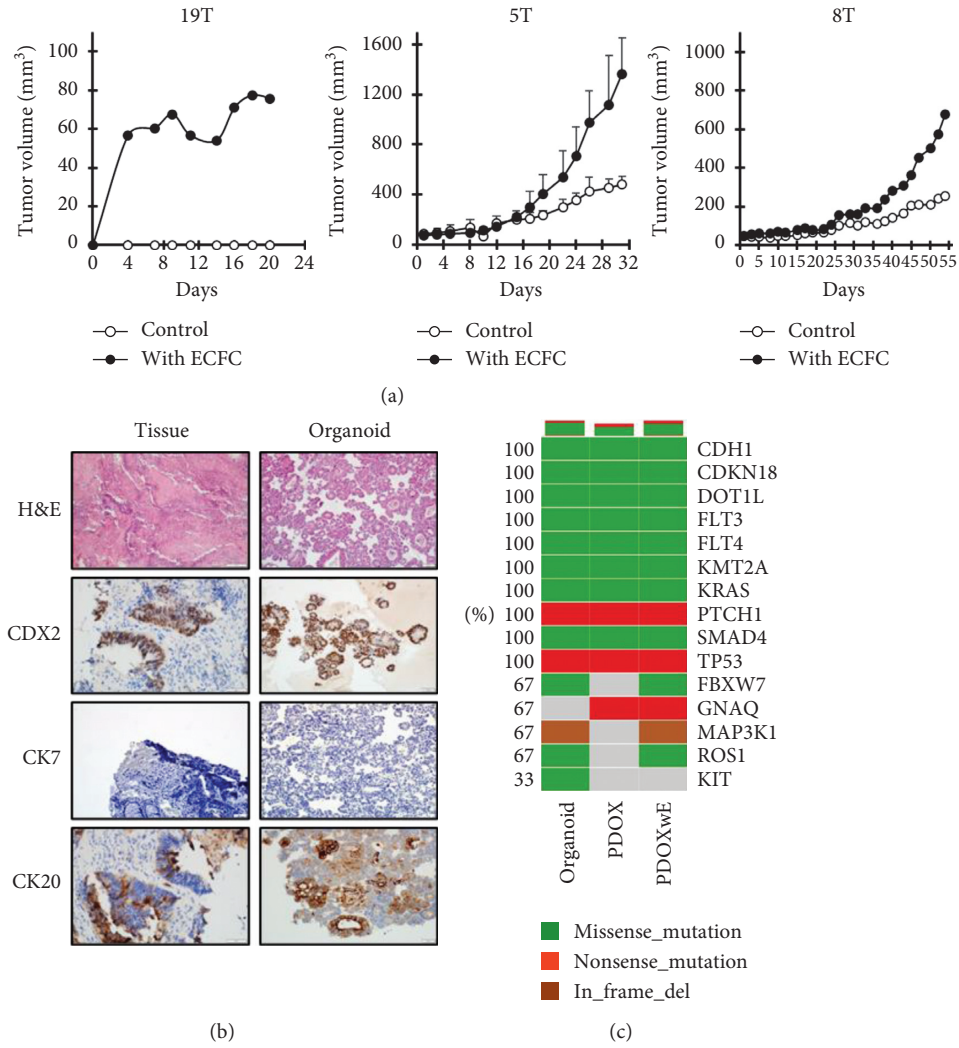

Figure 2: Enhancement of tumor growth in PDOX with ECFCs (PDOXwE). (a) Comparison of tumor growth between PDOX and PDOXwE. PDO only or PDO with ECFCs were transplanted in NRGA mice (G1 xenograft model; 19T patient) and Balb/c mice (G2 xenograft model; 5T patient, $n = 4$/group; 8T patient, $n = 1$/group) $^{*}p < 0.05$ (Student's t test). (b) Observation of the 5T patient's tumor tissue and organoid. Sections of the patient's tissue and patient-derived organoid were observed using H&E staining and immunohistochemistry (CDX2, CK7, and CK20). (c) Gene expression of the 5T patient's tumor-derived organoid, PDOX, and PDOXwE. The expression of fifteen major genes was analyzed by DNA sequencing.

could not show tumor-stroma interaction and the integratable immune system [13]. Therefore, indirect targeted anticancer agents, such as antiangiogenic agents and inhibitors of crosstalk between cancer cells and surrounding cells, are not suitable for evaluation in PDO.

To remedy PDO's shortcomings, the evaluation of anticancer agents in an *in vivo* model was required for development of chemotherapeutic agents. Transplanted materials of xenograft models for anticancer drug screening have been developed from human cancer cell lines to PDOs [4, 14]. Xenograft models could effectively evaluate the chemotherapeutic efficacy. In general, standard protocols have been established for human-cancer-cell-derived xenograft models. Thus, this model has been used easily for a long time in the field of anticancer drug development. However, this model could not show the diverse characteristics of cancer patients [15]. The PDX model improves the obstacles of the human-cancer-cell-derived xenograft model [14]. The PDX model as an avatar model represents genetic alterations and pathohistological characteristics of cancer patients [16]. Unfortunately, this model has several limitations including long establishment period and low engraftment rate [16], which may be one of the major hurdles to apply PDX models to the effective anticancer drug screening system. As an improving model, transplantation of PDO into immunodeficient mouse has been tried. The PDOX model retains the advantages of PDX. Thus, it could predict anticancer drug susceptibility just like in patients. However, these models could only be used with some organoids. Furthermore, an optimized protocol of PDOX for stable engraftment rate and rapid establishment period is not yet found. Unsolved limitations may be due to the insufficient blood supply to the cells within the PDO after implantation. Current methodologies have been improving on

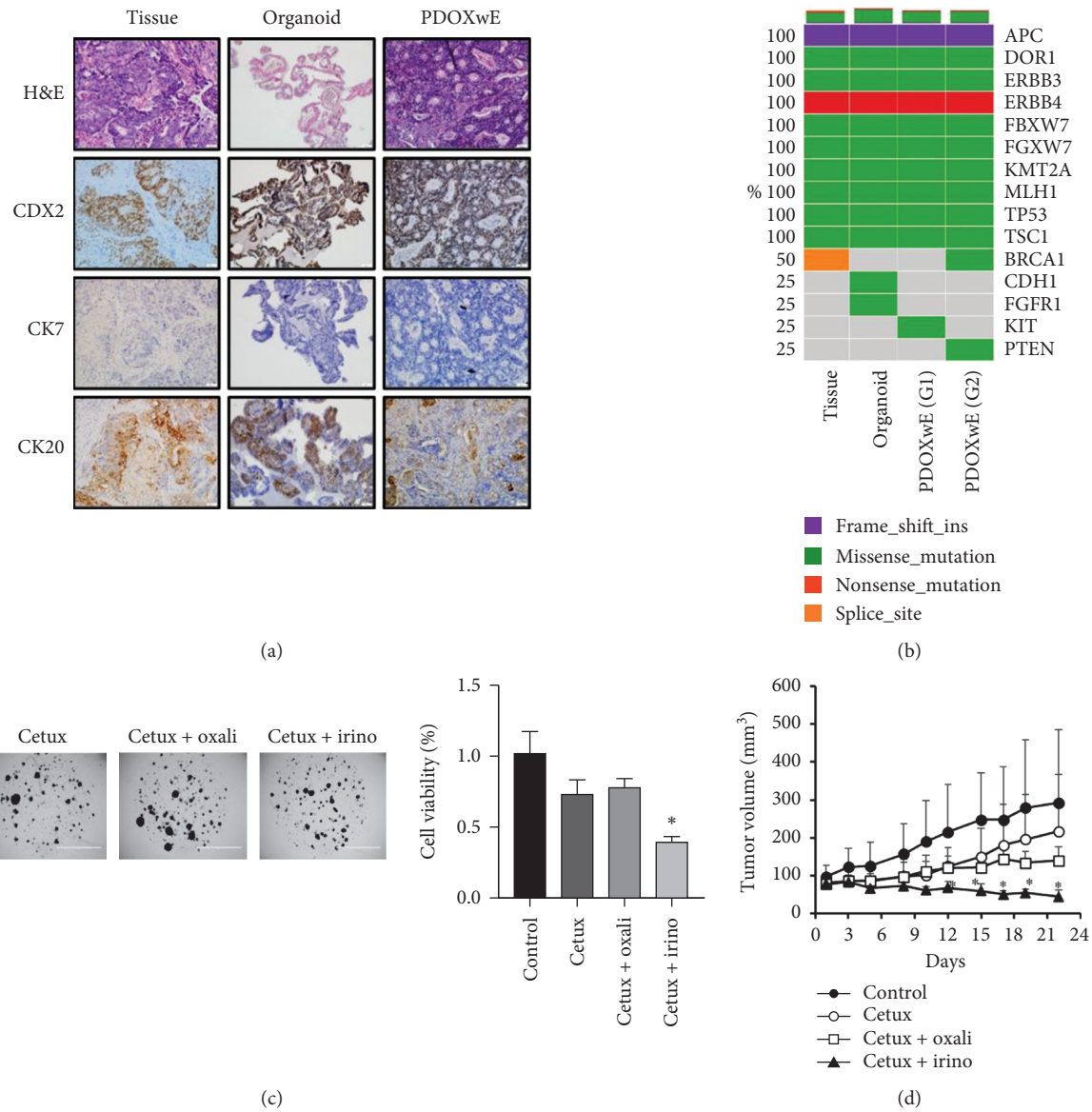

Figure 3: Continued.

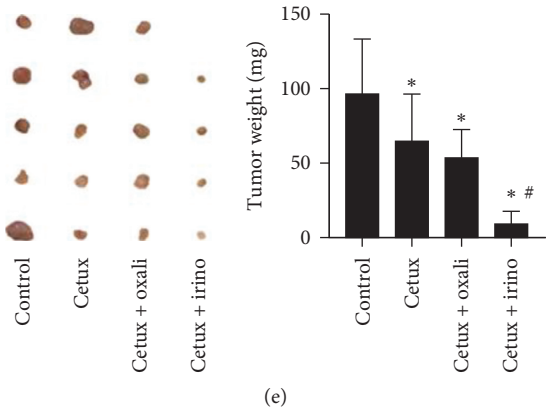

Figure 3: Combination therapeutic effect of cetuximab with irinotecan or oxaliplatin in organoids and PDOXwE of liver metastatic colorectal cancer. (a) Histopathology of the LMT patient's tumor tissue, organoid, and PDOXwE. Sections of the patient's tissue, patient-derived organoid, and PDOXwE were observed using H&E staining and immunohistochemistry (CDX2, CK7, and CK20). (b) Gene expression of the LMT patient's tumor tissue, organoid, and PDOXwE (each generation). The expression of fifteen major genes was analyzed by DNA sequencing. (c) Cytotoxicity of anticancer drugs in the organoid model. Cetuximab (oetux), oxaliplatin (oxali), and irinotecan (irino) (2.5 mg/mL, respectively) were used to treat the organoids for seven days. Organoids were photographed, and then, organoid cell viability was measured by the CellTiter 96 Aqueous One solution Cell Assay. $^{*}p < 0.05$ (one-way ANOVA test). (d) Efficacy test of anticancer drugs in PDOXwE. Cetux (10 mg/kg, two times/week), oxali (5 mg/kg, three times/week), and irino (20 mg/kg, five times/week) were intraperitoneally injected. Tumor volumes were measured three times per week. Data are expressed as the mean ± standard deviation ($n = 5$/group). $^{*}p < 0.05$ (one-way ANOVA test). (e) Comparison of tumor size and tumor weight. After measuring the final tumor volume, tumors were isolated, photographed, and weighed on a scale. $^{*}p < 0.05$ (vs. control); $^{\#}p < 0.05$ (vs. cetux) (one-way ANOVA test).

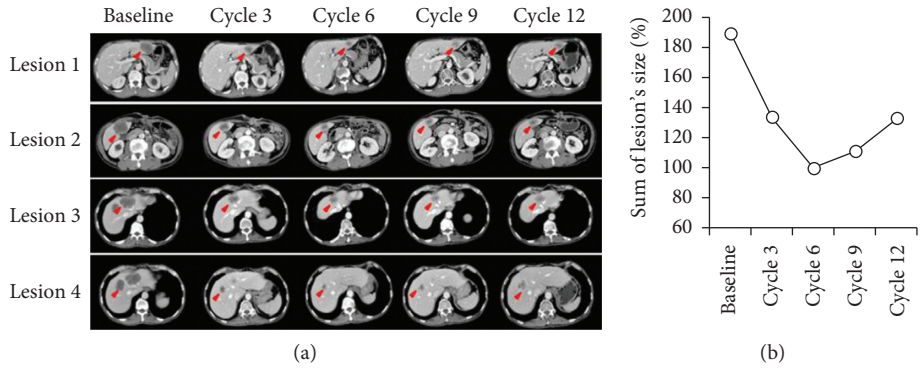

Figure 4: Chemotherapeutic efficacy in the LMT patient as observed by computed tomography (CT). (a) CT imaging of the LMT patient. The LMT patient received the FOLFIRI regimen, as described in Section 2. CT imaging was observed every three cycles of chemotherapy. Red arrows indicate cancer sites. (b) Sum of the lesions' sizes. The sizes of four lesions were summed, and then, percentage was calculated based on the sum of the lesion's size at cycle 6.

previous drawbacks, with the added advantage of being able to mimic the tumor microenvironment of patients. In this study, cotransplantation with ECFCs was tried to promote quick blood vessel formation surrounding PDO. In addition to the improvement of PDO progression, a newly formed vascular network surrounding PDO can facilitate drug delivery to the PDO and also provide the screening system to estimate indirect targeted anticancer agents. Our results indicated that the time required for PDOX establishment can be reduced by ECFCs.

ECFCs are circulating endothelial progenitor cells and contribute to neovascularization in many postnatal pathophysiological conditions. For example, circulating ECFCs are recruited into the ischemic tissues, where they are incorporated into the vascular endothelial lining and differentiate into endothelial cells to form new blood vessels [17]. Furthermore, it has been reported that about 40% of vascular endothelial cells within the tumor region are derived from ECFCs originated from the bone marrow [18]. Moreover, ECFCs have adhesiveness and migratory activities toward tumor [19]. Human-originated blood vessels are made to the vasculature of xenograft models by ECFCs around PDO. Similar to our results, human-derived blood vessels could be observed in tumor tissues of a breast cancer xenograft model by coinjection of MDA-MB-231 cells and ECFCs [20]. In our study, the transplanted PDO exhibited faster tumorigenicity and tumor growth through the blood vessels newly formed by ECFCs (Figure 2). Thus, by application of ECFCs to the PDOX models, PDOXwE can be a novel strategy to establish an effective and practicable

screening system for the personalized cancer medicine. Furthermore, our results showed that PDOXwE preserved patient genetic information, and some of the variations in gene expression were negligible (Figure 2). During anticancer drug screening, the drug sensitivity was observed to be coincident between PDO and PDOXwE (Figures 3(c) and 3(d)).

When the result of preclinical assessment was applied in chemotherapy, irinotecan was effective in the chemotherapy of the patient (Figure 4). These results indicated that PDO and PDOXwE models could predict chemotherapeutic efficacy in a patient.

5. Conclusions

In this study, PDOXwE as an advanced xenograft model was established by cotransplantation of organoids and ECFCs. The advanced xenograft model has a short establishment period and high success rate. The advanced xenograft model is an edge in preclinical modeling for precision medicine. Thus, the PDOXwE model is anticipated to be applied in precision medicine in the field of chemotherapy.

Data Availability

The data used to support the findings of this study are included within the article and the supplementary information file.

Conflicts of Interest

The authors declare that there are no conflicts of interest regarding the publication of this paper.

Acknowledgments

This work was supported by the Priority Research Centers Program through the National Research Foundation of Korea (NRF) funded by the Ministry of Education, Science, and Technology (No. 2016R1A6A1A03007648; K.T.K. and J.J.), NRF grant funded by the Ministry of Science and ICT (MSIT) (No. 2017R1A2B4008254; J.J, and 2017R1A2B4005463; K.T.K), and a grant of the Korea Institute of Radiological and Medical Sciences funded by the MSIT (No. 50542 2020; U.S.).

Supplementary Materials

Supplementary Figure 1. Sensitivity of oxaliplatin in PDOX oxaliplatin (5 mg/kg) was intraperitoneally injected in xenograft models bearing patient-derived organoids (left, 5T patient; right, 8T patient) 3 times per week for 3 weeks. Tumor size was measured 3 times per week by using a caliper. Tumor volume was calculated as follows: $0.5 \times$ (the longest diameter) $\times$ (the shortest diameter) 2. Data were presented as mean $\pm$ standard deviation ($n = 4$/group). Significance: $^{*}p < 0.05$ (Student's t test). . (*Supplementary Materials*)

References

[1] E. Driehuis, K. Kretzschmar, and H. Clevers, "Establishment of patient-derived cancer organoids for drug-screening applications," *Nature Protocols*, vol. 15, no. 10, pp. 3380–3409, 2020.

[2] L. Broutier, G. Mastrogiovanni, M. M. Verstegen et al., "Human primary liver cancer-derived organoid cultures for disease modeling and drug screening," *Nature Medicine*, vol. 23, no. 12, pp. 1424–1435, 2017.

[3] S. N. Ooft, F. Weeber, K. K. Dijkstra et al., "Patient-derived organoids can predict response to chemotherapy in metastatic colorectal cancer patients," *Science Translational Medicine*, vol. 11, no. 513, 2019.

[4] M. Jian, L. Ren, G. He et al., "A novel patient-derived organoids-based xenografts model for preclinical drug response testing in patients with colorectal liver metastases," *Journal of Translational Medicine*, vol. 18, no. 1, p. 234, 2020.

[5] X. Ji, S. Chen, Y. Guo et al., "Establishment and evaluation of four different types of patient-derived xenograft models," *Cancer Cell International*, vol. 17, no. 1, p. 122, 2017.

[6] Y. Y. Choi, J. E. Lee, H. Kim et al., "Establishment and characterisation of patient-derived xenografts as paraclinical models for gastric cancer," *Scientific Reports*, vol. 6, no. 1, p. 22172, 2016.

[7] R. L. Siegel, K. D. Miller, and A. Jemal, "Cancer statistics, 2019," *CA: A Cancer Journal for Clinicians*, vol. 69, no. 1, pp. 7–34, 2019.

[8] M. van de Wetering, H. E. Francies, J. M. Francis et al., "Prospective derivation of a living organoid biobank of colorectal cancer patients," *Cell*, vol. 161, no. 4, pp. 933–945, 2015.

[9] T. Sato, D. E. Stange, M. Ferrante et al., "Long-term expansion of epithelial organoids from human colon, adenoma, adenocarcinoma, and Barrett's epithelium," *Gastroenterology*, vol. 141, no. 5, pp. 1762–1772, 2011.

[10] M. Park, J. Kwon, H. J. Shin et al., "Butyrate enhances the efficacy of radiotherapy via FOXO3A in colorectal cancer patient-derived organoids," *International Journal of Oncology*, vol. 57, no. 6, pp. 1307–1318, 2020.

[11] J. M. Melero-Martin, M. E. De Obaldia, S.-Y. Kang et al., "Engineering robust and functional vascular networks *in vivo* with human adult and cord blood-derived progenitor cells," *Circulation Research*, vol. 103, no. 2, pp. 194–202, 2008.

[12] J. Kondo and M. Inoue, "Application of cancer organoid model for drug screening and personalized therapy," *Cells*, vol. 8, no. 5, 2019.

[13] M. Bleijs, M. van de Wetering, H. Clevers, and J. Drost, "Xenograft and organoid model systems in cancer research," *The EMBO Journal*, vol. 38, no. 15, Article ID e101654, 2019.

[14] J. Jung, "Human tumor xenograft models for preclinical assessment of anticancer drug development," *Toxicological Research*, vol. 30, no. 1, pp. 1–5, 2014.

[15] J. Jung, H. S. Seol, and S. Chang, "The generation and application of patient-derived xenograft model for cancer research," *Cancer Research and Treatment*, vol. 50, no. 1, pp. 1–10, 2018.

[16] G. J. Yoshida, "Applications of patient-derived tumor xenograft models and tumor organoids," *Journal of Hematology & Oncology*, vol. 13, no. 1, p. 4, 2020.

[17] K.-T. Kang, R.-Z. Lin, D. Kuppermann, J. M. Melero-Martin, and J. Bischoff, "Endothelial colony forming cells and mesenchymal progenitor cells form blood vessels and increase

blood flow in ischemic muscle," *Scientific Reports*, vol. 7, no. 1, p. 770, 2017.

[18] S. Rafii, D. Lyden, R. Benezra, K. Hattori, and B. Heissig, "Vascular and haematopoietic stem cells: novel targets for anti-angiogenesis therapy?" *Nature Reviews Cancer*, vol. 2, no. 11, pp. 826–835, 2002.

[19] K. Bieback, M. Vinci, S. Elvers-Hornung et al., "Recruitment of human cord blood-derived endothelial colony-forming cells to sites of tumor angiogenesis," *Cytotherapy*, vol. 15, no. 6, pp. 726–739, 2013.

[20] H. K. Lim, H. Lee, A. Moon, K.-T. Kang, and J. Jung, "Exploring protocol for breast cancer xenograft model using endothelial colony-forming cells," *Translational Cancer Research*, vol. 7, no. 5, pp. 1228–1234, 2018.

Hindawi
Journal of Oncology
Volume 2021, Article ID 6242798, 10 pages
https://doi.org/10.1155/2021/6242798

Research Article

LncRNA AFAP1-AS1 Promotes the Progression of Colorectal Cancer through miR-195-5p and WISP1

Yongsheng Li,[1] **Zhongpeng Zhu**,[2] **Xiaokun Hou**,[3] **and Yongjun Sun**[4]

[1]*Anal-Colorectal Surgery Department, Shengli Oil Field Central Hospital, Dongying 257000, China*
[2]*Oncology Department, Shengli Oil Field Central Hospital, Dongying 257000, China*
[3]*Medical Department, Shengli Oil Field Central Hospital, Dongying 257000, China*
[4]*Gastrointestinal Surgery Department, Shengli Oil Field Central Hospital, Dongying 257000, China*

Correspondence should be addressed to Yongjun Sun; yingjun530@sina.com

Yongsheng Li and Zhongpeng Zhu contributed equally to the work.

Received 26 May 2021; Accepted 25 June 2021; Published 13 July 2021

Academic Editor: Muhammad Wasim Khan

Objective. Colorectal cancer (CRC) is the most common cancer. But, the molecular mechanisms of CRC progression are not fully understood. This study was conducted to explore how the long noncoding RNA actin filament-associated protein 1-antisense RNA1 (lncRNA AFAP1-AS1) participates in CRC progression through the regulation of microRNA-195-5p (miR-195-5p) and wingless-type inducible signaling pathway protein-1 (WISP1). *Methods*. The expressions of AFAP1-AS1, miR-195-5p, and WISP1 were detected by RT-qPCR or western blot. A dual-luciferase assay confirmed the target relationship of AFAP1-AS1, miR-195-5p, and WISP1. Colony formation, wound-healing, and Transwell assays were used to detect the growth, migration, and invasion abilities of cells, respectively. *Results*. AFAP1-AS1 and WISP1 expressions were notably increased, and miR-195-5p expression was markedly reduced in CRC. The dual-luciferase assay verified that AFAP1-AS1 could bind to miR-195-5p. AFAP1-AS1 knockdown could inhibit the malignant behavior of CRC cells. miR-195-5p could target and regulate WISP1 expression. Overexpression of WISP1 or miR-195-5p inhibition reversed the inhibition effect of AFAP1-AS1 knockdown on the biological activity of CRC cells. *Conclusions*. AFAP1-AS1 knockdown may inhibit the proliferation, migration, and invasion of CRC cells through the miR-195-5p/WISP1 axis.

1. Introduction

Colorectal cancer (CRC) is a major cause of morbidity and mortality throughout the world. It accounts for over 9% of all cancer incidences and is the third most common cancer worldwide and the fourth most common cause of death [1]. In recent years, the incidence of CRC tends to be less, but the etiology is not clear. Advanced age, high-fat diet, obesity, smoking, familial polyposis, chronic inflammatory bowel disease, and other factors are considered as high-risk factors [2]. The invasion and metastasis of malignant tumors is often the main cause of treatment failure, and 40% to 50% of patients with CRC die from distant metastasis [3]. Radiotherapy and chemotherapy are used to improve symptoms and the quality of life of patients and prolong survival, but it is still not satisfactory [4]. Therefore, in-depth study on the etiology and pathogenesis of CRC is of great significance for clinical diagnosis and treatment.

LncRNAs, more than 200 nucleotide ncRNAs in length, are abnormally expressed in various types of tumor cells and involved in many malignant tumor biological behaviors [5]. With the in-depth research on lncRNAs, more and more lncRNAs were revealed to have a vital role in CRC pathogenesis and progression. Their biological functions include the regulation of proliferation, apoptosis, tumor resistance, and metastasis of CRC, which have great value in clinical diagnosis and prognosis judgment [6]. AFAP1-AS1, the antisense product of the gene encoding AFAP1, is a lncRNA with a length of 6810 nucleotides located on 4p16.1 of the human genome [7]. Recent studies have found that AFAP1-AS1 is highly expressed in many tumors and involved in the regulation of tumorigenesis and development [8]. Currently,

studies on AFAP1-AS1 have shown that AFAP1-AS1 is upregulated in CRC, suggesting that the high expression of AFAP1-AS1 involves CRC occurrence and development [9–11], but the specific mechanism of its involvement in tumor-related processes remains unclear.

As ceRNAs, lncRNAs can bind to miRNAs to affect miRNA target genes expression, thus exerting biological functions [5]. Bioinformatics software predicted that AFAP1-AS1 targets miR-195-5p and WISP1 is a miR-195-5p target gene. miR-195-5p was downregulated in CRC, and the overexpression of miR-195-5p obviously hampered the malignant behavior of CRC cells [12]. Wu et al. showed that the expression of WISP1 was increased in CRC tissues, and WISP1 downregulation could effectively hinder the cell proliferation and migration and tumor growth, providing a new target for CRC treatment [13]. Whether AFAP1-AS1 can affect the biological behavior of CRC cells through regulating miR-195-5p/WISP1 is still unknown. This study mainly explored the effects of AFAP1-AS1 on CRC progression and whether it plays a role by regulating miR-195-5p/WISP1, thus providing a target for molecular therapy of CRC.

2. Patients and Methods

2.1. Clinical Samples and Data Collection. Patients with CRC who underwent surgical treatment at Shengli Oil Field Central Hospital, Dongying, China, from January 2019 to October 2020, were selected as the research subjects. 26 pairs of CRC and matching paracancerous tissue samples were included. All samples were frozen in liquid nitrogen and stored at −80°C. This study was approved by the ethics committee of Shengli Oil Field Central Hospital. Inclusion criteria: (1) patients had not received any other form of antitumor therapy; (2) all patients had undergone surgery for the first time; (3) surgical resection was obtained, and the CRC tissue and paracancerous tissue were confirmed by pathologists; (4) complete clinicopathological data and follow-up data were obtained; and (5) the patient had no mental disorders. Exclusion criteria: (1) distant organ metastasis; (2) complicated with other types of tumors; (3) patients with severe organic diseases; and (4) ulcerative colitis, acute or chronic gastrointestinal inflammation, and autoimmune diseases. All patients signed informed consent.

2.2. Cell Culture and Transfections. Human normal colon cell lines NCM460 and CRC cell lines (SW480, SW620, HCT-8, and HCT-116) were purchased from the Cell Resource Center, Chinese Academy of Sciences (Shanghai, China). The abovementioned cells were conventionally cultured in the RPMI 1640 medium (Gibco, USA) with 10% fetal bovine serum (FBS, Gibco, USA) in a saturated humidity incubator at 37°C, 5% CO_2.

AFAP1-AS1 small interfering RNA (si-AFAP1-AS1) and disordered nonsense-negative sequence (si-NC), WISP1 overexpression vector (pc-WISP1) and empty vector (pc-NC), miR-195-5p mimic (mimic) and negative control (miR-NC), and miR-195-5p inhibitor (inhibitor) and negative control (anti-NC) were purchased from Shanghai Genepharma Co., Ltd. Cells at a logarithmic proliferative stage were inoculated into a 6-well plate at 5×10^6 cells/cm^2 that the confluence of cells at transfection was above 50%. The cells were transfected by using the Lipofectamine^{TM} 2000 liposome kit (Invitrogen, USA). After transfection for 6 h, the cells were replaced with fresh medium and cultured for 48 h.

2.3. Colony Formation Assay. Cells of each group (1×10^3 cells/well) were cultured in 6-well plates. After 14 days of culture, the medium was discarded and cells were fixed with paraformaldehyde (4%) and then stained with crystal violet (0.5%). After drying, photos were taken with a microscope and the clone numbers were observed. A colony larger than 50 cells is counted as a clone. The experiment was repeated three times independently.

2.4. Wound-Healing Assay. After trypsin digestion, cells were cultured with 6-well plates at 5×10^5 cells/ml. When the degree of cell fusion reached 100%, the cells were scratched at the bottom of the culture well with the tip of a 10 μl pipettor. After continuous culture for 48 h, the scar width was measured and the healing rate was calculated.

Scratch healing rate (%) = (scratch $\text{width}_{0\,\text{h}}$−scratch $\text{width}_{48\,\text{h}}$)/scratch $\text{width}_{0\,\text{h}} \times 100\%$. The experiment was conducted independently in triplicate.

2.5. Transwell Assay. An RPMI1640 medium without FBS was used to adjust the concentration of transfected cells to 5×10^4 cells/ml. The upper chamber of Transwell was precoated with matrigel, and 100 μl cell suspension was added. 500 μl RPMI 1640 medium containing FBS was added to the lower chamber. After incubation for 48 h, 4% paraformaldehyde was fixed for 30 min and stained with 0.4% crystal violet. An inverted microscope was selected to perform the observation and counting. The experiment was repeated three times.

2.6. Dual-Luciferase Reporter Assay. ENCORI (the encyclopedia of RNA interactomes) database (http://starbase.sysu.edu.cn/index.php) predicted that continuous binding sites exist between AFAP1-AS1 and miR-195-5p nucleotide sequences. The TargetScan database (http://www.targetscan.org/vert_72/) shows that there are miR-195-5p binding sites in the WISP1 3′UTR region. Fragments of the wild type (wt) and mutant type (mut) of AFAP1-AS1 and WISP1 were constructed and integrated into the pGL3 vector to construct a report vector (AFAP1-AS1-wt, AFAP1-AS1-mut, WISP1-wt, and WISP1-mut), respectively. Cells were transfected with miR-195-5p mimic or miR-NC with wt or mut reporter vectors, respectively. Luciferase activity was measured after 48 h transfection. Each experiment was repeated 3 times.

2.7. RT-qPCR. Total RNA was extracted from tissue and cells by the Trizol reagent (Takara, Japan) and reverse transcribed into cDNA using the RT-PCR kit (Invitrogen,

USA). RT-qPCR was performed with the SYBR Green kit (Takara, Japan) on ABI7500 Applied Biosystems. Primers are listed in Table 1. All data were calculated using the $2^{-\Delta\Delta CT}$ method. Data were obtained from three independent experiments.

2.8. Western Blot Assay. RIPA lysate (Beyotime, China) was used to extract the total protein from the cells, and a BCA kit (Beyotime, China) was used to detect the protein concentration. SDS-PAGE was performed with 30 μg protein per well. After electrophoresis, proteins were transferred to polyvinylidene fluoride (PVDF) membranes (Millipore, USA). Membranes were placed in 5% skimmed milk powder for sealing 1 h. Then, WISP1 and GAPDH antibodies were added, respectively. After incubation at 4°C overnight, horseradish peroxidase-labeled secondary antibody was incubated at room temperature for 1 h. A chemiluminescence reagent (Beyotime, China) was added to avoid light development, and exposure was taken by using a gel imaging system. The analysis was performed independently in triplicate.

2.9. Statistical Analysis. GraphPad Prism 6.0 was used for data analysis, and all data were expressed as mean ± standard deviation. The t test was used for comparison between the two groups. One-way analysis of variance was used for comparison between multiple groups. The significance level was $P < 0.05$.

3. Results

3.1. AFAP1-AS1 Expression Was Increased in CRC. As shown in Figure 1(a), AFAP1-AS1 expression was observably increased in CRC tissues versus paracancerous tissues. Similarly, AFAP1-AS1 expression in SW480, SW620, HCT116, and HT29 were also significantly increased versus NCM460 (Figure 1(b)). AFAP1-AS1 expression was the highest in SW480 cells, so SW480 cells were selected as the cell carrier for the subsequent experiments.

3.2. AFAP1-AS1 Knockdown Suppressed CRC Cell Malignant Behavior. To verify the role of AFAP1-AS1 in CRC, si-AFAP1-AS1 was transfected into SW480 cells, and AFAP1-AS1 expression was assessed by RT-qPCR. Results showed that AFAP1-AS1 expression of the si-AFAP1-AS1 group was obviously decreased versus si-NC (Figure 2(a)). The abovementioned results suggested si-AFAP1-AS1 has a good inhibitory efficiency and further experiments could be carried out.

After si-AFAP1-AS1 was transfected, the effects of AFAP1-AS1 inhibition on the malignant behavior of SW480 cells were verified by colony formation, wound-healing, and Transwell assay. Cell clone formation assay revealed the clone formation number of SW480 with si-AFAP1-AS1 was notably reduced versus si-NC (Figure 2(b)). This suggested that AFAP1-AS1 inhibition dramatically inhibits the proliferation of SW480 cells. The healing rate of the si-AFAP1-AS1 was memorably decreased versus si-NC at 48 h (Figure 2(c)). At the same time, the number of invading cells in si-AFAP1-AS1 was markedly reduced compared to si-NC (Figure 2(d)). We suggested that inhibition of AFAP1-AS1 expression hampered SW480 cell migration and invasion.

Table 1: Primer sequences for real-time fluorescence quantification PCR.

Gene name	Primer sequences (5′-3′)
GAPDH	F AAGGTGAAGGTCGGAGTCAA R AATGAAGGGGTCATTGATGG
U6	F GCTTCGGCAGCACATATACTAAAAT R CGCTTCACGAATTTGCGTGTCAT
AFAP1-AS1	F AGCCTTGGTGAGCAATAGGT R GGTATGAAGGGTGTGGGTGA
miR-195-5p	F GGGGTAGCAGCACAGAAAT R CAGTGCGTGTCGTGGAGT
WISP1	F GAAGCAGTCAGCCCTTATG R CTTGGGTGTAGTCCAGAAC

3.3. AFAP1-AS1 Directly Targeted miR-195-5p. The existence of binding sites between AFAP1-AS1 and miR-195-5p was predicted through the Starbase database (Figure 3(a)). miR-195-5p expression in tissues was detected by RT-qPCR. miR-195-5p expression was found to decrease in CRC tissues compared with paracancerous tissues (Figure 3(b)). Meanwhile, Pearson's correlation analysis results found AFAP1-AS1 expression was negatively correlated with miR-195-5p expression in tissues (Figure 3(c).

AFAP1-AS1 and miR-195-5p's relationship was further explored through dual-luciferase assay. The results showed that luciferase activity could be significantly inhibited by miR-195-5p mimic and AFAP1-AS1-wt, but it had no change of miR-195-5p mimic and AFAP1-AS1-mut (Figure 3(d)). Additionally, the miR-195-5p expression was promoted after AFAP1-AS1 knockdown (Figure 3(e)). In conclusion, AFAP1-AS1 targeted miR-195-5p and negative regulate its expression in CRC.

3.4. WISP1 Was a Target of miR-195-5p. According to TargetScan database analysis, binding sequences of miR-195-5p and WISP1 were found (Figure 4(a)). Whether WISP1 binds to miR-195-5p, detection of luciferase activity was performed through a dual-luciferase experiment. Compared with mutant WISP1-mut, luciferase activity of WISP1-wt was markedly reduced in the presence of mimic (Figure 4(b)). The results showed that miR-195-5p could specifically bind WISP1.

WISP1 mRNA expression in CRC and its adjacent tissues was detected by RT-qPCR, and then, Pearson's correlation analysis was used for correlation analysis. Compared with adjacent tissues, WISP1 mRNA expression was notably increased in CRC tissues (Figure 4(c)). Moreover, WISP1 mRNA expression was negatively correlated with miR-195-5p expression (Figure 4(d)), while the expression of AFAP1-AS1 and WISP1 mRNA has a positive correlation (Figure 4(e)).

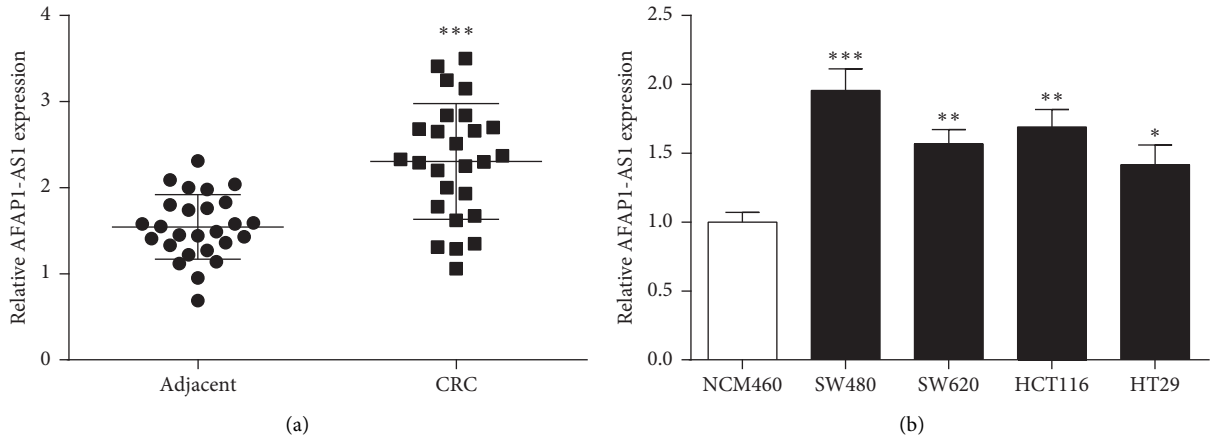

Figure 1: Expressions of AFAP1-AS1 in CRC. (a) Expression of AFAP1-AS1 in CRC tissues and adjacent tissues was detected by RT-qPCR. (b) Expression of AFAP1-AS1 in CRC cells was detected. $^{*}P < 0.05$, $^{**}P < 0.01$, and $^{***}P < 0.001$, compared with adjacent or human normal colon cell lines NCM460.

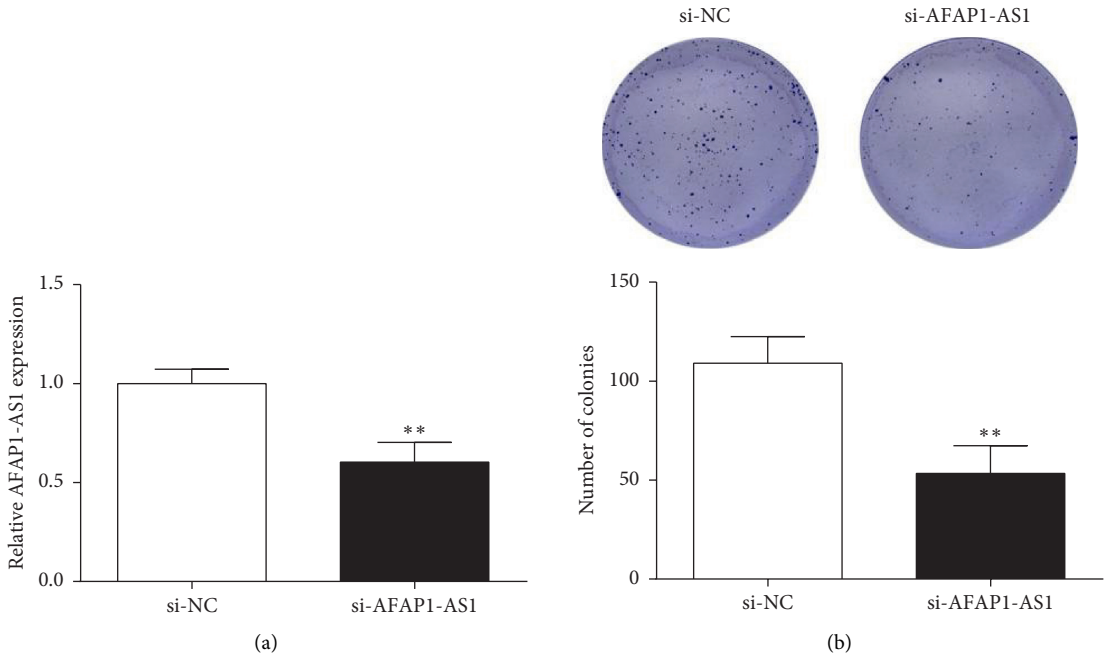

Figure 2: Continued.

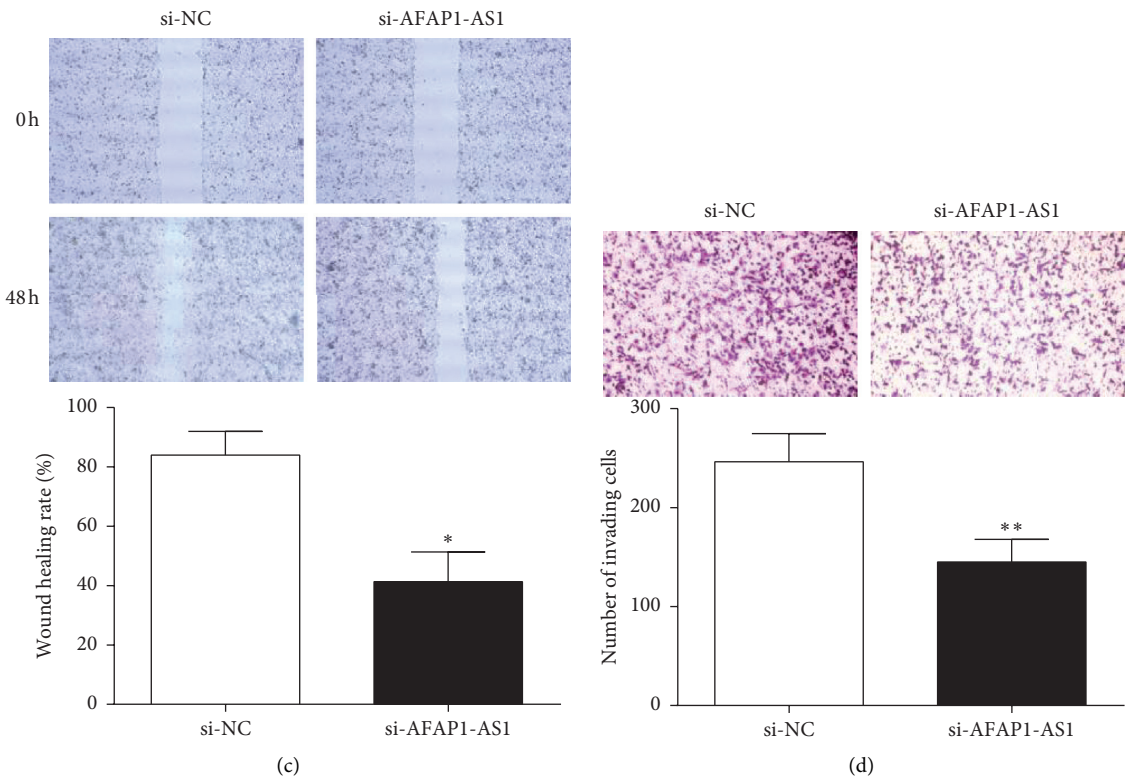

Figure 2: Effects of AFAP1-AS1 on CRC cell behavior. (a, b) The transfection efficiency of si-AFAP1-AS1 was detected by RT-qPCR. (b) Colony formation assay was conducted to evaluate the effect of si-AFAP1-AS1 on the proliferation of CRC cells (×200). (c) Wound-healing assay showed that si-AFAP1-AS1 inhibited migration of CRC cells (×200). (d) Effects of si-AFAP1-AS1 on the invasion of CRC cells were detected by Transwell assay (×200). $^{*}P < 0.05$ and $^{**}P < 0.01$, compared with the si-NC group.

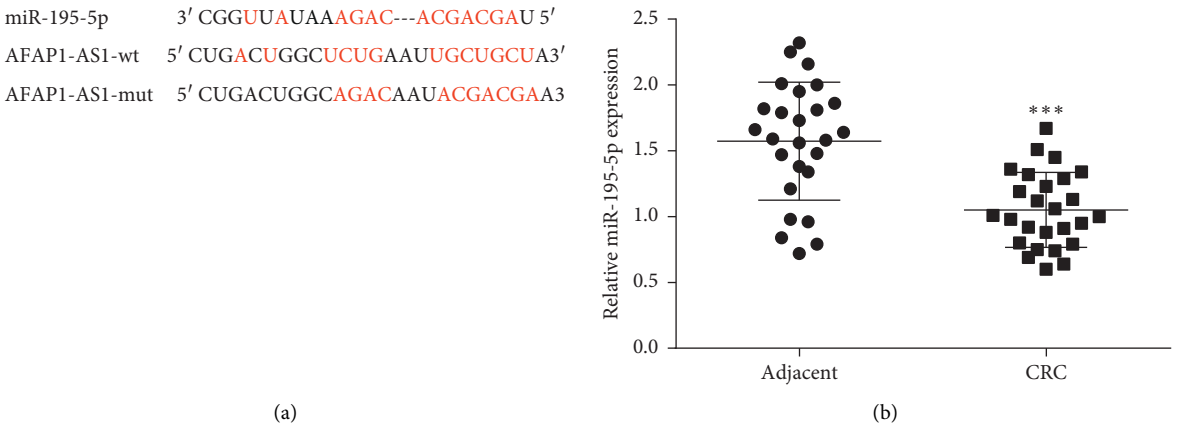

Figure 3: Continued.

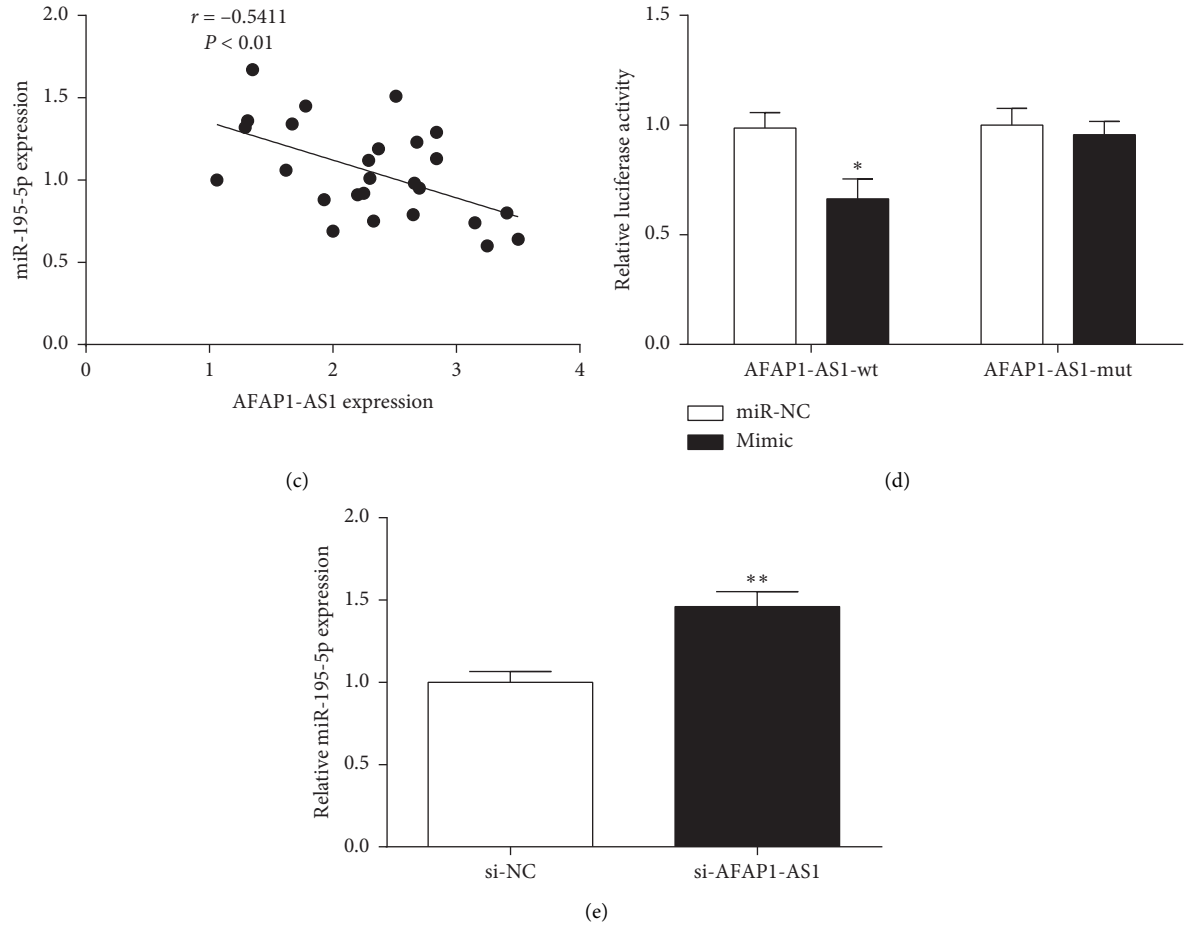

Figure 3: The relationship between AFAP1-AS1 and miR-195-5p. (a) Binding sites between AFAP1-AS1 and miR-195-5p were predicted by bioinformatics software. (b) The expression of miR-195-5p was decreased in CRC tissues. (c) Pearson correlation analysis revealed that a negative association existed between miR-195-5p and AFAP1-AS1 expression in CRC tissues. (d) Luciferase activity assay was performed to determine the relationship between AFAP1-AS1 and miR-195-5p. (e) The changes of miR-195-5p expression in CRC cells after AFAP1-AS1 knockdown. $^{*}P < 0.05$, $^{**}P < 0.01$, and $^{***}P < 0.001$, compared with the adjacent, miR-NC, or si-NC group.

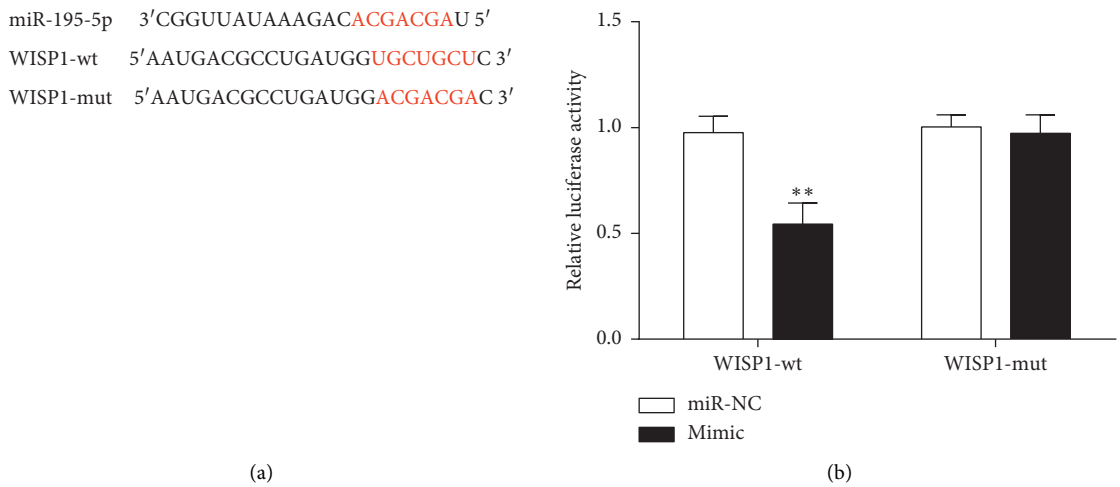

Figure 4: Continued.

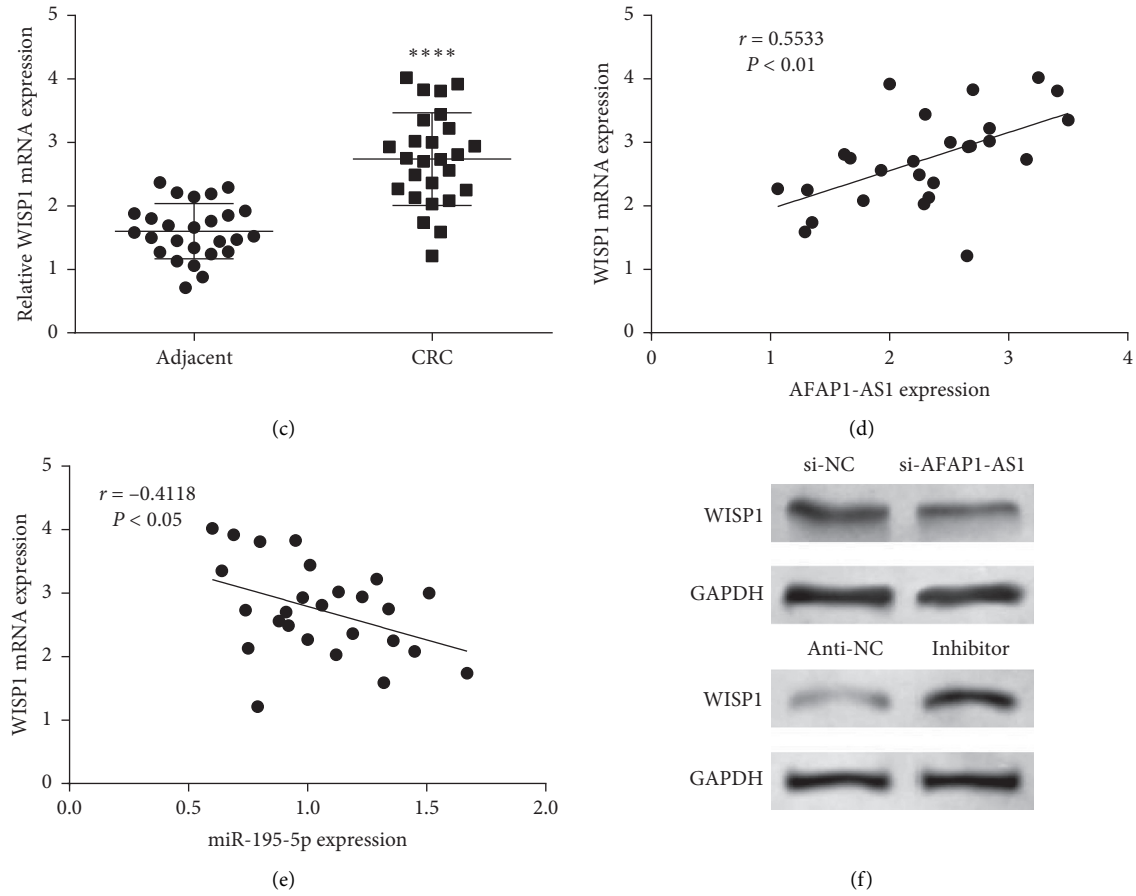

Figure 4: WISP1 was targeted by miR-195-5p. (a) TargetScan predicted the binding site between miR-195-5p and WISP1. (b) Dual-luciferase reporter gene assay determined WISP1 was targeted by miR-195-5p. (c) WISP1 was upregulated in CRC tissues. (d) Correlation analysis between AFAP1-AS1 and WISP1 expression in CRC tissues. (e) miR-195-5p expression was negatively correlated with WISP1 expression in CRC tissues. (f) Effects of AFAP1-AS1 and miR-195-5p on WISP1 protein expression. $^{**}P < 0.01$ and $^{****}P < 0.0001$, compared with the adjacent or miR-NC group.

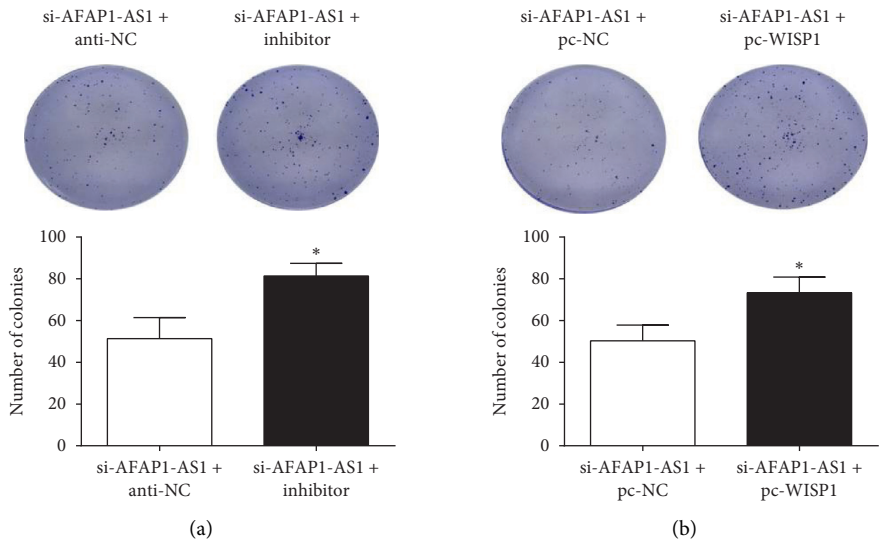

Figure 5: Continued.

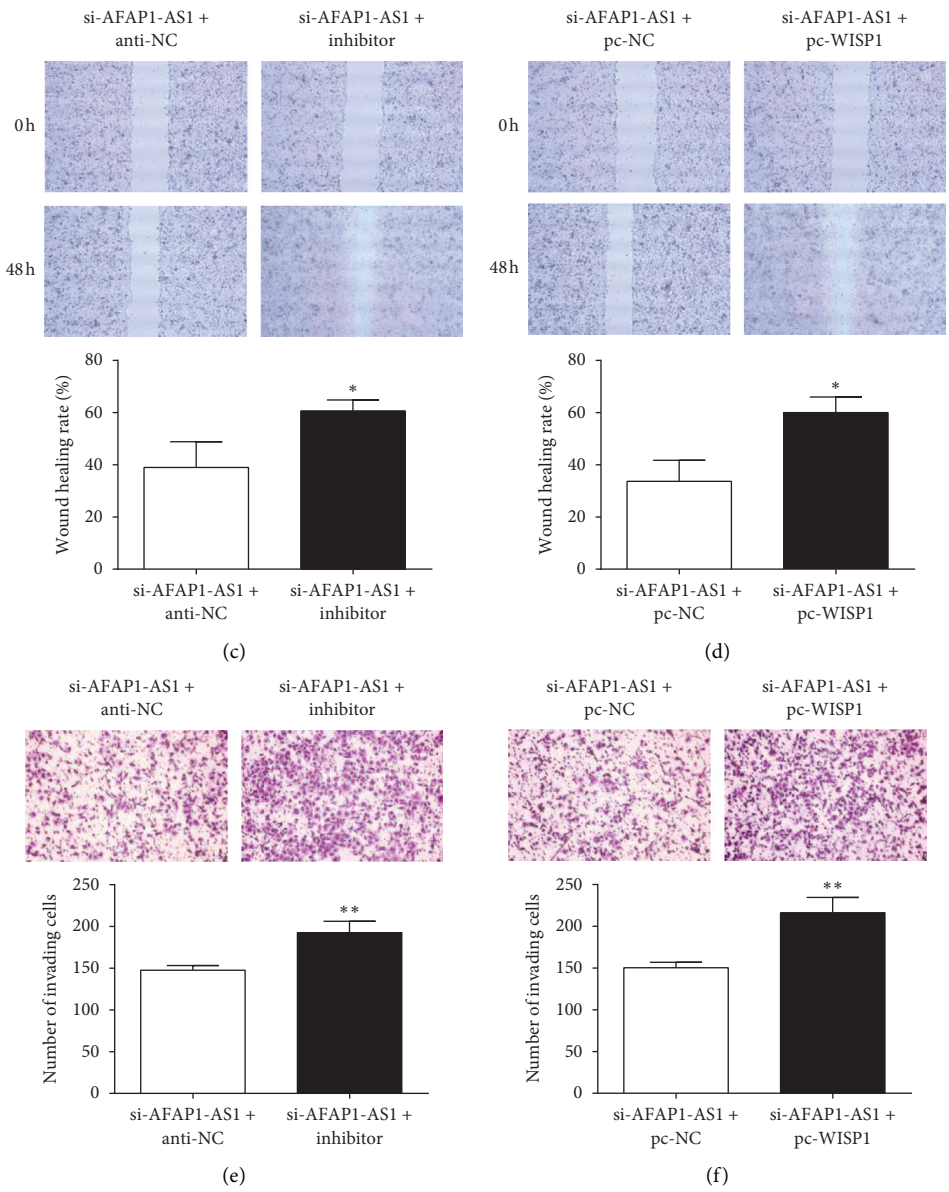

Figure 5: WISP1 overexpression or miR-195-5p inhibitor reverses the function of AFAP1-AS1 knockdown on the malignant behavior of CRC cell. (a, b) The proliferation of CRC cells was measured by colony formation assay (×200). (c, d) The migration ability of CRC cells was examined using a wound-healing assay (×200). (e, f) Transwell assay was conducted to assess the invasion of CRC cells (×200). $^{*}P < 0.05$ and $^{**}P < 0.01$, compared with the si-AFAP1-AS1 + anti-NC or si-AFAP1-AS1 + pc-NC group.

Western blotting results showed that AFAP1-AS1 knockdown could decrease WISP1 expression, while the miR-195-5p inhibitor could increase WISP1 expression (Figure 4(f)). Thus, it was speculated that WISP1 is a direct target of miR-195-5p and is negatively regulated by miR-195-5p and positively regulated by AFAP1-AS1.

3.5. AFAP1-AS1/miR-195-5p/WISP1 Facilitated CRC Progression. To further confirm the function of the AFAP1-AS1/miR-195-5p/WISP1 pathway in CRC, we performed the rescue experiment by colony formation, wound-healing, and Transwell assays. WISP1 overexpression or miR-195-5p inhibition rescued the cell malignant behavior induced by AFAP1-AS1 knockdown (Figure 5). Collectively, results verified that AFAP1-AS1 facilitated CRC progression through modulating miR-195-5p/WISP1 axis expression.

4. Discussion

The pathogenesis of CRC is still not very clear, and its occurrence and development involve the expression disorder or functional abnormality of several genes [14]. How to early diagnose and predict the poor prognosis of CRC and take intervention measures as early as possible is very important to reduce the mortality of patients. Hence, it has

great clinical significance in finding key molecules involved in the occurrence and development of CRC and in searching for biomarkers for early diagnosis and treatment of CRC.

LncRNAs play a vital role in tumor growth and can be used as molecular targets for the regulation of tumor progression [15]. Studies have shown that AFAP1-AS1 expression is increased, and its knockdown inhibits osteosarcoma progression by regulating miR-497/IGF1R [16]. In oral squamous cell carcinoma (OSCC), AFAP1-AS1 expression is enhanced and its inhibition can suppress the proliferation, migration, and invasion, while promoting cell apoptosis via affecting the miR-145/HOXA1 axis [17]. This study showed that AFAP1-AS1 expression was enhanced in CRC, suggesting that AFAP1-AS1 might involve in CRC occurrence and development. After transfection of si-AFAP1-AS1 into CRC cells, the cell survival, the number of clone formation, migration distance, and invaded cells number were decreased, which is consistent with previous reports [9–11]. However, research on the regulatory mechanism of AFAP1-AS1 in CRC cell biological behaviors is scarce.

In order to further explore the molecular mechanism by which AFAP1-AS1 affects CRC occurrence and development, this study confirmed that AFAP1-AS1 negatively regulates miR-195-5p expression by double-luciferase and RT-qPCR assays. Studies have shown that miR-195-5p overexpression inhibits the cell biological behaviors of cervical cancer, lung cancer, and other tumor cells and can be used as a potential molecular target for tumor therapy [18, 19]. Similarly, miR-195-5p also acts as a tumor suppressor in CRC [12]. More importantly, this study showed that inhibition of miR-195-5p reduced the inhibitory effect of AFAP1-AS1 knockdown on the proliferation, migration, and invasion of CRC cells, suggesting that AFAP1-AS1 affected the cell biological behaviors of CRC by regulating the expression of miR-195-5p.

In tumors, miRNA usually affects the cell's biological behaviors by targeting downstream target genes [20]. In this study, we found the binding site of miR-195-5p and WISP1 was existed according to bioinformatics analysis. WISP1 is a secreted extracellular-matrix-related protein and a member of the cellular communication network (CCN) growth factor family [21]. CCN protein is abnormally expressed in tumors [22]. As a member of this family, WISP1 has many developmental functions and may be related to tumorigenesis [23]. Thus, whether AFAP1-AS1 regulates proliferation, migration, and invasion of CRC cells through the regulation of WISP1 was further explored. In our double-luciferase report, the target relationship of miR-195-5p and WISP1 was confirmed. Additionally, AFAP1-AS1 expression has a positive correlation with WISP1 mRNA expression in CRC tissues. Moreover, AFAP1-AS1 inhibition could reduce WISP1 expression while miR-195-5p inhibition could enhance WISP1 expression. Moreover, WISP1 overexpression can offset the inhibitory effect of AFAP1-AS1 knockdown on CRC cells proliferation, migration, and invasion. We speculated that AFAP1-AS1 is involved in CRC progression, and the mechanism may be related to the regulation of the miR-195-5p/WISP1 pathway.

5. Conclusions

In conclusion, it was found that AFAP1-AS1 expression was increased in CRC. Further studies verified that AFAP1-AS1 knockdown inhibited the proliferation, invasion, and migration of CRC cells. Related mechanism experiments suggested that AFAP1-AS1 facilitated CRC progression by regulating the miR-195-5p/WISP1 axis. This study provides new insights into CRC pathogenesis and contributes to CRC diagnosis and treatment. However, there are still some shortcomings in this study. The study was limited to a small tissue sample, one cell line in functional experiments, and in vitro experiments. Further confirmation of the above-mentioned mechanisms is needed with larger samples (relationship of AFAP1-AS1 expression with clinicopathological characteristics and prognosis), two or more cell lines, and in vivo experiments. Also, more experimental exploration is needed to confirm whether it can be used in clinical diagnosis and targeted therapy.

Data Availability

The datasets used and/or analyzed during the present study are available from the corresponding author on reasonable request.

Conflicts of Interest

The authors declare that they have no conflicts of interest.

Authors' Contributions

Yongsheng Li and Zhongpeng Zhu contributed equally.

References

[1] F. Bray, J. Ferlay, I. Soerjomataram, R. L. Siegel, L. A. Torre, and A. Jemal, "Global cancer statistics 2018: GLOBOCAN estimates of incidence and mortality worldwide for 36 cancers in 185 countries," *CA: A Cancer Journal for Clinicians*, vol. 68, no. 6, pp. 394–424, 2018.

[2] G. Mauri, A. Sartore-Bianchi, A. G. Russo, S. Marsoni, A. Bardelli, and S. Siena, "Early-onset colorectal cancer in young individuals," *Molecular Oncology*, vol. 13, no. 2, pp. 109–131, 2019.

[3] H.-H. Oh and Y.-E. Joo, "Novel biomarkers for the diagnosis and prognosis of colorectal cancer," *Intestinal Research*, vol. 18, no. 2, pp. 168–183, 2020.

[4] V. Aran, A. P. Victorino, L. C. Thuler, and C. G. Ferreira, "Colorectal cancer: epidemiology, disease mechanisms and interventions to reduce onset and mortality," *Clinical Colorectal Cancer*, vol. 15, no. 3, pp. 195–203, 2016.

[5] J. Chan and Y. Tay, "Noncoding RNA:RNA regulatory networks in cancer," *International Journal of Molecular Sciences*, vol. 19, no. 5, p. 1310, 2018.

[6] A. Poursheikhani, M. R. Abbaszadegan, and M. A. Kerachian, "Mechanisms of long non-coding RNA function in colorectal cancer tumorigenesis," *Asia-Pacific Journal of Clinical Oncology*, vol. 17, no. 1, pp. 7–23, 2020.

[7] F. Zhang, J. Li, H. Xiao, Y. Zou, Y. Liu, and W. Huang, "AFAP1-AS1: a novel oncogenic long non-coding RNA in

human cancers," *Cell Proliferation*, vol. 51, no. 1, Article ID e12397, 2018.

[8] D. Ji, X. Zhong, X. Jiang et al., "The role of long non-coding RNA AFAP1-AS1 in human malignant tumors," *Pathology—Research and Practice*, vol. 214, no. 10, pp. 1524–1531, 2018.

[9] X. Han, L. Wang, Y. Ning, S. Li, and Z. Wang, "Long non-coding RNA AFAP1-AS1 facilitates tumor growth and promotes metastasis in colorectal cancer," *Biological Research*, vol. 49, no. 1, p. 36, 2016.

[10] W. Feng, H. Ni, S. Feng, L. Min, and C. Lin, "Overexpression of lncRNA AFAP1-AS1 correlates with poor prognosis and promotes tumorigenesis in colorectal cancer," *Biomedicine & Pharmacotherapy = Biomedecine & Pharmacotherapie*, vol. 81, pp. 152–159, 2016.

[11] J. Tang, G. Zhong, J. Wu, H. Chen, and Y. Jia, "Long non-coding RNA AFAP1-AS1 facilitates tumor growth through enhancer of zeste homolog 2 in colorectal cancer," *American Journal of Cancer Research*, vol. 8, no. 5, pp. 892–902, 2018.

[12] M. Sun, H. Song, S. Wang et al., "Integrated analysis identifies microRNA-195 as a suppressor of Hippo-YAP pathway in colorectal cancer," *Journal of Hematology & Oncology*, vol. 10, no. 1, pp. 1–16, 2017.

[13] J. Wu, Z. Long, H. Cai et al., "High expression of WISP1 in colon cancer is associated with apoptosis, invasion and poor prognosis," *Oncotarget*, vol. 7, no. 31, pp. 49834–49847, 2016.

[14] D. M. F. Palhares, R. Reis Figueiredo, K. R. Marchetti et al., "Stereotactic radiotherapy (SRT) in oligometastatic (OM) colorectal cancer (CRC): can we improve systemic therapy (ST) free interval?" *Journal of Clinical Oncology*, vol. 38, no. 4_ suppl, p. 154, 2020.

[15] Y.-H. Lin, "Crosstalk of lncRNA and cellular metabolism and their regulatory mechanism in cancer," *International Journal of Molecular Sciences*, vol. 21, no. 8, p. 2947, 2020.

[16] D. Fei, X. Zhang, Y. Lu, L. Tan, M. Xu, and Y Zhang, "Long noncoding RNA AFAP1-AS1 promotes osteosarcoma progression by regulating miR-497/IGF1R axis," *American Journal of Translational Research*, vol. 12, no. 5, pp. 2155–2168, 2020.

[17] M. Li, D. Yu, Z. Li, C. Zhao, C. Su, and J. Ning, "Long non-coding RNA AFAP1-AS1 facilitates the growth and invasiveness of oral squamous cell carcinoma by regulating the miR-145/HOXA1 axis," *Oncology Reports*, vol. 45, no. 3, pp. 1094–1104, 2020.

[18] Z. Long and Y. Wang, "miR-195-5p suppresses lung cancer cell proliferation, migration, and invasion via FOXK1," *Technology in Cancer Research Treatment*, vol. 19, pp. 1–9, 2020.

[19] X. Liu, Y. Zhou, Y. E. Ning, H. Gu, Y. Tong, and N. Wang, "MiR-195-5p inhibits malignant progression of cervical cancer by targeting YAP1," *OncoTargets and Therapy*, vol. 13, 2020.

[20] E. G. Nikitina, L. N. Urazova, and V. N. Stegny, "MicroRNAs and human cancer," *Experimental Oncology*, vol. 34, no. 1, pp. 2–8, 2012.

[21] K. Maiese, "WISP1: clinical insights for a proliferative and restorative member of the CCN family," *Current Neurovascular Research*, vol. 11, no. 4, pp. 378–389, 2014.

[22] A. Dhar and A. Ray, "The CCN family proteins in carcinogenesis," *Experimental Oncology*, vol. 32, no. 1, pp. 2–9, 2010.

[23] I. Gurbuz and C.-E. Ruth, "CCN4/WISP1 (WNT1 inducible signaling pathway protein 1): a focus on its role in cancer," *The International Journal of Biochemistry & Cell Biology*, vol. 62, pp. 142–146, 2015.

Hindawi
Journal of Oncology
Volume 2021, Article ID 8585371, 8 pages
https://doi.org/10.1155/2021/8585371

Research Article

The Clinical Value of the Combined Detection of Enhanced CT, MRI, CEA, and CA199 in the Diagnosis of Rectal Cancer

Cuijuan Hao, Yanbin Sui, Jian Li, Yunxia Shi, and Zhenxing Zou

Department of Medical Image, The Affiliated Yantai Yuhuangding Hospital of Qingdao University, Yantai 264000, China

Correspondence should be addressed to Zhenxing Zou; zouzhenxing@ytyhdyy.com.cn

Received 10 June 2021; Accepted 5 July 2021; Published 13 July 2021

Academic Editor: Muhammad Wasim Khan

Background. To explore the clinical value of enhanced computed tomography (enhanced CT), magnetic resonance imaging (MRI), carcinoembryonic antigen (CEA), and cancer antigen 199 (CA199) in the diagnosis of rectal cancer (RC). *Methods*. A total of 156 patients with RC confirmed by postoperative pathology admitted to the Affiliated Yantai Yuhuangding Hospital of Qingdao University from March 2018 to November 2020 were included in the malignant group, and 52 patients with chronic proctitis in the benign control group. All patients underwent preoperative enhanced CT, MRI scans, and serum CEA and CA199 tests. The accuracy, sensitivity, and specificity of single and combined enhanced CT, MRI, CEA, and CA199 tests for the clinical staging of RC were calculated. *Results*. The postoperative pathological diagnosis showed that 35 cases of 156 RC patients were at *T*1 stage, 29 cases were at *T*2 stage, 24 cases were at *T*3 stage, 11 cases were at *T*4 stage, 23 cases were at *N*0 stage, 21 cases were at *N*1 stage, 8 cases were at *N*2 stage, 3 cases were at *M*0 stage, and 2 cases were at *M*1 stage. The positive rate of MRI in the diagnosis of RC was higher than that of enhanced CT. Serum CEA and CA199 levels in the malignant group were significantly increased compared with the benign group. The sensitivity, specificity, and accuracy of the combined detection were significantly higher than those of the single detection. *Conclusion*. Compared with enhanced CT, MRI has a higher detection rate of *T* and *N* stage in patients with RC. Combined enhanced CT, MRI, CEA, and CA199 can provide more accurate diagnosis and preoperative staging of RC patients.

1. Introduction

Rectal cancer (RC) is one of the common clinical malignant tumors, which occurs in the mucosa or submucosa. The surface of the RC tumor is uneven, the texture is generally hard, and the growth rate is fast. RC has a high incidence and metastasis rate, which seriously threatens the health of patients and affects the quality of life [1, 2]. However, the early symptoms of RC are not obvious, and some RC patients have entered the advanced stage when seeking treatment and missed the best treatment opportunity, resulting in poor clinical efficacy [3]. The commonly used methods for the treatment of RC are surgical resection and adjuvant chemotherapy, local resection, and endoscopic treatment [4, 5]. Clinical results show that the treatment and prognosis of patients with RC are closely related to the preoperative staging, and the more accurate the preoperative staging judgment is, the more reasonable the treatment plan can be selected by physicians [6]. Therefore, accurate preoperative staging of RC is the key to the prognosis of patients and the formulation of the best treatment plan.

Studies have reported [7, 8] that imaging examinations, such as MSCT and MRI, have outstanding value in the diagnosis of preoperative staging of RC. At present, enhanced CT scan has been used more and more widely in clinical practice. Its advantages include high image definition and fast scanning speed, which can make a more effective judgment on the location, size, and degree of invasion of the tumor and can also clearly show the metastasis of distant organs [9]. Routine magnetic resonance imaging has been widely used in preoperative staging of RC, but its accuracy and imaging characteristics have not been accurately determined [10]. In recent years, studies have found that tumor markers [11] play an important role in the

occurrence and development of tumors. Oncoembryonic antigen (CEA) and carbohydrate antigen 19-9 (CA19-9) have been widely used in the diagnosis and prognosis follow-up of RC. But the sensitivity and specificity of the above indicators for single detection of RC are low [12–14]. Therefore, this study aims to explore the effectiveness of MSCT and MRI in the clinical staging of rectal cancer, and the clinical value of enhanced CT, MRI, CEA, and CA199 combined detection in the diagnosis of RC.

2. Materials and Methods

2.1. Study Design. A total of 156 patients with RC confirmed by postoperative pathology admitted to the Affiliated Yantai Yuhuangding Hospital of Qingdao University from March 2018 to December 2020 were included in this study. There were 95 males and 61 females. The average age was 52.5 ± 11.5 years from 27 to 69 years. There were 9 cases of highly differentiated adenocarcinoma, 124 cases of moderately differentiated adenocarcinoma, and 23 cases of poorly differentiated adenocarcinoma. There were 89 cases of middle and upper RC, and 67 cases of lower RC. The tumor diameter ranged from 1.5 to 7.7 cm, with an average of 4.9 cm. 52 patients with chronic proctitis were selected as the benign control group. Our study was approved by the medical ethics committee of the Affiliated Yantai Yuhuangding Hospital of Qingdao University.

Inclusion criteria: patients with RC met the relevant diagnostic criteria in Internal Medicine [15]; the patients and their family members provide informed consent, and all patients had no history of pelvic surgery and had not received pelvic radiotherapy or chemotherapy; also CT images, MRI images, and pathological data were clear and complete.

Exclusion criteria: patients with allergies to iodine contrast agents; patients with contraindications to MRI; patients with other benign and malignant tumors; patients with contraindications to examinations such as cardiac pacemakers and aneurysm clips.

2.2. Preparation before Inspection. All patients took liquid food two days before the examination, to avoid excessive feces accumulation in the body, which would affect the image quality. The day before the examination, patients took Senna granules (Z10910006, Yangzhou Xingdou Pharmaceutical Co., Ltd.) 10 g/time, twice/d, to clean the intestines. Eight hours *h* before the examination, patients were given a normal saline enema to maintain their intestinal cleanliness. One hour before the examination, the patients were given an intramuscular injection of 10 mg Racemic Anisodamine Hydrochloride Injection (H32024750, Xuzhou Lian Pharmaceutical Co., Ltd.) and drank 1000 ml water to make the bladder fully filled.

2.3. Enhanced CT Scanning. GE Light Speed 64-slice CT scanner was used for enhanced CT. Patients were placed in the left decubitus position and were supine after 800 ml of air was injected through the anus. After the plain scanning, patients were injected with 80 mL nonionic iodine contrast agent (3.5 mL/s). Dynamic enhanced CT scanning was performed at the intravenous phase (70 s after injection), arterial phase (30 s after injection), and balance phase (240 s after injection). After the scan, the data was transmitted to the CT postprocessing workstation.

2.4. MRI Scanning. Patients were placed in supine position and scanned the whole pelvic cavity. The scanning sequence was as follows: the sagittal T2WI sequence images were first scanned to observe the tumor size, scope, and distance from the tumor to the anus. Then, the axial high-resolution T2WI, T1WI sequence images perpendicular to the tumor segment, and the coronal T2WI parallel to the tumor segment were scanned. Finally, the DWI sequence images perpendicular to the tumor segment were scanned. After the plain scanning, sagittal, coronal, and cross-sectional enhanced scanning were performed. The total scanning time was controlled within 30 minutes. The data were transferred to the image processing workstation, and two physicians performed the staging diagnosis of the included patients.

2.5. CEA and CA199 Detection. 5 mL of fasting blood from the cubital vein of the patients was collected and centrifuged at 3000 r/min for 5 min. The levels of serum CEA and CA19-9 were detected by an automatic chemiluminescence immunoanalyzer (CENTAUR XP, Siemens, Germany). The operation process was strictly in accordance with the manufacturer's instructions.

2.6. HE Staining. After fixation and dehydration, the specimens were embedded in paraffin and sectioned with a thickness of 4 μm. The specimens were stained by hematoxylin-eosin staining [15] and observed under a microscope.

2.7. Evaluation Standard. Clinical staging of RC was determined according to the Updated Interpretation of the American Society of Oncology Colorectal Cancer Staging System [16]. Criteria for positive CEA and CA199: CEA > 5 ng/mL, CA199 > 37 U/mL. The sensitivity, specificity, and accuracy of enhanced CT, MRI, CEA, and CA199 alone and combined in the diagnosis of RC were compared and analyzed. Receiver operating curve (ROC) was used to calculate the diagnostic efficacy of CEA and CA19-9 in the diagnosis of RC. The positive criteria for the combined test: two or more positive results of enhanced CT, MRI, CEA, and CA199 tests.

2.8. Statistical Analysis. The data was analyzed by SPSS 23.0. Measurement data were expressed as mean ± SD, and enumeration data were expressed as number (%). $P < 0.05$ indicated that the difference was statistically significant.

3. Results

3.1. Postoperative TNM Staging Pathological Results of Rectal Cancer Patients. As shown in Figure 1, HE staining was performed on the specimens of patients with RC. The results

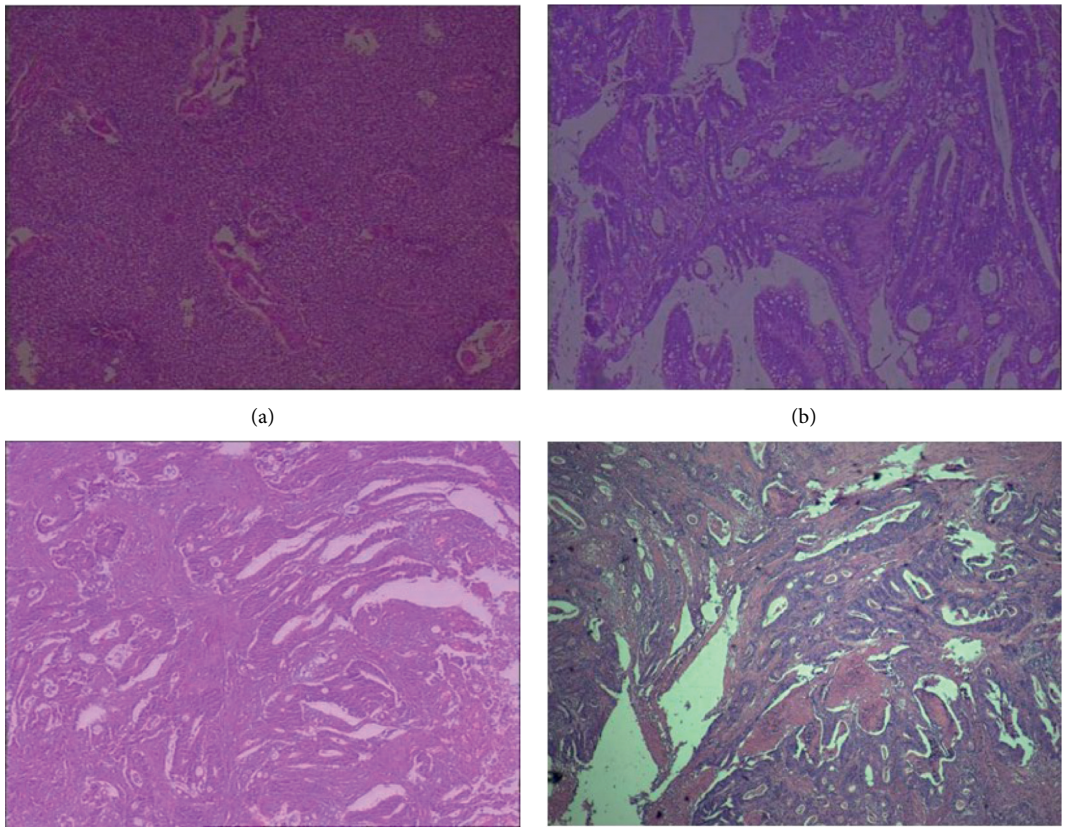

(a) (b) (c) (d)

Figure 1: TNM postoperative pathological staging images of RC patients. (a) The image of raised, moderately differentiated squamous cell carcinoma (size: $2 \times 2 \times 1$ cm). (b) The image of moderately differentiated ulcerative adenocarcinoma (size: $4.5 \times 3.5 \times 0.5$ cm). (c) The image of moderately differentiated ulcerative adenocarcinoma (size: $4 \times 3.5 \times 2$ cm). (d) The image of moderately differentiated ulcerative adenocarcinoma (size: $4.5 \times 3.5 \times 0.3$ cm).

displayed that 35 cases were *T*1 stage, 29 cases were *T*2 stage, 24 cases were *T*3 stage, 11 cases were *T*4 stage (Table 1), 23 cases were *N*0 stage, 21 cases were *N*1 stage, 8 cases were *N*2 stage (Table 2), and 3 cases were *M*0 stage, 2 cases of *M*1 stage (Table 3).

3.2. Contrast of the Diagnostic Results of Enhanced CT and MRI in Preoperative TNM Staging of RC Patients. According to enhanced CT and MRI image data, the preoperative TNM staging of RC patients was diagnosed (Figures 2(a)–2(d) and 3(a)–3(d)). The detection rate of MRI for *T* and *N* staging was higher than that of enhanced CT, and the detection rate of *M* staging was consistent. Therefore, MRI has a higher positive rate than enhanced CT in the diagnosis of RC (Tables 1–3).

3.3. Comparison of Serum CEA and CA199 Levels between the Two Groups. We detected the levels of serum CEA and CA199 in malignant group and benign group. The results displayed that serum CEA and CA199 levels in malignant group were significantly increased compared with benign group ($P < 0.001$, Table 4).

Table 1: Enhanced CT and MRI in the preoperative *T* staging of RC patients.

Item	Clinical staging	*T*1	*T*2	*T*3	*T*4	Total
Enhanced CT	*T*1	21	7	0	0	28
	*T*2	11	20	3	0	34
	*T*3	3	2	18	2	25
	*T*4	0	0	3	9	12
MRI	*T*1	26	3	0	0	29
	*T*2	8	23	3	0	34
	*T*3	1	3	20	1	25
	*T*4	0	0	1	10	11
Total		35	29	24	11	99

Table 2: Enhanced CT and MRI in the preoperative *N* staging of RC patients.

Item	Clinical staging	*N*0	*N*1	*N*2	Total
Enhanced CT	*N*0	17	3	0	20
	*N*1	6	17	1	24
	*N*2	0	1	7	8
MRI	*N*0	19	1	0	20
	*N*1	4	20	0	24
	*N*2	0	0	8	8
Total		23	21	8	52

Table 3: Enhanced CT and MRI in the preoperative *M* staging of RC patients.

Item	Clinical staging	*M*0	*M*1	Total
Enhanced CT	*M*0	3	0	3
	*M*1	0	2	2
MRI	*M*0	3	0	3
	*M*1	0	2	2
Total		3	2	5

3.4. ROC Curve of CA199 and CEA in the Diagnosis of RC. ROC curve indicated that the AUC was 0.713 (0.584–0.843), and Youden index was 0.331 for CEA diagnosis of RC (Figure 4(a)). The AUC of CA199 in the diagnosis of RC was 0.706 (0.575–0.836), and the Youden index was 0.274 (Figure 4(b)).

3.5. Comparison of Single and Combined Tests of Enhanced CT, MRI, CEA, and CA199 in the Diagnosis of RC. The sensitivity, specificity, and accuracy of enhanced CT in the diagnosis of RC were 73.08%, 78.85%, and 74.52%, respectively. The sensitivity, specificity, and accuracy of MRI in the diagnosis of RC were 83.97%, 86.54%, and 84.62%, respectively. The sensitivity, specificity, and accuracy of CA199 in the diagnosis of RC were 51.92%, 78.85%, and 58.65%, respectively. The sensitivity, specificity, and accuracy of CEA in the diagnosis of RC were 57.69%, 86.92%, and 62.50%, respectively. The sensitivity, specificity, and accuracy of combined detection in the diagnosis of RC were 94.23%, 98.08%, and 95.19%, respectively. As shown in Table 5, the sensitivity, specificity, and accuracy of combined diagnosis were significantly higher than those of a single diagnosis ($P < 0.05$, Table 5).

4. Discussion

At present, the incidence of RC in China is increasingly high, and it is more common in middle-aged and elderly groups [17]. Patients with early RC have no specific clinical manifestations and are often diagnosed in the middle and advanced stages, with unsatisfactory treatment and prognosis [3]. Therefore, it is of great significance for the early diagnosis of RC patients and the accurate judgment of postoperative staging.

Enhanced CT and MRI are widely used in preoperative staging detection [18, 19]. Enhanced CT has advantages of convenient operation, high spatial resolution, and good effect in the detection of distant metastasis [20]. Enhanced CT can also carry out a comprehensive scan of the tumor size, size, and infiltration in RC patients, and then quickly obtain comprehensive and detailed images [21]. Enhanced CT can be used to observe images through multiplanar recombination, thus obtaining images of any section of the patient's body. In addition, the diagnosis can help physicians have a deeper understanding of the patient's symptoms, the details of tumor lesions and the relationship between the patient's internal space anatomy, so as to improve the accuracy of malignant tumor staging [22, 23]. However, as the infiltration of RC in the early intestinal wall is not significant, and enhanced CT is difficult to stratify the patient's intestinal wall, preoperative staging diagnosis often lacks good accuracy, especially for the detection of early RC [24]. MRI can distinguish the three-layer structure of intestinal wall and the adjacent fat background rectal fascia, which is suitable for the benign and malignant differentiation and accurate staging of tumors [25, 26]. MRI can conduct comprehensive detection of tumor properties, layers of structure, lymph node metastasis, and organ infiltration in the patient's body and directly obtain comprehensive image information by skipping image and information reconstruction [27, 28]. Moreover, MRI also has multiple sequence imaging and a variety of image types, which can carry out in-depth and comprehensive detailed detection of rectum, bladder, vagina, and other areas of RC lesions. In this respect, the detection performance of MRI is significantly better than that of enhanced CT [29], which is consistent with the results of this study.

Studies have shown that CEA and CA199 play an important role in the diagnosis, prognosis, and recurrence monitoring of RC [30]. CEA, a high-molecular weight glycoprotein produced by normal colon cells, acts as an intercellular adhesion molecule and can promote the aggregation of RC cells. CEA is one of the most widely used tumor markers in RC [31]. However, due to the poor sensitivity and specificity of CEA, RC patients cannot be completely diagnosed by CEA content detection alone [32]. CA199 can be used as one of the common tumor markers of RC [33]. However, the sensitivity and accuracy of these two indicators in single detection of RC are poor, and the preoperative screening value is not high. However, it is helpful for early clinical detection of suspected RC patients and further combined with auxiliary detection methods such as preoperative imaging to improve the accuracy of preoperative staging of RC.

In this study, by comparison and analysis of examination results and postoperative pathological staging results, the sensitivity, specificity, and accuracy of MRI in the detection of preoperative TN staging of RC patients were significantly better than those of enhanced CT detection, and the obtained results were consistent with those of the above research reports [28]. The levels of CEA and CA199 in the malignant group were higher than those in the benign group, indicating that the levels of both indexes increased with the deepening of the malignant tumor. The sensitivity, specificity, and accuracy of the combined test for the preoperative staging of RC patients were significantly higher than those of the single test. It is suggested that the combined detection can make advantages complement each other and have higher diagnostic value and can provide data support for a more accurate diagnosis of RC.

In conclusion, the combined detection of enhanced CT, MRI, CEA, and CA199 levels can improve the detection rate of RC and make a more accurate judgment of preoperative staging. It has high diagnostic value and can provide the clinical basis for early diagnosis and treatment of RC patients, which is worthy of promotion and application. However, the sample size of this study was small, and the combined diagnosis in the clinical diagnosis of RC still needs further study.

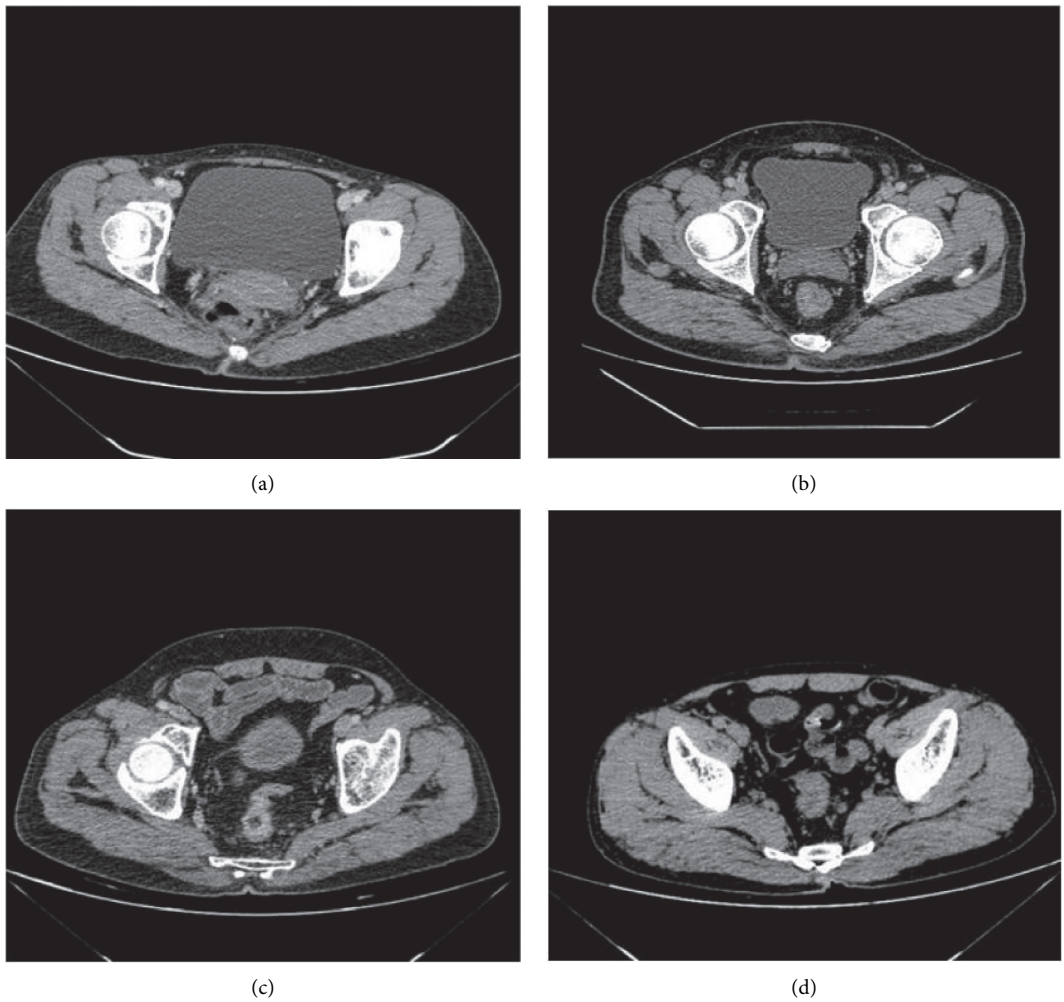

(a) (b)

(c) (d)

Figure 2: Enhanced CT image of patients with RC. (a) A 55-year-old woman in stage *T*1 RC presented with slight enhancement in submucosal lesions. (b) A 49-year-old man in stage *T*3 RC with involvement of the muscularis propria and perirectal tissues. (c) A 61-year-old female patient in stage *N*1 RC had subserosal invasion and lymph node metastasis. (d) A 37-year-old woman in stage *N*2 RC with invasion to the muscularis propria and lymph node metastasis.

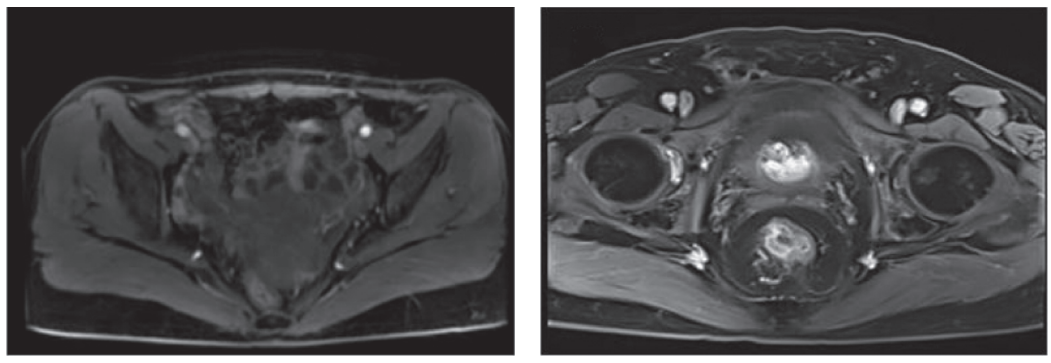

(a) (b)

Figure 3: Continued.

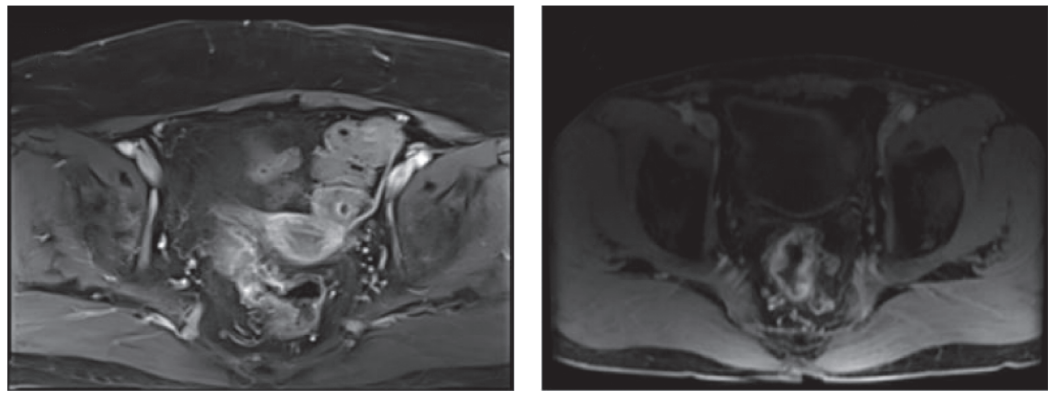

(c) (d)

Figure 3: MRI image of patients with RC. (a) The patient was in stage *T*1 RC with high signal submucosa below the lesion, and without involvement of muscularis propria. (b) The patient was in stage *T*3 RC with muscularis propria and perirectal adipose tissue, but not mesocrectum and fascia. (c) The patient was in stage *N*1 RC, and with lymph node metastasis. (d) The patient was in stage *N*2 RC with bilateral lymph node metastasis.

Table 4: Comparison of serum CEA and CA199 levels between the two groups ($\overline{x} \pm s$).

Group	*n*	CEA (ng/mL)	CA199 (U/mL)
Malignant group	156	5.63 ± 1.02	39.58 ± 3.47
Benign group	52	1.85 ± 0.64	12.33 ± 1.52
X^2		21.462	43.078
P value		<0.001	<0.001

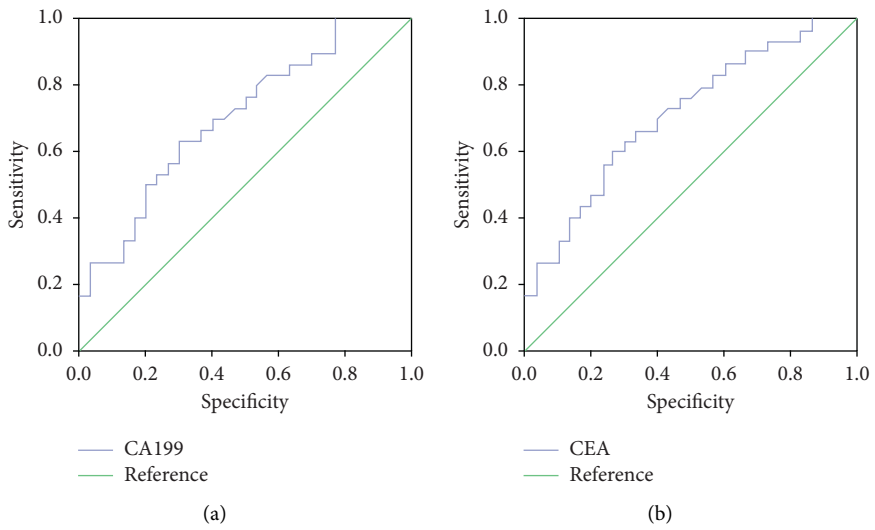

Figure 4: ROC curve of CA199 and CEA in diagnosis of RC. (a) CA199 curve of CEA in diagnosis of RC. (b) ROC curve of CEA in diagnosis of RC.

Table 5: Comparison of single and combined enhanced CT, MRI, CEA, and CA199 in the diagnosis of RC (%).

Item	Sensitivity	Specificity	Accuracy	Positive prediction rate	Negative prediction rate
Enhanced CT	73.08 (114/156)	78.85 (41/52)	74.52 (155/208)	91.20 (114/125)	49.40 (41/83)
MRI	83.97 (131/156)	86.54 (45/52)	84.62 (176/208)	94.93 (131/138)	64.29 (45/70)
CA199	51.92 (81/156)	78.85 (41/52)	58.65 (122/208)	88.04 (81/92)	35.34 (41/116)
CEA	57.69 (90/156)	86.92 (40/52)	62.50 (130/208)	88.24 (90/102)	37.74 (40/106)
Combined diagnosis	94.23 (147/156)	98.08 (51/52)	95.19 (198/208)	99.32 (147/148)	85.00 (51/60)

Data Availability

The data used to support the findings of this study are available from the corresponding author upon request.

Conflicts of Interest

The authors declare that they have no conflicts of interest.

Authors' Contributions

Cuijuan Hao, Yanbin Sui, Jian Li, and Yunxia Shi contributed equally to this work.

References

[1] K. Thanikachalam and G. Khan, "Colorectal cancer and nutrition," *Nutrients*, vol. 11, no. 1, p. 164, 2019.

[2] S. Haraldsdottir, H. M. Einarsdottir, A. Smaradottir, A. Gunnlaugsson, and T. R. Halfdanarson, "Colorectal cancer—review," *Laeknabladid*, vol. 100, no. 2, pp. 75–82, 2014.

[3] K. Heinimann, "Erblicher Darmkrebs: klinik, Diagnostik und Management," *Therapeutische Umschau*, vol. 75, no. 10, pp. 601–606, 2018.

[4] Y. Tian, L. Rong, W. D. Nian et al., "Clinical short-term and long-term efficacy of endoscopic submucosal dissection in the treatment of early low rectal cancer and precancerous lesions," *Zhonghua Wei Chang Wai Ke Za Zhi*, vol. 22, no. 7, pp. 639–642, 2019.

[5] L. Mitrogiannis, A. Barbouti, E. Theodorou et al., "Surgical treatment of juvenile idiopathic arthritis A review," *Bulletin of the Hospital for Joint Diseases*, vol. 77, no. 2, pp. 99–114, 2019.

[6] Y. Nasseri and S. J. Langenfeld, "Imaging for colorectal cancer," *Surgical Clinics of North America*, vol. 97, no. 3, pp. 503–513, 2017.

[7] X. L. Wen, L. Wang, X. Q. Song, Z. Zhang, X. F. Zhu, and S. P. Wu, "Clinical value of multi-slice spiral enhanced CT in diagnosing mild digestive tract hemorrhage," *Zhongguo Yi Xue Ke Xue Yuan Xue Bao*, vol. 40, no. 2, pp. 139–145, 2018.

[8] N. Horvat, C. Carlos Tavares Rocha, B. Clemente Oliveira, I. Petkovska, and M. J. Gollub, "MRI of rectal cancer: tumor staging, imaging techniques, and management," *Radiographics*, vol. 39, no. 2, pp. 367–387, 2019.

[9] J. H. Yoon, M. H. Yu, B. Y. Hur, C. M. Park, and J. M. Lee, "Detection of distant metastases in rectal cancer: contrast-enhanced CT vs whole body MRI," *European Radiology*, vol. 31, no. 1, pp. 104–111, 2021.

[10] M. Grunnet and J. B. Sorensen, "Carcinoembryonic antigen (CEA) as tumor marker in lung cancer," *Lung Cancer*, vol. 76, no. 2, pp. 138–143, 2012 May.

[11] M. Bacac, C. Klein, P. Umana, and T. C. B. CEA, "CEA TCB: a novel head-to-tail 2:1 T cell bispecific antibody for treatment of CEA-positive solid tumors," *Oncoimmunology*, vol. 5, no. 8, Article ID e1203498, 2016.

[12] J. Zhang, J. Ruan, W. Wang et al., "Prognostic value of the combination of CEA and fibrinogen/albumin ratio in resectable gastric cancer," *Cancer Management and Research*, vol. 12, pp. 2767–2775, 2020.

[13] P. Zeng, H. Li, Y. Chen, H. Pei, and L. Zhang, "Serum CA199 levels are significantly increased in patients suffering from liver, lung, and other diseases," *Progress in Molecular Biology and Translational Science*, vol. 162, pp. 253–264, 2019.

[14] V. Kraege, O. Aebischer, Y. Chocron et al., "The internal medicine articles that struck us the most in 2018," *Revue Médicale Suisse*, vol. 15, no. 634, pp. 146–148, 2019.

[15] K. J. Fowler, H. Kaur, B. D. Cash et al., "ACR appropriateness criteria() pretreatment staging of colorectal cancer," *Journal of the American College of Radiology*, vol. 14, no. 5, pp. S234–S244, 2017.

[16] N. I. Lindeman, P. T. Cagle, D. L. Aisner et al., "Updated molecular testing guideline for the selection of lung cancer patients for treatment with targeted tyrosine kinase inhibitors: guideline from the college of American pathologists, the international association for the study of lung cancer, and the association for molecular pathology," *Archives of Pathology & Laboratory Medicine*, vol. 142, no. 3, pp. 321–346, 2018.

[17] P. Wrobel and S. Ahmed, "Current status of immunotherapy in metastatic colorectal cancer," *International Journal of Colorectal Disease*, vol. 34, no. 1, pp. 13–25, Jan 2019.

[18] G. P. São Julião, A. Habr-Gama, B. B. Vailati, S. E. A. Araujo, L. M. Fernandez, and R. O. Perez, "New strategies in rectal cancer," *Surgical Clinics of North America*, vol. 97, no. 3, pp. 587–604, 2017.

[19] K. R. Kalisz, M. D. Enzerra, and R. M. Paspulati, "MRI evaluation of the response of rectal cancer to neoadjuvant chemoradiation therapy," *Radiographics*, vol. 39, no. 2, pp. 538–556, 2019.

[20] X. Wang, D. Lv, H. Song et al., "Multimodal preoperative evaluation system in surgical decision making for rectal cancer: a randomized controlled trial," *International Journal of Colorectal Disease*, vol. 25, no. 3, pp. 351–358, 2010.

[21] L. Lincender-Cvijetić, M. Banjin-Čardžić, S. Vegar-Zubović, and D. Vrcić, "Radiological imaging of rectal cancer," *Acta Medica Academica*, vol. 41, no. 2, pp. 199–209, 2012.

[22] D. S. Keller, M. Berho, R. O. Perez, S. D. Wexner, and M. Chand, "The multidisciplinary management of rectal cancer," *Nature Reviews Gastroenterology & Hepatology*, vol. 17, no. 7, pp. 414–429, 2020.

[23] R. Glynne-Jones, L. Wyrwicz, E. Tiret et al., "Rectal cancer: ESMO Clinical Practice Guidelines for diagnosis, treatment and follow-up," *Annals of Oncology*, vol. 28, no. s4, pp. iv22–iv40, 2017.

[24] B. Gürses, M. Böge, M. Boge, E. Altinmakas, and E. Balik, "Multiparametric MRI in rectal cancer," *Diagnostic and Interventional Radiology*, vol. 25, no. 3, pp. 175–182, 2019.

[25] D. Massihnia, E. G. Pizzutilo, A. Amatu et al., "Liquid biopsy for rectal cancer: a systematic review," *Cancer Treatment Reviews*, vol. 79, Article ID 101893, 2019.

[26] S. Balyasnikova and G. Brown, "Optimal imaging strategies for rectal cancer staging and ongoing management," *Current Treatment Options in Oncology*, vol. 17, no. 6, p. 32, 2016.

[27] C. Timmerman, L. R. Taveras, and S. Huerta, "Clinical and molecular diagnosis of pathologic complete response in rectal cancer: an update," *Expert Review of Molecular Diagnostics*, vol. 18, no. 10, pp. 887–896, 2018.

[28] Y. J. Wang, Y. Chen, X. T. Lyu, A. L. Ma, Y. P. He, and Z. L. Gao, "[Value and related factors of preoperative diagnosis of extramural vascular invasion of rectal cancer by 3.0T magnetic resonance imaging]," *Zhonghua Zhong Liu Za Zhi*, vol. 41, no. 8, pp. 610–614, 2019.

[29] F. Li, W. Zhang, J. Li et al., "The clinical application value of MR diffusion-weighted imaging in the diagnosis of rectal cancer," *Medicine*, vol. 97, no. 51, Article ID e13732, 2018.

[30] "Carcinoembryonic antigen (CEA) and hepatic metastasis in colorectal cancer: update on campos-da-paz M, dórea JG, galdino AS, Lacava ZGM, de Fatima menezes almeida santos

M. Biomarker for clinical and biotechnological approaches," *Recent Pat Biotechnol*, vol. 12, no. 4, pp. 269–279, 2018.

[31] C. Hao, G. Zhang, and L. Zhang, "Serum CEA levels in 49 different types of cancer and noncancer diseases," *Progress in Molecular Biology and Translational Science*, vol. 162, pp. 213–227, 2019.

[32] D. Teng, K. Wu, Y. Sun et al., "Significant increased CA199 levels in acute pancreatitis patients predicts the presence of pancreatic cancer," *Oncotarget*, vol. 9, no. 16, pp. 12745–12753, 2018.

[33] W.-Y. Xu, H.-H. Zhang, X.-B. Yang et al., "Prognostic significance of combined preoperative fibrinogen and CA199 in gallbladder cancer patients," *World Journal of Gastroenterology*, vol. 24, no. 13, pp. 1451–1463, 2018.

Hindawi
Journal of Oncology
Volume 2021, Article ID 4747843, 7 pages
https://doi.org/10.1155/2021/4747843

Research Article

Comparative Analysis of Clavien–Dindo Grade and Risk Factors of Complications after Dual-Port Laparoscopic Distal Gastrectomy and Hand-Assisted Laparoscopic Gastrectomy

Haihao Jin and Jianshan Geng

Department of Gastroenterology, Laiyang People's Hospital, Laiyang 265200, Shandong, China

Correspondence should be addressed to Jianshan Geng; sdlyjhh@163.com

Received 28 May 2021; Accepted 3 July 2021; Published 9 July 2021

Academic Editor: Alamgeer Yuchi

Objective. To compare the Clavien–Dindo grade and risk factors of complications after dual-port laparoscopic distal gastrectomy (DPLDG) and hand-assisted laparoscopic gastrectomy (HALG). *Methods*. The clinical data of 775 patients who underwent DPLDG or HALG in our hospital from May 2016 to May 2019 were retrospectively reviewed, and the patients were divided into the DPLDG group ($n = 386$) and HALG group ($n = 389$) according to the surgical method to explore the risk factors of postoperative complications by grading their postoperative complications according to the Clavien–Dindo classification system and single-factor and multivariate analysis of the association between variables in clinical data and complications. *Results*. Compared with the HALG group, the DPLDG group had significantly shorter surgical time, less intraoperative blood loss, and better postoperative exhaust time ($p < 0.05$), with no significant difference in other clinical indicators between the two groups ($p > 0.05$); the postoperative complication incidence rate of DPLDG group was significantly lower than that of the HALG group; it was shown in the single-factor analysis that the age, tumor length, intraoperative blood loss, pathological stages, and surgical method were related to the postoperative complications, and the results of multivariate analysis indicated that DPLDG was the protective factor for reducing postoperative complications, while age no less than 60 years old and intraoperative blood loss no less than 180 ml were the independent risk factors leading to complications; after surgery, the PNI level values at T1, T2, and T3 of DPLDG group were significantly higher than those of the HALG group ($p < 0.05$); and at 1 month after surgery, both groups obtained significantly higher GLQI scores than before, and the GLQI score of the DPLDG group was significantly higher in the between-group comparison ($p < 0.05$). *Conclusion*. The DPLDG has lower postoperative complication incidence rate than the HALG, but age no less than 60 years old and intraoperative blood loss not less than 180 ml are the independent risk factors for postoperative complications, so advanced prevention measures shall be taken to lower the incidence of complications.

1. Introduction

Gastric cancer is a kind of gastroenterological cancer originating from the gastric epithelial cell, which, according to related statistics [1, 2], ranks the fifth in the incidence and top three in the mortality among the new cancers worldwide. With the gradual development of clinical research, people have a deeper understanding of gastric cancer, and laparoscopy with the characteristics of less trauma and precise operative manipulation has been widely used in the treatment of gastric cancer, which can effectively remove lymph nodes and improve the survival outcome of patients [3]. In recent years, the totally laparoscopic distal gastrectomy (TLDG) has become more widely applied in the clinic, and studies have confirmed that TLDG has comparable long-term outcomes compared with open surgery. As an important branch of TLDG, hand-assisted laparoscopic gastrectomy (HALG) combines the advantages of TLDG with those of open surgery, thereby exerting the best therapeutic effect against gastric cancer [4–6]. In traditional TLDG, 5 ports plus auxiliary small incision reconstruction are usually needed, but with the continuous innovation and

development of minimal invasive technique, laparoscopic gastrectomy with less ports is applied. Theoretically speaking, with fewer ports, the operation will be less difficult and the patients are less traumatized. However, as D2 lymphadenectomy is difficult in surgery and the operation with single port is more complicated than that with 5 ports, the single-port laparoscopic radical gastrectomy is limited in application [7, 8]. On the basis of the single-port laparoscopy, the two-port method is conducted by adding an auxiliary operation port in the patient's right upper abdomen for laparoscopic drainage, which reduces trauma and lowers the difficulty of operation while not increasing the abdominal incision, which has been demonstrated in the clinical treatment of gastric cancer [9]. Previous literature is short of studies on Clavien–Dindo grade and risk factors of complications after DPLDG and HALG [10]. Based on this, the clinical data of 775 patients who underwent DPLDG or HALG in our hospital were retrospectively reviewed to analyze the effect of different surgical procedures on the Clavien–Dindo grade and risk factors of postoperative complications.

2. Materials and Methods

2.1. General Information. The clinical data of 775 patients who underwent distal gastrectomy in our hospital from May 2016 to May 2019 were retrospectively reviewed, and the patients were divided into the DPLDG group ($n = 386$) and HALG group ($n = 389$) according to the surgical method, with no significant difference in the baseline information between the two groups ($p > 0.05$), see Table 1.

2.2. Inclusion and Exclusion Criteria

2.2.1. Inclusion Criteria. (1) Patients met the clinical diagnosis criteria of gastric cancer in the *Surgery of Gastric Cancer* [11] and were confirmed to have gastric cancer by histopathological examination in vivo; (2) patients were not given chemoradiotherapy before surgery; (3) patients met the surgical indications; and (4) the study was reviewed and approved by the Hospital Ethics Committee, and patients and their family members signed the informed consent. *Exclusion Criteria*. (1) Patients had other malignant tumors; (2) patients had history of abdominal surgery or accepted the palliative resection of tumor before; (3) patients had serious brain, heart, lung, or kidney diseases; and (4) patients had coagulation disorders or serious basic diseases.

2.3. Methods. Both surgeries were performed by the same medical team, and the specific steps of DPLDG were as follows. After performing general anesthesia with tracheal intubation, the self-developed single-port multichannel operation device (made by Taizhou Roosin Medical Co., Ltd.) was used to make a 3-4 cm incision below or around the umbilicus on the left side. After the device entered the patient's abdominal cavity layer by layer, a matched incision protective sleeve was placed to hold the device and establish the pneumoperitoneum, with the pressure maintained at 12–15 mmHg. A 5 mm trocar was placed at the subcostal margin of right midclavicular line as the auxiliary operation hole to hang the liver. The ultrasound knife was used to free along the transverse colon to the splenic flexure to fully expose the pancreatic tail and the lower pole of the spleen, position the left gastroepiploic vessel, ligate the left gastroepiploic vessel at the root, and dissect the No. 4sb lymph node. The mesogastrium was separated from the transverse mesocolon, the right gastroomental vein was positioned at the inferior border of pancreas, the right gastroepiploic artery was positioned, and the root was ligated. The No. 6 lymph node was dissected by freeing along the subpyloric region to the suprapyloric region with the gastroduodenal artery as the clue. And the No. 5 lymph node was dissected by dividing the duodenal ampulla with the linear cutting closure and ligating the root. The No. 8a, No. 9, No. 11p, and No. 7 lymph nodes were dissected by freeing the splenic artery, common hepatic artery, and left gastric artery and vein, respectively, at the upper border of pancreas and retropancreatic space and ligating the left gastric vessel, the No. 12a lymph node was dissected by exposing the left portal vein wall, and the No. 3 and No. 1 lymph nodes were dissected after freeing along the lesser curvature of stomach; the gastric body was disconnected at 4-5 cm proximal to the tumor with the linear cutting closure, and the Roux-en-Y anastomosis or Billroth II anastomosis was performed in the cavity. Finally, a drainage tube was indwelled near the gastrointestinal anastomosis port through the auxiliary operation hole in the right upper abdomen.

The specific steps of performing HALG were as follows. General anesthesia was implemented in flat position; a disinfected drape was laid. The operator was standing on the right side of the patient to make an incision in the middle of the upper abdomen and then incised various layers of the abdominal wall sequentially to the abdomen and placed the lap disc base to explore the patient's abdominal cavity in order. The transverse colon was lifted and partial gastrocolic ligament was freed along the upper board of the transverse colon to expose the right crura of diaphragm. A 12 mm trocar was placed as the main operation hole, and the operator put his left hand into the abdominal cavity to install the lap disc and establish a pneumoperitoneum. A 12 mm trocar was placed at about 2 cm of subcostal margin of left anterior axillary line as the observation hole. The lymph node dissection was performed according to the tumor location and the relevant criteria in the latest *radical gastrectomy* [12]. The pneumoperitoneum was closed, and the digestive tract reconstruction was completed under euthyphoria. The Billroth I or II anastomosis was performed on patients who underwent distal gastrectomy, and the Roux-en-Y anastomosis was performed on patients who underwent oesophagus jejunum after total gastrectomy.

2.4. Evaluation Indexes. The surgical time, intraoperative blood loss, incision length, postoperative exhaust time, time to return to full-fluid diet for the first time after surgery, hospital stay after surgery, the off-bed ambulation time after surgery, the number of lymph nodes being dissected, and the

Table 1: Comparison of patients' baseline information between the two groups.

Item	DPLDG group ($n = 386$)	HALG group ($n = 389$)	X^2 (t)	p
Gender			0.101	0.750
Male	201 (52.07%)	207 (53.21%)		
Female	185 (47.93%)	182 (46.79%)		
Mean age ($\overline{x} \pm$ **s**, **years old**)	58.47 ± 5.71	58.52 ± 5.28	0.127	0.899
BMI (kg/m$^{2)}$	22.41 ± 1.62	22.43 ± 1.57	0.175	0.862
Tumor length (cm)	4.24 ± 1.03	4.29 ± 1.05	0.669	0.504
Pathological type				
Glandular carcinoma	214 (55.44%)	219 (56.30%)	0.058	0.810
Squamous cell carcinoma	114 (29.53%)	118 (30.33%)	0.059	0.808
Signet-ring cell carcinoma	58 (15.03%)	52 (13.37%)	0.438	0.508
Basic disease				
Diabetes	118 (30.57%)	120 (30.85%)	0.024	0.876
Hypertension	147 (38.08%)	153 (39.33%)	0.127	0.721
Kidney disease	121 (31.35%)	116 (29.82%)	0.213	0.645
Tumor location				
Antrum	207 (53.63%)	211 (54.24%)	0.030	0.864
Stomach body	146 (37.82%)	151 (38.82%)	0.081	0.776
Gastric angle	33 (8.55%)	27 (6.94%)	0.702	0.402
Range of gastrectomy			0.104	0.747
Total gastrectomy	195 (50.52%)	192 (49.36%)		
Partial gastrectomy	191 (49.48%)	197 (50.64%)		
TNM stage				
I	198 (51.30%)	201 (51.67%)	0.011	0.917
II	146 (37.82%)	149 (38.30%)	0.019	0.891
III	42 (10.88%)	39 (10.03%)	0.151	0.697
Differentiation type				
Low	189 (48.96%)	192 (49.36%)	0.012	0.913
Medium	152 (39.38%)	149 (38.30%)	0.094	0.759
High	45 (11.66%)	48 (12.34%)	0.085	0.770
Lymphatic metastasis rate (%)	46.11% (178/386)	46.53% (181/389)	0.014	0.908
Infiltrative depth				
T_1	134 (34.72%)	129 (33.16%)	0.208	0.648
T_2	95 (24.61%)	93 (23.91%)	0.052	0.819
T_3	121 (31.35%)	126 (32.39%)	0.097	0.755
T_{4a}	36 (9.33%)	41 (10.54%)	0.319	0.572
Number of lymph nodes submitted for inspection	24.41 ± 6.46	24.46 ± 6.48	0.108	0.914

time of removing the abdominal drainage tube of patients in both groups were recorded. The pain severity of patients in both groups was assessed by the numerical pain rating (NRS) scale [13] at 6 h, 12 h, 24 h, and 2 d postoperatively. The patients' self-evaluation to their incisions was assessed by the aesthetic scoring, which was composed of three parts, namely, the satisfaction of incision scar (1–7 points, with 1 point indicating unsatisfied and 7 points indicating fully satisfied), incision scar (1–7 points, with 1 point indicating disgusted and 7 points indicating enjoyed), and incision scar classification (1–10 points, with 1 point indicating the worst and 7 points indicating the best). The sum of the three parts was the final score of incision aesthetic, which was the basis for grading patients' satisfaction of incision as low (3–9 points), medium (10–17 points), and high (18–24 points).

The complication severity within 30 days after surgery was evaluated by the Clavien–Dindo classification system [14], and if the patient had more than one complication, the most severe one was recorded. IIIa complications or complications with higher grade were specified as severe.

The serum albumin (Alb, g/L) and peripheral blood lymphocyte count (Lymph, mm^3) of patients in both groups were tested before surgery and at 3 months, 6 months, and 12 months after surgery, and the prognosis nutrition index (PNI) was calculated by the formula (PNI) = (Alb) × 10 + (Lymph) × 0.005. The quality of life of patients in both groups before surgery and at 1 month after surgery was evaluated by the gastrointestinal quality of life index (GQLI) [15]. The maximum score was 145 points, with higher scores indicating better quality of life.

2.5. Statistical Methods. The experimental data were statistically analyzed and processed by the SPSS21.0, the picture drawing of data was completed by GraphPad Prism 7 (GraphPad Software, San Diego, USA), the enumeration data were examined by X^2 test and expressed by [n (%)], the measurement data were examined by t-test and expressed by ($\overline{x} \pm s$), the single-factor analysis and multivariate analysis of risk factors of postoperative complications were examined

by X^2 test and logistic regression model respectively, and differences were considered statistically significant at $p < 0.05$.

3. Results

3.1. Comparison of Patients' Clinical Effect Indexes between the Two Groups. Compared with the HALG group, the DPLDG group had significantly shorter surgical time, less intraoperative blood loss, and higher postoperative exhaust time ($p < 0.05$), with no significant difference in other clinical indexes ($p > 0.05$); see Table 2.

3.2. Comparison of Patients' Clavien–Dindo Grades of Postoperative Complications between the Two Groups. The overall incidence rate of postoperative complications of the DPLDG group was significantly lower than that of the HALG group ($p < 0.05$); see Table 3.

3.3. Single-Factor and Multivariate Analysis of Risk Factors of Postoperative Complications in Patients of Both Groups. It was showed in the single-factor analysis that the age, tumor length, intraoperative blood loss, pathological stages, and surgical method were related to the postoperative complications, and the results of multivariate analysis indicated that DPLDG was the protective factor for reducing postoperative complications, while age no less than 60 years old and intraoperative blood loss no less than 180 ml were the independent risk factors leading to complications; see Table 4.

3.4. Comparison of Patients' PNI Level Values before Surgery and at Different Moments after Surgery between the Two Groups. The PNI level values at T1, T2, and T3 after surgery of patients in the DPLDG group were significantly higher than those in the HALG group ($p < 0.05$); see Figure 1.

3.5. Comparison of Patients' GLQI Scores before Surgery and at 1 Month after Surgery between the Two Groups. At 1 month after surgery, both groups obtained significantly higher GLQI scores than before, and the GLQI score of the DPLDG group was significantly higher in the between-group comparison ($p < 0.05$); see Figure 2.

4. Discussion

Gastric cancer is a malignant tumor disease of the digestive tract. With the higher demand for the surgical efficacy of gastric cancer currently, an ideal surgical treatment regimen that aims to reduce the impact on the patient's body function and prolong survival time is needed [16, 17]. As surgery continuously becomes more standardized and less invasive, TLDG is applied, with the ultimate goal of providing painless and scarless clinical treatment. However, natural orifice transluminal endoscopic surgery has clinical application limits because of many factors, so the introduction of single-port laparoscopy is considered to be an excessive stage of traditional laparoscopic surgery to natural orifice transluminal endoscopic surgery. Some scholars [18, 19] believe that the single-port laparoscopy is limited in the operation scope, lacks antitraction, and has narrow surgical field, which will lead to an enlarged umbilical incision, etc., so an additional operation hole is added by attempt for countertraction and reducing the difficulty of operation. The efficacy of the two-port laparoscopy method has been proved in previous literature [20, 21], because compared with traditional laparoscopy, patients who underwent the two-port laparoscopy could get off bed and had their indwelling tube removed sooner. As the laparoscopic surgical technique has become more mature, although with some defects such as long surgical time and learning curve, and fatiguing the operator during surgery, most physicians recognize that this surgical approach is as safe and thorough as the open radical gastrectomy. Foreign literature [22] has reported that the HALG was successfully performed to 2 cases for the first time by the abdominal wall suspension technology and the operator putting his left hand into the patient's abdominal cavity through the incision in the right lower abdomen, which was promoted and applied in the clinic as it fully combined the advantages of laparoscopy and open surgery.

The Clavien–Dindo classification system is currently the most definitive criterion internationally for evaluating the postoperative complications including gastric cancer [23]. This study provided the basis for preventing complications after radical gastrectomy by comparing the impact of two surgical methods on the severity of postoperative complications and analyzing the risk factors of postoperative complications. The results showed that age not less than 60 years old was an independent risk factor for postoperative complications, which might be related to the poor body tolerance of the elderly patients, a view that was supported by other scholars [24]; on the other hand, intraoperative blood loss not less than 180 ml was another risk factor, which was proved in the study by FESCO et al. [25]. The study also found that compared with DPLDG, the surgical time of HALG was obviously longer, but the length of surgical time was confirmed to be not significantly associated with the postoperative complications. However, the definition of postoperative adverse events after different surgeries by the Clavien–Dindo classification system might not be consistent and cause bias in the grading of complications in reality. This study was conducted with fewer cases and lack of research on patients' long-term efficacy, so large sample and multicenter prospective studies are still needed in the future to further validate the application value of the Clavien–Dindo classification system in the assessment of postoperative complications of gastric cancer, so as to make a risk assessment and early intervention treatment for the occurrence of postoperative complications in patients and maximize the surgical treatment effect.

In conclusion, patients tend to have grade II complications or complications with lower grade after surgery, and age not less than 60 years old and intraoperative blood loss not less than 180 ml are the independent risk factors that cause postoperative complications. Therefore, we should focus on the high-risk group for complications, take corresponding prevention and treatment measures, and reduce the incidence of postoperative complications.

Table 2: Comparison of patients' clinical effect indexes between the two groups ($\overline{x} \pm s$).

Indicator	DPLDG group ($n = 386$)	HALG group ($n = 389$)	t	p
Surgical time (min)	173.25 ± 19.73	194.36 ± 23.65	13.497	≤0.001
Intraoperative blood loss (mL)	162.46 ± 25.36	171.35 ± 23.41	5.071	≤0.001
Incision length (cm)	5.73 ± 0.58	5.81 ± 0.62	1.854	0.064
Postoperative exhaust time (d)	2.67 ± 0.59	2.53 ± 0.62	3.220	0.001
Time to return to full-liquid diet for the first time after surgery (d)	2.36 ± 0.36	2.41 ± 0.43	1.754	0.080
Hospital stay after surgery (d)	9.35 ± .86	9.42 ± 1.73	0.543	0.588
Off-bed ambulation time after surgery (d)	2.74 ± 0.61	2.68 ± 0.58	1.403	0.161
Number of lymph nodes being dissected (n)	28.43 ± 3.27	28.51 ± 3.16	0.346	0.729
Time of removing the abdominal drainage tube (h)	4.15 ± 1.42	4.23 ± 1.38	0.795	0.427
NRS score (points)				
6 h after surgery	4.72 ± 0.82	4.68 ± 1.03	0.598	0.550
12 h after surgery	3.54 ± 0.75	3.62 ± 0.68	1.556	0.120
24 h after surgery	2.21 ± 0.53	2.28 ± 0.58	1.753	0.080
2 d after surgery	1.47 ± 0.45	1.51 ± 0.35	1.382	0.167
Aesthetic scoring (cases)				
Low	236 (61.14%)	241 (61.95%)	0.054	0.816
Medium	85 (22.02%)	87 (22.37%)	0.013	0.908
High	65 (16.84%)	61 (15.68%)	0.191	0.662

Table 3: Comparison of patients' Clavien–Dindo grades of postoperative complications between the two groups [n (%)].

Complication type	DPLDG group ($n = 386$)	HALG group ($n = 389$)	X^2	p
≤II	27 (36.00%)	53 (51.46%)	4.190	0.041
IIIa	15 (20.00%)	18 (17.48%)	0.183	0.669
IIIb	16 (21.33%)	12 (11.65%)	3.524	0.060
IVa	11 (14.67%)	10 (9.71%)	1.025	0.311
IVb	4 (5.33%)	7 (6.80%)	0.160	0.689
V	2 (2.67%)	3 (2.91%)	0.010	0.922
Overall complication incidence	75 (19.43%)	103 (26.48%)	5.440	0.020

Table 4: Single-factor and multivariate analysis of risk factors of postoperative complications in patients of both groups.

Item	Single-factor analysis		Multivariate analysis	
	Overall incidence rate of complications (%)	p	OR value (95% CI)	p
Gender		0.426		
Male	12.10			
Female	10.84			
Age		0.007	1	0.037
<60 years old	9.29		1.346 (1.048, 1.761)	
≥60 years old	13.68			
Range of gastrectomy		0.339		
Total gastrectomy	12.26			
Partial gastrectomy	10.71			
Surgical method		0.022	1	0.028
DPLDG	9.42		0.742 (0.562, 0.982)	
HALG	13.16			
Tumor length		0.010	1	0.462
<5 cm	9.55		1.137 (0.852, 1.525)	
≥5 cm	13.42			
Pathological stage		0.003	1	0.871
Stage I	9.06		1.051 (0.646, 1.751)	
Stages II-III	13.83			
Intraoperative blood loss (ml)		<0.001	1	<0.001
<180 ml	16.5		1.635 (1.249, 2.14)	
≥180 ml	27.4			

Table 4: Continued.

Item	Single-factor analysis		Multivariate analysis	
	Overall incidence rate of complications (%)	p	OR value (95% CI)	p
Number of lymph nodes submitted for inspection (n)		0.633		
<25	11.10			
≥25	11.87			
Surgical time		0.736		
Less than 180 min	12.31	<0.001		
No less than 180 min	11.27			

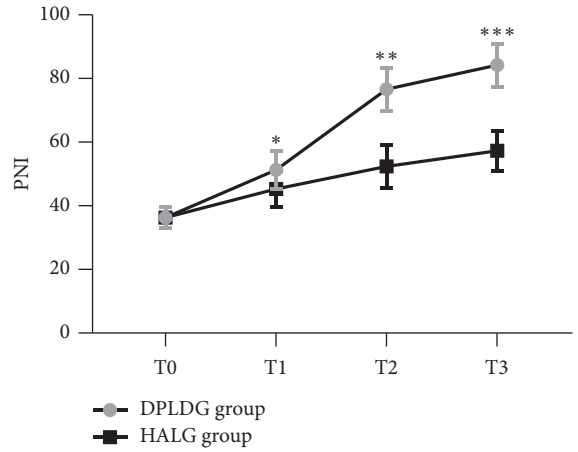

Figure 1: Comparison of patients' PNI level values before surgery and at different moments after surgery between the two groups ($\bar{x} \pm s$). *Note*. The horizontal axis indicated T0, T1, T2, and T3, and the vertical axis indicated the PNI level values. The PNI level values at T0, T1, T2, and T3 of patients in the DPLDG group were 36.26 ± 3.37, 51.26 ± 5.97, 76.63 ± 6.74, and 84.17 ± 6.69, respectively. The PNI level values at T0, T1, T2, and T3 of patients in the HALG group were 36.29 ± 3.41, 45.33 ± 5.63, 52.36 ± 6.81, and 57.26 ± 6.37, respectively. * indicates that the PNI level values at T1 of patients in the two groups were significantly different ($t = 14.227$, $p < 0.001$); ** indicates that the PNI level values at T2 of patients in the two groups were significantly different ($t = 49.861$, $p < 0.001$); and *** indicates that the PNI level values at T3 of patients in the two groups were significantly different ($t = 57.349$, $p < 0.001$).

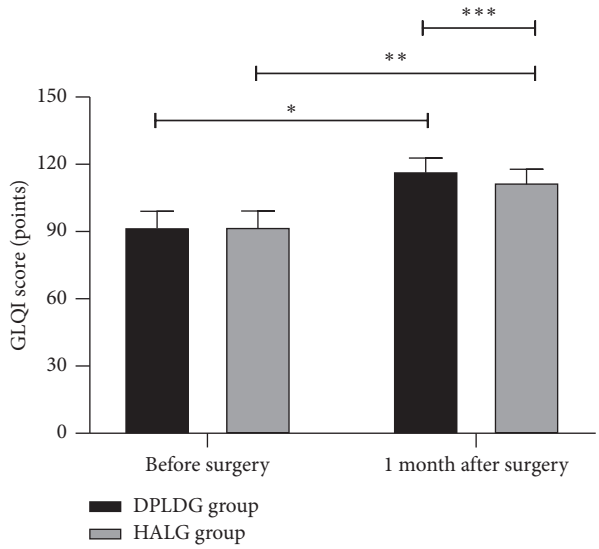

Figure 2: Comparison of patients' GLQI scores before surgery and at 1 month after surgery between the two groups ($\bar{x} \pm s$). *Note*. The horizontal axis indicated before surgery and 1 month after surgery, and the vertical axis indicated the GLQI score (points). The GLQI scores before surgery and at 1 month after surgery of patients in the DPLDG group were (92.35 ± 6.74) and (117.36 ± 5.43), respectively, and those of patients in the HALG group were (92.38 ± 6.79) and (112.36 ± 5.49), respectively. *indicates that the GLQI scores before surgery and at 1 month after surgery of patients in the DPLDG group were significantly different ($t = 56.771$, $p < 0.001$); **indicates that the GLQI scores before surgery and at 1 month after surgery of patients in the HALG group were significantly different ($t = 45.130$, $p < 0.001$); and ***indicates that the GLQI scores at 1 month after surgery of patients in the two groups were significantly different ($t = 12.746$, $p < 0.001$).

Data Availability

The datasets used and/or analyzed during the present study are available from the corresponding author upon reasonable request.

Conflicts of Interest

No conflicts of interest are associated with the publication of this work.

References

[1] G. Giuliani, A. Coratti, A. Patriti et al., "Pancreatic complications after conventional laparoscopic radical gastrectomy versus robotic radical gastrectomy: systematic review and meta-analysis," *Journal of Laparoendoscopic and Advanced Surgical Techniques, Part A*, vol. 28, no. 10, pp. 1207–1215, 2018.

[2] L. L. Cao, J. Lu, C. M. Huang et al., "Which method is more suitable for advanced gastric cancer with enlarged lymph nodes, laparoscopic radical gastrectomy or open gastrectomy?" *Gastric Cancer: Official Journal of the International Gastric Cancer Association and the Japanese Gastric Cancer Association*, vol. 21, no. 5, pp. 853–863, 2018.

[3] K. Nicolaus, S. Zschauer, D. Bräuer et al., "Extensive endometriosis surgery: rASRM and Enzian score independently relate to post-operative complication grade," *Archives of Gynecology and Obstetrics*, vol. 301, no. 3, pp. 699–706, 2020.

[4] P. Téoule, F. Bartel, E. Birgin, F. Rückert, and T. J. Wilhelm, "The Clavien-Dindo classification in pancreatic surgery: a clinical and economic validation," *Journal of Investigative Surgery*, vol. 32, no. 4, pp. 314–320, 2019.

[5] G. Vasileiou, M. Ray-Zack, M. Zielinski, S. Qian, D. D. Yeh, and M. Crandall, "Validation of the American association for the surgery of trauma emergency general surgery score for acute appendicitis-an EAST multicenter study," *Journal of Trauma and Acute Care Surgery*, vol. 87, no. 1, pp. 134–139, 2019.

[6] B. Bucher, N. Maldaner, L. Regli, J. Sarnthein, and C. Serra, "Standardized assessment of outcome and complications in chronic subdural hematoma: results from a large case series," *Acta Neurochirurgica*, vol. 161, no. 7, pp. 1297–1304, 2019.

[7] S. Chiappetta, C. Stier, and R. A. Weiner, "The Edmonton obesity staging system predicts perioperative complications and procedure choice in obesity and metabolic surgery-a German nationwide register-based cohort study (StuDoQ| MBE)," *Obesity Surgery*, vol. 29, no. 12, pp. 3791–3799, 2019.

[8] Y. Hirayama, J. Fujisaki, S. Yoshimizu et al., "Efficacy and safety of endoscopic resection for gastric tube cancer after surgical resection of esophageal squamous cell carcinoma," *Esophagus*, vol. 16, no. 2, pp. 194–200, 2019.

[9] A. Biondi, D. D'Ugo, F. Cananzi et al., "Prognostic indicators in stage IV surgically treated gastric cancer patients: a retrospective multi-institutional study," *Digestive Surgery*, vol. 36, no. 4, pp. 331–339, 2019.

[10] M. Uchida, Y. Kondo, S. Suzuki, and K. Hosohata, "Evaluation of acute kidney injury associated with anticancer drugs used in gastric cancer in the Japanese adverse drug event report database," *Annals of Pharmacotherapy*, vol. 53, no. 12, pp. 1200–1206, 2019.

[11] S. Lin, Y. Zhang, Y. Hu et al., "Epigenetic downregulation of MUC17 by *H. pylori* infection facilitates NF-κB-mediated expression of CEACAM1-3S in human gastric cancer," *Gastric Cancer*, vol. 22, no. 5, pp. 941–954, 2019.

[12] C. Zhang, D. Q. Dai, and Y. Zou, "Downregulation of microRNA-27b-3p via aberrant DNA methylation contributes to malignant behavior of gastric cancer cells by targeting GSPT1," *Biomedicine & pharmacotherapy = Biomedecine & Pharmacotherapie*, vol. 119, no. 119, Article ID 109417, 2019.

[13] F. Shen, P. Liu, Z. Xu et al., "CircRNA_001569 promotes cell proliferation through absorbing miR-145 in gastric cancer," *The Journal of Biochemistry*, vol. 165, no. 1, pp. 27–36, 2019.

[14] S. Komatsu, Y. Shioaki, H. Furuke et al., "Is curative gastrectomy justified for gastric cancer with cytology positive as the only stage IV factor?" *Langenbeck's Archives of Surgery*, vol. 404, no. 5, pp. 599–604, 2019.

[15] Y. Yoshida, T. Beppu, K. Kinoshita et al., "Five-year recurrence-free survival after surgery followed by oral chemotherapy for gastric cancer with portal vein tumor thrombosis," *Anticancer Research*, vol. 39, no. 4, pp. 2233–2238, 2019.

[16] M. Takeuchi, H. Takeuchi, H. Kawakubo et al., "Risk factors for lymph node metastasis in non-sentinel node basins in early gastric cancer: sentinel node concept," *Gastric Cancer*, vol. 22, no. 1, pp. 223–230, 2019.

[17] Y. Yamada, N. Boku, J. Mizusawa et al., "Docetaxel plus cisplatin and S-1 versus cisplatin and S-1 in patients with advanced gastric cancer (JCOG1013): an open-label, phase 3, randomised controlled trial," *The Lancet Gastroenterology & Hepatology*, vol. 4, no. 7, pp. 501–510, 2019.

[18] P. Chen, G. Chen, C. Wang, and C. Mao, "RAB13 as a novel prognosis marker promotes proliferation and chemotherapeutic resistance in gastric cancer," *Biochemical and Biophysical Research Communications*, vol. 519, no. 1, pp. 113–120, 2019.

[19] P. Kaurah, A. Talhouk, A. Macmillan et al., "Hereditary diffuse gastric cancer: cancer risk and the personal cost of preventive surgery," *Familial Cancer*, vol. 18, no. 4, pp. 429–438, 2019.

[20] T. Kumamoto, Y. Kurahashi, S. Haruta et al., "Laparoscopic modified lymphadenectomy in gastric cancer surgery using systematic mesogastric excision: a novel technique based on a concept," *Langenbeck's Archives of Surgery*, vol. 404, no. 3, pp. 369–374, 2019.

[21] P. Priego, M. Cuadrado, A. Ballestero, J. Galindo, and E. Lobo, "Comparison of laparoscopic versus open gastrectomy for treatment of gastric cancer: analysis of a textbook outcome," *Journal of Laparoendoscopic & Advanced Surgical Techniques*, vol. 29, no. 4, pp. 458–464, 2019.

[22] B.-B. Xu, J. Lu, Z.-F. Zheng et al., "Comparison of short-term and long-term efficacy of laparoscopic and open gastrectomy in high-risk patients with gastric cancer: a propensity score-matching analysis," *Surgical Endoscopy*, vol. 33, no. 1, pp. 58–70, 2019.

[23] X. Huang, H. Du, M. Aihemaiti et al., "Laparoscopic-assisted versus open D2 gastrectomy for advanced gastric cancer in highly selective patients," *American Journal of Clinical Oncology*, vol. 42, no. 5, pp. 459–465, 2019.

[24] T. Omori, Y. Fujiwara, K. Yamamoto et al., "The safety and feasibility of single-port laparoscopic gastrectomy for advanced gastric cancer," *Journal of Gastrointestinal Surgery*, vol. 23, no. 7, pp. 1329–1339, 2019.

[25] A. B. Fecso, J. A. Bhatti, P. K. Stotland, F. A. Quereshy, and T. P. Grantcharov, "Technical performance as a predictor of clinical outcomes in laparoscopic gastric cancer surgery," *Annals of Surgery*, vol. 270, no. 1, pp. 115–120, 2019.

Hindawi
Journal of Oncology
Volume 2021, Article ID 9918116, 17 pages
https://doi.org/10.1155/2021/9918116

Review Article

Colorectal Cancer: From Genetic Landscape to Targeted Therapy

Mouade El Bali, Joaira Bakkach, and Mohcine Bennani Mechita

Biomedical Genomics and Oncogenetics Research Laboratory, Faculty of Sciences and Techniques of Tangier, Abdelmalek Essaâdi University, Tetouan, Morocco

Correspondence should be addressed to Mouade El Bali; mouade.elbali@etu.uae.ac.ma

Received 10 March 2021; Accepted 25 June 2021; Published 6 July 2021

Academic Editor: Alamgeer Yuchi

Colorectal cancer (CRC) is the third most common cancer type and the second cause of death worldwide. The advancement in understanding molecular pathways involved in CRC has led to new classifications based on the molecular characteristics of each tumor and also improved CRC management through the integration of targeted therapy into clinical practice. In this review, we will present the main molecular pathways involved in CRC carcinogenesis, the molecular classifications. The anti-VEGF and anti-EGFR therapies currently used in CRC treatment and those under clinical investigation will also be outlined, as well as the mechanisms of primary and acquired resistance to anti-EGFR monoclonal antibodies (cetuximab and panitumumab). Targeted therapy has led to great improvement in the treatment of metastatic CRC. However, there has been variability in CRC treatment outcomes due to molecular heterogeneity in colorectal tumors, which underscores the need for identifying prognostic and predictive biomarkers for CRC-targeted drugs.

1. Introduction

Colorectal cancer (CRC) is considered the third most prevalent cancer and the second cause of death by cancer worldwide [1]. In 2018, 1.8 million new CRC cases were reported and 881,000 persons died of the disease, which accounted for 6.1% and 9.2% of new cases and deaths, respectively [2]. An increasing incidence trend of 2.5 million cases has been predicted in 2035 [3].

Currently, the 5-year overall survival (OS) rate of CRC is estimated at 64% for all stages in the United States, and this seems to decrease to nearly 12% for metastatic CRC (mCRC) [4, 5].

Surgery alone or in combination with chemotherapy and radiotherapy in the adjuvant setting remains the main treatment option in cases of early diagnosis, while surgery is no longer effective for advanced stages that represent 25% of CRCs cases [6]. Unfortunately, the efficacy of cytotoxic therapies may be altered by the rapid evolution of drug resistance and the occurrence of cancer recurrence [7]. Hence, developing other treatment options for CRC, especially for mCRC to increase its overall survival and reduce its severity, is highly needed.

With the advancement in our understanding of carcinogenesis mechanisms and the underlying molecular pathways, treatment of CRC, especially mCRC, has evolved considerably over the past years, which was reflected by using many chemotherapy combinations and integrating novel targeted drugs into clinical practice. This advancement in chemotherapy and targeted drugs has led to significantly improve OS to over 40 months for mCRC patients [8].

Cetuximab was the first targeted agent for CRC that has been approved by the Food and Drug Administration (FDA) in 2004, followed by bevacizumab in the same year. Since then, many other targeted drugs for CRC have been brought to market successively (Figure 1). Targeted agents currently used for the treatment of CRC may be divided into three categories: anti-Vascular Endothelial Growth Factor (VEGF) such as bevacizumab, aflibercept, and ramucirumab; anti-Epidermal Growth Factor Receptor (EGFR) antibodies such as cetuximab and panitumumab; and finally multikinase inhibitors like regorafenib [9].

The advancement in understanding molecular pathways involved in CRC carcinogenesis has also led to many molecular classification systems. The Cancer Genome Atlas (TCGA) and the Consensus Molecular Subtype (CMS) are

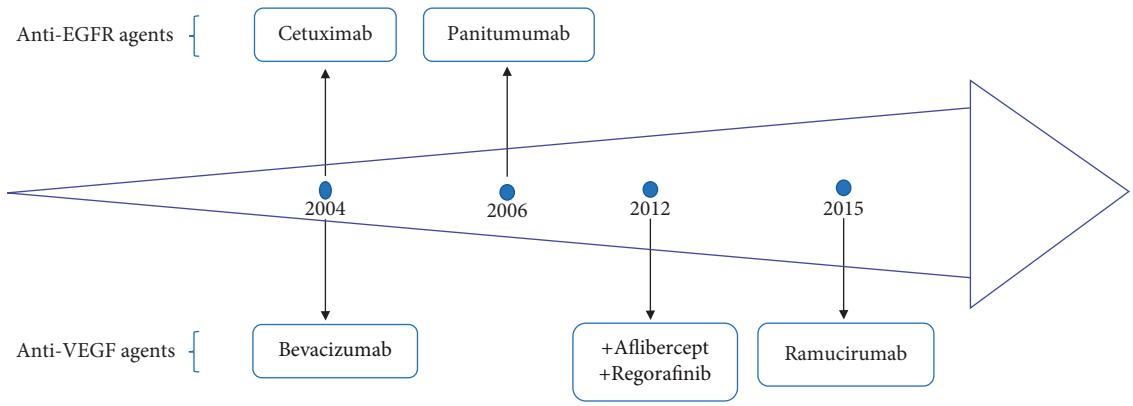

Figure 1: Targeted agent approved for colorectal cancer. EGFR: epidermal growth factor receptor; VEGF: vascular endothelial growth factor.

considered the main classifications. CMS classification has been proposed after analyzing the pathological and molecular profile of CRC patients from many studies. In addition to its potential prognostic and predictive value, CMS can also help to explain the CRC heterogeneity caused by genetic and epigenetic mechanisms [10].

The current review aims to provide an overview of molecular pathways involved in CRC carcinogenesis, as well as molecularly defined subtypes and their clinical implication. We will also summarize available and future CRC-targeted agents and discuss anti-EGFR resistance mechanisms.

2. Molecular Pathways in CRC

2.1. Inherited CRC. The etiologies of CRC are either genetic or environmental or both [11]. CRC is divided into hereditary and sporadic forms, with approximately 75–80% of sporadic forms [12].

Approximately 5% of all CRC cases are caused by inherited germline mutations in some key genes, leading to colorectal carcinogenesis. Approximately 20% of the remaining 95% of CRC cases present a positive family history, which cannot account as a true hereditary form of CRC. Many syndromes have been identified; the most frequent syndromes are Lynch Syndrome (Hereditary Nonpolyposis Colorectal Cancer (HNPCC)) and Familial Adenomatous Polyposis (FAP) [13, 14].

Lynch Syndrome (HNPCC) is the most common hereditary CRC syndrome representing 2-3% of all CRC patients [14]. It is an autosomal dominant syndrome, caused by germline mutations in DNA mismatch repair (MMR) genes, which lead to amplifying the replication errors, increasing rate, and the potential of malignancy. These genes included *MLH1*, *MSH2*, *PMS2*, and *MSH6* resulting in microsatellite instability (MSI) when mutated [15].

Familial Adenomatous Polyposis (FAP) is an autosomal dominant disorder, which is characterized by colorectal adenomatous polyps, which ranged from hundreds to thousands of polyps [16]. It is caused by germline mutations in the adenomatous polyposis coli (*APC*) gene with a frequency of 1% of all CRCs [14]. *APC* gene is a tumor suppressor gene, coding for a protein that regulates the cytoplasm degradation of β-catenin. These two molecules are essential components of the Wnt signaling pathway [17].

There are other rare forms of familial CRC including the *MYH-Associated Polyposis* (MAP), which is an autosomal recessive disorder caused by biallelic mutations in the *MYH* gene. Tumors in this form are commonly microsatellite stable and exhibit a high frequency of APC somatic mutations and a low rate of loss of heterozygosity (LOH) [14]. Additionally, the *Hamartomatous polyposis syndromes* that englobe the syndrome of *PeutzJeghers* (PJS), the syndrome of Juvenile Polyposis (JPS), and the syndrome of Cowden are autosomal dominant syndromes caused by germline mutations in *STK11/LKB1*, *BMPR1A/SMAD4*, and *PTEN*, respectively [18].

More details about these hereditary CRC syndromes, diagnosis, and management approaches have been well reviewed by Kastrinos and Syngal [19].

2.2. Sporadic CRC. With respect to sporadic CRC, Fearon et al. have suggested a colorectal carcinogenesis model that correlated specific genetic landscapes with changing tissue morphology, from adenomas to carcinomas [12, 20]. Genomic instability is considered an essential component of this transformation process [14]. There are three main categories of genomic instability in CRC. Chromosomal instability (CIN), the most frequent representing 70–85% of CRCs, is characterized by the accumulation of numerical or structural chromosomal abnormalities (aneuploidy). FAP is the inherited syndrome associated with these changes [21, 22]. Another type of genomic instability is the MSI, which is caused by MMR alteration [22]. With the increasing knowledge with regard to the involvement of epigenetic factors, particularly the promoter sequence methylation, in the development of certain subsets of cancers and polyps, the third pathway of genomic instability has emerged "CpG Island Methylator Phenotype (CIMP+)" [22]. All these alterations are presented in detail hereinafter.

2.2.1. Chromosome Instability. CIN accounts for 65–70% of sporadic CRCs. It is characterized by the high frequency of LOH, subchromosomal genomic amplifications, and

extensive chromosome imbalances (aneuploidy). In addition to these karyotypic abnormalities, the accumulation of particular mutations in some specific tumor suppressor genes and oncogenes activates CRC pathogenesis [23]. The main genes which are mutated during this pathway are as follows:

APC gene: It is a tumor suppressor gene located on chromosome 5q21. APC functional protein plays an important role in regulating differentiation, adhesion, apoptosis, development, migration, and chromosomal segregation. Mutations or loss of this gene have been found in 40–70% of CRCs and were considered the earliest genetic events in colorectal carcinogenesis [24, 25].

APC protein is a part of a complex that phosphorylates the β-catenin, which causes its ubiquitination and destruction in the proteosome. Truncated APC protein destabilizes the complex and increases the cytoplasmic β-catenin level, which translocates to the nucleus and activates the transcription of various genes involved in tumor growth and invasion, by interacting with the T-cell factor/lymphoid [24]. Half of CRC cases with intact *APC* have activating mutations in the *β-catenin* gene [26], which reflects the importance of the Wnt pathway.

KRAS oncogene: The frequency of *KRAS* proto-oncogene mutations is estimated to range from 30 to 60% in CRCs and large adenomas. Most activating mutations were found to be located in codons 12 and 13 of exon 1 [27]. Activation of K-Ras is known to affect various cellular pathways that regulate cellular growth, survival, proliferation, apoptosis, cytoskeleton organization, cell motility, differentiation, and inflammation [14, 23].

Activation of the *KRAS* gene has been suggested to play a significant role in the transition from adenoma to carcinoma [28].

SMAD2, SMAD4, and *DCC*: These three genes are located at chromosome 18q21. The allelic loss of this site has been found in 60% of CRCs [29]. *DCC* gene encodes for a transmembrane receptor that promotes apoptosis, whereas *SMAD2* and *SMAD4* are part of the transforming growth factor-β (TGF-β) signaling pathway, which regulates growth as well as apoptosis [22, 30].

TP53: It is located on 17p13.1 and encodes for a tumor suppressor protein p53 whose inactivation is usually a late event in the CRC carcinogenesis process [31]. It is widely known that p53 dysfunction is a universal biomarker of human tumors and the loss of its function has been reported in 4–26% of adenomas, 50% of adenomas with invasive foci, and 50–75% of CRCs, which define its role in the transition from adenoma to carcinoma [23, 32].

The CIN pathway is related to mutations in the *APC* gene or allelic loss at chromosome 5q (*APC, MCC* genes), followed by Kirsten rat sarcoma viral oncogene (*KRAS*) mutation, loss of 18q (*DCC, SMAD2,* and *SMAD4* genes), and finally, deletion of 17p, containing the famous tumor suppressor gene *TP53* [24].

2.2.2. Microsatellite Instability. Microsatellites are short sequences with repeated nucleotides, which are distributed across the entire human genome, and consist of mononucleotide, dinucleotide, or higher-order nucleotide repeats such as (A)n or (CA)n [33]. These microsatellites are especially motifs of mutation accumulations, due to the decreasing of DNA polymerase efficiency. The most common errors associated with microsatellites are base-base mismatches and insertion-deletion loops (IDLs) [33, 34].

MMR systems are charged to maintain genomic stability by identifying and repairing base-pair mismatches that occur during DNA replication. Mutator phenotype accompanied with MSI is a result of the MMR systems' inability to correct these errors. There are at least 7 proteins in the mismatch repair systems: hMLH1, hMLH3, hMSH2, hMSH3, hMSH6, hPMS1, and hPMS2, forming 5 protein dimers, which are the MutSα (MSH2, MSH6), MutSβ (MSH2, MSH3), MutLα (MLH1, PMS2), MutLβ (MLH1, PMS1), and finally MutLγ (MLH1, MLH3) [34, 35].

In order to test the MSI, there are two main methods: immunohistochemistry (IHC) which serves for the detection of the expression level of the four main MMR proteins (MSH2, MSH6, MLH1, and PMS2) directly from the tumor tissue. Loss of expression of at least one of these proteins means that the tumor is deficient MMR (dMMR) and as a consequence MSI [36]. The second method is based on testing a DNA microsatellite panel. In this method, MSI-High (MSI-H) is defined when 40% of the markers are unstable [36]. In 1998, a panel of five microsatellite markers called the Bethesda panel has been proposed for the first time by the "International Workshop on Microsatellite Instability and RER Phenotypes in Cancer Detection and Familial Predisposition," which includes two mononucleotides (BAT25 and BAT26) and three dinucleotides (D5S346, D2S123, and D17S250) [37]. Another panel called the Pentaplex panel, composed of five mononucleotides markers, has been proposed (BAT25, BAT26, NR21, NR24, and NR27), due to the high sensitivity of mononucleotides markers compared to dinucleotides. Based on the Pentaplex panel, two types of tumors have been established: MSI (MSI-High) with at least three unstable markers, and microsatellite stability (MSS) with no instability, or the instability in one marker [36].

Approximately 15% of CRC patients show an MSI, 3% of which are caused by germline mutations (Lynch Syndrome), and 12% are due generally to sporadic hypermethylation in the promoter of the *MLH1* gene [38]. Most studies suggested that MSS tumors had a worse prognosis than those with MSI. Additionally, a strong correlation has been found between sporadic MSI and the existence of V600E *BRAF* mutation [39, 40].

2.2.3. CpG Island Methylator Phenotype. Epigenetic regulation of gene expressions is defined as heritable changes without any alteration in the DNA sequence. These epigenetic changes are found to play an important role in the

carcinogenesis of many carcinomas including CRC and offer an explanation of some phenotypes of this disease. Histone modifications or DNA methylation are thought to be the most common cause of epigenetic alterations [41].

CpG island methylation is a typical epigenetic event in colorectal carcinogenesis, accounting for 20% in CRCs [42]. The concept of CIMP in CRC has been originally reported in 1999 by Toyota et al. [43]. It occurs generally by DNA hypermethylation at the 5′-CG-3′ (CpG) dinucleotide in the promoter region, resulting in gene silencing and the function loss of some tumor suppressor genes such as *MLH1, APC, MCC, MGMT*, and several others [44]. As the CIMP refers to the presence of multiple hypermutated genes, Weisenberger et al. have proposed a panel of five markers, which are CACNA1G, IGF2, NEUROG, RUNX3, and SOCS1. CIMP+ was defined by the methylation of 3 to 5 markers and CIMP- by the hypermethylation of 0 to 2 loci [45]. Other studies classified tumors to CIMP-high (CIMP-H) and CIMP-low (CIMP-L) or CIMP-0 [46].

Clinically, CIMP-H CRCs have been associated with female sex, older age, right-sided tumor location, and advanced stage. At the pathologic level, CIMP-H tumors showed higher rates of tumor-infiltrating lymphocytes, Crohn-like infiltrates, perineural, lymphovascular invasion, and higher levels of Fusobacterium nucleatum. With regard to molecular characteristics, this tumor subtype was shown to exhibit a higher prevalence of *BRAF* and *PIK3CA* mutation (OR: 20.17 (95% CI: 13.54–30.05); 1.61 (95% CI: 1.24–2.10), respectively) and more likely to have higher MSI status (OR: 10.95 (95% CI: 8.49–14.13)). Additionally, there was an inverse association of CIMP-H tumors with *TP53* and *KRAS* mutations, and no association has been reported with *APC* mutation [42].

Why CIMP is consistently associated with *BRAF* mutations has long been a debated question. In 2019, Tao et al. provided compelling evidence that solved this long-standing question suggesting that through the aging-like acquisition of DNA methylation, BRAF mutated cells may survive by suppressing senescence and activating stem cell pathways [47].

3. Molecular Classification of CRCs and Associated Features

3.1. Molecular Subtypes of CRC. As we reviewed earlier, there are three major mechanisms of genetic instability in CRC: CIN, MSI, and CIMP. Many studies have tried to establish a molecular classification for CRCs, but these did not lead to a single systematic classification [48].

A systematic molecular pathological classification has been proposed by The Cancer Genome Atlas (TCGA) in 2012 [49] and another one by the Consensus Molecular Subtype (CMS) Consortium in 2015 [50].

Despite the heterogeneity of CRCs, the ancient classification by TCGA has divided CRCs into two subtypes, which are characterized by a specific morphology and molecular alteration.

(i) The hypermutated cancers, representing 16% of CRCs. Three-quarters of this group have a high MSI as a result of dMMR, and the other one-quarter corresponds to ultramutated cancers with polymerase-ε *(POLE)* mutations.

(ii) The nonhypermutated cancers, which account for 84% of CRC cases. The tumors of this group are MSS, which harbors a higher frequency of alterations in somatic DNA and common mutations in *APC*, *TP53, KRAS, SMAD4*, and *PIK3CA* genes [48, 49].

In 2015, an international consortium has analyzed a large-scale data sharing, aiming to establish a new and universal molecular classification and facilitate its clinical implication. The panel experts evaluated six CRC subtyping algorithms from six studies [51–56] and also the data of TCGA, to develop a novel classification of four CMS groups (Figure 2) [50].

(i) CMS1 (microsatellite instability immune, 14%): Almost all patients with MSI were regrouped in this group, characterized by hypermutated profile, especially in *MLH1* gene, and high level of *BRAF* mutations. CMS1 patients have a strong immune activation, reflected by a high level in gene expression, associated with a diffuse immune infiltrate and upregulation in immune response pathways (PD1 activation, NK cells, Th1 cells, and cytotoxic T-cell infiltration signatures) [50]. This immune activation is a new feature of MSI CRCs [57]

(ii) CMS2 (canonical, 37%): It includes patients with higher CIN, which have a high level of somatic copy number alterations (SCNAs). Conversely to CMS1, CMS2 showed a strong upregulation of WNT and MYC downstream targets and epithelial differentiation. Compared with other groups, CMS2 exhibits more frequently copy number gain in oncogenes and copy number losses in tumor suppressor genes [50]

(iii) CMS3 (metabolic,13%): It is characterized by dysregulation of many metabolic pathways (glucose pentose, nitrogen, fatty acid, etc.), CIN with fewer SCANs, higher prevalence of CIMP-low, and higher *KRAS* mutations compared with other groups. Almost 30% of CMS3 was hypermutated, which results in more MSI samples compared with CMS2 and CMS4 [50]

(iv) CMS4 (mesenchymal, 23%): Higher CIN and increased level of SCNAs, with strong expression of epithelial-to-mesenchymal transition (EMT) genes and activation of TGF-β signaling. CMS4 overexpresses more commonly proteins that are implicated in stromal infiltration and angiogenesis and exhibits higher expression level of mesenchymal protein pathways [50]

Finally, there were tumors with mixed features (13%) that possibly represent either a transition phenotype or intratumoral heterogeneity [50].

3.2. Clinical and Prognostic Associations of the CMSs. CMS1 has been found to be significantly more common in females with higher histological grades and right-sided

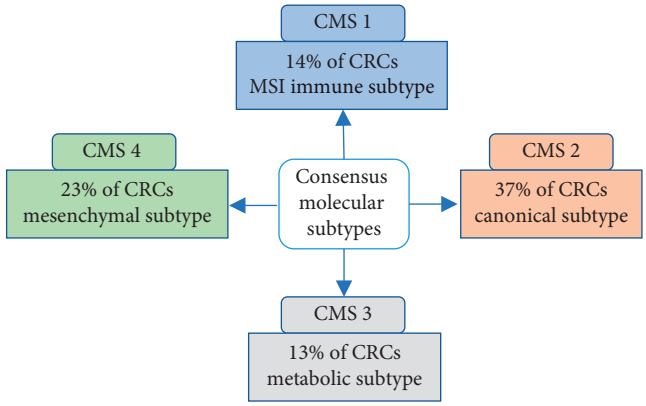

Figure 2: Consensus molecular subtypes classification of colorectal cancer. CMS: Consensus Molecular Subtype; CRCs: colorectal cancers; MSI: microsatellite instability.

lesions, conversely to CMS2 tumors which are more frequently left-sided. CMS4 is diagnosed often at advanced stages compared with other subtypes [50].

By analyzing data from patients enrolled in the PETACC-3 clinical trial [58], Guinney et al. [50] concluded that CMS can be used as a prognostic factor [59], and this was also supported by other studies [60–65]. However, as no targeted therapy regimens are available for primary CRC, stratifying tumors using CMS as a prognostic tool needs further evaluation [66]. In a recent large monocenter cohort study including 308 CRC tumors, Purcell et al. concluded that although CMS alone does not surpass TNM staging in terms of prognostication, their combination seems of interest [66]. CMS3 tumors showed lower OS of stage 2 CRCs than other subtypes, whereas stage 2 patients with a good prognosis exhibited immune activation and upregulation of tumor suppressor genes [66].

After analyzing data from the PETACC-3 clinical trial, CMS4 is reported to have the worst OS and relapse-free survival (RFS) in response to fluorouracil (FU)/leucovorin (LV) and irinotecan adjuvant regimen. CMS1 tumors have also a very poor survival rate after relapse, conversely to CMS2 that tends to have superior survival rates after relapse [50].

An *in vitro* study by Sveen et al. reported a strong response to EGFR and human epidermal growth factor receptor 2 (HER2) inhibitors for the CMS2 group, while CMS1 and CMS4 demonstrated higher sensitivity to HSP90 inhibitors [67]. CMS1 has shown worse PFS and OS in response to anti-EGFR therapy, whereas CMS2 showed particularly better PFS and OS compared with other groups [68]. This was supported by analyzing data from CALGB/SWOG 80405 phase III trial, which found more OS benefit after anti-VEGF than anti-EGFR treatments for the CMS1 group ($P < 0.001$) [60]. However, patients in the CMS2 group treated with cetuximab were found to have better OS compared to those treated with bevacizumab ($P = 0.0046$) [60]. Additionally, analysis of data from the FIRE-3 trial showed significantly better OS for CMS4 group after cetuximab plus FOLFIRI treatment compared to bevacizumab plus FOLFIRI in wild-type RAS mCRC [61].

4. Targeted Therapy in Metastatic CRC

5-fluorouracil (5-FU) was the first chemotherapy regimen used for the treatment of advanced CRC. After many failed combination regimens to improve its response rate, leucovorin has shown for the first time an advantage over 5-FU alone in terms of tumor response rate in 1992 [69]. Thereafter and over the past two decades, other drugs have shown more improvement in terms of survival, either with 5-FU or alone, such as irinotecan, capecitabine, and oxaliplatin [70]. With the understanding of molecular pathways in CRC, a number of targeted biologic therapies have been approved by the FDA. The first ones were the monoclonal antibodies (mAbs) targeting VEGF (bevacizumab) and the EGFR (cetuximab and panitumumab). The advancement in chemotherapy and targeted drugs has led to significantly improve overall survival to over 40 months for mCRC patients [8].

4.1. Antiangiogenic Inhibitors Targeting VEGF or Its Receptors. Angiogenesis is a mechanism that allows the creation of new blood vessels from preexisting ones to supply cancerous cells. It plays a crucial role in tumor initiation, growth, and metastasis [71]. For a long time, targeting the angiogenic pathway has been considered an important approach for cancer therapy. Although more than 40 molecules have been found to play an important role in blood vessel recruitment, most studies have focused on VEGF and its receptors [70]. VEGF signaling pathway is a key contributor in the process of angiogenesis, and high levels of VEGF ligands and its receptors activity were shown to be related to poor prognosis in CRC and other cancers [72–74].

Bevacizumab is the first anti-VEGF drug that has been approved by the FDA in 2004 for the treatment of patients with mCRC, initiating its use as standard first-line treatment in combination with chemotherapy. Bevacizumab is a humanized monoclonal antibody that binds to VEGF-A, preventing its binding on its receptors. According to a phase II clinical trial of Kabbinavar et al., bevacizumab with FU and LV, in the first line of mCRC treatment, was found to improve significantly the progression-free survival (PFS) and response rate (RR) compared to FU/LV plus placebo (PFS: 9 vs. 5.2 months; hazard ratio (HR), 0.005; $P < 0.001$; RR: 40% vs. 17%; $P = 0.029$) but did not improve the median OS (21.5 vs. 13.8 months; $P = 0.137$). The optimal dose of bevacizumab was 5 mg/kg [75]. In a phase III trial, significant improvement in OS was demonstrated with irinotecan, FU and LV (IFL), and bevacizumab compared to IFL plus placebo (20.3 vs. 15.6 months; HR, 0.66; $P < 0.001$) [76]. Other clinical trials have tested new combinations with bevacizumab in mCRC and showed a significant improvement in OS or PFS in first-line setting such as LV calcium, FU, and oxaliplatin-4/capecitabine and oxaliplatin (FOLFOX-4/Xelox), FU, LV, and irinotecan (FOLFIRI) and capecitabine [77–79]. Bevacizumab with FOLFIRI showed a better PFS and OS compared to bolus FU/LV with irinotecan (mIFL) and oral capecitabine with irinotecan (capeIRI) [80]. In the second-line setting, bevacizumab was tested with

FOLFOX-4 and was shown to improve the median PFS and the RR compared to FOLFOX-4 alone (PFS: 7.3 vs. 4.7 months; HR, 0.61; $P \leq 0.0001$; RR: 22.7% vs. 8.6%; $P \leq 0.0001$) [81]. The ML18147 phase III clinical trial concluded that the continuation of bevacizumab with switching second-line-based chemotherapy improved significantly OS compared to chemotherapy alone or bevacizumab alone [82]. Based on the positive results of these studies, the use of bevacizumab with fluoropyrimidine-oxaliplatin or fluoropyrimidine-irinotecan chemotherapy has been approved by the FDA as a second line for mCRC in 2013.

After bevacizumab, three other antiangiogenic agents have been approved for mCRC: aflibercept, regorafenib, and ramucirumab.

Aflibercept (also known as VEGF Trap, AVE0005) is a recombinant fusion protein that acts as a receptor, binding to human VEGF-A, VEGF-B, and placental growth factor (PGF). It is composed of extracellular domains of human VEGF receptors 1 and 2, fused to the Fc portion of human immunoglobulin (Ig)G1. Aflibercept has a high-affinity ligand trap and prevents these ligands to bind to their endogenous receptors [83]. VELOUR phase III trial showed that treatment with FOLFIRI and aflibercept conferred a significant benefit in terms of OS and PFS compared with FOLFIRI and placebo (OS: 13.5 vs. 12.1 months; HR, 0.82; $P = 0.0032$; PFS: 6.9 vs. 4.7 months; HR, 0.76; $P < 0.001$) [84]. Based on the positive results of this clinical trial, aflibercept has been approved after oxaliplatin failure as a second-line treatment in combination with FOLFIRI in mCRC patients by the FDA in August 2012 and by the European Medicines Agency (EMA) in February 2013.

Regorafenib is an oral multikinase inhibitor that inhibits angiogenic tyrosine kinases (vascular endothelial growth factor receptor 1 to 3 (VEGFR1-3), platelet-derived growth factor receptor (PDGFR- β), and fibroblast growth factor receptor (FGFR1)). It also blocks BRAF and oncogenic receptor tyrosine kinases (RTKs), such as RET and KIT [85]. The CORRECT phase III trial showed that treatment with regorafenib conferred a significant improvement in OS compared with the placebo arm, for mCRC that was refractory to standard therapy (6.4 vs. 5 months; HR, 0.77; $P = 0.0052$) [86]. Based on this trial, regorafenib has been approved by the FDA in September 2012 for the treatment of mCRC patients who have been treated previously with fluoropyrimidine-, oxaliplatin- and irinotecan-based chemotherapy, an anti-VEGF therapy, and an anti-EGFR therapy if KRAS wild type.

Ramucirumab is a monoclonal human antibody that has a high affinity to VEGFR-2, the essential receptor of the VEGF angiogenic signaling pathway. The RAISE phase III clinical trial has found that ramucirumab plus FOLFIRI as second-line treatment of mCRC improved significantly OS compared with FOLFIRI plus placebo (13.1 vs. 11.7 months, HR, 0.84; $P = 0.0219$) [87]. Based on these results, ramucirumab (Cyramza) in combination with FOLFIRI has been approved by the FDA as a second-line option for mCRC on April 24, 2015.

Other small multitargeted receptor tyrosine kinase inhibitors (RTKIs) are under investigation for mCRC treatment, such as Famitinib which targets VEGFR2, PDGFR, and c-Kit [88], as well as Fruquintinib and Cediranib which inhibit VEGF1-3 receptors [89, 90]. The main antiangiogenic RTKIs agents, which are under clinical investigation in mCRC, were summarized in Table 1.

4.2. Anti-EGFR Inhibitors. Epidermal growth factor receptor (EGFR/ERBB1) is a member of the erythroblastosis oncogene B (ERBB) family, which also consists of three other receptors, HER2 (ERBB2), HER3 (ERBB3), and HER4 (ERBB4) [91]. Ligands such as EGF, TGFα, Amphiregulin (AREG), and Epiregulin (EREG) activate EGFR by binding to its extracellular domain, leading to the activation of the tyrosine kinase domain in the cytoplasm, which stimulates two major signal-transduction pathways, RAS/RAF/MEK/ERK (mitogen-activated protein kinase (MAPK)) pathway and PI3K/AKT pathway. These two intracellular pathways play key roles in cell proliferation, survival, and migration [92, 93].

There is great evidence that ERBB family members have an important role in the initiation and survival of several solid cancers. Over the last years, many studies have shown the importance of constitutive activation of the EGFR pathway in cancer cell proliferation, stopping apoptosis, and activating metastasis [94–96]. This activation may occur through receptor overexpression and ligand-dependent and independent mechanisms [93]. After the research of Masui et al. in 1983 that provided evidence on the activity of anti-EGFR drugs against epidermoid carcinoma cell growth *in vivo* [97], many studies and clinical trials focused on two classes of anti-EFGR agents, which are the anti-EGFR monoclonal antibodies (cetuximab and panitumumab) and the small-molecule EGFR tyrosine kinase inhibitors [92].

Cetuximab is an anti-EGFR monoclonal antibody mAb (recombinant immunoglobulin G1 (IgG1)), which has been approved by the FDA in 2004, for the treatment of mCRC in combination with irinotecan after irinotecan-based refractory chemotherapy, or as a single agent for mCRC patients who are intolerant to irinotecan. This approval was based essentially on an open-label, randomized trial that showed a significant improvement in terms of RR and PFS for cetuximab with irinotecan, compared to cetuximab alone, in patients who were refractory to irinotecan-based chemotherapy (RR: 22.9 vs. 10.8%; P: 0.007; PFS: 4.1 vs. 1.5; $P < 0.001$) [98]. The CRYSTAL phase III clinical trial showed that cetuximab with FOLFIRI as a first line of treatment increased the RR by 10% (adjusted odds ratio (OR): 1.40; $P = 0.004$) and reduced the risk of mCRC tumor progression by 15% (HR, 0.85; $P = 0.048$) compared to FOLFIRI alone, and this benefit has been limited to KRAS wild-type groups (RR: 59.3% vs. 43.2% (OR, 1.9); PFS: 9.9 vs. 8.2; HR, 0.68; $P = 0.02$). No improvement in OS has been reported in this study, similarly to the previously mentioned trial [99]. Consequently, cetuximab in combination with FOLFIRI has been approved by the FDA for KRAS wild-type mCRC patients as a first-line treatment. FOLFOX4 has been tested in phase II of OPUS clinical trial and showed an improvement in overall response rate (ORR) and a lower risk of

Table 1: Antiangiogenic RTKIs agents under clinical trials investigation in mCRC.

Drugs	Target	Number of participants	Setting	Treatment	Primary outcome measures	Phase	Identifiers
Vatalanib (PTK787/ZK 222584)	VEGFR1-3, FGFR1-3, PDGFRα-β	1168	1st line mCRC	Oxaliplatin/5FU/ Leucovorin ± vatalanib	PFS	III	NCT00056459
		855	2nd line mCRC		OS		NCT00056446
Nintedanib (BIBF1120)	VEGFR1-3, FGFR1-3, PDGFRα-β	768	Refractory mCRC	BSC ± Nintedanib	PFS/OS	III	NCT02149108
		54	Refractory mCRC	mFOLFOX6 ± Nintedanib	PFS	III	NCT01362361
Semaxanib (SU5416)	VEGFR2	710	1st line mCRC	Leucovorin and Fluorouracil ± Semaxanib	OS	III	NCT00004252
Brivanib	VEGFR2/ FGFR1	750	mCRC kRAS wild-type (refractory)	Cetuximab ± Brivanib	OS	III	NCT00640471
Sunitinib	PDGFR-β, VEGFR2,	768	1st line mCRC	FOLFIRI ± Sunitinib	PFS	III	NCT00457691
Fruquintinib	VEGFR1-3	416	3rd line mCRC	Fruquintinib vs. placebo	OS	III	NCT02314819
Cediranib (AZD2171)	VEGFR1-3	1814	1st line mCRC	Beva + folfox vs. beva + Cediranib	PFS	II/III	NCT00384176
Sorafenib	VEGFR1-3 PDGFR-β BRAF	101	2nd line mCRC	FOLFOX6/ FOLFIRI ± Sorafenib	PFS	II	NCT00889343
Vanucizumab	VEGF-A Angiopoietin-2	197	1st line mCRC	mFOLFOX6 + beva vs. mFOLFOX6 + Vancizumab	PFS	II	NCT02141295
Famitinib	VEGFR2-3, c-Kit, PDGFR	154	3rd line advanced mCRC	Famitinib vs. placebo	PFS	II	NCT01762293
Axitinib	VEGFR1-3	70	1st line maintenance therapy	Axitinib alone after FOLFOX/ beva in 1st line	PFS	II	NCT01490866
Apatinib	VEGFR2	54	Refractory mCRC progressed after 2nd line	Apatinib alone	PFS	II	NCT03190616

mCRC: metastatic colorectal cancer; 5FU: 5-fluorouracil; FOLFOX: oxaliplatin in combination with 5-fluorouracil and folinic acid; FOLFIRI: irinotecan in combination with 5-fluorouracil and folinic acid; BSC: best supportive care; Beva: bevacizumab; PFS: progression-free survival; OS: overall survival; VEGFR: vascular endothelial growth factor receptor; FGFR: fibroblast growth factor receptor; PDGFR: platelet-derived growth factor receptor.

disease progression in patients with KRAS wild-type disease treated with cetuximab, as compared to those who received FOLFOX4 alone (ORR = 61 vs. 37%; OR: 2.54; $P = 0.011$; PFS: 7.7 vs. 7.2 months; HR, 0.57; $P = 0.0163$, respectively) [100]. A pooled analysis of the CRYSTAL and OPUS randomized clinical trials has shown that combining cetuximab to chemotherapy (FOLFIRI or FOLFOX4) in patients with KRAS wild-type disease improved significantly OS (HR, 0.81; $P = 0.0062$), PFS (HR, 0.66; $P < 0.0001$), and ORR (OR, 2.16; $P < 0.0001$), compared with chemotherapy alone. In contrast, BRAF mutation status did not show any significant difference in response to cetuximab, but it was a negative prognostic biomarker [101].

Recently, on April 8, 2020, the FDA approved encorafenib in combination with cetuximab for the treatment of mCRC with a BRAF V600E mutation, after prior therapy. This approval was based on the phase III BEACON CRC study, which showed an improvement of median OS for mCRC patients with BRAF V600E treated with cetuximab and encorafenib compared to cetuximab alone (8.4 vs. 5.4 months; HR, 0.6; $P < 0.001$) [102]. In the second-line setting, the phase III EPIC study has shown that cetuximab and irinotecan improved significantly PFS and RR and resulted in a better quality of life, after oxaliplatin and fluoropyrimidine failure, compared with irinotecan alone [103]. Additionally, cetuximab alone was shown to improve OS and PFS, in wild-type KRAS patients who failed all other treatments, compared with best supportive care (BSC) alone (9.5 vs. 4.8 months; HR, 0.55; $P < 0.001$ and 3.7 vs. 1.9 months; HR, 0.40; $P < 0.001$, respectively) [104].

Panitumumab is also an anti-EGFR monoclonal antibody. Conversely to cetuximab, it is a fully human IgG2, which has shown reduced immunogenic reactions and high affinity and specificity for the EGF receptors [105]. In phase III clinical trial, panitumumab and BSC showed a significant improvement in PFS for mCRC patients who had progressed after standard chemotherapy, compared with those receiving BSC alone [106]. PRIME phase III study has shown that panitumumab with FOLFOX4 as the first line of treatment for patients with wild-type KRAS mCRC improves significantly PFS compared with FOLFOX4 alone (10 vs. 8.6 months; HR, 0.8; $P = 0.01$) [107]. As a second-line

treatment, panitumumab with FOLFIRI has shown significant improvement in terms of PFS, compared with FOLFIRI alone for mCRC patients without KRAS mutations (5.9 vs. 3.9 months; HR, 0.71; $P = 0.004$) [108]. In 2006, the FDA approved panitumumab as a single agent for the treatment of mCRC KRAS wild-type after chemotherapy regimens failure, and in 2014, it was approved in combination with FOLFOX for patients with wild-type KRAS mCRC in the first-line setting.

5. Resistance to Anti-EGFR Therapy

Generally, resistance to targeted drugs englobes primary (de NOVO or innate) and secondary resistance (acquired resistance) [109]. Patients with primary resistance exhibit gene mutations, allelic loss, or gene overexpression, which inactivate or reduce the effectiveness of the drug targets. As an example, *RAS, BRAF,* and *PIK3CA* mutations and loss of PTEN and HER2 overexpression have been involved in the primary resistance to anti-EGFR therapy [110]. It has been shown that 40% of all mCRC patients will derive benefit from these agents [111]. Hence, identifying predictive biomarkers of response to anti-EGFR mAbs is of utmost importance. With regard to secondary resistance, the underlying mechanisms are the acquired EGFR (S492R) mutation, genetic alterations of RAS, BRAF, HER2, and MET, and the selection effect of preexisting subclones that confer primary resistance to anti-EGFR mAbs. These mechanisms and others have been reviewed by Misale et al. and Zhoa et al. [112, 113].

5.1. Primary Resistance. RAS mutations: the frequency of *KRAS* gene mutations is estimated at 40% in all CRCs. These mutations were shown to directly activate the MAP kinase signaling pathway, leading to anti-EGFR mAbs resistance [70]. Mutations located on exon2 (codon 12 or 13) were considered the first and the most important predictive biomarker for the nonresponse to anti-EGFR mAbs. These alterations represent 85–90% of *KRAS* mutations in CRC, and approximately 40% of mCRC patients were found to be mutation carriers [113, 114]. Based on the results of many studies that reported a nonbenefit from anti-EGFR mAbs and shorter PFS, OS, and RR for patients with *KRAS* exon2 mutations compared with wild-type patients [104, 115–117], the use of anti-EGFR mAbs has been limited by the FDA in 2009 to KRAS exon 2 wild-type mCRC patients [118]. Moreover, other *KRAS* mutations in exon 3 (codons 59 and 61) and exon 4 (codons 117 and 146) and mutations of the *NRAS* isoform (exons 2, 3, and 4) were identified in 15–20% of *KRAS* exon 2 wild-type patients and were found to be related to low PFS and OS in patients treated with cetuximab and panitumumab [119–122]. Of note, not all patients with wild-type RAS respond to anti-EGFR treatment; that is why research and identification of other biomarkers are of utmost importance.

BRAF mutations: BRAF is a downstream effector, which is directly regulated by RAS. Mutations in the *BRAF* gene represent 5–9% of CRCs and may lead to direct activation of the RAS/RAF/ERK pathway [123]. V600E is considered the most commonly reported mutation in BRAF, accounting for more than 95% of all identified mutations. This mutation causes direct activation of the MAP kinase pathway, leading to resistance to anti-EGFR mAbs [124]. Many studies reported that BRAF V600E has been associated with poorer PFS and OS in patients treated with anti-EGFR mAbs [125, 126]. However, a meta-analysis of eight randomized controlled trials by Rowland et al. concluded that there is insufficient evidence to consider BRAF as a predictive biomarker of benefit from anti-EGFR mAbs therapy for RAS wild-type mCRC, as there was no statistically significant difference in OS and PFS between RAS wild-type/BRAF wild-type and RAS wild-type/BRAF mutant [127].

PIK3CA mutations and PTEN loss: PI3K-AKT-mTOR signaling pathway is also known to be activated by EGFR, leading to cell proliferation, cell growth, and apoptosis suppression in CRCs [128]. Mutations on *PIK3CA*, which represent 10–18% of CRCs, can lead to direct activation of the PI3K/AKT pathway and cause resistance to anti-EGFR mAbs [113]. Mutations in exons 9 and 20 account for 80% of all *PIK3CA* mutations and result in its activation and the activation of its downstream signaling pathway [129]. A study by Sartore-Bianchi et al. including 110 mCRC-treated patients reported that *PIK3CA* mutations conferred significant clinical resistance to cetuximab and panitumumab [130]. Another large retrospective consortium analysis study showed that only *PIK3CA* exon 20 mutations have been associated with lower RR, PFS, and OS as a response to cetuximab plus chemotherapy compared with wild types, whereas exon 9 mutations showed no effect [131]. A meta-analysis by Mao et al., which included 576 mCRC patients, found that the objective response rate to anti-EGFR mAbs in the KRAS wild-type group was lower in patients with *PIK3CA* exon 20 mutations, but this difference was not significant due to the limited sample size. However, this study suggested that *PIK3CA* exon 20 mutations may predict the resistance to anti-EGFR mAbs in KRAS wild-type mCRC patients [132].

PTEN is considered a suppressor gene, due to its role in the negative regulation of AKT. Therefore, loss of *PTEN* expression or function leads to persistent activation of the PI3K-AKT-mTOR signaling pathway, which results in permanent cell proliferation and growth [133]. Some studies have found that *PTEN* can be a useful predictive biomarker for the response to anti-EGFR mAbs therapy, particularly in the KRAS wild-type [134–137]. In contrast, other studies did not find a significant difference in response to anti-EGFR therapy between PTEN-positive and PTEN-negative groups [138–140]. To confirm the role of PTEN in anti-EGFR resistance, other large clinical studies are warranted.

Level of EGFR ligand expression: in addition to studying the downstream EGFR signaling pathway in anti-EGFR resistance, the upregulation has also been investigated in some studies, especially in an intact downstream EGFR pathway [141–144]. In an exploratory cetuximab monotherapy clinical trial, cetuximab efficacy has been found to be related to KRAS wild-type and high gene expression levels of AREG and EREG in mCRC patients

[145], whereas other clinical trials confirmed that AREG and EREG expression levels have predictive power to anti-EGFR therapy only for KRAS wild-type patients [142, 146]. A recent study that analyzed tumor tissue of 688 patients participating in FIRE-1, CIOX, and FIRE-3 clinical trials has confirmed that AREG high level is a positive prognostic biomarker for anti-EGFR therapy in mCRC. AREG high level was significantly associated with high OS and PFS compared to a low level (26.2 vs. 21.5 months; $P = 0.007$) (10.0 vs. 8.1 months; $P = 0.001$), respectively [141]. EGFR ligand's high expression level can be related to tumors' dependence on the EGFR signaling pathway, which explains its predictive power in mCRC, but it can also occur as a consequence of epigenetic regulation [147].

STAT3: STAT3 is a transcription factor belonging to the STAT family. It is an essential component of the JAK/STAT signaling pathway, which is activated by EGFR and other receptors [148]. Phosphorylated by JAK, STAT3 plays an important role in cell proliferation, survival, and apoptosis activities [113, 149]. Persistent STAT3 activation may have a key role in anti-EGFR therapy resistance in mCRC. A retrospective study by Dobi et al. reported a significant improvement in time to progression (TTP) and OS for negative phospho-STAT3 compared to positive phospho-STAT3 group (TTP: 6.3 vs. 5.4 months; $P < 0.01$; OS: 13.1 vs. 9.4 months; $P = 0.02$), among 94 mCRC patients who were treated with cetuximab and chemotherapy in the second-line setting or beyond [150]. Another study by Ung et al. indicated a key role of STAT3 in promoting resistance to anti-EGFR treatment and showed that STAT3 activity can be inhibited by the anti-EGFR inhibitors in wild-type K-RAS colon cancer cell lines, suggesting that anti-EGFR therapy combined with STAT3 inhibitors may provide a therapeutic benefit for mCRC patients [151].

5.2. Secondary Resistance. Acquisition of KRAS mutation: as we mentioned previously, the RAS/RAF signaling pathway plays an important role in primary resistance to anti-EGFR mAbs in mCRC, but it has also been involved in acquired resistance [152]. A report by Diaz et al. found that 38% of KRAS wild-type patients who received panitumumab had KRAS mutations in their sera, occurring after five or six months of the treatment [153]. Interestingly, a mathematical model from this study showed that resistance mutations in KRAS were present in a clonal subpopulation within the tumors before initiating panitumumab therapy [153]. Another study reported that 55% (6/11) of patients who developed cetuximab or panitumumab resistance harbored secondary k-RAS mutations, and 9% (1/11) had K-RAS amplification [154]. KRAS variants were detectable in plasma of cetuximab-treated patients 10 months before radiographic documentation of disease progression [154].

EGFR S492R mutation: Montagut et al. were the first to report in 2012 that EGFR S492R mutation confers acquired resistance in mCRC patients treated with cetuximab, but not in those who were treated with panitumumab. In their study, 20% of patients who showed resistance to cetuximab harbored EGFR S492R mutation [155]. Later, a larger cohort study including 505 mCRC KRAS exon 2 wild-type patients suggested that EGFR S492R mutation was not involved in primary resistance to cetuximab [156]. In the ASPECCT study, a randomized controlled phase III trial, EGFR S492R mutation was detected, after analyzing liquid biopsies, in 16% of patients treated with cetuximab compared to 1% in those receiving panitumumab [157].

Amplification of HER2: HER2 can activate the RAS/RAF/ERK and PI3K/AKT pathways through its heterodimerization with EGFR and HER3, which are all members of the ERBB receptors tyrosine kinase family. For this reason, HER2 is considered a potential biomarker for the sensitivity to anti-EGFR therapy [91]. Studies using patient-derived xenografts showed that HER2 amplification or the overexpression of heregulin ligand leads to cetuximab resistance especially in KRAS and BRAF wild-type cancers [158, 159]. These findings have been supported by clinical data from a large retrospective cohort study by Martin et al. showing that HER2 gene copy number may confer resistance to anti-EGFR therapy in KRAS wild mCRC type [160]. HER2 amplification may also be involved in primary resistance, but considering its low frequency (2% of mCRC patients), it is mainly considered a mechanism of secondary resistance to anti-EGFR [113].

MET amplification: mesenchymal-epithelial transition factor (c-MET) is a tyrosine kinase receptor, which is encoded by the protooncogene *MET*. Binding to its ligand the hepatocyte growth factor (HGF), c-MET induces cell proliferation, growth, survival, and angiogenesis, through the activation of PI3K/AKT, RAS/RAF/ERK, STAT3, and nuclear factor-κB (NF-κB) signaling pathways [161]. Liska et al. have confirmed the importance of MET activation in restoring the MAPK and AKT pathways during anti-EGFR therapy in CRC cell lines [162]. In both *in vitro* and *in vivo* settings, Bardelli et al. demonstrated that MET amplification confers acquired resistance in patients who were KRAS wild-type during anti-EGFR therapy. Importantly, findings from this study supported using blood tests to monitor the emergence of MET amplification in patients undergoing anti-EGFR therapies, as the amplification of the MET locus has been present in circulating tumor DNA before any clinical evidence of relapse [163]. Another study by Troiani et al. showed that TGF-α overexpression induces the EGFR-MET interaction leading to subsequent MET pathway activation and MET acquired resistance and suggested that the inhibition of MET expression restores the sensitivity to cetuximab in CRC cell lines [164]. Nonetheless, MET amplification occurs only in 1% of unselected mCRC patients [163, 165], making it a weak predictive biomarker of primary resistance to anti-EGFR therapy in mCRC [113].

The subclone selection: the notion of secondary resistance not only consists of the development of new mutations during the therapy but can also include the selection of a low-frequency subclone that conferred primary resistance under the target therapy pressure [166]. To determine whether the acquired resistance to cetuximab in mCRC patients is due to novel mutations or the selection of pre-existing subclones, Misale et al. compared gene copy number and the mutational profile of parental and resistant cell lines

Table 2: mAbs targeting EGFR pathway under clinical investigation.

Drugs	Target	Setting	Treatment	Phase	Identifiers
Trastuzumab	HER2	HER2-positive wild KRAS mCRC	Trastuzumab + Lapatinib or Pertuzumab Trastuzumab + Tucatinib	II	NCT03225937 NCT03043313
Pertuzumab	HER2	2nd line of advanced or mCRC	Pertuzumab + cetuximab	I/II	NCT00551421
MEHD7945A (Duligotuzumab)	EGFR/ HER3	2nd line K-Ras wild-type mCRC	MEHD7945A + FOLFIRI vs. Cetuximab + FOLFIRI	II	NCT01652482
SYM004	EGFR	mCRC K-Ras WT acquired resistance to Anti-EGFR mAbs	SYM004 vs. BSC	II	NCT02083653
CPGJ 602	EGFR	2nd line mCRC KRAS WT	CPGJ 602 vs. Cetuximab	I	NCT03356158
Futuximab	EGFR	Chemotherapy-refractory mCRC	Futuximab vs. SYM004	II	NCT03549338
SCT 200	EGFR	Wild-type RAS and RAF mCRC	SCT200	II	NCT03405272
Dalotuzumab (MK-0646)	IGF-1R	Wild-type KRAS mCRC	Dalotuzumab + Cetuximab + irinotecan	II/III	NCT00614393
Ganitumab (AMG-479)	IGF-1R	Mutant KRAS mCRC	AMG-479 + FOLFIRI vs. FOLFIRI alone	II	NCT00813605
Cixutumumab (IMC-A12)	IGF-1R	2nd line mCRC kRAS wild-type	Irinotecan and Cetuximab ± IMC-A12	II	NCT00845039

mAbs: monoclonal antibodies; mCRC: metastatic colorectal cancer; FOLFIRI: irinotecan in combination with 5-fluorouracil and folinic acid; BSC: best supportive care; HER: human epidermal growth factor receptor; EGFR: epidermal growth factor receptor; IGF-1R: insulin-like growth factor 1 receptor; KRAS: Kirsten rat sarcoma viral oncogene.

Table 3: TKIs targeting EGFR pathway under clinical investigation.

Drugs	Target	Setting	Treatment	Phase	Identifiers
Erlotinib	EGFR	2nd line k-RAS WT mCRC	Erlotinib + panitumumab ± irinotecan	II	NCT00940316
Neratinib	EGFR/HER2	KRAS/NRAS/BRAF/ PIK3CA wild-type mCRC	Neratinib + Trastuzumb vs. Neratinib + Cetuximab	II	NCT03457896
Sapitinib (AZD8931)	EGFR/ HER2/3	Recurrent or metastatic CRC	AZD8931 + FOLFIRI	II	NCT01862003
Tucatinib	HER2	HER2 positive CRC	Tucatinib + trastuzumab	II	NCT03043313
Lapatinib (GSK572016)	EGFR/ HER2/erk-1/ 2	2nd line advanced or mCRC	Lapatinib + capecitabine	II	NCT00574171
Vemurafenib	BRAF (V600E)	BRAF V600E mutation and advanced CRC	FOLFIRI + Cetuximab + Vemurafenib	II	NCT03727763
Dabrafenib	BRAF (V600E)	BRAF V600E mutation mCRC	Dabrafenib + trametinib + spartalizumab	II	NCT03668431
Encorafenib (LGX-818)	BRAF (V600E)	MSS/BRAF V600E mCRC	Encorafenib + Cetuximab + nivolumab	I/II	NCT04017650
BMS-908662	BRAF	Mutant BRAF mCRC	BMS-908662 + cetuximab	I/II	NCT01086267
Binimetinib (MEK162)	MEK1/2	RAS positive mCRC	Binimetinib + mFOLFIRI	I	NCT02613650
Cobimetinib	MEK1	Locally advanced and metastatic CRC	Cobimetinib + Atezolizumab vs. Regorafenib	III	NCT02788279
Trametinib	MEK1/2	RAS/RAF mutant and TP53 WT mCRC	Trametinib + HDM201	I	NCT03714958
Selumetinib (AZD6244)	MEK1/2	2nd line k-RAS BRAF mCRC	Selumetinib + irinotecan	II	NCT01116271
Alpelisib (BYL719)	PI3K	BRAF mutant mCRC	Alpelisib + Cetuximab vs. BYL719 + Cetuximab + LGX818	I/II	NCT01719380
Buparlisib (BKM120)	PI3K	Wild-type RAS advanced or metastatic CRC	Panitumumab + BKM120	I/II	NCT01591421
Gedatolisib (PF05212384)	PI3K/mTOR	mCRC	Gedatolisib + FOLFIRI vs. FOLFIRI + Bevacizumab	I/II	NCT01937715
Nab-rapamycin (ABI-009)	mTOR	1st line advanced or metastatic CRC	ABI-009 + FOLFOX + bevacizumab	I/II	NCT03439462
Everolimus (RAD001)	mTOR	2nd line mCRC	Irinotecan + Cetuximab ± Everolimus	I/II	NCT00522665

Table 3: Continued.

Drugs	Target	Setting	Treatment	Phase	Identifiers
ONC201	AKT/ERK	MSS mCRC	ONC201 + Nivolumab	I/II	NCT03791398
MK2206	AKT	WT k-RAS/mutated PIK3CA mCRC	MK2206	II	NCT01186705
TTI-101	STAT3	Advanced CRC	TTI-101	I	NCT03195699
Ruxolitinib	JAK/STAT3	RAS mutant advanced CRC and pancreatic cancer	Ruxolitinib + trametinib	I	NCT04303403

mCRC: metastatic colorectal cancer; FOLFIRI: irinotecan in combination with 5-fluorouracil and folinic acid; MSS: microsatellite stability; FOLFOX: leucovorin calcium, fluorouracil, and oxaliplatin; KRAS: Kirsten rat sarcoma viral oncogene; WT Kras: wild-type Kras; HER: human epidermal growth factor receptor; EGFR: epidermal growth factor receptor; BRAF: v-raf murine sarcoma viral oncogene homolog B1; PIK3: phosphatidylinositol 3-kinase; mTOR: mammalian target of rapamycin. JAK: Janus kinase; STAT3: signal transducer and activator of transcription 3.

[154]. This study found that KRAS G13D mutation and KRAS amplification were present in parental cells with low frequency, which supports the theory of subclonal selection [154]. However, other mutations including KRAS G12R and EGFR S492R have been identified only in resistant cells [154, 156], which corroborates that some mutations may occur only during the EGFR mAbs treatment.

5.3. Overcoming Resistance to Anti-EGFR Therapy. In order to overcome resistance to cetuximab/panitumumab in mCRC patients, research studies have been focusing on widening therapeutic choices by testing new monoclonal antibodies against EGFR receptors (Duligotuzumab, Futuximab, etc.), as well as those against HER2, HER3, and IGF-1R receptors (Table 2). Using tyrosine kinase inhibitors to target the EGFR receptor and its downstream pathway is another promising active research area (Table 3).

6. Conclusion

The advancements in molecular technologies in recent decades, especially sequencing techniques, have led to a better understanding of the genomic landscape of CRC and hence increased dramatically our knowledge about the carcinogenesis process. This unprecedented information has been directly harnessed to establish molecular classifications that provide deeper insights into the biology of CRC. Available evidence suggests that the CMS classification might have a predictive and prognostic value, and also it can help to guide drug development and application.

The molecular understanding of CRC carcinogenesis has also led to developing targeted drugs such as anti-VEGF mAbs, anti-EGFR mAbs, and multikinase inhibitors, which improved the survival rates of mCRC patients. However, emerging primary or secondary resistance to current targeted therapies, especially to anti-EGFR mAbs, remains a major problem in clinical practice. Understanding resistance mechanisms, identifying new biomarkers and other targetable pathways is of paramount importance to optimize therapeutic choices and improve survival for resistant patients.

Abbreviations

APC: Adenomatous polyposis coli
AREG: Amphiregulin
BSC: Best supportive care
CapeIRI: Capecitabine and irinotecan
CIMP: CpG Island Methylator Phenotype
CIN: Chromosomal instability
c-MET: Mesenchymal epithelial transition factor
CMS: Consensus molecular subtype
CRC: Colorectal cancer
dMMR: Deficient mismatch repair
EGFR: Epidermal growth factor receptor
EMA: European medicines agency
EMT: Epithelial-to-mesenchymal transition
ERBB: Erythroblastosis oncogene B
EREG: Epiregulin
FAP: Familial adenomatous polyposis
FDA: Food drug administration
FGFR: Fibroblast growth factor receptor
FOLFIRI: Fluorouracil, leucovorin and irinotecan
FOLFOX: Leucovorin calcium, fluorouracil, and oxaliplatin
FU: Fluorouracil
HER: Human epidermal growth factor receptor
HGF: Hepatocyte growth factor
HNPCC: Hereditary nonpolyposis colorectal cancer
HR: Hazard ratio
IDLs: Insertion-deletion loops
IFL: Irinotecan, fluorouracil and leucovorin
IGF-1R: Insulin-like growth factor 1 receptor
IgG: Immunoglobulin G
IHC: Immunohistochemistry
JPS: Juvenile polyposis syndrome
KRAS: Kirsten rat sarcoma viral oncogene
LOH: Loss of heterozygosity
LV: Leucovorin
mAbs: Monoclonal antibodies
MAP: MYH-associated polyposis
MAPK: Mitogen-activated protein kinase
mCRC: Metastatic CRC
MMR: Mismatch repair
MSI: Microsatellite instability
MSI-H: Microsatellite instability high
OR: Odds ratio
ORR: Overall response rate
OS: Overall survival
PDGFR: Platelet-derived growth factor receptor
PFS: Progression-free survival
PGF: Placental growth factor

PJS: Peutz Jeghers
POLE: Polymerase-ε
RFS: Relapse-free survival
RR: Response rate
RTKs: Receptor tyrosine kinases
SCNAs: Somatic copy number alterations
TCGA: The cancer genome atlasTGF:
TGF: Transforming growth factor
TTP: Time to progression
VEGF: Vascular endothelial growth factor
VEGFR: Vascular endothelial growth factor receptor
XELOX: Capecitabine (xeloda) and oxaliplatin.

Conflicts of Interest

The authors declare that they have no conflicts of interest.

Authors' Contributions

Mouade El Bali was responsible for the conception and design of the study, analyzing literature data, and writing the manuscript. Joaira Bakkach drafted some parts of the work, participated in the design and the conception of the study, and revised it critically. Mohcine Bennani Mechita revised the manuscript. All authors read and approved the final version.

References

[1] N. Keum and E. Giovannucci, "Global burden of colorectal cancer: emerging trends, risk factors and prevention strategies," *Nature Reviews Gastroenterology & Hepatology*, vol. 16, no. 12, pp. 713–732, 2019.

[2] F. Bray, J. Ferlay, I. Soerjomataram, R. L. Siegel, L. A. Torre, and A. Jemal, "Global cancer statistics 2018: GLOBOCAN estimates of incidence and mortality worldwide for 36 cancers in 185 countries," *CA: A Cancer Journal for Clinicians*, vol. 68, no. 6, pp. 394–424, 2018.

[3] E. Dekker, P. J. Tanis, J. L. A. Vleugels, P. M. Kasi, and M. B. Wallace, "Colorectal cancer," *The Lancet*, vol. 394, no. 10207, pp. 1467–1480, 2019.

[4] Y.-H. Xie, Y.-X. Chen, and J.-Y. Fang, "Comprehensive review of targeted therapy for colorectal cancer," *Signal Transduction and Targeted Therapy*, vol. 5, no. 1, p. 22, 2020.

[5] R. L. Siegel, K. D. Miller, and A. Jemal, "Cancer statistics, 2019," *CA: A Cancer Journal for Clinicians*, vol. 69, no. 1, pp. 7–34, 2019.

[6] P. Rawla, T. Sunkara, and A. Barsouk, "Epidemiology of colorectal cancer: incidence, mortality, survival, and risk factors," *Gastroenterology Review*, vol. 14, no. 2, pp. 89–103, 2019.

[7] D. Colussi, G. Brandi, F. Bazzoli, and L. Ricciardiello, "Molecular pathways involved in colorectal cancer: implications for disease behavior and prevention," *International Journal of Molecular Sciences*, vol. 14, no. 8, pp. 16365–16385, 2013.

[8] D. M. Graham, V. M. Coyle, R. D. Kennedy, and R. H. Wilson, "Molecular subtypes and personalized therapy in metastatic colorectal cancer," *Current Colorectal Cancer Reports*, vol. 12, no. 3, pp. 141–150, 2016.

[9] H. Seow, W. K. Yip, and T. Fifis, "Advances in targeted and immunobased therapies for colorectal cancer in the genomic era," *OncoTargets and Therapy*, vol. 9, p. 1899, 2016.

[10] H. Sawayama, Y. Miyamoto, K. Ogawa, N. Yoshida, and H. Baba, "Investigation of colorectal cancer in accordance with consensus molecular subtype classification," *Annals of Gastroenterological Surgery*, vol. 4, no. 5, pp. 528–539, 2020.

[11] E. J. Kuipers, W. M. Grady, D. Lieberman et al., "Colorectal cancer," *Nature Reviews Disease Primers*, vol. 1, no. 1, p. 15065, 2015.

[12] A. Morán, "Differential colorectal carcinogenesis: molecular basis and clinical relevance," *World Journal of Gastrointestinal Oncology*, vol. 2, no. 3, p. 151, 2010.

[13] D. G. Power, E. Gloglowski, and S. M. Lipkin, "Clinical genetics of hereditary colorectal cancer," *Hematology/Oncology Clinics of North America*, vol. 24, no. 5, pp. 837–859, 2010.

[14] S. Al-Sohaily, A. Biankin, R. Leong, M. Kohonen-Corish, and J. Warusavitarne, "Molecular pathways in colorectal cancer," *Journal of Gastroenterology and Hepatology*, vol. 27, no. 9, pp. 1423–1431, 2012.

[15] K. Tamura, M. Kaneda, M. Futagawa et al., "Genetic and genomic basis of the mismatch repair system involved in Lynch syndrome," *International Journal of Clinical Oncology*, vol. 24, no. 9, pp. 999–1011, 2019.

[16] L. Valle, E. Vilar, S. V. Tavtigian, and E. M. Stoffel, "Genetic predisposition to colorectal cancer: syndromes, genes, classification of genetic variants and implications for precision medicine," *The Journal of Pathology*, vol. 247, no. 5, pp. 574–588, 2019.

[17] A. S. Aghabozorgi, A. Bahreyni, A. Soleimani et al., "Role of adenomatous polyposis coli (APC) gene mutations in the pathogenesis of colorectal cancer; current status and perspectives," *Biochimie*, vol. 157, pp. 64–71, 2019.

[18] F. G. Campos, "Colorectal cancer risk in hamartomatous polyposis syndromes," *World Journal of Gastrointestinal Surgery*, vol. 7, no. 3, p. 25, 2015.

[19] F. Kastrinos and S. Syngal, "Inherited colorectal cancer syndromes," *The Cancer Journal*, vol. 17, no. 6, pp. 405–415, 2011.

[20] E. R. Fearon and B. Vogelstein, "A genetic model for colorectal tumorigenesis," *Cell*, vol. 61, no. 5, pp. 759–767, 1990.

[21] E. A. H. Kheirelseid, N. Miller, and M. J. Kerin, "Molecular biology of colorectal cancer: review of the literature," *American Journal of Molecular Biology*, vol. 3, no. 2, pp. 72–80, 2013.

[22] D. L. Worthley, "Colorectal carcinogenesis: road maps to cancer," *World Journal of Gastroenterology*, vol. 13, no. 28, p. 3784, 2007.

[23] M. S. Pino and D. C. Chung, "The chromosomal instability pathway in colon cancer," *Gastroenterology*, vol. 138, no. 6, pp. 2059–2072, 2010.

[24] W. M. Grady, "Genomic instability and colon cancer," *Cancer and Metastasis Reviews*, vol. 23, no. 1-2, pp. 11–27, 2004.

[25] S. M. Powell, N. Zilz, Y. Beazer-Barclay et al., "APC mutations occur early during colorectal tumorigenesis," *Nature*, vol. 359, no. 6392, pp. 235–237, 1992.

[26] A. B. Sparks, P. J. Morin, B. Vogelstein, and K. W. Kinzler, "Mutational analysis of the APC//3-catenin/Tcf pathway in colorectal cancer," *Cancer Research*, vol. 58, pp. 1130–1134, 1998.

[27] M. Brink, "K-ras oncogene mutations in sporadic colorectal cancer in the Netherlands cohort study," *Carcinogenesis*, vol. 24, no. 4, pp. 703–710, 2003.

[28] J.-Y. Wang, Y.-H. Wang, S.-W. Jao et al., "Molecular mechanisms underlying the tumorigenesis of colorectal adenomas: correlation to activated K-ras oncogene," *Oncology Reports*, vol. 16, no. 6, pp. 1245–1252, 2006.

[29] G. Tarafa, A. Villanueva, L. Farré et al., "DCC and SMAD4 alterations in human colorectal and pancreatic tumor dissemination," *Oncogene*, vol. 19, no. 4, pp. 546–555, 2000.

[30] K. L. Woodford-Richens, A. J. Rowan, P. Gorman et al., "SMAD4 mutations in colorectal cancer probably occur before chromosomal instability, but after divergence of the microsatellite instability pathway," *Proceedings of the National Academy of Sciences*, vol. 98, no. 17, pp. 9719–9723, 2001.

[31] A. J. Cole, Y. Zhu, T. Dwight et al., "Comprehensive analyses of somatic TP53 mutation in tumors with variable mutant allele frequency," *Scientific Data*, vol. 4, no. 1, Article ID 170120, 2017.

[32] A. Leslie, F. A. Carey, N. R. Pratt, and R. J. C. Steele, "The colorectal adenoma-carcinoma sequence," *British Journal of Surgery*, vol. 89, no. 7, pp. 845–860, 2002.

[33] E. Vilar and S. B. Gruber, "Microsatellite instability in colorectal cancer-the stable evidence," *Nature Reviews Clinical Oncology*, vol. 7, no. 3, pp. 153–162, 2010.

[34] J. Jiricny, "The multifaceted mismatch-repair system," *Nature Reviews Molecular Cell Biology*, vol. 7, no. 5, pp. 335–346, 2006.

[35] M. Hewish, C. J. Lord, S. A. Martin, D. Cunningham, and A. Ashworth, "Mismatch repair deficient colorectal cancer in the era of personalized treatment," *Nature Reviews Clinical Oncology*, vol. 7, no. 4, pp. 197–208, 2010.

[36] C. Evrard, G. Tachon, V. Randrian, L. Karayan-Tapon, and D. Tougeron, "Microsatellite instability: diagnosis, heterogeneity, discordance, and clinical impact in colorectal cancer," *Cancers*, vol. 11, no. 10, p. 1567, 2019.

[37] C. R. Boland, S. N. Thibodeau, S. R. Hamilton et al., "A National Cancer Institute workshop on microsatellite instability for cancer detection and familial predisposition: development of international criteria for the determination of microsatellite instability in colorectal cancer," *Cancer Research*, vol. 58, pp. 5248–5257, 1998.

[38] C. R. Boland and A. Goel, "Microsatellite instability in colorectal cancer," *Gastroenterology*, vol. 138, no. 6, pp. 2073–2087, 2010.

[39] G. Deng, I. Bell, S. Crawley et al., "BRAF mutation is frequently present in sporadic colorectal cancer with methylated hMLH1, but not in hereditary nonpolyposis colorectal cancer," *Clinical Cancer Research*, vol. 10, no. 1, pp. 191–195, 2004.

[40] A. McGivern, C. V. A. Wynter, V. L. J. Whitehall et al., "Promoter hypermethylation frequency and BRAF mutations distinguish hereditary non-polyposis colon cancer from sporadic MSI-H colon cancer," *Familial Cancer*, vol. 3, no. 2, pp. 101–107, 2002.

[41] M. Esteller, "Epigenetics in cancer," *New England Journal of Medicine*, vol. 358, pp. 1148–1159, 2008.

[42] S. M. Advani, P. Advani, S. M. DeSantis et al., "Clinical, pathological, and molecular characteristics of CpG island methylator phenotype in colorectal cancer: a systematic review and meta-analysis," *Translational Oncology*, vol. 11, no. 5, pp. 1188–1201, 2018.

[43] M. Toyota, N. Ahuja, M. Ohe-Toyota, J. G. Herman, S. B. Baylin, and J.-P. J. Issa, "CpG island methylator phenotype in colorectal cancer," *Proceedings of the National Academy of Sciences of the United States of America*, vol. 96, pp. 8681–8686, 1999.

[44] J. J. L. Wong, N. J. Hawkins, and R. L. Ward, "Colorectal cancer: a model for epigenetic tumorigenesis," *Gut*, vol. 56, no. 1, pp. 140–148, 2007.

[45] D. J. Weisenberger, K. D. Siegmund, and M. Campan, "CpG island methylator phenotype underlies sporadic microsatellite instability and is tightly associated with BRAF mutation in colorectal cancer," *Nature Genetics*, vol. 38, no. 7, pp. 787–793, 2006.

[46] Y.-Y. Rhee, K.-J. Kim, and G. H. Kang, "CpG island methylator phenotype-high colorectal cancers and their prognostic implications and relationships with the serrated neoplasia pathway," *Gut Liver*, vol. 11, no. 1, pp. 38–46, 2017.

[47] Y. Tao, B. Kang, D. A. Petkovich et al., "Aging-like spontaneous epigenetic silencing facilitates Wnt activation, stemness, and BrafV600E-induced tumorigenesis," *Cancer Cell*, vol. 35, no. 2, pp. 315–328, 2019.

[48] M. F. Müller, A. E. K. Ibrahim, and M. J. Arends, "Molecular pathological classification of colorectal cancer," *Virchows Archiv*, vol. 469, no. 2, pp. 125–134, 2016.

[49] The Cancer Genome Atlas Network, "Comprehensive molecular characterization of human colon and rectal cancer," *Nature*, vol. 487, no. 7407, pp. 330–337, 2012.

[50] J. Guinney, R. Dienstmann, X. Wang et al., "The consensus molecular subtypes of colorectal cancer," *Nature Medicine*, vol. 21, no. 11, pp. 1350–1356, 2015.

[51] P. Roepman, A. Schlicker, J. Tabernero et al., "Colorectal cancer intrinsic subtypes predict chemotherapy benefit, deficient mismatch repair and epithelial-to-mesenchymal transition: molecular subtypes in colorectal cancer," *International Journal of Cancer*, vol. 134, no. 3, pp. 552–562, 2014.

[52] E. Budinska, V. Popovici, S. Tejpar et al., "Gene expression patterns unveil a new level of molecular heterogeneity in colorectal cancer: gene expression heterogeneity in colorectal cancer," *Journal of Pathology*, vol. 231, no. 1, pp. 63–76, 2013.

[53] A. Schlicker, G. Beran, C. M. Chresta et al., "Subtypes of primary colorectal tumors correlate with response to targeted treatment in colorectal cell lines," *BMC Medical Genomics*, vol. 5, no. 1, p. 66, 2012.

[54] A. Sadanandam, C. A. Lyssiotis, K. Homicsko et al., "A colorectal cancer classification system that associates cellular phenotype and responses to therapy," *Nature Medicine*, vol. 19, no. 5, pp. 619–625, 2013.

[55] F. D. S. E. Melo, X. Wang, M. Jansen et al., "Poor-prognosis colon cancer is defined by a molecularly distinct subtype and develops from serrated precursor lesions," *Nature Medicine*, vol. 19, no. 5, pp. 614–618, 2013.

[56] L. Marisa, A. de Reyniès, A. Duval et al., "Gene expression classification of colon cancer into molecular subtypes: characterization, validation, and prognostic value," *PLoS Medicine*, vol. 10, no. 5, Article ID e1001453, 2013.

[57] N. J. Llosa, M. Cruise, A. Tam et al., "The vigorous immune microenvironment of microsatellite instable colon cancer is balanced by multiple counter-inhibitory checkpoints," *Cancer Discovery*, vol. 5, no. 1, pp. 43–51, 2015.

[58] E. Van Cutsem, R. Labianca, G. Bodoky et al., "Randomized phase III trial comparing biweekly infusional fluorouracil/leucovorin alone or with irinotecan in the adjuvant treatment of stage III colon cancer: PETACC-3," *Journal of Clinical Oncology*, vol. 27, no. 19, pp. 3117–3125, 2009.

[59] E. Fontana, K. Eason, A. Cervantes, R. Salazar, and A. Sadanandam, "Context matters—consensus molecular subtypes of colorectal cancer as biomarkers for clinical trials," *Annals of Oncology*, vol. 30, no. 4, pp. 520–527, 2019.

[60] H.-J. Lenz, F.-S. Ou, A.-P. Venook et al., "Impact of consensus molecular subtype on survival in patients with metastatic colorectal cancer: results from CALGB/SWOG 80405 (alliance)," *Journal of Clinical Oncology*, vol. 37, no. 22, pp. 1876–1885, 2019.

[61] S. Stintzing, P. Wirapati, H. J. Lenz, D. Neureiter, L. Fischer von Weikersthal, and T. Decker, "Consensus molecular subgroups (CMS) of colorectal cancer (CRC) and 1st-line efficacy of FOLFIRI plus cetuximab or bevacizumab in the FIRE3 (AIO KRK-0306) trial," *Annals of Oncology*, vol. 30, pp. 1796–1803, 2019.

[62] J. K. Mooi, P. Virapati, R. Asher et al., "The prognostic impact of consensus molecular subtypes (CMS) and its predictive effects for bevacizumab benefit in metastatic colorectal cancer: molecular analysis of the AGITG MAX clinical trial," *Annals of Oncology*, vol. 29, no. 11, pp. 2240–2246, 2018.

[63] L. Marisa, M. Ayadi, R. Balogoun et al., "Clinical utility of colon cancer molecular subtypes: validation of two main colorectal molecular classifications on the PETACC-8 phase III trial cohort," *Journal of Clinical Oncology*, vol. 35, no. 15_ suppl, p. 3509, 2017.

[64] N. Song, K. L. Pogue-Geile, P. G. Gavin et al., "Clinical outcome from oxaliplatin treatment in stage II/III colon cancer according to intrinsic subtypes: secondary analysis of NSABP C-07/NRG oncology randomized clinical trial," *JAMA Oncology*, vol. 2, no. 9, p. 1162, 2016.

[65] N. Rodriguez-Salas, G. Dominguez, R. Barderas et al., "Clinical relevance of colorectal cancer molecular subtypes," *Critical Reviews in Oncology and Hematology*, vol. 109, pp. 9–19, 2017.

[66] R. V. Purcell, S. Schmeier, Y. C. Lau, J. F. Pearson, and F. A. Frizelle, "Molecular subtyping improves prognostication of Stage 2 colorectal cancer," *BMC Cancer*, vol. 19, no. 1, p. 1155, 2019.

[67] A. Sveen, J. Bruun, P. W. Eide et al., "Colorectal cancer consensus molecular subtypes translated to preclinical models uncover potentially targetable cancer cell dependencies," *Clinical Cancer Research*, vol. 24, no. 4, pp. 794–806, 2018.

[68] A. Okita, S. Takahashi, K. Ouchi et al., "Consensus molecular subtypes classification of colorectal cancer as a predictive factor for chemotherapeutic efficacy against metastatic colorectal cancer," *Oncotarget*, vol. 9, no. 27, 2018.

[69] "Modulation of fluorouracil by leucovorin in patients with advanced colorectal cancer: evidence in terms of response rate. advanced colorectal cancer meta-analysis project," *Journal of Clinical Oncology*, vol. 10, no. 6, pp. 896–903, 1992.

[70] J. Akkad, S. Bochum, and U. M. Martens, "Personalized treatment for colorectal cancer: novel developments and putative therapeutic strategies," *Langenbeck's Archives of Surgery*, vol. 400, no. 2, pp. 129–143, 2015.

[71] V. Loizzi, V. D. Vecchio, G. Gargano et al., "Biological pathways involved in tumor angiogenesis and bevacizumab based anti-angiogenic therapy with special references to ovarian cancer," *International Journal of Molecular Sciences*, vol. 18, no. 9, p. 1967, 2017.

[72] L. V. dos Santos, M. R. Cruz, G. de Lima Lopes, and J. P. d. S. N. Lima, "VEGF-A levels in bevacizumab-treated breast cancer patients: a systematic review and meta-analysis," *Breast Cancer Research and Treatment*, vol. 151, no. 3, pp. 481–489, 2015.

[73] J. M. Jürgensmeier, H.-J. Schmoll, J. D. Robertson et al., "Prognostic and predictive value of VEGF, sVEGFR-2 and CEA in mCRC studies comparing cediranib, bevacizumab and chemotherapy," *British Journal of Cancer*, vol. 108, no. 6, pp. 1316–1323, 2013.

[74] A. Lopez, K. Harada, M. Vasilakopoulou, N. Shanbhag, and J. A. Ajani, "Targeting angiogenesis in colorectal carcinoma," *Drugs*, vol. 79, no. 1, pp. 63–74, 2019.

[75] F. Kabbinavar, "Phase II, randomized trial comparing bevacizumab plus fluorouracil (FU)/Leucovorin (LV) with FU/LV alone in patients with metastatic colorectal cancer," *Journal of Clinical Oncology*, vol. 21, no. 1, pp. 60–65, 2003.

[76] H. Hurwitz, L. Fehrenbacher, W. Novotny et al., "Bevacizumab plus irinotecan, fluorouracil, and leucovorin for metastatic colorectal cancer," *New England Journal of Medicine*, vol. 350, no. 23, pp. 2335–2342, 2004.

[77] L. B. Saltz, S. Clarke, E. Díaz-Rubio et al., "Bevacizumab in combination with oxaliplatin-based chemotherapy as first-line therapy in metastatic colorectal cancer: a randomized phase III study," *Journal of Clinical Oncology*, vol. 26, no. 12, pp. 2013–2019, 2008.

[78] G. P. Stathopoulos, "Treatment of colorectal cancer with and without bevacizumab: a phase III study," *Oncology*, vol. 78, no. 5-6, pp. 376–381, 2010.

[79] N. C. Tebbutt, K. Wilson, V. J. Gebski et al., "Capecitabine, bevacizumab, and mitomycin in first-line treatment of metastatic colorectal cancer: results of the australasian gastrointestinal trials group randomized phase III MAX study," *Journal of Clinical Oncology*, vol. 28, no. 19, pp. 3191–3198, 2010.

[80] C. S. Fuchs, J. Marshall, and J. Barrueco, "Randomized, controlled trial of irinotecan plus infusional, bolus, or oral fluoropyrimidines in first-line treatment of metastatic colorectal cancer: updated results from the BICC-C study," *Journal of Clinical Oncology*, vol. 26, no. 4, pp. 689-690, 2008.

[81] B. J. Giantonio, P. J. Catalano, N. J. Meropol et al., "Bevacizumab in combination with oxaliplatin, fluorouracil, and leucovorin (FOLFOX4) for previously treated metastatic colorectal cancer: results from the eastern cooperative oncology group study E3200," *Journal of Clinical Oncology*, vol. 25, no. 12, pp. 1539–1544, 2007.

[82] J. Bennouna, J. Sastre, D. Arnold et al., "Continuation of bevacizumab after first progression in metastatic colorectal cancer (ML18147): a randomised phase 3 trial," *Lancet Oncology*, vol. 14, no. 1, pp. 29–37, 2013.

[83] A. Patel and W. Sun, "Ziv-aflibercept in metastatic colorectal cancer," *Biologics: Targets and Therapy*, vol. 8, pp. 13–25, 2013.

[84] E. Van Cutsem, J. Tabernero, R. Lakomy et al., "Addition of aflibercept to fluorouracil, leucovorin, and irinotecan improves survival in a phase III randomized trial in patients with metastatic colorectal cancer previously treated with an oxaliplatin-based regimen," *Journal of Clinical Oncology*, vol. 30, no. 28, pp. 3499–3506, 2012.

[85] S. M. Wilhelm, J. Dumas, L. Adnane et al., "Regorafenib (BAY 73-4506): a new oral multikinase inhibitor of angiogenic, stromal and oncogenic receptor tyrosine kinases with potent preclinical antitumor activity," *International Journal of Cancer*, vol. 129, no. 1, pp. 245–255, 2011.

[86] A. Grothey, E. V. Cutsem, A. Sobrero et al., "Regorafenib monotherapy for previously treated metastatic colorectal cancer (CORRECT): an international, multicentre,

randomised, placebo-controlled, phase 3 trial," *The Lancet*, vol. 381, no. 9863, pp. 303–312, 2013.

[87] M. Moore, S. Gill, T. Asmis et al., "Randomized phase II study of modified FOLFOX-6 in combination with ramucirumab or icrucumab as second-line therapy in patients with metastatic colorectal cancer after disease progression on first-line irinotecan-based therapy," *Annals of Oncology*, vol. 27, no. 12, pp. 2216–2224, 2016.

[88] R.-H. Xu, L. Shen, K.-M. Wang et al., "Famitinib versus placebo in the treatment of refractory metastatic colorectal cancer: a multicenter, randomized, double-blinded, placebo-controlled, phase II clinical trial," *Chinese Journal of Cancer*, vol. 36, no. 1, p. 97, 2017.

[89] J. Li, S. Qin, R.-H. Xu et al., "Effect of fruquintinib vs. placebo on overall survival in patients with previously treated metastatic colorectal cancer: the FRESCO randomized clinical trial," *JAMA*, vol. 319, no. 24, p. 2486, 2018.

[90] P. M. Hoff, A. Hochhaus, B. C. Pestalozzi et al., "Cediranib plus FOLFOX/CAPOX versus placebo plus FOLFOX/CAPOX in patients with previously untreated metastatic colorectal cancer: a randomized, double-blind, phase III study (horizon II)," *Journal of Clinical Oncology*, vol. 30, no. 29, pp. 3596–3603, 2012.

[91] C. L. Arteaga and J. A. Engelman, "ERBB receptors: from oncogene discovery to basic science to mechanism-based cancer therapeutics," *Cancer Cell*, vol. 25, no. 3, pp. 282–303, 2014.

[92] C. Fortunato and T. Giampaolo, "EGFR antagonists in cancer treatment," *New England Journal of Medicine*, vol. 358, pp. 1160–1174, 2008.

[93] M. Scaltriti and J. Baselga, "The epidermal growth factor receptor pathway: a model for targeted therapy," *Clinical Cancer Research*, vol. 12, no. 18, pp. 5268–5272, 2006.

[94] A. E. Koyen, G. Nabeta, S. Bienfait, A. J. Schlafstein, D. S. Yu, and W. Daddacha, "EGFR role in cancer: a potential therapeutic target," in *Role of Tyrosine Kinases in Gastrointestinal Malignancies*, G. P. Nagaraju, Ed., Springer, Singapore, pp. 225–234, 2018.

[95] A. B. Singh, "EGFR-signaling and autophagy: how they fit in the cancer landscape," *Journal of Adenocarcinoma*, vol. 1, no. 2, 2016.

[96] S. Sigismund, D. Avanzato, and L. Lanzetti, "Emerging functions of the EGFR in cancer," *Molecular Oncology*, vol. 12, no. 1, pp. 3–20, 2018.

[97] H. Masui, T. Kawamoto, J. D. Sato, B. Wolf, G. Sato, and J. Mendelsohn, "Growth inhibition of human tumor cells in athymic mice by anti-epidermal growth factor receptor monoclonal antibodies," *Journal of Urology*, vol. 132, no. 5, p. 1060, 1984.

[98] D. Cunningham, Y. Humblet, S. Siena et al., "Cetuximab monotherapy and cetuximab plus irinotecan in irinotecan-refractory metastatic colorectal cancer," *New England Journal of Medicine*, vol. 351, no. 4, pp. 337–345, 2004.

[99] E. V. Cutsem, C.-H. Köhne, E. Hitre et al., "Cetuximab and chemotherapy as initial treatment for metastatic colorectal cancer," *New England Journal of Medicine*, vol. 360, pp. 1408–1417, 2009.

[100] C. Bokemeyer, I. Bondarenko, A. Makhson et al., "Fluorouracil, leucovorin, and oxaliplatin with and without cetuximab in the first-line treatment of metastatic colorectal cancer," *Journal of Clinical Oncology*, vol. 27, pp. 663–671, 2009.

[101] C. Bokemeyer, E. V. Custem, P. Rougier et al., "Addition of cetuximab to chemotherapy as first-line treatment for KRAS wild-type metastatic colorectal cancer: pooled analysis of the CRYSTAL and OPUS randomised clinical trials," *European Journal of Cancer*, vol. 48, no. 10, pp. 1466–1475, 2012.

[102] S. Kopetz, A. Grothey, R. Yaeger et al., "Encorafenib, binimetinib, and cetuximab in BRAF V600E-mutated colorectal cancer," *New England Journal of Medicine*, vol. 381, no. 17, pp. 1632–1643, 2019.

[103] A. F. Sobrero, J. Maurel, L. Fehrenbacher et al., "EPIC: phase III trial of cetuximab plus irinotecan after fluoropyrimidine and oxaliplatin failure in patients with metastatic colorectal cancer," *Journal of Clinical Oncology*, vol. 26, pp. 2311–2319, 2008.

[104] C. S. Karapetis, S. Khambata-Ford, D. J. Jonker et al., "K-ras mutations and benefit from cetuximab in advanced colorectal cancer," *New England Journal of Medicine*, vol. 359, no. 17, pp. 1757–1765, 2008.

[105] M. Cohenuram and M. W. Saif, "Panitumumab the first fully human monoclonal antibody: from the bench to the clinic:," *Anti-Cancer Drugs*, vol. 18, no. 1, pp. 7–15, 2007.

[106] E. V. Cutsem, M. Peeters, S. Siena et al., "Open-label phase III trial of panitumumab plus best supportive care compared with best supportive care alone in patients with chemotherapy-refractory metastatic colorectal cancer," *Journal of Clinical Oncology*, vol. 25, no. 13, pp. 1658–1664, 2007.

[107] J. Y. Douillard, S. Siena, J. Cassidy et al., "Final results from PRIME: randomized phase 3 study of panitumumab with FOLFOX4 for first-line treatment of metastatic colorectal cancer," *Annals of Oncology*, vol. 25, pp. 1346–1355, 2014.

[108] M. Peeters, T. Jay Price, A. Cervantes et al., "Randomized phase III study of panitumumab with fluorouracil, leucovorin, and irinotecan (FOLFIRI) compared with FOLFIRI alone as second-line treatment in patients with metastatic colorectal cancer," *Journal of Clinical Oncology*, vol. 28, no. 31, pp. 4706–4713, 2010.

[109] S. Corso and S. Giordano, "Targeted therapies in cancer and mechanisms of resistance," *Journal of Molecular Medicine*, vol. 92, no. 7, pp. 677–679, 2014.

[110] V. Sforza, E. Martinelli, F. Ciardiello et al., "Mechanisms of resistance to anti-epidermal growth factor receptor inhibitors in metastatic colorectal cancer," *World Journal of Gastroenterology*, vol. 22, no. 28, p. 6345, 2016.

[111] A. Karani, T. C. Felismino, L. Diniz, M. Petaccia Macedo, V. Souza e Silva, and C. Abdon Mello, "Is there a role for rechallenge and reintroduction of anti-EGFR plus chemotherapy in later lines of therapy for metastatic colorectal carcinoma? A retrospective analysis," *Ecancermedicalscience*, vol. 14, 2020.

[112] S. Misale, F. Di Nicolantonio, A. Sartore-Bianchi, S. Siena, and A. Bardelli, "Resistance to anti-EGFR therapy in colorectal cancer: from heterogeneity to convergent evolution," *Cancer Discovery*, vol. 4, no. 11, pp. 1269–1280, 2014.

[113] B. Zhao, L. Wang, H. Qui et al., "Mechanisms of resistance to anti-EGFR therapy in colorectal cancer," *Oncotarget*, vol. 8, no. 3, pp. 3980–4000, 2017.

[114] V. K. Morris, F. A. San Lucas, M. J. Overman et al., "Clinicopathologic characteristics and gene expression analyses of non-KRAS 12/13, RAS-mutated metastatic colorectal cancer," *Annals of Oncology*, vol. 25, no. 10, pp. 2008–2014, 2014.

[115] E. V. Cutsem, I. Lang, G. D'haens et al., "KRAS status and efficacy in the first-line treatment of patients with metastatic colorectal cancer (mCRC) treated with FOLFIRI with or without cetuximab: the CRYSTAL experience," *Journal of Clinical Oncology*, vol. 26, no. 15_suppl, p. 2, 2008.

[116] C. Bokemeyer, I. Bondarenko, J. T. Hartmann et al., "KRAS status and efficacy of first-line treatment of patients with metastatic colorectal cancer (mCRC) with FOLFOX with or without cetuximab: the OPUS experience," *Journal of Clinical Oncology*, vol. 26, no. 15_suppl, p. 4000, 2008.

[117] C. J. Allegra, J. M. Jessup, M. R. Somerfield et al., "American Society of Clinical Oncology provisional clinical opinion: testing for KRAS gene mutations in patients with metastatic colorectal carcinoma to predict response to anti-epidermal growth factor receptor monoclonal antibody therapy," *Journal of Clinical Oncology*, vol. 27, no. 12, pp. 2091–2096, 2009.

[118] N. Piton, F. Borrini, A. Bolognese, A. Lamy, and J.-C. Sabourin, "KRAS and BRAF mutation detection: is immunohistochemistry a possible alternative to molecular biology in colorectal cancer?" *Gastroenterology Research and Practice*, vol. 2015, Article ID 753903, 8 pages, 2015.

[119] F. Loupakis, A. Ruzzo, C. Cremolini et al., "KRAS codon 61, 146 and BRAF mutations predict resistance to cetuximab plus irinotecan in KRAS codon 12 and 13 wild-type metastatic colorectal cancer," *British Journal of Cancer*, vol. 101, pp. 715–721, 2009.

[120] C. Bokemeyer, C.-H. Kohne, F. Ciardiello et al., "Treatment outcome according to tumor RAS mutation status in OPUS study patients with metastatic colorectal cancer (mCRC) randomized to FOLFOX4 with/without cetuximab," *Journal of Clinical Onclogy*, vol. 20, 2014.

[121] F. Ciardiello, H.-J. Lenz, C.-H. Kohne et al., "Treatment outcome according to tumor RAS mutation status in CRYSTAL study patients with metastatic colorectal cancer (mCRC) randomized to FOLFIRI with/without cetuximab," *Journal of Clinical Onclogy*, vol. 32, no. 15_suppl, p. 3506, 2014.

[122] J.-Y. Douillard, K. S. Oliner, S. Siena et al., "Panitumumab-FOLFOX4 treatment and RAS mutations in colorectal cancer," *New England Journal of Medicine*, vol. 369, no. 11, pp. 1023–1034, 2013.

[123] H. Davies, G. R. Bignell, C. Cox et al., "Mutations of the BRAF gene in human cancer," *Nature*, vol. 417, no. 6892, pp. 949–954, 2002.

[124] Z. Saridaki, M. Tzardi, M. Sfakianaki et al., "BRAFV600E mutation analysis in patients with metastatic colorectal cancer (mCRC) in daily clinical practice: correlations with clinical characteristics, and its impact on patients' outcome," *PLoS One*, vol. 8, no. 12, Article ID e84604, 2013.

[125] D. P. Modest, A. Jung, N. Moosmann et al., "The influence of KRAS and BRAF mutations on the efficacy of cetuximab-based first-line therapy of metastatic colorectal cancer: an analysis of the AIO KRK-0104-trial," *International Journal of Cancer*, vol. 131, no. 4, pp. 980–986, 2012.

[126] Q. Xu, A. T. Xu, M. M. Zhu, J. L. Tong, X. T. Xu, and Z. H. Ran, "Predictive and prognostic roles of BRAF mutation in patients with metastatic colorectal cancer treated with anti-epidermal growth factor receptor monoclonal antibodies: a meta-analysis: predictive and prognostic roles of BRAF," *Journal of Digestive Diseases*, vol. 14, no. 8, pp. 409–416, 2013.

[127] A. Rowland, M. M. Dias, M. D. Wiese et al., "Meta-analysis of BRAF mutation as a predictive biomarker of benefit from anti-EGFR monoclonal antibody therapy for RAS wild-type metastatic colorectal cancer," *British Journal of Cancer*, vol. 112, no. 12, pp. 1888–1894, 2015.

[128] S. A. Danielsen, P. W. Eide, A. Nesbakken, T. Guren, E. Leithe, and R. A. Lothe, "Portrait of the PI3K/AKT pathway in colorectal cancer," *Biochimica et Biophysica Acta*, vol. 1855, no. 1, pp. 104–121, 2015.

[129] J. A. Engelman, "Targeting PI3K signalling in cancer: opportunities, challenges and limitations," *Nature Reviews Cancer*, vol. 9, no. 8, pp. 550–562, 2009.

[130] A. Sartore-Bianchi, M. Martini, F. Molinari et al., "PIK3CA mutations in colorectal cancer are associated with clinical resistance to EGFR-targeted monoclonal antibodies," *Cancer Research*, vol. 69, no. 5, pp. 1851–1857, 2009.

[131] W. De Roock, B. Claes, D. Bernasconi et al., "Effects of KRAS, BRAF, NRAS, and PIK3CA mutations on the efficacy of cetuximab plus chemotherapy in chemotherapy-refractory metastatic colorectal cancer: a retrospective consortium analysis," *Lancet Oncology*, vol. 11, no. 8, pp. 753–762, 2010.

[132] C. Mao, Z. Y. Yang, X. F. Hu, Q. Chen, and J. L. Tang, "PIK3CA exon 20 mutations as a potential biomarker for resistance to anti-EGFR monoclonal antibodies in KRAS wild-type metastatic colorectal cancer: a systematic review and meta-analysis," *Annals of Oncology*, vol. 23, no. 6, pp. 1518–1525, 2012.

[133] V. Stambolic, A. Suzuki, J. L. de la Pompa et al., "Negative regulation of PKB/Akt-dependent cell survival by the tumor suppressor PTEN," *Cell*, vol. 95, no. 1, pp. 29–39, 1998.

[134] F. Loupakis, L. Pollina, I. Stasi et al., "PTEN expression and KRAS mutations on primary tumors and metastases in the prediction of benefit from cetuximab plus irinotecan for patients with metastatic colorectal cancer," *Journal of Clinical Oncology*, vol. 27, no. 16, pp. 2622–2629, 2009.

[135] M. Frattini, P. Saletti, E. Romagnani et al., "PTEN loss of expression predicts cetuximab efficacy in metastatic colorectal cancer patients," *British Journal of Cancer*, vol. 97, no. 8, pp. 1139–1145, 2007.

[136] Z.-H. Wang, Q.-Y. Gao, and J.-Y. Fang, "Loss of PTEN expression as a predictor of resistance to anti-EGFR monoclonal therapy in metastatic colorectal cancer: evidence from retrospective studies," *Cancer Chemotherapy and Pharmacology*, vol. 69, no. 6, pp. 1647–1655, 2012.

[137] E. Razis, E. Briasoulis, E. Vrettou et al., "Potential value of PTEN in predicting cetuximab response in colorectal cancer: an exploratory study," *BMC Cancer*, vol. 8, no. 1, p. 234, 2008.

[138] P. Laurent-Puig, A. Cayre, G. Manceau et al., "Analysis of PTEN, BRAF, and EGFR status in determining benefit from cetuximab therapy in wild-type KRAS metastatic colon cancer," *Journal of Clinical Oncology*, vol. 27, no. 35, pp. 5924–5930, 2009.

[139] E. I. Ágoston, T. Micsik, B. Ács et al., "In depth evaluation of the prognostic and predictive utility of PTEN immunohistochemistry in colorectal carcinomas: performance of three antibodies with emphasis on intracellular and intratumoral heterogeneity," *Diagnostic Pathology*, vol. 11, no. 1, p. 61, 2016.

[140] L. Salvatore, M. A. Calegari, F. Loupakis et al., "PTEN in colorectal cancer: shedding light on its role as predictor and target," *Cancers*, vol. 11, no. 11, p. 1765, 2019.

[141] A. Stahler, S. Stintzing, D. P. Modest et al., "Amphiregulin expression is a predictive biomarker for EGFR inhibition in metastatic colorectal cancer: combined analysis of three randomized trials," *Clinical Cancer Research*, vol. 26, pp. 6559–6567, 2020.

[142] J. F. Seligmann, F. Elliott, S. D. Richman et al., "Combined epiregulin and amphiregulin expression levels as a predictive biomarker for panitumumab therapy benefit or lack of

benefit in patients with RAS wild-type advanced colorectal cancer," *JAMA Oncology*, vol. 2, no. 5, p. 633, 2016.

[143] P. Llovet, J. Sastre, J. S. Ortega et al., "Prognostic value of BRAF, PI3K, PTEN, EGFR copy number, amphiregulin and epiregulin status in patients with KRAS codon 12 wild-type metastatic colorectal cancer receiving first-line chemotherapy with anti-EGFR therapy," *Molecular Diagnosis and Therapy*, vol. 19, no. 6, pp. 397–408, 2015.

[144] M. Yoshida, T. Shimura, M. Sato et al., "A novel predictive strategy by immunohistochemical analysis of four EGFR ligands in metastatic colorectal cancer treated with anti-EGFR antibodies," *Journal of Cancer Research and Clinical Oncology*, vol. 139, no. 3, pp. 367–378, 2013.

[145] S. Khambata-Ford, C. R. Garrett, N. J. Meropol et al., "Expression of epiregulin and amphiregulin and K-ras mutation status predict disease control in metastatic colorectal cancer patients treated with cetuximab," *Journal of Clinical Oncology*, vol. 25, no. 22, pp. 3230–3237, 2007.

[146] B. Jacobs, W. De Roock, H. Piessevaux et al., "Amphiregulin and epiregulin mRNA expression in primary tumors predicts outcome in metastatic colorectal cancer treated with cetuximab," *Journal of Clinical Oncology*, vol. 27, no. 30, pp. 5068–5074, 2009.

[147] F. Bormann, S. Stinzing, S. Tierling et al., "Epigenetic regulation of amphiregulin and epiregulin in colorectal cancer," *International Journal of Cancer*, vol. 144, no. 3, pp. 569–581, 2019.

[148] F. Laudisi, F. Cherubini, G. Monteleone, and C. Stolfi, "STAT3 interactors as potential therapeutic targets for cancer treatment," *International Journal of Molecular Sciences*, vol. 19, no. 6, p. 1787, 2018.

[149] F. M. Corvinus, C. Orth, R. Moriggl et al., "Persistent STAT3 activation in colon cancer is associated with enhanced cell proliferation and tumor growth," *Neoplasia*, vol. 7, no. 6, pp. 545–555, 2005.

[150] E. Dobi, F. Monnien, S. Kim et al., "Impact of STAT3 phosphorylation on the clinical effectiveness of anti-EGFR-based therapy in patients with metastatic colorectal cancer," *Clinical Colorectal Cancer*, vol. 12, no. 1, pp. 28–36, 2013.

[151] N. Ung, T. L. Putoczki, S. S. Stylli et al., "Anti-EGFR therapeutic efficacy correlates directly with inhibition of STAT3 activity," *Cancer Biology and Therapy*, vol. 15, no. 5, pp. 623–632, 2014.

[152] B. O. Van Emburgh, A. Sartore-Bianchi, F. Di Nicolantonio, S. Siena, and A. Bardelli, "Acquired resistance to EGFR-targeted therapies in colorectal cancer," *Molecular Oncology*, vol. 8, no. 6, pp. 1084–1094, 2014.

[153] L. A. Diaz Jr., R. T. Williams, J. Wu et al., "The molecular evolution of acquired resistance to targeted EGFR blockade in colorectal cancers," *Nature*, vol. 486, no. 7404, pp. 537–540, 2012.

[154] S. Misale, R. Yaeger, S. Hobor et al., "Emergence of KRAS mutations and acquired resistance to anti-EGFR therapy in colorectal cancer," *Nature*, vol. 486, no. 7404, pp. 532–536, 2012.

[155] C. Montagut, A. Dalmases, B. Bellosillo et al., "Identification of a mutation in the extracellular domain of the epidermal growth factor receptor conferring cetuximab resistance in colorectal cancer," *Nature Medicine*, vol. 18, no. 2, pp. 221–223, 2012.

[156] C. Esposito, A. M. Rachiglio, M. L. L. Porta et al., "The S492R EGFR ectodomain mutation is never detected in KRAS wild-type colorectal carcinoma before exposure to EGFR monoclonal antibodies," *Cancer Biology and Therapy*, vol. 14, no. 12, pp. 1143–1146, 2013.

[157] T. Price, A. Ang, M. Boedigheimer et al., "Frequency of S492R mutations in the epidermal growth factor receptor: analysis of plasma DNA from patients with metastatic colorectal cancer treated with panitumumab or cetuximab monotherapy," *Cancer Biology and Therapy*, vol. 21, pp. 891–898, 2020.

[158] K. Yonesaka, K. Zejnullahu, I. Okamoto et al., "Activation of ERBB2 signaling causes resistance to the EGFR-directed therapeutic antibody cetuximab," *Science Translational Medicine*, vol. 3, no. 99, 2011.

[159] A. Bertotti, G. Migliardi, F. Galimi et al., "A molecularly annotated platform of patient-derived xenografts ("xenopatients") identifies HER2 as an effective therapeutic target in cetuximab-resistant colorectal cancer," *Cancer Discovery*, vol. 1, no. 6, pp. 508–523, 2011.

[160] V. Martin, L. Landi, F. Molinari et al., "HER2 gene copy number status may influence clinical efficacy to anti-EGFR monoclonal antibodies in metastatic colorectal cancer patients," *British Journal of Cancer*, vol. 108, no. 3, pp. 668–675, 2013.

[161] W. Ariyawutyakorn, S. Saichaemchan, and M. Varella-Garcia, "Understanding and targeting MET signaling in solid tumors—are we there yet?" *Journal of Cancer*, vol. 7, no. 6, pp. 633–649, 2016.

[162] D. Liska, C.-T. Chen, T. Bachleitner-Hofmann, J. G. Christensen, and M. R. Weiser, "HGF rescues colorectal cancer cells from EGFR inhibition via MET activation," *Clinical Cancer Research*, vol. 17, no. 3, pp. 472–482, 2011.

[163] A. Bardelli, S. Corso, A. Bertotti et al., "Amplification of the MET receptor drives resistance to anti-EGFR therapies in colorectal cancer," *Cancer Discovery*, vol. 3, no. 6, pp. 658–673, 2013.

[164] T. Troiani, E. Martinelli, S. Napolitano et al., "Increased TGF- as a mechanism of acquired resistance to the anti-EGFR inhibitor cetuximab through EGFR-MET interaction and activation of MET signaling in colon cancer cells," *Clinical Cancer Research*, vol. 19, no. 24, pp. 6751–6765, 2013.

[165] F. Galimi, D. Torti, F. Sassi et al., "Genetic and expression analysis of MET, MACC1, and HGF in metastatic colorectal cancer: response to met inhibition in patient xenografts and pathologic correlations," *Clinical Cancer Research*, vol. 17, no. 10, pp. 3146–3156, 2011.

[166] N. C. Turner and J. S. Reis-Filho, "Genetic heterogeneity and cancer drug resistance," *Lancet Oncology*, vol. 13, no. 4, pp. e178–e185, 2012.

Hindawi
Journal of Oncology
Volume 2021, Article ID 5691982, 5 pages
https://doi.org/10.1155/2021/5691982

Research Article

Anticolon Cancer Properties of Pyrazole Derivatives Acting through Xanthine Oxidase Inhibition

Abdulrhman Alsayari, Yahya I. Asiri, Abdullatif Bin Muhsinah, and Mohd. Zaheen Hassan

College of Pharmacy, King Khalid University, Abha 61441, Saudi Arabia

Correspondence should be addressed to Mohd. Zaheen Hassan; zaheen@kku.edu.sa

Received 28 May 2021; Accepted 1 July 2021; Published 6 July 2021

Academic Editor: Alamgeer Yuchi

Background. Pyrazoles are an interesting class of compounds showing potent anticancer activities. Our previous studies have demonstrated the potent anticancer activity of pyrazole analogues. Therefore, we focused on developing anticancer agents through structure optimization of the pyrazolyl lead molecule. *Methods*. The pyrazole derivatives were prepared by the appropriate synthetic protocols. The antiproliferative activities were evaluated using a sulforhodamine B assay against three cancer cell lines. In vitro and in silico molecular docking studies employing xanthine oxidase were used to explore the mechanism by which pyrazole derivatives exert anticancer effects. *Results*. One of the pyrazole derivatives demonstrated the greatest promise as an anticancer agent against the human colon cancer cell line (IC_{50} 4.2 μM), with a potent xanthine oxidase inhibitory activity (IC_{50} 0.83 μM). *Conclusion*. In summary, our findings suggest that these pyrazolyl analogues containing a pyridine nucleus could serve as a promising lead molecule in the development of novel anticancer agents.

1. Introduction

Cancer is one of the four major types of noncommunicable diseases, along with cardiovascular disease, diabetes, and chronic respiratory diseases [1]. It is a disease in which abnormal cells divide without control and can invade nearby tissues [2]. The cancer burden continues to grow globally, with 18.1 million new cases and 9.6 million deaths in the preceding year [3]. Among males, the most prevalent cancers are lung, prostate, colorectal, stomach, and liver cancers, whereas among females, breast, colorectal, lung, cervical, and thyroid cancers are the most common [4]. This growing universal cancer burden is exerting huge physical, emotional, and financial strains on society. Moreover, chemotherapy resistance and its associated serious side effects, even with the targeted therapies, continue to be a major concern for oncologists [5]. Therefore, it is imperative that we develop safer and more effective anticancer agents acting through novel mechanisms and target only the cancer cells.

Pyrazoles are a promising scaffold for many anticancer agents. A number of clinical anticancer therapeutics, such as crizotinib, ruxolitinib, niraparib, encorafenib, and darolutamide, currently consist of a pyrazole moiety [6]. Therefore, in the past decades, a large number of pyrazolyl analogues were synthesized and tested as anticancer agents [7]. Our research group focused on the design and synthesis of pyrazole derivatives functionalized with aryldiazo pyrazoles. In our previous research, aryldiazo pyrazoles showed a very promising anticancer activity against MCF-7, HepG2, and HCT-116 cell lines. For instance, 4-[2-(4-nitrophenyl) hydrazono]-2-pyrazolin-5-one, as a lead molecule, showed an inhibition of cell proliferation with an IC_{50} value in the range of 0.2–3.4 μM [8]. Encouraged by these results, we further optimized the lead molecule through different substitutions on the aryl ring. These compounds were synthesized using our previously developed rapid one-pot three-component condensation method for the synthesis of pyrazolyl analogues [8] and then evaluated the resulting molecules for their anticancer potential.

Since cancer and oxidative stress share some aspects of their underlying pathophysiology, some antioxidants are equally effective as anticancer agents [9]. The cellular redox process produces reactive oxygen species (ROS) as by-products. These ROS exert beneficial effects on cellular response at low levels, whereas they can be deleterious and may cause DNA damage and cancer at high levels. Antioxidants have been shown to act as "free radical scavenger" by preventing damages caused by ROS and thus exert a protective effect against several different types of cancers [10]. Moreover, xanthine oxidase (XO) overexpression has been linked to the progress of oncogenesis through the generation of cytotoxic reactive oxygen species (ROS). Therefore, XO has been identified as a potential target for anticancer agents [11]. Recently, many studies have also reported that pyrazole derivatives are very promising XO inhibitors [12]. Therefore, these promising cytotoxic compounds were also subjected to further investigation for their XO inhibitory activities.

2. Materials and Methods

Pyrazolyl analogues **1** and **2** were synthesized using our previously described procedures [8]. These compounds were evaluated for their in vitro anticancer activity against HepG2, HCT-116, and MCF-7 cell lines by the sulforhodamine B assay (SRB).

2.1. Cell Culture. Human hepatocellular carcinoma cell line (HepG-2, ATCC HB-8065), colorectal adenocarcinoma cell line (HCT-116, ATCC CCL-247), and breast adenocarcinoma cell line (MCF-7, ATCC HTB-22) were obtained from the American type culture collection (ATCC). Cells were maintained in RPMI-1640 supplemented with (100 μg/ml) penicillin (100 units/ml) and heat-inactivated fetal bovine serum (10% v/v) in a humidified, 5% (v/v) CO_2 atmosphere at 37°C [13].

2.2. Cytotoxicity Assessment. The cytotoxicity of the different compounds was tested against human tumor cells using the sulforhodamine B assay (SRB). Healthy growing cells were cultured in a 96-well tissue culture plate (3000 cells/well) for 24 hours to allow attachment of the cells to the plate before treatment with the tested compounds. Cells were exposed to five different concentrations of each compound (0.01, 0.1, 1, 10, and 100 μM/ml); untreated cells (control) were also added. Triplicate wells were incubated with different concentrations for 72 h and subsequently fixed with TCA (10% w/v) for 1 h at 4°C. After several washings, cells were stained with 0.4% (w/v) SRB solution for 10 min in a dark place. Excess stain was washed with 1% (v/v) glacial acetic acid. After drying overnight, the SRB-stained cells were dissolved with tris-HCl and the color intensity was measured in a microplate reader at 540 nm. The linear relationship between the viability percentage of each tumor cell line and the compounds' concentrations was analyzed to obtain IC_{50} (dose of the drug which reduces survival to 50%) using SigmaPlot 12.0 software [14].

2.3. Xanthine Oxidase Assay. These compounds were further evaluated for their XO inhibitory potential by measuring the formation of uric acid concentration spectrophotometrically at 292 nm using a method previously described [15]. Solutions of the enzyme-drug complex were prepared by mixing freshly prepared XO enzyme solution (0.5 mL) with 1.0 mL solution of test compounds (at concentrations of 100, 50, 25, 12.5, 6.25, and 3.12 μM, dissolved in DMSO and diluted with a buffer) in a phosphate buffer (1.5 mL of 50 mM; pH 7.4) and incubated at 25°C for 15 min. Subsequently, 0.45 mL of the xanthine solution substrate was added and incubated at 25°C for another 30 min. The enzymatic reaction was stopped by adding 1 mL HCl (1 M). Allopurinol was used as a standard, and a phosphate buffer was substituted for xanthine as a blank. The XO inhibition was expressed as % inhibition and compared to the control with the following formula: % inhibition = $[(Ac - As)/Ac] \times 100$, where Ac indicates the absorbance of the control sample and As is the absorbance of the treated sample. Readings were taken in triplicate and represented as $IC_{50} \pm SD$. IC_{50} values were calculated using GraphPad Prism 8 software.

2.4. Molecular Docking Studies. Molecular docking studies were performed using AutoDock v. 4.2.2 to identify appropriate binding modes and conformation of the ligand molecules. The crystal structure of xanthine dehydrogenase (PDB code: 3BDJ, resolution: 2.0 Å) was retrieved from the RCSB Protein Data Bank as a PDB format [16]. The structures of all the ligands were drawn using ChemDraw Ultra 13.0 and converted into 3D structures using HyperChem Pro 8.0 software (http://www.hyper.com). AutoDock tools (ADT) version 1.5.6 (http://www.autodock.scrips.edu) was used to prepare the molecular docking. The active site was considered as a rigid molecule, while the ligands were treated as being flexible. Using default parameters, grid-based docking studies were carried out and docking was performed on all compounds using the standard ligand oxipurinol. The best binding conformation was selected from the docking log (.dlg) file for each ligand, and further interaction analysis was performed using PyMOL and Discovery Studio Visualizer 4.0.

3. Results and Discussion

Based on the encouraging results of 1-isonicotinoyl-3-methyl-4-[2-(4-nitrophenyl)hydrazono]-2-pyrazolin-5-one (IC_{50} 0.2–3.4 μM) as a potential anticancer lead molecule, we focused our attention on optimizing the anticancer potential of arylhydrazono-pyrazole derivatives with different substitutions at the phenyl ring (Figure 1). The newly synthesized compounds **1** and **2** were evaluated for the antiproliferative activity against three human tumor cell lines, namely, breast cancer (MCF-7), hepatocellular carcinoma (HepG2), and colorectal carcinoma (HCT-116), by the sulforhodamine B (SRB) assay. The SRB assay is the "gold-standard" assay and is extensively used in the high-throughput screening program at the National Cancer Institute (NCI), USA. The SRB uses an aminoxanthene dye,

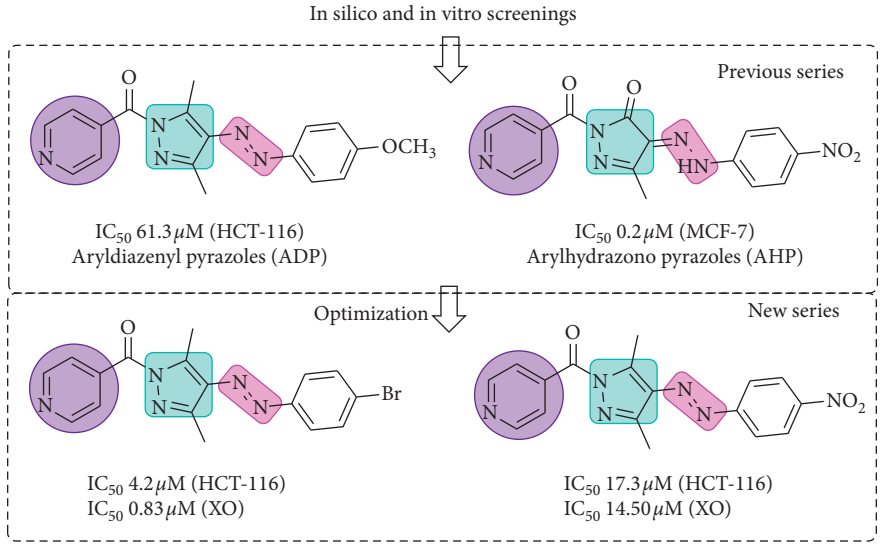

Figure 1: Design strategy and lead optimization of newer pyrazole analogues, showing the different bioactive pharmacophores essential for the anticancer activity.

which readily stains the cells through binding with the basic amino acids of cellular proteins. The SRB assay estimates the dye released from the stained cells after washing as stoichiometric proportions of cellular mass. In Table 1, the results of the SRB assay of the titled compounds are presented as 50% growth inhibitory concentration (IC_{50}) values. The IC_{50} values were determined by interpolation from dose-response curves. From the results, it was observed that most of the newly synthesized pyrazoles showed excellent to moderate antiproliferative activity against the three cell lines, especially against colorectal carcinoma (HCT-116). Compound **1** effectively inhibited cell growth at IC_{50} values of 17.8 ± 0.5, 4.4 ± 0.4, and $4.2 \pm 0.2\,\mu$M against the breast cancer (MCF-7), hepatocellular carcinoma (HepG2), and colorectal carcinoma (HCT-116) cell lines, respectively. The anticancer activity of compound **1** was comparable to the standard drug doxorubicin against the HepG2 (3.9 ± 0.06) and HCT-116 (4.4 ± 0.04) cell lines, but 3.7 times less potent in the MCF-7 (4.7 ± 0.08) cell lines. Compound **2** was found to be moderately effective, with IC_{50} values of 94.2 ± 0.3, 34.6 ± 2.6, and $17.3 \pm 0.5\,\mu$M against the MCF-7, HepG2, and HCT-116 cell lines, respectively. Our previous studies have shown that unsubstituted phenyl derivative of aryldiazenyl pyrazole had a poor antiproliferative activity ($IC_{50} > 100\,\mu$M) against all three cell lines [8]. This finding indicates that substitution with electron withdrawing groups such as bromo and nitro groups significantly improved the anticancer potential of aryldiazenyl pyrazole derivatives.

Pyrazolyl analogues have been reported as promising anticancer agents acting through xanthine oxidase (XO) inhibition [12]. The promising anticancer properties of pyrazole derivatives **1** and **2** further prompted us to assess their XO inhibitory activity to gain insight into the mechanism of the anticancer activity of these pyrazole derivatives. The assessment of the XO inhibitory activity was carried out spectrophotometrically by measuring the formation of uric acid at 290 nm. The results indicated that compound **1** (IC_{50} $0.83 \pm 1.36\,\mu$M) exhibited significant XO inhibition, 18.03 times more potent than the standard drug allopurinol (IC_{50} $14.97 \pm 1.61\,\mu$M) (Table 2), whereas compound **2** was equipotent (IC_{50} $14.50 \pm 2.25\,\mu$M) to allopurinol. These results confirm the XO inhibitory action of these compounds and suggest the possible influence of XO inhibition in the anticancer activity of pyrazoles. However, further kinetic studies are required to establish a more detailed mode of enzyme inhibition of these compounds.

Table 1: The IC_{50} (μM) of pyrazolyl derivatives against different tumor cell lines.

Compound	*R*	IC_{50} (μM)		
		MCF-7	HepG2	HCT-116
1	Br	17.8 ± 0.5	4.4 ± 0.4	4.2 ± 0.2
2	NO_2	94.2 ± 0.3	34.6 ± 2.6	17.3 ± 0.5
Doxorubicin	—	4.7 ± 0.08	3.9 ± 0.06	4.4 ± 0.04

Encouraged by the results of the in vitro anticancer and XO inhibitory activities of the newly synthesized pyrazolyl derivatives, molecular docking studies were carried out on xanthine dehydrogenase (XDH) using AutoDock. Both the enzymes XO and XDH are interconvertible forms of the same enzyme, known as xanthine oxidoreductase (XOR), with only slight differences in the FAD binding domain. The crystal structure of bovine milk XDH bound with oxipurinol was used in the current study and retrieved from the raw PDB structure 3BDJ, which has 90% similarity to the human liver enzyme [16]. Oxipurinol is a potent XOR inhibitor acting through a tight binding to the reduced molybdenum ion (Mo^{4+}) of the molybdopterin cofactor, which is essential for the mechanism-based inhibition. Furthermore, it forms hydrogen bonds with Glu802, Arg880, and Glu1261 in the active site of the enzyme (Figure 2). These binding interactions are concordant with previous reports. The results of the molecular docking studies of the two pyrazole derivatives revealed that they occupy the same narrow channel that

Table 2: Xanthine oxidase inhibition activities of pyrazole derivatives (1 and 2).

Compound	Binding free energy (kcal/mol)	IC_{50} (μM)
1	−7.6	0.83 ± 1.36
2	−6.1	14.50 ± 2.25
Allopurinol	—	14.97 ± 1.61

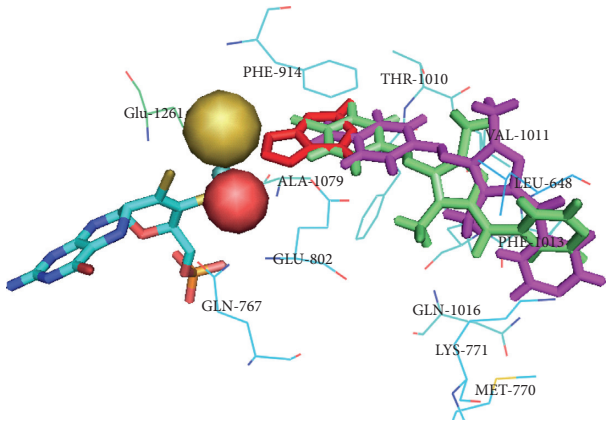

Figure 2: 3D view of docked pose of pyrazolyl analogues **1** (lime) and **2** (magenta), with oxipurinol (red) at the vicinity of the molybdopterin cofactor.

leads towards the molybdenum center in the active site; however, they do not interact with the cofactor. The binding free energy of these two compounds was in the range of −6.1 to −7.6 kcal/mol, indicating sufficient affinity between the enzyme and inhibitors (Table 2). The key interacting residues at the active site include Leu648, Phe649, Gln767, Met770, Glu802, Arg880, Phe914, Phe1009, Thr1010, Val1011, Phe1013, Leu1014, Glu1016, and Glu1261 (Figure 2). The results of the docking studies are consistent with the in vitro study and indicate the strong inhibitory activities of pyrazole derivatives against XO. Moreover, these data also indicate that the anticancer activity of pyrazolyl analogues might be due to XO inhibition.

After obtaining interesting results with arylhydrazonopyrazole analogues, different substitutions were made at the phenyl ring for optimizing the template. The analogues **1** and **2** were prepared by using the method described earlier [8]. Their antiproliferative activities were evaluated in comparison with the unsubstituted phenyl derivative ($IC_{50} > 100\,\mu$M), and compound **1** was about >22 folds more active than its unsubstituted derivative in the HepG2 and HCT-116 cell lines. These findings suggested that the electron withdrawing groups at the phenyl ring might be important for high potency. Furthermore, HCT-116 was the most sensitive cell line against these pyrazolyl analogues.

In conclusion, compound **1** emerged as a promising anticancer agent effective against the colorectal carcinoma cell lines (IC_{50} 4.2 μM) acting through xanthine oxidase inhibition (IC_{50} 0.83 μM). Results of in vitro and in silico xanthine oxidase inhibitory activities revealed that the anticancer activity of these pyrazolyl analogues might be due to XO inhibition.

Data Availability

The data used to support the findings of this study are available from the corresponding author upon request.

Conflicts of Interest

The authors declare that they have no conflicts of interest.

Acknowledgments

This work was financially supported by the Deanship of Scientific Research, King Khalid University (RGP. 1/136/42).

References

[1] H. C. Kim and S. M. Oh, "Noncommunicable diseases: current status of major modifiable risk factors in Korea," *Journal of Preventive Medicine & Public Health*, vol. 46, no. 4, pp. 165–172, 2013.

[2] National Cancer Institute, https://www.cancer.gov/about-cancer/understanding/what-is-cancer, April 2021.

[3] World Health Organization, *Global Health Observatory*, World Health Organization, Geneva, Switzerland, April 2021, http://who.int/gho/database/en/.

[4] X. Gu, R. Zheng, C. Xia et al., "Interactions between life expectancy and the incidence and mortality rates of cancer in China: a population-based cluster analysis," *Cancer Communications*, vol. 38, no. 1, pp. 1–15, 2018.

[5] H. Maeda and M. Khatami, "Analyses of repeated failures in cancer therapy for solid tumors: poor tumor-selective drug delivery, low therapeutic efficacy and unsustainable costs," *Clinical and Translational Medicine*, vol. 7, p. 11, 2018.

[6] S.-H. I. Ou, "Crizotinib: a novel and first-in-class multitargeted tyrosine kinase inhibitor for the treatment of anaplastic lymphoma kinase rearranged nonsmall cell lung cancer and beyond," *Drug Design, Development and Therapy*, vol. 5, pp. 471–485, 2011.

[7] F. E. Bennani, L. Doudach, Y. Cherrah et al., "Overview of recent developments of pyrazole derivatives as an anticancer agent in different cell line," *Bioorganic Chemistry*, vol. 97, p. 103470, 2020.

[8] A. Alsayari, A. B. Muhsinah, Y. I. Asiri et al., "Arylhydrazono/aryldiazenyl pyrazoles: green one-pot solvent-free synthesis and anticancer evaluation," *Letters in Organic Chemistry*, vol. 17, no. 10, pp. 772–778, 2020.

[9] A. Rauf, M. Imran, M. S. Butt et al., "Resveratrol as an anticancer agent: a review," *Critical Reviews in Food Science and Nutrition*, vol. 58, no. 9, pp. 1428–1447, 2018.

[10] L. Zewen, R. Zhangpin, Z. Jun et al., "Role of ROS and nutritional antioxidants in human diseases," *Frontiers in Physiology*, vol. 9, p. 477, 2018.

[11] H. Xu, C. Li, O. Mozziconacci et al., "Xanthine oxidase-mediated oxidative stress promotes cancer cell-specific apoptosis," *Free Radical Biology and Medicine*, vol. 139, pp. 70–79, 2019.

[12] J. Gaurav, S. Manisha, K. Sourav et al., "Design, synthesis, biological evaluation of 3,5-diaryl-4,5-dihydro-1H-pyrazole carbaldehydes as non-purine xanthine oxidase inhibitors: tracing the anticancer mechanism via xanthine oxidase inhibition," *Bioorganic Chemistry*, vol. 107, p. 104620, 2021.

[13] A. M. Mahmoud, A. M. Al-Abd, D. A. Lightfoot, and H. A. El-Shemy, "Anti-cancer characteristics of mevinolin against three different solid tumor cell lines was not solely p53-

dependent," *Journal of Enzyme Inhibition and Medicinal Chemistry*, vol. 27, no. 5, pp. 673–679, 2012.

[14] V. Vichai and K. Kirtikara, "Sulforhodamine B colorimetric assay for cytotoxicity screening," *Nature Protocols*, vol. 1, no. 3, pp. 1112–1116, 2006.

[15] M. Sun, J. Zhao, Q. Mao et al., "Synthesis and biological evaluation of 2-(4-alkoxy-3-cyano)phenylpyrimidine derivatives with 4-amino or 4-hydroxy as a pharmacophore element binding with xanthine oxidase active site," *Bioorganic & Medicinal Chemistry*, vol. 38, p. 116117, 2021.

[16] O. Ken, T. E. Bryan, N. Tomoko et al., "Mechanism of inhibition of xanthine oxidoreductase by allopurinol: crystal structure of reduced bovine milk xanthine oxidoreductase bound with oxipurinol," *Nucleosides, Nucleotides & Nucleic Acids*, vol. 27, pp. 888–893, 2008.

Hindawi
Journal of Oncology
Volume 2021, Article ID 9935410, 11 pages
https://doi.org/10.1155/2021/9935410

Research Article

LncRNA SNHG3 Promotes Gastric Cancer Cells Proliferation, Migration, and Invasion by Targeting miR-326

Jun Rao,[1] Jinjin Fu,[1] Chuchen Meng,[2] Jin Huang,[1] Xiangrong Qin,[1] and Shaohua Zhuang [1]

[1]*Department of Gastroenterology, Changzhou No. 2 People's Hospital, The Affiliated Hospital of Nanjing Medical University, No. 29 Xinglong District, Changzhou 213000, China*
[2]*Department of Endocrinology, Changzhou No. 2 People's Hospital, The Affiliated Hospital of Nanjing Medical University, Changzhou, China*

Correspondence should be addressed to Shaohua Zhuang; zhuangshaohua@czehospial.cn

Received 4 March 2021; Accepted 16 June 2021; Published 29 June 2021

Academic Editor: Muhammad Wasim Khan

The function and possible mechanism of lncRNA Small Nucleolar RNA Host Gene 3 (SNHG3) in GC have not been fully studied. The aim of our study was to investigate the role of SNHG3 in the proliferation, migration, and invasion of GC cell lines. The expressions of SNHG3, miR-326, and TWIST in GC9811-P GC cell lines were detected by RT-qPCR. Western blotting was performed to detect the protein levels of TWIST and EMT-related genes. Luciferase reporter gene analysis and RNA immunoprecipitation (RIP) analysis confirmed the interaction between lncRNA SNHG3, miR-326, and TWIST. CCK-8 and Transwell assays were performed to detect cell proliferation, invasion, and migration abilities. The results showed that lncRNA SNHG3 and TWIST were highly expressed in GC cell lines, while miR-326 was expressed to a low degree. Moreover, lncRNA SNHG3 knockdown or miR-326 overexpression significantly inhibited cell proliferation, migration, and invasion of GC cell lines. In addition, TWIST overexpression can reverse the inhibition of lncRNA SNHG3 knockdown or miR-326 overexpression on cell proliferation, migration, and invasion. In conclusion, lncRNA SNHG3 may promote GC progression through the miR-326/TWIST axis, which may provide a new diagnostic and prognostic biomarker for GC.

1. Introduction

Gastric cancer (GC) is a common malignancy in the world [1]. The most common cause of GC is *Helicobacter pylori* infection, accounting for more than half of the incidence. Other recognized risk factors include smoking, the intake of pickled vegetables in the diet, and the clinical management of obesity [2].The treatment of GC mainly includes surgery, chemotherapy, radiotherapy, and targeted therapy [3]. In the global scope, the overall results of GC are relatively poor, with a five-year survival of being lower than 10% [4]. Based on a comprehensive understanding of the biological basis of the disease, there is still an urgent need for accurate medicine. Long noncoding RNA (lncRNA) is more than 200 nucleotides in length without significant protein-coding potential [5]. It is worth noting that the accumulated evidence reveals that lncRNA plays an essential role in human malignant tumors [6]. SNHG3 is a new type of lncRNA, which may be related to Alzheimer's disease and colorectal cancer. For example, misaligned lncRNAs may act as oncogenes or tumor suppressor genes in the HCC process [7]. The results showed that the expression of Small Nucleolar RNA Host Gene 3 (SNHG3) was related to the malignant state, and the prognosis was relatively poor. SNHG3 was identified as a competitive endogenous RNA molecule to promote the malignant progression of colorectal cancer [8]. The abnormal upregulation of snhg3 in ovarian cancer is closely related to poor prognosis and malignant progression [9]. Systematic analysis of mitochondrial proteomics was performed [10]. LncRNA SNHG3 is also characterized by its involvement in the microRNA pathway of HCC, where miR-128/CD151 signaling of SNHG3 in-

duces epithelial mesenchymal transition (EMT). Although SNHG3 has been recognized as a carcinogenic gene in a series of human cancers, the mechanism of SNHG3 in GC remains elusive.

In addition, we try to understand the basic molecular mechanism behind the carcinogenicity of lncRNA. Like lncRNA, miRNA has been widely recognized in cancer. MiR-326 plays an anticancer role in a variety of malignant tumors and targets different genes in glioma, endometrial cancer, and cervical cancer [11–14]. However, the interaction between SNHG3 and miR-326 in GC has not been reported. It has been reported that miR-326 associates with bone metastasis, a biochemical marker of bone turnover in lung cancer, and promotes EMT-induced cellular lung adenocarcinoma infiltration [15]. Wang et al. reported that miR-326 is abnormally expressed in metastasis and non-metastasis tissues in non-small-cell lung cancer, providing an experimental basis for exploring the mechanism of non-small cell lung cancer metastasis and molecular diagnosis and treatment [16]. These results indicate that tumor suppresses the function of miR-326 in lung cancer. Our current goal is to investigate the biological function of miR-326 in GC and explore its potential mechanism.

TWIST, a transcription factor, plays an important role in the development and progression of cancer. The upregulation of TWIST inhibited the expression of E-cadherin in EMT, indicating that TWIST promoted metastasis by inducing EMT [17]. Previous investigations suggested that certain miRNA could regulate the expression level of TWIST through binding to TWIST mRNA [18, 19]. Previous reports have shown that miR-326 is dysfunctional and has various tumor developments. Nevertheless, the possible function and potential mechanism of miR-326 expression in GC have not been reported. In this study, we hypothesized that SNHG3 might promote HCC progression by targeting miR-326 expression. In order to clarify this problem, we analyzed the molecular expression mechanism of SNHG3 transcript in GC. The potential role of SNHG3 in tumor biology was studied.

2. Materials and Methods

2.1. Cell Culture and Transfection. Human immortalized gastric epithelial cell GES-1 and human gastric cancer cell lines HGC-27 and GC9811-P were cultured in DMEM medium containing 10% FBS (GIBCO, USA), 100 U/ml penicillin, and 100 μg/ml streptomycin (Solarbio, China). Cells were cultured in a 5% CO_2 at 37°C. For miRNA and siRNA transfection, HGC-27 and GC9811-P cells were laid in triplicate in a six-well plate. According to the manufacturer's procedures, miR-326 mimic or siRNA was transfected into GC cells using Lipofectamine 2000 (Invitrogen, USA).

2.2. CCK-8 Assay. According to manufacturer's instructions, cells were cultured in 96-well plates with a density of 2×10^3 cells/well. The cells were cultured at 37°C for 24, 48, and 72 hours in an incubator containing 5% CO_2. At different time points, 10 μl CCK-8 solution was added to every pore and cultured at 37°C for another 2 hours. The absorbance at 450 nm was recorded.

2.3. Transwell Analysis. The determination was carried out by using a polycarbonate filter (8 μm aperture). Twenty hours after miRNA transfection, cells were collected and 5×10^4 cells in 200 μl 0.1% serum medium were placed in the upper chamber. The lower chamber was full of 10% fetal bovine serum medium. After incubation for 24 hours and eliminating the cells in the upper chamber of the filter with cotton swabs, the cells below were fixed with 4% paraformaldehyde and stained with 0.1% crystal violet in 20% ethanol, and five phase contrast microscopes were randomly counted to observe the field of vision. Monitoring of migrating cells was performed by photographing with 400× magnification ICA microscope. The determination was carried out in triplicate.

2.4. Dual Luciferase Activity Assay. Shanghai gene Pharmaceutical Co. Ltd. (Shanghai, China) synthesized and confirmed the luciferase reporter vector pGL3-TWIST-3′UTR wild type (WT) and pGL3-TWIST-3′UTR mutant (MUT). GC cells were cotransfected with pGL3-TWIST-3′UTR WT or pGL3-TWIST-3′UTR MUT and miR-326 mimic or NC by Lipofectamine 2000. The transfected cells were harvested 48 hours after transfection, and luciferase activity was detected by a dual-luciferase reporter analysis system (Promega, Germany) according to the manufacturer's instructions.

2.5. RIP Assay. RIP analysis was performed using RIP Kit (Millipore, USA). HGC-27 and GC9811-P cell lines were lysed with RIP lysate buffer. The lysate was incubated overnight in RIP buffer with magnetic beads coupled to Ago2 or IgG antibodies (Sigma, USA) at 4°C. The expression of lncRNA SNHG3 and miR-326 was analyzed by RT-qPCR.

2.6. Quantitative Real-Time PCR. According to the manufacturer's instructions, total RNA was extracted from cultured cells using Trizol reagent (Invitrogen, USA). The RNA samples were then transcribed into cDNA in accordance with the manufacturer's instructions, with a total volume of 20 μL. The same amount of cDNA sample was used as the template of RT-qPCR to detect the expression level of TWIST. RT-qPCR was carried out with a light cycle real-time PCR system and SYBR Green Master Mix (Takara). GAPDH was used as an endogenous reference, and each sample was standardized to its GAPDH content. All experiments were carried out in duplicate and repeated twice. $2^{-\Delta\Delta Ct}$ method was used to express the induction multiple.

2.7. Western Blot. Western blotting was performed on 10% twelve alkyl sulfate polyacrylamide gel electrophoresis (SDS-PAGE). The cells were transfected with miR-NC or miR-326.72 hours after transfection and were collected and lysed.

The protein was separated and transferred to PVDF membrane by 10%SDS-PAGE gel. Then, 5% skim milk to block nonspecific connection was added. After incubation in dark for 1 hour at room temperature, rabbit anti-human TWIST polyclonal antibody was added in 1 : 200 dilutions. After washing 3 times with PBS, the membrane was mixed with the corresponding secondary antibody 1 hour at room temperature. For EMT-related proteins, the first antibody is used according to the specific protein. Finally, the strip was visualized by chemiluminescence after cleaning in TBS.

2.8. Statistical Analysis. Each experiment was repeated three times. SPSS 15.0 was used for statistical analysis. The Student–Newman–Keuls test is used as a posttest. $P < 0.05$ was supposed to indicate statistically significant differences.

3. Results

3.1. LncRNA SNHG3 and TWIST Were Upregulated while miR-326 Was Downregulated in HGC-27 and GC9811-P Cells. Firstly, SNHG3, miR-326 and TWIST were detected in GES-1, HGC-27, and GC9811-P cell lines. The results showed that the expression of lncRNA SNHG3 and TWIST in HGC-27 and GC9811-P cell lines was higher than control group (Figures 1(a)–1(c)). However, the expression of miR-326 in HGC-27 and GC9811-P cell lines was obviously lower than that in GES-1 cell line (Figure 1(d)). These results indicated that the unusual expression of lncRNA SNHG3, miR-326, and TWIST might be related to the progress of GC.

3.2. LncRNA SNHG3 Knockdown or miR-326 Overexpression Suppressed Cell Proliferation, Migration, and Invasion in HGC-27 and GC9811-P Cells. In order to study the functions of lncRNA SNHG3 and miR-326 in the development of GC, HGC-27 and GC9811-P cell lines were transfected with si SNHG3, miR-326 mimic, or their respective NC sequences, respectively. Compared with siNC, the expression of lncRNA SNHG3 was obviously decreased in cells transfected with siSNHG3 (Figure 2(a)). The influence of SNHG3 in protein levels of EMT-related proteins was detected by western blot. Results showed that the expressions of E-cadherin were significantly increased, while expressions of N-cadherin and vimentin were decreased (Figure 2(b)). In addition, cell migration and invasion were effectively reduced in HGC-27 and GC9811-P cell lines transfected with siSNHG3 (Figures 2(c) and 2(d)). CCK-8 assay showed that cell proliferation was significantly suppressed in cells transfected with siSNHG3 (Figures 2(e) and 2(f)).

miR-326 expression was obviously increased by miR-326 mimic in both HGC-27 and GC9811-P cell lines (Figure 3(a)). The protein level of EMT-related protein in cells transfected with miR-326 mimic was also detected (Figure 3(b)). Cell migration and invasion were effectively reduced by miR-326 mimic in HGC-27 and GC9811-P cell lines (Figures 3(c) and 3(d)). In the CCK-8 assay, cell proliferation of HGC-27 and GC9811-P cell lines was significantly suppressed by miR-326 mimic (Figures 3(e) and 3(f)).

3.3. LncRNA SNHG3 Targeted miR-326 and Negatively Regulated Its Expression. It is confirmed that lncRNA, which can act as ceRNA, can bind to miRNA and release target RNA transcripts. In order to explore the regulatory mechanism of lncRNA SNHG3, starstarv3.0 predicted the target sites between lncRNA SNHG3 and miR-326 (Figure 4(a)). The expression level of miR-326 in HGC-27 and GC9811-P cell lines was investigated by RT-qPCR when the lncRNA SNHG3 was knocked down. Our study showed that the expression of miR-326 in HGC-27 and GC9811-P cell lines transfected with siSNHG3 increased significantly (Figure 4(b)). Therefore, we proposed that lncRNA SNHG3 could be used as ceRNA of miR-326 in GC cells. In addition, we used luciferase reporter gene assay to confirm the direct interaction between lncRNA SNHG3 and miR-326. After cotransfection of fluorescent enzyme report vector (SNHG3-wt or SNHG3-mut) and miR-326 mimic or NC into the cell line, we found that in HGC-27 and GC9811-P cell lines, the activity of fluorescent enzyme transfected with SNHG3-wt and miR-326 mimic decreased significantly (Figures 4(c) and 4(d)). In addition, to further verify the interaction between lncRNA SNHG3 and miR-326, RIP analysis was carried out with antibodies against Ago2. We found that both SNHG3 and miR-326 were rich in Ago2 precipitates in HGC-27 and GC9811-P cell extracts (Figures 4(e) and 4(f)). In general, these results suggested that lncRNA SNHG3 can be used as a ceRNA to bind directly to miR-326 and negatively regulate its expression.

3.4. TWIST Was a Target of miR-326 and Promoted by lncRNA SNHG3. To further detect the molecular regulatory mechanism of lncRNA SNHG3 and miR-326, bioinformatics analysis was carried out to explore the potential target of miR-326 in GC cells. TWIST was predicted to be the main target gene of miR-326, and the target site was predicted by TargetScan (Figure 5(a)). In order to confirm the prediction of bioinformatics, we carried out luciferase reporter gene detection. Luciferase reporter vector (TWIST-wt or TWIST-mut) and miR-326 mimic or NC were cotransfected into HGC-27 and GC9811-P cells. Compared with the cotransfection of NC and TWIST-wt, the luciferase activity of cells cotransfected TWIST-wt and miR-326 mimic decreased significantly (Figures 5(b) and 5(c)). Furthermore, when the cells were transfected with miR-326 or NC, the expression of TWIST was measured. High expression of miR-326 effectively inhibited TWIST levels in HGC-27 and GC9811-P cells (Figures 5(d) and 5(e)). These data confirmed that TWIST was the target gene of miR-326 and was negatively controlled by miR-326. In addition, we found that cotransfection of miR-326 inhibitor and siSNHG3 could reverse the inhibition effects of siSNHG3 on TWIST expression (Figure 5(f)).

3.5. LncRNA SNHG3/miR-326/TWIST Axis Regulated Cell Proliferation, Migration, and Invasion in HGC-27 and GC9811-P Cells. According to the above experimental data, we speculated that the regulatory axis of lncRNA SNHG3-miR-326-TWIST might be related to the development of

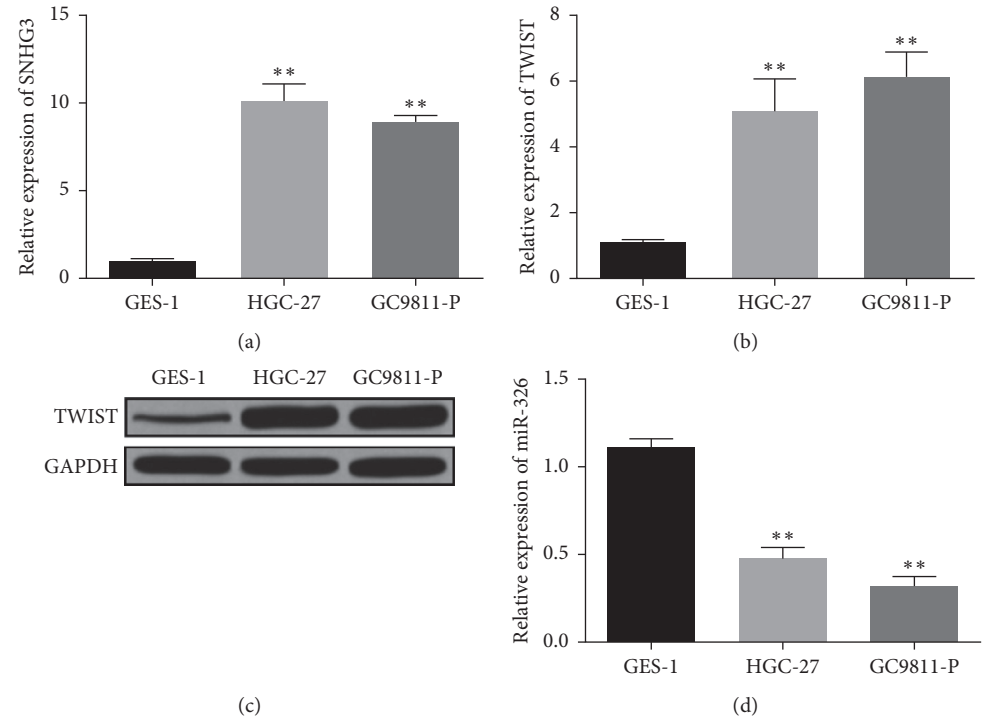

Figure 1: Expressions of lncRNA SNHG3, miR-326, and TWIST were examined in GC cells. (a) Expression of lncRNA SNHG3 in GC cells. (b) and (c) TWIST expression in GC cells. (d) MiR-326 expression in GC cells. $^{*}P < 0.05$ and $^{**}P < 0.01$.

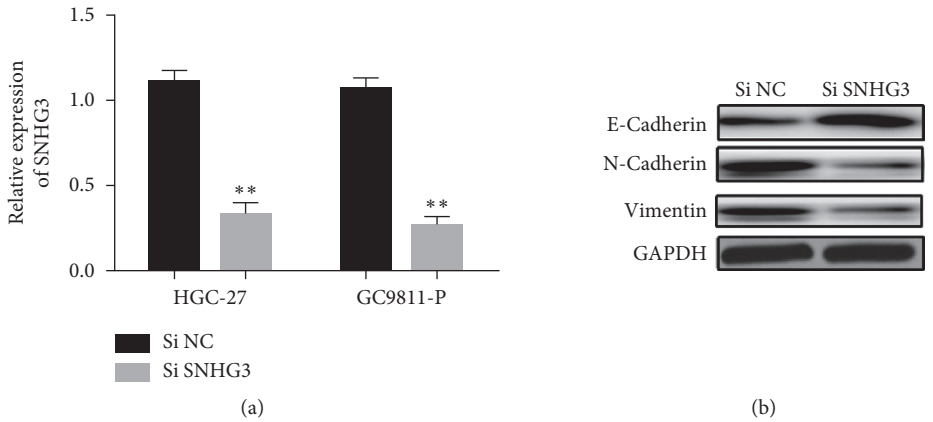

Figure 2: Continued.

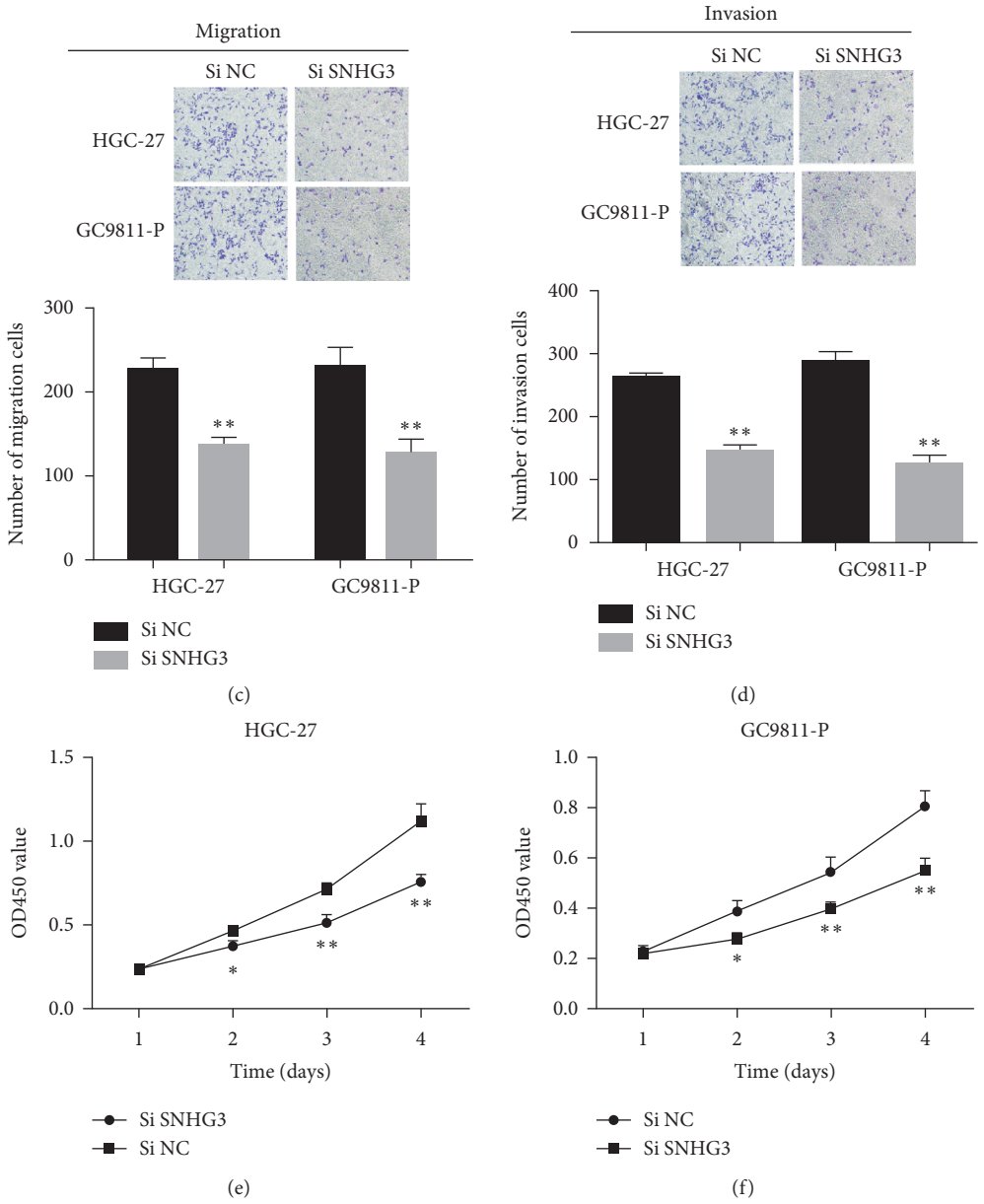

Figure 2: lncRNA SNHG3 knockdown suppressed HGC-27 and GC9811-P cell proliferation, migration, and invasion in vitro. (a) Expression of lncRNA SNHG3 in GC cells transfected with siSNHG3 or NC. (b) The protein level EMT-related marker in si NC and siSNHG3 groups. (c) and (d) Effect of lncRNA SNHG3 knockdown on cell migration and invasion. (e) and (f) Effect of lncRNA SNHG3 knockdown on cell proliferation. $^{*}P < 0.05$ and $^{**}P < 0.01$.

GC. As shown in Figures 6(a) and 6(b), the results showed that miR-326 overexpression significantly inhibited HGC-27 and GC9811-P cell proliferation, which could be partially reversed by TWIST overexpression. Furthermore, the inhibitory functions of si SNHG3 in HGC-27 and GC9811-P cell migration and invasion were also reversed by TWIST overexpression (Figures 6(c)–6(f)). It is suggested that lncRNA SNHG3 can promote cell proliferation, migration, and invasion by competitively binding and inhibiting miR-326 expression, thereby upregulating TWIST.

4. Discussion

GC is a major health problem and the second leading cause of cancer-related deaths worldwide. In Asia, about 60% of GC cases are diagnosed [20]. Despite improvements in surgical techniques and adjuvant therapies, GC is still highly lethal, with a 5-year survival rate of only 42% in China [21]. LncRNAs can mediate gene expression and affect tumor development, progression, and treatment. Huang et al. Snhg3 was identified as a competitive endogenous RNA

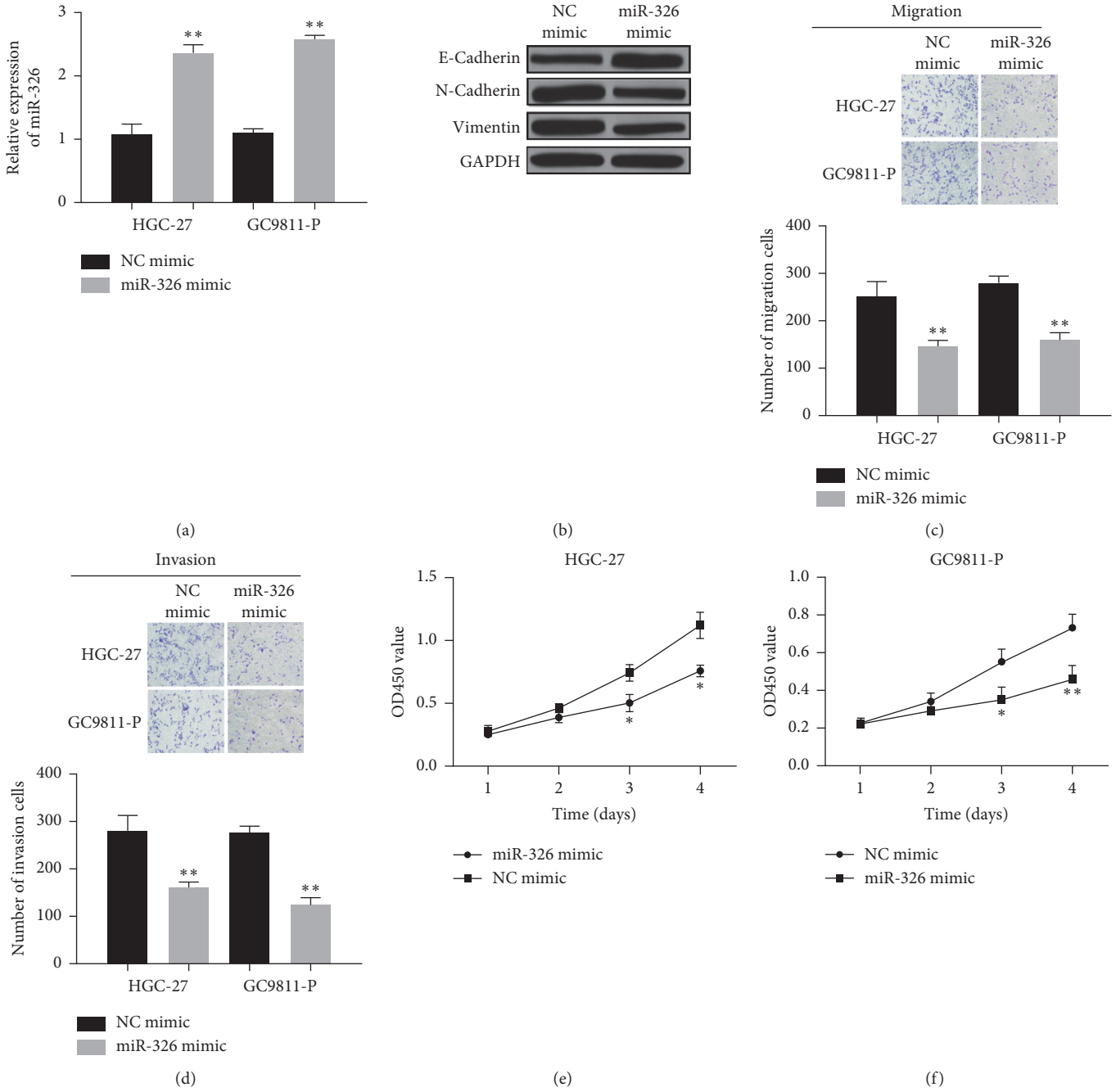

Figure 3: MiR-326 overexpression suppressed HGC-27 and GC9811-P cell proliferation, migration, and invasion in vitro. (a) Expression of miR-326 in GC cells transfected with miR-326 mimic or mimic NC. (b) The protein level expression of expression EMT-related marker in miR-326 mimic or mimic NC groups. (c) and (d) Effect of miR-326 overexpression on cell migration and invasion. (e) and (f) Effect of miR-326 overexpression on cell proliferation. $^{*}P < 0.05$ and $^{**}P < 0.01$.

molecule, which could promote the progression of colorectal cancer [22]. Hong et al. abnormal upregulation of snhg3 is closely related to poor prognosis in ovarian cancer [9]. However, many specific regulatory mechanisms of lncRNA in GC have not been studied. Therefore, exploring the potential molecular mechanism of lncRNA in GC may be helpful in the development of new diagnostic and therapeutic goals. Our study found that, according to RT-q PCR analysis, lncRNA SNHG3 was upregulated in GC cells compared to normal human immortalized gastric epithelial cells. CCK-8 and Transwell analysis showed that the inhibition of lncRNA SNHG3 could inhibit the proliferation, migration, and invasion of GC cells, which confirmed that lncRNA SNHG3 might affect the process of GC. Our results indicate that lncRNA SNHG3, which may be an oncogene, can be upregulated to benefit the development and progress

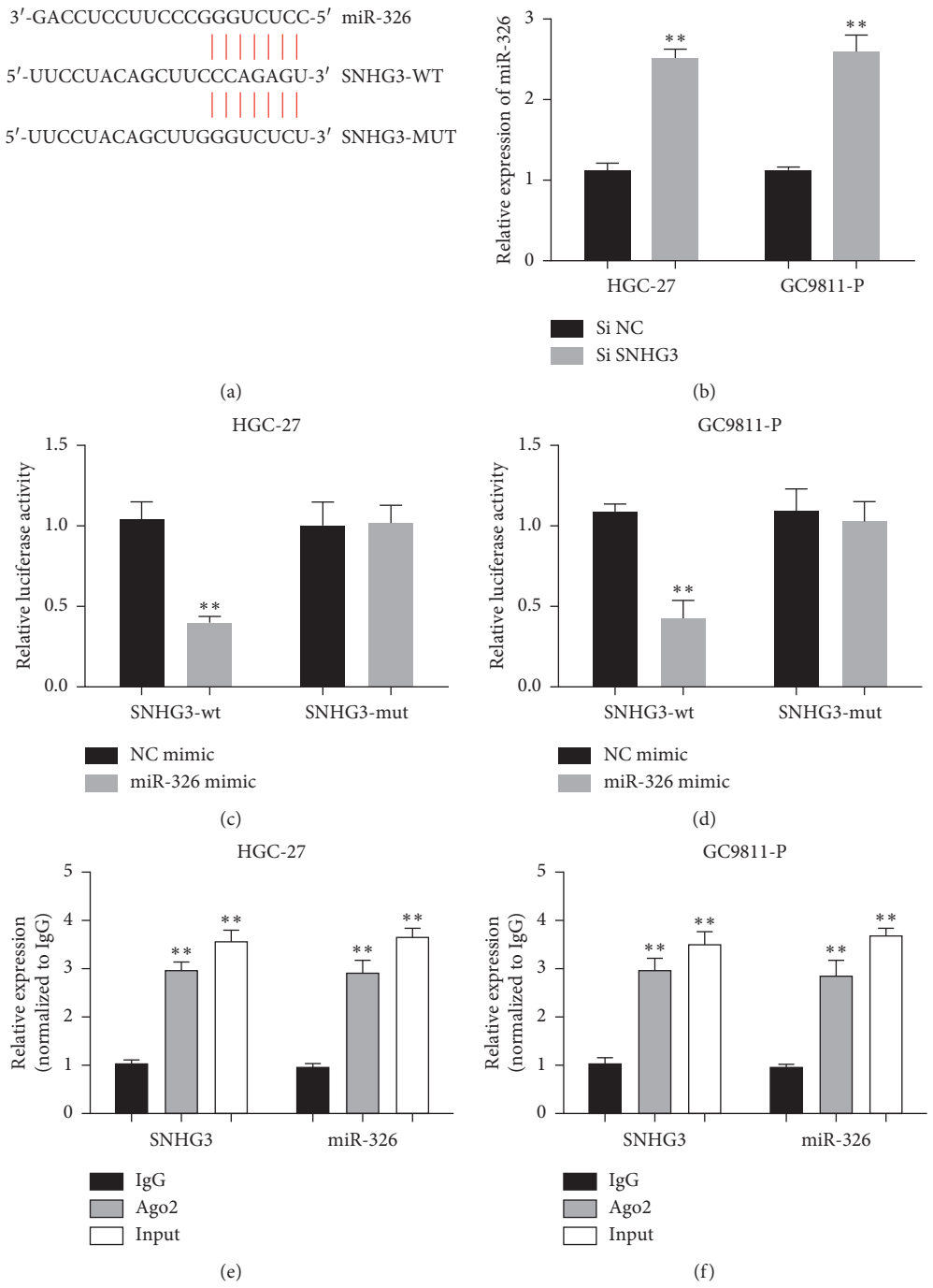

Figure 4: lncRNA SNHG3 functioned as an endogenous sponge to downregulate miR-326 by competitively binding to miR-326. (a) Putative binding sites between lncRNA SNHG3 and miR-326. (b) MiR-326 expression in GC cells transfected with siSNHG3 or siNC in HGC-27 and GC9811-P cell lines. (c) and (d) The luciferase activity was measured by a dual-luciferase reporter assay. (e) and (f) MiR-326 and lncRNA SNHG3 expressions in RIP assay. $^{**}P < 0.01$.

of GC. However, the specific mechanism of lncRNA SNHG3 in GC needs further study.

Like ceRNA, lncRNA plays a key role in cancer biology and pathology by competitively inhibiting miRNA and indirectly regulating mRNA. Wu et al. results suggest that SNHG15 is a competitive endogenous RNA (ceRNA) that participated in regulating the YAP1-hippo signaling pathway in thyroid papillary carcinoma through miR-200a-3p [23]. NORAD plays an important role in regulating the function of osteosarcoma cells by competing with hsa-miR-199a-3p [24]. He et al. demonstrated that NORAD overexpression promotes the growth, invasion, and migration of PTC cells by inhibiting miR-202-5p expression [25]. LncRNA HULC accelerates the proliferation of colon cancer cells by miR-613/RTKN 28, while lncRNA Xist, as the endogenous sponge of miR-137, upregulates Rac1, which is the

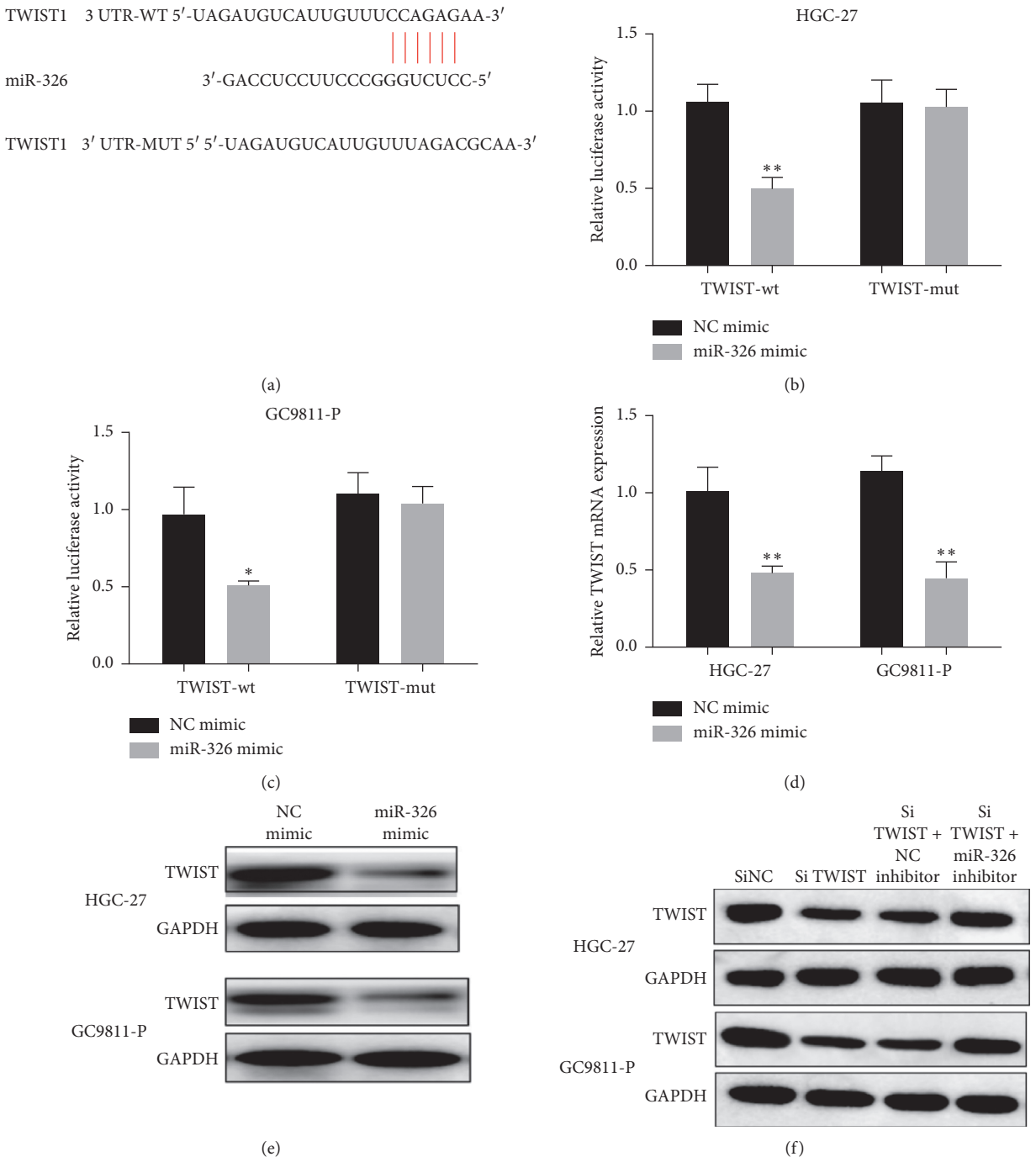

Figure 5: lncRNA SNHG3 regulated TWIST expression by competitively binding to miR-326. (a) Putative binding sites between miR-326 and TWIST. (b) and (c) The luciferase activity was measured by a dual-luciferase reporter assay. (d) and (e) TWIST expression in cells transfected with miR-326 mimic or NC. (f) The protein level of TWIST in HGC-27 and GC9811-P cells with different transfections. $^{*}P < 0.05$ and $^{**}P < 0.01$.

target gene of miR-137 and promotes the proliferation of glioma cells [26]. In our experiment, we found the expression of lncRNA SNHG3 and miR-326 and found that they showed a reverse expression trend in GC cells. In addition, according to bioinformatics analysis, we revealed that lncRNA SNHG3 contains a binding site with miR-326. Luciferase reporter gene and rip analysis showed that lncRNA SNHG3 interacted directly with miR-326 and regulated it. These results indicate that lncRNA SNHG3 acts as an endogenous sponge, competitively binds to miR-326, and negatively regulates its expression.

TWIST, a highly conserved transcription factor with a helical structure, is thought to regulate the carcinogenic properties essential for many cancer cells [27–29]. Recently, it was found that TWIST is involved in the transformation of breast cancer to stroma in vivo, which promotes epithelial

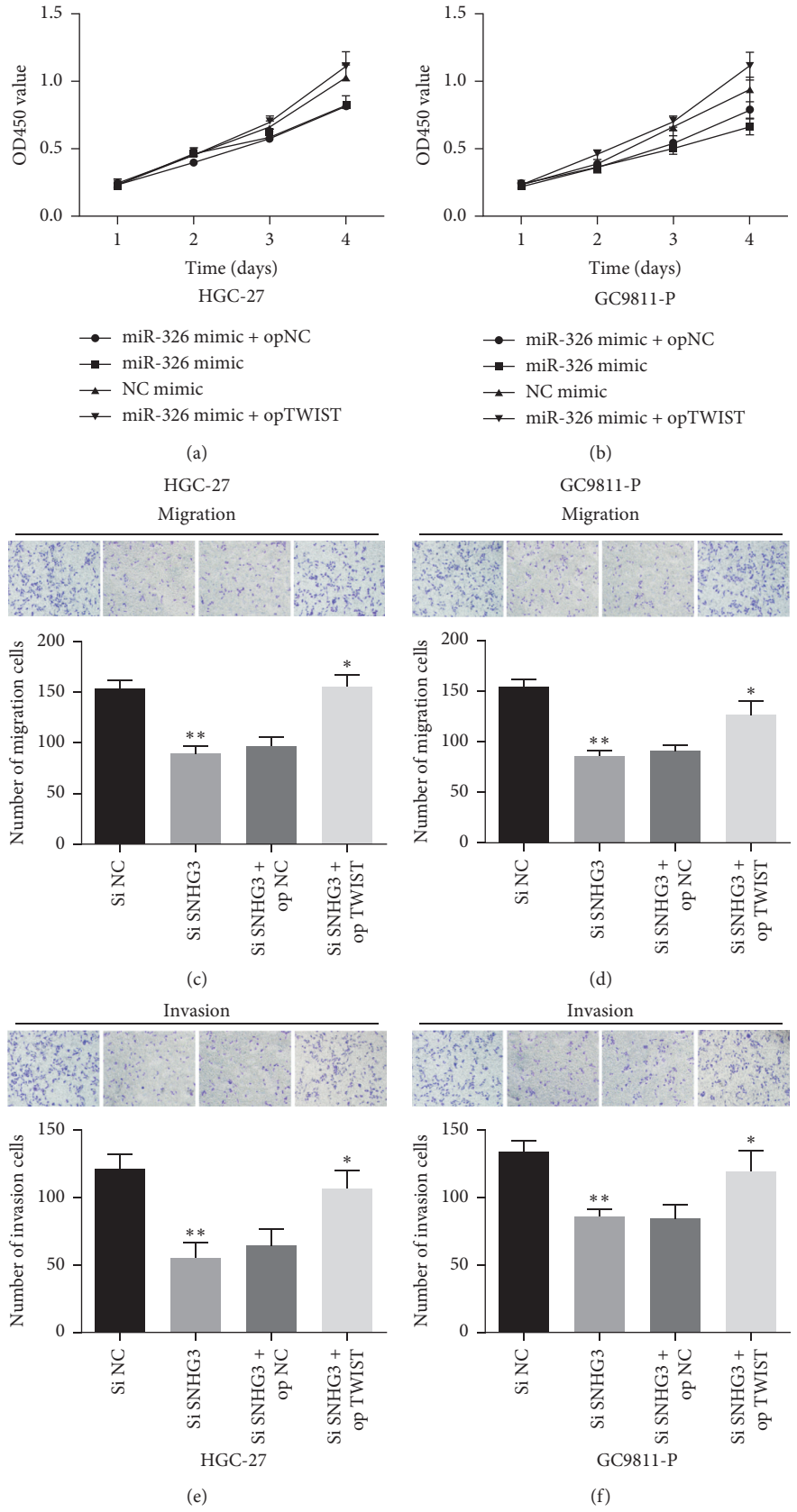

Figure 6: TWIST overexpression overturned lncRNA SNHG3 knockdown or miR-326 overexpression induced suppressive role on cell proliferation, migration, and invasion of GC cells. (a) and (b) TWIST overexpression overturned the suppressive functions of miR-326 overexpression in GC cell proliferation. ((c)–(f)) TWIST overexpression overturned the suppressive functions of SNHG3 knockdown in GC cell migration and invasion. $^{*}P < 0.05$ and $^{**}P < 0.01$.

formation [30]. It has also been reported that TWIST expression significantly enhances different types of cancer, such as prostate cancer, sarcoma, lymphoma, and melanoma [31–33]. In addition, TWIST also plays a significant role in many physiological processes, such as angiogenesis, visceral foot, exosmosis, and chromosome instability [31]. These findings indicate that TWIST is a new oncogene related to tumorigenesis and the progress of tumor. In order to investigate whether lncRNA SNHG3 and ceRNA can negatively regulate the release of miR-326, the upregulated target gene TWIST of miR-326 in GC cells was studied. Through bioinformatics analysis and luciferase reporter gene analysis, TWIST was proved to be the target of miR-326. More importantly, the overexpression of lncRNA SNHG3 reversed the luciferase activity of TWIST-wt inhibited by miR-326 mimic. Knockdown of lncRNA SNHG3 significantly reduced the expression of TWIST, which was reversed by miR-326 inhibitor. We suggest that lncRNA SNHG3 can regulate the expression of TWIST by negatively regulating miR-326. In addition, the overexpression of TWIST significantly overturned the inhibition of cell metastasis by knockdown of lncRNA SNHG3 or overexpression of miR-326, suggesting that the axis of lncRNA SNHG3-miR-326-TWIST may have participated in the development of GC.

5. Conclusion

In summary, our data showed that lncRNA SNHG3 promoted GC cell metastasis by regulating miR-326 and TWIST. This will help us to better understand the lncRNA, miRNA, and mRNA network in GC. However, the function of lncRNA SNHG3, miR-326, and TWIST was not tested in vivo. Moreover, we did not measure the expressions of SNHG3 in clinical patients. Further research should also be carried out to explore whether certain signaling pathways play a role in the mechanism of lncRNA SNHG3 in GC. Thus, the significance and robustness of SNHG3 as a biomarker for GC requires further confirmation.

Data Availability

All primary data are available from the corresponding author upon reasonable request.

Disclosure

Jun Rao and Jinjin Fu are co-first authors.

Conflicts of Interest

The authors declare that they have no conflicts of interest.

References

[1] A. Aiolfi, F. Lombardo, K. Matsushima et al., "Systematic review and updated network meta-analysis of randomized controlled trials comparing open, laparoscopic-assisted, and robotic distal gastrectomy for early and locally advanced gastric cancer," *Surgery*, vol. 21, 2021.

[2] N. Bizzaro, A. Antico, and D. Villalta, "Autoimmunity and gastric cancer," *International Journal of Molecular Sciences*, vol. 19, no. 2, 2018.

[3] S. Abi Doumeth, H. Bou Daher, A. El Mokahal, A. Tawil, and A. I. Sharara, "Prevalence and characteristics of post-gastroscopy gastric cancer: a retrospective study from an academic medical center," *Arab Journal of Gastroenterology*, vol. 2, 2021.

[4] A. Digklia and A. D. Wagner, "Advanced gastric cancer: current treatment landscape and future perspectives," *World Journal of Gastroenterology*, vol. 22, no. 8, pp. 2403–2414, 2016.

[5] J. J. Quinn and H. Y. Chang, "Unique features of long noncoding RNA biogenesis and function," *Nature Reviews Genetics*, vol. 17, no. 1, pp. 47–62, 2016.

[6] E. Abdi, S. Latifi-Navid, V. Kholghi-Oskooei, F. Pourfarzi, and A. Yazdanbod, "Interaction between lncRNAs HOTAIR and MALAT1 tagSNPs in gastric cancer," *British Journal of Biomedical Science*, vol. 78, no. 3, pp. 1–4, 2021.

[7] Y. Ge, X. Yan, Y. Jin et al., "MiRNA-192 [corrected] and miRNA-204 directly suppress lncRNA HOTTIP and interrupt GLS1-mediated glutaminolysis in hepatocellular carcinoma," *PLoS Genetics*, vol. 11, no. 12, Article ID e1005726, 2015.

[8] F.-T. Huang, W.-Y. Chen, Z.-Q. Gu et al., "The novel long intergenic noncoding RNA UCC promotes colorectal cancer progression by sponging miR-143," *Cell Death and Disease*, vol. 8, no. 5, p. e2778, 2017.

[9] L. Hong, W. Chen, D. Wu, and Y. Wang, "Upregulation of SNHG3 expression associated with poor prognosis and enhances malignant progression of ovarian cancer," *Cancer Biomarkers*, vol. 22, no. 3, pp. 367–374, 2018.

[10] N. Li, X. Zhan, and X. Zhan, "The lncRNA SNHG3 regulates energy metabolism of ovarian cancer by an analysis of mitochondrial proteomes," *Gynecologic Oncology*, vol. 150, no. 2, pp. 343–354, 2018.

[11] Y. Li, Y. Gao, Y. Xu, H. Ma, and M. Yang, "Down-regulation of miR-326 is associated with poor prognosis and promotes growth and metastasis by targeting FSCN1 in gastric cancer," *Growth Factors*, vol. 33, no. 4, pp. 267–274, 2015.

[12] X. Wu, X. Cao, and F. Chen, "Withdrawn: LncRNA-HOTAIR activates tumor cell proliferation and migration by suppressing MiR-326 in cervical cancer," *Oncology Research*, vol. 31, 2017.

[13] P. Zhang, F. Kong, X. Deng et al., "MicroRNA-326 suppresses the proliferation, migration and invasion of cervical cancer cells by targeting ELK1," *Oncology Letters*, vol. 13, no. 5, pp. 2949–2956, 2017.

[14] S. Yin, W. Du, F. Wang et al., "MicroRNA-326 sensitizes human glioblastoma cells to curcumin via the SHH/GLI1 signaling pathway," *Cancer Biology and Therapy*, vol. 19, no. 4, pp. 260–270, 2018.

[15] K. Valencia, M. Martín-Fernández, C. Zandueta et al., "miR-326 associates with biochemical markers of bone turnover in lung cancer bone metastasis," *Bone*, vol. 52, no. 1, pp. 532–539, 2013.

[16] R. Wang, X. F. Chen, and Y. Q. Shu, "Prediction of non-small cell lung cancer metastasis-associated microRNAs using bioinformatics," *American Journal of Cancer Research*, vol. 5, no. 1, pp. 32–51, 2015.

[17] L. Vermani, R. Kumar, R. R. Kannan, M. K. Deka, A. Talukdar, and N. S. Kumar, "Expression pattern of ALDH1, E-cadherin, vimentin and twist in early and late onset sporadic colorectal cancer," *Biomarkers in Medicine*, vol. 14, no. 14, pp. 1371–1382, 2020.

[18] X. F. Guo, A. Y. Wang, and J. Liu, "HIFs-MiR-33a-Twsit1 axis can regulate invasiveness of hepatocellular cancer cells," *European Review for Medical and Pharmacological Sciences*, vol. 20, no. 14, pp. 3011–3016, 2016.

[19] L. Jin, J. Zhang, H. Q. Fu, X. Zhang, and Y. L. Pan, "FOXO3a inhibits the EMT and metastasis of breast cancer by regulating TWIST-1 mediated miR-10b/CADM2 axis," *Translational Oncology*, vol. 14, no. 7, Article ID 101096, 2021.

[20] L. Shen, Y.-S. Shan, H.-M. Hu et al., "Management of gastric cancer in Asia: resource-stratified guidelines," *The Lancet Oncology*, vol. 14, no. 12, pp. e535–e547, 2013.

[21] V. E. Strong, A.-w. Wu, L. V. Selby et al., "Differences in gastric cancer survival between the U.S. and China," *Journal of Surgical Oncology*, vol. 112, no. 1, pp. 31–37, 2015.

[22] W. Huang, Y. Tian, S. Dong et al., "The long non-coding RNA SNHG3 functions as a competing endogenous RNA to promote malignant development of colorectal cancer," *Oncology Reports*, vol. 38, no. 3, pp. 1402–1410, 2017.

[23] D.-M. Wu, S. Wang, X. Wen et al., "LncRNA SNHG15 acts as a ceRNA to regulate YAP1-Hippo signaling pathway by sponging miR-200a-3p in papillary thyroid carcinoma," *Cell Death and Disease*, vol. 9, no. 10, p. 947, 2018.

[24] X. Wang, J. Zou, H. Chen et al., "Long noncoding RNA NORAD regulates cancer cell proliferation and migration in human osteosarcoma by endogenously competing with miR-199a-3p," *IUBMB Life*, vol. 71, no. 10, pp. 1482–1491, 2019.

[25] H. He, H. Yang, D. Liu, and R. Pei, "LncRNA NORAD promotes thyroid carcinoma progression through targeting miR-202-5p," *American Journal of Translational Research*, vol. 11, no. 1, pp. 290–299, 2019.

[26] S. Wu, N. Ai, Q. Liu, and J. Zhang, "MicroRNA448 inhibits the progression of retinoblastoma by directly targeting ROCK1 and regulating PI3K/AKT signalling pathway," *Oncology Reports*, vol. 39, no. 5, pp. 2402–2412, 2018.

[27] K. Ohuchida, K. Mizumoto, S. Ohhashi et al., "Twist, a novel oncogene, is upregulated in pancreatic cancer: clinical implication of twist expression in pancreatic juice," *International Journal of Cancer*, vol. 120, no. 8, pp. 1634–1640, 2007.

[28] R. Maestro, A. P. D. Tos, Y. Hamamori et al., "Twist is a potential oncogene that inhibits apoptosis," *Genes and Development*, vol. 13, no. 17, pp. 2207–2217, 1999.

[29] S. Raatikainen, S. Aaltomaa, J. J. Palvimo, V. Kärjä, and Y. Soini, "TWIST overexpression predicts biochemical recurrence-free survival in prostate cancer patients treated with radical prostatectomy," *Scandinavian Journal of Urology*, vol. 49, no. 1, pp. 51–57, 2015.

[30] J. Yang, S. A. Mani, J. L. Donaher et al., "Twist, a master regulator of morphogenesis, plays an essential role in tumor metastasis," *Cell*, vol. 117, no. 7, pp. 927–939, 2004.

[31] M. A. Khan, H.-c. Chen, D. Zhang, and J. Fu, "Twist: a molecular target in cancer therapeutics," *Tumor Biology*, vol. 34, no. 5, pp. 2497–2506, 2013.

[32] W. K. Kwok, M.-T. Ling, T.-W. Lee et al., "Up-regulation of TWIST in prostate cancer and its implication as a therapeutic target," *Cancer Research*, vol. 65, no. 12, pp. 5153–5162, 2005.

[33] S. Kyo, J. Sakaguchi, S. Ohno et al., "High twist expression is involved in infiltrative endometrial cancer and affects patient survival," *Human Pathology*, vol. 37, no. 4, pp. 431–438, 2006.

Hindawi
Journal of Oncology
Volume 2021, Article ID 3554219, 9 pages
https://doi.org/10.1155/2021/3554219

Research Article

MiR-466 Inhibits the Progression of Severe Hepatocellular Carcinoma via Regulating FMNL2-Mediated Activation of NF-κB and Wnt/β-Catenin Pathways

Jianwei Li[1] **and Su Yan**[2]

[1]*Department of Hepatology, Traditional Chinese Medicine Hospital of Rizhao City, Rizhao 276800, Shandong, China*
[2]*Department of Critical Care Medicine, Traditional Chinese Medicine Hospital of Rizhao City, Rizhao 276800, Shandong, China*

Correspondence should be addressed to Su Yan; yansu234@163.com

Received 25 April 2021; Revised 2 June 2021; Accepted 17 June 2021; Published 24 June 2021

Academic Editor: Muhammad Wasim Khan

Hepatocellular carcinoma (HCC) has threatened the health of humans, and some evidence has indicated that miR-466 involves the progressions of some cancers. This study focused on the role of miR-466 in the formation and development of HCC. The expression levels of miR-466 in the tissues of patients and HCC cell lines were measured by qRT-PCR, and CCK-8, transwell assay, and flow cytometry assay were used to observe the functions of miR-466 on the HCC cells. Moreover, the miRNA databases, dual-luciferase reporter assay, and Western blot were used for the investigation of the regulation mechanism of miR-466 on HCC cells. The results showed that miR-466 was significantly downregulated in HCC tissues and cell lines, and inhibited proliferation, invasion, and high apoptosis were found in HCC cells when miR-466 was overexpressed. The results confirmed that FMNL2 was a target of miR-466, and increased FMNL2 could reverse the effects of miR-466 on the phenotype of HCC cells. Besides, it was also found that miR-466 was involved in the regulation of NF-κB and Wnt/β-catenin pathways in HCC cells via targeting FMNL2. In conclusion, the results of this study suggest that miR-466 regulates the activities of NF-κB and Wnt/β-catenin pathways to inhibit the progression of HCC cells via targeting FMNL2.

1. Introduction

Hepatocellular carcinoma (HCC) is a malignant tumor with high morbidity and mortality, and up to 600000 people die from this disease worldwide every year [1, 2]. Recently, some significant improvements have been achieved in clinical diagnosis and treatment. However, the situations of more than half of patients have been developed to medium or late stage of HCC when they feel obvious discomfort, and the drugs-resistance and tumor invasion can also impede the healing of the patients [3, 4]. Thus, even with current therapeutic strategies, the prognosis and overall survival rates of HCC patients remain unsatisfactory [5, 6]. Although great achievements in the pathogenesis of HCC have been obtained in the last decade, the molecular mechanism on the progression of HCC is not completely illustrated [7, 8]. Therefore, there is an urgent demand to search for novel molecules and provide much more strategies for clinical diagnosis and treatment.

MicroRNAs (miRNAs), the single chain of noncoding RNA with 18–25 nucleotides, are characterized by regulating progressions of gene translations via interacting with the 3′-untranslated regions (3′-UTRs) of the related messenger RNAs (mRNAs) [9]. MiRNAs take part in the signal transmissions and regulate the life activities of cells such as proliferation, differentiation, and apoptosis [10]. Multiple studies have indicated that miRNAs dysfunction plays an important role in the formations and developments of many diseases ranging from cardiovascular deterioration to tumors [11, 12]. Therefore, regulating the expression of some special miRNAs has been proved as a promising diagnostic and therapeutic system for cancer in clinical treatment. The

studies have shown that the downregulation of miR-466 is related to the developments of epithelial ovarian cancer and colorectal cancer, while its role in HCC remains unclear [13, 14].

In this study, the exploration attempted to investigate the connection of miR-466 and HCC and reveal the effects of miR-466 on the phenotype of HCC cells and the regulation mechanism of miR-466 on the progression of HCC.

2. Materials and Methods

2.1. Clinical Tissues. This study was approved by the Ethics Committee of the Traditional Chinese Medicine Hospital of Rizhao, Rizhao, Shandong, China, and the prior consent of the patients and authorizations from hospitals were obtained. The tumor tissues and matched adjacent health tissues donated by the patients were used in this study. All tissues were stored at −80°C.

2.2. Cell Culture and Transfection. The normal human liver cell lines HL-7702 and the human hepatic carcinoma cell lines including Hep3B, Huh7, and HepG2 were used in this study. All cells were cultured with Dulbecco's modified eagle medium (DMEM, Procell Life Science and Technology Co., Ltd., China) containing 10% fetal bovine serum (FBS, ThermoFisher, USA) in an incubator with 37°C and 5% CO_2. The subculture of the cells was performed when the cellular confluence was at 90%.

The cells were seed into the 6-well plates, and cell transfection was performed when the confluences of the cells were at 70%. MiR-466 mimics, miRNA negative control (miR-NC), pcDNA-FMNL2, and pcDNA-NC were synthesized by Generay Biotech Co., Ltd. (Shanghai, China). In short, 4 g of DNA, 100 pmol RNA, or 10 μl lipofectamine 2000 (Beijing Noble Ryder Technology Co. Ltd., Beijing, China) were, respectively, diluted and incubated with 250 μL serum-free medium for 5 min. The diluted DNA or RNA was, respectively, mixed with isometric diluted lipofectamine 2000 and then was incubated at 25°C for 20 min. After that, 500 μL of the mixtures was added into each well, and then, the cells were cultured for 24 hours.

2.3. Real-Time Quantitative Reverse Transcription PCR (qRT-PCR). The miR-466 levels in the tissues and cell lines were measured by qRT-PCR. The TRIzol reagent was used to perform the extractions of the total RNAs in the tissues or HCC cell lines. The concentrations of the total RNAs were measured by spectrophotometry. After that, the total RNAs were transcribed as cDNA via PrimeScript® RT Reagent Kit (Thermo Fisher, Massachusetts, USA). The primers were synthesized and purified by Synbio Technology (Suzhou, China). The reaction systems (10 μL) of qRT-PCR were prepared according to the operational instruction of a KAPA qRT-PCR kit (Sigma-Aldrich, Missouri, USA). U6 was used as the endogenous control. The following conditions were used: denaturation at 95°C for 3 min, followed by amplification for 40 cycles at 95°C for 12 s, at 53°C for 40 s, and 70°C for 30 s. The relative levels of miRNAs were calculated with the $2^{-(\Delta\Delta Ct)}$ method. The primers of miR-466 and U6 were synthesized and purified by RiboBio Co., Ltd. (Guangzhou, China). The primer sequences of miR-466 and U6 are given in Table 1.

2.4. Western Blot. The total proteins in the tissues and cell lines were extracted with RIPA buffer on the ice box, and the concentrations of the extractions were measured by a BCA protein assay kit (ThermoFisher, Massachusetts, USA). The extracts were mixed with quadruple of SDS-PAGE sample loading buffer; then, the extracts were boiled at 100°C for 5 min. The proteins were separated by SDS-polyacrylamide gel electrophoresis (SDS-PAGE) and then transferred on the polyvinylidene fluoride (PVDF) membranes by the wet transfer method. After that, the membranes were blocked with 5% fat-free milk at 4°C for 1 hour, and then, membranes were incubated added with the related primary antibodies at 4°C overnight. The membranes were washed with Tris buffered saline-Tween (TBST) for three times (15 mins per time) and then were incubated with second antibodies at 25°C for 1 hour. Finally, the membranes were washed with TBST and added with ECL reagent (ThermoFisher, USA) for three times (10 mins per time). After that, the expressions of the proteins were observed under a chemiluminescence detection system. The antibodies were used under following conditions: anti-FMNL2 (1 : 1000, ab2540720, ThermoFisher, Massachusetts, USA); anti-β-catenin (1 : 1000, ab2533039, ThermoFisher, Massachusetts, USA); anti-Wnt (1 : 1000, ab11154198, ThermoFisher, Massachusetts, USA); anti-*P*65 (1 : 1000, ab2533893, ThermoFisher, Massachusetts, USA); anti-*p*-*P*65 (1 : 1000, ab10982265, ThermoFisher, Massachusetts, USA); and anti-β-actin (1 : 1000, ab2223496, ThermoFisher, Massachusetts, USA).

2.5. Transwell Assay. For the invasion assay, Matrigel was diluted with eight-time DMEM, and diluted Matrigel was added into the upper chambers of transwells. After drying, 5×10^4 cells and 200 μL of serum-free DMEM were added into the upper chambers, and 600 μL of DMEM containing 10% FBS was added into the cells in the lower chambers. The cells were cultured for 24 hours. After that, the cells on the upper surfaces of the chambers were removed by cotton buds, and the migrated cells on the lower surface of the upper chamber were fixed by methanol for 10 min; the cells were then dried at 25°C. The cells were stained with 0.1% w/v crystal violet (Solarbio, Beijing, China) for 30 mins and then washed with tap water. The invaded cells were calculated and photographed under a Leica DMi8 microscope.

2.6. CCK-8 Assay. The cells (3×10^3) were seeded into 96-well plates and incubated for 24 hours. After transfection, the cells were further incubated for 24 hours. Subsequently, the viability of the cells at 0, 24, 48, and 72 hours were measured by CCK-8 kit (Amyjet, Wuhan, China). In short, 10 μL of CCK-8 solution was added into each well, and then, the cells were incubated at 25°C in the dark for 4 hours.

Table 1: Primer sequence of miR-466 and U6.

Name of primer	Sequences
miR-466-F	5′-CACTAGTGGTTCCGTTTAGTAG-3′
miR-466-R	5′-TTGTAGTCA CTAGGGCACC-3′
FMNL2-F	5′-GCTATGAACCTACCTCCTGACA-3′
FMNL2-R	5′-AACACGCCGTCTGAATTTCTT-3′
U6–F	5′-CTCGCTTCGGCAGCACA-3′
U6-R	5′-AACGCTTCACGAATTTGCGT-3′

Finally, the absorbance value of the cells was measured by a microplate reader (Molecular Devices, Shanghai, China).

2.7. Dual-Luciferase Reporter Gene Assay. The mutant or wild 3′-UTR sequences of FMNL2 were inserted into the pmirGLO luciferase reporter vectors (Yanjiang Bio Co., Ltd., China) to establish the FMNL2-mutant type (FMNL2-mut) and FMNL2-wild type (FMNL2-wt), respectively. FMNL2-mut or FMNL2-wt was, respectively, cotransfected with miR-466 mimics or miR-NC into HEK-293T cells. After that, the cells were incubated for 48 hours. Finally, the binding effect of miR-466 and FMNL2 was observed by a dual-luciferase reporter assay system.

2.8. Flow Cytometry Assay. Huh7 cells were harvested by trypsinase (0.25%, EDTA-free). The harvested cells were washed by 3 mL of ice phosphate-buffered saline (PBS) for once and then were fixed by alcohol. After that, 1×10^6 of the cells were suspended with 100 μl of incubation buffer. 5 μL of ice Annexin V-FITC and 5 μL of propidium iodide (PI 20 μg/ml) were added into the tubes, and then, the cells were incubated in dark for 15 min. Finally, the apoptosis levels of the cells were instantly observed by flow cytometry equipment (BD Biosciences, State of New Jersey, USA).

2.9. Statistical Analysis. All experiments were performed at least 3 times, independently. The data were analyzed by SPSS 20.0, and the figures were charted by GraphPad Prism 8.0. The difference of the data was tested with the chi-squared test or ANOVA with Tukey's posthoc test. $P < 0.05$ means that the difference between the two groups was significant.

3. Results

3.1. MiR-466 was Significantly Downregulated in Tumor Tissues and Cell Lines. To observe the connection between miR-466 and hepatocellular carcinoma, the tissues of the patients and normal and tumor cell lines were used to measure the expression level of miR-466. The qRT-PCR showed that the miR-466 was significantly downregulated in the tumor tissues compared with the paracancerous tissues (Figure 1(a), $P < 0.01$). Besides, decreased miR-466 levels were also observed in the tumor cell lines including Hep3B, Huh7, and HepG2 compared with the normal cell line (Figure 1(b), $P < 0.01$).

3.2. MiR-466 Inhibited the Proliferation and Invasion of Hepatocellular Carcinoma Cells. To explore the functions of miR-466 in hepatocellular carcinoma cells, the miR-466 mimics were transfected into Huh7, and CCK-8 assay, transwell assay, and flow cytometry assay were used to reflect the changes in proliferation, invasion, and apoptosis levels of the cells. The CCK-8 assay showed that the proliferation of Huh7 transfected with miR-466 mimics was visibly inhibited compared with the cells transfected with miR-NC (Figure 2(a), $P < 0.01$). The transwell assay reflected that Huh7 cells transfected with miR-466 mimics expressed low invasive abilities compared with the cells transfected with miR-NC (Figure 2(c), $P < 0.01$). Moreover, the increased apoptosis levels were observed in the cells transfected with miR-466 mimics (Figure 2(b), $P < 0.01$).

3.3. MiR-466 Directly Targeted the 3′-UTR of FMNL2. To reveal the regulation mechanism of miR-466 on HCC, TargetScan, an online database, was used to search the downstream target of miR-466, and a dual-luciferase reporter assay was used to observe the binding effect of miR-466 and its target. The results showed that FMNL2 was one of the potential targets of miR-466. The dual-luciferase reporter assay showed that miR-466 significantly reduced the luciferase activity of the HEK-293T cells transfected with FMNL2 expressed vectors (Figure 3(a), $P < 0.01$). Besides, it was also observed that FMNL2 was extremely upregulated in Hep3B, Huh7, and HepG2 cells compared with normal cell lines (Figure 3(b), $P < 0.01$).

3.4. FMNL2 Reversed the Effects of miR-466 on HCC Cells. Although the connection of miR-466 and FMNL2 was proved above, whether FMNL2 was involved in the regulation of miR-466 on HCC cells remained unclear. The miR-466 mimics and FMNL2 expressed vectors were cotransfected into the HCC cells, and the changes in the proliferation, invasion, and apoptosis of the cells were observed. The CCK-8 assay showed that the weakened proliferation of the cells induced by miR-466 was reversed by FMNL2 upregulation (Figure 4(a), $P < 0.01$). The transwell assay showed that the inhibitory effect of miR-466 on the invasion of the cells was returned by FMNL2 (Figure 4(c), $P < 0.01$). Moreover, it was observed that the increased apoptosis levels of HCC cells including Hep3B, Huh7, and HepG2 induced by miR-466 were rescued by FMNL2 (Figure 4(b), $P < 0.01$). Those observations suggested that miR-466 could regulate the phenotype of the cells via targeting FMNL2.

3.5. MiR-466 Inactivated the Wnt/β-Catenin and NF-κB via Targeting FMNL2. FMNL2 was proved as a key factor in the regulation of miR-466 on HCC. To further analyze the regulation mechanism of miR-466 on HCC, the miR-466 mimics and FMNL2 were cotransfected into the cells, and the proteins in Wnt/β-catenin and NF-κB pathways were observed by Western blot. The results showed that miR-466 significantly inhibited the expressions of Wnt, β-catenin, and *p-P*65. However, the upregulations of those proteins

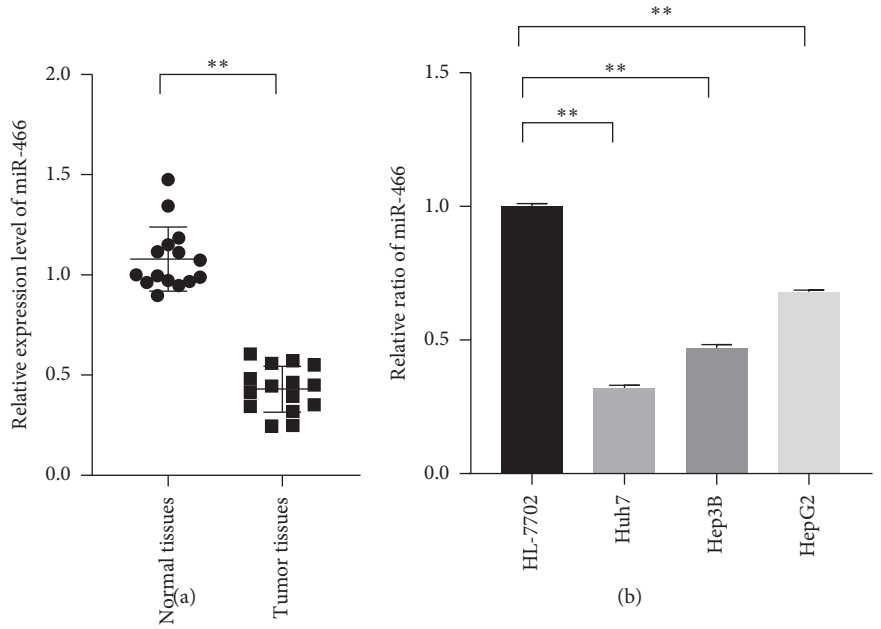

FIGURE 1: MiR-466 significantly downregulated in HCC tissues and cell lines. (a) The relative expression levels of miR-466 in the tumor and paracancerous tissues measured by qRT-PCR. (b) The relative expression levels of miR-466 normal human liver and HCC cell lines measured by qRT-PCR. $^{**}P < 0.05$.

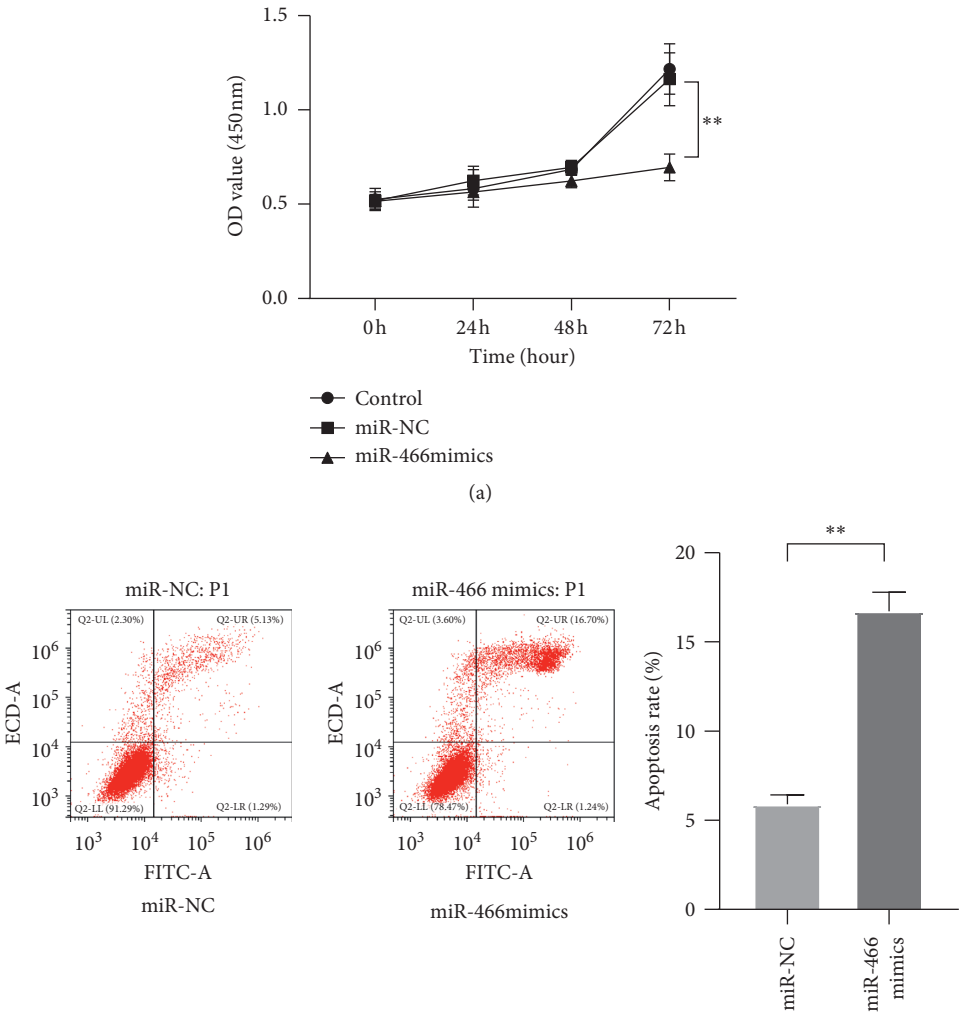

FIGURE 2: Continued.

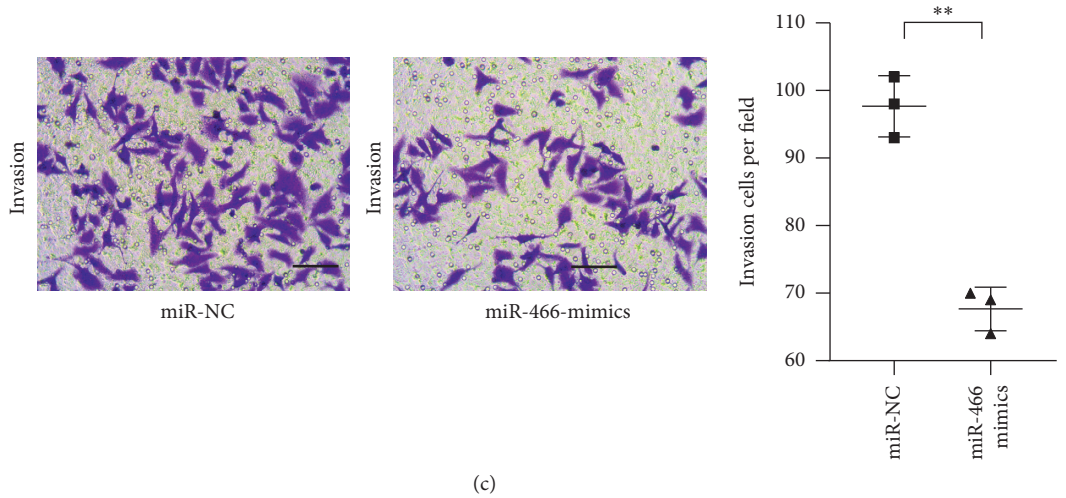

Figure 2: MiR-466 inhibited the proliferation, invasion, and apoptosis of Huh7. (a) The proliferation of Huh7 cells measured by CCK-8. (b) The apoptosis level of Huh7 cells observed by flow cytometry assay. (c) The invasion of Huh7 cells observed by transwell assay (scale bar = 50 μm). $^{**}P < 0.05$.

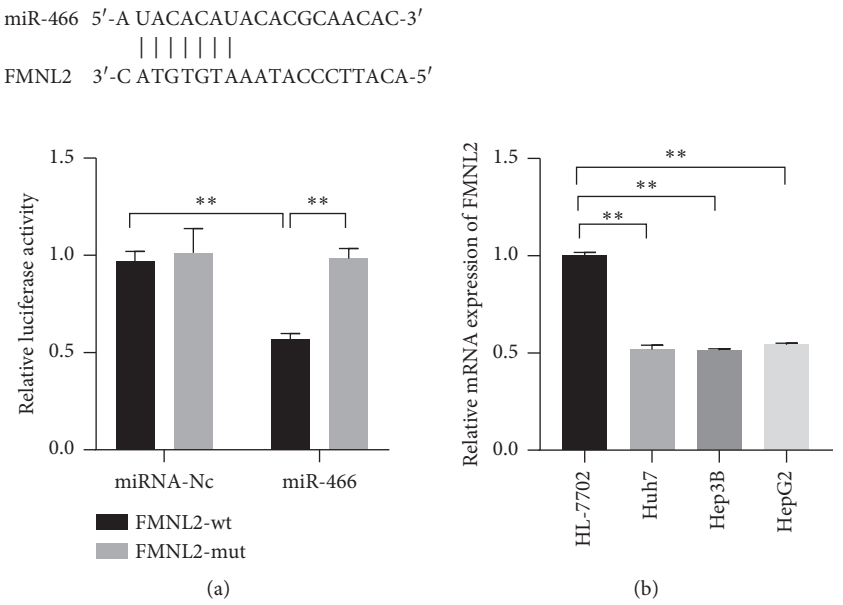

Figure 3: FMNL2 was a downstream target of miR-466 and upregulated in HCC tissues and cell lines. (a) The binding effect of miR-466 and FMNL2 measured by dual-luciferase reporter assay. (b) The expression levels of FMNL2 in HCC cell lines observed by Western blot. $^{**}P < 0.05$.

induced by miR-466 could be reversed by FMNL2 (Figure 5, $P < 0.01$).

4. Discussion

HCC is one of the malignant diseases which has threatened the health of human, and miRNA dysfunction has been found as a key cause of cancer formation [15]. MiR-466 locates on chromosome 3, and several studies have indicated that miR-466 is significantly downregulated in some tumor cells and involves the regulations of the proliferation and invasion of the tumors [16]. In this study, the expression levels of miR-466 in HCC tissues and cell lines were investigated, and the effects of miR-466 on the phenotype of HCC cells such as proliferation, invasion, and apoptosis were also explored. Subsequently, this study also researched the downstream target of miR-466 and further revealed the role of FMNL2 in HCC progression. Moreover, the effects of miR-466 on the activities of NF-κB and Wnt/β-catenin pathways were also illustrated in the present study.

MiRNAs dysfunction is a general event in multiple tumors, and some of them have emerged as keys players in cancer progressions, and intervention on the expressions of some special miRNAs has been considered as a promising

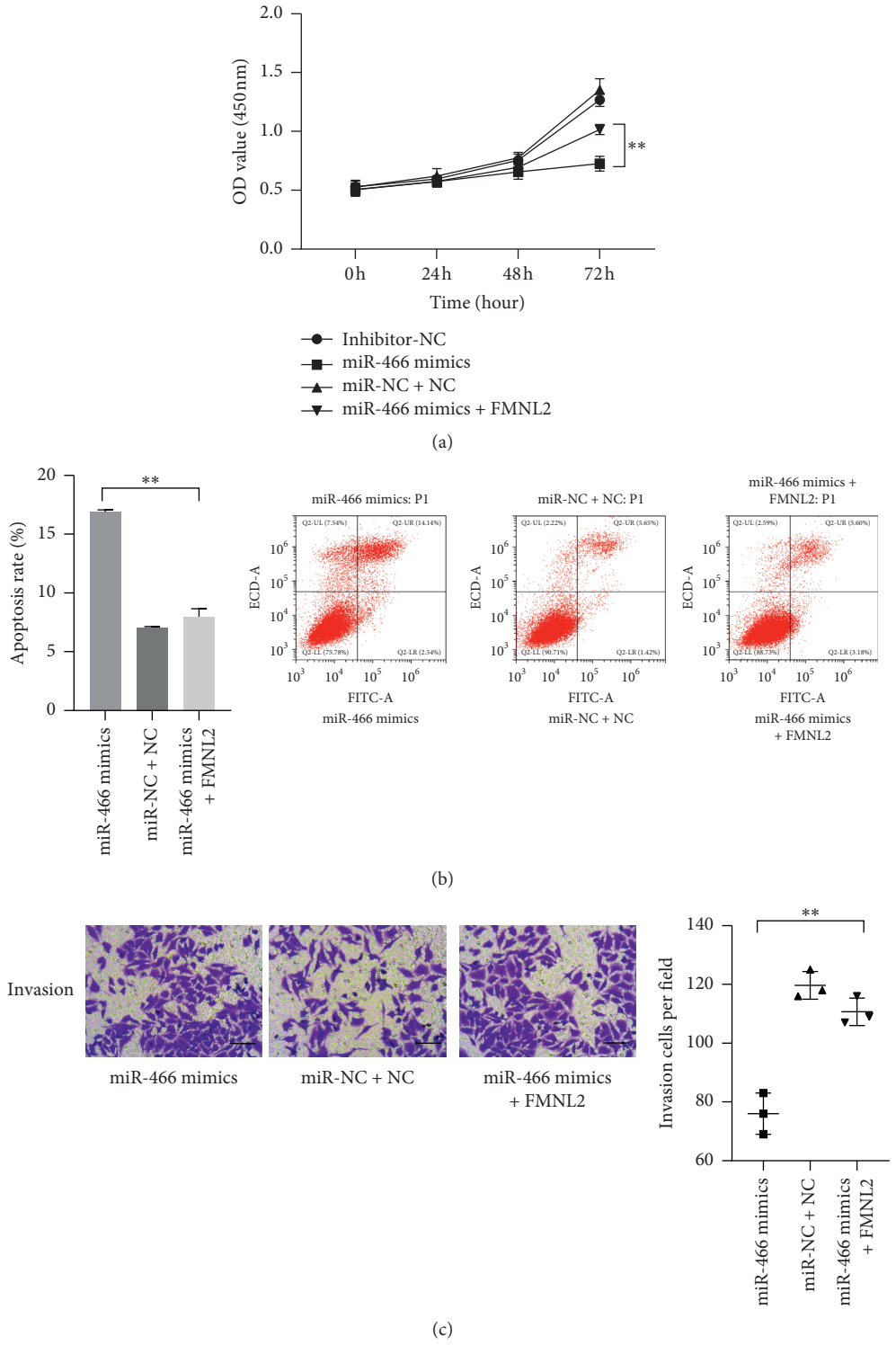

FIGURE 4: FMNL2 could reverse the effects of miR-466 on the proliferation, invasion, and apoptosis of Huh7. (a) The proliferation of Huh7 cells measured by CCK-8. (b) The apoptosis level of Huh7 cell observed by flow cytometry assay. (c) The invasion of Huh7 cells observed by transwell assay (scale bar = 50 μm). $^{**}P < 0.05$.

strategy for cancer treatment [17, 18]. Hence, the regulation of miRNAs in cancer has been increasingly appreciated [19]. This study determined that miR-466 was significantly downregulated in the HCC tissues and cell lines. MiRNAs contribute to affect the metabolism, resistance, and some other behaviors of tumor cells [20]. The downregulated miR-466 has been found in several cancers, and it plays an inhibitor role to suppress the proliferation and invasion of

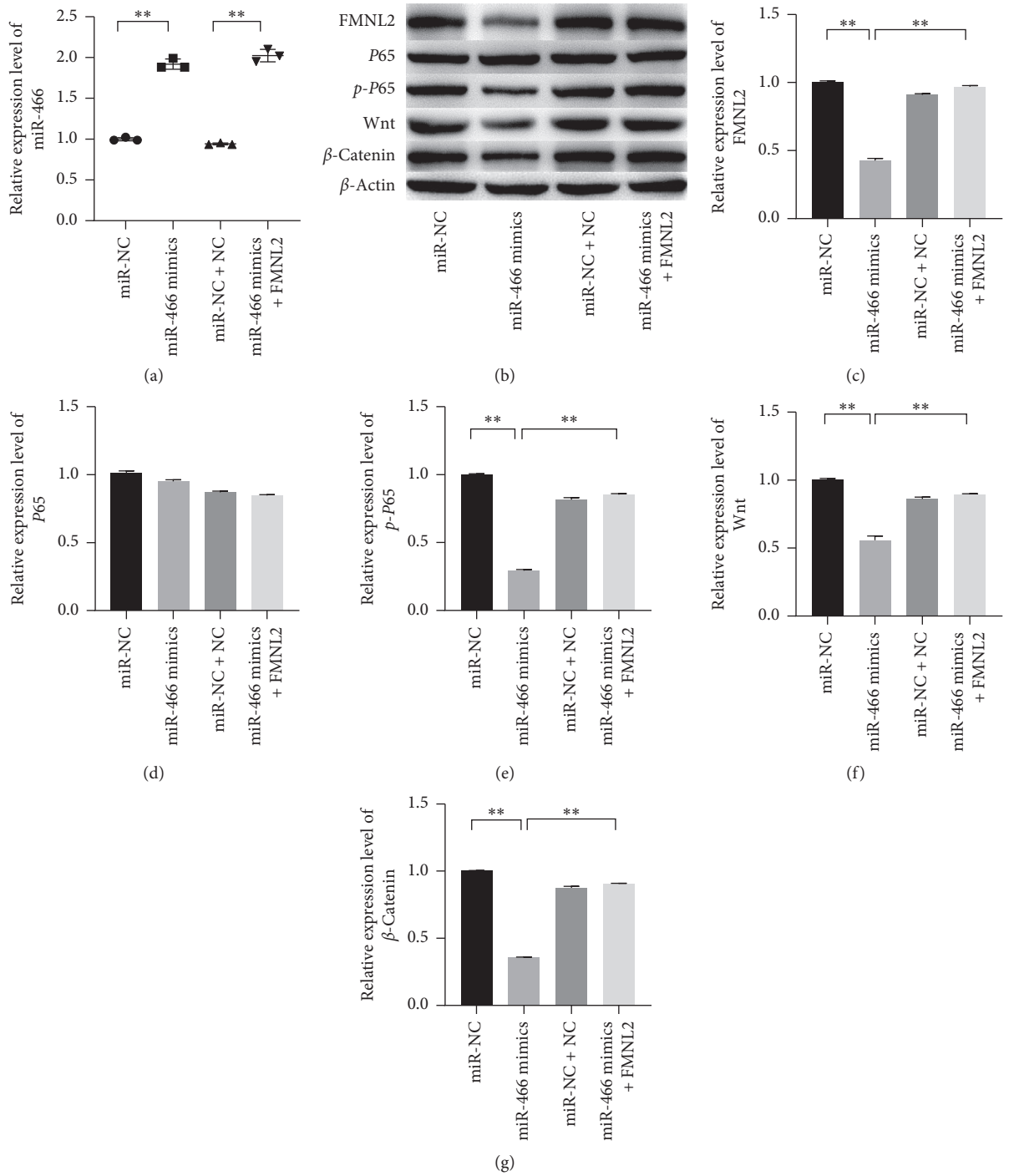

Figure 5: FMNL2 could reverse the effects of miR-466 on NF-κB and Wnt/β-catenin pathways in Huh7 cells. (a) The relative expression level of miR-466 tested by qRT-PCR. (b–g) The relative expression levels of FMNL2, *P*65, *p-P*65, Wnt, and β-catenin measured by Western blot. $^{**}P < 0.05$.

some tumors [21]. In this study, it was also found that miR-466 upregulation was adverse to the proliferation, invasion, and survival of HCC cells.

The consideration has been given in the character of miRNAs on regulating protein expression via interacting with the related mRNAs in this study. It was found that formin-like protein 2 (FMNL2) was a downstream factor of miR-466, and increased FMNL2 was also observed in HCC tissues and cell lines. FMNL2 is closely related to the formation and development of many tumors, and the carcinogenicity of FMNL2 has been corroborated by several studies. The study has pointed out that FMNL2 is significantly upregulated in colorectal cancer, and FMNL2 silence induced by miR-206 upregulation can visibly inhibit the proliferation and invasion of the tumor cells [22]. In this study, it was testified that increased FMNL2 could also

reverse the inhibitory effects of miR-466 on the proliferation, invasion, and survival of the HCC cells.

Molecular mechanisms underlying the growth, invasion, and chemotherapy resistance of HCC have been intensively studied. The aberrant activation of cellular signaling pathways plays a vital role in the deterioration of many types of cancer [23]. One study has indicated that miR-466 is sponged by LINC01152, and its downregulation is related to the dysfunction of the Notch pathway, and miR-466 downregulation indicates the poor prognosis and survival of the patients with glioblastoma multiform [24]. In this study, it was demonstrated that miR-466 upregulation could effectively inactivate the NF-κB and Wnt/β-catenin pathways. Aberrant NF-κB and Wnt/β-catenin and their downstream factors are widely implicated in numerous malignancies including HCC. A previous study has confirmed that the activated NF-κB induced by casein kinase II subunit beta (CSNK2B) upregulation can promote the unlimited growth and invasion of HCC [25]. This study discovered that miR-466 upregulation is an independent factor to mediate the inactivation of NF-κB and Wnt/β-catenin pathways. Moreover, the results also supported that the effects of miR-466 on NF-κB and Wnt/β-catenin pathways could be reversed by FMNL2. Yang et al. observed that FMNL2 was significantly upregulated in colorectal cancer cells, and it could further regulate the activation of NF-κB and mediate the invasion of the cancer cells via decreasing the stability of COMMD10 [26]. Moreover, one study has also indicated that FMNL2 could activate the Wnt/β-catenin to drive the progression of colorectal cancer [27]. Thus, those observations suggest that increased miR-466 can effectively inactivate the NF-κB and Wnt/β-catenin pathways of HCC cells via targeting FMNL2.

This study has revealed the role of miR-466 in the progression of HCC and confirmed the regulation effects of miR-466/FMNL2 on NF-κB and Wnt/β-catenin pathways. In summary, it suggests that miR-466 inactivates NF-κB and Wnt/β-catenin pathways to inhibit the progression of HCC via targeting FMNL2. However, whether the change of the FMNL2 level is an independent cause of miR-466 on regulating the phenotype and the signal pathways of HCC cells remains unknown. Therefore, more evidence is necessary from the experiments in vivo to corroborate the presumption in this study.

Data Availability

The data used to support the findings of this study are available from the corresponding author upon request.

Conflicts of Interest

The authors declare that they have no conflicts of interest.

References

[1] Z. Gong, J. Yu, S. Yang, P. B. S. Lai, and G. G. Chen, "FOX transcription factor family in hepatocellular carcinoma," *Biochimica et Biophysica Acta—Reviews on Cancer*, vol. 1874, no. 1, Article ID 188376, 2020.

[2] J. Chen, J. A. Gingold, and X. Su, "Immunomodulatory TGF-β signaling in hepatocellular carcinoma," *Trends in Molecular Medicine*, vol. 25, no. 11, pp. 1010–1023, 2019.

[3] L. Trevisan França de Lima, D. Broszczak, X. Zhang, K. Bridle, D. Crawford, and C. Punyadeera, "The use of minimally invasive biomarkers for the diagnosis and prognosis of hepatocellular carcinoma," *Biochimica et Biophysica Acta—Reviews on Cancer*, vol. 1874, no. 2, Article ID 188451, 2020.

[4] B. Hu, J. Z. Lin, X. B. Yang, and X. T. Sang, "Aberrant lipid metabolism in hepatocellular carcinoma cells as well as immune microenvironment: a review," *Cell Proliferation*, vol. 53, no. 3, Article ID e12772, 2020.

[5] S. M. Akula, S. L. Abrams, L. S. Steelman et al., "RAS/RAF/MEK/ERK, PI3K/PTEN/AKT/mTORC1 and TP53 pathways and regulatory miRs as therapeutic targets in hepatocellular carcinoma," *Expert Opinion on Therapeutic Targets*, vol. 23, no. 11, pp. 915–929, 2019.

[6] M. Pinter and M. Peck-Radosavljevic, "Review article: systemic treatment of hepatocellular carcinoma," *Alimentary Pharmacology Therapeutics*, vol. 48, no. 6, pp. 598–609, 2018.

[7] F. Zhou, W. Shang, X. Yu, and J. Tian, "Glypican-3: a promising biomarker for hepatocellular carcinoma diagnosis and treatment," *Medicinal Research Reviews*, vol. 38, no. 2, pp. 741–767, 2018.

[8] M. Abudoureyimu, H. Zhou, Y. Zhi et al., "Recent progress in the emerging role of exosome in hepatocellular carcinoma," *Cell Proliferation*, vol. 52, no. 2, Article ID e12541, 2019.

[9] M. Yang, H. C. Woolfenden, Y. Zhang et al., "Intact RNA structurome reveals mRNA structure-mediated regulation of miRNA cleavage in vivo," *Nucleic Acids Research*, vol. 48, no. 15, pp. 8767–8781, 2020.

[10] Q. Su and X. Lv, "Revealing new landscape of cardiovascular disease through circular RNA-miRNA-mRNA axis," *Genomics*, vol. 112, no. 2, pp. 1680–1685, 2020.

[11] K. A. Garbett, A. Vereczkei, S. Kálmán et al., "Coordinated messenger RNA/microRNA changes in fibroblasts of patients with major depression," *Biological Psychiatry*, vol. 77, no. 3, pp. 256–265, 2015.

[12] Y. J. Xu, Z. Zheng, C. Cao, J. Li, and Y. Liu, "Bioanalytical insights into the association between eicosanoids and pathogenesis of hepatocellular carcinoma," *Cancer and Metastasis Reviews*, vol. 37, no. 2-3, pp. 269–277, 2018.

[13] L. Tong, Y. Wang, Y. Ao, and X. Sun, "CREB1 induced lncRNA HAS2-AS1 promotes epithelial ovarian cancer proliferation and invasion via the miR-466/RUNX2 axis," *Biomedicine & Pharmacotherapy*, vol. 115, Article ID 108891, 2019.

[14] F. Tong, Y. Ying, H. Pan, W. Zhao, H. Li, and X. Zhan, "MicroRNA-466 (miR-466) functions as a tumor suppressor and prognostic factor in colorectal cancer (CRC)," *Bosnian Journal of Basic Medical Sciences*, vol. 18, no. 3, pp. 252–259, 2018.

[15] A. G. Singal, J. K. Lim, and F. Kanwal, "AGA clinical practice update on interaction between oral direct-acting antivirals for chronic hepatitis C infection and hepatocellular carcinoma: expert review," *Gastroenterology*, vol. 156, no. 8, pp. 2149–2157, 2019.

[16] Z. Zhihua, W. Weiwei, N. Lihua, Z. Jianying, and G. Jiang, "*p*53-induced long non-coding RNA PGM5-AS1 inhibits the progression of esophageal squamous cell carcinoma through regulating miR-466/PTEN axis," *IUBMB Life*, vol. 71, no. 10, pp. 1492–1502, 2019.

[17] Z. Yin, H. Ding, E. He, J. Chen, and M. Li, "Up-regulation of microRNA-491-5*p* suppresses cell proliferation and promotes apoptosis by targeting FOXP4 in human osteosarcoma," *Cell Proliferation*, vol. 50, no. 1, Article ID e12308, 2017.

[18] R. Martínez-Hernández, A. Serrano-Somavilla, A. Ramos-Leví et al., "Integrated miRNA and mRNA expression profiling identifies novel targets and pathological mechanisms in autoimmune thyroid diseases," *EBioMedicine*, vol. 50, pp. 329–342, 2019.

[19] N. S. Gandhi, R. K. Tekade, and M. B. Chougule, "Nanocarrier mediated delivery of siRNA/miRNA in combination with chemotherapeutic agents for cancer therapy: current progress and advances," *Journal of Controlled Release*, vol. 194, pp. 238–256, 2014.

[20] P. Vychytilova-Faltejskova and O. Slaby, "MicroRNA-215: from biology to theranostic applications," *Molecular Aspects of Medicine*, vol. 70, pp. 72–89, 2019.

[21] Q. Wu, J. Ma, J. Wei, W. Meng, Y. Wang, and M. Shi, "FOXD1-AS1 regulates FOXD1 translation and promotes gastric cancer progression and chemoresistance by activating the PI3K/AKT/mTOR pathway," *Molecular Oncology*, vol. 15, no. 1, pp. 299–316, 2021.

[22] H. J. Shao, Q. Li, T. Shi, G. Z. Zhang, and F. Shao, "LINC00707 promotes cell proliferation and invasion of colorectal cancer via miR-206/FMNL2 axis," *European Review for Medical and Pharmacological Sciences*, vol. 23, no. 9, pp. 3749–3759, 2019.

[23] M. Colden, A. A. Dar, S. Saini et al., "MicroRNA-466 inhibits tumor growth and bone metastasis in prostate cancer by direct regulation of osteogenic transcription factor RUNX2," *Cell Death and Disease*, vol. 8, no. 1, Article ID e2572, 2017.

[24] J. Wu, N. Wang, Y. Yang et al., "LINC01152 upregulates MAML2 expression to modulate the progression of glioblastoma multiforme via notch signaling pathway," *Cell Death and Disease*, vol. 12, no. 1, p. 115, 2021.

[25] Y. Xiao, S. Huang, F. Qiu et al., "Tumor necrosis factor *α*-induced protein 1 as a novel tumor suppressor through selective downregulation of CSNK2B blocks nuclear factor-*κ*B activation in hepatocellular carcinoma," *EBioMedicine*, vol. 51, Article ID 102603, 2020.

[26] S. S. Yang, X. M. Li, M. Yang et al., "FMNL2 destabilises COMMD10 to activate NF-*κ*B pathway in invasion and metastasis of colorectal cancer," *British Journal of Cancer*, vol. 117, no. 8, pp. 1164–1175, 2017.

[27] L. Shi, J. W. Huo, S. S. Chen et al., "MicroRNA-22 targets FMNL2 to inhibit melanoma progression via the regulation of the Wnt/*β*-catenin signaling pathway and epithelial-mesenchymal transition," *European Review for Medical and Pharmacological Sciences*, vol. 23, no. 12, pp. 5332–5342, 2019.

Hindawi
Journal of Oncology
Volume 2021, Article ID 3874478, 10 pages
https://doi.org/10.1155/2021/3874478

Research Article

Exosomes miR-22-3p Derived from Mesenchymal Stem Cells Suppress Colorectal Cancer Cell Proliferation and Invasion by Regulating RAP2B and PI3K/AKT Pathway

Yan Wang[1] **and Changkun Lin**[2]

[1]*Departmeng of Gastroenterology, Shengjing Hospital of China Medical University, Shenyang 110004, China*
[2]*College of Basic Medical Science, China Medical University, Shenyang 110122, China*

Correspondence should be addressed to Yan Wang; wangyan_cmusj@163.com

Received 18 May 2021; Accepted 2 June 2021; Published 21 June 2021

Academic Editor: Alamgeer Yuchi

Objective. Exosomes (exo) which contain proteins, microRNAs (miRNAs), and other bioactive substances can participate in intercellular signal transduction and material transport. Bone marrow mesenchymal stem cells (BMSCs) have a strong ability to produce exosomes. The purpose of this study was to observe the effect of hBMSCs-derived-exo miR-22-3p on proliferation and invasion of colorectal cancer (CRC) cells and to explore its mechanism. *Methods*. miR-22-3p and RAS oncogene family (RAP2B) expression was detected using qRT-PCR or Western blotting. Their interaction was confirmed by dual luciferase activity assay. Effects of miR-22-3p on cell proliferation and invasion were evaluated by CCK-8 and Transwell assay, respectively. Exosomes were extracted by the ultracentrifugation and identified through electron microscopy and Western blotting. *Results*. In CRC tissues and cells, downregulation of miR-22-3p and upregulation of RAP2B were observed. According to the analysis of dual luciferase activity, RAP2B was a target gene of miR-22-3p. In addition, miR-22-3p obviously repressed the cells proliferation and invasion via mediating RAP2B/PI3K/AKT pathway. Coculture experiments indicated that miR-22-3p derived from hBMSCs-exo had inhibition effects on SW480 cell proliferation and invasion. *Conclusions*. Collectively, miR-22-3p from hBMSCs-exo might impede CRC progression, which emphasized the potential of hBMSCs-exo-miR-22-3p as CRC treatment in the future.

1. Introduction

Colorectal cancer (CRC) is one of the common malignant tumors of the digestive tract with higher global morbidity and mortality [1]. With the changes in the diet structure of the Chinese people, the incidence of CRC has been increasing, and it has become a major tumor that threatens the health of our population [2]. Because of the relatively insidious onset and the atypical early symptoms of CRC, most patients are in the advanced stage of clinical diagnosis and miss the best opportunity for treatment [3]. Although the existing diagnosis and treatment methods have continued to be improved, the overall prognosis and the 5-year survival rate of the patient are still poor [4]. CRC is a complex process involving many factors and many steps, and an in-depth discussion of its pathogenesis has great significance for the early diagnosis and treatment of CRC patients [5].

Exosomes are vesicles with a size of 30–200 nm derived from the cell membrane of normal or cancerous cells and released into various body fluids, such as functional extracellular fluids (blood, lymph fluid, tissue fluid, etc.), urine, breast milk, saliva, and bile [6]. These vesicles can be transferred from the donor to the recipient cells and play a key role in intercellular communication [7]. The contents of exosomes have different components, such as DNA, RNA, lipids, and proteins, which can reflect the metabolism, cancerization, and apoptosis of cells to some extent [8]. Among them, miRNAs are the most studied exosomes-mediated small biomolecules. As a type of single-stranded noncoding RNA with a length of 18 to 25 nucleotides, miRNAs participate in different processes of malignant tumors, such as cancer cells proliferation, angiogenesis, and tumor metastasis [9]. Additionally, lots of researches reported that miRNAs regulated the progression of CRC and

cell proliferation, invasion, and metastasis by regulating specific target genes expression [10]. miR-22-3p, as a tumor suppressor, has been reported to repress HCC cell proliferation through downregulating the target gene Spl [11]. Moreover, miR-22-3p may inhibit NSCLC cell proliferation via targeting AEG-1 [12]. However, there are few studies on the role of miR-22-3p in CRC.

Mesenchymal stem cells (MSCs) with immunosuppressive, immunomodulatory, and therapeutic properties are the cells with the strongest ability to secrete exosomes, and MSC-exosomes have many biological functions similar to MSCs [13]. BMSCs, which have immunogenicity, high portability, and multidirectional differentiation ability, are an example of the most widely studied MSCs [14]. hBMSCs act as regulators of apoptosis, angiogenesis, and immune tolerance in tumors [15]. They have significant tumor localization and immune specificity and can be used as a carrier to deliver antitumor drugs to the tumor microenvironment [16]. In recent years, increasing researches were focused on the function of miRNAs derived from BMSCs exosome in various cancers progression, including CRC. For example, miR-16-5p derived from BMSCs-exosomes repressed CRC cell biological function via ITGA2 [17]. Meanwhile, Chen et al. found that BMSCs-derived exosome miR-4461 impeded CRC tumorigenesis through inhibiting the expression of COPB2 [18]. On the basis of previous researches, we supposed that hBMSCs-derived exosomes miR-22-3p might be concerned with CRC progression. Herein, we conducted this study to verify the above hypothesis and explore the potential mechanism.

2. Materials and Methods

2.1. Tissue Specimens. 36 pairs of CRC tissues (identified by pathological diagnosis) and matched adjacent tissue samples were obtained from Shengjing Hospital of China Medical University from August 2018 to June 2019. All patients received no radiotherapy or chemotherapy before treatment and had no history of other malignant tumors. All tissue samples were immediately snap-frozen using liquid nitrogen and preserved in −80°C for experiments. All patients provided written informed consent and the study was approved by the ethics committee of Shengjing Hospital of China Medical University.

2.2. Cell Culture. NCM460 cells (human normal colon mucosal epithelial cell line), human CRC cell lines (HT-29, SW620, HCT-116, SW480, and LoVo), and hBMSCs were purchased from American Type Culture Collection (MD, USA). hBMSCs were cultured in DMEM/F12 (supplemented with 10% fetal bovine serum (FBS, Gibco, USA)) and 1% penicillin-streptomycin) medium (Gibco, USA). Exosomes were removed from FBS by ultracentrifugation. The resuspended hBMSCs were placed in a humid environment at 37°C and 5% CO_2. When the adherent hBMSCs reached 80% confluence, the supernatant was collected and expanded to obtain hBMSCs. All the other cells were cultured in DMEM containing 10% FBS at 37°C in an incubator with 5% CO_2.

2.3. Transfection. Plasmids for SW480 cells transfection containing miR-22-3p mimic and inhibitor and their control (miR-NC and anti-NC), RAP2B overexpression vector pcDNA3.1-RAP2B (pc-RAP2B), and pcDNA3.1 empty vector (pc-NC) were obtained from Shanghai GenePharma in China. hBMSCs at passages 2-3 were transfected with miR-NC, anti-NC, and miR-22-3p mimic and inhibitor, respectively. All transfections were conducted by Lipofectamine 2000 (Invitrogen, USA). The exosomes isolated from transfected hBMSCs (exo-miR-NC, exo-anti-NC, exo-mimic, and exo-inhibitor) were cocultured with SW480 cells for 48 h, respectively.

2.4. Isolation of hBMSCs Exosomes. Transfected hBMSCs were inoculated into a culture flask with 5×10^6 cells/75 cm^2, and 10 ml serum-free medium was added. After 3 days of culture, serum-free medium was collected and centrifuged at 10,000 r/min for 30 minutes to remove cell residues and impurities, and the supernatant was aspirated. Then we added exosome extraction reagent to supernatant and mixed thoroughly to incubate at 4°C overnight. The precipitate obtained by centrifugation is exosome. The precipitate was resuspended in PBS and stored at −20°C. Finally, we observed and photographed with a transmission electron microscope and detected its antigen expression by Western bolt.

2.5. Cell Proliferation Assays. Cells of each group were seeded in 96-well plates with 2×10^4/well and cultured at 37°C with 5% CO_2. At 24, 48, 72, and 96 h of culture, 10 μl of CCK-8 solution (Sigma, USA) was added to each well and it was incubated for 2 h. Finally, a spectrophotometer was used to measure the absorbance at 450 nm.

2.6. Transwell Invasion Assay. 500 μl of RPMI 1640 culture medium containing 10% FBS was added to the lower chamber coated with Matrigel (Corning, USA), and 200 μl of serum-free cell suspension (2.5×10^5 cells/ml) was added to the upper chamber. Transwell chamber was cultured at 37°C, 5% CO_2 for 24 h. Then, cells were fixed with 4% paraformaldehyde solution for 20 min, washed with PBS, and stained with 0.1% crystal violet. We observed the cells under Olympus inverted fluorescence microscope and counted the number of cells passing through Matrigel polymer gel and cell microporous membrane.

2.7. Dual Luciferase Activity Assay. Bioinformatics prediction software TargetScan is used to predict the target genes of miR-22-3p. RAP2B was selected as the research object. In order to further verify the targeting relationship between miR-22-3p and RAP2B, 3'-UTR luciferase reporter vectors of wild-type RAP2B (RAP2B-wt) and mutant RAP2B (RAP2B-mut) were constructed and cotransfected with miR-22-3p mimic, respectively. The dual luciferase detection kit (Promega, USA) was used to detect the dual luciferase activity.

2.8. Quantitative Real-Time PCR. Total RNA was extracted by TRIzol reagent (Invitrogen, USA). According to the reverse transcription kit (TaKaRa, Japan) instructions, reverse transcription reaction was performed to synthesize cDNA strands, and SYBR green (TaKaRa, Japan) was added for qRT-PCR amplification on ABI 7500 System (ABI, USA). U6 or GAPDH was used as internal reference, and the relative expression of RNAs was calculated by the $2^{-\Delta\Delta Ct}$ method. Primers are listed in Table 1.

2.9. Western Blot. RIPA lysate was used to extract the total protein from cells, and the protein concentration was determined by BCA method. 30 μg protein was subjected to 10% SDS-PAGE. After protein separation, it was transferred to PVDF membranes. The transformed membrane was blocked with 5% skimmed milk. Then membranes were incubated with rabbit anti-CD9 (1 : 2000 dilution), rabbit anti-CD63(1 : 2000 dilution), rabbit anti-Hsp70 (1 : 2000 dilution), rabbit anti-RAP2B (1 : 1500), rabbit anti-PI3K (1 : 1500), rabbit anti-AKT (1 : 1500), rabbit anti-p-AKT (1 : 1500), and mouse anti-GAPDH (1 : 10,000 dilution) (Cambridge, USA) at 4°C overnight. After washing the membrane, incubation of HRP-labeled goat anti-rabbit or mouse secondary antibody (1 : 5000 dilution) was performed for 1 h at room temperature. Enhanced chemiluminescence (ECL) was used for development of the protein bands, and images were collected in the gel imaging system.

2.10. Statistical Analysis. GraphPad Prism v6.0 (GraphPad Software Inc, CA) software was used to do statistical analysis. Data in this study were expressed as mean ± standard deviation (SD). The *t*-test was used for comparison between two groups, and the one-way analysis of variance was used for comparison between multiple groups. The difference was statistically significant at $P < 0.05$.

3. Results

3.1. miR-22-3p Expression in CRC. The expression level of miR-22-3p in CRC tissues was lower than that in adjacent tissue through qRT-PCR detection (Figure 1(a)). The detection of miR-22-3p in CRC cells showed that the expressions of five types of CRC cells (HT-29, SW620, HCT-116, SW480, and LoVo) were downregulated versus NCM460 cells (Figure 1(b)). Data suggested that miR-22-3p has poor expression in CRC. Herein, SW480 cells with the lowest expression in the above five cells were selected for further experimentation.

3.2. miR-22-3p Suppressed CRC Cell Proliferation and Invasion. To investigate whether miR-22-3p dysregulation affects biological behavior of CRC cells, we transfected miR-22-3p mimic or inhibitor into SW480 cells to interfere in its expression. Compared to NC groups (miR-NC or anti-NC), miR-22-3p expression was increased in cells transfected with miR-22-3p mimics, while it was decreased by miR-22-3p inhibitor (Figure 2(a)). The CCK-8 assay was used to detect the cell proliferation of SW480 cells in each group. Results suggested that increasing miR-22-3p expression could inhibit the growth of SW480 cells, and miR-22-3p inhibition could significantly promote SW480 cell proliferation (Figure 2(b)). Similarly, Transwell experiments of each group showed that the number of cell invasions in mimic group was lower than that of miR-NC group, but it was higher in inhibitor group than in anti-NC group (Figure 2(c)). The results indicated that cell proliferation and invasion ability of SW480 was markedly enhanced after miR-22-3p expression was inhibited, while miR-22-3p overexpression reduced SW480 cell proliferation and invasion ability.

Table 1: Primer sequences for real-time fluorescence quantification PCR.

Gene name	Primer sequences (5′-3′)
GAPDH	F ACGCTGCATGTGTCCTTAG R GAGCCTCTTATAGCTGTTTG
U6	F CTCGCTTCGGCAGCACA R AACGCTTCACGAATTTGCGT
miR-22-3p	F AAGCTGCCAGTTGAAGAACTGTA R GCTGTCAACGATACGCTACGTAAC
RAP2B	F CTGCCCCTTCATGGAGACA R TGCGAATAGCTCATCCACTGA

3.3. miR-22-3p Regulated RAP2B Expression. Considering the effect of miR-22-3p on the behavior of CRC cells, we further analyzed its possible target genes and potential regulatory mechanisms. According to TargetScan online software analysis, we found that RAP2B may be one of the important target genes regulated by miR-22-3p. miR-22-3p can complementarily bind to the 3' UTR region of RAP2B (Figure 3(a)). The detection of luciferase activity revealed that miR-22-3p overexpression obviously reduced luciferase activity in the RAP2B-wt group but had no significant effect on the RAP2B-mut group (Figure 3(b)). This showed that miR-22-3p could bind to RAP2B.

To confirm the regulatory relationship of miR-22-3p and RAP2B, we detected the expression of RAP2B in SW480 cells overexpressing or silencing miR-22-3p. QRT-PCR results showed that the expression level of RAP2B was significantly elevated in miR-22-3p inhibition cells but was reduced by miR-22-3p overexpression (Figure 3(c)). This indicated that miR-22-3p may play a negative role in regulating RAP2B. Furthermore, RAP2B was also upregulated in CRC tissues (Figure 3(d)). More importantly, there was a negative correlation between RAP2B and miR-22-3p expression in CRC tissues (Figure 3(e)), suggesting that miR-22-3p may affect the occurrence and development of CRC by regulating RAP2B.

3.4. miR-22-3p Modulated Cell Proliferation and Invasion via RAP2B. Moreover, to verify whether miR-22-3p inhibited cell proliferation and invasion by RAP2B, SW480 cells were cotransfected with pc-RAP2B or pc-NC and miR-22-3p mimic or miR-NC. RAP2B expression was enhanced by pc-

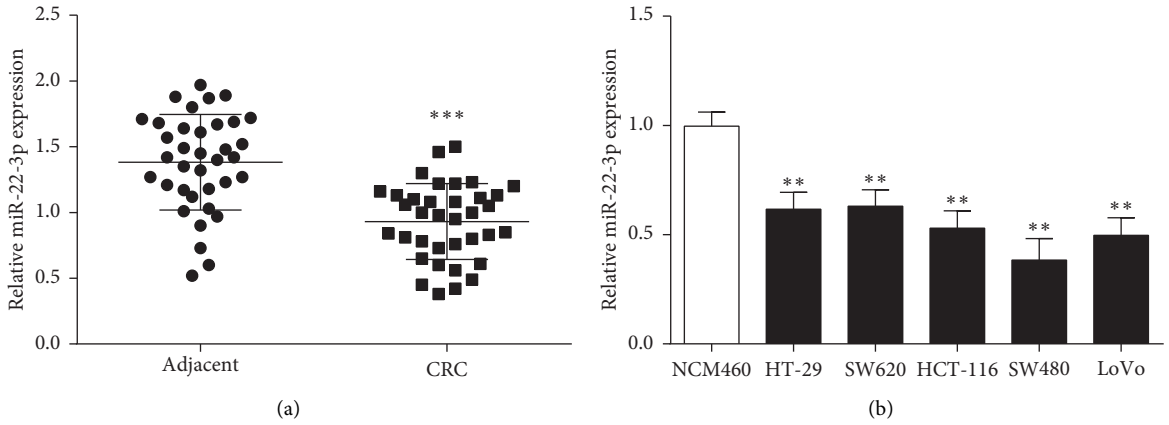

Figure 1: Expression of miR-22-3p was examined in CRC tissues and cells. (a) Expression of miR-22-3p was decreased in CRC tissues. (b) miR-22-3p expression in CRC cell lines. $^{**}P < 0.01$ and $^{***}P < 0.001$, compared with adjacent tissues or NCM460 group.

RAP2B, but enhancement was abolished by the cotransfection of pc-RAP2B and miR-22-3p inhibitor (Figures 4(a) and 4(b)). Additionally, PI3K and p-AKT protein levels were obviously increased in pc-RAP2B group, while this was reversed by miR-22-3p mimic cotransfection (Figure 4(b)); and there was no significant effect on AKT protein (Figure 4(b)). CCK-8 assay showed that miR-22-3p mimic abrogated the increasing cell proliferation caused by pc-RAP2B (Figure 4(c)). Additionally, miR-22-3p mimic also weakened the promotion of pc-RAP2B on cell invasion in SW480 cells (Figure 4(d)). To sum up, our data supported that miR-22-3p could contribute to CRC progression through RAP2B/PI3K/AKT pathway.

3.5. Identification of hBMSCs-Exosomes. Exosomes were extracted from the hBMSCs culture medium by the ultracentrifugation. The extracted exosomes were identified through electron microscopy and Western blot. The results suggested that the observation of morphologies under the transmission electron microscope showed a typical exosome structure, that is, a cup-shaped vesicle-like structure with a complete double-layer lipid membrane coating between 40 and 100 nm in diameter (Figure 5(a)). Western blot detection showed that exosome surface markers CD63, Hsp70, and CD9 were expressed higher in hBMSCs-exo than in hBMSCs (Figure 5(b)). The morphology and molecular level confirmed that the extracted vesicles were exosomes.

Subsequently, we detected miR-22-3p expression in hBMSCs and hBMSCs-exosomes. We found that miR-22-3p expression was enhanced in hBMSCs-exosomes (Figure 5(c)). To confirm whether hBMSCs-derived exosomes are rich in miR-22-3p, miR-22-3p expression was also measured in transfected hBMSCs. miR-22-3p was obviously upregulated in hBMSCs treated with miR-22-3p mimic, while it was downregulated in miR-22-3p inhibitor treatment hBMSCs (Figure 5(d)). In conclusion, exosomes derived from hBMSCs which were transfected with miR-22-3p mimics could effectively overexpress miR-22-3p, providing a good basis for subsequent experiment.

3.6. miR-22-3p from hBMSCs-Exosomes Inhibited Cell Proliferation and Invasion. To verify whether miR-22-3p from hBMSCs-exosomes regulate CRC cell biological function, CCK-8 and Transwell assays were conducted. Expression of miR-22-3p was markedly enhanced and RAP2B expression was notably reduced in SW480 cells treated with exo-mimic (Figures 6(a) and 6(b)). However, the opposite trend of miR-22-3p and RAP2B expression was observed in SW480 cells treated with exo-inhibitor (Figures 6(a) and 6(b)). Moreover, exo-mimic reduced RAP2B, PI3K, and p-AKT protein levels, all of which were opposite in exo-inhibitor group (Figure 6(c)). Besides, the cell proliferation and invasion of SW480 were observably decreased after exo-mimic treatment, while exo-inhibitor could notably promote SW480 cell proliferation and invasion (Figures 6(d) and 6(e)), suggesting that miR-22-3p derived from hBMSCs exosome repressed SW480 cell function.

4. Discussion

CRC is one of the most common malignant tumors in China, and its incidence and mortality have increased year by year [19]. CRC has high proliferative and antiapoptotic properties, and this is one of the main reasons for its poor prognosis [20, 21]. Although the progression of CRC is a multistage and multifactor participation process, gene mutations and epigenetic changes are still the decisive factors for starting and promoting the CRC progression [22]. Therefore, it has great significance to find effective diagnostic molecular biomarkers and therapeutic targets for CRC.

In recent years, more and more evidence indicated that MSCs play an important role in the development and metastasis of certain tumors and that paracrine factors secreted by them may participate in these reactions [23]. Exosomes, as paracrine factors, carry a large number of bioactive molecules and transfer their contents to adjacent tumor cells, thereby inducing phenotypic modification of the recipient cells [24, 25]. The research of the interaction between miRNAs from hBMSCs-exosomes and tumor has become a hot topic. Some functional RNAs can be transferred into tumor cells by exosomes and play roles in some

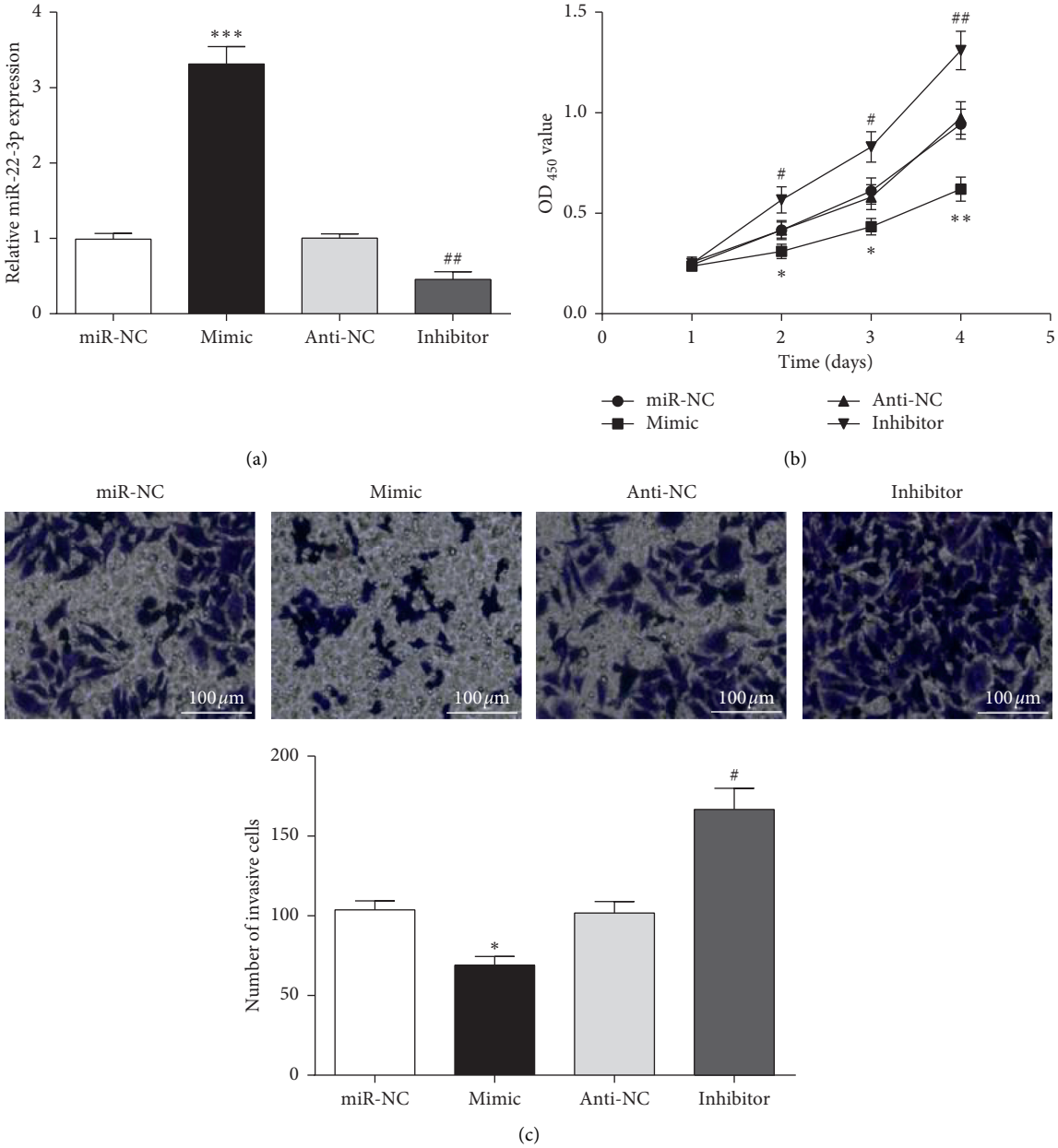

Figure 2: miR-22-3p regulated cell proliferation and invasion in CRC cells. (a) miR-22-3p expression in SW480 cells transfected with mimic or inhibitor. (b) Cell proliferation of SW480 cells after miR-22-3p knockdown or overexpression. (c) Cell invasion of SW480 cells after miR-22-3p knockdown or overexpression. $^{*}P < 0.05$, and $^{**}P < 0.01$, and $^{***}P < 0.001$, compared with miR-NC group; $^{\#}P < 0.05$ and $^{\#\#}P < 0.01$compared with anti-NC group.

physiological and pathological processes, including miRNAs [26]. Our current study explored the role of hBMSCs-exosome-miR-22-3p in CRC.

Currently, there are few studies on miR-22-3p in CRC, let alone its mechanism. Zhang et al. reported that miR-22 expression was reduced in CRC tissues, which was associated with liver metastasis and poor overall survival [27]. Sha et al. also found that miR-22-3p was downregulated in CRC and that LINC00858 could directly target it to regulate its target gene YWHAZ, thus promoting CRC progression [28]. Our results showed that the expression of miR-22-3p in CRC was decreased, which is in consistency with previous studies. In order to explore the mechanisms of miR-22-3p in CRC, RAP2B was predicted and confirmed as its target genes. Besides, RAP2B was upregulated and negatively correlated with miR-22-3p expression in CRC tissues. miR-22-3p overexpression inhibited the expression of RAP2B, suggesting that miR-22-3p targeted and negatively regulated RAP2B.

RAP2B located on 3q25.2 is an oncogene that is highly expressed in a variety of tumors and plays an important role in promoting biological processes (such as tumor cell proliferation, metastasis, etc.) [29, 30]. In this study, RAP2B overexpression notably promoted CRC cell proliferation and

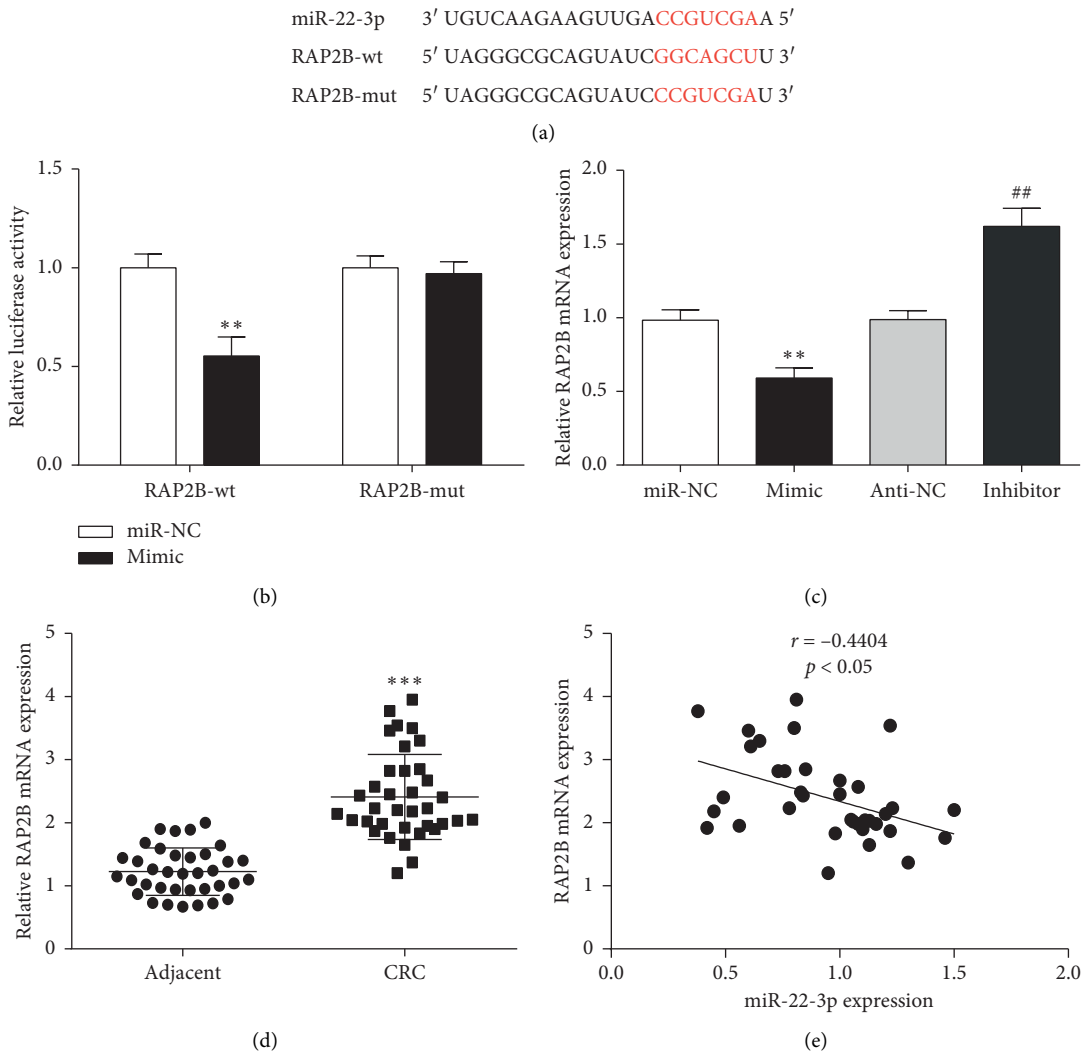

FIGURE 3: miR-22-3p directly targets RAP2B in CRC. (a) Predicted binding site between miR-22-3p and RAP2B. (b) The luciferase activity in SW480 cells. (c) RAP2B mRNA expression in SW480 cells after mimic or inhibitor transfection. (d) Expression of RAP2B in CRC tissue. (e) Correlation analysis between miR-22-3p and RAP2B in CRC tissues. $^{**}P < 0.01$ and $^{***}P < 0.001$, compared with miR-NC or adjacent group. $^{\#\#}P < 0.01$, compared with anti-NC group.

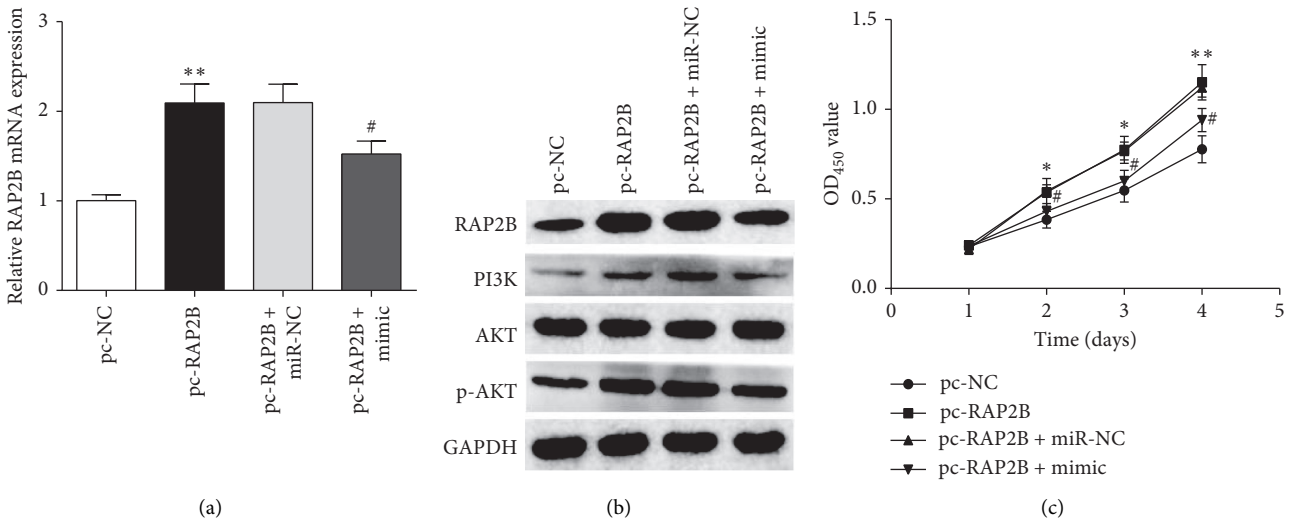

FIGURE 4: Continued.

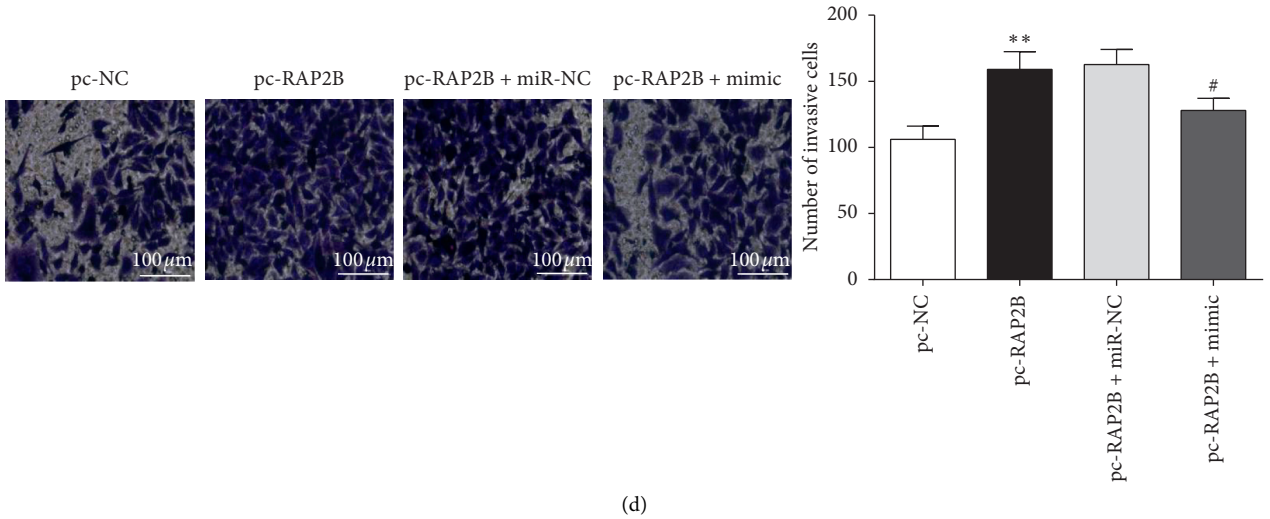

Figure 4: miR-22-3p could regulate SW480 cell proliferation and invasion through RAP2B. (a) RAP2B mRNA expression in SW480 cells after pc-PTEN and mimic cotransfection. (b) Protein levels of RAP2B, PI3K, AKT, and p-AKT in SW480 cells were determined by Western blot analysis. (c) Cell proliferation in SW480 cells cotransfected with miR-22-3p mimic and pc-RAP2B. (d) Cell invasion of SW480 cells cotransfected with miR-22-3p mimic and pc-RAP2B. $^{*}P < 0.05$, and $^{**}P < 0.01$ compared with pc-NC group; $^{\#}P < 0.05$ compared with pc-RAP2B + miR-NC group.

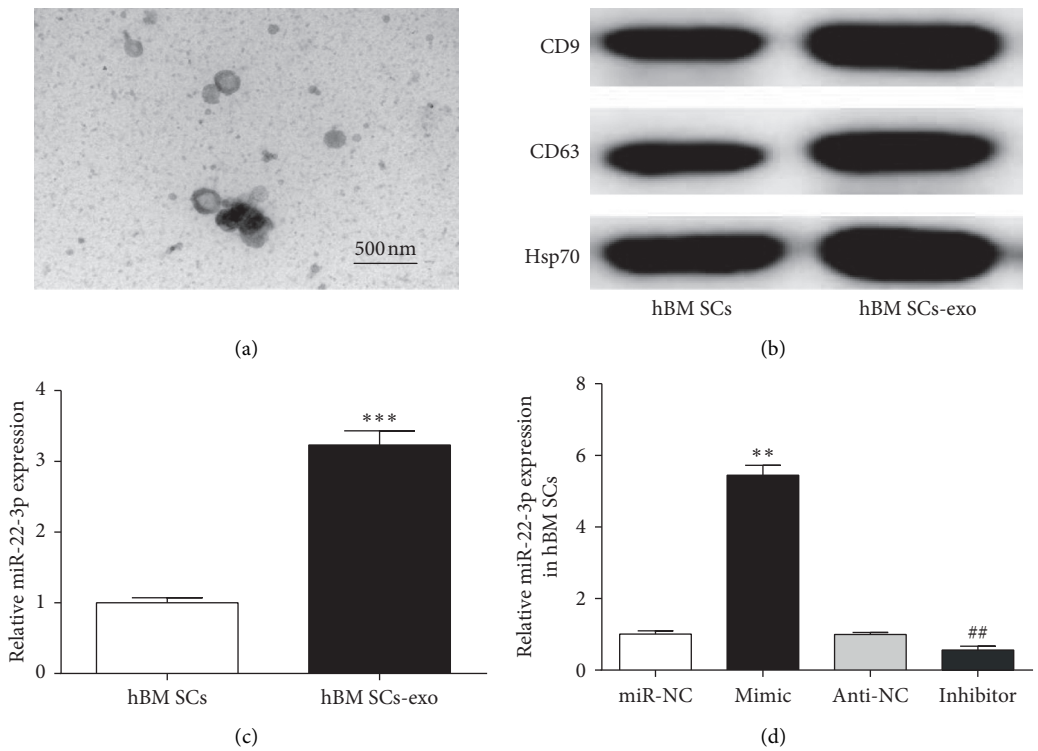

Figure 5: Identification of exosome sorted from hBMSCs. (a) The morphology of exosome was observed under transmission electron microscopy. (b) Surface markers (HSP70, CD63, and CD9) of hBMSCs-exosomes were detected by Western blot analysis. (c) miR-22-3p expression in hBMSCs and hBMSCs-exosomes. (d) miR-22-3p expression in hBMSCs treated with mimic or inhibitor. $^{**}P < 0.01$ and $^{***}P < 0.001$, compared with hBMSCs or miR-NC group; $^{\#\#}P < 0.01$, compared with anti-NC group.

invasion, and the facilitation was offset by miR-22-3p overexpression. Besides, PI3K and p-AKT protein levels were obviously increased by RAP2B overexpression, while this was reversed by miR-22-3p overexpression. Thus, we suggested that miR-22-3p overexpression repressed cell proliferation and invasion of CRC cells through RAP2B to inactive PI3K/AKT pathways.

Furthermore, we found that the exosomes derived from hBMSCs effectively expressed specific markers CD63, Hsp70, and CD9 and contained abundant miR-22-3p after

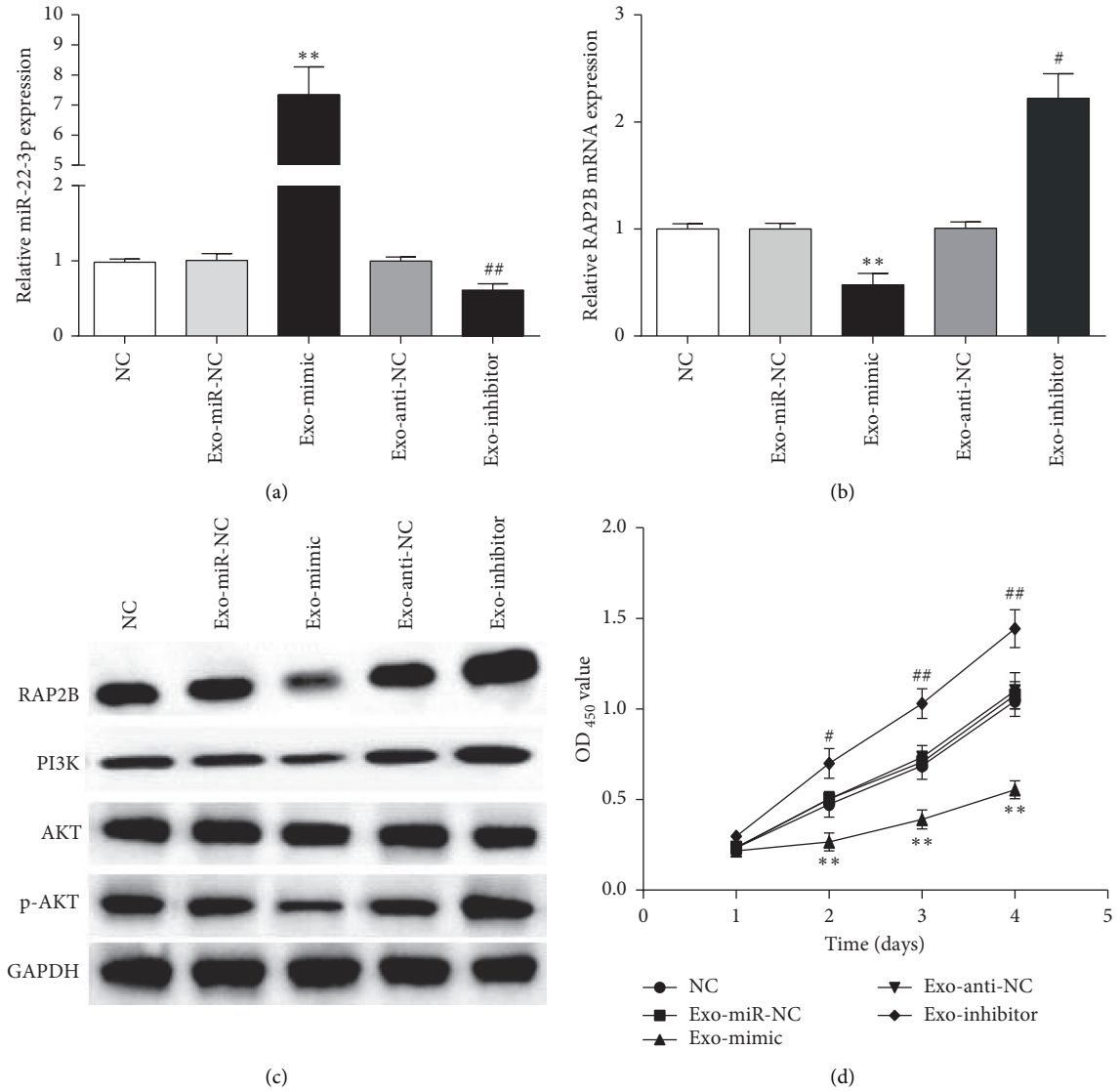

Figure 6: Continued.

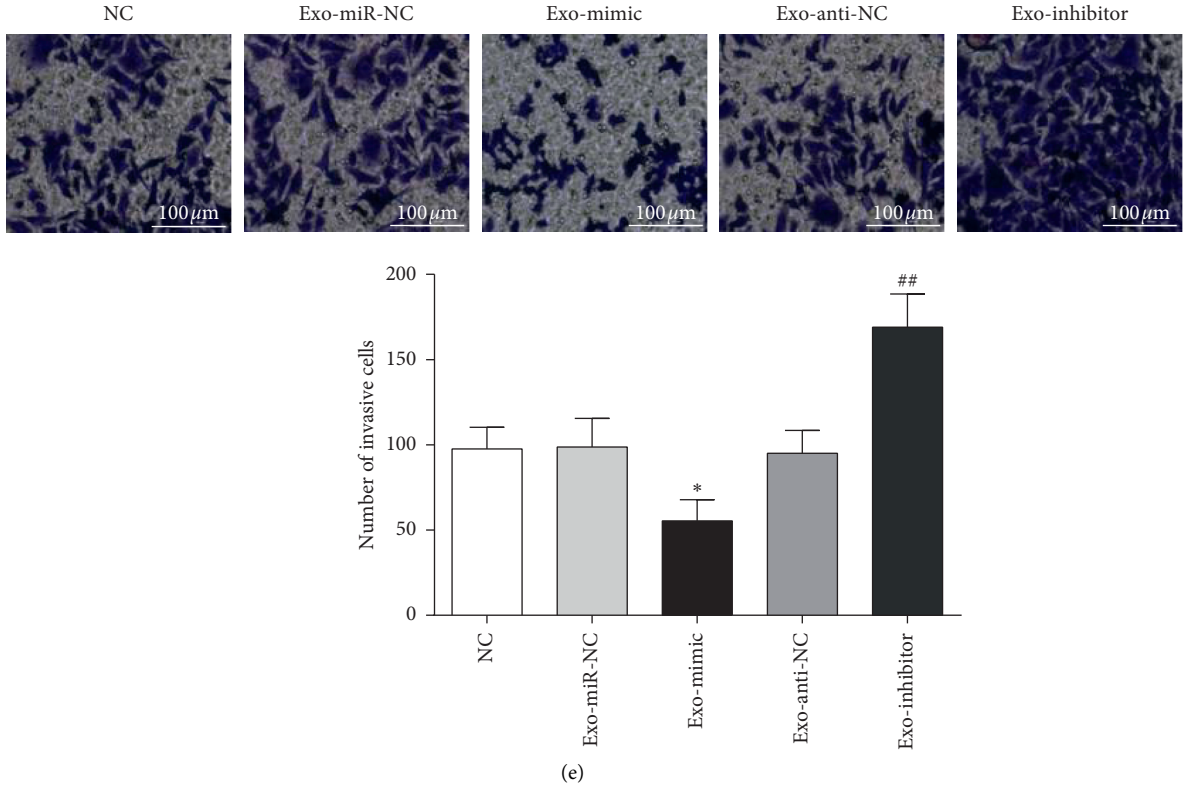

Figure 6: Exosomal miR-22-3p regulates SW480 cells proliferation and invasion via RAP2B. (a, b) miR-22-3p and RAP2B expression in SW480 cells. (c) Protein levels of RAP2B, PI3K, AKT, and p-AKT in SW480 cells. (d, e) SW480 cells proliferation and invasion were measured by CCK-8 and Transwell assays. $^{*}P < 0.05$ and $^{**}P < 0.01$, compared with exo-miR-NC group; $^{\#}P < 0.05$ and $^{\#\#}P < 0.01$, compared with exo-anti-NC group.

miR-22-3p mimic treatment. It was found that exosomes from hBMSCs treated by miR-22-3p mimic enhanced miR-22-3p and reduced RAP2B expression in CRC cells, while the opposite trend was observed for exosomes from hBMSCs treated with miR-22-3p inhibitor. Moreover, the cell proliferation and invasion ability of CRC cells were observably repressed by miR-22-3p derived from hBMSCs exosome. Besides, p-AKT protein level was also inhibited by hBMSCs-exosome-miR-22-3p. All of above results were similar to those in the transfection miR-22-3p mimic or inhibitor. The findings indicated that miR-22-3p carried by hBMSCs-exosome played a suppressor role of CRC via RAP2B/PI3K/AKT pathway.

Although our study verified that exosome-miR-22-3p exerted a suppressor role in CRC, some shortcomings still exist. If adequate clinical samples, in vivo animal experiments, and other potential target genes or signaling pathways (key protein expression level in pathway, especially in PI3K/AKT pathway) are added, the result could be more credible. Thus, there is still a need to conduct further clinical verification and experiments.

5. Conclusions

Collectively, we demonstrated that exosome-miR-22-3p derived from hBMSCs suppressed CRC cells proliferation and invasion via suppressing RAP2B expression to inhibit PI3K/AKT pathway, proposing that miR-22-3p might become a potential marker for early diagnosis and treatment of CRC patients.

Data Availability

The datasets used and/or analyzed during the present study are available from the corresponding author on reasonable request.

Conflicts of Interest

The authors declare that they have no conflicts of interest.

References

[1] R. L. Siegel, K. D. Miller, and A. Jemal, "Cancer statistics, 2019," *CA: A Cancer Journal for Clinicians*, vol. 69, no. 1, pp. 7–34, 2019.

[2] D. Wen, W. Zou, X. Wen et al., "Urban-rural disparity in colorectal cancer incidence and increasing trend in relation to socioeconomic development and urbanization in China," *Journal of International Medical Research*, vol. 46, no. 10, pp. 4181–4196, 2018.

[3] E. M. Corsini, K. G Mitchell, R. J. Mehran et al., "Colorectal cancer mutations are associated with survival and recurrence

after pulmonary metastasectomy," *Journal of Surgical Oncology*, vol. 120, no. 4, pp. 729–735, 2019.

[4] A. R. Marley and H. Nan, "Epidemiology of colorectal cancer," *International Journal of Molecular Epidemiology and Genetics*, vol. 7, no. 3, pp. 105–114, 2016.

[5] I. Mármol, C. Sánchez-de-Diego, A. Pradilla Dieste, E. Cerrada, and M. Rodriguez Yoldi, "Colorectal carcinoma: a general overview and future perspectives in colorectal cancer," *International Journal of Molecular Sciences*, vol. 18, no. 1, p. 197, 2017.

[6] D. M. Pegtel and S. J. Gould, "Exosomes," *Annual Review of Biochemistry*, vol. 88, no. 1, pp. 487–514, 2019.

[7] D. Song, D. Yang, C. A. Powell, and X. Wang, "Cell–cell communication: old mystery and new opportunity," *Cell Biology and Toxicology*, Springer, vol. 35, , 2019.

[8] S. Mousavi, R. Moallem, S. M. Hassanian et al., "Tumor-derived exosomes: potential biomarkers and therapeutic target in the treatment of colorectal cancer," *Journal of Cellular Physiology*, vol. 234, no. 8, pp. 12422–12432, 2019.

[9] A. Thind and C. Wilson, "Exosomal miRNAs as cancer biomarkers and therapeutic targets," *Journal of Extracellular Vesicles*, vol. 5, no. 1, Article ID 31292, 2016.

[10] N. Shirafkan, B. Mansoori, A. Mohammadi, N. Shomali, M. Ghasbi, and B. Baradaran, "MicroRNAs as novel biomarkers for colorectal cancer: new outlooks," *Biomedicine and Pharmacotherapy*, vol. 97, pp. 1319–1330, 2018.

[11] J. Chen, T. Bai, F. X. Wu et al., "miR-22-3p suppresses cell proliferation by regulating SP1 in hepatocellular carcinoma," *International Journal of Clinical and Experimental Pathology*, vol. 9, no. 5, pp. 5437–5444, 2016.

[12] Y. Chang et al., "MiR-22-3p suppresses cell proliferation by targeting AEG-1 in NSCLC," *The Journal of Practical Medicine*, vol. 33, no. 14, pp. 2267–2271, 2017.

[13] B. Yu, X. Zhang, and X. Li, "Exosomes derived from mesenchymal stem cells," *International Journal of Molecular Sciences*, vol. 15, no. 3, pp. 4142–4157, 2014.

[14] W. Yang and B. Ma, "A mini-review: the therapeutic potential of bone marrow mesenchymal stem cells and relevant signaling cascades," *Current Stem Cell Research and Therapy*, vol. 14, no. 3, pp. 214–218, 2019.

[15] P. Barcellos-de-Souza, V. Gori, F. Bambi, and P. Chiarugi, "Tumor microenvironment: bone marrow-mesenchymal stem cells as key players," *Biochimica et Biophysica Acta (BBA)—Reviews on Cancer*, vol. 1836, no. 2, pp. 321–335, 2013.

[16] S. A. Bergfeld and Y. A. DeClerck, "Bone marrow-derived mesenchymal stem cells and the tumor microenvironment," *Cancer and Metastasis Reviews*, vol. 29, no. 2, pp. 249–261, 2010.

[17] Y. Xu, L. Shen, F. Li, J. Yang, X. Wan, and M. Ouyang, "microRNA-16-5p-containing exosomes derived from bone marrow-derived mesenchymal stem cells inhibit proliferation, migration, and invasion, while promoting apoptosis of colorectal cancer cells by downregulating ITGA2," *Journal of Cellular Physiology*, vol. 234, no. 11, pp. 21380–21394, 2019.

[18] H.-L. Chen, J.-J. Li, F. Jiang, W.-J. Shi, and G.-Y. Chang, "MicroRNA-4461 derived from bone marrow mesenchymal stem cell exosomes inhibits tumorigenesis by downregulating COPB2 expression in colorectal cancer," *Bioscience, Biotechnology and Biochemistry*, vol. 84, no. 2, pp. 338–346, 2020.

[19] L. Shen, Q. Li, W. Wang et al., "Treatment patterns and direct medical costs of metastatic colorectal cancer patients: a retrospective study of electronic medical records from urban China," *Journal of Medical Economics*, vol. 23, pp. 456–463, 2020.

[20] Y. Jin, L. L. Yu, B. Zhang, C. F. Liu, and Y. Chen, "Circular RNA hsa_circ_0000523 regulates the proliferation and apoptosis of colorectal cancer cells as miRNA sponge," *Brazilian journal of medical and biological research = Revista brasileira de pesquisas medicas e biologicas*, vol. 51, no. 12, Article ID e7811, 2018.

[21] M. Huang, Z. Chen, D. Xu et al., "Adiponectin inhibits proliferation and induces apoptosis in colorectal cancer HCT116 cells," *Chinese Journal of Cellular and Molecular Immunology*, vol. 34, no. 3, pp. 253–259, 2018.

[22] S. N. Hong, "Genetic and epigenetic alterations of colorectal cancer," *Intestinal Research*, vol. 16, no. 3, p. 327, 2018.

[23] L. Zimmerlin, T. S. Park, E. T. Zambidis, V. S. Donnenberg, and A. D. Donnenberg, "Mesenchymal stem cell secretome and regenerative therapy after cancer," *Biochimie*, vol. 95, no. 12, pp. 2235–2245, 2013.

[24] H.-G. Zhang and W. E. Grizzle, "Exosomes and cancer: a newly described pathway of immune suppression," *Clinical Cancer Research*, vol. 17, no. 5, pp. 959–964, 2011.

[25] H.-G. Zhang and W. E. Grizzle, "Exosomes: a novel pathway of local and distant intercellular communication that facilitates the growth and metastasis of neoplastic lesions," *The American Journal of Pathology*, vol. 184, no. 1, pp. 28–41, 2014.

[26] M. Tomasetti, W. Lee, L. Santarelli, and J. Neuzil, "Exosome-derived microRNAs in cancer metabolism: possible implications in cancer diagnostics and therapy," *Experimental and Molecular Medicine*, vol. 49, no. 1, p. e285, 2017.

[27] G. Zhang, S. Xia, H. Tian, Z. Liu, and T. Zhou, "Clinical significance of miR-22 expression in patients with colorectal cancer," *Medical Oncology*, vol. 29, no. 5, pp. 3108–3112, 2012.

[28] Q.-K. Sha, L. Chen, J.-Z. Xi, and H. Song, "Long non-coding RNA LINC00858 promotes cells proliferation, migration and invasion by acting as a ceRNA of miR-22-3p in colorectal cancer," *Artificial Cells, Nanomedicine, and Biotechnology*, vol. 47, no. 1, pp. 1057–1066, 2019.

[29] L. Zhang, H.-b. Duan, and Y.-s. Yang, "Knockdown of Rap2B inhibits the proliferation and invasion in hepatocellular carcinoma cells," *Oncology Research Featuring Preclinical and Clinical Cancer Therapeutics*, vol. 25, no. 1, pp. 19–27, 2017.

[30] X. Zhang, Y. He, K.-H. Lee et al., "Rap2b, a novel p53 target, regulates p53-mediated pro-survival function," *Cell Cycle*, vol. 12, no. 8, pp. 1279–1291, 2013.

Hindawi
Journal of Oncology
Volume 2021, Article ID 9951010, 12 pages
https://doi.org/10.1155/2021/9951010

Research Article

Long Noncoding RNA WDFY3-AS2 Represses the Progression of Esophageal Cancer through miR-18a/PTEN Axis

Qingling Kong,[1] Guangcai Li,[2] Gang Yin,[3] Kun Li,[4] Dongqing Zhang,[5] and Weihao Xu[6]

[1]*Hospital Infection Control Office, Rizhao People's Hospital, Rizhao 276800, China*
[2]*China-Canada International Health Management Center, Rizhao Hospital of TCM, Rizhao 276800, China*
[3]*Department of Clinical Laboratory, Affiliated Qingdao Central Hospital, Qingdao University, Qingdao 266042, China*
[4]*Department of Anesthesia, Zhangqiu District People's Hospital, Jinan 250200, China*
[5]*Department of Public Health, Zhangqiu District People's Hospital, Jinan 250200, China*
[6]*Medical Laboratory Center, Yantai Yuhuangding Hospital, Yantai 264000, China*

Correspondence should be addressed to Weihao Xu; wogoumif61@163.com

Received 18 March 2021; Accepted 20 May 2021; Published 7 June 2021

Academic Editor: Alamgeer Yuchi

Background. Understanding the role of lncRNAs in the development of human malignancies is necessary for the targeted therapy of malignant tumors, including esophageal cancer (EC). Nevertheless, the specific role and regulatory mechanism of lncRNA WDFY3-AS2 in EC are still unclear. Here, we examined the functional role and regulatory mechanism of WDFY3-AS2 in EC. *Materials and Methods*. RT-qPCR assay was applied to measure the expression of WDFY3-AS2 and miR-18a in EC samples and cells. The luciferase reporter and RIP assays were used to check the relationship between WDFY3-AS2, miR-18a, and PTEN. Counting Clock Kit-8 (CCK-8) assay was carried out to detect cell viability, and transwell assays were used for measuring cell migration and invasion. *Results*. Underexpression of WDFY3-AS2 was found in EC specimens and cells, which predicted a poor prognosis of EC patients. Reexpression of WDFY3-AS2 repressed the progression of EC via inhibiting cell proliferation, migration, and invasion. Additionally, WDFY3-AS2 was negatively correlated with miR-18a and positively with PTEN. Furthermore, we discovered that the expression of PTEN decreased by miR-18a mimic was rescued by WDFY3-AS2 overexpression. *Conclusions*. WDFY3-AS2 modulates the expressional level of PTEN as a competitive endogenous RNA via sponging miR-18a in EC, which suggests that the WDFY3-AS2/miR-18a/PTEN pathway might be involved in the progression of EC.

1. Introduction

Esophageal cancer (EC) is a malignant tumor with rapid progression and poor prognosis and is one of the most fatal diseases worldwide [1]. EC-related risk factors include consumption of foods containing amines nitrite and fungal infection, as well as irritation from hot foods and drinks [2]. Although significant progress has been made in the treatment of EC, such as chemotherapy and surgical resection, the prognosis of EC patients is still poor, and the 5-year survival rate is low, only about 10% [3, 4]. Thus, it is essential to understand the pathogenesis of EC and discover the possible therapeutic targets for EC.

Long noncoding RNA (lncRNA) is a noncoding RNA that cannot encode proteins, and its length exceeds 200 base pairs [5]. Previous reports have discovered that LncRNAs play essential roles in the occurrence and development of EC [6]. In addition, there are enough pieces of evidence that dysregulation of lncRNAs that modulate cancer-related pathways could affect the progression of tumors, including EC [7]. For instance, ZNF750 was involved in ESCC progression and emphasized its significance as a biomarker for metastasis and prognosis [8]. Liang et al. discovered that lnc01980 acted as an oncogenic lncRNA in modulating ESCC proliferation, migration, and invasion [9]. Furthermore, Shen et al. verified that knockdown of AGAP2-AS1 showed suppressive effects on the migration and invasion of

EC through miR-195-5p/FOSL1 pathway [10]. LncRNA WDFY3-AS2 was first found to be increased in hepatocellular carcinoma [11]. Moreover, WDFY3-AS2 was decreased in triple-negative breast tumors and served as a potential prognostic factor in TNBC development [12]. Li et al. showed that overexpression of WDFY3-AS2 inhibited tumor growth, cell migration, and invasion [13]. To our knowledge, there are no reports on the role of WDFY3-AS2 in ESCC progression.

Previous literature demonstrated that miR-18a is significantly increased in hepatocellular cancer [14] and gliomas [15]. Also, miR-18a was reported to involve in nasopharyngeal carcinoma by suppressing SMG1 and activating the mTOR pathway [16]. Nair et al. displayed that miR-18a promoted the proliferative and migratory ability of ER-positive breast cancer cells via activating Wnt signaling [17]. In EC, miR-18a was highly expressed in plasma of EC patients [18]. However, there are few reports about the role of miR-18a in EC.

In the present study, we hypothesized that WDFY3-AS2 plays a critical role in regulating EC development with the implication of miR-18a and PTEN. Thus, we investigated the regulatory mechanism of WDFY3-AS2 in the regulation of EC cell proliferation, invasion, migration, and the relationships between WDFY3-AS2, miR-18a, and PTEN. Our findings may provide new insights into the role of lncRNA-miRNA-mRNA in EC.

2. Materials and Methods

2.1. Patients. Thirty-six EC tissue samples and the corresponding normal tissue samples were collected from EC patients at Rizhao People's Hospital, Rizhao, Shandong, China. None of EC patients received preoperative radiotherapy or chemotherapy before surgery. The tissue samples were stored at −80°C for further use. All patients provided written informed consent and the study was approved by the ethics committee of the Rizhao People's Hospital, Rizhao, Shandong, China (Approval no. 2018020078).

2.2. Cell Culture. Immortalized esophageal epithelial cell SHEE and human esophageal cancer cell lines (ECA109, YES2) were purchased from BeNa Culture Collection (Beijing, China). The cells were cultured in RPMI 1640 (Gibco, Invitrogen, Germany) medium containing 10% FBS at 37°C 5% CO_2. The complete medium was updated regularly every 2-3 days. When the degree of fusion reached 80%, the cells were separated and passaged as usual.

2.3. Cell Transfection. The siRNA for WDFY3-AS2 (si-WDFY3-AS2) or PTEN (si-PTEN) was used to knock down WDFY3-AS2 or PTEN. WDFY3-AS2 plasmid was subcloned into the pcDNA3.1 vector to overexpress WDFY3-AS2 (pcDNA3.1-WDFY3-AS2). MiR-18a mimic, miR-18a inhibitor, and corresponding negative controls (NC-mimic and NC-inhibitor) were purchased from GenePharma Company (Shanghai, China). The transfections were performed using by Lipofectamine 2000 reagent (Invitrogen) following the instructions of the manufacturer.

2.4. RNA Isolation and Quantitative Real-Time RT-PCR Assay. Total RNA was extracted using TRIzol kit (Invitrogen) following the instructions of the manufacturer. cDNA was generated by Transcriptor First Strand cDNA Synthesis Kit. GoTap®qPCRMaster Mix (Promega) was used to perform RT-PCR. GAPDH and U6 were employed as endogenous controls by using the $2^{-\Delta\Delta Ct}$ method.

2.5. Western Blot Analysis. RIPA lysis buffer was carried out to extract total proteins following the instructions of the manufacturer. BCA method was applied to determine the protein concentration. After electrophoresed on 10% SDS-PAGE gel and then transferred to PVDF membranes, the proteins were blocked with 5% skim milk, followed by the primary antibodies at 4°C overnight and secondary antibodies for 1 h at 37°C. Finally, an ECL detection reagent was used to visualize bands.

2.6. CCK-8 Assay. ECA109 cells were suspended in a culture medium containing 10% FBS and cultured for 24 h. Then, they were seeded in a 96-well plate with 1×10^3 per well. After incubation for 24, 48, 72, and 96 h, CCK-8 reagents were added and then incubated in a CO_2 incubator for 2 h. Finally, the optical density at 490 nm was measured.

2.7. Transwell Assays. 3×10^4 cells/well were added to the upper chamber with a serum-free medium. The lower chamber was fixed with a fresh medium supplement with 10% FBS. For migration assay, ECA109 cells were incubated at 37°C and 5% CO_2 for 24 h. The invasion test procedure was the same except that the upper chamber was coated with a matrix. After incubation for 48 h, the migration and invasion cells were stained with 0.1% crystal violet. Finally, a phase-contrast microscope was applied to observe EC cells.

2.8. RNA Immunoprecipitation (RIP) Assay. GFP antibody and the Magna RIP™ RNA Binding Protein Immunoprecipitation Kit were carried out to perform RNA immunoprecipitation (RIP) experiments following the manufacturer's instructions. The expressional levels of WDFY3-AS2 and miR-18a were measured by qRT-PCR assay. IgG was used as a negative control.

2.9. Luciferase Reporter Assay. The constructed pmirGLO-WDFY3-AS2-WT, pmirGLO-WDFY3-AS2-Mut, pmirGLO-PTEN-WT, or pmirGLO-PTEN-MuT with miR-18a mimic, miR-18a inhibitor, or negative control were cotransfected into ECA109 cells using lipofectamine 2000. After 48 h transfection, the firefly luciferase activity was measured with Dual-Luciferase Reporter Assay System.

2.10. Statistical Analysis. The data were shown as mean ± SD and analyzed using SPSS 19.0 or GraphPad Prism 8.0. The statistical differences were assessed by Student's *t*-test or one-way ANOVA. $P < 0.05$ was considered as statistically significant.

3. Results

3.1. Low Expression of WDFY3-AS2 in EC and Its Clinical Significance. We first investigated WDFY3-AS2 expression in EC tissue samples and cells by RT-qPCR. Downregulation of WDFY3-AS2 was found in EC tissue samples compared to corresponding normal tissue samples (Figure 1(a)). Moreover, the expression level of WDFY3-AS2 in EC cells was also higher than that in normal EC cells SHEE (Figure 1(b)). 36 EC patients were divided into a high expression group and a low expression group according to the average of WDFY3-AS2 expression. Results discovered that the higher expression of WDFY3-AS2, the higher the survival time of EC patients (Figure 1(c)). In addition, WDFY3-AS2 is closely associated with tumor grading and TNM stage (Table 1). All results indicate that WDFY3-AS2 is involved in the progress of EC.

3.2. Upregulation of WDFY3-AS2 Represses Proliferation, Migration, and Invasion of EC Cells. Next, we investigated the functional role of WDFY3-AS2 in EC cells. pcDNA3.1-WDFY3-AS2 and sh-WDFY3-AS2 vectors were adopted to overexpress and knockdown WDFY3-AS2 in ECA109 cells. As shown in Figure 2(a), WDFY3-AS2 expression was remarkably increased or decreased in ECA109 cells after overexpression or knockdown of WDFY3-AS2. Then, we detected the viability of EC cells by CCK-8 assay. The ECA109 cells transfected with pcDAN3.1-WDFY3-AS2 displayed significantly decreased cell viability compared to ECA109 cells transfected with pcDNA3.1-NC, while increased cell viability in ECA109 cells transfected with sh-WDFY3-AS2 (Figure 2(b)). Transwell migration and invasion assays displayed that overexpression of WDFY3-AS2 inhibited the migration and invasion of ECA109 cells, whereas knockdown of WDFY3-AS2 exerted the opposite effects (Figures 2(c) and 2(d)).

3.3. WDFY3-AS2 Acted as a Sponge for miR-18a in EC. To explore the molecular mechanism of WDFY3-AS2 in EC, bioinformatic analysis was first carried out to predict the possible binding site of WDFY3-AS2. miR-18a was obtained as the candidate miRNA, and the predicted binding site of miR-18a in WDFY3-AS2 is shown in Figure 3(a). Then, miR-18a was chosen for the subsequent investigations. Upregulation of WDFY3-AS2 decreased miR-18a expression and downregulation of WDFY3-AS2 increased the expression of miR-18a (Figure 3(b)). Afterwards, luciferase reporter assay and RIP assay were carried to verify the direct binding ability of miR-18a and WDFY3-AS2. The luciferase assay results displayed that the luciferase activity was inhibited or fortified by transfected with WDFY3-AS2-WT and miR-18a mimic or inhibitor (Figure 3(c)). However, there has no response to the alterations of miR-18a in WDFY3-AS2-Mut (Figure 3(d)). RIP assay showed that the expressions of WDFY3-AS2 and miR-18a were abundant in Ago2 groups versus IgG groups (Figure 3(e)). The results demonstrated that WDFY3-AS2 could directly bind to miR-18a in EC.

3.4. Overexpression of miR-18a Enhanced Proliferation, Migration, and Invasion of EC Cells. Next, we detected the expressional level of miR-18a in EC specimens and results found that miR-18a increased significantly in EC samples compared to the normal samples (Figure 4(a)). Considering the negative relationship between WDFY3-AS2 and miR-18a in EC tissues (Figure 4(b)), we investigated the functional role of miR-18a in EC proliferation, migration, and invasion. As shown in Figure 4(c), ECA109 cells transfected with miR-18a mimic displayed significantly increased cell viability compared to ECA109 cells transfected with NC-mimic, while decreased cell viability in ECA109 cells transfected with miR-18a inhibitor. Transwell migration and invasion assays displayed that overexpression of WDFY3-AS2 inhibited the migration and invasion of ECA109 cells, whereas knockdown of WDFY3-AS2 exerted the opposite effects (Figures 4(d) and 4(e)).

3.5. PTEN Served as the Target of miR-18a. TargetScan database was used to discover the target gene of miR-18a, and PTEN was screened as the candidate gene (Figure 5(a)). PTEN was reported to be highly expressed in diverse cancers as an oncogene [19, 20]. We then tested PTEN expression in EC tissue specimens. As shown in Figure 5(b), PTEN was significantly increased in EC tissues. Moreover, we found that miR-18a was negatively associated with PTEN in EC tissues (Figure 5(c)). Overexpression of miR-18a decreased the levels of PTEN in ECA109 cells, while knockdown of miR-18a increased PTEN expression (Figures 5(d) and 5(e)). The luciferase assay results showed that the luciferase activity was significantly inhibited or fortified by being transfected with miR-18a mimic or inhibitor in the PTEN-WT group (Figure 5(f)). These data suggested that PTEN was a direct target of miR-18a.

3.6. WDFY3-AS2 Attenuated the Development of EC via Modulating miR-18a/PTEN Axis. Next, rescue assays were conducted to verify the role of WDFY3-AS2/miR-18a/PTEN in EC development. CCK-8 assay discovered that the decreased cell viability caused by overexpression of WDFY3-AS2 was attenuated by upregulation of miR-18a or downregulation of PTEN (Figure 6(b)). Transwell migration and invasion assays demonstrated that EC invasion and migration were repressed by increasing WDFY3-AS2 and restored by upregulation of miR-18a or depletion of PTEN (Figures 6(c) and 6(d)). The results stated that WDFY3-AS2 might inhibit EC progression by regulating PTEN via miR-18a.

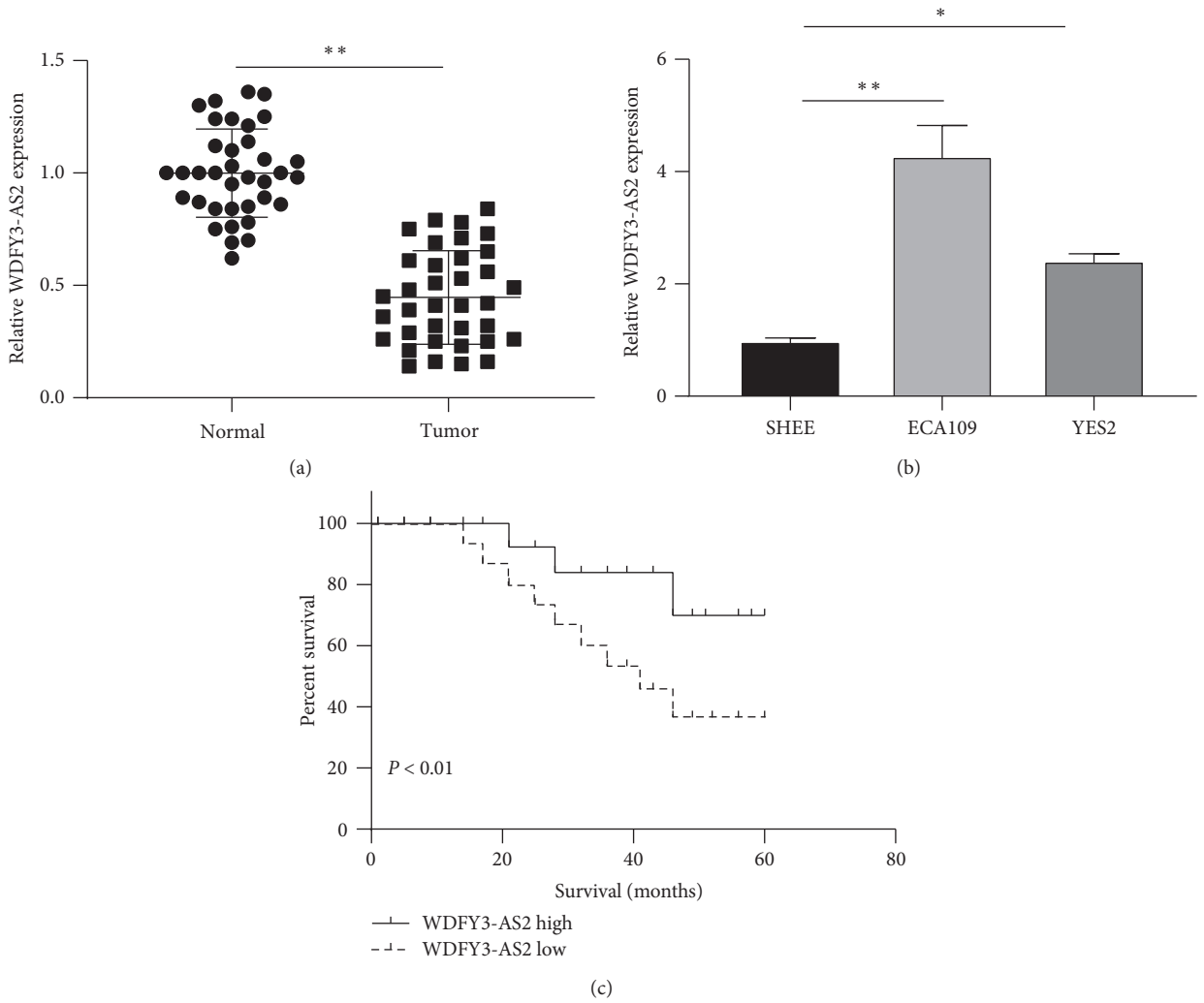

Figure 1: WDFY3-AS2 was decreased in EC. (a) Detection of WDFY3-AS2 expression in EC tissues by RT-PCR. (b) Detection of WDFY3-AS2 expression in EC cell lines by RT-PCR. (c) The overall survival of EC patients with high or low WDFY3-AS2 expression by the Kaplan–Meier analysis. $^{*}P < 0.05$, $^{**}P < 0.01$.

Table 1: Relationship between WDFY3-AS2 expression and clinical characteristics of EC patients.

Item	Cases ($n = 36$)	WDFY3-AS2		P value
		Low ($n = 17$)	High ($n = 19$)	
Age (years)				0.709
<60	16	7	9	
≥60	20	10	10	
Gender				0.194
Female	21	8	13	
Male	15	9	6	
Tumor location				0.342
Upper/middle	22	9	13	
Lower	14	8	6	
Tumor size				0.985
<4 cm	17	8	9	
≥4 cm	19	9	10	
Tumor grading				0.018 *
G1	12	9	3	
G2/3	24	8	16	
TNM stage				0.007 *
I-II	13	10	3	
III-IV	23	7	16	

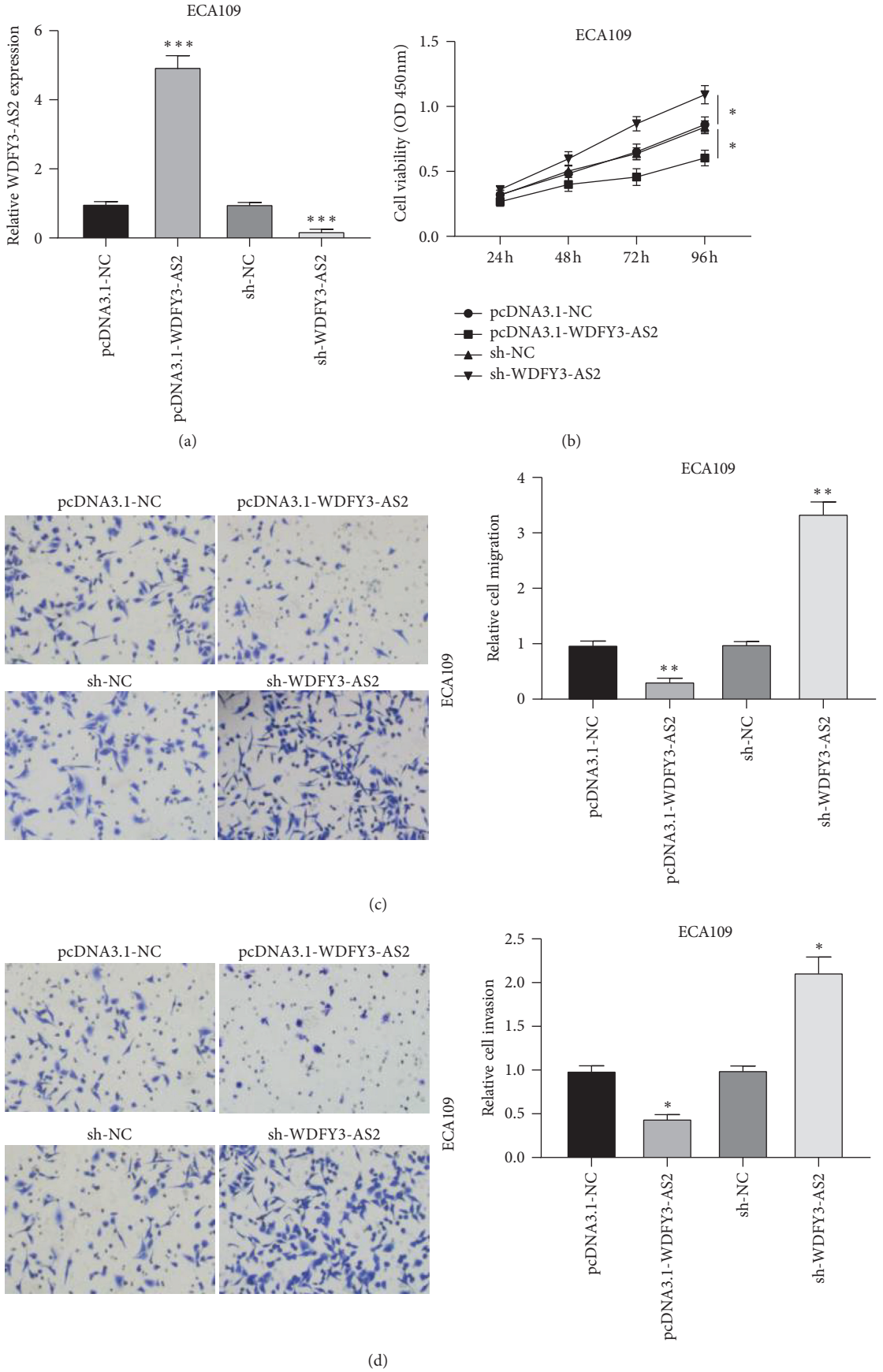

Figure 2: WDFY3-AS2 inhibited EC development. (a) The transfection efficiency of WDFY3-AS2 in ECA109 cells after knockdown and overexpression of WDFY3-AS2. (b) CCK-8 assay revealed WDFY3-AS2 effect on ECA109 cells proliferation. (c) Transwell migration assay revealed WDFY3-AS2 effect on ECA109 cells migration. (d) Transwell invasion assay revealed the cell invasion of ECA109 cells after overexpression or knockdown of WDFY3-AS2. $^{*}P < 0.05$, $^{**}P < 0.01$, and $^{***}P < 0.001$.

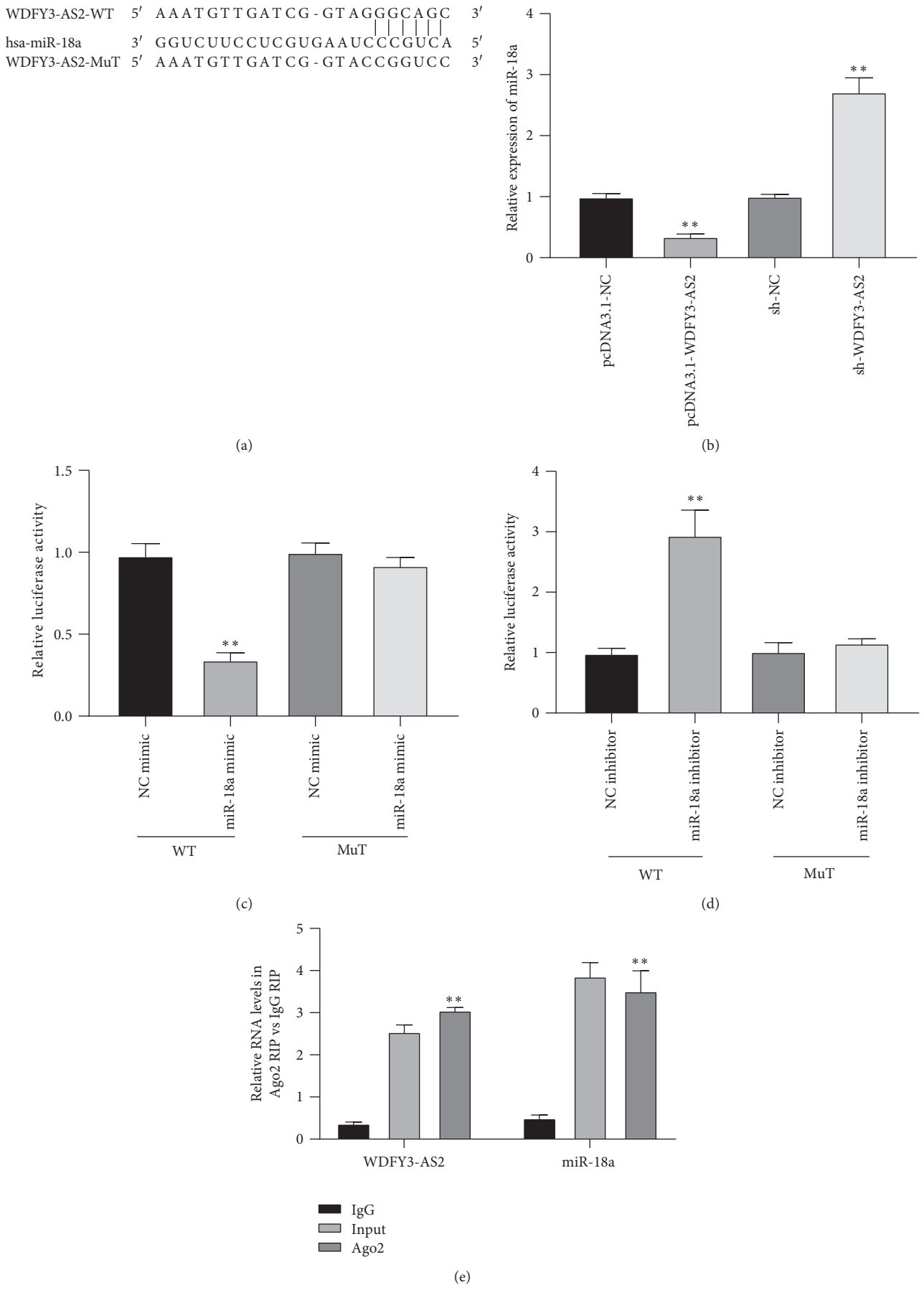

Figure 3: WDFY3-AS2 sponges for miR-18a. (a) The speculated binding sites of miR-18a for WDFY3-AS2. (b) The expressional level of miR-18a affected by WDFY3-AS2 alterations. (c) The luciferase activities of WDFY3-AS2 in response to miR-18a mimic or (d) miR-18a inhibitor. (e) The interplay between WDFY3-AS2 and miR-18a verified by RIP assay. $^{*}P < 0.05$, $^{**}P < 0.01$.

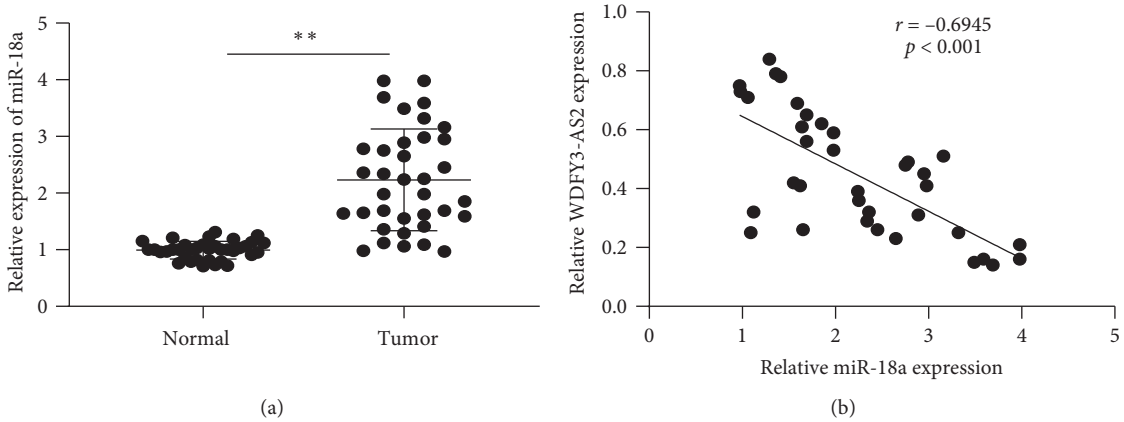

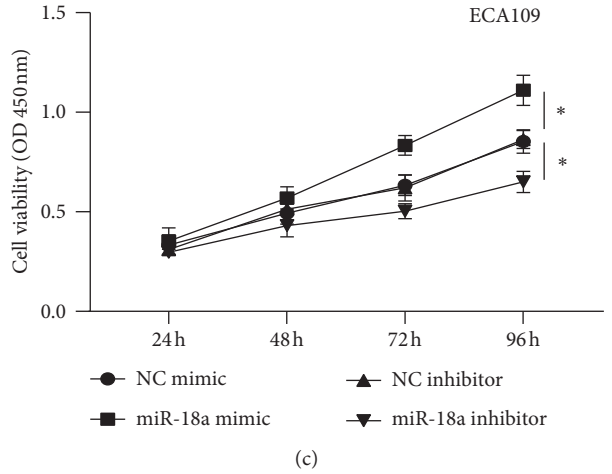

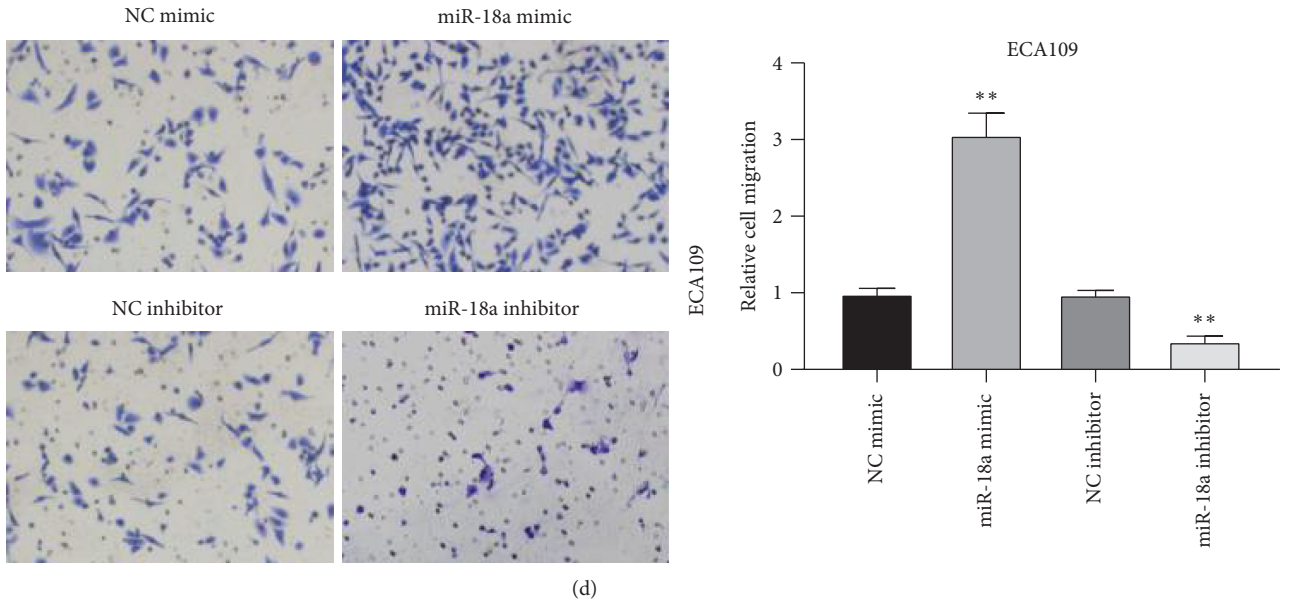

Figure 4: Continued.

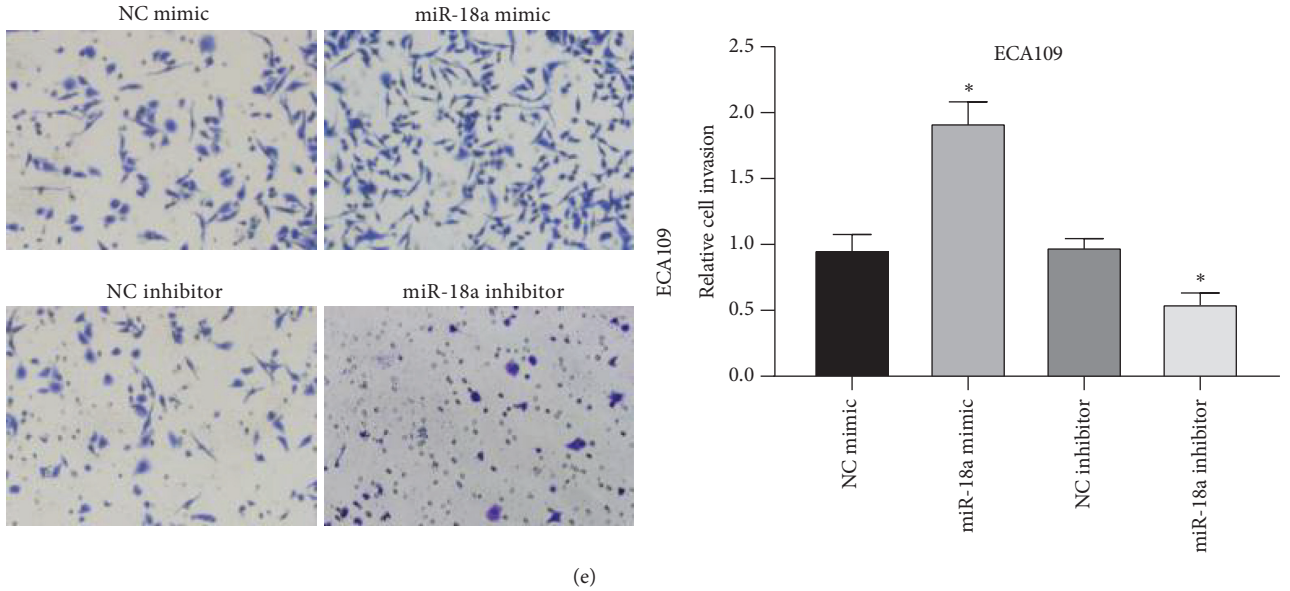

Figure 4: miR-18a enhanced EC development. (a) The expression level of miR-18a in EC tissues. (b) The negative relationship between miR-18a and WDFY3-AS2. (c) CCK-8 assay detected miR-18a effect on ECA109 cells viability. (d) Transwell migration assay revealed miR-18a effect on ECA109 cells migration. (e) Transwell invasion assay detected the cell invasion of ECA109 cells after overexpression or knockdown of miR-18a. $^{*}P < 0.05$, $^{**}P < 0.01$.

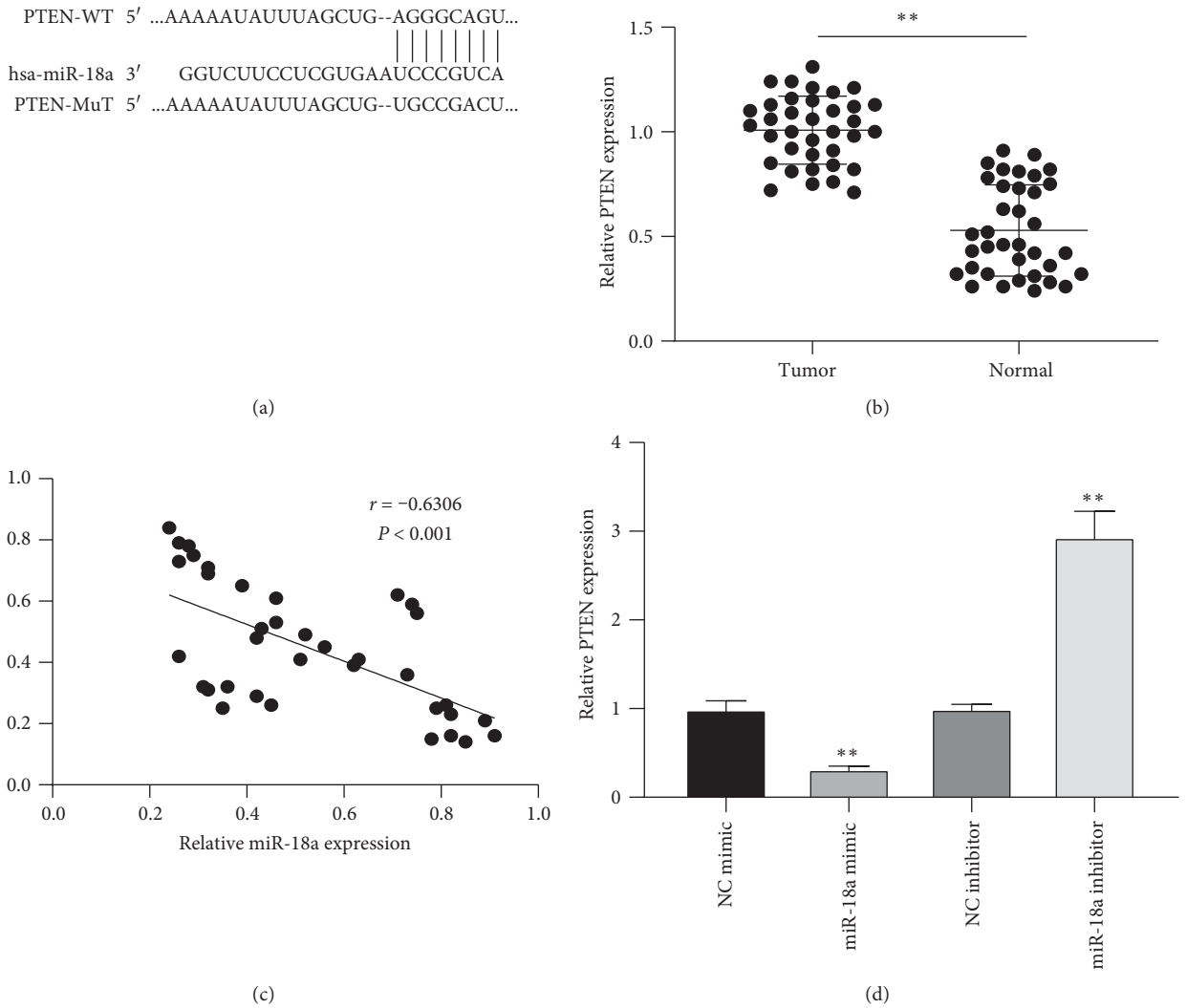

Figure 5: Continued.

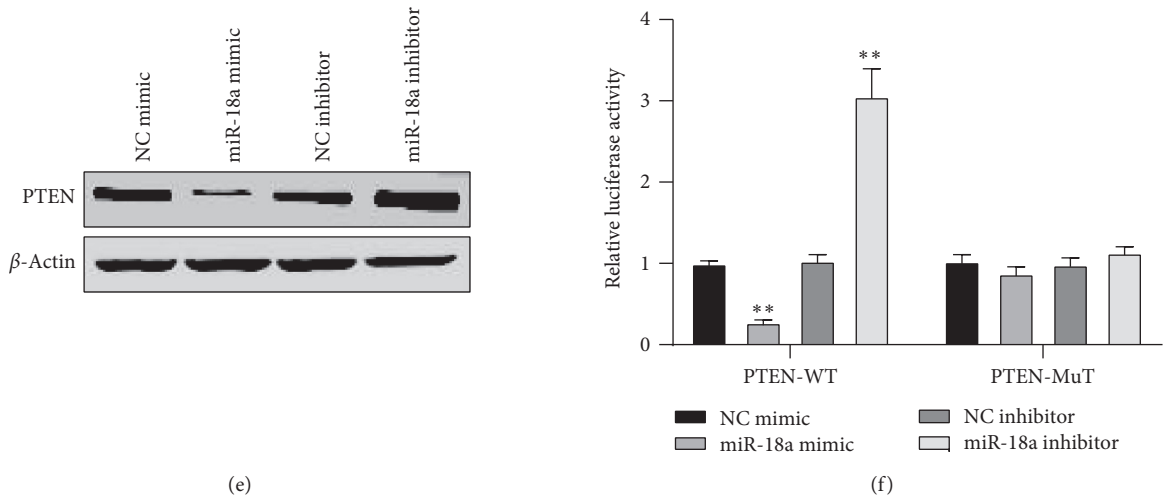

(e) (f)

Figure 5: PTEN acted as the target of miR-18a. (a) The prediction binding sites of miR-18a and PTEN. (b) Detection of the expression of PTEN in EC tissues. (c) Pearson's analysis of the relationship between PTEN and miR-18a. (d) The relative mRNA and (e) protein expression affected by miR-18a mimic or inhibitor. (f) The luciferase activity detected in ECA109 cells after treated with miR-18a mimic or inhibitor and PTEN-WT or PTEN-MuT.

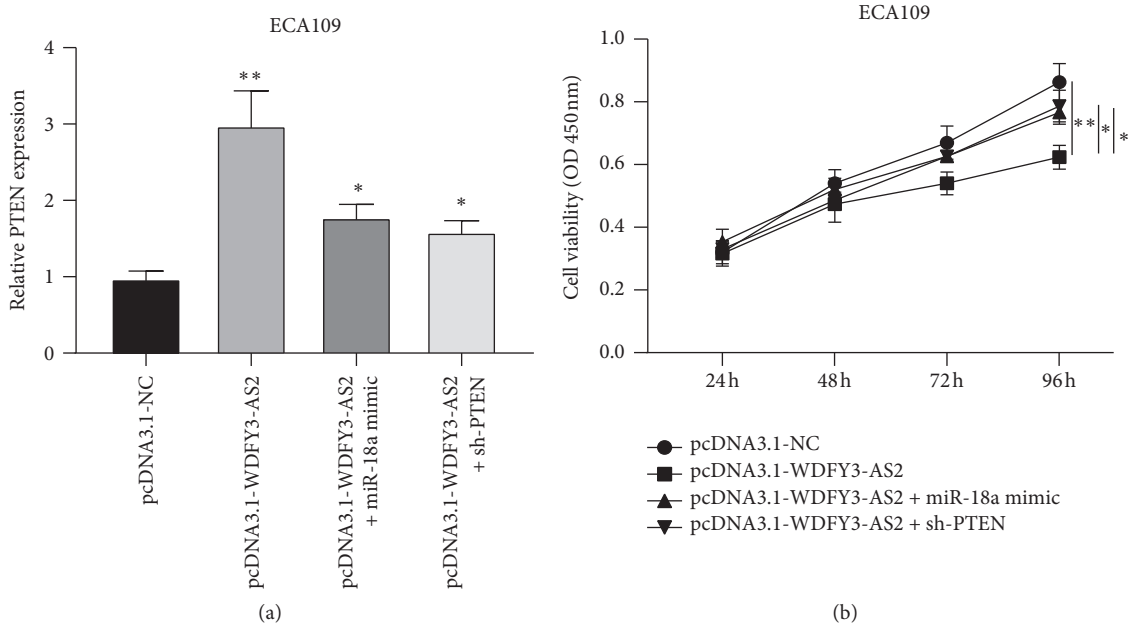

(a) (b)

Figure 6: Continued.

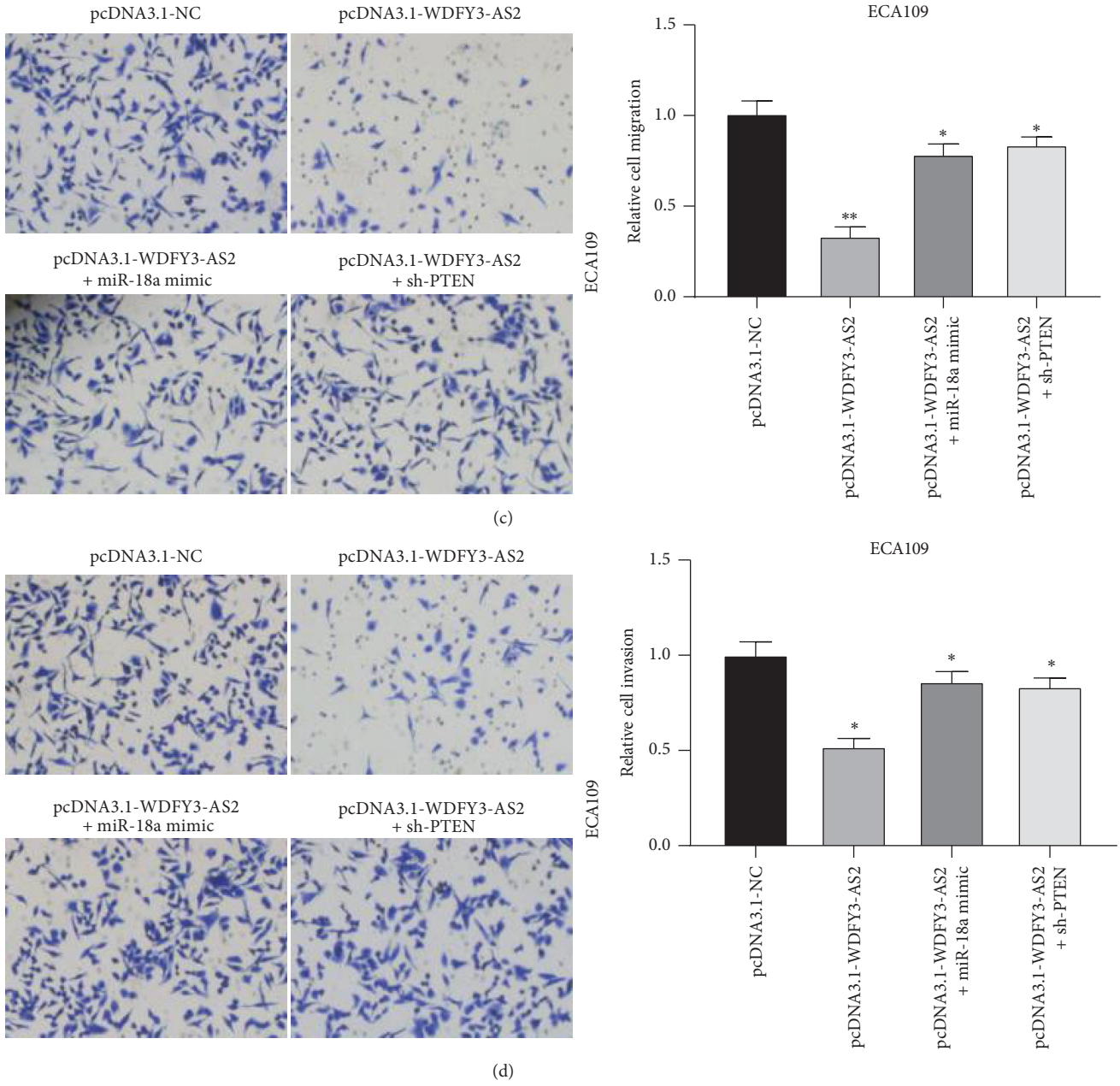

Figure 6: WDFY3-AS2/miR-18a/PTEN axis attenuated EC development. ECA109 cells were transfected with pcDAN3.1-WDFY3-AS2 alone or cotransfected with pcDAN3.1-WDFY3-AS2 and miR-18a mimic or sh-PTEN (a) RT-PCR analysis of PTEN expression. (b) CCK-8 assay to detect ECA109 cells proliferation. (c) Transwell migration assay was performed to investigate ECA109 cells migration. (d) Transwell invasion assay was performed to measure the cell invasion of ECA109 cells. $^{*}P < 0.05$, $^{**}P < 0.01$.

4. Discussion

Esophageal cancer is a malignant tumor occurring in the esophageal mucosa and is a common gastrointestinal tumor in China [21]. Lack of potential biomarkers and unnoticed early symptoms of potential EC patients often lead to delayed diagnosis [22]. LncRNA has been reported to be involved in the progression and prognosis of various human tumors. In recent years, although lncRNAs have been studied to assist in the clinical diagnosis of cancer as a potential molecular biomarker, the effect is not evident in EC. Previous studies have found that WDFY3-AS2 was underexpressed in EC patients [23], which was consistent with our findings that WDFY3-AS2 decreased in EC tissues and cells. Moreover, we revealed that overexpression of WDFY3-AS2 inhibited cell proliferation, invasion, and migration, whereas inhibited WDFY3-AS2 showed the opposite effect, suggesting the inhibitory role of WDFY3-AS2 in EC progression.

Previous literature has highlighted the critical role of lncRNAs and miRNAs in various biological processes of cancers, including EC [24, 25]. In the current study, we

demonstrated that miR-18a acted as a target of WDFY3-AS2. Moreover, WDFY3-AS2 increased PTEN expression by inhibiting miR-18a. These findings were consistent with the previous study that WDFY3-AS2 binds to miR-18a and WDFY3-AS2 negatively regulated miR-18a expression in ovarian cancer cells. MiR-18a was upregulated in various cancers, including EC [26]. However, its functional role in EC has not been clarified. In this study, we discovered that miR-18a was highly expressed in EC tissues and EC cells. MiR-18a promoted EC cells proliferation, invasion, and migration and WDFY3-AS2 attenuated the development of EC via miR-18a/PTEN axis.

The obtained results showed that PTEN was involved in EC progression. PTEN has been reported to have an oncogenic role in a variety of tumors. For instance, Xiang et al. discovered that PTEN repressed cell proliferation and inhibited apoptosis in lung cancer [27]. Besides, PTEN served as a promoter in gliomagenesis by facilitating cell proliferation, tumor growth, and inhibiting apoptosis [28]. Our study confirmed that the reexpression of WDFY3-AS2 suppressed EC cell proliferation, invasion, and migration by increasing PTEN expression via miR-18a. However, our research is in the preclinical stage; the mechanism of action involved is unclear. Therefore, further evaluation of other relevant biomarkers is recommended.

In conclusion, our study suggests that WDFY3-AS2 was underexpressed in EC samples and cells. Low expression of WDFY3-AS2 was associated with poor prognosis of EC patients. Additionally, the reexpression of WDFY3-AS2 suppressed EC progression by miR-18a/PTEN axis. WDFY3-AS2 may be a novel therapeutic and prognostic target for EC.

Data Availability

The datasets used and/or analyzed during the current study are available from the corresponding author on reasonable request.

Conflicts of Interest

The authors declare that they have no conflicts of interest.

Authors' Contributions

Qingling Kong guaranteed the integrity of the entire study and participated in writing the manuscript. Guangcai Li, Gang Yin, Kun Li, and Dongqing Zhang performed the experimental studies, data analysis, and statistical analysis. Weihao Xu designed, supervised the research, and participated in the writing and reviewing of the manuscript. All authors read and approved the final manuscript.

References

[1] H. Liang, J. H. Fan, and Y. L. Qiao, "Epidemiology, etiology, and prevention of esophageal squamous cell carcinoma in China," *Cancer Biology & Medicine*, vol. 14, pp. 33–41, 2017.

[2] Y. Zhang, "Epidemiology of esophageal cancer," *World Journal of Gastroenterology*, vol. 19, no. 34, pp. 5598–5606, 2013.

[3] F.-L. Huang and S.-J. Yu, "Esophageal cancer: risk factors, genetic association, and treatment," *Asian Journal of Surgery*, vol. 41, no. 3, pp. 210–215, 2018.

[4] C. Jiang, S. Li, Y. Li, and Y. Bai, "Anticancer effects of dihydroartemisinin on human esophageal cancer cells in vivo," *Analytical Cellular Pathology (Amsterdam)*, vol. 2018, Article ID 8759745, 7 pages, 2018.

[5] D.-H. Bach and S. K. Lee, "Long noncoding RNAs in cancer cells," *Cancer Letters*, vol. 419, pp. 152–166, 2018.

[6] L. Chen, E. E. Dzakah, and G. Shan, "Targetable long noncoding RNAs in cancer treatments," *Cancer Letters*, vol. 418, pp. 119–124, 2018.

[7] C. P. Ponting, P. L. Oliver, and W. Reik, "Evolution and functions of long noncoding RNAs," *Cell*, vol. 136, no. 4, pp. 629–641, 2009.

[8] Y. Bi, S. Guo, X. Xu et al., "Decreased ZNF750 promotes angiogenesis in a paracrine manner via activating DANCR/miR-4707-3p/$FOXC_2$ axis in esophageal squamous cell carcinoma," *Cell Death & Disease*, vol. 11, p. 296, 2020.

[9] X. Liang, Z. Wu, S. Shen et al., "LINC01980 facilitates esophageal squamous cell carcinoma progression via regulation of miR-190a-5p/MYO5A pathway," *Archives of Biochemistry and Biophysics*, vol. 686, Article ID 108371, 2020.

[10] S. Shen, K. Li, Y. Liu et al., "Silencing lncRNA AGAP2-AS1 upregulates miR-195-5p to repress migration and invasion of EC cells via the decrease of FOSL1 expression," *Molecular Therapy—Nucleic Acids*, vol. 20, pp. 331–344, 2020.

[11] Z. Zhang, S. Wang, and W. Liu, "EMT-related long noncoding RNA in hepatocellular carcinoma: a study with TCGA database," *Biochemical and Biophysical Research Communications*, vol. 503, no. 3, pp. 1530–1536, 2018.

[12] D. Rodrigues de Bastos and M. A. Nagai, "In silico analyses identify lncRNAs: WDFY3-AS2, BDNF-AS and AFAP1-AS1 as potential prognostic factors for patients with triple-negative breast tumors," *PLoS One*, vol. 15, no. 5, Article ID e0232284, 2020.

[13] W. Li, S. Ma, X. Bai, W. Pan, L. Ai, and W. Tan, "Long noncoding RNA WDFY3-AS2 suppresses tumor progression by acting as a competing endogenous RNA of microRNA-18a in ovarian cancer," *Journal of Cellular Physiology*, vol. 235, no. 2, pp. 1141–1154, 2020.

[14] Z. Zhang, J. Z. Li, Z. W. Wei et al., "Correlation between expression levels of lncRNA UCA1 and miR-18a with prognosis of hepatocellular cancer," *European Review for Medical and Pharmacological Sciences*, vol. 24, no. 7, pp. 3586–3591, 2020.

[15] M. K. Pandey, B. Sung, K. S. Ahn, A. B. Kunnumakkara, M. M. Chaturvedi, and B. B. Aggarwal, "Gambogic acid, a novel ligand for transferrin receptor, potentiates TNF-induced apoptosis through modulation of the nuclear factor-κB signaling pathway," *Blood*, vol. 110, no. 10, pp. 3517–3525, 2007.

[16] S. Mai, R. Xiao, L. Shi et al., "MicroRNA-18a promotes cancer progression through SMG1 suppression and mTOR pathway activation in nasopharyngeal carcinoma," *Cell Death & Disease*, vol. 10, no. 11, p. 819, 2019.

[17] M. G. Nair, J. S. Prabhu, A. Korlimarla et al., "miR-18a activates Wnt pathway in ER-positive breast cancer and is associated with poor prognosis," *Cancer Medicine*, vol. 9, no. 15, pp. 5587–5597, 2020.

[18] S. Hirajima, S. Komatsu, D. Ichikawa et al., "Clinical impact of circulating miR-18a in plasma of patients with oesophageal squamous cell carcinoma," *British Journal of Cancer*, vol. 108, no. 9, pp. 1822–1829, 2013.

[19] Z. Wang, F. Liu, W. Liao et al., "Curcumin suppress glioblastoma cell proliferation by p-AKT/mTOR pathway and increased the PTEN expression," *Archives of Biochemistry and Biophysics*, vol. 689, Article ID 108412, 2020.

[20] H. Izumi, Z. Wang, Y. Goto et al., "Pathway-specific genome editing of PI3K/mTOR tumor suppressor genes reveals that PTEN loss contributes to cetuximab resistance in head and neck cancer," *Molecular Cancer Therapeutics*, vol. 19, no. 7, pp. 1562–1571, 2020.

[21] M. L. Hemming, M. C. Heinrich, S. Bauer, and S. George, "Translational insights into gastrointestinal stromal tumor and current clinical advances," *Annals of Oncology*, vol. 29, no. 10, pp. 2037–2045, 2018.

[22] D. C. Codipilly, Y. Qin, S. M. Dawsey et al., "Screening for esophageal squamous cell carcinoma: recent advances," *Gastrointestinal Endoscopy*, vol. 88, no. 3, pp. 413–426, 2018.

[23] H. Liu, Q. Zhang, Q. Lou et al., "Differential analysis of lncRNA, miRNA and mRNA expression profiles and the prognostic value of lncRNA in esophageal cancer," *Pathology & Oncology Research*, vol. 26, no. 2, pp. 1029–1039, 2020.

[24] B. Feng, G. Wang, X. Liang et al., "LncRNA FAM83H-AS1 promotes oesophageal squamous cell carcinoma progression via miR-10a-5p/Girdin axis," *Journal of Cellular and Molecular Medicine*, vol. 24, no. 16, pp. 8962–8976, 2020.

[25] Q. Li, Z. Dai, C. Xia, L. Jin, and X. Chen, "Suppression of long non-coding RNA MALAT1 inhibits survival and metastasis of esophagus cancer cells by sponging miR-1-3p/CORO1C/TPM3 axis," *Molecular and Cellular Biochemistry*, vol. 470, no. 1-2, pp. 165–174, 2020.

[26] L. Jamali, R. Tofigh, S. Tutunchi et al., "Circulating microRNAs as diagnostic and therapeutic biomarkers in gastric and esophageal cancers," *Journal of Cellular Physiology*, vol. 233, no. 11, pp. 8538–8550, 2018.

[27] C. Xiang, Y. Zhang, Y. Zhang, C. Liu, Y. Hou, and Y. Zhang, "lncRNA LEF1-AS1 promotes proliferation and induces apoptosis of non-small-cell lung cancer cells by regulating miR-221/PTEN signaling," *Cancer Management and Research*, vol. 12, pp. 3845–3850, 2020.

[28] Y. Xie and Y. Cheng, "LINC01198 facilitates gliomagenesis through activating PI3K/AKT pathway," *RNA Biology*, vol. 17, no. 7, pp. 1040–1052, 2020.

Hindawi
Journal of Oncology
Volume 2021, Article ID 9972051, 6 pages
https://doi.org/10.1155/2021/9972051

Research Article

Clinical Effect of Radiotherapy Combined with Capecitabine after Neoadjuvant Therapy for Rectal Cancer

Qibo Zhang and Haibin Teng

Department of Nuclear Medicine, Linyi Central Hospital, Linyi 276400, Shandong Province, China

Correspondence should be addressed to Haibin Teng; haibinteng@yeah.net

Received 1 April 2021; Accepted 25 May 2021; Published 7 June 2021

Academic Editor: Muhammad Wasim Khan

Objective. The purpose of the study was to investigate the clinical effect of radiotherapy combined with capecitabine in rectal cancer patients after neoadjuvant therapy. *Methods*. 80 rectal cancer patients who underwent neoadjuvant therapy in our hospital from February 2016 to February 2018 were selected as the study subjects and divided into the control group ($n = 40$) and experimental group ($n = 40$) according to the order of admission. Among them, the control group was treated with radiotherapy, while the experimental group was treated with radiotherapy combined with capecitabine. The therapeutic efficacy, CEA levels, the incidence and recurrence rate of adverse reactions, as well as the progression-free survival and survival rate after 2-year treatment were analyzed in the two groups. *Results*. The effective rate of treatment in the experimental group of 87.5% (35/40) was significantly higher than 50% (20/40) in the control group, with statistical significance ($X^2 = 13.09$, $P < 0.001$). After treatment, the CEA levels in the two groups both decreased significantly, and the CEA level in the experimental group of 3.75 ± 1.76 ng/ml was significantly lower than 7.35 ± 2.11 ng/ml in the control group, with statistical significance ($T = 8.29$, $P < 0.001$). The incidence and the recurrence rate of adverse reactions of 5% (2/40) and 10% (4/40), respectively, in the experimental group were significantly lower than those of 40% (16/40) and 30% (12/40) in the control group, with statistical significance ($X^2 = 14.05$, 5.00, $P < 0.001$, 0.05). After the 2-year follow-up, it was found that the progression-free survival of 21.53 ± 6.23 months in the experimental group was significantly longer than that of 18.18 ± 5.41 months in the control group, with statistical significance ($T = 2.57$, $P < 0.05$), and the 2-year survival rate of 97.5% (39/40) in the experimental group was significantly higher than 80% (32/40) in the control group, with statistical significance ($T = 6.13$, $P < 0.05$). *Conclusion*. Radiotherapy combined with capecitabine in rectal cancer patients after neoadjuvant therapy can improve the therapeutic efficacy with fewer adverse reactions and longer patients' survival, which is worthy of popularization and application after neoadjuvant therapy for rectal cancer.

1. Introduction

Rectal cancer is a clinically common malignant tumor disease [1]. The location of rectal cancer is at the intersection of rectosigmoid colon and dentate line, which makes the anatomy more complex, with more difficulty in surgery. The majority of rectal cancer patients are middle-aged, and they are gradually progressing towards a younger age [2–4]. At present, the pathogenic factors of rectal cancer are still unclear, but mainly might be related to diet, society, and heredity. Because rectal cancer patients have no obvious symptoms in the early stage, with the continuous progression of disease, patients will have diarrhea, bloody stools, and other symptoms, which seriously threatens patients' health [5, 6]. In recent years, neoadjuvant therapy has played an active role in the clinical treatment of rectal cancer, but its clinical effect for rectal cancer patients is not ideal. With the continuous development of medical technology, radiotherapy is still an essential part of neoadjuvant therapy for rectal cancer, which can effectively inhibit tumor growth and improve patients' life quality. Capecitabine is an antimetabolic fluorouracil deoxynucleotide-based allophanate ester that is converted into 5-FU in vivo [7], which can inhibit protein synthesis and interfere with RNA and cell division. Nowadays, it has been widely used in the clinical treatment of breast cancer, gastric cancer, and rectal cancer [8]. This

Table 1: General clinical data of the two groups of patients.

Factors		Control group ($n = 40$)	Experimental group ($n = 40$)	X^2/T	P
Gender	Male	22	23	0.05	0.82
	Female	18	17		
Average age	—	55.32 ± 4.75	55.38 ± 4.26	0.06	0.95
Neoplasm staging	Stage II	26	25	0.05	0.82
	Stage III	14	15		
Pathological classification	Mucinous carcinoma	3	4	0.16	0.69
	Adenocarcinoma	37	36		
Differentiation	Poorly differentiated	11	12	0.22	0.90
	Moderately differentiated	15	13		
	Well differentiated	14	15		

study intended to investigate the clinical effect of radiotherapy combined with capecitabine in rectal cancer patients after neoadjuvant therapy and provide some references for rectal cancer treatment.

2. Materials and Methods

2.1. General Information. The patients with rectal cancer who underwent neoadjuvant therapy in our hospital from February 2016 to February 2018 were selected as the study subjects and divided into the control group and experimental group according to the order of admission. There were no significant differences between the two groups in general clinical data such as age and pathological classification, with comparability ($P > 0.05$), as given in Table 1.

2.2. Inclusion/Exclusion Criteria

2.2.1. Inclusion Criteria

(1) Patients who met the WHO diagnostic criteria for rectal cancer were clinically diagnosed as rectal cancer in our hospital and received neoadjuvant therapy

(2) Patients were or elder than 18 years old

(3) This study has been approved by the hospital ethics committee (no. 20160145)

(4) Patients and their family were informed of the whole process of treatment and signed the informed consent

2.2.2. Exclusion Criteria

(1) Patients had major organ diseases such as kidney, liver, and heart diseases

(2) Patients had mental, cognitive, and behavioral disorders

(3) Patients had the history of drug allergy

(4) Patients had inflammatory bowel disease and hereditary colorectal cancer

2.3. Methods. All patients were treated with radiation therapy after neoadjuvant therapy. The radiation instrument Varian Clinac CX 10MV medical electronic linear accelerator was adopted in this study. After simulated positioning, CT enhanced scanning was performed, with the slice thickness of 5 mm. In the emphasized planning system, coplanar multifield conformal irradiation was performed, with the total dose of 60 Gy~66 Gy (2 Gy/d, 1 time/d, 5 times/week). On the basis of that, the experimental group was treated with Xeloda capecitabine tablets (State Food and Drug Administration approval number: H20073024; manufacturer: Shanghai Roche Pharmaceutical Co., Ltd.), with a total daily dose of 2500 mg (1250 mg/time, once 30 minutes after breakfast and dinner by oral administration). After 14 days of continuous administration, the drug was discontinued for 7 days and 2 courses of treatment were carried out in succession with each course lasting 21 days.

2.4. Evaluation Indexes

2.4.1. Therapeutic Efficacy. The therapeutic efficacy was analyzed according to the response evaluation criteria in solid tumors which were divided into complete remission, partial remission, stable disease, and disease progression. Complete remission refers to the disappearance of all tumor lesions for 28 days. Partial remission refers to the reduction of tumor lesion long diameter by more than 30% for 28 days. Stable disease refers to the increase of tumor lesion long diameter by less than or equal to 20% or the reduction by less than or equal to 30%. Disease progression refers to the increase of tumor lesion long diameter more than 20%. The effective rate of treatment = (complete remission + partial remission)/total number of cases × 100%.

2.4.2. CEA Level. The CEA (serum carcinoembryonic antigen) levels before and after treatment were analyzed and compared between the two groups.

2.4.3. Incidence of Adverse Reactions. Adverse reactions such as nausea, vomiting, hand-foot syndrome, diarrhea, myelosuppression, and mucocutaneous impairments were analyzed and compared between the two groups.

2.4.4. Recurrence Rate. The recurrence rate in the two groups of patients was analyzed and compared.

Table 2: Therapeutic efficacy in the two groups of patients.

Group	Cases	Complete remission	Partial remission	Stable disease	Disease progression	Effective rate of treatment
Control group	40	0	20	15	5	50% (20/40)
Experimental group	40	3	32	5	0	87.5% (35/40)
X^2	—	—	—	—	—	13.09
P	—	—	—	—	—	$P < 0.01$

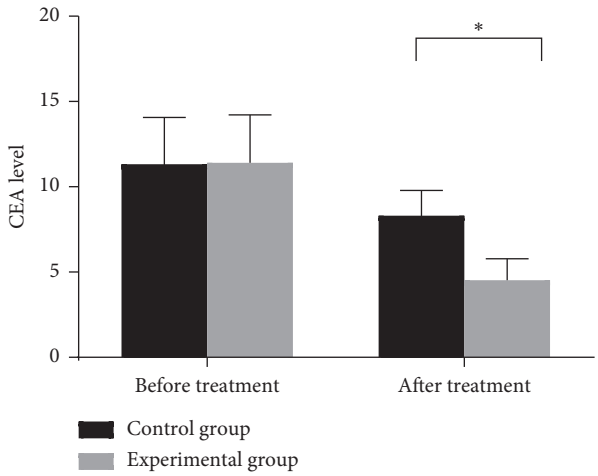

Figure 1: CEA levels in two groups. Note: the abscissa from left to right indicates before treatment and after treatment, while the ordinate indicates the CEA level (unit: ng/ml). The CEA level in the experimental group is significantly lower than that in the control group after treatment. *Statistical significance ($T = 8.29$, $P < 0.001$).

2.4.5. Progression-Free Survival and Survival Rate. Two-year follow-up was carried out for the two groups of patients, and the progression-free survival and 2-year survival rate in the two groups were analyzed.

2.5. Statistical Treatment. The data software SPSS18.0 was adopted in this study to process and analyze the research data. Measurement data were expressed by ($\overline{x} \pm s$) and tested by the t-test. Enumeration data were expressed as (n (%)) and tested by the X^2 test. The differences had statistical significance when $P < 0.05$.

3. Results

3.1. Analysis of Therapeutic Efficacy in the Two Groups of Patients. The effective rate of treatment in the experimental group was significantly higher than that in the control group, with statistical significance ($X^2 = 13.09$, $P < 0.001$), as given in Table 2.

3.2. Analysis of CEA Levels in the Two Groups of Patients. Before treatment, there were no significant differences in CEA levels between the experimental group of 9.53 ± 3.96 ng/ml and the control group of 9.49 ± 3.86 ng/ml ($T = 0.05$, $P = 0.96$), with no significant differences. After treatment, CEA levels in the two groups both decreased significantly, and the CEA level of 3.75 ± 1.76 ng/ml in the experimental group was significantly lower than 7.35 ± 2.11 ng/ml in the control group, with statistical significance ($T = 8.29$, $P < 0.001$), as shown in Figure 1.

3.3. Analysis of the Incidence of Adverse Reactions in the Two Groups of Patients. The incidence of adverse reactions in the experimental group was significantly lower than that in the control group, with statistical significance ($X^2 = 14.05$, $P < 0.001$), as given in Table 3.

3.4. Analysis of Recurrence Rate in the Two Groups of Patients. The recurrence rate of 10% (4/40) in the experimental group was significantly lower than 30% (12/40) in the control group, with statistical significance ($X^2 = 5.00$, $P < 0.05$), as shown in Figure 2.

3.5. Analysis of Progression-Free Survival and Survival Rate after 2-Year Treatment in the Two Groups of Patients. After two-year follow-up, it was found that the progression-free survival of 21.53 ± 6.23 months in the experimental group was significantly longer than 18.18 ± 5.41 months in the control group, with statistical significance ($T = 2.57$, $P < 0.05$). The 2-year survival rate of 97.5% (39/40) in the experimental group was significantly higher than 80% (32/40) in the control group, with statistical significance ($T = 6.13$, $P < 0.05$), as shown in Figures 3 and 4.

4. Discussion

Rectal cancer is a clinically common malignant tumor disease, which commonly affects rectum [9–11]. Because rectal cancer patients have no specific clinical symptoms in the early stage, with the progression of disease, patients will suffer from different degrees of constipation and diarrhea. Nowadays, rectal cancer diseases are mostly detected by proctoscope and digital rectal examination, and rectal cancer masses are characterized by rapid growth, uneven surface, and hard texture [12–14]. Surgical resection is currently one of the most commonly used methods in the clinical treatment of rectal cancer, but because most patients are diagnosed in the middle and late stage, the clinical efficacy of surgical resection is not ideal, with high postoperative recurrence rates. In recent years, with the continuous development of medical level, neoadjuvant therapy has been widely applied in clinical treatment. The study of Bushati et al. [15] has found that neoadjuvant therapy for patients with advanced rectal cancer can improve their life quality. At present, most scholars have pointed out that attention should be paid to the following two aspects in the adjuvant treatment of rectal cancer patients. One is that in the process

Table 3: Incidence of adverse reactions in the two groups of patients.

Group	Cases	Nausea/ vomiting	Hand-foot syndrome	Diarrhea	Myelosuppression	Mucocutaneous impairments	Incidence of adverse reactions
Control group	40	4	2	5	2	3	40% (16/40)
Experimental group	40	1	0	1	0	0	5% (2/40)
X^2	—	—	—	—	—	—	14.05
P	—	—	—	—	—	—	$P < 0.001$

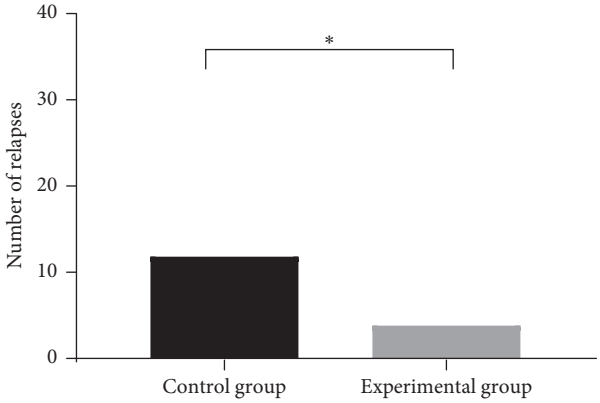

Figure 2: Groups of patients with recurrence rate. Note: the abscissa indicates the control group and experimental group, while the ordinate indicates number of relapses (unit: case). The number of relapses in the experimental group is significantly less than that in the control group. *Statistical significance ($X^2 = 5.00$, $P < 0.05$).

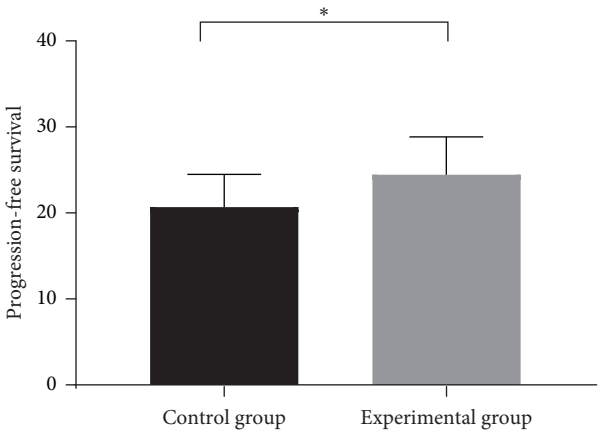

Figure 3: Progression-free survival of the two groups. Note: the abscissa from left to right indicates the control group and experimental group, while the ordinate indicates progression-free survival (unit: month). The progression free survival in the experimental group was significantly longer than that in the control group. *Statistical significance ($T = 2.57$, $P < 0.01$).

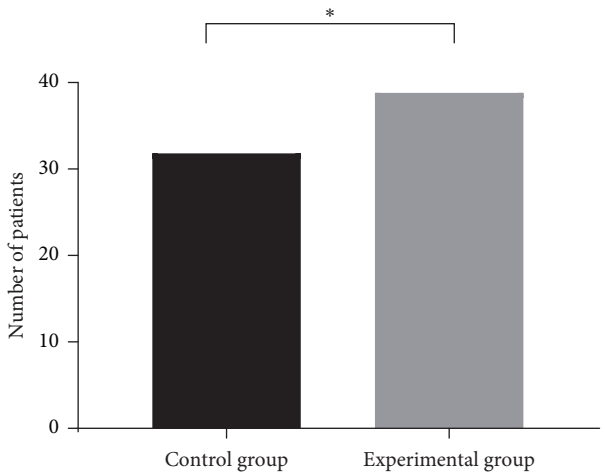

Figure 4: 2-year survival rate of the two groups. Note: the abscissa from left to right indicates the control group and experimental group, while the ordinate indicates number of patients (unit: case). The 2-year survival rate in the experimental group was significantly higher than that in the control group. *Statistical significance ($T = 6.13$, $P < 0.05$).

of neoadjuvant treatment, individual differences of rectal cancer patients should be paid much attention to, and disease stages, physical fitness, and treatment compliance of different patients should also be taken into consideration. Another is that radiotherapy or chemotherapy alone is not as effective as chemoradiotherapy because rectal cancer patients have distant metastases during the treatment. Therefore, chemoradiotherapy should be adopted for patients [16–18]. Although neoadjuvant therapy can improve patients' life quality, the recurrence rate after treatment is still very high and the survival rate is not ideal.

Capecitabine is a new 5-FU prodrug. After oral administration, patients convert fluoropyrimidine compounds into 5-FU under the action of thymidine phosphorylase (TP) in vivo. Due to the higher concentration of TP in tumor cells and the lower concentration of TP in normal cells, the activity of TP in tumor cells can be enhanced by radiotherapy, and the effect of 5-FU can be further improved. Therefore, radiotherapy combined with capecitabine in rectal cancer patients after neoadjuvant therapy has great advantages [19, 20]. In recent years, many scholars have proposed that radiotherapy combined with capecitabine in rectal cancer patients after neoadjuvant therapy can reduce patients' adverse reactions and has a positive effect on improving patients' survival rate [21, 22]. In this study, in order to investigate the clinical effect of radiotherapy combined with capecitabine in rectal cancer patients after neoadjuvant therapy, the patients in the control group were treated with radiotherapy, while the patients in the experimental group were treated with radiotherapy combined with capecitabine. The results showed that the therapeutic efficacy and CEA level in the experimental group were significantly better than those in the control group, with statistical significance ($P < 0.05$), indicating that the

radiotherapy combined with capecitabine can reduce the infiltration degree of tumor cells in patients.

Neoadjuvant therapy might increase adverse reactions, decrease therapeutic tolerance, and increase the recurrence rate in rectal cancer patients. This study found that the recurrence rate and the incidence of adverse reactions in the experimental group were significantly lower than those in the control group, with statistical significance ($P < 0.05$), which was similar to the conclusion of Yu et al. [23] and others. According to their study, radiotherapy combined with capecitabine under the basis of neoadjuvant therapy increased the safety of treatment and reduced the adverse reactions as well as recurrence rate of patients, which fully demonstrated that radiotherapy combined with capecitabine can reduce adverse reactions.

According to Velenik et al. [24], radiotherapy combined with capecitabine in patients after neoadjuvant treatment of rectal cancer can improve the survival rate. In this study, it was found that the progression-free survival and 2-year survival rate in the experimental group were significantly better than those in the control group, with statistical significance ($P < 0.05$), which indicated that radiotherapy combined with capecitabine can promote tumor regression, thereby improving patients' postoperative survival.

In conclusion, radiotherapy combined with capecitabine in rectal cancer patients after neoadjuvant therapy can improve the clinical efficacy with fewer adverse reactions and longer patients' survival, which is worthy of promotion and application after neoadjuvant therapy for rectal cancer.

Data Availability

The data used to support the findings of this study are available from the corresponding author upon request.

Conflicts of Interest

The authors declare that there are no conflicts of interest.

References

[1] G. Vanella, G. Capurso, and P. G. Arcidiacono, "Endosonography-guided radiofrequency ablation in pancreatic diseases," *Journal of Clinical Gastroenterology*, vol. 54, no. 7, pp. 591–601, 2020.

[2] G. J. L. H. Van Leenders, T. H. Van der Kwast, D. J. Grignon et al., "The 2019 international society of urological pathology (ISUP) consensus conference on grading of prostatic carcinoma," *American Journal of Surgical Pathology*, vol. 44, no. 8, pp. e87–e99, 2020.

[3] F. Veerankutty, N. Nair, S. Chacko et al., "Oncological adequacy of laparoscopic rectal cancer resection: an audit in Indian perspective," *Journal of Minimal Access Surgery*, vol. 16, no. 3, pp. 251–255, 2020.

[4] T. J. Chittleborough, I. Gutlic, J. F. Pearson et al., "Increasing incidence of young-onset colorectal carcinoma A 3-country population analysis," *Diseases of the Colon & Rectum*, vol. 63, no. 7, pp. 903–910, 2020.

[5] A. Shahnam, E. Paver, B. Nguyen, M. Fadia, and S. Ali, "Prognostic utility of CDX2 and PD-L1 in rectal cancer," *Applied Immunohistochemistry & Molecular Morphology*, vol. 28, no. 6, p. e53, 2020.

[6] F. H. Remzi, Y. Panis, A. Spinelli et al., "International organization for the study of IBD recommendations for surgery in patients with IBD during the coronavirus disease 2019 pandemic," *Diseases of the Colon & Rectum*, vol. 63, no. 7, pp. 870–873, 2020.

[7] A. M. Couwenberg, M. P. W. Intven, M. L. Gregorowitsch, C. Haaring, W. Van Grevenstein, and H. Marieke Verkooijen, "Patient-reported work ability during the first two years after rectal cancer diagnosis," *Diseases of the Colon & Rectum*, vol. 63, no. 5, pp. 578–587, 2020.

[8] D. S. Yang, J. A. Lee, W. S Yoon et al., "Sequential simulation computed tomography allows assessment of internal rectal movements during preoperative chemoradiotherapy in rectal cancer," *Journal of Cancer Research and Therapeutics*, vol. 15, no. 1, pp. 1–8, 2019.

[9] G. Ingrosso, R. Miceli, E. Ponti et al., "Interfraction prostate displacement during image-guided radiotherapy using intraprostatic fiducial markers and a cone-beam computed tomography system: a volumetric off-line analysis in relation to the variations of rectal and bladder volumes," *The Journal of Cancer Research and Therapeutics*, vol. 15, pp. S69–S75, 2019.

[10] J. Segelman, C. Buchli, A. Svanström Röjvall et al., "Effect of radiotherapy for rectal cancer on ovarian androgen production," *British Journal of Surgery*, vol. 106, no. 3, pp. 267–275, 2019.

[11] J. Erlandsson, D. Pettersson, B. Glimelius, T. Holm, and A. Martling, "Postoperative complications in relation to overall treatment time in patients with rectal cancer receiving neoadjuvant radiotherapy," *British Journal of Surgery*, vol. 106, no. 9, pp. 1248–1256, 2019.

[12] Y. Wang, M. Zhou, J. Yang et al., "Increased lymph node yield indicates improved survival in locally advanced rectal cancer treated with neoadjuvant chemoradiotherapy," *Cancer Medicine*, vol. 8, no. 10, pp. 4615–4625, 2019.

[13] K. Legge, D. Nguyen, J. A. Ng et al., "Real-time intrafraction prostate motion during linac based stereotactic radiotherapy with rectal displacement," *Journal of Applied Clinical Medical Physics*, vol. 18, no. 6, pp. 130–136, 2017.

[14] G. M. De Jong and N. Hugen, "Minimally invasive transanal surgery is safe after incomplete polypectomy of low risk T1 rectal cancer: a systematic review," *Colorectal Disease*, vol. 21, no. 10, pp. 1112–1119, 2019.

[15] M. Bushati, S. Pucciarelli, N. Gennaro et al., "Local excision in rectal cancer patients with major or complete clinical response after neoadjuvant therapy: a case-matched study," *International Journal of Colorectal Disease*, vol. 34, no. 12, pp. 2129–2136, 2019.

[16] A. Bausys, J. Kuliavas, A. Dulskas et al., "Early versus standard closure of temporary ileostomy in patients with rectal cancer: a randomized controlled trial," *Journal of Surgical Oncology*, vol. 120, no. 2, pp. 294–299, 2019.

[17] E. Luzietti, G. Pellino, S. Nikolaou et al., "Comparison of guidelines for the management of rectal cancer," *BJS Open*, vol. 2, no. 6, pp. 433–451, 2018.

[18] M. C. S. Babu, V. Asati, K. G. Babu, M. N. Suma, L. K. Rajeev, and K. N. Lokesh, "Synchronous primary cancers: renal cell carcinoma and rectal cancer," *Journal of Cancer Research and Therapeutics*, vol. 15, no. 1, pp. 250-251, 2019.

[19] L. Poynter, D. Galea, K. Veselkov et al., "Network mapping of molecular biomarkers influencing radiation response in rectal cancer," *Clinical Colorectal Cancer*, vol. 18, no. 2, pp. e210–e222, 2019.

[20] P. J. Brown, R. Hyland, A. J. Quyn et al., "Current concepts in imaging for local staging of advanced rectal cancer," *Clinical Radiology*, vol. 74, no. 8, pp. 623–636, 2019.

[21] J. De Leon, M. G. Jameson, D. Rivest-Henault et al., "Reduced motion and improved rectal dosimetry through endorectal immobilization for prostate stereotactic body radiotherapy," *The British Journal of Radiology*, vol. 92, no. 1098, p. 20190056, 2019.

[22] B. J. Quiram, J. Crippa, F. Grass et al., "Impact of enhanced recovery on oncological outcomes following minimally invasive surgery for rectal cancer," *British Journal of Surgery*, vol. 106, no. 7, pp. 922–929, 2019.

[23] X. Yu, Q.-X. Wang, W.-W. Xiao et al., "Neoadjuvant oxaliplatin and capecitabine combined with bevacizumab plus radiotherapy for locally advanced rectal cancer: results of a single-institute phase II study," *Cancer Communications*, vol. 38, no. 1, p. 24, 2018.

[24] V. Velenik, V. Zadnik, M. Omejc, J. Grosek, and M. Tuta, "Influence of concurrent capecitabine based chemoradiotherapy with bevacizumab on the survival rate, late toxicity and health-related quality of life in locally advanced rectal cancer: a prospective phase II CRAB trial," *Radiology and Oncology*, vol. 54, no. 4, pp. 461–469, 2020.

Hindawi
Journal of Oncology
Volume 2021, Article ID 1649344, 7 pages
https://doi.org/10.1155/2021/1649344

Research Article

Expression of the CLCA4 Gene in Esophageal Carcinoma and Its Impact on the Biologic Function of Esophageal Carcinoma Cells

Xin Song, Shuai Zhang, Shouchuan Li, Ye Wang, Xinming Zhang, and Feng Xue

Department of General Surgery, Qingdao Hospital of Traditional Chinese Medicine, Qingdao Hiser Hospital, Qingdao 266000, China

Correspondence should be addressed to Feng Xue; xuefeng@qdzyhospital.cn

Received 23 April 2021; Revised 25 May 2021; Accepted 26 May 2021; Published 7 June 2021

Academic Editor: Muhammad Wasim Khan

Background. Esophageal carcinoma (ESCA) is one of the malignant tumors with a high mortality rate worldwide, which seriously affects people's health. Calcium-activated chloride channel 4 (CLCA4) was reported to be a tumor inhibitor in hepatocellular carcinoma. Nevertheless, the role of CLCA4 in ESCA is still unclear. *Methods*. RT-qPCR and western blot assay were used to test the expression pattern of CLCA4 in ESCA tissues and cells. CCK-8 assay was performed to detect the effect of CLCA4 overexpression on cell proliferation in ESCA cells. Transwell assay was used to measure the effect of CLCA4 upregulation on migration and invasion abilities of ESCA cells. Animal experiments were conducted to investigate the role of CLCA4 upregulation in tumor growth in vivo. *Results*. CLCA4 was significantly reduced in ESCA tissues and correlated with *T* stage, differentiation, and lymph node metastasis. CLCA4 overexpression was found to inhibit cell proliferation, migration, invasion, and EMT progression in ESCA cells. Moreover, CLCA4 overexpression suppressed tumor growth in vivo. *Conclusion*. CLCA4 was suggested to act as a tumor inhibitor in ESCA and might be a therapeutic target gene for the treatment of patients with ESCA.

1. Introduction

Esophageal carcinoma (ESCA) is one of the common digestive tract tumors, mainly including esophageal squamous cell carcinoma and esophageal adenocarcinoma [1]. The incidence of ESCA in China is high, accounting for 46.6% of the world's ESCA patients. According to research reports, the 5-year survival rate of patients with ESCA is only 15 ~ 25% [2], which seriously affects people's health and life safety [3]. The occurrence and development of ESCA is a complex process including alcohol, smoking, dietary, multigene interaction [4, 5], and environmental factors [6]. At present, the treatment of ESCA mainly consists of surgery, radiotherapy, and chemotherapy, but the treatment effect is still not ideal, and the mortality rate is still high. Therefore, in-depth study on the pathogenesis of ESCA has become a hot topic, which provides a basis for early diagnosis, timely and effective treatment, and improving the survival rate of patients with ESCA.

The calcium-activated chloride channel (CLCA) gene family is located in the same region on chromosome p31-p22. The CLCA gene family has been reported to have a variety of functions, including cell adhesion, tumor inhibition, tumor promotion, and accessory molecules [7]. There are four kinds of CLCA regulatory proteins, namely, CLCA1, CLCA2, CLCA3, and CLCA4 [8]. CLCA1 is the first CLCA gene to be identified and cloned in human [9]. CLCA1 was reported to be closely related to the regulation of cell metastasis and immune invasion of colorectal cancer [10]. The CLCA2 gene can be used as a novel p53 inducible growth inhibitor, and downregulation can promote the proliferation of breast cancer cells [11]. CLCA3 may be involved in regulating the pathogenesis of allergic rhinitis [12]. CLCA4 has a similar cellular structure to CLCA2, and it has been found that CLCA4 plays a key role in EMT [13]. Yu et al. showed that CLCA4 was less expressed in breast cancer cells and CLCA4 downregulation promoted the proliferation of breast cancer cells and induced epithelial-mesenchymal transformation [13]. CLCA4 was found to repress cell migrated and invasive abilities by inhibiting the EMT pathway through the PI3K/AKT pathway in colorectal cancer [14]. Through a literature search, the expression and function of CLCA4 in esophageal cancer patients were not found.

In this study, through bioinformatics analysis, it was found that the expression of CLCA4 was low in esophageal cancer tissues. Moreover, the low expression of CLCA4 promoted the cell progression of esophageal cancer cells in vivo and in vitro. This study provides a theoretical basis for the development and prognosis of esophageal cancer.

2. Materials and Methods

2.1. Clinical Information. ESCA tissues and paracancerous tissues were collected from 84 patients at Qingdao Hospital of Traditional Chinese Medicine, Qingdao, Shandong, China. Among the 84 patients with ESCA (age: 36–72 years, mean: 54 years), 16 cases were female and 68 were male. All ESCA patients were diagnosed pathologically and had not received chemotherapy or radiotherapy before surgery. All patients have signed informed consent before surgery. This study was approved by the ethics committee of the Qingdao Hospital of Traditional Chines Medicine.

Inclusion criteria: ① all patients were diagnosed with ESCA by pathological biopsy; ② all patients were initially treated and had no family genetic history

Exclusion criteria: ① patients received radiotherapy, chemotherapy, or other targeted treatment before surgery; ② patients with other malignancies; and ③ patients with severe heart, liver, or renal insufficiency

2.2. Cell Culture and Cell Transfection. Esophageal epithelia cells HEEC and ESCA cell lines TE-1, Eca-109, TE-10, EC9706, and KYSE-150 were purchased from Shanghai JingKang Bioengineering CO., LTD. (Shanghai, China). All cells were cultured in the Roswell Park Memorial Institute 1640 (RPMI-1640) medium with 10% FBS at 37°C in a 5% CO_2 incubator.

Eca-109 cells and KYSE-150 cells were placed in a 6-well plate and infected with pcDNA3.1 vector or pcDNA3.1-CLCA4 vector. Cell transfection was performed by Lipofectamine 2000 according to the manufacturer's instructions. After infection for 72 h, cells were collected to detect the transfection efficiency by using RT-qPCR or for other experiments.

2.3. RT-qPCR Analysis. RT-qPCR analysis was used to detect the expression level of CLCA4 mRNA in ESCA tissues and cells. Total RNA was extracted by adding Trizol lysate. RNA concentration and purity were detected by using an ultraviolet spectrophotometer, and the RNA was stored in a −80°C refrigerator. The reaction system was configured according to the instructions of the reverse transfection kit, and the cDNA was obtained by PCR amplification. Subsequently, Ct values of each group were detected by RT-qPCR. GAPDH was used as the internal reference gene of CLCA4. The $2^{-\Delta\Delta Ct}$ method was carried out to calculate the relative mRNA expression of CLCA4. All primers were designed and synthesized by Shanghai Sangon Biological Engineering Co., Ltd. (Shanghai, China). The primer sequences used in this study were GAPDH, forward: 5′-TCCTCTGACTTCAACAGCGACAC-3′; reverse: 5′-TCTCTCTTCCTCTTGTGCTCTTGC-3′ and CLCA4 forward: 5′-TTTGGGGCTCTTACATCAGG-3′; reverse: 5′-GTGTCGTTCATCCAGGCATT-3′.

2.4. Western Blot Assay. Cells (1×10^7 cells/mL) were lysed with 100–150 μL lysate solution on ice for 1 h. Then, proteins were collected by centrifugation at low temperature and high speed. The protein concentration was determined by BCA protein quantitative assay. 30 μg protein was mixed with SDS buffer and boiled at 100°C for 5 min for denaturation. After 10% Sodium Dodecyl Sulfate Polyacrylamide Gel Electrophoresis (SDS-PAGE), proteins were transferred to the PVDF membrane. After blocked with 5% skim milk for 2 h, the membrane was incubated with the primary antibody at 37°C for 2 h. After washed with TBST solution 3 times, the membrane was incubated with the corresponding secondary antibody for 1 h. After washing with TBST solution 3 times, the protein expression of CLCA4 was detected by using the luminescence image system.

2.5. Cell Counting Kit-8 (CCK-8) Assay. Cell proliferation was measured by CCK-8 assay. 100 μL cells (1×10^5 cells/mL) were inoculated on a 96-well plate. 6 duplicate wells were set in the same detection time group. The plate was placed into an incubator (37°C and 5% CO_2). Then, 10 μL CCK-8 reagent was added to each group at 0, 24, 48, 72 h, respectively. The cells were cultured at 37°C for 1–4 h, until the color of the medium changed. The optical density of each well was measured by using a microplate analyzer at 450 nm.

2.6. Transwell Assay. ESCA cell motility was detected by Transwell assay. The frozen Matrigel was liquefied and diluted (1 mg/mL) and then added into the Transwell chamber. After incubation at 37°C for 1 h, the chamber was washed with the medium for 3 times. 100 μL cell suspensions (2.5×10^4 cells/mL) was added into the upper chamber previously uncoated with Matrigel (for the migration test) or coated with Matrigel (for the invasion test), respectively. The lower chamber was added with normal Dulbecco's Modified Eagle's Medium (DMEM) and cultured for 24 h (5% CO_2 and 37°C). The cells were absorbed, then fixed with paraformaldehyde, and stained with crystal violet. After rinsed with Phosphate Buffer Saline (PBS), the number of migrated or invaded cells was counted under a light microscope. Five fields were randomly selected to calculate the average value of each well.

2.7. Animal Experiments. The effect of CLCA4 on tumor growth in vivo was detected by the tumor xenograft model. Male BALB/C nude mice were obtained from Shanghai Slack Laboratory Anima Co., Ltd. (Shanghai, China). Eca-109 cells transfected with CLCA4 vector or vector were isolated by 0.25% trypsin and resuspended in phosphate buffered saline. Then, the cell suspension was injected into the flank of mice subcutaneously. The transplanted tumors were weighed and measured weekly. All mice were euthanized 5 weeks after

inoculation. Animal experiments were carried out in accordance with the Animal Protection Law of the People's Republic of China-2009.

2.8. Statistical Analysis. Data were analyzed by SPSS20.0 and GraphPad Prism 7.0 software. All data graphs were drawn by GraphPad Prism 7.0 software. The relationship between CLCA4 expression and clinicopathological data in patients with ESCA was determined by the rank-sum test. Differences between the two groups were detected by Student's *t*-test. $p < 0.05$ was considered statistically significant.

3. Results

3.1. CLCA4 Expression is Obviously Declined in ESCA. In order to identify the role of CLCA4 in ESCA, the expression level of CLCA4 was first tested in ESCA tissues and cells by RT-qPCR and western blot assay. RT-qPCR results indicated that CLCA4 expression was dramatically lower in ESCA tissues than in nontumor tissues (Figure 1(a)). Likewise, bioinformatics analysis displayed that CLCA4 was downregulated in ESCA tissues compared to the normal tissues (Figure 1(b)). Western blot assay showed that CLCA4 protein expression was downregulated in 69.05% (58/84) of ESCA samples (Figure 1(c)). As expected, we found that CLCA4 expression was lower in TE-1, Eca-109, TE-10, EC9706, and KYSE-150 cells than in esophageal epithelial cells HEEC (Figure 1(d)).

To evaluate the effect of CLCA4 in ESCA patients, the correlation between CLCA4 expression and clinicopathological factors in ESCA patients was analyzed. As shown in Table 1, the expression of CLCA4 was closely correlated with *T* stage ($p = 0.024$), differentiation ($p = 0.039$), and lymph node metastasis ($p = 0.048$). Inversely, CLCA4 expression was not significantly associated with tumor size ($p = 0.575$), age ($p = 0.513$), and gender ($p = 0.671$). Furthermore, univariate and multivariate logistic analyses were performed. The results displayed that CLCA4 expression was significantly related to differentiation (Table 2). Hence, our data indicated that CLCA4 was downregulated in ESCA and might be a diagnostic marker of ESCA.

3.2. CLCA4 Overexpression Inhibits Cell Viability and EMT Progression in ESCA Cells. Next, the biological function of CLCA4 on the progression of ESCA was detected. We transfected CLCA4 vector into KYSE-150 and Eca-109 cells. The transfection efficiency was detected by RT-qPCR assay. We noticed that the expression of CLCA4 was obviously elevated in KYSE-150 and Eca-109 cells after transfection with CLCA4 vector (Figure 2(a)). Then, cell proliferation of Eca-109 and KYSE-150 cells was explored by MTT assay. Overall, ESCA cell proliferation was significantly inhibited by overexpression of CLCA4 compared with the control group (Figure 2(b)). To investigate the effect of CLCA4 on EMT progression, western blot assay was carried out to detect the relative expressions of EMT-related proteins (E-cadherin, E-cadherin, and vimentin). Upregulation of E-cadherin and downregulation of vimentin and N-cadherin were detected in Eca-109 and KYSE-150 cells transfected with CLCA4 overexpression (Figure 2(c)). These findings indicated that CLCA4 might restrain cell viability and EMT progression in ESCA cells.

3.3. CLCA4 Overexpression Inhibits Cell Migration and Invasion Capabilities in ESCA Cells. Furthermore, cell migration and invasion in ESCA cells were measured by Transwell assay. In the migration experiment, after incubation in a serum-free medium for 24 h, we found that the number of migrated cells was remarkably reduced in KYSE-150and Eca-109 cells with CLCA4 vector (Figure 3(a)). Similarly, CLCA4 overexpression obviously decreased the cell invasion ability of KYSE-150 and Eca-109 cells through the basement membrane (Figure 3(b)). All data suggested that overexpression of CLCA4 might decrease the abilities of cell migration and invasion in ESCA cells.

3.4. CLCA4 Overexpression Impairs Tumorigenicity of ESCA Cells. To explore the function of CLCA4 on the tumorigenicity of ESCA cells, the tumor xenograft experiment was performed. Eca-109 cells transfected with CLCA4 vector or vector were injected into the flank of nude mice. Every 7 days, the growth conditions of the tumors were recorded. We noticed that the tumors with CLCA4 overexpression ($323.33 \pm 25.17\,mm^3$) were dramatically smaller than the control group ($460.72 \pm 36.06\,mm^3$) after 5 weeks (Figure 4(a)). After 5 weeks, all mice were euthanized, and the weight of CLCA4 vector tumors (0.68 ± 0.076 g) was dramatically smaller than in the control group (0.35 ± 0.095 g) (Figure 4(b)). Therefore, our results confirmed that the upregulation of CLCA4 inhibited tumorigenicity in ESCA cells.

4. Discussion

ESCA is one of the common malignant tumors that endanger human health. The incidence of ESCA is the tenth most common cancer worldwide, and the mortality rate of ESCA is the sixth in the world [15]. China is a region with a high incidence of ESCA, accounting for 53.7% of the global incidence of ESCA [16]. Although the incidence of ESCA has declined in recent years, the death rate remains high. In consequence, it is of great significance to further study the mechanism for early diagnosis and survival rate improvement of ESCA. Studying the pathogenesis of ESCA at the genetic level can provide some theoretical basis for the diagnosis and treatment of ESCA.

Researchers have found that multiple genes are closely related to the occurrence and development of human cancers [17]. Wang et al. reported that SPINK5 acted as a tumor suppressor by suppressing the Wnt/beta-catenin pathway in ESCA [18]. Lan et al. proved that TRPM8 facilitated cell growth and immune evasion in ESCA cells [19]. RSRC2 was proved to be a tumor inhibitor and a prognostic target gene inESCA [20]. In this article, we found that CLCA4 was obviously downregulated in ESCA tissues and cells. Simultaneously, CLCA4 expression was negatively

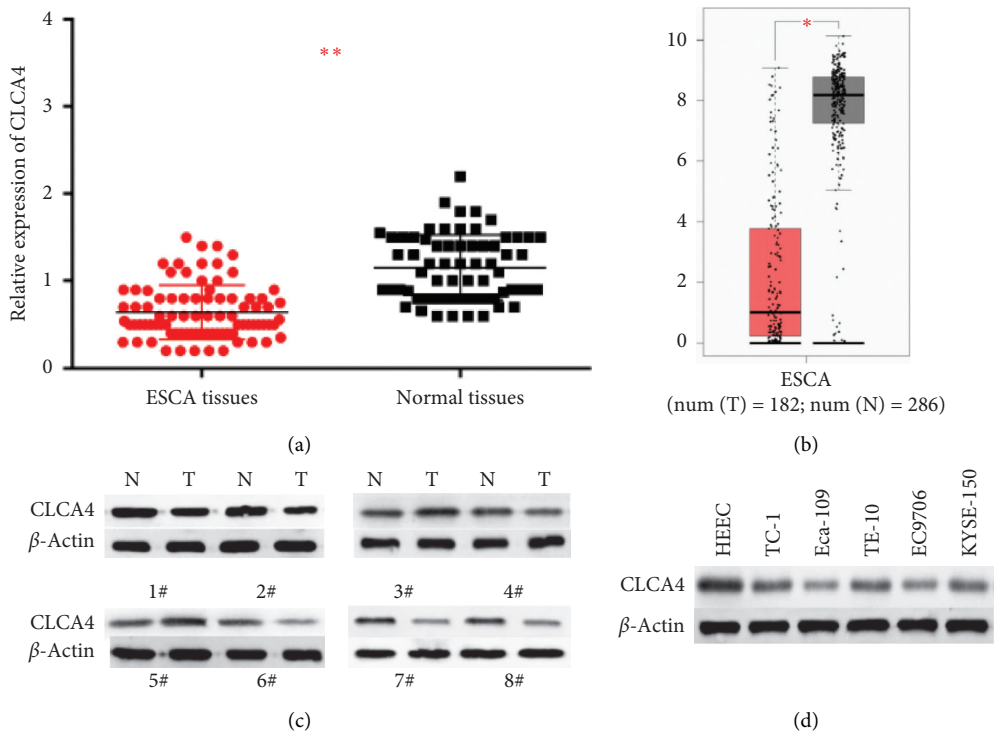

Figure 1: CLCA4 expression is obviously declined in ESCA. (a) The expression of CLCA4 in ESCA tissues was detected by RT-qPCR. (b) The GEPIA database displayed that the expression of CLCA4 was low in ESCA tissues. (c) The protein expression of CLCA4 in 8 ESCA tissues was detected by western blot. (d) The protein expression of CLCA4 in ESCA cells. $^{**}p < 0.01$.

Table 1: Association between CLCA4 expression and clinicopathological characteristics of patients with ESCA.

	Number of cases	CLCA4 expression		p value
		Low ($n = 46$)	High ($n = 38$)	
Age (years)				0.513
<60	30	15	15	
≥60	54	31	23	
Gender				0.671
Female	16	8	8	
Male	68	38	30	
Tumor size				0.757
<5 cm	56	30	26	
≥5 cm	28	16	12	
T stage				0.024*
I-II	55	35	20	
III-IV	29	11	18	
Differentiation				0.039*
Moderate/high	34	14	20	
Low	50	32	18	
Lymph node metastasis				0.048*
Present	27	19	8	
Absent	57	27	30	

* $p < 0.05$.

correlated with T stage, differentiation, and lymph node metastasis. Similar to our results, Hou et al. confirmed that CLCA4 was at a low level in bladder cancer [21]. Moreover, CLCA4 was reduced in colorectal cancer, and CLCA4 expression was associated with the overall survival rate of patients with breast cancer, stomach cancer, colorectal cancer, and head and neck cancer [22].

CLCA4 was reported to inhibited cell multiplication and metastasis by inhibiting the PI3K/AKT signaling pathway in bladder cancer [21]. CLCA4 was found to act as a tumor

Table 2: Univariate and multivariate Cox regression models for estimating the overall survival.

Variable	Univariate analysis		Multivariate analysis	
	HR (95% CI)	p value	HR (95% CI)	p value
Age (<60 vs. ≥60)	0.514 (0.347–1.647)	0.628	2.314 (1.345–3.547)	0.884
Tumor size (<5 vs. ≥5)	0.422 (0.214–0.847)	0.254	0.363 (0.094–0.921)	0.075
Gender (male vs. female)	0.647 (0.396–1.474)	0.341	0.421 (0.143–1.258)	0.069
T stage (I-II vs. III-IV)	1.671 (1.024–2.364)	0.044	0.694 (0.232–2.547)	0.055
Differentiation (moderate/high vs. low)	0.347 (0.127–0.843)	0.128	0.087 (0.029–0.647)	0.023*
Lymph node metastasis (present vs. absent)	1.694 (1.235–2.684)	0.034*	0.987 (0.348–1.874)	0.058
CLCA4 (low vs. high)	1.549 (1.146–2.647)	0.024*	1.124 (0.654–2.367)	0.018*

HR: hazard ratio; CI: confidence interval; * $p < 0.05$, ** $p < 0.01$.

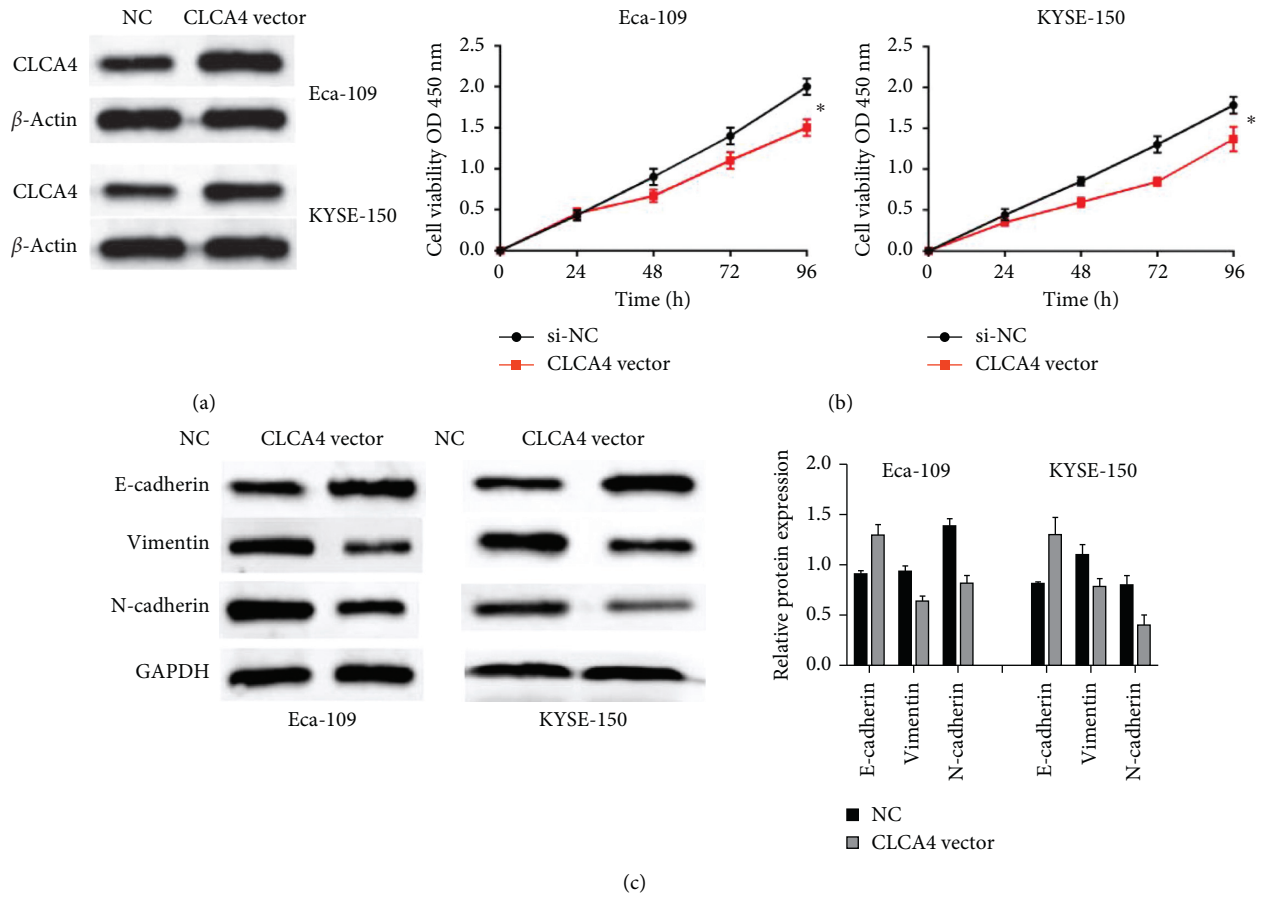

Figure 2: CLCA4 overexpression inhibits cell viability and EMT progression in ESCA cells. (a) The expression of CLCA4 in KYSE-150 and Eca-109 cells with CLCA4 vector. (b) Cell proliferation in KYSE-150 and Eca-109 cells with CLCA4 vector was detected by CCK-8 assay. (c) EMT progression in KYSE-150 and Eca-109 cells with CLCA4 vector was detected by western blot. * $p < 0.05$; ** $p < 0.01$.

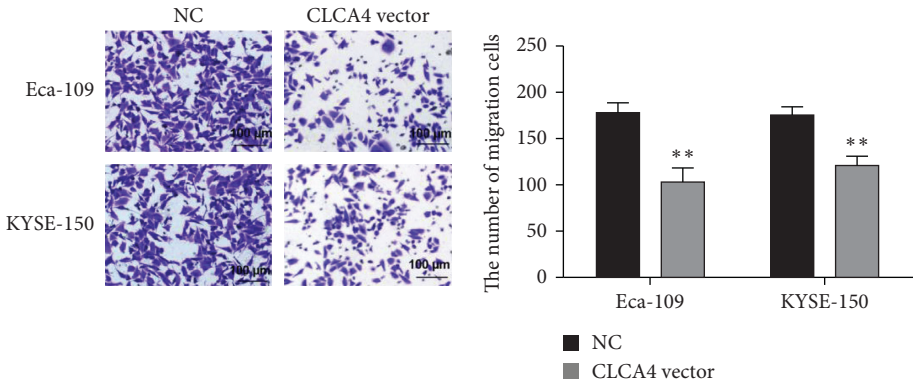

Figure 3: Continued.

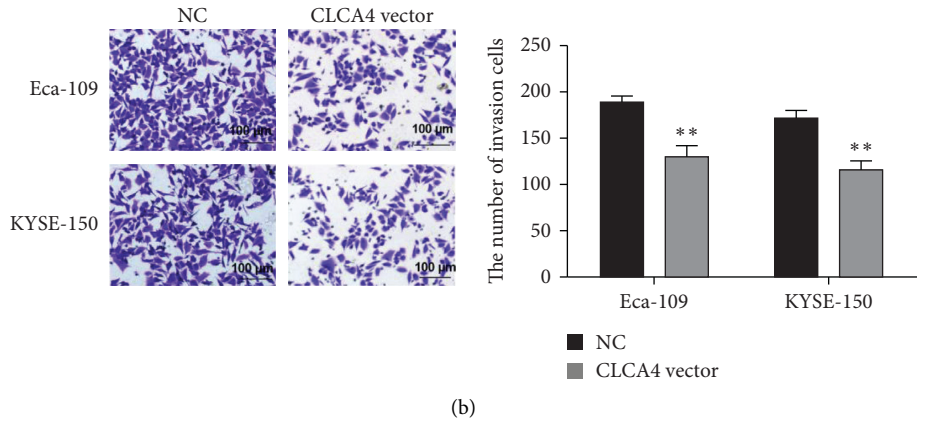

Figure 3: CLCA4 overexpression inhibits cell migration and invasion capabilities in ESCA cells. (a) Cell migration was inhibited in KYSE-150 and Eca-109 cells with CLCA4 vector (scale bar = 100 μm). (b) Cell invasion was inhibited in KYSE-150 and Eca-109 cells with CLCA4 vector (scale bar = 100 μm). $^{**}p < 0.01$.

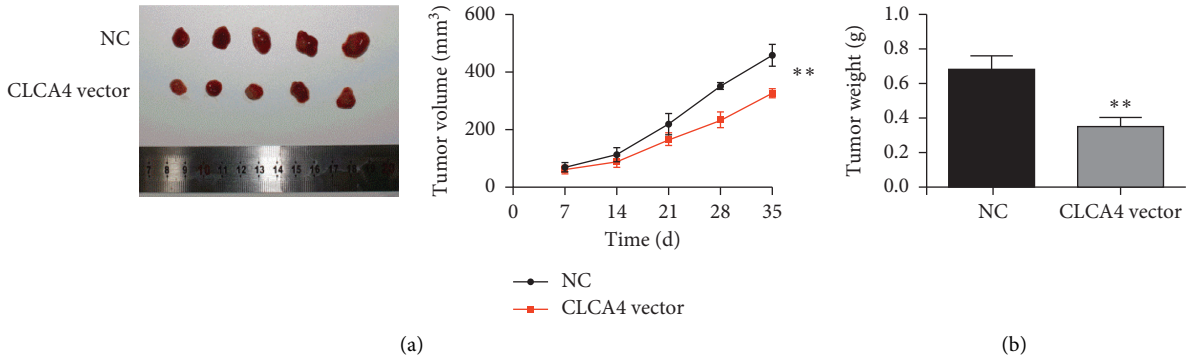

Figure 4: CLCA4 overexpression impairs tumorigenicity of ESCA cells. (a) CLCA4 overexpression suppressed tumor growth in vivo. (b) The weight of tumors with CLCA4 overexpression was dramatically smaller than in the control group. $^{**}p < 0.01$.

suppressor gene in some cancers, but its role in ESCA is still unclear. To investigate the role of CLCA4 in ESCA, the functional experiments were performed by Eca-109 and KYSE-150 cells. CCK-8 assay and Transwell assay were used to explore the effect of CLCA4 on cell proliferation, migration, and invasion abilities. We found that CLCA4 overexpression obviously suppressed cell proliferation, cell migration, cell invasion, and EMT progression in ESCA cells. Therefore, our findings confirmed that CLCA4 might block tumor growth and motility in ESCA. In line with our findings, CLCA4 was found to block cell migration and cell invasion by inhibiting the EMT pathway through the PI3K/ATK pathway in hepatocellular carcinoma [23]. CLCA4 overexpression was found to significantly decline the cell proliferation and metastasis ability in head and neck squamous cell carcinoma cells [24]. Furthermore, CLCA4 might be a target gene for primary colorectal cancer [25]. In addition, the tumor xenograft experiment was performed to detect the function of CLCA4 on the tumorigenicity in vivo. We found that both the weight and volume of tumors were significantly smaller than in the control group.

5. Conclusions

As far as we know, this is the first study to investigate the role of CLCA4 in ESCA. Our study verified that CLCA4 expression was obviously declined in ESCA tissues. Besides, the inhibitory effect of CLCA4 overexpression on cell progression in vivo and in vitro had also confirmed it. However, more studies are needed to confirm the specific mechanism of CLCA4 in ESCA. Collectively, our study confirmed that CLCA4 played a role as an antioncogene in ESCA and could provide a basis for a potential treatment approach for ESCA patients.

Data Availability

The data used to support the findings of this study are available from the corresponding author upon request.

Conflicts of Interest

The authors declare no conflicts of interest.

References

[1] Y. Zhang, "Epidemiology of esophageal cancer," *World Journal of Gastroenterology*, vol. 19, no. 34, pp. 5598–5606, 2013.

[2] R. L. Siegel, K. D. Miller, H. E. Fuchs, and A. Jemal, "Cancer statistics, 2021," *CA: A Cancer Journal for Clinicians*, vol. 71, no. 1, pp. 7–33, 2021.

[3] S. Liu, Z. Lin, J. Lin et al., "Health-related quality of life and treatment modality among esophageal squamous cell carcinoma survivors: a prospective study using time to deterioration model analysis," *Journal of Surgical Oncology*, vol. 123, no. 1, pp. 156–163, 2021.

[4] M. Tarazi, S. Chidambaram, and S. R. Markar, "Risk factors of esophageal squamous cell carcinoma beyond alcohol and smoking," *Cancers*, vol. 13, no. 5, p. 1009, 2021.

[5] T. Yu-Jing, T. Wen-Jing, and T. Biao, "Integrated analysis of hub genes and pathways in esophageal carcinoma based on NCBI's gene expression omnibus (geo) database: a bioinformatics analysis," *Medical Science Monitor*, vol. 26, Article ID e923934, 2020.

[6] M. Matejcic and M. Iqbal Parker, "Gene-environment interactions in esophageal cancer," *Critical Reviews in Clinical Laboratory Sciences*, vol. 52, no. 5, pp. 211–231, 2015.

[7] M. Abdel-Ghany, H.-C. Cheng, R. C. Elble, H. Lin, J. DiBiasio, and B. U. Pauli, "The interacting binding domains of the β4 integrin and calcium-activated chloride channels (CLCAs) in metastasis," *Journal of Biological Chemistry*, vol. 278, no. 49, pp. 49406–49416, 2003.

[8] M. Piirsoo, D. Meijer, and T. Timmusk, "Expression analysis of the CLCA gene family in mouse and human with emphasis on the nervous system," *BMC Developmental Biology*, vol. 9, no. 1, p. 10, 2009.

[9] A. D. Gruber, R. C. Elble, H.-L. Ji, K. D. Schreur, C. M. Fuller, and B. U. Pauli, "Genomic cloning, molecular characterization, and functional analysis of human CLCA1, the first human member of the family of Ca^{2+}-activated Cl^{-} channel proteins," *Genomics*, vol. 54, no. 2, pp. 200–214, 1998.

[10] F.-Z. Wei, S.-W. Mei, Z.-J. Wang et al., "Differential expression analysis revealing CLCA1 to be a prognostic and diagnostic biomarker for colorectal cancer," *Frontiers in Oncology*, vol. 10, Article ID 573295, 2020.

[11] Y. Sasaki, R. Koyama, R. Maruyama et al., "CLCA2, a target of the p53 family, negatively regulates cancer cell migration and invasion," *Cancer Biology & Therapy*, vol. 13, no. 14, pp. 1512–1521, 2012.

[12] H. Li, W. Wen, L. Cheng et al., "Expression of chloride channel protein CLC-3 in patients with allergic rhinitis," *Archives of Otolaryngology-Head & Neck Surgery*, vol. 134, no. 3, pp. 301–305, 2008.

[13] Y. Yu, V. Walia, and R. C. Elble, "Loss of CLCA4 promotes epithelial-to-mesenchymal transition in breast cancer cells," *PLoS One*, vol. 8, Article ID e83943, 2013.

[14] H. Chen, Y. Liu, C.-J. Jiang, Y.-M. Chen, H. Li, and Q.-A. Liu, "Calcium-activated chloride channel A4 (CLCA4) plays inhibitory roles in invasion and migration through suppressing epithelial-mesenchymal transition via PI3K/AKT signaling in colorectal cancer," *Medical Science Monitor*, vol. 25, pp. 4176–4185, 2019.

[15] H. Sung, J. Ferlay, R. L. Siegel et al., "Global cancer statistics 2020: GLOBOCAN estimates of incidence and mortality worldwide for 36 cancers in 185 countries," *CA: A Cancer Journal for Clinicians*, vol. 71, no. 3, pp. 209–249, 2021.

[16] F. He, J. Wang, L. Liu et al., "Esophageal cancer: trends in incidence and mortality in China from 2005 to 2015," *Cancer Medicine*, vol. 10, no. 5, pp. 1839–1847, 2021.

[17] X. Wang, Y. Zhang, Z.-G. Han, and K.-Y. He, "Malignancy of cancers and synthetic lethal interactions associated with mutations of cancer driver genes," *Medicine*, vol. 95, no. 8, p. e2697, 2016.

[18] Q. Wang, Q. Lv, H. Bian et al., "A novel tumor suppressor SPINK5 targets Wnt/β-catenin signaling pathway in esophageal cancer," *Cancer Medicine*, vol. 8, no. 5, pp. 2360–2371, 2019.

[19] X. Lan, J. Zhao, C. Song, Q. Yuan, and X. Liu, "TRPM8 facilitates proliferation and immune evasion of esophageal cancer cells," *Bioscience Reports*, vol. 39, no. 10, 2019.

[20] H. Kurehara, H. Ishiguro, M. Kimura et al., "A novel gene, RSRC2, inhibits cell proliferation and affects survival in esophageal cancer patients," *International Journal of Oncology*, vol. 30, no. 2, pp. 421–428, 2007.

[21] T. Hou, L. Zhou, L. Wang, G. Kazobinka, X. Zhang, and Z. Chen, "CLCA4 inhibits bladder cancer cell proliferation, migration, and invasion by suppressing the PI3K/AKT pathway," *Oncotarget*, vol. 8, no. 54, pp. 93001–93013, 2017.

[22] L. Wei, W. Chen, J. Zhao, Y. Fang, and J. Lin, "Down-regulation of CLCA4 expression is associated with the development and progression of colorectal cancer," *Oncology Letters*, vol. 20, no. 1, pp. 631–638, 2020.

[23] Z. Liu, M. Chen, L.-K. Xie et al., "CLCA4 inhibits cell proliferation and invasion of hepatocellular carcinoma by suppressing epithelial-mesenchymal transition via PI3K/AKT signaling," *Aging*, vol. 10, no. 10, pp. 2570–2584, 2018.

[24] B. Li, Y.-P. Jiang, J. Zhu, and L. Meng, "MiR-501-5p acts as an energetic regulator in head and neck squamous cell carcinoma cells growth and aggressiveness via reducing CLCA4," *Molecular Biology Reports*, vol. 47, no. 3, pp. 2181–2187, 2020.

[25] J. Han, X. Zhang, Y. Liu, L. Jing, Y.-B. Liu, and L. Feng, "CLCA4 and MS4A12 as the significant gene biomarkers of primary colorectal cancer," *Bioscience Reports*, vol. 40, no. 8, 2020.

Hindawi
Journal of Oncology
Volume 2021, Article ID 9919494, 10 pages
https://doi.org/10.1155/2021/9919494

Research Article

CXCL5/NF-κB Pathway as a Therapeutic Target in Hepatocellular Carcinoma Treatment

Xingqing Jia,[1] **Shuangqin Wei**,[1] **and Wujun Xiong**[2]

[1]*Department of Hepatology, Shanghai East Hospital, Tongji University School of Medicine, Shanghai 201399, China*
[2]*Department of Gastroenterology, Shanghai Pudong Hospital, Fudan University Pudong Medical Center, Shanghai 201399, China*

Correspondence should be addressed to Wujun Xiong; xiongwujun@shpdh.cn

Received 2 April 2021; Revised 8 May 2021; Accepted 21 May 2021; Published 31 May 2021

Academic Editor: Muhammad Wasim Khan

Background. Hepatocellular carcinoma (HCC) is a common malignant cancer worldwide. CXCL5 has a role in inhibiting cell viability and metastasis in many tumors. In the present study, we investigated the role of CXCL5 in HCC and explored the underlying mechanism. *Material and Methods*. RT-qPCR and western blot were performed to evaluate the mRNA and protein levels of CXCL5. CCK-8 and transwell assay were applied to measure the proliferative and invasive abilities. Meanwhile, the Kaplan–Meier method was used to assess the survival of HCC patients. *Results*. CXCL5 was upregulated in HCC tissues, which predicted a shorter overall survival in HCC. CXCL5 was a target gene of miR-577, and its expression was mediated by miR-577 in HCC. Knockdown of CXCL5 suppressed HuH-7 cell proliferation, invasion, and EMT and inhibited the NF-κB signaling pathway in cells. Moreover, knockdown of CXCL5 inhibited the xenograft growth of HuH-7 cells. *Conclusion*. Overexpression of CXCL5 predicts poor prognosis in HCC patients. Knockdown of CXCL5 inhibits cell proliferation and invasion through the NF-κB signaling pathway in HCC. The newly identified role of the CXCL5/miR-577/NF-κB axis provides novel insights into the targeted therapy of HCC.

1. Introduction

Hepatocellular carcinoma (HCC) is a major cause of cancer death, especially in Africa and Asia [1, 2]. Due to the hepatitis C virus epidemic, the incidence of HCC is increasing in Western countries [3]. The current treatment for HCC is limited to surgical resection, but resection results in a recurrence rate of more than 70% within 5 years, while about 80% are not suitable for surgery [4]. Therefore, it is urgent to explore potential biomarkers for the treatment.

C-X-C motif chemokine ligand 5 (CXCL5), known as ENA-78 or SCYB5, is a member of the CXC subfamily of chemokines; it binds the G-protein-coupled receptor chemokine (C-X-C motif) receptor-2 to recruit neutrophils, to promote angiogenesis and to remodel connective tissues [5]. CXCL5 was thought to play roles in cell proliferation, migration, and invasion of cancer [6, 7]. CXCL5 citrullination may exert inflammatory properties by recruiting monocytes to inflamed joint tissue in a mouse model of inflammatory arthritis [8]. CXCL5 acted as an important angiogenic factor in idiopathic pulmonary fibrosis and non-small-cell lung cancer [9, 10]. CXCL5 was involved in the interaction between cholangiocarcinoma cells and cancer-associated fibroblasts and inhibition of tumor-stromal interactions [7]. However, few studies have elucidated the roles of CXCL5 in HCC. Thus, the experiments were performed to explore the vital functions of CXCL5 in HCC.

The discovery of microRNAs (miRNAs) initiates a new generation of cognition in HCC [11, 12]. miRNAs negatively mediate gene expression through translational repression or mRNA degradation to be involved in tumor development [13]. According to a few reports, several miRNAs, including miR-122, miR-325, miR-206, miR-122, and miR-224 played crucial roles in HCC [14–17]. miR-577 acts as a tumor suppressor to suppress tumor growth and enhances chemosensitivity in colorectal cancer [18]. According to a

previous study, miR-577 regulated cell proliferation and promoted G1-S phase transition in esophageal squamous cell carcinoma [19]. Similarly, miR-577 inhibited pancreatic β-cell function and survival in pediatric diabetes [20]. Wang et al. reported that, in non-small-cell lung cancer, miR-577 suppressed cell growth and EMT in regulating WNT2B via the Wnt/β-catenin pathway [21]. We observed that CXCL5 promoted HCC growth, cell invasion, the EMT, and the NF-κB pathway in HCC. The expression of CXCL5 was regulated by miR-577 via directly targeting its 3'-UTR of mRNA.

2. Materials and Methods

2.1. Clinical Specimens. Pairs of HCC tissues and adjacent tissues were collected from 48 HCC patients at Shanghai East Hospital affiliated to Tongji University School of Medicine, Shanghai, China, from January 2016 to February 2021. Specimens were immediately frozen in liquid nitrogen and then stored at −80°C after surgery. All patients provided written informed consent, and the ethics committee of Shanghai East Hospital affiliated to Tongji University School of Medicine approved this study.

2.2. Cell Culture. HCC cells HuH-7 and a normal hepatocyte cell L-02 were purchased from the American Type Culture Collection (ATCC; Rockville, MD, USA). All cells were incubated in the DMEM medium (Invitrogen, Carlsbad, CA, USA) with 10% FBS (Sigma-Aldrich, Louis, MO, USA) at 37°C in a humidified chamber with 5 % CO_2.

2.3. Transfection. The specific plasmids of shRNA-CXCL5 and their negative control were designed and synthesized at Gene-Pharma (Shanghai, China). HuH-7 cells were transfected and incubated in a 6-well plate. The Lipofectamine 2000 Reagent (Invitrogen, USA) diluted using an Opti-MEM/Reduced serum medium (Thermo Scientific, Shanghai, China) was used to perform the transfection. Geneticin (G418; Thermo Scientific, Shanghai, China) was used to select the stable transfection cells, while the transient transfection cells were harvested after transfected for 48 h.

2.4. Quantitative Real-Time PCR. The TRIzol Reagent (Invitrogen) and miRNeasy Mini Kit (Qiagen, Hilden, Germany) were employed to extract total mRNAs and miRNAs from tissues or cells. The Omniscript Reverse Transcription Kit (Qiagen) and TaqMan miRNA Reverse Transcription Kit (Applied Biosystems, Foster City, CA, USA) were used for synthesizing the first cDNA chain; the QuantiTect SYBR Green PCR Kit (Qiagen) and miRNA-specific TaqMan miRNA Assay Kit (Applied Biosystems) were used to carry out the qPCR in a Quantitect SYBR green PCR system (Qiagen). The relative levels of mRNA and miRNA were derived using a $2^{-\Delta\Delta Ct}$ method, and the GAPDH and U6 small nuclear RNA were utilized for normalization. The primers used for RT-qPCR were as follows: CXCL5 forward 5'-AGCTGCGTTGCGTTTGTTTAC-3', reverse 5'-TGGCGAACACTTGCAGATTAC-3'; GAPDH forward 5'-AAGGTGAAGGTCGGAGTCAA-3', reverse 5'-AATGAAGGGGTCATTGATGG-3'; miR-577 forward 5'-TGCGGTAGATAAAATATTGG-3', reverse 5'-GTGCAGGGTCCGAGGT-3'; and U6 forward 5'-GCTTCGGCAGCACATATACTAAAAT-3', reverse 5'-CGCTTCACGAATTTGCGTGTCAT-3'.

2.5. Western Blot Analysis. The total proteins were lysed by RIPA Lysis Buffer (Sigma, USA) containing 10% PMSF (Sigma). SDS-PAGE was applied to separate the protein, and then, the blots were electrotransferred to PVDF membranes (Millipore, USA). After being blocked by 5% fat-free milk at room temperature for 1 h, the membranes were incubated with primary antibodies, such as CXCL5 (1 : 1000; Abcam, Cambridge, USA), E-cadherin (1 : 1000; Abcam), N-cadherin (1 : 1000; Abcam), Vimentin (1 : 1000; Abcam), p-P65 (1 : 1000, Abcam), and P65 (1 : 1000, Abcam). Next, the blots were incubated by a secondary anti-rabbit HRP-conjugated antibody (Cell Signaling). The protein signals were captured using an Enhanced Chemiluminescence Detection Kit (ECL, Pharmacia Biotech, Arlington, USA).

2.6. MTT Assay. The HuH-7 cells were plated into 96-well plates and cultivated for 24-, 48-, 72-, and 96 h. Total 20 μl of MTT (5 mg/ml, Sigma) was added into each well for 6 h of incubation. Next, the supernatant was discarded and 100 μl of DMSO (Sigma) was added to each well. After agitating for 10 min, the absorbance at a wavelength of 570 nm was evaluated using an ELISA reader (Bio-Rad, Hercules, CA, USA).

2.7. Transwell Assay. The transwell insert (8 μm membrane, Corning, Cambridge, MA) was placed in a 24-well plate to evaluate the cell invasive ability. The HuH-7 cells were suspended by the FBS-free RPMI-1640 medium and 200 μl was added in the upper chamber, whereas the lower chamber was filled with 500 μl medium containing 15% FBS, which acted as an inducer. After the cells were incubated for 24 h at 37°C, the noninvasive cells on the upper surface were removed by using cotton swabs. The invasive cells were fixed and stained using 4% paraformaldehyde and 10% crystal violet, respectively, and the cells were counted under a microscope (Olympus Corporation, Tokyo, Japan).

2.8. miRNA Target Prediction and Dual-Luciferase Reporter Assay. TargetScan was used to perform the prediction of target genes of miR-577, and we discovered that CXCL5 was one of the potential target genes. The binding sequence of UUUAUCU and AAAUAGA was mutated to confirm that miR-577 could not bind to the 3-UTR of CXCL5 mRNA in HCC cells. The wild type and the mutational 3'-UTR of CXCL5 were inserted into the dual-luciferase reporter vectors, which were named WT or MUT. The Lipofectamine 2000 Reagent (Invitrogen, USA) was used to cotransfect miR-577 mimic and WT or MUT vector into HuH-7 cells. Finally, the luciferase activity was measured using a dual-luciferase reporter assay system (Promega, USA).

2.9. Xenograft Assay in Nude Mice. All animal procedures were performed in accordance with protocols approved by the Institute Research Ethics Committee at Shanghai East Hospital affiliated to Tongji University School of Medicine, Shanghai, China. For the xenograft assay, 2×10^6 HuH-7 cells transfected with shRNA-CXCL5 or negative control were subcutaneously injected into the left armpit of 5-week-old BALB/C nude mice. Tumor volumes and body weights were measured every 3 days, and tumor volumes were calculated using the formula volume = 0.5 × tumor length- × tumor width^2. After 26 days, CO^2 was utilized for lethal anesthesia in mice; then, the weights of tumor were measured.

2.10. Statistical Analysis. All the statistical analyses were performed using SPSS 16.0 software (IBM, Armonk, NY, USA), and the data were presented as mean ± SD. Student's t test was performed to compare the differences between two groups; besides, one-way ANOVA was utilized to compare the differences between three or more groups. The association between CXCL5 expression and the overall survival for HCC patients was assessed by the Kaplan–Meier curve and log-rank test. $P < 0.05$ was considered to be statistically significant.

3. Results

3.1. Upregulation of CXCL5 Predicts Poor Prognosis of HCC Patients. The expression of CXCL5 in HCC tissues and normal tissues was detected in the GEPIA database; although the expression of CXCL5 has no significance in HCC tissues than in normal tissues (Figure 1(a)), we observed that the overexpression of CXCL5 in HCC patients predicted poor prognosis ($P < 0.05$) (Figure 1(b)). In this study, the mRNA level of CXCL5 was assessed in 48 pairs of HCC and adjacent normal tissue, and we found that the expression of CXCL5 was overexpressed in HCC tissues as compared to adjacent normal tissue ($P < 0.05$) (Figure 1(c)). The Kaplan–Meier method elucidated that the expression of CXCL5 was associated with poor overall survival of HCC patients ($P = 0.0208$) (Figure 1(d)).

3.2. Knockdown of CXCL5 Inhibits Cell Invasion, the EMT, and the NF-κB Signal Pathway in HuH-7 Cells. The expressions of CXCL5 were evaluated in HCC cells HuH-7 and a hepatocyte cell L-02. Moreover, we found that the expression of CXCL5 was lower in L-02 cells than that in HuH-7 cells ($P < 0.01$) (Figure 2(a)). To assess the roles of CXCL5, shRNA-CXCL5 was employed to downregulate CXCL5 in HuH-7 cells, and the transfection efficiency was calculated by RT-qPCR (Figure 2(b)). Transwell assay was utilized to measure the invasive ability after changing the expression of CXCL5 in HuH-7 cells, and we found that transfection of shRNA-CXCL5 enhanced the invasive ability ($P < 0.05$) (Figure 2(c)).

Moreover, the levels of EMT and pathway-associated proteins were assessed by western blot in HuH-7 cells. We found that knockdown of CXCL5 elevated the expression of E-cadherin, while suppressing N-cadherin and Vimentin expression in HuH-7 cells (Figure 2(d)), which suggested that knockdown of the CXCL5 suppressed the EMT. In addition, knockdown of CXCL5 inhibited the expression of P65 and p-P65 in HuH-7 cells (Figure 2(e)), which proved that knockdown of the CXCL5 inhibited the activation of the NF-κB pathway. All the results revealed that knockdown of CXCL5 inhibited cell invasion, the EMT, and the NF-κB signaling pathway.

3.3. Knockdown of CXCL5 Suppresses the Growth of HCC In Vitro and In Vivo. MTT assay was used to measure cell proliferation after knocking down CXCL5 in HuH-7 cells, and the results illuminated that transfection of shRNA-CXCL5 inhibited cell proliferative ability ($P < 0.05$) (Figure 3(a)). To further explore the functions of CXCL5 *in vivo*, HuH-7 cells transfected with shRNA-CXCL5 were used to perform tumor formation in nude mice. The HuH-7 cells that stably transfected shRNA-CXCL5 or control plasmid were subcutaneously injected into the nude mice. The volumes of xenograft tumors were measured every 3 days, and the group of transfecting shRNA-CXCL5 had a lower growth rate than the control group, which indicated that silencing of CXCL5 inhibited the HCC growth *in vivo* (Figure 3(b)). After 26 days, the nude mice were sacrificed. The weights of xenograft were calculated, and the tumor weights of the CXCL5 knockdown group were lower than that of the control group ($P < 0.05$) (Figure 3(c)), whereas the body weights were not significant between the CXCL5 knockdown group and control group (Figure 3(d)). The morphology of the xenograft is shown in Figure 3(e). All the findings indicated that silencing of CXCL5 inhibited the growth of HCC *in vitro* and *in vivo*.

3.4. CXCL5 Is a Target Gene of miR-577. CXCL5 was predicted to be a target gene of miR-577 using TargetScan, and the binding site was located at 249 to 255 on the 3'-UTR of CXCL5 mRNA. The potential binding sites were mutated to validate whether miR-577 directly binds to the potential binding site of CXCL5 (Figure 4(a)). Furthermore, the luciferase reporter assay results proved that miR-577 reduced the luciferase activity of HuH-7 cells that were transfected with wild-type CXCL5 3'-UTR ($P < 0.05$); however, it makes no difference on the luciferase activity of cells transfected with mutated CXCL5 3'-UTR ($P > 0.05$) (Figure 4(b)). RT-qPCR was employed to assess the expression of miR-577 in tissues and cells. Moreover, we found that the expression of miR-577 in HCC tissues was lower than that in peritumoral normal tissues ($P < 0.05$) (Figure 4(c)). Correlation analysis showed that the expression of CXCL5 was negatively correlated with miR-577 in tissues (Figure 4(d)). Similarly, miR-577 was less expressed in the HCC cell line HuH-7 compared with the hepatocyte cell line L-02 ($P < 0.05$) (Figure 4(e)). Moreover, the mRNA levels of CXCL5 were evaluated after transfecting miR-577 mimic in HuH-7 cells, and it showed that overexpression of miR-577 inhibited the expression of CXCL5 in HuH-7 cells ($P < 0.05$) (Figure 4(f)). All the results indicated that miR-577 regulated the expression of CXCL5 via directly targeting its 3'-UTR of mRNA in HCC cells HuH-7.

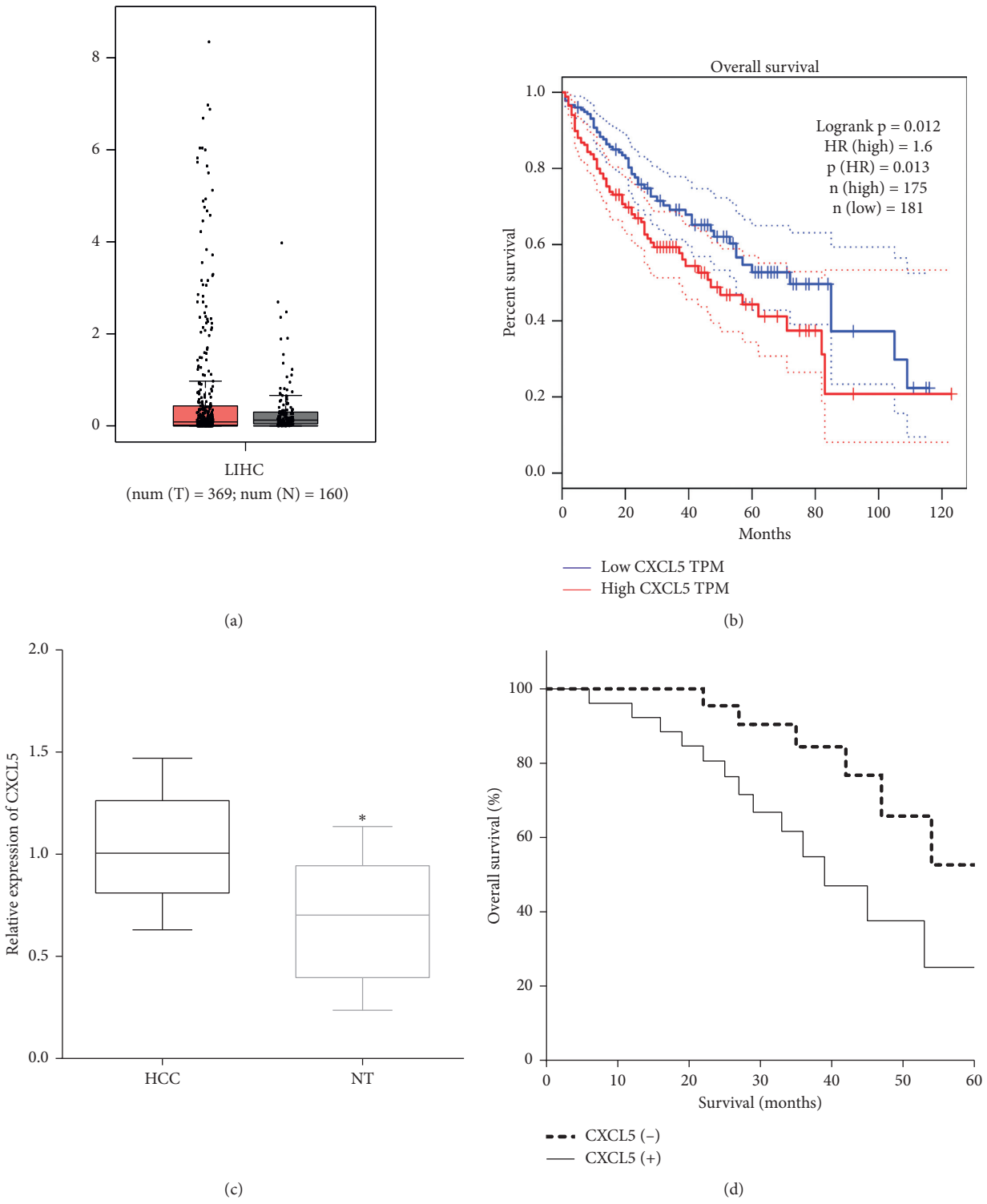

Figure 1: Upregulation of CXCL5 predicts poor prognosis of HCC. (a) The expression of CXCL5 in HCC tissues and normal tissues was detected in the GEPIA database. T: tumor tissues; N: normal tissues. (b) The GEPIA database showed that overexpression of CXCL5 predicted poor prognosis. (c) CXCL5 was less expressed in HCC tissues versus the corresponding peritumoral normal tissues vs. HCC, $^{*}P < 0.05$. (d) Upregulation of CXCL5 was associated with a poor 5-year survival of HCC patients.

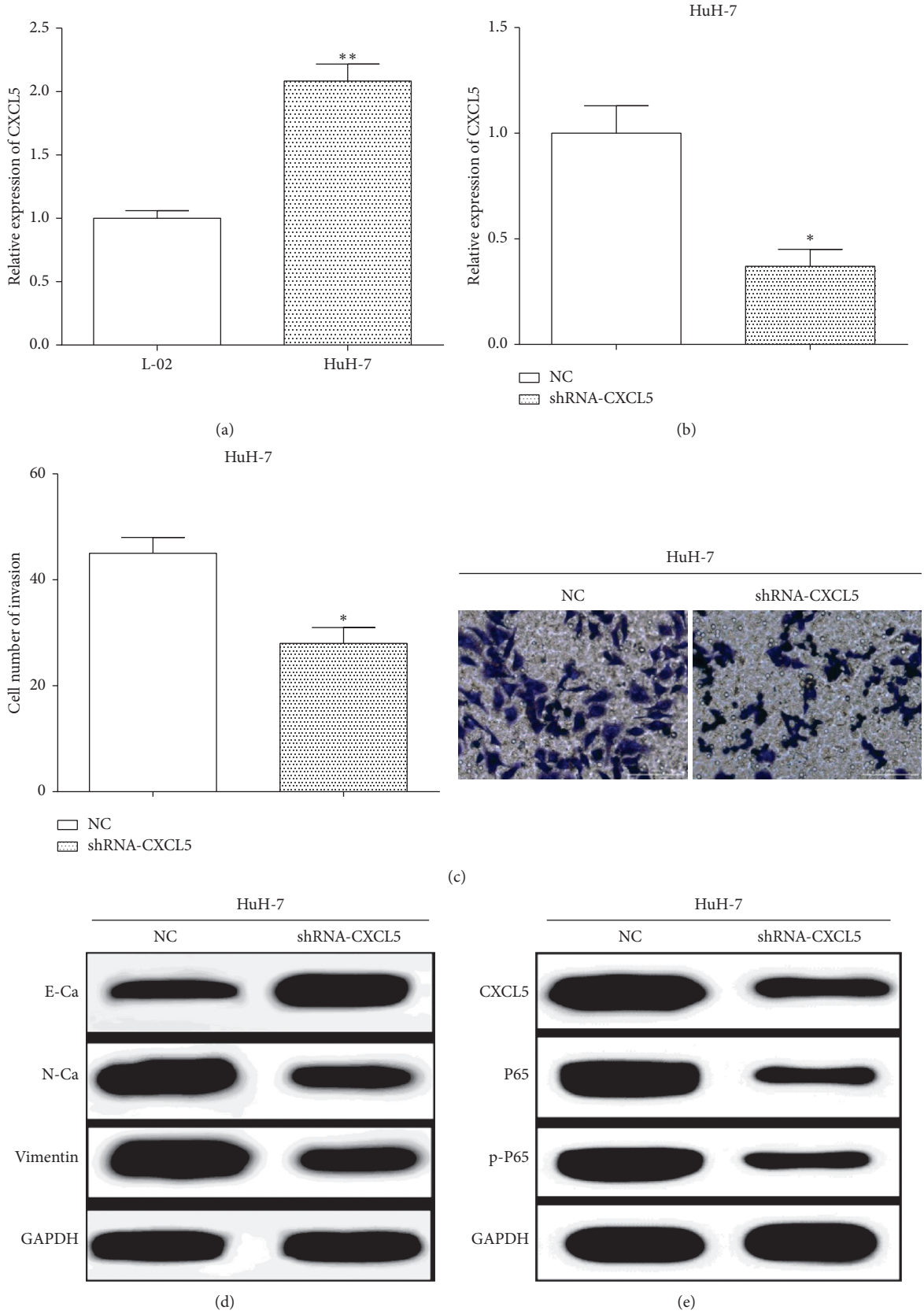

Figure 2: Knockdown of CXCL5 inhibits cell invasion, the EMT, and the NF-κB signal pathway in HuH-7 cells. (a) The expressions of CXCL5 in L-02 and HuH-7 cells were measured vs. L-02, $^{**}P < 0.01$. (b) The transfection efficiency of transfecting shRNA-CXCL5 in HuH-7 cells was calculated by RT-qPCR vs. NC group, $^{*}P < 0.05$. (c) The invasive ability after changing the expression of CXCL5 in HuH-7 cells was measured vs. NC, $^{*}P < 0.05$. (d) The levels of EMT-associated proteins were assessed by western blot in HuH-7 cells. (e) The expressions of P65 and p-P65 in HuH-7 cells were calculated in HuH-7 cells.

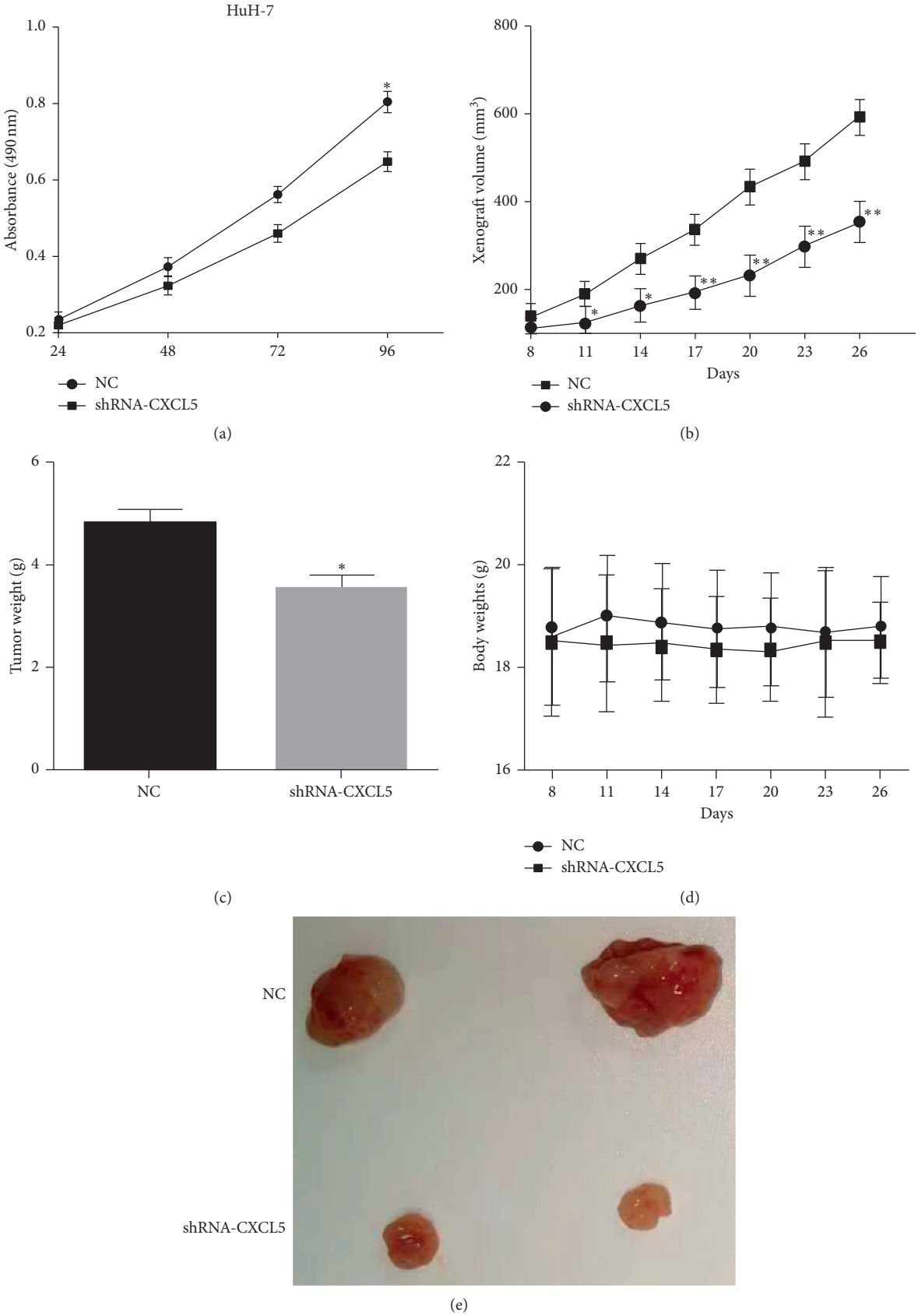

Figure 3: Knockdown of CXCL5 suppresses the growth of HCC *in vitro* and *in vivo*. (a) MTT assay was used to measure cell proliferation after silencing CXCL5 in HuH-7 cells vs. NC, $^{*}P < 0.05$. (b) The volumes of xenograft tumors were measured every 3 days in the group of transfecting shRNA-CXCL5 and the control group vs. NC, $^{*}P < 0.05$. (c) The weights of xenograft were calculated in the shRNA-CXCL5 and control group. vs. NC, $^{*}P < 0.05$. (d) The body weights of mice were measured in the shRNA-CXCL5 and control group. (e) The picture of the tumor in the shRNA-CXCL5 and control group.

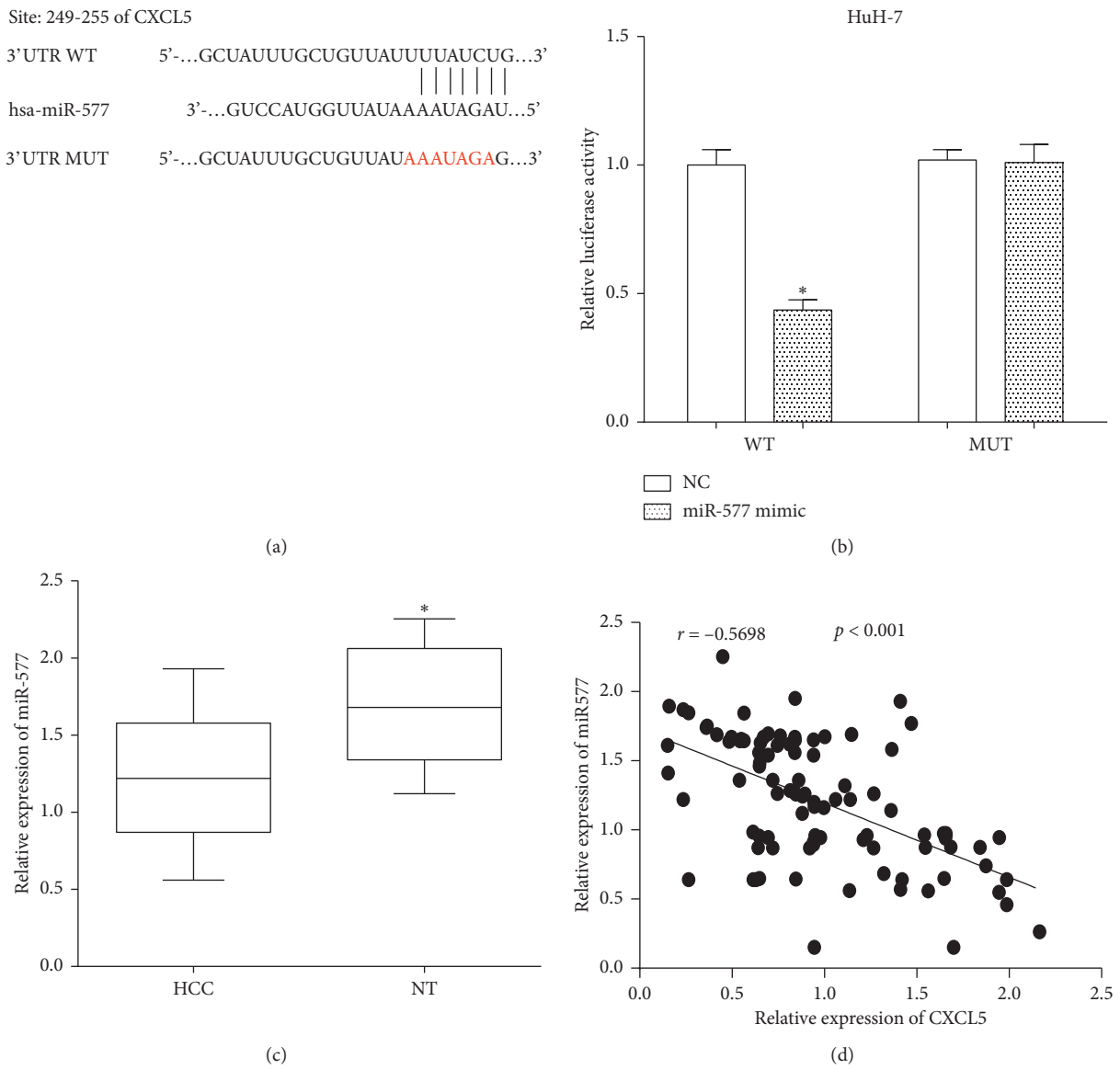

Figure 4: Continued.

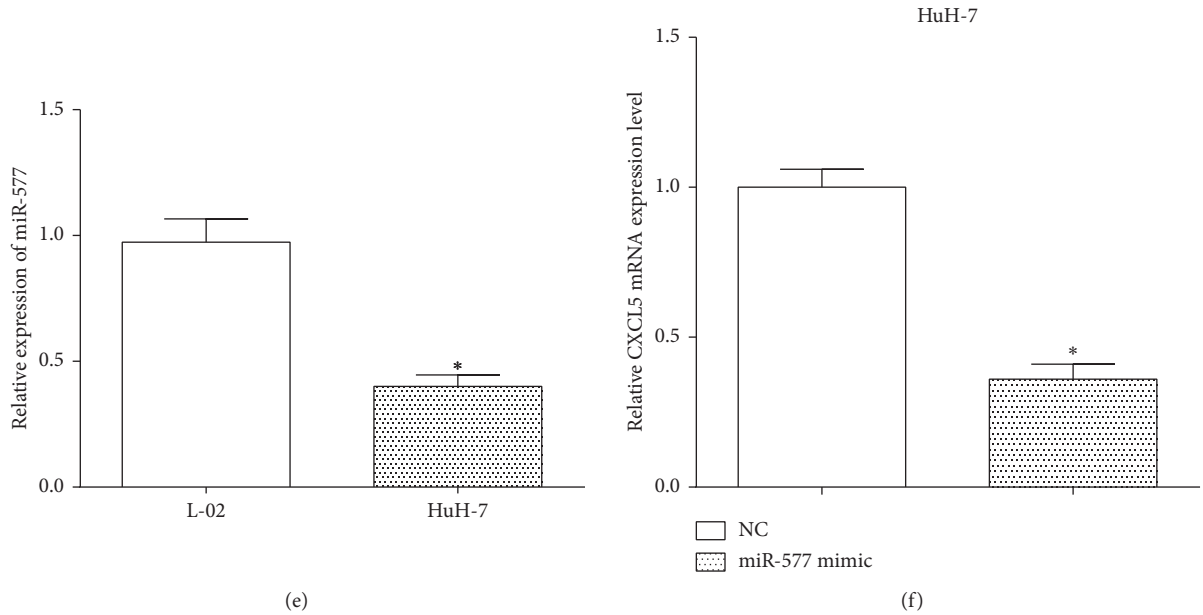

Figure 4: CXCL5 is a target gene of miR-577. (a) CXCL5 was predicted to be a target gene of miR-577 using TargetScan. (b) The luciferase activity was calculated using the luciferase reporter assay vs. NC, $^*P < 0.05$. (c) RT-qPCR was employed to assess the expression of miR-577 in tissues vs. HCC, $^*P < 0.05$. (d) The correlation analysis between CXCL5 and mir-577 in tissues. (e) The expression of miR-577 was measured in the HCC cell line HuH-7 and hepatocyte cell line L-02 vs. L-02, $^*P < 0.05$. (f) The mRNA levels of CXCL5 were evaluated after transfecting miR-577 mimic in HuH-7 cells vs. NC, $^*P < 0.05$.

4. Discussion

HCC is one of the most common causes of cancer-related deaths worldwide, with a lower 5-year survival rate [22, 23]. However, the molecular mechanisms involved in HCC remain poorly understood.

CXCL5 acts as an oncogene and enhances cell growth and metastasis in several tumors, including bladder cancer, pancreatic cancer, cervical cancer, and cutaneous melanoma [24–27]. Previous studies reported that CXCL5 was overexpressed in the intestinal epithelium in inflammatory bowel disease and also in malignant pancreatic diseases [28, 29]. CXCL5 directly enhances tumor cell survival and proliferation in gastric cancer [30]. Consistent with the previous studies, we observed that CXCL5 was upregulated in HCC tissues compared to the normal tissues. Overexpression of CXCL5 was associated with the poor prognosis of HCC patients. Consistent with all the findings, we proposed that CXCL5 was upregulated in the HCC cell line HuH-7 compared with the normal cell line L-02. Moreover, knockdown of CXCL5 inhibited cell invasiveness and the EMT abilities in the HCC line HuH-7. In colorectal cancer, CXCL5 promoted tumor angiogenesis via the AKT/NF-κB pathway [31]. We also revealed that knockdown of CXCL5 inhibited the NF-κB signaling pathway.

Numerous studies have shown that miRNAs were associated with translational repression and mRNA degradation at the posttranscriptional level [32, 33]. Xue et al. reported that miR-577 acted as a tumor suppressor to inhibit cell proliferation, migration, and invasion in papillary thyroid carcinoma [34]. Several reports showed that MiR-577 suppressed metastasis and EMT of breast cancer [35]. In addition, miR-577 suppressed tumor growth of HCC, which was consistent with the findings in glioblastoma [36]. It is the first time to propose that CXCL5 was a target gene of miR-577 in HCC.

5. Conclusions

Overexpression of CXCL5 predicts poor prognosis in HCC patients. Also, knockdown of CXCL5 impaired cell invasion and EMT via the NF-κB signaling pathway in HuH-7 cells. CXCL5 was a target gene of miR-577, and its expression was regulated by miR-577 in HCC. The newly identified role of the CXCL5/miR-577/NF-κB axis provides novel insights into the targeted therapy of HCC.

Data Availability

The data used to support the findings of this study are available from the corresponding author upon request.

Conflicts of Interest

The authors declare that they have no conflicts of interest.

Acknowledgments

The authors thank Dr. Lirui Tu and Dr. Jing Liu for helpful conversations and Dr. Wei Li, Dr. Xiuguang Song, and Dr. Hongwei Xu for assistance with the samples.

References

[1] F. X. Bosch, J. Ribes, M. Díaz, and R. Cléries, "Primary liver cancer: worldwide incidence and trends," *Gastroenterology*, vol. 127, no. 5 Suppl 1, pp. S5–S16, 2004.

[2] J. D. Yang and L. R. Roberts, "Epidemiology and management of hepatocellular carcinoma," *Infectious Disease Clinics of North America*, vol. 24, no. 4, pp. 899–919, 2010.

[3] H. B. El-Serag, J. A. Davila, N. J. Petersen, and K. A. McGlynn, "The continuing increase in the incidence of hepatocellular carcinoma in the United States: an update," *Annals of Internal Medicine*, vol. 139, no. 10, pp. 817–823, 2003.

[4] H. Imamura, Y. Matsuyama, E. Tanaka et al., "Risk factors contributing to early and late phase intrahepatic recurrence of hepatocellular carcinoma after hepatectomy," *Journal of Hepatology*, vol. 38, no. 2, pp. 200–207, 2003.

[5] B.-C. Lee and J. Lee, "Cellular and molecular players in adipose tissue inflammation in the development of obesity-induced insulin resistance," *Biochimica et Biophysica Acta (BBA) - Molecular Basis of Disease*, vol. 1842, no. 3, pp. 446–462, 2014.

[6] M. Kawamura, Y. Toiyama, K. Tanaka et al., "CXCL5, a promoter of cell proliferation, migration and invasion, is a novel serum prognostic marker in patients with colorectal cancer," *European Journal of Cancer*, vol. 48, no. 14, pp. 2244–2251, 2012.

[7] H. Okabe, T. Beppu, M. Ueda et al., "Identification of CXCL5/ENA-78 as a factor involved in the interaction between cholangiocarcinoma cells and cancer-associated fibroblasts," *International Journal of Cancer*, vol. 131, no. 10, pp. 2234–2241, 2012.

[8] K. Yoshida, O. Korchynskyi, P. P. Tak et al., "Citrullination of epithelial neutrophil-activating peptide 78/CXCL5 results in conversion from a non-monocyte-recruiting chemokine to a monocyte-recruiting chemokine," *Arthritis & Rheumatology*, vol. 66, no. 10, pp. 2716–2727, 2014.

[9] M. P. Keane, J. A. Belperio, M. D. Burdick, J. P. Lynch, M. C. Fishbein, and R. M. Strieter, "ENA-78 is an important angiogenic factor in idiopathic pulmonary fibrosis," *American Journal of Respiratory and Critical Care Medicine*, vol. 164, no. 12, pp. 2239–2242, 2001.

[10] D. A. Arenberg, M. P. Keane, B. DiGiovine et al., "Epithelial-neutrophil activating peptide (ENA-78) is an important angiogenic factor in non-small cell lung cancer," *Journal of Clinical Investigation*, vol. 102, no. 3, pp. 465–472, 1998.

[11] B. Mao and G. Wang, "MicroRNAs involved with hepatocellular carcinoma (Review)," *Oncology Reports*, vol. 34, no. 6, pp. 2811–2820, 2015.

[12] E. Chen, X. Xu, R. Liu, and T. Liu, "Small but heavy role: MicroRNAs in hepatocellular carcinoma progression," *BioMed Research International*, vol. 2018, Article ID 6784607, 2018.

[13] G. Meister, "miRNAs get an early start on translational silencing," *Cell*, vol. 131, no. 1, pp. 25–28, 2007.

[14] C. Turato, F. Fornari, D. Pollutri et al., "MiR-122 targets SerpinB3 and is involved in sorafenib resistance in hepatocellular carcinoma," *Journal of Clinical Medicine*, vol. 8, no. 2, p. 171, 2019.

[15] Z. Zhang, Y. Han, G. Sun, X. Liu, X. Jia, and X. Yu, "MicroRNA-325-3p inhibits cell proliferation and induces apoptosis in hepatitis B virus-related hepatocellular carcinoma by down-regulation of aquaporin 5," *Cellular & Molecular Biology Letters*, vol. 24, p. 13, 2019.

[16] Y. Wang, Q. Tai, J. Zhang et al., "miRNA-206 inhibits hepatocellular carcinoma cell proliferation and migration but promotes apoptosis by modulating cMET expression," *Acta Biochimica et Biophysica Sinica*, vol. 51, no. 3, pp. 243–253, 2019.

[17] K. S. Amr, H. A. Elmawgoud Atia, R. A. Elazeem Elbnhawy, and W. M. Ezzat, "Early diagnostic evaluation of miR-122 and miR-224 as biomarkers for hepatocellular carcinoma," *Genes & Diseases*, vol. 4, no. 4, pp. 215–221, 2017.

[18] H. Jiang, H. Ju, L. Zhang, H. Lu, and K. Jie, "microRNA-577 suppresses tumor growth and enhances chemosensitivity in colorectal cancer," *Journal of Biochemical and Molecular Toxicology*, vol. 31, no. 6, p. e12888, 2017.

[19] X. Yuan, J. He, F. Sun, and J. Gu, "Effects and interactions of MiR-577 and TSGA10 in regulating esophageal squamous cell carcinoma," *International Journal of Clinical and Experimental Pathology*, vol. 6, no. 12, pp. 2651–2667, 2013.

[20] X. Y. Chen, G. M. Li, Q. Dong, and H. Peng, "miR-577 inhibits pancreatic β-cell function and survival by targeting fibroblast growth factor 21 (FGF-21) in pediatric diabetes," *Genetics and Molecular Research*, vol. 14, no. 4, pp. 15462–15470, 2015.

[21] B. Wang, L. Sun, J. Li, and R. Jiang, "miR-577 suppresses cell proliferation and epithelial-mesenchymal transition by regulating the WNT2B mediated Wnt/beta-catenin pathway in non-small cell lung cancer," *Molecular Medicine Reports*, vol. 18, no. 3, pp. 2753–2761, 2018.

[22] Y. A. Ghouri, I. Mian, and B. Blechacz, "Cancer review: cholangiocarcinoma," *Journal of Carcinogenesis*, vol. 14, p. 1, 2015.

[23] J. Tejeda-Maldonado, I. García-Juárez, J. Aguirre-Valadez et al., "Diagnosis and treatment of hepatocellular carcinoma: an update," *World Journal of Hepatology*, vol. 7, no. 3, pp. 362–376, 2015.

[24] Y. Gao, Z. Guan, J. Chen et al., "CXCL5/CXCR2 axis promotes bladder cancer cell migration and invasion by activating PI3K/AKT-induced upregulation of MMP2/MMP9," *International Journal of Oncology*, vol. 47, no. 2, pp. 690–700, 2015.

[25] A. Li, J. King, A. Moro et al., "Overexpression of CXCL5 is associated with poor survival in patients with pancreatic cancer," *The American Journal of Pathology*, vol. 178, no. 3, pp. 1340–1349, 2011.

[26] X. Feng, D. Zhang, X. Li et al., "CXCL5, the upregulated chemokine in patients with uterine cervix cancer, in vivo and in vitro contributes to oncogenic potential of Hela uterine cervix cancer cells," *Biomedicine & Pharmacotherapy*, vol. 107, pp. 1496–1504, 2018.

[27] A. Forsthuber, K. Lipp, L. Andersen et al., "CXCL5 as regulator of neutrophil function in cutaneous melanoma," *Journal of Investigative Dermatology*, vol. 139, no. 1, pp. 186–194, 2019.

[28] K. Z'Graggen, A. Walz, L. Mazzucchelli, R. Strieter, and C. Mueller, "The C-X-C chemokine ENA-78 is preferentially expressed in intestinal epithelium in inflammatory bowel disease," *Gastroenterology*, vol. 113, no. 3, pp. 808–816, 1997.

[29] V. O. Frick, C. Rubie, M. Wagner et al., "Enhanced ENA-78 and IL-8 expression in patients with malignant pancreatic diseases," *Pancreatology*, vol. 8, no. 4-5, pp. 488–497, 2008.

[30] H. Verbeke, V. Hannelien, K. Geboes et al., "The role of CXC chemokines in the transition of chronic inflammation to esophageal and gastric cancer," *Biochimica et Biophysica Acta*, vol. 1825, no. 1, pp. 117–129, 2012.

[31] C. Chen, Z.-Q. Xu, Y.-P. Zong et al., "CXCL5 induces tumor angiogenesis via enhancing the expression of FOXD1

mediated by the AKT/NF-kappaB pathway in colorectal cancer," *Cell Death & Disease*, vol. 10, no. 3, p. 178, 2019.

[32] D. P. Bartel, "MicroRNAs: target recognition and regulatory functions," *Cell*, vol. 136, no. 2, pp. 215–233, 2009.

[33] D. P. Bartel, "MicroRNAs," *Cell*, vol. 116, no. 2, pp. 281–297, 2004.

[34] K. C. Xue, D. D. Hu, L. Zhao, N. Li, and H. Y. Shen, "MiR-577 inhibits papillary thyroid carcinoma cell proliferation, migration and invasion by targeting SphK2," *European Review for Medical and Pharmacological Sciences*, vol. 21, no. 17, pp. 3794–3800, 2017.

[35] C. Yin, Q. Mou, X. Pan, G. Zhang, H. Li, and Y. Sun, "MiR-577 suppresses epithelial-mesenchymal transition and metastasis of breast cancer by targeting Rab25," *Thoracic Cancer*, vol. 9, no. 4, pp. 472–479, 2018.

[36] W. Zhang, C. Shen, C. Li et al., "miR-577 inhibits glioblastoma tumor growth via the Wnt signaling pathway," *Molecular Carcinogenesis*, vol. 55, no. 5, pp. 575–585, 2016.

Hindawi
Journal of Oncology
Volume 2021, Article ID 6839555, 6 pages
https://doi.org/10.1155/2021/6839555

Research Article

Effect and Nursing Satisfaction of Bedside Nursing Combined with Detail Nursing in Clinical Nursing of Gastroenterology Department

Hongyan Ai[1] **and Shuqin Peng**[2]

[1]*Department of Gastroenterology, Linyi Central Hospital, Linyi 276400, Shandong Province, China*
[2]*Department of Traditional Chinese Medicine, Second Hospital of Liaocheng, Linqing, Liaocheng 252600, Shandong Province, China*

Correspondence should be addressed to Hongyan Ai; lxfahy@163.com

Received 12 April 2021; Accepted 25 May 2021; Published 31 May 2021

Academic Editor: Muhammad Wasim Khan

Objective. The purpose of the study was to investigate the therapeutic effect and nursing satisfaction of bedside nursing combined with detail nursing in the gastroenterology department. *Methods*. 112 patients with gastrointestinal diseases admitted to our hospital from November 2018 to November 2019 were selected as the study subjects and randomly divided into a research group ($n = 56$) and reference group ($n = 56$). The reference group received routine clinical nursing, while on this basis, the research group received bedside nursing combined with detail nursing. After that, the clinical nursing effects of the two groups were compared. *Results*. There were no significant differences in sex ratio, age, BMI, smoking history, drinking history, marital status, and disease types between the two groups ($P > 0.05$). The VAS scores in the two groups after intervention were significantly lower than those before intervention ($P < 0.01$), and the VAS scores in the research group after intervention were significantly lower than those in the reference group ($P < 0.01$). The nursing ability, nursing skills, and nursing responsibility in the research group were significantly higher than those in the reference group ($P < 0.01$). There were no significant differences between the two groups in the number of patients who were satisfied and needed improvement ($P > 0.05$). Besides, the number of very satisfied cases in the research group was significantly higher than that in the reference group ($P < 0.05$), and the number of unsatisfied cases was significantly lower than that in the reference group ($P < 0.05$). The total incidence of clinical adverse events in the research group was significantly lower than that in the reference group ($P < 0.01$). The gastrointestinal diseases related knowledge scores after intervention were significantly higher than those before intervention ($P < 0.01$), and the gastrointestinal diseases related knowledge scores after intervention in the research group were significantly higher than those in the reference group ($P < 0.01$). The GQOLI-74 scores after intervention in the two groups were significantly higher than those before intervention ($P < 0.01$), and the GQOLI-74 scores after intervention in the research group were significantly higher than those in the reference group ($P < 0.01$). *Conclusion*. The application of bedside nursing mode combined with detail nursing in gastrointestinal diseases can effectively reduce patients' pains, as well as the incidence of clinical adverse events, and improve patients' life quality, with definite curative effect, which is worthy of promotion and application.

1. Introduction

With the accelerating rhythm of people's life, the number of patients with digestive diseases has been increasing. Gastroenterology refers to the three-level clinical disciplines with stomach, esophagus, large and small intestines, gallbladder, and other diseases as the main contents, covering a wide range of diseases, and it has complex and sophisticated clinical treatment and nursing operation [1–3]. At present, patients not only put forward higher requirements for clinical treatment effect but also have higher requirements for daily nursing care. Due to the

characteristics of high incidence and wide coverage, gastroenterology commonly occurs in all age groups; therefore, with improved treatment effect, the quality and level of clinical nursing care cannot be ignored [4–6]. Detail nursing complies with this requirement, and its measures can effectively improve patients' negative moods and make patients satisfied with the high-quality nursing services in hospital. Detail nursing is the inheritance and innovation based on the traditional clinical nursing, and it has been recognized by the society through optimizing the nursing process, changing the traditional doctor-patient communication mode, paying more attention to clinical details, improving the satisfaction of clinical nursing, creating a good nurse-patient relationship, and improving the overall treatment level of the hospital [7–9]. Bedside nursing is a brand-new nursing method that establishes responsibility system groups and carries out level-to-level administration, which can improve the responsibility consciousness of nursing staff to a certain extent, reduce the incidence of clinical adverse events, provide guarantee for clinical treatment, make hospital nursing services closer to patients, and establish a harmonious nurse-patient relationship. Based on this, this study further explores the clinical effect of bedside nursing combined with detail nursing in digestive diseases, and now the summary reports are as follows.

2. Materials and Methods

2.1. General Information. This study was approved by the Hospital Ethics Committee. 112 patients with gastrointestinal diseases admitted to our hospital from November 2018 to November 2019 were selected as the study subjects and randomly divided into a research group ($n = 56$) and control group ($n = 56$).

2.2. Inclusion Criteria. ① Patients met the diagnostic criteria of digestive diseases. ② Patients had complete clinical data. ③ The patients and their families were informed of the purpose and process of this study and signed the informed consent.

2.3. Exclusion Criteria. ① Patients had other organic lesions in the brain, heart, kidney, and liver. ② Patients had cognitive or communication disorders such as mental disorders. ③ Patients refused to cooperate with the study.

2.4. Methods. The clinical nursing was carried out in the reference group through advising patients to take medicine on time, keeping the ward environment clean and tidy, implementing dietary intervention for patients, and monitoring various vital signs.

The research group received bedside nursing combined with detail nursing on the basis of routine clinical nursing. Bedside nursing: ① primary nursing groups were established, whose members were composed of a head nurse and 3 or 4 nurses. The head nurse, serving as the group leader, arranged specific work according to the working ability of each nurse. Besides, the primary nurses performed comprehensive nursing in clinical propaganda and education, psychological counseling, medication guidance, and dietary intervention. ② Three-level quality control was adopted. The first level referred to that nurses timely found existing problems through self-inspection, self-evaluation, and other ways and then took effective measures to solve them. The second level referred to that the team leader timely checked each team member's nursing record sheets, patients' medication records, snd so forth, to supervise and correct their work. The third level referred to that department leaders developed specific work assessment mechanisms and guided the daily work of each nurse. ③ Departments equipped each group with a treatment vehicle and with the drugs and instruments needed in the treatment process. Detail nursing: ① medical staff should actively communicate with patients, eliminate their negative emotions, and explain the relevant precautions during hospitalization. In addition, medical staff should act gently with smiling when nursing patients so as to establish a good doctor-patient relationship and make them feel more love and care. ② Medical staff should pay attention to appearance, face patients with a positive and enthusiastic attitude, and leave a good mark for patients. ③ Medical staff should pay attention to their own language expression and tone of voice in clinical nursing to make patients more acceptable.

2.5. Observation Indexes. The clinical data of the two groups were compared and analyzed, which included gender, age, body mass index (BMI), smoking history, drinking history, marital status, and disease types.

The pain degree before and after intervention was evaluated by referring to the visual analogue scale (VAS) [10], with the total score of 10 points, and higher scores indicated higher pain degree.

The Clinical Nursing Quality Scale made by the department was adopted to evaluate the clinical nursing quality of the two groups, which included three items, such as nursing ability, nursing skills, and nursing responsibility, with each item totally scoring 50 points, and higher scores indicated better nursing quality.

The Patient Clinical Satisfaction Questionnaire prepared by the hospital was used, and the patients were guided to fill in it truthfully. According to the satisfaction level of clinical nursing, the questionnaire can be classified as being very satisfied, satisfied, needing improvement, and unsatisfied.

The incidence of clinical adverse events during hospitalization was statistically compared between the two groups.

The Patient Disease Related Knowledge Scale prepared by the department was adopted to evaluate the knowledge mastery of gastrointestinal diseases in the two groups before and after intervention, with the total score of 100 points, and higher scores indicated better patients' knowledge mastery of gastrointestinal diseases.

Referring to Generic Quality of Life Inventory-74 [11] (GQOLI-74), the life quality of the patients in the two groups before and after intervention was evaluated. The scale was

composed of four scoring factors, such as psychological function, physical function, social function, and material life state, with the total score of 100 points, and higher scores indicated patients' better life quality.

2.6. Statistical Methods. SPSS21.0 software was adopted to statistically analyze and process the data in this study. GraphPad Prism 6 (GraphPad Software, San Diego, USA) was also used to draw pictures of the data. Measurement data were expressed by ($\overline{x} \pm s$) and tested by t-test. Enumeration data were expressed as [n (%)] and tested by X^2 test. The differences had statistical significance when $P < 0.05$.

3. Results

3.1. Comparison of Clinical Data between the Two Groups. There were no significant differences in sex ratio, age, BMI, smoking history, drinking history, marital status, and disease types between the two groups ($P > 0.05$), as shown in Table 1.

3.2. Comparison of VAS Scores between the Two Groups before and after Intervention. The VAS scores after intervention in both groups were significantly lower than those before intervention ($P < 0.05$), and the VAS scores after intervention in the research group were significantly lower than those in the reference group ($P < 0.05$), as shown in Figure 1.

3.3. Comparison of Clinical Nursing Quality between the Two Groups. The nursing ability, nursing skills, and nursing responsibility in the research group were significantly higher than those in the reference group ($P < 0.05$), as shown in Figure 2.

3.4. Comparison of Clinical Nursing Satisfaction between the Two Groups. There were no significant differences between the two groups in the number of patients who were satisfied and needed improvement ($P > 0.05$). The number of very satisfied cases in the research group was significantly higher than that in the reference group ($P < 0.05$), and the number of unsatisfied cases was significantly lower than that in the reference group ($P < 0.05$), as shown in Table 2.

3.5. Comparison of Clinical Adverse Events between the Two Groups. The total incidence of clinical adverse events in the research group was significantly lower than that in the reference group ($P < 0.05$), as shown in Table 3.

3.6. Comparison of Gastrointestinal Disease Related Knowledge Scores between the Two Groups before and after Intervention. The gastrointestinal disease related knowledge scores in the two groups after intervention were significantly higher than those before intervention ($P < 0.05$), and the gastrointestinal disease related knowledge scores in the research group after intervention were significantly higher than those in the reference group ($P < 0.05$), as shown in Figure 3.

3.7. Comparison of Life Quality Scores between the Two Groups before and after Intervention. The GQOLI-74 scores in the two groups after intervention were significantly higher than those before intervention ($P < 0.05$), and the GQOLI-74 scores in the research group after intervention were significantly higher than those in the reference group ($P < 0.05$), as shown in Figure 4.

4. Discussion

The gastroenterology department is one of the important departments in the hospital which can treat a wide range of diseases, with a high recurrence rate. Therefore, while treating gastrointestinal diseases, patients should be given scientific and precise clinical nursing care [11–14]. Detail nursing, as a patient-centered nursing concept and a nursing standard, requires nurses to do their utmost to nurse patients and make patients feel more care from hospitals, which can improve the clinical treatment effect and gain acceptance from patients and their families on hospital nursing work, thus promoting the improvement of hospital nursing service quality [15, 16]. If the patients with digestive system diseases are in critical conditions, there might be so many risks in clinical nursing management; therefore, it is particularly important to do a good job in basic nursing. Traditional clinical nursing just simply divides nurses' work into different types, which results in confusion of responsibilities, difficulty in adapting to the needs of clinical nursing management, and irritation of nurse-patient conflicts, adversely affecting treatment [17]. In bedside nursing, primary nursing teams are established and nurses are assigned with different tasks according to their working ability and patients' needs so that each patient is nursed by a primary nurse. In addition, the implementation of three-level quality control and supervision system can effectively improve the working ability of the nursing staff, and reduce or avoid the occurrence of clinical adverse events, thereby improving the nursing quality and ensuring the clinical treatment effect [18, 19]. In this study, after the implementation of combined nursing intervention for patients with gastrointestinal diseases, the VAS scores in the research group were significantly lower than those in the reference group. Pains would lead to adverse emotions which were partly negative to the prognosis of the patients. Moreover, the results of GQOLI-74 scores showed that the patients who received combined nursing intervention express satisfactory prognosis. The combined nursing intervention can relieve the negative moods by communicating with the patients and distracting patients' attention to alleviate the pains.

In addition, bedside nursing and optimization of hierarchical nursing management should also be implemented. Primary nurses should not only take charge of patient care and treatment but also promptly carry out self-examination and self-correction. The team leaders need to supervise the work of primary nurses to correct deficiencies. For the

Table 1: Comparison of clinical data between the two groups [n (%), ($\overline{x} \pm s$)].

Types	n	Research group ($n = 56$)	Reference group ($n = 56$)	χ^2/t	P
Gender				0.146	0.703
Male		31 (55.36%)	33 (58.93%)		
Female		25 (44.64%)	23 (41.07%)		
Average age (years old)		40.73 ± 4.31	40.77 ± 4.35	0.049	0.961
BMI (kg/m^2)		22.42 ± 1.65	22.46 ± 1.63	0.129	0.898
Smoking history				0.148	0.701
No		34 (60.71%)	32 (57.14%)		
Yes		22 (39.29%)	24 (42.86%)		
Drinking history				0.156	0.693
No		37 (66.07%)	35 (62.50%)		
Yes		19 (33.93%)	21 (37.50%)		
Marital status				0.373	0.541
Unmarried		49 (87.50%)	51 (91.07%)		
Married		7 (12.50%)	5 (8.93%)		
Disease types					
Gastric polyps		16 (28.57%)	18 (32.14%)	0.169	0.681
Duodenal ulcer		19 (33.93%)	16 (28.57%)	0.374	0.541
Gastric ulcer		14 (25.00%)	17 (30.36%)	0.401	0.526
Esophagitis		7 (12.50%)	5 (8.93%)	0.373	0.541

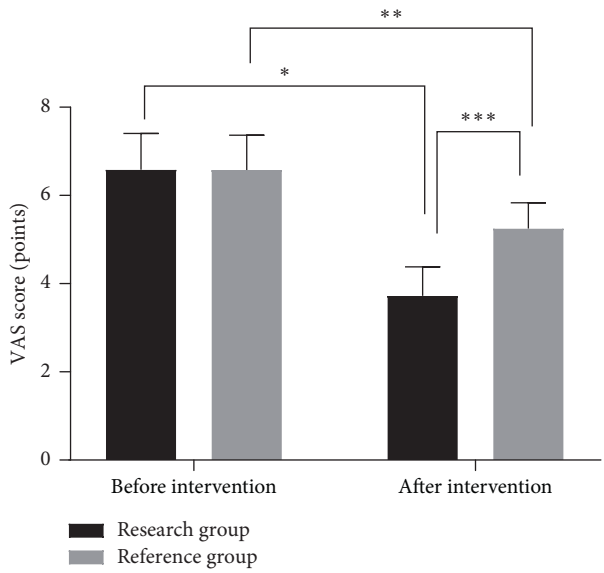

Figure 1: Comparison of VAS scores between the two groups before and after intervention ($\overline{x} \pm s$). Note: the abscissa indicates before and after intervention, while the ordinate indicates the VAS score. The VAS scores in the research group before and after intervention were (6.03 ± 1.17) points and (3.27 ± 0.94) points, while the VAS scores in the reference group before and after intervention were (6.05 ± 1.12) points and (4.86 ± 0.83) points. *indicates that there were significant differences in VAS scores in the research group before and after intervention ($t = 13.762$, $P < 0.001$). **indicates that there were significant differences in VAS scores in the reference group before and after intervention ($t = 6.388$, $P < 0.001$). ***indicates that there were significant differences in VAS scores between the two groups before and after intervention ($t = 9.488$, $P < 0.001$).

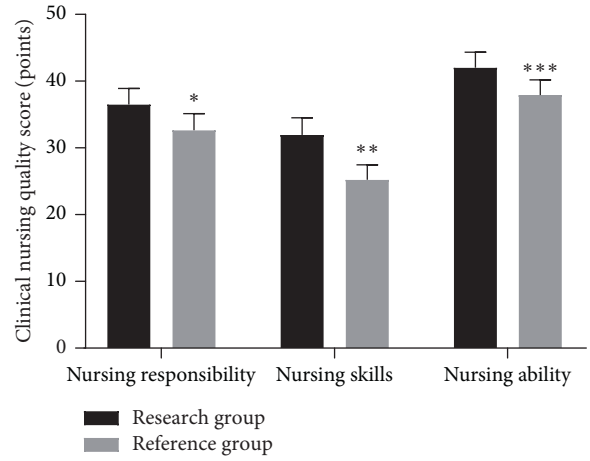

Figure 2: Comparison of clinical nursing quality between the two groups ($\overline{x} \pm s$). Note: the abscissa indicates nursing responsibility, nursing skills, and nursing ability, while the ordinate indicates clinical nursing quality score (points). The scores of nursing responsibility, nursing skills, and nursing ability in the research group were (34.94 ± 3.46), (30.28 ± 3.64), and (40.62 ± 3.25), respectively. The scores of nursing responsibility, nursing skills, and nursing ability in the reference group were (31.05 ± 3.53), (23.74 ± 3.19), and (36.51 ± 3.21), respectively. *indicates that there were significant differences in nursing responsibility between the two groups ($t = 5.889$, $P < 0.001$). **indicates that there were significant differences in nursing skills between the two groups ($t = 10.112$, $P < 0.001$). ***indicates that there were significant differences in nursing ability between the two groups ($t = 6.733$, $P < 0.001$).

department leaders, they should supervise the daily work of primary nursing, conduct a check-up system to comprehensively grasp the causes of clinical adverse events, analyze the risk factors affecting the quality of care, and fundamentally ensure the smooth development of nursing services [18, 20, 21]. This study showed that the incidence of clinical adverse events in the research group was significantly lower than that in the reference group, suggesting that the

Table 2: Comparison of clinical nursing satisfaction between the two groups [n (%)].

Satisfaction	Research group ($n = 56$)	Reference group ($n = 56$)	χ^2	P
Very satisfied	33 (58.93%)	18 (32.14%)	8.1000	0.004
Satisfied	13 (23.21%)	15 (26.79%)	0.191	0.663
Needing improvement	7 (12.50%)	9 (16.07%)	0.292	0.589
Unsatisfied	3 (5.36%)	14 (25.00%)	8.391	0.004

Table 3: Comparison of clinical adverse events between the two groups [n (%)].

Group	n	Medication errors	Aspiration	Empyrosis	Falling down	Total incidence
Research group	56	0 (0.00%)	1 (1.79%)	0 (0.00%)	1 (1.79%)	3.57% (2/56)
Reference group	56	2 (3.57%)	3 (5.36%)	2 (3.57%)	1 (1.79%)	14.29% (8/56)
χ^2						3.953
P						0.047

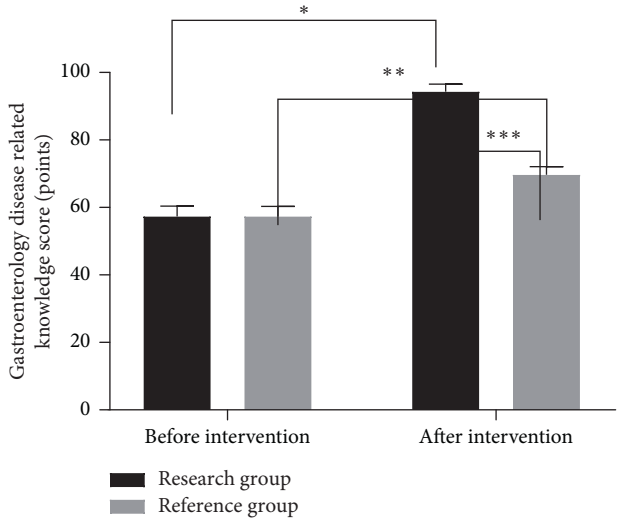

Figure 3: Comparison of gastrointestinal disease related knowledge scores between the two groups ($\overline{x} \pm s$). Note: the abscissa indicates before and after intervention, while the ordinate indicates the gastrointestinal disease related knowledge scores. The gastrointestinal disease related knowledge scores in the research group before and after intervention were (55.47 ± 4.36) points and (93.23 ± 3.17) points, respectively. The gastrointestinal disease related knowledge scores in the reference group before and after intervention were (55.51 ± 4.23) points and (68.35 ± 3.43) points, respectively. *indicates that there were significant differences in the gastrointestinal disease related knowledge scores in the research group before and after intervention ($t = 52.419$, $P < 0.01$). **indicates that there were significant differences in the gastrointestinal disease related knowledge scores in the reference group before and after intervention ($t = 17.419$, $P < 0.001$). ***indicates that there were significant differences in the gastrointestinal disease related knowledge scores between the two groups after intervention ($t = 39.864$, $P < 0.001$).

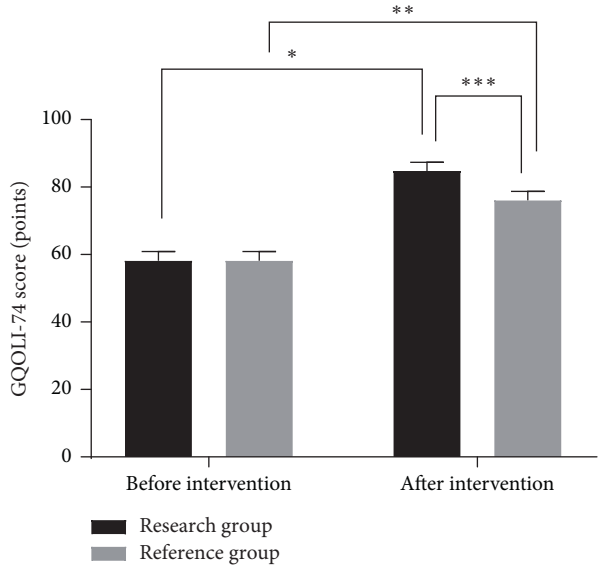

Figure 4: Comparison of life quality scores between the two groups before and after intervention ($\overline{x} \pm s$). Note: the abscissa indicates before and after intervention, while the ordinate indicates GQOLI-74 score. The GQOLI-74 scores in the research group before and after intervention were (56.54 ± 3.86) points and (83.47 ± 3.55) points, respectively. The GQOLI-74 scores in the reference group before and after intervention were (56.51 ± 3.90) points and (74.53 ± 3.84) points, respectively. *indicates that there were significant differences in GQOLI-74 scores in the research group before and after intervention ($t = 38.428$, $P < 0.01$). **indicates that there were significant differences in the GQOLI-74 scores in the reference group before and after intervention ($t = 24.638$, $P < 0.01$). ***indicates that there were significant differences in GQOLI-74 scores between the two groups after intervention ($t = 12.793$, $P < 0.01$).

combined nursing intervention can effectively improve the responsibility consciousness of nursing staff and reduce the incidence of clinical adverse events. This study also revealed that the combined nursing mode can significantly improve patients' clinical nursing satisfaction. Maddock et al. [22] believed that digestive system diseases, due to the long disease course, repeated medication, and high recurrence rate, easily led to patients' loss of confidence in treatment and fear of their own diseases. With the application of bedside nursing in patients with acute pancreatitis, it was found that the number of patients who were very satisfied with this nursing mode was 36, which was significantly higher than 20 in the control group, and the number of

patients who were unsatisfied was 4, which was significantly lower than 18 in the control group, showing that the bedside nursing could promote the establishment of a good nurse-patient relationship and improve the patients' nursing satisfaction. In addition, the combined nursing intervention can also improve the patients' understanding of their own diseases, improve their life quality, and increase the life happiness index to a certain extent [23].

In conclusion, bedside nursing combined with detail nursing can effectively reduce patients' pains of gastrointestinal diseases, improve nursing quality and nursing satisfaction, and reduce the incidence of clinical adverse events, which is worthy of popularization and application. This study investigated the effect of bedside nursing combined with detail nursing in clinical nursing of the gastroenterology department and provide some reference for nursing improvement.

Data Availability

The primary data to support the results of this study are available at reasonable request to the corresponding author.

Conflicts of Interest

The authors declare that there are no conflicts of interest regarding the publication of this paper.

References

[1] H. Thomas, "Improving veterans' access to gastroenterology clinical care," *Journal of the American Academy of Physician Assistants*, vol. 31, no. 3, pp. 47–49, 2018.

[2] T. Suzuki, T. Kato, R. Ohnishi et al., "Clinical characteristics of nursing- and healthcare-associated tuberculosis," *Diseases*, vol. 6, no. 4, p. 101, 2018.

[3] Y. Ang, P. Bhandari, S. S. Sami et al., "UK guidelines on oesophageal dilatation in clinical practice," *Gut: Journal of the British Society of Gastroenterology*, vol. 67, no. 6, pp. 1000–1023, 2018.

[4] C. Cuerda, S. M. Schneider, and A. Van Gossum, "Reply, letter to the editor- undergraduate nutrition education of health professionals in Greek medical, dentistry, pharmacy, nursing and midwifery departments," *Clinical Nutrition*, vol. 37, no. 1, p. 399, 2018.

[5] K. Gerasimidis, K. Zafeiropoulou, M. Mackinder et al., "Comparison of clinical methods with the faecal gluten immunogenic peptide to assess gluten intake in coeliac disease," *Journal of Pediatric Gastroenterology & Nutrition*, vol. 67, no. 3, pp. 356–360, 2018.

[6] V. Bressan, L. Sasso, F. Timmins et al., "Ethical dimensions of paediatric nursing: a rapid evidence assessment," *Nursing Ethics*, vol. 25, no. 1, pp. 111–122, 2018.

[7] P. Hunt, "Professional growth is a personal responsibility," *Nursing Management*, vol. 49, no. 9, pp. 5-6, 2018.

[8] A.-C. Blomberg, B. Bisholt, and L. Lindwall, "Responsibility for patient care in perioperative practice," *Nursing Open*, vol. 5, no. 3, pp. 414–421, 2018.

[9] E. Rosser and B. G. Thomas, "Responsibility, research and reasoning: nursing through 70 years of the NHS," *British Journal of Nursing: BJN*, vol. 27, no. 13, pp. 784–786, 2018.

[10] C. P. Caldas and C. Berterö, "Taking the responsibility in dementia care: a concept analysis about facticity," *Nursing Open*, vol. 5, no. 3, pp. 310–316, 2018.

[11] J. H. Flaskerud, "Individual responsibility vs. System failure," *Issues in Mental Health Nursing*, vol. 39, no. 3, pp. 275–278, 2018.

[12] A. J. Barton, "Academic freedom and educational responsibility," *Journal of Nursing Education*, vol. 57, no. 2, pp. 67-68, 2018.

[13] H. Cho and K. Han, "Associations among nursing work environment and health-promoting behaviors of nurses and nursing performance quality: a multilevel modeling approach," *Journal of Nursing Scholarship*, vol. 50, no. 4, pp. 403–410, 2018.

[14] B. Foss, K. Eriksson, and D. Nåden, "Love and responsibility: a new understanding of leadership," *Nursing Science Quarterly*, vol. 31, no. 2, pp. 148–156, 2018.

[15] S. Knippa, C. A. Rauen, and M. Muller, "Attention to detail," *Critical Care Nurse*, vol. 39, no. 3, pp. 67–71, 2019.

[16] Modern Tire Dealer Group, "Attention to detail WTC'S wheel care guide will help YOU complete the job," *Modern Tire Dealer*, vol. 100, no. 4 Suppl, pp. 6-7, 2019.

[17] J. M. Phillips, A. M. Stalter, J. S. Ruggiero et al., "Systems thinking for transitions of care," *Clinical Nurse Specialist*, vol. 33, no. 3, pp. 128–135, 2019.

[18] S. A. Ellis and L. Dalke, "Midwifery care for transfeminine individuals," *Journal of Midwifery & Women's Health*, vol. 64, no. 3, pp. 298–311, 2019.

[19] G. Fitzgerald, R. N. Kerley, and T. J. Kiernan, "High-sensitivity troponin assays: development and utility in a modern health-care system," *Expert Review of Cardiovascular Therapy*, vol. 17, no. 10, pp. 763–770, 2019.

[20] N. Hyland, M. B. Smith, B. Gribben, and W. M. Thomson, "The residual dentition among New Zealanders in aged residential care," *Gerodontology*, vol. 36, no. 3, pp. 216–222, 2019.

[21] M. H. E. Hermans, "An introduction to burn care," *Advances in Skin & Wound Care*, vol. 32, no. 1, pp. 9–18, 2019.

[22] B. Maddock, A. Kumar, and F. Kent, "Creating a collaborative care curriculum framework," *The Clinical Teacher*, vol. 16, no. 2, pp. 120–124, 2019.

[23] M. Dee and V. L. Hanson, "Effectively including the voice of residents in care home design," *Design for Health*, vol. 3, no. 2, pp. 283–304, 2019.

Hindawi
Journal of Oncology
Volume 2021, Article ID 9923454, 10 pages
https://doi.org/10.1155/2021/9923454

Research Article

miR-455 Inhibits the Viability and Invasion by Targeting RAB18 in Hepatocellular Carcinoma

Chenghong Wang,[1] **Guicai Zhu**,[2] **Miaolin Yu**,[3] **Xiufang Mi**,[4] **and Honghua Qu**[5]

[1]*Department of Clinical Laboratory, Yantaishan Hospital, Yantai 264000, China*
[2]*Department of Surgery, Rizhao Hospital of TCM, Rizhao 276800, China*
[3]*Department of Chinese Medicine, Qingdao Central Hospital, Qingdao University, Qingdao 266042, China*
[4]*Department of Internal Medicine, Zhangqiu District People's Hospital, Jinan 250200, China*
[5]*Department of Medical Insurance Office, Qilu Hospital of Shandong University, Jinan 250012, China*

Correspondence should be addressed to Honghua Qu; quhonghua@sdqiluhospital.cn

Received 29 March 2021; Accepted 19 May 2021; Published 28 May 2021

Academic Editor: Alamgeer Yuchi

Background. Hepatocellular carcinoma (HCC) has been regarded as the fifth most common cancer worldwide with a low prognosis. miR-455 usually played the role of a tumor suppressor in multiple cancers. The aim of this study was to investigate the roles of miR-455 in HCC. *Materials and Methods*. Cell viability and invasion were measured by CCK8 and Transwell assays. Luciferase reporter assay was performed to verify that miR-455 directly binds to the 3′-noncoding region (UTR) of RAB18 mRNA in Huh7 cells. *Results*. The expression of miR-455 was lower in HCC tissues and cell lines than in nontumor tissues and normal cell line, and downregulation of miR-455 was connected with worse outcome of HCC patients. miR-455 suppressed cell proliferation in vitro and in vivo, and it inhibited the abilities of cell invasion and EMT in HCC. RAB18 was upregulated in HCC tissues and cell lines, and the expression of RAB18 was regulated by miR-455. RAB18 reversed partial roles of miR-455 on cell viability and invasion in HCC. *Conclusion*. miR-455 inhibited cell viability and invasion by directly targeting the 3′-UTR of RAB18 mRNA of hepatocellular carcinoma.

1. Introduction

Hepatocellular carcinoma (HCC), the third major cause of cancer-related death, is the fifth most common cancer worldwide [1]. In recent years, the increase in the incidence of HCC has been the result of a combination of factors, especially the phenotype caused by hepatitis B or C virus (HBV or HCV) infection [2, 3]. Despite significant advances in treatment and diagnosis, surgery is the primary treatment for patients with HCC. About half of HCC cases are advanced unresectable HCC, resulting in a poor prognosis [4]. Thus, it is necessary to investigate the biomarkers for the treatment and the pathogenesis of HCC.

MicroRNAs (miRNAs) are small noncoding endogenous RNAs containing 19 to 25 nucleotides that promote post-transcriptional control in regulating the expression of target gene by binding to the 3′-UTR sequences of its mRNA [5]. Recently, increasing evidences elucidated that miRNAs was involved in the cancer pathogenesis, including cell proliferation, metastasis, and apoptosis [6]. Most reports found that multiple miRNAs that include miR-548a, miR-1246, miR-632, and miR-5692a played pivotal roles in HCC [7–10]. miR-455 has been reported to act as a tumor suppressor to inhibit cap-dependent translation and the proliferation in prostate cancer [11]. Also, in gastric cancer, miR-455 inhibited human cell proliferation and invasion and promoted cell apoptosis [12]. In addition, miR-455 inhibited cell viability, while it induced cell apoptosis in colorectal cancer [13]. However, miR-455 promoted cell invasion and migration in triple-negative breast cancer [14]. Thus, the pivotal roles of miR-455 in cell viability and metastasis in HCC still needed to be explored.

RAB18, a member of Ras-related small GTPases family, belongs to members of the Ras oncogene superfamily of small guanosine triphosphatases [15]. Accumulating evidences have elucidated connection between the expression of GTPases members and several diseases, including colorectal cancer, lung cancer, and prostate cancer [16–18]. RAB18 regulates membrane trafficking in organelles and transport vesicles, leading to a reduction in mature LDs and lipid storage [19]. RAB18 binds to NS5A to improve the interaction between sites of viral replication and lipid droplets [20]. RAB18 is reduced in pituitary tumors, resulting in acromegaly and restoration of excessive growth hormone hypersecretion [21]. RAB18 was associated with lipogenesis, lipolysis, and obesity in adipocytes [22]. However, the functions of RAB18 in HCC remain unclear; thus, in the present study, we discovered that miR-455 inhibited cell viability, invasion, and EMT by directly targeting to the 3′-UTR of RAB18 mRNA in hepatocellular carcinoma.

2. Materials and Methods

2.1. Patients and Tissue Samples. A cohort of 98 patients who underwent HCC were harvest from Yantaishan Hospital during the period from January 2016 to November 2018. None of the patients received preoperative treatment such as chemotherapy and radiotherapy before surgery. All the fresh tissues were snap-frozen in liquid nitrogen and stored at −80°C until RNA extraction. The project protocol was reviewed and approved by the Ethics Committee of Zhangjiagang Hospital. All participants signed the written informed consents before inclusion in this study.

2.2. Cell Culture. HCC cell lines HCC-LM3, Huh7, and Bel-7402 and a normal liver cell L-O2 were obtained from American Type Culture Collection (ATCC, Rockville, MD, USA). All cells were cultured with Dulbecco's modified Eagle's medium (DMEM, Invitrogen, CA, USA) supplemented with 10% FBS (Gibco, USA) at 37°C in a humidified atmosphere containing 5% CO_2.

2.3. Western Blot. Radioimmunoprecipitation assay (RIPA, Thermo Fisher Scientific, Waltham, MA, USA) lysis buffer containing PMSF was employed to separate total protein on ice for 37°C. After centrifugation at 12,000 × g for 20 min at 4°C, the concentration of the protein was then quantified using BCA Protein Assay Reagent Kit (Beyotime, Shanghai, China). Equal amounts of protein for each sample were loaded and separated on a 10% sodium dodecyl sulphate-polyacrylamide gel (SDS-PAGE) before being transferred onto a polyvinylidene difluoride (PVDF, Roche Diagnostics) membrane. After blocking in 5% skim milk powder at room temperature for 1 h, the membrane was incubated by primary antibodies overnight at 4°C. The primary antibodies were RAB18 (1 : 1000, Santa Cruz Biotechnology, Santa Cruz, CA, USA), E-cadherin, N-cadherin, and glyceraldehyde-3-phosphate dehydrogenase (GAPDH). Next, horseradish peroxidase- (HRP-) conjugated secondary antibody (1 : 5000) was conducted to incubate the membrane at room temperature for 1 h. The Enhanced Chemiluminescence (ECL) Kit (KeyGen Biotech, China) was applied to measure the bands and imaged on a Tanon-5200 Chemiluminescent Imaging System (Millipore, Bedford, MA, USA).

2.4. RNA Isolation and qRT-PCR. TRIzol reagent (Invitrogen, USA) was used to extract the total RNAs from tissues and cell lines. The miRNA was reverse-transcribed using miRNA first-strand complementary DNA (cDNA) synthesis kit (Poly A Tailing; Sangon, China), while mRNA was reverse-transcribed using RevertAid First-Strand cDNA Synthesis Kit (Thermo Fisher Scientific). Subsequently, qRT-PCR was carried out using SYBR Premix Ex Taq kit (Takara) on an ABI PRISM 7900 Sequence Detection System (Applied Biosystems). The $2^{-\Delta\Delta Cq}$ method was applied to analyze the miRNA or mRNA expression with GAPDH or U6 was the normalization. The primer pairs are shown in Table 1.

2.5. Cell Proliferation Assay. The cell proliferation was calculated using cell counting kit-8 (CCK-8) assay (Dojindo Laboratories, Kumamoto, Japan) in 96-well plates. After 24, 48, 72, or 96 h of culture, CCK-8 solution was added to each well and cultivated for 3 h at 37°C. The plates were shook for 20 min, followed by measuring the absorbance at 450 nm using automatic multiwell spectrophotometer (Bio-Rad, Richmond, CA, USA).

2.6. Invasion Assay. Invasive ability was evaluated using Transwell insert (Corning Incorporated, Corning, New York) covered with Matrigel (BD Biosciences). Briefly, the cells were suspended in DMEM medium without FBS and the cell suspension was placed in the upper well, while the bottom well was filled with medium with 20% FBS that acted as chemoattractant. After incubation at 37°C with 5% CO_2 for 24 h, the cells that failed to pass through the membrane were removed with cotton swabs. Meanwhile, the cells that passed through the membrane were fixed with 100% methanol for 15 min and stained using 0.1% crystal violet solution for 30 min. Finally, a microscope (Olympus, Tokyo, Japan) was utilized to count the invaded cells.

2.7. Cell Transfection. The miR-455 mimic, miR-455 inhibitor, and RAB18 overexpression plasmids, as well as corresponding negative control, were obtained from GenePharma (Shanghai, China). Cells were placed in a 6-well plate, and the transfections of special vectors were performed using Lipofectamine 2000 Reagent (Invitrogen, Carlsbad, CA, USA) following the manufacturer's instruction.

2.8. Dual-Luciferase Reporter Gene Assay. TargetScan predicted the miR-455 binding site at 3′-UTR of RAB18 mRNA. The putative sequences of miR-455 on RAB18 mRNA were mutated from GCACAUA to CGUGUAU. The wild type or the mutated sequences of RAB18 mRNA were cloned into pmiRGLO Vector, which were designated as pmiRGLO-

Table 1: Primer sequences for RT-qPCR.

Gene		Primer sequences
miR-455	Forward	5′-CGAGCTTCCTTCTGCAGGT-3′
	Reverse	5′-CACCACTGCCATCCCACA-3′
U6	Forward	5′-TGCGGGTGCTCGCTTCGCAGC-3′
	Reverse	5′-CCAGTGCAGGGTCCGAGGT-3′
RAB18	Forward	5′-CAGGGAAGAAGGCCAAGGAG-3′
	Reverse	5′-CCCGGGGTCGATGGAGT-3′
GAPDH	Forward	5′-GAAGGTGAAGGTCGGAGTC-3′
	Reverse	5′-GAAGATGGTGATGGGATTTC-3′

RAB18-WT (WT) and pmiRGLO-RAB18-MUT (MUT), respectively. The Huh7 cells were seeded and cotransfected with pmiRGLO-RAB18-WT or pmiRGLO-RAB18-MUT plasmid and miR-455 mimic or miR-455 NC using Lipofectamine 2000 (Invitrogen, Carlsbad, CA, USA). Firefly luciferase activity was assessed by dual-luciferase reporter assay system (Promega, Madison, WI, USA), with Renilla luciferase activity acting as normalization.

2.9. Construction of the Mice Xenograft Model. Four-week-old nude mice were purchased from Vital River Laboratory Animal Technology (Beijing, China). Huh7 cells that transfected miR-455 mimic or control plasmids were subcutaneously inoculated in the mice to build xenograft tumor model. The volumes were calculated as $1/2 \times \text{length} \times \text{width}^2$ of the tumor, which were measured every 3 days. After cultivation for 26 days, the mice were executed and the tumors dissected out. The animal study was also approved by the Research Ethics Committee of Zhangjiagang Hospital.

2.10. Statistical Analysis. The data were indicated as means ± SD. The SPSS statistical software version 19.0 (IBM Corp, Armonk, NY, USA) and GraphPad Prism 7.0 (GraphPad, San Diego, CA) were used to analyze all the data. The differences between two or more groups were compared by Student's *t*-test or one-way analysis of variance (ANOVA) followed by the Student-Newman-Keuls post hoc test. Values of $P < 0.05$ were considered to be statistically significant.

3. Results

3.1. The Expression of miR-455 in HCC. To investigate the functions of miR-455 in HCC, qRT-PCR was conducted to measure the expression of miR-455 in tissues or cell lines. As a result, miR-455 had a low expression in HCC tissues versus noncancerous tissues ($P < 0.05$) (Figure 1(a)). The expression of miR-455 was also evaluated in HCC cell lines HCC-LM3, Huh7, and Bel-7402 and normal liver cell L-O2. As expected, the expression of miR-455 was lower in HCC cell lines HCC-LM3 ($P < 0.05$), Huh7 ($P < 0.01$), and Bel-7402 ($P < 0.05$) than in L-O2 cells (Figure 1(b)).

3.2. miR-455 Inhibits Cell Viability of HCC In Vitro and In Vivo. To explore the roles of miR-455 in cell proliferation, miR-455 mimic and miR-455 inhibitor were utilized to upregulate ($P < 0.01$) or downregulate ($P < 0.05$) the expression of miR-455 in HCC cells Huh7, which was measured by RT-qPCR (Figure 2(a)). CCK8 assay showed that the proliferative ability was decreased by transfecting miR-455 mimic ($P < 0.05$) (Figure 2(b)). On the contrary, miR-455 inhibitor increased the proliferative ability in comparison with normal control ($P < 0.05$) (Figure 2(c)).

In addition, Huh7 cells stably transfected with miR-455 mimic had a slower growth rate in vivo (Figure 2(d)). After 26 days of cultivation, the nude mice were executed and the volume of the xenograft tumor was calculated. Not unfortunately, tumors of miR-455 overexpressed group had a smaller volume than that of control group ($P < 0.05$) (Figure 2(e)). All results elucidated that miR-455 suppressed the growth of HCC in vitro and in vivo.

3.3. miR-455 Impairs Cell Invasion and the EMT in HCC Cells. Transwell assay was performed to calculate cell invasion in Huh7 cells transfected with miR-455 mimic or miR-455 inhibitor. As expected, the invasive ability was reduced by miR-455 mimic ($P < 0.05$), while it was improved by miR-455 inhibitor in Huh7 cells ($P < 0.05$) (Figure 3(a)). Furthermore, proteins associated with EMT markers, such as E-cadherin and N-cadherin, were measured using western blot. As a result, the expression of N-cadherin was inhibited, while the expression of E-cadherin was improved by miR-455 mimic. On the contrary, miR-455 inhibitor enhanced the expression of N-cadherin, whereas it decreased the expression of E-cadherin in Huh7 cells (Figure 3(b)).

3.4. miR-455 Directly Targets the 3′-UTR of RAB18 mRNA. TargetScan predicted RAB18 was a potential target of miR-455 at 96–102 on the 3′-UTR. To verify miR-455 binding to the 3′-UTR of RAB18 mRNA, the putative binding sequences were mutated from GCACAUA to CGUGUAU, as shown in Figure 4(a). The miR-455 mimic and the wild type or the mutant 3′-UTR were cotransfected in Huh7 cells, followed by calculating the luciferase ability. As expected, miR-455 mimic reduced the luciferase ability of wild type mRNA 3′-UTR ($P < 0.05$), whereas it did not alter the mutant 3′-UTR ($P > 0.05$) (Figure 4(b)). Furthermore, the expression of RAB18 was assessed after transfection with miR-455 mimic or inhibitor. The expression of RAB18 was decreased by miR-455 mimic ($P < 0.05$), while it was enhanced by miR-455 inhibitor in Huh7 cells ($P < 0.05$) (Figure 4(c)).

3.5. RAB18 Restores Partial Functions of miR-455 on Cell Viability and Invasion. To investigate the roles of RAB18 in HCC, the expression of RAB18 was assessed in tissues and cell lines by RT-qPCR. Not unfortunately, RAB18 was overexpressed in HCC tissues versus nontumor tissues (Figure 5(a)). In cells, the expression of RAB18 was higher in HCC-LM3 ($P < 0.05$), Huh7 ($P < 0.01$), and Bel-7402 ($P < 0.05$) cells than in L-O2 cells (Figure 5(b)). To investigate the inhibitory effect of miR-455 on cell proliferation and invasion CCK8 and

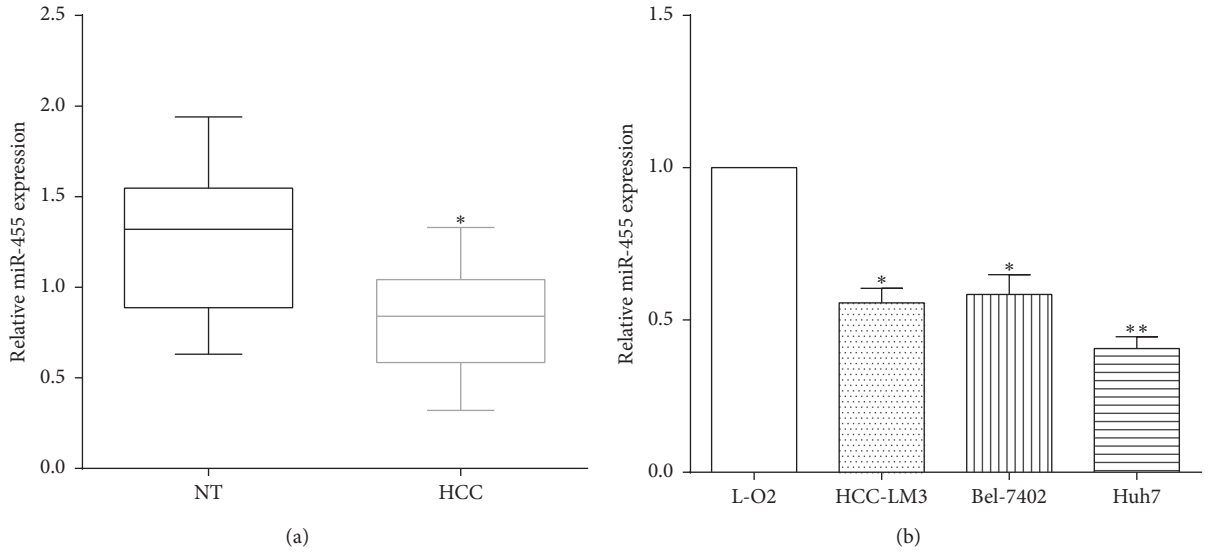

Figure 1: The expression of miR-455 in HCC. (a) The expression of miR-455 was low in HCC tissues versus noncancerous tissues vs NT, $^{*}P < 0.05$. (b) The expression of miR-455 was lower in HCC cells than in normal cells vs L-O2, $^{*}P < 0.05$; $^{**}P < 0.01$.

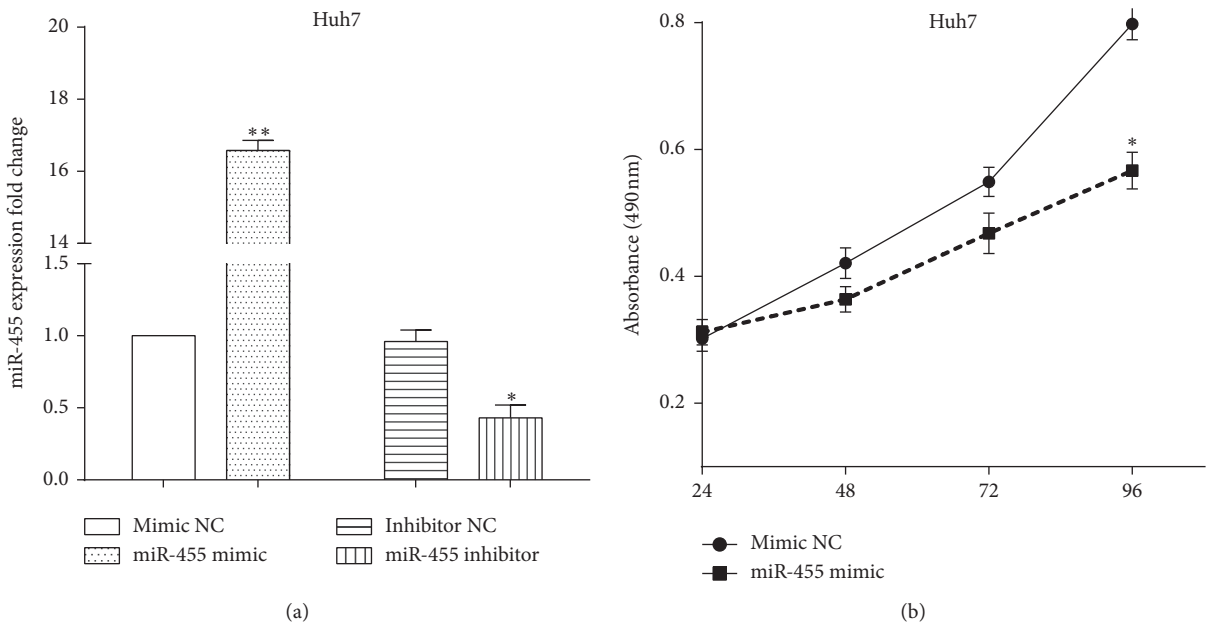

Figure 2: Continued.

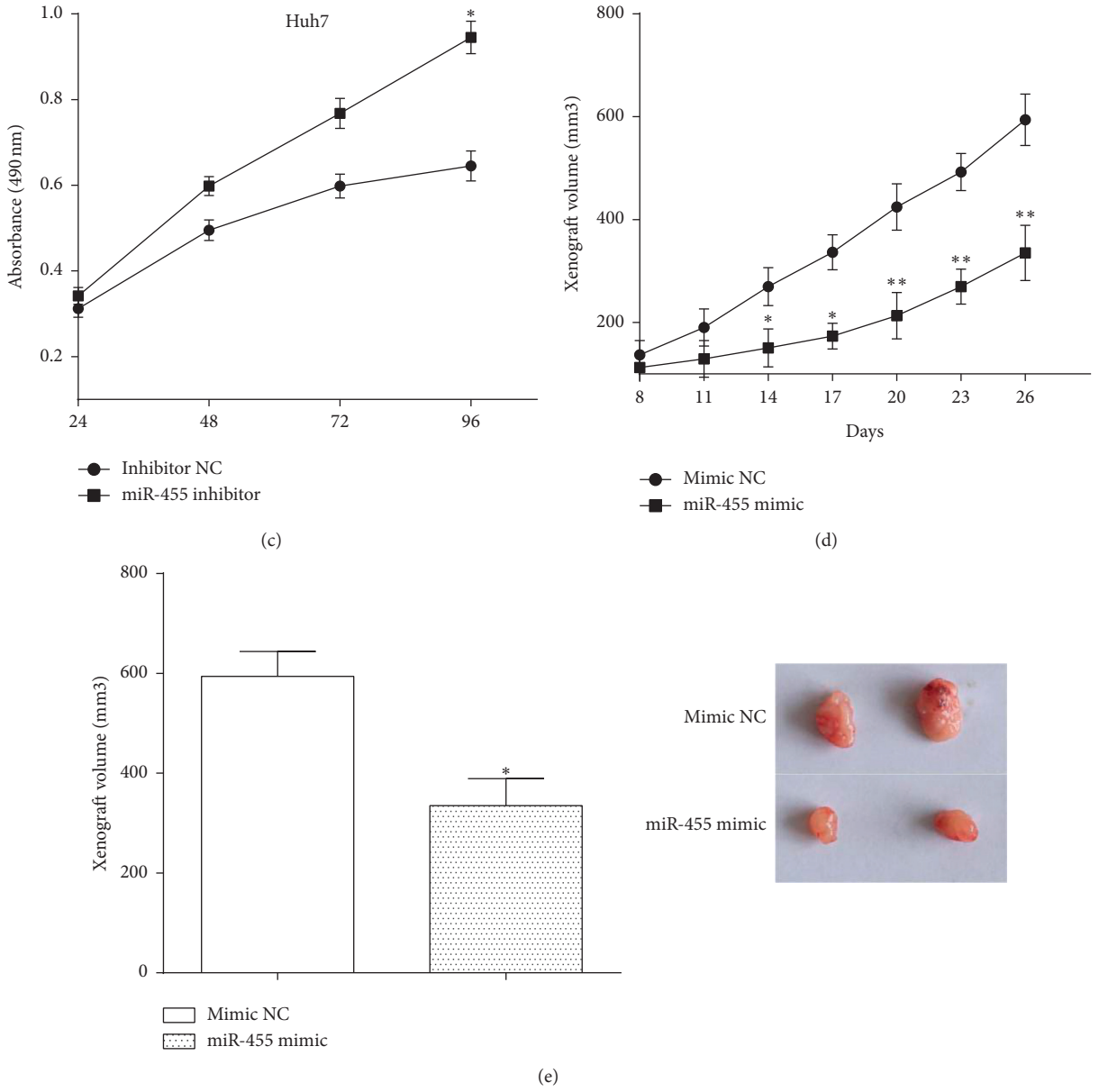

Figure 2: miR-455 inhibits cell viability of HCC in vitro and in vivo. (a) miR-455 mimic and miR-455 inhibitor were used to upregulate or downregulate the expression of miR-455 vs mimic NC or inhibitor NC, $^{*}P < 0.05$, $^{**}P < 0.01$. (b) The proliferative ability was decreased after transfection with miR-455 mimic vs mimic NC, $^{*}P < 0.05$. (c) miR-455 inhibitor increased proliferative ability in comparison with normal control vs inhibitor NC, $^{*}P < 0.05$. (d) miR-455 suppressed the growth of HCC in vivo vs inhibitor NC, $^{*}P < 0.05$; $^{**}P < 0.01$. (e) Tumors of miR-455 overexpressed group had a smaller volume than that of control group vs inhibitor NC, $^{*}P < 0.05$.

Transwell assays were performed in miR-455 mimic-transfected Huh7 cells. RAB18 overexpressed plasmid was transfected in miR-455 mimic-transfected cells and the efficiency was calculated by RT-qPCR (Figure 5(c)). CCK8 result revealed that cotransfection with RAB18 overexpressed plasmid and miR-455 mimic increased cell proliferation versus only transfected miR-455 mimic ($P < 0.05$) (Figure 5(d)). Moreover, Transwell assay elucidated that overexpressing RAB18 improved cell invasive ability in miR-455 mimic-transfected cells ($P < 0.05$) (Figure 5(e)). All results validated that RAB18 reversed partial functions of miR-455 on cell viability and invasion in HCC cells.

4. Discussion

Although treatment with HCC has improved, recurrence and metastasis often occur, and the 5-year overall survival rate remains low [23, 24]. Therefore, it is important to identify growth and metastasis mechanisms and develop biomarkers that improve patient outcomes.

Increasing evidence indicates that miRNAs have a major impact on cancer growth and metastasis and are associated with tumor development and progression [25, 26]. A previous study showed that miR-455 functioned as a tumor suppressor to inhibit cell proliferation and migration in

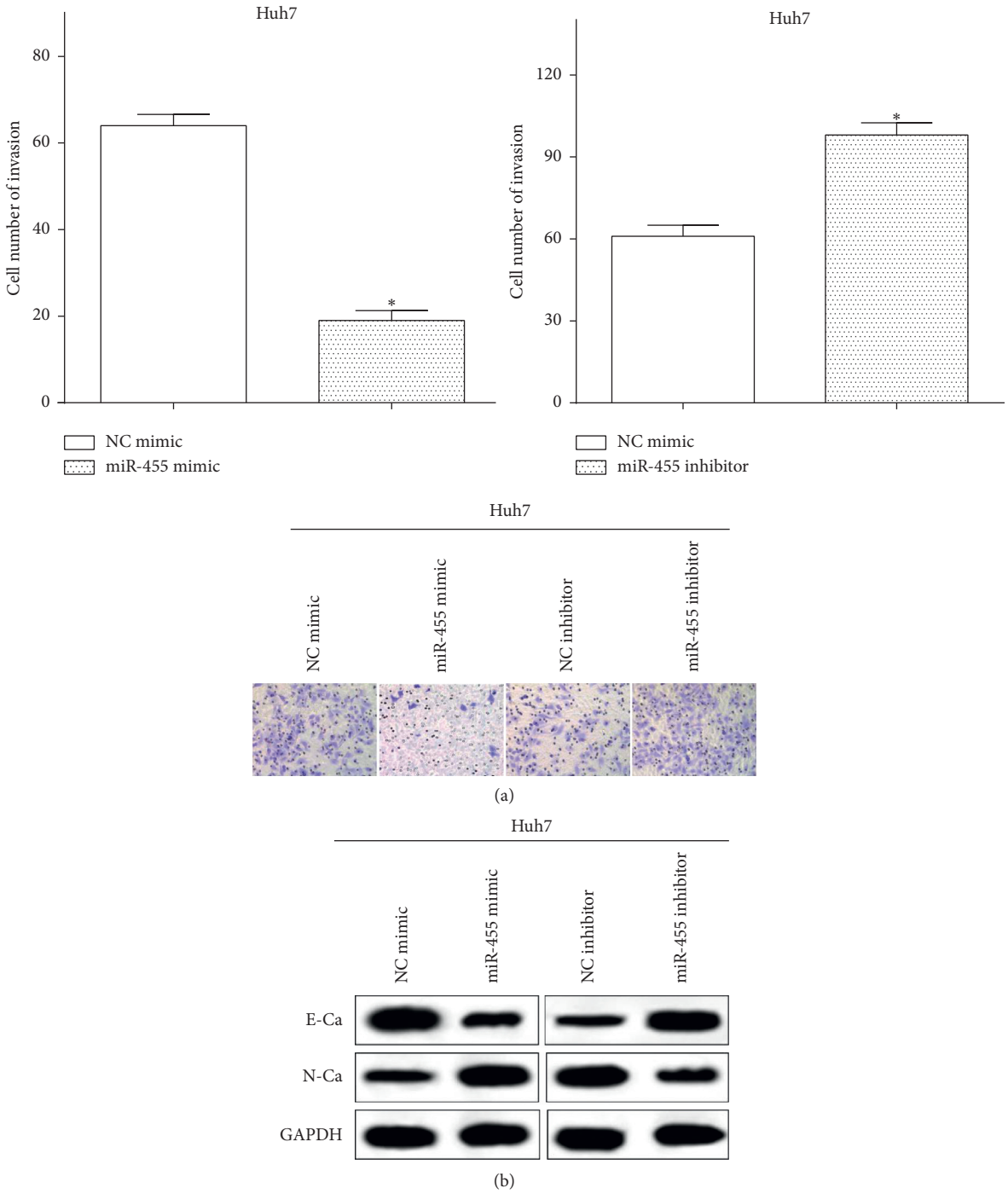

Figure 3: miR-455 impairs cell metastasis of HCC cells. (a) miR-455 mimic reduced the invasive ability, while miR-455 inhibitor improved that in Huh7 cells vs mimic NC, $^{*}P < 0.05$. (b) miR-455 inhibited the EMT ability in Huh7 cells.

colorectal cancer [27]. Methods were referred to previous studies [28]. Consistent with the findings in colorectal cancer, we discovered that the expression of miR-455 was low in HCC tissues and cell lines versus the nontumor tissues and normal cells. What is more, our results were consistent with the findings in esophageal squamous cell carcinoma, miR-455 acted as a prognostic marker, and downregulation of miR-455 was connected with worse outcome of HCC patients [29]. miR-455 suppressed cell proliferation of HCC in vitro and in vivo, which was consistent with the findings in breast cancer [30]. What is more, miR-455 impaired cell proliferation and invasion in colorectal cancer [31]. We also found that miR-455 suppressed cell invasive ability in HCC. In addition, miR-455 suppressed the EMT phenomenon of HCC by downregulating N-cadherin expression but upregulating E-cadherin.

RAB18 promoted cell viability, invasion, and migration and impaired cell apoptosis in gastric cancer [32]. In addition,

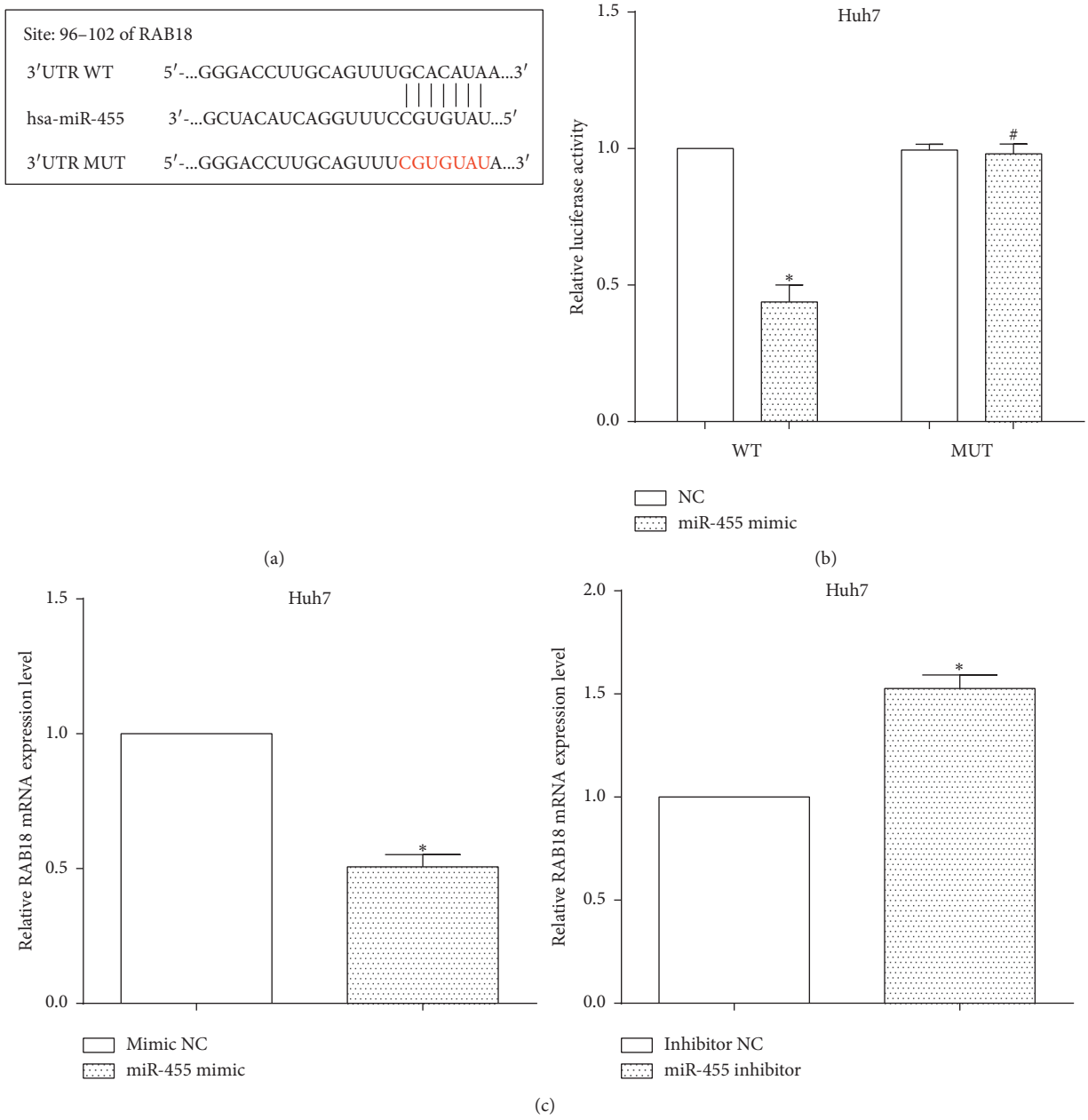

Figure 4: miR-455 targets RAB18 and regulates its expression. (a) TargetScan predicted that RAB18 was a potential target of miR-455. (b) miR-455 mimic reduced the luciferase ability of wild type mRNA 3′-UTR, whereas it did not alter the mutant 3′-UTR vs WT-NC, $^{*}P < 0.05$ and vs MUT-NC, $^{\#}P < 0.05$. (c) The expression of RAB18 was decreased by miR-455 mimic, while it was promoted by miR-455 inhibitor in Huh7 cells vs mimic NC, $^{*}P < 0.05$ and vs inhibitor NC, $^{*}P < 0.05$.

interference of RAB18 suppressed cell viability of non-small-cell lung cancer [33]. In this study, the expression of RAB18 was significantly mediated by miR-455, which was consistent with the findings in gastric cancer where miR-455 targeted RAB18 through directly binding to the 3′-UTR of RAB18 mRNA [34]. What is more, we discovered that RAB18 was overexpressed in HCC tissues and cell lines. RAB18 reversed partial roles of miR-455 on cell viability and invasion in HCC.

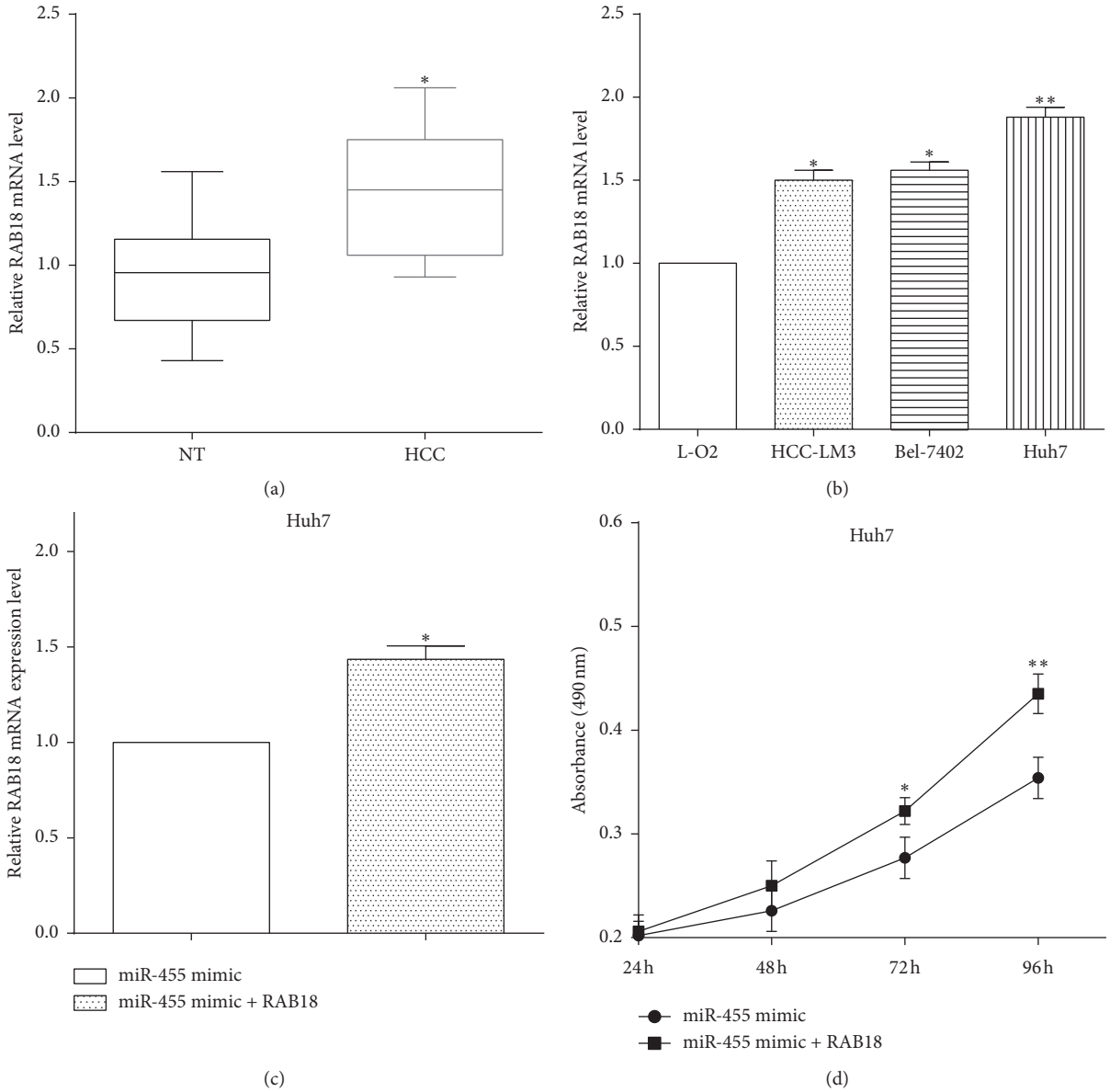

Figure 5: Continued.

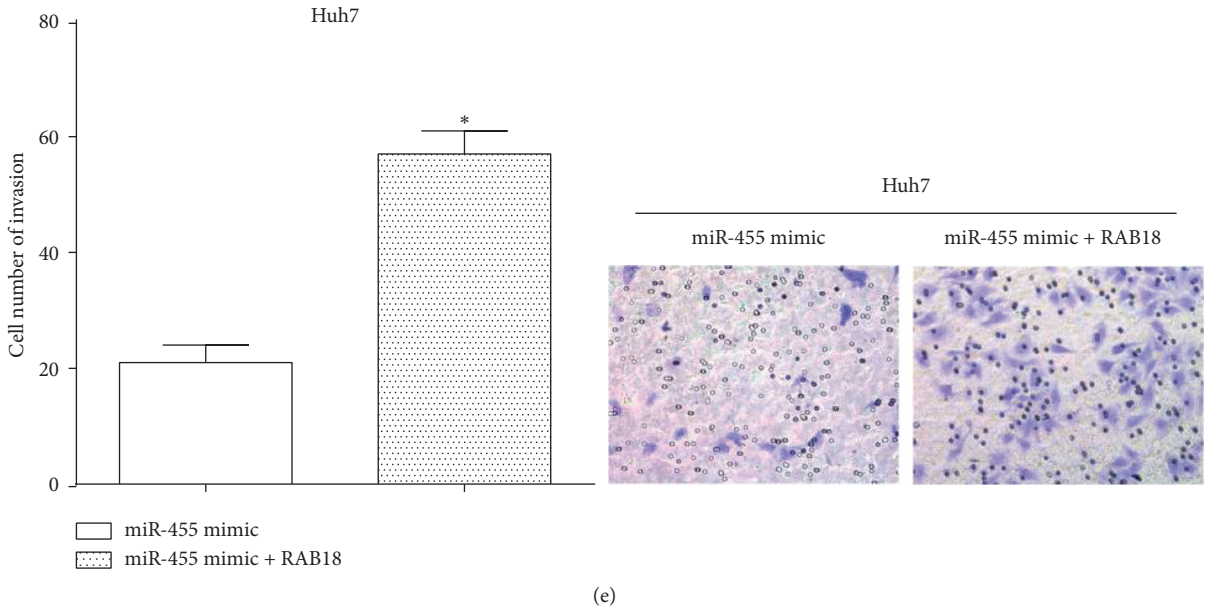

Figure 5: RAB18 restores partial functions of miR-455 on cell viability and invasion. (a) RAB18 was overexpressed in HCC tissues versus nontumor tissues vs NT, $^{*}P < 0.05$. (b) The expression of RAB18 was higher in HCC-LM3, Huh7, and Bel-7402 than in L-O2 cells vs L-O2, $^{*}P < 0.05$; $^{**}P < 0.01$. (c) RT-qPCR revealed the transfection efficiency of overexpressing RAB18 in miR-455 mimic-tranfected cells vs miR-455 mimic, $^{*}P < 0.05$. (d) RAB18 reversed partial functions of miR-455 on cell viability vs miR-455 mimic, $^{*}P < 0.05$. (e) Overexpressing RAB18 improved cell invasive ability in miR-455 mimic-transfected cells vs miR-455 mimic, $^{*}P < 0.05$.

5. Conclusion

The expression of miR-455 was low in HCC tissues and cell lines, and downregulation of miR-455 was connected with worse outcome of HCC patients. miR-455 suppressed cell growth in vitro and in vivo and suppressed the abilities of cell invasion and EMT in HCC. miR-455 regulated cell viability and invasion by directly targeting the 3′-UTR of RAB18 mRNA. RAB18 reversed partial roles of miR-455 on cell viability and invasion in HCC.

Data Availability

The data used to support the findings of this study are available from the corresponding author upon request.

Conflicts of Interest

The authors declare that they have no conflicts of interest.

References

[1] A. Forner and J. Bruix, "Biomarkers for early diagnosis of hepatocellular carcinoma," *The Lancet Oncology*, vol. 13, no. 8, pp. 750-751, 2012.

[2] H. C. Spangenberg, R. Thimme, and H. E. Blum, "Targeted therapy for hepatocellular carcinoma," *Nature Reviews Gastroenterology and Hepatology*, vol. 6, no. 7, pp. 423–432, 2009.

[3] S. Kakar, J. P. Grenert, V. Paradis, N. Pote, S. Jakate, and L. D. Ferrell, "Hepatocellular carcinoma arising in adenoma: similar immunohistochemical and cytogenetic features in adenoma and hepatocellular carcinoma portions of the tumor," *Modern Pathology*, vol. 27, no. 11, pp. 1499–1509, 2014.

[4] A. P. Venook, C. Papandreou, J. Furuse, and L. Ladrón de Guevara, "The incidence and epidemiology of hepatocellular carcinoma: a global and regional perspective," *The Oncologist*, vol. 15, no. S4, pp. 5–13, 2010.

[5] L. Liu, L. Chen, X. Wu et al., "Low-dose DNA-demethylating agent enhances the chemosensitivity of cancer cells by targeting cancer stem cells via the upregulation of microRNA-497," *Journal of Cancer Research and Clinical Oncology*, vol. 142, no. 7, pp. 1431–1439, 2016.

[6] S. M. Hartig, M. P. Hamilton, D. A. Bader, and S. E. McGuire, "The miRNA interactome in metabolic homeostasis," *Trends in Endocrinology and Metabolism*, vol. 26, no. 12, pp. 733–745, 2015.

[7] A. Habieb, M. Matboli, H. El-Tayeb, and F. El-Asmar, "Potential role of lncRNA-TSIX, miR-548-a-3p, and SOGA1 mRNA in the diagnosis of hepatocellular carcinoma," *Molecular Biology Reports*, vol. 46, pp. 4581–4590, 2019.

[8] M. Chuma, H. Toyoda, J. Matsuzaki et al., "Circulating microRNA-1246 as a possible biomarker for early tumor recurrence of hepatocellular carcinoma," *Hepatology Research: The Official Journal of the Japan Society of Hepatology*, vol. 49, pp. 810–822, 2019.

[9] J. Pu, J. Wang, Z. Xu et al., "miR-632 functions as oncogene in hepatocellular carcinoma via targeting MYCT1," *Human Gene Therapy. Clinical development*, vol. 30, pp. 67–73, 2019.

[10] S. Sun, N. Wang, Z. Sun, X. Wang, and H. Cui, "MiR-5692a promotes proliferation and inhibits apoptosis by targeting HOXD8 in hepatocellular carcinoma," *Journal of B.U.ON.: Official Journal of the Balkan Union of Oncology*, vol. 24, pp. 178–186, 2019.

[11] Y. Zhao, M. Yan, Y. Yun et al., "MicroRNA-455-3p functions as a tumor suppressor by targeting eIF4E in prostate cancer," *Oncology Reports*, vol. 37, no. 4, pp. 2449–2458, 2017.

[12] T. Ning, Z. Peng, S. Li et al., "miR-455 inhibits cell proliferation and migration via negative regulation of EGFR in human gastric cancer," *Oncology Reports*, vol. 38, no. 1, pp. 175–182, 2017.

[13] Q. D. Mao, W. Zhang, K. Zhao et al., "MicroRNA-455 suppresses the oncogenic function of HDAC2 in human colorectal cancer," *Brazilian Journal of Medical and Biological Research*, vol. 50, Article ID e6103, 2017.

[14] Z. Li, Q. Meng, A. Pan et al., "MicroRNA-455-3p promotes invasion and migration in triple negative breast cancer by targeting tumor suppressor EI24," *Oncotarget*, vol. 8, no. 12, pp. 19455–19466, 2017.

[15] W. J. Chia and B. L. Tang, "Emerging roles for Rab family GTPases in human cancer," *Biochimica et Biophysica Acta (BBA)—Reviews on Cancer*, vol. 1795, no. 2, pp. 110–116, 2009.

[16] M. Huang and Y. Wang, "Targeted quantitative proteomic approach for probing altered protein expression of small GTPases associated with colorectal cancer metastasis," *Analytical Chemistry*, vol. 91, pp. 6233–6241, 2019.

[17] V. Casado-Medrano, L. Barrio-Real, A. Wang, M. Cooke, C. Lopez-Haber, and M. G. Kazanietz, "Distinctive requirement of PKCε in the control of Rho GTPases in epithelial and mesenchymally transformed lung cancer cells," *Oncogene*, vol. 38, pp. 5396–5412, 2019.

[18] P. Seshacharyulu, S. Rachagani, S. Muniyan et al., "FDPS cooperates with PTEN loss to promote prostate cancer progression through modulation of small GTPases/AKT axis," *Oncogene*, vol. 38, pp. 5265–5280, 2019.

[19] D. Xu, Y. Li, L. Wu et al., "Rab18 promotes lipid droplet (LD) growth by tethering the ER to LDs through SNARE and NRZ interactions," *Journal of Cell Biology*, vol. 217, no. 3, pp. 975–995, 2018.

[20] S. Salloum, H. Wang, C. Ferguson, R. G. Parton, and A. W. Tai, "Rab18 binds to hepatitis C virus NS5A and promotes interaction between sites of viral replication and lipid droplets," *PLoS Pathogens*, vol. 9, Article ID e1003513, 2013.

[21] R. Vazquez-Martinez, A. J. Martinez-Fuentes, M. R. Pulido et al., "Rab18 is reduced in pituitary tumors causing acromegaly and its overexpression reverts growth hormone hypersecretion," *The Journal of Clinical Endocrinology & Metabolism*, vol. 93, no. 6, pp. 2269–2276, 2008.

[22] M. R. Pulido, A. Diaz-Ruiz, Y. Jimenez-Gomez et al., "Rab18 dynamics in adipocytes in relation to lipogenesis, lipolysis and obesity," *PLoS One*, vol. 6, Article ID e22931, 2011.

[23] J. Bruix, G. J. Gores, and V. Mazzaferro, "Hepatocellular carcinoma: clinical frontiers and perspectives," *Gut*, vol. 63, no. 5, pp. 844–855, 2014.

[24] G. Ferrin, M. de la Mata, J. L. Montero-Álvarez, P. Aguilar-Melero, and M. Rodríguez-Perálvarez, "Biomarkers for hepatocellular carcinoma: diagnostic and therapeutic utility," *Hepatic Medicine: Evidence and Research*, vol. 7, pp. 1–10, 2015.

[25] D. P. Bartel, "MicroRNAs: target recognition and regulatory functions," *Cell*, vol. 136, no. 2, pp. 215–233, 2009.

[26] G. A. Calin and C. M. Croce, "MicroRNA signatures in human cancers," *Nature Reviews Cancer*, vol. 6, no. 11, pp. 857–866, 2006.

[27] H. Yunqi, Y. Fangrui, Y. Yongyan et al., "miR-455 functions as a tumor suppressor through targeting GATA6 in colorectal cancer," *Oncology Research Featuring Preclinical and Clinical Cancer Therapeutics*, vol. 27, no. 3, pp. 311–316, 2019.

[28] Y. Jiao, G. Zhu, J. Yu et al., "miR-1271 inhibits growth, invasion and epithelial-mesenchymal transition by targeting ZEB1 in ovarian cancer cells," *OncoTargets and Therapy*, vol. 12, pp. 6973–6980, 2019.

[29] H. Yang, Y. N. Wei, J. Zhou, T. T. Hao, and X. L. Liu, "MiR-455-3p acts as a prognostic marker and inhibits the proliferation and invasion of esophageal squamous cell carcinoma by targeting FAM83F," *European Review for Medical and Pharmacological Sciences*, vol. 21, pp. 3200–3206, 2017.

[30] B. Wang, A. Zou, L. Ma et al., "miR-455 inhibits breast cancer cell proliferation through targeting CDK14," *European Journal of Pharmacology*, vol. 807, pp. 138–143, 2017.

[31] J. Chai, S. Wang, D. Han, W. Dong, C. Xie, and H. Guo, "MicroRNA-455 inhibits proliferation and invasion of colorectal cancer by targeting RAF proto-oncogene serine/threonine-protein kinase," *Tumor Biology*, vol. 36, no. 2, pp. 1313–1321, 2015.

[32] B. Wu, R. Qi, X. Liu, L. Qian, and Z. Wu, "Rab18 overexpression promotes proliferation and chemoresistance through regulation of mitochondrial function in human gastric cancer," *OncoTargets and Therapy*, vol. 11, pp. 7805–7820, 2018.

[33] K. Zhong, K. Chen, L. Han, and B. Li, "MicroRNA-30b/c inhibits non-small cell lung cancer cell proliferation by targeting Rab18," *BMC Cancer*, vol. 14, p. 703, 2014.

[34] J. Liu, J. Zhang, Y. Li, L. Wang, B. Sui, and D. Dai, "MiR-455-5p acts as a novel tumor suppressor in gastric cancer by down-regulating RAB18," *Gene*, vol. 592, no. 2, pp. 308–315, 2016.

Hindawi
Journal of Oncology
Volume 2021, Article ID 9961189, 10 pages
https://doi.org/10.1155/2021/9961189

Research Article

Long Noncoding RNA HCG11 Acts as a Tumor Suppressor in Gastric Cancer by Regulating miR-942-5p/BRMS1 Axis

Qingmei Zhang,[1] **Keli Yang**,[2] **Jie Li**,[3] **Fang Chen**,[4] **Yan Li**,[5] **and Qiuju Lin**[6]

[1]*Emergency Ward, Qingdao Hospital of Traditional Chinese Medicine, Qingdao Hiser Hospital, Qingdao 266033, China*
[2]*Gastroenterology Department, People's Hospital of Chiping, Chiping 252100, China*
[3]*Department of Oncology, People's Hospital of Rizhao, Rizhao 276800, China*
[4]*ICU, the People's Hospital of Zhangqiu Area, Jinan 250200, China*
[5]*Interventional Vascular Department, the People's Hospital of Zhangqiu Area, Jinan 250200, China*
[6]*Oncology Department (II), Qingdao Central Hospital, Qingdao University, Qingdao 266042, China*

Correspondence should be addressed to Qiuju Lin; linqiuju@sdqdzxyy.cn

Received 19 March 2021; Accepted 30 April 2021; Published 11 May 2021

Academic Editor: Muhammad Wasim Khan

The functions of long noncoding RNAs (lncRNAs) have been widely investigated in human cancers, including gastric cancer (GC). The purpose of this study was to elucidate the role of lncRNA HCG11 in GC. In this study, mRNA and protein expressions were detected by quantitative real-time polymerase chain reaction assays (RT-qPCR) and Western blot analysis. The proliferation ability of GC cells was examined by (3-(4,5-Dimethylthiazol-2-yl)-2,5-Diphenyl Tetrazolium Bromide) MTT assays. The invasion and migration abilities of GC cells were evaluated by Transwell assays. The binding sites between miR-942-5p and HCG11/BRMS1 were confirmed by dual-luciferase reporter assays. Results showed that LncRNA HCG11 was downregulated in GC cells. Functionally, overexpression of HCG11 inhibited GC cell proliferation, migration, and invasion. In addition, lncRNA HCG11 was found to act as a molecular sponge of miR-942-5p. Furthermore, miR-942-5p promoted GC progression by suppressing lncRNA HCG11 expression. Besides that, BRMS1 was confirmed as a direct target of miR-942-5p. More importantly, breast cancer metastasis suppressor 1 (BRMS1) inhibited GC progression by upregulating lncRNA HCG11 and downregulating miR-942-5p. In conclusion, LncRNA HCG11 inhibited cell proliferation, migration, and invasion in GC by sponging miR-942-5p and upregulating BRMS1.

1. Introduction

Gastric cancer (GC) is a malignant tumor originating from the gastric mucosal epithelium, and its incidence has been increasing in recent years. Moreover, GC not only causes damage to the digestive system but also may cause metastasis, affecting liver, kidney, and respiratory function [1]. Previous studies have shown that the tumorigenesis of GC may be related to smoking, high salt intake, viral infection, and heredity [2]. Although the current medical technology has made significant progress, the five-year overall survival rate of GC patients in China is still not optimistic, maintaining around 30% [3]. Recently, targeted therapy has become a hot spot for the treatment of cancer, including GC. Therefore, finding effective therapeutic targets is of great significance for improving the survival rate of GC patients.

As widely recognized targets, long noncoding RNAs (lncRNAs) have been reported to act as tumor suppressors and oncogenes in human cancers [4]. In addition, the functions of lncRNAs have been identified in GC [5]. For example, upregulation of lncRNA AWPPH inhibited proliferation and invasion of GC cells via miR-203a/DKK2 axis [6]. On the contrary, lncRNA SNHG8 promoted proliferation and invasion of GC cells by targeting the miR-491/PDGFRA axis [7]. Recently, the specific roles of lncRNA

HCG11 in other cancers caught our attention. Low expression of lncRNA HCG11 has been found in glioma and prostate cancer. Furthermore, lncRNA HCG11 inhibited the progression of glioma and prostate cancer [8, 9]. However, the dysregulation of HCG11 in GC remains unrevealed and needs to be illuminated. To further explore the regulatory mechanism of HCG11 in GC, miR-942-5p was predicted to be a downstream regulator of HCG11.

Previous studies have reported that miR-942-5p can be involved in the pathogenesis of human cancers. Upregulation of miR-942-5p has been detected in Huntington's disease and Kaposi's sarcoma and metastatic renal cell carcinoma [10, 11]. Functionally, miR-942-5p has been reported to promote proliferation and metastasis of hepatocellular carcinoma cells by inhibiting RRM2B [12]. More importantly, lncRNA Linc00675 suppressed cell proliferation and metastasis in colorectal cancer via targeting miR-942 [13]. These findings suggest that miR-942-5p acts as a tumor promoter in cancers. However, little is known about the regulatory mechanism of lncRNA HCG11/miR-942-5p in GC. Besides that, it is well known that miRNAs regulate human cancers by interacting with target genes. In this study, breast cancer metastasis suppressor 1 (BRMS1) was found to have a binding site with miR-942-5p.

BRMS1 was initially identified in breast carcinoma and suppressed breast cancer metastasis [14]. Recently, the function of BRMS1 has been identified in other cancers. For example, BRMS1 can suppress metastasis and correlate with improved patient survival in non-small cell lung cancer [15]. Besides, BRMS1 can coordinately regulate miRNA expression to participate in tumorigenesis [16]. For example, Guo *et al.* reported that miR-346 promoted hepatocellular carcinoma progression by suppressing BRMS1 expression [17]. In particular, downregulation of BRMS1 has been found in GC tissues [18]. Nevertheless, the function of BRMS1 in GC remains largely unknown.

Therefore, we explored the role of BRMS1 as well as its interaction with lncRNA HCG11/miR-942-5p in GC. Simultaneously, the regulatory mechanism of lncRNA HCG11/miR-942-5p was also investigated in GC. This study will provide a novel regulatory network in GC.

2. Materials and Methods

2.1. Cell Culture. Normal human gastric epithelium cell line GES-1 and GC cell line AGS and HGC-27 were purchased from BeNa Culture Collection (BNCC, Beijing, China). These cells were seeded in RPMI-1640 medium with 10% FBS and incubated in a humid atmosphere with 5% CO_2 at 37°C.

2.2. Cell Transfection. The pcDNA3.1 vector containing HCG11 complementary DNA, HCG11 siRNA, BRMS1 siRNA, miR-942-5p mimic, and miR-942-5p inhibitor were purchased from GenePharma (Shanghai, China). Next, they were transfected into AGS cells using Lipofectamine 2000 (Invitrogen/Thermo Fisher Scientific).

2.3. RT-qPCR. Total RNA extraction was performed using TRIzol reagent (Invitrogen, USA). The cDNA solution was synthesized using a PrimeScript RT reagent kit (Takara, Dalian, China). RT-qPCR assay was performed on ABI 7300 real-time PCR system (Applied Biosystems, Waltham, MA) using SYBR Green Master Mix II (Takara). HCG11 and miR-942-5p expression were normalized to U6, while BRMS1 was normalized to GAPDH. Their expressions were quantified with the $2^{-\triangle\triangle cq}$ method. The primers used were as follows: HCG11 forward 5′-AGG AGT GGT TGC ATT TGG GA-3′′; HCG11 reverse 5′′-CCC ACC ACG CAG TGA ATA GT-3′; miR-942-5p forward: 5′-GCC AGA TCT TGA TTG ACT TAC AGC CCA GTT-3′ and reverse, 5′-GCC GAA TTC CAC CTG TCT TTA TTC CAC CC-3′; U6-forward: 5′-GCT TCG GCA GCA CAT ATA CTA AAA T-3′ and reverse, 5′-CGC TTC ACG AAT TTG CGT GTC AT-3′; BRMS1 forward: 5′-CAG CCT CCA AGC AAA GAC AC-3′ and reverse, 5′-GCG GCG TCG CTC ATA GTC-3′; GAPDH forward: 5′-ACA ACT TTG GTA TCG TGG AAG G-3′, and reverse, 5′-GCC ATC ACG CCA CAG TTT C-3′.

2.4. MTT Assay. Transfected AGS cells (3×10^3 cells/well) were incubated in RPMI-1640 medium containing 10% FBS for 24, 48, 72, or 96 h. Then, AGS cells were incubated with 20 μl of MTT for 4 h. Next, 150 μl of dimethyl sulfoxide was added to the medium. After 10 minutes, we evaluated the cell viability using a spectrophotometer (Olympus Corp., Tokyo, Japan) to determine the optical density at 490 nm.

2.5. Transwell Assay. Cell invasion was detected in the upper chamber with Matrigel. Cell migration experiment was performed without Matrigel. Next, AGS cells (3×10^3 cells/well) were added to Transwell upper chamber. RPMI-1640 medium with 10% FBS was added to the lower chamber. After 24 h, the moving cells were fixed and stained for 30 mins. Observation and photographing were performed by a light microscope.

2.6. Western Blot Analysis. The protein was lysed using RIPA lysis buffer (Beyotime, Shanghai, China). Next, the protein was electrophoresed by 10% SDS-PAGE. Protein samples were blocked with 5% nonfat milk and transferred into PVDF membranes. Protein samples were then incubated with E-cadherin, N-cadherin, Bcl-2, Bax, and GAPDH primary antibodies (Abcam, Shanghai, China) overnight at 4°C. Secondary antibodies were added to incubate the protein for 1 h. Finally, the protein was examined using an ECL kit (Beyotime).

2.7. Dual-Luciferase Reporter Assay. The 3′-UTR of wild-type and mutant HCG11 (wt-HCG11 and mut-HCG11) or BRMS1 (wt-BRMS1 and mut-BRMS1) was inserted into pmiR-GLO vector (Promega Beijing Biotech Co., Beijing, China). Next, the above reporter plasmids or miR-942-5p mimics were transfected into AGS cells. After 48 h, luciferase activities were determined by a dual-luciferase reporter assay system (Promega, USA).

2.8. Statistical Analysis. Data are shown as mean ± SD and analyzed using Student's *t*-test or one-way ANOVA in SPSS 19.0 or Graphpad Prism 6. $P < 0.05$ was defined as a statistical difference.

3. Results

3.1. LncRNA HCG11 Inhibits Cell Proliferation, Migration, and Invasion in GC. First, the expression of HCG11 was detected in GES-1, AGS, and HGC-27 cells. RT-qPCR showed that HCG11 was downregulated in AGS and HGC-27 GC cells compared to GES-1 cells (Figure 1(a)). Furthermore, the expression of HCG11 is significantly decreased in AGS cells compared to HGC-27 cells. Thus, AGS cells were used to explore the role of HCG11 in GC. Next, HCG11 vector or siRNA was transfected into AGS cells, respectively. We found that HCG11 expression was inhibited by HCG11 siRNA and promoted by HCG11 vector (Figure 1(b)). MTT assay indicated that overexpression of HCG11 inhibited cell proliferation, while knockdown of HCG11 promoted cell proliferation in AGS cells (Figure 1(c)). Additionally, HCG11 vector promoted E-cadherin and Bax expression and inhibited N-cadherin and Bcl-2 expressions, while HCG11 siRNA showed an opposite effect on these genes in AGS cells (Figure 1(d)). Next, the Transwell assay showed that cell migration and invasion were restrained by HCG11 overexpression and promoted by HCG11 siRNA (Figures 1(e) and 1(f)). These results imply that lncRNA HCG11 inhibits cell proliferation, migration, and invasion in GC.

3.2. LncRNA HCG11 Acts as a Molecular Sponge of miR-942-5p. Next, starBase version 2.0 (http://starbase.sysu.edu.cn/) predicts that lncRNA HCG11 has a binding site with miR-942-5p (Figure 2(a)). Besides, the dual-luciferase reporter suggested that miR-942-5p mimics reduced the luciferase activity of wt-HCG11 but had little effect on mut-HCG11 luciferase activity in AGS cells (Figure 2(b)). Next, miR-942-5p expression was examined in AGS cells with HCG11 siRNA and vector. We found that HCG11 overexpression decreased miR-942-5p expression, while HCG11 downregulation promoted miR-942-5p expression in AGS cells (Figure 2(c)). Meanwhile, HCG11 expression was detected in AGS cells with miR-942-5p mimics or inhibitors. HCG11 expression was found to be reduced by miR-942-5p mimics and enhanced by a miR-942-5p inhibitor (Figure 2(d)). Based on these results, lncRNA HCG11 was considered to act as a molecular sponge of miR-942-5p.

3.3. MiR-942-5p Is Involved in GC Progression by Mediating lncRNA HCG11. The expression of miR-942-5p was detected in GC cells. We found that miR-942-5p was upregulated in AGS and HGC-27 GC cells compared to GES-1cells (Figure 3(a)). To explore the interaction between miR-942-5p and lncRNA HCG11, miR-942-5p mimics, miR-942-5p inhibitor, or HCG11 siRNA was transfected into AGS cells. RT-qPCR showed that miR-942-5p mimics enhanced its expression, whereas miR-942-5p inhibitor decreased its expression in AGS cells. However, HCG11 siRNA recovered the decreased expression of miR-942-5p induced by its inhibitor (Figure 3(b)). Additionally, miR-942-5p mimics were found to promote N-cadherin and Bcl-2 expressions and suppress E-cadherin and Bax expression, while miR-942-5p inhibitor exerted the opposite effect on these genes. HCG11 siRNA exerted a reverse effect on the expression of these genes regulated by miR-942-5p inhibitor in AGS cells (Figure 3(c)). Functionally, cell proliferation, migration, and invasion were promoted by miR-942-5p overexpression and inhibited by miR-942-5p downregulation. Furthermore, the reverse effect of HCG11 siRNA on cell proliferation, migration, and invasion was also found in AGS cells with miR-942-5p inhibitor (Figures 3(d)–3(f)). Collectively, miR-942-5p promotes cell proliferation, migration, and invasion by downregulating lncRNA HCG11.

3.4. BRMS1 is a Direct Target of miR-942-5p. Further, TargetScan (http://www.targetscan.org) predicts that miR-942-5p has a binding site on the 3′-UTR of BRMS1 (Figure 4(a)). Luciferase reporter assay indicated that miR-942-5p mimics reduced the luciferase activity of wt-BRMS1 but had no effect on mut-BRMS1 luciferase activity (Figure 4(b)). In addition, BRMS1 expression was found to be reduced by miR-942-5p mimics and promoted by miR-942-5p inhibitor in AGS cells (Figure 4(c)). On the contrary, the expression level of BRMS1 was enhanced by upregulation of HCG11 and decreased by downregulation of HCG11 in AGS cells (Figure 4(d)). These results demonstrate that BRMS1 is a direct target of miR-942-5p and can be regulated by lncRNA HCG11 in GC.

3.5. BRMS1 Is Involved in GC Progression by Affecting lncRNA HCG11/miR-942-5p Axis. To further explore the interaction between lncRNA HCG11/miR-942-5p axis and BRMS1, HCG11 vector or miR-942-5p inhibitor was transfected into AGS cells with BRMS1 siRNA. First, we found that BRMS1 expression was lower in AGS and HGC-27 GC cells than GES-1 cells (Figure 5(a)). After transfection of BRMS1 siRNA, BRMS1 expression was decreased in AGS cells. However, HCG11 vector or miR-942-5p inhibitor recovered the decreased expression of BRMS1 (Figure 5(b)). Moreover, BRMS1 downregulation promoted N-cadherin and Bcl-2 expressions and restrained E-cadherin and Bax expression in AGS cells. HCG11 vector or miR-942-5p inhibitor reversely regulated the effect of BRMS1 siRNA on these genes (Figure 5(c)). Besides, knockdown of BRMS1 was found to promote cell proliferation, migration, and invasion in AGS cells. Similarly, HCG11 vector or miR-942-5p inhibitor abolished the promoting effect of BRMS1 siRNA on AGS cell proliferation, migration, and invasion (Figures 5(d)–5(f)). Taken together, BRMS1 is involved in GC progression by affecting lncRNA HCG11/miR-942-5p axis.

4. Discussion

Recently, various lncRNAs have been demonstrated to regulate tumorigenesis of GC. For example, lncRNA

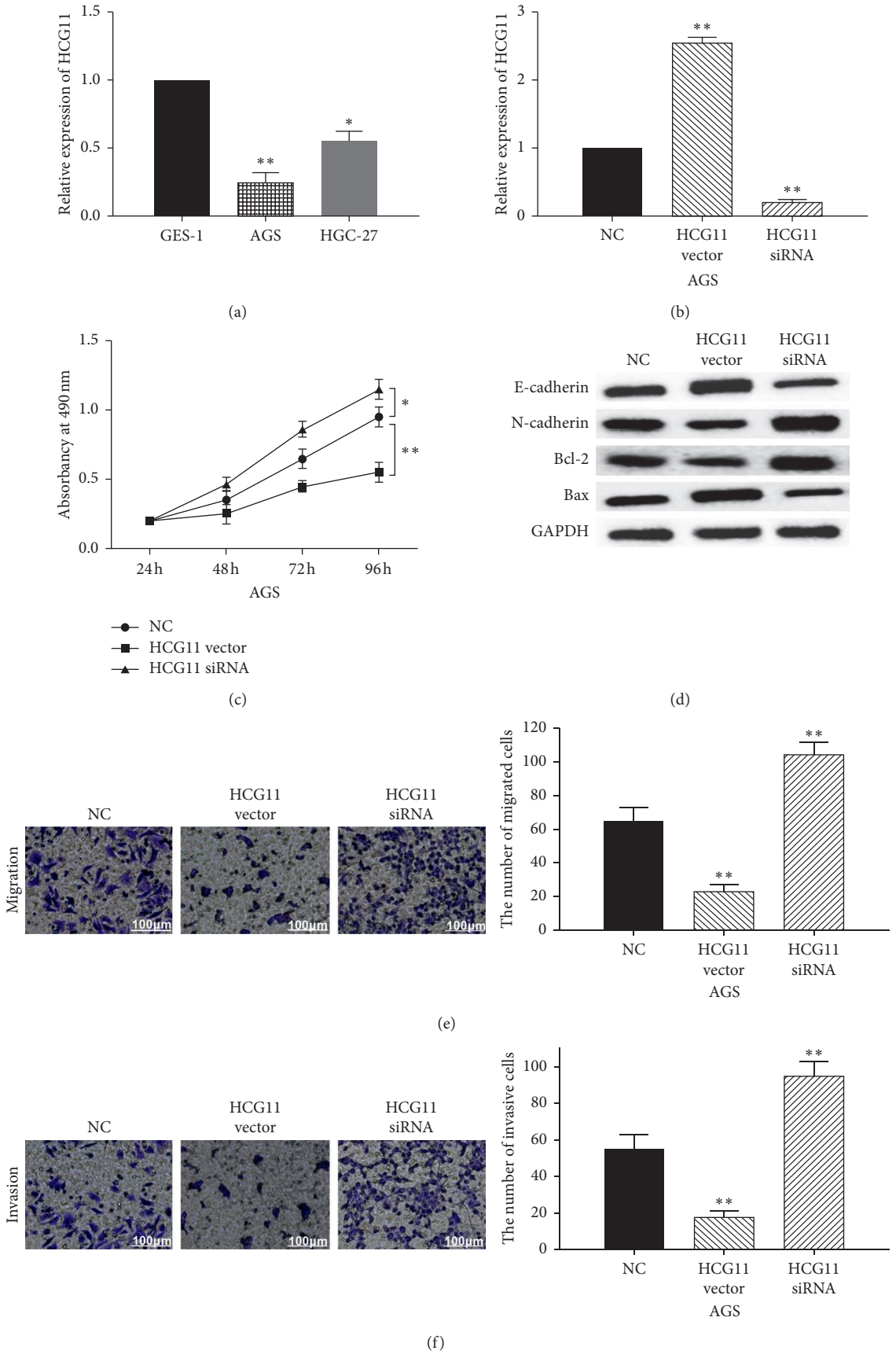

Figure 1: LncRNA HCG11 inhibits cell proliferation, migration, and invasion in GC. (a) The expression of HCG11 was detected in GES-1, AGS, and HGC-27 cells. (b) LncRNA HCG11 expression in AGS cells with its vector or siRNA. (c) Cell proliferation in AGS cells with HCG11 vector or siRNA. (d) The protein expressions of E-cadherin, N-cadherin, Bax, and Bcl-2 in AGS cells with HCG11 vector or siRNA. (e, f) Cell migration and invasion in AGS cells with HCG11 vector or siRNA. $^{*}P < 0.05$, $^{**}P < 0.01$.

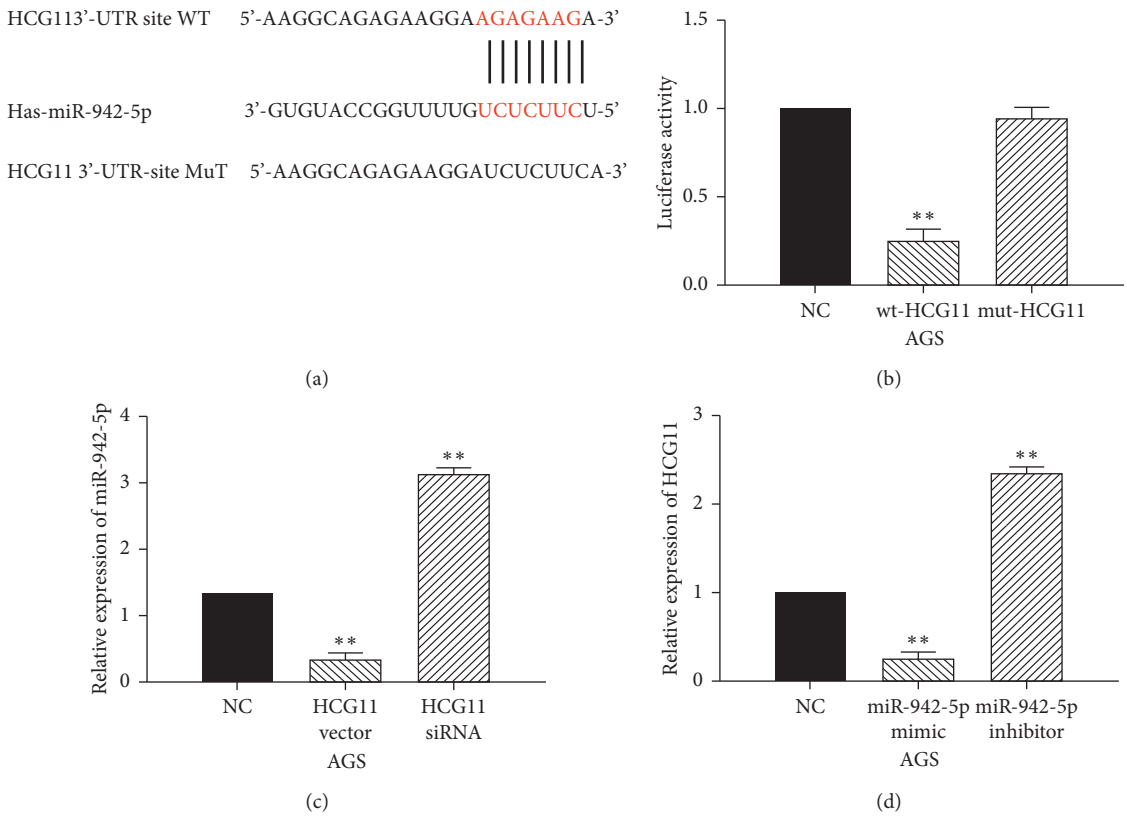

Figure 2: LncRNA HCG11 acts as a molecular sponge of miR-942-5p. (a) The binding sites of HCG11 with miR-942-5p. (b) Luciferase reporter assay. (c) MiR-942-5p expression regulated by HCG11 siRNA and vector in AGS cells. (d) HCG11 expression in AGS cells containing miR-942-5p mimics or inhibitor. $^{**}P < 0.01$.

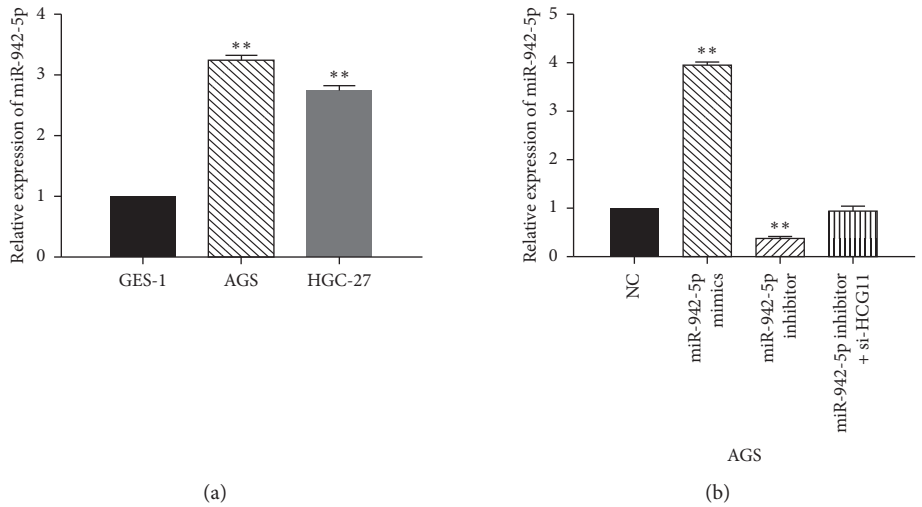

Figure 3: Continued.

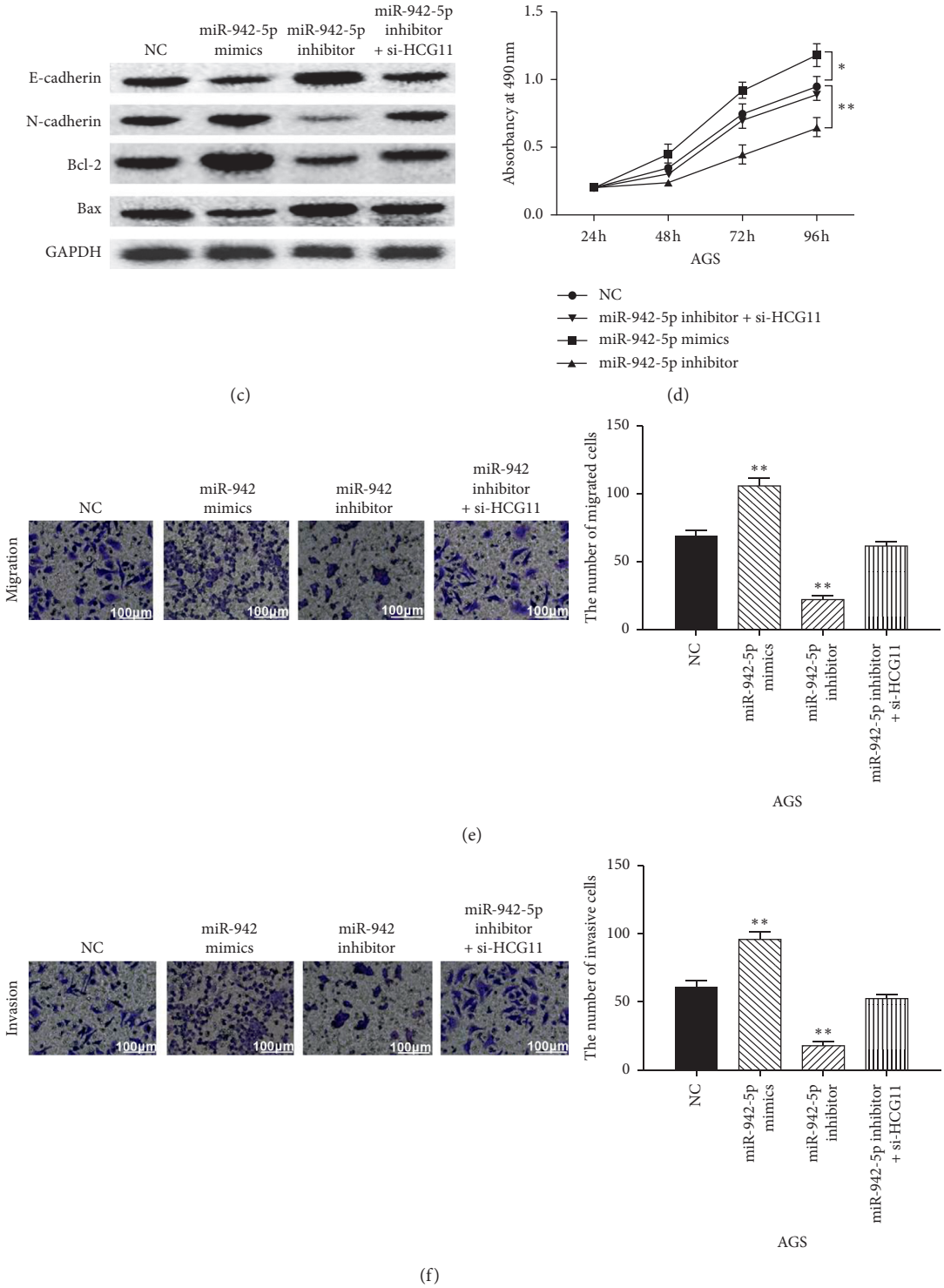

Figure 3: MiR-942-5p is involved in GC progression by mediating lncRNA HCG11. (a) The expression of miR-942-5p was detected in GES-1, AGS, and HGC-27 cells. (b) MiR-942-5p expression in AGS cells with miR-942-5p mimics, miR-942-5p inhibitor, or HCG11 siRNA. (c) The protein expressions of E-cadherin, N-cadherin, Bax, and Bcl-2 in AGS cells with miR-942-5p mimics, miR-942-5p inhibitor, or HCG11 siRNA. (d, e, f) Cell proliferation, migration, and invasion in AGS cells with miR-942-5p mimics, miR-942-5p inhibitor, or HCG11 siRNA. $^{*}P < 0.05$, $^{**}P < 0.01$.

LUCAT1 was upregulated in GC and promoted GC cell proliferation and invasion [19]. In addition, lncRNA MEG-3 was downregulated in GC. Overexpression of MEG-3 suppressed GC cell growth, invasion, and migration [20]. These findings suggest that lncRNAs are important regulators in GC progression. This study aimed to investigate the

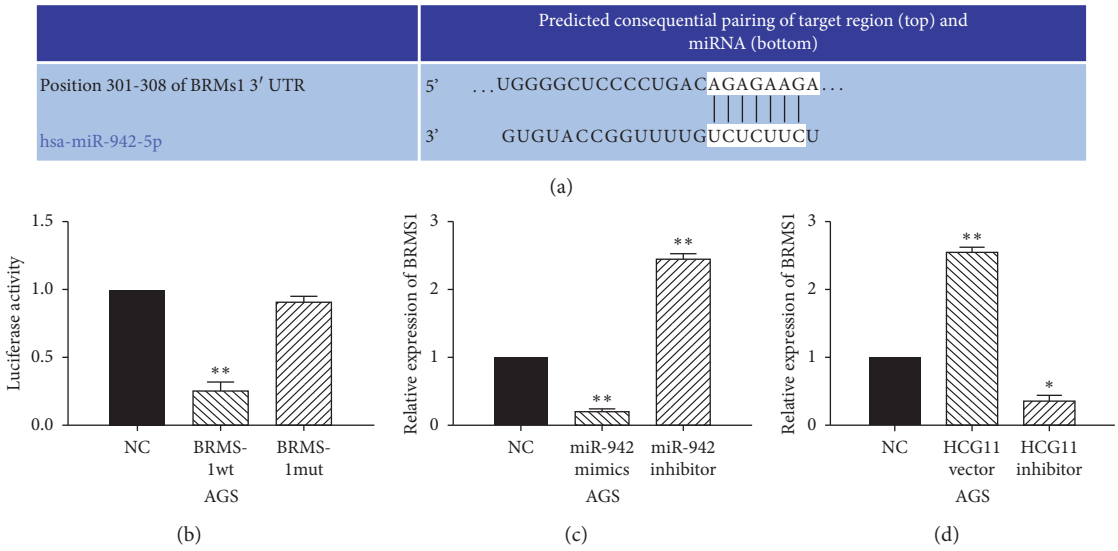

FIGURE 4: BRMS1 is a direct target of miR-942-5p. (a) The binding sites of BRMS1 and miR-942-5p. (b) Luciferase reporter assay. (c) BRMS1 expression in AGS cells with miR-942-5p mimics or inhibitor. (d) BRMS1 expression in AGS cells with HCG11 siRNA or vector. $^{*}P < 0.05$, $^{**}P < 0.01$.

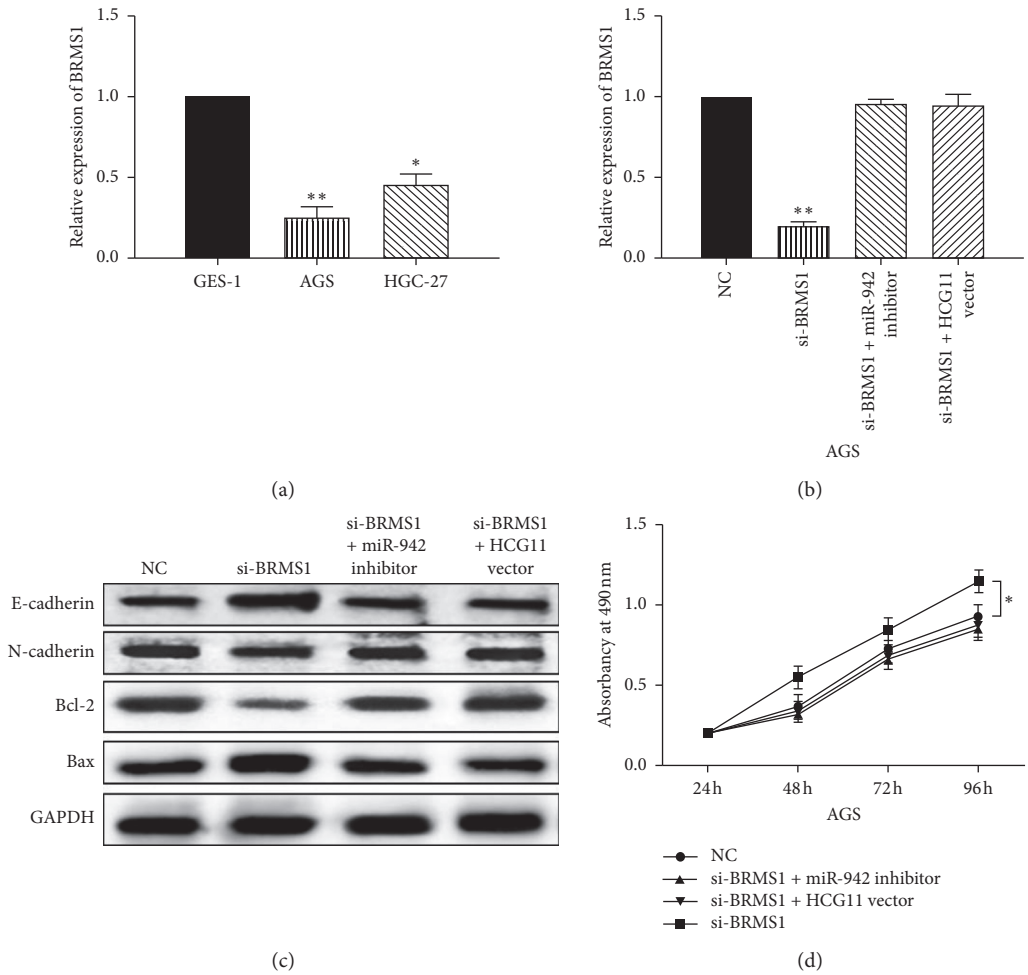

FIGURE 5: Continued.

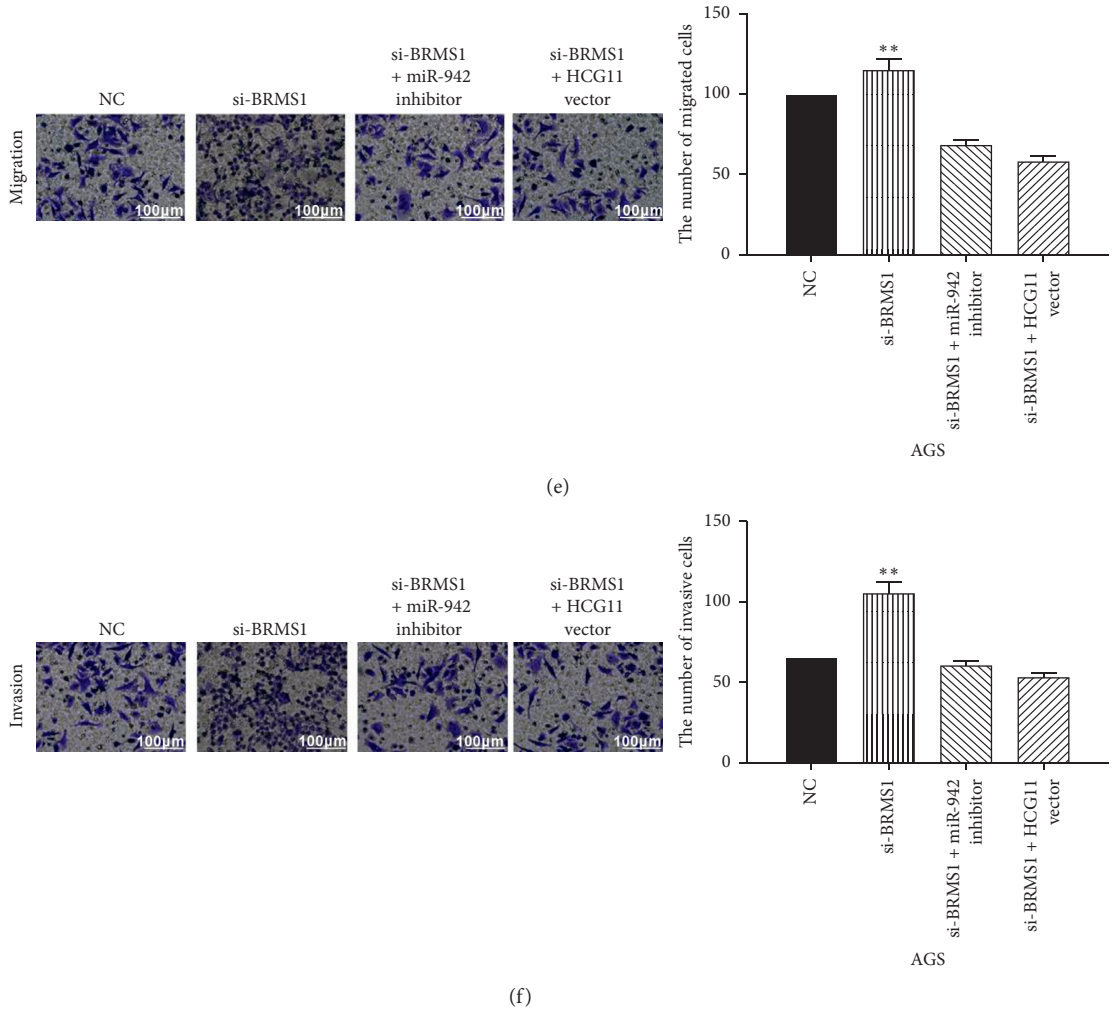

Figure 5: BRMS1 is involved in GC progression by affecting lncRNA HCG11/miR-942-5p axis. (a) The expression of BRMS1 was detected in GES-1, AGS, and HGC-27 cells. (b) BRMS1 expression in AGS cells with BRMS1 siRNA, BRMS1 siRNA + miR-942-5p inhibitor, or BRMS1 siRNA + HCG11 vector. (c) The protein expressions of E-cadherin, N-cadherin, Bax, and Bcl-2 in AGS cells with BRMS1 siRNA, BRMS1 siRNA + miR-942-5p inhibitor, or BRMS1 siRNA + HCG11 vector. (d, e, f) Cell proliferation, migration, and invasion in AGS cells with BRMS1 siRNA, BRMS1 siRNA + miR-942-5p inhibitor, or BRMS1 siRNA + HCG11 vector. $^{*}P < 0.05$, $^{**}P < 0.01$.

regulatory mechanism of lncRNA HCG11 in GC. We found that the downregulation of HCG11 expression was decreased in GC cells. Furthermore, HCG11 overexpression inhibited cell proliferation, migration, and invasion in GC. Consistent with our results, downregulation of HCG11 has been identified in prostate cancer and predicted a poor prognosis [21]. Additionally, HCG11 has been proposed to suppress the growth of glioma through cooperating with miR-4425/MTA3 axis [22]. Here, HCG11 was found to inhibit GC progression by interacting with miR-942-5p/BRMS1 axis.

It is widely recognized that lncRNAs can interact with miRNAs, thereby regulating the downstream genes. In the present study, we found that lncRNA HCG11 directly targets miR-942-5p and acts as a molecular sponge of miR-942-5p. At the same time, the role of miR-942-5p was also explored in GC. In contrast to HCG11, miR-942-5p was upregulated in GC cells. Upregulation of miR-942-5p promoted cell proliferation, migration, and invasion in GC. Similarly, Ge et al. found that miR-942-5p expression was also increased in esophageal squamous cell carcinoma and promoted cancer stem cell-like traits [23]. These findings demonstrate that miR-942-5p acts as a tumor promoter in GC. Meanwhile, we found that lncRNA HCG11 could interact with miR-942-5p in GC cells. Furthermore, HCG11 can exert a reverse effect on cell proliferation, migration, and invasion regulated by miR-942-5p in GC cells, which has not been reported in previous studies. Further, miR-942-5p was confirmed to target BRMS1 directly. Furthermore, lncRNA HCG11 can positively regulate BRMS1 expression in GC cells.

In this study, we found that BRMS1 expression was increased in GC cells. Knockdown of BRMS1 promoted cell proliferation, migration, and invasion in GC cells. In addition, BRMS1 has been found to upregulate miR-146 and suppress breast cancer metastasis [24]. Based on these results, we consider that BRMS1 plays an inhibitory effect

on GC progression. Besides that, miR-346 has been demonstrated to promote migration and invasion of nasopharyngeal carcinoma cells via targeting BRMS1 [25]. Here, miR-942-5p was also found to promote GC progression by targeting BRMS1. At the same time, we also found that BRMS1 competed with HCG11 to bind with miR-942-5p, which is firstly proposed. Rescue assays showed that HCG11 inhibited GC progression by upregulating BRMS1. Collectively, lncRNA HCG11 acts as a ceRNA to regulate GC progression by mediating the miR-942-5p/BRMS1 axis. This study firstly reveals the potential involvement of HCG11 in the pathogenesis of GC and investigates its correlation with miR-942-5p/BRMS1 hitherto unreported in GC.

5. Conclusion

To conclude, lncRNA HCG11 inhibited cell proliferation, migration, and invasion in GC by downregulating miR-942-5p and upregulating BRMS1. Our study reveals that lncRNA HCG11 may be a potential target for GC treatments. Although the regulatory mechanism of lncRNA HCG11 has been initially elucidated in this study, the further functional mechanism of HCG11 still needs to be investigated in GC by independent cohorts and prospective trials, such as EMT and the *in vivo* study.

Data Availability

The data used to support the findings of this study are available from the corresponding author upon request.

Conflicts of Interest

The authors declare that they have no conflicts of interest.

References

[1] A. E. Russo and V. E. Strong, "Gastric cancer etiology and management in asia and the west," *Annual Review of Medicine*, vol. 70, no. 1, pp. 353–367, 2019.

[2] S. Ge, "Association between habitual dietary salt intake and risk of gastric cancer: a systematic review of observational studies," *Gastroenterology Research and Practice*, vol. 2012, Article ID 808120, 11 pages, 2012.

[3] T. Aoyama and T. Yoshikawa, "Adjuvant therapy for locally advanced gastric cancer," *Surgery Today*, vol. 47, no. 11, pp. 1295–1302, 2017.

[4] R. L. Mather, "The evolutionarily conserved long non-coding RNA LINC00261 drives neuroendocrine prostate cancer proliferation and metastasis via distinct nuclear and cytoplasmic mechanisms," *Molecular Oncology*, 2021.

[5] J. Zou, K. Wu, C. Lin, and Z.-G. Jie, "LINC00319 acts as a microRNA-335-5p sponge to accelerate tumor growth and metastasis in gastric cancer by upregulating ADCY3," *American Journal of Physiology-Gastrointestinal and Liver Physiology*, vol. 318, no. 1, pp. G10–G22, 2020.

[6] D. Rong, C. Dong, K. Fu, H. Wang, W. Tang, and H. Cao, "Upregulation of circ_0066444 promotes the proliferation, invasion, and migration of gastric cancer cells," *OncoTargets and Therapy*, vol. 11, pp. 2753–2761, 2018.

[7] P. Zhang, S. Li, Z. Chen, Y. Lu, and H. Zhang, "LncRNA SNHG8 promotes proliferation and invasion of gastric cancer cells by targeting the miR-491/PDGFRA axis," *Human Cell*, vol. 33, no. 1, pp. 123–130, 2020.

[8] Y. Chen, "Long non-coding RNA HCG11 modulates glioma progression through cooperating with miR-496/CPEB3 axis," *Cell Proliferation*, vol. 52, no. 5, Article ID e12615, 2019.

[9] Y. C. Wang, W. Y. He, C. H. Dong, L. Pei, and Y. L. Ma, "lncRNA HCG11 regulates cell progression by targeting miR-543 and regulating AKT/mTOR pathway in prostate cancer," *Cell Biology International*, vol. 43, no. 12, pp. 1453–1462, 2019.

[10] E. R. Reed, J. C. Latourelle, J. H. Bockholt et al., "MicroRNAs in CSF as prodromal biomarkers for Huntington disease in the PREDICT-HD study," *Neurology*, vol. 90, no. 4, pp. e264–e272, 2018.

[11] C. Prior, "Identification of tissue microRNAs predictive of sunitinib activity in patients with metastatic renal cell carcinoma," *PLoS One*, vol. 9, no. 1, Article ID e86263, 2014.

[12] Q. Zhang, B. Zhu, J. Qian, K. Wang, and J. Zhou, "miR-942 promotes proliferation and metastasis of hepatocellular carcinoma cells by inhibiting RRM2B," *OncoTargets and Therapy*, vol. 12, pp. 8367–8378, 2019.

[13] Z. Shan, N. An, J. Qin, J. Yang, H. Sun, and W. Yang, "Long non-coding RNA Linc00675 suppresses cell proliferation and metastasis in colorectal cancer via acting on miR-942 and Wnt/β-catenin signaling," *Biomedicine & Pharmacotherapy*, vol. 101, pp. 769–776, 2018.

[14] C. Gong, "BRMS1L suppresses breast cancer metastasis by inducing epigenetic silence of FZD10," *Nature Communications*, vol. 5, p. 5406, 2014.

[15] P. W. Smith, Y. Liu, S. A. Siefert, C. A. Moskaluk, G. R. Petroni, and D. R. Jones, "Breast cancer metastasis suppressor 1 (BRMS1) suppresses metastasis and correlates with improved patient survival in non-small cell lung cancer," *Cancer Letters*, vol. 276, no. 2, pp. 196–203, 2009.

[16] M. D. Edmonds, D. R. Hurst, K. S. Vaidya, L. J. Stafford, D. Chen, and D. R. Welch, "Breast cancer metastasis suppressor 1 coordinately regulates metastasis-associated microRNA expression," *International Journal of Cancer*, vol. 125, no. 8, pp. 1778–1785, 2009.

[17] Z. Guo, J. Li, J. Sun, L. Sun, Y. Zhou, and Z. Yu, "miR-346 promotes HCC progression by suppressing breast cancer metastasis suppressor 1 expression," *Oncology Research Featuring Preclinical and Clinical Cancer Therapeutics*, vol. 26, no. 7, pp. 1073–1081, 2018.

[18] Y. Cao, S. Tan, Y Tu et al., "MicroRNA-125a-5p inhibits invasion and metastasis of gastric cancer cells by targeting BRMS1 expression," *Oncology Letters*, vol. 15, no. 4, pp. 5119–5130, 2018.

[19] J. Chi, T. Liu, C. Shi et al., "Long non-coding RNA LUCAT1 promotes proliferation and invasion in gastric cancer by regulating miR-134-5p/YWHAZ axis," *Biomedicine & Pharmacotherapy*, vol. 118, Article ID 109201, 2019.

[20] J. Jiao and S. Zhang, "Long noncoding RNA MEG3 suppresses gastric carcinoma cell growth, invasion and migration via EMT regulation," *Molecular Medicine Reports*, vol. 20, no. 3, pp. 2685–2693, 2019.

[21] Y. Zhang, P. Zhang, X. Wan et al., "Downregulation of long non-coding RNA HCG11 predicts a poor prognosis in prostate cancer," *Biomedicine & Pharmacotherapy*, vol. 83, pp. 936–941, 2016.

[22] L. Zhang, "Long non-coding RNA HCG11 suppresses the growth of glioma by cooperating with the miR-4425/MTA3

axis," *Journal of Gene Medicine*, vol. 21, no. 4, Article ID e3074, 2019.

[23] C. Ge, S. Wu, W. Wang et al., "miR-942 promotes cancer stem cell-like traits in esophageal squamous cell carcinoma through activation of Wnt/β-catenin signalling pathway," *Oncotarget*, vol. 6, no. 13, pp. 10964–10977, 2015.

[24] D. R. Hurst, M. D. Edmonds, G. K. Scott, C. C. Benz, K. S. Vaidya, and D. R. Welch, "Breast cancer metastasis suppressor 1 up-regulates miR-146, which suppresses breast cancer metastasis," *Cancer Research*, vol. 69, no. 4, pp. 1279–1283, 2009.

[25] H.-L. Yan, L. Li, S.-J. Li, H.-S. Zhang, and W. Xu, "miR-346 promotes migration and invasion of nasopharyngeal carcinoma cells via targeting BRMS1," *Journal of Biochemical and Molecular Toxicology*, vol. 30, no. 12, pp. 602–607, 2016.

Hindawi
Journal of Oncology
Volume 2021, Article ID 9954214, 10 pages
https://doi.org/10.1155/2021/9954214

Research Article

LncRNA MSC-AS1 Promotes Colorectal Cancer Progression by Regulating miR-325/TRIM14 Axis

Changhong He,[1] **Xia Wang**,[2] **Meichun Du**,[3] **and Yanjun Dong**[4]

[1]*Department of Clinical Laboratory, Yantaishan Hospital, Yantai 264000, China*
[2]*Blood Purification Centre, East Hospital, Qingdao Municipal Hospital, Qingdao 266071, China*
[3]*PICC Clinic, Qingdao Central Hospital Affiliated to Qingdao University, Qingdao 266042, China*
[4]*Department of Clinical Laboratory, People's Hospital of Rizhao, Rizhao 276800, China*

Correspondence should be addressed to Yanjun Dong; dongyanjun@sdrzph.cn

Received 29 March 2021; Accepted 29 April 2021; Published 11 May 2021

Academic Editor: Alamgeer Yuchi

Background. LncRNA MSC-AS1 has been reported to be a tumor promoter in hepatocellular carcinoma. However, the function of MSC-AS1 in colorectal cancer (CRC) has not been elucidated. It is designed to study the expression level of MSC-AS1 and investigate its biological effect on the progression of CRC. *Methods*. The expression patterns of MSC-AS1, miR-325, and TRIM14 were explored by RT-qPCR in CRC tissues and cells. The protein expression of TRIM14 was tested by Western blot assay. The association between MSC-AS1 expression and clinicopathological data was analyzed by chi-squared test. CCK-8 assay, colony formation, and Transwell assay were used to investigate the effect of MSC-AS1 on cell growth, invasion, and migration in CRC cells. The correlations among MSC-AS1, miR-325, and TRIM14 were analyzed by Pearson's correlation coefficient analysis. *Results*. We found that MSC-AS1 and TRIM14 were upregulated in CRC tissues, while miR-325 was downregulated in CRC tissues. Functional experiments demonstrated that MSC-AS1 knockdown inhibited cell proliferation, migration, and invasion abilities in CRC cells. Additionally, miR-325 was proved to be a target miRNA of MSC-AS1, and TRIM14 might be a downstream gene of miR-325. Besides that, MSC-AS1 counteracted the inhibitory effect of miR-325 on the cell progression and TRIM14 expression. *Conclusion*. Our results indicated that MSC-AS1 facilitated CRC progression by sponging miR-325 to upregulate TRIM14 expression. We suggested that MSC-AS1 might be a potential lncRNA-target for CRC therapy.

1. Introduction

Colorectal cancer (CRC) is one of the most common gastrointestinal malignancies, which seriously threatens human health. The incidence of CRC has been on the rise worldwide. In 2020, about 1.9 million patients were diagnosed with CRC worldwide, and more than 935,000 patients died directly or indirectly from CRC [1]. A large number of studies have shown that dietary habits (alcohol consumption, red meat, processed meat, and refined grains, etc.), lifestyle (low physical labor, smoking, etc.), obesity, diabetes, and genetic factors are the most important causes of CRC [2, 3]. The treatment of CRC is generally based on surgery, followed by radiotherapy, chemotherapy, or other treatments [4]. Although the survival rate of CRC has been improved in recent years, the economic burden of CRC ranks first among malignancies. In recent years, molecular targeted therapy has become a hot spot in tumor therapy.

These non-protein-coding RNAs are called noncoding RNAs, including long noncoding RNAs (lncRNAs) with a length of more than 200 nucleotides. Although the mode and regulatory mechanism of lncRNAs in tumors have not been thoroughly studied, lncRNAs are verified to play a vital role in the occurrence and development of human cancers [5]. At present, it has been found that related lncRNAs are involved in the occurrence, metastasis and invasion, early diagnosis, prognosis evaluation, and radiotherapy and chemotherapy efficacy of CRC [6, 7]. LncNEAT1 was reported to promote CRC progression by suppressing miR-486-5p expression and regulating NR4A1/Wnt/β-catenin pathway [8]. LncHSD17B11-1:1 acted as a tumor enhancing factor by regulating miR-338-3p and MACC1 in CRC [9]. In addition,

lncGNAT1-1 acted as a tumor inhibitor in CRC by modulating RKIP-NF-kappaB-Snail pathway [10]. LncRNA MSC antisense RNA 1 (MSC-AS1) has been reported to accelerate osteogenic differentiation by regulating miR-140e-5p and BMP2 [11]. Moreover, MSC-AS1 promoted tumor progression in kidney renal clear cell carcinoma [12]. Nevertheless, the role of MSC-AS1 in CRC remains unclear.

Plentiful reports have confirmed that lncRNAs act as miRNA sponges to upregulate downstream genes to affect tumor progression. For example, lncRNA UCA1 was found to promote CRC cell proliferation and 5-FU resistance by suppressing miR-204-5p [13]. KCNQ1OT1 was reported to facilitate CRC cell progression by inhibiting miR216b-5p to increase ZNF146 expression [14]. Zhang et al. found that LINC00152 was downregulated in CRC and induced cell apoptosis in CRC cells by regulating miR-376c-3p [15]. miR-325 was found to inhibit cell growth and metastasis by targeting MT3 in bladder cancer [16]. In the current work, bioinformatics analysis confirmed that miR-325 might be a target miRNA of MSC-AS1.

In this article, we explored the expression of MSC-AS1 in CRC tissues. In the meantime, the function of MSC-AS1 knockdown on cell proliferation, migration, and invasion was also detected. Most importantly, we demonstrated that MSC-AS1 influenced the tumor progression by regulating miR-325/TRIM14 axis in CRC.

2. Materials and Methods

2.1. Clinical Specimens. 46 tissues from patients with CRC were obtained from Yantaishan Hospital. The CRC tissues and paracancerous tissues were surgically collected and stored in liquid nitrogen. All patients did not receive any preoperative treatment (radiotherapy or chemotherapy). Before surgery, the purpose and significance of this study were introduced to all patients or their family members; and we have obtained the informed consents signed by all patients or their family members. This study was approved by the Ethics Committee of Yantaishan Hospital.

2.2. Cell Culture and Cell Transfection. CRC cell lines HT29, SW620, HCT116, and SW480 and normal human epithelial cells NCM460 were obtained from TongPai (Shanghai) Biotechnology Co., LTD (Shanghai, China). The frozen CRC cells were placed in a 37°C water bath until they were completely dissolved. Cells were resuspended with DMEM containing 10% PBS. Then, CRC cells were cultured in an incubator at 37°C and 5% CO_2. Cell passage was carried out when the cell confluence reached 70–80%.

CRC cells (2×10^5 cells/well) in logarithmic growth phase were cultured into 6-well plate. MSC-AS1 siRNA, negative control (si-NC), pcDNA3.1-MSC-AS1 (MSC-AS1 vector), miR-325 mimic, and NC mimic were transfected into cells by Lipofectamine 2000. After culturing at 37°C and 5% CO_2 for 48 h, follow-up experiments were carried out.

2.3. Quantitative Real-Time Polymerase Chain Reaction (qRT-PCR). TRIzol reagent was performed to extract total RNA from CRC tissues and cells. Then, the concentration of RNA was determined by ultraviolet spectrophotometer. According to the instructions of PrimeScript RT reagent kit, the cDNA was synthesized by reverse transcription. RT-qPCR was performed according to the instructions of SYBR Premix Ex Taq^{TM}. The ABI software was used to analyze and process the data to obtain the Ct value. Finally, $2^{-\triangle\triangle Ct}$ method was used to calculate the relative expression of target gene.

2.4. Dual-Luciferase Reporter Assay. StarBase (http://starbase.sysu.edu.cn/) was performed to seek the potential binding miRNAs of MSC-AS1. TargetScan (http://www.targetscan.org/vert_72/) was used to explore the potential downstream genes of miR-325. The mutant and wild sequence fragments of MSC-AS1 and TRIM14 were cloned and combined with the Promega vector. MSC-AS1-Mut and MSC-AS1-Wt and TRIM14-Mut and TRIM14-Wt were transfected into cells with miR-325 mimic or NC mimic, respectively. After transfection for 48 h, the relative luciferase activity of target gene was detected by dual-luciferase reporter assay kit.

2.5. MTT Assay. The cells in logarithmic phase were resuspended. 100 μl cell suspension (1×10^4 cells/ml) was inoculated in 96-well plate at 37°C and 5% CO_2. After incubation for 24, 48, 72, and 96 h, the plates were added with 20 μl MTT solution (5 mg/ml, Sigma) and incubated for another 4 h. Then, 200 μl DMSO was added and shook on the shaker for 10 min. The absorbance value was measured by using a microplate analyzer at 490 nm. According to the experimental data, the growth curve was plotted.

2.6. Transwell Assay. For cell migration, after transfection for 48 h, cells were digested with trypsin and resuspended with 400 μl serum-free medium. Cell suspension (1×10^5 cells/ml) was seeded in a 24-well plate. Cells in each group were added to the upper chamber of Transwell chamber, and 600 μL DMEM with 10% FBS was added to the lower chamber of Transwell chamber. Cells were cultured in a constant temperature incubator containing 5% CO_2 at 37°C for 24 h. Then, the chamber was fixed with 4% formaldehyde for 15 min and stained with crystal violet for 20 min. The migratory cells were observed and photographed under a light microscope. 5 high-power visual fields were randomly selected to count the number of migratory cells.

For cell invasion, 50 μl Matrigel blue was diluted and spread in the upper chamber of Transwell chamber. The remaining steps were the same as those in the cell migration experiment. The invaded cells were observed under a light microscope and photographed. 5 high-power fields were randomly selected to count the number of invaded cells.

2.7. Western Blot Assay. Total protein was extracted from CRC cells by TRIzol. The protein samples (30 μg) were boiled at 100°C for 5 min. After SDS-PAGE gel electrophoresis, the protein samples were transferred to the PVDF

membranes. After blocking with 5% skim milk for 2 hours, the membranes were incubated with antibodies overnight at 4°C. After incubation with secondary antibodies for another 1 h, the protein signal of CLCA4 was detected by ECL reagent.

2.8. Statistical Analysis. All data were expressed as mean ± SD and analyzed by using SPSS 22.0 and GraphPad Prism 6.0. The differences between the two groups were detected by Student's *t*-test. The differences among multiple groups were detected by one-way ANOVA. The correlations between MSC-AS, miR-325, and TRIM14 were detected by Pearson's correlation analysis. $p < 0.05$ was considered statistically significant.

3. Results

3.1. MSC-AS1 Overexpression Was Discovered in CRC Tissues and Cells. First, GEPIA database showed that MSC-AS1 was upregulated in colon adenocarcinoma (COAD) (Figure 1(a)). Next, RT-qPCR assay was used to detect the expression pattern of MSC-AS1 in 46 CRC tissues from Yantaishan Hospital. It is noted that there was an upward trend of MSC-AS in CRC tissues compared with control tissues (Figure 1(b)). Next, we measured the expression level of MSC-AS1 in CRC cells (HT29, SW620, HCT116, and SW480) and normal human epithelial cells NCM460. As expected, the expression of MSC-AS1 was obviously higher in CRC cells than in NCM460 cells (Figure 1(c)). Furthermore, MSC-AS1 was closely associated with lymph node metastasis ($p = 0.014$) and TNM stage ($p = 0.040$) (Table 1). Our data indicated that MSC-AS1 was involved in the progression of CRC and might be a potential diagnosis target in patient with CRC.

3.2. MSC-AS1 Might Be a Carcinogen in CRC Cells. In order to investigate the function of MSC-AS1 in CRC, MSC-AS1 siRNA was transfected into HCT116 cells (Figure 2(a)). Then, CCK-8 assay and Transwell assay were performed. CCK-8 results displayed that MSC-AS1 downregulation weakened cell proliferative ability in HCT116 cells (Figure 2(b)). Moreover, Transwell assay displayed that cell migration was obviously inhibited by MSC-AS1 knockdown in HCT116 cells (Figure 2(c)). Similarly, cell invasion ability of CRC cells was blocked by MSC-AS1 knockout (Figure 2(d)). Altogether, our results indicated that MSC-AS1 silencing blocked cell progression in CRC cells.

3.3. MSC-AS1 Acted as a Sponge of miR-325 in CRC. In our study, StarBase database was performed to seek the potential miRNAs of MSC-AS1. As shown in Figure 3(a), there were special binding sites between MSC-AS1 and miR-325. Dual-luciferase reporter assay and RT-qPCR assay were performed. We found that the luciferase activity of MSC-AS1-WT was obviously reduced when cells were transfected with miR-325 mimic. However, the luciferase activity of MSC-AS1-MUT was not significantly changed in mimic cells (Figure 3(b)). Next, the expression level of miR-325 in CRC tissues and cells was detected. Results indicated that miR-325 was significantly downregulated in CRC tissues and cells compared with normal groups (Figures 3(c) and 3(d)). Additionally, the expression of miR-325 was increased in HCT116 cells with MSC-AS1 knockdown (Figure 3(e)). Nevertheless, RT-qPCR results indicated that the expression of MSC-AS1 was reduced in CRC cells with miR-325 mimic (Figure 3(f)). Besides, Pearson's correlation analysis was used to detect the relationship between MSC-AS and miR-325 in CRC tissues. The results showed that MSC-AS1 expression was inversely related with miR-325 expression in CRC (Figure 3(g)). In sum, our findings suggested that MSC-AS1 might be a sponge of miR-325.

3.4. TRIM14 Might Be a Target Gene of miR-325. Subsequently, we seek out downstream target gene of miR-325. The StarBase software showed that TRIM14 might be a potential target gene of miR-325 (Figure 4(a)). Dual-luciferase reporter results displayed that miR-325 mimic led to decrease in TRIM14-Wt but not TRIM14-Mut (Figure 4(b)). Then, the mRNA expression of TRIM14 in CRC tissues and cells was detected. We found that TRIM14 was obviously upregulated in CRC tissues compared with nontumor tissues (Figure 4(c)). Furthermore, the expression of TRIM14 was reduced in HT29 and HCT116 cells (Figure 4(d)). Furthermore, there was a negative correlation between miR-325 and TRIM14 in CRC tissues (Figure 4(e)). Our results confirmed that TRIM14 might be a target gene of miR-325.

3.5. MSC-AS1 Regulated CRC Progression by Inhibiting miR-325 Expression. To investigate the mechanism of MSC-AS1/miR-325, MSC-AS1 vector was transfected into CRC cells with miR-325 mimic. RT-qPCR results displayed that the expression of miR-325 was significantly increased in cells when they are transfected with miR-325 mimic, while it declined when mimic cells were transfected with MSC-AS1 vector (Figure 5(a)). Next, CCK-8 assay and Transwell assay were used to measure the function of MSC-AS1/miR-325 in CRC cells. We found that cell proliferative ability was dramatically declined in cells with miR-325 mimic. However, MSC-AS1 overexpression weakened the inhibitory effect of miR-325 mimic on cell proliferation (Figure 5(b)). Furthermore, Transwell results indicated that miR-325 mimic reduced cell migration capability in HCT116 and SW480 cells, while MSC-AS1 transfection reversed the effect of miR-325 (Figure 5(c)). Likewise, MSC-AS1 upregulation destroyed the inhibitory effect of miR-325 mimic on cell invasion ability (Figure 5(d)). Therefore, our data suggested that MSC-AS1 regulated CRC progression by restraining miR-325 expression.

3.6. MSC-AS1 Accelerated TRIM14 Expression by Sponging miR-325 in CRC Cells. Next, we explored how MSC-AS1 regulated the TRIM14 expression by targeting miR-325. As shown in Figure 6(a), the mRNA expression of TRIM14 was significantly reduced by miR-325 mimic, while the

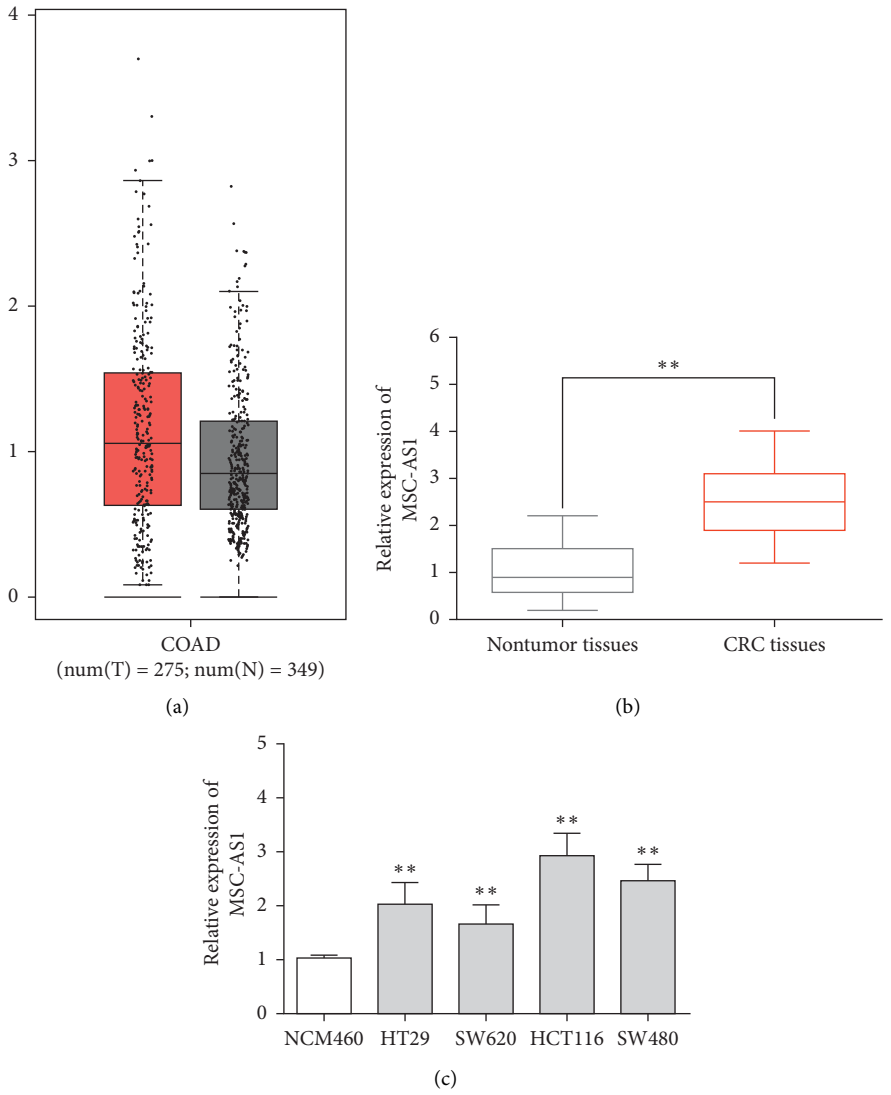

Figure 1: MSC-AS1 expression in CRC tissues and cells. (a) The expression level of MSC-AS1 in GEPIA database. (b) The expression of MSC-AS1 in 46 CRC tissues from Yantaishan Hospital. (c) The expression of MSC-AS1 in CRC cells (HT29, SW620, HCT116, and SW480). ** $p < 0.01$.

Table 1: Correlation between the expression level of MSC-AS1 and clinical characteristics of CRC patients ($n = 46$).

Clinical characteristics	Number of cases $n = 46$	MSC-AS1 expression		p value
		Low ($n = 22$)	High ($n = 24$)	
Age (years)				0.619
≤60	12	5	7	
>60	34	17	17	
Gender				0.351
Male	26	14	12	
Female	20	8	12	
Tumor size				0.382
≤5 cm	24	10	14	
>5 cm	22	12	10	
Location				0.229
Proximal	11	7	4	
Distal	35	15	20	
TNM stage				0.040*
I-II	18	12	6	
III-IV	28	10	18	
Lymph node metastasis				0.014*
Absent	27	17	10	
Present	19	5	14	

* $p < 0.05$: the difference is significant.

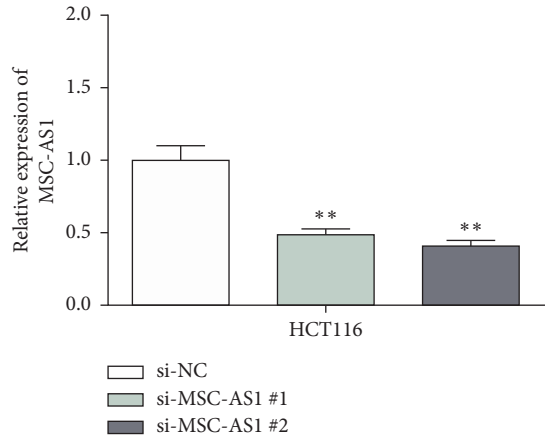

(a)

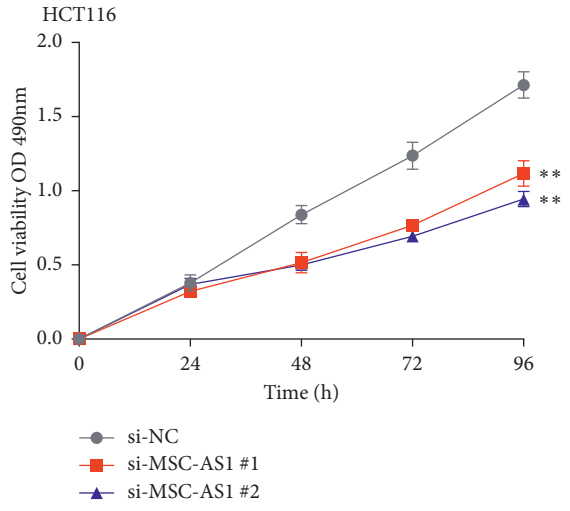

(b)

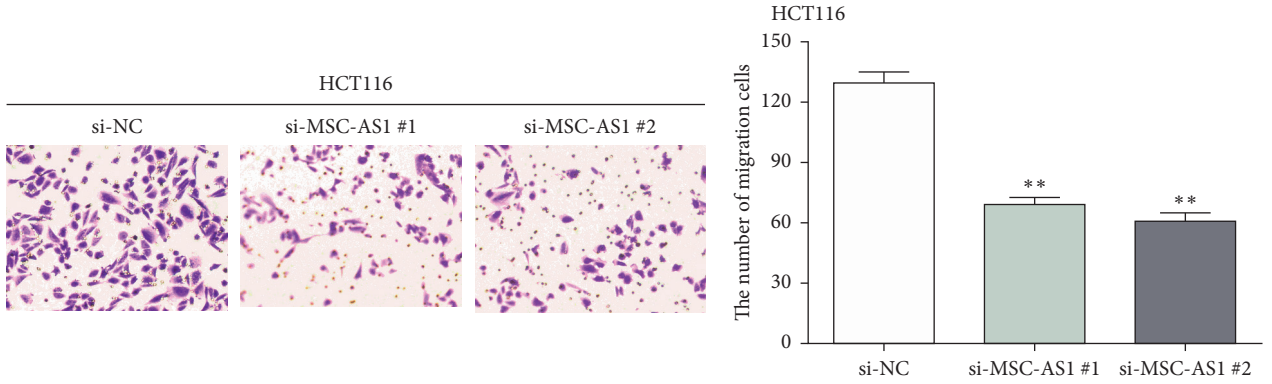

(c)

Figure 2: Continued.

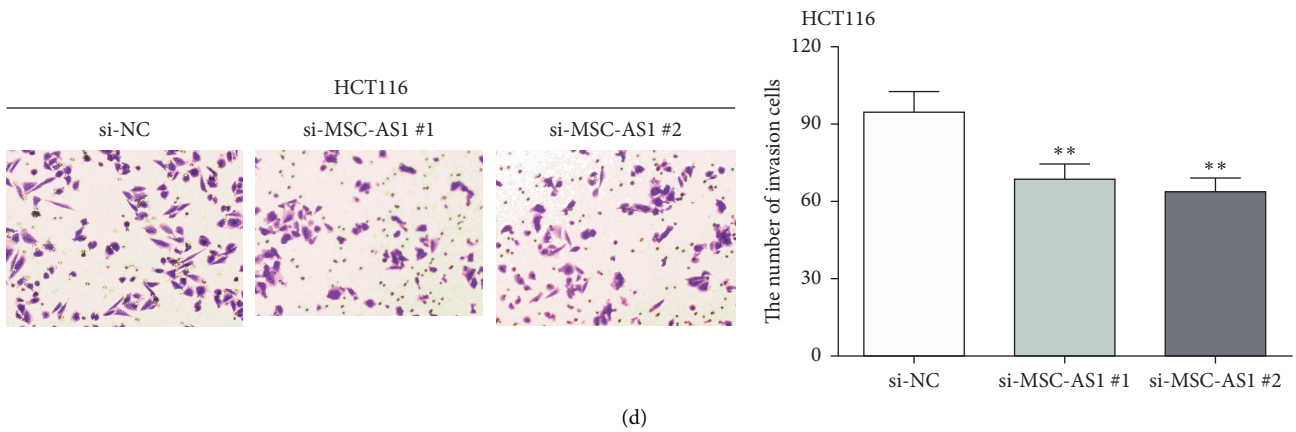

Figure 2: MSC-AS1 might be a carcinogen in CRC cells. (a) The expression of MSC-AS1 was reduced by MSC-AS1 siRNAs. (b) MSC-AS1 knockdown obviously suppressed cell proliferation in HCT116 cells. ((c) and (d)) MSC-AS1 knockdown inhibited cell migration and invasion abilities in HCT116 cells. ** $p < 0.01$.

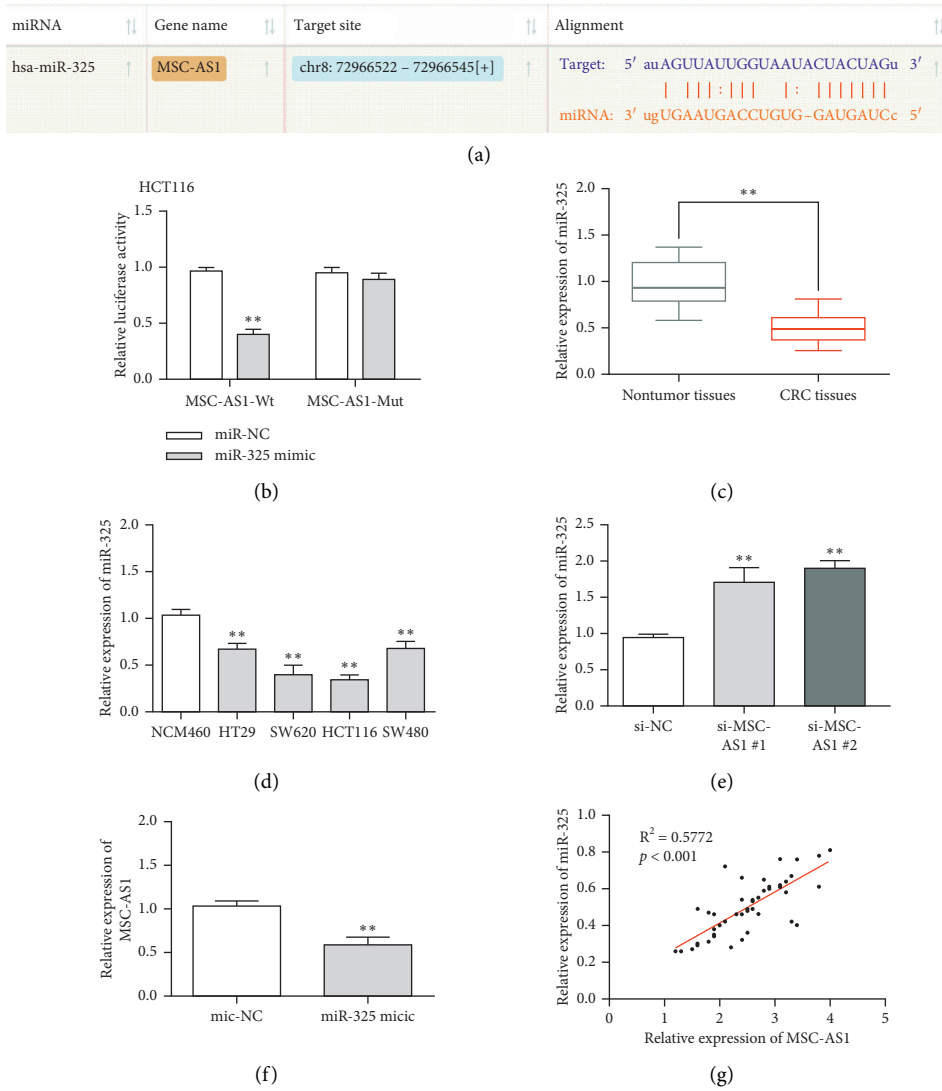

Figure 3: MSC-AS1 acted as a sponge of miR-325 in CRC cells. (a) StarBase showed that there were special binding sites between MSC-AS1 and miR-325. (b) The relative luciferase activity of MSC-AS1-Wt and MSC-AS1-Mut. (c) The expression of miR-325 in CRC tissues. (d) The expression of miR-325 in CRC cells. (e) The expression of miR-325 was increased by MSC-AS1 knockdown. (f) The expression of MSC-AS1 was reduced by miR-325 mimic. (g) Correlation analysis between MSC-AS1 and miR-325 expression in 46 CRC tissues. ** $p < 0.01$.

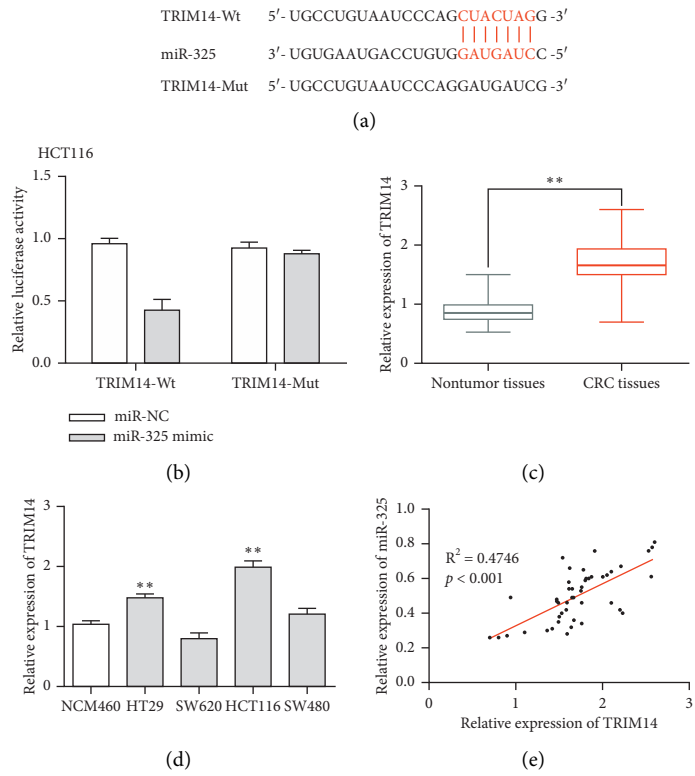

Figure 4: TRIM14 might be a target gene of miR-325. (a) There were special binding sites between miR-325 and TRIM14. (b) The luciferase activity of TRIM14-Wt and TRIM14-Mut. (c) The expression of TRIM14 in CRC tissues. (d) The expression of TRIM14 in CRC cells. (e) Correlation analysis between TRIM14 and miR-325 expression in 46 CRC tissues. ** $p < 0.01$.

suppression effect of miR-325 mimic on TRIM14 expression was counteracted by MSC-AS1 vector. In addition, MSC-AS1 vector impaired the inhibitory effect of miR-325 on the protein expression of TRIM14 (Figure 6(b)). Therefore, our data suggested that MSC-AS1 regulated TRIM14 expression by restraining miR-325 expression.

4. Discussion

Recently, the mortality and incidence of CRC have been on the rise worldwide, posing a serious threat to human health. Due to the lack of effective CRC prevention and low rate of early diagnosis, most patients are already in the mid and late stages when they are diagnosed. The IARC estimates that, by 2025, there will be more than 20 million new cases of CRC worldwide. In order to find out the effective treatment, it is urgent to study the mechanism of CRC by using molecular biology technology.

At present, the role of lncRNAs in tumor progression has become a research hotspot. Studies have found abnormal expression of lncRNAs in various human cancers, which play a key role in tumor development, metastasis, early diagnosis, prognosis evaluation, radiotherapy and chemotherapy efficacy, etc. Alaiyan et al. reported that CCAT1 was gradually upregulated during the progression of CRC and was associated with tumor metastasis [17]. HAGLR was proved to promote cell growth, migration, and invasion viabilities and inhibit cell apoptosis in CRC [18]. LncRNA MSC-AS1 is a new lncRNA that has been discovered in recent years, which is first found to be overexpressed in hepatocellular carcinoma tissues [19]. Cao et al. confirmed that MSC-AS1 played a carcinogenic lncRNA role in hepatocellular carcinoma by increasing PGK1 expression [20]. As we have mentioned, MSC-AS1 expression was increased in CRC; and we discovered that depletion of MSC-AS1 suppressed tumor progression in CRC. Therefore, our results indicated that MSC-AS1 might be carcinogenic lncRNA in CRC.

Accumulating studies have manifested that lncRNAs can act as ceRNAs to sponge miRNAs and thus upregulate target genes. MSC-AS1 was found to regulate the tumor progression by inhibiting miR-124 expression to increase CDK6 expression in osteosarcoma [21]. Moreover, MSC-AS1 acted as a role of carcinogenic factor in glioma by sponging miR-373-3p and upregulating CPEB4 [22]. Li et al. reported that the expression of miR-325 was reduced in CRC [23]. Similarly, the low expression of miR-325 in CRC was discovered in our study. Additionally, we confirmed that MSC-AS1 might act as a sponge of miR-325 in CRC. Functionally, MSC-AS1 promoted cell proliferation, invasion, and migration in CRC cells by sponging miR-325.

Tripartite motif containing 14 (TRIM14) is a member of the TRIM family. Studies have found that TRIM14 was involved in a variety of biological functions, including cell proliferation, cell apoptosis, inflammatory response, cell metastasis, and immune response [24–26]. TRIM14 was confirmed to facilitate cell proliferation, migration, and invasion and block cell apoptosis in CRC cells [27, 28].

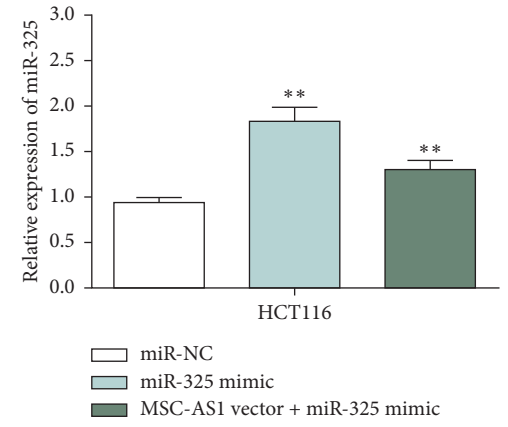

(a)

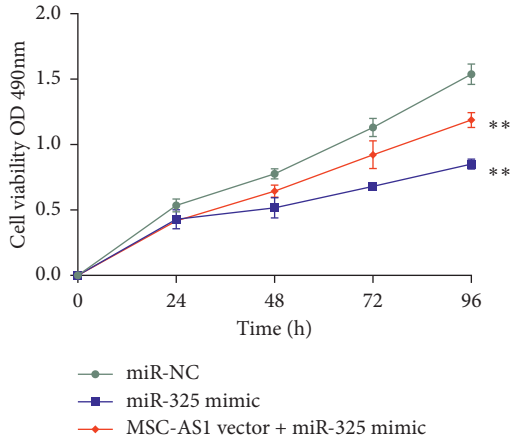

(b)

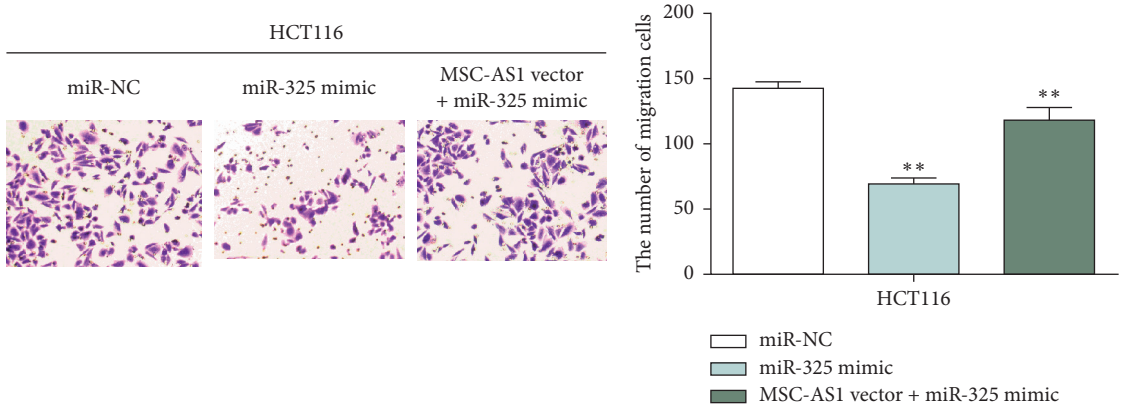

(c)

Figure 5: Continued.

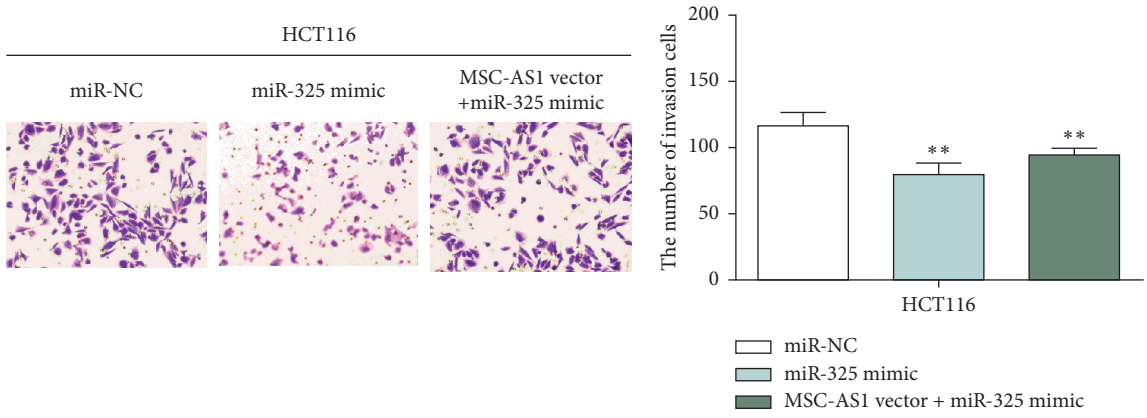

(d)

Figure 5: MSC-AS1 regulated CRC progression by inhibiting miR-325 expression. (a) The expression of miR-325 in HCT116 cells transfected with miR-325 mimic or MSC-AS1 vector. (b) miR-325 mimic suppressed cell proliferation, while MMSC-AS1 impaired the inhibitory effect of miR-325. (c, d) miR-325 mimic suppressed cell migration and invasion, while MMSC-AS1 impaired the inhibitory effect of miR-325. ** $p < 0.01$.

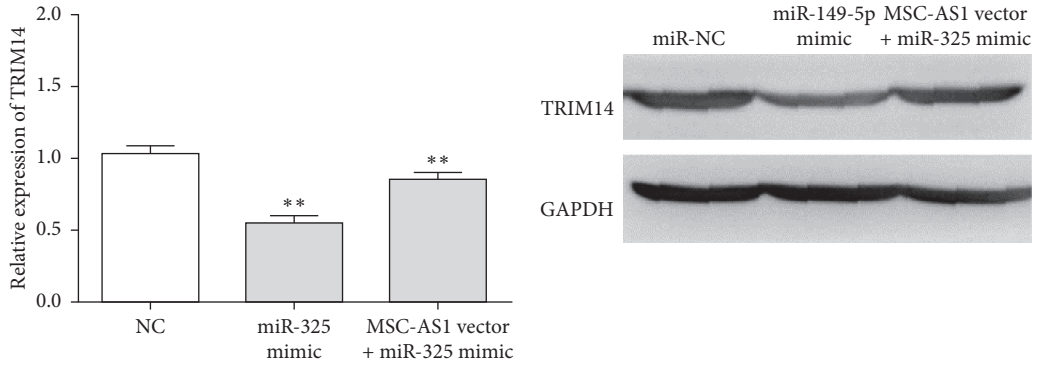

(a) (b)

Figure 6: MSC-AS1 accelerated TRIM14 expression by sponging miR-325 in CRC cells. (a) miR-325 mimic reduced the mRNA expression of TRIM14, while MMSC-AS1 impaired the inhibitory effect of miR-325. (b) miR-325 mimic reduced the protein expression of TRIM14, while MMSC-AS1 impaired the inhibitory effect of miR-325. ** $p < 0.01$.

Therefore, TRIM14 was confirmed to play a role as an oncogene in CRC. In the current work, we confirmed that TRIM14 might be a downstream target gene of miR-325. Most importantly, our findings demonstrated that MSC-AS1 regulated TRIM14 expression by restraining miR-325 expression.

Above all, we demonstrated that MSC-AS1 promoted tumor progression by sponging miR-325 to increase TRIM14 expression in CRC. Our results provided a basis for further understanding of CRC progression and supported the potential role of MSC-AS1 as a target for CRC treatment.

Data Availability

The data used to support the findings of this study are available from the corresponding author upon request.

Conflicts of Interest

The authors declare that they have no conflicts of interest.

References

[1] H. Sung, J. Ferlay, R. L Siegel et al., "Global cancer statistics 2020: GLOBOCAN estimates of incidence and mortality worldwide for 36 cancers in 185 countries," *CA: A Cancer Journal for Clinicians*, vol. 71, no. 3, pp. 209–249, 2021.

[2] G. Breau and U. Ellis, "Risk factors associated with young-onset colorectal adenomas and cancer: a systematic review and meta-analysis of observational research," *Cancer Control : Journal of the Moffitt Cancer Center*, vol. 27, no. 1, Article ID 1073274820976670, 2020.

[3] K. Leong, J. Hartley, and S. Karandikar, "Association of coloproctology of great britain & Ireland (ACPGBI): guidelines for the management of cancer of the colon, rectum and anus (2017) - follow up, lifestyle and survivorship," *Colorectal Disease*, vol. 19, pp. 67–70, 2017.

[4] C. Carvalho and R. Glynne-Jones, "Challenges behind proving efficacy of adjuvant chemotherapy after preoperative chemoradiation for rectal cancer," *The Lancet Oncology*, vol. 18, no. 6, pp. e354–e363, 2017.

[5] A. Nandwani, S. Rathore, and M. Datta, "LncRNAs in cancer: regulatory and therapeutic implications," *Cancer Letters*, vol. 501, pp. 162–171, 2021.

[6] M. Bermudez, M. Aguilar-Medina, E. Lizarraga-Verdugo et al., "LncRNAs as regulators of autophagy and drug resistance in colorectal cancer," *Frontiers in Oncology*, vol. 9, p. 1008, 2019.

[7] N. Dastmalchi, R. Safaralizadeh, and M. M. Nargesi, "LncRNAs: potential novel prognostic and diagnostic biomarkers in colorectal cancer," *Current Medicinal Chemistry*, vol. 27, no. 30, pp. 5067–5077, 2020.

[8] Z. Liu, Y. Gu, X. Cheng et al., "Upregulation Lnc-NEAT1 contributes to colorectal cancer progression through Sponging miR-486-5p and Activating NR4A1/Wnt/beta-Catenin pathway," *Cancer Biomarkers*, vol. 30, 2020.

[9] W. Zhang, B. Wang, Q. Wang et al., "Lnc-HSD17B11-1:1 functions as a competing endogenous RNA to promote colorectal cancer progression by sponging miR-338-3p to upregulate MACC1," *Frontiers in Genetics*, vol. 11, p. 628, 2020.

[10] C. Ye, Z. Shen, B. Wang et al., "A novel long non-coding RNA lnc-GNAT1-1 is low expressed in colorectal cancer and acts as a tumor suppressor through regulating RKIP-NF-kappaB-Snail circuit," *Journal of Experimental & Clinical Cancer Research : CR*, vol. 35, no. 1, p. 187, 2016.

[11] N. Zhang, X. Hu, S. He et al., "LncRNA MSC-AS1 promotes osteogenic differentiation and alleviates osteoporosis through sponging microRNA-140-5p to upregulate BMP2," *Biochemical and Biophysical Research Communications*, vol. 519, no. 4, pp. 790–796, 2019.

[12] Z. Hu, L. Li, P. Cheng et al., "lncRNA MSC-AS1 activates Wnt/β-catenin signaling pathway to modulate cell proliferation and migration in kidney renal clear cell carcinoma via miR-3924/WNT5A," *Journal of Cellular Biochemistry*, vol. 121, no. 10, pp. 4085–4093, 2020.

[13] Z. Bian, L. Jin, J. Zhang et al., "LncRNA-UCA1 enhances cell proliferation and 5-fluorouracil resistance in colorectal cancer by inhibiting miR-204-5p," *Scientific Reports*, vol. 6, Article ID 23892, 2016.

[14] S. Zhu, C. Y. Chen, and Y. Hao, "LncRNA KCNQ1OT1 acts as miR-216b-5p sponge to promote colorectal cancer progression via up-regulating ZNF146," *Journal of Molecular Histology*, 2021.

[15] Y. H. Zhang, J. Fu, Z. J. Zhang, C. C. Ge, and Y. Yi, "LncRNA-LINC00152 down-regulated by miR-376c-3p restricts viability and promotes apoptosis of colorectal cancer cells," *American Journal of Translational Research*, vol. 8, no. 12, pp. 5286–5297, 2016.

[16] S. Sun, F. Liu, S. Xian, and D. Cai, "miR-325-3p overexpression inhibits proliferation and metastasis of bladder cancer cells by regulating MT3," *Medical Science Monitor : International Medical Journal of Experimental and Clinical Research*, vol. 26, Article ID e920331, 2020.

[17] B. Alaiyan, N. Ilyayev, A. Stojadinovic et al., "Differential expression of colon cancer associated transcript1 (CCAT1) along the colonic adenoma-carcinoma sequence," *BMC Cancer*, vol. 13, p. 196, 2013.

[18] W. Sun, W. Nie, Z. Wang, H. Zhang, Y. Li, and X. Fang, "Lnc HAGLR promotes colon cancer progression through sponging miR-185-5p and activating CDK4 and CDK6 in vitro and in vivo," *OncoTargets and Therapy*, vol. 13, pp. 5913–5925, 2020.

[19] J.-X. Gu, X. Zhang, R.-C. Miao et al., "Six-long non-coding RNA signature predicts recurrence-free survival in hepatocellular carcinoma," *World Journal of Gastroenterology*, vol. 25, no. 2, pp. 220–232, 2019.

[20] C. Cao, Q. Zhong, L. Lu et al., "Long noncoding RNA MSC-AS1 promotes hepatocellular carcinoma oncogenesis via inducing the expression of phosphoglycerate kinase 1," *Cancer Medicine*, vol. 9, no. 14, pp. 5174–5184, 2020.

[21] L. Zhang, G. Zhao, S. Ji, Q. Yuan, and H. Zhou, "Down-regulated long non-coding RNA MSC-AS1 inhibits osteosarcoma progression and increases sensitivity to cisplatin by binding to MicroRNA-142," *Medical Science Monitor : International Medical Journal of Experimental and Clinical Research*, vol. 26, Article ID e921594, 2020.

[22] C. Li, S. Feng, and L. Chen, "MSC-AS1 knockdown inhibits cell growth and temozolomide resistance by regulating miR-373-3p/CPEB4 axis in glioma through PI3K/Akt pathway," *Molecular and Cellular Biochemistry*, vol. 476, no. 2, pp. 699–713, 2021.

[23] L. Zhang, H. Chen, Y. Song et al., "MiR-325 promotes oxaliplatin-induced cytotoxicity against colorectal cancer through the HSPA12B/PI3K/AKT/Bcl-2 pathway," *Digestive diseases and sciences*, vol. 66, 2020.

[24] M. Chen, Q. Meng, Y. Qin et al., "TRIM14 inhibits cGAS degradation mediated by selective autophagy receptor p62 to promote innate immune responses," *Molecular Cell*, vol. 64, no. 1, pp. 105–119, 2016.

[25] Z. Tan, L. Song, W. Wu et al., "TRIM14 promotes chemoresistance in gliomas by activating Wnt/β-catenin signaling via stabilizing Dvl2," *Oncogene*, vol. 37, no. 40, pp. 5403–5415, 2018.

[26] J. Hai, C. Q. Zhu, T. Wang, S. L. Organ, F. A. Shepherd, and M. S. Tsao, "TRIM14 is a putative tumor suppressor and regulator of innate immune response in non-small cell lung cancer," *Scientific Reports*, vol. 7, p. 39692, 2017.

[27] Z. Jin, H. Li, X. Hong et al., "TRIM14 promotes colorectal cancer cell migration and invasion through the SPHK1/STAT3 pathway," *Cancer Cell International*, vol. 18, p. 202, 2018.

[28] W. Shen, Z. Jin, X. Tong et al., "TRIM14 promotes cell proliferation and inhibits apoptosis by suppressing PTEN in colorectal cancer," *Cancer Management and Research*, vol. 11, pp. 5725–5735, 2019.

Hindawi
Journal of Oncology
Volume 2021, Article ID 9944132, 10 pages
https://doi.org/10.1155/2021/9944132

Research Article

Knockdown of NOLC1 Inhibits PI3K-AKT Pathway to Improve the Poor Prognosis of Esophageal Carcinoma

Fanguo Kong,[1] **Yansheng Shang**,[1] **Xingyuan Diao**,[1] **Jiaguo Huang**,[1] **and Hui Liu**[2]

[1]*Department of Gastroenterology, Jinan City People's Hospital, Jinan People's Hospital Affiliated to Shandong First Medical University, Jinan 271199, China*
[2]*Department of Gastroenterology, Shandong Provincial Hospital Affiliated to Shandong First Medical University, Jinan 271199, China*

Correspondence should be addressed to Hui Liu; liuhui@sdphospital.cn

Received 18 March 2021; Accepted 30 April 2021; Published 10 May 2021

Academic Editor: Muhammad Wasim Khan

Objective. Esophageal carcinoma (ESCA) is a common malignant gastrointestinal tumor. The abnormal expression of NOLC1 is involved in the tumorigenesis of various human tumors, whereas the function and mechanism of NOLC1 in ESCA remain unclear. In this study, we explored the relationship between NOLC1 and poor prognosis of ESCA, and its role and mechanism in the occurrence of ESCA. *Methods*. The NOLC1 expression in ESCA tissues and cell lines was determined by qRT-PCR, immunohistochemistry, or western blot. The Kaplan–Meier method was conducted to estimate the overall survival. Cox regression analysis was carried out to examine the association between patient characteristics and prognosis. A recombined lentiviral vector containing NOLC1 was applied for transfecting ESCA cells (Eca109 and TE-13) and established a stable cell line with low NOLC1 expression or high NOLC1 expression, in the absence or presence of PI3K inhibitor (LY294002) treatment. Cell proliferation, apoptosis rate, invasion ability, migration ability, and PI3K/AKT pathway were detected by CCK8 assay, flow cytometry, Transwell assay, wound-healing assay, and western blot. *Results*. NOLC1 overexpression was observed in ESCA tissues and ESCA cell lines (EC9706, Eca109, TE-13, Kyse170, T.TN) compared with adjacent normal tissues and normal esophageal cell line HEEC. NOLC1 overexpression was markedly associated with bigger tumor size, lymph node metastasis, and advanced TNM stage. Patients with NOLC1 overexpression have shorter overall survival than that of those with low NOLC1 expression. NOLC1 overexpression was considered to be an independent poor prognostic factor affecting overall survival. NOLC1 knockdown inhibited proliferation, migration, invasion, and cyclin B1 expression and promoted the apoptosis and cleaved-caspase-3 expression of Eca109 and TE-13 cells. NOLC1 overexpression accelerated proliferation, migration, invasion, and cyclin B1 expression and inhibited the apoptosis and cleaved-caspase-3 expression of ESCA cells via activating PI3K/AKT pathway. Rescue experiments showed that PI3K inhibitor (LY294002) could reverse the phenomenon caused by NOLC1 overexpression. *Conclusion*. NOLC1 may be a marker for poor prognosis. It can participate in the occurrence and development of ESCA via the PI3K/AKT pathway.

1. Introduction

Esophageal carcinoma (ESCA) is a common malignant gastrointestinal tumor, which is the sixth leading cause of mortality among all kinds of tumors worldwide. Because the incidence of ESCA is relatively insidious and the early clinical symptoms are not typical, the majority of patients are already in the middle and advanced stages of treatment [1, 2]. Although resection operation is currently the main therapeutic schedule, comprehensive treatment including chemotherapy and radiotherapy is difficult to provide a survival benefit and improved quality of life. The 5-year survival rate of patients with ESCA remain poor, <20%, and the recurrence rate is more than 40% [3]. The cause of death is tumor recurrence or metastasis in patients with ESCA. However, the etiology and pathogenesis of ESCA remain ambiguous, which may be mediated by the cumulative effect of multiple genes [4, 5]. Therefore, it is urgently required to develop effective biomarkers for diagnosing, and new treatment strategies, such as targeted therapy, for preventing malignancy in patients with ESCA.

Nucleolar and coiled-body phosphoprotein 1 (NOLC1), a phosphoprotein, consists of a unique central repeat domain, and C-terminal and N-terminal domains [6–8]. Huang et al. reported that NOLC1 was positively correlated with the tumorigenesis of non-small cell lung cancer (NSCLC) and might be utilized as biomarkers for the early diagnosis of NSCLC [9]. Additionally, Hwang et al. showed that NOLC1 cooperates with TP53 synergistically to activate a cellular proto-oncogene MDM2, leading to cell growth and impediment of apoptosis in nasopharyngeal carcinoma [7, 10], whereas the function and mechanism of NOLC1 in the occurrence of ESCA remain unknown.

In the current study, we analyzed the gene expression profiling interactive analysis (GEPIA) database and discovered that, compared with normal esophageal epithelial tissues, ESCA tissues tend to have a relatively higher of NOLC1 expression. Thus, we measured NOLC1 expression in ESCA tissues and investigated the clinical and prognostic significance of NOLC1 expression in patients with ESCA, and a transfected recombinant lentiviral vector containing NOLC1 into ESCA cell lines with or without PI3K inhibitor (LY294002), to further investigate the function and mechanism of NOLC1 expression in ESCA.

2. Methods

2.1. Clinical Specimens. In this study, a total of 45 patients with ESCA who underwent surgical resection were recruited between January 2010 and December 2015 from Jinan City People's Hospital, Jinan People's Hospital Affiliated to Shandong First Medical University, Jinan City, Shandong Province, China. And 19 adjacent normal tissue specimens 3 cm away from the edge of the primary tumor were excised as control. In all cases, the diagnosis of each clinical specimen was verified by two pathologists at Jinan City People's Hospital. International Union Against Cancer (UICC) guidance was utilized for tumor staging. Gene expression profiling of interactive analysis website was carried out to analyze NOLC1 expression in ESCA tissues and normal tissues. The clinical parameters from the patients' medical records are analyzed in Table 1. All patients signed informed consent, and the ethics committee of Jinan City People's Hospital approved this study.

2.2. QRT-PCR. Total RNA was obtained from tissue specimens and cells using TRIzol (Thermo Fisher, Shanghai, China). The purity and concentration of RNA samples were determined using spectrophotometry (Bio-Tek, Vermont, USA). Subsequently, 300 ng RNA samples were reverse-transcribed into cDNAs and amplificated by using a One Step SuperRT-PCR Mix Kit (Solarbo, Shanghai, China). GAPDH was utilized as an expression control. NOLC1 mRNA levels were analyzed with the $2^{-\Delta\Delta Ct}$ method. Fold changes were calculated for Ct values of amplified NOLC1 mRNA compared with those of GAPDH.

(1) NOLC1 primer: F 5′-AGCTGGCCTGACGGTATG-3′, R 5′-TTGGTCTGGCTGAGTACCG-3′

(2) GAPDH primer: F 5′-TCACCAGGGCTGCTTTTA-3′, R 5′-TTCACACCCATGACGAACA-3′

2.3. Immunohistochemical Staining. Routine immunohistochemical staining of esophageal cancer biopsy specimens was performed using an anti-NOLC1 monoclonal antibody. Specimens embedded in paraffin wax were cut onto slides. Subsequently, slides were dewaxed, hydrated, and stained with the 3,3′-diaminobenzidine (DAB). Additionally, slides were counterstained with hematoxylin. The number of NOLC1-positive and the number of NOLC1-negative ESCA cells were counted at a magnification of ×400 under a light microscope. Cells on the section with brown nucleoli were considered positive for NOLC1. Positive scores were divided into 4 groups: "0" (no expression), "1+" (weak staining, only one nucleolus staining), "2+" (moderate staining, multiple nucleolar staining), and "3+" (strong staining, cell nuclei and nucleoli staining).

2.4. Western Blot. Tissues and cells were lysed in RIPA lysis buffer to isolate protein (Beyotime, Shanghai, China). Subsequently, samples were separated using 10% SDS-PAGE, transferred to PVDF membranes, and blocked in 5% BSA for 1 h. Membranes were incubated with primary antibodies, including rabbit monoclonal antibody NOLC1 (1 : 1000, Abcam, CA, USA), cleaved-caspase-3 (1 : 1000, Abcam), cyclin B1 (1 : 1000, Abcam), AKT (1 : 1000, Abcam), PI3K (1 : 1000, Abcam), p-PI3K (1 : 1000, Cell Signaling Technology, Shanghai, China), p-AKT (1 : 1000, Abcam), and rabbit polyclonal antibody GAPDH (1 : 10000, Abcam) overnight at 4°C. Membranes were washed 3 times and labeled with the HRP conjugated secondary antibodies (1 : 2000, Abcam) at room temperature for 1 h. Protein bands were visualized using an ECL system (Tannon, Beijing, China).

2.5. Cell Culture and Lentivirus Infection. Normal esophageal cell line HEEC and five esophageal cancer cell lines (EC9706, Eca109, TE-13, Kyse170, T.TN) were obtained from Cell Resource Center, Shanghai Institute for Biological Sciences, Chinese Academy of Sciences. All cells were cultured in RPMI-1640 medium (Gibco, Rockville, USA) containing 10% FBS (Gibco, Rockville, USA) at 37°C and 5% CO_2 incubator. The NOLC1 overexpression and knockdown lentiviral vector were purchased from GenePharma (Shanghai, China). The cells were transduced with lentiviral vectors at a multiplicity of infection (MOI) of 10 in a serum-free medium for 12 h. Subsequently, the cells were harvested and cultured with a complete medium for further study.

2.6. CCK8 (Cell Counting Kit-8) Assay. CCK8 assay was carried out to examine the cell viability. After lentivirus infection, Eca109 and TE-13 cells (2×10^3 cells/well) with or without PI3K inhibitor (LY294002) were resuspended and plated in 96-well plates for 0-, 24-, 48-, and 72 h incubation.

Table 1: Relationship between the expression of NOLC1 and the clinicopathological variables of ESCC patients.

Variables	Case number ($n = 45$)	NOLC1 expression		p-value
		Low ($n = 20$)	High ($n = 25$)	
Sex				
Male		8	12	0.601
Female		12	13	
Age (years)				
<60		9	10	0.743
≥60		11	15	
Tumor size (cm)				
<3		13	8	0.027
≥3		7	17	
TNM stage				
I + II		11	6	0.033
III + Iv		9	19	
Lymph node metastasis				
Yes		15	10	0.018
No		5	15	

Subsequently, 10 μL of CCK8 solution (Beyotime, Shanghai, China) was added, dropwise, into each well and incubated for 2 h. The absorbance at a wavelength of 450 nm was measured using a microplate reader (BioTek, Vermont, USA).

2.7. Flow Cytometry. After lentivirus infection, Eca109 and TE-13 cells with or without LY294002 were harvested and stained with Annexin V-FITC/PI (BD Biosciences, Bedford, USA) in the dark for 15 min. Cell apoptosis was analyzed using flow cytometry.

2.8. Invasion Assay. Transwell chamber was applied to measure the cell invasion ability. Matrigel matrix (Becton, Dickinson and Company, Bedford, USA) was diluted with serum-free medium at a ratio of 1 : 10. Then, Matrigel was evenly added to the upper chamber. After lentivirus infection, 5×10^4 Eca109 and TE-13 cells with or without LY294002 in 200 μL of serum-free medium were added to the apical chamber, and 600 μL of medium containing 15% FBS was supplied to the bottom chamber for 48 h. Cells in apical chamber were wiped off, fixed with 5% paraformaldehyde, and then stained with 0.1% crystal violet solution for 15 minutes. Finally, cell invasion was evaluated by counting under the microscope field (Olympus, Tokyo, Japan).

2.9. Wound-Healing Assay. Wound-healing assay was carried out to detect cell migration. After lentivirus infection, Eca109 and TE-13 cells (5×10^5 cells) with or without LY294002 were resuspended and seeded in six-well plates. The cells were cultured until confluent, and the monolayer in each was scratched using a 200 μL pipette tip. The detached cells were washed using PBS. Cells were cultured with 2 mL medium at 37°C and 5% CO_2. Photos for wounded cells were taken at 0 and 48 h under an optical microscope, and the gap distance was measured by Image J software.

2.10. Statistical Analysis. All data were expressed as the mean ± SD. All statistical analyses were carried out by SPSS Statistics 21.0. Student's t-test was applied for comparisons between two groups, while ANOVA was utilized to analyze the significant differences among multiple groups. Comparisons between NOLC1 subgroup (low vs. high) in patient survival were analyzed using the Kaplan–Meier method and assessed using the Cox regression analysis. p value < 0.05 was indicative of statistical significance.

3. Results

3.1. The Overexpression of NOLC1 in ESCA Tissues and Cells. Gene expression profiling interactive analysis (GEPIA) database was conducted to analyze the expression pattern of NOLC1 in ESCA tissues and normal esophageal epithelial tissues. The data revealed that ESCA tissues have a trend of relatively higher levels of NOLC1 expression compared with normal esophageal epithelial tissues (Figure 1(a)). In order to verify whether it was consistent with the database, the expression of NOLC1 was detected in 45 cases of ESCC tissues and 19 cases of adjacent normal tissues by QRT-PCR and immunohistochemical staining. The QRT-PCR results showed that NOLC1 mRNA was overexpressed in ESCA tissues than that in adjacent normal tissues (Figure 1(b), $p < 0.05$). The immunoreactivity of NOLC1 was observed in the brown nucleus. High NOLC1 expression was observed in ESCA tissues (55.6%) compared with normal tissues. The immunoreactivity of the low NOLC1 expression and high NOLC1 expression is shown in Figure 1(c). For further analysis, ESCA tissues were divided into 2 group on the basis of the immunohistochemical score: low NOLC1 expression group ("0" and "1+" expression of NOLC1) and high NOLC1 expression group ("2+" and "3+" expression of NOLC1). We further measured the expression of NOLC1 in five esophageal cancer cell lines (EC9706, Eca109, TE-13, Kyse170, T.TN) and normal esophageal cell line HEEC by QRT-PCR and western blot assay. QRT-PCR results showed that NOLC1 mRNA expression in five ESCA cell lines was

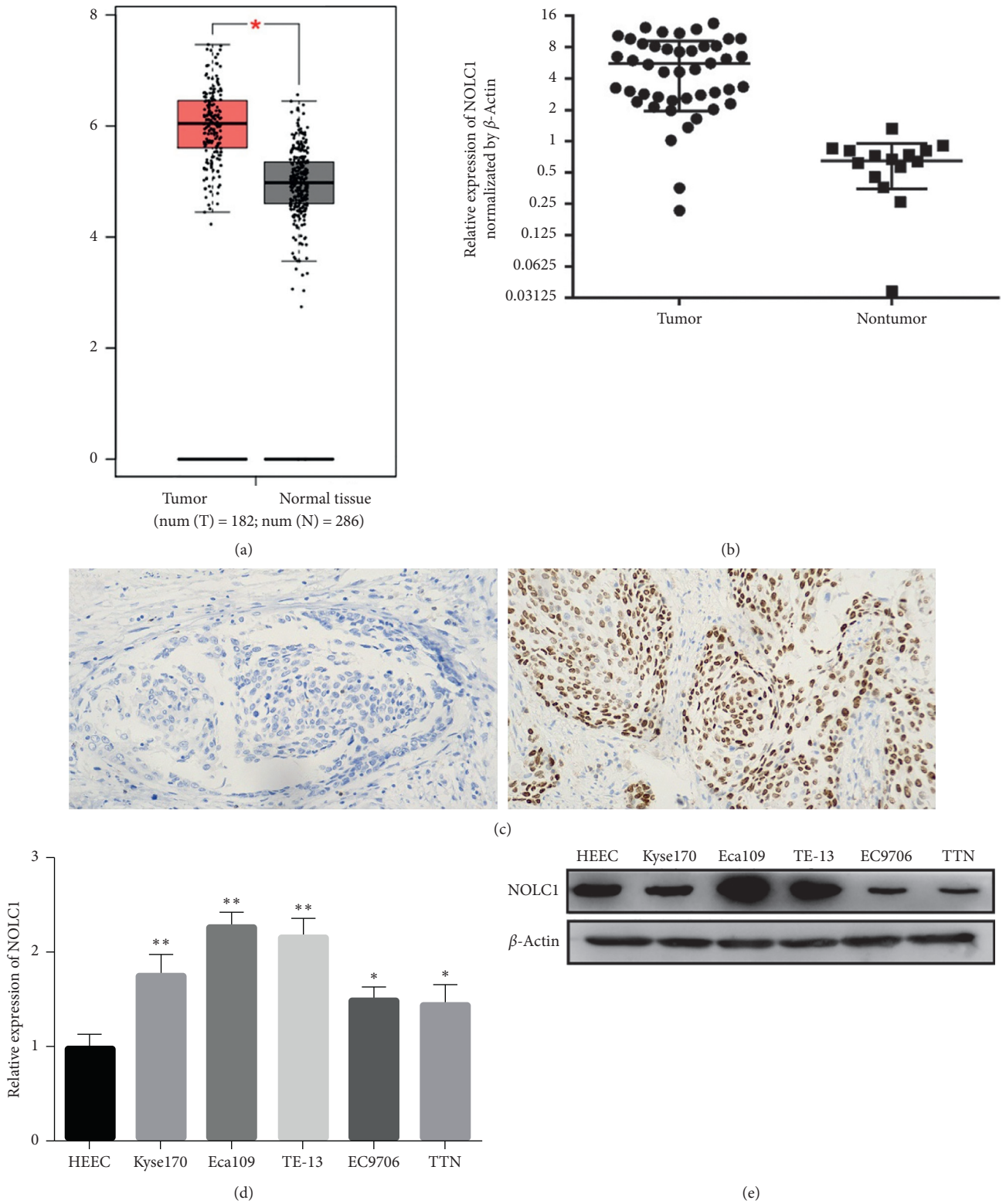

Figure 1: The NOLC1 expression in ESCA tissues and cell lines. (a) The expression pattern of NOLC1 in ESCA tissues and normal esophageal epithelial tissues was analyzed by GEPIA database. (b) The NOLC1 mRNA in ESCC tissues and adjacent normal tissues was measured by QRT-PCR. (c) The NOLC1 expression in ESCC tissues was evaluated by immunohistochemical staining: (1) No expression, (2) high expression. (d) The NOLC1 expression in five esophageal cancer cell lines (EC9706, Eca109, TE-13, Kyse170, T.TN) and normal esophageal cell line HEEC was detected by QRT-PCR. vs si-NC group, $^{*}p < 0.05$, $^{**}p < 0.01$. (e) The NOLC1 expression in five esophageal cancer cell lines (EC9706, Eca109, TE-13, Kyse170, T.TN) and normal esophageal cell line HEEC was detected by western blot.

predominantly higher than that of HEEC cells (Figure 1(d)). Consistently, western blot results indicated that NOLC1 protein levels in ESCC cell lines (Eca109 and TE-13) were notably higher than those of HEEC cells (Figure 1(e)). NOLC1 expression in Eca109 and TE-13 cells was more dramatic than that in other ESCA cell lines, so that Eca109 and TE-13 cells were utilized in subsequent experiments. These results revealed that NOLC1 was overexpressed in ESCA tissues and cell lines.

3.2. NOLC1 Overexpression Is Associated with Poor Prognosis of ESCA. The relationship between the NOLC1 overexpression and the clinical parameters of the patients with ESCA is listed in Table 1. There was statistically significant correlation between the overexpression of NOLC1 and bigger tumor size ($p = 0.027$), lymph node metastasis ($p = 0.018$), and advanced TNM stage ($p = 0.033$), while there was no significant correlation between NOLC1 overexpression and patients' gender and age. Kaplan–Meier analysis revealed that patients with NOLC1 overexpression have shorter survival time compared with those with low NOLC1 expression (Figure 2, $p < 0.01$). The 5-year survival rate of ESCA patients with low NOLC1 expression was 70.0% (14/20), while that of patients with high NOLC1 expression was 32% (8/25). Univariate COX regression analysis suggested that NOLC1 was negatively correlated with overall survival ($p = 0.029$, Table 2). Otherwise, multivariate COX regression analysis demonstrated that the expression level of NOLC1 was a significant independent prognostic factor for the overall survival of ESCA patients ($p = 0.032$, Table 2).

3.3. NOLC1 Knockdown Inhibits the Proliferation, Migration, and Invasion and Promotes the Apoptosis of ESCA Cells. In order to explore whether NOLC1 affects the development of ESCA, Eca109 and TE-13 cells were transduced with lentiviral vectors to knock down NOLC1 expression. The western blot displayed that NOLC1 expression in the sh-NOLC1-1 group and sh-NOLC1-2 group was declined compared to that in the sh-NC group ($p < 0.05$), and NOLC1 expression in the sh-NOLC1-1 group was the lowest (Figure 3(a)). Therefore, the lentiviral vectors of sh-NOLC1-1 group were selected to knock down NOLC1 in the subsequent experiments and it was named sh-NOLC1. CCK8 assays revealed that NOLC1 knockdown abrogated the proliferation of Eca109 and TE-13 cells compared to sh-NC group in a time-dependent manner (Figure 3(b), $p < 0.05$). Consistent with the impediment proliferation rate, NOLC1 knockdown encouraged the apoptotic rate of Eca109 and TE-1 cells compared to that of the sh-NC group (Figure 3(c), $p < 0.05$). Additionally, NOLC1 knockdown of Eca109 and TE-13 cells resulted in a significant impediment in invasion compared to that of sh-NC group (Figure 3(d), $p < 0.05$). Consistently, wound-healing assay revealed that the scratch in NOLC1 knockdown group of Eca109 and TE-13 cells was remarkably larger than that of the sh-NC group at 48h (Figure 3(e)). Moreover, NOLC1 knockdown depleted cyclin B1 protein level while NOLC1 knockdown elevated cleaved-caspase-3 expression. Overall, our data indicated that depletion of NOLC1 inhibits the proliferation, invasion, and migration and promotes the apoptosis of ESCA cells (Figure 3(f)).

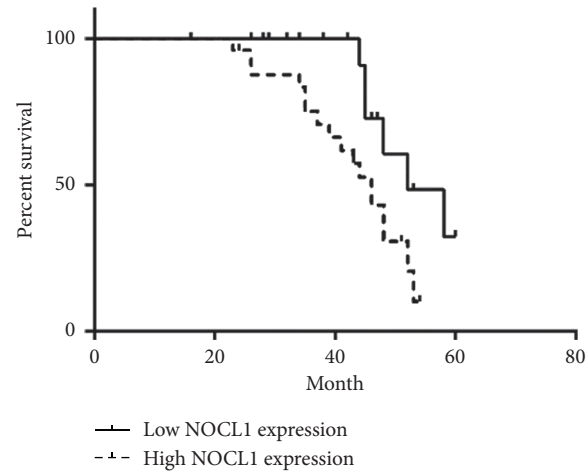

Figure 2: The association between NOLC1 expression and overall survival.

3.4. NOLC1 Overexpression Promotes Oncogenesis and Progression of ESCA via Activating PI3K/AKT Pathway. To further investigate the mechanism by which NOLC1 exerted function on ESCA cells, we first focused on the PI3K/AKT signaling pathway, which is considered to be involved in tumorigenesis and metastasis [11, 12]. Eca109 and TE-13 cells were transduced with lentiviral vectors to overexpress NOLC1. The western blot displayed that NOLC1 overexpression elevated AKT and PI3K phosphorylation, whereas the total PI3K and AKT level remained unchanged in both Eca109 and TE-13 cells (Figure 4(a)). In order to further explore the association between NOLC1 and AKT, after NOLC1 overexpression lentivirus infection, the PI3K inhibitor LY294002 (25 μmol/L) was utilized to treat Eca109 and TE-13 cells. NOLC1 overexpression significantly promoted the cell proliferation rate compared with vector group, while LY294002 deeply blocked cell proliferation mediated by NOLC1 overexpression (Figure 4(b), $p < 0.01$). Likewise, NOLC1 overexpression notably restrained the apoptosis rate of Eca109 and TE-13 cells compared with vector group, while LY294002 treatment attenuated the impediment effects on apoptosis rate caused by NOLC1 overexpression (Figure 4(c)). Additionally, NOLC1 overexpression accelerated the invasion ability of Eca109 and TE-13 cells compared with vector group, while LY294002 treatment abrogated invasion ability caused by NOLC1 overexpression (Figure 4(d)). Consistently, NOLC1 overexpression encouraged the migration ability compared with vector group in Eca109 and TE-13 cells, while LY294002 abolished the promotion effects on migration ability induced by NOLC1 overexpression (Figure 4(e)). Moreover, NOLC1 overexpression elevated cyclin B1 protein level while it depleted cleaved-caspase-3

Table 2: Univariate and multivariate analysis of survival associated factors.

Parameters	Univariate analysis		Multivariate analysis	
	HR (95% CI)	*p*-value	HR (95% CI)	*p*-value
Sex (male vs. female)	2.011 (0.777–5.204)	0.150		
Age (<60 vs. ≥60 years)	2.333 (0.776–7.017)	0.132		
Tumor size (<3 vs. ≥3 cm)	2.239 (0.745–6.735)	0.151		
TNM stage (I + II vs. III + IV)	1.351 (0.438–4.168)	0.601		
Lymph node metastasis (yes vs. no)	2.351 (0.919–6.011)	0.074		
NOLC1 expression (low vs. high)	3.078 (1.125–8.423)	0.029	3.522 (1.114–11.141)	0.032

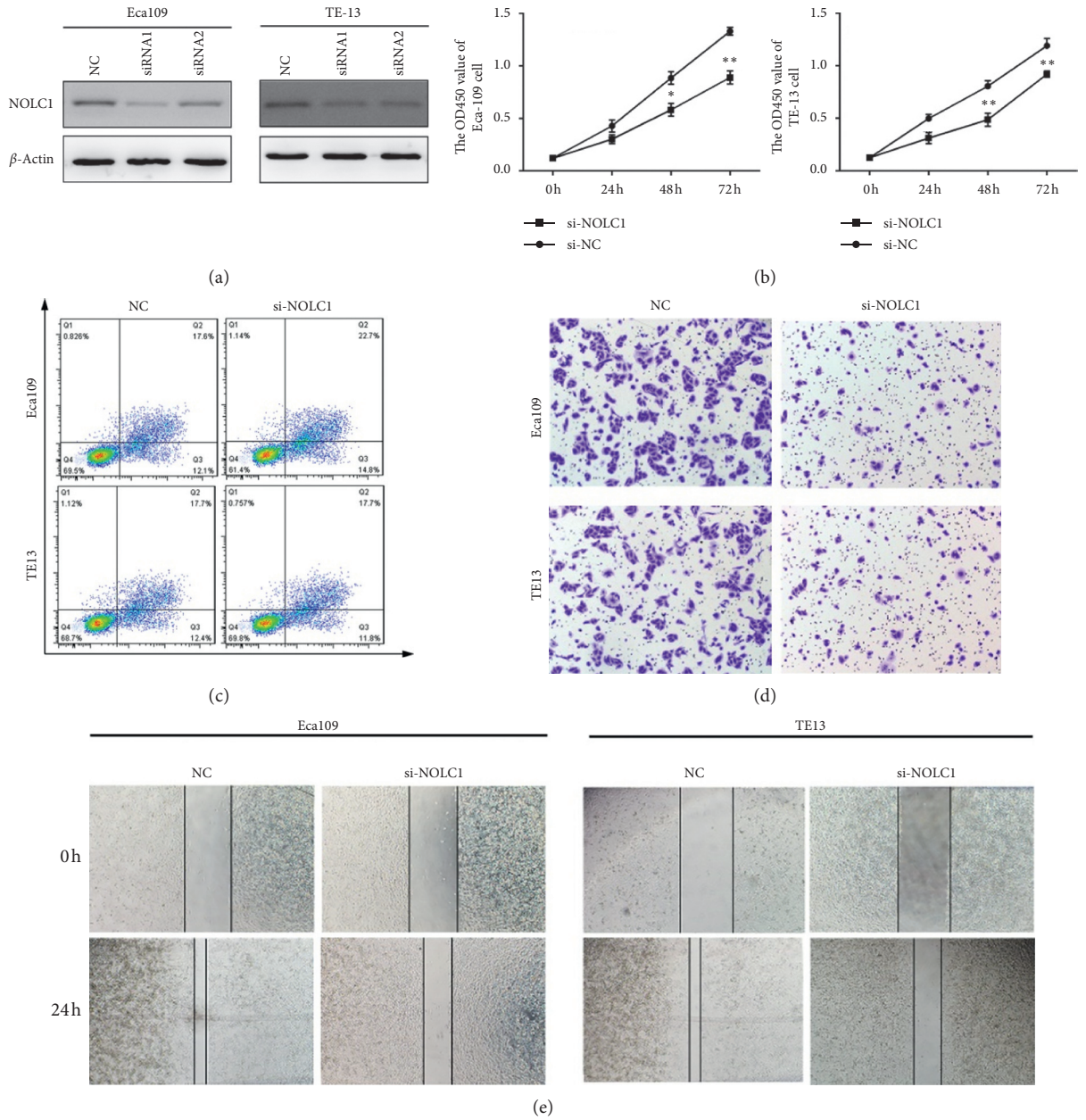

Figure 3: Continued.

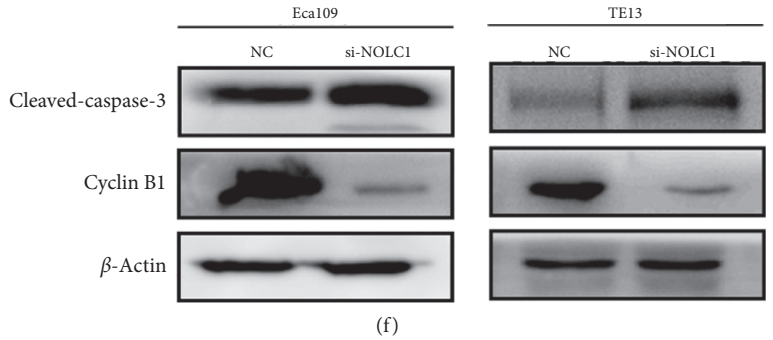

(f)

Figure 3: NOLC1 overexpression promotes oncogenesis and progression of ESCC. (a) The NOLC1 expression of Eca109 and TE-13 cells after NOLC1 knockdown. (b) The proliferation rate of Eca109 and TE-13 cells after NOLC1 knockdown vs. si-NC group, $^{*}p < 0.05$, $^{**}p < 0.01$. (c) The apoptotic rate of Eca109 and TE-13 cells after NOLC1 knockdown. (d) The invasion ability of Eca109 and TE-13 cells after NOLC1 knockdown. (e) The migration capacity of Eca109 and TE-13 cells after NOLC1 knockdown. (f) The protein level of cleaved-caspase-3 and cyclin B1 in Eca109 and TE-13 cells after NOLC1 knockdown.

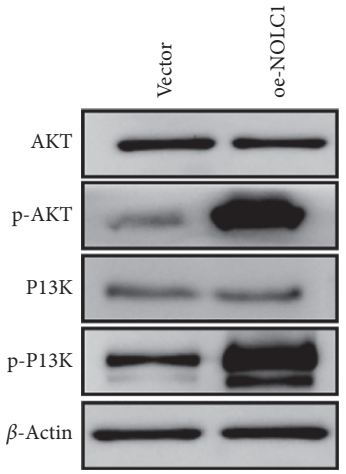

(a)

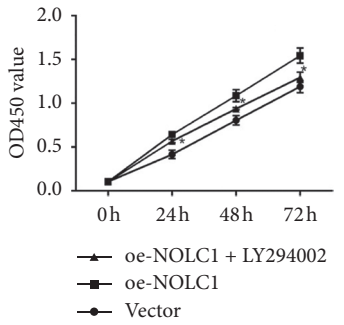

(b)

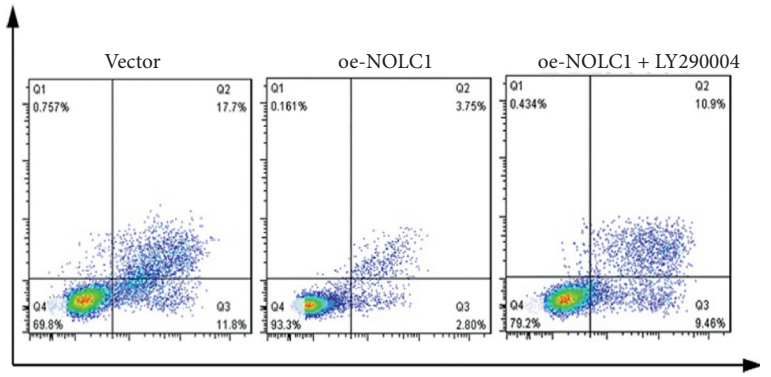

(c)

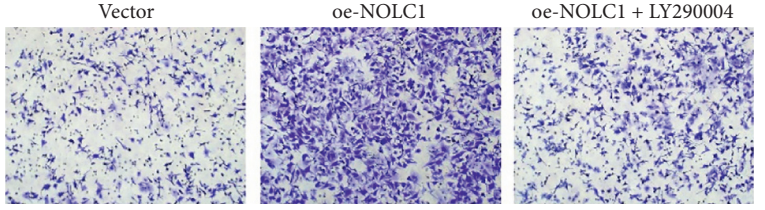

(d)

Figure 4: Continued.

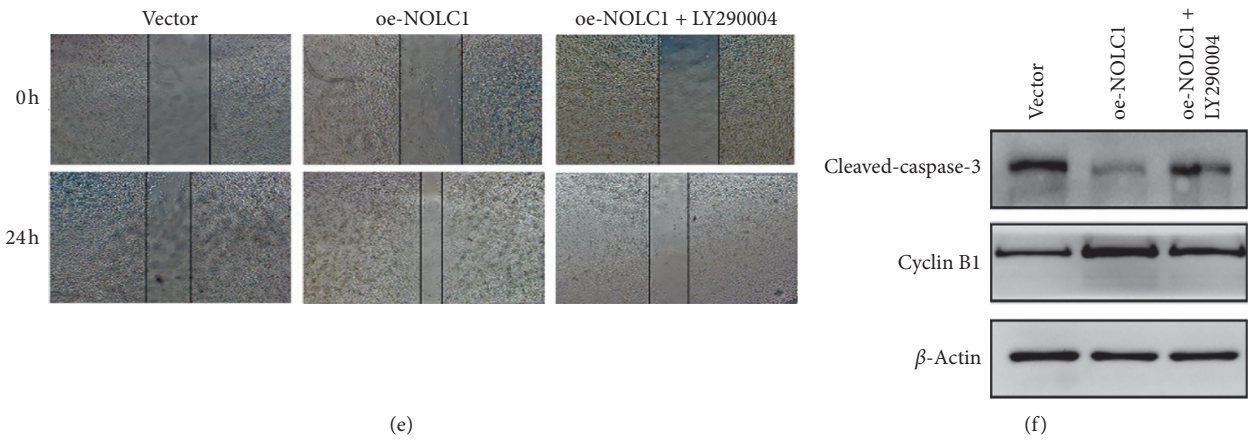

Figure 4: NOLC1 overexpression promotes oncogenesis and progression of ESCC via activating PI3K/AKT pathway. (a) The activation of PI3K/AKT pathway in Eca109 and TE-13 cells. (b) PI3K inhibitor LY294002 blocked cell proliferation mediated by NOLC1 overexpression vs. oe-NOLC1 group, $* p < 0.05$. (c) LY294002 impeded apoptosis rate caused by NOLC1 overexpression. (d) LY294002 abrogated invasion ability caused by NOLC1 overexpression. (e) LY294002 abolished migration ability induced by NOLC1 overexpression. (f) LY294002 reversed the expression of cyclin B1 and cleaved-caspase-3 induced by NOLC1 overexpression.

expression. However, this phenomenon could be reversed by LY294002 (Figure 4(f)). Collectively, these bodies of evidence indicated that NOLC1 overexpression promotes oncogenesis and progression of ESCA through activating the PI3K/AKT signaling pathway.

4. Discussion

Deregulation of NOLC1 has been observed in various cancer types, which is associated with poor prognosis in patients with nasopharyngeal carcinoma or lung cancer. In this study, our data provided further evidence that NOLC1 expression levels were overexpressed in ESCC tissues compared to normal adjacent tumor and correlated with poor prognosis. Additionally, NOLC1 knockdown inhibited proliferation, migration, invasion, and protein expression, such as cyclin B1, and promoted the apoptosis and cleaved-caspase-3 expression of Eca109 and TE-13 cells. NOLC1 overexpression accelerated proliferation, migration, invasion, and cyclin B1 expression and inhibited the apoptosis and cleaved-caspase-3 expression of ESCA cells via activating PI3K/AKT pathway. Rescue experiments show that PI3K inhibitor (LY294002) could reverse the phenomenon caused by NOLC1 overexpression.

Targeted therapy and molecular targeted therapy are the basis of sophisticated basic medicine, leading to the improved prognosis of patients with ESCC and also leading to resurgent research interest in the research of targeted agents in ESCA. NOLC1 exerts multiple functions, such as cell differentiation regulation [13] and rRNA transcription [6]. Few pieces of research have demonstrated that it has a function correlated with tumorigenesis [14]. For example, Hwang YC et al. showed that NOLC1 is more highly expressed in nasopharyngeal carcinoma compared with normal tissues and participates in tumorigenesis together with TP53 [7]. Krastev DB et al. have further confirmed that NOLC1 can be suppressed by p53 and contributed to molecular pathways of tumor suppressor genes [15]. In addition, Huaping Huang et al. showed that NOLC1 knockdown can enhance the drug sensitivity of NSCLC chemotherapy-resistant (A549/MDR) cells to multidrug response by inhibiting cell viability and accelerating cell apoptosis [9]. However, the exact functions of NOLC1 on tumorigenesis in ESCA remain elusive. Consistent with these facts, through GEPIA database, we found high expression of NOLC1 in ESCA tissues, but the expression was comparatively weak in normal adjacent tissues. Subsequently, we detected the NOLC1 expression in ESCA tissues and cell lines. The results confirmed that NOLC1 mRNA and protein levels were abundant in both ESCA tissue specimens and cell lines. The mRNA expression of NOLC1 in cancer cells, Kyse170, ECA9706, and T.TN is different from the protein expression, which may be due to post-transcriptional regulatory mechanisms such as translation and post-translational modifications. These data by themselves are certainly not enough to explain the exact mechanism of regulation, but they do provide a direction for us to conduct more targeted experiments. Moreover, NOLC1 overexpression was associated with bigger tumor size, lymph node metastasis, and advanced TNM stage in ESCA patients. Additionally, ESCA patients with NOLC1 overexpression have shorter overall survival than that of those with low NOLC1 expression. Moreover, NOLC1 overexpression was considered as an independent poor prognostic factor affecting overall survival. Based on these pieces of evidence, it was speculated that the NOLC1 overexpression might be involved in the tumorigenesis of ESCA. To verify this hypothesis, we conducted a loss of function experiment in vitro. Results showed that NOLC1 knockdown inhibited proliferation, migration, invasion, and protein expression, such as cyclin B1, and promoted the apoptosis and cleaved-caspase-3 expression of Eca109 and TE-13 cells. Collectively,

our research indicated that NOLC1 may serve as an oncogene by accelerating the proliferation, metastasis, and invasion of ESCA cells.

The specific mechanism by which NOLC1 contributed to tumorigenesis remains unclear. Intriguingly, it was recently reported that lncRNAs (TROLL-2 and TROLL-3) could counteract the interaction between WDR26 and NOLC1, while promoting the combination of WDR26 and AKT to activate the PI3K/AKT pathway in lung cancer cells, human breast carcinoma cells, and human melanoma cell lines [16]. PI3K/AKT pathway is dysregulated in various cancer cells. The PI3K/AKT pathway plays an important role in the internalization of membrane tyrosine kinases and external growth factors. Membrane kinases including epidermal growth factor receptor (EGFR) are activated by external growth factors, which initiate receptor dimerization and subsequent events to activate these intracellular pathways. AKT has multiple targets to modulate a variety of proliferative and antiproliferative signaling processes, such as survival, apoptosis, angiogenesis, cell cycle, cell-cycle energy, and DNA repair [17–22]. Additionally, Lianghai Wang et al. showed that the elevation of SOX9 inhibits the transcription of miR-203a by binding to the miR-203a promoter, thereby abolishing miR-203a-mediated impediment of PI3K/AKT/mTOR pathway [23]. Furthermore, Konstantia E. Tasioudi et al. reported that 90.5% of esophagus cancer (EC) patients expressed p-AKT mainly in the nucleus. Even in the absence of mutations in PIK3CA and Akt1, the expression of PI3K/AKT/mTOR pathway components is also expressed in EC and is associated with tumor grade, tumor stage, and clinicopathologic feature [24]. Consistent with previous research, in this study, NOLC1 overexpression elevated PI3K and AKT phosphorylation, which suggested that PI3K/AKT may be the downstream pathway of NOLC1. To verify this hypothesis, we conducted a series of rescue experiments. NOLC1 overexpression accelerated proliferation, migration, invasion, and cyclin B1 expression and inhibited the apoptosis and cleaved-caspase-3 expression in ESCA cells. Rescue experiments show that PI3K inhibitor (LY294002) could reverse the phenomenon caused by NOLC1 overexpression. Thus, NOLC1 can participate in the occurrence and development of ESCA via the PI3K/AKT pathway.

Although our research has further deepened our understanding of the function of NOLC1, this study also has some limitations that have not been clarified. However, the detailed interaction mechanism between NOLC and AKT pathway still needs to be explored, and the biological functions and mechanisms of NOLC and downstream pathways in the occurrence and development of ESCA still need further experimental exploration.

In conclusion, inhibition of NOLC1 expression may play an important role in regulating the occurrence and development of ESCA by inhibiting the proliferation, invasion, and migration, promoting the apoptosis, and regulating drug resistance-related molecules, which will provide a new perspective for the development of targeted drugs for the treatment of ESCA.

Data Availability

The data used to support the findings of this study are available from the corresponding author upon request.

Conflicts of Interest

The authors declare that they have no conflicts of interest.

References

[1] L. Ma, N. Yao, P. Chen, and Z. Zhuang, "TRIM27 promotes the development of esophagus cancer via regulating PTEN/AKT signaling pathway," *Cancer Cell International*, vol. 19, p. 283, 2019.

[2] J. Lv, L. Guo, J.-J. Liu, H.-P. Zhao, J. Zhang, and J.-H. Wang, "Alteration of the esophageal microbiota in Barrett's esophagus and esophageal adenocarcinoma," *World Journal of Gastroenterology*, vol. 25, no. 18, pp. 2149–2161, 2019.

[3] J. D. Bradley, C. Hu, R. R. Komaki et al., "Long-term results of NRG oncology RTOG 0617: standard- versus high-dose chemoradiotherapy with or without cetuximab for unresectable stage III non-small-cell lung cancer," *Journal of Clinical Oncology*, vol. 38, no. 7, pp. 706–714, 2020.

[4] Z. W. Reichenbach, M. G. Murray, R. Saxena et al., "Clinical and translational advances in esophageal squamous cell carcinoma," *Advances in Cancer Research*, vol. 144, pp. 95–135, 2019.

[5] A. Fatehi Hassanabad, R. Chehade, D. Breadner, and J. Raphael, "Esophageal carcinoma: towards targeted therapies," *Cellular Oncology*, vol. 43, no. 2, pp. 195–209, 2020.

[6] X. Gao, Q. Wang, W. Li et al., "Identification of nucleolar and coiled-body phosphoprotein 1 (NOLC1) minimal promoter regulated by NF-κB and CREB," *BMB Reports*, vol. 44, no. 1, pp. 70–75, 2011.

[7] Y.-C. Hwang, T.-Y. Lu, D.-Y. Huang et al., "NOLC1, an enhancer of nasopharyngeal carcinoma progression, is essential for TP53 to regulate MDM2 expression," *The American Journal of Pathology*, vol. 175, no. 1, pp. 342–354, 2009.

[8] Y. Chen, X. Shao, J. Cao et al., "Phosphorylation regulates cullin-based ubiquitination in tumorigenesis," *Acta Pharmaceutica Sinica B*, vol. 11, no. 2, pp. 309–321, 2021.

[9] H. Huang, T. Li, M. Chen et al., "Identification and validation of NOLC1 as a potential target for enhancing sensitivity in multidrug resistant non-small cell lung cancer cells," *Cellular and Molecular Biology Letters*, vol. 23, p. 54, 2018.

[10] X. Duan, J. Zhang, S. Liu, M. Zhang, Q. Wang, and J. Cheng, "Methylation of nucleolar and coiled-body phosphoprotein 1 is associated with the mechanism of tumorigenesis in hepatocellular carcinoma," *Oncology Reports*, vol. 30, no. 5, pp. 2220–2228, 2013.

[11] M. Zhang, S. Liu, M. S Chua et al., "SOCS5 inhibition induces autophagy to impair metastasis in hepatocellular carcinoma cells via the PI3K/Akt/mTOR pathway," *Cell Death and Disease*, vol. 10, no. 8, p. 612, 2019.

[12] H. Jiang, Z. Zhou, S. Jin et al., "PRMT 9 promotes hepatocellular carcinoma invasion and metastasis via activating PI 3K/Akt/GSK -3β/Snail signaling," *Cancer Science*, vol. 109, no. 5, pp. 1414–1427, 2018.

[13] A. Werner, S. Iwasaki, C. A. McGourty et al., "Cell-fate determination by ubiquitin-dependent regulation of translation," *Nature*, vol. 525, no. 7570, pp. 523–527, 2015.

[14] F. Yuan, G. Li, and T. Tong, "Nucleolar and coiled-body phosphoprotein 1 (NOLC1) regulates the nucleolar retention of TRF2," *Cell Death Discovery*, vol. 3, p. 17043, 2017.

[15] D. B. Krastev, M. Slabicki, M. Paszkowski-Rogacz et al., "A systematic RNAi synthetic interaction screen reveals a link between p53 and snoRNP assembly," *Nature Cell Biology*, vol. 13, no. 7, pp. 809–818, 2011.

[16] M. Napoli, X. Li, H. D Ackerman et al., "Pan-cancer analysis reveals TAp63-regulated oncogenic lncRNAs that promote cancer progression through AKT activation," *Nature Communications*, vol. 11, no. 1, p. 5156, 2020.

[17] S. A. Javadinia, S. Shahidsales, A. Fanipakdel et al., "The esophageal cancer and the PI3K/AKT/mTOR signaling regulatory microRNAs: a novel marker for prognosis, and a possible target for immunotherapy," *Current Pharmaceutical Design*, vol. 24, no. 39, pp. 4646–4651, 2018.

[18] Z. Wang, L. Kang, H. Zhang et al., "AKT drives SOX2 overexpression and cancer cell stemness in esophageal cancer by protecting SOX2 from UBR5-mediated degradation," *Oncogene*, vol. 38, no. 26, pp. 5250–5264, 2019.

[19] M. Song, X. Liu, K. Liu et al., "Targeting AKT with oridonin inhibits growth of esophageal squamous cell carcinoma in vitro and patient-derived xenografts in vivo," *Molecular Cancer Therapeutics*, vol. 17, no. 7, pp. 1540–1553, 2018.

[20] X. Fu, G. Cui, S. Liu, and S. Zhao, "Linc01014 regulates gefitinib resistance in oesophagus cancer via EGFR-PI3K-AKT-mTOR signalling pathway," *Journal of Cellular and Molecular Medicine*, vol. 24, no. 2, pp. 1670–1675, 2020.

[21] X. Deng, J. Zhao, L. Qu et al., "Ginsenoside Rh4 suppresses aerobic glycolysis and the expression of PD-L1 via targeting AKT in esophageal cancer," *Biochemical Pharmacology*, vol. 178, Article ID 114038, 2020.

[22] C. C. Liu, K. T. Chou, J. W. Hsu et al., "High metabolic rate and stem cell characteristics of esophageal cancer stem-like cells depend on the Hsp27-AKT-HK2 pathway," *International Journal of Cancer*, vol. 145, no. 8, pp. 2144–2156, 2019.

[23] L. Wang, Z. Zhang, X. Yu et al., "SOX9/miR-203a axis drives PI3K/AKT signaling to promote esophageal cancer progression," *Cancer Letters*, vol. 468, pp. 14–26, 2020.

[24] K. E. Tasioudi, S. Sakellariou, G. Levidou et al., "Immunohistochemical and molecular analysis of PI3K/AKT/mTOR pathway in esophageal carcinoma," *Apmis*, vol. 123, no. 8, pp. 639–647, 2015.

Hindawi
Journal of Oncology
Volume 2021, Article ID 9966744, 9 pages
https://doi.org/10.1155/2021/9966744

Research Article

MicroRNA-552 Accelerates the Progression of Gastric Cancer by Targeting FOXO1 and Regulating PI3K/AKT Pathway

Yuguo Zhao, Jianwen Zhang, Wenbin Yang, Zhao Yang, and Kaikai Zhou

Department of Gastrointestinal Surgery, The First People's Hospital of Chenzhou, Chenzhou, Hunan Province 423000, China

Correspondence should be addressed to Jianwen Zhang; h6041897js@163.com

Received 19 March 2021; Revised 19 April 2021; Accepted 26 April 2021; Published 5 May 2021

Academic Editor: Muhammad Wasim Khan

The specific function of microRNA-552 (miR-552) has been investigated in several malignancies, except gastric cancer (GC). Therefore, this study was performed to determine the role of miR-552 in GC.GC tissues and adjacent non-tumor tissues were collected to determine the expressions of miR-552. Quantitative real-time polymerase chain reaction assays (RT-qPCR) and Western blot analysis were carried out to measure expression levels. The regulatory mechanism of miR-552 was explored by (3-(4,5-dimethylthiazol-2-yl)-2,5-diphenyl tetrazolium bromide) MTT Assay, and Transwell assays. The binding site between miR-552 and FOXO1 was verified by dual-luciferase reporter assays. Upregulation of miR-552 expression was detected and associated with worse clinical outcomes in GC. Furthermore, high miR-552 expression predicted poor prognosis in GC patients. Functionally, upregulation of miR-552 promoted cell viability, metastasis, epithelial-mesenchymal transition (EMT), and phosphatidylinositol 3-kinase and protein kinase B (PI3K/AKT) pathway in GC. In addition, miR-552 was confirmed to target forkhead box O1 (FOXO1) directly and inversely regulate its expression in GC. Upregulation of FOXO1 reversed the carcinogenesis of miR-552 in GC. In conclusion, miR-552 serves as a tumor promoter in GC through targeting FOXO1 and regulating EMT and PI3K/AKT pathway.

1. Introduction

Gastric cancer (GC) is the second largest cancer, second only to lung cancer. Most patients with GC are over 50 years old, and men are twice as likely to have GC as women [1]. GC is more common in Japan and China, mainly due to dietary reasons. Moreover, the development of GC is extremely fast, and the current treatment can only control the spread of GC [2]. The therapeutic effect of GC is related to the onset, the pathological type, the thoroughness of surgical radicalization, and the comprehensive treatments [3]. Early GC has the best therapeutic effect, but there is a risk of recurrence. Nearly two-thirds of recurrence will lead to distant metastasis of GC, and distant metastasis is the biggest cause of death in GC patients [4]. Therefore, it is of great significance to explore potential molecular markers for the early diagnosis and treatment of GC.

MicroRNAs (miRNAs) are well-known to be involved in human diseases and cancers [5]. Moreover, many miRNAs have been reported to regulate biological activities in GC. For example, miR-423-5p was upregulated in GC and promoted cancer growth and metastasis [6]. An et al. proposed that miR-1236-3p was downregulated in GC and inhibited invasion and metastasis [7]. Now, the dysregulation of miR-552 caught our attention, which has not been investigated in GC. Miao et al. reported that miR-552 suppressed both transcription and translation of cytochrome P450 2E1 [8]. In addition, miR-552 can distinguish primary lung adenocarcinoma and colorectal cancer metastases [9]. MiR-552 was upregulated in osteosarcoma and hepatocellular carcinoma and promoted cell viability and metastasis [10, 11]. Besides that, increased expression of miR-552 was found to act as a potential predictor biomarker for poor prognosis of colorectal cancer [12]. Previous studies indicate that miR-552 participates in the pathogenesis of human cancers.

As a forkhead box transcription factor, forkhead box O1 (FOXO1) has been found to participate in cancer

development [13]. For example, the expression of FOXO1 predicted disease-free survival in breast cancer [14]. Xie et al. found that FOXO1 was a tumor suppressor in classical Hodgkin lymphoma [15]. Moreover, FOXO1 controlled thyroid cell proliferation and was involved in thyroid tumorigenesis [16, 17]. In the meantime, the interaction between FOXO1 and miRNAs has been detected in some malignancies, such as bladder cancer and breast cancers [17, 18]. FOXO1 has been proposed to play an essential role in PI3K/AKT signaling and regulate many biological activities in cancers [19]. It was reported that miR-132 played an oncogenic role in laryngeal squamous cell carcinoma by targeting FOXO1 and activating the PI3K/AKT pathway [20]. However, the regulatory mechanism of miR-552/FOXO1/PI3K/AKT remains unclear in GC. Therefore, the dysregulation of miR-552 and its regulatory mechanism in GC were evaluated in this study. These findings could provide new insights into GC treatment.

2. Materials and Methods

2.1. Sample Collection. In this study, GC specimens and normal specimens were obtained from 84 patients at The First People's Hospital of Chenzhou, Chenzhou, Hunan, China. Before the experiment, written informed consent was provided by all GC patients. The participants did not receive any treatment except for surgery. This study was approved by the Institutional Ethics Committee of The First People's Hospital of Chenzhou.

2.2. Cell Lines and Transfection. Normal gastric cell GES-1 and MKN-45, MGC-803 GC cell lines (BNCC, Beijing, China) were seeded in RPMI-1640 medium containing 10% fetal bovine serum (FBS). These cells were cultured at 37°C in 5% CO_2.

MiR-552 mimics or inhibitor, FOXO1 vector (RiboBio, Guangzhou, China) were severally transferred into MKN-45 cells using Lipofectamine 2000 (Invitrogen, Carlsbad, USA). Untreated MKN-45 cells were set as the control.

2.3. RT-qPCR. The extraction of total RNA was performed using TRIzol reagent (Invitrogen, Carlsbad, USA). The cDNA was synthesized by PrimeScript RT reagent (Takara, Dalian, China). We conducted RT-qPCR using SYBR Green Master Mix II (Takara) based on the manufacturer's instructions. MiR-552 or FOXO1 was normalized by U6 or GAPDH as the internal reference. Their expression levels were calculated using the $2^{-\triangle\triangle ct}$ method. The primers used in our work were as follows: miR-552, forward primer: 5′-GTT TAA CCT TTT GCC TGT TGG-3′, reverse primer: 5′-CGA ACG CTT CAC GAA TTT G-3'; U6, forward primer: 5′-CTC GCT TCG GCA GCA CA-3′, reverse primer: 5′-AAC GCT TCA CGA ATT TGC GT-3'; FOXO1 forward primer: 5′-AGG GTT AGT GAG CAG GTT ACA C-3′, reverse primer: 5′-TGC TGC CAA GTC TGA CGA AA-3'; GAPDH forward, 5′-ACA TCG CTC AGA CAC CAT G-3′, reverse, 5′-TGT AGT TGA GGT CAA TGA AGG G-3'.

2.4. MTT Assay. Transfected MKN-45 cells (4×10^3 cells/well) were seeded in RPMI-1640 with 10% FBS for 24, 48, 72 or 96 h. Next, the suspension of MKN-45 cells was added with 20 μl of MTT for 4 h. Then, 150 μl of dimethyl sulfoxide was added to the medium. After 10 minutes, cell viability was assessed using a microplate reader (Olympus Corp., Tokyo, Japan) to determine the optical density at 490 nm.

2.5. Transwell Assay. Transwell assay was used to assess cell migration and invasion abilities. Next, upper chamber was added with Matrigel (BD Biosciences, Franklin Lakes, NJ, USA) to detect MKN-45 cell invasion. The transfected cells (5×10^3 cells/well) were put in the upper chamber, and lower chamber filled with 10% FBS. The migrated or invaded cells were fixed with methanol and stained with 0.1% crystal violet for 30 mins. Finally, migrated or invaded cells were examined under a light microscope (Olympus Corporation, Tokyo, Japan). Cell migration assay was performed without Matrigel, and other process was the same as cell invasion assay.

2.6. Western Blot Analysis. First, the protein sample was lysed using RIPA buffer (Beyotime, Shanghai, China). Then, the supernatant was collected as the total protein. The protein was electrophoresed by 10% SDS-PAGE. The protein was blocked by 5% non-fat milk for 1 h. After incubating the protein with the following primary antibodies (Bax, Bcl-2, E-cadherin, N-cadherin, PI3K, AKT and GAPDH) overnight at 4°C, the diluted secondary antibodies were added to incubate protein for another 1 h. Finally, the protein was examined by an ECL reagent (Millipore, MA, USA).

2.7. Luciferase Reporter Assay. Dual-luciferase reporter assay (Promega, Madison, WI, USA) was performed to verify the relationships between miR-552 and FOXO1.The 3′-UTR of wild or mutant FOXO1 was inserted into pcDNA3.1 plasmid vector (Promega, Madison, USA) to construct the luciferase reporter vectors of Wt-FOXO1 and Mut-FOXO1. The above vectors were then severally transfected into MKN-45 cells with miR-552 mimics or NC-mimics using Lipofectamine 2000 (Invitrogen) to execute the dual-luciferase reporter assay. After incubation of 48 h, a dual-luciferase assay system (Promega, USA) was used to detect luciferase activities.

2.8. Statistical Analysis. Data are shown as mean ± SD, which were analyzed using SPSS 17.0 or Graphpad Prism 6. Chi-squared test, one-way analysis of variance with Tukey's post hoc test, and univariate Kaplan–Meier method with the log-rank test were applied to calculate differences between groups. Differences were considered as significant at $p < 0.05$.

3. Results

3.1. The Expression of miR-552 Was Increased in GC Tissues. The alternation of miR-552 expression was initially detected in GC tissues. RT-qPCR showed that miR-552 expression

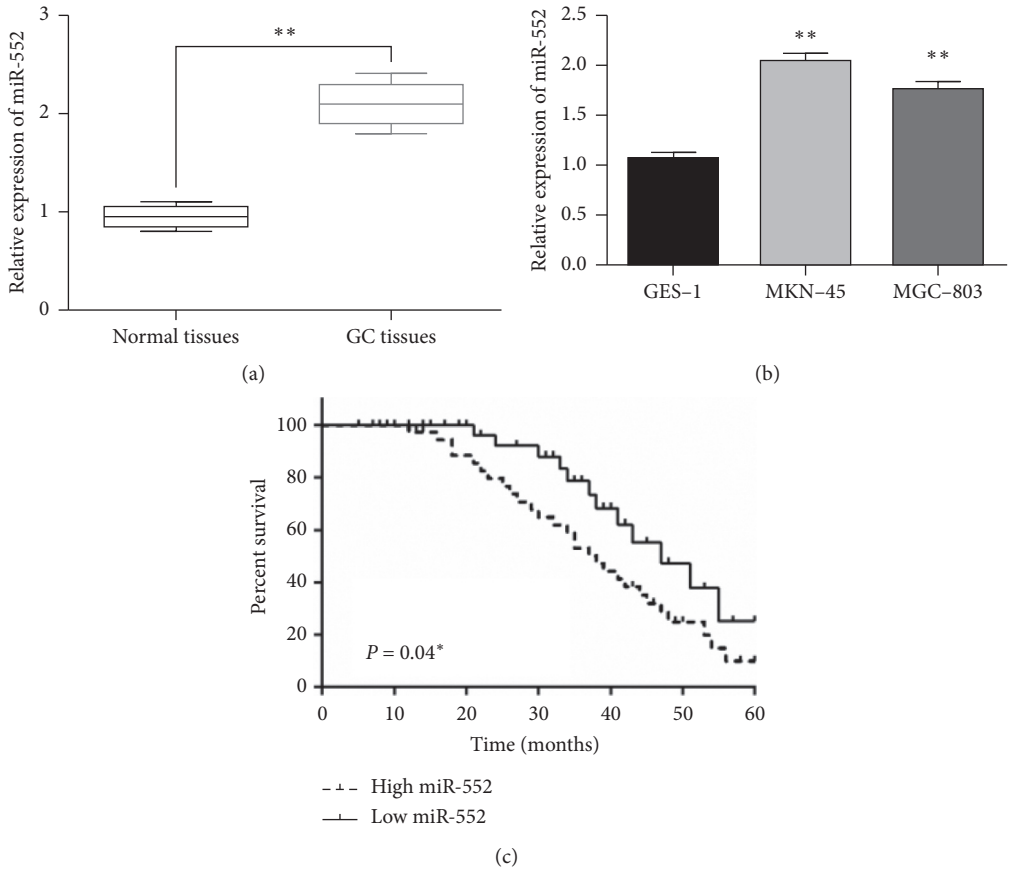

Figure 1: The expression of miR-552 was increased in GC tissues. (a) MiR-552 expressions in GC tissues. (b) The miR-552 expression in MKN-45 and MGC-803 cells compared to that in GES-1 cells. (c) High miR-552 expression was associated with poor prognosis in GC patients. * * $p < 0.01$.

was increased in GC tissues compared to normal tissues ($p < 0.01$, Figure 1(a)). Similarly, miR-552 was higher in MKN-45 and MGC-803 cells than in GES-1 cells ($p < 0.01$, Figure 1(b)). MKN-45 cells were selected for the functional assay due to the significant difference in miR-552 expression. In addition, we analyzed the correlation between abnormal miR-552 expression and clinical features in GC patients. GC patients were assigned into high and low miR-552 groups based on the median miR-552 expression level. As shown in Table 1, the dysregulation of miR-552 was associated with differentiation ($p < 0.01$), TNM stage ($p < 0.05$), and lymph node metastasis ($p < 0.05$). Furthermore, GC patients with high miR-552 expression showed a shorter overall survival, indicating that upregulating of miR-552 predicted poor prognosis in GC patients ($p < 0.01$, Figure 1(c)). These results indicated that miR-552 might function as an important regulator in the pathogenesis of GC.

3.2. Upregulation of miR-552 Promoted Cell Viability and Metastasis in GC. Next, miR-552 mimics or inhibitor was transfected into MKN-45 cells to perform a gain-loss experiment. MiR-552 expression was promoted by its mimics and inhibited by its inhibitor in MKN-45 cells ($p < 0.01$, Figure 2(a)). MTT assay revealed that overexpression of miR-552 promoted cell proliferation, whereas downregulation of miR-552 restrained MKN-45 cell proliferation ($p < 0.05$, Figure 2(b)). Transwell assay displayed that cell migration was accelerated by miR-552 mimics and repressed by miR-552 inhibitor in MKN-45 cells ($p < 0.01$, Figure 2(c)). Similarly, upregulation of miR-552 facilitated cell invasion, while downregulation of miR-552 inhibited cell invasion in MKN-45 cells ($p < 0.01$, Figure 2(d)). Taken together, miR-552 promoted the viability and metastasis of GC cells.

3.3. MiR-552 Activated EMT and PI3K/AKT Pathway in GC. In addition, the effect of miR-552 on the EMT and PI3K/AKT pathway was investigated to further illuminate its role in GC. As for EMT, miR-552 mimics were found to promote N-cadherin expression and inhibit the expression of E-cadherin. However, miR-552 inhibitor reduced N-cadherin expression and facilitated E-cadherin expression in MKN-45 cells (Figure 3). Next, expressions of apoptosis-associated proteins (Bcl-2/Bax) were measured in MKN-45 cells with miR-552 mimics or inhibitor. The results showed that miR-552 mimics declined Bax expression and promoted survival gene Bcl-2 expression. Furthermore, miR-552 inhibitor promoted Bax expression and reduced Bcl-2

Table 1: Relationship between miR-552 expression and their clinic-pathological characteristics in GC patients.

Characteristics	Cases	miR-552		p-value
		High	Low	
Age (years)				0.08
≥60	38	20	18	
<60	46	30	16	
Gender				0.15
Male	58	32	26	
Female	26	18	8	
Tumor size (mm)				0.21
≤5.0	31	19	12	
>5.0	53	31	22	
Differentiation				0.009*
Well/moderate	24	18	6	
Poor	60	32	28	
Lymph node metastasis				0.04*
Yes	62	42	20	
No	22	8	14	
TNM stage				0.02*
I-II	28	18	10	
III-IV	56	32	24	

Statistical analyses were performed by the χ^2 test. * $p < 0.05$ was considered significant.

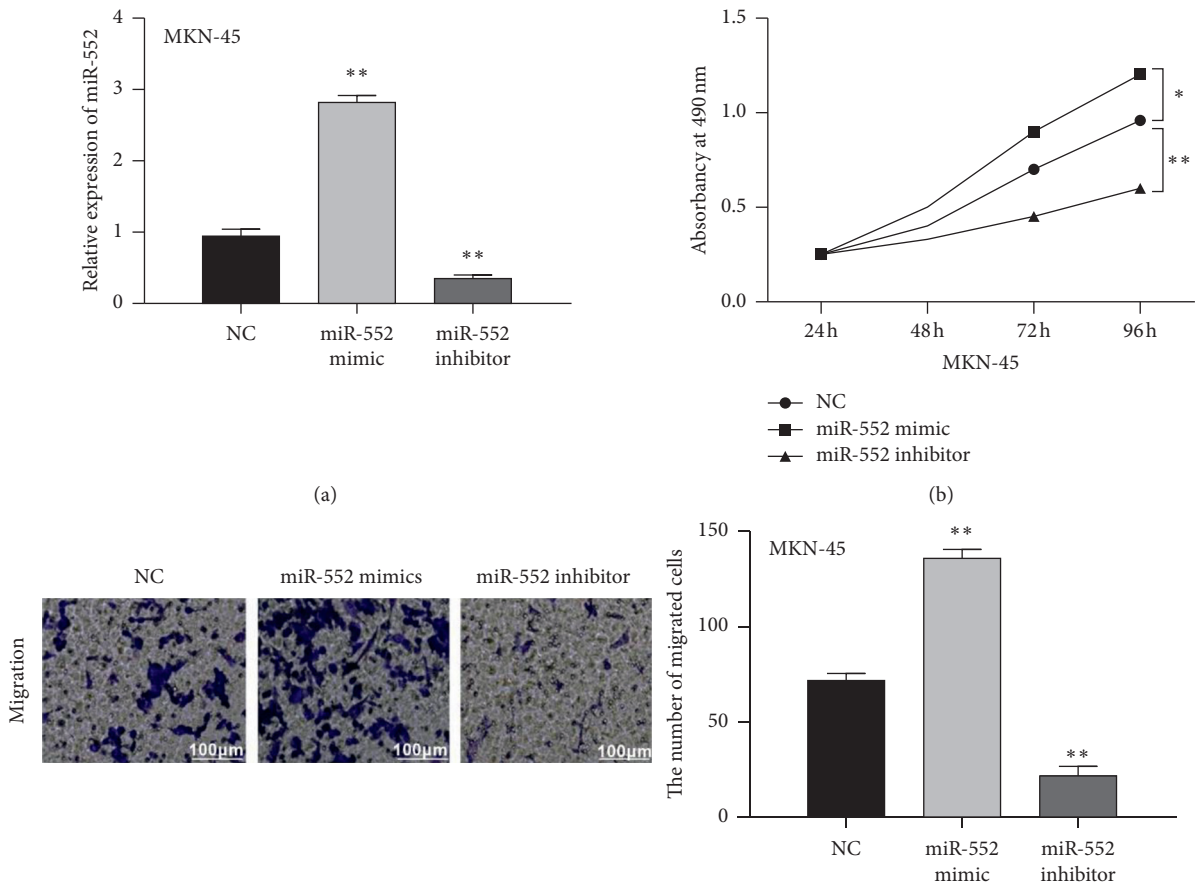

Figure 2: Continued.

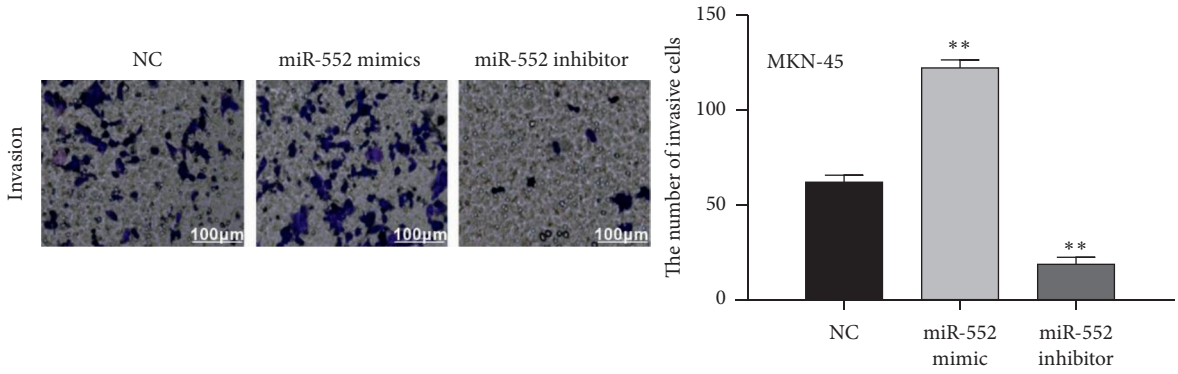

(d)

Figure 2: Upregulation of miR-552 promoted cell viability and metastasis in GC. (a) MiR-552 expression in MKN-45 cells with its mimics or inhibitor. (b–d) Cell proliferation, migration, and invasion regulated by miR-552 mimics or inhibitor. $^{*}p < 0.05$, $^{**}p < 0.01$.

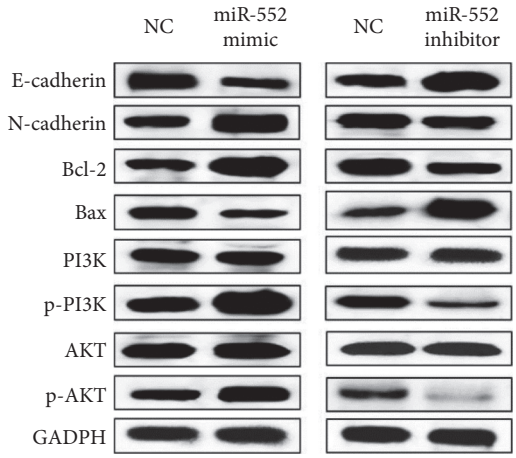

Figure 3: MiR-552 activated EMT and PI3K/AKT pathway in GC. MiR-552 regulated expressions of E-cadherin, N-cadherin, Bax, Bcl-2, PI3K, and AKT in MKN-45 cells.

expression (Figure 3). Besides that, expressions of p-PI3K and p-AKT were found to be promoted by the upregulation of miR-552 and suppressed by the downregulation of miR-552. However, expressions of PI3K and AKT were not affected by miR-552 in MKN-45 cells (Figure 3). Combining all these results, miR-552 was considered to serve as a cancerogenic factor in GC progression.

3.4. FOXO1 Is a Direct Target of miR-552. The downstream target of miR-552 was searched in TargetScan (http://www.targetscan.org/) databases to explain its regulatory mechanism in GC. It predicts that miR-552 has binding sites with the 3′-UTR of FOXO1 (Figure 4(a)). Luciferase reporter assay was designed to confirm this prediction. We found that miR-552 mimics decreased Wt-FOXO1 luciferase activity but had no effect on Mut-FOXO1 luciferase activity in MKN-45 cells ($p < 0.01$, Figure 4(b)). Furthermore, miR-552 has a negative correlation with FOXO1 expression in GC tissues ($p < 0.0001$, $R^2 = 0.7298$; Figure 4(c)). In addition, the expression level of FOXO1 was reduced by upregulation of miR-552 and enhanced by downregulation of miR-552 in MKN-45 cells ($p < 0.01$, Figures 4(d) and 4(e)). Briefly, miR-552 directly targets FOXO1 and has negative association with FOXO1 expression in GC.

3.5. Upregulation of FOXO1 Reversed the Carcinogenesis of miR-552 in GC. Finally, the interaction between miR-552 and FOXO1 was investigated in MKN-45 cells with miR-552 mimics and FOXO1 vector. RT-qPCR displayed that the FOXO1 vector restored its decreased expression induced by miR-552 mimics (Figure 5(a)). Functionally, upregulation of FOXO1 impaired the promoted effect of miR-552 on cell proliferation (Figure 5(b)). Similarly, the promoted effect of miR-552 on cell migration and invasion was also abolished by the FOXO1 vector (Figures 5(c) and 5(d)). In addition, the reverse effect of FOXO1 on EMT and PI3K/AKT pathway was also identified in MKN-45 cells (Figure 5(e)). Collectively, upregulation of FOXO1 weakened the carcinogenesis of miR-552 in GC.

4. Discussion

Recently, various miRNAs have been found to participate in tumorigenesis of GC. For example, miR-208a was upregulated and acted as a tumor promoter in GC [21]. In the current study, the expression of miR-552 was increased in GC tissues, which was related to worse clinical outcomes. Furthermore, high miR-552 expression predicted poor prognosis in GC patients. Functionally, upregulation of miR-552 promoted cell viability and metastasis in GC. Moreover, miR-552 activated EMT and enhanced p-PI3K and p-AKT expression in GC. In addition, miR-552 overexpression was found to reduce Bax expression and promote survival gene Bcl-2 expression in GC cells. Briefly, miR-552 plays a carcinogenic role in the progression of GC.

Consistent with our results, upregulation of miR-552 had been examined in colorectal cancer and osteosarcoma [10, 22]. In addition, increased expression of miR-552 was associated with a poor prognosis of colorectal cancer [12], which is the same as our results. Functionally, miR-552 was

	Predicted consequential pairing of target region (top) and miRNA (bottom)
Position 1706-1712 of FOXO1 3'UTR	5' . . .UAUUACUUUCCAAUUACCUGUAA. . .
hsa-miR-552-3p	3' AACAGAUUGGUCAGUGGACAA

(a)

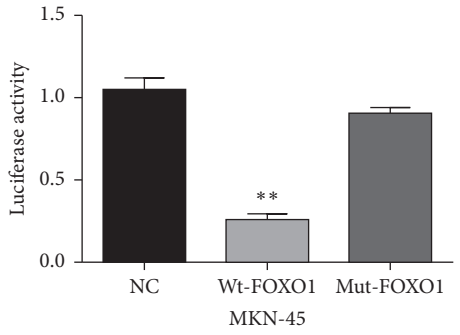

(b)

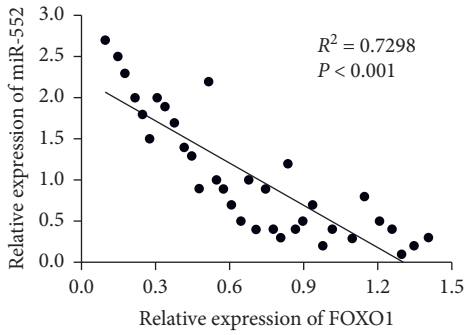

(c)

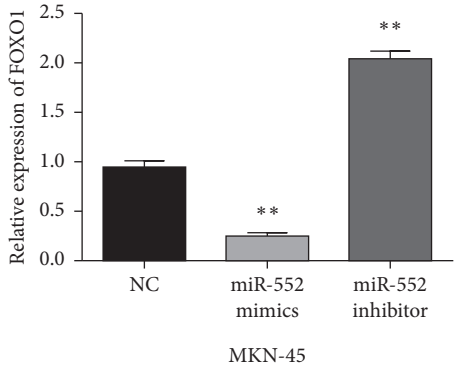

(d)

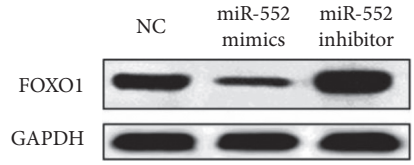

(e)

Figure 4: FOXO1 is a direct target of miR-552. (a) The binding sites between miR-552 and FOXO1. (b) Luciferase reporter assay. (c) A negative correlation between miR-552 and FOXO1. (d, e) FOXO1 expression in MKN-45 cells with miR-552 mimics or inhibitor. $^{**}p < 0.01$.

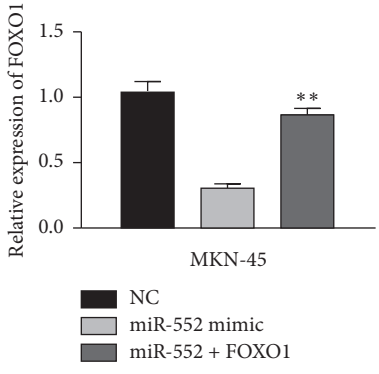

(a)

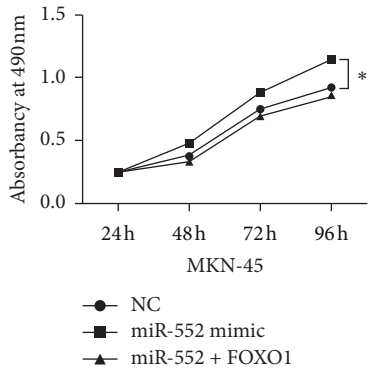

(b)

Figure 5: Continued.

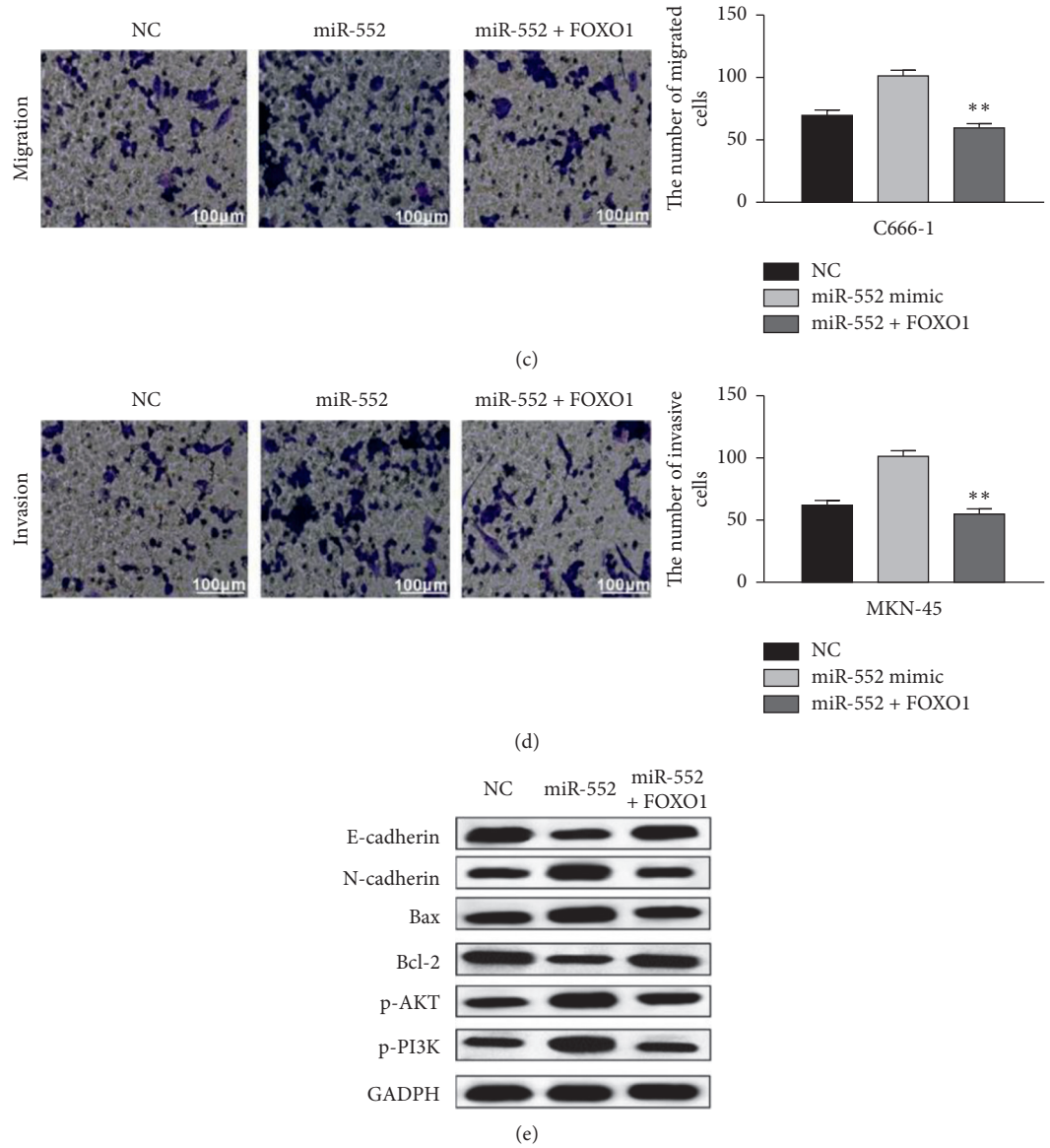

Figure 5: Upregulation of FOXO1 reversed the carcinogenesis of miR-552 in GC. (a) FOXO1 expression in MKN-45 cells with miR-552 mimics and FOXO1 vector. (b–d) Cell proliferation, migration, and invasion in MKN-45 cells with miR-552 mimics and FOXO1 vector. (e) Expressions of E-cadherin, N-cadherin, Bax, Bcl-2, PI3K, and AKT in MKN-45 cells with miR-552 mimics and FOXO1 vector. $^{*}p < 0.05$, $^{**}p < 0.01$.

reported to promote the proliferation and EMT of hepatocellular carcinoma cells [23]. Wang et al. demonstrated that miR-552 enhanced the metastatic capacity of colorectal cancer cells [24]. Here, the acceleration of proliferation, migration, and invasion of GC cells as well as EMT was also induced by miR-552. In addition, we also found that miR-552 regulated apoptosis-associated proteins (Bcl-2/Bax) and PI3K/AKT pathway to be involved in GC progression, which has not been reported in previous studies. Besides that, miR-552 was confirmed to target FOXO1 directly and inversely regulated its expression in GC.

FOXO1, as a target gene, is regulated by some miRNAs in human cancers, such as miR-9 and miR-135a [25, 26]. In particular, miR-132 upregulation was found to promote GC cell growth through suppression of FOXO1 translation [27]. In this study, the upregulation of FOXO1 reversed the carcinogenesis induced by miR-552 in GC. Furthermore, miR-552 overexpression suppressed FOXO1 expression in GC. It indicated that upregulation of miR-552 accelerated GC progression by downregulation of FOXO1. Besides that, FOXO1 has been shown to function as a tumor inhibitor in many cancers, including GC [28, 29]. These results also indicated that miR-552 served as a tumor promoter in GC by inhibiting FOXO1 expression. In addition, previous studies showed that miR-96 played an oncogenic role in papillary thyroid carcinoma by regulating AKT/FOXO1 pathway [30]. In our study, miR-552 also accelerated the progression of GC by regulating the FOXO1/PI3K/AKT pathway.

5. Conclusion

In summary, this study proposed the upregulation of miR-552 in GC, which was related to poor prognosis in GC patients. Functionally, miR-552 promoted cell viability and metastasis and activated EMT and I3K/AKT in GC via targeting FOXO1. Although we have preliminarily evaluated the regulatory mechanism of miR-552, a more in-depth study of miR-552 in GC is still essential.

Data Availability

The datasets used and/or analyzed during the current study are available from the corresponding author on reasonable request.

Ethical Approval

The study was approved by the Ethics Committee of The First People's Hospital of Chenzhou, Chenzhou, Hunan, China.

Conflicts of Interest

The authors declare that they have no competing interests.

Acknowledgments

This research did not receive any specific grant from funding agencies in the public, commercial, or not-for-profit sectors.

References

[1] M. Arnold, S. P. Moore, S. Hassler, L. Ellison-Loschmann, D. Forman, and F. Bray, "The burden of stomach cancer in indigenous populations: a systematic review and global assessment," *Gut*, vol. 63, no. 1, pp. 64–71, 2014.

[2] K. M. Fock and T. L. Ang, "Epidemiology ofHelicobacter pyloriinfection and gastric cancer in Asia," *Journal of Gastroenterology and Hepatology*, vol. 25, no. 3, pp. 479–486, 2010.

[3] J. G. Kim, B. Y. Ryoo, Y. H. Park et al., "Prognostic factors for survival of patients with advanced gastric cancer treated with cisplatin-based chemotherapy," *Cancer Chemotherapy and Pharmacology*, vol. 61, no. 2, pp. 301–307, 2008.

[4] A. Cervantes, D. Roda, N. Tarazona, S. Roselló, and J. A. Pérez-Fidalgo, "Current questions for the treatment of advanced gastric cancer," *Cancer Treatment Reviews*, vol. 39, no. 1, pp. 60–67, 2013.

[5] H. Liu, C. Lei, Q. He, Z. Pan, D. Xiao, and Y. Tao, "Nuclear functions of mammalian MicroRNAs in gene regulation, immunity and cancer," *Molecular Cancer*, vol. 17, p. 64, 2018.

[6] H. Yang, H. Fu, B. Wang et al., "Exosomal miR-423-5p targets SUFU to promote cancer growth and metastasis and serves as a novel marker for gastric cancer," *Molecular Carcinogenesis*, vol. 57, no. 9, pp. 1223–1236, 2018.

[7] J. X. An, M. H. Ma, C. D. Zhang, S. Shao, N. M. Zhou, and D. Q. Dai, "miR-1236-3p inhibits invasion and metastasis in gastric cancer by targeting MTA2," *Cancer Cell International*, vol. 18, p. 66, 2018.

[8] L. Miao, H. Yao, C. Li et al., "A dual inhibition: microRNA-552 suppresses both transcription and translation of cytochrome P450 2E1," *Biochimica et Biophysica Acta (BBA)—Gene Regulatory Mechanisms*, vol. 1859, no. 4, pp. 650–662, 2016.

[9] H. K. Kim, N. J. Lim, S. G. Jang, G. K. Lee, and G. K. Lee, "miR-592 and miR-552 can distinguish between primary lung adenocarcinoma and colorectal cancer metastases in the lung," *Anticancer Research*, vol. 34, no. 5, pp. 2297–2302, 2014.

[10] Y. Chao, K. Hu, X. Wang, and L. Wang, "MicroRNA-552 promotes migration and invasion of osteosarcoma through targeting TIMP2," *Biochemical and Biophysical Research Communications*, vol. 511, no. 1, pp. 63–68, 2019.

[11] W. Cai, Y. Xu, J. Yin, W. Zuo, and Z. Su, "miR-552-5p facilitates osteosarcoma cell proliferation and metastasis by targeting WIF1," *Experimental and Therapeutic Medicine*, vol. 17, no. 5, pp. 3781–3788, 2019.

[12] N. Wang and W. Liu, "Increased expression of miR-552 acts as a potential predictor biomarker for poor prognosis of colorectal cancer," *European Review for Medical and Pharmacological Sciences*, vol. 22, no. 2, pp. 412–416, 2018.

[13] A. Coomans de Brachène and J.-B. Demoulin, "FOXO transcription factors in cancer development and therapy," *Cellular and Molecular Life Sciences*, vol. 73, no. 6, pp. 1159–1172, 2016.

[14] Y. Wu, Y. Elshimali, M. Sarkissyan, H. Mohamed, S. Clayton, and J. V. Vadgama, "Expression of FOXO1 is associated with GATA3 and Annexin-1 and predicts disease-free survival in breast cancer," *American Journal of Cancer Research*, vol. 2, no. 1, pp. 104–115, 2012.

[15] L. Xie, A. Ushmorov, F. Leithäuser et al., "FOXO1 is a tumor suppressor in classical Hodgkin lymphoma," *Blood*, vol. 119, no. 15, pp. 3503–3511, 2012.

[16] M. A. Zaballos and P. Santisteban, "FOXO1 controls thyroid cell proliferation in response to TSH and IGF-I and is involved in thyroid tumorigenesis," *Molecular Endocrinology*, vol. 27, no. 1, pp. 50–62, 2013.

[17] I. K. Guttilla and B. A. White, "Coordinate regulation of FOXO1 by miR-27a, miR-96, and miR-182 in breast cancer cells," *Journal of Biological Chemistry*, vol. 284, no. 35, pp. 23204–23216, 2009.

[18] Y. Guo, H. Liu, H. Zhang, C. Shang, and Y. Song, "miR-96 regulates FOXO1-mediated cell apoptosis in bladder cancer," *Oncology Letters*, vol. 4, no. 3, pp. 561–565, 2012.

[19] B. M. T. Burgering and R. H. Medema, "Decisions on life and death: FOXO Forkhead transcription factors are in command when PKB/Akt is off duty," *Journal of Leukocyte Biology*, vol. 73, no. 6, pp. 689–701, 2003.

[20] R. Lian, B. Lu, L. Jiao et al., "MiR-132 plays an oncogenic role in laryngeal squamous cell carcinoma by targeting FOXO1 and activating the PI3K/AKT pathway," *European Journal of Pharmacology*, vol. 792, pp. 1–6, 2016.

[21] H.-B. Cui, H.-E. Ge, Y.-S. Wang, and X.-Y. Bai, "MiR-208a enhances cell proliferation and invasion of gastric cancer by targeting SFRP1 and negatively regulating MEG3," *The International Journal of Biochemistry & Cell Biology*, vol. 102, pp. 31–39, 2018.

[22] B. Kwak, D. U. Kim, T. O. Kim, H. S. Kim, and S. W. Kim, "MicroRNA-552 links Wnt signaling to p53 tumor suppressor in colorectal cancer," *International Journal of Oncology*, vol. 53, no. 4, pp. 1800–1808, 2018.

[23] W. Qu, X. Wen, K. Su, and W. Gou, "MiR-552 promotes the proliferation, migration and EMT of hepatocellular carcinoma cells by inhibiting AJAP1 expression," *Journal of Cellular and Molecular Medicine*, vol. 23, no. 2, pp. 1541–1552, 2019.

[24] J. Wang, H. Li, Y. Wang et al., "MicroRNA-552 enhances metastatic capacity of colorectal cancer cells by targeting a

disintegrin and metalloprotease 28," *Oncotarget*, vol. 7, no. 43, pp. 70194–70210, 2016.

[25] D.-Z. Liu, B. Chang, X.-D. Li, Q.-H. Zhang, and Y.-H. Zou, "MicroRNA-9 promotes the proliferation, migration, and invasion of breast cancer cells via down-regulating FOXO1," *Clinical and Translational Oncology*, vol. 19, no. 9, pp. 1133–1140, 2017.

[26] Y. B. Zeng, X. H. Liang, G. X. Zhang et al., "miRNA-135a promotes hepatocellular carcinoma cell migration and invasion by targeting forkhead box O1," *Cancer Cell International*, vol. 16, p. 63, 2016.

[27] W. Li, J. Zhang, T. Chen, P. Yin, J. Yang, and Y. Cao, "miR-132 upregulation promotes gastric cancer cell growth through suppression of FoxO1 translation," *Tumor Biology*, vol. 37, pp. 15551–15557, 2015.

[28] Y. Zang, T. Wang, J. Pan, and F. Gao, "miR-215 promotes cell migration and invasion of gastric cancer cell lines by targeting FOXO1," *Neoplasma*, vol. 64, no. 4, pp. 579–587, 2017.

[29] X. W. Yang, G. Z. Shen, L. Q. Cao et al., "MicroRNA-1269 promotes proliferation in human hepatocellular carcinoma via downregulation of FOXO1," *BMC Cancer*, vol. 14, p. 909, 2014.

[30] H. M. Song, Y. Luo, D. F. Li et al., "MicroRNA-96 plays an oncogenic role by targeting FOXO1 and regulating AKT/FOXO1/Bim pathway in papillary thyroid carcinoma cells," *International Journal of Clinical and Experimental Pathology*, vol. 8, no. 9, pp. 9889–9900, 2015.